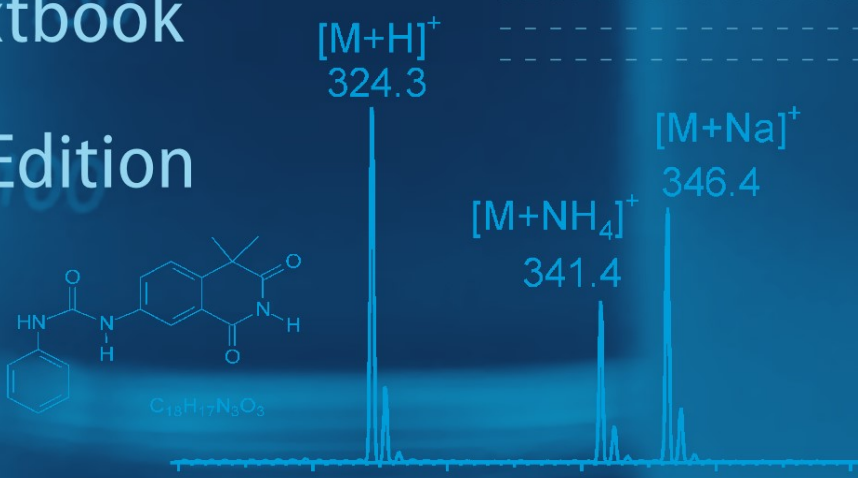
Jürgen H. Gross

Mass Spectrometry

A Textbook

2nd Edition



Springer

Mass Spectrometry

Second Edition

Jürgen H. Gross

Mass Spectrometry

A Textbook

Second Edition

Foreword by Peter Roepstorff

Springer

Jürgen H. Gross
Institute of Organic Chemistry
Heidelberg University
Im Neuenheimer Feld 270
69120 Heidelberg
Germany
email: author@ms-textbook.com

ISBN 978-3-642-10709-2 e-ISBN 978-3-642-10711-5
DOI 10.1007/978-3-642-10711-5
Springer Heidelberg Dordrecht London New York

© Springer-Verlag Berlin Heidelberg 2004, 2011
This work is subject to copyright. All rights are reserved, whether the whole or part of the material is concerned, specifically the rights of translation, reprinting, reuse of illustrations, recitation, broadcasting, reproduction on microfilm or in any other way, and storage in data banks. Duplication of this publication or parts thereof is permitted only under the provisions of the German Copyright Law of September 9, 1965, in its current version, and permission for use must always be obtained from Springer. Violations are liable to prosecution under the German Copyright Law.
The use of general descriptive names, registered names, trademarks, etc. in this publication does not imply, even in the absence of a specific statement, that such names are exempt from the relevant protective laws and regulations and therefore free for general use.

Cover design: WMXDesign GmbH, Heidelberg

Printed on acid-free paper

Springer is part of Springer Science+Business Media (www.springer.com)

Foreword

Shortly after having graduated in 1966 and just employed as a research assistant in a protein chemistry laboratory, my very first contact with mass spectrometry happened when I stumbled on a paper by Michael Barber, the later discoverer of fast atom bombardment (FAB). Together with a French group he had determined the covalent structure of an almost 1.4 kDa complex peptidolipid called fortuitine by using mass spectrometry. Fascinated by this to me unknown technique, I felt that MS would be a future key analytical method in protein studies. At that time, the only ionization method available was electron ionization, which required a sample to be in the gaseous state in the ion source. Therefore most mass spectrometric analyses were dealing with small organic molecules – and peptides and proteins were not volatile. Fortuitine was a very fortuitous sample, because it was naturally derivatized with the consequence that it could be volatilized into the ion source. Nevertheless, I went into mass spectrometry. My first mass spectrometer was installed in our laboratory in 1968. Mass spectrometers at that time were complex fully manually operated instruments most of them magnetic/electrostatic sector instruments, and the operator needed to know the instrument well in order to avoid catastrophes by opening wrong valves at the wrong moment. Spectra were recorded on UV paper with a galvanometer recorder or on photographic plates and mass assignment was performed manually. During the 1970s a number of new ionization methods and mass analyzers became available. These included ionization by chemical ionization and by field ionization/desorption as well as mass analyses by quadrupoles and ion traps. Computers became available for data acquisition and mass assignment. Life became easier but the requirement for volatile samples was still there.

The 1980s revolutionized the possibilities for mass spectrometric analysis. In the early half of the decade introduction of FAB and commercialization of the 10 years earlier developed plasma desorption mass spectrometry allowed for analyses of nonvolatile samples such as peptides, proteins, and nucleic acids. The first commercial fully automated mass spectrometer, the BioIon plasma desorption mass spectrometer, became available and the time-of-flight analyzer, which had unlimited mass range, was revived. Late in the decade the two new and now dominating ionization methods electrospray ionization (ESI) and matrix-assisted laser desorption ionization (MALDI) were introduced. These two ionization methods opened a new era for mass spectrometry. Now all the large nonvolatile biological molecules could be analyzed. Till then GC-MS had been extensively used for analysis of complex mixtures in environmental and clinical sciences, but due to its nature it was limited to small volatile molecules. ESI made coupling of LC with MS possible allowing for entirely new applications of mass spectrometry. Proteomics now became a big move forward with mass spectrometry as the key analytical tool. Thousands of scientists took up mass spectrometric analysis and

the instrument manufacturers realized that a new market had emerged and that the new generation of users were different from the previous technically skilled specialists. The new generation of instruments therefore became computer controlled, equipped with safety features to avoid any erroneous operation and with fully computerized data acquisition. The requirement from the biological sciences for high speed, sensitivity, and mass accuracy resulted in dramatic improvements of the performance of the instruments. Hybrid instruments combining the well-known mass analyzers were constructed, the FT-ICR mass spectrometer, which till then had only been available in highly specialized mass spectrometry laboratories, moved into the biological laboratory. Lately, the orbitrap analyzer, also based on Fourier transformation, has become standard in advanced biological research laboratories. Biological mass spectrometry and especially analysis of proteins and proteomics now dominate mass spectrometry conferences and mass spectrometry has a strong position in biological conferences, where these subjects ten years earlier were only marginally present.

What are the consequences of this development? For me, having tried to get mass spectrometry into protein science for more than 40 years it is of course encouraging. Mass spectrometry is without any doubt now the most versatile analytical technique available. It is used in a wide variety of areas from inorganic, nuclear chemistry, and geochemistry over organic chemistry, environmental analyses, clinical chemistry, to molecular and cell biology. Online separation of complex mixtures is possible using either GC-MS or LC-MS. Almost all commercial instruments are highly automated. However, this development also rises serious concerns. Many of the new users consider the mass spectrometer as a black box where they put in the sample in one end and get a result from the computer in the other end. They do not or only marginally understand the principles in their instrument and rarely look at the raw data. They are satisfied with computer prints with lists of identified compounds. Sample preparation often follows standard protocols and the understanding of the need for optimized sample preparation for each analytical task is often ignored. As a result, a considerable amount of the data obtained are questionable either due to poor sample preparation, poor instrument performance, or suboptimal use of the instruments. It is my wish that the new generation of mass spectrometry users will spend time to understand their instruments and the requirements for optimal preparation of the samples and it is my hope that this book will be read by many of them so that they can use their techniques to the best of the equipment's potential.

Odense, 2010

Peter Roepstorff
Department of Biochemistry and Molecular Biology
University of Southern Denmark

Preface to the Second Edition

To all readers of the first edition of *Mass Spectrometry – A Textbook* I would like to express my deepest gratitude. Without their interest in wanting to learn more about mass spectrometry by use of this book, all the efforts in writing it would have been a mere waste of time, and moreover, without their demand for updates, there would be no next edition. I would also like to thank the instructors all over the world who adopted and recommended this book for their own mass spectrometry courses.

Preparing the second edition of *Mass Spectrometry – A Textbook* was not an easy task. The years have witnessed a flood of innovations and detailed knowledge of interrelationships that were previously hardly understood. The time between the editions may have appeared a bit long for many eager scholars. But the author has used the time effectively to improve and update the entire contents, hopefully to the benefit of all who have been patiently bearing with me in anticipation.

So, what's new? The book now comprises fifteen instead of twelve chapters, each of them headed by essential "Learning Objectives". Chapter 9 inserts methods of ion activation such as CID, ECD, ETD, and IRMPD closely related to the instrumental approaches to tandem mass spectrometry. A second additional chapter deals with sampling and ion generation from surfaces under ambient conditions as afforded by DART and DESI, to name the most relevant methods. Finally, a new chapter on inorganic mass spectrometry has been added, for one, to include element speciation that bridges the gap between biomedical and trace elemental analysis and, also, to open a perspective extending beyond the key topics of this book. The chapter on instrumentation has been significantly expanded to cover orbitrap, linear ion traps, TOF/TOF, FT-ICR, and the ever-changing hybrid instruments including IMS-MS systems. More detailed attention is drawn to applications regarding biopolymers, especially in those chapters dealing with MALDI and ESI.

Overall, the book has been expanded by more than 200 pages. No chapter has remained untouched. Numerous passages have been rewritten to improve the clarity of explanations while keeping them short and concise. Care has been taken not only to explain how, but also to why things are done a certain way. Several schemes have been added to clarify interrelationships between different techniques. Tables compiling data for general reference where transferred to the expanded appendix. The book's website has been updated providing new exercises and supplementary material (http://www.ms-textbook.com).

Many kind people have supported me in the process of compiling this second edition. I appreciate the detailed knowledge and great thoroughness of Kenzo Hiraoka, Yasuhide Naito, Takemichi Nakamura, and Hiroaki Sato allocated to the translation of the first edition into Japanese. The valuable and welcome comments from readers from all over the world, and in particular, from book reviewers and colleagues have revealed some shortcomings in the first edition, which now have been eliminated to the improvement of the resulting new edition.

As in the first edition, several well-respected colleagues have contributed to this book by carefully checking contents in their fields of expertise. For the second edition, I want to express special thanks to Jürgen Grotemeyer, Universität Kiel, for checking Chap. 2 (*Principles of Ionization and Ion Dissociation*), Alexander Makarov, Thermo Fisher Scientific, Bremen (Chap. 4, *Instrumentation*), Christoph A. Schalley, Freie Universität Berlin (Chap. 9, *Tandem Mass Spectrometry*), Belá Paizs, German Cancer Research Center, Heidelberg (Chap. 11, *Matrix-Assisted Laser Desorption/Ionization*), Zoltán Takáts, Universität Gießen (Chap. 13, *Ambient Mass Spectrometry*), and Detlef Günther, ETH Zürich (Chap. 15, *Inorganic Mass Spectrometry*). Without their care and help the many new parts would not have reached the present level of accuracy. Despite intense reviewing and proofreading some errors inevitably may have remained. I apologize for these in advance and would highly appreciate any feedback from the readership in trying to identify and correcting them.

I am indebted to Peter Roepstorff, Odense University, for writing the Foreword with such a personal connotation. Permission to prepare this 2nd edition, alongside my official professional duties, by A. Stephen K. Hashmi, Director of OCI, and Heinfried Schöler, Dean of the Faculty of Chemistry and Earth Sciences is sincerely acknowledged. Many thanks to Doris Lang, Iris Mitsch, and Norbert Nieth, for smoothly running the routine analyses in our MS facility. And again, several mass spectrometry companies are acknowledged for supplying new instrument schemes and other figures for inclusion in the 2nd edition. Theodor C. H. Cole accomplished a great job in polishing up my English. Finally, I am immeasurably grateful to my family for their patience and solidarity in times when I had to come home late or needed to vanish on Saturdays during the writing of this book.

Have a good time studying, learning, and enjoying the world of mass spectrometry!

Heidelberg, 2010

Jürgen H. Gross
Institute of Organic Chemistry
Heidelberg University
Im Neuenheimer Feld 270
69120 Heidelberg
Germany
email: author@ms-textbook.com

Preface

When non-mass spectrometrists are talking about mass spectrometry it rather often sounds as if they were telling a story out of Poe's *Tales of Mystery and Imagination.* Indeed, mass spectrometry appears to be regarded as a mysterious method, just good enough to supply some molecular weight information. Unfortunately, this rumor about the dark side of analytical methods reaches students much earlier than their first contact with mass spectrometry. Possibly, some of this may have been bred by mass spectrometrists themselves who tended to celebrate each mass spectrum they obtained from the gigantic machines of the early days. Of course, there were also those who enthusiastically started in the 1950s to develop mass spectrometry out of the domain of physics to become a new analytical tool for chemistry.

Nonetheless, some oddities remain and the method which is to be introduced herein is not always straightforward and easy. If you had asked me, the author, just after having finished my introductory course whether mass spectrometry would become my preferred area of work, I surely would have strongly denied. On the other hand, J. J. Veith's mass spectrometry laboratory at Darmstadt University was bright and clean, had no noxious odors, and thus presented a nice contrast to a preparative organic chemistry laboratory. Numerous stainless steel flanges and electronics cabinets were tempting to be explored and – whoops – infected me with CMSD (chronic mass spectrometry disease). Staying with Veith's group slowly transformed me into a mass spectrometrist. Inspiring books such as *Fundamental Aspects of Organic Mass Spectrometry* or *Metastable Ions*, out of stock even in those days, did help me very much during my metamorphosis. Having completed my doctoral thesis on fragmentation pathways of isolated immonium ions in the gas phase, I assumed my current position. Since 1994, I have been head of the mass spectrometry laboratory at the Chemistry Department of Heidelberg University where I teach introductory courses and seminars on mass spectrometry.

When students ask what books to read on mass spectrometry, there are various excellent monographs, but the ideal textbook still seemed to be missing – at least in my opinion. Finally, encouraged by many people including P. Enders, Springer-Verlag Heidelberg, two years of writing began.

The present volume would not have its actual status without the critical reviews of the chapters by leading experts in the field. Their thorough corrections, remarks, and comments were essential. Therefore, P. Enders, Springer-Verlag Heidelberg (*Introduction*), J. Grotemeyer, University of Kiel (*Gas Phase Ion Chemistry*), S. Giesa, Bayer Industry Services, Leverkusen (*Isotopes*), J. Franzen, Bruker

Daltonik, Bremen (*Instrumentation*), J. O. Metzger, University of Oldenburg (*Electron Ionization* and *Fragmentation of Organic Ions and Interpretation of EI Mass Spectra*), J. R. Wesener, Bayer Industry Services, Leverkusen (*Chemical Ionization*), J. J. Veith, Technical University of Darmstadt (*Field Desorption*), R. M. Caprioli, Vanderbilt University, Nashville (*Fast Atom Bombardment*), M. Karas, University of Frankfurt (*Matrix-Assisted Laser Desorption/Ionization*), M. Wilm, European Molecular Biology Laboratory, Heidelberg (*Electrospray Ionization*) and M. W. Linscheid, Humboldt University, Berlin (*Hyphenated Methods*) deserve my deep gratitude.

Many manufacturers of mass spectrometers and mass spectrometry supply are gratefully acknowledged for sending large collections of schemes and photographs for use in this book. The author wishes to express his thanks to those scientists, many of them from the University of Heidelberg, who generously allowed to use material from their actual research as examples and to those publishers, who granted the numerous copyrights for use of figures from their publications. The generous permission of the National Institute of Standards and Technology (G. Mallard, J. Sauerwein) to use a large set of electron ionization mass spectra from the NIST/EPA/NIH Mass Spectral Library is also gratefully acknowledged. My thanks are extended to the staff of my facility (N. Nieth, A. Seith, B. Flock) for their efforts and to the staff of the local libraries for their friendly support. I am indebted to the former director of our institute (R. Gleiter) and to the former dean of our faculty (R. N. Lichtenthaler) for permission to write a book besides my official duties.

Despite all efforts, some errors or misleading passages will still have remained. Mistakes are an attribute that make us human, but unfortunately, they do not contribute to the scientific or educational value of a textbook. Therefore, please do not hesitate to report errors to me or to drop a line of comment in order to allow for corrections in a future edition.

Hopefully, *Mass Spectrometry – A Textbook* will introduce you to the many facets of mass spectrometry and will satisfy your expectations.

Heidelberg, 2003

Jürgen H. Gross
Institute of Organic Chemistry
Heidelberg University
Im Neuenheimer Feld 270
69120 Heidelberg
Germany
email: author@ms-textbook.com

Table of Contents

Table of Contents ..... **XI**

1 Introduction **1**
Learning Objectives 1
1.1 Aims and Scope 3
1.1.1 Filling the Black Box 5
1.2 What Is Mass Spectrometry? 5
1.2.1 Mass Spectrometry 6
1.2.2 Mass Spectrometer 7
1.2.3 Mass Scale 8
1.2.4 Mass Spectrum 9
1.3 Ion Chromatograms 11
1.4 Performance of Mass Spectrometers 13
1.4.1 Sensitivity 13
1.4.2 Detection Limit 14
1.4.3 Signal-to-Noise Ratio 14
1.5 Terminology – General Aspects 15
1.5.1 Basic Terminology in Describing Mass Spectra 16
1.6 Units, Physical Quantities, and Physical Constants 17
References 17

2 Principles of Ionization and Ion Dissociation **21**
Learning Objectives 21
2.1 Gas Phase Ionization by Energetic Electrons 21
2.1.1 Formation of Ions 22
2.1.2 Processes Accompanying Electron Ionization 23
2.1.3 Ions Generated by Penning Ionization 24
2.1.4 Ionization Energy 25
2.1.5 Ionization Energy and Charge-Localization 25
2.2 Vertical Transitions 27
2.3 Ionization Efficiency and Ionization Cross Section 29

2.4 Internal Energy and the Further Fate of Ions 30
2.4.1 Degrees of Freedom 31
2.4.2 Appearance Energy 32
2.4.3 Bond Dissociation Energies and Heats of Formation 33
2.4.4 Randomization of Energy 35
2.5 Quasi-Equilibrium Theory 37
2.5.1 QET's Basic Premises 37
2.5.2 Basic QET 38
2.5.3 Rate Constants and Their Meaning 39
2.5.4 $k_{(E)}$ Functions – Typical Examples 40
2.5.5 Reacting Ions Described by $k_{(E)}$ Functions 40
2.5.6 Direct Cleavages and Rearrangement Fragmentations 40
2.6 Time Scale of Events 42
2.6.1 Stable, Metastable, and Unstable Ions 43
2.6.2 Time Scale of Ion Storage Devices 44
2.7 Internal Energy – Practical Implications 45
2.8 Reverse Reactions and Kinetic Energy Release 46
2.8.1 Activation Energy of the Reverse Reaction 46
2.8.2 Kinetic Energy Release 48
2.8.3 Energy Partitioning 49
2.9 Isotope Effects 49
2.9.1 Primary Kinetic Isotope Effects 50
2.9.2 Measurement of Isotope Effects 51
2.9.3 Secondary Kinetic Isotope Effects 53
2.10 Determination of Ionization Energies 54
2.10.1 Conventional Determination of Ionization Energies 54
2.10.2 Improved *IE* Accuracy from Data Post-Processing 54
2.10.3 *IE* Accuracy – Experimental Improvements 55
2.10.4 Photoionization Processes 55
2.11 Determining the Appearance Energies 58
2.11.1 Kinetic Shift 58
2.11.2 Breakdown Graphs 59
2.12 Gas Phase Basicity and Proton Affinity 61
References 62

3 Isotopic Composition and Accurate Mass 67
Learning Objectives 67
3.1 Isotopic Classification of the Elements 67
3.1.1 Monoisotopic Elements 68
3.1.2 Di-isotopic Elements 68
3.1.3 Polyisotopic Elements 69
3.1.4 Representation of Isotopic Abundances 69
3.1.5 Calculation of Atomic, Molecular, and Ionic Mass 71
3.1.6 Natural Variations in Relative Atomic Mass 73
3.2 Calculation of Isotopic Distributions 74
3.2.1 Carbon: An X+1 Element 74

3.2.2 Terms Related to Isotopic Composition 77
3.2.3 Binomial Approach 77
3.2.4 Halogens 78
3.2.5 Combinations of Carbon and Halogens 80
3.2.6 Polynomial Approach 81
3.2.7 Oxygen, Silicon, and Sulfur 81
3.2.8 Polyisotopic Elements 84
3.2.9 Practical Aspects of Isotopic Patterns 84
3.2.10 Bookkeeping with Isotopic Patterns in Mass Spectra 85
3.2.11 Information from Complex Isotopic Patterns 86
3.3 Isotopic Enrichment and Isotopic Labeling 87
3.3.1 Isotopic Enrichment 87
3.3.2 Isotopic Labeling 88
3.4 Resolution and Resolving Power 88
3.4.1 Definitions 88
3.4.2 Resolution and its Experimental Determination 90
3.4.3 Resolving Power and its Effect on Relative Peak Intensity 91
3.5 Accurate Mass 92
3.5.1 Exact Mass and Molecular Formulas 92
3.5.2 Mass Defect 93
3.5.3 Mass Accuracy 95
3.5.4 Accuracy and Precision 96
3.5.5 Mass Accuracy and the Determination of Molecular Formulas 97
3.5.6 Extreme Mass Accuracy – Special Considerations 98
3.6 Applied High-Resolution Mass Spectrometry 99
3.6.1 External Mass Calibration 99
3.6.2 Internal Mass Calibration 101
3.6.3 Compiling Mass Reference Lists 103
3.6.4 Specification of Mass Accuracy 104
3.6.5 Deltamass 104
3.6.6 Kendrick Mass Scale 105
3.6.7 Van Krevelen Diagrams 106
3.7 Resolution Interacting with Isotopic Patterns 107
3.7.1 Multiple Isotopic Compositions at Very High Resolution 107
3.7.2 Isotopologs and Accurate Mass 110
3.7.3 Large Molecules – Isotopic Patterns at Sufficient Resolution 110
3.7.4 Large Molecules – Isotopic Patterns at Low Resolution 112
3.8 Charge State and Interaction with Isotopic Patterns 112
References 114

4 Instrumentation 117
Learning Objectives 117
4.1 How to Create a Beam of Ions 119
4.2 Time-of-Flight Instruments 120
4.2.1 Time-of-Flight – Basic Principles 120
4.2.2 TOF Instruments – Velocity of Ions and Time-of-Flight 121
4.2.3 Linear Time-of-Flight Analyzer 123

4.2.4 Reflector Time-of-Flight Analyzer 126
4.2.5 Higher Vacuum Improves Resolving Power 128
4.2.6 Delay Before Extraction to Improve Resolving Power 128
4.2.7 Analog-to-Digital Conversion 131
4.2.8 Orthogonal Acceleration TOF Analyzers 132
4.2.9 Operation of the oaTOF Analyzer 133
4.2.10 Duty Cycle 134
4.2.11 Time-to-Digital Conversion 135
4.3 Magnetic Sector Instruments 135
4.3.1 Evolution of Magnetic Sector Instruments 135
4.3.2 Principle of the Magnetic Sector 136
4.3.3 Focusing Action of the Magnetic Field 138
4.3.4 Double-Focusing Sector Instruments 139
4.3.5 Geometries of Double-Focusing Sector Instruments 141
4.3.6 Adjusting the Resolving Power of a Sector Instrument 143
4.3.7 Innovations in Sector Instruments 144
4.4 Linear Quadrupole Instruments 146
4.4.1 Introduction 146
4.4.2 The Linear Quadrupole 147
4.4.3 Resolving Power of Linear Quadrupoles 151
4.4.4 RF-Only Quadrupoles, Hexapoles, and Octopoles 152
4.5 Linear Quadrupole Ion Traps 155
4.5.1 Linear RF-Only Multipole Ion Traps 155
4.5.2 Mass-Analyzing Linear Quadrupole Ion Trap with Axial Ejection 158
4.5.3 Mass-Analyzing Linear Ion Trap with Radial Ejection 160
4.6 Three-Dimensional Quadrupole Ion Trap 164
4.6.1 Introduction 164
4.6.2 The Quadrupole Ion Trap 164
4.6.3 Visualization of Ion Motion in the Ion Trap 167
4.6.4 Mass-Selective Stability Mode 168
4.6.5 Mass-Selective Instability Mode 168
4.6.6 Resonant Ejection 169
4.6.7 Axial Modulation and Automatic Gain Control 170
4.6.8 Nonlinear Resonances 171
4.6.9 Digital Waveform Quadrupole Ion Trap 172
4.6.10 External Ion Sources for the Quadrupole Ion Trap 173
4.7 Fourier Transform Ion Cyclotron Resonance 174
4.7.1 Ion Cyclotron Resonance 174
4.7.2 Ion Cyclotron Motion 174
4.7.3 Cyclotron Motion – Excitation and Detection 175
4.7.4 Cyclotron Frequency Bandwidth and Energy-Time Uncertainty 177
4.7.5 Fourier Transform – Basic Properties 179
4.7.6 Nyquist Criterion 181
4.7.7 Excitation Modes in FT-ICR-MS 182
4.7.8 Axial Trapping and Design of ICR Cells 183
4.7.9 Magnetron Motion and Reduced Cyclotron Frequency 184

4.7.10 Detection and Accuracy in FT-ICR-MS 186
4.7.11 FT-ICR Instruments 187
4.8 Orbitrap Analyzer 189
4.8.1 Orbitrap – Principle of Operation 189
4.8.2 Ion Detection and Resolving Power of the Orbitrap 191
4.8.3 Ion Injection into the Orbitrap 192
4.8.4 Hybridization with a Linear Quadrupole Ion Trap 193
4.9 Hybrid Instruments 194
4.9.1 Evolution of Hybrid Mass Spectrometers 196
4.9.2 Ion Mobility-Mass Spectrometry Systems 198
4.10 Detectors 202
4.10.1 Discrete Dynode Electron Multipliers 203
4.10.2 Channel Electron Multipliers 204
4.10.3 Microchannel Plates 205
4.10.4 Post-Acceleration and Conversion Dynode 206
4.10.5 Focal Plane Detectors 207
4.11 Vacuum Technology 208
4.11.1 Basic Mass Spectrometer Vacuum System 209
4.11.2 High Vacuum Pumps 209
4.12 Purchasing an Instrument 210
References 210

5 Practical Aspects of Electron Ionization 223
Learning Objectives 223
5.1 Electron Ionization Ion Sources 223
5.1.1 Layout of an Electron Ionization Ion Source 223
5.1.2 Generation of Primary Electrons 225
5.1.3 Overall Efficiency and Sensitivity of an El Ion Source 226
5.1.4 Optimization of Ion Beam Geometry 227
5.2 Sample Introduction 228
5.2.1 Reservoir or Reference Inlet System 228
5.2.2 Direct Insertion Probe 231
5.2.3 Sample Vials for Use with Direct Insertion Probes 232
5.2.4 Fractionation When Using Direct Insertion Probes 233
5.2.5 Direct Exposure Probe 235
5.3 Pyrolysis Mass Spectrometry 237
5.4 Gas Chromatograph 237
5.5 Liquid Chromatograph 238
5.6 Low-Energy Electron Ionization Mass Spectra 239
5.7 Analytes for EI 241
5.8 Mass Analyzers for EI 241
5.9 Mass Spectral Databases for EI 242
5.9.1 NIST/EPA/NIH Mass Spectral Database 243
5.9.2 Wiley Registry of Mass Spectral Data 244
5.9.3 Mass Spectral Databases – General Aspects 244
References 245

6 Fragmentation of Organic Ions and Interpretation of EI Mass Spectra ... 249
Learning Objectives ... 249
6.1 Cleavage of a Sigma-Bond ... 250
6.1.1 Writing Conventions for Molecular Ions ... 250
6.1.2 σ-Bond Cleavage in Small Nonfunctionalized Molecules ... 251
6.1.3 Even-Electron Rule ... 252
6.1.4 σ-Bond Cleavage in Small Functionalized Molecules ... 254
6.2 Alpha-Cleavage ... 255
6.2.1 α-Cleavage of Acetone Molecular Ion ... 255
6.2.2 Stevenson's Rule ... 257
6.2.3 α-Cleavage of Nonsymmetrical Aliphatic Ketones ... 259
6.2.4 Acylium Ions and Carbenium Ions ... 260
6.2.5 α-Cleavage When Heteroatoms Belong to the Aliphatic Chain ... 262
6.2.6 α-Cleavage of Aliphatic Amines ... 262
6.2.7 Nitrogen Rule ... 265
6.2.8 α-Cleavage of Aliphatic Ethers and Alcohols ... 266
6.2.9 Charge Retention at the Heteroatom ... 268
6.2.10 α-Cleavage of Thioethers ... 269
6.2.11 α-Cleavage of Halogenated Hydrocarbons ... 269
6.2.12 Double α-Cleavage ... 271
6.2.13 Double α-Cleavage for the Identification of Regioisomers ... 272
6.3 Distonic Ions ... 273
6.3.1 Definition of Distonic Ions ... 273
6.3.2 Formation and Properties of Distonic Ions ... 274
6.3.3 Distonic Ions as Intermediates ... 275
6.4 Benzylic Bond Cleavage ... 275
6.4.1 Cleavage of the Benzylic Bond in Phenylalkanes ... 275
6.4.2 The Further Fate of $[C_6H_5]^+$ and $[C_7H_7]^+$ ... 277
6.4.3 Isomerization of $[C_7H_8]^{+\bullet}$ and $[C_8H_8]^{+\bullet}$ Ions ... 279
6.4.4 Rings Plus Double Bonds ... 280
6.5 Allylic Bond Cleavage ... 281
6.5.1 Cleavage of the Allylic Bond in Aliphatic Alkenes ... 281
6.5.2 Methods for the Localization of the Double Bond ... 283
6.6. Cleavage of Non-Activated Bonds ... 284
6.6.1 Saturated Hydrocarbons ... 284
6.6.2 Carbenium Ions ... 286
6.6.3 Very Large Hydrocarbons ... 287
6.6.4 Recognition of the Molecular Ion Peak ... 288
6.7 McLafferty Rearrangement ... 290
6.7.1 McL of Aldehydes and Ketones ... 290
6.7.2 Fragmentation of Carboxylic Acids and Their Derivatives ... 293
6.7.3 McL of Aromatic Hydrocarbons ... 296
6.7.4 McL with Double Hydrogen Transfer ... 297
6.8 Retro-Diels-Alder Reaction ... 300
6.8.1 Properties of the Retro-Diels-Alder Reaction ... 300

6.8.2 Influence of Positional Isomerism on the RDA Reaction 302
6.8.3 RDA Reaction in Natural Products 303
6.8.4 Widespread Occurrence of the RDA Reaction 303
6.9 Elimination of Carbon Monoxide 304
6.9.1 CO Loss from Phenols 304
6.9.2 CO and C_2H_2 Loss from Quinones 307
6.9.3 Fragmentation of Arylalkylethers 308
6.9.4 CO Loss from Transition Metal Carbonyl Complexes 310
6.9.5 CO Loss from Carbonyl Compounds 311
6.9.6 Differentiation Between Loss of CO, N_2, and C_2H_4 311
6.10 Thermal Degradation vs. Ion Fragmentation 312
6.10.1 Decarbonylation and Decarboxylation 312
6.10.2 Retro-Diels-Alder Reaction 312
6.10.3 Loss of H_2O from Alkanols 312
6.10.4 EI Mass Spectra of Organic Salts 314
6.11 Alkene Loss from Onium Ions 315
6.11.1 McL of Onium Ions 316
6.11.2 Onium Reaction 319
6.12 Ion-Neutral Complexes 322
6.12.1 Evidence for the Existence of Ion-Neutral Complexes 322
6.12.2 Attractive Forces in Ion-Neutral Complexes 323
6.12.3 Criteria for Ion-Neutral Complexes 324
6.12.4 Ion-Neutral Complexes of Radical Ions 325
6.13 *Ortho* Elimination (*Ortho* Effect) 326
6.13.1 *Ortho* Elimination from Molecular Ions 327
6.13.2 *Ortho* Elimination from Even-Electron Ions 328
6.13.3 *Ortho* Elimination in the Fragmentation of Nitroarenes 331
6.14 Heterocyclic Compounds 332
6.14.1 Saturated Heterocyclic Compounds 333
6.14.2 Aromatic Heterocyclic Compounds 336
6.15 Guide to the Interpretation of Mass Spectra 340
6.15.1 Summary of Rules 340
6.15.2 Systematic Approach to Mass Spectra 341
References 342

7 Chemical Ionization 351
Learning Objectives 351
7.1 Basics of Chemical Ionization 351
7.1.1 Formation of Ions in Positive-Ion Chemical Ionization 351
7.1.2 Chemical Ionization Ion Sources 352
7.1.3 Sensitivity of Chemical Ionization 353
7.1.4 Chemical Ionization Techniques and Terms 353
7.2 Protonation in Chemical Ionization 354
7.2.1 Source of Protons 354
7.2.2 Methane Reagent Gas Plasma 355
7.2.3 CH_5^+ and Related Ions 356

7.2.4 Energetics of Protonation 356
7.2.5 Impurities of Higher *PA* than the Reagent Gas 357
7.2.6 Methane Reagent Gas PICI Spectra 358
7.2.7 Other Reagent Gases in PICI 359
7.3 Proton Transfer Reaction Mass Spectrometry 361
7.3.1 Reactant Ion Formation in PTR-MS 362
7.3.2 Analyte Ion Formation in PTR-MS 362
7.4 Charge Exchange Chemical Ionization 364
7.4.1 Energetics of CE 365
7.4.2 Reagent Gases for CE-CI 365
7.4.3 Compound Class-Selective CE-CI 366
7.4.4 Regio- and Stereoselectivity in CE-CI 368
7.5 Negative-Ion Chemical Ionization 368
7.6 Electron Capture 370
7.6.1 Ion Formation by Electron Capture 370
7.6.2 Energetics of EC 370
7.6.3 Creating Thermal Electrons 372
7.6.4 Appearance of EC Spectra 373
7.6.5 Applications of EC 373
7.7 Desorption Chemical Ionization 374
7.8 Analytes for CI 375
References 376

8 Field Ionization and Field Desorption 381
Learning Objectives 381
8.1 Field Ionization Process 382
8.2 FI and FD Ion Sources 383
8.3 Field Emitters 385
8.3.1 Blank Metal Wires as Emitters 385
8.3.2 Activated Emitters 385
8.3.3 Emitter Temperature 386
8.3.4 Handling of Activated Emitters 387
8.4 Field Ionization Mass Spectrometry 388
8.4.1 Origin of $[M+H]^+$ Ions in FI-MS 389
8.4.2 Multiply-Charged Ions in FI-MS 389
8.4.3 Field-Induced Dissociation 390
8.4.4 Accurate Mass FI Spectra 390
8.4.5 Coupling Gas Chromatography to FI-MS 391
8.5 FD Spectra 392
8.5.1 Ion Formation by Field Ionization in FD-MS 393
8.5.2 Desorption of Preformed Ions in FD-MS 394
8.5.3 Cluster Ion Formation in FD-MS 396
8.5.4 FD-MS of Ionic Analytes 397
8.5.5 Best Anode Temperature and Thermal Decomposition 399
8.5.6 FD-MS of Polymers 400
8.5.7 Types of Ions in FD-MS 401

8.6 Liquid Injection Field Desorption Ionization 402
8.7 General Properties of FI-MS and FD-MS 405
8.7.1 Sensitivity of FI-MS and FD-MS 405
8.7.2 Analytes and Practical Considerations for FI, FD, and LIFDI 407
8.7.3 Mass Analyzers for FI and FD 407
References 408

9 Tandem Mass Spectrometry 415
Learning Objectives 415
9.1 Concepts of Tandem Mass Spectrometry 415
9.1.1 Tandem-in-Space and Tandem-in-Time 416
9.1.2 Pictograms for MS/MS Experiments 418
9.2 Metastable Ion Dissociation 420
9.3 Collision-Induced Dissociation 420
9.3.1 Effecting Collisions in a Mass Spectrometer 420
9.3.2 Energy Transfer During Collisions 421
9.3.4 Single and Multiple Collisions in CID 424
9.3.5 Time Scale of Ion Activating Processes 426
9.4 Surface-Induced Dissociation 426
9.5 Tandem MS on TOF Instruments 427
9.5.1 Utilizing a ReTOF for Tandem MS 427
9.5.2 Curved-Field Reflectron 429
9.5.3 Tandem MS on True Tandem TOF Instruments 429
9.6 Tandem MS with Magnetic Sector Instruments 431
9.6.1 Dissociations in the FFR Preceding the Magnetic Sector 431
9.6.2 Mass-Analyzed Ion Kinetic Energy Spectra 432
9.6.3 Determination of Kinetic Energy Release 432
9.6.4 B/E = *Const.* Linked Scan 434
9.6.5 Additional Linked Scan Functions 434
9.6.6 Multi-Sector Instruments 436
9.7 Tandem MS with Linear Quadrupole Analyzers 437
9.7.1 Triple Quadrupole Mass Spectrometers 437
9.7.2 Scan Modes for Tandem MS with Triple Quadrupole Instruments 438
9.7.3 Penta Quadrupole Instruments 438
9.8 Tandem MS with the Quadrupole Ion Trap 439
9.9 Tandem MS with Linear Quadrupole Ion Traps 443
9.9.1 Tandem MS on QqLIT Instruments 444
9.9.2 Tandem MS on LITs with Radial Ejection 444
9.10 Tandem MS with Orbitrap Instruments 445
9.10.1 Higher-Energy C-Trap Dissociation 446
9.10.2 Extended LIT-Orbitrap Hybrid Instruments 446
9.11 Tandem MS with FT-ICR Instruments – Part I 448
9.11.1 Sustained Off-Resonance Irradiation-CID in ICR Cells 448
9.12 Infrared Multiphoton Dissociation 451
9.12.1 IRMPD in QITs and LITs 452
9.13 Electron Capture Dissociation 452

9.13.1 Principles of Electron Capture Dissociation 452
9.13.2 Peptide Ion Cleavages Upon ECD 454
9.14 Tandem MS with FT-ICR Instruments – Part II 455
9.14.1 IRMPD for Tandem FT-ICR-MS 455
9.14.2 Infrared Photodissociation Spectroscopy 456
9.14.3 Blackbody Infrared Radiative Dissociation 457
9.14.4 ECD for Tandem FT-ICR-MS 458
9.15 Electron Transfer Dissociation 459
9.16 Electron Detachment Dissociation 461
9.17 Summary of Ion Activation Techniques 462
9.18 Special Applications of Tandem MS 463
9.18.1 Ion–Molecule Reactions in Catalytic Studies 464
9.18.2 Gas Phase Hydrogen–Deuterium Exchange 464
9.18.3 Determination of Gas Phase Basicities and Proton Affinities 466
9.18.4 Neutralization-Reionization Mass Spectrometry 467
References 468

10 Fast Atom Bombardment 479
Learning Objectives 479
10.1 Ion Sources for FAB and LSIMS 480
10.1.1 FAB Ion Sources 480
10.1.2 LSIMS Ion Sources 482
10.1.3 FAB Probes 482
10.2 Ion Formation in FAB and LSIMS 483
10.2.1 Ion Formation from Inorganic Samples 483
10.2.2 Ion Formation from Organic Samples 484
10.3 Liquid Matrices for FAB and LSIMS 486
10.3.1 The Role of the Liquid Matrix 486
10.3.2 FAB Matrix Spectra – General Characteristics 487
10.3.3 Unwanted Reactions in FAB-MS 487
10.4 Applications of FAB-MS 488
10.4.1 FAB-MS of Analytes of Low to Medium Polarity 488
10.4.2 FAB-MS of Ionic Analytes 490
10.4.3 High-Mass Analytes in FAB-MS 491
10.4.4 Accurate Mass Measurements in FAB Mode 492
10.4.5 Continuous-Flow FAB 494
10.4.6 Low-Temperature FAB 495
10.4.7 FAB-MS and Peptide Sequencing 496
10.5 FAB and LSIMS – General Characteristics 496
10.5.1 Sensitivity of FAB-MS 496
10.5.2 Types of Ions in FAB-MS 497
10.5.3 Analytes for FAB-MS 497
10.5.4 Mass Analyzers for FAB-MS 497
10.6 Massive Cluster Impact 498
10.7 ^{252}Californium Plasma Desorption 498
References 499

11 Matrix-Assisted Laser Desorption/Ionization 507
Learning Objectives 507
11.1 Ion Sources for LDI and MALDI 508
11.2 Ion Formation 509
11.2.1 Ion Yield and Laser Fluence 510
11.2.2 Effect of Laser Irradiation on the Surface 511
11.2.3 Temporal Evolution of a Laser Desorption Plume 512
11.2.4 Processes of Ion Formation in MALDI 513
11.2.5 "Lucky Survivor" Model of Ion Formation 514
11.3 MALDI Matrices 516
11.3.1 Role of the Solid Matrix 516
11.3.2 Matrices in UV-MALDI 516
11.3.3 Characteristics of MALDI Matrix Spectra 519
11.4 Sample Preparation 519
11.4.1 MALDI Target 519
11.4.2 Standard Sample Preparation 520
11.4.3 Cationization 522
11.4.4 Cation Removal 524
11.4.5 Solvent-Free Sample Preparation 526
11.4.6 Additional Methods of Sample Supply 527
11.5 Applications of LDI 527
11.6 Applications of MALDI 529
11.6.1 Protein Analysis by MALDI-MS 529
11.6.2 Peptide Sequencing and Proteomics 531
11.6.3 Carbohydrate Analysis by MALDI-MS 536
11.6.4 Oligonucleotide Analysis by MALDI-MS 538
11.6.5 MALDI-MS of Synthetic Polymers 539
11.7 Special Surfaces to Mimic the Matrix 541
11.7.1 Desorption/Ionization on Silicon 541
11.7.2 Nano-Assisted Laser Desorption/Ionization 542
11.7.3 Further Variations of the MALDI Theme 543
11.8 MALDI Imaging 544
11.9 Atmospheric Pressure MALDI 546
11.10 General Characteristics of MALDI 547
11.10.1 Sample Consumption and Detection Limit 547
11.10.2 Analytes for MALDI 547
11.10.3 Types of Ions in LDI and MALDI-MS 548
11.10.4 Mass Analyzers for MALDI-MS 548
References 549

12 Electrospray Ionization 561
Learning Objectives 561
12.1 Development of ESI and Related Methods 562
12.1.1 Atmospheric Pressure Ionization 563
12.1.2 Thermospray 564
12.1.3 Electrohydrodynamic Ionization 565

12.1.4 Electrospray Ionization 565
12.2 Ion Sources for ESI 566
12.2.1 Basic Design Considerations 566
12.2.2 Adaptation to Different Flow Rates 568
12.2.3 Improved Electrospray Configurations 569
12.2.4 Advanced Electrospray Interface Designs 571
12.2.5 Nozzle-Skimmer Dissociation 573
12.3 Nanoelectrospray 574
12.3.1 Practical Considerations for NanoESI 575
12.3.2 Spray Modes of NanoESI 576
12.3.3 Nanoelectrospray from a Chip 577
12.4 Ion Formation in ESI 578
12.4.1 Formation of the Electrospray Plume 578
12.4.2 Disintegration of Charged Droplets 581
12.4.3 Formation of Ions from Charged Droplets 582
12.5 Multiply Charged Ions and Charge Deconvolution 585
12.5.1 Dealing with Multiply Charged Ions 585
12.5.2 Mathematical Charge Deconvolution 587
12.5.3 Computerized Charge Deconvolution 588
12.5.4 Hardware Charge Deconvolution 590
12.5.5 Controlled Charge Reduction in ESI 592
12.6 Applications of ESI-MS 593
12.6.1 ESI-MS of Small Molecules 593
12.6.2 ESI of Metal Complexes 594
12.6.3 ESI of Surfactants 596
12.6.4 Oligonucleotides, DNA, and RNA 596
12.6.5 ESI-MS of Oligosaccharides 599
12.6.6 High-Mass Proteins and Protein Complexes 600
12.7 Summary of ESI Characteristics 601
12.7.1 Sample Consumption 603
12.7.2 Types of Ions in ESI 603
12.7.3 Mass Analyzers for ESI 603
12.8 Atmospheric Pressure Chemical Ionization 604
12.8.1 Ion Sources for APCI 604
12.8.2 Ion Formation in APCI 605
12.8.3 APCI Spectra 605
12.9 Atmospheric Pressure Photoionization 608
12.9.1 Ion Formation in APPI 608
12.9.2 APPI Spectra 610
References 612

13 Ambient Mass Spectrometry 621
Learning Objectives 621
13.1 Desorption Electrospray Ionization 622
13.1.1 Experimental Setup for DESI 622
13.1.2 Mechanisms of Ion Formation in DESI 626

13.1.3 Analytical Features of DESI 627
13.2 Desorption Atmospheric Pressure Chemical Ionization 631
13.3 Desorption Atmospheric Pressure Photoionization 632
13.4 Other Methods Related to DESI 634
13.4.1 Desorption Sonic Spray Ionization 635
13.4.2 Extractive Electrospray Ionization 635
13.4.3 Electrospray-Assisted Laser Desorption/Ionization (ELDI) 637
13.4.4 Laser Ablation Electrospray Ionization 638
13.4.5 Atmospheric Pressure Solids Analysis Probe 640
13.5 Direct Analysis in Real Time 640
13.5.1 Experimental Setup for DART 640
13.5.2 Ion Formation in DART 642
13.5.3 Analytical Applications of DART 642
13.6 Overview of Ambient Mass Spectrometry 644
References 645

14 Hyphenated Methods 651
Learning Objectives 651
14.1 Concept of Chromatography-Mass Spectrometry 652
14.1.1 Ion Chromatograms 653
14.1.2 Repetitive Acquisition of Mass Spectra During Elution 654
14.1.3 Selected Ion Monitoring 656
14.1.4 Selected Reaction Monitoring 658
14.2 Quantitation 659
14.2.1 Quantitation by External Standardization 659
14.2.2 Quantitation by Internal Standardization 660
14.2.3 Quantitation by Isotope Dilution 661
14.2.4 Retention Times of Isotopologs 663
14.3 Gas Chromatography-Mass Spectrometry 663
14.3.1 GC-MS Interfaces 663
14.3.2 Volatility and Derivatization 664
14.3.3 Column Bleed 665
14.3.4 Fast GC-MS 667
14.3.5 Multiplexing for Increased Throughput 667
14.4 Liquid Chromatography-Mass Spectrometry 668
14.4.1 Multiplexed LC-ESI-MS 671
14.5 Ion Mobility Spectrometry-Mass Spectrometry 673
14.6 Tandem MS as a Complement to LC-MS 675
14.7 Ultrahigh-Resolution Mass Spectrometry 678
References 680

15 Inorganic Mass Spectrometry 685
Learning Objectives 685
15.1 Thermal Ionization Mass Spectrometry 689
15.2 Spark Source Mass Spectrometry 691
15.3 Glow Discharge Mass Spectrometry 694

15.4 Inductively Coupled Plasma Mass Spectrometry 697
15.4.1 Laser Ablation ICP-MS 700
15.5 Secondary Ion Mass Spectrometry 701
15.5.1 Atomic SIMS 702
15.5.2 Instrumentation for Atomic SIMS 702
15.5.3 Molecular SIMS 704
15.5.4 Polyatomic Primary Ion Beams 705
15.6 Accelerator Mass Spectrometry 707
15.7 Conclusion 710
References 711

Appendix 717
A.1 Units, Physical Quantities, and Physical Constants 717
A.2 Isotopic Composition of the Elements 718
A.3 Carbon Isotopic Patterns 725
A.4 Chlorine and Bromine Isotopic Patterns 726
A.5 Silicon and Sulfur Isotopic Patterns 727
A.6 Isotopologs and Accurate Mass 727
A.7 Characteristic Ions 728
A.8 Common Impurities 729
A.9 Amino Acids 730
A.10 Method Selection Guide 731
A.11 How to Recognize Cationization 732
A.12 Systematic Approach to Mass Spectra 733
A.13 Rules for the Interpretation of Mass Spectra 733
A.14 Nobel Prizes for Mass Spectrometry 734

Subject Index 735

1 Introduction

Learning Objectives

- The relevance of mass spectrometry
- Mass spectrometry – Basic concepts
- How mass spectra are displayed and communicated
- The performance features of mass spectrometry
- Basic terminology and conventions in data presentation

Mass spectrometry is an indispensable analytical tool in chemistry, biochemistry, pharmacy, medicine, and many related fields of science. No student, researcher or practitioner in these disciplines can really get by without a substantial knowledge of mass spectrometry. Can this statement be approved?

Mass spectrometry (MS) is employed to analyze combinatorial libraries [1,2] sequence biomolecules [3], and help explore single cells [4,5] or objects from outer space [6]. Structure elucidation of unknown substances, environmental and forensic analytes, quality control of drugs, foods, and polymers: they all rely to a great extent on mass spectrometry [7-13]. Today, "mass spectrometry is interwoven with biology to an extent that basic considerations of proteomics research are dealt with in a MS journal" [14].

Whatever the analytical interest may be: mass spectrometry aims to identify a compound from the molecular or atomic mass(es) of its constituents. The information delivered by mass alone can be sufficient for the identification of elements and the determination of the molecular formula of an analyte. The relative abundance of isotopologs helps to decide which elements contribute to such a formula and to estimate the number of atoms of a contributing element. Under the conditions of certain mass spectrometric experiments, fragmentation of ions can deliver information on ionic structure. Thus, MS elucidates the connectivity of atoms within smaller molecules, identifies functional groups, determines the (average) number and eventually the sequence of constituents of macromolecules, and in some cases even yields their three-dimensional structure. From the 1950s to the present, mass spectrometry has developed in big strides and innovations are still being made at an enormous rate [15,16]. The pioneering mass spectrometrist worked with home-built rather than commercial instruments. These machines, typically magnetic sector instruments using electron ionization, delivered a few mass spectra per day, providing that the device was delicately handled. Intimate knowledge of such an instrument and interpretation skills of the according EI spectra would provide the mass spectrometrist with a previously unknown wealth

J. Gross, *Mass Spectrometry*, 2nd ed., DOI 10.1007/978-3-642-10711-5_1,
© Springer-Verlag Berlin Heidelberg 2011

of insight into structural details [17-22]. In particular the life sciences gave a great impetus for new developments for expanding the mass range to higher molecular weights and increasingly fragile molecules.

Table 1.1. Fields of application of mass spectrometry

Key application and field of application	Explanation
Elemental and isotopic analysis Physics Radiochemistry Geochemistry	Elemental identification and isotopic abundance measurement of both short-lived and stable species in physics and radiochemistry (nuclear waste), in geochemistry and more recently in the life sciences.
Organic and bio-organic analysis Organic chemistry Polymer chemistry Biochemistry and medicine	Identification and structural characterization of molecules from small to very large as provided either by chemistry, physiological processes, or polymer chemistry.
Structure elucidation Organic chemistry Polymer chemistry Biochemistry and medicine	Mass spectrometric experiments can be arranged consecutively to study mass-selected ions in tandem mass spectrometry (MS/MS or MS^2). Eventually products are subjected to a third level (MS^3) and so forth (MS^n).
Characterization of ionic species and chemical reactions Physical chemistry Thermochemistry	Tandem MS provides an elegant means for the study of unimolecular or bimolecular reactions of gas phase ions and for the determination of ion energetics.
Coupling to separation techniques Quality control Environmental analysis Complex mixture analysis Petroleum chemistry Food chemistry	MS can be coupled to separation methods such as gas chromatography (GC) and liquid chromatography (LC). 'Hyphenation', i.e., as GC-MS or LC-MS, delivers high selectivity and low detection limits for the analysis of trace compounds in complicated matrices or the deconvolution of complex mixtures.
Mass spectral imaging Biomedical studies Material sciences	Mass spectra can be obtained from micrometer-sized areas on surfaces, translating the lateral distribution of compounds on surfaces (microelectronics, slices of tissue) into images, which in turn can be correlated to optical images.
Miniaturization Field portable MS Space missions Military applications	Mass spectrometers can be very small. Portable instruments allow for environmental on-site analysis, detection systems for explosives and warfare chemicals, and last but not least for many space missions.

Environmental and pharmaceutical research has been a driving force in reaching even lower limits of detection. Current research is aimed at methods of ion sampling, ion generation, and subsequent ion transfer into mass analyzers for superior performance.

Nowadays, the output of mass spectra has reached an unprecedented level. Highly automated systems produce thousands of spectra per day when running a routine application where samples of the very same type are to be treated by an analytical protocol that has been carefully elaborated by an expert beforehand. A large number of ionization methods and types of mass analyzers has been developed and combined in various ways. Thus, people sometimes feel overwhelmed by the mere task of selecting one out of about a dozen of promising techniques available for their particular sample. It is precisely this diversity that makes a basic understanding of the concepts and tools of mass spectrometry more important than ever. On the other extreme, there are mass spectrometry laboratories specialized on employing only one particular method – preferably matrix-assisted laser desorption/ionization (MALDI) or electrospray ionization (ESI). In contrast to some 50 years ago, the instrumentation is now concealed in a sort of "black box", more appealingly designed to resemble an espresso machine or tumble dryer. Let us take a look inside!

1.1 Aims and Scope

This book is tailored to be your guide to mass spectrometry – from the first steps to your daily work in research. Starting from the very principles of gas phase ion chemistry and isotopic properties, it leads you through the design of mass analyzers, mass spectral interpretation, and applied ionization methods. The book closes with chapters on chromatography–mass spectrometry coupling and one on inorganic mass spectrometry. In total, it comprises fifteen chapters that can be read independently from each other. However, for the novice it is recommended to work through from start to finish, occasionally skipping over more advanced sections (Table 1.1). Now in its 2nd edition, "Mass Spectrometry – A Textbook" continues to be your companion from undergraduate to graduate studies in chemistry, biochemistry, and other natural sciences, and aims to hold its value when serving as a hands-on reference in the course of professional life.

Step by step you will understand how mass spectrometry works and what it can do as a powerful tool in your hands – equally well for analytical applications as for basic research. A clear layout and many high-quality figures will make is easier to acquire the new knowledge. Many tables have been included, compiling facts and comparing topics. Interrelationships are pointed to where appropriate. The correctness of scientific content has been examined by leading experts. Each chapter begins with a set of Learning Objectives and closes by providing an elaborate list of references, emphasizing tutorial and review articles, book chapters, and monographs in the respective field. Titles are included with all citations to help

with the evaluation of useful further reading [23]. References for general further reading on mass spectrometry are compiled at the end of this Introduction.

The coverage of this book is basically restricted to what is called “organic mass spectrometry” in a broad sense. It includes the ionization methods and mass analyzers currently in use, and in addition to classical organic compounds it covers applications to bio-organic samples such as peptides and oligonucleotides. Of course, transition metal complexes, synthetic polymers, and fullerenes are discussed as well as environmental or forensic applications. Elemental analysis, the classical field of inorganic mass spectrometry has been added to get a taste of mass spectrometry beyond molecular species.

Table 1.2. Chapters of this book: overview for orientation

No.	Chapter Title	Comment
1	Introduction	Getting ready, getting started
2	Principles of Ionization and Ion Dissociation	Tools of the trade. Basics needed for the understanding of any of the subsequent chapters
3	Isotopic Composition and Accurate Mass	
4	Instrumentation	
5	Practical Aspects of Electron Ionization	Electron ionization: the classical key to organic MS and indispensable part of every introductory course
6	Fragmentation of Organic Ions and Interpretation of EI Mass Spectra	
7	Chemical Ionization	Traditional, nonetheless still highly relevant soft ionization methods
8	Field Ionization and Field Desorption	
9	Tandem Mass Spectrometry	Fully controlled dissociation of mass-selected ions for many interesting purposes
10	Fast Atom Bombardment	More soft ionization methods. The latter two represent today's most relevant techniques in MS
11	Matrix-Assisted Laser Desorption/Ionization	
12	Electropray Ionization	
13	Ambient Mass Spectrometry	Exciting new field based on advances in atmospheric pressure ionization methods
14	Hyphenated Methods	Coupling of separation techniques to MS
15	Inorganic Mass Spectrometry	There is even more: a glimpse beyond the horizon of organic and biomedical MS

Note: "Problems and solutions" sections are omitted from the printed book. These are available free of charge at **http://www.ms-textbook.com**.

1.1.1 Filling the Black Box

There is no single "golden rule" in approaching the wide field of mass spectrometry. In any case, it is necessary to learn about the ways of sample introduction, generation of ions, their mass analysis, and their detection as well as about data redording and presentation of mass spectra – and what's more is the art of interpreting mass spectra. All these aspects are correlated to each other in many ways and in their entirety contribute to what is referred to as mass spectrometry (Fig. 1.1). In other words, mass spectrometry is multifacet rather than to be viewed from a single perspective. Like a view onto a globe does not reveal the complete surface of our planet, but roughly just one continent at a time, mass spectrometry needs to be explored from various vantage points [24].

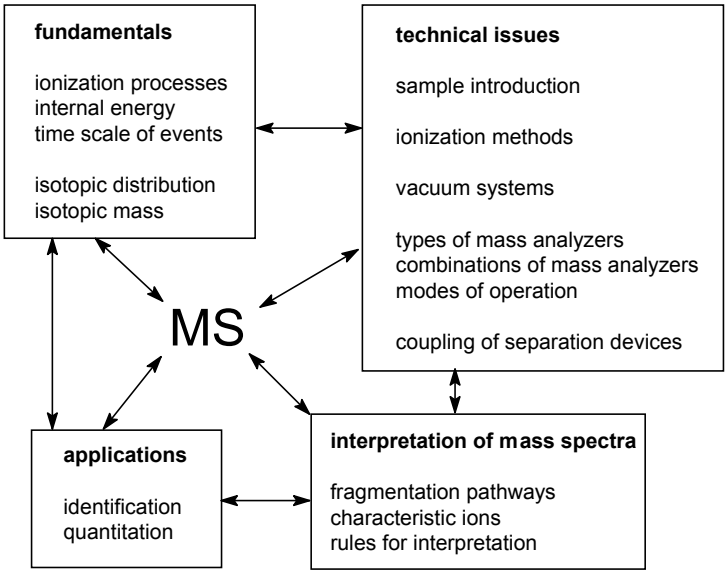


Fig. 1.1. The main domains of mass spectrometry. Each block is correlated to the others in various ways.

1.2 What Is Mass Spectrometry?

Now, what is mass spectrometry? Well in any case, mass spectrometry is special in many ways. Up front, most *mass spectrometrists* do not fathom to be addressed as *mass spectroscopists*.

Hint: “First of all, never make the mistake of calling it 'mass spectroscopy'. Spectroscopy involves the absorption of electromagnetic radiation, and mass spectrometry is different, as we will see. The mass spectrometrists sometimes get upset if you confuse this issue” [25].

Indeed, there is almost no book using the term *mass spectroscopy* and all scientific journals in the field bear *mass spectrometry* in their titles. You will find such highlighted rules, hints, notes, and definitions throughout the book. This more amusing one – we might call it the “zeroth law of mass spectrometry” – has been taken from a standard organic chemistry textbook. The same author completes his chapter on mass spectrometry with the conclusion that “despite occasional mysteries, mass spectrometry is still highly useful” [25].

Historical Remark: Another explanation for this terminology originates from the historical development of our instrumentation [16]. The device employed by Thomson for the first mass-separating experiments was a type of *spectroscope* showing blurred signals on a fluorescent screen [26]. Dempster constructed an instrument with a deflecting magnetic field angled at 180°. In order to detect different masses, it could either be equipped with a photographic plate – a so-called *mass spectrograph* – or it could have a variable magnetic field to detect different masses by focusing them successively onto an electric point detector [27]. Later, the term *mass spectrometer* was coined for the latter type of instruments using a *scanning* magnetic field [28].

1.2.1 Mass Spectrometry

“The basic principle of *mass spectrometry* (MS) is to generate ions from either inorganic or organic compounds by any suitable method, to separate these ions by their *mass-to-charge ratio* (*m/z*) and to detect them qualitatively and quantitatively by their respective *m/z* and abundance. The analyte may be ionized thermally, by electric fields or by impacting energetic electrons, ions or photons. The ... ions can be single ionized atoms, clusters, molecules or their fragments or associates. Ion separation is effected by static or dynamic electric or magnetic fields.” Although this definition of mass spectrometry dates back to 1968 when organic mass spectrometry was in its infancy [29], it is still valid. However, some additions should be made. First, ionization of a sample can be effected not only by electrons, but also by (atomic) ions or photons, energetic neutral atoms, electronically excited atoms, massive cluster ions, and even electrostatically charged microdroplets can also be used to effect. Second, as demonstrated with great success by the time-of-flight analyzer, ion separation by *m/z* can also be effected in field-free regions, provided the ions possess a well-defined kinetic energy at the entrance of the flight path.

The large variety of ionization techniques and their key applications can be roughly classified by their relative hardness or softness and (molecular) mass of suitable analytes (Fig. 1.2).

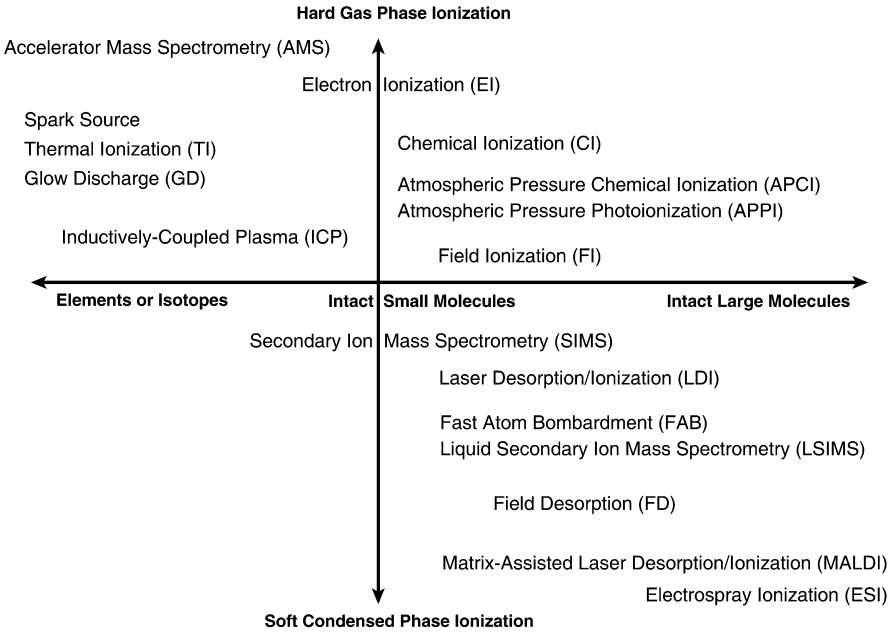


Fig. 1.2. Mass spectrometric techniques for different needs arranged by main fields of application and estimated relative hardness or softness. Reproduced from Ref. [24] by permission. © Wiley-VCH, Weinheim, 2009.

1.2.2 Mass Spectrometer

Obviously, almost any technique to achieve the goals of ionization, separation and detection of ions in the gas phase can be applied – and actually has been applied – in mass spectrometry. Fortunately, there is a simple basic scheme that all mass spectrometers follow. A mass spectrometer consists of an *ion source*, a *mass analyzer*, and a *detector* which are operated under high vacuum conditions. A closer look at the front end of such a device might separate the steps of *sample introduction*, *evaporation*, and successive *ionization* or *desorption/ionization*, respectively, but it is not always trivial to identify each of these steps as clearly separated from each other. If the manufacturing date of the instrument is relatively recent, it will have a data system which collects and processes data from the detector. Since the 1990s, mass spectrometers are fully equipped and controlled by data systems (Fig. 1.3).

The *consumption of analyte* by its examination in the mass spectrometer is an aspect deserving our attention: Whereas other spectroscopic methods such as nuclear magnetic resonance (NMR), infrared (IR) or Raman spectroscopy do allow for sample recovery, mass spectrometry is destructive, i.e., it consumes the analyte. This is apparent from the process of ionization and translational motion through the mass analyzer to the detector during analysis. Although some sample is consumed, it may still be regarded as practically nondestructive, however, because the amount of analyte needed is in the low microgram range or even by several orders of magnitude below. In turn, the extremely low sample consumption of mass spectrometry makes it the method of choice when most other analytical techniques fail because they are not able to yield analytical information from nanogram amounts of sample.

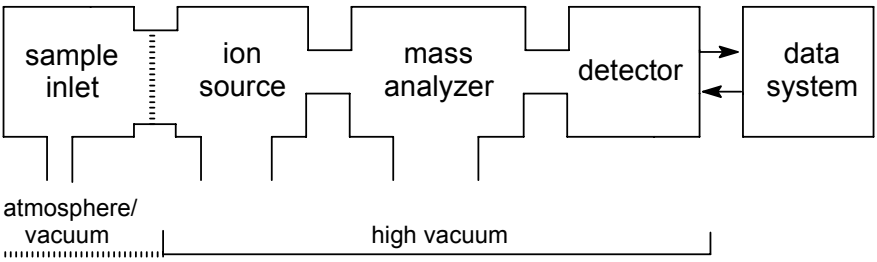


Fig. 1.3. General scheme of any mass spectrometer. Often, several types of sample inlets are attached to the ion source housing. Transfer of the sample from atmospheric pressure to the high vacuum of the ion source and mass analyzer is accomplished by use of a vacuum lock (Chap. 5.2).

1.2.3 Mass Scale

Plotting mass spectra on a physical scale of mass per electric charge (kg C^{-1}) would be very inconvenient to use. Thus, mass spectrometrists have adopted the use of a scale of atomic mass per number of elementary charges and termed it *mass-to-charge ratio*, *m/z*, (read "m over z" and write *m/z*) [30]. There is only one correct writing convention: the location of a peak on the abscissa is to be reported as "at *m/z x*".

Unfortunately, *m/z* is a rather artificial construct as it has not received the status of a physical unit. Instead, *m/z* is dimensionless by definition. It may be understood as the ratio of the numerical value of ionic mass on the atomic mass scale and the number of elementary charges of the respective ion. The number of elementary charges is often, but by far not necessarily, equal to one. As long as only singly charged ions are observed ($z = 1$) the *m/z* scale directly reflects the atomic mass scale. However, there can be conditions where doubly, triply, or even highly charged ions are being created from the analyte depending on the ionization method employed.

Note: Some mass spectrometrists use the unit *thomson* [Th] (to honor J. J. Thomson) instead of the dimensionless quantity *m/z*. Although the thomson is widely accepted (or tolerated), it is not an SI unit. The thomson is equivalent to *m/z* in that there is no conversion factor between these units.

The distance between peaks on that axis has the meaning of a neutral loss from the ion at higher *m/z* to produce the fragment ion at lower *m/z*. Therefore, the amount of this neutral loss is given as "*x* u", where the symbol u stands for *unified atomic mass*. It is important to notice that the mass of the neutral is only reflected by the difference between the corresponding *m/z* values, i.e., $\Delta(m/z)$. This is because the mass spectrometer detects only charged species, i.e., the charge-retaining group of a fragmenting ion. Since 1961 the *unified atomic mass* [u] has been defined as $^{1}/_{12}$ of the mass of one single atom of the nuclide ^{12}C which by convention has been set to precisely 12 u (Chap. 3).

Note: Mass spectrometrists working in the biomedical field tend to use the *dalton* [Da] (to honor J. Dalton) instead of the *unified atomic mass* [u]. The dalton also is not an SI unit. The dalton is equivalent to unified atomic mass in that there is no conversion factor between these units.

1.2.4 Mass Spectrum

A *mass spectrum* is the two-dimensional representation of signal intensity (ordinate) versus *m/z* (abscissa). The position of a *peak*, as signals are usually called, reflects the *m/z* of an ion that has been created from the analyte within the ion source. The *intensity* of this peak correlates to the *abundance* of that ion.

Often but not necessarily, the peak at highest *m/z* results from the detection of the intact ionized molecule, the *molecular ion*, $M^{+\bullet}$. The *molecular ion peak* is usually accompanied by several peaks at lower *m/z* caused by fragmentation of the molecular ion to yield *fragment ions*. Consequently, the respective peaks in the mass spectrum may be referred to as *fragment ion peaks*.

The most intense peak of a mass spectrum is called *base peak*. In most representations of mass spectral data the intensity of the base peak is normalized to 100% *relative intensity*. This largely helps to make mass spectra more easily comparable. The normalization can be done because the relative intensities are basically independent from the absolute ion abundances registered by the detector.

Note: There is an upper limit for the number of ions and neutrals per volume inside the ion source where the appearance of spectra will significantly change due to ion–molecule reactions. One should also be aware of the fact that a single molecule only yields one ion of one *m/z* value. To build a useful mass spectrum requires the statistics of thousands of ion formations and eventual fragmentations to result in signals at different *m/z* where each of them can be assigned a relevant intensity.

Example: In the electron ionization mass spectrum of a particular hydrocarbon, the molecular ion peak and the base peak of the spectrum happen to correspond to the same ionic species at *m/z* 16 (Fig. 1.4). The fragment ion peaks at *m/z* 12–15 are spaced at $\Delta(m/z) = 1$. Obviously, the molecular ion, $M^{+\bullet}$, fragments by loss of $H^{\bullet}$ which is the only possibility to explain the peak at *m/z* 15 by loss of a neutral of 1 u mass. Accordingly, the peaks at lower *m/z* might arise from loss of an H_2 molecule (2 u) and so forth. It is rather obvious that this spectrum corresponds to methane, CH_4, showing its molecular ion peak at *m/z* 16 because the atomic mass of carbon is 12 u and that of hydrogen is 1 u, and therefore 12 u + 4 × 1 u = 16 u. Removal of one electron from a 16 u neutral yields a singly-charged radical ion that is detected at *m/z* 16 by the mass spectrometer. Of course, most mass spectra are not that simple, but this is how it works.

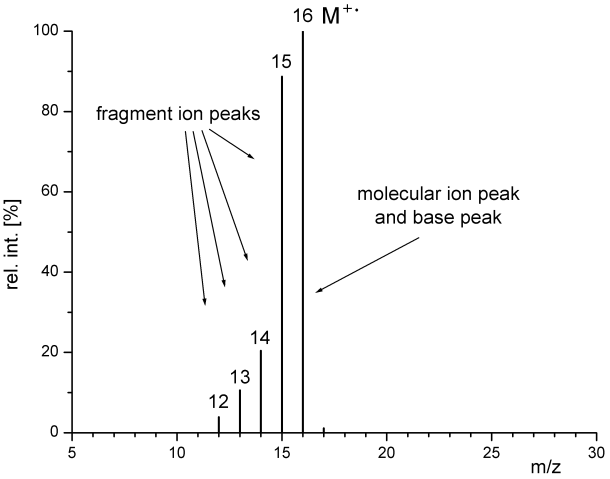


Fig. 1.4. Electron ionization mass spectrum of a hydrocarbon. Adapted with permission. © National Institute of Standards and Technology, NIST, 2002.

The above spectrum is represented as a *bar graph* or *histogram*. Such *data reduction* is common in mass spectrometry and useful as long as peaks are well resolved. The intensities of the peaks can be obtained either from measured peak heights or more correctly from peak areas. The position, i.e., the *m/z* ratio, of the signal is determined from its centroid. Noise below some user-defined cut level is usually subtracted from the bar graph spectrum. If peak shape and peak width become important, e.g., in case of high-mass analytes or high-resolution measurements, spectra should be represented as *profile data* as initially acquired by the mass spectrometer. *Tabular listings* of mass spectra are used to report mass and intensity data more accurately (Fig. 1.5).

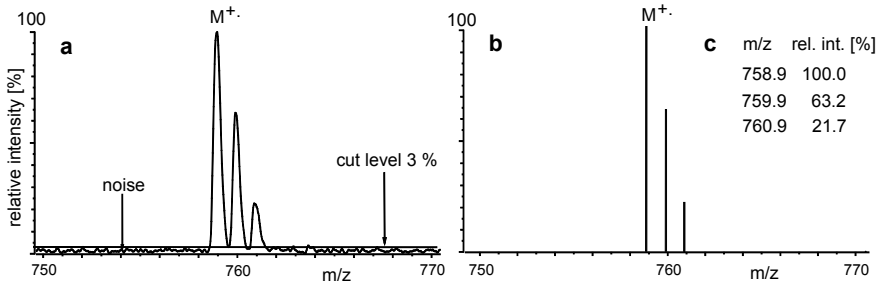


Fig. 1.5. Tetrapentacontane, $C_{54}H_{110}$: Three representations of the molecular ion signal in the field desorption mass spectrum (Chap. 8) (**a**) profile spectrum, (**b**) bar graph representation, and (**c**) tabular listing.

1.3 Ion Chromatograms

In gas and liquid chromatographs the components of a mixture are eluted at different *retention times* from the chromatographic column. When a mass spectrometer is employed as the chromatographic detector (GC-MS and LC-MS, Chaps. 5.4, 5.5 and 14) its output must somehow represent the chromatogram that would have been obtained with other chromatographic detectors (FID, TCD, UV). The chromatogram as produced by the mass spectrometer is composed of a large *set of consecutively acquired mass spectra*, each of which containing spectral data of the eluting species, i.e., each component can be identified from its mass spectrum. Because mass spectral chromatograms represent ionic abundances as a function of retention time, these are termed *ion chromatograms*. To a certain degree fractionation is also observed during evaporation of mixtures from a direct insertion probe, though the separation by far can not be compared to that of chromatographic systems.

Note: The terms *ion profile* and *ion pherogram* have been suggested in place of *ion chromatogram* when DIPs or electrophoresis are used, respectively, as these cannot produce chromatograms in the strict sense [31,32]. However, this would add yet more terms to one of the rather vague areas of our terminology which is even insufficiently covered by official recommendations [31-36].

The *total ion current* (TIC) can either be measured by a *hardware TIC monitor* before mass analysis (nA to µA range), or its equivalent can be *reconstructed* or *extracted* after mass analysis [33]. Both adjectives, reconstructed and extracted, serve to illustrate that the chromatogram has been obtained from a set of spectra by a computational process that selects user-defined signals to build the trace.

Thus, the TIC represents a measure of the overall intensity of ion production or of mass spectral output as a function of time, respectively. The TIC obtained by means of *data reduction* [34], i.e., by summation of peak intensities of each mass spectrum as successively acquired during analysis, is termed *total ion chroma-*

togram (TIC). For this purpose, the sum of all ion intensities belonging to each of the spectra is plotted as a function of time or scan number, respectively. The term *total ion current chromatogram* (TICC) refers to a chromatogram obtained by plotting the total ion current detected in each of a series of mass spectra recorded as a function of retention times of the chromatographically separated components of a mixture (which essentially is implicated by: TIC). Sometimes we find combinations such as *reconstructed total ion current* (RTIC) or *reconstructed total ion current chromatogram* (RTICC).

Note: Modern instruments do not support hardware TIC measurements, but until the 1970s, there used to be a hardware TIC monitor on the electronics panel. The TIC was obtained by measuring the ion current caused by those ions hitting the ion source exit plate instead of passing through its slit.

The term *reconstructed ion chromatogram* (RIC) was and still is used by many to describe the intensity of a given *m/z* or *m/z* range plotted as a function of time or scan number. Recently, the term *extracted ion chromatogram* (EIC) has been used to describe a chromatogram created by plotting the intensity of the signal observed at a chosen *m/z* value or set of values in a series of mass spectra recorded as a function of retention time. Plotting RICs or EICs is especially useful to identify a target compound of known *m/z* from complex GC-MS or LC-MS data. In other words, the RIC allows to retrieve the retention time of the target compound. RICs can also be used to uncover the relationship of certain *m/z* values to different mass spectra obtained from the measurement of a single (impure) sample. Thus, RICs (EICs) often reveal valuable information on impurities accompanying the main product, e.g., remaining solvents, plasticizers, vacuum grease, or synthetic by-products (Chap. 5.2.4).

Finally, the *base peak chromatogram* (BPC) is a chromatogram obtained by plotting the signal of the ions giving the base peak detected in each of a series of mass spectra recorded as a function of retention time.

Example: Polycyclic and nitro musks are frequently used as fragrances in cosmetic products. A GC-MC procedure for their identification and quantitation employs the characteristic RICs (EICs) of tonalide (AHTN), $C_{18}H_{26}O^{+\bullet}$, *m/z* 258, and xylene musk (MX), $C_{12}H_{15}N_3O_6^{+\bullet}$, *m/z* 297 [37]. Although eluting simultaneously (peak **3** in Fig. 1.6), EICs allow to separate both components by choosing characteristic *m/z* values, e.g., of the respective molecular ions or abundant fragment ions. The concentration of the solution injected was in the order of 1 μg ml^{-1} per component.

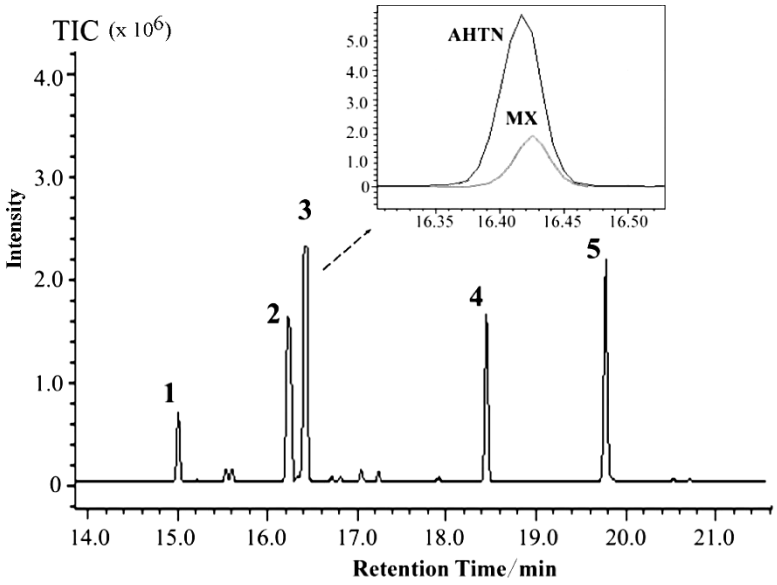


Fig. 1.6. Typical GC-MS chromatogram, i.e., TIC (TICC) in full scan mode for synthetic musks and some standards. The inset shows the characteristic RICs (EICs) of tonalide (AHTN), $C_{18}H_{26}O^{+\bullet}$, *m/z* 258, and xylene musk (MX), $C_{12}H_{15}N_3O_6^{+\bullet}$, *m/z* 297. Reproduced from Ref. [37] with permission. © The Japan Society for Analytical Chemistry, 2009.

1.4 Performance of Mass Spectrometers

1.4.1 Sensitivity

The term *sensitivity* specifies the overall response of any analytical system for a certain analyte when operated under well-defined conditions. The *sensitivity* is defined as the slope of a plot of analyte amount vs. signal strength. In mass spectrometry, sensitivity is reported as electric charge of a specified ion species reaching the detector per mass of analyte used. The sensitivity is given in units of C μg^{-1} for solids [33]; for gaseous analytes, it can be specified as the ratio of ion current to analyte partial pressure in units of A Pa^{-1} [31,34].

According to the above definition, sensitivity does not only depend on the ionization efficiency of EI or any other ionization method. Also relevant are the extraction of ions from the ion source, the mass range acquired during the experiment, and the transmission of the mass analyzer. Therefore, the complete experimental conditions have to be stated with sensitivity data.

Example: Modern magnetic sector instruments are specified to have a sensitivity of about 4×10^{-7} C μg^{-1} for the molecular ion of methylstearate, *m/z* 298, at $R = 1000$ in 70 eV EI mode. The charge of 4×10^{-7} C corresponds to 2.5×10^{12}

electron charges. One microgram of methylstearate is equivalent to 3.4×10^{-9} mol or 2.0×10^{15} molecules.

1.4.2 Detection Limit

The term *detection limit* or *limit of detection* (LOD) is almost self-explanatory, yet it is often confused with sensitivity. The detection limit defines the smallest flow or the lowest amount of analyte necessary to obtain a signal that can be distinguished from the background noise. The detection limit is valid for one well-specified analyte upon treatment according to a certain analytical protocol [31,33,34].

Of course, the sensitivity of an instrumental setup is of key importance to low detection limits; nevertheless, the detection limit is a clearly different quantity. The detection limit may either be stated as a relative measure in trace analysis, e.g., 1 ppb of dioxin in waste oil samples (equivalent to 1 μg kg^{-1} of sample), or as an absolute measure, e.g., 1 femtomol of substance P in MALDI-MS.

1.4.3 Signal-to-Noise Ratio

The *signal-to-noise ratio* (S/N) describes the uncertainty of an intensity measurement and provides a quantitative measure of a signal's quality by quantifying the ratio of the intensity of a signal relative to noise.

Noise results from the electronics of an instrument, and thus noise is not only present *between* the signals but also *on* the signals. Consequently, intensity measurements are influenced by noise. Real and very numerous background signals of various origin, e.g., FAB or MALDI matrices, GC column bleed and impurities, can appear as if they were electronic noise, so-called "chemical" noise. In the strict sense, this should be distinct from electronic noise and should be reported as *signal-to-background ratio* (S/B) [31]. In practice, this can be difficult to do.

Noise is statistical in nature, and therefore can be reduced by elongated data acquisition and subsequent summing or averaging of the spectra, respectively. Accordingly, an intensive peak has a better S/N than a low-intensity peak within the same spectrum. The reduction of noise is proportional to the square root of acquisition time or number of single spectra that are averaged [38], e.g., the noise is reduced by a factor of 3.16 by averaging 10 spectra or by a factor of 10 by averaging 100 spectra, respectively.

Example: A signal may be regarded to be clearly visible at $S/N \geq 10$, a value often stated with detection limits. A mass spectrometer in good condition yields $S/N > 10^4$ which means in turn that even isotopic peaks of low relative intensity can be reliably measured, provided there is no interference with background signals (Fig. 1.7).

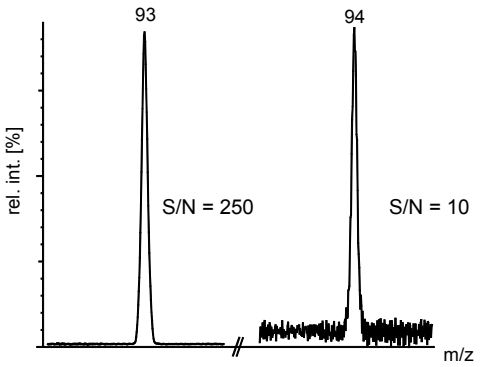


Fig. 1.7. Signal-to-noise ratio. The first isotopic peak of toluene molecular ion, *m/z* 93, (70 eV EI, $R = 4000$) shows about S/N = 250, whereas the second isotopic peak at *m/z* 94 has S/N = 10. The theoretical ratio of intensities of *m/z* 92 : 93 : 94 = 100 : 7.7 : 0.3, i.e., the ratio of intensities also reflects the S/N ratio.

1.5 Terminology – General Aspects

Agreement on terms, acronyms, and symbols are of paramount importance for proper communication in mass spectrometry. The current terminology is chiefly defined by three authoritative publications: *i*) a compilation by Price under the guidance of the *American Society for Mass Spectrometry* (ASMS) [39], *ii*) one by Todd representing the official recommendations of the *International Union of Pure and Applied Chemistry* (IUPAC), [40] and *iii*) an independent one by Sparkman [32,41]. A project to update terms and definitions has been commissioned by IUPAC. A task group has been set up to prepare a new document in conjunction with mass spectrometry journals, national mass spectrometry societies, and the International Mass Spectrometry Foundation [35]. Comments and suggestions regarding the terms and definitions are being collected [36,42,43].

IUPAC in its 1995 version, for example, stays in opposition to the vast majority of practitioners, journals, and books when talking about *mass spectroscopy*, while both, Price and Sparkman are using *mass spectrometry*. IUPAC accepts terms such as *daughter ion* and *parent ion* as equivalent to *product ion* and *precursor ion*, respectively. Sparkman discourages the use of *daughter ion* and *parent ion* as these are archaic and gender-specific terms. None of these collections is fully comprehensive. Nevertheless, there is about 95% agreement between these guidelines to terminology in mass spectrometry and their overall coverage can be regarded as highly sufficient, making the application of any of these beneficial to oral and written communication.

One cannot ignore the existence of multiple terms for one and the same thing sometimes just coined for commercial reasons, e.g., *mass-analyzed ion kinetic energy spectrometry* (MIKES, correct) and *direct analysis of daughter ions* (DADI, archaic company term). Another prominent example concerns the use of MS as an

acronym for *mass spectrometry*, *mass spectrometer*, and *mass spectrum*, too. This is misleading. The acronym MS should only be used to abbreviate *mass spectrometry*. Unfortunately, misleading and redundant terms are used throughout the literature, and thus, we need at least to understand their intention even if we are not going to use them actively. Terminology in this book avoids outdated or vague terms and special notes are given for clarification where ambiguities might arise.

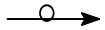
We mass spectrometrist like to communicate our work using countless acronyms [44,45], and there is no intention of avoiding them here. They are all explained when used for the first time in a chapter and they are included in the subject index for reference. A glossary of terms has deliberately been omitted here, as most terms are already referred to in the contents of this book and according sources are readily available in the book by Sparkman [41].

1.5.1 Basic Terminology in Describing Mass Spectra

One should be aware of some basic, nonetheless often mistaken, rules of terminology when describing mass spectra. Common symbols are collected in Table 1.3.

1. We talk about a *xyz-type (mass) spectrum*, e.g., an *EI mass spectrum*. MS means *mass spectrometry*, and thus, the term *MS spectrum* is clearly incorrect.
2. Ions are detected *at* a certain *m/z* value. Correct phrasings are "the molecular ion at *m/z* 16" or "$M^{+\bullet}$, *m/z* 16" or "$CH_4^{+\bullet}$, *m/z* 16", for example.
3. Only ions may be correlated with peaks in a spectrum. This is already an act of interpretation.
4. Neutral losses (rarely called *dark matter* [32]) are exclusively recognized from the distance between peaks expressed in terms of difference in *m/z*. The mass of the corresponding neutral is then given in units of u.
5. A signal or peak is only the graphical representation of the mass spectrometer's detector output. It can be observed, but not act by itself in any way.
6. Ions can act, typically they fragment, dissociate, rearrange, react, isomerize etc.

Table 1.3. Symbols

Symbol	Meaning
•	unpaired electron in radicals
+	positive even-electron ions
–	negative even-electron ions
+•	positive radical ions
–•	negative radical ions
	arrow for transfer of an electron pair
	single-barbed arrow for transfer of a single electron
	indicates the position of a cleaved bond
	fragmentation or reaction
	occasionally for rearrangement fragmentation

1.6 Units, Physical Quantities, and Physical Constants

The consistent use of units for physical quantities is a prerequisite in science, because it simplifies the comparison of physical quantities, e.g., temperature, pressure, or physical dimensions. Therefore, the *International System of Units* (SI) is used throughout the book. This system is based on seven units that can be combined to form any other unit needed. Nevertheless, mass spectrometers often have long lifetimes and 20-year-old instruments being scaled in inches and having pressure readings in Torr or psi may still be in use. In the Appendix you will find tables providing collections of SI units together with frequently needed conversion factors and a collection of physical constants and quantities (Tables A.1–A.4).

References

Direct Reference

1. Enjalbal, C.; Maux, D.; Martinez, J.; Combarieu, R.; Aubagnac, J.L. Mass Spectrometry and Combinatorial Chemistry: New Approaches for Direct Support-Bound Compound Identification. *Comb. Chem. High Throughput Screening* **2001,** *4*, 363-373.
2. Enjalbal, C.; Maux, D.; Combarieu, R.; Martinez, J.; Aubagnac, J.L. Imaging Combinatorial Libraries by MS: From Peptide to Organic-Supported Syntheses. *J. Comb. Chem.* **2003,** *5*, 102-109.
3. Maux, D.; Enjalbal, C.; Martinez, J.; Aubagnac, J.L.; Combarieu, R. Static Secondary Ion MS to Monitor Solid-Phase Peptide Synthesis. *J. Am. Soc. Mass Spectrom.* **2001,** *12*, 1099-1105.
4. Beverly, M.B.; Voorhees, K.J.; Hadfield, T.L. Direct Mass Spectrometric Analysis of *Bacillus* Spores. *Rapid Commun. Mass Spectrom.* **1999,** *13*, 2320-2326.
5. Jones, J.J.; Stump, M.J.; Fleming, R.C.; Lay, J.O., Jr.; Wilkins, C.L. Investigation of MALDI-TOF and FT-MS Techniques for Analysis of *Escherichia coli* Whole Cells. *Anal. Chem.* **2003,** *75*, 1340-1347.
6. Fenselau, C.; Caprioli, R. Mass Spectrometry in the Exploration of Mars. *J. Mass Spectrom.* **2003,** *38*, 1-10.
7. He, F.; Hendrickson, C.L.; Marshall, A.G. Baseline Mass Resolution of Peptide Isobars: A Record for Molecular Mass Resolution. *Anal. Chem.* **2001,** *73*, 647-650.
8. Cooper, H.J.; Marshall, A.G. Electrospray Ionization FT-ICR Analysis of Wine. *J. Agric. Food Chem.* **2001,** *49*, 5710-5718.
9. Hughey, C.A.; Rodgers, R.P.; Marshall, A.G. Resolution of 11,000 Compositionally Distinct Components in a Single Electrospray Ionization FT-ICR Mass Spectrum of Crude Oil. *Anal. Chem.* **2002,** *74*, 4145-4149.
10. Mühlberger, F.; Wieser, J.; Ulrich, A.; Zimmermann, R. Single Photon Ionization (SPI) Via Incoherent VUV-Excimer Light: Robust and Compact TOF Mass Spectrometer for On-Line, Real-Time Process Gas Analysis. *Anal. Chem.* **2002,** *74*, 3790-3801.
11. Glish, G.L.; Vachet, R.W. The Basics of MS in the Twenty-First Century. *Nat. Rev. Drug Discovery* **2003,** *2*, 140-150.
12. Zuccato, E.; Chiabrando, C.; Castiglioni, S.; Calamari, D.; Bagnati, R.; Schiarea, S.; Fanelli, R. Cocaine in Surface Waters: a New Evidence-Based Tool to Monitor Community Drug Abuse. *Environmental Health: A Global Access Science Source* **2005,** *4*, doi:10.1186/1476-069X-4-14.
13. Harris, W.A.; Reilly, P.T.A.; Whitten, W.B. Detection of Chemical Warfare-Related Species on Complex Aerosol Particles Deposited on Surfaces Using an Ion Trap-Based Aerosol Mass Spectrometer. *Anal. Chem.* **2007,** *79*, 2354-2358.
14. Aebersold, R. A Mass Spectrometric Journey into Protein and Proteome Re-

search. *J. Am. Soc. Mass Spectrom.* **2003,** *14*, 685-695.
15. Busch, K.L. Synergistic Developments in MS. A 50-Year Journey From "Art" to Science. *Spectroscopy* **2000,** *15*, 30-39.
16. *Measuring Mass - From Positive Rays to Proteins;* Grayson, M.A., editor; ASMS and CHF: Santa Fe/Philadelphia, 2002.
17. Meyerson, S. Reminiscences of the Early Days of MS in the Petroleum Industry. *Org. Mass Spectrom.* **1986,** *21*, 197-208.
18. Quayle, A. Recollections of MS of the Fifties in a UK Petroleum Laboratory. *Org. Mass Spectrom.* **1987,** *22*, 569-585.
19. Maccoll, A. Organic MS – the Origins. *Org. Mass Spectrom.* **1993,** *28*, 1371.
20. Meyerson, S. MS in the News, 1949. *Org. Mass Spectrom.* **1993,** *28*, 1373..
21. Meyerson, S. From Black Magic to Chemistry. The Metamorphosis of Organic Mass Spectrometry. *Anal. Chem.* **1994,** *66*, 960A-964A.
22. Nibbering, N.M.M. Four Decades of Joy in MS. *Mass Spectrom. Rev.* **2006,** *25*, 962-1017.
23. Gross, M.L.; Sparkman, O.D. The Importance of Titles in References. *J. Am. Soc. Mass Spectrom.* **1998,** *9*, 451.
24. Gross, J.H. Mass Spectrometry, in *Encyclopedia of Applied Spectroscopy*, Andrews, D.L., editor; Wiley-VCH: Berlin, 2009; Chap. 29, pp. 989-1054.
25. Jones, M., Jr. Mass Spectrometry, in *Organic Chemistry*, 2nd ed.; W.W. Norton: New York, 2000; pp. 641-649.
26. Griffiths, I.W., J. J. Thomson: the Centenary of His Discovery of the Electron and His Invention of MS. *Rapid Commun. Mass Spectrom.* **1997,** *11*, 1-16.
27. Dempster, A.J. A New Method of Positive Ray Analysis. *Phys. Rev.* **1918,** *11*, 316-325.
28. Nier, A.O. Some Reflections on the Early Days of Mass Spectrometry at the University of Minnesota. *Int. J. Mass Spectrom. Ion Proc.* **1990,** *100*, 1-13.
29. Kienitz, H. Einführung, in *Massenspektrometrie*; Kienitz, H., editor; Verlag Chemie: Weinheim, 1968.
30. Busch, K.L. Units in Mass Spectrometry. *Spectroscopy* **2001,** *16*, 28-31.
31. Sparkman, O.D. *Mass Spec Desk Reference*; Global View Publ.: Pittsburgh, 2000.
32. Sparkman, O.D. *Mass Spectrometry Desk Reference;* 2nd ed.; Global View Publ.: Pittsburgh, 2006.
33. Price, P. Standard Definitions of Terms Relating to MS. A Report From the Committee on Measurements and Standards of the Amercian Society for Mass Spectrometry. *J. Am. Chem. Soc. Mass Spectrom.* **1991,** *2*, 336-348.
34. Todd, J.F.J. Recommendations for Nomenclature and Symbolism for MS Including an Appendix of Terms Used in Vacuum Technology. *Int. J. Mass Spectrom. Ion Proc.* **1995,** *142*, 211-240.
35. Murray, K. K.; Boyd, R. K.; Eberlin, M. N.; Langley, G. J.; Li, L.; Naito, Y.; Tabet, J. C. *IUPAC Standard Definitions of Terms Relating to Mass Spectrometry*; 2005; pp. ANYL-212.
36. Murray, K. Web Glossaries the Wiki Way. *Chem. Intl.* **2007,** *29*, 23-25.
37. Lv, Y.; Yuan, T.; Hu, J.; Wang, W. Simultaneous Determination of Trace Polycyclic and Nitro Musks in Water Samples Using Optimized Solid-Phase Extraction by Gas Chromatography and MS. *Anal. Sci.* **2009,** *25*, 1125-1130.
38. Kilburn, K.D.; Lewis, P.H.; Underwood, J.G.; Evans, S.; Holmes, J.; Dean, M. Quality of Mass and Intensity Measurements From a High Performance Mass Spectrometer. *Anal. Chem.* **1979,** *51*, 1420-1425.
39. Price, P. Standard Definitions of Terms Relating to MS. Report from the Committee on Measurements and Standards of the Am. Soc. Mass Spectrom. *J. Am. Soc. Mass Spectrom.* **1991,** *2*, 336-348.
40. Todd, J.F.J. Recommendations for Nomenclature and Symbolism for MS Including an Appendix of Terms in Vacuum Technol. *Int. J. Mass Spectrom. Ion. Proc.* **1995,** *142*, 211-240.
41. Sparkman, O.D. *Mass Spectrometry Desk Reference*; 2nd ed.; Global View Publ.: Pittsburgh, 2006.
42. Naito, Y. Commentary on Terms and Definitions Relating to MS. *J. Mass Spectrom. Soc. Japan* **2007,** *55*, 149-156.
43. Murray, K.K.; Boyd, R.K.; Eberlin, M.N.; Langley, J.G.; Li, L.; Naito, Y. Standard Definitions of Terms Relating to MS (IUPAC Recommendations). *Pure and Applied Chemistry* **2009,** *provisional recommendations in state of review*.
44. Busch, K.L. SAMS: Speaking with Acronyms in MS. *Spectroscopy* **2002,** *17*, 54-62.
45. Busch, K.L. A Glossary for MS. *Spectroscopy* **2002,** *17*, S26-S34.

Classical Mass Spectrometry Books

46. Field, F.H.; Franklin, J.L. *Electron Impact Phenomena and the Properties of Gaseous Ions*; Academic Press: New York, 1957.
47. Beynon, J.H. *Mass Spectrometry and Its Applications to Organic Chemistry*; Elsevier: Amsterdam, 1960.
48. Biemann, K. *Mass Spectrometry*; McGraw-Hill: New York, 1962.
49. Biemann, K. *Mass Spectrometry – Organic Chemical Applications*; McGraw-Hill: New York, 1962.
50. Biemann, K.; Dibeler, V.H.; Grubb, H.M.; Harrison, A.G.; Hood, A.; Knewstubb, P.F.; Krauss, M.; McLafferty, F.W.; Melton, C.E.; Meyerson, S.; Reed, R.I.; Rosenstock, H.M.; Ryhage, R.; Saunders, R.A.; Stenhagen, E.; Williams, A.E. *Mass Spectrometry of Organic Ions*; McLafferty, F.W., editor; Academic Press: London, 1963.
51. Kiser, R.W. *Introduction to Mass Spectrometry and Its Applications;* Prentice-Hall: Englewood Cliffs, 1965.
52. Budzikiewicz, H.; Djerassi, C.; Williams, D.H. *Mass Spectrometry of Organic Compounds*; Holden-Day: San Francisco, 1967.
53. Aulinger, F.; Kienitz, H.; Franke, G.; Habfast, K.; Spiteller, G. *Massenspektrometrie*; Kienitz, H., editor; Verlag Chemie: Weinheim, 1968.
54. Cooks, R.G.; Beynon, J.H.; Caprioli, R.M. *Metastable Ions*; Elsevier: Amsterdam, 1973.
55. Levsen, K. *Fundamental Aspects of Organic Mass Spectrometry*; Verlag Chemie: Weinheim, 1978.

Other Introductory Texts

56. Howe, I.a.o. *Mass Spectrometry: Principles and Applications;* 2nd ed.; McGraw-Hill: New York, 1981.
57. Chapman, J.R. *Practical Organic Mass Spectrometry: A Guide for Chemical and Biochemical Analysis;* 2nd ed.; Wiley: Chichester, 1993.
58. McLafferty, F.W.; Turecek, F. *Interpretation of Mass Spectra;* 4th ed.; University Science Books: Mill Valley, 1993.
59. Budzikiewicz, H.; Schäfer, M. *Massenspektrometrie – Eine Einführung;* 5th ed.; Wiley-VCH: Weinheim, 2005.
60. De Hoffmann, E.; Stroobant, V. *Mass Spectrometry – Principles and Applications;* 3rd ed.; Wiley: Chichester, 2007.
61. Watson, J.T.; Sparkman, O.D. *Introduction to Mass Spectrometry;* 4th ed.; Wiley: Chichester, 2007.
62. Ekman, R.; Silberring, J.; Westman-Brinkmalm, A.M.; Kraj, A. *Mass Spectrometry: Instrumentation, Interpretation, and Applications;* Wiley: Hoboken, 2009.

Monographs

63. Porter, Q.N.; Baldas, J. *Mass Spectrometry of Heterocyclic Compounds*; Wiley: New York, 1971.
64. Dawson, P.H. *Quadrupole Mass Spectrometry and Its Applications*; Elsevier: New York, 1976.
65. Beckey, H.D. *Principles of Field Desorption and Field Ionization Mass Spectrometry*; Pergamon Press: Oxford, 1977.
66. *Tandem Mass Spectrometry*; McLafferty, F.W., editor; Wiley: New York, 1983.
67. Castleman Jr., A.W.; Futrell, J.H.; Lindinger, W.; Märk, T.D.; Morrison, J.D.; Shirts, R.B.; Smith, D.L.; Wahrhaftig, A.L. *Gaseous Ion Chemistry and Mass Spectrometry;* Futrell, J.H., editor; Wiley: New York, 1986.
68. Benninghoven, A.; Werner, H.W.; Rudenauer, F.G. *Secondary Ion Mass Spectrometry: Basic Concepts, Instrumental Aspects, Applications and Trends*; Benninghoven, A., editor; Wiley: New York, 1987.
69. Busch, K.L.; Glish, G.L.; McLuckey, S.A. *Mass Spectrometry/Mass Spectrometry*; Wiley VCH: New York, 1988.
70. Briggs, D.; Brown, A.; Vickerman, J.C. *Handbook of Static Secondary Ion Mass Spectrometry;* Wiley: Chichester, 1989.
71. March, R.E.; Hughes, R.J. *Quadrupole Storage Mass Spectrometry;* Wiley: Chichester, 1989.
72. Wilson, R.G.; Stevie, F.A.; Magee, C.W. *Secondary Ion Mass Spectrometry: A Practical Handbook for Depth Profiling and Bulk Impurity Analysis;* Wiley: Chichester, 1989.
73. *Continuous-Flow Fast Atom Bombardment Mass Spectrometry;* Caprioli, R.M., editor; Wiley: Chichester, 1990.

74. Prókai, L. *Field Desorption MS*; Marcel Dekker: New York, 1990.
75. *Analytical Applications of FT-ICR-MS;* Assamoto, B., ed.; VCH: Weinheim, 1991.
76. Harrison, A.G. *Chemical Ionization Mass Spectrometry;* 2nd ed.; CRC Press: Boca Raton, 1992.
77. *Applications of Mass Spectrometry to Organic Stereochemistry*; Splitter, J.S.; Turecek, F., editors; Verlag Chemie: Weinheim, 1994.
78. *Forensic Applications of Mass Spectrometry;* Yinon, J., editor; CRC Press: Boca Raton, 1994.
79. *Time of Flight Mass Spectrometry and Its Applications*; Schlag, E.W., editor; Elsevier: Amsterdam, 1994.
80. Lehmann, W.D. *Massenspektrometrie in der Biochemie*; Spektrum Akademischer Verlag: Heidelberg, 1996.
81. *Electrospray Ionization Mass Spectrometry – Fundamentals, Instrumentation and Applications*; Dole, R.B., editor; Wiley: Chichester, 1997.
82. Cotter, R.J. *Time-of-Flight Mass Spectrometry: Instrumentation and Applications in Biological Research*; American Chemical Society: Wash., DC, 1997.
83. Platzner, I.T.; Habfast, K.; Walder, A.J.; Goetz, A. *Modern Isotope Ratio Mass Spectrometry*; Platzner, I.T., editor; Wiley: Chichester, 1997.
84. *Current Practice of Liquid Chromatography-Mass Spectrometry;* Niessen, W.M.A.; Voyksner, R.D., editors; Elsevier: Amsterdam, 1998.
85. Tuniz, C.; Bird, J.R.; Fink, D.; Herzog, G.F. *Accelerator Mass Spectrometry - Ultrasensitive Analysis for Global Science;* CRC Press: Boca Raton, 1998.
86. Roboz, J. *Mass Spectrometry in Cancer Research*; CRC: Boca Raton, 1999.
87. *Mass Spectrometry of Proteins and Peptides;* Chapman, J.R., editor; Humana Press: Totowa, 2000.
88. Kinter, M.; Sherman, N.E. *Protein Sequencing and Identification Using Tandem MS;* Wiley: Chichester, 2000.
89. Snyder, A.P. *Interpreting Protein Mass Spectra*; Oxford Univ. Press: New York, 2000.
90. Taylor, H.E. *Inductively Coupled Plasma Mass Spectroscopy*; Academic Press: London, 2000.
91. *Mass Spectrometry of Polymers*; Montaudo, G.; Lattimer, R.P., editors; CRC Press: Boca Raton, 2001.
92. Budde, W.L. *Analytical Mass Spectrometry*; ACS and Oxford Univ. Press: Wash., D.C. and Oxford, 2001.
93. de Laeter, J.R. *Applications of Inorganic MS*; Wiley: New York, 2001.
94. *Mass Spectrometry in Drug Discovery;* Rossi, D.T.; Sinz, M.W., editors; Marcel Dekker: New York, 2002.
95. *Applied Electrospray Mass Spectrometry;* Pramanik, B.N.; Ganguly, A.K.; Gross, M.L., editors; Marcel Dekker: New York, 2002.
96. Ardrey, R.E. *Liquid Chromatography-Mass Spectrometry – An Introduction;* Wiley: Chichester, 2003.
97. Pasch, H.; Schrepp, W. *MALDI-TOF Mass Spectrometry of Synthetic Polymers;* Springer: Heidelberg, 2003.
98. Henderson, W.; McIndoe, S.J. *Mass Spectrometry of Inorganic and Organometallic Compounds;* Wiley: Chichester, 2005.
99. Kaltashov, I.A.; Eyles, S.J. *Mass Spectrometry in Biophysics: Conformation and Dynamics of Biomolecules;* Wiley: Hoboken, 2005.
100. March, R.E.; Todd, J.F.J. *Quadrupole Ion Trap Mass Spectrometry*; Wiley: Hoboken, 2005.
101. Siuzdak, G. *The Expanding Role of Mass Spectrometry in Biotechnology*; 2nd ed.; MCC Press: San Diego, 2006.
102. *MALDI-MS. A Practical Guide to Instrumentation, Methods and Applications*; Hillenkamp, F.; Peter-Katalinic, J., editors; Wiley-VCH: Weinheim, 2007.
103. Becker, J.S. *Inorganic Mass Spectrometry: Principles and Applications*; Wiley: Chichester, 2008.
104. Boyd, R.K.; Basic, C.; Bethem, R.A. *Trace Quantitative Analysis by Mass Spectrometry;* Wiley: Chichester, 2008.
105. *Miniaturization and Mass Spectrometry;* Le Gac, S.; van den Berg, A., editors; The Royal Society of Chemistry: Cambridge, 2009.
106. *Mass Spectrometry in Drug Metabolism and Pharmacokinetics*; Ramanathan, R., editor; Wiley: Hoboken, 2009.
107. Schalley, C.A.; Springer, A. *Mass Spectrometry and Gas-Phase Chemistry of Non-Covalent Complexes*; Wiley: Hoboken, 2009.

2 Principles of Ionization and Ion Dissociation

Learning Objectives

- Ionization process and ionization energy
- Internal energy of ions and internal energy distribution
- Energetic considerations governing the fragmentation of excited ions
- Quasi-equilibrium theory and rates of unimolecular dissociations
- Time scale of mass spectrometry
- Selected tools of gas phase ion chemistry

The mass spectrometer can be regarded as a kind of chemical laboratory, especially designed to study ions in the gas phase [1,2]. In addition to the task it is commonly used for – creation of mass spectra for a generally analytical purpose – it allows for the examination of fragmentation pathways of selected ions, for the study of ion–neutral reactions and more. Understanding these fundamentals is prerequisite for the proper application of mass spectrometry with all technical facets available, and for the successful interpretation of mass spectra because "analytical chemistry is the application of physical chemistry to the real world" [3].

In the first place, this chapter deals with the fundamentals of gas phase ion chemistry, i.e., with ionization, excitation, ion thermochemistry, ion lifetimes, and reaction rates of ion dissociation. The final sections are devoted to more practical aspects of gas phase ion chemistry such as the determination of ionization and appearance energies or of gas phase basicities and proton affinities.

Brief discussions of some topics of this chapter may also be found in physical chemistry textbooks; however, much better introductions are given in the specialized literature [4-11]. Detailed compound-specific fragmentation mechanisms, ion–molecule complexes, and more are dealt with later (Chap. 6).

2.1 Gas Phase Ionization by Energetic Electrons

Besides some rare experimental setups the mass analyzer of any mass spectrometer can only handle charged species, i.e., ions that have been created from atoms or molecules, occasionally also from radicals, zwitterions or clusters. It is the task of the ion source to perform this crucial step and there is a wide range of ionization methods in use to achieve this goal for the whole variety of analytes.

J. Gross, *Mass Spectrometry*, 2nd ed., DOI 10.1007/978-3-642-10711-5_2,
© Springer-Verlag Berlin Heidelberg 2011

The classical procedure of ionization involves shooting energetic electrons on a gaseous neutral. This is called *electron ionization* (EI). Electron ionization has formerly been termed *electron impact ionization* or simply *electron impact* (EI). For EI, the neutral previously must have been transferred into the highly diluted gas phase, which is done by means of any sample inlet system suitable for the evaporation of the respective compound. In practice, the gas phase may be regarded highly diluted when the mean free path for the particles becomes long enough to make bimolecular interactions almost impossible within the lifetime of the particles concerned. This is easily achieved at pressures in the range of 10^{-4} Pa usually realized in electron ionization ion sources. Here, the description of EI is restricted to what is essential for an understanding of the ionization process as such [12,13] and the consequences for the fate of the freshly created ions.

2.1.1 Formation of Ions

When a neutral is hit by an energetic electron carrying several tens of electronvolts (eV) of kinetic energy, some of the energy of the electron is transferred to the neutral. If the electron, in terms of energy transfer, collides very effectively with the neutral, the energy transferred can exceed the *ionization energy* (*IE*) of the neutral. Then – from the mass spectrometric point of view – the most desirable process can occur: ionization by ejection of one electron generating a *molecular ion*, a positive *radical ion*:

$$M + e^- \rightarrow M^{+\bullet} + 2e^- \tag{2.1}$$

Depending on the analyte and on the energy of the primary electrons, doubly charged and even triply charged ions may be observed

$$M + e^- \rightarrow M^{2+} + 3e^- \tag{2.2}$$

$$M + e^- \rightarrow M^{3+\bullet} + 4e^- \tag{2.3}$$

While the doubly charged ion, M^{2+}, is an *even-electron ion*, the triply charged ion, $M^{3+\bullet}$, again is an *odd-electron ion*. In addition, there are several other events possible from the electron–neutral interaction, e.g., a less effective interaction will bring the neutral into an electronically excited state without ionizing it.

Examples: EI predominantly creates singly charged ions from the precursor neutral. If the neutral was a molecule as in most cases, it started as having an even number of electrons, i.e., it was an *even-electron* (*closed-shell*) *molecule*. The molecular ion formed must then be a radical cation or an *odd-electron* (*open-shell*) *ion* as these species are termed. For methane we obtain:

$$CH_4 + e^- \rightarrow CH_4^{+\bullet} + 2e^- \tag{2.4}$$

In the rare case the neutral was a radical, the ion created by electron ionization would be even-electron, e.g., for nitric oxide:

$$NO^{\bullet} + e^- \rightarrow NO^+ + 2e^- \tag{2.5}$$

Example: The EI mass spectrum of a phenanthroperylene derivative shows a series of comparatively intensive doubly-charged ions, the one at *m/z* 178 being the doubly-charged molecular ion, the others representing doubly-charged fragment ions (Fig. 2.1) [14]. The occurrence of doubly-charged ions of moderate abundance is quite common in the mass spectra of polycyclic aromatic hydrocarbons (PAHs). For another example of multiply-charged ions in EI spectra cf. Chap. 3.5, for the LDI spectrum of this compound cf. Chap. 11.4.

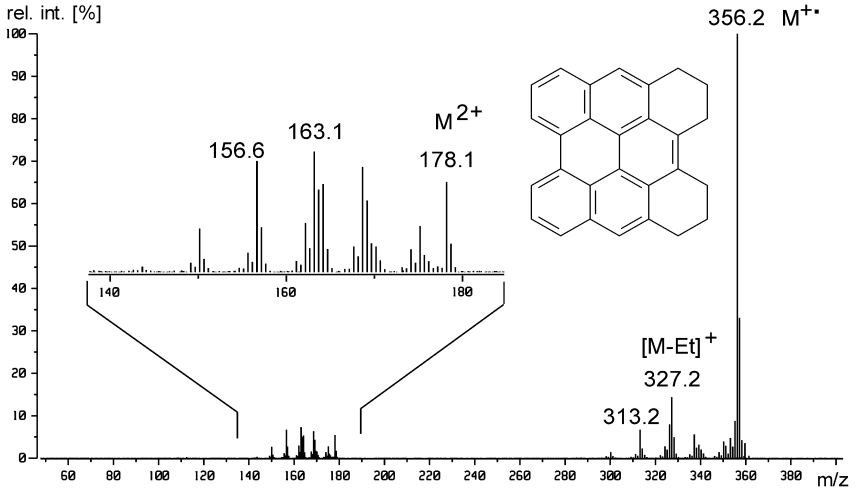


Fig. 2.1. EI mass spectrum of 1,2,3,4,5,6-hexahydrophenanthro[1,10,9,8-*opqra*]perylene. All signals in the expanded inset correspond to doubly-charged ions. Adapted from Ref. [14] with permission. © Elsevier Science, 2002.

2.1.2 Processes Accompanying Electron Ionization

In addition to the desired generation of molecular ions, several other events can result from electron-neutral interactions (Fig. 2.2). A less effective interaction brings the neutral into an electronically excited state without ionizing it. As the energy of the primary electrons increases, the abundance and variety of the ionized species will also increase, i.e., electron ionization may occur via different channels, each of which gives rise to characteristic ionized and neutral products. This includes the production of the following type of ions: molecular ions, fragment ions, multiply charged ions, metastable ions, rearrangement ions, and ion pairs [12].

The electron could also be captured by the neutral to form a negative radical ion. However, *electron capture* (EC) is rather unlikely to occur with electrons of 70 eV since EC is a resonance process because no electron is produced to carry away the excess energy [16]. Thus, EC only proceeds effectively with electrons of very low energy, preferably with thermal electrons (Chap. 7.4). Nonetheless,

molecules containing strongly electronegative elements may form negative ions with low effectivity.

Exceptions: The generation of negative ions from tungsten hexafluoride, WF_6, has been studied under conventional EI conditions. At higher electron energies, $WF_6^{-\bullet}$, WF_5^-, and F^- ions have been found [17]. Organic analytes such as perfluorokerosene also yield negative ions, but sensitivity is lower by some orders of magnitude than for positive-ion EI.

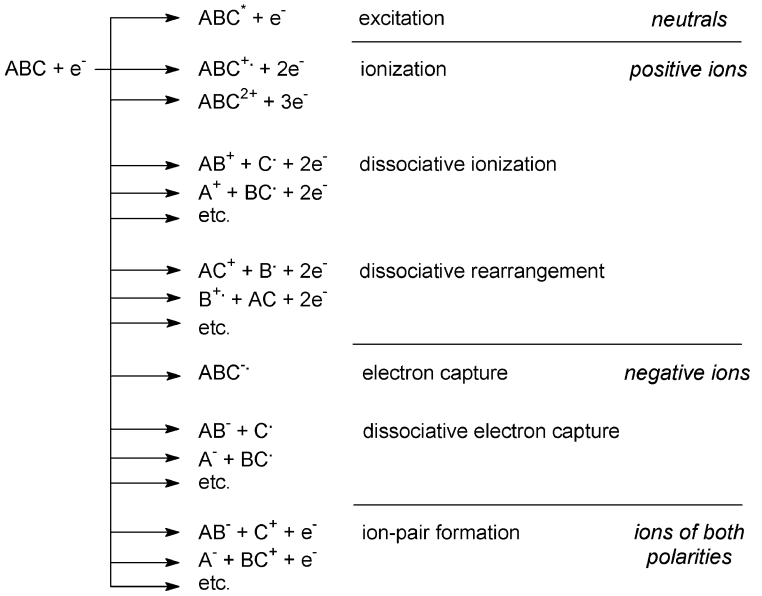


Fig. 2.2. Processes under electron ionization conditions. Under certain conditions, Penning ionization could also play a role. Adapted from Ref. [15] with permission. © Springer-Verlag Heidelberg, 1991.

2.1.3 Ions Generated by Penning Ionization

Non-ionizing electron–neutral interactions create electronically excited neutrals. The ionization reactions occurring when electronically excited neutrals like noble gas atoms, A*, collide with a ground state molecule, M, can be divided into two classes [18]. The first process is *Penning ionization* (Eq. 2.6) [19], the second is *associative ionization*, also known as the *Hornbeck-Molnar process* (Eq. 2.7) [20].

$$A^* + M \rightarrow A + M^{+\bullet} + e^- \tag{2.6}$$

$$A^* + M \rightarrow AM^{+\bullet} + e^- \tag{2.7}$$

Penning ionization occurs with the (trace) gas M having an ionization energy lower than the energy of the metastable state of the excited (noble gas) atoms A*. The above ionization processes have also been employed to construct ion sources [18,21], but until the advent of *direct analysis in real time* (DART, Chap. 13.5), Penning ionization sources were not widely used in analytics.

2.1.4 Ionization Energy

It is obvious that ionization of the neutral can only occur when the energy deposited by the electron-neutral collision is equal to or greater than the *ionization energy* (*IE*) of the corresponding neutral. Formerly, ionization energy has erroneously been termed *ionization potential* (*IP*), as derived from the technique for its experimental determination (Chap. 2.10)..

Definition: The *ionization energy* (*IE*) is defined as the minimum amount of energy that needs to be absorbed by an atom or molecule in its electronic and vibrational ground states in order to form an ion that is also in its ground states by ejection of an electron.

Lone pairs are good sources of an ejectable electron, thus the *IE* of ethanol and dimethylether is lower than that of ethane. It has been shown that the *IE* of a polysubstituted alkane is in principle equal to the *IE* of a structurally otherwise identical monosubstituted alkane bearing the sort of heteroatom which is energetically least demanding for electron loss [22]. The other substituent, provided it is separated by at least two carbon atoms, exerts a very small effect upon the IE. For example, the *IE* of dimethylsulfide, CH_3SCH_3, 8.7 eV, almost equals that of the larger methionine, $CH_3SCH_2CH_2CH(NH_2)COOH$. Introduction of an oxygen decreases the *IE* to a lesser extent than nitrogen, sulfur or even selenium, since these elements have lower electronegativities and thus, are even better sources of the ejected electron. The bottom line of *IE*s is reached when π-systems and heteroatoms are combined in the same molecule.

Note: Ionization energies of most molecules are in the range of 7–15 eV.

2.1.5 Ionization Energy and Charge-Localization

Removal of an electron from a molecule can formally be considered to occur at a σ-bond, a π-bond, or at a lone electron pair with the σ-bond being the least favored and the lone electron pair being the most favored position for *charge-localization* within the molecule, an assumption directly reflected in the *IE*s (Table 2.1). Nobel gases do exist as atoms having closed electron shells and therefore, they exhibit the highest *IE*s. They are followed by diatomic molecules with fluorine, nitrogen, and hydrogen at the upper limit. The *IE* of methane is lower than

Table 2.1. Ionization energies of selected compounds[a]

Compound	IE[b] [eV]	Compound	IE[b] [eV]
Hydrogen, H_2	15.4	Helium, He	24.6
Methane, CH_4	12.6	Neon, Ne	21.6
Ethane, C_2H_6	11.5	Argon, Ar	15.8
Propane, *n*-C_3H_8	10.9	Krypton, Kr	14.0
Butane, *n*-C_4H_{10}	10.5	Xenon, Xe	12.1
Pentane, *n*-C_5H_{12}	10.3		
Hexane, *n*-C_6H_{14}	10.1	Nitrogen, N_2	15.6
Decane, *n*-$C_{10}H_{22}$	9.7	Oxygen, O_2	12.1
		Carbon monoxide, CO	14.0
Ethene, C_2H_4	10.5	Carbon dioxide, CO_2	13.8
Propene, C_3H_6	9.7		
(*E*)-2-Butene, C_4H_8	9.1	Fluorine, F_2	15.7
		Chlorine, Cl_2	11.5
Benzene, C_6H_6	9.2	Bromine, Br_2	10.5
Toluene, C_6H_8	8.8	Iodine, I_2	9.3
Indene, C_9H_8	8.6		
Naphthalene, $C_{10}H_8$	8.1	Ethanol, C_2H_6O	10.5
Biphenyl, $C_{12}H_{10}$	8.2	Dimethylether, C_2H_6O	10.0
Anthracene, $C_{14}H_{10}$	7.4	Ethanethiol, C_2H_6S	9.3
Aniline, C_6H_7N	7.7	Dimethylsulfide, C_2H_6S	8.7
Triphenylamine, $C_{18}H_{15}N$	6.8	Dimethylamine, C_2H_7N	8.2

[a] *IE* data taken from Ref. [23] with permission. © NIST 2002.
[b] All values have been rounded to the first digit.

that of molecular hydrogen but still higher than that of ethane and so forth until the *IE* of long-chain alkanes approaches a lower limit [24]. The more atoms are contained within a molecule the easier it finds a way for stabilization of the charge, e.g., by delocalization or hyperconjugation. Molecules with π-bonds have lower IEs than those without, causing the *IE* of ethene to be lower than that of ethane. Again the *IE* is reduced further with increasing size of the alkene. Aromatic hydrocarbons can stabilize a single charge even better and expanding π-systems also help making ionization easier.

Once the molecular ion is formed, the electron charge is never really localized in a single orbital, although assuming so is often a good working hypothesis for mass spectral interpretation [25,26]. Nonetheless, the concept of charge localization is contradictory to electronegativity that dictates the positive center of an ion should not reside on the more electronegative atom [27]. In case of the molecular ion of pyrrole only 5% of the positive charge reside on the nitrogen, while the adjacent two carbons take about 20% each, and the five hydrogens compensate for the remainder by almost equally contributing ~10% each [27]. Whatever species, it turns out that the charge is delocalized over the whole molecular ion [28-30].

Example: For the *para*-tolyl ion only ~36% of the electron charge rests at the *para*-carbon atom (Fig. 2.3) [31]. In addition, the ionic geometry loses the symmetry of the corresponding neutral molecule.

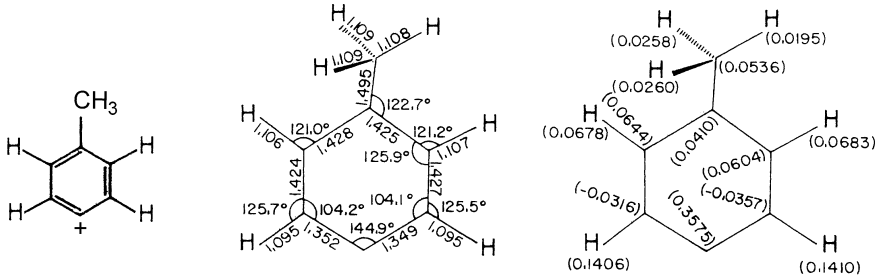


Fig. 2.3. *para*-Tolyl ion, $[C_7H_7]^+$: structural formula (*left*), calculated geometries (*center*) and calculated distributions of formal charge (*right*). Reproduced from Ref. [31] with permission. © American Chemical Society, 1977.

2.2 Vertical Transitions

Electron ionization occurs extremely fast. The time needed for an electron of 70 eV to travel 1 nm through a molecule, a distance roughly corresponding to half a dozen bond lengths, is only about 2×10^{-16} s, and even larger molecules can be traversed in the low femtosecond range. The molecule being hit by the electron can be considered to be at rest because the thermal velocity of a few 100 m s^{-1} is negligible compared to the speed of the electron rushing through. Vibrational motions are slower by at least two orders of magnitude, e.g., even the fast C–H stretching vibration takes 1.1×10^{-14} s per cycle as can be calculated from its IR absorbance at around 3000 cm^{-1}.

According to the *Born-Oppenheimer approximation*, electronic motions and nuclear motions can be separated due to the large mass difference between nuclei and electrons [32-34]. Furthermore, the *Franck-Condon principle* states that electronic transitions will occur on a much faster timescale than it takes the nuclei to move to their new equilibrium positions [34-36]. Applied to the interaction of an energetic electron with a gaseous molecule this means that the positions of the atoms and thus bond lengths remain unaltered during ionization. In diagrams where energy is plotted on the ordinate and bond length on the abscissa, such transitions are represented as *vertical transitions* (Fig. 2.4).

The probability of a particular transition from the ground state neutral to a certain vibrational level of the ion is expressed by its *Franck-Condon factor*. The Franck-Condon factors originate from the fact that the probability for a transition is highest where the electronic wave functions of both ground state and excited state have maximum overlap. While for the ground state this is at equilibrium po-

sition, the wave functions of higher vibrational states have their maxima at the turning points of the motion.

No matter where the electron has formally been taken from, ionization tends to cause weakening of the bonding within the ion as compared to the precursor neutral. Weaker bonding means longer bond lengths on the average and this goes with a higher tendency toward dissociation of a bond. In terms of potential energy surfaces, the situation can easiest be visualized by focusing on just one bond within the molecule or simply by discussing a diatomic molecule. A diatomic molecule has only one vibrational motion, its bond stretching vibration, and therefore its potential energy can be represented by potential energy curves rather than potential energy surfaces. The minimum of the potential energy curve of the neutral, which is assumed to be in its vibrational ground state, is located at shorter bond length, r_0, than the minimum of the radical ion in its ground state, r_1 (Fig. 2.4). Consequently, ionization is accompanied by vibrational excitation because the transitions are vertical, i.e., because the positions of the atoms are actually fixed during this short period.

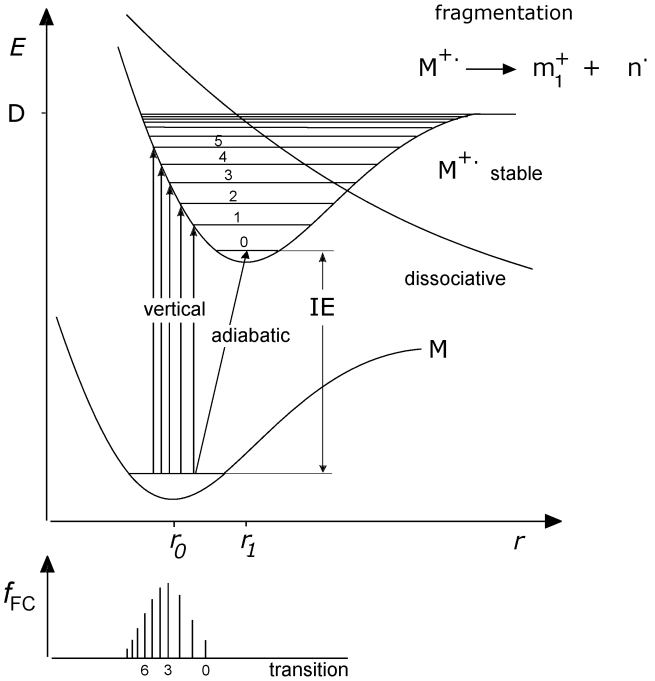


Fig. 2.4. Illustration of the transitions from the neutral to the ionic state for a diatomic molecule. Electron ionization can be represented by a vertical line in this diagram. Thus, ions are formed in a vibrationally excited state if the internuclear distance of the ionic state, r_1, is longer than in the ground state, r_0. Ions having internal energies below the dissociation energy D remain stable, whereas fragmentation will occur above. In few cases, ions are unstable, i.e., there is no minimum on their potential energy curve. The lower part schematically shows the distribution of Franck-Condon factors, f_{FC}, for various transitions.

The distribution of Franck-Condon factors, f_{FC}, describes the distribution of vibrational states for an excited ion [37]. The larger r_1 is, as compared to r_0, the more probable will be the generation of ions excited even well above the dissociation energy. Photoelectron spectroscopy allows for both the determination of adiabatic ionization energies and of Franck-Condon factors (Chap. 2.10.4).

The counterpart of the vertical ionization is a process where ionization of the neutral in its vibrational ground state would yield the radical ion also in its vibrational ground state, i.e., the $(0 \leftarrow 0)$ transition. This is termed *adiabatic ionization* and should be represented by a diagonal line in the diagram. The difference $IE_{vert} - IE_{ad}$ can lead to errors in ionization energies in the order of 0.1–0.7 eV [7].

The further fate of the ion depends on the shape of its potential energy surface. In case there is a minimum and the level of excitation is below the energy barrier for dissociation, D, the ion can exist for a very long time. Ions having an *internal energy* above the dissociation energy level will dissociate at some point leading to causing fragment ions within a mass spectrum. In some unfavorable cases, ions bear no minimum on their energy surface at all. These will suffer spontaneous dissociation and consequently, there is no chance to observe a molecular ion.

Note: To understand the situation of the molecule imagine an apple through which a bullet is being shot: the impacting bullet passes through the apple, transfers an amount of energy, tears some of the fruit out and has long left it when the perforated apple finally drops or breaks into pieces.

2.3 Ionization Efficiency and Ionization Cross Section

The ionization energy represents the absolute minimum energy required for ionization of the neutral concerned. This means in turn that in order to effect ionization, the impacting electrons need to carry at least this amount of energy. If this energy were then to be quantitatively transferred during the collision, ionization would take place. Obviously, such an event is of rather low probability and therefore, the *ionization efficiency* is close to zero with electrons carrying just the *IE* of the pertinent neutral. However, a slight increase in electron energy brings about a steady increase in ionization efficiency.

Strictly speaking, every molecular species has an ionization efficiency curve of its own depending on the *ionization cross section* of the specific molecule. In the case of methane, this issue has been studied repeatedly (Fig. 2.5) [12]. The ionization cross section describes an area through which the electron must travel in order to effectively interact with the neutral and consequently, the ionization cross section is given in units of square-meters.

Fortunately, the curves of ionization cross section vs. electron energy are all of the same type, exhibiting a maximum at electron energies around 70 eV (Fig. 2.5). This explains why EI spectra are almost always acquired at 70 eV.

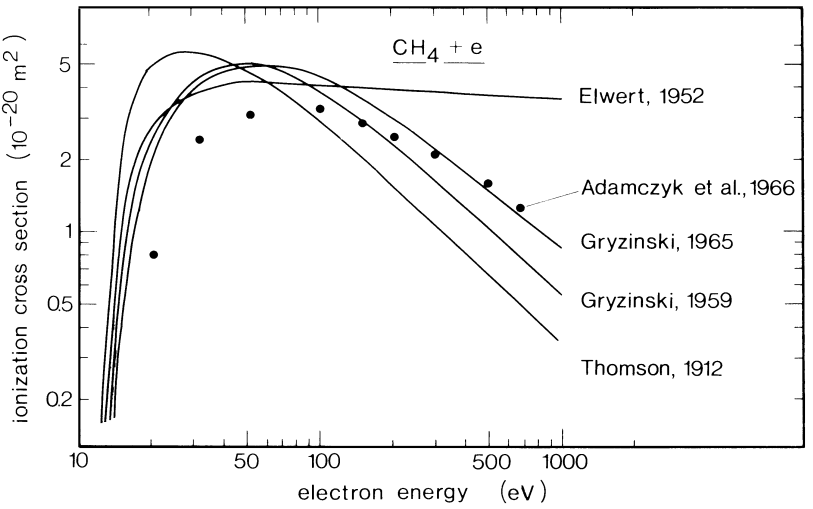


Fig. 2.5. Ionization cross sections for CH_4 upon electron ionization as obtained by several research groups. Reproduced from Ref. [12] with permission. © Elsevier Science, 1982.

Reasons for measuring EI spectra at 70 eV:

- All atoms or molecules can be ionized at 70 eV, whereas at 15 eV such gases as He, Ne, Ar, H_2, and N_2 are not.
- The plateau of the ionization efficiency curve at ~70 eV implies small that variations in electron energy are negligible; actually EI at 60–80 eV work just as well.
- Therefore: better reproducibility of spectra, allowing comparison of spectra obtained from different mass spectrometers or from mass spectral databases (Chap 5.8).

2.4 Internal Energy and the Further Fate of Ions

When an analyte is transferred into the ion source by means of any kind of sample introduction system it is in thermal equilibrium with this inlet device. As a result, the energy of the incoming molecules is represented by their thermal energy. This is the last opportunity to control the temperature, being a macroscopic property. After that, gas phase dilution would preclude any further collisions from taking place, and accordingly, any intermolecular energy transfer that would provide the basis for reaching thermal equilibrium and the validity of the *Boltzmann distribution* governing condensed phases and normal pressure gas phases. Thus, ionization changes the situation dramatically, as comparatively large amounts of energy need to be "handled" internally by the freshly formed ion. Even though part of this energy will contribute to translational or rotational energy of the molecule as a whole, the major fraction has to be stored in internal modes. Among the internal

modes rotational excitation cannot store significant amounts of energy, whereas vibration and especially electronic excitation are capable of an uptake of several electronvolts each [38,39].

2.4.1 Degrees of Freedom

Any atom or molecule in the gas phase has *external degrees of freedom*, because atoms and molecules as a whole can move along all three dimensions in space (along x, y, and z directions). This yields three *translational degrees of freedom*. From the kinetic gas theory the average translational energy can easily be estimated as $^3/_2kT$ delivering 0.04 eV at 300 K and 0.13 eV at 1000 K.

In case of diatomic and other linear molecules there are two rotations (around the x and y axes) and for all other molecules three rotations (around the x, y, and z axes). Thus, we have two or three more degrees of freedom contributing another kT or $^3/_2kT$ of energy, respectively, for the latter summing up to 0.08 eV at room temperature and 0.26 eV at 1000 K. This does not change independently of the number of atoms of the molecule or of their atomic masses.

In contrast to the external degrees of freedom, the number of *internal degrees of freedom*, notably *vibrational degrees of freedom*, s, increases with the number of atoms within the molecule, N. These internal degrees of freedom represent the number of vibrational modes a molecule can access. In other words, each of N atoms can move along three coordinates in space yielding $3N$ degrees of freedom in total, but as explained in the preceding paragraph, three of them have to be subtracted for the motion of the molecule as a whole and an additional two (linear) or three (nonlinear) have to be subtracted for rotational motion as a whole. Thus, we obtain for the number of vibrational modes

$$s = 3N - 5 \quad \text{in case of diatomic or linear molecules} \tag{2.8}$$

$$s = 3N - 6 \quad \text{in case of nonlinear molecules.} \tag{2.9}$$

It is obvious that even relatively small molecules possess a considerable number of vibrational modes.

Example: The thermal energy distribution curves for 1,2-diphenylethane, $C_{14}H_{14}$, $s = 3 \times 28 - 6 = 78$, have been calculated at 75 and 200 °C [40]. Their maxima were obtained at ~0.3 and ~0.6 eV, respectively, with almost no molecules exceeding twice that energy of maximum probability. At 200 °C, the most probable energy roughly corresponds to 0.008 eV per vibrational degree of freedom, which is a very small as compared to binding energies.

This indicates that excited vibrational states are almost fully unoccupied at room temperature and only the energetically much lower-lying internal rotations are effective under these conditions. Upon electron ionization, the situation changes quite dramatically as can be concluded from the Franck-Condon principle and therefore, energy storage in highly excited vibrational modes becomes of key importance for the further fate of ions in a mass spectrometer. In case of an indene

molecule having 45 vibrational modes, the storage of 10 eV would mean roughly 0.2 eV per vibration, i.e., roughly a 20-fold value of thermal energy, provided the energy is perfectly randomized among the bonds.

2.4.2 Appearance Energy

As explained by the Franck-Condon diagram, hardly any molecular ions will be generated in their vibrational ground state. Instead, the majority of the ions created by EI is vibrationally excited and many of them are well above the dissociation energy level, the source of this energy being the 70 eV electrons. Dissociation of $M^{+\bullet}$, or fragmentation as it is usually referred to in mass spectrometry, leads to the formation of a fragment ion, m_1^+, and a neutral, generally referred to as

$$M^{+\bullet} \rightarrow m_1^+ + n^\bullet \tag{2.10}$$

$$M^{+\bullet} \rightarrow m_1^{+\bullet} + n \tag{2.11}$$

Reaction 2.10 describes the loss of a radical, whereas reaction 2.11 corresponds to the loss of a molecule, thereby conserving the radical cation property of the molecular ion in the fragment ion. Bond breaking is a endothermal process and thus the potential energy of the fragment ion is usually located at a higher energy level (Fig. 2.6).

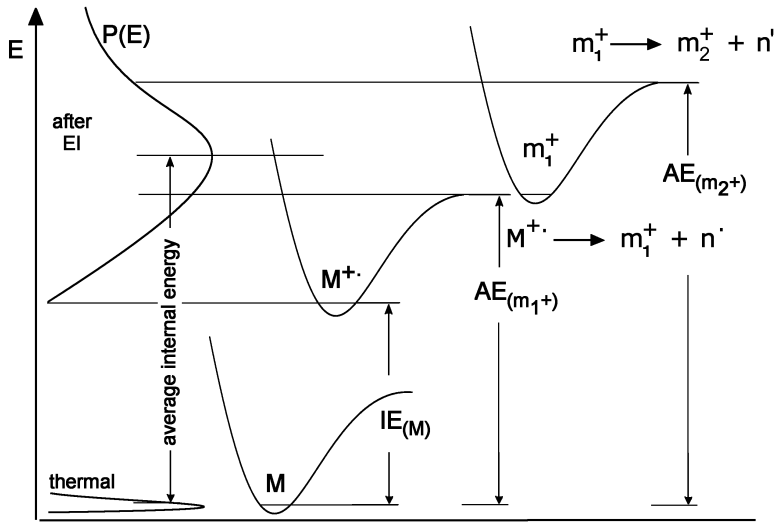


Fig. 2.6. Definition of the appearance energy and visualization of changes in internal energy distributions, $P_{(E)}$, of relevant species upon electron ionization and subsequent fragmentation (energy scale compressed for the ions).

Definition: The amount of energy needed to be transferred to the neutral M to allow for the detection of the fragment ion m_1^+ is called the *appearance energy* (*AE*) of that fragment ion. The old, and also incorrect, term *appearance potential* (*AP*) is still found in the literature.

In fact, the ions are not generated by one specific internal energy applying for all ions, but via a broad energy distribution $P_{(E)}$. One should keep in mind, however, that such a distribution is only valid for a large set of ions as each individual one bears a defined internal energy, ranging from just above *IE* to well beyond 10 eV for certain ones. Fragmentation of those highly excited ions from the tail of the $P_{(E)}$ curve yields fragment ions having still enough energy for a second dissociation step, $m_1^+ \rightarrow m_2^+ + n'$ or even a third one. Each of the subsequent steps can in principle also be characterized by an appearance energy value.

2.4.3 Bond Dissociation Energies and Heats of Formation

Great efforts have been made to generate accurate and reliable ion thermochemistry data. Once such data is available, it can be employed to elucidate fragmentation mechanisms and in addition, it is useful for obtaining some background on the energetic dimensions in mass spectrometry.

Heats of formation of neutral molecules, $\Delta H_{f(RH)}$, can be obtained from combustion data with high accuracy. Bond dissociation energies can either be derived for *homolytic bond dissociation*

$$R\text{–}H \rightarrow R^{\bullet} + H^{\bullet}, \ \Delta H_{Dhom} \tag{2.12}$$

or *heterolytic bond dissociation*

$$R\text{–}H \rightarrow R^{+} + H^{-}, \ \Delta H_{Dhet} \tag{2.13}$$

The homolytic bond dissociation enthalpies give the energy needed to cleave a bond of the neutral molecule which, in the gas phase is in its vibrational and electronic ground states, to obtain a pair of radicals which also are not in excited modes. Homolytic bond dissociation enthalpies are in the range of 3–5 eV (Table 2.2). The heterolytic bond dissociation energies apply for the case of creating a cation and an anion in their ground states from the neutral precursor which means that these values include the amount of energy needed for charge separation; they are in the order of 10–13 eV (Table 2.3). Due to the significantly altered bonding situation, breaking of a bond is clearly less demanding in molecular ions than in neutral molecules.

Example: The minimum energy needed to form a CH_3^+ ion and a hydrogen radical from the methane molecular ion can be estimated from the heat of reaction, ΔH_r, of this process. According to Fig. 2.6, $\Delta H_r = AE_{(CH3+)} - IE_{(CH4)}$. In order to calculate the missing $AE_{(CH3+)}$ we use the tabulated values of $\Delta H_{f(H^{\bullet})} = 218.0$ kJ mol^{-1}, $\Delta H_{f(CH3+)} = 1093$ kJ mol^{-1}, $\Delta H_{f(CH4)} = -74.9$ kJ mol^{-1}, and $IE_{(CH4)} = 12.6$ eV

= 1216 kJ mol^{-1}. First, the heat of formation of the methane molecular ion is determined:

$$\Delta H_{f(CH4+\bullet)} = \Delta H_{f(CH4)} + IE_{(CH4)} \tag{2.14}$$

$$\Delta H_{f(CH4+\bullet)} = -74.9 \text{ kJ mol}^{-1} + 1216 \text{ kJ mol}^{-1} = 1141.1 \text{ kJ mol}^{-1}$$

Then, the heat of formation of the products is calculated from

$$\Delta H_{f(prod)} = \Delta H_{f(CH3+)} + \Delta H_{f(H\bullet)} \tag{2.15}$$

$$\Delta H_{f(prod)} = 1093 \text{ kJ mol}^{-1} + 218 \text{ kJ mol}^{-1} = 1311 \text{ kJ mol}^{-1}$$

Now, the heat of reaction is obtained from the difference

$$\Delta H_r = \Delta H_{f(prod)} - \Delta H_{f(CH4+\bullet)} \tag{2.16}$$

$$\Delta H_r = 1311 \text{ kJ mol}^{-1} - 1141.1 \text{ kJ mol}^{-1} = 169.9 \text{ kJ mol}^{-1}$$

The value of 169.9 kJ mol^{-1} (1.75 eV) corresponds to $AE_{(CH3+)} = 14.35$ eV which is in good agreement with published values of about 14.3 eV [23,45]. In addition, this is only 40% of the homolytic C–H bond dissociation enthalpy of the methane molecule, thereby indicating the weaker bonding in the molecular ion.

Table 2.2. Homolytic bond dissociation enthalpies, ΔH_{Dhom}, and heats of formation, $\Delta H_{f(X\bullet)}$, of some selected bonds and radicals [kJ mol^{-1}] [a]

	X$^\bullet$	H$^\bullet$	$CH_3^\bullet$	Cl$^\bullet$	OH$^\bullet$	$NH_2^\bullet$
	$\Delta H_{f(X\bullet)}$	218.0	143.9	121.3	37.7	197.5
R$^\bullet$	$\Delta H_{f(R\bullet)}$					
H$^\bullet$	218.0	436.0	435.1	431.4	497.9	460.2
$CH_3^\bullet$	143.9	435.1	373.2	349.8	381.2	362.8
$C_2H_5^\bullet$	107.5	410.0	354.8	338.1	380.3	352.7
i-$C_3H_7^\bullet$	74.5	397.5	352.3	336.4	384.5	355.6
t-$C_4H_9^\bullet$	31.4	384.9	342.3	335.6	381.6	349.8
$C_6H_5^\bullet$	325.1	460.1	417.1	395.4	459.0	435.6
$C_6H_5CH_2^\bullet$	187.9	355.6	300.4	290.4	325.9	300.8
$C_6H_5CO^\bullet$	109.2	363.5	338.1	336.8	440.2	396.6

[a] Values from Ref. [41]

The heat of formation of organic radicals and positive ions decreases with their size and even more importantly with their degree of branching at the radical or ionic site. A lower heat of formation is equivalent to a higher thermodynamic stability of the respective ion or radical. The corresponding trends are clearly expressed by the values given in Tables 2.2 and 2.3. This causes the fragmentation pathways of molecular ions proceeding by formation of secondary or tertiary radi-

cals and/or ions to become dominant over those leading to smaller and/or primary radical and ionic fragments, respectively (Chap. 6.2.2).

Example: An impressive case showing the effects of isomerization upon thermal stability is that of butyl ions, $C_4H_9^+$. This carbenium ion can exist in four isomeric states with heats of formation that range from 837 kJ mol^{-1} in the case of *n*-butyl over 828 kJ mol^{-1} for *iso*-butyl (also primary) to 766 kJ mol^{-1} for *sec*-butyl to 699 kJ mol^{-1} in the case of *t*-butyl, meaning an overall increase in thermodynamic stability by 138 kJ mol^{-1} (Chap. 6.6.2) [42].

Table 2.3. Heterolytic bond dissociation enthalpies, ΔH_{Dhet}, and heats of formation of some molecules and ions [kJ mol^{-1}] [a]

Ion	ΔH_{Dhet}	$\Delta H_{f(R+)}$	$\Delta H_{f(RH)}$
Proton, H^+	1674	1528	0.0
Methyl, CH_3^+	1309	1093	–74.9
Ethyl, $C_2H_5^+$	1129	903	–84.5
n-Propyl, $CH_3CH_2CH_2^+$	1117	866	–103.8
i-Propyl, $CH_3CH^+CH_3$	1050	802	–103.8
n-Butyl, $CH_3CH_2CH_2CH_2^+$	1109	837	–127.2
sec-Butyl, $CH_3CH_2CH^+CH_3$	1038	766	–127.2
i-Butyl, $(CH_3)_2CHCH_2^+$	1109	828	–135.6
t-Butyl, $(CH_3)_3C^+$	975	699	–135.6
Phenyl, $C_6H_5^+$	1201	1138	82.8

[a] Values from Refs. [8,42-44]

2.4.4 Randomization of Energy

The best evidence for randomization of internal energy over all vibrational modes of a molecular ion prior to any fragmentation is delivered by EI mass spectra themselves. If there was no randomization, fragmentation would occur directly at any bond that immediately suffers from the withdrawal of an electron. As a result, mass spectra would show an almost statistical bond breaking throughout the molecular ion. Instead, mass spectra reveal a great deal of selectivity of the molecular ion when choosing fragmentation pathways. This means the molecular ion explores many pathways up to its respective transition states and prefers the thermodynamically (and as we will see, also kinetically) more favorable ones. The same is true for fragment ions.

From a purely thermodynamic point of view the situation can be elucidated by considering a hypothetical molecular ion having some internal energy and being faced to the selection of a fragmentation pathway (Fig. 2.7).

a) The molecular ion $ABC^{+\bullet}$ has an internal energy E_{inta} being slightly above the activation energy, E_{02}, required to cross the transition state TS_2 leading to the

formation of $A^{\bullet}$ and BC^{+}, but definitely more than needed to dissociate into AB^{+} and $C^{\bullet}$. The difference between the energy content E_{inta} and E_{01} is termed *excess energy*, $E_{ex} = E_{int} - E_0$, of the transition state TS_1. In this case either ionic product would be observed, but the third pathway could not be accessed.

b) The molecular ion $ABC^{+\bullet}$ has an internal energy E_{intb} being clearly higher than any of the three activation energies. Here, formation of all possible products should occur.

A simple comparison of activation energies does not allow, however, to predict the relative intensities of the ions AB^{+} and BC^{+} or of AB^{+}, BC^{+}, and A^{+}, respectively. In fact, from this model one would expect similar or even equal abundances of all accessible fragment ions. Actual mass spectra show greatly differing intensities of signals resulting from competing decomposition pathways. This reveals the oversimplification of the preceding passage.

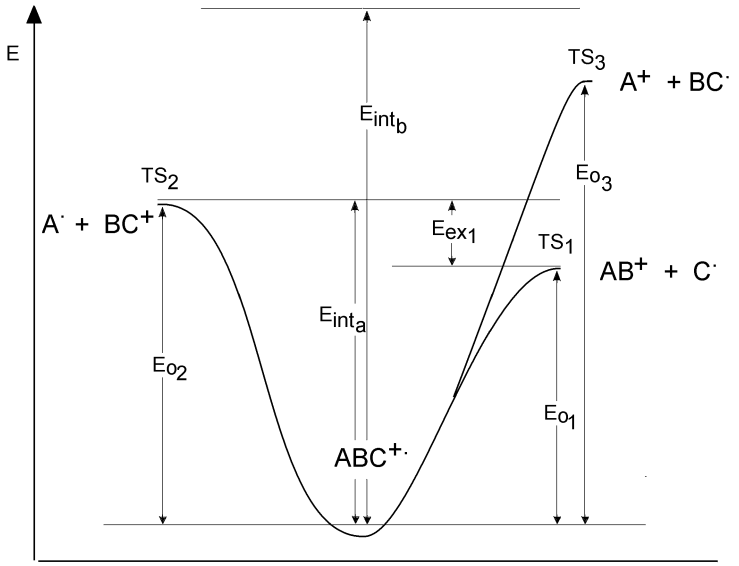


Fig. 2.7. Competition of fragmentation pathways strongly depends on the internal energy of the fragmenting ion and on the activation energies, E_0, of the transition states, i.e., the "energy barriers" of the respective reactions.

Note: Thermodynamic data such as heats of formation and activation energies alone are not sufficient to adequately describe the unimolecular fragmentations of excited ions.

2.5 Quasi-Equilibrium Theory

The *quasi-equilibrium theory* (QET) of mass spectra is a theoretical approach for describing the unimolecular decompositions of ions and hence their mass spectra [46-48]. QET is an extention of the Rice-Ramsperger-Marcus-Kassel (RRKM) theory with the aim of accommodating the conditions of mass spectrometry and marks a landmark in the theory of mass spectra [11]. Within the mass spectrometer almost all processes occur under high vacuum, i.e., in the highly diluted gas phase – one needs to be aware of how this contrasts to chemical reactions in the condensed phase as usually carried out in the laboratory [49,50]. In essence, bimolecular reactions rarely occur in a mass spectrometer and we are rather dealing with the chemistry of *isolated ions in the gas phase*. Isolated ions are not in thermal equilibrium with their surrounds as assumed by the RRKM theory. Instead, to be isolated in the gas phase means for an ion that it may only internally redistribute energy and that it may only undergo unimolecular reactions such as isomerization or dissociation. This is why the theory of unimolecular reactions is of paramount importance in mass spectrometry.

QET is not the sole theory in the field; indeed, there are several apparently competitive statistical theories for describing rate constants of unimolecular reactions [10,48]. However, none of these theories has been able to quantitatively describe all reactions of a given ion. QET, however, is well established and even in its simplified form allows sufficient insight into the behavior of isolated ions. Thus, we start out the chapter from the basic assumptions of QET. Along this scheme we will be led from the neutral molecule to ions, and from transition states and reaction rates to fragmentation products and thus, through the basic concepts and definitions of gas phase ion chemistry.

2.5.1 QET's Basic Premises

According to QET the rate constant, k, of a unimolecular reaction is basically a function of excess energy, E_{ex}, of the reactants in the transition state and thus $k_{(E)}$ strongly depends on the internal energy distribution of any particular ion. QET is thus based on the following essential premises [46,51]:

1. The initial ionization is "vertical", i.e., there is no change of position or kinetic energy of the nuclei while it is taking place. With the usual electron energy any valence shell electron may be removed.
2. The molecular ion will be of low symmetry and have an odd electron. It will have as many low-lying excited electronic states as necessary to form essentially a continuum. Radiationless transitions then will result in transfer of electronic energy into vibrational energy at times comparable to the periods of nuclear vibrations.
3. These low-lying excited electronic states will in general not be repulsive; hence, the molecular ions will not dissociate immediately, but rather remain to-

gether for a time sufficient for the excess electronic energy to become randomly distributed as vibrational energy over the ion.
4. The rates of dissociation of the molecular ion are determined by the probabilities of the energy randomly distributed over the ion becoming concentrated in the particular fashions required to give several activated complex configurations yielding the dissociations.
5. Rearrangements of the ions can occur in a similar fashion.
6. If the initial molecular ion has sufficient energy, the fragment ion will in turn have enough energy to undergo further decomposition.

The characteristics of the ionization process as described in Chap. 2.2 justify the first assumption of QET. Further, it is obvious that electronic excitation occurs together with vibrational excitation and thus, the second assumption of QET is met.

2.5.2 Basic QET

QET focuses on the dynamic aspects of ion fragmentation. It describes the *rate constants* for the dissociation of isolated ions as a function of internal energy, E_{int}, and activation energy of the reaction, E_0. By doing so, it compensates for the shortcomings of the merely thermodynamic treatment above.

QET delivers the following expression for the unimolecular rate constant

$$k_{(E)} = \int_0^{E-E_0} \frac{1}{h} \times \frac{\rho^*_{(E_{\text{int}},E_0,E_t)}}{\rho_{(E)}} dE_t \tag{2.17}$$

In this equation, $\rho_{(\text{E})}$ is the density of energy levels for the system with total energy E_{int}, and $\rho_{(\text{E,E0,Et})}$ is the density of energy levels in the activated complex, i.e., transition state, with activation energy E_0 and translational energy E_{t} in the reaction coordinate. The reaction coordinate represents the bond which is actually being broken. The expression is slightly simplified by approximating the system by as many harmonic oscillators as there are vibrational degrees of freedom

$$k_{(E)} = \left(\frac{E_{\text{int}} - E_0}{E_{\text{int}}} \right)^{s-1} \frac{\prod_{j=1}^{s} \nu_j}{\prod_{i=1}^{s-1} \nu_i^*} \tag{2.18}$$

Then, the exponent is given by the number of degrees of freedom, s, minus 1 for the breaking bond. For a strict treatment of fragmenting ions by QET one would need to know the activation energies of all accessible reactions and the probability functions describing the density of energy levels.

In the most simplified form, the rate constant $k_{(\text{E})}$ can be expressed as

$$k_{(E)} = \nu \times \left(\frac{E_{\text{int}} - E_0}{E_{\text{int}}} \right)^{s-1} \tag{2.19}$$

where ν is a frequency factor which is determined by the number and density of vibrational states. The frequency factor thereby replaces the complex expression of probability functions. Now, it becomes clear that a reaction rate considerably increases with growing E_{ex}.

$$k_{(E)} = \nu \times \left(\frac{E_{ex}}{E_{\text{int}}} \right)^{s-1} \tag{2.20}$$

Unfortunately, as with all oversimplified theories, there are limitations for the application of the latter equation to ions close to the dissociation threshold. In these cases, the number of degrees of freedom has to be replaced by an effective number of oscillators which is obtained by use of an arbitrary correction factor [7]. However, as long as we are dealing with ions having internal energies considerably above the dissociation threshold, i.e., where $(E - E_0)/E \approx 1$, the relationship is valid and can even be simplified to give the quasi-exponential expression

$$k_{(E)} = \nu \times e^{-(s-1)E_0/E} \tag{2.21}$$

Example: For $\nu = 10^{15}$ s^{-1}, $s = 15$, $E_{\text{int}} = 2$ eV, and $E_0 = 1.9$ eV the rate constant is calculated as 3.0×10^{-5} s^{-1}. For the same parameters but $E_{\text{int}} = 4$ eV we obtain $k = 6.3 \times 10^{10}$ s^{-1} being a 2.1×10^{15}-fold increase. This means that a reaction is extremely slow at small excess energies but becomes very fast as soon as there is some substantial excess energy available.

2.5.3 Rate Constants and Their Meaning

The rate constants of unimolecular reactions have the dimension *per second* (s^{-1}). This means the process can happen x times per second, e.g., $k = 6.3 \times 10^{10}$ s^{-1} being equivalent to 1.6×10^{-11} s *per fragmentation on the average*. Note the emphasis "on the average", because rate constants are macroscopic and statistical in nature as they get their meaning only from considering a very large number of reacting particles. A single ion will have a lifetime of 1.6×10^{-11} s *on the average* in this case; however, a specific one in consideration might also decay much sooner or later, with the actual decay occurring at the speed of vibrational motions. The dimension s^{-1} also means there is no dependence on concentration as it is the case with second- or higher order reactions. This is because the ions are isolated in the gas phase, alone for their entire lifetime, and the only chance for change is by means of unimolecular reaction.

2.5.4 $k_{(E)}$ Functions – Typical Examples

Although the general shape of any $k_{(E)}$ function resembles the ionization efficiency curve to the left of the maximum, these must not be confused. At an excess energy close to zero, the rate constant is also close to zero but it rises sharply upon slight increase of the excess energy. However, there is an upper limit for the rate of a dissociation that is defined by the vibrational frequency of the bond to be cleaved. The fragments are not able to fly apart at a higher velocity than determined by their vibrational motion (Fig. 2.8).

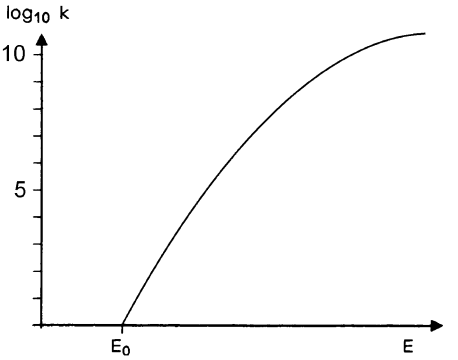


Fig. 2.8. General shape of a log k vs. E plot as determined by the simplified QET. At $E = E_0$ the reaction is extremely slow. A slight increase in energy causes k to rise sharply.

2.5.5 Reacting Ions Described by $k_{(E)}$ Functions

According to our knowledge of rate constants, Fig. 2.7 requires a different interpretation. At an internal energy E_{inta} the molecular ion $ABC^{+\bullet}$ can easily cross the transition state TS_1 to form AB^+ and $C^\bullet$. The products of the second reaction can in principle be formed, even though the excess energy at TS_2 is so small that the product ion BC^+ will almost be negligible. The third pathway is still not accessible. At an internal energy E_{intb} the excess energy is assuredly high enough to allow for any of the three pathways with realistic rates to observe the products. Nevertheless, due to the strong dependence of the rate constant on E_{ex}, the reaction over TS_3 will be by far the least important.

2.5.6 Direct Cleavages and Rearrangement Fragmentations

The reactions of excited ions are not always as straightforward as expected. Of course, the existence of multiple fragmentation pathways for an ion consisting of several tens of atoms brings about different types of reactions all of which certainly will not lead to the same $k_{(E)}$ function [52].

The $k_{(E)}$ functions of two reactions of the same type, appear to be "parallel" in comparison, starting out at different activation energies (Fig. 2.9a), whereas different types of reactions will show a crossover of their $k_{(E)}$ functions at intermediate excess energy (Fig. 2.9b).

For example, case (**a**) depicts two competing homolytic bond cleavages. Homolytic bond cleavages are simple fragmentations of molecular ions creating an even-electron ion and a radical. One cleavage might require a somewhat higher activation energy than the other ($E_{02} > E_{01}$) because of the difference between the bonds to be cleaved, but once having enough excess energy their rates will rise sharply. The more energy is pushed into the ion, the faster the bond rupture can occur. A further increase of excess energy will become ineffective onlywhen the rate approaches the upper limit as defined by the vibrational frequency of the bond to be cleaved.

Case (**b**) compares a *rearrangement fragmentation* (reaction 1) with a *homolytic bond cleavage* (reaction 2). During a rearrangement fragmentation the precursor ion expels a neutral fragment which is an intact molecule after having rearranged in an energetically favorable manner. Rearrangements begin at low excess energy, but then the rate approaches the limit relatively soon, while cleavage starts out later, then overrunning the other at higher excess energy. The differences can be explained by the different transition states of both types of reactions. The cleavage has a *loose transition state* [40], i.e., there is no need for certain parts of the molecule to assume a specific position while the cleavage proceeds. The dissociation merely requires enough energy in the respective bond so that the binding forces can be overcome. Once the bond is stretched too far, the fragments drift apart. The rearrangement demands less excess energy to proceed, because the energy for a bond rupture on one side is compensated for by the energy received

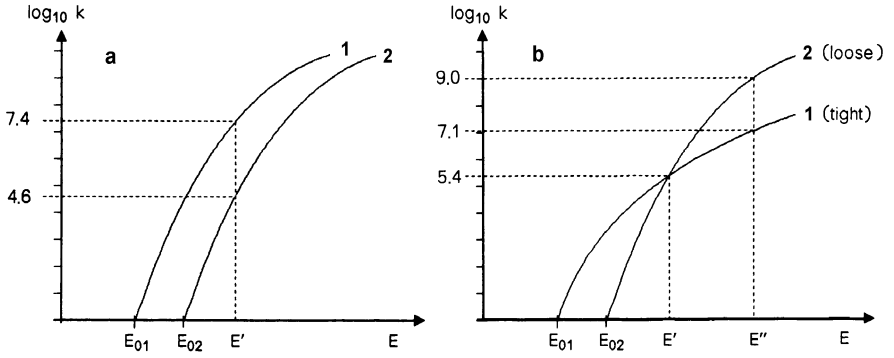


Fig. 2.9. Comparison of different types of reactions by their $k_{(E)}$ functions. (**a**) Reactions of the same type show $k_{(E)}$ functions that are "parallel", whereas (**b**) $k_{(E)}$ functions of different types tend to cross over at intermediate excess energy. In (**a**), reaction **1** would proceed $10^{2.8}$ (630) times faster at an internal energy E' than would reaction **2**. In (**b**), both reactions have the same rate constant, $k = 10^{5.4}$ s^{-1}, at an internal energy E', whereas reaction **2** becomes $10^{1.9}$ (80) times faster at E''.

when a new bond is formed by the accepting position. Compared to the simple cleavage, such a transition state is usually termed *tight transition state* (cf. Chap. 6.12.2). Then, the neutral is expelled in a second step. Such a reaction obviously depends on the suitable conformation for rearrangement at the same time when sufficient energy is put into the bond to be cleaved. Furthermore, the second step has to follow in order to yield the products. Overall, there is no use in having more than enough energy until the ion reaches the conformation needed. Thus, after considering either basic type of fragmentation, the fifth assumption of QET is justified, because there is no reason why rearrangements should not be treated by QET.

2.6 Time Scale of Events

We have just learned that ionization occurs on the low femtosecond timescale, direct bond cleavages require between some picoseconds to several tens of nanoseconds, and rearrangement fragmentations usually proceed in much less than a microsecond (Fig. 2.10). All those chemical reactions are strictly unimolecular, because the reacting ions are created in the highly diluted gas phase – circumstances that prevent bimolecular reactions of the ions during their residence time within the ion source. This dwell time is determined by the extraction voltages applied to accelerate and focus ions to form a beam and by the dimensions of that ion source. In standard EI sources the ions spend about 1 µs before they are ejected by action of the accelerating potential [53].

Therefore, a reaction needs to proceed within that certain period of time to make the products detectable in the mass spectrum, and for this purpose there is a need for some excess energy in the transition state.

Finally, some fragment ions may even be formed after the excited species has left the ion source, so to speak in the "afterglow", giving rise to metastable ion dissociation. As the ions then travel at speeds of some 10^4 m s^{-1} they pass the mass analyzer in the order of 10–50 µs (Fig. 2.11) [9]. Even though this particular case has been adapted for a double-focusing magnetic sector mass spectrometer, an ion of *m/z* 100, and an acceleration voltage of 8 kV, the effective time scales for other types of beam instruments (quadrupole, time-of-flight) are very similar under their typical conditions of operation (Table 2.4).

Table 2.4. Typical ion flight times in different types of mass spectrometers

Mass analyzer	Flight path [m]	Acceleration voltage [V]	Typical *m/z*	Flight time [µs]
Quadrupole	0.2	10	500	57
Magnetic sector	2.0	5000	500	45
Time-of-flight	2.0	20,000	2000	45

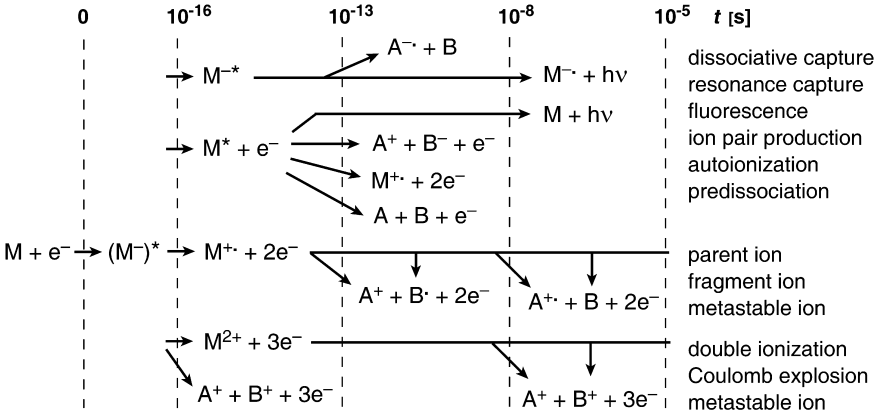


Fig. 2.10. Schematic time chart of possible electron ionization processes. Adapted from Ref. [39] with permission. © Wiley & Sons, 1986.

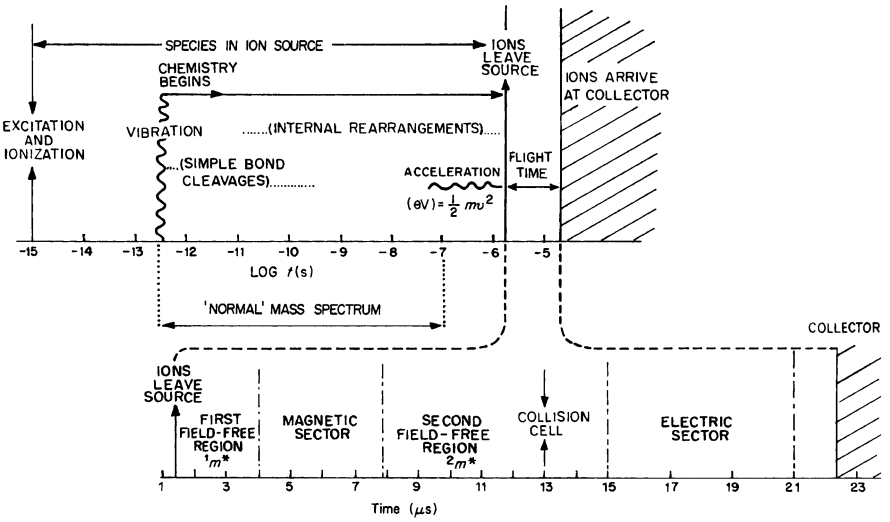


Fig. 2.11. The mass spectrometric time scale and its correlation to the classical instrumental framework. Note the logarithmic time scale for the ion source that spans nine orders of magnitude. Reproduced from Ref. [9] with permission. © John Wiley & Sons, Ltd., 1985.

2.6.1 Stable, Metastable, and Unstable Ions

The terminology for ions has been coined as a direct consequence of the classical mass spectrometric time scale. Nondecomposing molecular ions and molecular ions decomposing at rates below about $10^5\ s^{-1}$ will reach the detector without fragmentation and are therefore termed *stable ions*. Consequently, ions dissociat-

ing at rates above 10^6 s^{-1} cannot reach the detector. Instead, their fragments will be detected and thus they are called *unstable ions*. A small percentage, however, decomposing at rates of 10^5–10^6 s^{-1} will just fragment on transit through the mass analyzer – those are termed *metastable ions* (Figs. 2.10–2.12) [4,5,9].

Definition:	*stable ions*, $k < 10^5$ s^{-1} *metastable ions*, 10^5 $s^{-1} < k < 10^6$ s^{-1} *unstable ions*, $k > 10^6$ s^{-1}

There is no justification for such a classification of ion stabilities outside the mass spectrometer because almost all ions created under the conditions inside a mass spectrometer would spontaneously react in the atmosphere or in solvents. Nevertheless, this classification is useful as far as ions isolated in the gas phase are concerned and is valid independently of the type of mass analyzer or ionization method employed.

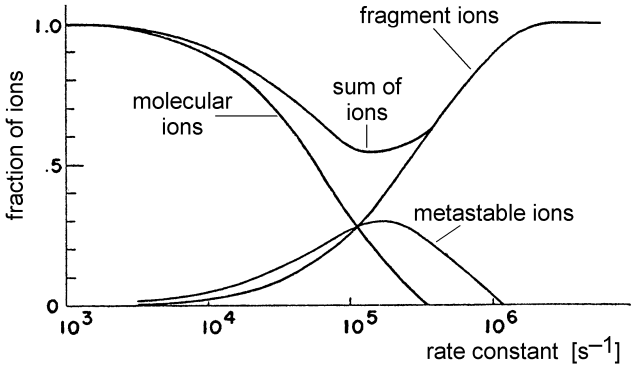


Fig. 2.12. Correlation between rate constants of ion dissociations and terminology referring to ion stability as employed in mass spectrometry. Adapted from Ref. [54] with permission. © The American Institute of Physics, 1959.

2.6.2 Time Scale of Ion Storage Devices

Many modern instruments make use of ion storage in some way. Linear radiofrequency multipoles can be axially segmented or equipped with trapping plates to their ends to raise switchable potential walls that allow to accumulate, store and eject ion packages as required. The most prominent of those devices is the *linear (quadrupole) ion trap* (LIT). The other type, the so-called *three-dimensional quadrupole ion trap* (QIT) stores ion clouds to have them ready for mass analysis by bringing them successively from stable to unstable ion trajectories that end up with ejection from the trap onto a detector. *Fourier transform ion cyclotron resonance* (FT-ICR) relies on storage of ions on circular paths to detect the angular frequencies of coherent ion packages as they repeatedly pass a pair of detection plates. The recent *orbitrap* mass analyzer employs a different operational concept

but shares the time frame with FT-ICR. Even during their transport from the ion source to the mass analyzer of the above instruments, ions are often repeatedly being accumulated, stored and passed to another section of the instrument before they finally enter the compartment for *m/z* analysis. (For details of mass analyzers refer to Chap. 4.)

The time span of ion accumulation can easily extend from milliseconds to seconds, the passage between functional units of the instrument may take tens of microseconds to milliseconds, and the *m/z* analysis requires storage times from milliseconds (QIT, LIT) to seconds (FT-ICR, orbitrap).

This way, modern mass spectrometry instrumentation has gone beyond the classical mass spectrometric time scale. Especially the time frame after leaving the ion source has drastically been extended. It is still important, however, to understand the considerations of the classical mass spectrometric time scale as it governs the processes in many types of ion sources (electron ionization, chemical ionization, field ionization and field desorption, laser desorption) and as it is still basically valid for a wide range of mass analyzers. One should be aware though of the 10^3–10^6-fold expansion of the time scale for cases where ion storage is involved. Furthermore, the handling of ions on the extended time scale is only possible if they are stable, i.e., nondecomposing, and this is in accordance with our previous definition of ion stability in terms of being just below threshold for dissociation during their dwell time in the instrument. Without the use of extremely soft ionization techniques (such as electrospray ionization), those ion-storing instruments would not have any ions to store nor to be analyzed.

2.7 Internal Energy – Practical Implications

Even comparatively small molecular ions can exhibit a substantial array of first-, second-, and higher-generation fragmentation pathways due their internal energy in the order of several electronvolts [52]. Typically, ion dissociations are endothermic, and thus each fragmentation step consumes some of the ions' internal energy. Highly excited ions may carry enough internal energy to allow for several consecutive cleavages, whereas others may just undergo one or even none (Chap. 2.4.2). The latter reach the detector as still intact molecular ions. The fragmentation pathways of the same generation compete with each other, their products being potential precursors for the next generation of fragmentation processes.

Example: Imagine the hypothetical molecular ion $ABYZ^{+\bullet}$ undergoing three competing first-generation fragmentations, two of them rearrangements, one a homolytic bond cleavage (Fig. 2.13). Next, three first-generation fragment ions have several choices each, and thus the second-generation fragment ions $Y^{+\bullet}$ and YZ^+ are both formed on two different pathways. The formation of the same higher-generation fragment ion on two or more different pathways is a widespread phenomenon. A closer look reveals that $Y^{+\bullet}$ and Y^+ are different although having identical empirical formulas, because one of them is an odd-electron and the other

an even-electron species. Nevertheless, they would both contribute to one common peak at the same nominal *m/z* in a mass spectrum of ABYZ (Chap. 3.1.4).

In an EI mass spectrum of ABYZ, all ionic species would be detected which are formed as a result of numerous competing and consecutive reactions, but there is no simple rule which of them should give rise to intensive peaks and which of them would be hardly noticed.

Obviously, the first-generation fragment ions should be more closely related to the initial structure of ABYZ than those of the second or even third generation. Fortunately, such higher generation (and therefore low-mass) fragment ions can also reveal relevant information on the constitution of the analyte. In particular, they yield reliable information on the presence of functional groups (Chap. 6).

Fragmentation trees similar to that shown here can be constructed from any EI mass spectrum, providing ten thousands of examples for the sixth assumption of QET, that fragment ions may again be subject to dissociation, provided their internal energy suffices.

Note: The assumptions of QET have turned into basic statements governing the behavior of isolated ions in the gas phase and thus, in mass spectrometry in general.

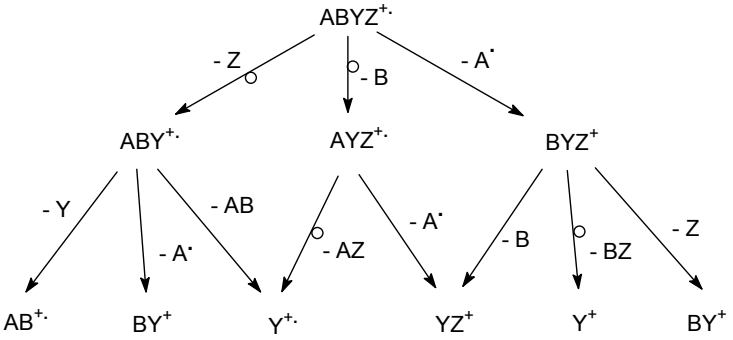


Fig. 2.13. Possible fragmentation pathways for hypothetical molecular ions $ABYZ^{+\bullet}$ having internal energies typical for EI.

2.8 Reverse Reactions and Kinetic Energy Release

2.8.1 Activation Energy of the Reverse Reaction

By merely considering thermodynamic and kinetic models we may be able to understand how ions are formed and what parameters are effective to determine their further fate in the mass spectrometer. However, the potential energy surfaces considered in this context only reached up to the transition state (Fig. 2.6). Without explicitly mentioning it, we assumed the curves to stay on the same energetic level between transition state and the products of ion dissociation, i.e., the sum of heats

of formation of the products would be equal to the energy of the transition state. This assumption is almost correct for homolytic bond cleavages in molecular ions because the recombination of an ion with a radical proceeds with almost negligible activation energy [4,5]. In other words, the *activation energy of the reverse reaction*, E_{0r} (or often simply called *reverse activation energy*) is then close to zero. This explains why the result of our simple estimation of the activation energy for hydrogen radical loss from the molecular ion of methane could be realistic (Chap. 2.4.3).

In case of rearrangement fragmentations the situation is quite different, because one of the products is an intact neutral molecule of comparatively high thermodynamic stability, i.e., having negative or at least low values of ΔH_f (Table 2.5). Once the transition state is crossed, the reaction proceeds by formation of products energetically much lower than the transition state. In case of the reverse reaction, this would require some or even substantial activation energy transfer to the fragments to allow their recombination, and thus $E_{0r} > 0$ (Fig. 2.14).

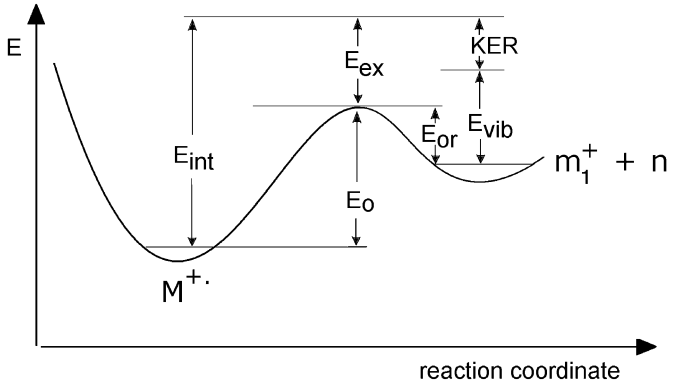


Fig. 2.14. Definition of E_{0r} and origin of KER. The excess energy of the decomposing ion in the transition state relative to the sum of the heats of formation of the ionic and neutral product is partitioned into vibrational excitation of the products plus KER.

Table 2.5. Gas phase heats of formation, ΔH_f, of some frequently eliminated molecules[a]

Molecule	ΔH_f [kJ mol^{-1}][b]	Molecule	ΔH_f [kJ mol^{-1}][b]
CO_2	–393.5	H_2CO	–115.9
HF	–272.5	HCl	–92.3
H_2O	–241.8	NH_3	–45.9
CH_3OH	–201.1	C_2H_4	52.5
CO	–110.5	HCN	135.1

[a] *IE* data extracted from Ref. [23] with permission. © NIST 2002.
[b] All values have been rounded to one digit.

2.8.2 Kinetic Energy Release

The total excess energy, E_{extot}, of the precursor ion relative to the heats of formation of the products in their ground state, comprises the excess energy in the transition state, E_{ex}, plus the activation energy of the reverse reaction, E_{0r}:

$$E_{extot} = E_{ex} + E_{0r} \tag{2.22}$$

Although most ion fragmentations are endothermic, there is still a significant amount of energy to be redistributed among the reaction products. Much of E_{extot} is redistributed as vibrational energy, E_{vib}, among the internal modes, thereby supplying the energy for consecutive fragmentation of the fragment ion. Nonetheless, some of the energy is converted into translational motion of the fragments relative to their center of gravity. This portion of E_{extot} is released in the direction of the bond that is being cleaved, in other words, into separation from each other. This is termed *kinetic energy release*, KER (Fig. 2.14) [4,5,9,55,56].

The larger the sum of $E_{ex} + E_{0r}$ the larger is the expected KER. Large reverse activation energy, especially when combined with repulsive electronic states in the transition state, will cause significant KER that has been observed up to 1.64 eV [57-60]. Significant KER also has been measured in the rare case of exothermic fragmentations [61]. On the other hand, homolytic cleavages and ion–neutral complex-mediated reactions tend to proceed with very small KER in the range of 1–50 meV (Fig. 2.15).

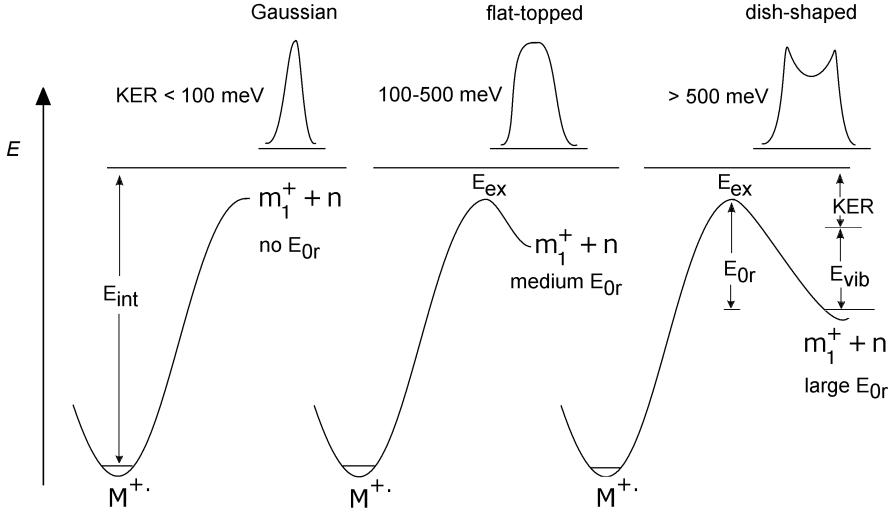


Fig. 2.15. Influence of the reverse activation energy on KER and thus, on peak shapes in metastable ion decompositions (suitable experimental setup being a prerequisite). *From left*: no or small reverse barrier causes Gaussian peak shape, whereas medium E_{0r} yields flat-topped peaks and large E_{0r} causes dish-shaped peaks.

Note: The importance of KER measurements results from the fact that the potential energy surface between transition state and products of a reaction can be reconstructed [55]. Thus, KER and *AE* data are complementary in determining the energy of the transition state.

2.8.3 Energy Partitioning

The observed KER consists of two components, one from E_{ex} and one from E_{0r}. This splitting becomes obvious from the fact that even if there is no E_{0r}, a small KER is always observed, thus demonstrating partitioning of E_{ex} between E_{vib} and E_{trans*} (KER):

$$E_{ex} = E_{vib} + E_{trans*} \tag{2.23}$$

Diatomic molecular ion dissociations represent the only case with clear energy partitioning, as all excess energy of the decomposition has to be converted to translational energy of the products ($E_{ex} = E_{trans*}$). For polyatomic ions the partitioning of excess energy can be described by a simple empirical relationship between E_{ex} and the number of degrees of freedom, s [6,62]:

$$E_{trans*} = \frac{E_{ex}}{\alpha \times s} \tag{2.24}$$

with the empirical correction factor $\alpha = 0.44$ [62]. According to Eq. 2.24 the ratio E_{trans*}/E_{ex} decreases as the size of the fragmenting ion increases. This influence has been termed *degrees of freedom effect* (DOF) [63-65].

Consequently, E_{trans*} becomes rather small for substantial values of s, e.g., 0.3 eV/(0.44 × 30) = 0.023 eV. Therefore, any observed KER in excess of E_{trans*} must originate from E_{0r} being the only alternative source [61]. The analogous partitioning of E_{0r} is described by:

$$E_{trans} = \beta E_{or} \tag{2.25}$$

with $\beta = 0.2–0.4$ and $^1/_3$ being a good approximation in many cases.

Note: In practice, most of the observed KERs (except at < 50 meV), can be attributed to E_{trans} from E_{0r} [61], and as a rule of thumb, $E_{trans} \approx 0.33\ E_{or}$

2.9 Isotope Effects

Most elements are composed of more than one naturally occurring *isotope*, i.e., having nuclei of the same *atomic number* but different *mass numbers* due to different numbers of neutrons [66]. The mass number of an isotope is given as a superscript preceding the element symbol, e.g., ^{1}H and ^{2}H (D) or ^{12}C and ^{13}C

(Chap. 3). Obviously, mass spectrometry is ideally suited for distinguishing between isotopic species, and isotopic labeling is used for mechanistic as well as analytical applications (Chap. 3.2.9). However, isotopic substitution not only affects ionic mass, but rather "isotopic substitution can have several simultaneous effects, and this complication sometimes produces results which are at first sight curious" [67].

Any effect exerted by the introduction of isotopes are termed *isotope effects*. Isotope effects can be *intermolecular*, e.g., upon $D^{\bullet}$ loss from $CD_4^{+\bullet}$ vs. $H^{\bullet}$ loss from $CH_4^{+\bullet}$, or *intramolecular*, e.g., upon $H^{\bullet}$ loss versus $D^{\bullet}$ loss from $CH_2D_2^{+\bullet}$.

2.9.1 Primary Kinetic Isotope Effects

Kinetic isotope effects represent one particular type of isotope effect. They are best rationalized when considering the potential energy diagram of both $H^{\bullet}$ and $D^{\bullet}$ loss from equivalent positions in the same isotopically labeled (e.g., deuterated) molecular ion (Fig. 2.16) [4,5,68]. The diagram is essentially symmetric, with the only differences arising from the zero-point energy (ZPE) terms. Since $H^{\bullet}$ and $D^{\bullet}$ are being lost from the same molecular ion, the single ZPE to start from is defined by this species. The transition states leading up to $H^{\bullet}$ and $D^{\bullet}$ loss possess ZPE terms associated with all the degrees of freedom of the dissociating ion except the one involved in that particular reaction. The transition state corresponding to $H^{\bullet}$ loss must therefore have a lower ZPE because it contains a C–D bond that is not involved in the actual cleavage. This corresponds to a lower ZPE than is provided by the C–H bond-retaining transition state that leads to $D^{\bullet}$ loss. Therefore, an ion with an internal energy E_{int} has a larger excess energy E_{exH} when it is about to eliminate $H^{\bullet}$ than if it cleaved off a $D^{\bullet}$. The activation energy for $H^{\bullet}$ loss is thereby lowered making it proceed faster than $D^{\bullet}$ loss ($k_H/k_D > 1$).

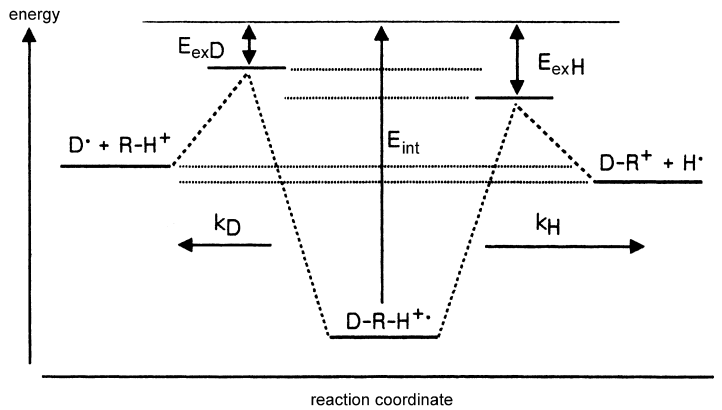


Fig. 2.16. Origin of kinetic isotope effects [4,5,68]. The change in vibrational frequencies, and thus in density of states causes somewhat higher activation energy and consequently smaller excess energy for the reaction of the deuterated bond, and thus reduces k_D.

The reason for the lower ZPE of the deuterium-retaining species is found in its lower vibrational frequencies due to the double mass of D as compared to H at almost identical binding forces. According to classical mechanics the vibrational frequency ν_D should therefore be lower by the inverse ratio of the square roots of their masses, i.e., $\nu_D / \nu_H \approx 1/1.41 \approx 0.71$ [69].

Example: Isotopic labeling does not only reveal the original position of a rearranging atom, but can also reveal the rate-determining step of multi-step reactions by its marked influence on reaction rates. Thus, the examination of H/D and $^{12}C/^{13}C$ isotope effects led to the conclusion that the McLafferty rearrangement of aliphatic ketones (Chap. 6.7) rather proceeds stepwise than concerted. [70]

Notes: *i*) The isotope effects dealt with in mass spectrometry are usually *intramolecular kinetic isotope effects*, i.e., two competing fragmentations only differing in the isotopic composition of the products exhibit different rate constants k_H and k_D [71]. *ii*) The kinetic isotope effect is called *normal* if $k_H/k_D > 1$ and *inverse* if $k_H/k_D < 1$. *iii*) Isotope effects can also be observed on KER [60,72], e.g., the KER accompanying H_2 loss from methylene immonium ion varies between 0.61 and 0.80 eV upon D labeling at various positions [60].

The term *primary kinetic isotope effect* applies if the effect is exerted on a bond where the isotope itself is involved during the reaction. It seems clear that there is no single well-defined value of the kinetic isotope effect of a reaction (Fig. 2.17) and that it strongly depends on the internal energy of the decomposing ions. In the rare case when E_{int} is just above the activation energy for $H^\bullet$ loss but still below that for $D^\bullet$ loss, the isotope effect would be infinite. As ions in a mass spectrometer usually exhibit comparatively wide distributions of E_{int}, the probability for such a case is extremely low. However, kinetic isotope effects can be large in case of decomposing metastable ions ($k_H/k_D \approx 2$–4) because these ions possess only small excess energies. Such circumstances make them sensitive to the difference between E_{exD} and E_{exH}. On the other hand, ions that decompose in the ion source usually have high internal energies, and thus smaller isotope effects are observed ($k_H/k_D \approx 1$–1.5).

While the mass of H remarkably differs from that of D (2 u/1 u = 2), the relative increase in mass is much lower for heavier elements such as carbon (13 u/12 u ≈ 1.08) [70] or nitrogen (15 u/14 u ≈ 1.07). In consequence, kinetic isotope effects of those elements are particularly small and special attention has to be devoted for their proper determination.

2.9.2 Measurement of Isotope Effects

Mass spectrometry measures the abundance of ions vs. their *m/z* ratio, and it is common practice to use the ratio $I_{mH}/I_{mD} = k_H/k_D$ as a direct measure of the isotope effect. The typical procedure for determining isotope effects from intensity ratios is to solve a set of simultaneous equations [73-76].

Example: The transfer of a D compared to the transfer of an H during propene loss from partially labeled phenylpropylethers is accompanied by an isotope effect, the approximate magnitude of which was estimated as follows [76]:

$$[1,1-D_2]: \quad \frac{[C_6H_6O]^+}{[C_6H_5OD]^+} = \frac{\alpha\, i}{1-\alpha} \tag{2.28}$$

$$[2,2,3,3,3-D_5]: \quad \frac{[C_6H_6O]^+}{[C_6H_5OD]^+} = \frac{(1-\alpha)\, i}{\alpha} \tag{2.29}$$

where α is the total fraction of H transferred from positions 2 and 3 and i is the isotope effect favoring H over D transfer. Unfortunately, the situation is more complicated if more than just one complementary pair is being studied, and an exact solution will no longer be feasible. Then, a numerical approach is required to approximate the i value [76,77].

Also, a rigorous treatment of isotope effects within the framework of QET reveals that the assumption $I_{mH}/I_{mD} = k_H/k_D$ represents a simplification [71]. It is only valid for when the studied species populate a small internal energy distribution, e.g., as metastable ions do, whereas wide internal energy distributions, e.g., those of ions fragmenting in the ion source after 70 eV electron ionization, may cause erroneous results. This is because the $k_{(E)}$ functions of isotopic reactions are not truly parallel [78], but they do fulfill this requirement over a small range of internal energies (Figs. 2.16 and 2.17)

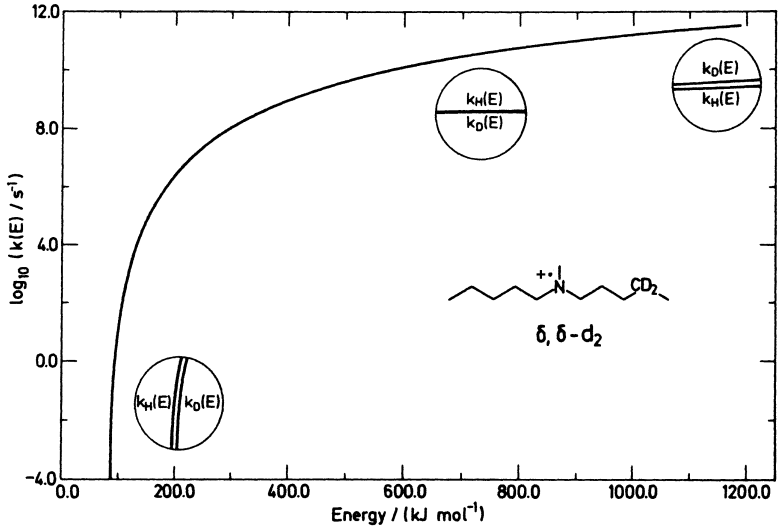


Fig. 2.17. Calculated $k_{H(E)}$ and $k_{D(E)}$ curves for the α-cleavage of deuterated amine molecular ions. The curves can be regarded as parallel over a small range of internal energies, but they are not in the strict sense. They may even cross to cause inverse isotope effects in the domain of highly excited ions. Reproduced from Ref. [78] with permission. © Wiley & Sons, 1991.

2.9.3 Secondary Kinetic Isotope Effects

Secondary kinetic isotope effects are observed if an isotopic label is located adjacent to or remote from the bond that is being broken or formed during the reaction. Again, these depend on the internal energy of the decomposing ions. Secondary kinetic isotope effects, i_{sec}, are generally much smaller than their primary analogs.

Example: The ratio $[M–CH_3]^+/[M–CD_3]^+$ from isopropylbenzene molecular ions decomposing by benzylic cleavage (Chap. 6.4) vary from 1.02 for ion source fragmentations (70 eV EI) over 1.28 for metastable ions in the 1st FFR to 1.56 in the 2nd FFR, thus clearly demonstrating the dependence of the secondary kinetic isotope effect on internal energy [79].

It is convenient to specify the value normalized *per heavier isotope present*, $i_{secnorm}$, because of the possible presence of a number of heavier isotopes, n_D [68,78]:

$$i_{sec\,norm} = \sqrt[n_D]{i_{sec}} \tag{2.30}$$

Example: Effects of a secondary kinetic isotope on the α-cleavage of tertiary amine molecular ions occurring after deuterium labeling both adjacent to and remote from the cleaved bond (Chap. 6.2.6). This reduces the fragmentation rate relative to the nonlabeled chain by factors of 1.08–1.30 per D in case of metastable ion decompositions (Fig. 2.18), but the isotope effect vanished for ion source processes [80]. The reversal of these kinetic isotope effects for short-lived ions (10^{-11}–10^{-10} s) could be demonstrated by field ionization kinetic measurements, i.e., then the deuterated species decomposed slightly faster than their nonlabeled isotopologs [68,78].

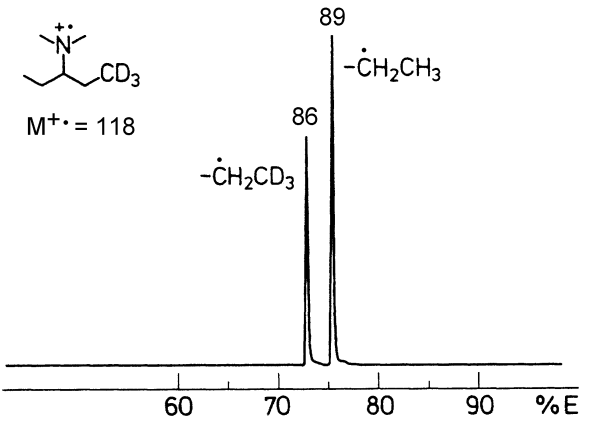


Fig. 2.18. Observation of secondary H/D isotope effects on the α-cleavage of tertiary amine molecular ions. For convenience, *m/z* labels have been added to the original energy scale of the MIKE spectrum. Adapted from Ref. [80] with permission. © American Chemical Society, 1988.

2.10 Determination of Ionization Energies

2.10.1 Conventional Determination of Ionization Energies

Ionization energies [81] can rather easily be determined – one simply needs to read out the lower limit of the electron energy at a vanishing molecular ion signal. Unfortunately, doing so yields only coarse approximations of the real ionization energy of a molecule. The accuracy of *IE* data obtained by this simple procedure will be about ± 1 eV. One of the associated problems is measuring the electron energy itself. The electrons are thermally emitted from a hot metal filament (1600–2000 °C), and therefore, their total kinetic energy is not only defined by the potential applied to accelerate them, but also by their thermal energy distribution [24]. In addition, electron ionization preferably creates vibrationally excited ions (Chap. 2.1), because ionization is a threshold process, i.e., it will take place not just when the energy needed to accomplish the process is reached, but also for all higher energies [82]. This causes a systematic error in that vertical IEs are obtained being higher than the adiabatic IEs one would like to measure. Further drawbacks are: *i*) Due to inhomogeneous electric fields within the ionization volume, the actual electron energy also depends on the location where ionization takes place. *ii*) The fact that the low electron acceleration voltages of 7–15 V have to be superimposed on the ion acceleration voltage of several kilovolts causes low precision of the voltage settings in commercial magnetic sector instruments. *iii*) There is additional thermal energy of the neutrals roughly defined by the temperature of the inlet system and the ion source.

2.10.2 Improved *IE* Accuracy from Data Post-Processing

The slightly diffuse energy of the electrons effects that the ionization efficiency curves do not approach zero in a straight line; they rather bend close to the ionization threshold and exponentially approximate zero. Even if the electron energy scale of the instrument is properly calibrated against IEs of established standards, the accuracy of the *IE* data obtained from direct readout is only ± 0.3 eV (Fig. 2.19a).

To overcome the unpredictability of the actual onset of ionization, , the *critical slope method* has been developed [24,84], among several other methods [83]. It makes use of the fact that, according to theory, realistic values of *IE* are expected at the position of the ionization efficiency curve where the slope of a semilog plot of the curve is

$$\frac{d}{dV}(\ln N_i) = \frac{n}{n+1}\,\frac{1}{kT} \tag{2.31}$$

with N_i being the total number of ions produced at an electron acceleration voltage V, and with an empirical value of $n = 2$ (Fig. 2.19b).

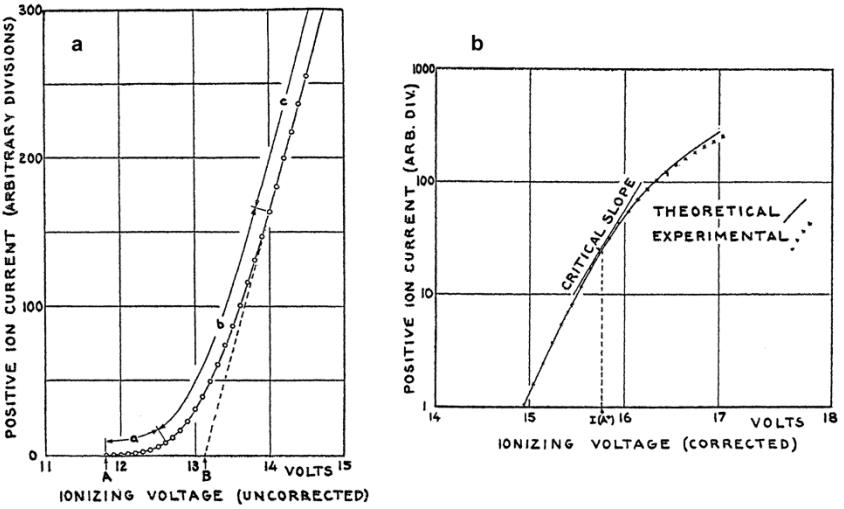


Fig. 2.19. Ionization efficiency curve of argon (**a**) plotted on a linear scale and (**b**) as semilog plot. Extrapolation of the linear portion of (**a**) gives erroneous IEs, whereas the *x*-position of the tangent of an empirical critical slope to the semilog plot yields accuracies of ± 0.05 eV. Reproduced from Ref. [24] by permission. © American Chemical Society, 1948.

2.10.3 *IE* Accuracy – Experimental Improvements

If reliable thermochemical data [23,85] is required, the above disturbing effects have to be substantially reduced. [81] One way is to use an *electron monochromator* (accuracy up to ± 0.1 eV) [86,87]. An electron monochromator is a device for selecting nearly monoenergetic electrons from an electron beam [88]. Alternatively, *photoionization* (PI) may be employed instead of EI. Photoionization yields even more accurate results (± 0.05 eV) than the electron monochromator [89]. In any case, the half width of the electron or photon energy distribution becomes small enough to detect detailed structural features of the ionization efficiency curves such as electronic transitions. Both techniques have been widely employed to obtain *IE* data (Table 1.1).

2.10.4 Photoionization Processes

The absorption of UV light by a neutral can result in electronically excited states that undergo relaxation either by emission of light or by emission of an electron. Thus, the photon in *photoionization* (PI) serves the same purpose as the energetic electron in EI.

$$M + h\nu \rightarrow M^* \rightarrow M^{+\bullet} + e^- \qquad (2.32)$$

Of course, the energy absorbed must lead into in a continuum state, i.e., at least provide the ionization energy of the neutral. Typical photon sources for PI are frequency-quadrupled Nd:Yag lasers delivering photons at 266 nm wavelength (4.6 eV) and ArF excimer lasers at 193 nm (6.3 eV). Both light sources clearly deliver photons well below the *IE* of most molecules. Fortunately, the absorption of energy has not to be a one-photon process. Instead, stepwise accumulation of energy from less energetic photons is also feasible. Thus, the normal procedure to achieve PI is *multiphoton ionization* (MUPI) [90].

The next stepping-stone to photoionization is finding the electronic levels of the neutral, because nonresonant ionization has rather low cross-sections that translate into poor ionization efficiencies along with high photon flux requirements. Resonant absorption of photons is more effective by several orders of magnitude [91]. Ideally, resonant absorption of the first photon leads to an intermediate state from where absorption of a second photon can forward the molecule into a continuum. This technique is known as 1 + 1 *resonance-enhanced multiphoton ionization* (REMPI). From a practical point of view, the second photon should be, but not necessarily has to be, of the same wavelength (Fig. 2.20) [92]. Proper selection of the laser wavelengths provides compound-selective analysis at extremely low detection limits [90,91,93,94].

Ultrashort laser pulses in the picosecond rather than the conventional nanosecond regime prevent the molecules from unwanted relaxation or fragmentation prior to molecular ion formation. The REMPI mass spectra of diphenylmercury, for example, only exhibit a molecular ion peak when sub-picosecond laser ionization is employed [95].

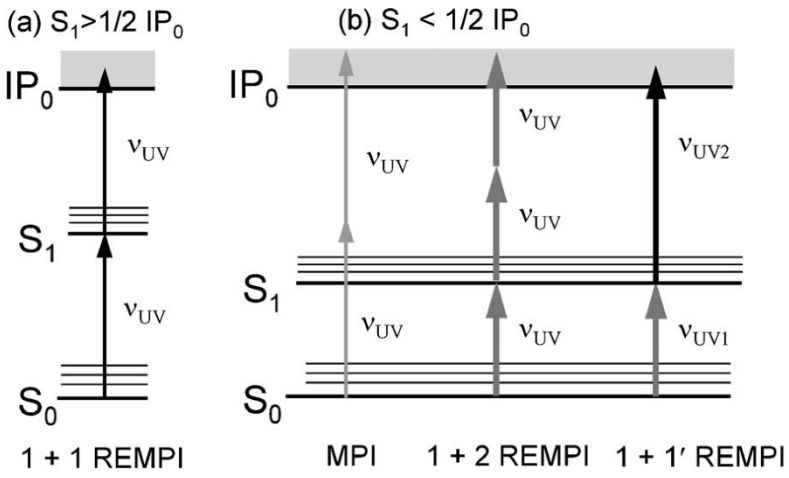


Fig. 2.20. Photoionization schemes. (**a**) Resonant 1 + 1 REMPI, (**b**) nonresonant MPI, resonant 1 + 2 REMPI, and resonant 1 + 1' REMPI with two different wavelengths. Reproduced from Ref. [92] with permission. © The Vacuum Society of Japan, 2007.

Example: The electronic and vibrational states of the oxygen molecular ion has been perfectly resolved by *photoelectron spectroscopy* (PES) (Fig. 2.21), thus allowing to directly read out the Franck-Condon factors and to identify the $(0 \leftarrow 0)$ transitions corresponding to adiabatic ionization [100].

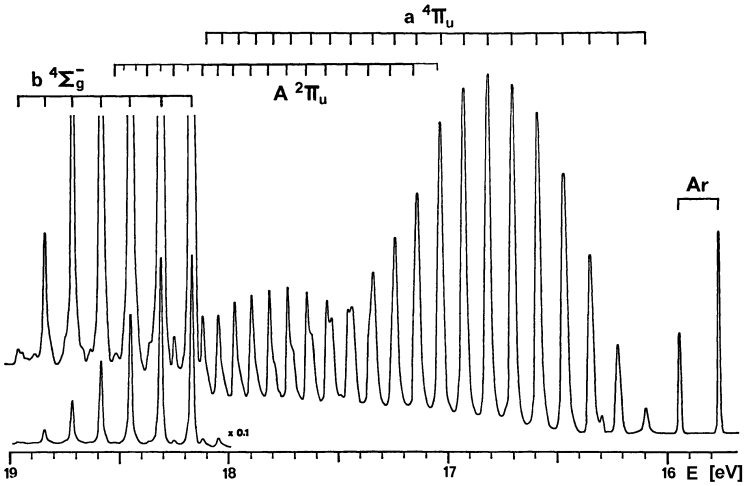


Fig. 2.21. High-resolution photoelectron spectrum of O_2, showing overlapping vibrational progressions from transitions to different electronic states of the ion (range of *IE* not shown). Reproduced from Ref. [100] with permission. © Royal Swedish Academy of Sciences, 1970.

The main disadvantage of PES and ZEKE experiments lies in the detection of electrons making the measurements sensitive to impurities, because the electrons could arise from these instead of the intended sample. This can be avoided by detecting the produced ions instead – the corresponding technique is known as *mass-analyzed threshold ionization* (MATI) [101]. In MATI experiments, the neutrals are excited in a field-free environment by means of a tunable light source (usually a multi-photon laser process) very close to the ionization threshold. Possible prompt ions are removed after about 0.1 μs by a weak positive electric field. Then, the near-threshold Rydberg species are ionized by applying a negative electric field pulse also effecting acceleration of those ions towards a time-of-flight mass analyzer [101-103]. Thus, we are finally back to a real mass spectral technique. In contrast to ZEKE, the mass selectivity of MATI allows not only for the study of molecules [101,103], but also consideration of dissociating complexes and clusters [82,104,105].

Example: The ionization spectra at the first ionization threshold of pyrazine as obtained by PI, MATI, and ZEKE-PES are clearly different (Fig. 2.22) [101]. The PI spectrum is a plot of ion current vs. wavelength of the probe laser. PI spectra show a simple rise of the curve at IE, while MATI and ZEKE yield a sharp peak at ionization threshold plus additional signals from lower vibrational ionization thresholds.

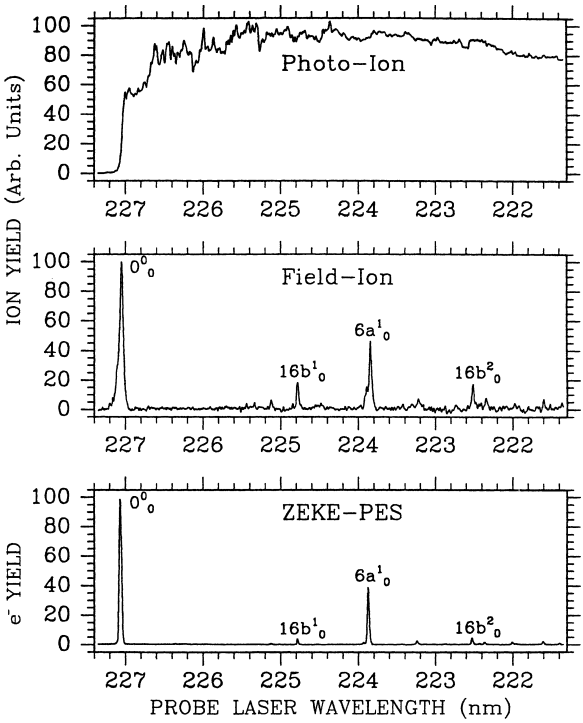


Fig. 2.22. Comparison of PI, MATI and ZEKE spectra of pyrazine. Reproduced from Ref. [101] with permission. © American Institute of Physics, 1991.

2.11 Determining the Appearance Energies

The techniques used for the determination of appearance energies are essentially identical to those described above for IEs. However, even when using the most accurately defined electron or photon energies, great care has to be taken when determining *AE*s because of the risk of overestimation due to kinetic shift. Provided that there is no reverse activation energy for the particular reaction, the *AE* value also delivers the sum of heats of formation of the dissociation products. If substantial KER is observed, the *AE* may still be used to determine the activation energy of the process.

2.11.1 Kinetic Shift

Fragment ion abundances observed by means of any mass spectrometer strongly depend on ion lifetimes within the ion source and on ion internal energy distributions, i.e., kinetic aspects play an important role for a mass spectrum's appearance.

As explained by QET the rate constant of an ion dissociation is a function of excess energy in the transition state of the respective reaction, and there is a need of substantial excess energy to make the rate constant exceed the critical 10^6 s^{-1} needed to dissociate during the residence times within the ion source. Therefore, appearance and activation energies are always in excess of the true values by the above amount. This phenomenon is known as *kinetic shift* (Fig. 2.23) [40,54]. Often, kinetic shifts are almost negligible (0.01–0.1 eV), but they can be as large as 2 eV, [40] e.g. an activation energy of 2.07 eV for $C_3H_6^{+\bullet} \rightarrow C_3H_5^+ + H^\bullet$ is accompanied by a kinetic shift of 0.19 eV [81]. As $k_{(E)}$ functions greatly differ between reactions and especially between homogeneous bond cleavages and rearrangement fragmentations, it is not an easy task to correct the experimental *AE*s by subtraction of E_{ex}. The influence of the kinetic shift can be minimized by increasing the ion source residence time and/or by increasing the detection sensitivity of the instrument.

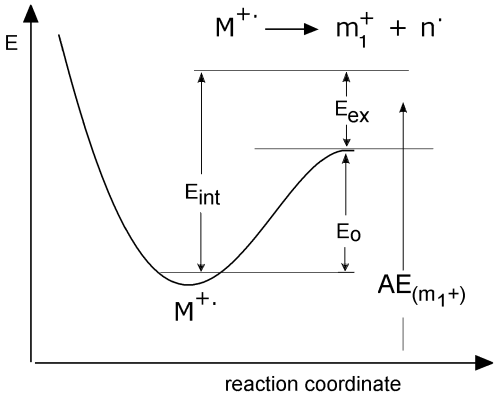


Fig. 2.23. Kinetic shift. The excess energy in the transition state affects *AE* measurements such that it always causes experimental values to be too high.

Note: The *kinetic shift* denotes the overestimation of *AE*s due to the contribution of excess energy in the transition state necessary to yield rate constants larger than 10^6 s^{-1}. The determination of IEs is not negatively affected by kinetic shift as kinetics is not involved in electron or photon ionization.

2.11.2 Breakdown Graphs

Employing the above techniques, one can examine the fragmentations of a molecular ion as a function of internal energy by constructing a so-called *breakdown graph*. This involves plotting the ion intensities of interest, i.e., those of a certain *m/z*, vs. electron energy or vs. ion internal energy if the *IE* has been subtracted before [106]. Typically, a molecular ion can access a considerable number of fragmentation pathways as soon as there are some 1–3 eV of internal energy available.

Breakdown graphs can be used to compare the energetic demands of those different fragmentation pathways. In addition, breakdown graphs help to correlate ion internal energy distributions derived from other methods such as photoelectron spectroscopy [107] with mass spectral data.

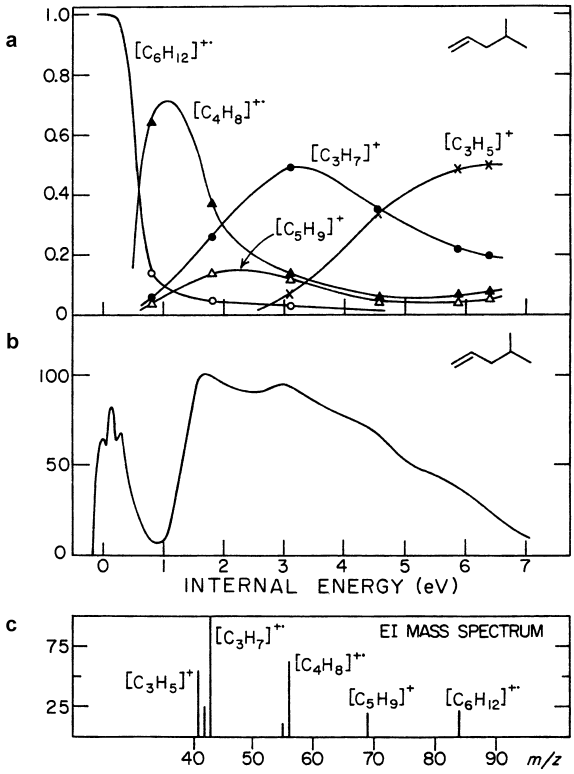


Fig. 2.24. 4-Methyl-1-pentene: (**a**) relationship of breakdown graph, (**b**) internal energy distribution from PES, and (**c**) mass spectrum. Reproduced from Ref. [108] by permission. © Wiley & Sons, 1982.

Example: For 4-methyl-1-pentene, the breakdown graph, the internal energy distribution from the PE spectrum, and the 70-eV EI mass spectrum are compared (Fig. 2.24) [108]. From the fragmentation threshold to about 2 eV of internal energy the breakdown graph is dominated by the $[C_4H_8]^{+\bullet}$ ion, *m/z* 56. In the range 2–4.5 eV the $[C_3H_7]^+$ ion, *m/z* 43, becomes most prominent. However, $[C_4H_8]^{+\bullet}$ only has 60% of the intensity of $[C_3H_7]^+$. It is obvious that the 0.5–1 eV energy region where the $[C_4H_8]^{+\bullet}$ fragment ion predominates corresponds to a region of the internal energy distribution that has a low ion population. This explains why $[C_3H_7]^+$ constitutes the base peak of the spectrum. Beyond 5 eV of internal energy, the $[C_3H_5]^+$ ion, *m/z* 41, becomes the most prominent fragment ion.

2.12 Gas Phase Basicity and Proton Affinity

Not all ionization methods rely on unimolecular conditions as strictly as EI does. Chemical ionization (CI, Chap. 7), for example, makes use of reactive collisions between ions generated from a reactant gas and the neutral analyte to achieve its ionization by some bimolecular process such as proton transfer. The question which reactant ion can protonate a given analyte can be answered from *gas phase basicity* (*GB*) or *proton affinity* (*PA*) data. Proton transfer, and thus the relative proton affinities of the reactants, also play an important role in many ion–neutral complex-mediated reactions (Chap. 6.12). In the last decade, *proton transfer reaction* (PTR) MS has emerged as a tool for analyzing *volatile organic compounds* (VOCs) in air. Therefore, PTR-MS is interesting for analytical work concerning environmental issues and in occupational health and safety (Chap. 7.3).

Here, we deal with proton affinity and gas phase basicity as thermodynamic quantities. Consider the following gas phase reaction of a (basic) molecule, B:

$$B_g + H_g^+ \rightarrow [BH]_g^+ \tag{2.34}$$

The tendency of B to accept a proton is then quantitatively described by

$$-\Delta G_r^0 = GB_{(B)} \quad \text{and} \quad -\Delta H_r^0 = PA_{(B)}\,, \tag{2.35}$$

i.e. the gas phase basicity $GB_{(B)}$ is defined as the negative free energy change for the proton transfer, $-\Delta G_r^0$, whereas the proton affinity $PA_{(B)}$ is the negative enthalpy change, $-\Delta H_r^0$, for the same reaction [109,110]. From the relation

$$\Delta G^0 = \Delta H^0 - T\,\Delta S^0 \tag{2.36}$$

we obtain the expression

$$PA_{(B)} = GB_{(B)} - T\,\Delta S^0 \tag{2.37}$$

with the entropy term $T\Delta S^0$ usually being relatively small (25–40 kJ mol^{-1}). Furthermore, in case of an equilibrium

$$[AH]^+ + B \rightleftharpoons A + [BH]^+ \tag{2.38}$$

with the equilibrium constant K_{eq} for which we have

$$K_{eq} = [BH^+]/[AH^+] \times [A]/[B] \tag{2.39}$$

the gas phase basicity is related to K_{eq} by [113,114]

$$GB_{(B)} = -\Delta G^0 = RT \ln K_{eq} \tag{2.40}$$

For the experimental determination of *GB*s and *PA*s refer to Chap. 9.18.3. Some representative *PA* and *GB* values are collected in Table 2.6.

Table 2.6. Selected proton affinities and gas phase basicities [23,109,113]

Molecule	$PA_{(B)}$ [kJ mol^{-1}]	$GB_{(B)}$ [kJ mol^{-1}]
H_2	424	396
CH_4	552	527
C_2H_6	601	558
H_2O	697	665
$H_2C{=}O$	718	685
$CH_3CH{=}CH_2$	751	718
C_6H_6 (benzene)	758	731
$(CH_3)_2C{=}CH_2$	820	784
$(CH_3)_2C{=}O$	823	790
$C_{14}H_{10}$ (phenanthrene)	831	802
C_4H_8O (tetrahydrofurane)	831	801
$C_2H_5OC_2H_5$	838	805
NH_3	854	818
CH_3NH_2	896	861
C_5H_5N (pyridine)	924	892
$(CH_3)_3N$	942	909

References

1. Porter, C.J.; Beynon, J.H.; Ast, T. The Modern Mass Spectrometer. A Complete Chemical Laboratory. *Org. Mass Spectrom.* **1981,** *16*, 101-114.
2. Schwarz, H. The Chemistry of Naked Molecules or the Mass Spectrometer As a Laboratory. *Chem. Unserer Zeit* **1991,** *25*, 268-278.
3. Kazakevich, Y. Citation Used by Permission. *http://hplc.chem.shu.edu/* **1996,** Seton Hall Univ., South Orange, NJ.
4. Cooks, R.G.; Beynon, J.H.; Caprioli, R.M. *Metastable Ions*; Elsevier: Amsterdam, 1973.
5. Levsen, K. *Fundamental Aspects of Organic Mass Spectrometry;* VCH: Weinheim, 1978.
6. Franklin, J.L. Energy Distributions in the Unimolecular Decomposition of Ions, in *Gas Phase Ion Chemistry*; Bowers, M.T. (ed.); Academic Press: New York, 1979; Vol. 1, Chap. 7, pp. 272-303.
7. Beynon, J.H.; Gilbert, J.R. Energetics and Mechanisms of Unimolecular Reactions of Positive Ions: Mass Spectrometric Methods, in *Gas Phase Ion Chemistry*; Bowers, M.T. (ed.); Academic Press: New York, 1979; Vol. 2, Chap. 13, pp. 153-179.
8. Vogel, P. The Study of Carbocations in the Gas Phase, in *Carbocation Chemistry*; Elsevier: Amsterdam, 1985; Chap. 2, pp. 61-84.
9. Holmes, J.L. Assigning Structures to Ions in the Gas Phase. *Org. Mass Spectrom.* **1985,** *20*, 169-183.
10. Lorquet, J.C. Basic Questions in MS. *Org. Mass Spectrom.* **1981,** *16*, 469-481.
11. Lorquet, J.C. Landmarks in the Theory of Mass Spectra. *Int. J. Mass Spectrom.* **2000,** *200*, 43-56.
12. Märk, T.D. Fundamental Aspects of Electron Impact Ionization. *Int. J. Mass Spectrom. Ion Phys.* **1982,** *45*, 125-145.
13. Märk, T.D. Electron Impact Ionization, in *Gaseous ion Chemistry and Mass Spectrometry*, Futrell, J.H. (ed.); Wiley: New York, 1986; pp. 61-93.
14. Wolkenstein, K.; Gross, J.H.; Oeser, T.; Schöler, H.F. Spectroscopic Characterization and Crystal Structure of the 1,2,3,4,5,6-Hexahydrophen-anthro-[1,10,9,8-*opqra*]Perylene. *Tetrahedron Lett.* **2002,** *43*, 1653-1655.

15. Schröder, E. *Massenspektrometrie – Begriffe und Definitionen*; Springer-Verlag: Heidelberg, 1991.
16. Harrison, A.G. Fundamentals of Gas Phase Ion Chemistry, in *Chemical Ionization Mass Spectrometry*, 2nd ed.; CRC Press: Boca Raton, 1992; Chap. 2, pp. 26.
17. De Wall, R.; Neuert, H. The Formation of Negative Ions From Electron Impact With Tungsten Hexafluoride. *Z. Naturforsch.,A.* **1977,** *32A*, 968-971.
18. Jones, E.G.; Harrison, A.G. Study of Penning Ionization Reactions Using a Single-Source Mass Spectrometer. *Int. J. Mass Spectrom. Ion Phys.* **1970,** *5*, 137-156.
19. Penning, F.M. Ionization by Metastable Atoms. *Naturwissenschaften* **1927,** *15*, 818.
20. Hornbeck, J.A.; Molnar, J.P. Mass-Spectrometric Studies of Molecular Ions in the Noble Gases. *Phys. Rev.* **1951,** *84*, 621-625.
21. Faubert, D.; Paul, G.J.C.; Giroux, J.; Betrand, M.J. Selective Fragmentation and Ionization of Organic Compounds Using an Energy-Tunable Rare-Gas Metastable Beam Source. *Int. J. Mass Spectrom. Ion Proc.* **1993,** *124*, 69-77.
22. Svec, H.J.; Junk, G.A. Electron-Impact Studies of Substituted Alkanes. *J. Am. Chem. Soc.* **1967,** *89*, 790-796.
23. NIST Chemistry Webbook. *http://webbook. nist.gov/* **2002**.
24. Honig, R.E. Ionization Potentials of Some Hydrocarbon Series. *J. Chem. Phys.* **1948,** *16*, 105-112.
25. Baldwin, M.; Kirkien-Konasiewicz, A.; Loudon, A.G.; Maccoll, A.; Smith, D. Localized or Delocalized Charges in Molecule-Ions? *Chem. Commun.* **1966,** 574.
26. McLafferty, F.W. Generalized Mechanism for Mass Spectral Reactions. *Chem. Commun.* **1966,** 78-80.
27. Wellington, C.A.; Khowaiter, S.H. Charge Distributions in Molecules and Ions: MINDO 3 Calculations. An Alternative of the Charge Localization Concept in Mass Spectrometry. *Tetrahedron* **1978,** *34*, 2183-2190.
28. Baldwin, M.A.; Welham, K.J. Charge Localization by Molecular Orbital Calculations. I. Urea and Thiourea. *Rapid. Commun. Mass Spectrom.* **1987,** *1*, 13-15.
29. Baldwin, M.A.; Welham, K.J. Charge Localization by Molecular Orbital Calculations. II. Formamide, Thioformamide and *N*-Methylated Analogs. *Org. Mass Spectrom.* **1988,** *23*, 425-428.
30. Weinkauf, R.; Lehrer, F.; Schlag, E.W.; Metsala, A. Investigation of Charge Localization and Charge Delocalization in Model Molecules by Multiphoton Ionization Photoelectron Spectroscopy and DFT Calculations. *Faraday Discussions* **2000,** *115*, 363-381.
31. Cone, C.; Dewar, M.J.S.; Landman, D. Gaseous Ions. 1. MINDO/3 Study of the Rearrangement of Benzyl Cation to Tropylium. *J. Am. Chem. Soc.* **1977,** *99*, 372-376.
32. Born, M.; Oppenheimer, J.R. Zur Quantentheorie Der Molekeln. *Annalen der Physik* **1927,** *84*, 457-484.
33. Seiler, R. Born-Oppenheimer Approximation. *International Journal of Quantum Chemistry* **1969,** *3*, 25-32.
34. Lipson, R.H. Ultraviolet and Visible Absorption Spectroscopy, in *Encyclopedia of Applied Spectroscopy*, Andrews, D.L. (ed.); Wiley-VCH: Berlin, 2009; Chap. 11, pp. 353-380.
35. Franck, J. Elementary Processes of Photochemical Reactions. *Trans. Faraday Soc.* **1925,** *21*, 536-542.
36. Condon, E.U. Theory of Intensity Distribution in Band Systems. *Phys. Rev.* **1926,** *28*, 1182-1201.
37. Dunn, G.H. Franck-Condon Factors for the Ionization of H_2 and D_2. *J. Chem. Phys.* **1966,** *44*, 2592-2594.
38. Märk, T.D. Fundamental Aspects of Electron Impact Ionization. *Int. J. Mass Spectrom. Ion Phys.* **1982,** *45*, 125-145.
39. Märk, T.D. Electron Impact Ionization, in *Gaseous ion Chemistry and MS*, Futrell, J.H. (ed.); Wiley: New York, 1986; pp. 61-93.
40. McLafferty, F.W.; Wachs, T.; Lifshitz, C.; Innorta, G.; Irving, P. Substituent Effects in Unimolecular Ion Decompositions. XV. Mechanistic Interpretations and the Quasi-Equilibrium Theory. *J. Am. Chem. Soc.* **1970,** *92*, 6867-6880.
41. Egger, K.W.; Cocks, A.T. Homopolar- and Heteropolar Bond Dissociation Energies and Heats of Formation of Radicals and Ions in the Gas Phase. I. Data on Organic Molecules. *Helv. Chim. Acta* **1973,** *56*, 1516-1536.

42. Lossing, F.P.; Semeluk, G.P. Free Radicals by Mass Spectrometry. XLII. Ionization Potentials and Ionic Heats of Formation for C_1-C_4 Alkyl Radicals. *Can. J. Chem.* **1970,** *48*, 955-965.
43. Lossing, F.P.; Holmes, J.L. Stabilization Energy and Ion Size in Carbocations in the Gas Phase. *J. Am. Chem. Soc.* **1984,** *106*, 6917-6920.
44. Cox, J.D.; Pilcher, G. *Thermochemistry of Organic and Organometallic Compounds*; Academic Press: London, 1970.
45. Chatham, H.; Hils, D.; Robertson, R.; Gallagher, A. Total and Partial Electron Collisional Ionization Cross Sections for Methane, Ethane, Silane, and Disilane. *J. Chem. Phys.* **1984,** *81*, 1770-1777.
46. Wahrhaftig, A.L. Ion Dissociations in the Mass Spectrometer, in *Advances in Mass Spectrometry*, Waldron, J.D (ed.); Pergamon: Oxford, 1959; pp. 274-286.
47. Wahrhaftig, A.L. Unimolecular Dissociations of Gaseous Ions, in *Gaseous ion Chemistry and MS*, Futrell, J.H. (ed.); Wiley: New York, 1986; pp. 7-24.
48. Rosenstock, H.M.; Krauss, M. Quasi-Equilibrium Theory of Mass Spectra, in *Mass Spectrometry of Organic Ions*; McLafferty, F.W. (ed.); Academic Press: London, 1963; pp. 1-64.
49. Bohme, D.K.; Mackay, G.I. Bridging the Gap Between the Gas Phase and Solution: Transition in the Kinetics of Nucleophilic Displacement Reactions. *J. Am. Chem. Soc.* **1981,** *103*, 978-979.
50. Speranza, M. Gas Phase Ion Chemistry Versus Solution Chemistry. *Int. J. Mass Spectrom. Ion Proc.* **1992,** *118/119*, 395-447.
51. Rosenstock, H.M.; Wallenstein, M.B.; Wahrhaftig, A.L.; Eyring, H. Absolute Rate Theory for Isolated Systems and the Mass Spectra of Polyatomic Molecules. *Proc. Natl. Acad. Sci. U.S.A.* **1952,** *38*, 667-678.
52. McAdoo, D.J.; Bente, P.F.I.; Gross, M.L.; McLafferty, F.W. Metastable Ion Characteristics. XXIII. Internal Energy of Product Ions Formed in Massspectral Reactions. *Org. Mass Spectrom.* **1974,** *9*, 525-535.
53. Meier, K.; Seibl, J. Measurement of Ion Residence Times in a Commercial Electron Impact Ion Source. *Int. J. Mass Spectrom. Ion Phys.* **1974,** *14*, 99-106.
54. Chupka, W.A. Effect of Unimolecular Decay Kinetics on the Interpretation of Appearance Potentials. *J. Chem. Phys.* **1959,** *30*, 191-211.
55. Holmes, J.L.; Terlouw, J.K. The Scope of Metastable Peak Shape Observations. *Org. Mass Spectrom.* **1980,** *15*, 383-396.
56. Williams, D.H. A Transition State Probe. *Acc. Chem. Res.* **1977,** *10*, 280-286.
57. Williams, D.H.; Hvistendahl, G. Kinetic Energy Release in Relation to Symmetry-Forbidden Reactions. *J. Am. Chem. Soc.* **1974,** *96*, 6753-6755.
58. Williams, D.H.; Hvistendahl, G. Kinetic Energy Release As a Mechanistic Probe. The Role of Orbital Symmetry. *J. Am. Chem. Soc.* **1974,** *96*, 6755-6757.
59. Hvistendahl, G.; Williams, D.H. Partitioning of Reverse Activation Energy Between Kinetic and Internal Energy in Reactions of Simple Organic Ions. *J. Chem. Soc.,Perkin Trans. 2* **1975,** 881-885.
60. Hvistendahl, G.; Uggerud, E. Secondary Isotope Effect on Kinetic Energy Release and Reaction Symmetry. *Org. Mass Spectrom.* **1985,** *20*, 541-542.
61. Kim, K.C.; Beynon, J.H.; Cooks, R.G. Energy Partitioning by Mass Spectrometry. Chloroalkanes and Chloroalkenes. *J. Chem. Phys.* **1974,** *61*, 1305-1314.
62. Haney, M.A.; Franklin, J.L. Correlation of Excess Energies of Electron Impact Dissociations With the Translational Energies of the Products. *J. Chem. Phys.* **1968,** *48*, 4093-4097.
63. Cooks, R.G.; Williams, D.H. The Relative Rates of Fragmentation of Benzoyl Ions Generated Upon Electron Impact From Different Precursors. *Chem. Commun.* **1968,** 627-629.
64. Lin, Y.N.; Rabinovitch, B.S. Degrees of Freedom Effect and Internal Energy Partitioning Upon Ion Decomposition. *J. Phys. Chem.* **1970,** *74*, 1769-1775.
65. Bente III., P.F.; McLafferty, F.W.; McAdoo, D.J.; Lifshitz, C. Internal Energy of Product Ions Formed in Mass Spectral Reactions. The Degrees of Freedom Effect. *J. Phys. Chem.* **1975,** *79*, 713-721.
66. Todd, J.F.J. Recommendations for Nomenclature and Symbolism for Mass Spectroscopy Including an Appendix of Terms Used in Vacuum Technology. *Int. J. Mass Spectrom. Ion. Proc.* **1995,** *142*, 211-240.
67. Robinson, P.J.; Holbrook, K.A. Unimolecular Reactions, in *Unimolecular*

Re-actions, Wiley: London, 1972; Chap. 9.

68. Ingemann, S.; Hammerum, S.; Derrick, P.J.; Fokkens, R.H.; Nibbering, N.M.M. Energy-Dependent Reversal of Secondary Isotope Effects on Simple Cleavage Reactions: Tertiary Amine Radical Cations With Deuterium at Remote Positions. *Org. Mass Spectrom.* **1989,** *24*, 885-889.
69. Lowry, T.H.; Schueller Richardson, K. Isotope Effects, in *Mechanism and Theory in Organic Chemistry*; Harper and Row: New York, 1976; Chap. 1.7.
70. Stringer, M.B.; Underwood, D.J.; Bowie, J.H.; Allison, C.E.; Donchi, K.F.; Derrick, P.J. Is the McLafferty Rearrangement of Ketones Concerted or Stepwise? The Application of Kinetic Isotope Effects. *Org. Mass Spectrom.* **1992,** *27*, 270-276.
71. Derrick, P.J. Isotope Effects in Fragmentation. *Mass Spectrom. Rev.* **1983,** *2*, 285-298.
72. Hvistendahl, G.; Uggerud, E. Deuterium Isotope Effects and Mechanism of the Gas-Phase Reaction $[C_3H_7]^+ \rightarrow [C_3H_5]^+ + H_2$. *Org. Mass Spectrom.* **1986,** *21*, 347-350.
73. Howe, I.; McLafferty, F.W. Unimolecular Decomposition of Toluene and Cycloheptatriene Molecular Ions. Variation of the Degree of Scrambling and Isotope Effect With Internal Energy. *J. Am. Chem. Soc.* **1971,** *93*, 99-105.
74. Bertrand, M.; Beynon, J.H.; Cooks, R.G. Isotope Effects Upon Hydrogen Atom Loss From Molecular Ions. *Org. Mass Spectrom.* **1973,** *7*, 193-201.
75. Lau, A.Y.K.; Solka, B.H.; Harrison, A.G. Isotope Effects and H/D Scrambling in the Fragmentation of Labeled Propenes. *Org. Mass Spectrom.* **1974,** *9*, 555-557.
76. Benoit, F.M.; Harrison, A.G. Hydrogen Migrations in Mass Spectrometry. I. The Loss of Olefin From Phenyl-*n*-Propyl Ether Following Electron Impact Ionization and Chemical Ionization. *Org. Mass Spectrom.* **1976,** *11*, 599-608.
77. Veith, H.J.; Gross, J.H. Alkene Loss From Metastable Methyleneimmonium Ions: Unusual Inverse Secondary Isotope Effect in Ion–Neutral Complex Intermediate Fragmentations. *Org. Mass Spectrom.* **1991,** *26*, 1097-1105.
78. Ingemann, S.; Kluft, E.; Nibbering, N.M.M.; Allison, C.E.; Derrick, P.J.; Hammerum, S. Time-Dependence of the Isotope Effects in the Unimolecular Dissociation of Tertiary Amine Molecular Ions. *Org. Mass Spectrom.* **1991,** *26*, 875-881.
79. Nacson, S.; Harrison, A.G. Dependence of Secondary Hydrogen/Deuterium Isotope Effects on Internal Energy. *Org. Mass Spectrom.* **1985,** *20*, 429-430.
80. Ingemann, S.; Hammerum, S.; Derrick, P.J. Secondary Hydrogen Isotope Effects on Simple Cleavage Reactions in the Gas Phase: The α-Cleavage of Tertiary Amine Cation Radicals. *J. Am. Chem. Soc.* **1988,** *110*, 3869-3873.
81. Rosenstock, H.M. The Measurement of Ionization and Appearance Potentials. *Int. J. Mass Spectrom. Ion Phys.* **1976,** *20*, 139-190.
82. Urban, B.; Bondybey, V.E. Multiphoton Photoelectron Spectroscopy: Watching Molecules Dissociate. *Phys. Chem. Chem. Phys.* **2001,** *3*, 1942-1944.
83. Nicholson, A.J.C. Measurement of Ionization Potentials by Electron Impact. *J. Chem. Phys.* **1958,** *29*, 1312-1318.
84. Barfield, A.F.; Wahrhaftig, A.L. Determination of Appearance Potentials by the Critical Slope Method. *J. Chem. Phys.* **1964,** *41*, 2947-2948.
85. Levin, R.D.; Lias, S.G. Ionization Potential and Appearance Potential Measurements, 1971-1981. *National Standard Reference Data Series* **1982,** *71*, 634 pp.
86. Harris, F.M.; Beynon, J.H. Photodissociation in Beams: Organic Ions, in *Gas Phase Ion Chemistry – Ions and Light*; Bowers, M.T. (ed.); Academic Press: New York, 1985; Vol. 3, Chap. 19, pp. 99-128.
87. Dunbar, R.C. Ion Photodissociation, in *Gas Phase Ion Chemistry*; Bowers, M.T. (ed.); Academic Press: New York, 1979; Vol. 2, Chap. 14, pp. 181-220.
88. Maeda, K.; Semeluk, G.P.; Lossing, F.P. A Two-Stage Double-Hemispherical Electron Energy Selector. *Int. J. Mass Spectrom. Ion Phys.* **1968,** *1*, 395-407.
89. Traeger, J.C.; McLoughlin, R.G. A Photoionization Study of the Energetics of the $C_7H_7^+$ Ion Formed from C_7H_8 Precursors. *Int. J. Mass Spectrom. Ion Phys.* **1978,** *27*, 319-333.
90. Boesl, U. Laser MS for Environmental and Industrial Chemical Trace Analysis. *J. Mass Spectrom.* **2000,** *35*, 289-304.

91. Wendt, K.D.A. The New Generation of Resonant Laser Ionization Mass Spectrometers: Becoming Competitive for Selective Atomic Ultra-Trace Determination? *Eur. J. Mass Spectrom.* **2002,** *8*, 273-285.
92. Matsumoto, J.; Misawa, K.; Ishiuchi, S.I.; Suzuki, T.; Hayashi, S.I.; Fujii, M. On-Site and Real-Time Mass Spectrometer Utilizing the Resonance-Enhanced Multiphoton Ionization Technique. *Shinku* **2007,** *50*, 241-245.
93. Thanner, R.; Oser, H.; Grotheer, H.-H. Time-Resolved Monitoring of Aromatic Compounds in an Experimental Incinerator Using an Improved Jet-Resonance-Enhanced Multi-Photon Ionization System Jet-REMPI. *Eur. Mass Spectrom.* **1998,** *4*, 215-222.
94. Zenobi, R.; Zhan, Q.; Voumard, P. Multiphoton Ionization Spectroscopy in Surface Analysis and Laser Desorption MS. *Mikrochimica Acta* **1996,** *124*, 273-281.
95. Weickhardt, C.; Grun, C.; Grotemeyer, J. Fundamentals and Features of Analytical Laser MS With Ultrashort Laser Pulses. *Eur. Mass Spectrom.* **1998,** *4*, 239-244.
96. Turner, D.W.; Al Jobory, M.I. Determination of Ionization Potentials by Photoelectron Energy Measurement. *J. Chem. Phys.* **1962,** *37*, 3007-3008.
97. Müller-Dethlefs, K.; Sander, M.; Schlag, E.W. Two-Color Photoionization Resonance Spectroscopy of Nitric Oxide: Complete Separation of Rotational Levels of Nitrosyl Ion at the Ionization Threshold. *Chem. Phys. Lett.* **1984,** *112*, 291-294.
98. Müller-Dethlefs, K.; Sander, M.; Schlag, E.W. A Novel Method Capable of Resolving Rotational Ionic States by the Detection of Threshold Photoelectrons With a Resolution of 1.2 Cm^{-1}. *Z. Naturforsch.* **1984,** *39a*, 1089-1091.
99. Schlag, E.W. *ZEKE Spectroscopy*; Cambridge Univ. Press: Cambridge, 1998.
100. Edqvist, O.; Lindholm, E.; Selin, L.E.; Åsbrink, L. Photoelectron Spectrum of Molecular Oxygen. *Phys. Scr.* **1970,** *1*, 25-30.
101. Zhu, L.; Johnson, P. Mass Analyzed Threshold Ionization Spectroscopy. *J. Chem. Phys.* **1991,** *94*, 5769-5771.
102. Weickhardt, C.; Moritz, F.; Grotemeyer, J. Time-of-Flight MS: State-of-the-Art in Chemical Analysis and Molecular Science. *Mass Spectrom. Rev.* **1997,** *15*, 139-162.
103. Gunzer, F.; Grotemeyer, J. New Features in the Mass Analyzed Threshold Ionization (MATI) Spectra of Alkyl Benzenes. *Phys. Chem. Chem. Phys.* **2002,** *4*, 5966-5972.
104. Peng, X.; Kong, W. Zero Energy Kinetic Electron and Mass-Analyzed Threshold Ionization Spectroscopy of $Na\times(NH_3)_n$ (n=1,2,and 4) Complexes. *J. Chem. Phys.* **2002,** *117*, 9306-9315.
105. Haines, S.R.; Dessent, C.E.H.; Müller-Dethlefs, K. Mass Analyzed Threshold Ionization of Phenol×CO: Intermolecular Binding Energies of a Hydrogen-Bonded Complex. *J. Chem. Phys.* **1999,** *111*, 1947-1954.
106. Lavanchy, A.; Houriet, R.; Gäumann, T. The Mass Spectrometric Fragmentation of *N*-Heptane. *Org. Mass Spectrom.* **1978,** *13*, 410-416.
107. Meisels, G.G.; Chen, C.T.; Giessner, B.G.; Emmel, R.H. Energy-Deposition Functions in Mass Spectrometry. *J. Chem. Phys.* **1972,** *56*, 793-800.
108. Herman, J.A.; Li, Y.-H.; Harrison, A.G. Energy Dependence of the Fragmentation of Some Isomeric $C_6H_{12}^{+\cdot}$ Ions. *Org. Mass Spectrom.* **1982,** *17*, 143-150.
109. Lias, S.G.; Liebman, J.F.; Levin, R.D. Evaluated Gas Phase Basicities and Proton Affinities of Molecules; Heats of Formation of Protonated Molecules. *J. Phys. Chem. Ref. Data* **1984,** *13*, 695-808.
110. Harrison, A.G. The Gas-Phase Basicities and Proton Affinities of Amino Acids and Peptides. *Mass Spectrom. Rev.* **1997,** *16*, 201-217.
111. Kukol, A.; Strehle, F.; Thielking, G.; Grützmacher, H.-F. Methyl Group Effect on the Proton Affinity of Methylated Acetophenones Studied by Two MS Techniques. *Org. Mass Spectrom.* **1993,** *28*, 1107-1110.
112. McMahon, T.B. Thermochemical Ladders: Scaling the Ramparts of Gaseous Ion Energetics. *Int. J. Mass Spectrom.* **2000,** *200*, 187-199.
113. Lias, S.G.; Bartmess, J.E.; Liebman, J.F.; Holmes, J.L.; Levin, R.D.; Mallard, W.G. Gas-Phase Ion and Neutral Thermochemistry. *J. Phys. Chem. Ref. Data* **1988,** *17, Supplement 1*, 861 pp.

3 Isotopic Composition and Accurate Mass

Learning Objectives

- Isotopes and their effects on mass spectra
- Translation of isotopic abundances into mass spectral patterns
- Analytical information from isotopic patterns
- Nominal and accurate mass of molecules and ions
- Mass resolution and its effects on isotopic patterns and mass accuracy
- Accurate mass as a tool for determining molecular formulas
- Ultra-high resolution – aspects and applications.

In the context of general chemistry we rarely pay attention to the different isotopes of the individual elements involved in a reaction. For instance, the molecular mass of tribromomethane, $CHBr_3$, is usually calculated as 252.73 g mol^{-1} on the basis of relative atomic mass from the Periodic Table. In mass spectrometry, however, we need to more accurately consider individual isotopes, because mass spectrometry is based upon the separation of ions by mass-to-charge ratio, *m/z*. [1-3]. Thus, there actually is no signal at *m/z* 252.73 in the mass spectrum of tribromomethane. Instead, major peaks occur at *m/z* 250, 252, 254, and 256 accompanied by some minor other ones.

In order to successfully interpret a mass spectrum, one needs to understand isotopic masses and their relation to the atomic weights, isotopic abundances, and the resulting isotopic patterns, and finally, high-resolution and accurate mass measurements. These issues are closely related to each other, offer a wealth of analytical information, and are valid for any type of mass spectrometer and any ionization method employed.

3.1 Isotopic Classification of the Elements

An element is specified by the number of protons in its nucleus. This equals the *atomic number Z* of the respective element and determines its place within the periodic table of the elements. The atomic number is given as a subscript preceding the elemental symbol, e.g., $_6C$ in case of carbon. Atoms with nuclei of the same atomic number differing in the number of neutrons are termed *isotopes*. One isotope differs from another isotope of the same element in that it possesses a differ-

J. Gross, *Mass Spectrometry*, 2nd ed., DOI 10.1007/978-3-642-10711-5_3,
© Springer-Verlag Berlin Heidelberg 2011

ent *number of neutrons N*, i.e., by the *mass number A* or *nucleon number*. The mass number of an isotope is given as a superscript preceding the elemental symbol, e.g., ^{12}C. The mass number A is the sum of the total number of protons and neutrons in an atom, molecule, or ion [4].

$$A = Z + N \tag{3.1}$$

Note: The *mass number* must not be confused with the *atomic number* of an element. For the heavier atoms there can be isotopes of the same mass number belonging to different elements, e.g., the most abundant isotopes of both $_{18}Ar$ and $_{20}Ca$ have mass number 40.

3.1.1 Monoisotopic Elements

Among 83 naturally occurring stable elements, 20 elements do exist in the form of only one single naturally occurring stable isotope. Therefore, they are termed *monoisotopic elements*, i.e., all of their atoms have equal A. Among the monoisotopic elements, fluorine (^{19}F), sodium (^{23}Na), phosphorus (^{31}P), and iodine (^{127}I) belong to the more prominent examples in organic mass spectrometry. Nonetheless, there are many more such as beryllium (^{9}Be), aluminum (^{27}Al), manganese (^{55}Mn), cobalt (^{59}Co), arsenic (^{75}As), niobium (^{93}Nb), rhodium (^{103}Rh), cesium (^{133}Cs), and gold (^{197}Au). The monoisotopic elements are also referred to as A or X elements. [5,6] If radioactive isotopes were also taken into account, not a single monoisotopic element would remain.

3.1.2 Di-isotopic Elements

Several elements exist naturally in two isotopes and within the context of mass spectrometry it is useful to deal with them as a class of their own. Nevertheless, the term *di-isotopic element* is not an official one. These elements can even be sub-classified into those having one isotope that is 1 u heavier than the most abundant isotope and those having one isotope that is 2 u heavier than the most abundant isotope. The first group has been termed A+1 or X+1 elements, the latter ones have been termed A+2 or X+2 elements, respectively [5,6]. If we do not restrict our view to the elements typically encountered in organic mass spectrometry, one should add the class of X–1 elements with one minor isotope of 1 u lower mass than the most abundant one.

Prominent examples of X+1 elements are hydrogen (^{1}H, $^{2}H \equiv D$), carbon (^{12}C, ^{13}C), and nitrogen (^{14}N, ^{15}N). Deuterium (D) is of low abundance (0.0115%) and therefore, hydrogen is usually treated as a monoisotopic or as an X element, which is a valid approximation, even if a hundred hydrogens are contained in a molecule.

Among the X+2 elements, chlorine (^{35}Cl, ^{37}Cl) and bromine (^{79}Br, ^{81}Br) are relatively common, but copper (^{63}Cu, ^{65}Cu), gallium (^{69}Ga, ^{71}Ga), silver (^{107}Ag, ^{109}Ag), indium (^{113}In, ^{115}In), and antimony (^{121}Sb, ^{123}Sb) also belong to this group.

Even though occurring in more than two isotopes, some other elements such as oxygen, sulfur, and silicon, can be dealt with as X+2 elements for practical reasons. As long as only a few oxygens are part of a formula, oxygen might even be treated as an X element because of the low abundances of ^{17}O and ^{18}O.

Finally, the elements lithium (^{6}Li, ^{7}Li), boron (^{10}B, ^{11}B), and vanadium (^{50}V, ^{51}V) come along with a lighter isotope of lower abundance than the heavier one and thus, they can be grouped together as X–1 elements.

3.1.3 Polyisotopic Elements

The majority of elements are grouped as *polyisotopic elements* because they consist of three or more isotopes showing a wide variety of isotopic distributions.

3.1.4 Representation of Isotopic Abundances

Isotopic abundances are listed either as their sum being 100% or with the abundance of the most abundant isotope normalized to 100%. The latter is used throughout this book because this is consistent with the custom of reporting mass spectra normalized to the base peak (Chap. 1). The isotopic classifications and *isotopic compositions* of some common elements are listed below (Table 3.1).

Bar graph representations are much better suited for visualization of isotopic compositions than tables, and in fact they exactly show how such a distribution would appear in a mass spectrum (Fig. 3.1). This appearance coined the term *isotopic pattern*.

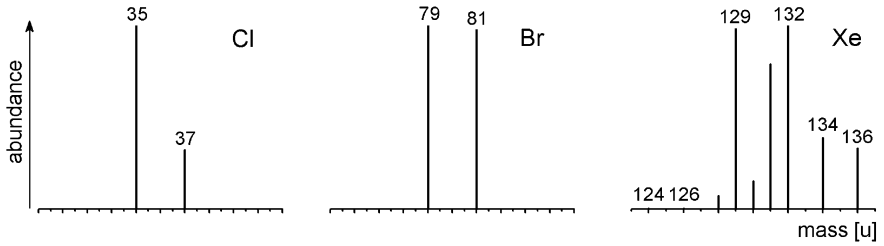


Fig. 3.1. Isotopic patterns of chlorine, bromine, and xenon. The bar graph representations of the isotopic distributions have the same optical appearance as mass spectra.

Note: Some authors use the term *isotopic cluster*, which is incorrect, as *cluster* refers to an associate of more atoms, molecules, or ions of the same species, sometimes associated with one other species, e.g., $[Ar_n]^{+\bullet}$, $[(H_2O)_nH]^+$, and $[I(CsI)_n]^-$ are cluster ions.

Table 3.1. Isotopic classifications and isotopic compositions of some common elements. A complete table is provided in the Appendix. © IUPAC 2001 [7,8]

Classification	Atomic symbol	Atomic number Z	Mass number A	Isotopic composition	Isotopic mass [u]	Relative atomic mass [u]
(X)[a]	H	1	1	100	1.007825	1.00795
			2	0.0115	2.014101	
X	F	9	19	100	18.998403	18.998403
X	Na	11	23	100	22.989769	22.989769
X	P	15	31	100	30.973762	30.973762
X	I	53	127	100	126.904468	126.904468
X+1	C	6	12	100	12.000000[b]	12.0108
			13	1.08	13.003355	
X+1	N	7	14	100	14.003074	14.00675
			15	0.369	15.000109	
(X+2)[a]	O	8	16	100	15.994915	15.9994
			17	0.038	16.999132	
			18	0.205	17.999116	
(X+2)[a]	Si	14	28	100	27.976927	28.0855
			29	5.0778	28.976495	
			30	3.3473	29.973770	
(X+2)[a]	S	16	32	100	31.972071	32.067
			33	0.80	32.971459	
			34	4.52	33.967867	
			36	0.02	35.967081	
X+2	Cl	17	35	100	34.968853	35.4528
			37	31.96	36.965903	
X+2	Br	35	79	100	78.918338	79.904
			81	97.28	80.916291	
X–1	Li	3	6	8.21	6.015122	6.941
			7	100	7.016004	
X–1	B	5	10	24.8	10.012937	10.812
			11	100	11.009306	
poly	Xe	54	124	0.33	123.905896	131.29
			126	0.33	125.904270	
			128	7.14	127.903530	
			129	98.33	128.904779	
			130	15.17	129.903508	
			131	78.77	130.905082	
			132	100	131.904154	
			134	38.82	133.905395	
			136	32.99	135.907221	

[a] Classification in parentheses ≡ "not in the strict sense". [b] Standard of atomic mass scale.

Note: Care has to be taken when comparing isotopic abundances from different sources as they might be compiled using one *or* the other procedure of normalization. Never mix normalization modes in your calculations!

3.1.5 Calculation of Atomic, Molecular, and Ionic Mass

3.1.5.1 Nominal Mass

In order to calculate the approximate mass of a molecule we usually sum up integer masses of the elements encountered, e.g., for CO_2 we calculate the mass as 12 u + 2 × 16 u = 44 u. The result of this simple procedure is not particularly precise but provides acceptable values for simple molecules. This is called *nominal mass* [6].

The nominal mass of an element is defined as the *integer mass* of its most abundant naturally occurring stable isotope [6]. The nominal mass of an element is often equal to the integer mass of the lowest mass isotope of that element, e.g., for H, C, N, O, S, Si, P, F, Cl, Br, I (Table 3.1). The nominal mass of an ion is the sum of the nominal masses of its constituent elements.

Example: To calculate the nominal mass of $SnCl_2$, the masses of ^{120}Sn and ^{35}Cl have to be used, i.e., 120 u + 2 × 35 u = 190 u. While the ^{35}Cl isotope represents the most abundant as well as the lowest mass isotope of chlorine, ^{120}Sn is the most abundant but not the lowest mass isotope of tin which is ^{112}Sn.

Note: When dealing with nominal mass, mass number and nominal mass both have the same numerical value. However, the *mass number* is dimensionless and must not be confused with *nominal mass* in units of u.

3.1.5.2 Isotopic Mass

The *isotopic mass* is the exact mass of an isotope. It is very close to but not equal to the nominal mass of the isotope (Table 3.1). The only exception is the carbon isotope ^{12}C which has an isotopic mass of 12.000000 u. The *unified atomic mass* [u] is defined as $^1/_{12}$ of the mass of one atom of nuclide ^{12}C which has been assigned precisely 12 u, where 1 u = 1.660538 × 10^{-27} kg [4,6,9,10]. This convention dates back to 1961 [2].

Note: Mass values from dated literature can be ambiguous. Prior to 1961 physicists defined the *atomic mass unit* [amu] based on $^1/_{16}$ of the mass of one atom of nuclide ^{16}O. The definition of chemists was based on the relative atomic mass of oxygen which is somewhat higher resulting from the nuclides ^{17}O and ^{18}O contained in natural oxygen [2].

3.1.5.3 Relative Atomic Mass

The *relative atomic mass* or the *atomic weight* as it is also often imprecisely termed is calculated as the weighted average of the naturally occurring isotopes of an element [6]. The weighted average M_r is calculated from

$$M_r = \frac{\sum_{i=1}^{i} A_i \times m_i}{\sum_{i=1}^{i} A_i} \tag{3.2}$$

with A_i being the abundances of the isotopes and m_i their respective isotopic masses [11]. For this purpose, the abundances can be used in any numerical form or normalization as long as they are used consistently.

Example: The relative atomic mass of chlorine is 35.4528 u. However, there is no atom of this mass. Instead, chlorine is composed of ^{35}Cl (34.968853 u) and ^{37}Cl (36.965903 u) making up 75.78% and 24.22% of the total or having relative abundances of 100% and 31.96%, respectively (cf. Table 3.1 and Fig 3.1). According to Eq. 3.2, we can now calculate the relative atomic mass of chlorine
$M_r = (100 \times 34.968853\ u + 31.96 \times 36.965903\ u)/(100 + 31.96) = 35.4528\ u$.

3.1.5.4 Monoisotopic Mass

The exact mass of the most abundant isotope of an element is termed *monoisotopic mass* [6]. The monoisotopic mass of a molecule is the sum of the monoisotopic masses of the elements in its empirical formula. As mentioned before, the mono- isotopic mass is not necessarily the naturally occurring isotope of lowest mass. However, for the common elements in organic mass spectrometry the monoisotopic mass is obtained using the mass of the lowest mass isotope of that element, because this is also the most abundant isotope of the respective element (Chap. 3.1.5.1).

3.1.5.5 Relative Molecular Mass

The *relative molecular mass*, M_r, or *molecular weight* is calculated from the relative atomic masses of the elements contributing to the empirical formula [6].

3.1.5.6 Exact Ionic Mass

The *exact mass* or *accurate mass* of a positive ion formed by the removal of one or more electrons from a molecule is equal to its monoisotopic mass minus the mass of the electron(s), m_e [4]. For negative ions, the electron mass (0.000548 u) has to be added accordingly.

Example: The exact mass of the carbon dioxide molecular ion, $CO_2^{+\bullet}$, is calculated as 12.000000 u + 2 × 15.994915 u – 0.000548 u = 43.989282 u.

3.1.5.7 Role of the Electron Mass When Calculating Exact Mass

The question remains whether the mass of the electron m_e (5.48×10^{-4} u) has really to been taken into account. This issue was of almost pure academic interest as long as mass spectrometry was limited to mass accuracies of several 10^{-3} u. As FT-ICR, orbitrap, and even recent oaTOF instruments deliver mass accuracies in the order of $< 10^{-3}$ u, one should routinely include the electron mass in calculations [12,13]. Here, neglecting the electron mass would cause a systematic error of the size of m_e, which is unacceptable when mass measurement accuracies in the order of $< 10^{-3}$ u are to be achieved.

3.1.5.8 Number of Decimal Places When Calculating Exact Mass

The isotopic masses provided in this book are listed with six decimal places corresponding to an accuracy of 10^{-6} u (Tab. 3.1 and Appendix), which is about three orders of magnitude below typical mass errors in mass spectrometry (± 0.001 u).

The number of decimal places one should employ in mass calculations depends on the purpose they are used for. In the *m/z* range of up to about 500 u, the use of isotopic mass with four decimal places may provide sufficient accuracy. Above that, at least five decimal places are required, because the increasing number of atoms results in an unacceptable multiplication of many small mass errors. The results of those calculations may again be reported with only four decimal places (± 0.0001 u), because this is sufficient for most applications.

3.1.6 Natural Variations in Relative Atomic Mass

The masses of isotopes can be measured with accuracies better than *parts per billion* (ppb), e.g., $m_{^{40}Ar} = 39.9623831235 \pm 0.000000005$ u. Unfortunately, determinations of abundance ratios are less accurate, causing errors of several *parts per million* (ppm) in relative atomic mass. The real limiting factor, however, comes from the variation of isotopic abundances from natural samples, e.g., in case of lead (Pb) which is the final product of radioactive decay of uranium, the atomic weight varies by 500 ppm depending on the Pb/U ratios in the lead ore [11]. Variations in natural isotopic distributions are also responsible for the varying number of decimal places stated with the relative atomic masses in Table 3.1.

For organic mass spectrometry the case of carbon is of highest relevance. Carbon is ubiquitous in metabolic processes and the most prominent example of variations in the $^{13}C/^{12}C$ isotopic ratio is presented by the different pathways of CO_2 fixation during photosynthesis, causing $^{13}C/^{12}C$ ratios of 0.01085–0.01115. Petroleum, coal, and natural gas yield very low $^{13}C/^{12}C$ ratios of 0.01068–0.01099 and carbonate minerals, on the other side, set the upper limit at about 0.01125

[11]. Even proteins of different origin (plants, fish, mammals) can be distinguished by their $^{13}C/^{12}C$ ratios [14,15].

Isotope ratio mass spectrometry (IR-MS) makes use of these facts to determine the origin or the age of a sample. For convenience, the minor changes in isotopic ratios are expressed using the *delta notation* stating the deviation of the isotopic ratio from a defined standard in parts per thousand (‰) [11,16]. The delta value of carbon, for example, is calculated from

$$\delta^{13}C\ (‰) = [(^{13}C/^{12}C_{sample})/(^{13}C/^{12}C_{standard}) - 1] \times 1000 \qquad (3.3)$$

The internationally accepted value for $^{13}C/^{12}C_{standard}$ is 0.0112372 from a belemnite fossil from the Pee Dee formation in South Carolina (PDB standard). Naturally occurring $^{13}C/^{12}C$ ratios range from about $\delta^{13}C = -50$ to +5‰.

As an example, the origin of food can be determined by employing $\delta^{13}C$ measurements, e.g., fruit/vegetables by country or whether the source of ethanol in alcoholic beverages is sugar cane, sugar beet, cereal starch, or obtained by synthetic processes [14,16,17].

Note: A ^{13}C content of 1.1%, equalling a $^{13}C/^{12}C$ ratio of 0.0111 has proven to be most useful in the majority of mass spectrometric applications.

3.2 Calculation of Isotopic Distributions

As long as we are dealing with molecular masses in a range of up to some 10^3 u, it is possible to separate ions which differ by 1 u in mass. The upper mass limit for their separation depends on the resolution of the instrument employed. Consequently, the isotopic composition of the analyte is directly reflected in the mass spectrum – it can be regarded as an elemental fingerprint.

Even if the analyte is chemically perfectly pure it represents a mixture of different isotopic compositions, provided it is not composed of monoisotopic elements only. Therefore, a mass spectrum normally superimposes the mass spectra of all isotopic species involved [18]. The *isotopic distribution* or *isotopic pattern* of molecules containing one chlorine or bromine atom is listed in Table 3.1. But what about molecules containing two or more di-isotopic or even polyisotopic elements? While it may seem, at the first glance, to complicate the interpretation of mass spectra, isotopic patterns are in fact an ideal source of analytical information.

3.2.1 Carbon: An X+1 Element

In the mass spectrum of methane (Fig. 1.4), there is a tiny peak at *m/z* 17 that has not been mentioned in the introduction. As one can infer from Table 3.1 this should result from the ^{13}C content of natural carbon which is an X+1 element according to our classification.

Example: Imagine a total of 1000 CH_4 molecules. Due to a content of 1.1% ^{13}C, there will be 11 molecules containing ^{13}C instead of ^{12}C; the remaining 989 molecules are $^{12}CH_4$. Therefore, the ratio of relative intensities of the peaks at *m/z* 16 and *m/z* 17 is defined by the ratio 989/11 or by usual normalization 100/1.1.

In a more general way, carbon consists of ^{13}C and ^{12}C in a ratio r that can be written as $r = c/(100 - c)$ where c is the abundance of ^{13}C. Then, the probability to have only ^{12}C in a molecular ion M consisting of w carbons, i.e., the probability of monoisotopic ions P_M is given by [19]

$$P_M = \left(\frac{100 - c}{100}\right)^w \tag{3.4}$$

The probability of having exactly one ^{13}C atom in an ion with w carbon atoms is therefore

$$P_{M+1} = w\left(\frac{c}{100 - c}\right)\left(\frac{100 - c}{100}\right)^w \tag{3.5}$$

and the ratio P_{M+1}/P_M is given as

$$\frac{P_{M+1}}{P_M} = w\left(\frac{c}{100 - c}\right) \tag{3.6}$$

In case of a carbon-only molecule such as the buckminster fullerene C_{60}, the ratio P_{M+1}/P_M becomes $60 \times 1.1/98.9 = 0.667$. If the monoisotopic peak at *m/z* 720 due to $^{12}C_{60}$ is regarded as 100%, the M+1 peak due to $^{12}C_{59}{}^{13}C$ will have 66.7% relative intensity.

Note: For the $^{13}C/^{12}C$ ratio, the M+1 peak intensity can be easily estimated in percent in a simplified manner, and with an insignificant error, by multiplying the number of carbon atoms by 1.1%, e.g., $60 \times 1.1\% = 66\%$.

There is again a certain probability for one of the remaining 59 carbon atoms to be ^{13}C rather than ^{12}C. After simplification of Beynon's approach [19] to be used for one atomic species only, the probability that there will be an ion containing two ^{13}C atoms is expressed by

$$\frac{P_{M+2}}{P_M} = \frac{w}{2}\left(\frac{c}{100 - c}\right)(w - 1)\left(\frac{c}{100 - c}\right) = \frac{w(w - 1)c^2}{2(100 - c)^2} \tag{3.6}$$

For C_{60} the ratio P_{M+2}/P_M now becomes $(60 \times 59 \times 1.1^2)/(2 \times 98.9^2) = 0.219$, i.e., the M+2 peak at *m/z* 722 due to $^{12}C_{58}{}^{13}C_2$ ions will show as 21.9% relative to the M peak, which definitely can not be neglected. By extension of this principle, equations for the P_{M+3}/P_M ratio representing the third isotopic peak can be derived and so forth.

The calculation of isotopic patterns as just shown for the carbon-only molecule C_{60} can be done analogously for any X+1 element. Furthermore, the application of this scheme is not restricted to molecular ions, but can also be used for fragment ions. Nevertheless, care should be taken to assure that the presumed isotopic peak is not partially or even completely due to a different fragment ion, e.g., an ion containing one hydrogen more than the presumed X+1 composition.

Note: It is very helpful to read out the P_{M+1}/P_M ratio from a mass spectrum to calculate the approximate number of carbon atoms. Provided no other element contributing to M+1 is present, an M+1 intensity of 15%, for example, indicates the presence of 14 carbons. (For possible overestimation due to autoprotonation cf. Chap. 7.2.1)

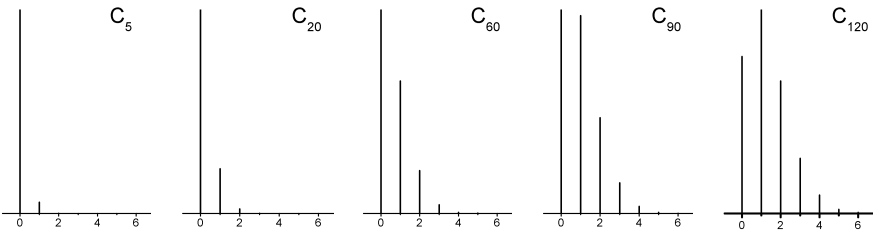


Fig. 3.2. Calculated isotopic patterns for carbon. Note the steadily expanding width of the pattern as X+2, X+3, X+4,... become visible. At about C_{90} the X+1 peak reaches the same intensity as the X peak. At higher carbon numbers it becomes the base peak of the pattern.

It is interesting how the width of the isotopic pattern increases as X+2, X+3, X+4 ... become detectable. In principle, the isotopic pattern of C_w expands up to X+*w*, because even the composition $^{13}C_w$ is possible. As a result, the isotopic pattern of *w* atoms of a di-isotopic element consists at least theoretically of *w*+1 peaks. However, the probability of extreme combinations is negligible and even somewhat more probable combinations are of no importance as long they are below about 0.1%. In practice, the interpretation of the carbon isotopic pattern is limited by experimental errors in relative intensities rather than by detection limits for peaks of low intensity. Such experimental errors can be due to poor signal-to-noise ratios (Chap. 1.4.3), autoprotonation (Chap.7), or interference with other peaks.

At about C_{90} the X+1 peak reaches the same intensity as the X peak, and at higher carbon number *w*, it becomes the base peak of the pattern, because the probability that an ion contains at least one ^{13}C becomes larger than that for the monoisotopic ion. A further increase in *w* makes the X+2 signal stronger than the X and X+1 peak and so on. A table with representative carbon isotopic abundances is provided in the Appendix.

3.2.2 Terms Related to Isotopic Composition

Molecules and ions of identical elemental composition but differing in isotopic composition are termed *isotopic homologs* or simply *isotopologs*. For example, $H_3C\text{-}CH_3$ and $H_3C\text{-}^{13}CH_3$ are isotopologs. Molecules and ions of identical isotopic composition but differing in position of the isotopes are termed *isotopomers*. For example, $H_2C{=}CD_2$ and HDC=CHD are isotopomers.

The *isotopic molecular ion* (M+1, M+2, ...) is a molecular ion containing one or more of the less abundant naturally occurring isotopes of the atoms that make up the molecular structure [4]. This term can be generalized for any non-monoisotopic ion. Thus, *isotopic ions* are those ions containing one or more of the less abundant naturally occurring isotopes of the atoms that make up the ion.

The position of the most intensive peak of an isotopic pattern is termed *most abundant mass* [6], and the corresponding ion should be named *most abundant isotopolog* (*ion*). For example, the most abundant mass in case of C_{120} is 1441 u corresponding to M+1 (Fig. 3.2). The most abundant mass is relevant in the case of large ions (Chap. 3.4.3).

3.2.3 Binomial Approach

The above stepwise treatment of X+1, X+2, and X+3 peaks has the advantage that it can be followed easier, but it bears the disadvantage that an equation needs to be solved for each individual peak. Alternatively, one can calculate the relative abundances of the isotopic species for a di-isotopic element from a binomial expression [20-22]. In the term $(a + b)^n$ the isotopic abundances of both isotopes are given as a and b, respectively, and n is the number of this species in the molecule.

$$(a+b)^n = a^n + na^{n-1}b + n(n-1)a^{n-2}b^2/(2!) + n(n-1)(n-2)a^{n-3}b^3/(3!) + \ldots \tag{3.8}$$

For $n = 1$ the isotopic distribution can of course be directly obtained from the isotopic abundance table (Table 3.1 and Fig. 3.1) and in case of $n = 2$, 3, or 4 the expression can easily be solved by simple multiplication, e.g.,

$$(a+b)^2 = a^2 + 2ab + b^2 \tag{3.9}$$
$$(a+b)^3 = a^3 + 3a^2b + 3ab^2 + b^3$$
$$(a+b)^4 = a^4 + 4a^3b + 6a^2b^2 + 4ab^3 + b^4$$

Again, we obtain w+1 terms for the isotopic pattern of w atoms. The binomial approach works for any di-isotopic element, regardless of whether it is of X+1, X+2, or X–1 type. However, as the number of atoms increases above 4 it is also no longer suitable for manual calculations.

3.2.4 Halogens

The halogens Cl and Br occur in two isotopic forms, each of them being of significant abundance, whereas F and I are monoisotopic (Table 3.1). In most cases there are only a few Cl and/or Br atoms in a molecule and this predestinates the binomial approach for this purpose.

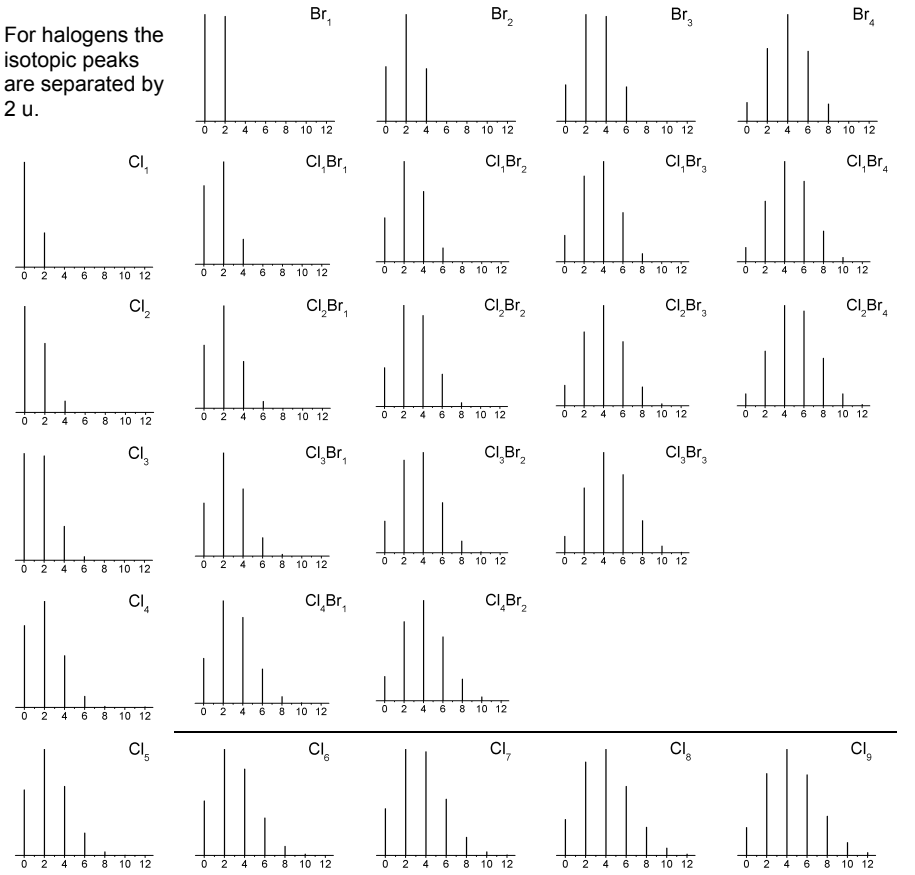


Fig. 3.3. Calculated isotopic patterns for combinations of bromine and chlorine. The peak shown at zero position corresponds to the monoisotopic ion at *m/z* X. The isotopic peaks are then located at *m/z* = X+2, 4, 6, ... The numerical value of X is given by the mass number of the monoisotopic combination, e.g., 70 u for Cl_2.

Example: The isotopic pattern of Cl_2 is calculated from Eq. 3.9 with the abundances $a = 100$ and $b = 31.96$ as $(100 + 31.96)^2 = 10{,}000 + 6392 + 1019$. After normalization we obtain 100 : 63.9 : 10.2 as the relative intensities of the three peaks. Any other normalization for the isotopic abundances would give the same result, e.g., $a = 0.7578$, $b = 0.2422$. The calculated isotopic pattern of Cl_2 can be understood from the following practical consideration: The two isotopes ^{35}Cl and

^{37}Cl can be combined in three different ways: *i*) $^{35}Cl_2$ giving rise to the monoisotopic composition, *ii*) $^{35}Cl^{37}Cl$ yielding the first isotopic peak which is here X+2, and finally *iii*) $^{37}Cl_2$ giving the second isotopic peak X+4. The combinations with a higher number of chlorine atoms can be explained accordingly.

Note: Rapid estimation of the isotopic patterns of chlorine and bromine can be achieved with good results by using the approximate isotope ratios $^{35}Cl/^{37}Cl = 3 : 1$ and $^{79}Br/^{81}Br = 1 : 1$. Visual comparison with calculated patterns is also suitable (Fig. 3.3).

It is helpful to have frequent isotopic distributions at hand. For some Cl_x, Br_y, and Cl_xBr_y combinations these are tabulated in the Appendix. Tables are useful for the construction of isotopic patterns from "building blocks". Nevertheless, as visual information is easier to compare with a plotted spectrum, these patterns are also shown below (Fig. 3.3). In case of Cl and Br the peaks are always separated from each other by 2 u, i.e., the isotopic peaks are located at X+2, 4, 6 and so on.

If there are two bromine or four chlorine atoms contained in the formula, the isotopic peaks become stronger than the monoisotopic peak, because the second isotope is of much higher abundance than in case of the ^{13}C isotope.

Hint: One may want to seek advice on how to distinguish between those patterns. For example, the patterns of Cl_2Br and Cl_3Br or of Cl_2Br_3 and Cl_3Br_3 closely resemble each other. To distinguish such pairs it is helpful to construct orientation lines between signal peak tips of comparable intensity. Generally these will decline with one pattern but can be positively inclined or even close to horizontal in others (Fig. 3.4).

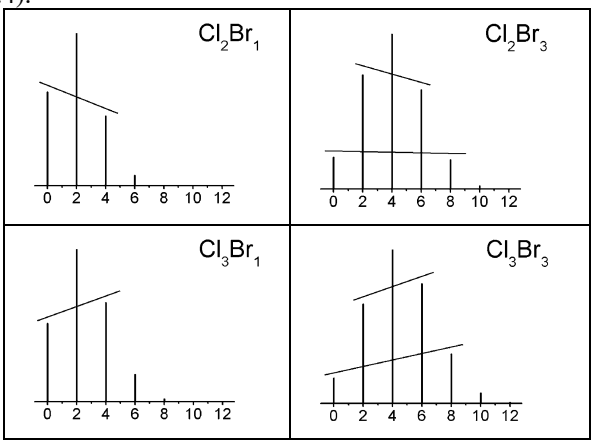


Fig. 3.4. Aid in distinguishing isotopic patterns by using orientation lines. *Left side:* patterns with four peaks each; *right side*: patterns with six peaks.

3.2.5 Combinations of Carbon and Halogens

So far we have treated the X+1 and the X+2 elements separately, admittedly a rather artificial approach. The combination of C, H, N, and O with the halogens F, Cl, Br, and I covers a large fraction of the molecules one usually has to deal with. When regarding H, O, and N as X elements, which is a valid approximation for not too large molecules, the construction of isotopic patterns can be conveniently accomplished. By use of the isotopic abundance tables of the elements or of tables of frequent combinations of these as provided in this chapter or in the Appendix, the building blocks can be combined to obtain more complex isotopic patterns.

Example: Let us construct the isotopic pattern of $C_9N_3Cl_3$ restricting ourselves to the isotopic contributions of C and Cl, i.e., with N as an X element. Here, the isotopic pattern of chlorine can be expected to be dominant over that of carbon. First, from the cubic form of Eq. 3.9 the Cl_3 pattern is calculated as follows: $(0.7578 + 0.2422)^3 = 0.435 + 0.417 + 0.133 + 0.014$ and after normalization this becomes 100 : 95.9 : 30.7 : 3.3. Of course, using the tabulated abundances of the Cl_3 distribution (Appendix) would be faster. The result is then plotted with 2 u distance, beginning at the nominal mass of the monoisotopic ion, i.e., $9 \times 12\ u + 3 \times 14\ u + 3 \times 35\ u = 255\ u$. The contribution of C_9 to the pattern is mainly at X+1 where we have $9 \times 1.1\% = 9.9\%$, whereas its contribution to X+2 (0.4%, Appendix) is negligible in this simple estimation. Finally, the X+1 contribution of C_9 is placed into the gaps of the Cl_3 pattern each with 9.9% relative to the preceding peak of the chlorine isotopic distribution (Fig. 3.5).

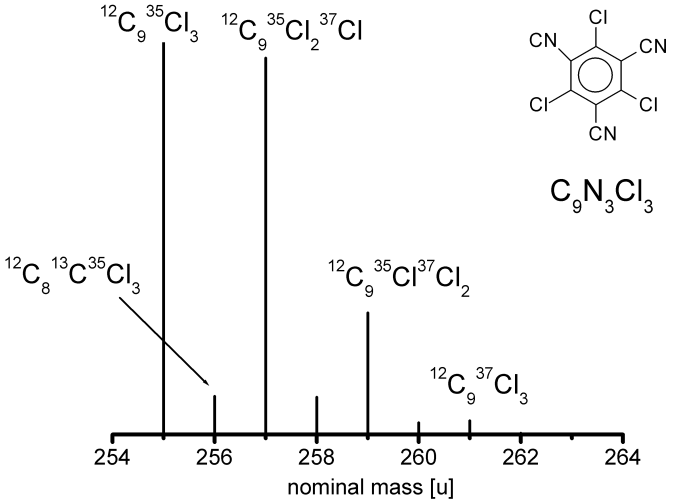


Fig. 3.5. The isotopic pattern of $C_9N_3Cl_3$ as constructed in the example above. The first ^{13}C isotopic peaks are located between the X+2, 4, and 6 peaks of the dominant Cl_3 pattern. Nitrogen is treated as an X element and has been omitted from the peak labels for clarity.

3.2.6 Polynomial Approach

The polynomial approach is the logical expansion of the binomial approach. It is useful for the calculation of isotopic distributions of polyisotopic elements or for formulas composed of several non-monoisotopic elements [21,22]. In general, the isotopic distribution of a molecule can be described by a product of polynominals

$$(a_1 + a_2 + a_3 + ...)^m \; (b_1 + b_2 + b_3 + ...)^n \; (c_1 + c_2 + c_3 + ...)^o + ... \qquad (3.10)$$

where a_1, a_2, a_3 etc. represent the individual isotopes of one element, b_1, b_2, b_3 etc. represent those of another and so on until all elements are included. The exponents m, n, o etc. give the number of atoms of these elements as contained in the empirical formula.

Example: The complete isotopic distribution of stearic acid trichloromethylester, $C_{19}H_{35}O_2Cl_3$, is obtained from Eq. 3.10 from the polynomial expression

$$(A_{12C} + A_{13C})^{19} \; (A_{1H} + A_{2H})^{35} \; (A_{16O} + A_{17O} + A_{18O})^2 \; (A_{35Cl} + A_{37Cl})^3$$

with A_x representing the relative abundances of the isotopes involved for each element. The problem with the calculation of isotopic patterns resides in the enormous number of terms obtained for larger molecules. Even for this simple example, the number of terms would be $(2)^{19} \times (2)^{35} \times (3)^2 \times (2)^3 = 1.297 \times 10^{18}$. The number is dramatically reduced if like terms are combined which describe the same isotopic composition regardless where the isotopes are located in the molecule. However, manual calculations are prone to become tedious if not impractical; computer programs now simplify the process [23,24].

Note: Mass spectrometers usually are delivered with the software for calculating isotopic distributions. Such programs are also offered as internet-based or shareware solutions. While such software is freely accessible, it is still necessary to obtain a thorough understanding of isotopic patterns as a prerequisite for adequately interpreting mass spectra.

3.2.7 Oxygen, Silicon, and Sulfur

Oxygen, silicon, and sulfur are polyisotopic elements in the strict sense – oxygen as ^{16}O, ^{17}O, and ^{18}O, sulfur as ^{32}S, ^{33}S, ^{34}S, and ^{36}S, and silicon as ^{28}Si, ^{29}Si, and ^{30}Si. The isotopic patterns of sulfur and silicon are by far not as prominent as those of chlorine and bromine, but still important (Fig. 3.6).

^{17}O (0.038%) and ^{18}O (0.205%) are so rare that the occurrence of oxygen usually cannot be detected from the isotopic pattern in routine spectra because the experimental error in relative intensities tends to be larger than the contribution of ^{18}O. Therefore, oxygen is frequently treated as an X type element although X+2 would be a more appropriate but practically rather useless classification. In oligo-

saccharides, for instance, a substantial number of oxygen atoms contribute to the X+2 signal.

Sulfur can be classified as an X+2 element as long as few sulfur atoms are present in a molecule. However, the 0.8% contributed by ^{33}S to the X+1 is almost comparable to the situation with ^{13}C (1.1% per atom). If the X+1 peak is used for estimating the number of carbons present, then for ^{33}S this would cause an overestimation of the number of carbon atoms by roughly one carbon per sulfur.

In the case of silicon the ^{30}Si isotope contributes a "mere" 3.4% to the X+2 signal, and ^{29}Si even 5.1% to X+1. So, neglecting ^{29}Si would cause an overestimation of the carbon number by 5 per Si present, which is unacceptable.

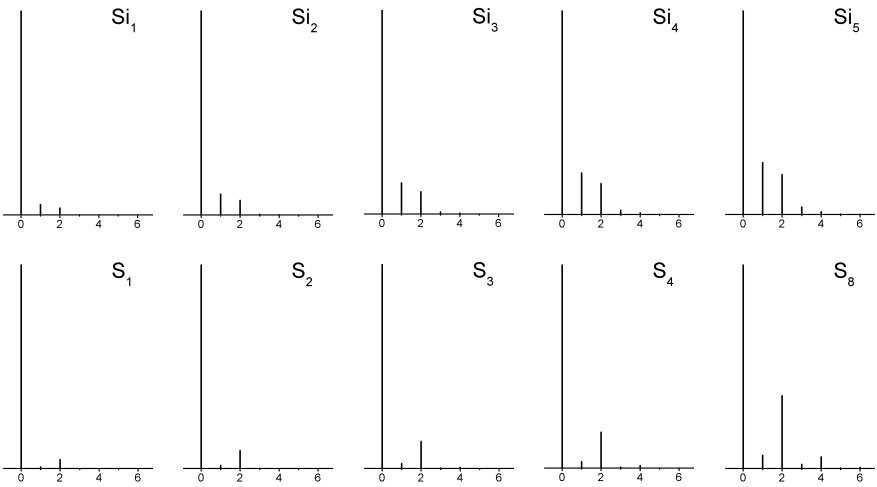


Fig. 3.6. Calculated isotopic patterns for combinations of elemental silicon and sulfur. The peak shown at zero position corresponds to the monoisotopic ion at *m/z* X. The isotopic peaks are then located at *m/z* X+1, 2, 3, ...

Note: The presence of S and Si in a mass spectrum is best revealed by carefully examining the X+2 intensity: this signal's intensity will be too high to be caused by the contribution of $^{13}C_2$ alone, even if the number of carbons has been obtained from X+1 without prior subtraction of the S or Si contribution.

Example: Ethyl propyl thioether, $C_5H_{12}S$: the isotopic pattern of its elemental composition and.the relative contributions of ^{33}S and ^{13}C to the M+1 and of ^{34}S and $^{13}C_2$ to the M+2 signal.(see Fig. 3.7 and Chap. 6.12). If the M+1 peak resulted from ^{13}C alone, this would rather indicate the presence of 6 carbon atoms, which in turn would imply an M+2 intensity of only 0.1% instead of the actually observed 4.6%. Consideration of Si for explaining the isotopic pattern would still fit the M+2 intensity, however with relatively low accuracy, while for M+1 the situa-

tion would be quite different. As ^{29}Si itself demands 5.1% at M+1, there would be no or one carbon maximum allowed to explain the observed M+1 intensity.

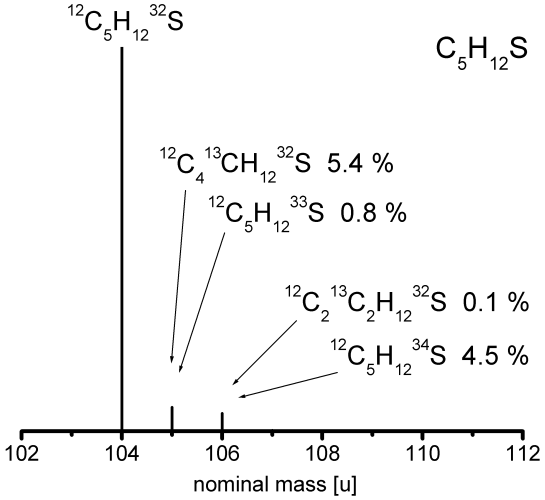


Fig. 3.7. Ethyl propyl thioether, $C_5H_{12}S$ – calculated isotopic pattern of the molecular ion indicating the respective contributions of ^{33}S and ^{13}C to the M+1 and of ^{34}S and $^{13}C_2$ to the M+2 signal.

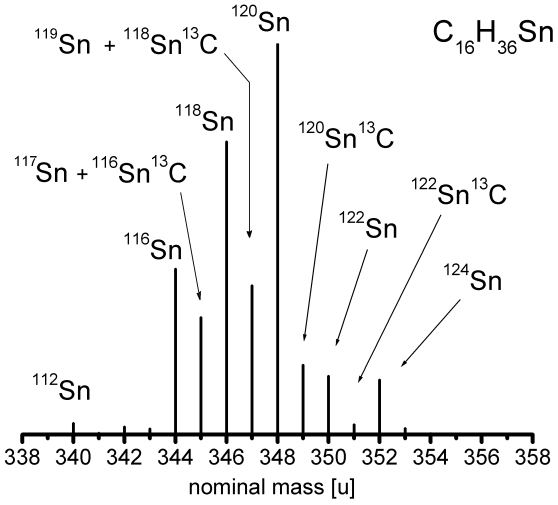


Fig. 3.8. Tetrabutyltin, $C_{16}H_{36}Sn$ – calculated isotopic pattern..

3.2.8 Polyisotopic Elements

The treatment of polyisotopic elements does not require other techniques as far as calculation or construction of isotopic patterns are concerned. However, isotopic patterns can differ largely from what has been considered so far and it is worth mentioning their peculiarities.

Example: Tin (Sn) – the presence or absence of this polyisotopic element can readily be detected from its characteristic isotopic pattern. For tetrabutyltin, $C_{16}H_{36}Sn$, the lowest mass isotopic composition is $^{12}C_{16}H_{36}{}^{112}Sn$, 340 u. Regarding the 16 carbon atoms, the ^{13}C isotopic abundance is about 17.5%. This is superimposed on the isotopic pattern of elemental Sn, which becomes especially obvious at 345 and 347 u (Fig. 3.7). The bars labeled with a tin isotope alone are almost solely due to $^{x}Sn^{12}C$ species. Tin neither has an isotope ^{121}Sn nor ^{123}Sn, and therefore the contributions at 349 and 351 u must be due to $^{120}Sn^{13}C$ and $^{122}Sn^{13}C$, respectively.

3.2.9 Practical Aspects of Isotopic Patterns

The recognition of isotopic patterns bears some potential pitfalls. Particularly, if signals from compounds differing by two or four hydrogens are superimposed or if such a superimposition can not a priori be excluded, the observed pattern has to be stepwise carefully checked to avoid misinterpretation of mass spectral data. When isotopically labeled compounds are involved similar care also becomes necessary.

Example: 1-Butene (EI spectrum) – Supposing it to be an unknown, the peaks in the *m/z* 50–57 range could be misinterpreted as a complex isotopic pattern (Fig. 3.9). However, there is no element having a comparable isotopic pattern, and in addition, all elements exhibiting broad isotopic distributions have much higher mass. Instead, the 1-butene molecular ion loses $H^{\bullet}$, H_2, and multiple H_2. The peak at *m/z* 57, of course, results from ^{13}C. Similarly, the peaks at *m/z* 39 and 41 erroneously seem to result from the isotopic distribution of iridium, which is not the case however (^{191}Ir and ^{193}Ir); rather, these peaks originate from the formation of an allyl cation, $C_3H_5^+$, *m/z* 41, which fragments further by loss of H_2 to form the $C_3H_3^+$ ion, *m/z* 39 (Chap. 6.2.4).

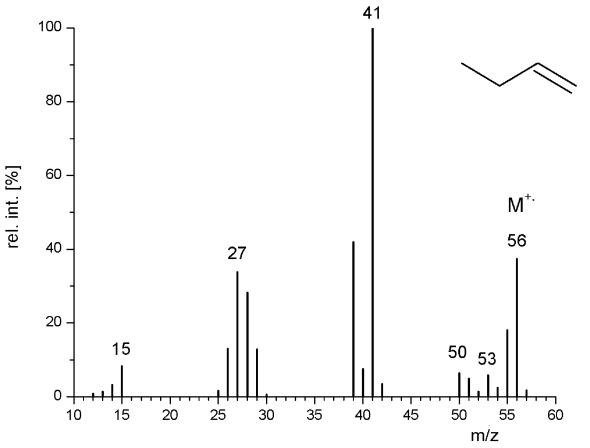


Fig. 3.9. 1-Butene EI mass spectrum. Adapted with permission. © NIST, 2002.

3.2.10 Bookkeeping with Isotopic Patterns in Mass Spectra

Proving the identity of isotopic patterns requires careful comparison with calculated patterns. The mass differences must be consistent with the mass of the presumed neutral losses. In order to hold true, a pattern can only be assigned to signals at or above the mass given by the sum of all contributing atoms.

In calculating the mass differences between peaks from different isotopic patterns it is strongly recommended to proceed from the monoisotopic peak of one group to the monoisotopic peak of the next. Accordingly, the mass difference obtained also owes to the loss of a monoisotopic fragment. Otherwise, one bears the risk of erroneously omitting or adding hydrogens in a formula.

Example: The EI mass spectrum of tribromomethane is dominated by the bromine isotopic distribution (Fig. 3.10). At first, there is no need to wonder *why* bromoform fragments like it does upon EI (Chap. 6.1.4). Let us simply accept this fragmentation and focus on the isotopic patterns. By referring to Fig. 3.3 one can identify the patterns of Br_3, Br_2, and Br. As a matter of fact, the molecular ion must contain the full number of bromine atoms (*m/z* 250, 252, 254, 256).

The primary fragment ion due to $Br^{\bullet}$ loss will then show a Br_2 pattern (*m/z* 171, 173, 175). A mass difference of 79 u is calculated between *m/z* 250 and *m/z* 171, owing to ^{79}Br, and thus identifying the process as a loss of $Br^{\bullet}$. Starting from the $CH^{79}Br_2{}^{81}Br$ isotopic ion at *m/z* 252 would yield the same information if ^{81}Br was used for the calculation. Here, ^{79}Br would wrongly indicate loss of H_2Br.

Subsequent elimination of HBr leads to CBr^+ at *m/z* 91, 93. Alternatively, the molecular ion can eliminate Br_2 to form $CHBr^{+\bullet}$, *m/z* 92, 94, overlapping with the *m/z* 91, 93 doublet, or it may lose CHBr to yield $Br_2{}^{+\bullet}$, causing the peaks at *m/z*

158, 160, 162. The peaks at *m/z* 79, 81 are due to Br^+ and those at *m/z* 80, 82 result from $HBr^{+\bullet}$ formed by CBr_2 loss from the molecular ion.

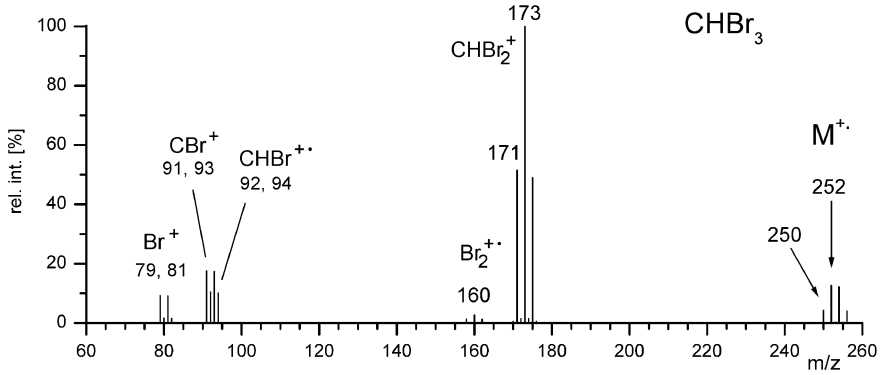


Fig. 3.10. Tribromomethane EI mass spectrum. Adapted with permission. © NIST, 2002.

3.2.11 Information from Complex Isotopic Patterns

If the isotopic distribution is very broad and/or there are elements encountered that have a lowest mass isotope of very low abundance, recognition of the monoisotopic peak would become rather uncertain. However, there are ways to cope with that situation.

Example I: The ^{112}Sn isotopic peak of tin compounds can easily be overlooked or simply could be superimposed by background signals (Fig. 3.8). Here, one should identify the ^{120}Sn peak from its unique position within the characteristic pattern before screening the spectrum from peak to peak. For all other elements contained in the respective ions still the lowest mass isotope would be used in calculations.

Example II: Ruthenium exhibits a wide isotopic distribution of which the ^{102}Ru isotope can be used as a marker during assignment of mass differences. Moreover, the strong isotopic fingerprint of Ru makes it easily detectable from mass spectra and even compensates for a lack of information resulting from moderate mass accuracy (Fig. 3.11).

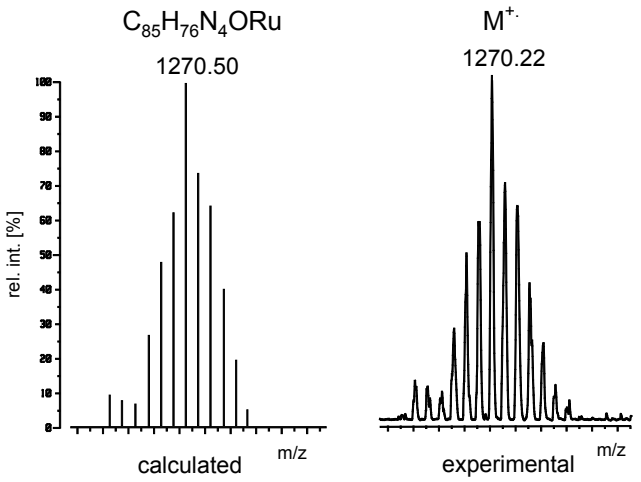


Fig. 3.11. Ruthenium carbonyl porphyrin complex – calculated and experimental isotopic pattern (FD-MS, cf. Chap. 8.5.5). The isotopic pattern supports the presumed molecular composition. The labeled peak corresponds to the ^{102}Ru-containing ion. Adapted from Ref. [25] with permission. © IM Publications, 1997.

Note: If the isotopic distribution is broad and/or there are elements encountered that have a lowest mass isotope of very low abundance, it is recommended to base calculations on the most abundant isotope of the respective element.

3.3 Isotopic Enrichment and Isotopic Labeling

3.3.1 Isotopic Enrichment

If the abundance of a particular nuclide is higher than the natural level in an ion, the term *isotopically enriched ion* is used to describe any ion enriched in the isotope [4]. The degree of *isotopic enrichment* is best determined by MS.

Example: Isotopic enrichment is a standard means to enhance the response of an analyte in nuclear magnetic resonance (NMR). Such measures gain importance if extremely low solubility is combined with a large number of carbons, as is often the case with [60]fullerene compounds [26]. The molecular ion signals, $M^{+\bullet}$, of C_{60} with natural isotopic abundance and of ^{13}C-enriched C_{60} are shown below (Fig. 3.11; for EI-MS of [60]fullerenes cf. Refs. [27-29]). From these mass spectra, the ^{13}C enrichment can be determined by use of Eq. 3.2. For C_{60} of natural isotopic abundance we obtain $M_{rC60} = 60 \times 12.0108$ u = 720.65 u. Applying Eq. 3.2 to the isotopically enriched compound yields $M_{r13C\text{-}C60} = (35 \times 720 + 65 \times 721 + 98 \times 722 + 100 \times 723 + 99 \times 724 + 93 \times 725 + ...)$u/(35 + 65 + 98 + 100 + 99 + 93

+ ...) = 724.10 u. (Integer mass and intensity values are used here for clarity.) This result is equivalent to an average content of 4.1 ^{13}C atoms per [60]fullerene molecule which on the average means 3.45 ^{13}C atoms more than the natural content of 0.65 ^{13}C atoms per molecule.

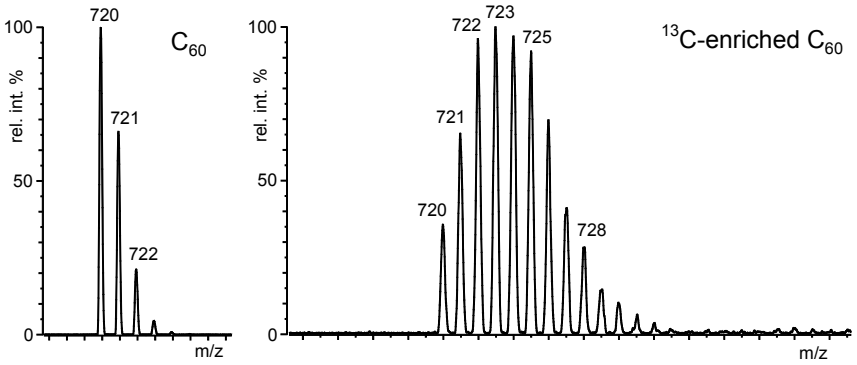


Fig. 3.12. [60]Fullerene – comparison of the molecular ion signals, $M^{+\bullet}$, with natural isotopic abundance and of ^{13}C-enriched C_{60}. By courtesy of W. Krätschmer, Max Planck Institute for Nuclear Physics, Heidelberg.

3.3.2 Isotopic Labeling

If the abundance of a particular nuclide is higher than the natural level at one or more (specific) positions within an ion, the term *isotopically labeled ion* is used to describe such an ion. Among other applications, *isotopic labeling* is used in order to track metabolic pathways, to serve as internal standard for quantitative analysis, or to elucidate fragmentation mechanisms of ions in the gas phase. In mass spectrometry, the nonradiating isotopes ^{2}H (deuterium, D), ^{13}C, and ^{18}O are preferably employed and thus, a rich methodology to incorporate isotopic labels has been developed [30]. Isotopic labeling is rather a mass spectrometric research tool [31] than mass spectrometry being a tool to control the quality of isotopic labeling. As a result, isotopic labeling is used in many applications; examples are given throughout the book.

3.4 Resolution and Resolving Power

3.4.1 Definitions

So far, we have taken for granted that mass spectra separate isotopic patterns; now we want to quantify this degree of separation. The separation observed in a mass spectrum is termed *mass resolution*, *R*, or simply *resolution*. Mass resolution is given as the smallest difference in *m/z* ($\Delta m/z$) that can be separated for a given signal, i.e., at a given *m/z* value:

$$R = \frac{m}{\Delta m} = \frac{m/z}{\Delta m/z} \tag{3.11}$$

Accordingly resolution is dimensionless. The ability of an instrument to resolve neighboring peaks is called its *mass resolving power* or simply *resolving power*. It is obtained from the peak width at a specific percentage of the peak height expressed as a function of mass [4].

Two neighboring peaks are assumed to be sufficiently separated when the valley separating their maxima has decreased to 10% of their intensity. Hence, this is known as *10% valley definition of resolution*, $R_{10\%}$. The 10% valley conditions are fulfilled if the peak width at 5% relative height equals the mass difference of the corresponding ions, because then the 5% contribution of each peak to the same point of the *m/z* axis adds up to 10% (Fig. 3.13). With the advent of linear quadrupole analyzers the *full width at half maximum (FWHM) definition* of resolution became widespread especially among instruments manufacturers. It is also commonly used for time-of-flight and quadrupole ion trap mass analyzers. With Gaussian peak shapes, the ratio of R_{FWHM} to $R_{10\%}$ is 1.8. The resolution for a pair of peaks at different *m/z* and its practical implications are illustrated below (Fig. 3.14).

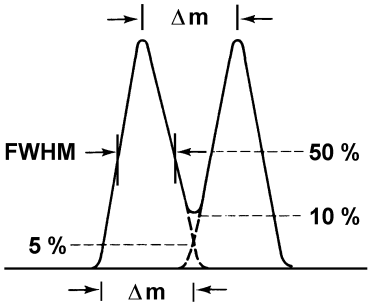


Fig. 3.13. The 10% valley and full width at half maximum (FWHM) definitions of resolution. Peak heights are not to scale.

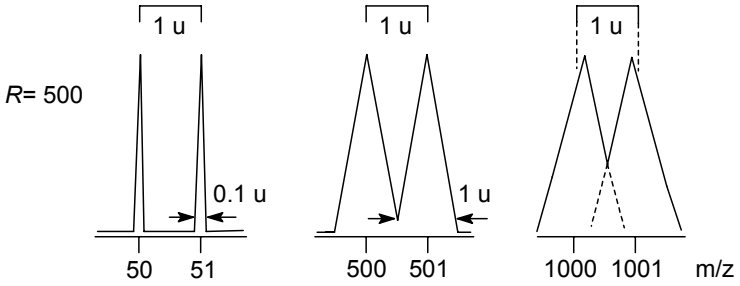


Fig. 3.14. Signals at *m/z* 50, 500, and 1000 as obtained at R = 500. At *m/z* 1000 the peak maxima shift towards each other due to superimposing peaks, thus approximating the expected value of R_{FWHM} = 900.

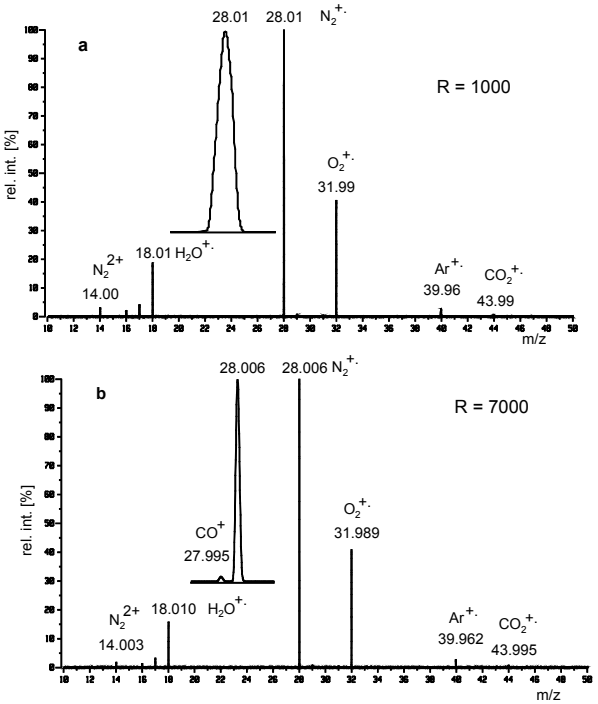


Fig. 3.15. Residual air – EI mass spectra (**a**) at $R = 1000$ and (**b**) at $R = 7000$. The relative intensities are not affected by different resolution. The decimal digits of the mass labels indicate achievable mass accuracies under the respective conditions.

Example: The changes in the electron ionization spectra of residual air nicely show the effect of higher resolution (Fig. 3.15). Setting $R = 1000$ yields a peak width of 0.028 u for the signal at *m/z* 28. An increase to $R = 7000$ perfectly separates the minor contribution of CO^+, *m/z* 27.995, from the predominating $N_2^{+\bullet}$ at *m/z* 28.006 (The CO^+ ion rather results from fragmenting $CO_2^{+\bullet}$ ions than from carbon monoxide in laboratory air.)

Note: The attributive *low resolution* (LR) is generally used to describe spectra obtained at $R = 500–2000$. *High resolution* (HR) is appropriate for $R > 5000$. However, there is no exact definition of these terms.

3.4.2 Resolution and its Experimental Determination

In principle, resolution is always determined from the peak width of some signal at a certain relative height and therefore, any peak can serve this purpose. As the exact determination of a peak width is not always easy to perform, certain doublets of known Δm are being used.

The minimum resolution to separate CO^+ from $N_2^{+\bullet}$ is 28/0.011 ≈ 2500. The doublet from the pyridine molecular ion, $C_5H_5N^{+\bullet}$, *m/z* 79.0422, and from the first isotopic peak of the benzene molecular ion, $^{13}CC_5H_6^{+\bullet}$, *m/z* 79.0503, necessitates $R = 9750$ to be separated. Finally, the doublet composed of the first isotopic ion of $[M–CH_3]^{+\bullet}$ from xylene, $^{13}CC_6H_7^+$, *m/z* 92.0581, and toluene molecular ion, $C_7H_8^{+\bullet}$, *m/z* 92.0626, requires $R = 20{,}600$ for separation (Fig 3.16).

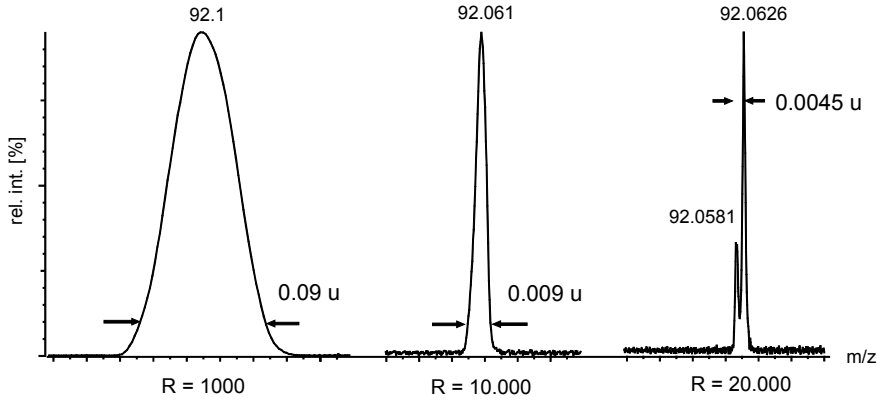


Fig. 3.16. The peak at *m/z* 92 from a mixture of xylene and toluene at different settings of resolution. At $R = 10{,}000$ some separation of the lower mass ion can already be presumed from a slight asymmetry of the peak. $R = 20{,}600$ is needed to fully separate $^{13}CC_6H_7^+$, *m/z* 92.0581, from $C_7H_8^{+\bullet}$, *m/z* 92.0626. The *m/z* scale is the same for all of the signals.

Note: There is no need to use a more accurate value of *m/z* than nominal and likewise, there is no use of reporting $R = 2522.52$ exactly as obtained for the $CO^+/N_2^{+\bullet}$ pair. It is fully sufficient to know that setting $R = 3000$ is sufficient for one specific task or that $R = 10{,}000$ is suitable for another.

With magnetic sector instruments a resolving power of up to $R = 10{,}000$ can routinely be employed, even $R = 15{,}000$. In practice, those instruments are rarely adjusted to resolve beyond $R = 10{,}000$, e.g., only when interferences of ions of the same nominal *m/z* need to be excluded. With an instrument in perfect condition, it is possible to achieve higher resolving power; typically they are specified to deliver about $R \approx 60{,}000$ (on intensive peaks).

3.4.3 Resolving Power and its Effect on Relative Peak Intensity

Increasing resolution does not affect the relative intensities of the peaks, i.e., the intensity ratios for *m/z* 28 : 32 : 40 : 44 in the spectrum of air generally remain constant (Fig. 3.15). However, increased settings of *resolving power* are usually obtained at the cost of transmission of the analyzer, thereby reducing the absolute signal intensity. Accordingly, isotopic patterns are not affected by increasing reso-

lution up to $R \approx 10{,}000$; beyond, there can be changes in isotopic patterns due to the separation of different isotopic species of the same nominal mass (Chap. 3.7).

3.5 Accurate Mass

The section on high resolution (HR) already anticipated *accurate mass* to a certain extent. In fact, HR and accurate mass measurements are closely related and depend on each other, because mass accuracy tends to improve as peak resolution is improved. Nevertheless, they should not be confused, as performing a measurement at *high resolution* alone does not equally imply measuring the *accurate mass*. High resolution separates adjacent signals, accurate mass can deliver molecular formulas [32-34].

Until the early 1980s, accurate mass measurements were nearly restricted to electron ionization, and for a while, the technique even seemed to become abandoned. New options available through FT-ICR instrumentation then revived the value of accurate mass measurements. The newly developed orbitrap and a new generation of oaTOF analyzers contributed to an increased demand for accurate mass data. Nowadays, formula elucidation can be performed using any ionization method [35], their widespread application thus demanding a thorough understanding of their potential and limitations [33].

3.5.1 Exact Mass and Molecular Formulas

Let us briefly repeat: *i*) the *isotopic mass* is also the *exact mass* of an isotope; *ii*) the isotopic mass is very close but not equal to the *nominal mass* of that isotope; *iii*) accordingly, the calculated exact mass of a molecule or of a monoisotopic ion equals its monoisotopic mass; *iv*) due to the definition of our mass scale, the isotope ^{12}C represents the only exception from non-integer isotopic mass. As a consequence of these individual non-integer isotopic masses, almost no combination of elements in a molecular or ionic formula has the same *calculated exact mass*, or simply *exact mass* as it is often referred to, as any other one [36].

Example: The molecular ions of nitrogen, $N_2^{+\bullet}$, carbon monoxide, $CO^{+\bullet}$, and ethene, $C_2H_4^{+\bullet}$, have the same nominal mass of 28 u, i.e., they are so-called *isobaric ions*. The isotopic masses of the most abundant isotopes of hydrogen, carbon, nitrogen, and oxygen are 1.007825 u, 12.000000 u, 14.003074 u, and 15.994915 u, respectively. Thus, the calculated ionic masses are 28.00559 u for $N_2^{+\bullet}$, 27.99437 u for $CO^{+\bullet}$, and 28.03075 u for $C_2H_4^{+\bullet}$. This means they differ by several 10^{-3} u, and none of these isobaric ions has precisely 28.00000 u (Chaps. 3.3.4 and 6.9.6).

Note: Historically, 10^{-3} u is referred to as 1 *millimass unit* (mmu). There is still use of mmu in the MS community because of its convenience in dealing with small differences in mass. The mmu is in no way an SI unit.

3.5.2 Mass Defect

The deviation of exact mass from nominal mass can be to either side, higher or lower, depending on the isotopes encountered. While the matter itself can be easily understood, existing terminology here is somewhat unfortunate. The term *mass defect*, m_{defect}, defined as the difference between integer mass, m_{nominal}, and exact mass, m_{exact}, is used to describe this deviation [6].

$$m_{\text{defect}} = m_{\text{nominal}} - m_{\text{exact}} \tag{3.12}$$

Application of this concept leads to *positive* and *negative mass* defects. The hydrogen atom, for example, has a negative mass defect, $m_{\text{defectH}} = -7.825 \times 10^{-3}$ u. In addition, the association of something being "defective" with certain isotopic masses can be misleading. The mass defect was unveiled by Aston [2,3] who already had discovered 212 of the total 287 stable isotopes.

The term *mass deficiency* better describes the fact that the exact mass of an isotope or a complete molecule is lower than the corresponding nominal mass. In case of ^{16}O, for example, the isotopic mass is 15.994915 u, being 5.085×10^{-3} u deficient as compared to the nominal value ($m_{\text{defectO}} = 5.085 \times 10^{-3}$ u). Most isotopes are more or less mass deficient with a tendency towards larger mass defect for the heavier isotopes, e.g., $M_{35\text{Cl}}$ = 34.96885 u (-3.115×10^{-2} u) and $M_{127\text{I}}$ = 129.90447 u (-9.553×10^{-2} u).

Mass–energy equivalence is a key postulate of Einstein's theory of relativity as expressed by his famous equation $E = mc^2$. It explains the conversion of mass into energy during nucleation, and thus, the increasing mass deficiency of the heavier isotopes caused by their larger nuclear binding energy. The binding energy per nucleon steeply increases along the mass numbers from ^{2}H to its maximum around ^{56}Fe and then decreases again somewhat up to ^{238}U (Fig. 3.17). Translation into isotopic mass reveals that for light elements mass is by some 10^{-3} u above the nominal value (^{1}H or ^{14}N) whereas some 10^{-3} u (^{19}F) to almost 10^{-1} u (^{127}I) below for heavier elements [34]. This also complies with the fact that the radioactive isotopes of thorium and uranium have isotopic masses above the nominal value, thus reflecting their comparatively unstable nuclei (Appendix). The numerical values of mass deficiency, however, are merely defined by the "arbitrary" setting of ^{12}C as the standard in the atomic mass scale.

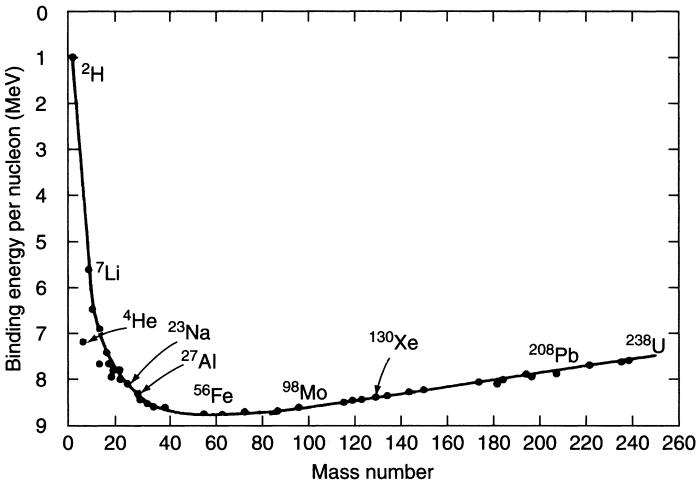


Fig. 3.17. Plot of binding energy per nucleon vs. mass number. Reproduced from Ref. [1] by permission. © John Wiley & Sons, 1992.

Among the elements frequently encountered in mass spectrometry, only H, He, Li, Be, B, and N exhibit isotopic masses larger than their nominal value. Among the isotopes with negative mass defect, ^{1}H is the most important one, because each hydrogen adds 7.825×10^{-3} u. Thereby, it significantly contributes to the mass of larger hydrocarbon molecules [37]. In general, the ubiquitous occurrence of hydrogen in organic molecules causes most of them to exhibit considerable negative mass defects, which again decreases with the number of mass-deficient isotopes, e.g., from halogens, oxygen, or metals.

Example: Plotting the deviations from nominal mass of different oligomers as a function of nominal mass, one finds only pure carbon molecules (such as fullerenes) to be located on the *x*-axis. Hydrocarbons, due to their large number of hydrogens, receive roughly 1 u from negative mass defect per 1000 u in molecular mass. Halogenated oligomers, on the other hand, are more or less mass deficient and those oligomers containing some oxygen are located in between (Fig. 3.18).

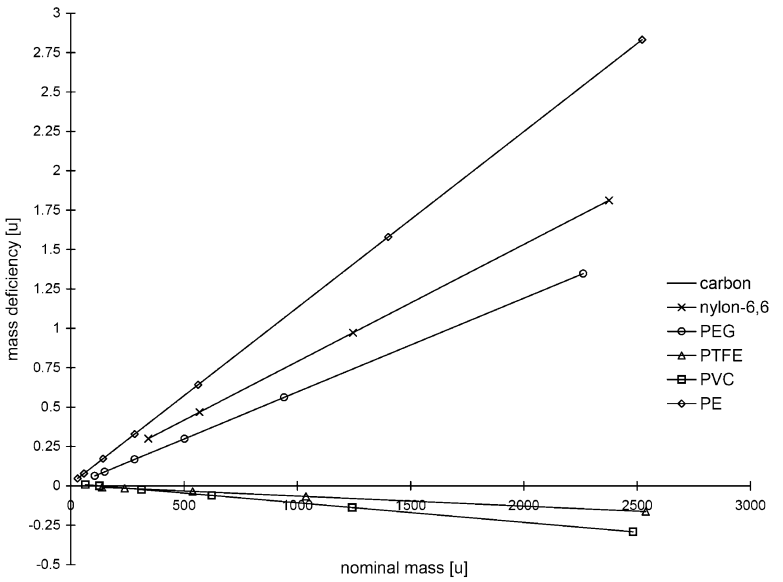


Fig. 3.18. Deviation from nominal mass for some oligomers as a function of nominal mass. PE: polyethylene, PEG: polyethyleneglycol, PTFE: polytetrafluoroethylene, PVC: polyvinylchloride.

Note: The use of nominal mass is limited to the low mass range. Above about 500 u the first decimal of isotopic mass can be larger than .5 causing it to be rounded up to 501 u instead of the expected value of 500 u. This will in turn lead to severe misinterpretation of a mass spectrum (Chap. 6).

3.5.3 Mass Accuracy

The *absolute mass accuracy*, $\Delta m/z$, is defined as the difference between *measured accurate mass* and *calculated exact mass*:

$$\Delta m/z = m/z_{\text{experimental}} - m/z_{\text{calculated}} \tag{3.13}$$

Instead of stating the absolute mass accuracy in units of u, it can also be given as *relative mass accuracy*, $\delta m/m$, i.e., absolute mass accuracy divided by the mass it is determined for:

$$\delta m/m = (\Delta m/z) / (m/z) \tag{3.14}$$

The *relative mass accuracy*, $\delta m/m$, is normally given in *parts per million* (ppm). As mass spectrometers tend to have similar absolute mass accuracies over a comparatively wide range, absolute mass accuracy represents a more meaningful way of stating mass accuracies than the use of ppm.

Note: *Parts per million* (1 ppm = 10^{-6}) is simply a relative measure as are percent (%) or permill (parts per thousand, ‰). In addition, *parts per billion* (1 ppb = 10^{-9}), and *parts per trillion* (1 ppt = 10^{-12}) are in use.

Example: A magnetic sector mass spectrometer allows for an absolute mass accuracy of $\Delta m/z$ = 0.002–0.005 u in scanning mode over a range of about m/z 50–1500. At m/z 1200 an error of $\Delta m/z$ = 0.003 u corresponds to inconspicuous $\delta m/m$ = 2.5 ppm, whereas the same error yields 60 ppm at m/z 50, which appears to be unacceptably high.

3.5.4 Accuracy and Precision

The concepts of *accuracy* and *precision* can best be illustrated using the analogy to a target where the center represents the true value of some physical quantity [38]. Accuracy describes the deviation of the experimental value from the true value, which normally is rather an accepted reference value than a "true" one in the strict sense. Accuracy is high (A+ in Fig. 3.19) if the values from several measurements are close to the reference value. Accuracy depends on systematic errors of an experiment. Precision describes the deviation within a group of determinations and it is high (P+ in Fig. 3.19) if the values from several measurements are in close proximity to but not necessarily identical with the reference value. Precision is an expression of random error, e.g., as introduced by noise, variation in injection volumes or times. *Repeatability* and *reproducibility* are two aspects of precision. Repeatability is connected to the repetition of the same measurement on the same setup within a short time frame while reproducibility is related to long term stability of a setup and inter-platform or inter-operator effects. Suitable statistical evaluation of a widespread dataset can result in an accurate determination of a quantity at the cost of lower precision (P– A?), e.g., root-mean-square deviation (Chap. 3.6.4) [39,40].

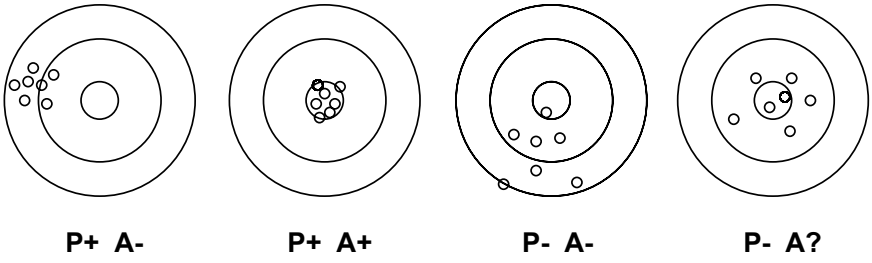


Fig. 3.19. Precision (**P**) and accuracy (**A**), along with seven hits on a target.

3.5.5 Mass Accuracy and the Determination of Molecular Formulas

Assuming infinite mass accuracy, we should be able to identify the molecular formula of any ion merely on the basis of its exact mass – the emphasis is on *infinite* mass accuracy (Chap. 3.5.1). In reality we are dealing with errors in the order of one to several ppm depending on the type of instrument and the mode of its operation.

Example: The number of possible even-electron ionic formulas based on an unrestricted selection among the elements C, H, N, and O as a function of relative mass error strongly depends on the *m/z* value of the ion. Here, the formulas proposed for the measured signals from $[(\text{arginine})_{1–5}+\text{H}]^+$ cluster ions, *m/z* 175.1189, 349.2309, 523.3427, 697.4548, and 871.5666 were counted for different relative mass error. While the lowest-mass ion is undoubtedly identified up to 5 ppm, the second ion is only unambiguously identified up to 2 ppm (Fig. 3.20). Allowing sulfur ($S_{0–2}$) in addition would already result in 18 rather than the 7 hits shown for the $[(\text{arginine})_3+\text{H}]^+$ ion, *m/z* 523.3427, at 2 ppm error. Taking also odd-electron ions into account would contribute another 15 compositions to this selection. In case of the $[(\text{arginine})_5+\text{H}]^+$ ion, *m/z* 871.5666, the number of C, H, N, O hits reaches 26 at 1 ppm error and even 232 at 10 ppm.

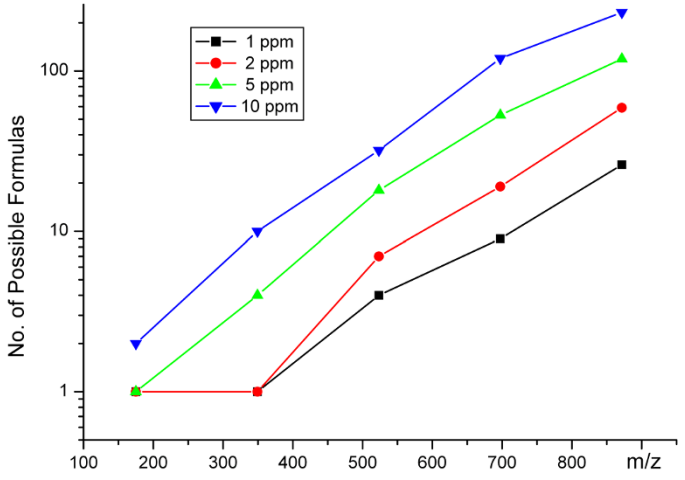


Fig. 3.20. Number of possible even-electron ionic formulas based on a free selection among the elements C, H, N, O as a function of relative mass error vs. *m/z*. The data points correspond to $[(\text{arginine})_{1–5}+\text{H}]^+$ cluster ions, *m/z* 175.1189, 349.2309, 523.3427, 697.4548, and 871.5666. The lines are meant as visual guides.

Unequivocal formula assignment by accurate mass alone only works in a range up to about *m/z* 500 depending on the particular restrictions [41]. Obviously, for ions of larger *m/z* the number of hits rapidly increases beyond a reasonable limit. Even at a high mass accuracy of 1 ppm and with the particular case of peptides the elemental composition can only be unambiguously identified up to about 800 u

[42-44]. Determining the formula of a peptide among all natural peptide compositions possible at *m/z* 1005.4433 requires $\delta m/m = 0.1$ ppm [45].

The situation becomes more complicated as more elements and fewer limitations of their number must be taken into account. In practice, one must try to restrict oneself to certain elements and a maximum and/or minimum number of certain isotopes to assure a high degree of confidence in the assignment of formulas. Isotopic patterns provide a prime source of such additional information. Combining the information from accurate mass data and experimental peak intensities with calculated isotopic patterns allows to significantly reduce the number of potential elemental compositions of a particular ion [46,47].

3.5.6 Extreme Mass Accuracy – Special Considerations

Even when we have determined a molecular formula, it does not tell us much about the structure of the molecule. According to the *mass–energy equivalence* (1 u = 931.5 MeV), a mass accuracy of 1 ppm ($\delta m/m = 10^{-6}$) roughly corresponds to an energy of 100 keV if an ion of *m/z* 100 is considered. A mass accuracy of 1 ppb ($\delta m/m = 10^{-9}$) still corresponds to an energy of 100 eV, and thus, 1 ppt ($\delta m/m = 10^{-12}$) would be required to approach energy differences of 0.1 eV, i.e., between isomers. Obviously, isomers are (almost) perfect isobars [48]. Nonetheless, it is worth noting that physicist are approaching 10 ppt, at least in the case of single atomic species (Fig. 3.21).

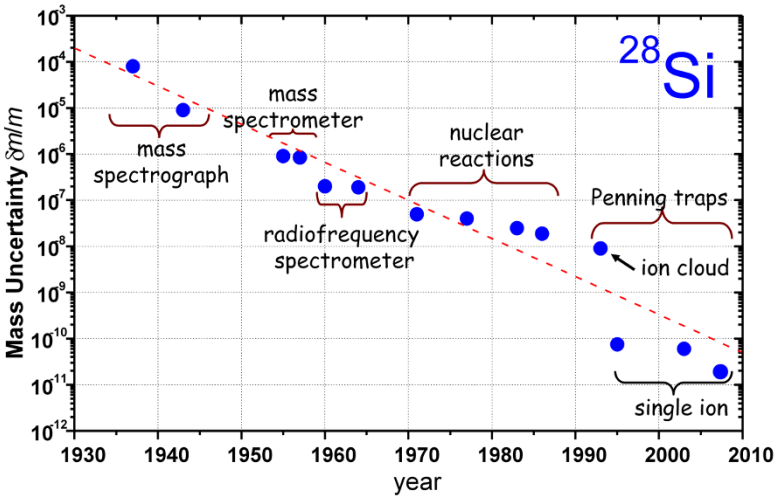


Fig. 3.21. Relative mass uncertainty $\delta m/m$ for ^{28}Si as a function of time. The most accurate mass of ^{28}Si so far is $m_{(28Si)} = 27.876\ 926\ 534\ 96(62)$ u corresponding to an uncertainty of 0.2 ppt. The *dashed line* serves as a visual orientation and reveals an improvement in accuracy by about one order of magnitude per decade. By courtesy of H.-J. Kluge, GSI Helmholtz Centre for Heavy Ion Research GmbH, Darmstadt, Germany.

3.6 Applied High-Resolution Mass Spectrometry

Generally, *high-resolution mass spectrometry* (HR-MS) aims to achieve both high mass resolution and high mass accuracy. These quantities have been introduced without considering the means by which they can be measured. The key to this problem is *mass calibration*. Resolution alone can separate ions with *m/z* in close proximity, but it does not automatically reveal where on the *m/z* axis the respective signals are located. This section deals with the techniques for establishing accurate mass data and their analytical evaluation [32,33].

3.6.1 External Mass Calibration

All mass spectrometers require mass calibration before they are put to use. However, proper procedures and the number of required calibration points may largely differ between different types of mass analyzers. Typically, this necessitates several peaks of well-known *m/z* values evenly distributed over the mass range of interest. These are supplied from a well-known *mass calibration compound* or *mass reference compound*. Calibration is then performed by recording a mass spectrum of the *calibration compound* and subsequent correlation of experimental *m/z* values to the *mass reference list* [33,49,50]. Usually, this conversion of the mass reference list to a calibration is accomplished by the mass spectrometer's software. Thus, the mass spectrum is recalibrated by interpolation of the *m/z* scale between the assigned calibration peaks to obtain the best match. The mass calibration obtained may then be stored in a *calibration file* and used for future measurements without the presence of a calibration compound. This procedure is termed *external mass calibration*.

Note: The numerous ionization methods and mass analyzers in use have created a demand for a large number of calibration compounds to suit their specific needs. Therefore, mass calibration will variously be addressed at the end of the chapters on ionization methods. It is also not possible to specify a general level of mass accuracy with external calibration. Depending on the type of mass analyzer and on the frequency of recalibration, mass accuracy can vary from mediocre 0.5 u to perfect 10^{-3} u.

Example: *Perfluorokerosene* (PFK) is a well-established mass calibration standard in EI-MS. It provides evenly spaced $C_xF_y^+$ fragment ions over a wide range (Figs. 3.22 and 3.23). The major ions are all mass deficient, with CHF_2^+, *m/z* 51.0046, being the only exception. PFK mixtures are available from low-boiling to high-boiling grades which may be used up to *m/z* 700–1100. Apart from the highest boiling grades, PFK is suitable to be introduced by the reference inlet (Chap. 5.2.1), a property making it attractive for internal calibration as well. Perfluorotributylamine, PFTBA (more often termed FC-43) is another frequently used calibrant, a pure compound delivering peaks up to *m/z* 614 in EI spectra [40,50].

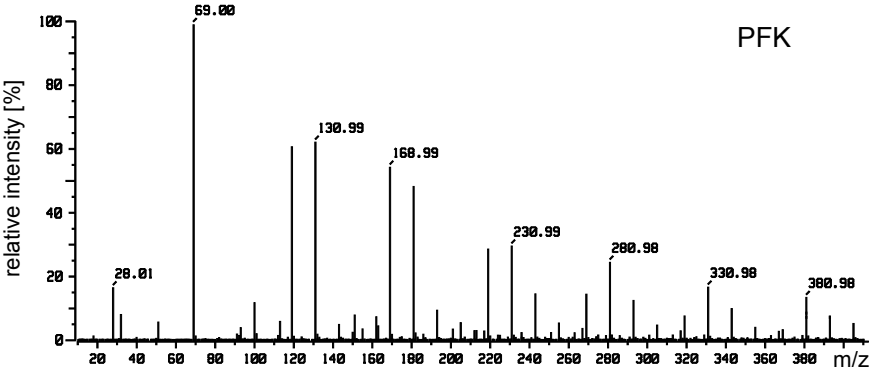


Fig. 3.22. Perfluorokerosene, PFK: partial 70-eV EI mass spectrum. The peaks are evenly distributed over a wide *m/z* range. Also, peaks from residual air occur in the low *m/z* range.

calculated m/z of mass reference

not assigned as reference masses

relative intensity of peaks

assigned value of magnet current in arbitrary units

No.	STD-m/z	Int.	Pos.
1	1.0078	0.0	0
2	4.0026	0.0	0
3	18.0106	1.1	155289
4	28.0061	12.4	307693
5	31.9898	6.1	360716
6	39.9624	0.8	457947
7	43.9898	0.0	0
8	51.0046	4.4	578153
9	68.9952	100.0	749596
10	92.9952	3.1	947601
11	99.9936	8.9	1000568
12	118.9920	45.4	1136056
13	130.9920	46.5	1216350
14	142.9920	3.8	1293209
15	154.9920	2.8	1367064
16	168.9888	40.6	1449851
17	180.9888	36.1	1518276
18	192.9888	7.2	1584564
19	204.9888	4.3	1648914
20	218.9856	21.5	1721755
21	230.9856	22.2	1782476
22	242.9856	11.0	1841691
23	254.9856	4.2	1899529
24	268.9824	10.9	1965392
25	280.9824	18.4	2020563
26	292.9824	9.5	2074630
27	304.9824	3.7	2127653
28	318.9792	5.8	2188219
29	330.9792	12.6	2239166
30	342.9792	7.5	2289210
31	354.9792	3.1	2338447
32	366.9792	2.2	2386888
33	380.9760	10.1	2442422
34	392.9760	5.8	2489260
35	404.9760	4.0	2535438

Fig. 3.23. Reproduction of a partial PFK calibration table (*m/z* 1–305 range) of a magnetic sector instrument. In order to expand the PFK reference peak list to the low *m/z* range, ^{1}H, ^{4}He, and peaks from residual air are included, but for intensity reasons ^{1}H, ^{4}He, and CO_2 have not been assigned in this particular case.

3.6.2 Internal Mass Calibration

Elemental compositions are preferably assigned via *internal mass calibration*. The calibration compound can be introduced from a second inlet system or be mixed with the analyte prior to analysis. Mixing calibration compounds with the analyte requires some operational skills in order for it not to modify the analyte or to be modified itself. Therefore, a separate inlet for introducing the calibration compound is preferred. This can be done by introducing volatile standards such as PFK from a reference inlet system in electron ionization, by use of a dual-target probe in fast atom bombardment, or by use of a second sprayer in electrospray ionization.

Internal mass calibration typically affords mass accuracies in the order of 0.1–0.5 ppm with FT-ICR, 0.5–1 ppm with orbitrap, 0.5–5 ppm with magnetic sector, and 1–10 ppm with time-of-flight analyzers. Mass accuracy strongly depends on various parameters such as resolving power, scan rate, scanning method, signal-to-noise ratio of the peaks, peak shapes, overlap of isotopic peaks at same nominal mass, mass difference between adjacent reference peaks etc. The experimentally determined accurate mass should be within a reasonable error range independent of the ionization method and the instrument used [51]. The correct (expected) composition is not necessarily the one with the least error.

Note: Mass accuracy may suffer from too high settings of resolving power if this causes noisy peaks. Often centroids are determined more accurately from smooth and symmetrically shaped peaks at moderate HR. One should be aware of the fact that the position of a peak of 0.1 u width, for example, has to be determined to $^1/_{50}$ of its width to obtain 0.002 u accuracy [32].

Example: For zirconium complexes the molecular ion range of an HR-EI spectrum is typified by the isotopic pattern of zirconium and chlorine (Fig. 3.24). ^{90}Zr represents the most abundant zirconium isotope which is accompanied by ^{91}Zr, ^{92}Zr, ^{94}Zr, and ^{96}Zr, all of them having considerable abundances. If the peak at *m/z* 414.9223 represents the monoisotopic ion, then the elemental composition containing ^{90}Zr and ^{35}Cl is the only correct interpretation. Thus, the formula $C_{16}H_{14}NCl_3Zr$ can be identified from the composition list (Fig. 3.25). Next, the X+2 and X+4 compositions should mainly be due to $^{35}Cl_2{}^{37}Cl$ and $^{35}Cl_{37}Cl_2$, respectively, leading to their identification. All formulas must have a remainder of $C_{16}H_{14}N$ in common. In this example, $R = 8000$ is the minimum to separate the PFK reference peak at *m/z* 417 from that of the analyte. Otherwise, the mass assignment would have been wrong because the peak at *m/z* 417 would then be centered at a weighted mass average of its two contributors. Alternatively, such a peak may be omitted from both reference list and composition list.

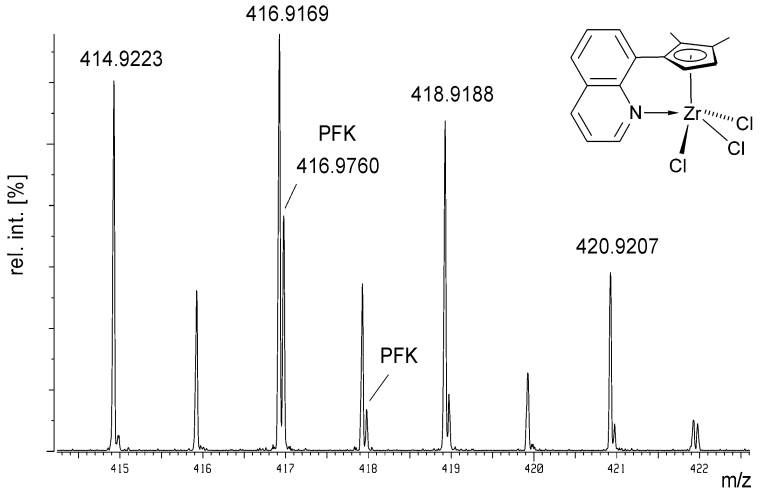


Fig. 3.24. Partial high-resolution EI mass spectrum in the molecular ion region of a zirconium complex. At $R = 8000$ the PFK ion can barely be separated from the slightly more mass-deficient analyte ion. By courtesy of M. Enders, Heidelberg University.

Observed m/z	Int%	Err[ppm / mmu]	U.S.	Composition
414.9223	7.5	-0.4 / -0.2	22.5	C 23 H 2 N 2 35Cl 37Cl 2
	→	-3.9 / -1.6	10.0	C 16 H 14 N 35Cl 3 Zr
		-15.3 / -6.3	15.0	C 19 H 11 N 35Cl 37Cl Zr
		-0.8 / -0.3	15.5	C 20 H 11 37Cl 2 Zr
416.9169	8.9	-6.2 / -2.6	22.5	C 23 H 2 N 2 37Cl 3
		+3.1 / +1.3	28.0	C 26 H N Zr
	→	-9.7 / -4.0	10.0	C 16 H 14 N 35Cl 2 37Cl Zr
		+9.1 / +3.8	15.5	C 18 H 9 N 2 37Cl 2 Zr
		+4.8 / +2.0	10.5	C 17 H 14 35Cl 37Cl 2 Zr
418.9188	7.5	-8.2 / -3.4	24.5	C 26 H 2 35Cl 3
		+0.2 / +0.1	27.5	C 25 H N 2 Zr
		-4.2 / -1.7	22.5	C 24 H 6 35Cl Zr
	→	+1.8 / +0.8	10.0	C 16 H 14 N 35Cl 37Cl 2 Zr

Fig. 3.25. Suggested elemental compositions of the Zr complex shown in Fig. 3.24. The error for each proposal is listed in units of ppm and mmu (0.001 u). U.S. = "unsaturation", i.e., the number of rings and/or double bonds (Chap. 6.4.4). Here the correct assignments are highlighted with an *arrow*. By courtesy of M. Enders, Heidelberg University.

Basic Rules: The assignment of molecular formulas from accurate mass
- must always be in accordance with the experimentally observed and the calculated isotopic pattern for the assumed composition,
- the formula has to obey the nitrogen rule (Chap. 6.2.7),
- depending on the ionization method, even-electron or odd-electron ions may be formed exclusively, and thus can rule out some compositions, and
- formulas in contradiction to one of these points are erroneous.

3.6.3 Compiling Mass Reference Lists

A reference list may be compiled once the mass spectrum of a calibration standard is known and the elemental composition of the ions that are to be included in the mass reference list are established by an independent measurement,.For this purpose, the listed reference masses should be calculated using six decimal digits. Otherwise, one runs a chance of obtaining erroneous reference values, especially when masses of ion series are calculated by multiplication of a subunit. This can easily be done using conventional spreadsheet applications.

Example: Cesium iodide is frequently used for mass calibration in fast atom bombardment (FAB) mass spectrometry (Chap. 10) because it yields cluster ions of the general formula $[Cs(CsI)_n]^+$ in positive-ion and $[I(CsI)_n]^-$ in negative-ion mode. For the $[Cs(CsI)_{10}]^+$ cluster ion, *m/z* 2730.9 is calculated instead of the correct value *m/z* 2731.00405 by applying only one decimal digit rather than the exact values M_{133Cs} = 132.905447 and M_{127I} = 126.904468. The error of 0.104 u is acceptable for LR work, but definitely unacceptable if accurate mass measurements are needed.

```
[ Elemental Composition ]
Data  : JMS18120_009                  Date : 14-May-2002 08:20
Sample: CHCl3
Elements : C 10/1(12C 10/0, 13C 1/0), H 10/0, Cl 4/0(35Cl 4/0, 37Cl 4/0)
Mass Tolerance      : 10mmu
Unsaturation (U.S.) : -200.0 - 200.0

Observed m/z Int%   Err[ppm / mmu]    U.S.  Composition
   82.9433   100.0    +27.5 /  +2.3    1.0  13C 35Cl 2
                      -26.4 /  -2.2    0.5  12C H 35Cl 2

   84.9406    62.5    +29.5 /  +2.5    1.0  13C 35Cl 37Cl
                      -23.2 /  -2.0    0.5  12C H 35Cl 37Cl

   86.9379    10.1    +31.6 /  +2.7    1.0  13C 37Cl 2
                      -19.9 /  -1.7    0.5  12C H 37Cl 2

Observed m/z Int%   Err[ppm / mmu]    U.S.  Composition
   82.9449   100.0    +45.8 /  +3.8    1.0  13C 35Cl 2
                       -8.1 /  -0.7    0.5  12C H 35Cl 2

   84.9422    66.0    +48.0 /  +4.1    1.0  13C 35Cl 37Cl
                       -4.7 /  -0.4    0.5  12C H 35Cl 37Cl

   86.9404    11.2    +60.3 /  +5.2    1.0  13C 37Cl 2
                       +8.9 /  +0.8    0.5  12C H 37Cl 2

Observed m/z Int%   Err[ppm / mmu]    U.S.  Composition
   82.9447   100.0    +43.7 /  +3.6    1.0  13C 35Cl 2
                      -10.2 /  -0.8    0.5  12C H 35Cl 2

   84.9419    65.1    +44.6 /  +3.8    1.0  13C 35Cl 37Cl
                       -8.1 /  -0.7    0.5  12C H 35Cl 37Cl

   86.9391    10.8    +45.1 /  +3.9    1.0  13C 37Cl 2
                       -6.3 /  -0.6    0.5  12C H 37Cl 2
```

Fig. 3.26. Chloroform – Printout of elemental compositions of $[M–Cl]^+$ ions as obtained from three subsequent measurements (70 eV EI, R = 8000). The error for each proposal is listed in units of ppm and "mmu". U.S. ("unsaturation") is the number of rings and/or double bonds (Chap. 6.4.4).

3.6.4 Specification of Mass Accuracy

Measured accurate masses, when used to assign molecular formulas, should always be accompanied by their mass accuracies. [52]. Ideally, this can be done by giving the mean mass value and the corresponding error in terms of standard deviation through several repeated measurements of the same ion. [40] This is definitely not identical to the error usually provided with a mass spectrometer's software, where the error is based on the difference of a single pair of calculated and measured values. The reduction of the average mass error goes with the square root of the number of determinations (Chap. 3.5.4) [39].

Example: The $[M\text{-}Cl]^+$ ion, $[CHCl_2]^+$, represents the base peak in the EI spectrum of chloroform. The results of three subsequent determinations for the major peaks of the isotopic pattern are listed below (Fig. 3.26). The typical printout of a mass spectrometer's data system provides experimental accurate mass and relative intensity of the signal along with absolute and relative mass error as calculated for a set of suggested formulas. Here, the experimentally accurate mass values yield a root-mean-square of 82.9442 ± 0.0006 u for the $[^{12}CH^{35}Cl_2]^+$ ion. The comparatively small standard deviation of 0.0006 u corresponds to a relative error of 7.5 ppm.

3.6.5 Deltamass

The term *deltamass* has been coined to define the mass value following the decimal point [53] thereby elegantly circumventing the somewhat unfortunate terminology related to the mass defect. The deltamass concept is only valid in the context for which it has been developed, i.e., to describe mass deviations of peptides from average values. Beyond this context, ambiguities arise from its rigorous application because *i*) a mass defect would then be expressed the same way as larger values of negative mass defect, e.g., in case of $^{127}I^+$ as 0.9045 u and in case of $C_{54}H_{110}^{+\bullet}$ as 0.8608 u, respectively, and *ii*) deviations of more than 1 u would be expressed by the same numerical value as those of less than 1 u.

Example: The magnitude of mass defect can provide an idea of what compound class is being analyzed (Chap. 3.5.2). At a sufficient level of sophistication, mass defect can even reveal more detail [43]. Peptides consist of amino acids and therefore, their elemental compositions are rather similar independent of their size or sequence. This results in a characteristic relationship of formulas and deltamass values. Phosphorylation and more pronounced glycosylation cause lower deltamass, because they introduce mass-deficient atoms (P, O) into the molecule. The large number of hydrogens associated with lipidation, on the other side, contributes to a deltamass above normal level. On the average, an unmodified peptide of 1968 u, for example, shows a deltamass of 0.99 u, whereas a glycosylated peptide of the same nominal mass will have a value of 0.76 u. Thus, the deltamass can be employed to obtain information on the type of covalent protein modification [53].

3.6.6 Kendrick Mass Scale

The intention of the *Kendrick mass scale* is to provide data reduction in a way that homologs can be recognzed by their identical *Kendrick mass defect* (KMD). Due to the steadily increasing resolution and mass accuracy of modern instrumentation this issue is again gaining importance for complex mixture analysis by MS. The Kendrick mass scale is based on the definition $M_{(CH_2)} = 14.0000$ u [54]. The conversion factor from the IUPAC mass scale, m_{IUPAC}, to the Kendrick mass scale, $m_{Kendrick}$, is therefore 14.000000/14.015650 = 0.9988834:

$$m_{Kendrick} = 0.9988834\ m_{IUPAC} \tag{3.15}$$

Next, we define the *Kendrick mass defect*, $m_{defectKendrick}$, as

$$m_{defectKendrick} = m_{nomKendrick} - m_{Kendrick} = \text{KMD} \tag{3.16}$$

where $m_{nomKendrick}$ is the *nominal Kendrick mass*, the closest integer to Kendrick mass (cf. example next page).

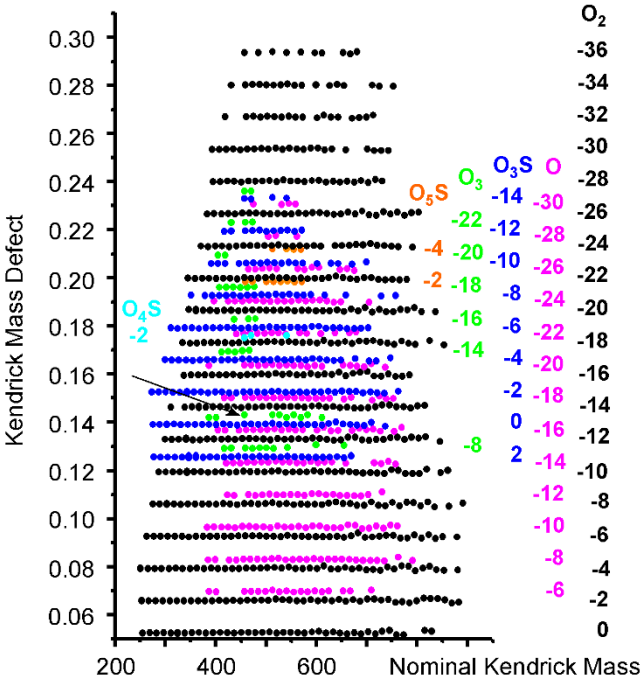


Fig. 3.27. Kendrick mass defect vs. nominal Kendrick mass for odd-mass $^{12}C_x$ ions ($[M–H]^-$ ions). The compound classes (O, O_2, O_3S, and O_4S) and the different numbers of rings plus double bonds (Chap. 6.4.4) are separated vertically. Horizontally, the points are spaced by CH_2 groups along a homologous series [55]. By courtesy of A.G. Marshall, NHFL, Tallahassee.

Example: The IUPAC mass of $[C_{30}H_{49}O_3]^-$ is 457.3687 u. The Kendrick mass of this ion is calculated as 457.3687 u × 0.9988834 = 456.8580 u. From this it follows that $m_{\text{nomKendrick}}$ = 457 u. The Kendrick mass defect of this ion is thus obtained as $m_{\text{defectKendrick}}$ = 457 u – 456.8580 u = 0.1419 u.

To translate spectral data into a useful *Kendrick mass plot*, a high-resolution mass spectrum is broken into segments of 1 u, which are aligned on the abscissa. Then, the Kendrick mass defect of the isobaric ions contained in the respective segment is plotted onto the ordinate. The resulting graph preserves not only the "coarse" spacing, e.g., about 1 u between odd and even mass values, but also the "fine structure", i.e., different Kendrick mass defects (KMDs) for different elemental compositions across each segment. Homologs are now easily recognized as horizontal rows in the plot [55].

Example: Crude oil / diesel fuel – In a Kendrick plot the composition of complex systems can be conveniently displayed. Several thousand elemental compositions in the ultra-high resolution spectrum of petroleum crude oil [55] or diesel fuel [56] may be resolved. Such samples consist of numerous compound classes and/or alkylation series with some 30 homologs each that can be visually identified (Fig. 3.27). The formula employed for the preceding example is marked in the plot by an arrow.

3.6.7 Van Krevelen Diagrams

There is yet another tool for the display of composition characteristics of complex mixtures, the *van Krevelen diagram* [57]. The van Krevelen diagram is a plot of the atomic H/C ratio against the atomic O/C ratio. This plot causes the products related by reactions such as decarboxylation, dehydration, dehydrogenation, or oxidation to be displayed along straight lines. Along with KMD plots, the van Krevelen plot is therefore a major tool for the assessment of complex organic mixtures such as crude oil and its refinery products or the wide field of *natural organic matter* (NOM) that represents the largest share of biomass on earth [58-62].

Example: Deep-sea *dissolved organic matter* (DOM) – The van Krevelen diagrams show a group of molecules having low H/C (< 0.9) and low O/C (< 0.25) ratios clearly separated from each other (Fig. 3.28) [61]. An enlarged view of this group shows that it comprises 224 different molecular formulas corresponding to molecules that contain up to 35 rings and/or double bonds (r+d, Chap. 6.4.4). Homologous series can be identified along straight lines. Still this does not tell the complete structure of those molecules, but it delivers much more insight into the composition of DOM than pure accurate mass data alone.

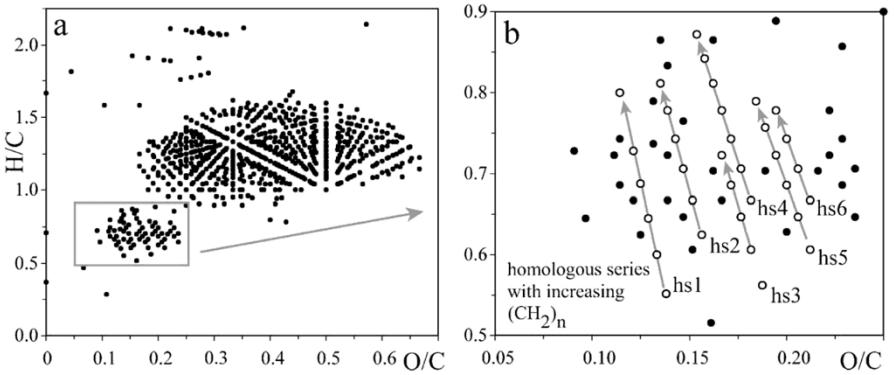


Fig. 3.28. Van Krevelen diagrams of deep-sea DOM. (**a**) Presentation of all molecules in 3500 m and 4600 m water depth. (**b**) Enlarged region of condensed polyaromatics where the members of the homologous series $(CH_2)_n$ with $n \geq 4$ are shown as *white circles* and connected along a *gray line*. Reproduced from Ref. [61] with permission. © Elsevier Science Publishers, 2006.

3.7 Resolution Interacting with Isotopic Patterns

3.7.1 Multiple Isotopic Compositions at Very High Resolution

We started our lesson on isotopic patterns with the unspoken assumption of nominal mass resolution, which makes it much easier to understand how isotopic patterns are formed. The procedure of summing up all isotopic abundances contributing to the same nominal mass is correct as long as very high resolution is not employed. In that case, following such a simplified protocol is acceptable, because generally isobaric isotopolog ions are very similar in mass [24].

In the earlier introduction of resolution it should have become clear that very high resolution is capable of separating different isotopic compositions of the same nominal mass, thereby giving rise to multiple peaks on the same nominal *m/z* (Figs. 3.15, 3.16, 3.24). In molecules with masses of around 10,000 u, a single unresolved isotopic peak may consist of as many as 20 different isotopic compositions (also cf. Fig. 3.31) [63,64].

Example: $C_{16}H_{20}OSi$ – Numerous isotopologs contribute to its isotopic pattern. Among them the monoisotopic ion at *m/z* 256.1283 is the most abundant (Fig. 3.29). For the first isotopic peak at *m/z* 257 the major contribution derives from ^{13}C, but ^{29}Si and ^{17}O also play a role. Actually, ^{2}H should also be considered, but has been omitted due to its extremely low isotopic abundance. As the isotopologs of the same nominal *m/z* are not true isobars, their intensities will not sum up in one common peak. Instead, they are detected side by side provided sufficient resolving power is available. The pair $^{13}C^{12}C_{15}H_{20}{}^{16}OSi$, *m/z* 257.13171, and $^{12}C_{16}H_{20}{}^{17}OSi$, *m/z* 257.13257, roughly necessitates 3×10^5 resolution

(R = 257/0.00086 = 299,000). There are six different compositions contributing to the second isotopic peak at *m/z* 258 and even eight for the third isotopic peak at *m/z* 259. Again, it is the merit of FT-ICR-MS that resolutions in the order of several 10^5 are now available although *ultrahigh resolution*, as this is termed, is still not fully routine on those instruments (Chap. 4).

m/z	composition	rel.int. [%]	
256.12836	C16.H20.O.Si	100.00000	monoisotopic
257.12790	C16.H20.O.29Si	5.10957	1st isotopic
257.13171	C15.13C.H20.O.Si	17.92663	
257.13257	C16.H20.17O.Si	0.03709	
258.12518	C16.H20.O.30Si	3.38468	2nd isotopic
258.13126	C15.13C.H20.O.29Si	0.91597	
258.13214	C16.H20.17O.29Si	0.00190	
258.13260	C16.H20.18O.Si	0.20449	
258.13507	C14.13C2.H20.O.Si	1.50639	
258.13593	C15.13C.H20.17O.Si	0.00665	
259.12854	C15.13C.H20.O.30Si	0.60676	3rd isotopic
259.12939	C16.H20.17O.30Si	0.00126	
259.13214	C16.H20.18O.29Si	0.01045	
259.13461	C14.13C2.H20.O.29Si	0.07697	
259.13550	C15.13C.H20.17O.29Si	0.00034	
259.13596	C15.13C.H20.18O.Si	0.03666	
259.13843	C13.13C3.H20.O.Si	0.07876	
259.13928	C14.13C2.H20.17O.Si	0.00056	
260.12943	C16.H20.18O.30Si	0.00692	4th isotopic
260.13190	C14.13C2.H20.O.30Si	0.05099	
260.13275	C15.13C.H20.17O.30Si	0.00023	
260.13550	C15.13C.H20.18O.29Si	0.00187	
260.13797	C13.13C3.H20.O.29Si	0.00402	
260.13885	C14.13C2.H20.17O.29Si	0.00003	
260.13931	C14.13C2.H20.18O.Si	0.00308	
260.14175	C12.13C4.H20.O.Si	0.00287	
260.14264	C13.13C3.H20.17O.Si	0.00003	

Fig. 3.29. $C_{16}H_{20}OSi$ – Tabular representation of the theoretical isotopic distribution at infinite resolution. The contribution of ^2H is not considered, and isotopic peaks above *m/z* 260 are omitted due to their minor intensities.

Example: Peptides often contain sulfur from cysteine. Provided there are at least two cysteines in the peptide molecule, sulfur can be in the form of thiol group (SH, reduced) or sulfur bridges (S–S, oxidized). Often, both forms are contained in the same sample. At ultrahigh resolution, the contributions of these compositions to the same nominal *m/z* can be distinguished. The ultrahigh-resolution matrix-assisted laser desorption/ionization (MALDI) FT-ICR mass spectrum of native and reduced [D-Pen^{2,5}]enkephalin is an example of such a separation (Fig. 3.30) [65]. The left expanded view shows fully resolved peaks due to ^{34}S and $^{13}C_2$ isotopomers of the native and the all-^{12}C peak of the reduced compound at *m/z* 648. The right expansion reveals the $^{13}C_1{}^{34}S$ peak of the native plus the $^{13}C_1$ signal of the reduced form at *m/z* 649. Here, R_{FWHM} is more than 9×10^5.

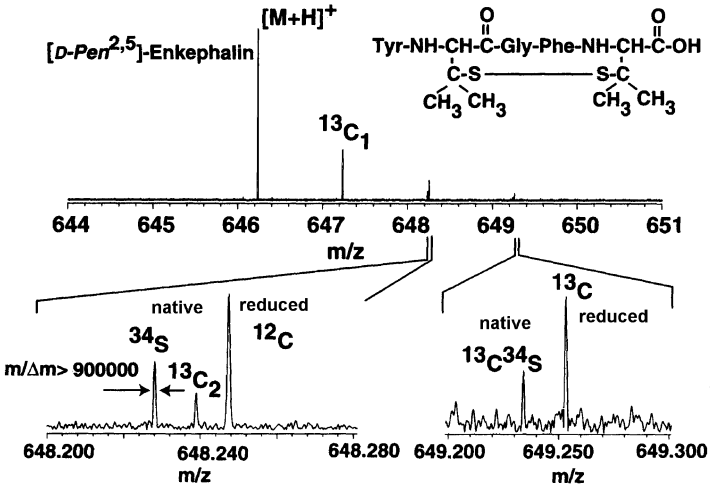


Fig. 3.30. [D-Pen^{2,5}]Enkephalin – Ultrahigh-resolution MALDI-FT-ICR mass spectrum of native (S–S) and reduced (2 × SH).forms. The expanded *m/z* views of the second and third isotopic peak show fully mass-resolved signals. Reproduced from Ref. [65] with permission. © American Chemical Society, 1997.

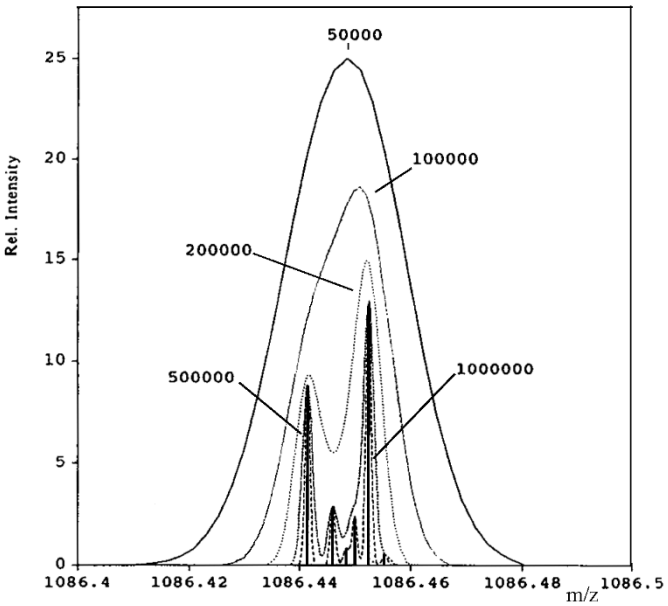


Fig. 3.31. Arg^8 vasopressin – Theoretical effect of resolution on the shape of the M+2 peak at *m/z* 1086.4. Theoretical mass spectra of the [vasopressin+H]$^+$ ion and the five indicated resolution values (FWHM) have been superimposed and the bar spectrum corresponds to infinite resolution. Adapted from Ref. [64] with permission. © John Wiley and Sons Ltd., 1994.

3.7.2 Isotopologs and Accurate Mass

It has been pointed out that routine accurate mass measurements are conducted at resolutions which are normally too low to separate isobaric isotopologs. Unfortunately, multiple isotopic compositions under the same signal tend to distort the peak shape (Fig. 3.31) [64]. This effect causes problems when elemental compositions have to be determined from such multi-isotopolog peaks, e.g., if the monoisotopic peak is too weak as in case of many transition metals. Generally, the observed decrease in mass accuracy is not dramatic and is somewhat counterbalanced by the information derived from the isotopic pattern. However, it can be observed that mass accuracy decreases by about 50% on such unresolved signals.

If isotopolog ions are resolved or if certain isotopologs are free from interference, and provided sufficient mass accuracy is available, the distance between isotopic peaks can yield a new type of analytical information. As are the isotopic masses themselves, the differences between isotopic masses are characteristic for certain elements. Boron for example, has a small mass difference of just 0.9964 u between ^{10}B and ^{11}B, whereas the pair of ^{191}Ir and ^{193}Ir presents a rare example of a difference clearly above 2 u, which is still distinguishable from hydrogenation. Determination of $\Delta m/z$ values can thus help to distinguish between hydrogenation and X+2 element isotopic peaks can ascertain the presence of boron vs. loss of a hydrogen radical etc. Some helpful values are compiled in Table 3.2. Obviously, there are also limits to this approach, for example, when a decision between M+2 due to ^{37}Cl or ^{65}Cu is called for, in particular, as their isotopic abundances are also similar.

Table 3.2. Characteristic mass differences to identify the presence of elements

Pair of isotopes or modification	Δm [u]
^{6}Li vs. ^{7}Li	1.0009
^{10}B vs. ^{11}B	0.9964
^{12}C vs. ^{13}C	1.0033
^{32}S vs. ^{34}S	1.9958
^{35}Cl vs. ^{37}Cl	1.9970
^{58}Ni vs. ^{60}Ni	1.9955
^{63}Cu vs. ^{65}Cu	1.9982
^{79}Br vs. ^{81}Br	1.9980
^{191}Ir vs. ^{193}Ir	2.0023
gain or loss of H	1.0078
gain or loss of H_2	2.0156

3.7.3 Large Molecules – Isotopic Patterns at Sufficient Resolution

Terms such as *large molecules* or *high mass* are subject to steady change in mass spectrometry as new techniques for analyzing high-mass ions are being developed or improved [66]. Here, the focus is on masses in the range of 10^3–10^4 u.

With increasing *m/z* the center of the isotopic pattern, i.e., the *average molecular mass*, is shifted to values higher than the *monoisotopic mass*. The center, i.e., the average mass, may not be represented by a real peak, but it tends to be close to the peak of *most abundant mass* (Fig. 3.32). The monoisotopic mass is of course still related to a real signal, but it may be of such a low intensity that it is difficult to recognize. Finally, the *nominal mass* becomes a mere number which is no longer useful to describe the molecular weight [37,63].

The calculation of isotopic patterns of molecules of several 10^3 u is not a trivial task, because slight variations in the relative abundances of the isotopes encountered gain relevance and may shift the most abundant mass and the average mass up or down by 1 u. In a similar fashion the algorithm and the number of iterations employed to perform the actual calculation affect the final result [24].

Note: The calculation of relative molecular mass, M_r, of organic molecules exceeding 2000 u is significantly influenced by the basis it is performed on. Both the atomic weights of the constituent elements and the natural variations in isotopic abundance contribute to the differences between *monoisotopic*- and *relative atomic mass-based* M_r values. In addition, they tend to characteristically differ between major classes of biomolecules. This is primarily because of molar carbon content, e.g., the difference between polypeptides and nucleic acids is about 4 u at M_r = 25,000 u. Considering terrestrial sources alone, variations in the isotopic abundance of carbon lead to differences of about 10–25 ppm in M_r which is significant with respect to mass measurement accuracy in the region up to several 10^3 u [37].

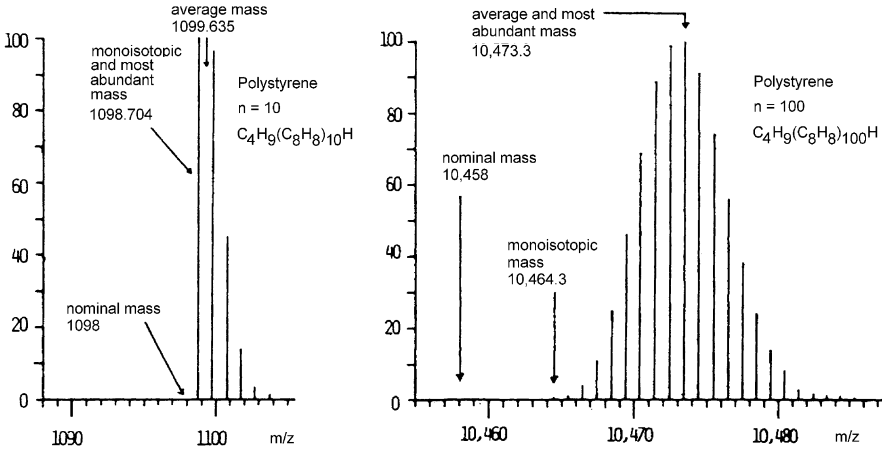


Fig. 3.32. Polystyrene – calculated isotopic patterns of. large ions. Adapted from Ref. [63] with permission. © American Chemical Society, 1983.

3.7.4 Large Molecules – Isotopic Patterns at Low Resolution

It is certainly desirable to have at least sufficient resolution to resolve isotopic patterns to their nominal mass contributions. However, not every mass analyzer is capable of doing so with any ion it can pass through. Such conditions often occur when ions of several thousand u are being analyzed by quadrupole, time-of-flight or quadrupole ion trap analyzers, and hence it is useful to know about the changes in spectral appearance and their effect on peak width and detected mass [64].

Example: $[C_{254}H_{378}N_{65}O_{75}S_6]^+$ of Bovine Insulin – isotopic pattern of the $[M+H]^+$ ion calculated for $R_{10\%} = 1000$, 4000, and 10,000. At $R = 1000$ the isotopic peaks are not resolved (Fig. 3.33) and an envelope smoothly covering the isotopic peaks is observed instead; it is even slightly wider than the real isotopic pattern. The maximum of this envelope is in good agreement with the calculated average mass, i.e., the molecular weight (Eq. 3.2). At $R = 4000$ the isotopic peaks become sufficiently resolved to be recognized as such. The *m/z* values are very close to the corresponding isotopic masses; however, there can be some minor shifts due to their still significant overlap. Finally, at $R = 10{,}000$ the isotopic pattern is well resolved and interferences between isotopic peaks are avoided. The next step, i.e., to resolve the multiple isotopic contributions to each of the peaks would require $R > 10^6$.

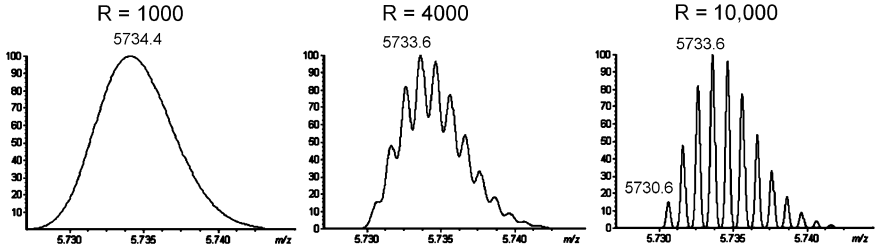


Fig. 3.33. Bovine insulin – the isotopic pattern calculated for $[M+H]^+$ at different resolutions ($R_{10\%}$). Note that the envelope at $R = 1000$ is wider than the real isotopic pattern.

3.8 Charge State and Interaction with Isotopic Patterns

Even though singly charged ions seem to be the dominant species in mass spectrometry at first sight, there are many applications where doubly and multiply charged ions are of utmost importance. In electrospray ionization (Chap. 12) even extremely high *charge states* can be observed, e.g., up to 60-fold in case of proteins of about 60,000 u molecular weight. Doubly and triply charged ions are also common in electron ionization (Chaps. 5, 6) and field desorption (Chap. 8).

The effect of higher charge states are worth considering. As z increases from 1 to 2, 3 etc., the numerical value of *m/z* is reduced by a factor of 2, 3 etc., i.e., the ion will be detected at lower *m/z* than the corresponding singly charged ion of the same mass. In general, the entire *m/z* scale is compressed by a factor of z if $z > 1$.

Consequently, the isotopic peaks are then located at $^1/_z$ u distance. Vice versa, the charge state is obtained from the reciprocal value of the distance between adjacent peaks, e.g., peaks at $^1/_3$ u correspond to triply charged ions. The reasons for the compression of the *m/z* scale are discussed later (Chap. 4).

Example: C_{60} – EI mass spectrum, also showing an abundant doubly charged molecular ion, C_{60}^{2+}, at *m/z* 360 with its isotopic peaks located at $\Delta m/z = 0.5$ distance and a $C_{60}^{3+\bullet}$ signal at *m/z* 240 of very low intensity (Fig. 3.34) [29]. The isotopic pattern remains unaffected by the charge state. As a consequence of the compressed *m/z* scale, the doubly charged C_{58}^{2+} fragment ion is detected at *m/z* 348.

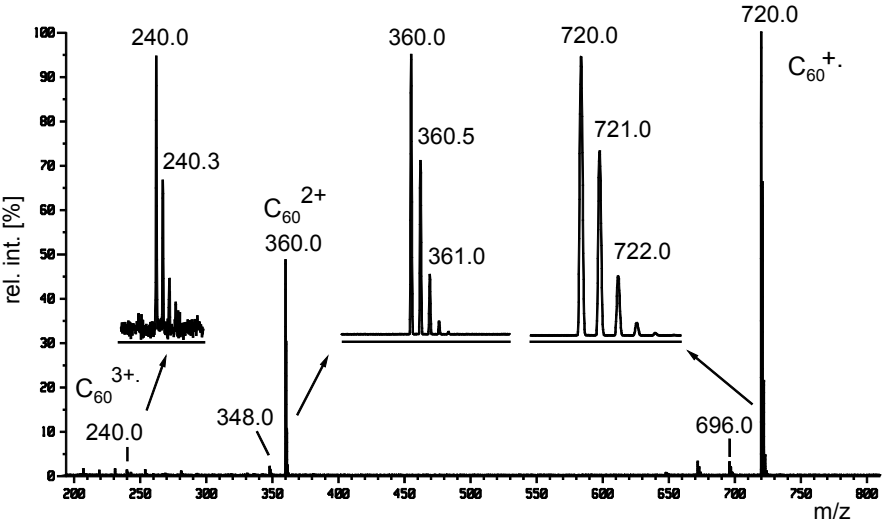


Fig. 3.34. [60]Fullerene – EI mass spectrum.. The insets show the expanded signals of $M^{+\bullet}$, M^{2+}, and $M^{3+\bullet}$ ions. The signals of the patterns are $\Delta m/z = 1$, 0.5, and 0.33, respectively. The intensity scale has been normalized in the insets to allow for easier comparison of the isotopic patterns. By courtesy of W. Krätschmer, Max Planck Institute for Nuclear Physics, Heidelberg.

Note: Isotopic distributions remain unaffected by the charge state of an ion as far as the relative intensities are concerned. However, the distance between the peaks is reduced by $^1/_z$, thus allowing multiply charged ions to be easily distinguished from singly charged ions and their charge state to be determined.

References

1. de Laeter, J.R.; De Bièvre, P.; Peiser, H.S. Isotope Mass Spectrometry in Metrology. *Mass Spectrom. Rev.* **1992,** *11*, 193-245.
2. Audi, G. The History of Nuclidic Masses and of Their Evaluation. *Int. J. Mass Spectrom.* **2006,** *251*, 85-94.
3. Budzikiewicz, H.; Grigsby, R.D. Mass Spectrometry and Isotopes: A Century of Research and Discussion. *Mass Spectrom. Rev.* **2006,** *25*, 146-157.
4. Todd, J.F.J. Recommendations for Nomenclature and Symbolism for Mass Spectroscopy Including an Appendix of Terms Used in Vacuum Technology. *Int. J. Mass Spectrom. Ion. Proc.* **1995,** *142*, 211-240.
5. McLafferty, F.W.; Turecek, F. *Interpretation of Mass Spectra;* 4th ed.; University Science Books: Mill Valley, 1993.
6. Sparkman, O.D. *Mass Spec Desk Reference*; Global View Publ: Pittsburgh, 2000.
7. IUPAC Isotopic Composition of the Elements 1997. *Pure Appl. Chem.* **1998,** *70*, 217-235.
8. IUPAC; Coplen, T.P. Atomic Weights of the Elements 1999. *Pure Appl. Chem.* **2001,** *73*, 667-683.
9. Price, P. Standard Definitions of Terms Relating to Mass Spectrometry. A Report From the Committee on Measurements and Standards of the Amercian Society for Mass Spectrometry. *J. Am. Soc. Mass Spectrom.* **1991,** *2*, 336-348.
10. Busch, K.L. Units in Mass Spectrometry. *Spectroscopy* **2001,** *16*, 28-31.
11. Platzner, I.T. Applications of Isotope Ratio Mass Spectrometry, in *Modern Isotope Ratio Mass Spectrometry*; Wiley: Chichester, 1997; pp. 403-447.
12. Ferrer, I.; Thurman, E.M. Measuring the Mass of an Electron by LC/TOF-MS: A Study of "Twin Ions". *Anal. Chem.* **2005,** *77*, 3394-3400.
13. Ferrer, I.; Thurman, E.M. Importance of the Electron Mass in the Calculations of Exact Mass by Time-of-Flight Mass Spectrometry. *Rapid Commun. Mass Spectrom.* **2007,** *21*, 2538-2539.
14. Schmidt, H.L. Food Quality Control and Studies on Human Nutrition by Mass Spectrometric and Nuclear Magnetic Resonance Isotope Ratio Determination. *Fresenius' Zeitschrift für Analytische Chemie* **1986,** *324*, 760-766.
15. Beavis, R.C. Chemical Mass of Carbon in Proteins. *Anal. Chem.* **1993,** *65*, 496-497.
16. Carle, R. Isotopen-Massenspektrometrie: Grundlagen Und Anwendungsmöglichkeiten. *Chem. Unserer Zeit* **1991,** *20*, 75-82.
17. Förstel, H. The Natural Fingerprint of Stable Isotopes - Use of IRMS to Test Food Authenticity. *Anal. Bioanal. Chem.* **2007,** *388*, 541-544.
18. Busch, K.L. Isotopes and Mass Spectrometry. *Spectroscopy* **1997,** *12*, 22-26.
19. Beynon, J.H. The Compilation of a Table of Mass and Abundance Values, in *Mass spectrometry and its applications to organic chemistry*; Elsevier: Amsterdam, 1960; Chapter 8.3, pp. 294-302.
20. McLafferty, F.W.; Turecek, F. *Interpretation of Mass Spectra;* 4th ed.; University Science Books: Mill Valley, 1993.
21. Margrave, J.L.; Polansky, R.B. Relative Abundance Calculations for Isotopic Molecular Species. *J. Chem. Educ.* **1962,** 335-337.
22. Yergey, J.A. A General Approach to Calculating Isotopic Distributions for Mass Spectrometry. *Int. J. Mass Spectrom. Ion Phys.* **1983,** *52*, 337-349.
23. Hsu, C.S. Diophantine Approach to Isotopic Abundance Calculations. *Anal. Chem.* **1984,** *56*, 1356-1361.
24. Kubinyi, H. Calculation of Isotope Distributions in Mass Spectrometry. A Trivial Solution for a Non-Trivial Problem. *Anal. Chim. Acta* **1991,** *247*, 107-119.
25. Frauenkron, M.; Berkessel, A.; Gross, J.H. Analysis of Ruthenium Carbonyl-Porphyrin Complexes: a Comparison of Matrix-Assisted Laser Desorption/Ionization Time-of-Flight, Fast-Atom Bombardment and Field Desorption Mass Spectrometry. *Eur. Mass Spectrom.* **1997,** *3*, 427-438.
26. Giesa, S.; Gross, J.H.; Hull, W.E.; Lebedkin, S.; Gromov, A.; Krätschmer, W.; Gleiter, R. $C_{120}OS$: the First Sulfur-Containing Dimeric [60]Fullerene Derivative. *Chem. Commun.* **1999,** 465-466.
27. Luffer, D.R.; Schram, K.H. Electron Ionization Mass Spectrometry of Syn-

thetic C_{60}. *Rapid Commun. Mass Spectrom.* **1990,** *4*, 552-556.
28. Srivastava, S.K.; Saunders, W. Ionization of C_{60} (Buckminsterfullerene) by Electron Impact. *Rapid Commun. Mass Spectrom.* **1993,** *7*, 610-613.
29. Scheier, P.; Dünser, B.; Märk, T.D. Production and Stability of Multiply-Charged C_{60}. *Electrochem. Soc. Proc.* **1995,** *95-10*, 1378-1394.
30. Thomas, A.F. *Deuterium Labeling in Organic Chemistry;* Appleton-Century-Crofts: New York, 1971.
31. Kaltashov, I.A.; Eyles, S.J. *Mass Spectrometry in Biophysics: Conformation and Dynamics of Biomolecules;* Wiley: Hoboken, 2005.
32. Balogh, M.P. Debating Resolution and Mass Accuracy in Mass Spectrometry. *Spectroscopy* **2004,** *19*, 34-38,40.
33. Bristow, A.W.T. Accurate Mass Measurement for the Determination of Elemental Formula - a Tutorial. *Mass Spectrometry Reviews* **2006,** *25*, 99-111.
34. Leslie, A.D.; Volmer, D.A. Dealing With the Masses: a Tutorial on Accurate Masses, Mass Uncertainties, and Mass Defects. *Spectroscopy* **2007,** *22*, 32,34-32,39.
35. Busch, K.L. The Resurgence of Exact Mass Measurement With FTMS. *Spectroscopy* **2000,** *15*, 22-27.
36. Beynon, J.H. Qualitative Analysis of Organic Compounds by Mass Spectrometry. *Nature* **1954,** *174*, 735-737.
37. Pomerantz, S.C.; McCloskey, J.A. Fractional Mass Values of Large Molecules. *Org. Mass Spectrom.* **1987,** *22*, 251-253.
38. Boyd, R.K.; Basic, C.; Bethem, R.A. *Trace Quantitative Analysis by Mass Spectrometry;*Wiley: Chichester, 2008.
39. Kilburn, K.D.; Lewis, P.H.; Underwood, J.G.; Evans, S.; Holmes, J.; Dean, M. Quality of Mass and Intensity Measurements From a High Performance Mass Spectrometer. *Anal. Chem.* **1979,** *51*, 1420-1425.
40. Sack, T.M.; Lapp, R.L.; Gross, M.L.; Kimble, B.J. A Method for the Statistical Evaluation of Accurate Mass Measurement Quality. *Int. J. Mass Spectrom. Ion Proc.* **1984,** *61*, 191-213.
41. Kim, S.; Rodgers, R.P.; Marshall, A.G. Truly "Exact" Mass: Elemental Composition Can Be Determined Uniquely From Molecular Mass Measurement at Approximately 0.1 mDa Accuracy for Molecules up to Approximately 500 Da. *Int. J. Mass Spectrom.* **2006,** *251*, 260-265.
42. Zubarev, R.A.; Demirev, P.A.; Håkansson, P.; Sundqvist, B.U.R. Approaches and Limits for Accurate Mass Characterization of Large Biomolecules. *Anal. Chem.* **1995,** *67*, 3793-3798.
43. Zubarev, R.A.; Håkansson, P.; Sundqvist, B. Accuracy Requirements for Peptide Characterization by Monoisotopic Molecular Mass Measurements. *Anal. Chem.* **1996,** *68*, 4060-4063.
44. Clauser, K.R.; Baker, P.; Burlingame, A. Role of Accurate Mass Measurement (±10 Ppm) in Protein Identification Strategies Employing MS or MS/MS and Database Searching. *Anal. Chem.* **1999,** *71*, 2871-2882.
45. Spengler, B. De Novo Sequencing, Peptide Composition Analysis, and Composition-Based Sequencing: a New Strategy Employing Accurate Mass Determination by Fourier Transform Ion Cyclotron Resonance Mass Spectrometry. *J. Am. Soc. Mass Spectrom.* **2004,** *15*, 703-714.
46. Roussis, S.G.; Proulx, R. Reduction of Chemical Formulas From the Isotopic Peak Distributions of High-Resolution Mass Spectra. *Anal. Chem.* **2003,** *75*, 1470-1482.
47. Stoll, N.; Schmidt, E.; Thurow, K. Isotope Pattern Evaluation for the Reduction of Elemental Compositions Assigned to High-Resolution Mass Spectral Data From Electrospray Ionization Fourier Transform Ion Cyclotron Resonance Mass Spectrometry. *J. Am. Soc. Mass Spectrom.* **2006,** *17*, 1692-1699.
48. Marshall, A.G.; Hendrickson, C.L.; Shi, S.D.H. Scaling MS Plateaus With High-Resolution FT-ICR-MS. *Anal. Chem.* **2002,** *74*, 252A-259A.
49. Busch, K.L. Masses in Mass Spectrometry: Balancing the Analytical Scales. *Spectroscopy* **2004,** *19*, 32-34.
50. Busch, K.L. Masses in Mass Spectrometry: Perfluors and More. Part II. *Spectroscopy* **2005,** *20*, 76-81.
51. Bristow, A.W.T.; Webb, K.S. Intercomparison Study on Accurate Mass Measurement of Small Molecules in Mass Spectrometry. *J. Am. Soc. Mass Spectrom.* **2003,** *14*, 1086-1098.

52. Gross, M.L. Accurate Masses for Structure Confirmation. *J. Am. Soc. Mass Spectrom.* **1994,** *5*, Editorial.
53. Lehmann, W.D.; Bohne, A.; von der Lieth, C.W. The Information Encrypted in Accurate Peptide Masses-Improved Protein Identification and Assistance in Glycopeptide Identification and Characterization. *J. Mass Spectrom.* **2000,** *35*, 1335-1341.
54. Kendrick, E. Mass Scale Based on CH_2 = 14.0000 for High-Resolution Mass Spectrometry of Organic Compounds. *Anal. Chem.* **1963,** *35*, 2146-2154.
55. Hughey, C.A.; Hendrickson, C.L.; Rodgers, R.P.; Marshall, A.G. Kendrick Mass Defect Spectrum: A Compact Visual Analysis for Ultrahigh-Resolution Broadband Mass Spectra. *Anal. Chem.* **2001,** *73*, 4676-4681.
56. Hughey, C.A.; Hendrickson, C.L.; Rodgers, R.P.; Marshall, A.G. Elemental Composition Analysis of Processed and Unprocessed Diesel Fuel by Electrospray Ionization Fourier Transform Ion Cyclotron Resonance Mass Spectrometry. *Energy Fuels* **2001,** *15*, 1186-1193.
57. van Krevelen, D.W. Graphical-Statistical Method for the Study of Structure and Reaction Processes of Coal. *Fuel* **1950,** *29*, 269-284.
58. Wu, Z.; Rodgers, R.P.; Marshall, A.G. Two- and Three-Dimensional Van Krevelen Diagrams: A Graphical Analysis Complementary to the Kendrick Mass Plot for Sorting Elemental Compositions of Complex Organic Mixtures Based on Ultrahigh-Resolution Broadband Fourier Transform Ion Cyclotron Resonance Mass Measurements. *Anal. Chem.* **2004,** *76*, 2511-2516.
59. Kim, S.; Kramer, R.W.; Hatcher, P.G. Graphical Method for Analysis of Ultrahigh-Resolution Broadband Mass Spectra of Natural Organic Matter, the Van Krevelen Diagram. *Anal. Chem.* **2003,** *75*, 5336-5344.
60. Hertkorn, N.; Benner, R.; Frommberger, M.; Schmitt-Kopplin, P.; Witt, M.; Kaiser, K.; Kettrup, A.; Hedges, J.I. Characterization of a Major Refractory Component of Marine Dissolved Organic Matter. *Geochimica et Cosmochimica Acta* **2006,** *70*, 2990-3010.
61. Dittmar, T.; Koch, B.P. Thermogenic Organic Matter Dissolved in the Abyssal Ocean. *Marine Chemistry* **2006,** *102*, 208-217.
62. Koch, B.P.; Dittmar, T. From Mass to Structure: an Aromaticity Index for High-Resolution Mass Data of Natural Organic Matter. *Rapid Commun. Mass Spectrom.* **2005,** *20*, 926-932.
63. Yergey, J.; Heller, D.; Hansen, G.; Cotter, R.J.; Fenselau, C. Isotopic Distributions in Mass Spectra of Large Molecules. *Anal. Chem.* **1983,** *55*, 353-356.
64. Werlen, R.C. Effect of Resolution on the Shape of Mass Spectra of Proteins: Some Theoretical Considerations. *Rapid Commun. Mass Spectrom.* **1994,** *8*, 976-980.
65. Solouki, T.; Emmet, M.R.; Guan, S.; Marshall, A.G. Detection, Number, and Sequence Location of Sulfur-Containing Amino Acids and Disulfide Bridges in Peptides by Ultrahigh-Resolution MALDI-FTICR Mass Spectrometry. *Anal. Chem.* **1997,** *69*, 1163-1168.
66. Matsuo, T.; Sakurai, T.; Ito, H.; Wada, Y. "High Masses". *Int. J. Mass Spectrom. Ion Proc.* **1991,** *118/119*, 635-659.

4 Instrumentation

Learning Objectives

- Separating ions by *m/z* – basic principles
- Mass analyzers as designed from basic principles
- Types of mass analyzers and their modes of operation
- Guiding, collimating, and focusing ions along a path
- Hybrid instruments
- Detectors for mass-analyzed ions
- Vacuum generation for mass spectrometry
- Ability to judge fitness for purpose of commercial instruments

"A modern mass spectrometer is constructed from elements which approach the state-of-the-art in solid-state electronics, vacuum systems, magnet design, precision machining, and computerized data acquisition and processing" [1]. This is and has ever been a fully valid statement about mass spectrometers.

Table 4.1. Common mass analyzers

Type	Acronym	Principle
Time-of-flight	TOF	Time dispersion of a pulsed ion beam; separation by time-of-flight
Magnetic sector	B	Deflection of a continuous ion beam; separation by momentum in magnetic field due to Lorentz force
Linear quadrupole	Q	Continuous ion beam in linear radio frequency quadrupole field; separation due to instability of ion trajectories
Linear quadrupole ion trap	LIT	Continuous ion beam delivers ions for trapping; storage, and eventually separation in linear radio frequency quadrupole field by resonant excitation
Quadrupole ion trap	QIT	Trapped ions; separation in three-dimensional radio frequency quadrupole field by resonant excitation
Fourier transform-ion cyclotron resonance	FT-ICR	Trapped ions in magnetic field (Lorentz force); separation by cyclotron frequency, image current detection and Fourier transformation of transient signal
Orbitrap	orbitrap	Axial oscillation in inhomogeneous electric field; detection of frequency after Fourier transformation of transient signal

J. Gross, *Mass Spectrometry*, 2nd ed., DOI 10.1007/978-3-642-10711-5_4,
© Springer-Verlag Berlin Heidelberg 2011

Under the headline of instrumentation we shall mainly discuss the different types of mass analyzers in order to understand their basic principles of operation, their specific properties, and their performance characteristics. Of course, this is only one aspect of instrumentation; hence topics such as ion detection and vacuum generation will also be addressed in brief.

As a matter of fact, sample introduction is more closely related to particular ionization methods than to the type of mass analyzer employed, and therefore, this issue is treated in the corresponding chapters on ionization methods. The order of treatment in this chapter neither reflects their ever-changing individual predominance in mass spectrometry nor does it follow a strictly historic time line. Rather, an attempt is made to follow a trail of easiest understanding.

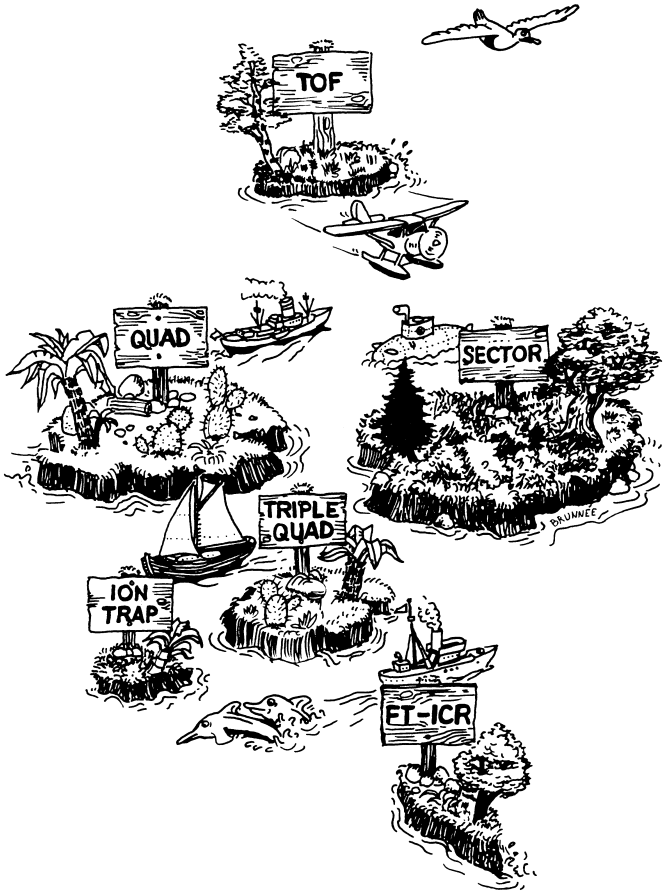


Fig. 4.1. Mass spectrometer islands as presented in a cartoon by C. Brunnée in 1987. The actual situation is quite different, however: much of the cliffs of the sector and quad islands have vanished in the sea while all others have gained new land, and moreover, the orbitrap island has been given birth in the south east. Reproduced from Ref. [2] with permission. © Elsevier Science, 1987.

From the very beginning to the present almost any physical principle ranging from time-of-flight to cyclotron motion has been employed to construct mass-analyzing devices (Fig 4.1). Some were extremely successful at the time of their invention, for others it took decades until their potential had fully been recognized. The basic types of mass analyzers employed for analytical mass spectrometry are summarized in Table 4.1.

The properties of an ideal mass analyzer are well described [2], but despite the tremendous improvements made, still no mass analyzer is perfect. To reach a deeper insight into the evolution of mass spectrometers the articles by Beynon [3], Habfast and Aulinger [4,5], Brunnée [6,7], Chapman et al. [8], and McLuckey [9] are recommended for further reading. In recent years, there has been a growing interest in employing miniature mass analyzers for *in situ* analysis [10], for instance in environmental [11] and biochemical applications [12], for process monitoring, for detection of chemical warfare agents, for extraterrestrial applications [13], and for improving the safety of the Space Shuttle [14]. The most promising development, however, has been a new mass analyzer – the orbitrap by Makarov [15].

4.1 How to Create a Beam of Ions

Consider an ion that is brought into or generated within an electric field between two oppositely charged plates of a capacitor. Such an ion will be accelerated towards the plate of opposite charge. If the attracting plate has a hole or a slit, an ion beam is produced by this simple ion source. Assuming the spread in ion kinetic

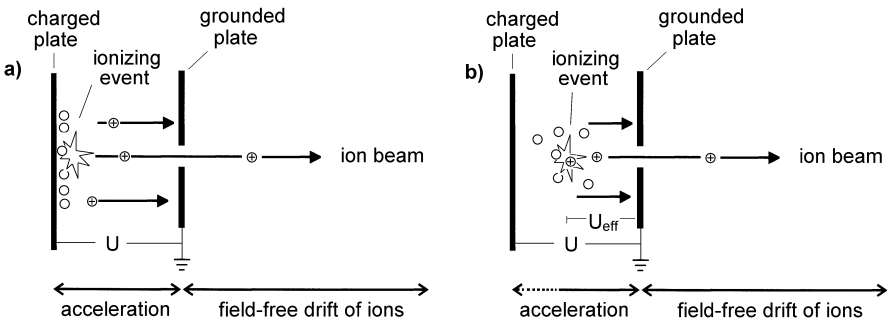


Fig. 4.2. Simple single-stage ion sources. (**a**) Ionization from a surface or probe where the ionizing event is located on the charged plate; in reality ionizing events in a spatially confined volume above the surface have to be taken into account. (**b**) Gas phase ionization, where the effective accelerating voltage U_{eff} depends on the actual position of the ion between the plates. After a neutral has been ionized (positive in this illustration), it is attracted by the opposite grounded plate. Those ions passing through a hole of the grounded electrode create an ion beam emerging into the field-free region behind. The ion beam produced by such a primitive ion source is not parallel, but has some angular spread.

energy to be small as compared to the total ion kinetic energy, i.e., $\Delta E_{kin} << E_{kin}$, the beam can be considered to be monoenergetic. The actual charge of an ion may be either positive or negative depending on the ionization method employed. Changing the polarity of the plates causes a switch from the extraction of positive ions to negative ions or vice versa. For practical reasons, the attracting electrode is usually grounded and the pushing plate is set to high voltage. Doing so allows to keep the whole mass analyzer grounded, thereby contributing substantially to safety of operation (Fig. 4.2). The extraction of ions and the shape of the ion beam can largely be improved if the acceleration voltage is applied in two [16] or more successive stages instead of a single one and if ion optical lenses are part of the ion acceleration assembly.

4.2 Time-of-Flight Instruments

4.2.1 Time-of-Flight – Basic Principles

The first *time-of-flight* (TOF) analyzer was constructed and published in 1946 by W. E. Stephens [17]. The principle of TOF is quite simple: ions of different *m/z* are dispersed in time during their flight along a field-free drift path of known length. Provided all the ions start their journey at the same time or at least within a sufficiently short time interval, the lighter ones will arrive earlier at the detector than the heavier ones. This demands that they emerge from a pulsed ion source which can be realized either by pulsing ion packages out of a continuous beam or more conveniently by employing a true pulsed ionization method.

Soon, other groups embarked on Stephens' concept [18] and increasingly useful TOF instruments were designed and constructed [16,19,20] leading to their first commercialization by Bendix in the mid-1950s. These first-generation TOF instruments were designed for gas chromatography-mass spectrometry (GC-MS) coupling [21,22]. Their performance was poor as compared to modern TOF analyzers, but the specific advantage of TOF over the competing magnetic sector instruments was the rate of spectra they were able to deliver per second (Fig. 4.3). In GC-MS the TOF analyzer soon became superseded by linear quadrupole analyzers and it was not until the late 1980s that development of TOF analyzers encountered a revival [23,24] – the success of pulsed ionization methods, especially of matrix-assisted laser desorption/ionization (MALDI), made this possible (Chap. 10). Therefore, we will repeatedly refer to MALDI in our discussion of TOF analyzers.

MALDI generated a great demand for mass analyzers which are suitable to be used in conjunction with a naturally pulsed ion source and capable of transmitting ions of extremely high mass up to several 10^5 u [25]. Since then, the performance of TOF instruments has tremendously increased [26,27]. TOF analyzers have been adapted for use with other ionization methods and – together with orbitraps and FT-ICR instruments – have superseded the established magnetic sector instruments in most applications [26,28].

The main advantages of TOF instruments are: *i*) that in principle, the *m/z* range is unlimited [29,30]; *ii*) from each ionizing event, i.e., a single laser shot in MALDI, a complete mass spectrum is obtained within several tens of microseconds; *iii*) improved transmission of TOF analyzers, with high sensitivity; *iv*) TOF instrument design and construction is comparatively simple and inexpensive; and *v*) recent instruments allow for accurate mass measurements and tandem MS experiments [31].

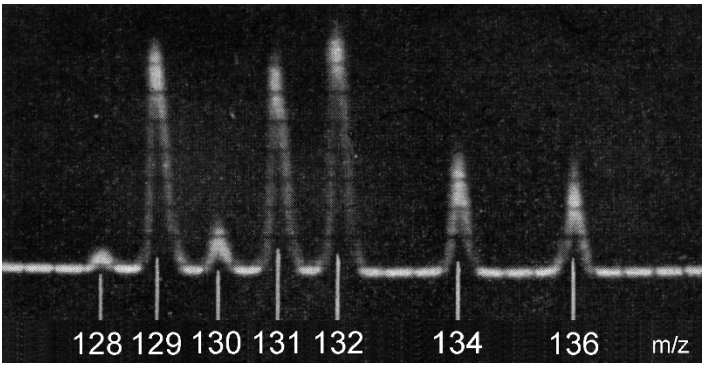


Fig. 4.3. Oscilloscope output of the electron ionization TOF spectrum of xenon on a Bendix TOF-MS. The *dark lines* are a grid on the oscilloscopic screen. (For the isotopic pattern of Xe cf. Fig. 3.1.) Adapted from Ref. [21] with permission. © Pergamon Press, 1959.

4.2.2 TOF Instruments – Velocity of Ions and Time-of-Flight

Independent of the ionization method, the electric charge q of an ion of mass m_i is equal to an integer number z of electron charges e, and thus $q = ez$. The energy uptake E_{el} by moving through a voltage U is given by

$$E_{el} = qU = ezU \tag{4.1}$$

Thereby, the former potential energy of a charged particle in an electric field is converted into kinetic energy E_{kin}, i.e., into translational motion

$$E_{el} = ezU = \frac{1}{2} m_i v^2 = E_{kin} \tag{4.2}$$

Assuming that the ion was initially at rest, which holds by first approximation, the velocity attained is calculated by rearranging Eq. 4.2 into

$$v = \sqrt{\frac{2ezU}{m_i}} \tag{4.3}$$

i.e., v is inversely proportional to the square root of mass.

Example: The velocity of the [60]fullerene molecular ion, $C_{60}^{+\bullet}$, after acceleration by 19.5 kV is obtained from Eq. 4.3 as

$$v = \sqrt{\frac{2 \cdot 1.6022 \times 10^{-19}\,\mathrm{C} \times 19{,}500\,\mathrm{V}}{1.1956 \times 10^{-24}\,\mathrm{kg}}} = 72{,}294\,\mathrm{m\,s^{-1}}$$

An ion velocity of 72,294 m s^{-1} appears rather high, but merely is 0.0024% of the speed of light. The acceleration voltages and thus, the ion velocities are the highest in TOF-MS, although magnetic sector instruments are operated with kilo-electron-volt ion beams, too (Chap. 4.3). The other types of mass analyzers require ions to enter at much lower kinetic energies.

Note: Equation 4.3 describes the velocity of any ion after acceleration in an electric field, and therefore it is valid not only for TOF-MS, but for any part of a mass spectrometer handling beams of ions.

One now can quite easily imagine measuring the time for an ion of unknown m/z in traveling a distance s after being accelerated by a voltage U. The relationship between velocity and time t needed for traveling the distance s is

$$t = \frac{s}{v} \tag{4.4}$$

which upon substitution of v by Eq. 4.3 becomes

$$t = \frac{s}{\sqrt{\frac{2ezU}{m_i}}} \tag{4.5}$$

Equation 4.5 yields the time needed for the ion to travel the distance s at constant velocity, i.e., in a *field-free* environment after the process of acceleration has been completed. Rearrangement of Eq. 4.5 reveals the relationship between the instrumental parameters s and U, the experimental value of t and the ratio m_i/z

$$\frac{m_i}{z} = \frac{2\,e\,U t^2}{s^2} \tag{4.6}$$

It is also obvious from Eq. 4.5 that the time to drift through a fixed length of field-free space is proportional to the square root of m_i/z

$$t = \frac{s}{\sqrt{2eU}} \sqrt{\frac{m_i}{z}} \tag{4.7}$$

and thus, the time interval Δt between the arrival times of ions of different m/z is proportional to $s \times (m_i/z_1^{\,½} - m_i/z_2^{\,½})$.

Note: Here, the ratio m_i/z denotes ion mass [kg] per number of electron charges. The index i at the mass symbol is used to avoid confusion with the *mass-to-charge ratio*, *m/z*, as used to specify the position of a peak on the abscissa of a mass spectrum (Chap. 1.2.3).

Example: According to Eq. 4.7 the $C_{60}^{+\bullet}$ ion, *m/z* 720, of the preceding example will travel through a field-free flight path of 2.0 m in 27.665 µs, while it takes slightly longer for its isotopolog $^{13}C^{12}C_{59}^{+\bullet}$, *m/z* 721. The proportionality to the square root of *m/z* gives (use of m_i/z values yields identical results as the dimension is cancelled)

$$\frac{t_{721}}{t_{720}} = \frac{\sqrt{721}}{\sqrt{720}} = 1.000694$$

Thus, t_{721} = 27.684 µs. This corresponds to a difference in time-of-flight of 19 ns under these conditions (cf. Fig. 4.7).

The proportionality of time-of-flight to the square root of *m/z* causes Δt for a given $\Delta m/z$ to decrease with increasing *m/z*: under otherwise the same conditions Δt per 1 u is calculated as 114 ns at *m/z* 20, 36 ns at *m/z* 200, and just 11 ns at *m/z* 2000. Therefore, the realization of a time-of-flight mass analyzer depends on the ability to measure short time intervals with sufficient accuracy [32-34]. At this point it becomes clear that the performance of the early TOF analyzers – among other reasons – suffered from the low-efficiency electronics of their time. It took until the mid-1990s to overcome this barrier [27].

The time-of-flight of multicharged ions ($z > 1$) explains the outcome of higher charge states for isotopic patterns (Chap. 3.8). As *z* increases to 2, 3 etc., the numerical value of *m/z* is reduced by a factor of 2, 3 etc., i.e., the ion will be detected at lower *m/z* than the corresponding single-charged ion of the same mass. According to Eq. 4.7, the time-of-flight is reduced by a factor of 1.414 (the square root of 2) for doubly charged ions which is the same time-of-flight as for a singly-charged ion of half of its mass. Accordingly, the time-of-flight is reduced by a factor of 1.732 (the square root of 3), for triply charged ions corresponding to a single-charged ion of one third of its mass.

Note: For multicharged ions, the *m/z* scale is compressed by a factor of *z* equal to the charge state of the ion. Isotopic patterns remain unaffected as far as the relative intensities are concerned. As the distance between isotopic peaks is reduced inversely proportional to *z*, the charge state can readily be assigned.

4.2.3 Linear Time-of-Flight Analyzer

Restricting its use to laser desorption/ionization (LDI) and matrix-assisted laser desorption/ionization (MALDI, Chap. 11), a simple TOF instrument can be set up as follows (Fig. 4.4): The analyte is supplied as a thin layer on a *sample holder* or

target upon which a pulsed laser is focused. The acceleration voltage U is applied between this target and a grounded counter electrode. Ions formed and desorbed during the laser pulse are continuously extracted and accelerated as they emerge from the target into the gas phase. When leaving the acceleration region s_0 the ions should possess equal kinetic energies. They drift down a field-free flight path s in the order of 1–2 m and finally hit the detector. Typically, *microchannel plate* (MCP) detectors are employed to compensate for the angular spread of the ion beam (Chap. 4.8.3). A fast *time-to-analog converter* (8 bit ADC) transforms the analog output of the detector for computer-based data storage and data processing. Such an instrumental setup where the ions are traveling on a straight line from the point of their creation to the detector is called *linear TOF*.

In principle, any other ionization method can be combined with a TOF analyzer even if it is not an intrinsically pulsed technique, provided there are means to extract ions in a pulsed manner from such an ion source (Chap. 4.2.6).

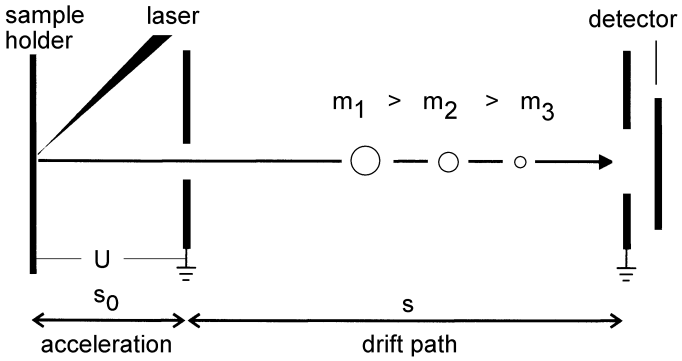


Fig. 4.4. Scheme of a linear TOF instrument. Once created during a laser pulse onto the sample layer, ions are continuously accelerated by a voltage U. While drifting along the field-free drift path s, they are dispersed in time. Lighter ions reach the detector first.

The drift time t_d as calculated by means of Eq. 4.7 is not fully identical to the total time-of-flight. Obviously, the time needed for acceleration of the ions t_a has to be added. Furthermore, a short period of time t_0 may be attributed to the laser pulse width and the process of desorption/ionization, which is typically in the order of a few nanoseconds. Thus, the total time-of-flight t_{total} is given by

$$t_{total} = t_0 + t_a + t_d \tag{4.8}$$

A rigorous mathematical treatment of the TOF analyzers as needed for the construction of such instruments of course has to include all contributions to the total time-of-flight [27,31-33,35-37].

The transmittance of a linear TOF analyzer approaches 90% because ion losses are solely caused by collisional scattering due to residual gas or by poor spatial focusing of the ion source. With a sufficiently large detector surface located at a short distance from the ion source exit, a very high fraction of the ions will be collected by the detector.

Even metastable decompositions during the flight do not reduce the intensity of a molecular ion signal, because the fragments formed conserve the velocity of the fragmenting ion and are therefore detected simultaneously with their intact precursors. In such a case, the ionic *and* the neutral fragment cause a response at the detector. These properties make the linear TOF analyzer the ideal device for analyzing easily fragmenting and/or high-mass analytes [38].

Note: The detection of neutrals formed by metastable fragmentation in linear TOF analyzers is one of the few exceptions where neutrals are handled and give rise to a signal in mass spectrometry.

The example in Chap. 4.2.2 demonstrates that the differences in time-of-flight of ions differing by 1 u in mass are in the order of about 10 ns at about *m/z* 1000. The time elapsing during desorption/ionization is roughly 10–50 ns in case of standard UV lasers, but can be longer with IR lasers. Consequently, the variation in starting times for ions of the same *m/z* value is often larger than the difference in time-of-flight of neighboring *m/z* values, thereby limiting the resolution.

Another effect is even worse: Laser-desorbed ions, for example, possess comparatively large initial kinetic energies of some 10 eV that are superimposed on the kinetic energy provided by the acceleration voltage, which is typically in the order of 10–30 kV. Obviously, higher acceleration voltages are advantageous in that they diminish the relative contribution of the energy distribution caused by the ionization process. Figure 4.5 illustrates the possible effects of deviations from the assumption that ions initially are at rest on an equipotential surface [34]. All these effects together limit resolution to $R \approx 500$ for continuous extraction linear TOF analyzers.

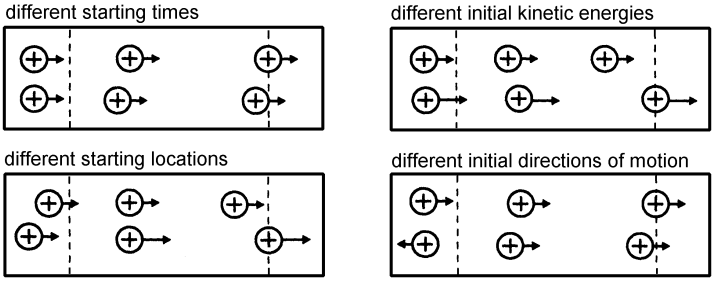


Fig. 4.5. Effects of initial time, space, and kinetic energy distributions on mass resolution in TOF-MS. Adapted from Ref. [34] with permission. © American Chemical Society, 1992.

Note: The spread in ion kinetic energies from thermal energy as well as from inhomogeneous acceleration presents a general problem in the construction of mass analyzers. Accordingly, there are numerous approaches to narrow down the kinetic energy distributions of ions or to compensate for their effects.

4.2.4 Reflector Time-of-Flight Analyzer

The *reflector* or *reflectron* was devised by Mamyrin in 1994 [39]. In the reflector TOF analyzer – often abbreviated *ReTOF* – the reflector acts as an ion mirror that focuses ions of different kinetic energies in time. Its performance is improved by using two-stage or even multistage reflector designs.

Commonly, reflector instruments are also equipped with a detector behind the reflector allowing linear mode operation simply by switching off the reflector voltage. A complete mathematical treatment of single-stage and two-stage reflectors is found in the literature [31-33,37]. Here, we will restrict ourselves to a qualitative explanation of the reflector.

A simple reflector consist of a retarding electric field located behind the field-free drift region opposed to the ion source. In practice, a reflector is comprised of a series of ring-shaped electrodes at increasing potential. The reflection voltage U_r is set to about 1.05–1.10 times the acceleration voltage U in order to ensure that all ions are reflected within the homogeneous portion of the electric field of the device (Fig. 4.6). The ions penetrate the reflectron until they reach zero kinetic energy and are then expelled from the reflector in opposite direction. The kinetic energy of the leaving ions remains unaffected, however their flight paths vary according to their differences in kinetic energy. Ions carrying more kinetic energy will fly deeper into the decelerating field, and thus spend more time within the reflector than less energetic ions. Thereby, the reflector effects a correction in time-

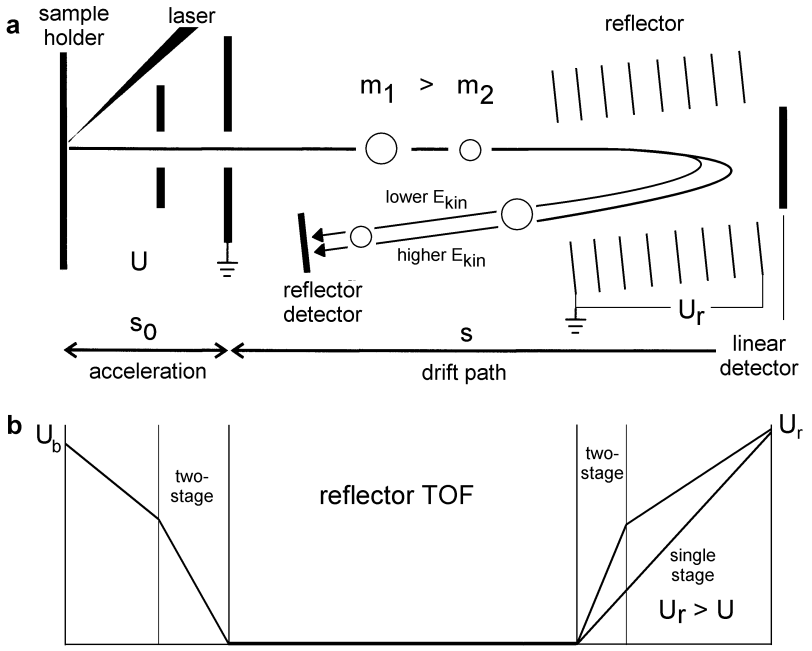


Fig. 4.6. ReTOF analyzer. (**a**) Principle of operation, (**b**) potentials along the instrument.

of-flight that substantially improves the resolving power of the TOF analyzer [27,32-34]. In addition, the reflector provides (imperfect) focusing with respect to angular spread of the ions leaving the source and it corrects for their spatial distribution [32,39]. Adjusting the reflector at a small angle with respect to the ions exiting from the source allows the reflector–detector to be placed adjacent to the ion source (Mamyrin design). Alternatively, a detector with a central hole to transmit the ions leaving the ion source has to be used in *coaxial reflectrons* (cf. Chap. 9.5.2).

Although the reflector elongates the flight path and hence the dispersion in time-of-flight, this effect is of lower importance than its capability to compensate for initial energy spread. Simple elongation of the flight path can also be achieved with longer flight tubes in linear instruments. However, too long flight paths may even decrease the overall performance of TOF analyzers due to loss of ions by angular spread of the ion beam and scattering of ions after collisions with residual gas.

The ability of the ReTOF to compensate for the initial energy spread of ions largely increases the resolving power of TOF instruments. While a typical continuous extraction TOF instrument in linear mode cannot resolve isotopic patterns of analytes above about *m/z* 500, it will do when operated in reflector mode (Fig. 4.7). At substantially higher *m/z*, the ReTOF still fails to resolve isotopic patterns, even though its resolution is still better than that of a linear TOF analyzer.

In case of metastable fragmentations, the ReTOF behaves different from the linear TOF. If fragmentation occurs between ion source and reflector, the ions will be lost by the reflector due to their change in kinetic energy. Only fragments still having kinetic energies close to that of the precursor, e.g., $[M+H–NH_3]^+$ in case of

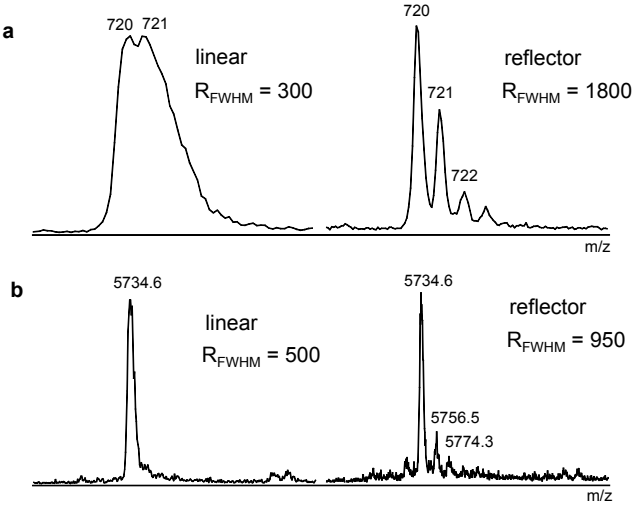


Fig. 4.7. The (**a**) C_{60} molecular ion signal of at *m/z* 720 and (**b**) the $[M+H]^+$ ion signal of bovine insulin, *m/z* 5734.6, as obtained on a TOF instrument in linear mode (*left*) and reflector mode (*right*). All other experimental parameters remained unchanged.

a peptide of about *m/z* 2000, are transmitted due to the energy tolerance of the reflector. However, such ions are not detected at correct *m/z*, thereby giving rise to a "tailing" of the signal. Ions fragmenting in transit from reflector to detector are treated the same way as ions in the linear TOF. Thus, the elongated flight path of the ReTOF, which is equivalent to more time for fragmentation, and the above property complicate the detection of very labile analytes in the ReTOF.

4.2.5 Higher Vacuum Improves Resolving Power

Improved vacuum conditions result in an elongated mean free path for the ions and thus reduce the risk of collisions in transit through the analyzer. The resolving power of a TOF analyzer clearly depends on the background pressure [40]. Despite improvements of resolving power in the order of a factor of two can be realized (Fig. 4.8), enhanced pumping systems alone are not able to effect a breakthrough in resolving power.

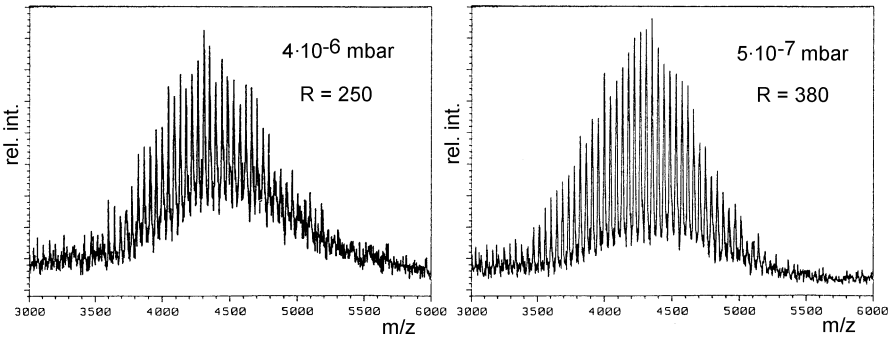


Fig. 4.8. Dependence of resolution on analyzer pressure: linear MALDI-TOF spectra of polyethylene glycol 4000 recorded at a pressure of 4×10^{-4} Pa (*left*) and 5×10^{-5} Pa (*right*). Adapted from Ref. [40] with permission. © John Wiley & Sons, 1994.

Note: With the exception of the quadrupole ion trap which uses buffer gas to damp ion trajectories, a reduced background pressure, i.e., better vacuum, is always beneficial or even essential for any type of mass analyzer.

4.2.6 Delay Before Extraction to Improve Resolving Power

In MALDI-TOF-MS, the energy spread of the emerging ions is of significant magnitude as a result of the MALDI process, which in addition, creates a temporal distribution of ion formation. The most successful approach of handling such conditions is presented by ion sources allowing a delay between generation and extraction/acceleration of the ions. *Time-lag focusing* (TLF) dates back to 1955 [16] and since then has been adapted to the needs of MALDI-TOF-MS by several

groups [41-44]. (The concept of using a time delay to separate charged species in space is also employed in ZEKE-PES and MATI, Chap. 2.10.5).

The advantage of pulsed acceleration is its capability to focus the ions in time thereby reducing the effect of initial position and initial velocity on resolution. In addition, the delay permits the plume generated upon laser irradiation to disperse while still in a field-free region prior to acceleration. This avoids collisions of energetic ions with neutrals in the initially dense plume that could broaden the translational energy distribution and cause fragmentation due to CID (Chap. 9). Continuous extraction MALDI ion sources had to be operated with laser fluences close to the threshold for ion formation in order not to sacrifice the limited resolution any further. With pulsed acceleration, this effect is greatly reduced.

After allowing the ions to separate in space according to their different initial velocities during a delay of some hundreds of nanoseconds the acceleration voltage is switched on with a fast pulse. This procedure also ensures that laser-induced reactions have terminated before ion acceleration begins. A minimum delay of about 200 ns was empirically found to be required to realize the desired effect [31,37]. Longer delays allow to achieve very high resolving power at the focused mass, but outside the optimized *m/z* range resolution remains limited. More recently, the so-called *panoramic pulsed ion extraction* (PAN) was introduced (Bruker Daltonik) that makes use of a time-modulated extraction pulse to stretch the optimum resolution over a wide *m/z* range.

Note: Unfortunately, establishing patents and trademarks has caused redundant names for almost the same thing: *time lag focusing* (TLF, Micromass); *delayed extraction* (DE, Applied Biosystems); *pulsed ion extraction* (PIE), and more recently *panoramic pulsed ion extraction* (PAN, Bruker Daltonik).

Using a two-stage acceleration ion source allows the electric field between target (repeller) and extraction plate P_1 to be varied. The remaining fraction of the acceleration voltage is applied in the second stage. At the onset of extraction, ions with high initial velocities have traveled farther than slower ones, and therefore experience only a fraction of the extraction voltage dV between target and extraction plate P_1. The voltage of the second stage is the same for all ions. As a result, the fastest ions receive less energy from the accelerating field than the slowest. Thereby, such ion sources compensate for the initial energy distribution [44].

The optimum settings of the delay time and of the ratio of pulsed to fixed voltage (V_1/V_2) depend on *m/z* with a tendency towards longer delays and/or a larger V_1/V_2 ratio for heavier ions. In practice, the variation of potentials in pulsed ion extraction with time can be handled as follows (Fig. 4.9): target and extraction plate P_1 are maintained at the same potential during the delay time, thereby creating a field-free region d_1. After the delay has passed, P_1 switches from V_1 by a variable value dV to V_2 causing extraction of the ions.

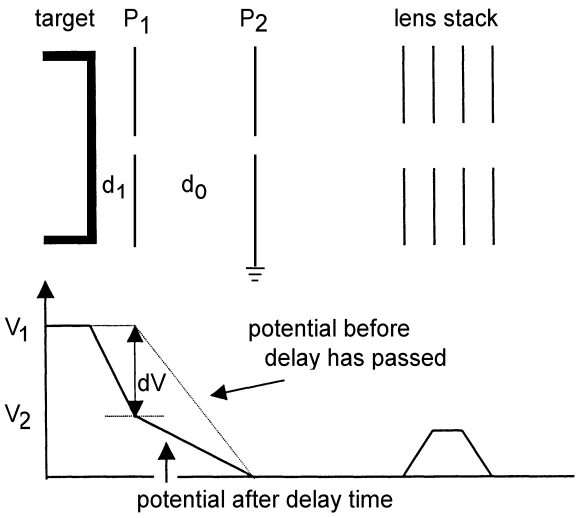


Fig. 4.9. Variation of potentials in pulsed ion extraction with time. The lens stack acts as angular focusing device for the ion beam. By courtesy of Bruker Daltonik, Bremen.

Example: Regardless of the manufacturer of the hardware, the effect of a time lag on resolution is quite dramatic. The resolving power of linear instruments is improved by a factor of 3–4 and reflector instruments become better by a factor of about 2–3 [44]. The advantages are obvious by comparison of the molecular ion signal of C_{60} as obtained from a ReTOF instrument with continuous extraction (Fig. 4.7) and from the same instrument after upgrading with PIE (Fig. 4.11), or by examination of MALDI-TOF spectra of substance P, a low mass peptide, as obtained in continuous extraction mode and after PIE upgrade of the same instrument (Fig. 4.10). Modern mid-class MALDI-TOF instruments easily deliver twice that resolution.

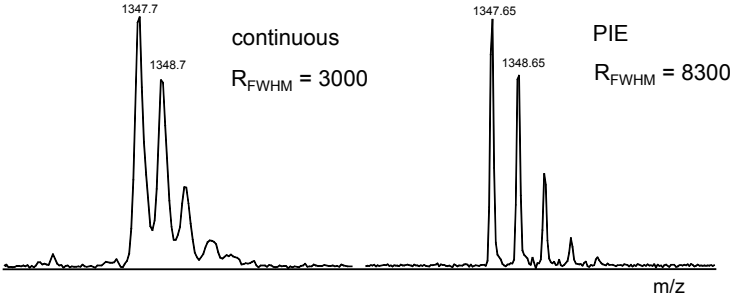


Fig. 4.10. MALDI-TOF spectra of substance P, a low-mass peptide, as obtained from a Bruker Biflex ReTOF in continuous extraction mode (1995, *left*) and after PIE upgrade (2001, *right*).

4.2.7 Analog-to-Digital Conversion

In a TOF analyzer, ion packages of adjacent *m/z* values hit the detector in very short time intervals causing the signal to change extremely fast in time, which makes the *analog-to-digital conversion* a technically demanding task. It can easily be shown that the final peak shape directly depends on the speed of the *analog-to-digital converter* (ADC) [40]. Vice versa, the resolving power of advanced TOF analyzers creates a need for high-speed ADCs. In actual TOF instruments, 8-bit ADCs with a digitization rate of 4 GHz are available to suit their resolving power of up to $R = 45{,}000$. The *digitization rate* or *sampling rate* of an ADC may be reported as dwell time per data point, e.g., 1 ns, or as sampling frequency, e.g., 1 GHz (Fig. 4.11).

Note: The dependence of the signal output on the sampling rate, i.e., on the frequency at which data points are recorded, presents a general concern for any (mass spectrometer) detector system (cf. Chap. 4.6).

In case of 8-bit ADCs as typically used in MALDI-TOF instruments, the intensity of the detector output is converted into a numerical value of 0–255 [45]. The *dynamic range* is the ratio obtained by dividing the intensity of the most intense signal by that of the weakest while both are correctly detected in the same spectrum. To improve the small dynamic range delivered by 8-bit ADCs (0–255) several tens to a few hundred single spectra are usually summed up.

Slower scanning instruments such as quadrupole, quadrupole ion trap, and magnetic sector instruments are typically equipped with 16–20-bit ADCs corresponding to intensity values of 0–65535 (2^{16}–1) and 0–1048575 (2^{20}–1), respectively. This explains their superiority when a high linear dynamic range is required, e.g., for quantitation.

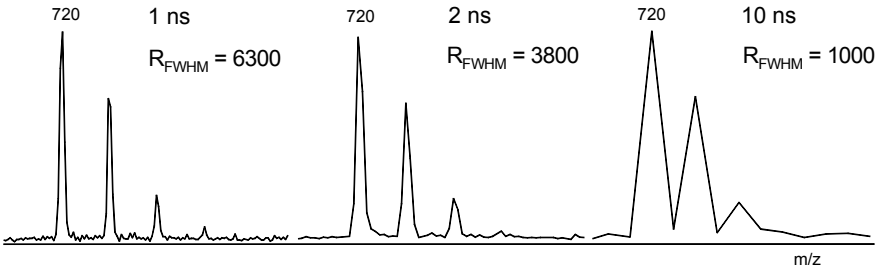


Fig. 4.11. [60]Fullerene molecular ion peak at different settings of the dwell time per data point of the analog-to-digital converter obtained on the aforementioned instrument after PIE upgrade. At 1 ns per data point (1 GHz) the peaks are well resolved and resolution is limited by the analyzer, at 2 ns (500 MHz) some broadening occurs and at 10 ns (100 MHz) peak shapes are reduced to triangles because detection yields just about two points per *m/z*.

4.2.8 Orthogonal Acceleration TOF Analyzers

Up to here, the TOF analyzer has been under consideration bearing MALDI-TOF equipment in mind, just because MALDI as a pulsed ionization method delivers ions to a TOF analyzer in an ideal manner. In fact, MALDI initiated such tremendous improvements of TOF analyzers that it became attractive to combine these compact but powerful analyzers with other, inherently nonpulsed, ionization methods. The major breakthrough for generalized use of TOF analyzers arose from the design of the *orthogonal acceleration* TOF analyzer (oaTOF). In an oaTOF analyzer, pulses of ions are extracted orthogonally from a continuous ion beam (Fig. 4.12) [46,47]. The oaTOF analyzer can be of linear or ReTOF type. Although different problems have to be overcome for each ionization method, the oaTOF analyzer is in principle suited for any of them [24,48,49]. More recently, an oaTOF analyzer has even been adapted to a MALDI ion source [50].

The advantages of oaTOF analyzers are: *i*) high sensitivity due to good duty cycle and high transmission of TOF analyzers, *ii*) high rate of spectra per second even after pre-averaging, *iii*) high mass-resolving power, *iv*) mass accuracies even up to 1 ppm for formula determination, and *v*) compact design. Therefore, it is not

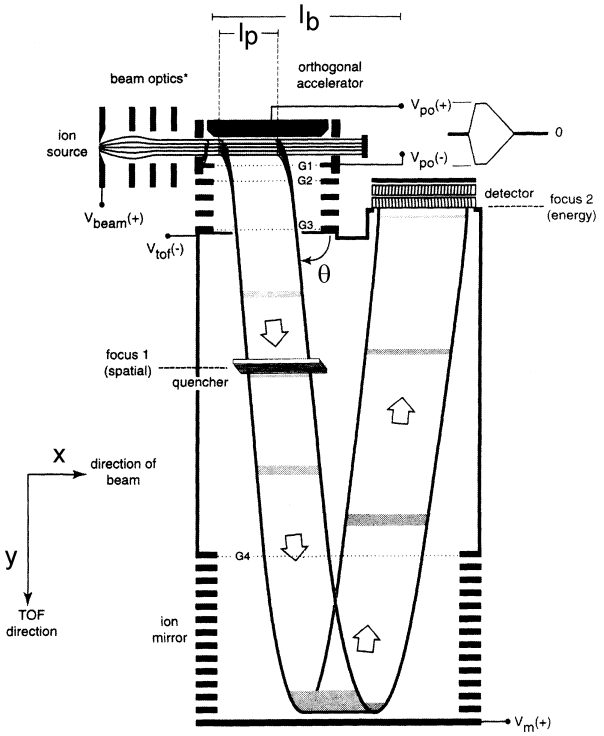


Fig. 4.12. An orthogonal acceleration reflector TOF instrument. See text for discussion. Reproduced from Ref. [49] by permission. © John Wiley & Sons, 2000.

astonishing that oaTOF instruments are currently widespread in use for numerous kinds of applications. Electrospray ionization (ESI) oaTOF instruments with accurate mass capabilities represent the majority of these systems [51-53], but gas chromatography–mass spectrometry (GC-MS) instruments are also available. In particular for *fast GC* applications [54,55] and for HR-GC-MS [56] oaTOF systems are advantageous. Today, a large portion of the instruments incorporating oaTOF analyzers are hybrids mostly of the quadrupole-oaTOF type. We will therefore deal with them in the section on hybrid instruments.

4.2.9 Operation of the oaTOF Analyzer

Ions leaving the ion source are focused to form an almost parallel ion beam, i.e., to minimize ion motion orthogonal to the ion beam axis. Then, the ion beam enters the orthogonal accelerator (*x*-axis) [24,48,49]. The ion kinetic energy in this beam is only in the range of 10–20 eV. A package of ions of length l_p is pushed out orthogonally from its initial direction by a sharp pulse, and is thus accelerated into the TOF analyzer (*y*-axis) by a voltage of 5–10 kV. From the TOF analyzer's point of view the orthogonal acceleration unit can be regarded as the ion source. Usually, ions are accelerated through a two-stage setup analogous to the Wiley-McLaren ion source [16].

The design of the TOF analyzer itself is similar to those discussed before, but its diameter is much wider because the velocity of the ions in *x*-direction, v_{beam}, is not affected by the orthogonal push-out process. Therefore, the detector needs to be comparatively wide in *x*-direction to enable ions extracted anywhere from the whole path l_p to hit its surface. In practice, the detector needs to be several centimeters in length. The angle θ between the *x*-direction and the flight axis into the TOF analyzer is given by

$$\theta = \tan^{-1}\sqrt{\frac{-V_{tof}}{V_{beam}}} = \tan^{-1}\left(\frac{v_{tof}}{v_{beam}}\right) \tag{4.9}$$

where V_{tof} and V_{beam} are the acceleration voltages for ion beam and orthogonal accelerator, respectively, and v_{tof} and v_{beam} are the corresponding ion velocities.

While one ion package travels through the TOF analyzer and is being dispersed in time, the accelerator is refilled with new ions from the ion source (the time-of-flight to cover an *m/z* range up to about 5000 by the oaTOF is about 100 µs). During the drift time of an ion through the oaTOF, it travels a distance l_b. The ratio of the length of the orthogonal accelerator l_p to l_b determines the efficiency of the mass analyzer in terms of the ratio of ions used to ions created. This efficiency is known as the *duty cycle* of an instrument (next paragraph). The duty cycle of an oaTOF instrument is at an optimum if the time-of-flight to pass the TOF analyzer is slightly longer than the time needed for the continuous ion beam to refill the orthogonal accelerator. As soon as the heaviest ions have reached the detector, the next package is pulsed into the analyzer, giving rise to 10,000 complete mass spectra per second. In order to reduce the amount of data and to improve the sig-

nal-to-noise ratio, summation of several single spectra is done by an acquisition processing unit before the spectra are passed to a computer for data storage and post-processing.

4.2.10 Duty Cycle

In mass spectrometry the term *duty cycle* is used to specify the fraction of time of an ion current as continuously delivered from an ion source that is finally used for mass analysis. The duty cycle of scanning instruments is intrinsically low as only ions of one *m/z* value hit the detector at a time while all others are discarded by the analyzer, e.g., at $R = 1000$ only a fraction of 10^{-3} of the *m/z* range reaches the detector corresponding to a duty cycle of just 10^{-3}. Linear and ReTOF analyzers, on the other side, are capable of using almost all ions that are created from a pulsed ionizing event, and thus, these allow duty cycles in the order of 0.9. Although the oaTOF analyzer is by far better than scanning devices, it has to deal with a batch operation of the ion pulser. Fast (low-mass) ions traverse the orthogonal accelerator in a shorter time span than slow (high-mass) ions, thereby causing discrimination of low-mass ions. This behavior poses limitations on the mass range that can be simultaneously pulsed into the TOF analyzer. Depending on the axial velocity distribution of the ions and on the *m/z* range to be analyzed, the duty cycle of oaTOF analyzers is in the 3–30% range.

Example: In oaTOF operation, the frequency between acceleration pulses is selected as to avoid spectral overlap due to mixing of subsequent ion packages traveling along the TOF analyzer. The slowest ions arrive at the detector at a time that is determined by the ratio of the length of the ion entrance window, l_p, to the distance between the midpoints of this window and the detector, l_b. The duty cycle (*Du*) for the heaviest ion at m/z_{max} is therefore given by $Du = l_p / l_b$ (Fig. 4.12) [57]. Furthermore, as the velocity of ions is proportional $(m/z)^{-2}$ (Eq. 4.3) the duty cycle for low-mass ions at m/z_{low} is given by

$$Du = \frac{l_p}{l_b}\sqrt{\frac{m/z_{low}}{m/z_{max}}} \tag{4.10}$$

In practice, the ratio l_p / l_b is about 0.25, and thus, for $m/z_{low} = 100$ and $m/z_{max} = 2000$ one obtains $Du = 0.056$ for the low-mass ion.

Two measures to improve the duty cycle of oaTOF analyzers are described here in brief. First, *Hadamard Transform TOF-MS* employs modulation of the ion beam by pseudorandom on/off pulses. The data acquisition is operated synchronously with this modulation. Deconvolution of the raw data using a fast Hadamard transform (FHT) algorithm yields the normal TOF spectra [58-60]. HT-TOF improves the duty cycle to better than 0.5 [59,60], but still is not being much applied. Second, one may aim at bunching or thermalizing the ions prior to orthogonal acceleration as to reduce losses from passing the pulsed pusher. Third, one can incorporate some preselection to improve the duty cycle in target analysis [61]. Such

approaches often make use of ion-trapping devices that usually can also act in manifold additional ways to manipulate the ions. As quadrupoles and quadrupole ion traps are dealt with later in this chapter, the discussion of such hybrid instruments is postponed until Chap. 4.9.

Note: It is not the duty cycle alone that reduces the transmission of oaTOF analyzers. In practice, the overall sensitivity of instruments is also influenced by ion losses during entrance into the orthogonal accelerator, divergence of ions prior to pulsing, eventual grids in the flight path, etc.

4.2.11 Time-to-Digital Conversion

Time-to-digital converters (TDC) are sometimes employed in oaTOF instruments instead of analog-to-digital converters because of the much higher speed of TDCs. Speed in terms of sampling rate is needed to get access to the high resolution of oaTOF analyzers, and speed in terms of data flow is a prerequisite to handle the enormous number of spectra per second. However, a TDC is a pulse-counting device that offers only 1 bit dynamic range (value 0 or 1) [45]. Detector–TDC combinations easily suffer from saturation effects as they cannot distinguish the arrival of a single ion from that of several ions at a time. The TDC response is therefore not proportional to ion flux. Thus, summation of many single spectra is also necessary to obtain a higher dynamic range via improved signal statistics. Nevertheless, the result is still unsatisfactory for quantitative analysis and for correct isotopic patterns. Furthermore, the dead time between subsequent counting events causes the second of a pair of ions having almost equal arrival times to remain undetected. Dead time effects within ion packages of a given *m/z* even cause *m/z* values to shift to the low-mass side (detection of early incoming ions only), which makes empirical dead-time corrections necessary for accurate mass measurements [45,62]. Most recent oaTOF instruments are therefore equipped with 8-bit ADCs to provide a dynamic range of up to 10^4 after summation of several single spectra (JEOL AccuTOF, Bruker microTOF).

4.3 Magnetic Sector Instruments

4.3.1 Evolution of Magnetic Sector Instruments

Magnetic sector instruments paved the road to organic mass spectrometry. “Whereas mass spectrometry was still very an art rather than a science in 1940, the picture changed drastically during the war years. Vacuum and electronic techniques had matured” [63]. It took until the 1950s for magnetic sector instruments to become commercially available [7,8]. These pioneering instruments were fairly bulky and not very easy to use [63-65]. Nevertheless, they provided analytical information of a kind that chemists had long been seeking for. They continuously

became faster, more accurate, with higher resolving power [3,5,9,66]. The first instruments used a single magnetic sector (symbol B) to effect separation of the ions. Later, the introduction of *double-focusing instruments* which in addition were equipped with an *electrostatic sector* or *electrostatic analyzer* (ESA, symbol E) in addition defined a standard which is still valid. With few exceptions, magnetic sector instruments are comparatively large devices capable of high resolution and accurate mass determination, and suited for a wide variety of ionization methods.

Until a decade ago, double-focusing sector instruments were the choice of MS laboratories with a large chemical diversity of samples. In recent years, however, there has been a strong tendency to substitute sector instruments by TOF, orbitrap, or FT-ICR instruments, and moreover, to even substitute classical ionization methods such as EI, CI, or FAB with APCI or ESI just to redirect the stream of samples to those preferable modern mass analyzers.

4.3.2 Principle of the Magnetic Sector

The *Lorentz Force Law* can be used to describe the effects exerted onto a charged particle entering a constant magnetic field. The Lorentz force F_L depends on the velocity v, the magnetic field B, and the charge q of an ion. In the simplest form the force is given by the scalar equation [3,4,67,68]

$$F_L = qvB \tag{4.11}$$

which is valid if v and B (both are vectors) are perpendicular to each other. Otherwise, the relationship becomes

$$F_L = qvB(\sin\alpha) \tag{4.11a}$$

where α is the angle between v and B. Figure 4.13 demonstrates the relationship between the direction of the magnetic field, the direction of the ionic motion, and the direction of the resulting Lorentz force. Each of them is at right angles to the others. An ion of mass m and charge q traveling at a velocity v in a direction perpendicular to an homogeneous magnetic field will follow a circular path of radius r_m that fulfills the condition of equilibrium of F_L and centripetal force F_c

$$F_L = qvB = \frac{m_i v^2}{r_m} = F_c \tag{4.12}$$

Upon rearrangement we obtain the radius r_m of this circular motion

$$r_m = \frac{m_i v}{qB} \tag{4.13}$$

This shows the working principle of a magnetic sector where the radius r_m depends on the momentum mv of an ion, which itself depends on m/z.

Note: The magnetic sector is a momentum analyzer rather than a direct mass analyzer as commonly assumed.

Finally, dispersion in momentum causes a dependence of r_m on the square root of mass becoming obvious by substitution of v from Eq. 4.3 and $q = ez$

$$r_m = \frac{m_i}{ezB}\sqrt{\frac{2ezU}{m_i}} = \frac{1}{B}\sqrt{\frac{2m_iU}{ez}} \tag{4.13a}$$

Alternatively, the ratio m_i/q can be expressed by rearranging Eq. 4.13

$$\frac{m_i}{q} = \frac{r_m B}{v} \tag{4.14}$$

which upon substitution of v as performed above becomes

$$\frac{m_i}{q} = \frac{r_m B}{\sqrt{\frac{2qU}{m_i}}} \quad \Rightarrow \quad \frac{m_i}{q} = \frac{{r_m}^2 B^2}{2U} \tag{4.14a}$$

For singly charged ions ($z = 1$, $q = e$) we obtain the more widespread form

$$\frac{m_i}{e} = \frac{{r_m}^2 B^2}{2U} \tag{4.14b}$$

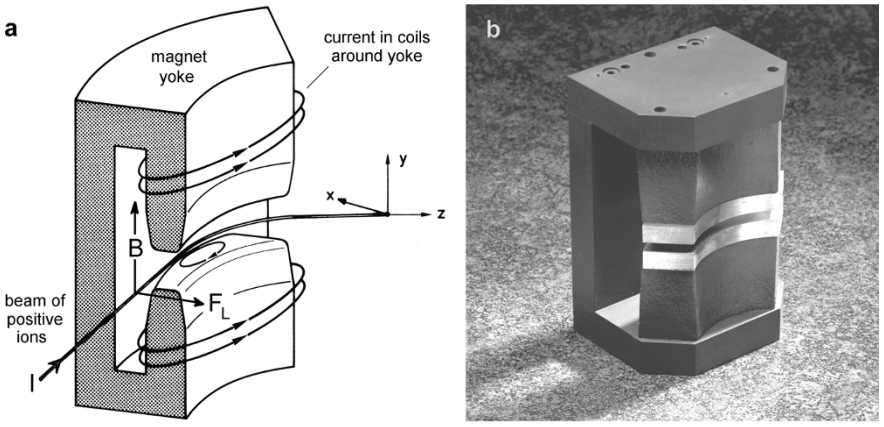


Fig. 4.13. The Right Hand Rule (I thumb, B index finger, F_L middle finger) to determine the direction of the Lorentz force (**a**), where the current corresponds to the direction where positive charges move, i.e., the figure directly applies for positive ions. (**b**) A real magnet yoke without coils and flight tube. With kind permission of Thermo Electron (Bremen) GmbH, (left) and Waters Corporation, MS Technologies, Manchester, UK (right).

Note: Equation 4.14b has become known as the *basic equation of mass spectrometry*. Nowadays, there is no more justification for a single basic equation of mass spectrometry because of the large variety of mass analyzers employed.

4.3.3 Focusing Action of the Magnetic Field

The focusing action of an homogeneous magnetic field on a beam of ions having the same *m/z* and the same kinetic energy can best be illustrated by a 180° sector (Fig. 4.14). If the beam is divergent by a half-angle α, the collector slit must be $\alpha^2 r_m$ wide to pass all ions after suffering 180° deflection. This is because the ions come to a first order, i.e., imperfect, focus as they all traverse the magnetic field at the same radius but not all of them entered the field at right angles. Ions of different *m/z* fly at a different radius, e.g., the lighter ions of m/z_1 hit the wall while ions of m/z_2 reach the collector slit. To allow for detection of various masses, such an analyzer could either be equipped with a photographic plate in the focal plane to become a so-called *mass spectrograph*, or it could be designed with variable magnetic field to detect different masses at the same point by bringing them subsequently to the collector slit. Indeed, such a 180° geometry with *scanning* magnetic field has been used by Dempster [69]. Later, the term *mass spectrometer* was coined for this type of instruments [65].

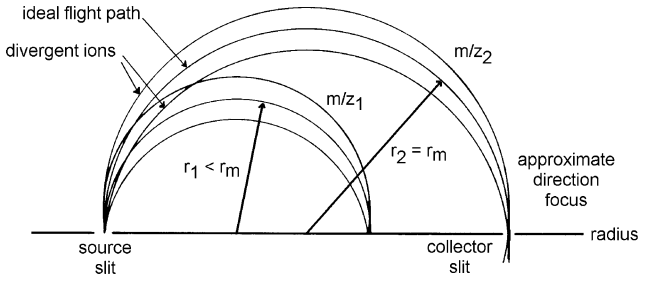


Fig. 4.14. Direction focusing properties of a 180° magnetic sector on a diverging beam of ions of the same *m/z* and the same kinetic energy and effect on ions of different *m/z*. In this illustration, *B* has to come out of the plane towards the reader for positive ions.

Among other complications, the 180° design requires large and heavy magnetic sectors. It is by far more elegant to employ magnetic sectors of smaller angles (Figs. 4.15, 4.16). An optimized magnetic sector alone can provide resolutions of $R = 2000–7000$ depending on its radius. The limitation arises from the fact that ions emerging from the ion source are not really monoenergetic. This way, ions of different *m/z* can obtain the same momentum and thus cause overlap of adjacent ion beams at the detector.

Example: Equation 4.13a describes the radius r_m in the magnetic field. Obviously, the value r_m remains constant as long as $m_i U = const$. If the instrument is set to pass an ion of say *m/z* 500 and 3000 eV kinetic energy, it will simultaneously

allow the passage for ions of *m/z* 501 having 2994 eV or of *m/z* 499 having 3006 eV of kinetic energy. This is why high resolving power demands narrow kinetic energy distributions.

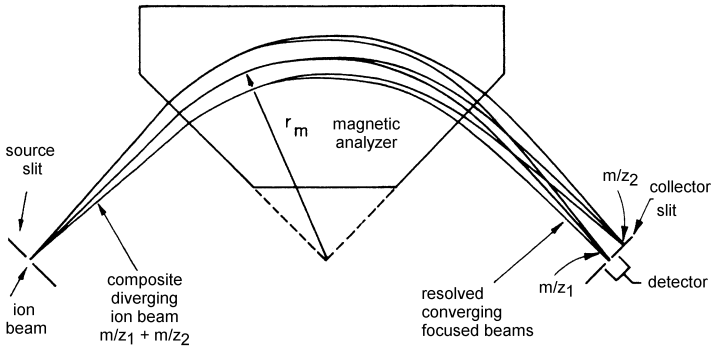


Fig. 4.15. A 90° magnetic sector illustrating *m/z* separation and direction focusing in a plane (angles are shown exaggerated). Reprinted from Ref. [1] with permission. © American Association for the Advancement of Science, 1979.

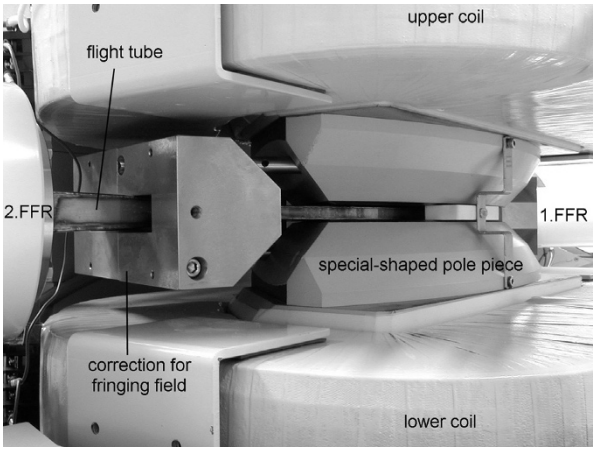


Fig. 4.16. Flight tube passing through the gap of the magnetic sector of a JEOL JMS-700 instrument seen from the ESA side. The shapes of the pole pieces of the yoke and the additional blocks around the tube are designed to minimize fringing fields. In addition the pole faces are rotated to increase the mass range.

4.3.4 Double-Focusing Sector Instruments

The *electrostatic sector* or *electrostatic analyzer* (ESA) produces a radial electric field between two oppositely charged plates extending over the ESA angle ϕ (Fig. 4.17). An ion passes the ESA midway on a circular path if

$$F_e = qE = \frac{m_i v^2}{r_e} = F_c \tag{4.15}$$

where F_e represents the electric force, E the electric field strength, and r_e the radius of the ESA. Rearrangement of Eq. 4.15 demonstrates that the ESA acts as an energy dispersive device

$$r_e = \frac{m_i v^2}{qE} = \frac{m_i v^2}{ezE} \tag{4.16}$$

Note: The ESA effects energy dispersion. Thus, the kinetic energy distribution of an ion beam can be reduced. The ESA does not allow for mass separation among monoenergetic ions.

Upon substitution of Eq. 4.3 for v one obtains the simple relationship

$$r_e = \frac{2U}{E} \tag{4.17}$$

to describe the radius of the ESA. As with the magnetic sector before, the ESA has direction-focusing properties in one plane (Fig. 4.17). Ions entering the ESA in the middle and at right angles to the field boundaries pass through on a path of equipotential, whereas ions with a velocity component towards one of the capacitor plates are brought into focus at the focal length l_e. To understand this, imagine an ion drifting towards the outer plate having the same charge sign as the ion. As it approaches the plate it is decelerated by the opposed electric field and finally reflected towards the center of the beam. With its radial component of v inverted it crosses the ideal path at l_e. In an analogous fashion an ion approaching the inner plate becomes accelerated by the attractive force. The resulting higher velocity causes an increase in centripetal force, and thereby effects a correction of the flight path in the appropriate sense.

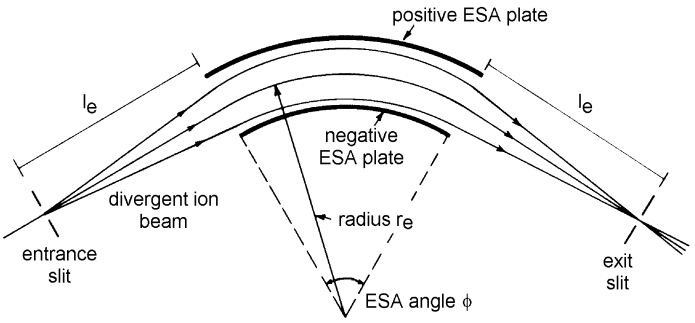


Fig. 4.17. Direction focusing of a radial electric field. Ions of appropriate kinetic energy are focused at the exit slit. Divergent ions pass the ESA close to either plate. Here, the electric potentials are set to transmit positive ions. The image distance l_e depends on the ESA angle.

Energy focusing is achieved by combining a magnetic sector and an electric sector in a way that the energy dispersion of the magnetic field is just compensated by the energy dispersion of the electric field. Additional direction focusing is obtained if the radii and angles of these fields and their mutual alignment does not diminish the focusing properties of each of them. Then, an ion optical system is obtained that is able to focus ions onto a single image point, although these were emerging from the ion source in (slightly) different directions and with (slightly) different kinetic energies. This is called *double focusing*. Double focusing can improve the resolving power of a magnetic sector instrument more than ten times.

4.3.5 Geometries of Double-Focusing Sector Instruments

The following passages present examples of particular double-focusing geometries that either have been milestones in instrument design [3,5] or still are incorporated in modern mass spectrometers.

The EB design by Mattauch and Herzog combines a 31° 50' ESA with a 90° magnetic sector producing an image plane that allows for simultaneous photographic detection of a comparatively large *m/z* range [70]. This mass spectrograph attains double-focusing over the total image plane resulting in resolving powers of $R > 10{,}000$. Thus, it became the basis for numerous commercial instruments (Fig. 4.18). The *Mattauch-Herzog geometry* has survived until today in dedicated instruments for spark source (SS)-MS (Chap.15.2).

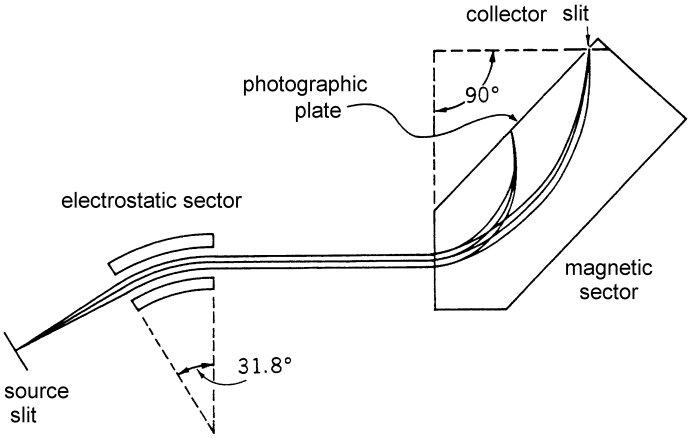


Fig. 4.18. Mattauch-Herzog double-focusing mass spectrograph providing direction and momentum focusing of ions on a plane [70]. Reprinted from Ref. [1] with permission. © American Association for the Advancement of Science, 1979.

An EB design effecting an image plane of 140 mm in length with a linear mass scale for detection on a photographic plate has been published by Bainbridge and Jordan (*Bainbridge-Jordan geometry*) [71]. Their paper is especially recommended as it also nicely illustrates the use of photographic plates in those days.

The third famous type of EB arrangement has become known as *Nier-Johnson geometry* (Fig. 4.19) [72]. Here, the ion beam first passes through the electrostatic analyzer producing energy-resolved beams without mass dispersion in the plane of an intermediate slit located at the focal point of the ESA. It then passes through a magnetic analyzer to achieve mass dispersion of the ions. Different from the Mattauch-Herzog *mass spectrograph*, the Nier-Johnson *mass spectrometer* was constructed to be used in conjunction with a *scanning magnet* to focus one specific *m/z* after the other onto a point detector. This presented a major advantage for the use of UV recorders or electronic data acquisition as well as for the achievement of better ion optics.

Note: Typically, on magnetic sector mass spectrometers a spectrum is produced by varying the strength of the magnetic field to successively pass through ions of different *m/z*. This is termed *magnetic field scan* [73]. For scans *linear in time*, the *scan rate* is given in units of *m/z* s^{-1}, e.g., 500 *m/z* s^{-1}. For scans *exponential in time*, the *scan rate* is reported in units of s per decade, e.g., 10 s/decade means 10 s from *m/z* 30 to 300 or from *m/z* 100 to 1000.

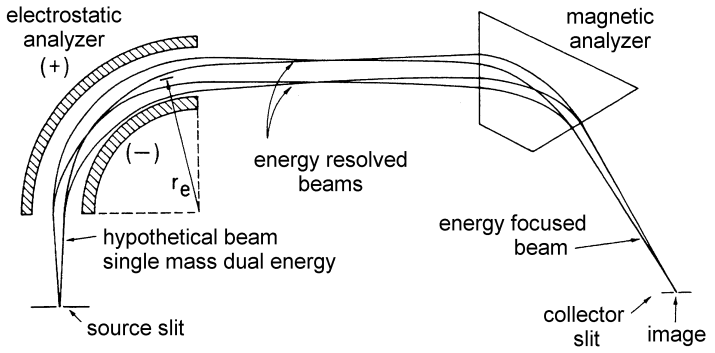


Fig. 4.19. Nier–Johnson geometry (EB) [72]. Direction and velocity focusing are shown exaggerated. Reprinted from Ref. [1] with permission. © American Association for the Advancement of Science, 1979.

Later EB instrument models are often constructed to be used in combination with an (optional) array detector, e.g., the JEOL HX-110 (EB), the Thermo Finnigan MAT 900 (EB), and the Micromass Autospec (EBE) instruments can be equipped in that way. The array detector is then located at the focus plane of the magnet, in contrast to the Mattauch-Herzog design it only covers a comparatively small *m/z* range simultaneously.

Successful constructions of *reversed geometry*, i.e., BE instead of *forward* EB design, have been presented in the form of the MAT 311 in the mid-1970s and shortly after by the VG Analytical ZAB-2F instrument [74] based on a proposal by Hintenberger and König [75]. The first generation ZABs were based on a magnetic sector of 30 cm radius followed by an ESA of 38 cm radius. The specified resolving power (of a new instrument) was R > 70,000.

More recent BE geometry instruments are presented by the Thermo Finnigan MAT 90 and 95 series (Fig. 4.20), the JEOL JMS-700, and although not strictly due to its EBE geometry [76], the Micromass Autospec. However, the only instrument of this millennium incorporating a redesigned BE geometry has been the Thermo Scientific DSF introduced in 2005. In inorganic MS, double-focusing designs are still more widespread (Chap. 15).

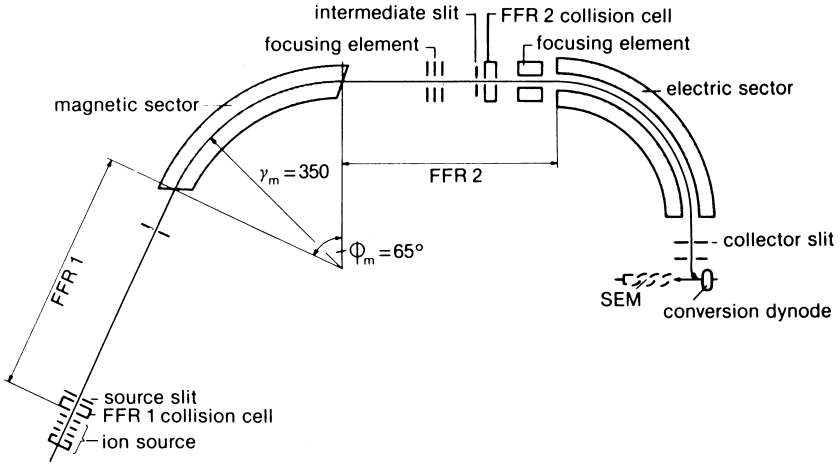


Fig. 4.20. The Finnigan MAT 90 double-focusing mass spectrometer with rotated pole faces of the magnetic sector. Reproduced from Ref. [2] with permission. © Elsevier Science, 1987.

4.3.6 Adjusting the Resolving Power of a Sector Instrument

The ion optics of a sector instrument are the analog to a cylindrical lens in light optics. Accordingly, the reduction of an aperture can be used to obtain a sharper image, i.e., to increase resolution (Chap 3.4). Slits are used instead of circular apertures to comply with the cylindrical properties of the ion optical system. Most important are the settings of the *object slit* (*source slit*, *entrance slit*) and the *image slit* (*collector slit*, *exit slit*, *detector slit*). Intermediate slits may be used in addition. Unfortunately, closing slits also means cutting off ions from the beam, and thus reduction of the transmission of the mass analyzer. In the ideal case, the improvement of resolution by a factor of 10 goes along with a reduction in transmission to 10%, in reality the effect is often worse.

Example: The influence of relative slit width on peak shape and resolution is demonstrated on the second isotopic peak of toluene molecular ion, $^{13}C_2{}^{12}C_5H_8^{+\bullet}$, *m/z* 94 (Fig. 4.21). With the entrance slit at 50 µm and the exit slit at 500 µm the peak is flat-topped (*left*), because a narrow beam from the entrance sweeps over the wide open detector slit keeping the intensity constant as the scan proceeds until the beam passes over the other edge of the slit. Closing the exit slit to 100 µm

increases resolution to 2000 without affecting the peak height (*center)*, but reduces the peak area by a factor of 4 in accordance with an increase in resolution by the same factor. Further reduction of the exit slit width to 30 µm improves resolution at the cost of peak height (*right*). (Any sector instrument must behave alike, otherwise, cleaning or other maintenance are required.)

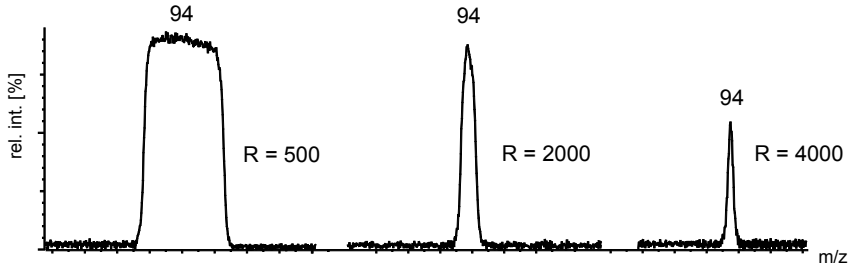


Fig. 4.21. The influence of relative slit width settings on peak shape and resolution on a magnetic sector instrument. The peak shape first changes from flat-topped (*left*) to Gaussian (*center*) and finally resolution improves at cost of peak height (*right*).

Note: The ultimate resolution of a magnetic sector mass spectrometer is reached when the slits are closed to a width of a few micrometers. Often, the slit height is also reduced, e.g., from 5 to 1 mm. In daily work, the resolution will be set to fit the actual task, e.g., R = 1000–2000 for low-resolution work, R = 3000–5000 if accurate mass determination at high scan rates is needed (GC-MS, Chap. 14) or isotopic patterns of high mass analytes have to be resolved, or R = 7000–15,000 in slow-scanning accurate mass measurements.

4.3.7 Innovations in Sector Instruments

To further improve the performance of sector instruments in terms of scan speed, resolving power, transmission, and mass range, the construction, in particular that of the magnet, needs some additional refining.

The rapid change of a magnetic field suffers from hysteresis, i.e., the magnetic flux does not exactly follow the change of the electric current through the coils in time, but lags behind due to the induction of eddy currents. On one side, this causes problems in creating a scan perfectly linear in time, on the other this prevents high scan rates as required for GC-MS. Lamination of the yoke substantially reduces these problems [77] and is now part of all modern sector instruments.

Another problem is due to fringing fields. To reduce these defocusing effects at the entrance and exit of the field, the pole pieces of the yoke of the electromagnet generally have specially shaped edges (Fig. 4.16).

In order to extend the mass range one either has to increase the field strength or the radius of the magnet. However, there are limitations of the field strength with nonsuperconducting magnets at about 2.4 T. Instead of simply enlarging the ra-

dius, the pole faces of the magnet can be rotated to preserve a compact design by reduction of its focal length (Figs. 4.20, 4.22, 4.24) [2].

Furthermore, pure EB and BE designs are somewhat limited concerning the transmittance through a narrow magnet gap as compared to instrument designs using some quadrupole (q) or hexapole (h) lenses to form the ion beam (Figs. 4.22–24) [78,79]. However, quadrupole and hexapole lenses do not alter the effective instrument geometry, i.e., a qqBqE analyzer behaves like a pure BE analyzer in any mode of operation.

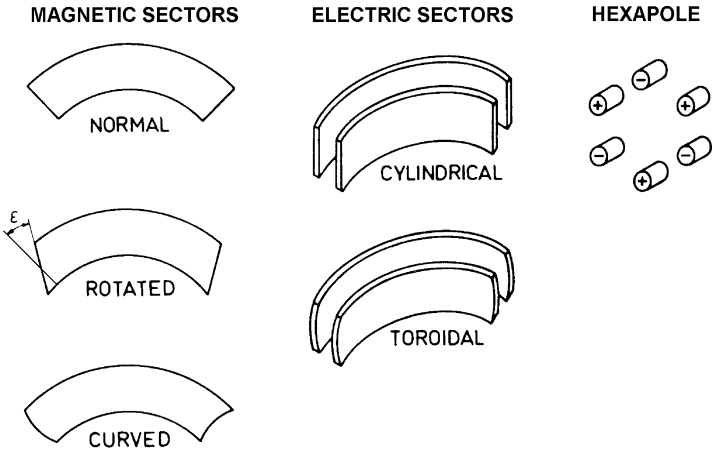


Fig. 4.22. Types and shapes of ion optical elements used in magnetic sector instruments. By courtesy of Thermo Fisher Scientific, Bremen.

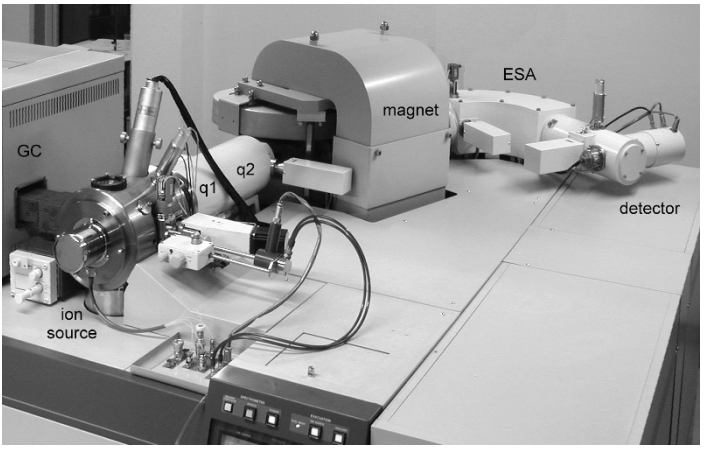


Fig. 4.23. The JEOL JMS-700 double-focusing magnetic sector instrument; for a scheme of this instrument design cf. Fig. 4.24.

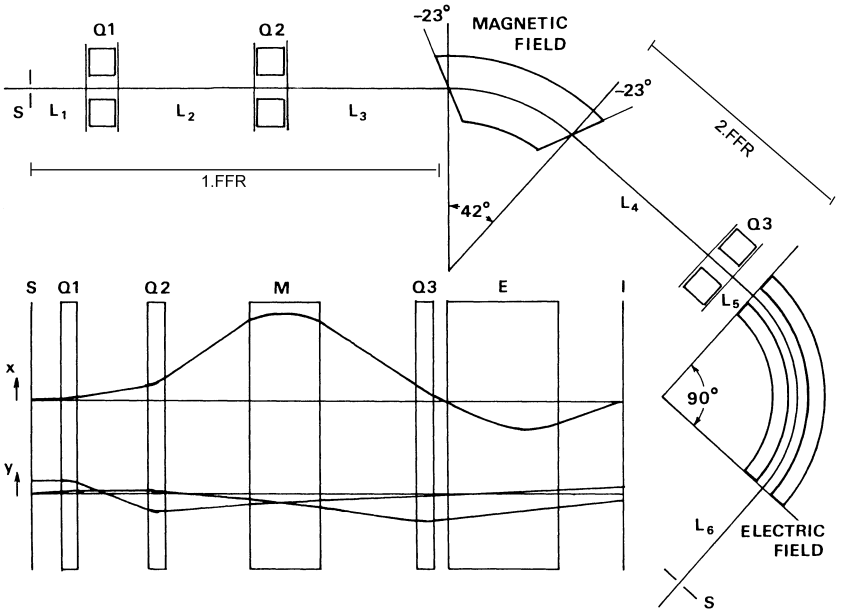


Fig. 4.24. Layout of the above instrument. Horizontal (x) and vertical (y) trajectories are also shown. Quadrupole lenses are used to improve the transmission of the magnetic sector, thus resulting in a qqBqE geometry. Adapted from Ref. [78] with permission. © Elsevier Science, 1985.

4.4 Linear Quadrupole Instruments

4.4.1 Introduction

Since the Nobel Prize-awarded discovery of the mass-analyzing and ion-trapping properties of two- and three-dimensional electric quadrupole fields [80,81] and the concomitant construction of a *quadrupole* (Q) *mass spectrometer* [82,83], this type of instrument has steadily gained importance. Chiefly starting from GC-MS that demanded for rapid scanning analyzers, quadrupole instruments made their way into the MS laboratories [84-87], although those early systems offered poor resolving power and low mass range, e.g., *m/z* 1–200. Modern quadrupole instruments cover up to *m/z* 2000 or even higher with good resolving power and represent some kind of standard device in LC-MS. The advantages of quadrupoles are that they *i*) have high transmission, *ii*) are light-weighted, very compact and comparatively low-priced, *iii*) have low ion acceleration voltages, and *iv*) allow high scan speeds, since scanning is realized by solely sweeping electric potentials.

4.4.2 The Linear Quadrupole

A linear quadrupole mass analyzer consists of four hyperbolically or cylindrically shaped rod electrodes extending in the *z*-direction and mounted in a square configuration (*xy*-plane, Figs. 4.25, 4.26). The pairs of opposite rods are each held at the same potential which is composed of a DC and an AC component.

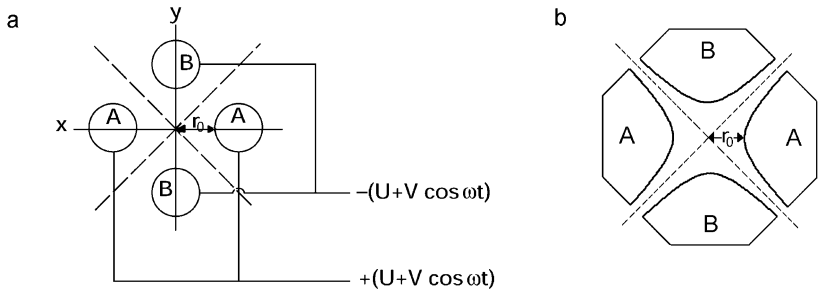


Fig. 4.25. Cross section of a quadrupole (**a**) for the cylindrical approximation and (**b**) for the hyperbolic profile of the rods. The electric field is zero along the *dotted lines*, i.e., along the asymptotes in (**b**). (**a**) Courtesy of Waters Corp., MS Technologies, Manchester, UK.

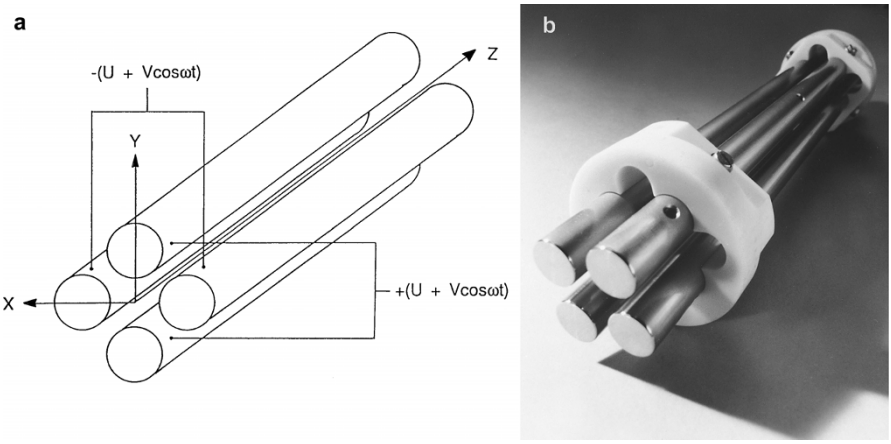


Fig. 4.26. Linear quadrupole mass analyzer: (**a**) schematic and (**b**) photograph. By courtesy of (**a**) JEOL, Tokyo and (**b**) Waters Corp., MS Technologies, Manchester, UK.

As an ion enters the quadrupole assembly in the *z*-direction, an attractive force is exerted on it by one of the rods with its charge actually opposite to the ionic charge. If the voltage applied to the rods is periodic, attraction and repulsion in both the *x*- and *y*-directions will alternate in time, because the sign of the electric force also changes periodically in time. If the applied voltage is composed of a DC voltage U and a radiofrequency (RF) voltage V with the frequency ω the total potential Φ_0 is given by

$$\Phi_0 = U + V\cos\omega t \tag{4.18}$$

Thus, the equations of motion are

$$\frac{d^2x}{dt^2} + \frac{e}{m_i {r_0}^2}(U + V\cos\omega t)x = 0 \tag{4.19}$$

$$\frac{d^2y}{dt^2} - \frac{e}{m_i {r_0}^2}(U + V\cos\omega t)y = 0$$

In case of an inhomogeneous periodic field such as the above quadrupole field, there is a small average force which is always in the direction of the lower field. The electric field is zero along the dotted lines in Fig. 4.25, i.e., along the asymptotes in case of the hyperbolic electrodes. It is therefore possible that an ion may traverse the quadrupole without hitting the rods, provided its motion around the *z*-axis is stable with limited amplitudes in the *xy*-plane. Such conditions can be derived from the theory of the *Mathieu equations*.

Note: The Mathieu functions were originally derived in 1868 by Émile Léonard Mathieu, a French mathematician, to describe the vibrations of elliptical drumheads. It turned out that they are also useful to treat quadrupole mass filters and several other physical phenomena.

Now, writing Eq. 4.19 in dimensionless form yields

$$\frac{d^2x}{d\tau^2} + (a_x + 2q_x\cos 2\tau)x = 0 \tag{4.20}$$

$$\frac{d^2y}{d\tau^2} + (a_y + 2q_y\cos 2\tau)y = 0$$

The parameters *a* and *q* can now be obtained by comparing with Eq. 4.19

$$a_x = -a_y = \frac{4eU}{m_i {r_0}^2\omega^2}, \quad q_x = -q_y = \frac{2eV}{m_i {r_0}^2\omega^2}, \quad \tau = \frac{\omega t}{2} \tag{4.21}$$

For a given set of *U*, *V*, and ω the overall ion motion can result in a stable trajectory causing ions of a certain *m/z* value or *m/z* range to pass the quadrupole. Ions oscillating within the distance $2r_0$ between the electrodes will have stable trajectories. These are transmitted through the quadrupole and detected thereafter. The path stability of a particular ion is defined by the magnitude of the RF voltage *V* and by the ratio *U*/*V*.

By plotting the parameter *a* (ordinate, time invariant field) vs. *q* (abscissa, time variant field) one obtains the stability diagram of the two-dimensional quadrupole field. This reveals the existence of regions where *i*) both *x*- and *y*-trajectories are stable, *ii*) either *x*- or *y*-trajectories are stable, and *iii*) no stable ion motion occurs

(Fig. 4.27) [86]. Among the four stability regions of the first category, region I is of special interest for the normal mass-separating operation of the linear quadrupole (Fig. 4.28) [80,81].

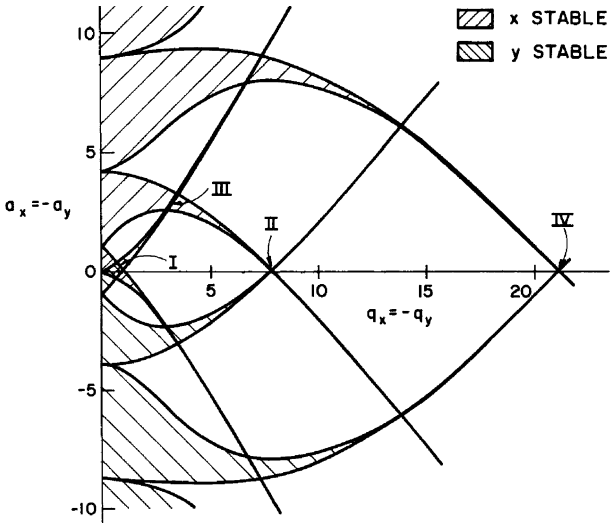


Fig. 4.27. Stability diagram for a linear quadrupole analyzer showing four stability regions (I–IV) for *x*- and *y*-motion. Reproduced from Ref. [86] with permission. © John Wiley & Sons Inc., 1986.

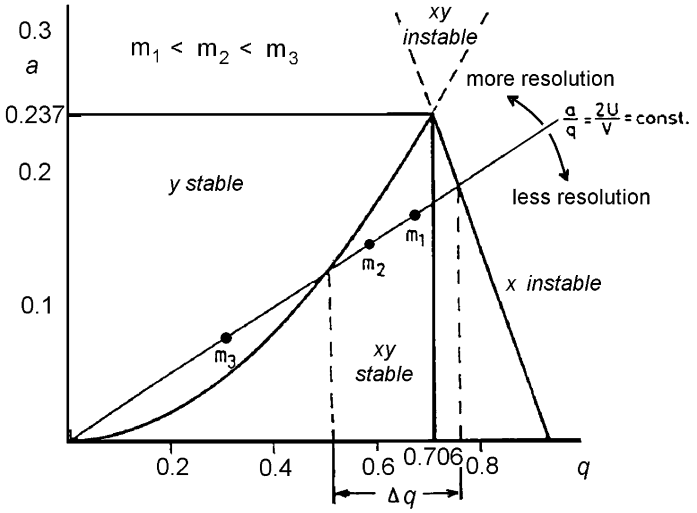


Fig. 4.28. Detail of the upper half of region I of the stability diagram for a linear quadrupole analyzer. Reproduced from Ref. [81] with permission. © World Scientific Publishing, 1993.

If the ratio a/q is chosen so that $2U/V = 0.237/0.706 = 0.336$, the *xy*-stability region shrinks to one point, the apex, of the diagram (cf. Eq. 4.21, Fig. 4.28). By reducing a at constant q, i.e., reducing U relative to V, an increasingly wider m/z range can be transmitted simultaneously. Sufficient resolving power is achieved as long as only a small m/z range remains stable, e.g., one specific $m/z \pm 0.5$ for *unit resolution* (Chap. 4.4.3). Thus, the width (Δq) of the stable region determines the resolving power (Fig. 4.29). By varying the magnitude of U and V at constant U/V ratio an $U/V = constant$ linked scan is obtained allowing ions of increasingly higher m/z to pass the quadrupole.

Overall, the quadrupole analyzer rather acts as a mass filter than as a momentum (B sector) or energy (ESA) spectrometer; hence the widespread use of the term *quadrupole mass filter*.

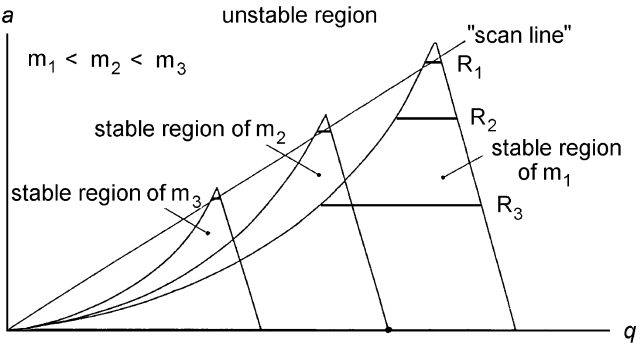


Fig. 4.29. Scanning of linear quadrupoles means performing a $U/V = constant$ linked scan. Resolution is adjusted by variation of the a/q ratio: higher a/q ratio means higher resolving power and is represented by a steeper "scan line"; $R_1 > R_2 > R_3$.

Note: Scanning of any quadrupole means shifting the whole stability diagram along a "scan line", because each m/z value has a stability diagram of its own (Figs. 4.28, 4.29). The representation of a scan by a "scan line" would only be correct in case of infinite resolving power, i.e., if the apices were connected. Any real resolving power is represented by a horizontal line across the stability region, where only ions falling in the region above that line are transmitted.

Ion trajectory simulations allow for the visualization of the ion motions while traveling through a quadrupole mass analyzer (Fig. 4.30). Furthermore, the optimum number of oscillations to achieve a certain level of performance can be determined. It turns out that best performance is obtained when ions of about 10 eV kinetic energy undergo approximately a hundred oscillations [88].

Note: Standard quadrupole analyzers have rods of 10–20 mm in diameter and 15–25 cm in length. The radiofrequency is in the order of 1–4 MHz, and the DC and RF voltages are in the range of some 10^2–10^3 V. Thus, ions of about 10 eV kinetic energy undergo about 100 oscillations during their passage.

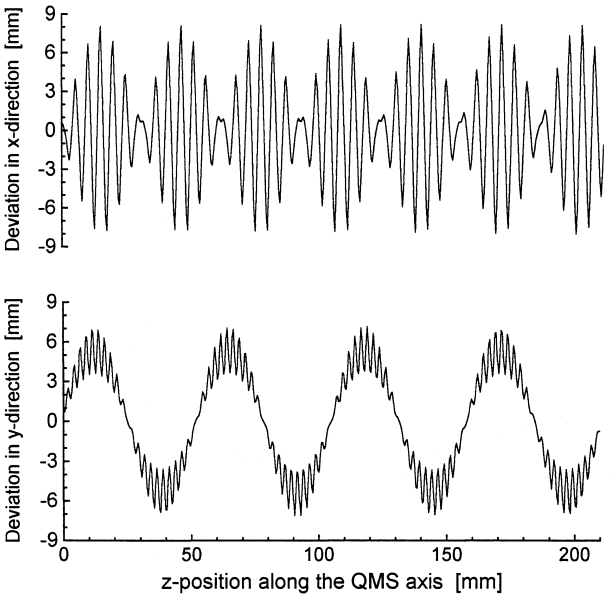


Fig. 4.30. Projection of a 3D trajectory simulation of a stable ion onto the *x*- and *y*-coordinates. Reproduced from Ref. [88] with permission. © Elsevier Science, 1998.

4.4.3 Resolving Power of Linear Quadrupoles

Quadrupole analyzers generally are operated at so-called *unit resolution*, normally restricting their use to typical low resolution (LR) applications [89,90]. At unit resolution adjacent peaks are just separated from each other over the entire *m/z* range, i.e., $R = 20$ at *m/z* 20, $R = 200$ at *m/z* 200, and $R = 2000$ at *m/z* 2000 (Fig. 4.31).

The resolution as adjusted by the *U*/*V* ratio cannot arbitrarily be increased, but is ultimately limited by the mechanical accuracy with which the rods are constructed and supported (± 10μm) [89]. Above an *m/z* value characteristic of each quadrupole assembly, any further improvement of resolution can only be achieved at the cost of significantly reduced transmission. High-performance quadrupoles allowing for about 10-fold unit resolution have only recently been developed [90].

Theoretically, the electrodes of a quadrupole mass filter should have a hyperbolic cross section for optimized geometry of the resulting quadrupole field, and thus for optimized performance [80,81]. However, for ease of manufacture, cylindrical rods are often employed instead. By adjusting the radius of the rods carefully ($r = 1.1468 \times r_0$), a hyperbolic field may be approximated [91]. However, even slight distortions of the ideal quadrupole field either from interference with external fields or due to low mechanical precision or inadequate shape of the device cause severe losses of transmission and resolution [92]. The expected advan-

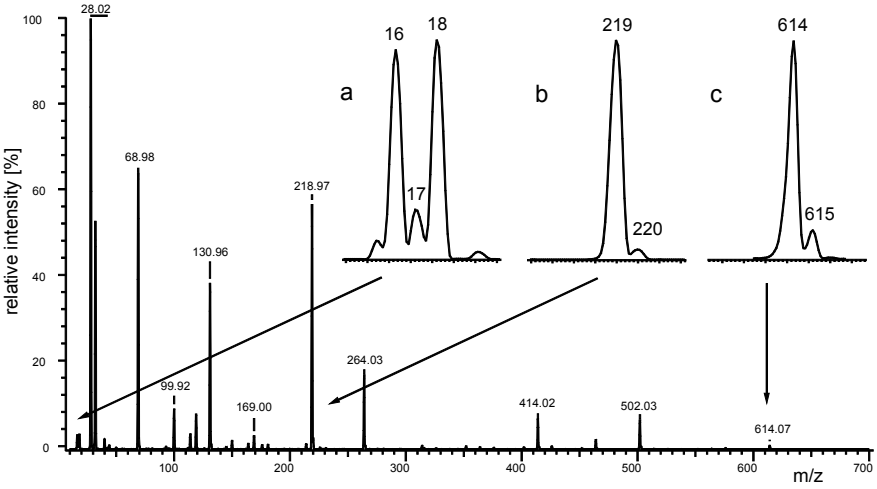


Fig. 4.31. Perfluorotributylamine (mass calibrant FC43). EI mass spectrum demonstrating the unit resolution of a quadrupole analyzer. The expanded views (**a–c**) show peaks separated to almost identical degree.

tages of hyperbolic rods [93] have been demonstrated by ion trajectory calculations [88,94]: circular rods cause a reduction in macromotion frequency because of an increased residence time of the ions in close vicinity to the rods; this in turn means reduced resolution.

Besides optimization of mechanical accuracy, the resolving power of quadrupoles can be improved by innovative modes of operation. The operation as a multiple pass system with ion reflection at either end extends the flight path and thus the number of RF cycles. The same effect can be obtained from increased radiofrequency and for ions traveling slower through the device [89]. Alternatively, the quadrupole may be operated in stability regions other than the first, e.g., in the second or fourth [89,95]; doing so requires higher ion kinetic energies of about 750 eV.

4.4.4 RF-Only Quadrupoles, Hexapoles, and Octopoles

Setting the DC voltage U to zero transforms the quadrupole into a wide band pass for ions. In the stability diagram this mode of operation is represented by an operation line equivalent to the q-axis (Fig. 4.28). Such devices are commonly knownas *RF-only quadrupoles* (q); *RF-only hexapoles* (h) and *octopoles* (o) are used analogously. Generally, higher-order RF 2N-multipoles differ from quadrupoles in that they do not exhibit a sharp *m/z* cutoff in transmission, because x and y motions are strongly coupled, which causes the boundaries of ion stability to become rather diffuse. For low trapping voltages, the ion trajectories in an RF 2N-multipole are approximated by an effective mechanical potential, $U_{\mathrm{eff(r)}}$, given by [87,96]:

$$U_{eff(r)} = \frac{N^2}{4} \frac{(ze)^2}{m_i \Omega^2} \frac{V^2}{r_0^2} \left(\frac{r}{r_0} \right)^{2N-2} \tag{4.22}$$

where N is the order of the multipole, e.g., $N = 3$ for a hexapole. According to Eq. 4.22, higher-order multipoles exhibit increasingly steeper potential wells, offer better ion-guiding capabilities and better wide-band pass characteristics, i.e., wider *m/z* range acceptance (Fig. 4.32). This property led to the widespread application of electric quadrupoles, hexapoles, and octopoles as *ion guides* and *collision cells* [97].

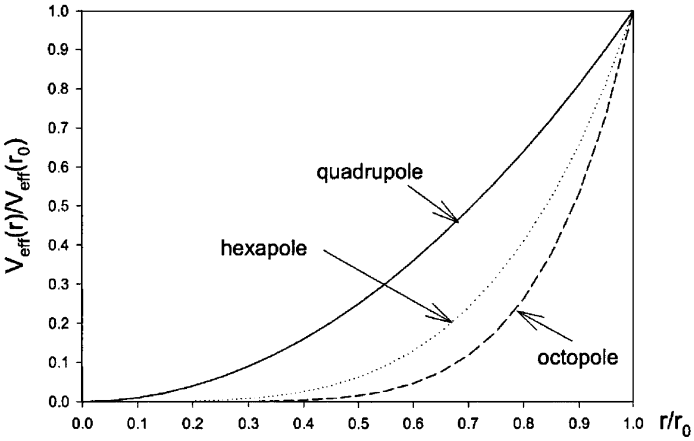


Fig. 4.32. Comparison of effective potentials for quadrupole (r^2), hexapole (r^4) and octopole fields (r^6). Reproduced from [96] with permission. © Wiley Periodicals, Inc., 2005.

RF ion guides are employed in many ways to transfer ions of low kinetic energy, typically of 1–50 eV, from one functional unit to another without substantial losses [96,98]. Ion guides are used to adapt atmospheric pressure ion sources to mass analyzers, e.g., for ESI, APCI, and ambient MS (Chaps. 12, 13). From the viewpoint of the ions, they act like a hose or pipe while being fully permeable for neutrals. Thus, the RF ion guide allows residual gas to effuse through the gaps between the rods into the vacuum pumps, whereas ions are escorted into the mass analyzer. Examples for RF ion guide usage will be given in the instrument schemes to follow later in this chapter.

In contrast to expectations based on scattering by collisions with residual gas, RF-only multipoles deliver even improved transmission at moderate vacuum conditions in the range of 10^{-3}–10^{-2} mbar. This is due to a reduction in ion kinetic energy and concomitant collisional damping of ion motion toward the central axis of the device, so-called *collisional cooling* [87,99-101]. It has been shown that ions of 25 eV kinetic energy are slowed down to 0–2 eV upon passing through a 15-cm-long RF-only quadrupole ion guide at 8×10^{-3} mbar [99,102]. Ions of higher mass (not higher *m/z*) are more prone to this effect, e.g., a 7-fold increase was found for ions of about 200 u, whereas ions of about 17,000 u showed 80-fold im-

provement in transmission [99]. Here, collisional cooling causes a confinement of the ion beam towards the central axis of the quadrupole which in turn increases the transmission efficiency through an exit aperture. This phenomenon is known as *collisional focusing* (cf. Fig. 4.35 in Chap. 4.5.1) [87,101,103].

It is even more interesting that the cooled ion cloud forms concentric cylindrical layers inside the RF-only multipole, each of those layers being composed of ions of the same *m/z* value with higher *m/z* ions gathering in more outward radial layers. This behavior is due to more effective RF focusing for ions of lower *m/z* that pushes these ions closer towards the center. Multiply charged ions form more distinct radial boundaries of the layers as compared to singly charged ion clouds of the same *m/z* and charge density (Fig. 4.33). The gaps of low ion population between the layers result from space charge repulsion [100]. Formation of such *m/z*-stratified structures requires sufficiently high charge density and effective collisional damping. Both RF-only collision multipoles and linear quadrupole ion traps as employed for external ion accumulation fulfill those criteria. When the linear ion density increases, the maximum ion cloud radius also increases. Overfilling of the multipole capacity results in a strong discrimination against high *m/z* ions, because the ion clouds expand to larger radii causing outer layers (high *m/z* ions) to hit the multipole rods [100].

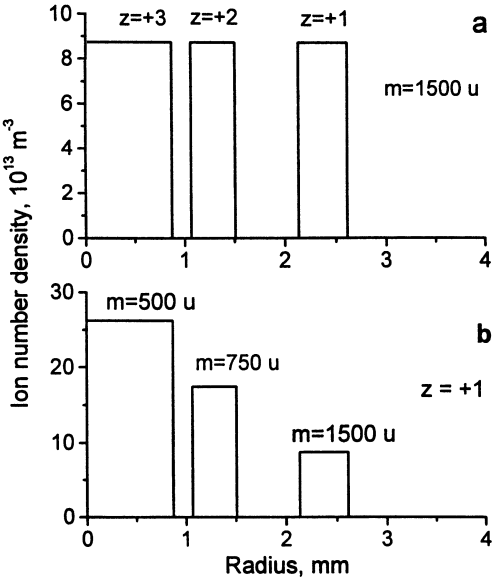


Fig. 4.33. Calculated number density distributions of ions stored in a collisional cooling RF-only quadrupole ion guide having an inner radius of 4 mm and being operated at 1 MHz. (**a**) Radial positions of ions of 1500 u bearing 1, 2, and 3 positive charges. (**b**) Radial position of ion clouds of singly charged ions of *m/z* 500, 1000, and 1500. Reproduced from Ref. [100] with permission. © John Wiley & Sons, Ltd, 2000.

Note: From the work by Douglas [99] a rule of thumb can be derived to judge whether thermalization occurs. This $p \times d$ *rule* demands the product of pressure (p in Torr) times path length (l in mm) to be larger than 0.2 mmTorr. For example, at 2×10^{-3} Torr a RF-only device of 100 mm length is just sufficient for effective ion cooling as we have 2×10^{-3} Torr $\times$ 100 mm = 0.2 mmTorr.

RF-only *quadrupole*, *hexapole*, or *octopole collision cells* [96,104,105] are part of so-called *triple quadrupole mass spectrometers*, which essentially represent QqQ, QhQ, or QoQ instruments, respectively, depending on the type of RF-only collision cell actually in place. They are efficient tools for tandem mass spectrometry (Chap. 9).

Different from magnetic sector or TOF instruments having collimated beams of energetic ions, the ions are exiting from quadrupoles in almost any direction on the *xy*-plane. Thus, real field-free regions as employed in sector or TOF instruments have to be replaced by ion-guiding collision cells to allow CID of ions of 5–100 eV kinetic energy. RF-only collision cells need not to be straight: starting from the Finnigan TSQ700 bent geometries were introduced, and 90° cells (Thermo Scientific TSQ Quantum™ series) or 180° cells (Varian 1200L™, 320-MS™, 325-MS™) are nowadays common. Besides a reduced footprint of the instrument, the bent geometries have other beneficial effects such as the elongation of the flight path through the collision region for improved fragmentation efficiency and the exclusion of neutrals or photons from hitting the detector, and thus, reduced noise levels.

Note: The initial kinetic energy of slow ions can be lost upon several collisions. At 5×10^{-3} mbar (0.5 Pa) fragment ion kinetic energies are reduced to about 1 eV [102]. The ions may even stop their motion along the cell [100,103]. Under such conditions, the continuous ion current into the cell is the only impetus to push the ions through as a result of space-charge effects. The resulting dwell time of about 10 ms allows up to about 5000 (reactive) collisions to take place at about 5×10^{-2} mbar (5 Pa) collision gas (or reagent gas) pressure in an octopole collision cell [106].

4.5 Linear Quadrupole Ion Traps

4.5.1 Linear RF-Only Multipole Ion Traps

As we have just learned, collisional cooling may bring translational ion motion along the axis of an RF-only multipole almost to a halt, thereby transforming such an RF-only multipole ion guide into an ion storage device [100]. To prevent ions inside the multipole from escaping via either open end, one creates a trapping potential well by placing electrodes of slightly higher potential adjacent to the front and rear ends of the multipole [107]. Such devices are known as *linear (quadrupole) ion traps* (LIT).

Note: Quadrupoles are the only devices capable of mass-selective operation, whereas higher-order RF ion guides or higher-order LITs can only guide, accumulate, store, and finally release ions for subsequent *m/z* analysis.

While the entrance plate of the LIT is held at low potential, ions may enter the radially ion-confining RF field. The time span for ion accumulation is limited by reflection of the fast ions at the backside potential wall affording that the entrance gate has to be closed before the lightest ions to be stored can exit the trap via the entrance (Fig. 4.34). Storage of ions in the presence of some buffer gas, e.g., argon or nitrogen at 10^{-3}–10^{-2} mbar, then allows for their thermalization and collisional focusing towards the LIT axis (Fig. 4.35). Both actual ion kinetic energy of the entering ion beam and the degree of thermalization directly influence the potential required to stop axial ion motion [101]. Vice versa, the trapping efficiency of an LIT for faster ions improves with rising pressure (Fig. 4.36) [108]. Finally, the ions can be axially ejected at any convenient point in time. Alternatively, the RF multipole may be segmented, typically into a longer middle and two shorter ends, which are operated at the same RF drive frequency and amplitude but at a DC offset voltage to create the switchable trapping potential well analogous to the trapping plates [109].

LITs are a rapidly expanding field of instrumentation; they have been established to collect ions externally before injecting them in bunches into an FT-ICR [110] or oaTOF analyzer [101,107]. In those instruments the LIT serves *i*) to accumulate ions until a population suitable for the respective analyzer is reached, *ii*) to thermalize the ions in order to have narrow kinetic energy distributions, and *iii*) to deliver this package to a mass analyzer operating in batch mode. Even extensive H/D exchange in the gas phase prior to mass analysis can be accomplished in a LIT if D_2O vapor is admitted instead of inert buffer gas [110,111]. LITs can be build to store ions of very high *m/z*, e.g., singly charged ions of bovine serum albumine, *m/z* 66.000, or even charged particulate matter [112].

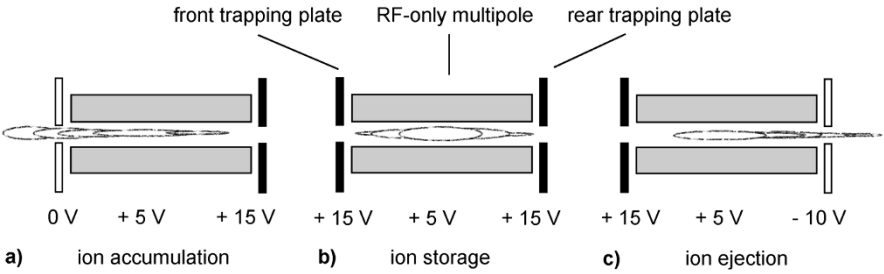


Fig. 4.34. Operation of a linear RF multipole ion trap illustrated using typical DC voltage offsets for positive ions. (**a**) Ion accumulation with backside potential wall up, (**b**) storage of ions with both trapping potentials up, and (**c**) axial ejection of ions from trap using an attractive exit plate potential. The trapping RF multipole section is held at constant DC offset of + 5 V in this example.

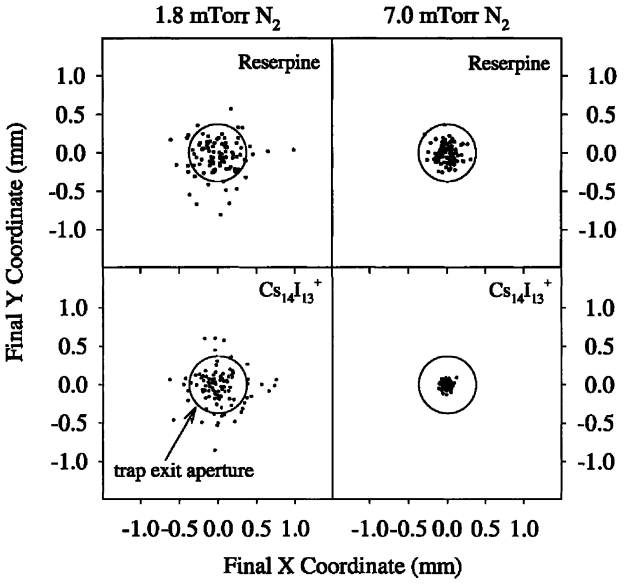


Fig. 4.35. Radial distribution of 100 ion trajectories at the LIT exit aperture (*circle* indicates 0.7 mm aperture hole) for ions of reserpine and $Cs_{14}I_{13}^+$ cluster ions. Collisional focusing is well improved when raising the LIT pressure from 1.8 mTorr (2.4×10^{-3} mbar) to 7.0 mTorr (9.3×10^{-3} mbar). Adapted from Ref. [101] with permission. © John Wiley & Sons, Ltd., 2001.

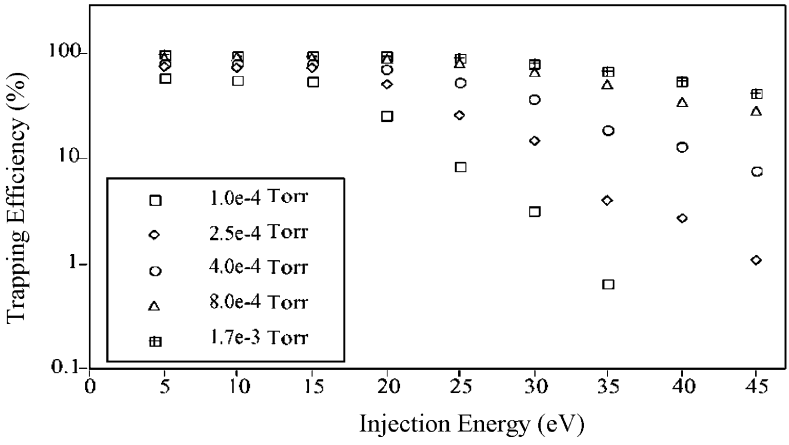


Fig. 4.36. Dependence of the trapping efficiency of an LIT on ion injection energy (reserpine $[M+H]^+$ ions, *m/z* 609) for varying LIT pressures (from the top 1.3×10^{-4} mbar, 3.3×10^{-4} mbar, 5.3×10^{-4} mbar, 1.1×10^{-3} mbar, 2.3×10^{-3} mbar). Reproduced from Ref. [108] with permission. © John Wiley & Sons, Ltd., 2002.

LITs capable of scanning by either axial or radial excitation of the ions and even capable of precursor ion selection for MS/MS experiments [108,109,113] have lately been incorporated in commercial mass spectrometers [96,114-116].

Note: Here, we have gone beyond the domain of the classical mass spectrometric time scale (Chap. 2.6.2). In ion trapping devices, ions are stored for milliseconds to seconds, i.e., 10^3–10^6 times longer than their lifetimes in beam instruments.

4.5.2 Mass-Analyzing Linear Quadrupole Ion Trap with Axial Ejection

Linear ion traps provide high capacities as far as the number of trapped ions is concerned, because the ion cloud can expand along the entire device. It is thus desirable to operate such an LIT not only for ion thermalization and ion accumulation but also as a mass analyzer. In principle, there are two modes possible: one employs excitation of the ions to achieve mass-selective ejection in radial direction [117], the other uses mass-selective axial ejection by application of an auxiliary AC field to the rods of the LIT [108]. The latter mode makes use of the fact that near the exit of the LIT radial ion motion (RF-controlled) and axial ion motion (trapping potential-controlled) are coupled via the fringing fields. When the ion radial secular frequency (governed by the stability parameters and the drive RF) matches that of the auxiliary AC field, ion excitation is effected in a way that also enhances its axial kinetic energy, and thus, leads to ejection from the LIT ([118] and Chap. 5 in [119]). Such an instrument has been developed by Hager by replacing either the RF-only collision quadrupole or the second mass-analyzing

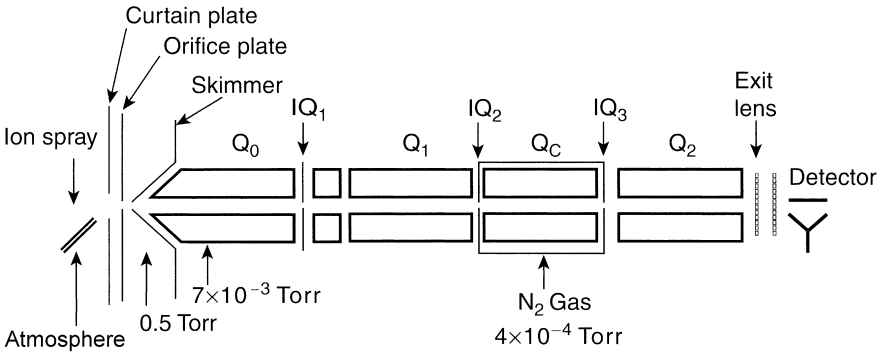


Fig. 4.37. A quadrupole-LIT hybrid instrument. In this scheme, the RF-only collision quadrupole has been replaced by the LIT. The other option, replacement of Q2 by a LIT, is finally in commercial use. Adapted from Ref. [108] with permission. © John Wiley & Sons, Ltd., 2002.

quadrupole of a QqQ instrument with an LIT. The attained configurations are Q-LIT-Q (Fig. 4.37) and QqLIT, respectively [108,115,116]. The QqLIT offers enhanced sensitivity as compared to its QqQ precursor model and offers new modes of operation ([115] and Chap. 3 in [120]). The QqLIT has been commercialized by Applied Biosystems as their Q-Trap series.

As with the linear quadrupole before, the potential $\Phi_{(x,y,z,t)}$ in the two-dimensional quadrupole field of the LIT is expressed by a DC voltage U and an RF drive voltage V with the frequency Ω ([108,118] and Chap. 5 in [119])

$$\Phi_{(x,y,z,t)} = (U - V\cos\Omega t)\frac{(x^2 - y^2)}{r_0^2} \tag{4.23}$$

from which the equations of motion can be derived

$$\begin{aligned} &\frac{d^2x}{dt^2} + \frac{e}{m_i {r_0}^2}(U - V\cos\Omega t)x = 0 \\ &\frac{d^2y}{dt^2} - \frac{e}{m_i {r_0}^2}(U - V\cos\Omega t)y = 0 \\ &\frac{d^2z}{dt^2} = 0 \end{aligned} \tag{4.24}$$

where m_i is the mass of the ion, r_o is the distance between the central axis of the LIT and the surface of the rod. At least, these relationships hold valid as long as ions are sufficiently distant to the fringing fields at the end of the rods.

In practice, there is no DC component, and thus, only the Mathieu parameter q is required, which is obtained by solving the above equations

$$q_x = \frac{4eV}{m_i {r_0}^2 \Omega^2} \tag{4.25}$$

The voltage V is the zero-to-peak amplitude of the RF drive voltage. For an ion inside the quadrupole field the fundamental resonant frequency ω_n is obtained as

$$\omega_n = (2n + \beta)\left(\frac{\Omega}{2}\right) \tag{4.26}$$

For $n = 0$ Eq. 4.26 simplifies to become

$$\omega = \frac{\beta\Omega}{2} \tag{4.26a}$$

which for $q_x < 0.4$ can be approximated by the relationship

$$\omega \approx \frac{q_x}{\sqrt{8}}\Omega \tag{4.27}$$

The stability diagram for the LIT is analogous to that of the linear quadrupole (Figs. 4.27, 4.28). While a description of the scanning of the LIT to achieve mass-selective axial ejection requires complex mathematics [118], the practical application of LIT can easier be understood. The scan function of such an instrument can be displayed in four time slices comprising *i*) ion injection until enough ions are accumulated, *ii*) trapping and thermalization, *iii*) mass scan by linear alteration of RF drive and auxiliary AC voltage, and finally *iv*) a short blanking pulse to reset the LIT prior to the next scan cycle (Fig. 4.38).

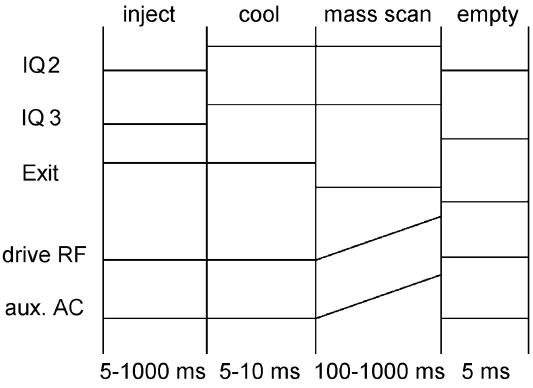


Fig. 4.38. Scan function as used in the QqLIT instrument. IQ2, IQ3, and Exit belong to the trapping plates and the exit lens. Vertical displacements of lines indicate changes of the respective voltages. Note that the time slices are not to scale and that the duration of ion accumulation and mass scan may vary substantially. Adapted from Ref. [108] with permission. © John Wiley & Sons, Ltd., 2002.

Note: The QqLIT setup combines into one single instrument different kinds of mass analyzers, a scanning linear quadrupole, and a scanning linear quadrupole ion trap all connected via an RF-only ion guide. Instruments combining different types of mass analyzers are termed *hybrid instruments*. Most modern mass spectrometers are assembled from different elements to achieve optimum capabilities in the sense of creating instruments uniting the best of two worlds [114]. An overview of hybrids is presented at the end of the analyzer section.

4.5.3 Mass-Analyzing Linear Ion Trap with Radial Ejection

A scanning LIT [109] can alternatively be realized using a mass-selective radial ejection mode of operation. Such a LIT can either serve as a stand-alone mass analyzer (Thermo Scientific LTQ™ series) or can be combined into a hybrid LIT-FT-

ICR instrument (Thermo Scientific LTQ-FT™ series). In the LTQ-FT instruments, the LIT shields the ultrahigh vacuum of the FT-ICR from collision gas and decomposition products in order to operate under optimum conditions. More importantly from the analytical point of view, the LIT can accumulate, mass-select and fragment selected ions prior to the next FT-ICR cycle while the ICR cell is still busy with the previous ion package (FT-ICR cf. Chap. 4.7). By using an orbitrap analyzer (Chap. 4.8) in place of the FT-ICR cell, the same company offers the Thermo Scientific LTQ-Orbitrap™ series as an economical nonetheless powerful alternative to their LTQ-FT.

The LIT is composed of a quadrupole with hyperbolic rods that is cut into three segments of 12 mm in length for both trapping sections and 37 mm in length for the ion storage compartment (Fig. 4.39) [109]. The segmented design avoids fringing fields from the trapping plates as obvious from the electric field calculations using the SIMION software package (Fig. 4.40) [121,122]. Although necessary for the axial ejection scan mode discussed in the preceding section, the radial excitation scanning requires the absence of fringing fields in the trapping zone. One pair of opposite storage compartment rods has cut a slit of 0.25 mm width and 30 mm length to allow for radial ejection of ions onto a conversion dynode. The conversion dynode is held at –15 kV (for positive-ion operation), and upon ion impact it delivers secondary electrons to an electron multiplier. In the commercial variant of the instrument, two detectors are in use to double the sensitivity of the device. The field inhomogeneity introduced by cutting slits into the rods is counterbalanced by aligning them slightly outward from their theoretical *x*-position [109]. To operate as an *m/z* analyzer, the assembly of rods needs *i*) a DC voltage supply to create the axial trapping field (*z*-coordinate), *ii*) an RF voltage supply (1 MHz, ± 5 kV rod to ground) to deliver the radial quadrupolar trapping field (*x,y*-plane), and *iii*) two phases of supplemental AC voltage (5–500 kHz, ± 80 V) that is applied across the *x*-rods for ion isolation, activation, and mass-selective ejection.

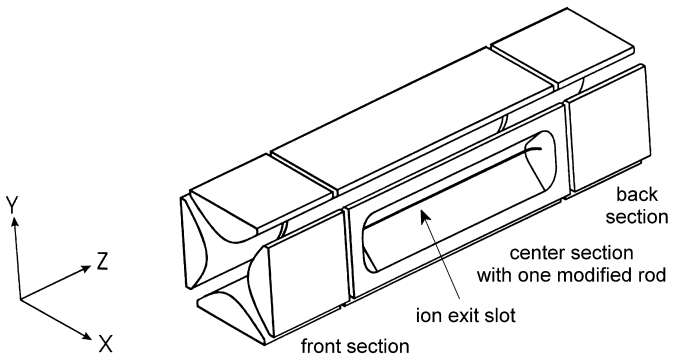


Fig. 4.39. A segmented linear quadrupole ion trap with mass-selective radial ejection capability. Applying higher potential to the front and back sections creates an axial trapping potential for ions in the center section. Radial trapping is again provided by the RF quadrupolar field. Ions are exiting through the slot in one of the four rods. The commercial design offers doubled sensitivity by using two detectors at opposite rods. Adapted from Ref. [109] by permission. © Elsevier Science, 2002.

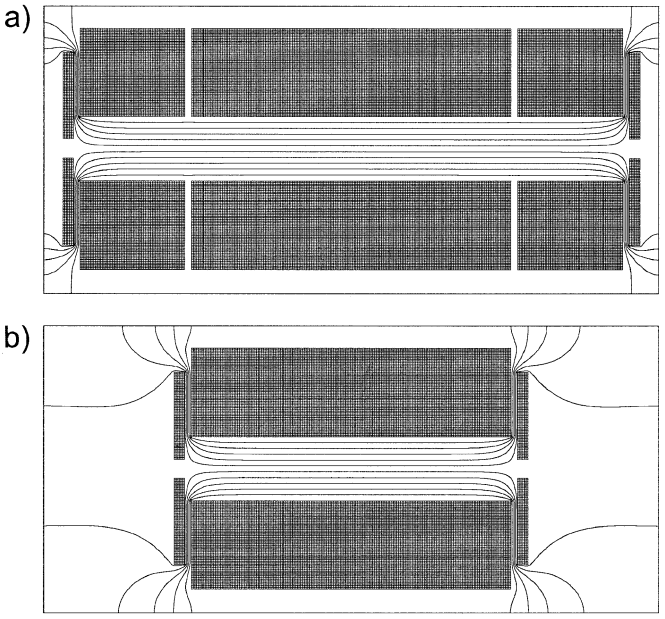


Fig. 4.40. SIMION simulation of the resonance excitation field comparing (**a**) a three-section ion trap and (**b**) a single-section device with end plates for trapping. In (**a**) the field remains unperturbed from fringing fields. Adapted with permission from Ref. [109]. © Elsevier Science Publishers, 2002.

Note: It takes more than just a nicely working *m/z* analyzer to put together a real-world instrument. Thus, the example in the next short paragraph presents a typical technical approach relevant for any type of mass spectrometer.

Example: To build a useful mass spectrometer, the above LIT is connected to an electrospray ionization (ESI, Chap. 12) source using RF-only ion guides to bridge the distance from the source orifice to the entrance of the LIT. As the ESI process starts at atmospheric pressure, the incipient ions need to be continuously transferred from outside the mass spectrometer into the high vacuum of the *m/z* analyzer. This can be achieved by so-called *differential pumping*. Differential pumping makes use of the fact that macroscopic flow is only sustained as long as the mean free path of a molecule is shorter than the average dimension of the aperture it has to pass or of the vessel where it is contained. In practice, a powerful rotary pump (30 $m^3\ h^{-1}$) maintains a pressure in the order of 1 mbar behind a 0.4–0.5 mm orifice. The next stages of the differentially pumped system are usually pumped by turbomolecular pumps. In modern instruments one split-flow turbomolecular pump often serves for both ports. In case of the LIT instrument the intermediate region is thus evacuated to about 2×10^{-3} mbar and the LIT itself to 2.6×10^{-5} mbar (Fig. 4.41). The resulting mass spectrometer is able to deliver unit

resolution over an *m/z* 150–2000 range at about 3 scans per second (Fig. 4.42) and even to provide higher resolution at lower scan rates ([109,123] and Chap. 5 in [119]).

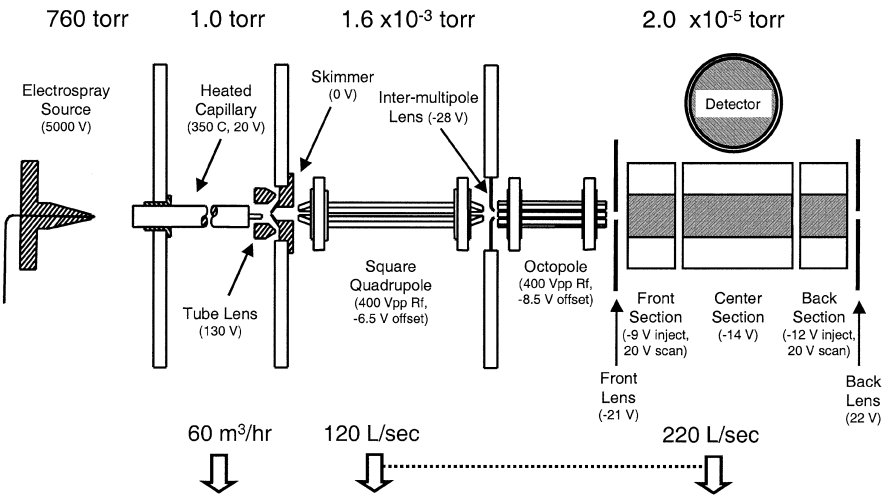


Fig. 4.41. Radial ejection LIT mass spectrometer with ESI source. Typical operating voltages and pressures are given. Reprinted with permission from Ref. [109]. © Elsevier Science Publishers, 2002.

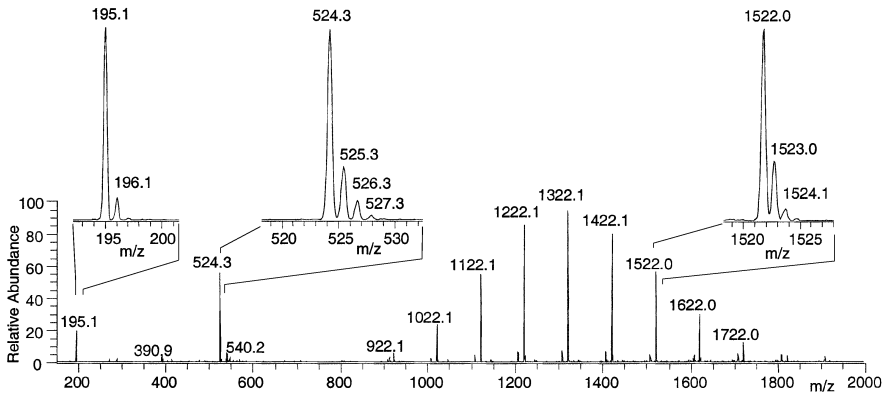


Fig. 4.42. Full scan mass spectrum of a calibration mixture containing caffeine, $[M+H]^+$ at *m/z* 195, the peptide MRFA, $[M+H]^+$ at *m/z* 524, and Ultramark 1621 yielding a series of ions from *m/z* 922 to 1722. The expanded views of selected signals show uniform resolution over the whole range. Adapted with permission from Ref. [109]. © Elsevier Science Publishers, 2002.

4.6 Three-Dimensional Quadrupole Ion Trap

4.6.1 Introduction

In contrast to the linear two-dimensional quadrupole field of the LIT, the three-dimensional *quadrupole ion trap* (QIT) developed by Wolfgang Paul creates a three-dimensional RF quadrupole field of rotational symmetry to store ions within defined boundaries. Its invention goes back to 1953 [80-82]; however, it took until the mid-1980s to access the full analytical potential of quadrupole ion traps [119,124-128].

Note: Wolfgang Paul himself preferred to call the device *"Ionenkäfig"* (ion cage) rather than the nowadays accepted term *quadrupole ion trap* because it does not actively act to catch ions from outside. The acronym QUISTOR derived from *quadrupole ion store* was also in use for a while.

The first commercial quadrupole ion traps were incorporated in GC-MS benchtop instruments (Finnigan MAT ITD and ITMS). Electron ionization was effected inside the trap by admitting the GC effluent and a beam of electrons directly into the storage volume of the trap. Later, external ion sources became available, and soon a large number of ionization methods could be fitted to the QIT analyzer [129-131]. Modern QITs cover ranges up to about *m/z* 3000 with fast scanning at unit resolution, and in addition, offer *"zoom scans"* over smaller *m/z* ranges at higher resolution; instruments delivering resolving power up to 5-fold unit resolution are commercially available. Accurate mass measurements with QITs were expected [127] but not realized so far. The tandem-in-time capabilities of QITs can be employed to conveniently perform MS^n experiments [125,126], and their compact size is ideal for field applications [11].

Note: Historically, both the linear quadrupole analyzer and the quadrupole ion trap originate from the early 1950s (even from the same inventor), whereas the scanning linear ion trap is a product of the 1990s. A detailed timeline of the development of quadrupole ion traps can be found in the comprehensive monographs by March and Todd [119,124]. However, from a teaching perspective, it appears advisable to align the explanations in the logical order as presented here. Once the concepts of trapping and mass-selective release from a quadrupole ion trap have been understood, the step from linear to rotational symmetry should be comparatively easy.

4.6.2 The Quadrupole Ion Trap

The QIT consists of two hyperbolic electrodes serving as end caps along with a ring electrode that replaces two of the linear quadrupole rods, i.e., it could theoretically be obtained by rotating a linear quadrupole with hyperbolic rods by 360° (Fig. 4.43, 4.44). Thus, a section through the *rz*-plane of the QIT closely resem-

bles that of the entrance of a linear quadrupole with hyperbolic rods (cf. Fig. 4.25b) [84,129]. However, the angle between the asymptotes enclosing the ring electrode is 70.5° (2 × arctan(1/√2)) instead of 90°. The end caps are electrically connected and the DC and RF potentials are applied between them and the ring electrode. The working principle of the QIT is based on creating stable trajectories for ions of a certain *m/z* or *m/z* range while removing unwanted ions by letting them collide with the walls or by axial ejection from the trap due to their unstable trajectories [119,124,128].

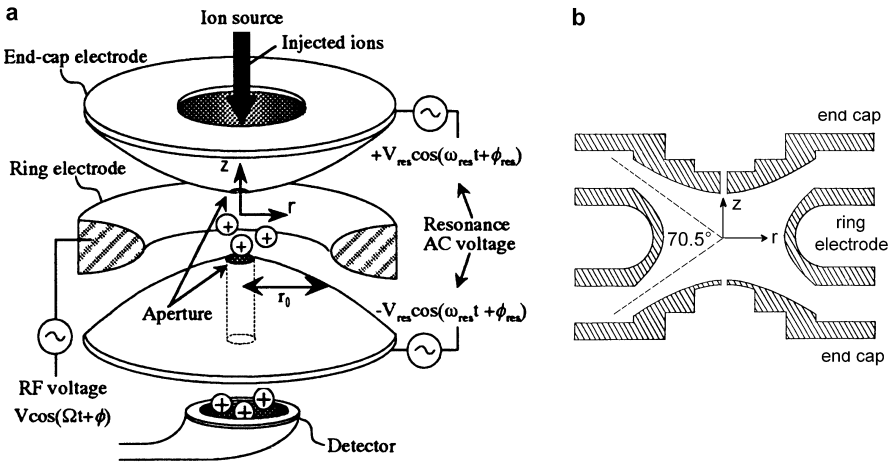


Fig. 4.43. A quadrupole ion trap. (**a**) QIT with external ion source (illustration stretched in *z*-direction) and (**b**) section in the *rz*-plane (in scale). (**a**) Reproduced from Ref. [132] by permission. © John Wiley & Sons, 2000.



Fig. 4.44. Electrodes of the Finnigan MAT ITS40 quadrupole ion trap. By courtesy of Thermo Electron (Bremen) GmbH.

For the QIT, the electric field has to be considered in three dimensions. Let the potential Φ_0 be applied to the ring electrode while the hyperbolic end caps are grounded. The axial coordinate of the trap is designated as the z-axis, the value z_0 defines the physical dimension of the trap (center to cap), and z presents the actual position of an ion with respect to the z-axis. The x,y-plane is resolved into the cell radius r_0 where r analogously defines the actual radial position of an ion. With the pair of end caps grounded the potential inside the trap is given as

$$\Phi_0 = U + V\cos\Omega t \tag{4.28}$$

Then, the field can be described in cylindrical coordinates (using the standard transformations $x = r\cos\theta$, $y = r\sin\theta$, *and* $z = z$) by the expression [124,129]

$$\Phi_{x,y,z} = \frac{\Phi_0}{r_0^2}(r^2\cos^2\theta + r^2\sin^2\theta - 2z^2) \tag{4.29}$$

Because of $\cos^2 + \sin^2 = 1$ this reduces to

$$\Phi_{r,z} = \frac{\Phi_0}{r_0^2}(r^2 - 2z^2) \tag{4.30}$$

The equations of motion of an ion in such a field are

$$\begin{aligned} \frac{d^2z}{dt^2} - \frac{4e}{m_i\left(r_0^2 + 2z_0^2\right)}(U - V\cos\Omega t)z = 0 \\ \frac{d^2r}{dt^2} + \frac{2e}{m_i\left(r_0^2 + 2z_0^2\right)}(U - V\cos\Omega t)r = 0 \end{aligned} \tag{4.31}$$

Solving these differential equations which are again of the Mathieu type, finally yields the parameters a_z and q_z

$$\begin{aligned} a_z &= -2a_r = -\frac{16eU}{m_i\left(r_0^2 + 2z_0^2\right)\Omega^2} \\ q_z &= -2q_r = \frac{8eV}{m_i\left(r_0^2 + 2z_0^2\right)\Omega^2} \end{aligned} \tag{4.32}$$

where $\Omega = 2\pi f$ and f is the fundamental RF frequency of the trap ($\approx$ 1 MHz). To remain stored in the QIT, an ion has to be simultaneously stable in the r and z directions. The occurrence of stable ion trajectories is determined by the stability parameters β_r and β_z which depend on the parameters a and q. The borders of the first stability region are defined by $0 < \beta_r, \beta_z < 1$ [133].

A stability diagram can be drawn where the stability region closest to its origin is of greatest importance for the operation of the QIT (Fig. 4.45). At a given U/V ratio, ions of different m/z are located along a straight line crossing the stability region; ions of higher m/z are nearer to the origin than lighter ones. The regions of

stability as plotted in the *a/q* plane are represented as envelopes of characteristic shape. Ions with their *m/z* value inside the boundaries are stored in the QIT. The low-mass limit of the trapped *m/z* range is strictly defined by $q_z = 0.908$.

Collisional cooling (Chap. 4.4.4) by several tens of soft collisions during the dwell time of the ions inside the QIT significantly enhances its resolving power and sensitivity [134,135]. The light buffer gas, normally helium at 0.1 Pa, serves to dampen the ion motion towards the center of the trap, and thus, keeps them away from the electrode surfaces and from field inhomogeneities as induced by the entrance and exit holes of the QIT [136].

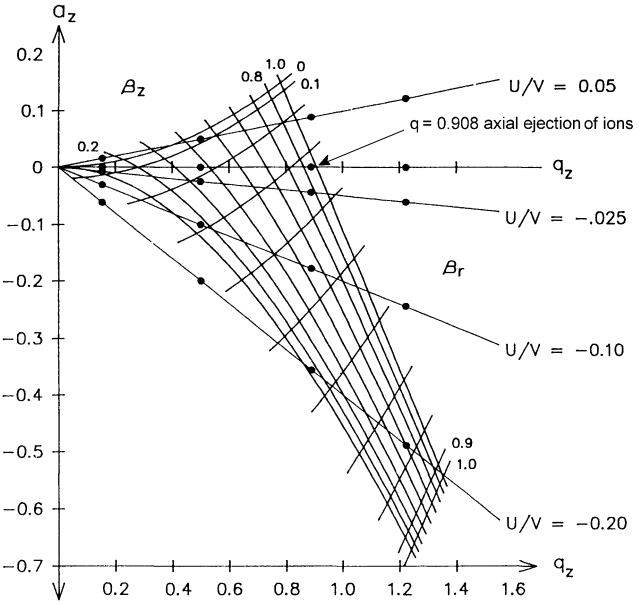


Fig. 4.45. Stability diagram for the quadrupole ion trap. The points collected on a common line mark the *a/q* values of a set of ions. Each line results from different settings of the *U/V* ratio. Reproduced from Ref. [124] by permission. © John Wiley and Sons, 1989.

4.6.3 Visualization of Ion Motion in the Ion Trap

The way the three-dimensional quadrupole field acts to keep ions within a certain volume, i.e., within a potential well some electron volts in depth, can be illustrated by a mechanical analog: A ball can be prevented from rolling from a saddle by rotating the saddle just right to bring the ball back to the middle before it can leave the surface via one of the steeply falling sides (Fig. 4.46a). Paul demonstrated the dynamic stabilization of up to three steel balls by such a device in his Nobel lecture [80,81].

The trajectories of low-mass ions in a QIT were shown to be similar to those observed for charged aluminum dust particles [137-140]. Wuerker recorded Lissa-

jous trajectories, superimposed by the RF drive frequency, as a photomicrograph (Fig. 4.46b) [137]. The complex motion of the ions is the result of the two superimposed secular oscillations in r and z direction. Calculations of the trajectories yield the same results [141].

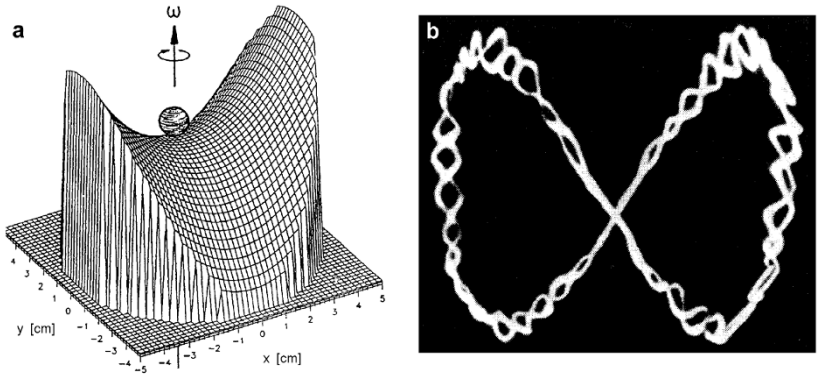


Fig. 4.46. Visualization of ion motion in the ion trap. (**a**) Mechanical analog of the QIT. (**b**) Photograph of ion trajectories of charged aluminum particles in a quadrupole ion trap. (**a**) Reproduced from Ref. [81] with permission. © World Scientific Publishing, 1993. (**b**) Reproduced from Ref. [137] with permission. © American Institute of Physics, 1959.

4.6.4 Mass-Selective Stability Mode

The whole range of ions is generated within or admitted to the QIT, but solely ions of one particular *m/z* are trapped at a time by setting appropriate parameters of the QIT. Then, the stored ions are pulsed out of the storage volume by applying a negative pulse to one of the end caps [142,143]. Thus, they hit the detector located behind a hole in the center of one of the end caps. A full-scan mass spectrum is obtained by addition of several hundred single steps, one for each nominal *m/z* value. This is the so-called *mass-selective stability* mode of the QIT [144,145]. The mass-selective stability mode is no longer in use, because it is too slow and provides poor sensitivity as most ions are wasted.

4.6.5 Mass-Selective Instability Mode

First, the full *m/z* range of interest is trapped within the QIT. The trapped ions may either be created inside the QIT or externally. Then, with the end caps grounded an RF-voltage scan (V) is applied to the ring electrode causing consecutive ejection of ions in the order of their *m/z* values. This is known as *mass-selective instability* (*ejection*) mode [134,146]. It can be represented in the stability diagram by a horizontal line from the origin to the point of axial ejection at $q_z = 0.908$. The timing sequence is shown in Fig. 4.47.

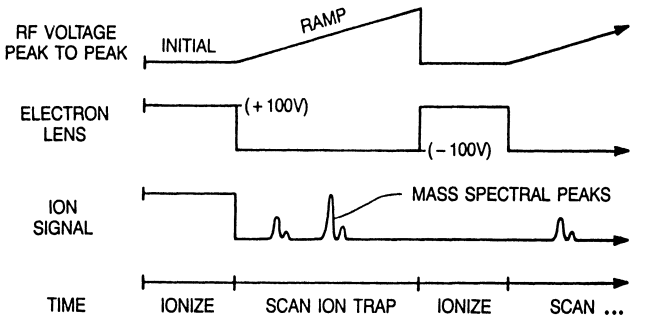


Fig. 4.47. Timing sequence used for mass-selective instability mode (about 1.5 cycles shown). With an external ion source the ionization time is replaced by the ion injection pulse. Reproduced from Ref. [134] by permission. © Elsevier Science, 1984.

4.6.6 Resonant Ejection

Modern QITs employ the effects of *resonant ejection* to remove ions of successively increasing *m/z* value from the storage volume, i.e., to achieve a scan. In an ideal QIT, the motions of the ions in radial and axial directions are mutually independent. Their oscillations can be described by a radial and an axial secular frequency, each of them being a function of the Mathieu trapping parameters a and q. If a supplementary RF voltage which matches the axial secular frequency is applied to the end caps, resonant ejection of ions occurs at $q < 0.908$ (Fig. 4.45) [147]. Excitation occurs when the frequency of a supplementary RF signal matches the secular frequency of a trapped ion in z direction. The secular frequency components in axial direction (ω_z) are given by $\omega_z = (n + \beta_z/2)\Omega$, where Ω represents the angular frequency, n is an integer, and β_z is determined by the working point of an ion within the stability diagram [148]. In the special case when $\beta_z = 1$ and $n = 0$, the fundamental secular frequency is exactly half of the RF drive frequency applied between ring electrode and end caps.

Example: To effect resonant ejection for the set of $\beta_z = 0.5$ and $n = 0$ we have $\omega_z = (0 + 0.5/2) = 0.25\Omega$, i.e., $^1/_4$ of the RF drive frequency has to be applied to eject ions at the $\beta_z = 0.5$ borderline. By scanning the voltage of the RF drive frequency upwards, ions of increasing *m/z* ratio are successively ejected.

Scans based on resonant ejection may either be carried out in a forward, i.e., from low to high mass, or a reverse direction. However, the scan direction has significant influence on the attainable resolving power, the reverse direction being clearly inferior in that respect. [149,150] The combination of forward and reverse scanning allows for the selective storage of ions of a certain *m/z* value by elimination of ions below and above that *m/z* value from the trap. Thus, it can serve for precursor ion selection in tandem MS experiments [147,149]. Axial excitation can also be used to cause collision-induced dissociation (CID) of the ions as a result of

collisions with the helium buffer gas [134,147]. A substantial increase of the mass range is realized by reduction of both the RF frequency of the modulation voltage and the physical size of the QIT [145,151,152].

4.6.7 Axial Modulation and Automatic Gain Control

Ion trapping devices are sensitive to overload because of the detrimental effects of coulombic repulsion on ion trajectories. The maximum number of ions that can be stored in a QIT is about 10^6–10^7, but it reduces to about 10^3–10^4 if unit mass resolution in an RF scan is desired. *Axial modulation*, a subtype of resonant ejection, allows to increase the number of ions stored in the QIT by one order of magnitude while maintaining unit mass resolution [152,153]. During the RF scan, the modulation voltage with a fixed amplitude and frequency is applied between the end caps. Its frequency is chosen slightly below $^1/_2$ of the fundamental RF frequency, because for $\beta_z \leq 1$, e.g., $\beta_z = 0.98$, we have $\Omega_z = (0 + 0.98/2) \times \Omega = 0.49 \times \Omega$. At the stability boundary, ion motion is in resonance with this modulation voltage, and thus ion ejection is facilitated. Axial modulation basically improves the mass-selective instability mode of operation.

If resolving power is not a major concern, scanning of QITs can be very fast, a property that can be employed to make a *pre-scan*. The actual ion current into the trap is then determined from the pre-scan and the result is used to adjust the number of ions admitted to the QIT by a timed ion gate for the subsequent analytical scan. Thus, the number of ions, and hence, charge density inside the QIT are continously held close to the optimum. This is known as *automatic gain control* (AGC) [125,154]. AGC gives increased sensitivity at low sample flow and avoids overload of the QIT at high sample flow.

Note: AGC is not only relevant for QITs but also for all other types of ion traps. AGC is well implemented in LITs that are not only employed as stand-alone devices but also in conjunction with FT-ICR analyzers to serve for ion selection and dosing into the ICR cell (Chap. 4.9.1).

Provided sufficiently high scan rates are also available whilst resolution is preserved, the pre-scan can be omitted. Instead, a trend analysis based on a set of two or three preceding analytical scans can be performed. This procedure avoids wasting of ions and results in further optimization of the filling level of the QIT. The exploitation of the phenomenon of nonlinear resonances turned out to be of key importance for the realization of this method.

Example: Tandem mass spectrometric experiments in quadrupole ion traps (more in Chap. 9.8) are performed by combining the techniques of resonant ejection, and forward and reverse scanning to achieve an optimum in precursor ion selection, ion activation, and fragment ion scanning (Fig. 4.48) [147].

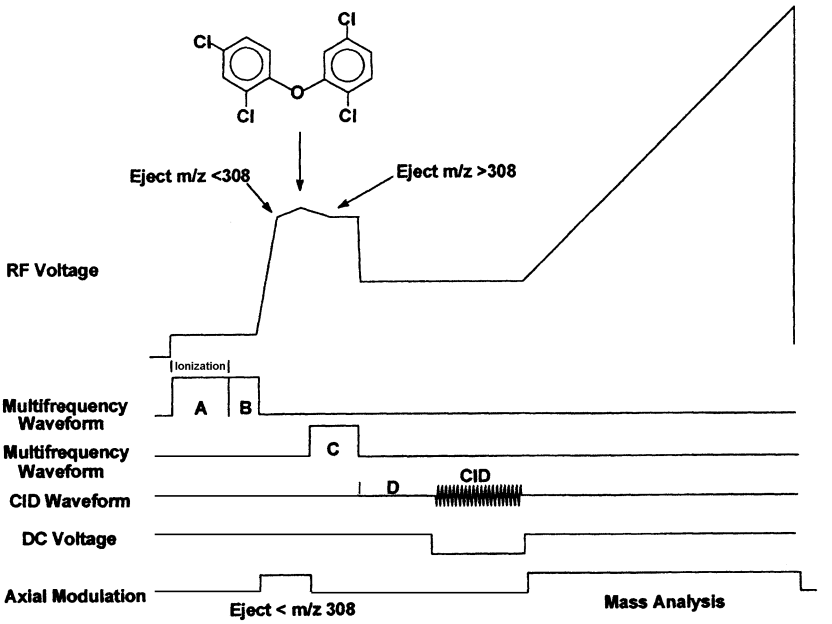


Fig. 4.48. Complex scan function used for a tandem mass spectrometric study of 2,4,3',6'-tetrachlorodiphenylether. Reproduced from Ref. [147] by permission. © John Wiley and Sons, 1997.

4.6.8 Nonlinear Resonances

Higher multipole fields, in particular octopole fields, are induced in any real ion trap by deviations from the ideal electrode structure. The trapping potential may then be represented as a sum of an ideal quadrupole field and weak higher order field contributions [133,155,156]. Application of an excitation voltage across the end caps induces dipole and hexapole fields in addition. Those higher order fields in the QIT may have beneficial effects such as increase in mass resolution in the resonant ejection mode, but may also result in losses of ions due to nonlinear resonances [157]. Nonlinear resonances have been known for long [158,159], but useful theoretical descriptions were only recently developed [133,156,160,161]. The condition for the appearance of instabilities is related to certain frequencies through the stability parameters β_r and β_z and the integer multiples n_r and n_z. The locations of instability spread like a net over the stability diagram and have been experimentally verified with astonishing accuracy (Fig. 4.49) [133]. Excitation of ions with a suitable frequency can cause their fast ejection from the trap due to the sudden shift to nonlinear stability. Nonlinear resonances can thus be exploited to realize very fast scans of the QIT (26,000 u s^{-1}) while maintaining good resolving power [161], e.g., irradiation of $0.33 \times \Omega$ amplifies hexapole resonances and causes sudden ejection at the $\beta_z = 0.66$ borderline.

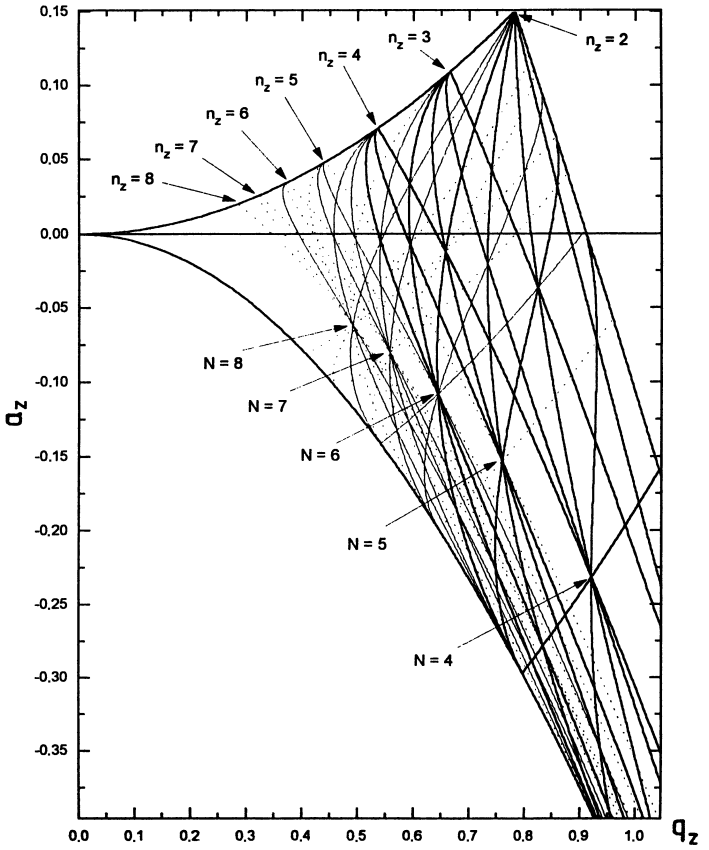


Fig. 4.49. Plot of theoretical lines of instability corresponding to the relation $n_r/2\beta_r + n_z/2\beta_z = 1$ for different orders $N = n_r + n_z$ (strong resonances represented by *solid lines*, weak ones by *dotted lines*). Reproduced from Ref. [133] by permission. © Elsevier Science, 1996.

4.6.9 Digital Waveform Quadrupole Ion Trap

In almost all QITs, the *m/z* range is extended by lowering the RF drive frequency and/or by resonant ejection at a low q value, e.g., Thermo Fisher Scientific QITs eject the ions at $q = 0.78–0.80$ rather than the classical $q = 0.908$. Alternatively to a scan of the drive voltage at constant RF, a frequency scan at constant voltage can be applied to realize scans over an extended *m/z* range of up to about *m/z* 20,000. This demands a waveform generator coupled with a power amplifier, which is associated with excessive power consumption and difficulties in obtaining a high voltage output without waveform distortion [150].

The concept of the *digital ion trap* (DIT) makes use of a digital waveform to trap the ions. In this context, the terms *digital ion trap* and *digital waveform* describe a waveform composed of simple rectangular pulses applied to the ring electrode [150,162]. In practice, a switching circuit is used to generate a pulsed waveform by rapid alternation between discrete DC high-voltage levels (± 250 to ± 1000 V). The digital mode of pulse generation affords precise control of the timing. Furthermore, the AC excitation voltage connected across the end-cap electrodes can be delivered by the same digital circuitry. Interestingly, the ion motion under the influence of a digital waveform may still be expressed in terms of the conventional Mathieu parameters [150,162,163].

The development of the DIT has been pursued by Shimadzu and has reached a quite impressive level. Recently, an array of DITs, termed *ion trap array* (ITA), has been developed allowing multiple steps of isolation, activation, or scanning in parallel [164].

4.6.10 External Ion Sources for the Quadrupole Ion Trap

Chemical ionization (CI) mass spectra were first obtained by using the mass-selective instability mode of the QIT [145,146,165]. The reagent gas was admitted into the QIT, ionized and then allowed to react with the analyte.

With external ion sources it became feasible to interface any ionization method to the QIT mass analyzer. [166] However, commercial QITs are chiefly offered for two fields of applications: *i*) GC-MS systems with EI and CI, because they are either inexpensive or capable of MS/MS to improve selectivity of the analysis (Chap. 14); and *ii*) instruments equipped with atmospheric pressure ionization (API) methods (Chaps. 12, 13) offering higher mass range, and some 5-fold unit resolution to resolve isotopic patterns of multiply charged ions (Fig. 4.50) [140,154,167,168].

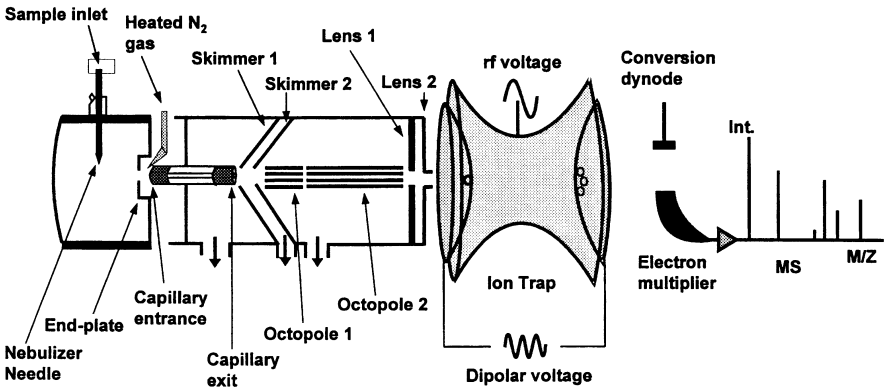


Fig. 4.50. Layout of a quadrupole ion trap instrument equipped with an external ESI ion source. The analogy to the ESI-LIT configuration shown in Fig. 4.41 is striking. Reproduced from Ref. [168] by permission. © John Wiley & Sons, 2000.

4.7 Fourier Transform Ion Cyclotron Resonance

4.7.1 Ion Cyclotron Resonance

The development that led to modern *Fourier transform ion cyclotron resonance* (FT-ICR) mass spectrometers began in 1932 when E. O. Lawrence applied a transverse alternating electric field orthogonally to a magnetic field to build a particle accelerator [169,170]. It was demonstrated that in *ion cyclotron resonance* (ICR) the angular frequency of the circular motion of ions is independent of the radius they are traveling on. Later, this principle was applied to construct an ICR mass spectrometer [171,172]. ICR mass spectrometers measuring the power absorption from the exciting oscillator were commercialized in the mid-1960s by Varian. Starting from their application to gas phase ion chemistry [173], ICR instruments made their way into analytical mass spectrometry. [174] However, it was the introduction of FT-ICR in 1974 that initiated the major breakthrough [175,176]. Ever since, the performance of FT-ICR instruments has steadily improved [177,178] to reach unprecedented levels of resolving power and mass accuracy when superconducting magnets are employed [179-184].

Note: Modern FT-ICR mass spectrometers offer ultrahigh resolving power ($R = 10^5$–10^6) [185,186] and highest mass accuracy ($\Delta m = 10^{-4}$–10^{-3} u, cf. Chaps. 3.5, 3.6) [183,184], attomol detection limits (with nanoESI or MALDI sources), high mass range and MS^n capabilities [187]. Most of the modern FT-ICR instruments actually represent some sort of hybrids with linear quadrupole or LIT front ends.

4.7.2 Ion Cyclotron Motion

As we know from the discussion of magnetic sectors, an ion of velocity v entering a uniform magnetic field B perpendicular to its direction will, by action of the Lorentz force (Chap. 4.3.2), immediately move on a circular path. Contemplating the path in the direction of the magnetic field reveals that negative ions circulate clockwise while positive ions move counterclockwise (Figs. 4.13, 4.51).

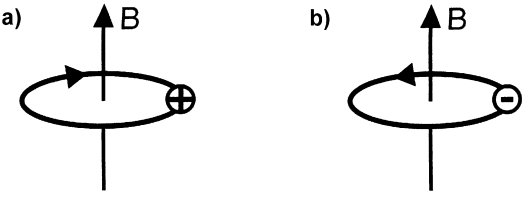


Fig. 4.51. Circular motion of ions in a magnetic field. Viewing along the direction of the magnetic field one observes (**a**) a counterclockwise motion for positive ions and (**b**) a clockwise motion for negative ions. Adapted from Ref. [188] with permission. © Elsevier Science Publishers, 2002.

The radius r_m of the ions' circular motion is determined by Eq. 4.13:

$$r_m = \frac{m_i v}{qB} \tag{4.13}$$

Upon substitution with $v = r_m\omega$ and rearrangement of the resulting term, *the cyclotron angular frequency* ω_c is obtained as:

$$\omega_c = \frac{qB}{m_i} \tag{4.33}$$

and by substituting with the cyclotron frequency ($f_c = \omega_c/2\pi$) Eq. 4.33 becomes

$$f_c = \frac{qB}{2\pi m_i} \tag{4.34}$$

One realizes that the cyclotron frequency is independent of the ions' initial velocity, but proportional to its charge and the magnetic field, and inversely proportional to its mass. Of any physical quantity, frequencies can be measured at the highest accuracy, and thus, cyclotron frequency measurements appear as ideal premises for building powerful *m/z* analyzers.

4.7.3 Cyclotron Motion – Excitation and Detection

Gaseous ions are not at rest but at least move arbitrarily at their thermal velocities. When such a package of thermal ions is generated within a magnetic field or is injected into it, the resulting small ion cloud contains ions that are all spinning at their respective cyclotron frequencies (circular micromotion) while the cloud as a whole remains stationary provided it has been brought to a halt within the field boundaries. Therefore, the magnetic field not only acts in an *m/z*-sensitive way by imposing the cyclotron motion on the ions, but also provides ion trapping in a plane perpendicular to its field lines (*xy*-plane, cf. action of the quadrupolar field in a LIT).

Upon excitation, the circular micromotion is superimposed by the macroscopic cyclotron motion of the whole ion cloud, i.e., the RF excitation field preserves the coherence of ion packages composed of ions of the same *m/z* value. As the initial kinetic energy of the ions is small as compared to the energy uptake from the RF field, it is of minor importance for the experiment [189]. Nonetheless, the complexity of the overall motion affects frequency-to-mass calibration if accurate results are required [190].

In practice, mass-selective excitation, so-called *resonant excitation*, is achieved by applying a transverse electric field alternating at the cyclotron frequency f_c ($\omega_c = 2\pi f_c$) to accelerate the ions. Such a field can be applied by a pair of RF electrodes placed on opposite sides of the orbit. As the ions accelerate, the radius of their orbit increases, and the resulting overall motion is a spiral (Fig. 4.52a)

[170,178]. For lighter ions, the spiral reaches the same radius with fewer cycles than in case of heavier ones, i.e., the spiral is steeper, because low-mass ions need less energy than high-mass ions to accelerate to a certain velocity.

Example: Consider a singly charged ion of a mass of 100 u at thermal energy. Assuming a temperature of 300 K, its average velocity (Boltzmann distribution) is about 230 m s^{-1}. In a 3-T magnetic field it will circulate at $r_m \approx 0.08$ mm. To increase the radius to 1 cm, Eq. 4.13 demands the velocity to rise by a factor of 125, i.e., to 28,750 m s^{-1}. Rearranging Eq. 4.3 delivers $eU = v^2 m_i/2$, and thus, we calculate a kinetic energy of about 430 eV. Definitely, the translational energy of ions in an ICR cell is high enough to effect activating collisions (Fig. 4.53 and Chap. 9) [189].

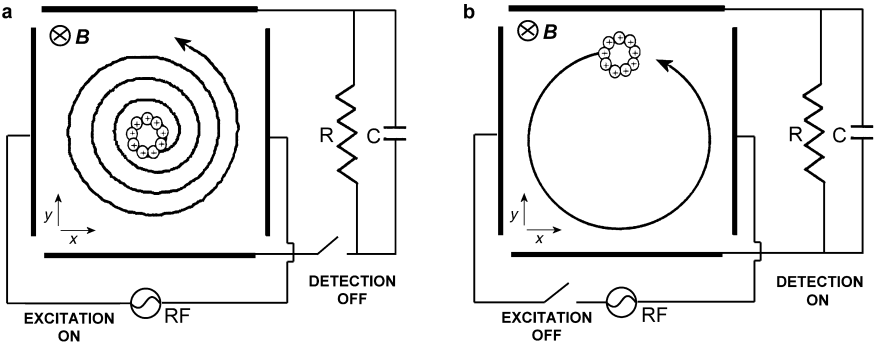


Fig. 4.52. The sequence of (**a**) excitation (**b**) and image current detection in ICR-MS. The ionic micromotion is indicated by the small circle of ions. The cell is shown along the direction of the magnetic field. (**a**) Illustrates the spiral trajectory of the ion cloud as induced by excitation of the ions by an RF electric field oscillating at the cyclotron resonance frequency. Note that the radius is a function of ion velocity, but the frequency f_c of circulation is not and that the radius remains constant during detection.

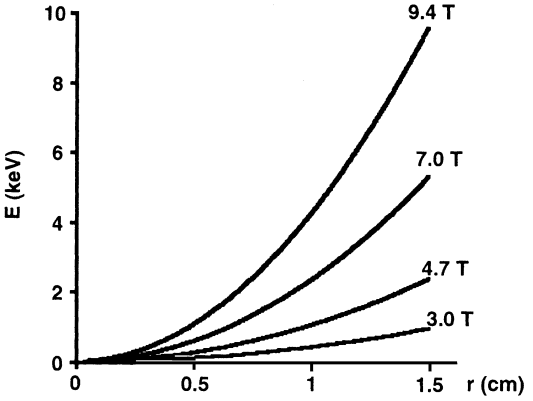


Fig. 4.53. Kinetic energy of *m/z* 100 ions in an ICR cell vs. orbital radius at magnetic field strengths from 3.0 to 9.4 T. Adapted from Ref. [189] with permission. © John Wiley and Sons, Inc., 1998.

The first-generation ICR instruments essentially performed an energy scan: the *m/z* value was obtained from the number of half cycles, until the ions struck an electrometer plate at $r = r_{cell}$ [171,172]. The disadvantages of this concept are clear: *i*) mass accuracy and resolution are limited to $1/N_c$ (N_c = number of half cycles); *ii*) the electric signal for ion detection is solely due to neutralization of the ions, and there is no amplification as obtained with multiplier-type detectors used with all other analyzers; and *iii*) the ions are removed from the cell upon detection precluding its use for MS/MS.

Moving from destructive detection by discharging the ions on the detection plates to nondestructive *image current detection* allows to switch from energy scanning to cyclotron frequency measurement (Fig. 4.52b) [191,192]. Image current detection relies on the fact that an ion cloud repeatedly attracts (positive ions) or repels (negative ions) the electrons of the detection electrodes upon its passage. The resulting minuscule image current can be amplified, transformed into a voltage signal and recorded as long as the ion motion exhibits sufficient coherence.

Note: In ICR cells, the ions circulate like separate swarms of birds rather than like matter in the rings of Saturn. If ions of the same *m/z* noncoherently circulated at the same frequency and radius, but occupied the total orbit rather than a small sector of it, there would be no image current induced upon their passage at the detector plates, i.e., coherence of the circulating ion motion is crucial.

4.7.4 Cyclotron Frequency Bandwidth and Energy-Time Uncertainty

The *frequency bandwidth* to be covered by an ICR instrument is governed by the *m/z* range to be analyzed. Assuming a 9.4-T superconducting magnet, which currently represents the "upper-middle class", we may now use Eq. 4.34 to calculate f_c for singly charged ions of *m/z* 50 ($m_i = 8.30 \times 10^{-26}$ kg) as $f_c = (1.66 \times 10^{-19}\ \text{C} \times 9.4\ \text{T})/(2\pi \times 8.30 \times 10^{-26}\ \text{kg}) = 3.00$ MHz. For an ion of *m/z* 500 (8.30×10^{-25} kg) we get a 10 times lower value, $f_c = 300$ kHz, and for an ion of *m/z* 5000 (8.30×10^{-24} kg) we arrive at 30 kHz. To handle ions in the range *m/z* 50–5000, the ICR frequency band has to span from 30 kHz to 3.0 MHz. In other words, an ICR instrument needs to cover a frequency range from several tens of kilohertz to a few megahertz (Fig. 4.54). The large bandwidth has severe implications on both the mode of operation to achieve homogeneous excitation and detection and on the electronics to deliver the required level of performance over the entire range.

Note: FT-ICR instruments from any vendor are exclusively equipped with superconducting magnets, with 7 T and 9.4 T as the usual field strengths, 12 T and 15 T have now become available. The advantages of increased field strength are numerous, e.g., resolving power and scan speed increase linearly with B. Moreover, upper mass limit, ion trapping time, ion energy, and number of trapped ions even increase with B^2.

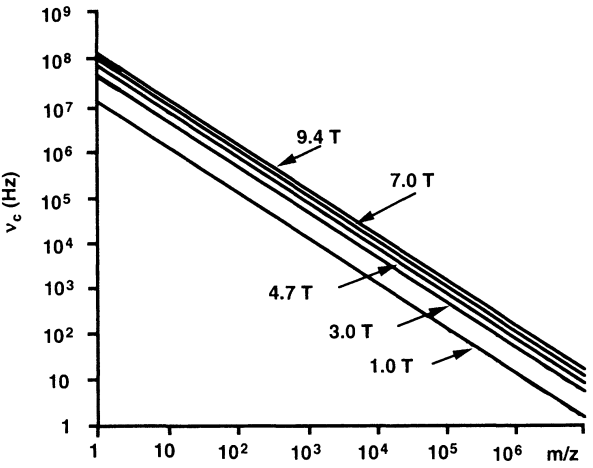


Fig. 4.54. Plot of ICR frequencies vs. *m/z* for different magnetic field strengths from 1.0 to 9.4 T. Reproduced from Ref. [189] with permission. © John Wiley and Sons, Inc., 1998.

Following the above calculation, it takes a frequency resolution of 3 Hz (300 kHz/100,000) to achieve a resolving power of $R = 100{,}000$ at *m/z* 500. The *energy-time uncertainty principle* states that $\Delta E \times \Delta t \approx h$. With $\Delta E = h\Delta\nu$ we derive $h\Delta\nu \times \Delta t \approx h$ or $\Delta\nu \times \Delta t \approx 1$. Accordingly, the above frequency resolution of 3 Hz in 0.3 MHz corresponds to a measurement time of 0.33 s per data point of the scan range. Operation of an ICR instrument in *continuous wave mode*, i.e., scanning in the frequency domain, is obviously unrealistic as soon as high resolving power is to be achieved. Therefore, the only practical way to acquire high-resolution ICR spectra would be to realize a broad band detection of all frequencies in parallel.

Although discouraging for ion detection, the energy-time uncertainty principle opens up new perspectives for ion excitation. According to $\Delta\nu \times \Delta t \approx 1$, a rectangular pulse of 1 ms duration covers a frequency bandwidth of 1000 Hz; a pulse of even 1 µs should correspond to a bandwidth (frequency uncertainty) of 1 MHz, i.e., shorter pulses cover increasingly broader ranges. This has been employed in so-called *pulse excitation*.

Note: The "bell" model: To understand pulse excitation, it is helpful to consider a mechanical comparison – a bell, for example, does not require excitation at its resonance frequency. Instead, a short strike with a hammer (pulse excitation) is fully sufficient. The bell takes up the energy with no specified frequency (all potential frequencies are contained) and automatically "finds" its own frequency plus its overtones to resonate and, thus, to sound.

4.7.5 Fourier Transform – Basic Properties

Some knowledge of the basic properties of the *Fourier transform* (FT) will be helpful prior to discussing FT-ICR instrumentation [193]. The Fourier transform is a mathematical operation that transforms one complex-valued function of a real variable into another. The domain of the original function is typically time (as is here) and accordingly is termed the *time domain*. The domain of the function generated upon FT is frequency. The product of FT then is the *frequency domain* representation of the original function. The frequency domain function describes which frequencies are contained in the original function. For example, FT applied to a chord of music comprising several fundamental frequencies (and overtones) as represented by the notes would deliver all contributing frequencies and their amplitudes. The Fourier transform makes the move from a wave and its amplitude to its frequency and its amplitude (Fig. 4.55a,b).

FT of a transient signal, i.e., a signal vanishing to zero amplitude at the end of the observation time span, delivers a Lorentzian curve in the frequency domain (Fig. 4.55c,d). In accordance with the energy-time uncertainty principle, the frequency domain output becomes increasingly sharper the longer the observation time span, because the frequency is more accurately determined the more cycles are recorded in the transient.

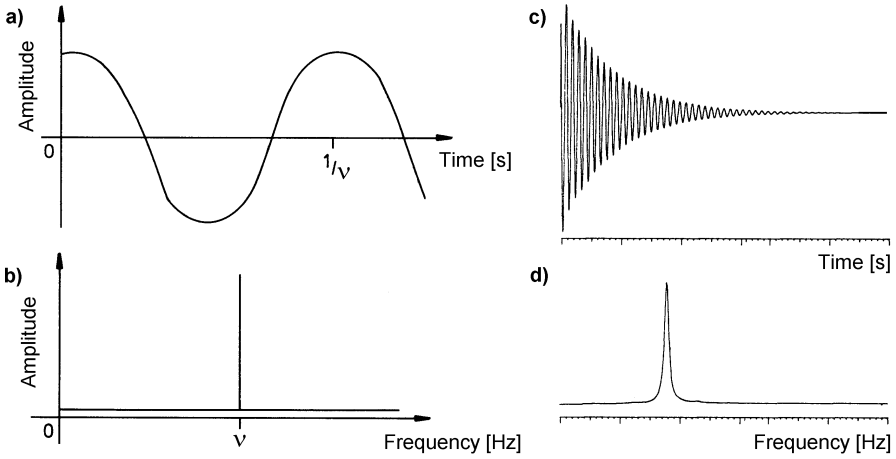


Fig. 4.55. Illustration of the FT principle. (**a**) A time domain wave, infinite in time, is transformed by FT to (**b**) reveal its frequency. The amplitude is conserved. (**c**) FT of a transient time domain signal into (**d**) a frequency domain signal of Lorentzian shape. FT also works when a large number of frequencies and amplitudes is contained in the time domain signal.

Note: Jean-Baptiste Joseph Fourier, French mathematician (1768–1830). Besides Fourier transformation, his influential work concerns the mathematical description of the conduction of heat in solids and the development of infinite series (Fourier series). He witnessed the French revolution and accompanied Napoleon on his expedition to Egypt.

In FT-ICR experiments, the observation time span is normally shorter than the time required to damp down the transient to zero. Instead, the detection is abruptly ended when the preset transient length is reached. The duration of the transient is generally determined by the product of the number of data points that is to be recorded and the rate at which those data points are being sampled. The minimum *sampling rate* is in turn determined by the highest cyclotron frequency to be observed. Typical values in FT-ICR-MS are 0.5–2 s transients of 512 k to 2 M (2×10^6) data points at 250 kHz to 1 MHz sampling frequency. Thus, the arbitrary truncation of the transient causes the transient to represent a combination of a step function and a perfectly dampened signal (Fig. 4.56). As FT yields sinc (x) from a step function, the FT output from a truncated signal is a Lorentzian main peak accompanied by side bands, so-called *wiggles*.

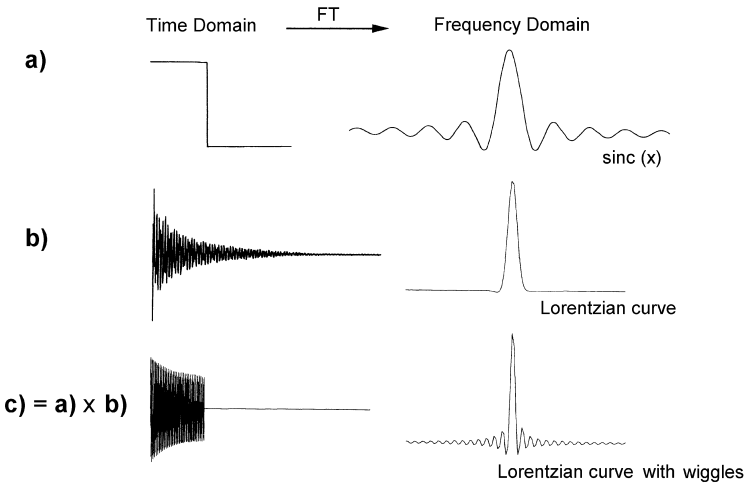


Fig. 4.56. The effects of Fourier transforms on different input signals. (**a**) A step function is converted to sinc (x), (**b**) a fully dampened transient signal containing only one frequency yields a single Lorentzian curve, and (**c**) the truncated transient can be regarded as a combination of (**a**) and (**b**) and yields a Lorentzian curve accompanied by "wiggles".

To reduce the side band-creating effect of truncation, the transient is normally subjected to *apodization* prior to FT. Apodization means the multiplication of the signal by a mathematical function that causes the values to smooth out to zero. Some sophisticated apodization methods are in use to deliver the ultimate resolution, nonetheless, simple sin (x) or $\sin^2$ (x) functions work well.

Another feature of FT is to yield better resolved frequency spectra from larger data sets, which not necessarily need to contain real data. Simply adding a row of zeros to the end of the experimental transient is beneficial in that it smoothes the peak shape by increasing the number of data points per *m/z* interval. This "trick" is known as *zero-filling*. The number of attached zeros normally equals the number of data points, sometimes even twice as many are filled in (*double zero-filling*).

4.7.6 Nyquist Criterion

As we know from Chap. 4.2.7 the shape of a signal depends heavily on the sampling rate. The sampling rate is even more relevant for periodic signals such as from the cyclotron motion in FT-ICR. The minimum sampling rate needed to correctly detect any periodic signal is governed by the *Nyquist criterion*, according to which the sampling rate, ν_{samp}, must have at least twice the frequency of the process, ν_{proc}, that is to be recorded

$$\nu_{samp} \geq 2 \times \nu_{proc} \tag{4.35}$$

Vice versa, the *Nyquist limit frequency*, ν_{nyq}, up to which a process can just be correctly detected is given as

$$\nu_{nyq} = \nu_{samp} / 2 \tag{4.36}$$

aliasing (or *folding back*) occurs beyond the Nyquist limit. Then, the detected signal pretends the process to proceed at a foldback frequency, ν_{fold}, described by

$$\nu_{fold} = |n \times \nu_{samp} - \nu_{proc}| \tag{4.37}$$

where the factor n is an integer selected as to fulfill the condition $0 < \nu_{fold} \leq \nu_{nyq}$ An illustration of the folding back phenomenon is given in Fig. 4.57.

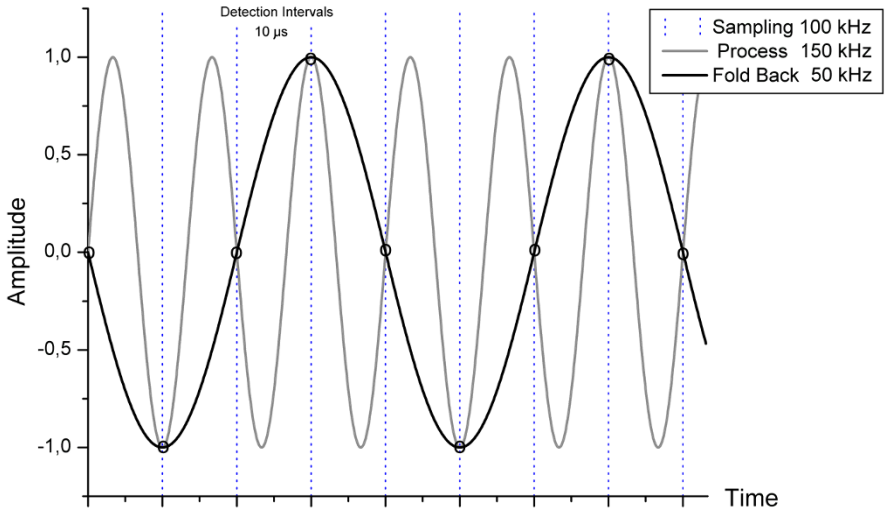


Fig. 4.57. The aliasing phenomenon. Detection points are where the *dotted* verticals cross the *light gray* signal curve (**o**). The process (150 kHz) occurs at $\nu_{proc} = 1.5 \times \nu_{samp}$ (100 kHz or 10 µs per point) instead of $\leq 0.5\ \nu_{samp}$. This causes the output of an aliased signal at $\nu_{fold} = 50$ kHz as determined by Eq. 4.37 (*dark curve*). In this special case setting n =1 just delivers $\nu_{fold} = \nu_{nyq}$.

4.7.7 Excitation Modes in FT-ICR-MS

In the ICR cell, there is a stringent correlation of cyclotron frequency f_c and *m/z* value. For simplicity, the very first FT-ICR experiment was therefore performed with an excitation pulse of a fixed f_c tailored to fit the model analyte, methane molecular ion [175]. However, useful measurements require the simultaneous excitation of all ions in the cell, and this in turn demands for a large RF bandwidth.

Several excitation methods have been developed to cope with this technically nontrivial task. The differences between these methods can easily be judged from the shape of the frequency-domain excitation waveforms (Fig. 4.58) [178,189]. The simplest approach is to irradiate a single frequency (resonant excitation) for some time, i.e., as a *rectangular pulse*, but this selectively excites ions of a single mass [175]. Applying such a narrow band excitation as a short pulse yields some expansion of the range. The effect of a *frequency sweep* or *"chirp" excitation* is much better [176]. Chirp excitation sequentially affects ions across the *m/z* range although it never delivers a defined frequency. Instead, the chirp exploits the wide band character of rushing across the frequencies. Chirp excitation is not perfectly

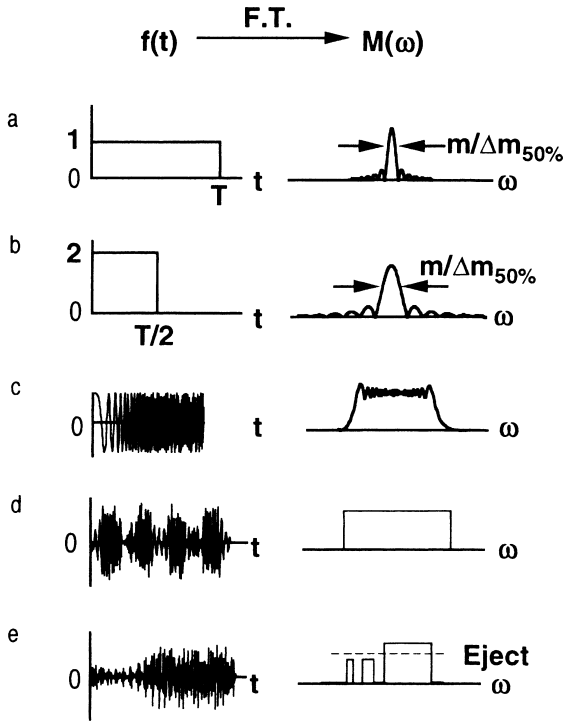


Fig. 4.58. Time-domain (*left*) and frequency-domain (*right*) excitation waveforms: (**a**), (**b**) rectangular pulses yield inhomogeneous and rather narrow excitation windows; (**c**) "chirp" excitation; (**d**), (**e**) SWIFT excitations, with (**e**) designed to eject a certain mass range from the cell. Reproduced from Ref. [189] by permission. © John Wiley & Sons, 1998.

homogeneous as it gives some distortions close to the borders of the range, nonetheless is it successfully employed in commercial FT-ICR instruments.

The best results are to be expected from *stored waveform inverse Fourier transform* (SWIFT) excitation [194]. First, the ideal excitation waveform is tailored to the needs of the intended experiment and then produced by an RF generator. SWIFT excitation also allows to remove ions of predefined *m/z* ranges from the ICR cell. This results in storage of a small *m/z* range, or after repeated SWIFT pulsing of a single nominal mass out of a broad band spectrum. Those ions are then accessible for ultrahigh resolution measurements or as precursors for tandem MS.

4.7.8 Axial Trapping and Design of ICR Cells

Our basic considerations of ICR (Chap. 4.7.3 and Fig. 4.52) were restricted to the *xy*-plane of a cell. Two of the four side walls (*x*-axis) of the ICR cell are connected to the RF power supply during the period of excitation. Then, the image current induced in the detector plates (*y*-axis) is recorded as transient signal for some period of time (0.5–30 s). The excitation of the ions within the ICR cell has to stop at a level low enough to avoid wall collisions of the lightest ions to be measured [181,188,189].

At a first glance, the *z*-dimension of the cell seems to be of no importance for the function of an FT-ICR mass spectrometer. However, the *z*-component of thermal energy and the kinetic energy of ion injection into the ICR cell in case of an external ion source both would lead to rapid loss of the *xy*-trapped ions along that axis, because they would pass through the cell along the *z*-axis on a helical trajectory. It is therefore important to establish a trapping potential in *z*-direction. The simplest way is to place DC trapping electrodes at the open ends [172]. Furthermore, our initial treatment of the ICR cell was also done with the implicit understanding that this would be a cubic cell.

However, due to field imperfections of simple cubic cells, other designs offering enormous improvements over the cubic cell have been developed [188,189]. As in case of the LIT with radial ejection (Chap. 3.5.3 and Figs. 4.39, 4.40), the distortion of the electric field can be avoided when the trapping sections are properly designed and operated. Then the ICR cell appears to the ions as of virtually infinite length (Fig. 4.59). Such improved geometries make use of segmented end caps on cylindrical cells (*Infinity Cell*™ [195]), thrice segmented cylindrical cells [196], and many others [197].

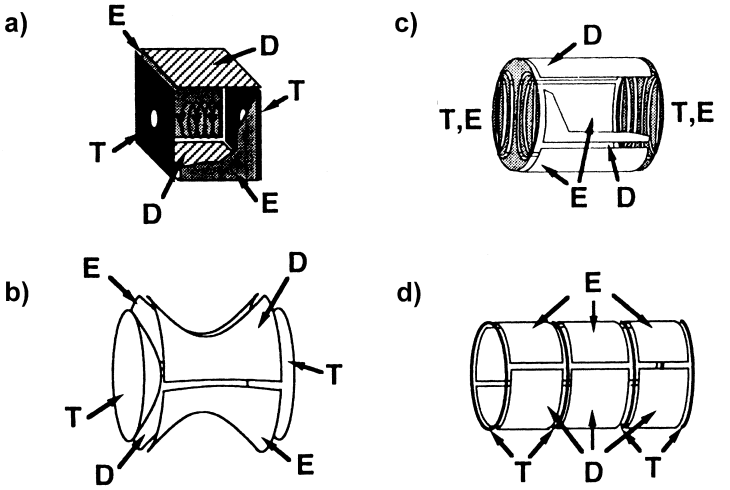


Fig. 4.59. Important ICR cell types; electrodes are labeled with **E**: excitation, **D**: detection, **T**: trapping; (**a**) classic cubic cell, (**b**) Penning cell with hyperbolic electrodes, (**c**) infinity Cell™ with segmented trapping plates, and (**d**) triple cell. The latter two aim at virtually expanding the potentials in the trapping zone along the *z*-axis. Adapted from Ref. [197] with permission. © Elsevier Science Publishers, 1995.

4.7.9 Magnetron Motion and Reduced Cyclotron Frequency

Trapping of ions in a potential well implies reflection of ions between the trapping plates that induces an oscillatory motion along the *z*-axis the frequency ω_z of which is given by

$$\omega_z = \sqrt{\frac{2qV_{trap}\alpha}{ma^2}} \tag{4.38}$$

where a is the physical z-dimension of the trap and α represents a shape parameter that depends on the trap design [189]. The curved electric field close to the borders also produces an outward-bound radial force $F_r = qE_{(r)}$ opposed to the action of the Lorentz force F_L that is given by

$$F_r = q\,E_{(r)} = \frac{qV_{trap}\alpha}{a^2}r \tag{4.39}$$

The magnetic field now acts by transforming the radial force component into another circular motion of the trapped ions. The total force on an ion then is

$$F_{tot} = F_L - F_r = m_i \omega^2 r = q B \omega r - \frac{q V_{trap} \alpha}{a^2} r \tag{4.40}$$

which can be rewritten to reveal its character of a quadratic equation in ω

$$\omega^2 - \frac{q B \omega}{m_i} + \frac{q V_{trap} \alpha}{a^2} = 0 \tag{4.41}$$

This quadratic equation has two solutions, the first of them representing the *reduced cyclotron frequency* ω_+

$$\omega_+ = \frac{\omega_c}{2} + \sqrt{\left(\frac{\omega_c}{2}\right)^2 - \frac{\omega_z^2}{2}} \tag{4.42}$$

and the second the *magnetron frequency* ω_-

$$\omega_- = \frac{\omega_c}{2} - \sqrt{\left(\frac{\omega_c}{2}\right)^2 - \frac{\omega_z^2}{2}} \tag{4.43}$$

where ω_z is obtained from Eq. 4.38 and ω_c from Eq. 4.33. The obvious consequence for the ionic motion in an ICR cell is that the simple description of ω_c by Eq. 4.33 only yields the so-called *unperturbed cyclotron frequency*, whereas the real motion is by far more complex. Figure 4.60 shows the overall motion of ions in an ICR cell taking ω_z, ω_+ and ω_- into account [198]. In many cases the magnetron motion also causes a small side peak in the vicinity of the main peak.

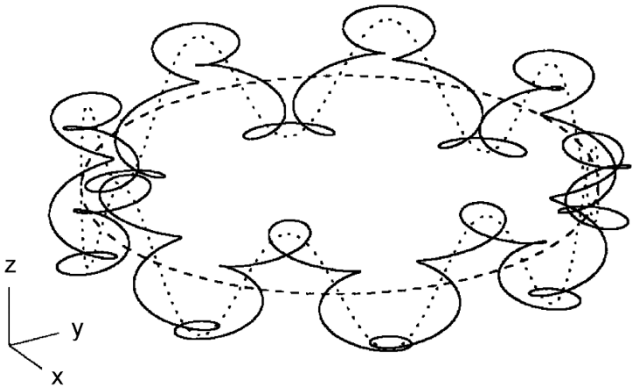


Fig. 4.60. Ion motion for $\omega_+ = 4\omega_z$ and $\omega_z = 8\omega_-$ in an ICR cell. Pure magnetron motion (*dashed*), magnetron plus trapping motion (*dotted*), and the resulting overall motion (*solid*). Reproduced from Ref. [198] by permission. © Elsevier Science Publishers, 1995.

4.7.10 Detection and Accuracy in FT-ICR-MS

An FT-ICR experiment requires full temporal separation of excitation and subsequent detection of the trapped ions. Detection is based on the measurement of image currents in the detector plates. An image current is induced by each ion package when repeatedly passing the detector plates at its individual cyclotron frequency, i.e., detection in FT-ICR means "listening to the circulating ions". The transient *free induction decay* (FID) is recorded, and afterwards, the FID is converted from the *time domain* to the *frequency domain* by means of Fourier transformation. This means that the complex FID caused by superimposition of many single frequencies is deconvoluted to reveal the single contributing frequencies and their respective amplitudes. Using Eq. 4.34, the frequencies are converted to *m/z* values; their amplitudes now representing the abundances of the corresponding ions (Fig. 4.61) [170,175,178,199,200].

The detection efficiency is greatly improved for cylindrical cells as compared to cubic cells, because the ions pass the detection electrodes at almost constant distance to their surface. This results in stronger image currents due to on the average closer passages and sharper detection wave forms as their entering and exiting from the detection zone causes more sudden changes.

The ICR voltage signal strength at the detector plates is inversely proportional to ion mass if the monitoring circuit is predominantly resistive, and is independent of ion mass if the circuit is predominantly capacitive [200]. Image current detection at room temperature is typically less sensitive than ion counting techniques in

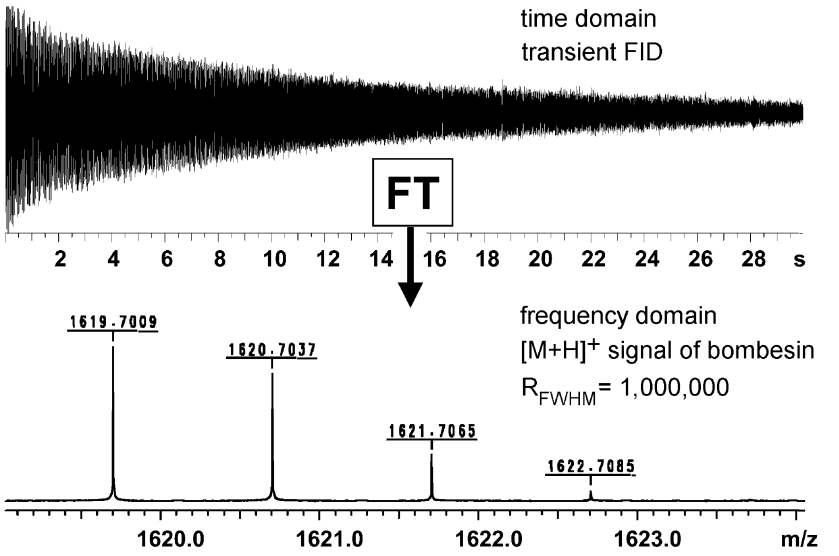


Fig. 4.61. The principle of FT-ICR-MS. In detail, the procedure includes recording the transient, apodization of the transient, zero-filling, FT, and finally the calculation of *m/z* values from the cyclotron frequencies. The longer the detection interval the higher the attainable resolving power. By courtesy of Bruker Daltonik, Bremen.

beam instruments. However, for a modern FT-ICR instrument equipped with typical detection circuits, the detection limit to yield a signal-to-noise ratio of 3:1 corresponds to roughly 200 ions, provided these are excited to travel at half of the maximum cyclotron radius [188].

There is a correlation between the transient signal and the pressure in the ICR cell [189,199]. In perfect vacuum, the orbiting motion would solely be dampened by induction, whereas in the presence of residual gas collisions will finally slow down the ions to thermal energy. As the resolving power in FT-ICR-MS is also proportional to the acquisition time of the FID signal, ultrahigh vacuum in the range of $\approx 10^{-10}$ mbar is a prerequisite in the ICR cell.

Some advantages of FT-ICR-MS are obvious: *i*) the $1/N_c$ limit vanishes because every ion makes some 10^4–10^8 cycles during the detection interval; *ii*) sensitivity improves because the ions give rise to a detectable image charge during each passage of a detector plate; and *iii*) ion detection is nondestructive, i.e., ions are not lost upon detection allowing the performance of MS/MS experiments. In addition, elongated recording of the FID provides for extremely precise determination of all cyclotron frequencies, thereby yielding the highest values of resolution and mass accuracy available [185,186,201].

External calibration is most effective when the level of excitation and the number of trapped ions of calibrant ions closely approaches that of the analyte ions [188]. The latest FT-ICR instruments can routinely attain mass accuracies of better than 1 ppm. Internal calibration can yield further improvement.

Although resolution and mass accuracy are already high in broadband spectra ($R = 3 \times 10^4$–10^5, $\Delta m < 10^{-3}$ u), the performance of FT-ICR instruments further improves by storing only narrow *m/z* ranges, because fewer ions in the cell mean less distortion by coulombic interactions.

Note: The need for almost perfect vacuum, i.e., extremely long mean free paths, in FT-ICR mass spectrometers arises from the combination of high ion velocities of several 10^3 m s^{-1}, observation intervals in the order of seconds, and the effect of collisions on peak shape.

4.7.11 FT-ICR Instruments

Ion traps, ICR cells as well as QITs, are best operated with the number of trapped ions close to their respective optimum, because otherwise ion trajectories are distorted by coulombic repulsion. Hence, external ion sources in combination with ion transfer optics capable of controlling the number of injected ions are ideally attached to ion traps. Currently, MALDI [202] and even more so ESI [182,185,186,201,203] ion sources predominate in FT-ICR. The ion current is not solely regulated by the source but by some device to collect and store the desired amount of ions until the package is ready for injection into the ICR cell. Linear RF-multipole ion traps are normally employed for that purpose (Chap. 4.4.6) [98,204], but other systems are also in use [187]. RF-only multipoles are com-

monly used to transfer the ions through the boundaries of the magnetic field into the ICR cell (Chap. 4.4.4). For their injection, it is important to adjust the conditions so that the ions have low kinetic energy in *z*-direction in order not to overcome the shallow trapping potential. While some buffer gas is beneficial in case of LITs and QITs, ICR cells are operated at the lowest achievable pressure. The typical path from an external ion source into the ICR cell is therefore characterized by multistep differential pumping to achieve some 10^{-8}–10^{-7} Pa inside the ICR cell (Fig. 4.62).

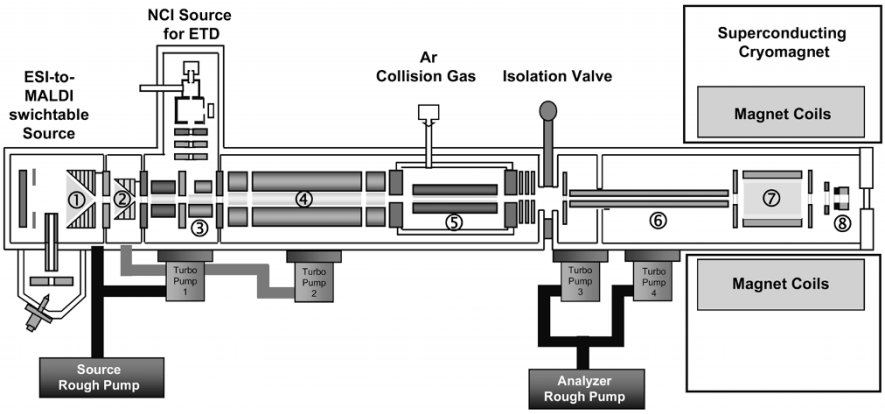


Fig. 4.62. hQh-ICR hybrid instrumentation. This instrument is equipped with an ESI-to-MALDI switchable ion source that makes use of a two-stage ion funnel (①, ②) to focus ions into a RF hexapole ion guide (h, ③). The ions then pass a quadrupole (④) that may either be run as band pass (q) or as mass-selective device (Q) and then reach a multifunctional RF hexapole ion trap (h, ⑤) where they can be *i*) accumulated, *ii*) collisionally activated, or *iii*) reacted with radical anions from the NCI source to effect ETD as required. For mass analysis the ions are then guided via an RF-only hexapole (⑥) into the ICR cell (⑦) where a hollow cathode (⑧) is attached for ECD. Schematic of Bruker Solarix instrument series by courtesy of Bruker Daltonik, Bremen.

Note: Occasionally, FT-ICR-MS is inaccurately referred to as FTMS. Of course, ICR without Fourier transformation would not have become as successful as it has, but Fourier transformation alone cannot separate ions according to *m/z*. With the advent of the orbitrap analyzer (below), there is a second system that makes use of Fourier transformation. Hence, the acronym FT-MS is proposed for all FT-based methods such as FT-ICR and orbitrap.

4.8 Orbitrap Analyzer

The *orbitrap* analyzer incorporates a completely new concept of *m/z* analysis [15,205]. Commercialized by Thermo Fisher Scientific in 2005, the Orbitrap™ delivers high resolving power and accurate mass measurement at a level rivaling FT-ICR to a certain extent [15,206-210]. It is the special charm of the orbitrap to operate without a magnetic field, and therefore, to be available at a much lower price and lower installation room requirements than FT-ICR instruments. Nonetheless, it has one important feature with FT-ICR in common: the orbitrap also employs image current detection of ion oscillations and Fourier transformation for the conversion of the transient into the frequency domain.

Note: The orbitrap is also an ion trap, but there is neither RF nor a magnet to hold ions inside. Instead, moving ions are trapped in an electrostatic field. The electrostatic attraction towards the central electrode is compensated by a centrifugal force that arises from the initial tangential velocity of ions: very much like a satellite in orbit [206].

4.8.1 Orbitrap – Principle of Operation

In 1923, Kingdon constructed an ion trapping device based on a straight wire along the axis of a surrounding cylindrical electrode having flanges that enclosed the trapping volume. Ions tangentially approaching the wire that is set to attractive electric potential would not hit the wire but become captured in a rotational motion around it. Their trajectory is then defined by an equilibrium of the centrifugal force and the electrostatic force generated by applying a voltage between wire and enclosing cylinder. Axial motion along the wire is confined by the field curvature introduced by the flanges of the cylinder. This became known as the *Kingdon trap* [211]. Later, Knight refined the outer electrode shapes to a design with large radius in the center that continuously decreased toward both ends. The outer electrode was symmetrically split into halves in a fashion similar to the end caps of the QIT. This trap design is often called *ideal Kingdon trap* [212]. Knight's trap could store ions and eject them onto a detector, but did not perform any *m/z* analysis [210]. The first proposal to build a Kingdon trap-based mass analyzer with image current detection addressed the ion rotational frequencies, but it suffered from the poor definition of those frequencies due to the influence of initial ion velocity upon entering the trap [213]. Finally, the concept of Makarov exploited the periodic back and forth motion of ions along the central electrode [205]. This setup requires a precisely defined field composed of a quadrupole field of the ion trap and the logarithmic field of a cylindrical capacitor that is split into two halves. This mass analyzer was termed *orbitrap* [205] and can be considered as a refined Knight-style Kingdon trap. It has a spindle-like central electrode and a barrel-like outer electrode (Fig. 4.63) [210].

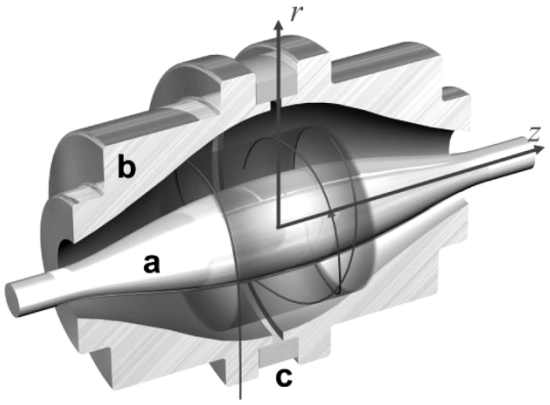


Fig. 4.63. A cut-away view of the Thermo Fisher Orbitrap™ mass analyzer. Ions are moving in spirals around a spindle-like-shaped central electrode (**a**) that creates an axial field gradient. An outer electrode (**b**) is split in half by an insulating ceramic ring (**c**). An image current induced by moving ions is detected via a differential amplifier between the two halves of the outer orbitrap electrode. The *m/z* of different ions in the orbitrap can be determined from respective frequencies of oscillation after a Fourier transform. Reproduced from Ref. [206] with permission. © Wiley-VCH, Weinheim, 2006.

The electric field resulting from the complex shape of the orbitrap electrodes may be termed quadrologarithmic field and has the potential distribution $U(r,z)$

$$U(r,z) = \frac{k}{2}\left(z^2 - \frac{r^2}{2}\right) + \frac{k}{2}\left(R_m\right)^2 \ln\left[\frac{r}{R_m}\right] + C \tag{4.44}$$

where r and z are cylindrical coordinates ($z = 0$ being the plane of symmetry of the field), k is the field curvature, R_m the characteristic radius, and C is a constant [205,214]. Equation 4.44 determines the electrostatic field experienced by ions inside the orbitrap that forces them to move in complex spiral patterns. Stable ion trajectories combine rotation around the central axis with axial oscillations, the frequency ω_z of which solely depends on the ratio of ionic charge q to ionic mass m_i and the field curvature, but is independent of the tangential velocity and spatial spread of the ions [206].

A detailed mathematical treatment of the orbitrap can be found in Refs. [15,205]. It delivers this important frequency of axial oscillations ω_z (in rad/s) as given by

$$\omega_z = \sqrt{k\left(\frac{q}{m_i}\right)} \tag{4.45}$$

The frequency of the harmonic axial oscillation ω_z is inversely proportional to the square root of the mass-to-charge ratio of the ions.

Another two characteristic frequencies can be derived for ions inside the orbitrap. First the frequency of rotation ω_φ around the central electrode

$$\omega_\varphi = \frac{\omega_z}{\sqrt{2}} \sqrt{\left(\frac{R_m}{R}\right)^2 - 1} \tag{4.46}$$

and second, the frequency of radial oscillation ω_r, i.e., the "pumping motion" of the orbit as the ions move along the variable radius of the central electrode:

$$\omega_r = \omega_z \sqrt{\left(\frac{R_m}{R}\right)^2 - 2} \tag{4.47}$$

4.8.2 Ion Detection and Resolving Power of the Orbitrap

The frequency of the harmonic axial oscillation ω_z can be determined by image current detection from a differential amplifier connected to the halves of the outer electrode; for each *m/z* value a sine wave is produced. Analogous to FT-ICR, the image current signal is monitored, stored, and translated into a frequency domain signal by fast Fourier transform resulting in an accurate reading of their *m/z* (Fig. 4.64) [206,215]. Different from FT-ICR, there is no excitation prior to the detection period. Instead, the electric field gradient induces the axial oscillation when ions are injected tangentially but off-center with respect to plane of symmetry. All ions have exactly the same amplitude whereas the frequency of axial motion is dictated by their *m/z* value. Again, there is an analogy to FT-ICR in that packets of ions of common *m/z* exhibit discrete motions with some interference by interpenetration of ion clouds of different *m/z* that are simultaneously occupying the trapping volume [15].

In an orbitrap, the mass resolving power *R* is half the frequency resolving power due to the square root in Eq. 4.45 [210,214]. It can be calculated as

$$R = \frac{m}{\Delta m} = \frac{1}{2\,\Delta\omega_z} \sqrt{\frac{kq}{m}} \tag{4.48}$$

Note: While the frequency of the axial oscillation ω_z in an orbitrap is proportional to $(q/m)^{1/2}$, the cyclotron frequency ω_c in FT-ICR is proportional to q/m. As a consequence, FT-ICR offers better resolving power for lower *m/z* ions whereas the orbitrap may outperform it at high *m/z* values, e.g., above *m/z* 800 in case of an FT-ICR instrument with a 7-T magnet [206,210].

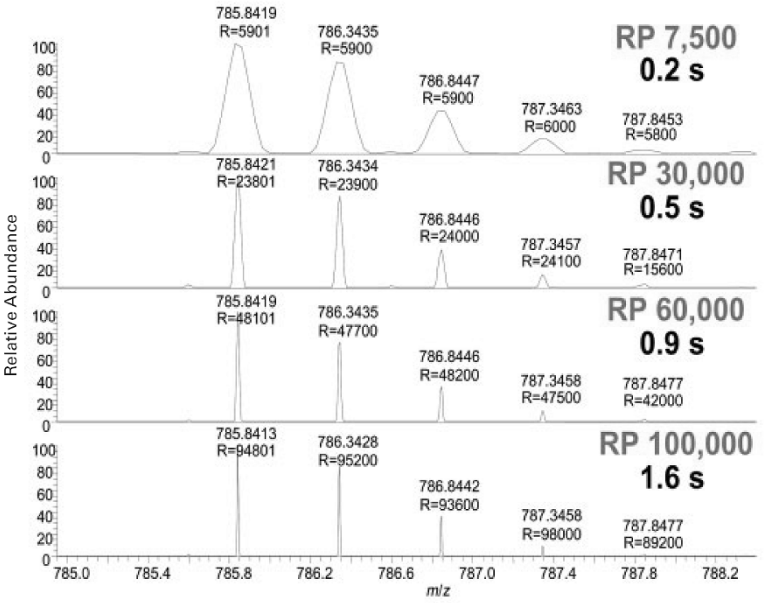


Fig. 4.64. Resolving power of a commercial orbitrap instrument as achieved for doubly charged peptide ions at detection intervals ranging from 95 ms to 1267 ms resulting in cycle times from 0.2 to 1.6 s. The cycle times are longer than pure detection intervals due to preparation of ion packets, data processing etc. The values specified are calculated with reference to the manufacturer's standard value of *m/z* 400. Reproduced from Ref. [206] with permission. © Wiley-VCH, Weinheim, 2006.

4.8.3 Ion Injection into the Orbitrap

The orbitrap alone does not present a very practical instrument. While it serves as a high performance *m/z* analyzer, its operation demands for proper ion injection and it requires ultra-high vacuum in order to realize sufficiently long transients. Ion injection has several aspects: *i*) geometric prerequisites such as injection angle, angular spread, and position with respect to the electrodes; *ii*) energetic requirements as far the initial ion velocity and the velocity distribution is concerned; *iii*) temporal in terms of timing of the injection and its duration, and *iv*) quantitative as far as dosage of ions is concerned. The ultra-high vacuum is needed to warrant the mean free path for tens to hundreds of thousands of undisturbed revolutions around the center electrode.

Thus, a bent RF-only quadrupole is employed to accumulate, store, and thermalize the ions by a low pressure of nitrogen prior to injection. Derived from the shape of the RF section in the form of the letter "C" this part has been termed the *C-trap*. The C-trap can be filled with about a million elementary charges. Collisional damping is important, because this way the ions are brought to rest in the

middle of the C-trap. Nitrogen is used for that purpose as it is already used in the source region of the instrument and it is efficient at capturing and cooling the ions. In other words, the C-trap decouples the orbitrap from all preceding steps of ion generation, desolvation, and eventually precursor ion selection [215].

High-voltage electric pulses with short rise times in the order of few hundreds of nanoseconds serve to eject the ions from the C-trap through the gap between the inner pair of quadrupole rods along lines converging on the entrance of the orbitrap. By lowering the electric potential of the central electrode simultaneously with the entry of the ion packets, ions are captured and start circling. Typically, the ions are injected at kinetic energies of about 1.3 keV while the central electrode is set to –3.4 kV (for positive-ion mode) [210]. The initial bunches become reshaped into rings that oscillate axially along the central electrode. The amplitude of these oscillations is determined by the initial offset of ion injection from the orbitrap center, whereas coherency of axial oscillations, i.e., maintenance of thin rings, is ensured by the short temporal duration of ion packet injection (Fig. 4.65).

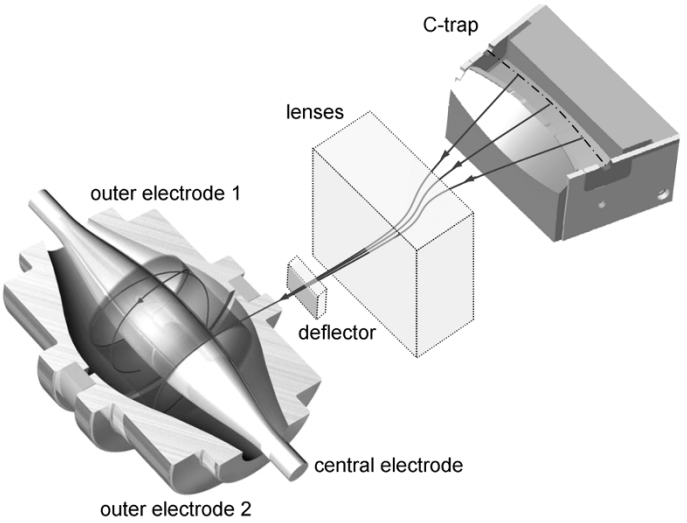


Fig. 4.65. The orbitrap mass analyzer with ions being injected from the C-trap through lenses and a deflector. During injection, the C-trap acts as a convex lens with the outer rods pushing and the inner short rods pulling the ions by a DC pulse. Trapping voltage is applied to the central electrode. Courtesy of A. Makarov, Thermo Fisher Scientific.

4.8.4 Hybridization with a Linear Quadrupole Ion Trap

To become an analytically useful mass spectrometer, the above combination still needs to be interfaced to an ion source. The prototype implementation of the orbitrap made use of laser desorption/ionization in the immediate vicinity of the orbitrap [205], but soon, an external electrospray ion source followed [214]. For highest versatility, the orbitrap has been attached to the rear of a fully functional

Thermo Fisher LTQ instrument (cf. Chap. 4.5.3 and Fig. 4.41). The LIT may either be operated on its own as it still is equipped with SEM detectors or it may be axially emptied into the C-trap via an RF-only transfer octopole. The whole setup, dubbed LTQ-orbitrap, is shown in Fig. 4.66. This instrument offers both low-resolution MS and MS^n operation in the LTQ section and final high-resolving *m/z* analysis at ppm-accuracy of whatever ions decided to be sent into the orbitrap [206-209,215]. A differential pumping system reduces the pressure along the instrument to achieve about 2×10^{-10} mbar in the orbitrap. Although the orbitrap has reached a certain maturity, there is still ongoing research for further improvement [216-218] and the series of instruments featuring an orbitrap analyzer is being expanded (Chap. 9.10).

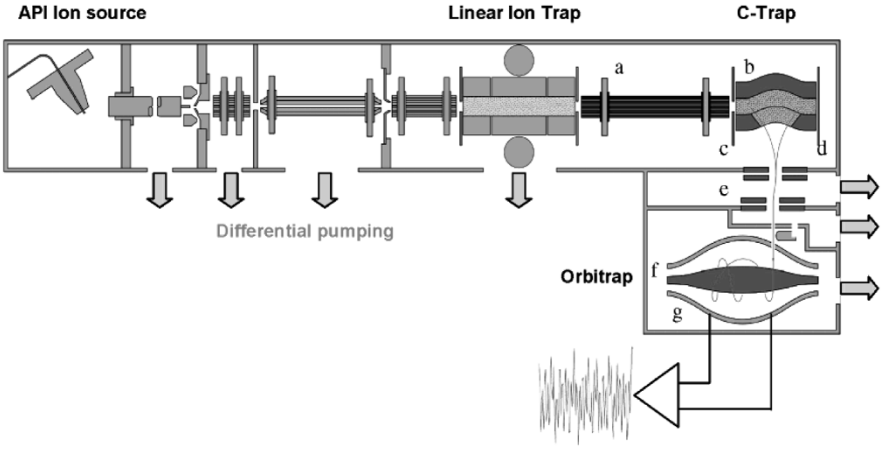


Fig. 4.66. The Thermo Scientific LTQ orbitrap mass spectrometer. The front end up to the LIT is identical to the LTQ instrument introduced in Chap. 4.5.3 and Fig. 4.41. Ions axially ejected from the LIT are entering (**a**) a transfer octopole to (**b**) a curved RF-only quadrupole known as C-trap, from where they are injected via (**c**) gate electrode, (**d**) trap electrode, and (**e**) ion optics into the orbitrap comprising (**f**) the inner electrode and (**g**) outer electrodes for detection. Note that there are four ports for differential pumping along the LTQ section and another three sideways to reduce the pressure from the C-trap to the orbitrap. Adapted from Ref. [208] with permission. © American Chemical Society, 2006.

4.9 Hybrid Instruments

As anticipated in the sections on linear ion traps (Chap. 4.4.6), modern Fourier transform-ion cyclotron resonance (Chap. 4.7.11), and LIT-orbitrap mass spectrometers (Chap. 4.8.4), our instrumentation may efficiently be constructed by combining different types of mass analyzers and ion-guiding devices in a single so-called *hybrid instrument* [219,220]. The driving force to do so is the desire to obtain mass spectrometers that unite the advantageous properties of each mass

analyzer they are composed of in order to have the most powerful machines for tandem mass spectrometry. In tandem mass spectrometers the first stage of *m/z* analysis (MS1) is used to select ions for further fragmentation and subsequent analysis of the product ions in a second *m/z* analyzer (MS2, Chap. 9). Budgetary aspects are another issue in favor of hybridization, because in a hybrid instrument each stage is selected as to deliver optimum performance at lowest cost. Cost is not only affected by the price of acquisition of a mass spectrometer but also by operation in that it may have highly variable requirements of room, power, and operational skills (Table 4.2).

Table 4.2. Rough estimates correlating instrumentation and factors affecting its cost[a]

	Acquisition	Installation room requirements		Operation and long-term usage	
	Price of instrument	Footprint and weight	Power consumption, air condition load	Qualification of personnel	Maintenance
Time-of-flight	S – L	S – L	S – M	S – L	S – L
Magnetic sector	L – XL	L – XL	L – XL	L – XL	L
Linear quadrupole	S – M	S – M	S – M	S – M	S – M
Quadrupole ion trap	S – M	S – M	S – M	S – M	S – M
Linear quadrupole ion trap	M – L	S – M	S – M	M – L	M
Fourier transform-ion cyclotron resonance	XL – XXL	XL – XXL	XL – XXL	L – XL	XL – XXL
Orbitrap	L – XL	L	L	L – XL	L
Quadrupole-TOF hybrid	M – XL	M – L	L	M – L	L
Ion mobility-TOF hybrid	XL	L	L	L – XL	L – XL

[a] classified in the format of American dress sizes as S, M, L, XL, XXL

4.9.1 Evolution of Hybrid Mass Spectrometers

The development of hybrid instruments started from magnetic sector-quadrupole hybrids, either BqQ [221,222], EBqQ, [223] or BEqQ [224-226]. Numerous other systems such as magnetic sector-QIT [227], magnetic sector-oaTOF [228,229], QITTOF [138,230,231], QqTOF [49,232-234], QqLIT [108], LITICR, and QqICR followed (Table 4.3).

The adaptation of conceptually different mass analyzers to each other may demand for sophisticated interfaces, because of the largely differing requirements concerning ion kinetic energies. The magnetic sector-quadrupole or magnetic sector-QIT hybrids, for example, require keV ions exiting the sector to be decelerated to some 10 eV before entering the qQ section, or to be slowed down and pulsed into the QIT, respectively. Due to the bulky and demanding magnetic sector analyzer, hybrids of that type do not anymore play a role.

Geometries composed of an oaTOF as second analyzer bear the advantage that advanced TOFs offer accurate mass measurements equaling the accuracy of magnetic sector instruments. Currently, QqTOF systems are among the commercially most successful hybrids. While their linear quadrupole front end serves as MS1 in tandem MS experiments, it is operated in RF-only mode when tandem MS is not intended, because this allows to acquire full-range spectra at high resolution using the TOF analyzer (MS2, Fig. 4.67).

The next higher level of performance can be achieved by replacing the oaTOF section with a FT-ICR analyzer. Those high-end instruments are either available as Qh-ICR by employing a quadrupole as first mass analyzer (Bruker Daltonik

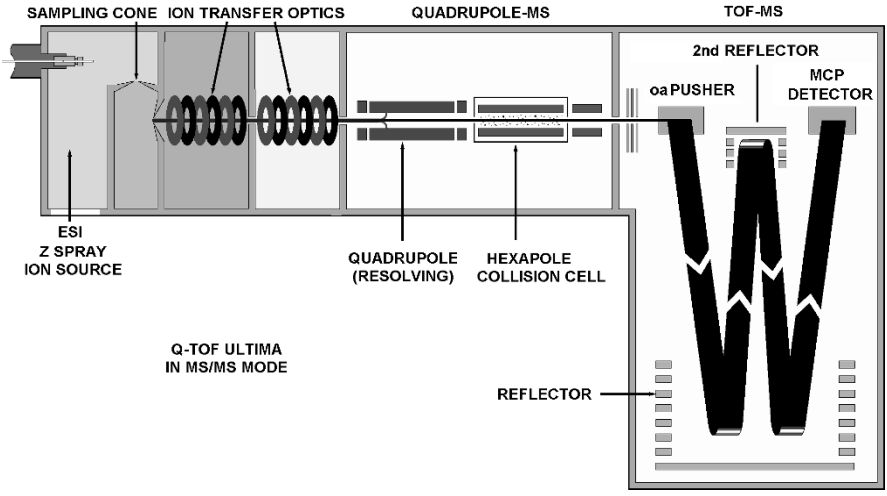


Fig. 4.67. The Q-TOF Ultima, Qh-oaTOF design, with ESI ion source in MS/MS mode. The TOF analyzer has a reflector that can either be operated using the large reflector alone (V-mode) or adding a second stage of ion reflection (W-mode) for higher resolving power. Courtesy of Waters Corporation, MS Technologies, Manchester, UK.

APEX-Q and Solarix instruments, Fig. 4.62) or as LIT-ICR, i.e., with a linear ion trap in front of the ICR cell (Thermo Fisher LTQ-FT series, Fig. 4.68).

Note: Besides accommodating to their versatility, there is nothing new to understand with hybrid instruments. Exotic at a first glance, hybrids are governing today's market of mass spectrometers [114-116].

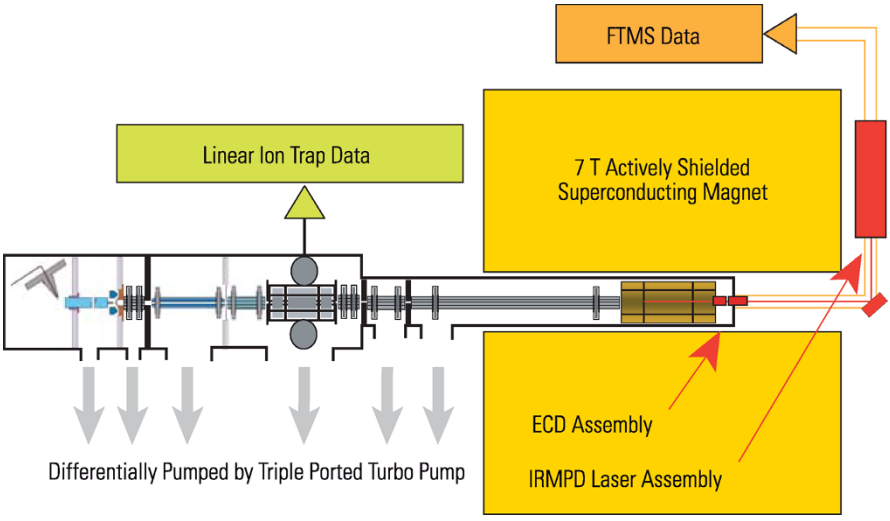


Fig. 4.68. Schematic of a LIT-FT-ICR hybrid instrument, the Thermo Scientific LTQ FT Ultra, incorporating a fully functional LTQ front end (as in LTQ Orbitrap) for highest versatility. Courtesy of Thermo Fisher Scientific, Bremen.

Table 4.3. Hybrid mass analyzers

MS1	Properties of MS1	MS2	Properties of MS2
BE or EB	LR and HR	Q	LR, low energy CID
BE or EB	LR and HR	QIT	LR, low energy CID, MS^n
EB or EBE	LR and HR	oaTOF	LR, low energy CID, high sensitivity
Q	LR, low-energy CID	oaTOF	HR, high sensitivity
Q	LR, low-energy CID	LIT	LR, higher sensitivity than QqQ, MS/MS in LIT
QIT	LR, low-energy CID, MS^n	TOF	HR, high sensitivity
Q	LT, low-energy CID, MS^2	ICR	Ultrahigh resolution and mass accuracy, MS/MS in ICR
LIT	LR, low-energy CID, MS^n	ICR	Ultrahigh resolution and mass accuracy, MS/MS in ICR

4.9.2 Ion Mobility-Mass Spectrometry Systems

Recently, there is an increasing interest in *ion mobility spectrometry* (IMS) as it presents an effective means of separating gaseous ions. In IMS an electric field forces the ions to drift along a path through a countercurrent inert gas atmosphere whereby they are separated due to their collision cross sections. IMS does for gaseous ions what gas chromatography does for gaseous neutrals, and in fact, IMS was initially referred to as *plasma chromatography* (PC). IMS can separate isobaric ions of different charge state (size-to-charge ratio) resulting from their distinct speed of propagation along the electric field of the ion mobility tube or distinguish isobars of the same charge state by their steric properties, i.e., it separates isomers and conformers alike. Thus, IMS is a valuable aid in biomolecular analysis [235-237].

Mass spectrometry obviously is an ideal detection method for gaseous ions eluting from an ion mobility device. Therefore, the *ion mobility-mass spectrometry* (IM-MS) coupling has received considerable attention since the 1970s [238-240].

Note: A detailed treatment of ion mobility spectrometry is beyond the scope of this book, nonetheless, a brief description of the method is required. While IM-MS systems can in principle be regarded as hyphenated instrumentation (treated in more detail in Chap. 14), the peculiarities of ion mobility demand for an integrated instrumental approach rather than gas or liquid chromatography couplings that can rapidly be attached and removed from a mass spectrometer as required [235,241]. Therefore, IM-MS is dealt with here as a special case under the heading of instrumentation.

Ion mobility effects separation of ions based on their different velocities when accelerated by a constant electric field along a drift tube with a countercurrent inert gas, typically helium or nitrogen. The average velocity, v_D, of a drifting ion is then governed by the number of soft collisions it experiences within the drift tube. This number of collisions with the neutrals is directly proportional to the electric field strength, E, and the ion mobility constant K (in $cm^2\ V^{-1}\ s^{-1}$)

$$v_D = K\,E \tag{4.49}$$

The value of K depends on the ion and the drift gas. Equation 4.49 is only valid up to field strengths of about 1000 V cm^{-1}, whereas above that electric field strength the proportionality between K and E is canceled [235].

The electric field needs to be weak enough so that collisions at given gas density dampen the ions to achieve an internal ion energy in equilibrium with the temperature of the bath gas [237]. Furthermore, gas discharges have strictly to be avoided. In the high-pressure regime (100–760 Torr or 133–1013 mbar) drift tubes are operated at 100–300 V cm^{-1} to deliver what in IMS is considered as high resolving power of 100–300. In the low-pressure regime, field strengths are limited to 10–30 V cm^{-1}. Unfortunately, lower pressure goes along with reduced resolving power of the device while coupling to mass analyzers is simplified [237].

In the low-field regime, the value of K can be calculated from

$$K = \frac{3q}{16N}\sqrt{\frac{2\pi}{kT}}\sqrt{\left(\frac{m+M}{mM}\right)}\left(\frac{1}{\Omega}\right) \tag{4.50}$$

where q is the ionic charge, N the number density of the buffer gas, k is Boltzmann's constant, T is the absolute temperature, m is the mass of the buffer gas, and M is the mass of the ions that have the collision cross section Ω [236,241]. In the IM-MS experiment, q and Ω are a priori unknown, but M is derived from m/z as soon as the charge state z has been identified, which in turn delivers q from $q = ze$. As hundreds of TOF mass spectra can be acquired during the tens of milliseconds required for one ion mobility run, the setup easily delivers high-quality MS data to identify the drift time-separated ions (Fig. 4.69).

Often, the *reduced mobility*, K_0, is calculated for comparing IMS data between different instruments, by using the relation

$$K_0 = \frac{{l_D}^2}{t_D U_D}\ \frac{273.2}{T}\ \frac{P}{760} \tag{4.51}$$

where l_D is the length of the drift tube and U_D the voltage applied along it; the temperature is given in units of Kelvin and the pressure in Torr [237].

For this classical approach to IMS, the theory of ion propagation is very well developed and allows to calculate the orientationally averaged collision cross sections with high confidence [236].

As an alternative to RF-only multipole ion guides, the *stacked ring ion guide* (SRIG) has been newly recognized since 2004. Ring electrodes (2–3 mm i.d.) are aligned with 1–2 mm insulating ceramics spacers in between them and supplied with an RF drive voltage ($U_{RF} \approx 100$ V at 1 MHz) that is reversed in phase between adjacent rings (Fig. 4.70) [97,242]. Ions entering the SRIG experience a deep radial potential well with comparatively steep walls towards the inner ring surfaces when traveling though the apertures. The SRIG offers high transmission if operated with a thermalizing buffer gas at around 3 mbar. Interestingly, the SRIG not merely forms a kind of pipe for the ions, its effective potential more resembles a corrugated hose where the grooves act as low potential wells in axial direction, which are deep enough to restrain axial drift of thermalized ions by soft trapping.

To avoid stopping of the ions, a DC pulse can be delivered to a pair of rings causing the ions to move forth to the next potential groove. If the DC pulse makes a progression from pair to pair it creates a *traveling wave* (T-wave) that makes the ions "surf" along the SRIG (Fig. 4.71). Such *traveling wave ion guides* (TWIGs) are now used in many Waters instruments to replace the more traditional RF-only multipoles as ion guides and collision cells, e.g., in the "triplequadrupoles" of the Xevo™ and Quattro Premier™ series that essentially are of Q-TWIG-Q design. The wave created by a potential of about 2 V is generally propagating at around 300 m s^{-1}. This provides an effective means of minimizing dwell times in the corresponding compartment.

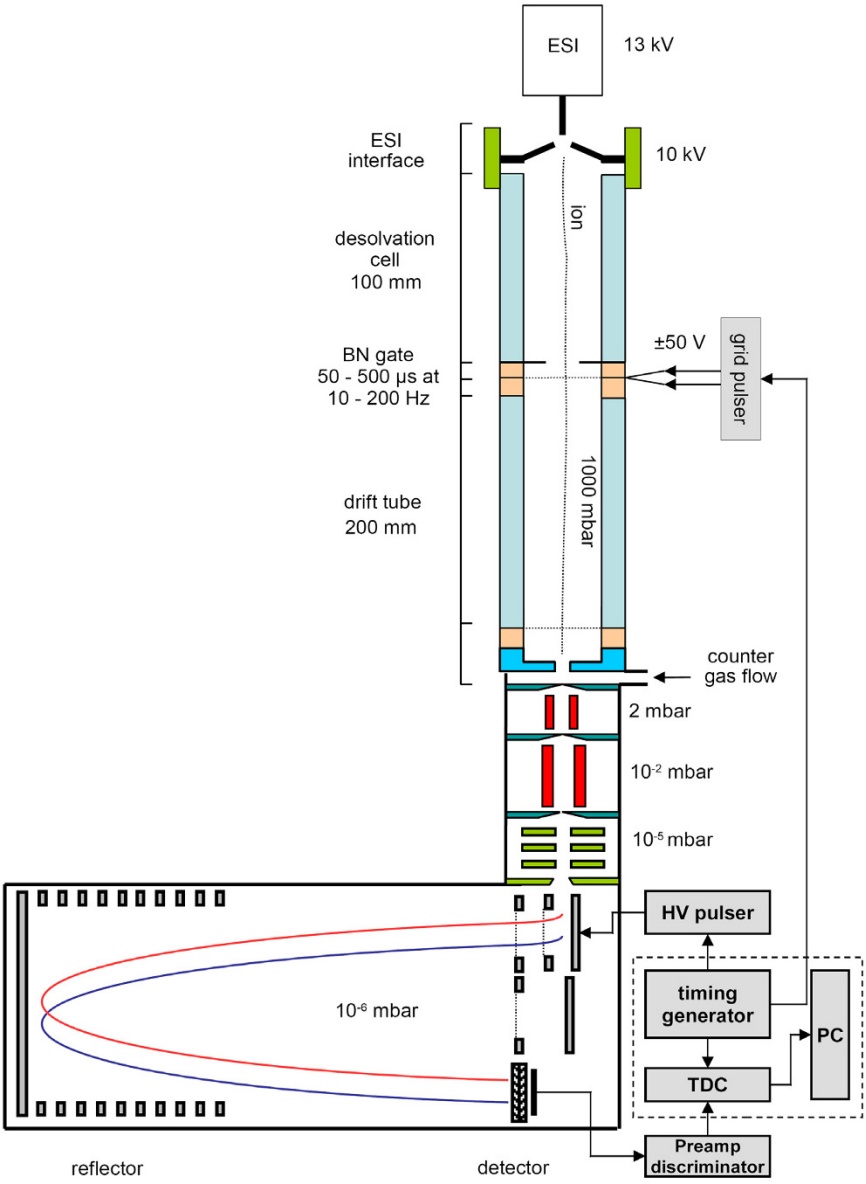


Fig. 4.69. Basic design of an ambient-pressure IMS-TOF mass spectrometer. Ions from an electrospray source are entering a desolvation chamber from where packets are pulsed into the ion mobility tube (uneven ion path to indicate diffusion of ions) by means of an ion gate. After ion mobility separation the ions are transferred into the W-type double reflector oaTOF analyzer via a differentially pumped interface. Courtesy of TofWerk AG, Thun, Switzerland.

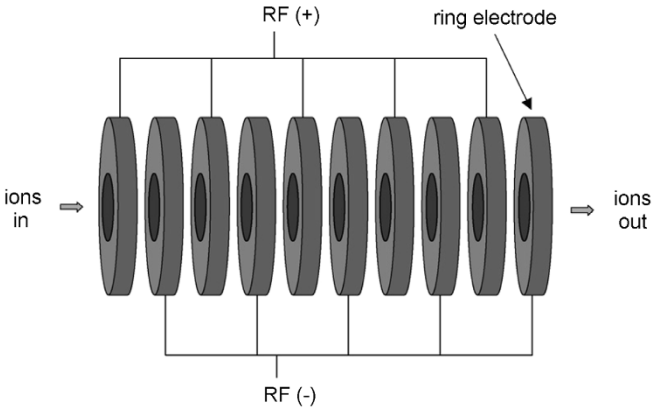


Fig. 4.70. A stacked ring ion guide. Rings are connected to an RF drive voltage in alteration of the phase. Normally tens of pairs are used to build one ion guide. Ions entering from the left experience a deep radial potential well with comparatively steep walls toward the inner ring surfaces when traveling though the apertures. Reproduced from Ref. [242] with permission. © Elsevier Science Publishers, 2007.

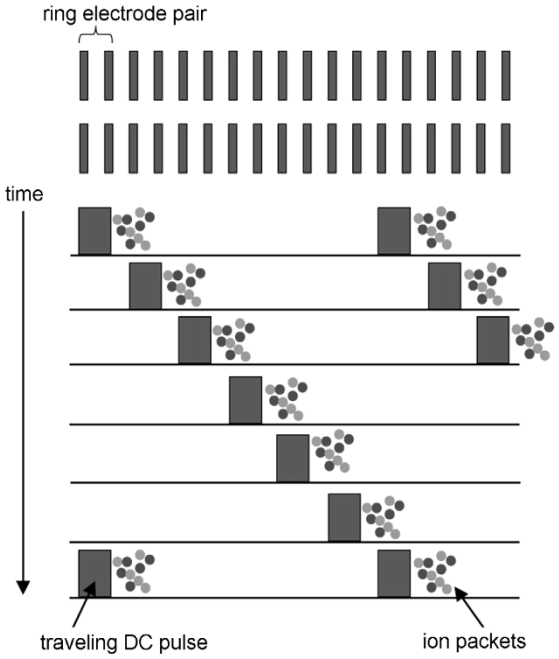


Fig. 4.71. Effect of a traveling wave DC pulse along a stacked ring ion guide. Ions in front of the DC pulse are moving along from stack to stack and are thus propulsed through the device (T-wave ion guide). A buffer gas is required to narrow down the thermal energy distribution. Reproduced from Ref. [242] with permission. © Elsevier Science Publishers, 2007.

When ions differing either in charge state or collision cross sections, or both, are entering the TWIG, the less mobile ones may occasionally transverse a wave in backward direction. Those ions lagging behind the traveling wave will exit later than those surfing on the wave. This makes the TWIG become an ion mobility separator. A hybrid instrument comprising a mass-selecting quadrupole, a traveling wave ion mobility separator, and an oaTOF analyzer has been marketed by Waters as Synapt HDMS™ (Fig. 4.72), and more recently as Synapt G2™ instrument [97,242].

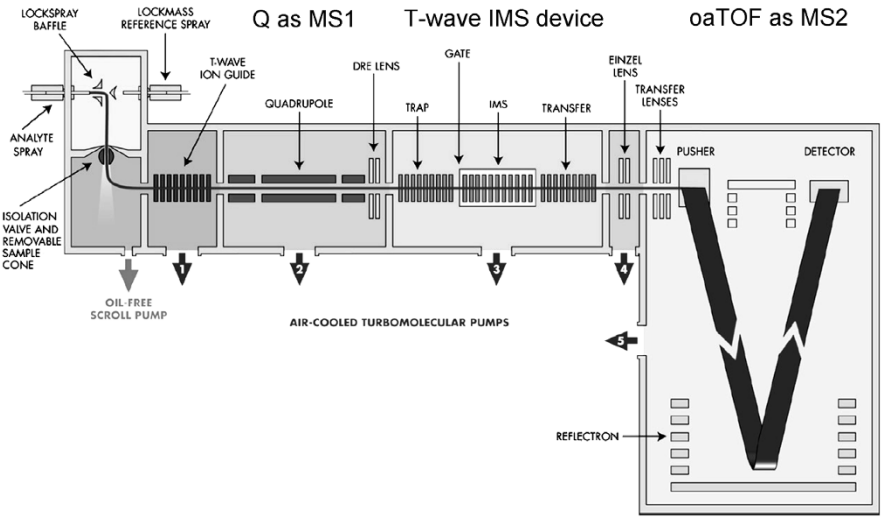


Fig. 4.72. The Waters Synapt HDMS instrument, a Q-IMS-oaTOF hybrid. The combination of three ring ion guide sections is used to build a complete IMS device comprising a trap at the entrance to supply ion packages, the IMS itself, and an ion guide for transfer to the mass analyzer. Adapted from Ref. [242] with permission. © Elsevier Science Publishers, 2007.

Note: A specific type of IM-MS instrumentation using a *traveling-wave* (T-wave™) approach is available from Waters. In a T-wave ion mobility device ions are pushed by low-voltage waves established along a large stack of paired ring electrodes. However, the theory of ion mobility separation in the T-wave is not as fully understood as in traditional IMS devices [236,241].

4.10 Detectors

The simplest detector is a *Faraday cup*, i.e., an electrode where the ions deposit their charge. The electric current flowing away from that electrode results in a voltage when passing through a resistor of high impedance. Faraday cups are still

in use to measure abundance ratios with highest accuracy in *isotope ratio mass spectrometry* (IR-MS) [243]. In the era of Mattauch-Herzog-type instruments, the *photographic plate* has been the standard detection system (Chap. 4.3.5). With the advent of scanning mass spectrometers, *secondary electron multipliers* (SEM) became predominant [244]. These rely on the emission of secondary electrons from surfaces upon impact of energetic ions. Progress has been made to employ *cryogenic detectors*, a rather special type of ion-counting detector for high-mass ions in TOF-MS [245]. The first commercial cryogenic detector TOF instrument has been released (Comet Macromizer, Flamatt, Switzerland). Ion-counting detectors are not used in FT-ICR and orbitrap instruments where *image current detection* is employed instead.

Note: Ion counting detectors also give signals upon impact of energetic neutrals, electrons, or photons. Therefore, care has to be taken, not to allow other particles than the mass-analyzed ions to hit the detector.

4.10.1 Discrete Dynode Electron Multipliers

When an energetic particle impinges on the surface of a metal or a semiconductor, secondary electrons are emitted from that surface. The ease of such an emission is determined by the *electron(ic) work function* of the respective material, e.g., BeCu alloy oxide ($w_e \approx 2.4$ eV) [246]. The higher the velocity of the impacting particle [244,247] and the lower the electron work function of the surface, the larger the number of secondary electrons. If an electrode opposite to the location of emission is held at more positive potential, all emitted electrons will be accelerated towards and hit that surface where they in turn cause the release of several electrons each. The avalanche of electrons produced over 12–18 discrete dynode stages held at about 100 V more positive potential each causes an electric current large enough to be detected by a sensitive preamplifier. Such a detector is called *secondary electron multiplier* (SEM, Fig. 4.73) [248]. The dynodes are normally cup-shaped, but stacks of Venetian blind-like dynodes have also been in use. Due to a certain air sensitivity of the emissive layer and in order to prevent arcing due to the high voltage, electron multipliers require operation in high vacuum.

The ion currents actually reaching the first dynode are chiefly in the picoampere range, but may span over a 10^{-18}–10^{-9} A range. Depending on the applied voltage, SEMs provide a gain of 10^6–10^8 [248]. The resulting current at the electron trap is the input of a nearby preamplifier providing another 10^6–10^9 gain. Its output current is then converted to a voltage signal which finally can be translated to an intensity value by means of an analog-to-digital converter (ADC, Chap. 4.2.7).

Example: A singly-charged ion corresponds to a charge of 1.6×10^{-19} C, and 1 A is equal to 1 C s^{-1}. Thus, an ion current of 10^{-15} A = 10^{-15} C s^{-1} is provided by about 6000 ions per second. If the detection of these ions during a scan in a GC-MS run taking 1 s over the *m/z* 40–400 range yields a mass spectrum consisting of

some 30–60 peaks, this corresponds to 100–200 ions per peak. Such conditions define the detection limit of a scanning mass spectrometer.

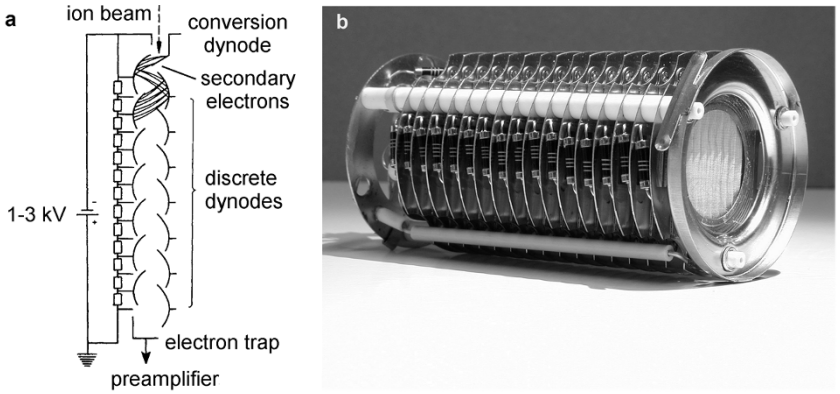


Fig. 4.73. Discrete dynode electron multipliers. (**a**) Schematic of a 14-stage SEM. (**b**) An old-fashioned 16-stage Venetian blind-type SEM clearly showing the resistors and ceramics insulators between the stacking dynodes at its side. (**a**) Adapted from Ref. [249] by permission. © Springer-Verlag Heidelberg, 1991.

Note: All types of secondary electron multipliers have limited life-time. They can deliver 0.1–10 C of extracted charge and are also limited by beam-induced destruction of the first dynode.

4.10.2 Channel Electron Multipliers

The cascade of secondary electrons can also be produced in a continuous tube. Such detectors, known as *channel electron multipliers* (CEM) or just *channeltrons*, are more compact and less expensive than discrete dynode SEMs. CEMs are preferably used in benchtop instruments. Their gain depends on the length-to-diameter ratio with an optimum ratio around 40–80 [250]. In a CEM, the high voltage drops continuously from the ion entrance to the electron exit of the tube requiring a sufficiently high resistance of the semiconducting material to withstand high voltage of about 2 kV. This is accomplished by an emissive layer of silicon dioxide overlying a conductive layer of lead oxide on the supporting heavily lead-doped glass tube [248,251]. Straight CEMs are unstable at gains exceeding 10^4 because positive ions created inside by EI of residual gas are accelerated towards the input side of the tube where they randomly contribute to the signal causing spurious output pulses [251,252]. A curved design shortens the free path for ion acceleration thereby suppressing noise from this so-called *ion-feedback*. Curved CEMs provide gains of up to 10^8 (Figs. 4.74, 4.75).

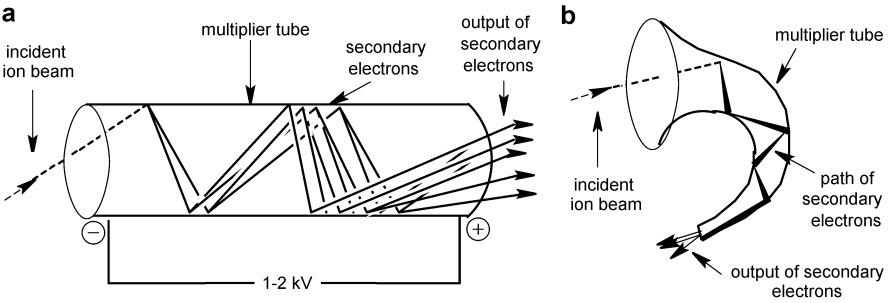


Fig. 4.74. Multipliers: (**a**) Linear channel electron multiplier and (**b**) curved channel electron multiplier. By courtesy of Waters Corporation, MS Technologies, Manchester, UK.

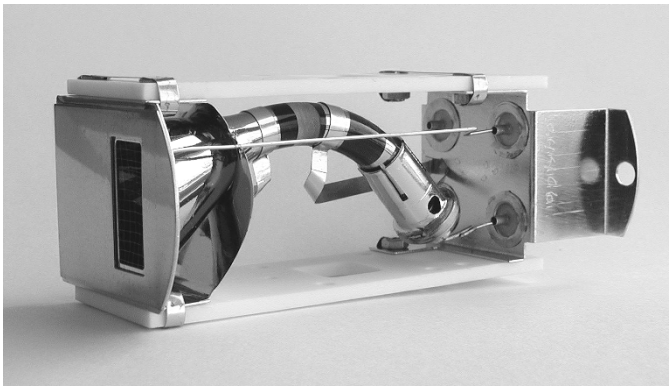


Fig. 4.75. Channeltron multiplier.

4.10.3 Microchannel Plates

An extreme reduction of the size of a linear channeltron tube to some micrometers in diameter can be achieved. The cross section of such a single tube is by far too small to be of any use, however, millions of these tubes put together in a "bundle" yield a *channel electron multiplier array*; more common terms are *microchannel plate* or *multichannel plate* (MCP, Fig. 4.76). To avoid that the ions enter the microchannels parallel to their axis, these are inclined by some degrees from the perpendicular to the plate's surface. The gain of an MCP is 10^3–10^4, i.e., much lower than that of a SEM or CEM. Instead of a single MCP, two MCPs are often sandwiched together in such a way that the small angles oppose each other (*Chevron plate*, Fig. 4.77) to obtain gains of 10^6–10^7. Occasionally, even three MCPs are stacked analogously (*z-stack*, gain up to 10^8) [252,253].

MCPs are produced as round plates of various sizes. Those of 2–5 cm in diameter are typically employed in mass spectrometers. An MCP may either be operated to give an integral output for all incident ions during a certain time interval, or the

location of the impact may be conserved by connecting sectors of the MCP to individual registration channels. The first setup is more widespread, e.g., in TOF-MS to detect the electron current every nanosecond while the ions are arriving at the detector. The second setup can be used for imaging purposes, e.g., to construct an array detector (below).

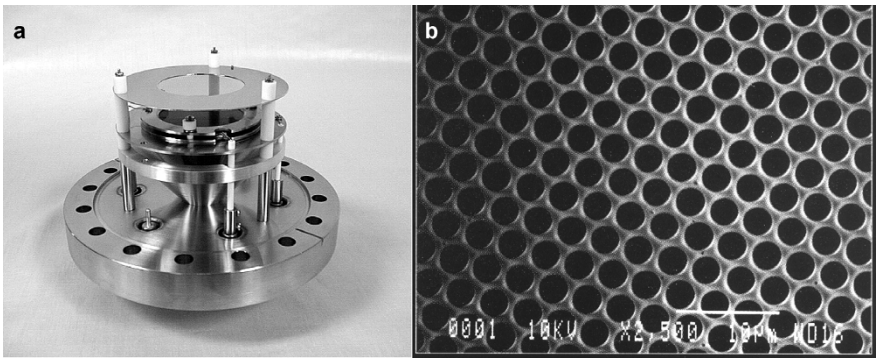


Fig. 4.76. (**a**) MCP detector (top inner, glossy disk) mounted on top of a flange and (**b**) SEM micrograph of a high-resolving MCP showing channels of 2 μm diameter. Courtesy of (**a**) R.M. Jordan Company, Grass Valley, and of (**b**) Burle Industries, Baesweiler.

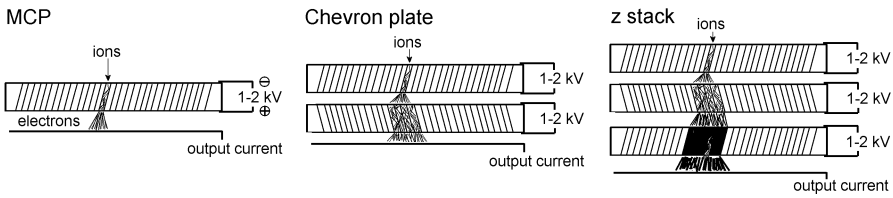


Fig. 4.77. Stacking of MCPs to increase gain. *From left*: single MCP, Chevron plate, and z-stack configuration. Note the loss of spatial resolution upon stacking.

4.10.4 Post-Acceleration and Conversion Dynode

Discrimination of slower ions as compared to faster ions is observed with SEMs [254], CEMs, and MCPs as well [250,255,256]. This means a reduction in sensitivity upon reduction of the acceleration voltage of a mass spectrometer, and of course, with increasing ion mass. *Post-acceleration detectors* can reduce such effects and especially help to improve the sensitivity for high-mass ions [247,256]. In post-acceleration detectors the ions are accelerated immediately in front of the detector by a voltage of 10–30 kV before they hit the first dynode or the first MCP.

The electron output of ion-counting detectors is usually measured with reference to ground potential, i.e., the first dynode is set to negative high voltage as to achieve acceleration of the electrons down the dynode assembly. In case of sector

or TOF instruments, the deceleration of keV negative ions by the detector voltage is of comparatively minor importance. However, the slow ions exiting from quadrupole mass analyzers would stop before they reached the detector. Therefore, *conversion dynodes* are frequently placed in front of the SEM or CEM (Fig. 4.78) [248]. These are robust electrodes set to high potential (5–20 kV) of a polarity suitable to attract the ions actually exiting from the mass analyzer. Their impact on the conversion dynode creates secondary ions or electrons that can be used for subsequent detection. A conversion dynode detector also serves as a post-acceleration detector and gives almost equal sensitivity for positive and negative ion detection. In addition, neutrals and photons cannot reach the detector if the conversion dynode is placed out of the line of sight.

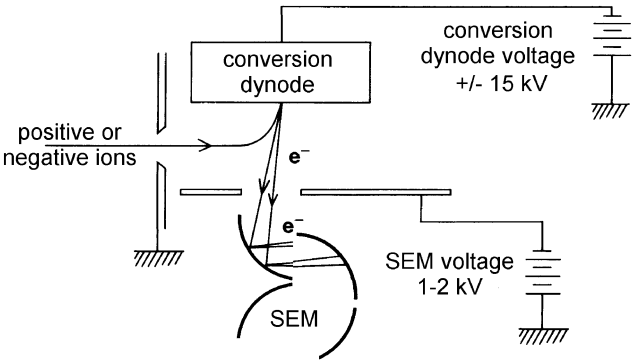


Fig. 4.78. Detector configuration with conversion dynode. By courtesy of JEOL, Tokyo.

4.10.5 Focal Plane Detectors

Magnetic sector instruments are scanning devices usually focusing ions of one *m/z* value after the other onto a point detector. However, the mass-dispersive element of these instruments, i.e., the magnetic sector, is capable of producing an image of several neighboring *m/z* values simultaneously. *Focal plane detectors* (FPD) or *array detectors*, as they are often termed, can detect a small *m/z* range, i.e., ± 2–5% of the center mass, at a time [250,257,258]. The ions impinging along the focal plane on the surface of an MCP (usually a Chevron plate) are converted to electrons. The electrons from the backside of the MCP stack are then converted into photons by a phosphor screen, and the light image is guided onto a photodiode array or a CCD detector by means of a fiber optical device. Such a multichannel electro-optical detection system typically improves sensitivity or signal-to-noise ratio, respectively, by a factor of 20–100, because less of the ion current is lost without being detected and fluctuations in the ion current are compensated [259,260].

The resolution of an FPD is theoretically limited by the number of channels (512–2048). In practice, it is even less because the image suffers some broadening as it passes from the first MCP to the photodiode array (Fig. 4.79). Therefore, in-

struments with FPD can normally be switched from FPD to SEM detection, e.g., by vertical electrostatic deflection of the ion beam (Finnigan MAT900). Furthermore, quadrupole lenses or an inhomogeneous ESA behind the magnet are employed to achieve variable dispersion, i.e., to zoom the *m/z* range of simultaneous detection. Recent developments point towards fully integrated FPDs on a silicon chip [261].

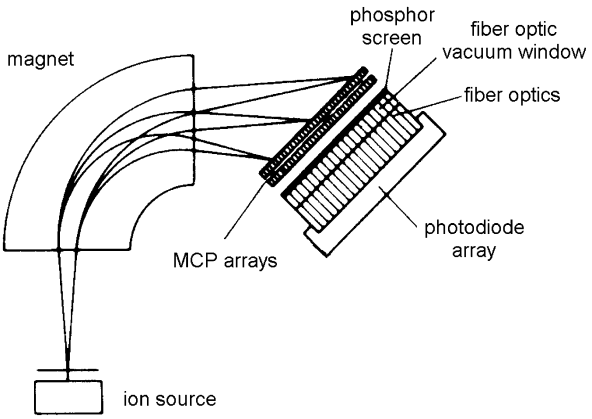


Fig. 4.79. Array detector in the focal plane of a magnetic sector to detect a small mass range simultaneously. By courtesy of Thermo Electron (Bremen) GmbH.

4.11 Vacuum Technology

Vacuum systems are integral parts of any mass spectrometer, but vacuum technology definitely is a field of its own [262-266]. Thus, the discussion of mass spectrometer vacuum systems will be restricted to the very basics.

Table 4.4. Pressure ranges in vacuum technology

Pressure range [Pa]	Pressure range [mbar]	Pressure range [mtorr]	Vacuum	Gas flow
$10^5 - 10^2$	1 bar – 1 mbar	750 torr – 750 mtorr	Rough vacuum (RV)	Viscous flow
$10^2 - 10^{-1}$	$1 - 10^{-3}$	750 – 0.75	Medium vacuum (MV)	Knudsen flow
$10^{-1} - 10^{-5}$	$10^{-3} - 10^{-7}$	$0.75 - 7.5\times10^{-5}$	High vacuum (HV)	Molecular flow
$< 10^{-5}$	$< 10^{-7}$	$< 7.5 \times 10^{-5}$	Ultrahigh vacuum (UHV)	Molecular flow

4.11.1 Basic Mass Spectrometer Vacuum System

Generally, two pumping stages are employed to generate the high vacuum of a mass spectrometer. Usually, *rotary vane pumps* having *pumping speeds* of about 4–16 $m^3\,h^{-1}$ are used to generate a medium vacuum of several Pascals. They are then connected to high-vacuum pumps in a way that their high-pressure side exhales into the medium vacuum of the rotary vane pumps, i.e., they are operated as *backing pumps*. This way, each pumping stage contributes a compression of some 10^4–10^5 to the total factor of 10^9–10^{10} between atmospheric pressure and the high vacuum of 10^{-4}–10^{-5} Pa (Table 4.4). The high-vacuum pumps can either be *turbomolecular pumps*, *oil diffusion pumps*, or *cryopumps* [267,268].

Example: The vacuum system of non-benchtop mass spectrometers consists of one to three rotary vane pumps and two or three turbo pumps. Rotary vane pumps are used for the inlet system(s) and as backing pumps for the turbo pumps. One turbo pump is mounted to the ion source housing, another one or two are operated at the analyzer. Thereby, a differentially pumped system is provided where local changes in pressure, e.g., from reagent gas in CI or collision gas in CID, do not have a noteworthy effect on the whole vacuum chamber.

4.11.2 High Vacuum Pumps

Turbomolecular pumps or *turbo pumps* having pumping speeds of 200–500 $l\,s^{-1}$ are currently the standard high vacuum pumps in mass spectrometry. A high-speed rotor (50,000–60,000 rpm) is employed to transport the molecules out of the *vacuum manifold (vacuum chamber)*. Turbo pumps can be switched on and off in minutes, have low power consumption (about 100 W), and thus can be operated either air- or water cooled. Furthermore, they provide clean, in particular oil-free, high vacuum, are compact, and can be mounted either vertically below or horizontally at the sides of the vacuum manifold. Their disadvantages are the risk of sudden damage (similar to hard disk drives) and potential high frequency noise. Fortunately, modern turbo pumps run for many years and their noise is negligible.

Oil diffusion pumps offer high pumping speeds (600–2000 $l\,s^{-1}$) at the cost of high power consumption (0.4–2 kW) and the need for a strong cooling water flow. The oil (perfluoropolypropylene glycols; Fomblin™, Santovac™) is thermally evaporated and the oil vapor supplies transport of gas molecules that enter it by diffusion. The gas-loaded oil vapor is condensed and the gas is removed from the liquid by the action of the backing pump. As diffusion pumps have no moving mechanical parts they are highly reliable and extremely silent. However, elongated use as well as sudden venting causes severe oil contaminations of the vacuum manifold. Diffusion pumps have almost been abandoned from modern mass spectrometers.

Cryopumps adsorb (freeze) residual gas to a surface cooled to the temperature of liquid nitrogen. They are highly efficient and silent and provide clean vacuum, but cannot be operated without interruptions to recover the adsorber. Cryopumps

are typically operated in combination with turbo pumps because they are only started after high-vacuum conditions are reached. Otherwise, the adsorber would soon be saturated.

4.12 Purchasing an Instrument

To some of us it can unexpectedly happen that we are faced with the task of having to buy a mass spectrometer, eventually for ourselves or on behalf of someone else. References to certain commercial instruments made in this chapter were in no way intended to preclude such a 100,000–600,000 € decision. The below guide may be useful in selecting an instrument that meets your requirements best:

- Define the tasks the mass spectrometer is to be acquired for: *i*) Need for one or several ionization methods? *ii*) GC-MS or LC-MS required? *iii*) High resolution and accurate mass desirable? *iv*) Is tandem MS an issue? *v*) What sensitivity is needed? *vi*) Is quantitative work important?
- Check your budget. A powerful and versatile second-hand machine from a proven company can be better than a toy-like single-purpose benchtop system.
- Get into contact with sales persons of all manufacturers offering suitable systems. Compare prices and modalities of customer training and support.
- Use independent information from the published literature and ask current users of your top-choice mass spectrometers for the special strengths and shortcomings of those systems.
- Modern instruments form a unit with their data system. Does this offer the features you want? Does it allow for "manual" settings or corrections?
- Make appointments for demonstration of those instruments that are likely to be acquired, e.g., for the top three of your ranking. Do not use completely unknown samples for this purpose. Otherwise, problems associated with your analyte might erroneously be regarded as a lack of instrumental performance.

References

1. Ligon, W.V., Jr. Molecular Analysis by Mass Spectrometry. *Science* **1979,** *205*, 151-159.
2. Brunnée, C. The Ideal Mass Analyzer: Fact or Fiction? *Int. J. Mass Spectrom. Ion Proc.* **1987,** *76*, 125-237.
3. Beynon, J.H. Instruments, in *Mass Spectrometry and its Applications to Organic Chemistry*, Elsevier: Amsterdam, 1960; pp. 4-27.
4. Habfast, K.; Aulinger, F. Massenspektrometrische Apparate, in *Massenspektrometrie*, Kienitz, H., editor; Verlag Chemie: Weinheim, 1968; pp. 29-124.
5. Aulinger, F. Massenspektroskopische Geräte, in *Massenspektrometrie*, Kienitz, H., editor; Verlag Chemie: Weinheim, 1968; pp. 125-154.
6. Brunnée, C. New Instrumentation in Mass Spectrometry. *Int. J. Mass Spectrom. Ion Phys.* **1982,** *45*, 51-86.
7. Brunnée, C. 50 Years of MAT in Bremen. *Rapid Commun. Mass Spectrom.* **1997,** *11*, 694-707.
8. Chapman, J.R.; Errock, G.A.; Race, J.A. Science and Technology in Manchester: the Nuture of Mass Spectrometry. *Rapid*

Commun. Mass Spectrom. **1997,** *11*, 1575-1586.
9. McLuckey, S.A. Intrumentation for Mass Spectrometry: 1997, 14 ed.; Karjalainen, E.J.; Hesso, A.E.; Jalonen, J.E.; Karjalainen, U.P., editors; Elsevier: Amsterdam, 1998; pp. 153-196.
10. Badman, E.R.; Cooks, R.G. Miniature Mass Analyzers. *J. Mass Spectrom.* **2000,** *35*, 659-671.
11. Baykut, G.; Franzen, J. Mobile Mass Spectrometry; a Decade of Field Applications. *Trends Anal. Chem.* **1994,** *13*, 267-275.
12. Prieto, M.C.; Kovtoun, V.V.; Cotter, R.J. Miniaturized Linear Time-of-Flight Mass Spectrometer With Pulsed Extraction. *J. Mass Spectrom.* **2002,** *37*, 1158-1162.
13. Fenselau, C.; Caprioli, R. Mass Spectrometry in the Exploration of Mars. *J. Mass Spectrom.* **2003,** *38*, 1-10.
14. Arkin, C.R.; Griffin, T.P.; Ottens, A.K.; Diaz, J.A.; Follistein, D.W.; Adams, F.W.; Helms, W.R. Evaluation of Small Mass Spectrometer Systems for Permanent Gas Analysis. *J. Am. Soc. Mass Spectrom.* **2002,** *13*, 1004-1012.
15. Hu, Q.; Noll, R.J.; Li, H.; Makarov, A.; Hardman, M.; Cooks, R.G. The Orbitrap: A New Mass Spectrometer. *J. Mass Spectrom.* **2005,** *40*, 430-443.
16. Wiley, W.C.; McLaren, I.H. Time-of-Flight Mass Spectrometer With Improved Resolution. *Rev. Sci. Instrum.* **1955,** *26*, 1150-1157.
17. Stephens, W.E. A Pulsed Mass Spectrometer With Time Dispersion. *Phys. Rev.* **1946,** *69*, 691.
18. Cameron, A.E.; Eggers, D.F. An Ion "Velocitron". *Rev. Sci. Instrum.* **1948,** *19*, 605-607.
19. Wolff, M.M.; Stephens, W.E. A Pulsed Mass Spectrometer With Time Dispersion. *Rev. Sci. Instrum.* **1953,** *24*, 616-617.
20. Wiley, W.C.; McLaren, I.H. Reprint of: Time-of-Flight Mass Spectrometer With Improved Resolution. *J. Mass Spectrom.* **1997,** *32*, 4-11.
21. Harrington, D.B. The Time-of-Flight Mass Spectrometer, in *Advances in Mass Spectrometry*, Waldron, J.D., editor; Pergamon Press: Oxford, 1959; pp. 249-265.
22. Gohlke, R.S.; McLafferty, F.W. Early Gas Chromatography/Mass Spectrometry. *J. Am. Soc. Mass Spectrom.* **1993,** *4*, 367-371.
23. Guilhaus, M. The Return of Time-of-Flight to Analytical Mass Spectrometry. *Adv. Mass Spectrom.* **1995,** *13*, 213-226.
24. Guilhaus, M.; Mlynski, V.; Selby, D. Perfect Timing: Time-of-Flight Mass Spectrometry. *Rapid Commun. Mass Spectrom.* **1997,** *11*, 951-962.
25. Karas, M.; Hillenkamp, F. Laser Desorption Ionization of Proteins With Molecular Masses Exceeding 10000 Daltons. *Anal. Chem.* **1988,** *60*, 2299-2301.
26. Weickhardt, C.; Moritz, F.; Grotemeyer, J. Time-of-Flight Mass Spectrometry: State-of-the-Art in Chemical Analysis and Molecular Science. *Mass Spectrom. Rev.* **1997,** *15*, 139-162.
27. Cotter, R.J. *Time-of-Flight Mass Spectrometry: Instrumentation and Applications in Biological Research;* American Chemical Soc.: Washington, DC, 1997.
28. Enke, C.G. The Unique Capabilities of Time-of-Flight Mass Analyzers. *Adv. Mass Spectrom.* **1998,** *14*, 197-219.
29. Fuerstenau, S.D.; Benner, W.H. Molecular Weight Determination of Megadalton DNA Electrospray Ions Using Charge Detection Time-of-Flight Mass Spectrometry. *Rapid Commun. Mass Spectrom.* **1995,** *9*, 1528-1538.
30. Fuerstenau, S.D.; Benner, W.H.; Thomas, J.J.; Brugidou, C.; Bothner, B.; Suizdak, G. Mass Spectrometry of an Intact Virus. *Angew. Chem., Int. Ed.* **2001,** *40*, 541-544.
31. Vestal, M.L. Modern MALDI Time-of-Flight Mass Spectrometry. *J. Mass Spectrom.* **2009,** *44*, 303-317.
32. Guilhaus, M. Principles and Instrumentation in Time-of-Flight Mass Spectrometry. Physical and Instrumental Concepts. *J. Mass Spectrom.* **1995,** *30*, 1519-1532.
33. Ioanoviciu, D. Ion-Optical Solutions in Time-of-Flight Mass Spectrometry. *Rapid Commun. Mass Spectrom.* **1995,** *9*, 985-997.
34. Cotter, R.J. Time-of-Flight Mass Spectrometry for the Analysis of Biological Molecules. *Anal. Chem.* **1992,** *64*, 1027A-1039A.
35. Takach, E.J.; Hines, W.M.; Patterson, D.H.; Juhasz, P.; Falick, A.M.; Vestal, M.L.; Martin, S.A. Accurate Mass Measurements Using MALDI-TOF With De-

Delayed Extraction. *J. Prot. Chem.* **1997,** *16*, 363-369.
36. Vestal, M.; Juhasz, P. Resolution and Mass Accuracy in Matrix-Assisted Laser Desorption Ionization-Time-of-Flight. *J. Am. Soc. Mass Spectrom.* **1998,** *9*, 892-911.
37. Vestal, M.; Hayden, K. High Performance MALDI-TOF Mass Spectrometry for Proteomics. *Int. J. Mass Spectrom.* **2007,** *268*, 83-92.
38. Beavis, R.C.; Chait, B.T. Factors Affecting the Ultraviolet Laser Desorption of Proteins. *Rapid Commun. Mass Spectrom.* **1989,** *3*, 233-237.
39. Mamyrin, B.A. Laser Assisted Reflectron Time-of-Flight Mass Spectrometry. *Int. J. Mass Spectrom. Ion Proc.* **1994,** *131*, 1-19.
40. Schuerch, S.; Schaer, M.; Boernsen, K.O.; Schlunegger, U.P. Enhanced Mass Resolution in Matrix-Assisted Laser Desorption/Ionization Linear Time-of-Flight Mass Spectrometry. *Biol. Mass Spectrom.* **1994,** *23*, 695-700.
41. Brown, R.S.; Lennon, J.J. Mass Resolution Improvement by Incorporation of Pulsed Ion Extraction in a Matrix-Assisted Laser Desorption/Ionization Linear Time-of-Flight Mass Spectrometer. *Anal. Chem.* **1995,** *67*, 1998-2003.
42. Colby, S.M.; King, T.B.; Reilly, J.P. Improving the Resolution of Matrix-Assisted Laser Desorption/Ionization Time-of-Flight Mass Spectrometry by Exploiting the Correlation Between Ion Position and Velocity. *Rapid Commun. Mass Spectrom.* **1994,** *8*, 865-868.
43. Whittal, R.M.; Li, L. High-Resolution Matrix-Assisted Laser Desorption-Ionization in a Linear Time-of-Flight Mass Spectrometer. *Anal. Chem.* **1995,** *67*, 1950-1954.
44. Vestal, M.L.; Juhasz, P.; Martin, S.A. Delayed Extraction Matrix-Assisted Laser Desorption Time-of-Flight Mass Spectrometry. *Rapid Commun. Mass Spectrom.* **1995,** *9*, 1044-1050.
45. Weaver, P.J.; Laures, A.M.F.; Wolff, J.C. Investigation of the Advanced Functionalities of a Hybrid Quadrupole Orthogonal Acceleration Time-of-Flight Mass Spectrometer. *Rapid Commun. Mass Spectrom.* **2007,** *21*, 2415-2421.
46. Dawson, J.H.J.; Guilhaus, M. Orthogonal-Acceleration Time-of-Flight Mass Spectrometer. *Rapid Commun. Mass Spectrom.* **1989,** *3*, 155-159.
47. Mirgorodskaya, O.A.; Shevchenko, A.A.; Chernushevich, I.V.; Dodonov, A.F.; Miroshnikov, A.I. Electrospray-Ionization Time-of-Flight Mass Spectrometry in Protein Chemistry. *Anal. Chem.* **1994,** *66*, 99-107.
48. Coles, J.; Guilhaus, M. Orthogonal Acceleration - a New Direction for Time-of-Flight Mass Spectrometry: Fast, Sensitive Mass Analysis for Continuous Ion Sources. *Trends Anal. Chem.* **1993,** *12*, 203-213.
49. Guilhaus, M.; Selby, D.; Mlynski, V. Orthogonal Acceleration Time-of-Flight Mass Spectrometry. *Mass Spectrom. Rev.* **2000,** *19*, 65-107.
50. Selby, D.S.; Mlynski, V.; Guilhaus, M. A 20 KV Orthogonal Acceleration Time-of-Flight Mass Spectrometer for Matrix-Assisted Laser Desorption/Ionization. *Int. J. Mass Spectrom.* **2001,** *210/211*, 89-100.
51. Selditz, U.; Nilsson, S.; Barnidge, D.; Markides, K.E. ESI/TOF-MS Detection for Microseparation Techniques. *Chimia* **1999,** *53*, 506-510.
52. Charles, L. Influence of Internal Standard Charge State on the Accuracy of Mass Measurements in Orthogonal Acceleration Time-of-Flight Mass Spectrometers. *Rapid Commun. Mass Spectrom.* **2008,** *22*, 151-155.
53. Guo, C.; Huang, Z.; Gao, W.; Nian, H.; Chen, H.; Dong, J.; Shen, G.; Fu, J.; Zhou, Z. A Homemade High-Resolution Orthogonal-Injection Time-of-Flight Mass Spectrometer With a Heated Capillary Inlet. *Rev. Sci. Instrum.* **2008,** *79*, 013109-1-013109/8.
54. Prazen, B.J.; Bruckner, C.A.; Synovec, R.E.; Kowalski, B.R. Enhanced Chemical Analysis Using Parallel Column Gas Chromatography With Single-Detector Time-of-Flight Mass Spectrometry and Chemometric Analysis. *Anal. Chem.* **1999,** *71*, 1093-1099.
55. Hirsch, R.; Ternes, T.A.; Bobeldijk, I.; Weck, R.A. Determination of Environmentally Relevant Compounds Using Fast GC/TOF-MS. *Chimia* **2001,** *55*, 19-22.
56. Hsu, C.S.; Green, M. Fragment-Free Accurate Mass Measurement of Complex Mixture Components by Gas Chromatography/Field Ionization-Orthogonal

Acceleration Time-of-Flight Mass Spectrometry: an Unprecedented Capability for Mixture Analysis. *Rapid Commun. Mass Spectrom.* **2001,** *15*, 236-239.
57. Chernushevich, I.V. Duty Cycle Improvement for a Quadrupole-Time-of-Flight Mass Spectrometer and Its Use for Precursor Ion Scans. *Eur. J. Mass Spectrom.* **2000,** *6*, 471-479.
58. Brock, A.; Rodriguez, N.; Zare, R.N. Hadamard Transform Time-of-Flight Mass Spectrometry. *Anal. Chem.* **1998,** *70*, 3735-3741.
59. Zare, R.N.; Fernandez, F.M.; Kimmel, J.R. Hadamard Transform Time-of-Flight Mass Spectrometry: More Signal, More of the Time. *Angew. Chem. , Int. Ed.* **2003,** *42*, 30-35.
60. Trapp, O.; Kimmel, J.R.; Yoon, O.K.; Zuleta, I.A.; Fernandez, F.M.; Zare, R.N. Continuous Two-Channel Time-of-Flight Mass Spectrometric Detection of Electrosprayed Ions. *Angew. Chem. , Int. Ed.* **2004,** *43*, 6541-6544.
61. Brenton, A.G.; Krastev, T.; Rousell, D.J.; Kennedy, M.A.; Craze, A.S.; Williams, C.M. Improvement of the Duty Cycle of an Orthogonal Acceleration Time-of-Flight Mass Spectrometer Using Ion Gates. *Rapid Commun. Mass Spectrom.* **2007,** *21*, 3093-3102.
62. Colombo, M.; Sirtori, F.R.; Rizzo, V. A Fully Automated Method for Accurate Mass Determination Using High-Performance Liquid Chromatography With a Quadrupole/Orthogonal Acceleration Time-of-Flight Mass Spectrometer. *Rapid Commun. Mass Spectrom.* **2004,** *18*, 511-517.
63. Nier, A.O. The Development of a High Resolution Mass Spectrometer: a Reminiscence. *J. Am. Soc. Mass Spectrom.* **1991,** *2*, 447-452.
64. Nier, A.O. Some Reminiscences of Mass Spectrometry and the Manhattan Project. *J. Chem. Educ.* **1989,** *66*, 385-388.
65. Nier, A.O. Some Reflections on the Early Days of Mass Spectrometry at the University of Minnesota. *Int. J. Mass Spectrom. Ion Proc.* **1990,** *100*, 1-13.
66. Duckworth, H.E.; Barber, R.C.; Venkatasubramanian, V.S. *Mass Spectroscopy;* 2nd ed.; Cambridge University Press: Cambridge, 1986.
67. Cooks, R.G.; Beynon, J.H.; Caprioli, R.M. Instrumentation, in *Metastable Ions*, Elsevier: Amsterdam, 1973; pp. 5-18.
68. Morrison, J.D. Ion Focusing, Mass Analysis, and Detection, in *Gaseous Ion Chemistry and Mass Spectrometry*, Futrell, J.H., editor; Wiley: New York, 1986; pp. 107-125.
69. Dempster, A.J. A New Method of Positive Ray Analysis. *Phys. Rev.* **1918,** *11*, 316-325.
70. Mattauch, J.; Herzog, R. Über Einen Neuen Massenspektrographen. *Z. Phys.* **1934,** *89*, 786-795.
71. Bainbridge, K.T.; Jordan, E.B. Mass-Spectrum Analysis. 1. The Mass Spectrograph. 2. The Existence of Isobars of Adjacent Elements. *Phys. Rev.* **1936,** *50*, 282-296.
72. Johnson, E.G.; Nier, A.O. Angular Aberrations in Sector Shaped Electromagnetic Lenses for Focusing Beams of Charged Particles. *Phys. Rev.* **1953,** *91*, 10-17.
73. Todd, J.F.J. Recommendations for Nomenclature and Symbolism for Mass Spectroscopy Including an Appendix of Terms Used in Vacuum Technology. *Int. J. Mass Spectrom. Ion Proc.* **1995,** *142*, 211-240.
74. Morgan, R.P.; Beynon, J.H.; Bateman, R.H.; Green, B.N. The MM-ZAB-2F Double-Focussing Mass Spectrometer and MIKE Spectrometer. *Int. J. Mass Spectrom. Ion Phys.* **1978,** *28*, 171-191.
75. Hintenberger, H.; König, L.A. Über Massenspektrometer Mit Vollständiger Doppelfokussierung Zweiter Ordnung. *Z. Naturforsch.* **1957,** *12A*, 443.
76. Guilhaus, M.; Boyd, R.K.; Brenton, A.G.; Beynon, J.H. Advantages of a Second Electric Sector on a Double-Focusing Mass Spectrometer of Reversed Configuration. *Int. J. Mass Spectrom. Ion Proc.* **1985,** *67*, 209-227.
77. Bill, J.C.; Green, B.N.; Lewis, I.A.S. A High Field Magnet With Fast Scanning Capabilities. *Int. J. Mass Spectrom. Ion Phys.* **1983,** *46*, 147-150.
78. Matsuda, H. High-Resolution High-Transmission Mass Spectrometer. *Int. J. Mass Spectrom. Ion Proc.* **1985,** *66*, 209-215.
79. Matsuda, H. Double-Focusing Mass Spectrometers of Short Path Length. *Int. J. Mass Spectrom. Ion Proc.* **1989,** *93*, 315-321.

80. Paul, W. Elektromagnetische Käfige Für Neutrale Und Geladene Teilchen (Nobel-Vortrag). *Angew. Chem.* **1990,** *102*, 780-789.
81. Paul, W. Electromagnetic Traps for Charged and Neutral Particles, in *Nobel Prize Lectures in Physics 1981-1990*, World Scientific Publishing: Singapore, 1993; pp. 601-622.
82. Paul, W.; Steinwedel, H. A New Mass Spectrometer Without Magnetic Field. *Z. Naturforsch.* **1953,** *8A*, 448-450.
83. Paul, W.; Raether, M. Das Elektrische Massenfilter. *Z. Phys.* **1955,** *140*, 262-273.
84. Lawson, G.; Todd, J.F.J. Radio-Frequency Quadrupole Mass Spectrometers. *Chem. Brit.* **1972,** *8*, 373-380.
85. Dawson, P.H. *Quadrupole Mass Spectrometry and Its Applications;* Elsevier: New York, 1976.
86. Dawson, P.H. Quadrupole Mass Analyzers: Performance, Design and Some Recent Applications. *Mass Spectrom. Rev.* **1986,** *5*, 1-37.
87. Douglas, D.J. Linear Quadrupoles in Mass Spectrometry. *Mass Spectrom. Rev.* **2009,** *28*, 937-960.
88. Blaum, K.; Geppert, C.; Müller, P.; Nörtershäuser, W.; Otten, E.W.; Schmitt, A.; Trautmann, N.; Wendt, K.; Bushaw, B.A. Properties and Performance of a Quadrupole Mass Filter Used for Resonance Ionization Mass Spectrometry. *Int. J. Mass Spectrom.* **1998,** *181*, 67-87.
89. Amad, M.H.; Houk, R.S. High-Resolution Mass Spectrometry With a Multiple Pass Quadrupole Mass Analyzer. *Anal. Chem.* **1998,** *70*, 4885-4889.
90. Liyu, Y.; Amad, M.H.; Winnik, W.M.; Schoen, A.E.; Schweingruber, H.; Mylchreest, I.; Rudewicz, P.J. Investigation of an Enhanced Resolution Triple Quadrupole Mass Spectrometer for High-Throughput Liquid Chromatography/Tandem Mass Spectrometry Assays. *Rapid Commun. Mass Spectrom.* **2002,** *16*, 2060-2066.
91. Denison, D.R. Operating Parameters of a Quadrupole in a Grounded Cylindrical Housing. *J. Vac. Sci. Technol.* **1971,** *8*, 266-269.
92. Dawson, P.H.; Whetten, N.R. Nonlinear Resonances in Quadrupole Mass Spectrometers Due to Imperfect Fields. II. Quadrupole Mass Filter and the Monopole Mass Spectrometer. *Int. J. Mass Spectrom. Ion Phys.* **1969,** *3*, 1-12.
93. Brubaker, W.M. Comparison of Quadrupole Mass Spectrometers With Round and Hyperbolic Rods. *J. Vac. Sci. Technol.* **1967,** *4*, 326.
94. Gibson, J.R.; Taylor, S. Prediction of Quadrupole Mass Filter Performance for Hyperbolic and Circular Cross Section Electrodes. *Rapid Commun. Mass Spectrom.* **2000,** *14*, 1669-1673.
95. Chen, W.; Collings, B.A.; Douglas, D.J. High-Resolution Mass Spectrometry With a Quadrupole Operated in the Fourth Stability Region. *Anal. Chem.* **2000,** *72*, 540-545.
96. Douglas, D.J.; Frank, A.J.; Mao, D. Linear Ion Traps in Mass Spectrometry. *Mass Spectrom. Rev.* **2005,** *24*, 1-29.
97. Giles, K.; Pringle, S.D.; Worthington, K.R.; Little, D.; Wildgoose, J.L.; Bateman, R.H. Applications of a Traveling Wave-Based Radio-Frequency-Only Stacked Ring Ion Guide. *Rapid Commun. Mass Spectrom.* **2004,** *18*, 2401-2414.
98. Huang, Y.; Guan, S.; Kim, H.S.; Marshall, A.G. Ion Transport Through a Strong Magnetic Field Gradient by Radio Frequency-Only Octupole Ion Guides. *Int. J. Mass Spectrom. Ion Proc.* **1996,** *152*, 121-133.
99. Douglas, D.J.; French, J.B. Collisional Focusing Effects in Radiofrequency Quadrupoles. *J. Am. Soc. Mass Spectrom.* **1992,** *3*, 398-408.
100. Tolmachev, A.V.; Udseth, H.R.; Smith, R.D. Radial Stratification of Ions As a Function of Mass to Charge Ratio in Collisional Cooling Radio Frequency Multipoles Used As Ion Guides or Ion Traps. *Rapid Commun. Mass Spectrom.* **2000,** *14*, 1907-1913.
101. Collings, B.A.; Campbell, J.M.; Mao, D.; Douglas, D.J. A Combined Linear Ion Trap Time-of-Flight System With Improved Performance and MS^n Capabilities. *Rapid Commun. Mass Spectrom.* **2001,** *15*, 1777-1795.
102. Douglas, D.J. Applications of Collision Dynamics in Quadrupole Mass Spectrometry. *J. Am. Soc. Mass Spectrom.* **1998,** *9*, 101-113.
103. Thomson, B.A. 1997 McBryde Medal Award Lecture Radio Frequency Quadrupole Ion Guides in Modern Mass

Spectrometry. *Can. J. Chem.* **1998,** *76*, 499-505.
104. Lock, C.M.; Dyer, E. Characterization of High Pressure Quadrupole Collision Cells Possessing Direct Current Axial Fields. *Rapid Commun. Mass Spectrom.* **1999,** *13*, 432-448.
105. Lock, C.M.; Dyer, E. Simulation of Ion Trajectories Through a High Pressure Radio Frequency Only Quadrupole Collision Cell by SIMION 6.0. *Rapid Commun. Mass Spectrom.* **1999,** *13*, 422-431.
106. Adlhart, C.; Hinderling, C.; Baumann, H.; Chen, P. Mechanistic Studies of Olefin Metathesis by Ruthenium Carbene Complexes Using Electrospray Ionization Tandem Mass Spectrometry. *J. Am. Chem. Soc.* **2000,** *122*, 8204-8214.
107. Mao, D.; Douglas, D.J. H/D Exchange of Gas Phase Bradykinin Ions in a Linear Quadrupole Ion Trap. *J. Am. Soc. Mass Spectrom.* **2003,** *14*, 85-94.
108. Hager, J.W. A New Linear Ion Trap Mass Spectrometer. *Rapid Commun. Mass Spectrom.* **2002,** *16*, 512-526.
109. Schwartz, J.C.; Senko, M.W.; Syka, J.E.P. A Two-Dimensional Quadrupole Ion Trap Mass Spectrometer. *J. Am. Soc. Mass Spectrom.* **2002,** *13*, 659-669.
110. Hofstadler, S.A.; Sannes-Lowery, K.A.; Griffey, R.H. Enhanced Gas-Phase Hydrogen-Deuterium Exchange of Oligonucleotide and Protein Ions Stored in an External Multipole Ion Reservoir. *J. Mass Spectrom.* **2000,** *35*, 62-70.
111. Mao, D.; Ding, C.; Douglas, D.J. Hydrogen/Deuterium Exchange of Myoglobin Ions in a Linear Quadrupole Ion Trap. *Rapid Commun. Mass Spectrom.* **2002,** *16*, 1941-1945.
112. Koizumi, H.; Whitten, W.B.; Reilly, P.T.A. Trapping of Intact, Singly-Charged, Bovine Serum Albumin Ions Injected From the Atmosphere With a 10-cm Diameter, Frequency-Adjusted Linear Quadrupole Ion Trap. *J. Am. Soc. Mass Spectrom.* **2008,** *19*, 1942-1947.
113. Collings, B.A.; Scott, W.R.; Londry, F.A. Resonant Excitation in a Low-Pressure Linear Ion Trap. *J. Am. Soc. Mass Spectrom.* **2003,** *14*, 622-634.
114. Aebersold, R.; Mann, M. Mass Spectrometry-Based Proteomics. *Nature* **2003,** *422*, 198-207.
115. Hopfgartner, G.; Husser, C.; Zell, M. Rapid Screening and Characterization of Drug Metabolites Using a New Quadrupole-Linear Ion Trap Mass Spectrometer. *J. Mass Spectrom.* **2003,** *38*, 138-150.
116. Hager, J.W. Recent Trends in Mass Spectrometer Development. *Anal. Bioanal. Chem.* **2004,** *378*, 845-850.
117. Welling, M.; Schuessler, H.A.; Thompson, R.I.; Walther, H. Ion/Molecule Reactions, Mass Spectrometry and Optical Spectroscopy in a Linear Ion Trap. *Int. J. Mass Spectrom. Ion Proc.* **1998,** *172*, 95-114.
118. Londry, F.A.; Hager, J.W. Mass Selective Axial Ion Ejection From a Linear Quadrupole Ion Trap. *J. Am. Soc. Mass Spectrom.* **2003,** *14*, 1130-1147.
119. March, R.E.; Todd, J.F.J. *Quadrupole Ion Trap Mass Spectrometry;* Wiley: Hoboken, 2005.
120. *Mass Spectrometry in Drug Metabolism and Pharmacokinetics;* Ramanathan, R., editor; Wiley: Hoboken, 2009.
121. Dahl, D.A.; Delmore, J.E.; Appelhans, A.D. SIMION PC/PS2 Electrostatic Lens Design Program. *Rev. Sci. Instrum.* **1990,** *61*, 607-609.
122. Dahl, D.A. SIMION for the Personal Computer in Reflection. *Int. J. Mass Spectrom.* **2000,** *200*, 3-25.
123. Magparangalan, D.P.; Garrett, T.J.; Drexler, D.M.; Yost, R.A. Analysis of Large Peptides by MALDI Using a Linear Quadrupole Ion Trap With Mass Range Extension. *Anal. Chem.* **2010,** *82*, 930-934.
124. March, R.E.; Hughes, R.J. *Quadrupole Storage Mass Spectrometry;* Wiley: Chichester, 1989.
125. March, R.E. Quadrupole Ion Trap Mass Spectrometry: Theory, Simulation, Recent Developments and Applications. *Rapid Commun. Mass Spectrom.* **1998,** *12*, 1543-1554.
126. March, R.E. Quadrupole Ion Trap Mass Spectrometry. A View at the Turn of the Century. *Int. J. Mass Spectrom.* **2000,** *200*, 285-312.
127. Stafford, G., Jr. Ion Trap Mass Spectrometry: a Personal Perspective. *J. Am. Soc. Mass Spectrom.* **2002,** *13*, 589-596.
128. March, R.E. Quadrupole Ion Traps. *Mass Spectrom. Rev.* **2009,** *28*, 961-989.
129. *Practical Aspects of Ion Trap Mass Spectrometry;* March, R.E.; Todd, J.F.J., editors; CRC Press: Boca Raton, 1995; Vol. 1 Fundamentals of Ion Trap Mass Spectrometry.

130. *Practical Aspects of Ion Trap Mass Spectrometry;* March, R.E.; Todd, J.F.J., editors; CRC Press: Boca Raton, 1995; Vol. 2, Ion Trap Instrumentation.
131. *Practical Aspects of Ion Trap Mass Spectrometry;* March, R.E.; Todd, J.F.J., editors; CRC Press: Boca Raton, 1995; Vol. 3 Chemical, Environmental, and Biomedical Applications.
132. Yoshinari, K. Theoretical and Numerical Analysis of the Behavior of Ions Injected into a Quadrupole Ion Trap Mass Spectrometer. *Rapid Commun. Mass Spectrom.* **2000,** *14*, 215-223.
133. Alheit, R.; Kleinadam, S.; Vedel, F.; Vedel, M.; Werth, G. Higher Order Non-Linear Resonances in a Paul Trap. *Int. J. Mass Spectrom. Ion Proc.* **1996,** *154*, 155-169.
134. Stafford, G.C., Jr.; Kelley, P.E.; Syka, J.E.P.; Reynolds, W.E.; Todd, J.F.J. Recent Improvements in and Analytical Applications of Advanced Ion Trap Technology. *Int. J. Mass Spectrom. Ion Proc.* **1984,** *60*, 85-98.
135. Wu, H.F.; Brodbelt, J.S. Effects of Collisional Cooling on Ion Detection in a Quadrupole Ion Trap Mass Spectrometer. *Int. J. Mass Spectrom. Ion Proc.* **1992,** *115*, 67-81.
136. Plass, W.R.; Li, H.; Cooks, R.G. Theory, Simulation and Measurement of Chemical Mass Shifts in RF Quadrupole Ion Traps. *Int. J. Mass Spectrom.* **2003,** *228*, 237-267.
137. Wuerker, R.F.; Shelton, H.; Langmuir, R.V. Electrodynamic Containment of Charged Particles. *J. Appl. Phys.* **1959,** *30*, 342-349.
138. Ehlers, M.; Schmidt, S.; Lee, B.J.; Grotemeyer, J. Design and Set-Up of an External Ion Source Coupled to a Quadrupole-Ion-Trap Reflectron-Time-of-Flight Hybrid Instrument. *Eur. J. Mass Spectrom.* **2000,** *6*, 377-385.
139. Forbes, M.W.; Sharifi, M.; Croley, T.; Lausevic, Z.; March, R.E. Simulation of Ion Trajectories in a Quadrupole Ion Trap: a Comparison of Three Simulation Programs. *J. Mass Spectrom.* **1999,** *34*, 1219-1239.
140. Coon, J.J.; Steele, H.A.; Laipis, P.; Harrison, W.W. Laser Desorption-Atmospheric Pressure Chemical Ionization: A Novel Ion Source for the Direct Coupling of Polyacrylamide Gel Electrophoresis to Mass Spectrometry. *J. Mass Spectrom.* **2002,** *37*, 1163-1167.
141. Nappi, M.; Weil, C.; Cleven, C.D.; Horn, L.A.; Wollnik, H.; Cooks, R.G. Visual Representations of Simulated Three-Dimensional Ion Trajectories in an Ion Trap Mass Spectrometer. *Int. J. Mass Spectrom. Ion Proc.* **1997,** *161*, 77-85.
142. Dawson, P.H.; Hedman, J.W.; Whetten, N.R. Mass Spectrometer. *Rev. Sci. Instrum.* **1969,** *40*, 1444-1450.
143. Dawson, P.H.; Whetten, N.R. Miniature Mass Spectrometer. *Anal. Chem.* **1970,** *42*, 103A-108A.
144. Griffiths, I.W.; Heesterman, P.J.L. Quadrupole Ion Store (QUISTOR) Mass Spectrometry. *Int. J. Mass Spectrom. Ion Proc.* **1990,** *99*, 79-98.
145. Griffiths, I.W. Recent Advances in Ion-Trap Technology. *Rapid Commun. Mass Spectrom.* **1990,** *4*, 69-73.
146. Kelley, P.E.; Stafford, G.C., Jr.; Syka, J.E.P.; Reynolds, W.E.; Louris, J.N.; Todd, J.F.J. New Advances in the Operation of the Ion Trap Mass Spectrometer, 1986; Chapter 10B, pp. 869-870.
147. Splendore, M.; Lausevic, M.; Lausevic, Z.; March, R.E. Resonant Excitation and/or Ejection of Ions Subjected to DC and RF Fields in a Commercial Quadrupole Ion Trap. *Rapid Commun. Mass Spectrom.* **1997,** *11*, 228-233.
148. Creaser, C.S.; Stygall, J.W. A Comparison of Overtone and Fundamental Resonances for Mass Range Extension by Resonance Ejection in a Quadrupole Ion Trap Mass Spectrometer. *Int. J. Mass Spectrom.* **1999,** *190/191*, 145-151.
149. Williams, J.D.; Cox, K.A.; Cooks, R.G.; McLuckey, S.A.; Hart, K.J.; Goeringer, D.E. Resonance Ejection Ion Trap Mass Spectrometry and Nonlinear Field Contributions: The Effect of Scan Direction on Mass Resolution. *Anal. Chem.* **1994,** *66*, 725-729.
150. Ding, L.; Sudakov, M.; Brancia, F.L.; Giles, R.; Kumashiro, S. A Digital Ion Trap Mass Spectrometer Coupled With Atmospheric Pressure Ion Sources. *J. Mass Spectrom.* **2004,** *39*, 471-484.
151. Cooks, R.G.; Amy, J.W.; Bier, M.; Schwartz, J.C.; Schey, K. New Mass Spectrometers, 1989; Chapter 11A, pp. 33-52.
152. Kaiser, R.E., Jr.; Louris, J.N.; Amy, J.W.; Cooks, R.G. Extending the Mass

Range of the Quadrupole Ion Trap Using Axial Modulation. *Rapid Commun. Mass Spectrom.* **1989,** *3*, 225-229.
153. Weber-Grabau, M.; Kelley, P.; Bradshaw, S.; Hoekman, D.; Evans, S.; Bishop, P. Recent Advances in Ion-Trap Technology, 1989; Chapter 11A, pp. 152-153.
154. Siethoff, C.; Wagner-Redeker, W.; Schäfer, M.; Linscheid, M. HPLC-MS With an Ion Trap Mass Spectrometer. *Chimia* **1999,** *53*, 484-491.
155. Eades, D.M.; Johnson, J.V.; Yost, R.A. Nonlinear Resonance Effects During Ion Storage in a Quadrupole Ion Trap. *J. Am. Soc. Mass Spectrom.* **1993,** *4*, 917-929.
156. Makarov, A.A. Resonance Ejection From the Paul Trap: A Theoretical Treatment Incorporating a Weak Octapole Field. *Anal. Chem.* **1996,** *68*, 4257-4263.
157. Doroshenko, V.M.; Cotter, R.J. Losses of Ions During Forward and Reverse Scans in a Quadrupole Ion Trap Mass Spectrometer and How to Reduce Them. *J. Am. Soc. Mass Spectrom.* **1997,** *8*, 1141-1146.
158. von Busch, F.; Paul, W. Nonlinear Resonances in Electric Mass-Filters As a Consequence of Field Irregularities. *Z. Phys.* **1961,** *164*, 588-594.
159. Dawson, P.H.; Whetten, N.R. Nonlinear Resonances in Quadrupole Mass Spectrometers Due to Imperfect Fields. I. Quadrupole Ion Trap. *Int. J. Mass Spectrom. Ion Phys.* **1969,** *2*, 45-59.
160. Wang, Y.; Franzen, J. The Non-Linear Ion Trap. Part 3. Multipole Components in Three Types of Practical Ion Trap. *Int. J. Mass Spectrom. Ion Proc.* **1994,** *132*, 155-172.
161. Franzen, J. The Non-Linear Ion Trap. Part 5. Nature of Non-Linear Resonances and Resonant Ion Ejection. *Int. J. Mass Spectrom. Ion Proc.* **1994,** *130*, 15-40.
162. Berton, A.; Traldi, P.; Ding, L.; Brancia, F.L. Mapping the Stability Diagram of a Digital Ion Trap (DIT) Mass Spectrometer Varying the Duty Cycle of the Trapping Rectangular Waveform. *J. Am. Soc. Mass Spectrom.* **2008,** *19*, 620-625.
163. Ding, L.; Kumashiro, S. Ion Motion in the Rectangular Wave Quadrupole Field and Digital Operation Mode of a Quadrupole Ion Trap Mass Spectrometer. *Rapid Commun. Mass Spectrom.* **2006,** *20*, 3-8.
164. Li, X.; Jiang, G.; Luo, C.; Xu, F.; Wang, Y.; Ding, L.; Ding, C. Ion Trap Array Mass Analyzer: Structure and Performance. *Anal. Chem.* **2009,** *81*, 4840-4846.
165. Brodbelt, J.S.; Louris, J.N.; Cooks, R.G. Chemical Ionization in an Ion Trap Mass Spectrometer. *Anal. Chem.* **1987,** *59*, 1278-1285.
166. Doroshenko, V.M.; Cotter, R.J. Injection of Externally Generated Ions into an Increasing Trapping Field of a Quadrupole Ion Trap Mass Spectrometer. *J. Mass Spectrom.* **1997,** *31*, 602-615.
167. Van Berkel, G.J.; Glish, G.L.; McLuckey, S.A. Electrospray Ionization Combined With Ion Trap Mass Spectrometry. *Anal. Chem.* **1990,** *62*, 1284-1295.
168. Wang, Y.; Schubert, M.; Ingendoh, A.; Franzen, J. Analysis of Non-Covalent Protein Complexes Up to 290 kDa Using Electrospray Ionization and Ion Trap Mass Spectrometry. *Rapid Commun. Mass Spectrom.* **2000,** *14*, 12-17.
169. Lawrence, E.O.; Livingston, M.S. The Production of High-Speed Light Ions Without the Use of High Voltages. *Phys. Rev.* **1932,** *40*, 19-35.
170. Comisarow, M.B.; Marshall, A.G. The Early Development of Fourier Transform Ion Cyclotron Resonance (FT-ICR) Spectroscopy. *J. Mass Spectrom.* **1996,** *31*, 581-585.
171. Smith, L.G. New Magnetic Period Mass Spectrometer. *Rev. Sci. Instrum.* **1951,** *22*, 115-116.
172. Sommer, H.; Thomas, H.A.; Hipple, J.A. Measurement of E/M by Cyclotron Resonance. *Phys. Rev.* **1951,** *82*, 697-702.
173. Baldeschwieler, J.D. Ion Cyclotron Resonance Spectroscopy. *Science* **1968,** *159*, 263-273.
174. *Analytical Applications of Fourier Transform Ion Cyclotron Resonance Mass Spectrometry;* Assamoto, B., editor; VCH: Weinheim, 1991.
175. Comisarow, M.B.; Marshall, A.G. Fourier Transform Ion Cyclotron Resonance Spectroscopy. *Chem. Phys. Lett.* **1974,** *25*, 282-283.
176. Comisarow, M.B.; Marshall, A.G. Frequency-Sweep Fourier Transform Ion Cyclotron Resonance Spectroscopy. *Chem. Phys. Lett.* **1974,** *26*, 489-490.
177. Wanczek, K.-P. ICR Spectrometry - A Review of New Developments in The-

ory, Instrumentation and Applications. I. 1983-1986. *Int. J. Mass Spectrom. Ion Proc.* **1989,** *95*, 1-38.
178. Marshall, A.G.; Grosshans, P.B. Fourier Transform Ion Cyclotron Resonance Mass Spectrometry: the Teenage Years. *Anal. Chem.* **1991,** *63*, 215A-229A.
179. Amster, I.J. Fourier Transform Mass Spectrometry. *J. Mass Spectrom.* **1996,** *31*, 1325-1337.
180. Dienes, T.; Salvador, J.P.; Schürch, S.; Scott, J.R.; Yao, J.; Cui, S.; Wilkins, C.L. Fourier Transform Mass Spectrometry-Advancing Years (1992-Mid. 1996). *Mass Spectrom. Rev.* **1996,** *15*, 163-211.
181. Marshall, A.G. Milestones in Fourier Transform Ion Cyclotron Resonance Mass Spectrometry Technique Development. *Int. J. Mass Spectrom.* **2000,** *200*, 331-356.
182. Smith, R.D. Evolution of ESI-Mass Spectrometry and Fourier Transform Ion Cyclotron Resonance for Proteomics and Other Biological Applications. *Int. J. Mass Spectrom.* **2000,** *200*, 509-544.
183. Marshall, A.G.; Hendrickson, C.L.; Shi, S.D.H. Scaling MS Plateaus With High-Resolution FT-ICR-MS. *Anal. Chem.* **2002,** *74*, 252A-259A.
184. Schaub, T.M.; Hendrickson, C.L.; Horning, S.; Quinn, J.P.; Senko, M.W.; Marshall, A.G. High-Performance Mass Spectrometry: Fourier Transform Ion Cyclotron Resonance at 14.5 Tesla. *Anal. Chem.* **2008,** *80*, 3985-3990.
185. He, F.; Hendrickson, C.L.; Marshall, A.G. Baseline Mass Resolution of Peptide Isobars: A Record for Molecular Mass Resolution. *Anal. Chem.* **2001,** *73*, 647-650.
186. Bossio, R.E.; Marshall, A.G. Baseline Resolution of Isobaric Phosphorylated and Sulfated Peptides and Nucleotides by Electrospray Ionization FT-ICR-MS: Another Step Toward MS-Based Proteomics. *Anal. Chem.* **2002,** *74*, 1674-1679.
187. White, F.M.; Marto, J.A.; Marshall, A.G. An External Source 7 T Fourier Transform Ion Cyclotron Resonance Mass Spectrometer With Electrostatic Ion Guide. *Rapid Commun. Mass Spectrom.* **1996,** *10*, 1845-1849.
188. Marshall, A.G.; Hendrickson, C.L. Fourier Transform Ion Cyclotron Resonance Detection: Principles and Experimental Configurations. *Int. J. Mass Spectrom.* **2002,** *215*, 59-75.
189. Marshall, A.G.; Hendrickson, C.L.; Jackson, G.S. Fourier Transform Ion Cyclotron Resonance Mass Spectrometry: a Primer. *Mass Spectrom. Rev.* **1998,** *17*, 1-35.
190. Shi, S.D.H.; Drader, J.J.; Freitas, M.A.; Hendrickson, C.L.; Marshall, A.G. Comparison and Interconversion of the Two Most Common Frequency-to-Mass Calibration Functions for Fourier Transform Ion Cyclotron Resonance Mass Spectrometry. *Int. J. Mass Spectrom.* **2000,** *195/196*, 591-598.
191. Nikolaev, E.N.; Gorshkov, M.V. Dynamics of Ion Motion in an Elongated Cylindrical Cell of an ICR Spectrometer and the Shape of the Signal Registered. *Int. J. Mass Spectrom. Ion Proc.* **1985,** *64*, 115-125.
192. Pan, Y.; Ridge, D.P.; Wronka, J.; Rockwood, A.L. Resolution Improvement by Using Harmonic Detection in an Ion Cyclotron Resonance Mass Spectrometer. *Rapid Commun. Mass Spectrom.* **1987,** *1*, 120-121.
193. Derome, A.E. *Modern NMR Techniques for Chemistry Research;* Pergamon Press: Oxford, 1987.
194. Guan, S.; Marshall, A.G. Stored Waveform Inverse Fourier Transform (SWIFT) Ion Excitation in Trapped-Ion Mass Spectrometry: Theory and Applications. *Int. J. Mass Spectrom. Ion Proc.* **1996,** *157/158*, 5-37.
195. Caravatti, P.; Allemann, M. The Infinity Cell: a New Trapped-Ion Cell With Radiofrequency Covered Trapping Electrodes for FT-ICR-MS. *Org. Mass Spectrom.* **1991,** *26*, 514-518.
196. Huang, Y.; Li, G.-Z.; Guan, S.; Marshall, A.G. A Combined Linear Ion Trap for Mass Spectrometry. *J. Am. Soc. Mass Spectrom.* **1997,** *8*, 962-969.
197. Guan, S.; Marshall, A.G. Ion Traps for Fourier Transform Ion Cyclotron Resonance Mass Spectrometry: Principles and Design of Geometric and Electric Configurations. *Int. J. Mass Spectrom. Ion Proc.* **1995,** *146/147*, 261-296.
198. Schweikhard, L.; Ziegler, J.; Bopp, H.; Luetzenkirchen, K. The Trapping Condition and a New Instability of the Ion Motion in the Ion Cyclotron Resonance Trap. *Int. J. Mass Spectrom. Ion Proc.* **1995,** *141*, 77-90.

199. Comisarow, M.B.; Marshall, A.G. Theory of Fourier Transform Ion Cyclotron Resonance Mass Spectroscopy. I. Fundamental Equations and Low-Pressure Line Shape. *J. Chem. Phys.* **1976,** *64*, 110-119.
200. Comisarow, M.B. Signal Modeling for Ion Cyclotron Resonance. *J. Chem. Phys.* **1978,** *69*, 4097-4104.
201. Hughey, C.A.; Rodgers, R.P.; Marshall, A.G. Resolution of 11,000 Compositionally Distinct Components in a Single Electrospray Ionization FT-ICR Mass Spectrum of Crude Oil. *Anal. Chem.* **2002,** *74*, 4145-4149.
202. Solouki, T.; Emmet, M.R.; Guan, S.; Marshall, A.G. Detection, Number, and Sequence Location of Sulfur-Containing Amino Acids and Disulfide Bridges in Peptides by Ultrahigh-Resolution MALDI FTICR Mass Spectrometry. *Anal. Chem.* **1997,** *69*, 1163-1168.
203. Wu, Z.; Hendrickson, C.L.; Rodgers, R.P.; Marshall, A.G. Composition of Explosives by Electrospray Ionization Fourier Transform Ion Cyclotron Resonance Mass Spectrometry. *Anal. Chem.* **2002,** *74*, 1879-1883.
204. Wang, Y.; Shi, S.D.H.; Hendrickson, C.L.; Marshall, A.G. Mass-Selective Ion Accumulation and Fragmentation in a Linear Octopole Ion Trap External to a Fourier Transform Ion Cyclotron Resonance Mass Spectrometer. *Int. J. Mass Spectrom.* **2000,** *198*, 113-120.
205. Makarov, A. Electrostatic Axially Harmonic Orbital Trapping: A High-Performance Technique of Mass Analysis. *Anal. Chem.* **2000,** *72*, 1156-1162.
206. Scigelova, M.; Makarov, A. Orbitrap Mass Analyzer - Overview and Applications in Proteomics. *Practical Proteomics* **2006,** *6*, 16-21.
207. Makarov, A.; Denisov, E.; Lange, O.; Horning, S. Dynamic Range of Mass Accuracy in LTQ Orbitrap Hybrid Mass Spectrometer. *J. Am. Chem. Soc.* **2006,** *17*, 977-982.
208. Makarov, A.; Denisov, E.; Kholomeev, A.; Balschun, W.; Lange, O.; Strupat, K.; Horning, S. Performance Evaluation of a Hybrid Linear Ion Trap/Orbitrap Mass Spectrometer. *Anal. Chem.* **2006,** *78*, 2113-2120.
209. Macek, B.; Waanders, L.F.; Olsen, J.V.; Mann, M. Top-Down Protein Sequencing and MS^3 on a Hybrid Linear Quadrupole Ion Trap-Orbitrap Mass Spectrometer. *Mol. Cell. Proteomics* **2006,** *5*, 949-958.
210. Perry, R.H.; Cooks, R.G.; Noll, R.J. Orbitrap Mass Spectrometry: Instrumentation, Ion Motion and Applications. *Mass Spectrom. Rev.* **2008,** *27*, 661-699.
211. Kingdon, K.H. A Method for Neutralizing the Electron Space Charge by Positive Ionization at Very Low Pressures. *Phys. Rev.* **1923,** *21*, 408-418.
212. Knight, R.D. Storage of Ions From Laser-Produced Plasmas. *Appl. Phys. Lett.* **1981,** *38*, 221-223.
213. Oksman, P. A Fourier Transform Time-of-Flight Mass Spectrometer. A SIMION Calculation Approach. *Int. J. Mass Spectrom. Ion Proc.* **1995,** *141*, 67-76.
214. Hardman, M.; Makarov, A.A. Interfacing the Orbitrap Mass Analyzer to an Electrospray Ion Source. *Anal. Chem.* **2003,** *75*, 1699-1705.
215. Olsen, J.V.; de Godoy, L.M.F.; Li, G.; Macek, B.; Mortensen, P.; Pesch, R.; Makarov, A.; Lange, O.; Horning, S.; Mann, M. Parts Per Million Mass Accuracy on an Orbitrap Mass Spectrometer Via Lock Mass Injection into a C-Trap. *Mol. Cell. Proteomics* **2005,** *4*, 2010-2021.
216. Perry, R.H.; Hu, Q.; Salazar, G.A.; Cooks, R.G.; Noll, R.J. Rephasing Ion Packets in the Orbitrap Mass Analyzer to Improve Resolution and Peak Shape. *J. Am. Soc. Mass Spectrom.* **2009,** *20*, 1397-1404.
217. Makarov, A.; Denisov, E. Dynamics of Ions of Intact Proteins in the Orbitrap Mass Analyzer. *J. Am. Soc. Mass Spectrom.* **2009,** *20*, 1486-1495.
218. Makarov, A.; Denisov, E.; Lange, O. Performance Evaluation of a High-Field Orbitrap Mass Analyzer. *J. Am. Soc. Mass Spectrom.* **2009,** *20*, 1391-1396.
219. Amy, J.W.; Baitinger, W.E.; Cooks, R.G. Building Mass Spectrometers and a Philosophy of Research. *J. Am. Soc. Mass Spectrom.* **1990,** *1*, 119-128.
220. Futrell, J.H. Development of Tandem Mass Spectrometry. One Perspective. *Int. J. Mass Spectrom.* **2000,** *200*, 495-508.
221. McLuckey, S.A.; Glish, G.L.; Cooks, R.G. Kinetic Energy Effects in Mass Spectrometry/Mass Spectrometry Using a Sector/Quadrupole Tandem Instru-

ment. *Int. J. Mass Spectrom. Ion Phys.* **1981,** *39*, 219-230.
222. Glish, G.L.; McLuckey, S.A.; Ridley, T.Y.; Cooks, R.G. A New "Hybrid" Sector/Quadrupole Mass Spectrometer for Mass Spectrometry/Mass Spectrometry. *Int. J. Mass Spectrom. Ion Phys.* **1982,** *41*, 157-177.
223. Bradley, C.D.; Curtis, J.M.; Derrick, P.J.; Wright, B. Tandem Mass Spectrometry of Peptides Using a Magnetic Sector/Quadrupole Hybrid-the Case for Higher Collision Energy and Higher Radio-Frequency Power. *Anal. Chem.* **1992,** *64*, 2628-2635.
224. Schoen, A.E.; Amy, J.W.; Ciupek, J.D.; Cooks, R.G.; Dobberstein, P.; Jung, G. A Hybrid BEQQ Mass Spectrometer. *Int. J. Mass Spectrom. Ion Proc.* **1985,** *65*, 125-140.
225. Ciupek, J.D.; Amy, J.W.; Cooks, R.G.; Schoen, A.E. Performance of a Hybrid Mass Spectrometer. *Int. J. Mass Spectrom. Ion Proc.* **1985,** *65*, 141-157.
226. Louris, J.N.; Wright, L.G.; Cooks, R.G. New Scan Modes Accessed With a Hybrid Mass Spectrometer. *Anal. Chem.* **1985,** *57*, 2918-2924.
227. Loo, J.A.; Münster, H. Magnetic Sector-Ion Trap Mass Spectrometry With Electrospray Ionization for High Sensitivity Peptide Sequencing. *Rapid Commun. Mass Spectrom.* **1999,** *13*, 54-60.
228. Strobel, F.H.; Solouki, T.; White, M.A.; Russell, D.H. Detection of Femtomole and Sub-Femtomole Levels of Peptides by Tandem Magnetic Sector/Reflectron Time-of-Flight Mass Spectrometry and Matrix-Assisted Laser Desorption Ionization. *J. Am. Soc. Mass Spectrom.* **1991,** *2*, 91-94.
229. Bateman, R.H.; Green, M.R.; Scott, G.; Clayton, E. A Combined Magnetic Sector-Time-of-Flight Mass Spectrometer for Structural Determination Studies by Tandem Mass Spectrometry. *Rapid Commun. Mass Spectrom.* **1995,** *9*, 1227-1233.
230. Aicher, K.P.; Müller, M.; Wilhelm, U.; Grotemeyer, J. Design and Setup of an Ion Trap-Reflectron-Time-of-Flight Mass Spectrometer. *Eur. Mass Spectrom.* **1995,** *1*, 331-340.
231. Wilhelm, U.; Aicher, K.P.; Grotemeyer, J. Ion Storage Combined With Reflectron Time-of-Flight Mass Spectrometry: Ion Cloud Motions As a Result of Jet-Cooled Molecules. *Int. J. Mass Spectrom. Ion Proc.* **1996,** *152*, 111-120.
232. Morris, H.R.; Paxton, T.; Dell, A.; Langhorne, J.; Berg, M.; Bordoli, R.S.; Hoyes, J.; Bateman, R.H. High Sensitivity Collisionally-Activated Decomposition Tandem Mass Spectrometry on a Novel Quadrupole/Orthogonal-Acceleration Time-of-Flight Mass Spectrometer. *Rapid Commun. Mass Spectrom.* **1996,** *10*, 889-896.
233. Shevchenko, A.; Chernushevich, I.V.; Ens, W.; Standing, K.G.; Thompson, B.; Wilm, M.; Mann, M. Rapid 'De Novo' Peptide Sequencing by a Combination of Nanoelectrospray, Isotopic Labeling and a Quadrupole/Time-of-Flight Mass Spectrometer. *Rapid Commun. Mass Spectrom.* **1997,** *11*, 1015-1024.
234. Hopfgartner, G.; Chernushevich, I.V.; Covey, T.; Plomley, J.B.; Bonner, R. Exact Mass Measurement of Product Ions for the Structural Elucidation of Drug Metabolites With a Tandem Quadrupole Orthogonal-Acceleration Time-of-Flight Mass Spectrometer. *J. Am. Soc. Mass Spectrom.* **1999,** *10*, 1305-1314.
235. Collins, D.C.; Lee, M.L. Developments in Ion Mobility Spectrometry-Mass Spectrometry. *Anal. Bioanal. Chem.* **2002,** *372*, 66-73.
236. Mukhopadhyay, R. IMS/MS: Its Time Has Come. *Anal. Chem.* **2008,** *80*, 7918-7920.
237. Bohrer, B.C.; Merenbloom, S.I.; Koeniger, S.L.; Hilderbrand, A.E.; Clemmer, D.E. Biomolecule Analysis by Ion Mobility Spectrometry. *Ann. Rev. Anal. Chem.* **2008,** *1*, 293-327.
238. Karasek, F.W. Drift-Mass Spectrometer. *Res. Development* **1970,** *21*, 25-27.
239. Karasek, F.W. Plasma Chromatograph. *Res. Development* **1970,** *21*, 34-37.
240. Karasek, F.W.; Cohen, M.J.; Carroll, D.I. Trace Studies of Alcohols in the Plasma Chromatograph-Mass Spectrometer. *J. Chromatogr. Sci.* **1971,** *9*, 390-392.
241. Kanu, A.B.; Dwivedi, P.; Tam, M.; Matz, L.; Hill, H.H., Jr. Ion Mobility-Mass Spectrometry. *J. Mass Spectrom.* **2008,** *43*, 1-22.
242. Pringle, S.D.; Giles, K.; Wildgoose, J.L.; Williams, J.P.; Slade, S.E.; Thalassinos, K.; Bateman, R.H.; Bowers, M.T.; Scrivens, J.H. An Investigation of the Mobility Separation of Some Peptide and Pro-

and Protein Ions Using a New Hybrid Quadrupole/Travelling Wave IMS/Oa-ToF Instrument. *Int. J. Mass Spectrom.* **2007,** *261*, 1-12.
243. Platzner, I.T.; Habfast, K.; Walder, A.J.; Goetz, A. *Modern Isotope Ratio Mass Spectrometry;* Platzner, I.T., editor; Wiley: Chichester, 1997.
244. Stanton, H.E.; Chupka, W.A.; Inghram, M.G. Electron Multipliers in Mass Spectrometry; Effect of Molecular Structure. *Rev. Sci. Instrum.* **1956,** *27*, 109.
245. Frank, M. Mass Spectrometry With Cryogenic Detectors. *Nucl. Instrum. Methods Phys. Res. ,A* **2000,** *444*, 375-384.

246. Allen, J.S. An Improved Electron-Multiplier Particle Counter. *Rev. Sci. Instrum.* **1947,** *18*, 739-749.
247. Wang, G.H.; Aberth, W.; Falick, A.M. Evidence Concerning the Identity of Secondary Particles in Post-Acceleration Detectors. *Int. J. Mass Spectrom. Ion Proc.* **1986,** *69*, 233-237.
248. Busch, K.L. The Electron Multiplier. *Spectroscopy* **2000,** *15*, 28-33.
249. Schröder, E. *Massenspektrometrie - Begriffe und Definitionen;* Springer-Verlag: Heidelberg, 1991.
250. Boerboom, A.J.H. Array Detection of Mass Spectra, a Comparison With Conventional Detection Methods. *Org. Mass Spectrom.* **1991,** *26*, 929-935.
251. Kurz, E.A. Channel Electron Multipliers. *Am. Laboratory* **1979,** *11*, 67-82.
252. Wiza, J.L. Microchannel Plate Detectors. *Nucl. Instrum. Methods* **1979,** *162*, 587-601.
253. Laprade, B.N.; Labich, R.J. Microchannel Plate-Based Detectors in Mass Spectrometry. *Spectroscopy* **1994,** *9*, 26-30.
254. Alexandrov, M.L.; Gall, L.N.; Krasnov, N.V.; Lokshin, L.R.; Chuprikov, A.V. Discrimination Effects in Inorganic Ion-Cluster Detection by Secondary-Electron Multiplier in Mass Spectrometry Experiments. *Rapid Commun. Mass Spectrom.* **1990,** *4*, 9-12.
255. Geno, P.W.; Macfarlane, R.D. Secondary Electron Emission Induced by Impact of Low-Velocity Molecular Ions on a Microchannel Plate. *Int. J. Mass Spectrom. Ion Proc.* **1989,** *92*, 195-210.
256. Hedin, H.; Håkansson, K.; Sundqvist, B.U.R. On the Detection of Large Organic Ions by Secondary Electron Production. *Int. J. Mass Spectrom. Ion Proc.* **1987,** *75*, 275-289.
257. Hill, J.A.; Biller, J.E.; Martin, S.A.; Biemann, K.; Yoshidome, K.; Sato, K. Design Considerations, Calibration and Applications of an Array Detector for a Four-Sector Tandem Mass Spectrometer. *Int. J. Mass Spectrom. Ion Proc.* **1989,** *92*, 211-230.
258. Birkinshaw, K. Fundamentals of Focal Plane Detectors. *J. Mass Spectrom.* **1997,** *32*, 795-806.
259. Cottrell, J.S.; Evans, S. The Application of a Multichannel Electro-Optical Detection System to the Analysis of Large Molecules by FAB Mass Spectrometry. *Rapid Commun. Mass Spectrom.* **1987,** *1*, 1-2.
260. Cottrell, J.S.; Evans, S. Characteristics of a Multichannel Electrooptical Detection System and Its Application to the Analysis of Large Molecules by Fast Atom Bombardment Mass Spectrometry. *Anal. Chem.* **1987,** *59*, 1990-1995.
261. Birkinshaw, K.; Langstaff, D.P. The Ideal Detector. *Rapid Commun. Mass Spectrom.* **1996,** *10*, 1675-1677.
262. Hucknall, D.J. *Vacuum Technology and Applications*; Butterworth-Heinemann: Oxford, 1991.
263. Pupp, W.; Hartmann, H.K. *Vakuum-Technik – Grundlagen und Anwendungen;* Fachbuchverlag Leipzig: Leipzig, 1991.
264. Wutz, M.; Adam, H.; Walcher, W. *Theory and Practice of Vacuum Technology,* 5th ed.; Vieweg: Braunschweig, 1992.
265. *Foundations of Vacuum Science and Technology*; Lafferty, J.M., editor; Wiley: New York, 1998.
266. *Leybold Vacuum Products and Reference Book*; Umrath, W., editor; Leybold Vacuum GmbH: Köln, 2001.
267. Busch, K.L. Vacuum in Mass Spectroscopy. Nothing Can Surprise You. *Spectroscopy* **2000,** *15*, 22-25.
268. Busch, K.L. High-Vacuum Pumps in Mass Spectrometers. *Spectroscopy* **2001,** *16*, 14-18.

5 Practical Aspects of Electron Ionization

Learning Objectives

- Electron ionization ion sources – construction and operation
- Generating primary electrons for electron ionization
- Sample introduction into EI ion sources – methods and devices
- Databases of EI mass spectra

The use of *electron ionization* (EI) [1] dates back to the infancy of mass spectrometry in the early 20th century. Before, only *spark source* (SS), *glow discharge* (GD), and *thermal ionization* (TI) had been in use (Chap. 15) [2]. In electron ionization, energetic electrons are shot onto gaseous neutrals to effect their ionization. EI definitely represents the classical approach to ionization in organic mass spectrometry. EI still remains an important technique for analyzing low- to medium-polarity, non-ionic organic compounds of molecular weights in the range of up to $M_r \approx 1000$ u. EI formerly has been referred to as *electron impact ionization* or simply *electron impact* (EI).

The physicochemical aspects of the ionization process in general, ion internal energy, and the principles determining the reaction pathways of excited ions have already been addressed (Chap. 2). Here, we will discuss practical aspects concerning the construction of EI ion sources and sample introduction systems. Finally, by considering EI mass spectral databases, this chapter directly leads over to the interpretation of EI mass spectra (Chap. 6).

5.1 Electron Ionization Ion Sources

5.1.1 Layout of an Electron Ionization Ion Source

The basic layout of any ion source has already been introduced (Chap. 4.1). The design is arranged so that an ion generated within an electric field as realized between two oppositely charged plates, will be accelerated towards the plate of opposite charge sign. If the attracting plate has a hole or a slit, a beam of approximately monoenergetic ions is produced. For practical reasons, the attracting electrode is usually grounded and the location of ion generation is set to high po-

J. Gross, *Mass Spectrometry*, 2nd ed., DOI 10.1007/978-3-642-10711-5_5,
© Springer-Verlag Berlin Heidelberg 2011

tential. Doing so allows to keep the whole mass analyzer grounded, thereby contributing substantially to safety of operation (Fig. 5.1).

The beam of neutral gaseous analyte molecules enters the *ionization chamber* or *ion volume*, i.e., the actual region of ionization within the *ion source block*, in a line vertical to the paper plane and crosses the electron beam in the center. In order to reduce loss of ions by neutralizing collisions with the walls, the ions are pushed out immediately after generation by action of a low voltage applied to the *repeller* electrode [3,4]. They are then accelerated and focused towards the mass analyzer. Efficient ionization and ion extraction are of key importance for the construction of ion sources producing focusable ion currents in the nanoampere range [5].

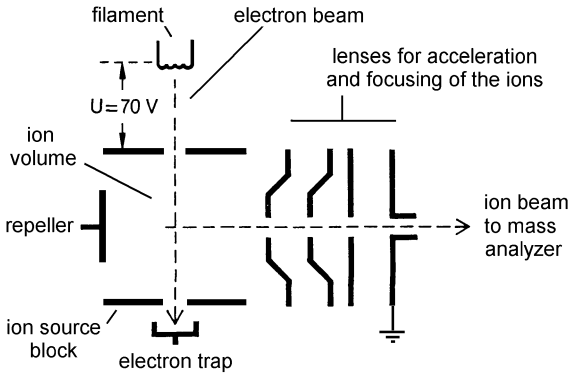


Fig. 5.1. Principle layout of an EI ion source. Adapted from Ref. [6] with permission. © Springer-Verlag Heidelberg, 1991.

Modern ion sources are of compact design to simplify the handling during exchange and cleaning (Fig. 5.2). They are usually constructed as *combination ion sources*, that can be switched from EI to *chemical ionization* (CI), *fast atom bombardment* (FAB), or *field ionization/field desorption* (FI/FD) with EI/CI/FAB and EI/FI/FD [7,8] ion sources being most commonly encountered. Some instruments are equipped with ion sources having ion volumes that are exchangeable via a (separate) vacuum lock to allow for their exchange without breaking the high vacuum, e.g., Micromass Autospec, Finnigan MAT 95 and MAT 900 series. Unfortunately, more recent developments of EI ion sources are mainly communicated in patents.

Hint: System contamination – For a high vacuum system and for the ion source in particular *any sample* introduction also means introduction of *contamination*. Even though ion sources are operated at 150–250°C, decomposition products of low volatility cannot be removed by pumping. Instead, they form semiconducting layers on the surfaces which in turn cause defocusing due to badly defined potentials. Therefore, cleaning of an ion source is necessary on a regular basis. This includes disassembling, use of fine abrasives to polish the lenses, baking of the insulating ceramics, and thorough washing of the parts.

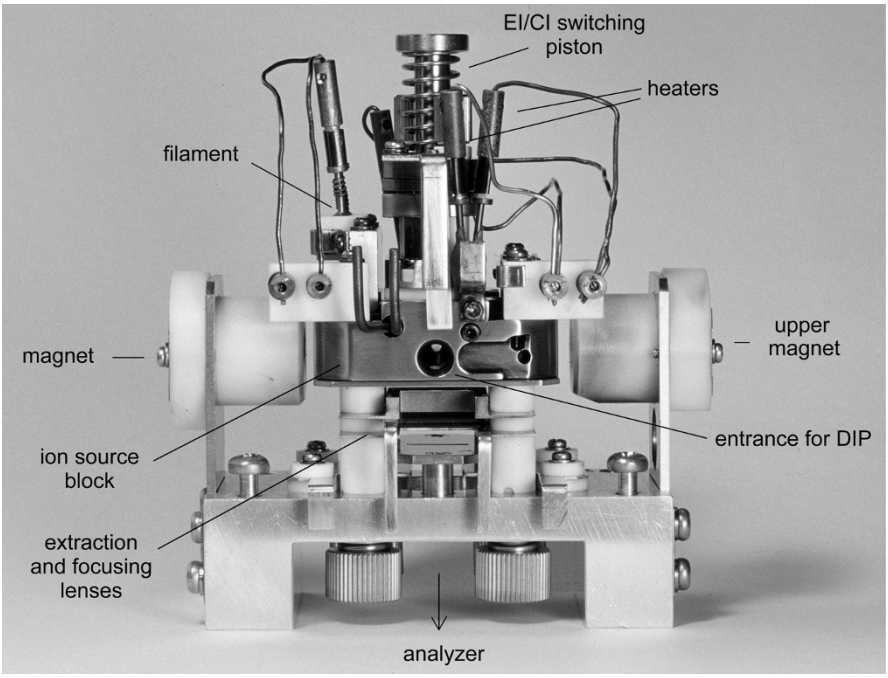


Fig. 5.2. EI/CI/FAB combination ion source of a JEOL JMS-700 sector instrument.

5.1.2 Generation of Primary Electrons

The beam of ionizing electrons is produced by *thermionic emission* from a resistively heated metal wire or *filament* typically made of rhenium or tungsten. The filament reaches up to 2000°C during operation. Some reduction of the working temperature without loss of electron emission (1–10 mA mm^{-2}) can be achieved by use of thoriated iridium or thoriated rhenium filaments [9]. There is a wide variety of filaments available from different manufacturers working almost equally well, e.g., the filament can be a straight wire, a ribbon, or a small coil (Fig. 5.3).

The potential for acceleration of the primary electrons has to be carefully shielded from the acceleration voltage for the ions. Otherwise, badly defined ion kinetic energies cause substantial loss of resolution and mass accuracy. In addition, a pair of permanent magnets with their field aligned in parallel to the electron beam is attached above the filament and below the electron trap, thus preventing the electrons from spreading all over the ion volume (Fig. 5.2). This is achieved by action of the Lorentz force on divergent electrons which are forced to travel on helical paths; the resulting electron beam is about 1 mm in diameter. These features developed by Bleakney [10], and refined by Nier [11] were destined to direct the design of EI ion sources ever since [2,4,12] (the basic EI ion source is sometimes referred to as “Nier-type” ion source). Further improvements can be ob-

tained by *i*) more efficient shielding of the ion volume from the filament, a measure also reducing thermal decomposition of the analyte, and *ii*) by use of stronger ion source magnets [3].

To achieve a more stable mode of operation, in modern instruments the heating current for the filament is *emission-controlled*, i.e., the current of the electron trap is used to keep emission comparatively independent from actual ion source conditions. Typical emission currents are in the range of 50–400 μA.

Note: The lifetime of a filament is several weeks under proper operating conditions. However, this may become drastically shortened by the harsh conditions of aggressive analytes or reagent gases in chemical ionization, too high emission current, and in particular sudden breakdown of the high vacuum.

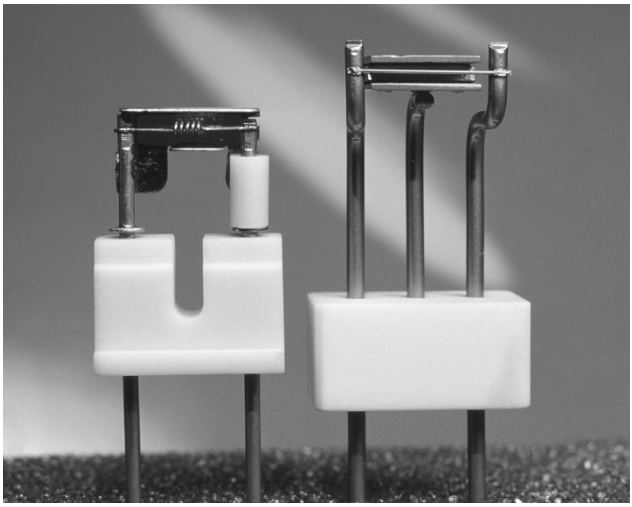


Fig. 5.3. Filaments for EI/CI ion sources. A coiled filament of the VG ZAB-2F (*left*) and a straight wire filament of the JEOL JMS-700 (*right*). The shields behind the filament are at the same potential as the wire itself and the white parts are made of ceramics for insulation.

5.1.3 Overall Efficiency and Sensitivity of an EI Ion Source

The overall efficiency of an EI ion source depends on the intrinsic properties of the ionization process, the ion source design, and the actual operation parameters. The most astonishing fact is the extremely low ionization probability for a neutral entering the ion source. Only a minor fraction of the sample introduced becomes ionized, whereas the vast majority gets lost via the vacuum pumps. This is due to the disadvantageous combination of long mean free paths for ions and electrons and the low collision cross section of the electron itself. Remember, the path

through the effective ionization volume is merely about 1 mm long. Nonetheless, EI provides high sensitivity as compared to other ionization methods.

In 70 eV EI mode, modern magnetic sector instruments are specified to have a sensitivity of about 4×10^{-7} C μg^{-1} for the molecular ion of methylstearate, *m/z* 298, at $R = 1000$. The charge of 4×10^{-7} C corresponds to 2.5×10^{12} electron charges. One microgram of methylstearate is equivalent to 3.4×10^{-9} mol or 2.0×10^{15} molecules. For a molecule entering the ionization volume one therefore calculates a chance of 1 : 800 to become ionized and to reach the detector as a molecular ion. The fraction of the neutrals that become ionized is definitely larger, maybe 1 : 100, because a significant fraction of them will dissociate to form fragment ions of other *m/z* values. Even then, a ratio of about 1 : 100 indicates an almost perfect ion source design as compared to 1 : 10^4–10^5 in the 1970s. (For a comparison of EI to other ionization methods refer to Chap. 8.7.1.)

5.1.4 Optimization of Ion Beam Geometry

The extraction of ions and the shape of the ion beam can largely be improved if the acceleration voltage is applied in two or more successive stages instead of a single stage. In addition, by dividing the plates into an upper and a lower half or a left and a right one, the ion beam can be directed up and down or adjusted from right to left, respectively, by applying slightly different voltages to the corresponding halves (Figs. 5.1 and 5.2). This also allows for focusing of the ion beam.

In practice, the ion optical properties of an ion source are optimized by means of ion trajectory calculations. [13]. The standard tool for this task is the SIMION software suite [14-17], while there are others, too [18]. Thus one can determine the optimum number, positions, voltages, and eventually shapes of the plates (Fig. 5.4). In order to compensate for slight mechanical deviations from theory and for effects exerted by contamination of the plates during elongated use, the voltages can be adjusted to yield optimum conditions.

Note: Usually, some *tuning* of the instrument is performed before actually starting measurements. Such a tuning procedure mainly means adjusting the voltages applied to the ion acceleration lenses of the ion source and eventually of some additional components of the ion optical system. Modern instruments have automatic tuning routines that are often faster and even more thorough than routine manual tuning would be. In any case, a reasonable mass spectrometer data system will also allow for manual corrections.

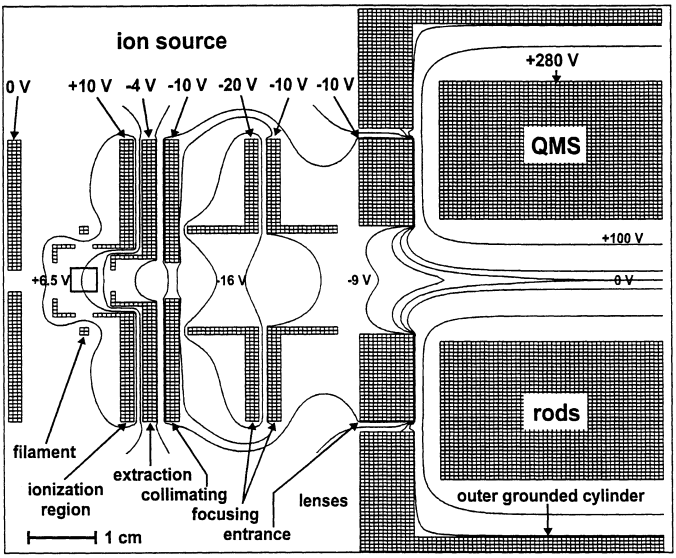


Fig. 5.4. The EI ion source of a quadrupole mass spectrometer with equipotentials as calculated by the computer simulation program SIMION three-dimensional version 6.0. Reproduced from Ref. [15] with permission. © Elsevier Science, 1998.

5.2 Sample Introduction

For the purpose of sample introduction, any *sample introduction system* (also *sample inlet system* or *inlet*) can be employed that is suitable for the respective compound. Hence, *direct probes*, *reservoir inlets*, *gas chromatographs*, and even *liquid chromatographs* can be attached to an EI ion source. The preferable inlet systems is to be preferred depends on the type of sample to be analyzed. Whatever type the inlet system may be, it has to manage the same basic task, i.e., the transfer of the analyte from atmospheric conditions into the high vacuum of the EI ion source; Table 5.1 provides an overview.

Note: The below-mentioned sample introduction systems (reservoir inlets, various direct insertion probes, and chromatographs) are of equal importance to other ionization methods.

5.2.1 Reservoir or Reference Inlet System

Highly volatile samples cannot be introduced into the ion source by means of a direct insertion probe even when cooling is applied. A *reference inlet system* or *reservoir inlet system* is better suited for that purpose [19]. The name of this type of

inlet has been coined by the fact that reference inlets have been intended – and often are used for – the introduction of a mass calibrant (or *reference*) independent of the analyte in order to achieve internal mass calibration in accurate mass measurements (Chap. 3.3). Fluorocarbons such as perfluorotributylamine (FC43) or perfluorokerosene (PFK) can be admitted to the ion source in this way.

Reference inlets serve equally well for the analysis of gases, solvents, and similar volatile samples. They are especially convenient when a continuous signal is desired for instrument tuning or long-lasting MS/MS experiments in ion chemistry. In addition, the components of a mixture are admitted to the ion source without fractionation, i.e., without affecting their partial pressures. This property of reservoir inlets has extensively been used in the petroleum industry. A reference inlet system basically consists of a vessel heated to 80–200°C that *i*) can be filled via a septum port, *ii*) can be connected to the ion source via a toggle valve and a needle valve to adjust the partial pressure in the ion source housing, and *iii*) can be connected to some vacuum pump to remove the sample after completion of the measurement. Typically, reference inlets have volumes of 30–100 ml and are filled with a few microliters of liquid sample by means of a microliter syringe. Heating is applied to suppress adsorption of the analytes to the walls and thus, to speed up the final removal of sample (Fig. 5.5). As the analyte is exposed to elongated heating, the application of reference inlet systems should be restricted to thermally stable analytes. To reduce the risks of catalytic degradation and selective adsorption of components of mixtures on the walls of the reservoir, an *all-glass heated inlet system* (AGHIS) [20,21] and a teflon-coated reservoir inlet system have been commercially available as an alternative to stainless steel systems. To this end, *dynamic batch inlet systems* (DBIS) have been developed, where the analyte is transferred from the reservoir into the ion source by means of a capillary and where a carrier gas (H_2, He) can be used to reduce fractionation of mixtures having an extremely wide range of boiling points [21].

Table 5.1. Sample introduction systems for EI-MS

Inlet system	Principle	Analytes
Reservoir/reference inlet	heated reservoir with sample vapor	low to medium boiling liquids
Direct insertion probe, DIP	sample in heated/cooled glass/metal vial as particles or film of analyte	solids, waxes or high-boiling liquids
Direct exposure probe, DEP	sample particles or film of analyte on resistively heated metal filament	solids of extremely low volatility, especially if thermally labile
Gas chromatograph, GC	elutes directly into ion source	volatile components of mixtures
Liquid chromatograph, LC	connected via particle beam interface	analytes suitable for EI that cannot be separated by GC due to high polarity

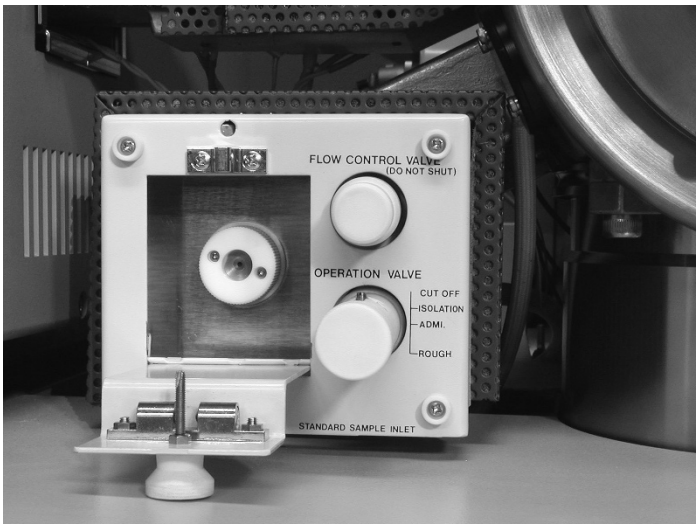


Fig. 5.5. Reservoir inlet of a JEOL JMS-700 sector instrument with the septum injection port opened. The "operation valve" switches between evacuation, isolation, and admission of the sample; a needle valve allows regulation of the sample flow. The GC transfer line crosses in the upper background from the GC (*left*) to the ion source housing (*upper right*).

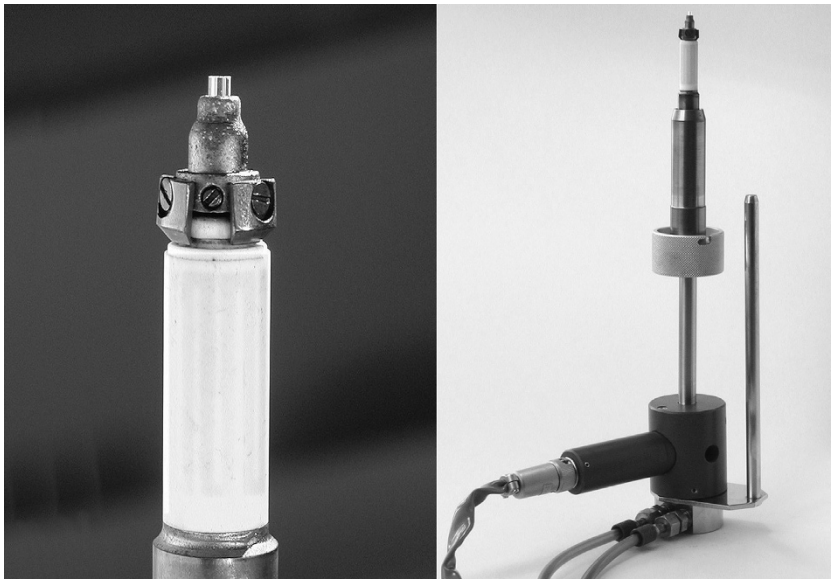


Fig. 5.6. DIP of a JEOL JMS-700 sector instrument for use with EI, chemical ionization (CI) and field ionization (FI). The copper probe tip holds the glass sample vial and is fitted to a temperature-controlled heater (*left*). The heater, a thermocouple, and circulation water cooling are provided inside. The (*white*) ceramics insulator protects the operator from the high voltage of the ion source.

The *liquid introduction system* represents another variation of reservoir inlets. Here, the ion source housing serves as the reservoir into which a few microliters of liquid are introduced by means of a kind of "micro DIP" [22].

5.2.2 Direct Insertion Probe

The "traditional" way of introducing solids into a mass spectrometer is by directly placing them inside an ion source, which is mounted to the instrument thereafter and heated [23]. Definitely, the most convenient procedure is to involve a micro *sample vial* or *crucible* containing some 0.1–2 µg of the analyte that can be directly applied close to the ion source by means of a *direct insertion probe* (DIP) (Fig. 5.6). DIPs have been devised from the late 1950s and were in common use by the mid-1960s [24-26].

A DIP consists of a stainless steel shaft with a tip suitable to insert the sample vial. The shaft is polished to allow installation an effective vacuum seal against the O-rings of a vacuum lock. Being transferred into the high vacuum of the ion source housing through the *vacuum lock* [26], the probe is pushed in, eventually until it contacts the ion source block (Fig. 5.7). Spectra are then acquired while the

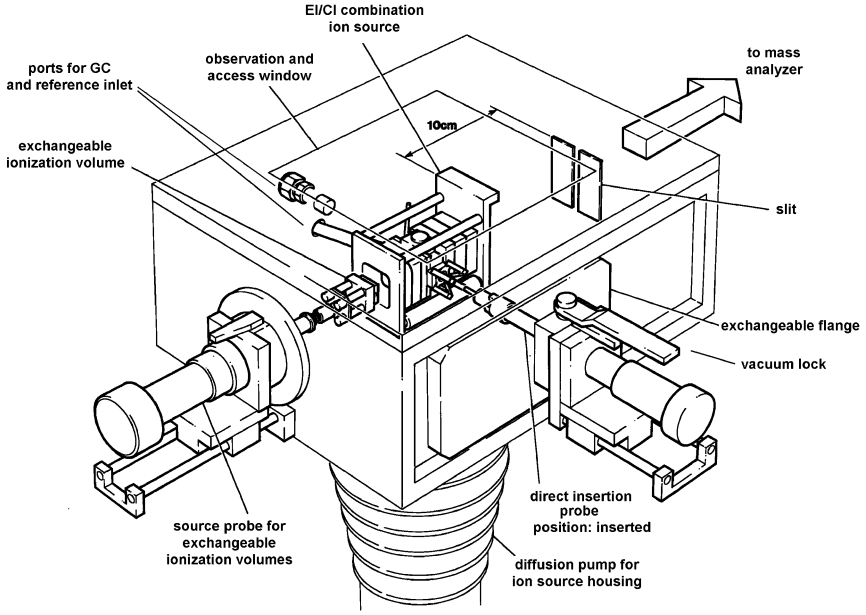


Fig. 5.7. Ion source housing of a Waters Micromass Autospec™ magnetic sector instrument. The ion source can be accessed from several directions to allow for simultaneous connection to DIP/DEP, GC and reference inlet system. By courtesy of Waters Corporation, MS Technologies, Manchester, UK.

analyte evaporates or sublimes from the vial directly into the ionization volume of the ion source. Typically, the sample holder can be heated up to about 500°C can be applied to enforce evaporation of the sample, which sometimes is accompanied by decomposition prior to evaporation.

Special high-temperature probes reaching up to 1000°C are also available. Modern direct probes have *temperature programed heaters* [27] allowing to set rates of 5–150°C min^{-1} or are equipped with *ion current-controlled heaters* [28].

To prevent more volatile samples from suddenly evaporating a circulation watercooling is often incorporated in the DIP, and refrigerated probes for more volatile samples have also been developed [29]. Sometimes, glass wool is placed into the sample vial to increase the surface for adsorption, and thus to slow down evaporation of the sample. Sudden evaporation causes distorted spectra and may even result in a temporary breakdown of the high vacuum.

5.2.3 Sample Vials for Use with Direct Insertion Probes

Sample vials for use with DIPs usually are about 2 mm in outer diameter and 10–20 mm in length. They are made from borosilicate glass or aluminum (Fig. 5.8). In general, the vials are disposed after use. However, although bearing the risk of memory effects or adsorption of analyte to residual pyrolysis products from previous samples, reusable quartz vials have also been employed in the past. The analyte may either be loaded in solution into the vial or as a tiny piece if solid or waxy (Fig. 5.9). Using solutions of known concentration allows for more reproducible loading of the vials which in other cases is not a prerequisite. The solvent should then be evaporated before insertion of the probe into the vacuum lock, but it may also be removed by carefully opening the rough evacuation valve.

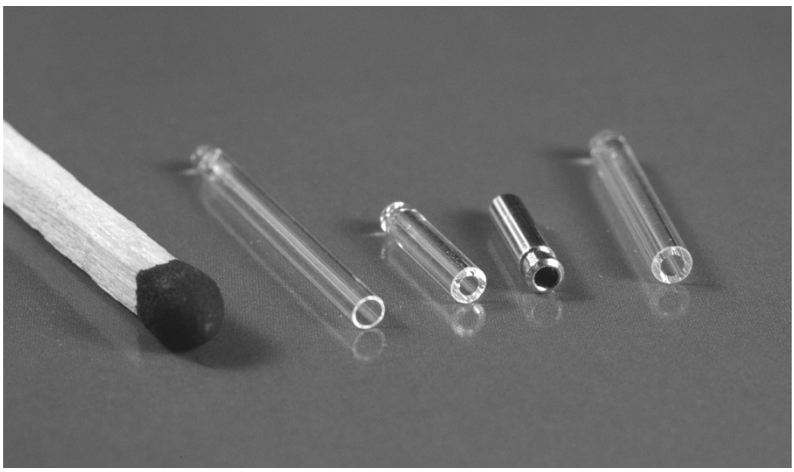


Fig. 5.8. Sample vials for different DIPs. From *left*: VG ZAB-2F, Finnigan TSQ700 glass and aluminum version, and JEOL JMS-700 (*right*). The match illustrates the scale.

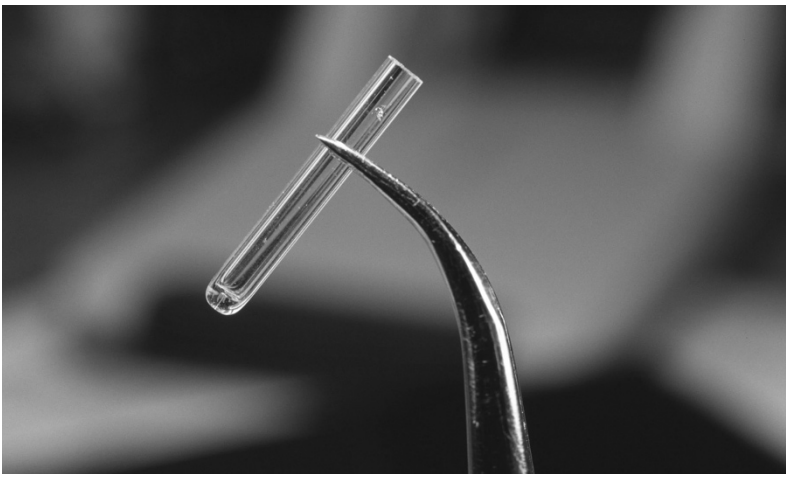


Fig. 5.9. Sample vial filled with analyte. The bright spot halfway between the tip of the tweezers and upper rim of the vial is the piece of solid material to be analyzed. Use of additional amount of sample does not bear any advantage; rather, it may only cause ion source contamination.

Note: Disposable vials devoid of memory effects. Glass vials bear the additional advantage of revealing the amount and position of sample within the vial. Afterwards, it is also possible that the analyte decomposes during the measurement yielding a black residue.

5.2.4 Fractionation When Using Direct Insertion Probes

The evaporation process out of the sample vial causes a certain degree of sample fractionation that can often be recognized from the *total ion chromatogram* (TIC) alone. Employing *reconstructed ion chromatograms* (RICs) in addition presents a valuable tool in identifying components of a simple mixture and in assigning their corresponding mass spectra. Generally, residual solvent is observed during the first few scans, while all other components appear more or less in order of increasing molecular weight as evaporation progresses.

Example: The TIC of an EI measurement using a DIP already reveals ion formation during the first scans. After some period of relatively low TIC, heating of the DIP to about 200°C finally led to evaporation of the major fraction of the sample, and thus produced a steeply rising TIC (Fig. 5.10). The TIC decreased again as all sample had evaporated. Thus, two different spectra were extracted from the data. The first was obtained by averaging scans 2–4, the second by averaging scans 20–29 (Fig. 5.11). Spectrum (**a**) corresponds to some impurities, whereas spectrum (**b**) represents the target compound, $C_{28}H_{47}NSi_2$.

Using RICs, the ions belonging to the same component can readily be identified from their parallel dependence in time (Fig. 5.10). The increase of the signal at *m/z* 194 in the chromatogram during late scans results from the presence of a minor signal at *m/z* 194 in the mass spectrum of the target compound. (More examples for the use of RICs are presented in Chap. 14.)

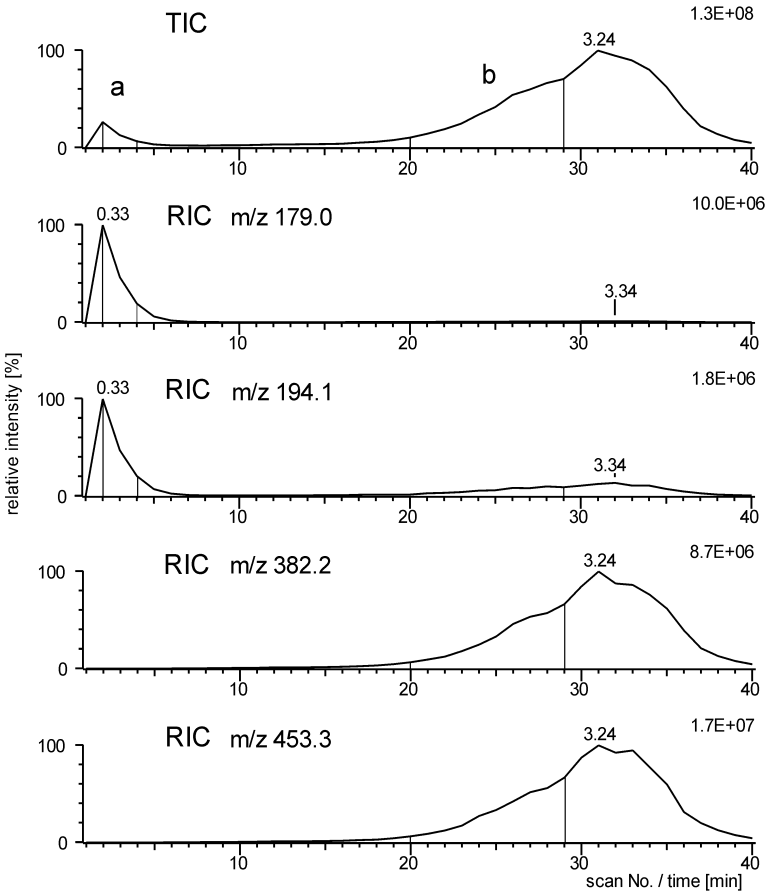


Fig. 5.10. Ion chromatograms from a DIP measurement. The TIC (*upper trace*) shows a bump during early scans that is also reflected in the RICs of *m/z* 179.0 and 194.1. Spectrum (**a**) corresponds to volatile impurities, whereas the RICs of *m/z* 382.2 and 453.3 are related to the target compound (**b**) that evaporates upon heating (cf. Fig. 5.11). By courtesy of R. Gleiter, Heidelberg University.

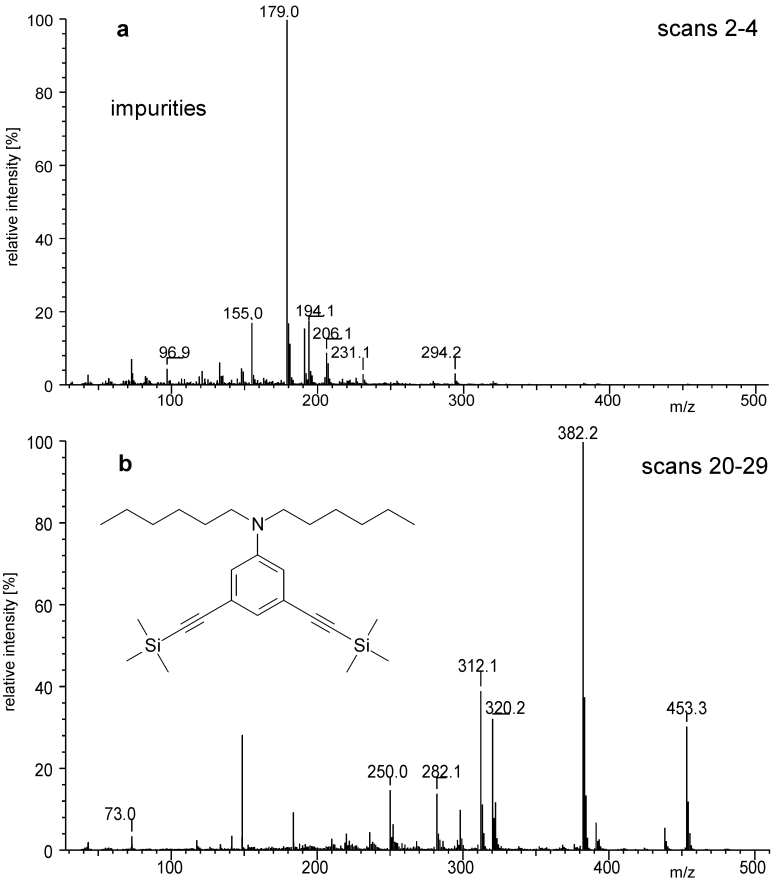


Fig. 5.11. Two EI mass spectra from the same sample. The spectrum (**a**) obtained from scans 2–4 corresponds to some volatile impurities, while spectrum (**b**) from scans 20–29 represents the target compound (cf. TIC and RICs in Fig. 5.10). By courtesy of R. Gleiter, Heidelberg University.

5.2.5 Direct Exposure Probe

Employing a *direct exposure probe* (DEP) may be helpful in case of analytes that cannot be evaporated from a sample vial without complete decomposition [30]. Here, the analyte is applied from solution or suspension to the outside of a thin wire loop or pin which is then directly exposed to the ionizing electron beam. This method has also been termed *in-beam* electron ionization. Early work describing the direct exposure of a sample to the electron beam came from Ohashi [31,32], Constantin, [33] and Traldi [34,35]. The idea behind the rapid heating of a DEP is

to achieve evaporation faster than thermal degradation of the sample [36,37]. This principle is realized in perfection with *energy-sudden methods* (Chaps. 10, 11).

If the analyte is exposed to energetic electrons the method is called *direct electron ionization* (DEI) or *desorption electron ionization* (DEI), and accordingly it is termed *direct* or *desorption chemical ionization* (DCI) if the analyte is immersed in the reagent gas under conditions of chemical ionization (Chap. 7). There are different types of DEPs in that some of them rely on the heated tip of a modified DIP [35], and others – widespread in use – that are capable of rapid resistive heating of a small loop made of chemically inert metal wire (rhenium). Resistively heated probes allow rates of several hundred °C s^{-1} and temperatures up to about 1500°C (Fig. 5.12). As a consequence of rapid heating, fast scanning, e.g., 1 s per scan over the *m/z* range of interest, is required to follow the evaporation of the analyte. In either case, the use of a DEP allows to extend the temperature range for evaporation. In addition, it reduces thermal degradation as a result of heating the

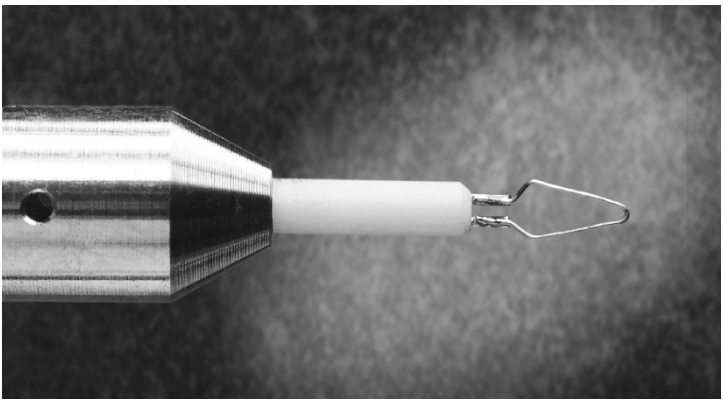


Fig. 5.12. Tip of a direct exposure probe of a GC-oaTOF mass spectrometer for EI, CI, FI). By courtesy of Waters Corporation, MS Technologies, Manchester, UK.

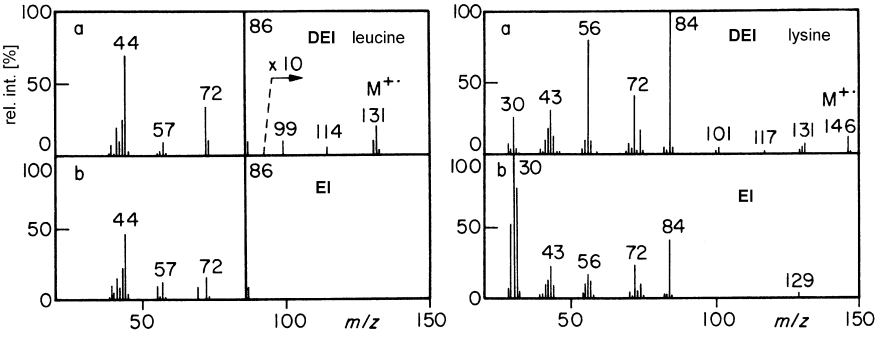


Fig. 5.13. Comparison of DEI (*upper*) and EI spectra (*lower*) of the amino acids leucine and lysine. In the leucine DEI spectrum the intensities above *m/z* 90 are shown in 10-fold expansion. Adapted from Ref. [35] with permission. © John Wiley & Sons, 1982.

analyte faster than its thermal decomposition usually proceeds, and therefore expands the range of applications for EI and CI to some extent. In any case, employing direct exposure probes is by far no alternative to real desorption ionization methods [38,39].

Example: The DEI technique has been applied to obtain mass spectra of four underivatized amino acids [35]. The method allowed for the observation of molecular ions and some primary fragment ions in contrast to conventional EI conditions which do not yield molecular ions. However, these additional signals are comparatively weak (Fig. 5.13).

5.3 Pyrolysis Mass Spectrometry

The enormous temperatures attained on resistively heated sample holders can also be used to intentionally enforce the decomposition of nonvolatile samples, thereby yielding characteristic pyrolysis products. *Pyrolysis mass spectrometry* (Py-MS) can be applied to synthetic polymers [40], fossil biomaterial [41], food [42], and soil [43] analysis and even to characterize whole bacteria [44]. In polymer analysis, for example, Py-MS does of course not yield molecular weight distributions, though the type of polymer and the monomer units it is based on can usually be identified by Py-MS [40,45]. Often, pyrolysis products are not directly introduced into the ion source but separated by GC beforehand. A detailed treatment of this branch of mass spectrometry is beyond the scope of the present book.

5.4 Gas Chromatograph

The *gas chromatograph* (GC) can be used for chromatographic separation of volatile analytes in complex mixtures prior to mass spectrometric analysis. This becomes especially advantageous if the GC elutes directly into the ion source of a mass spectrometer, so-called *GC-MS coupling* [46-48]. Packed GC columns with a high throughput rate can be connected via a jet-separator, but these have now been abandoned [49]. Capillary columns provide gas flow rates in the order of a few milliliters per minute, therefore their back end can be directly fitted into the entrance of the ion volume. In fact, the nano-LC-EI interface described in the next section is inspired by the standard direct coupling of capillary columns into EI ion sources.

EI is idealy suited as an ionization method for GC-MS applications. The specific properties of GC-MS are discussed later (Chap. 14). For the moment, it is sufficient to notice that proper coupling of a GC to an EI ion source neither exerts substantial effects on the EI process nor does it alter the fragmentation pathways of the ions.

5.5 Liquid Chromatograph

The *liquid chromatograph* (LC) can be used for chromatographic separation of polar analytes of low volatility prior to mass spectrometric analysis. Usually, atmospheric pressure ionization methods are employed when direct coupling of a liquid chromatograph to a mass spectrometer is required, so-called *LC-MS coupling* (Chap. 14) However, it can be desirable to obtain EI spectra of LC-separated analytes or of dissolved analytes in general, e.g., where the analyte is only accessible by EI or where EI spectra are required for mass spectral database searches.

The 'historic' *moving belt interface* seems rather a curiosity. The LC effluent is deposited onto a metal wire or belt which is heated thereafter to desolvate the sample. Then, the belt traverses a region of differential pumping before it enters an EI/CI ion source where the analyte is rapidly evaporated from the belt by further heating (Fig. 5.14) [50-54].

A *particle beam interface* (PBI) better serves the purpose of LC-EI-MS [55-57]. The PBI removes the solvent by nebulization into an evacuated desolvation chamber from where the evolving microscopic sample particles are transferred into an EI ion source via a jet separator (Fig. 5.14). Designs different from PBI have also been developed [57]. The PBI is comparatively robust and attained popularity in particular for low- to medium-polarity analytes, but has some drawbacks such as poor sensitivity especially with water-rich mobile phases, moderate linearity with polar compounds, and low tolerance for heat-sensitive compounds [58,59]. The most recent addition to LC-EI interfaces, also the simplest and most elegant solution, makes use of the very low liquid flow rates of nano-LC equipment [60,61]. The flow from a 30 μm i.d. fused silica capillary column is passed

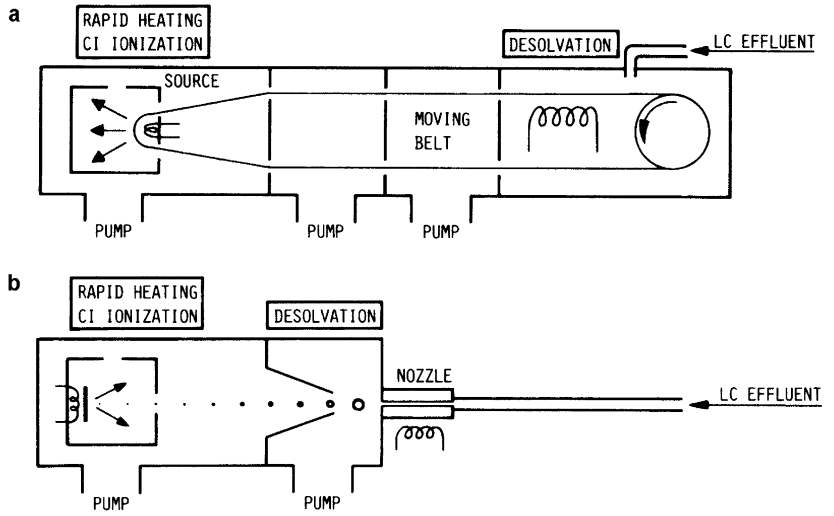


Fig. 5.14. LC-MS interfaces for EI mode; (**a**) moving belt interface, (**b**) particle beam interface. By courtesy of Thermo Finnigan, Bremen.

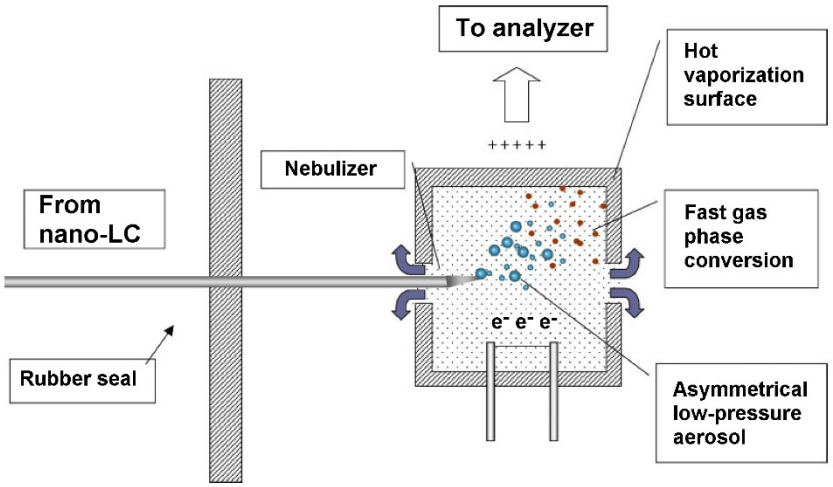


Fig. 5.15. Nano-LC-EI interface with direct connection of the LC capillary to a slightly modified EI ion source. Reproduced from Ref. [61] with permission. © Wiley Periodicals, Inc., 2005.

through a 5 µm i.d. micro-nebulizer with its orifice slightly bent sideways as to spray the droplets towards the opposite ion source wall (Fig. 5.15). The high ion source temperature of 200–300°C serves to provide heat for solvent and analyte evaporation. The open source construction keeps a low solvent partial pressure in the ionization volume, and thus, prevents $[M+H]^+$ ion formation that would deteriorate the EI character of the spectra. Due to gas flow rates from solvent vaporization similar to capillary GC flow rates, the nano-LC liquid flow of less than 1 µl min^{-1} can easily be accommodated by any ion source vacuum pump.

5.6 Low-Energy Electron Ionization Mass Spectra

Low-energy primary electrons limit the excess energy deposited onto a molecular ion. Using 12–15 eV instead of 70 eV electrons still ionizes most compounds while disadvantageous fragmentations are reduced. Superior EI mass spectra of large hydrocarbons can be obtained [62], even more so if the ion source is operated at 70°C instead of 200°C (Fig. 5.16). The concept of recording *low-energy, low-temperature EI mass spectra* has been postulated long ago [63] and has been extensively investigated since then [64-66]. Low-energy, low-temperature mass spectra are much easier to interpret than their conventional 70 eV counterparts for three reasons,: *i*) the relative intensity of the molecular ion peak is enhanced, thus permitting this important peak to be identified more easily, *ii*) less fragmentation also means a simpler overall appearance of the spectrum, and *iii*) the fragmentation pattern is dominated by a few characteristic primary fragmentations carrying the largest portion of structural information.

Unfortunately, there are some disadvantages: *i*) the decreased ionization efficiency at 12–15 eV goes along with a significant loss of sensitivity (Chap. 2.3), *ii*) low ion source temperatures cause long-lasting "memory" of previous samples due to slow desorption from the surfaces that have been in contact with the sample vapor, and *iii*) a weak molecular ion peak may well be enhanced, however, a spectrum showing no molecular ion peak at 70 eV will not turn into a spectrum exhibiting a strong molecular ion peak at 12 eV.

Nonetheless, during the first decades of analytical mass spectrometry, low-energy EI spectra were the only way to minimize fragmentation, and thereby to increase the relative intensity of a weak molecular ion peak. Nowadays, EI mass spectra are preferably complemented with spectra obtained from so-called *soft ionization methods* (Chaps. 7–13).

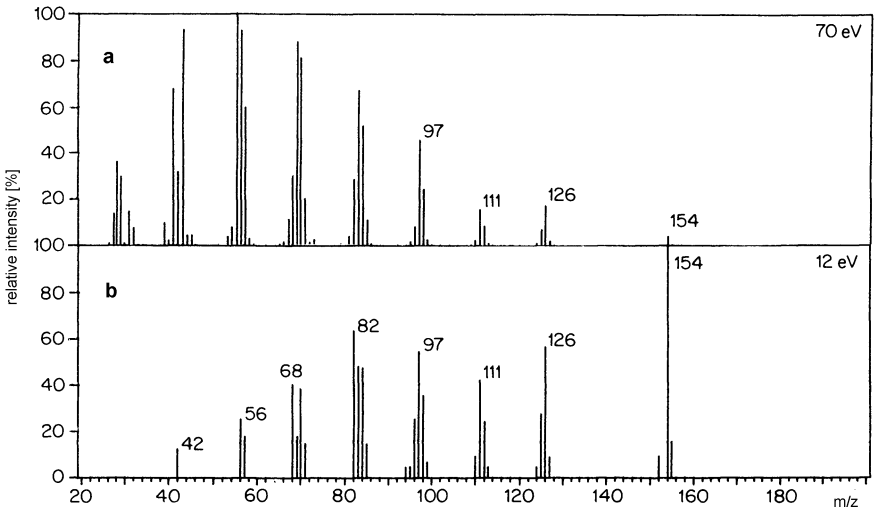


Fig. 5.16. Undecan-1-ol, $C_{11}H_{24}O$, $M_r = 172$ u: Comparison of (**a**) 70 eV and (**b**) 12 eV EI mass spectra. The molecular ion peak is absent in both spectra, but the $[M–H_2O]^{+\bullet}$ peak and the primary fragments become more prominent at 12 eV. (The detailed fragmentation pathways of aliphatic alcohols are discussed in Chaps. 6.2.5, 6.10.3) Reproduced from Ref. [65] with permission. © John Wiley & Sons, 1988.

Note: Signals from previous samples in the mass spectrum of the actual analyte are usually termed *memory*. Memory is caused by contamination of ion source or sample introduction system. To reduce memory one should use the lowest amount of sample necessary to produce good spectra, keep the ion source around 200°C, and allow some pumping between measurements.

5.7 Analytes for EI

Classical organic chemistry provides a wide variety of potential analytes for electron ionization, the only limitation being that the analyte should be able to evaporate or sublime without significant thermal decomposition. These requirements are usually met by saturated and unsaturated aliphatic and aromatic hydrocarbons and their derivatives such as halides, ethers, acids, esters, amines, amides etc. Heterocycles generally yield useful EI spectra, and flavones, steroids, terpenes and comparable compounds can successfully be analyzed by EI, too. Therefore, EI represents *the standard method* for such kinds of samples.

GC-EI-MS can be used for the direct analysis of mixtures, e.g., to analyze synthetic by-products; an advantage that made GC-EI-MS benchtop instruments become widespread in modern synthetic laboratories. The GC-EI-MS combination is especially successful in monitoring environmental pollutants such as polycyclic aromatic hydrocarbons (PAHs), polychlorinated biphenyls (PCBs), polychlorinated dibenzodioxins (PCDDs), polychlorinated dibenzofuranes (PCDFs), or other volatile organic compounds (VOCs).

While low- and medium-polarity analytes are usually well suited for EI, highly polar or even ionic compounds, e.g., diols or polyalcohols, amino acids, nucleosides, peptides, sugars, and organic salts should not be subjected to EI unless properly derivatized prior to EI-MS [67-72].

There is – as with any other ionization method – no strict upper limit for molecular mass, a range of up to 800–1000 u being a realistic estimate. There are exceptions of up to 1300 u if the analyte is extremely nonpolar, e.g., from numerous fluoroalkyl or trialkylsilyl groups which also significantly contribute to molecular mass.

5.8 Mass Analyzers for EI

In case of EI, there is no restriction as to type of mass analyzer (Chap. 4). Magnetic sector instruments used to dominate EI applications in the early days of mass spectrometry. With the increasing application of GC-MS, single quadrupole instruments became more popular because of significantly higher scan speeds. The demand for improved analytical selectivity in MS/MS favored the use of triple quadrupole instruments and quadrupole ion traps. In recent years, accurate mass measurements have become a nessecity thus increasing the demand for oaTOF and magnetic sector analyzers in contrast to quadrupole systems of either type. ICR analyzers may also be used in conjunction with EI, but due of their high cost they are rarely employed.

5.9 Mass Spectral Databases for EI

EI mass spectra are excellently reproducible when measured under standard conditions (70 eV, ion source at 150–250°C, pressure in the order of 10^{-4} Pa). This is not only the case for repeated measurements on the same instrument, but also between different types and brands of mass spectrometers. Large EI mass spectral libraries exist in either printed [73-75] or digitized form [76]. The most comprehensive EI mass spectral databases are the NIST/EPA/NIH Mass Spectral Database and the Wiley/NBS Mass Spectral Database [77-80].

Searching for a mass spectrum of an unknown substance in a mass spectral database often very quickly identifies the unknown, provided the corresponding spectrum is already available in the database. However, even if this is not case, the search might deliver similar spectra of closely related compounds, thus facilitating structure elucidation [81].

The obvious approach of comparing a mass spectrum of an unknown with a library spectrum is termed *forward library search* [82]. Normally, only a subset of the measured spectrum, i.e., a set of signals having intensities above a threshold value or a set of signals as defined by user input, is used to search the database. Database spectra closely matching that of the unknown are then displayed with a points score to judge the probability of the respective hit. In a so-called *reverse library search*, a library spectrum is compared to the mass spectra of unknowns in a way disregarding all peaks of the unknown's spectrum that are absent in the library spectrum. This prevents a misled search by background signals that might derive from column bleed, impurities, residual solvent, or memory. Typically, a mass spectral database offers a variety of search modes (Table 5.2).

Table 5.2. Types of searches in the NIST/EPA/NIH Mass Spectral Database

Type of Search	Explanation
Formula	Searches spectra corresponding to a chemical formula. Parentheses are resolved, e.g., $CH_3CH(C(CH_3)_3)_2$ is converted to $C_{10}H_{22}$. Constraints like name fragment or certain peaks can be selected.
Molecular weight	Searches for spectra belonging to a defined molecular weight. Constraints like elements, required peaks etc. may be selected.
Any peaks	A search based on a small number of peaks. Spectra can be searched using the largest peaks, or peaks in certain ranges of total intensity.
Sequential search	Search through database for matches that satisfy the constraints selected by the user.
CAS number	Search for compounds with specified CAS number.
NIST number	The NIST number identifies a unique spectrum. Search used to retrieve such a spectrum for repeated examination.
ID number	Each library spectrum has an additional identification number to correctly deal with user-edited spectra.

5.9.1 NIST/EPA/NIH Mass Spectral Database

The 2008 version of the NIST/EPA/NIH Mass Spectral Database [77,83] contains about 222,000 EI spectra of more than 192,000 compounds plus roughly 28,000 replicate spectra. For almost 43,000 compounds there is a compilation of 293,000 *Kovats retention index* (KRI) values as determined on nonpolar and polar columns. Since 2005, this database also offers CID spectra, which actually sum up to 14,800 spectra of about 5,300 different ions. The reason for the larger number of spectra over the number of ions is the inclusion of multiple spectra for a given ionic species as obtained by nozzle–skimmer dissociatio and CID on triplequadrupole or quadrupole ion trap instruments, respectively [84]. The NIST/EPA/NIH Mass Spectral Database is available as a stand-alone version or with – most probably – any commercial mass spectrometer that can be equipped with an EI ion source.

Example: The NIST/EPA/NIH mass spectral database (V 2.0, 2005) was searched for spectra corresponding to the molecular formula $C_8H_{10}ClN$. Eleven compounds were found, two of which were present with replicate spectra from different sources. Figure 5.17 shows the screenshot where the second spectrum

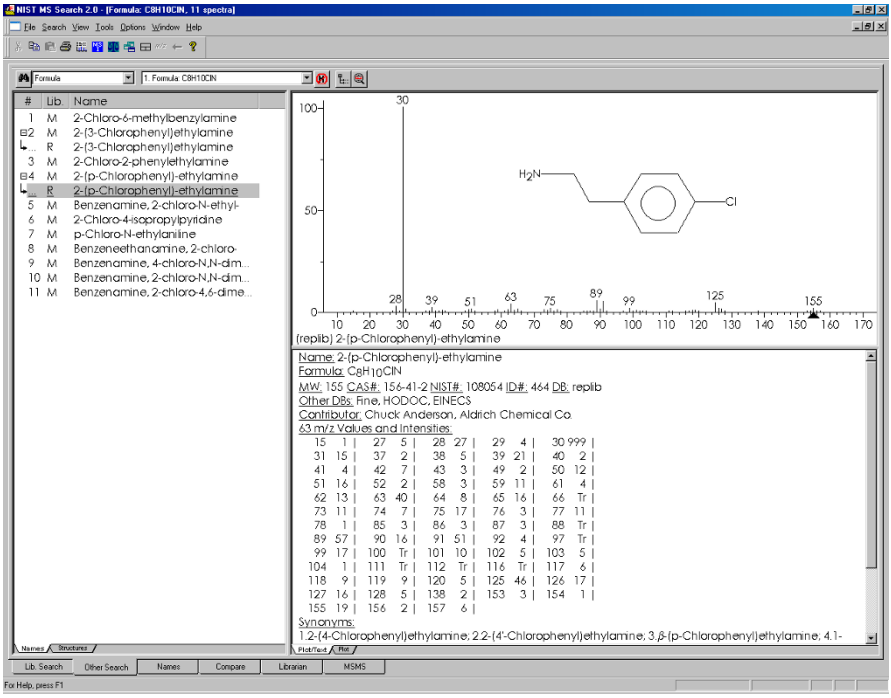


Fig. 5.17. Screenshot of NIST/EPA/NIH mass spectral database (V 2.0, 2005) after a formula search for spectra corresponding to $C_8H_{10}ClN$. The second of two replicate spectra of 2-(*p*-chlorophenyl)-ethylamine has been selected.

available of 2-(*p*-chlorophenyl)-ethylamine was selected for spectrum display. The structural formula is included in the spectral plot, while compound name, formula, molecular weight, CAS number, a tabular listing of the peaks, and a (here truncated) collection of synonyms are presented in the text window. It is possible to a certain extent to customize the information to be displayed in a specified window and how this is formatted.

Note: EI mass spectral databases can optionally be included in the software package of mass spectrometers. Thus, the EI spectra measured are directly searchable in the database by similarity search typically yielding a list of several hits. Alternatively, stand-alone solutions allow for sophisticated search algorithms and strategies (Table 5.2) [85-87].

5.9.2 Wiley Registry of Mass Spectral Data

The Wiley Registry of Mass Spectral Data dates back to the early 1960s when Stenhagen, Abrahamsson, and McLafferty started collecting mass spectra to be published in printed volumes of the Atlas of Mass Spectral Data in 1968 [73-75]. Different from the American Petroleum Institute's (API) spectral library, this project collected more spectra while applying lower restrictions to spectral quality. The reasoning behind that concept being that the probability to find a spectrum similar to that just measured in ones own laboratory would be higher and that the spectrum of a similar compound may also provide useful guidance for the final elucidation of the unknown structure.

The Wiley Registry 9th Edition as of autumn 2009 contains 662,780 spectra of 590,000 compounds. It may be obtained in a package combined with NIST08 spectra and search software to provide the largest available general-purpose MS library.

In addition, specialty libraries for compound classes are available, e.g., the Mass Spectra of Pharmaceuticals and Agrochemicals by Kühnle, the Maurer/Pfleger/Weber Mass Spectral & GC Data of Drugs, Poisons, Pesticides, Pollutants, and their Metabolites or the Mass Spectra of Designer Drugs [88].

5.9.3 Mass Spectral Databases – General Aspects

Although the coverage of these databases is enormous, and an easy-to-use interface is provided, one should be aware of potential pitfalls. The high score of a hit can be wrong, simply because the spectrum of the actual compound is still not included in database. A spectrum may be flawed by superimposition with some impurity peaks, which can in turn mislead the search. As a result, the unknown can generally not be perfectly identified by simple comparison with a library spectrum [83]. Nonetheless, mass spectral databases are highly useful, because even under unfavorable circumstances, they deliver spectra of similar compounds or isomers

for comparison, or at least afford some characteristics of spectra of a compound class under investigation [81]. Ultimately, one should always cross check the hits from the database. Again: even the highest score hit can be wrong, so adequate interpretational skills are still indispensible ...

Note: There are several mass spectral databases available on the market today [88]. As collections and packages in the software world are subject to rapid changes, it is recommended to do a quick internet search for something like "EI mass spectral database" to identify current options in this field.

References

1. Field, F.H.; Franklin, J.L. *Electron Impact Phenomena and the Properties of Gaseous Ions*; Academic Press: New York, 1957.
2. Nier, A.O. Some Reflections on the Early Days of Mass Spectrometry at the University of Minnesota. *Int. J. Mass Spectrom. Ion Proc.* **1990,** *100*, 1-13.
3. Schaeffer, O.A. An Improved Mass Spectrometer Ion Source. *Rev. Sci. Instrum.* **1954,** *25*, 660-662.
4. Fock, W. Design of a Mass Spectrometer Ion Source Based on Computed Ion Trajectories. *Int. J. Mass Spectrom. Ion Phys.* **1969,** *3*, 285-291.
5. Koontz, S.L.; Denton, M.B. A Very High Yield Electron Impact Ion Source for Analytical MS. *Int. J. Mass Spectrom. Ion Phys.* **1981,** *37*, 227-239.
6. Schröder, E. *Massenspektrometrie - Begriffe Und Definitionen*; Springer-Verlag: Heidelberg, 1991.
7. Hogg, A.M.; Payzant, J.D. Design of a Field Ionization/Field Desorption/Electron Impact Ion Source and Its Performance on a Modified AEIMS9 Mass Spectrometer. *Int. J. Mass Spectrom. Ion Phys.* **1978,** *27*, 291-303.
8. Brunnée, C. A Combined Field Ionisation-Electron Impact Ion Source for High Molecular Weight Samples of Low Volatility. *Z. Naturforsch. ,B* **1967,** *22*, 121-123.
9. Habfast, K. Massenspektrometrische Funktionselemente: Ionenquellen, in *Massenspektrometrie*; Kienitz, H., editor; Verlag Chemie: Weinheim, 1968; Chap. B 1.2, pp. 43-74.
10. Bleakney, W. A New Method of Positive-Ray Analysis and Its Application to the Measurement of Ionization Potentials in Mercury Vapor. *Phys. Rev.* **1929,** *34*, 157-160.
11. Nier, A.O. Mass Spectrometer for Isotope and Gas Analysis. *Rev. Sci. Instrum.* **1947,** *18*, 398-411.
12. Nier, A.O. The Development of a High Resolution Mass Spectrometer: a Reminiscence. *J. Am. Soc. Mass Spectrom.* **1991,** *2*, 447-452.
13. Morrison, J.D. Ion Focusing, Mass Analysis, and Detection, in *Gaseous Ion Chemistry and Mass Spectrometry*, Futrell, J.H., editor; Wiley: New York, 1986; pp. 107-125.
14. Dahl, D.A.; Delmore, J.E.; Appelhans, A.D. SIMION PC/PS2 Electrostatic Lens Design Program. *Rev. Sci. Instrum.* **1990,** *61*, 607-609.
15. Blaum, K.; Geppert, C.; Müller, P.; Nörtershäuser, W.; Otten, E.W.; Schmitt, A.; Trautmann, N.; Wendt, K.; Bushaw, B.A. Properties and Performance of a Quadrupole Mass Filter Used for Resonance Ionization Mass Spectrometry. *Int. J. Mass Spectrom.* **1998,** *181*, 67-87.
16. Ehlers, M.; Schmidt, S.; Lee, B.J.; Grotemeyer, J. Design and Set-Up of an External Ion Source Coupled to a Quadrupole-Ion-Trap Reflectron-Time-of-Flight Hybrid Instrument. *Eur. J. Mass Spectrom.* **2000,** *6*, 377-385.
17. Dahl, D.A. SIMION for the Personal Computer in Reflection. *Int. J. Mass Spectrom.* **2000,** *200*, 3-25.
18. Forbes, M.W.; Sharifi, M.; Croley, T.; Lausevic, Z.; March, R.E. Simulation of

Ion Trajectories in a Quadrupole Ion Trap: a Comparison of Three Simulation Programs. *J. Mass Spectrom.* **1999,** *34*, 1219-1239.
19. Caldecourt, V.J. Heated Sample Inlet System for Mass Spectrometry. *Anal. Chem.* **1955,** *27*, 1670.
20. Peterson, L. Mass Spectrometer All-Glass Heated Inlet. *Anal. Chem.* **1962,** *34*, 1850-1851.
21. Roussis, S.G.; Cameron, A.S. Simplified Hydrocarbon Compound Type Analysis Using a Dynamic Batch Inlet System Coupled to a Mass Spectrometer. *Energy & Fuels* **1997,** *11*, 879-886.
22. Pattillo, A.D.; Young, H.A. Liquid Sample Introduction System for a Mass Spectrometer. *Anal. Chem.* **1963,** *35*, 1768.
23. Cameron, A.E. Electron-Bombardment Ion Source for MS of Solids. *Rev. Sci. Instrum.* **1954,** *25*, 1154-1156.
24. Reed, R.I. Electron Impact and Molecular Dissociation. Part I. Some Steroids and Triterpenoids. *J. Chem. Soc.* **1958,** 3432-3436.
25. Gohlke, R.S. Obtaining the Mass Spectra of Non-Volatile or Thermally Unstable Compounds. *Chem. Industry* **1963,** 946-948.
26. Junk, G.A.; Svec, H.J. A Vacuum Lock for the Direct Insertion of Samples into a Mass Spectrometer. *Anal. Chem.* **1965,** *37*, 1629-1630.
27. Kankare, J.J. Simple Temperature Programmer for a Mass Spectrometer Direct Insertion Probe. *Anal. Chem.* **1974,** *46*, 966-967.
28. Franzen, J.; Küper, H.; Riepe, W.; Henneberg, D. Automatic Ion Current Control of a Direct Inlet System. *Int. J. Mass Spectrom. Ion Phys.* **1973,** *10*, 353-357.
29. Sawdo, R.M.; Blumer, M. Refrigerated Direct Insertion Probe for MS. *Anal. Chem.* **1976,** *48*, 790-791.
30. Cotter, R.J. Mass Spectrometry of Nonvolatile Compounds by Desorption From Extended Probes. *Anal. Chem.* **1980,** *52*, 1589A-1602A.
31. Ohashi, M.; Nakayama, N. In-Beam Electron Impact Mass Spectrometry of Aliphatic Alkohols. *Org. Mass Spectrom.* **1978,** *13*, 642-645.
32. Ohashi, M.; Tsujimoto, K.; Funakura, S.; Harada, K.; Suzuki, M. Detection of Pseudomolecular Ions of Tetra- and Pentasaccharides by in-Beam EI-MS. *Spectroscopy Int. J.* **1983,** *2*, 260-266.
33. Constantin, E.; Nakatini, Y.; Ourisson, G.; Hueber, R.; Teller, G. Spectres De Masse De Phospholipides Et Polypeptides Non Proteges. Une Méthode Simple D'Obtention Du Spectre Complet. *Tetrahedron Lett.* **1980,** *21*, 4745-4746.
34. Traldi, P.; Vettori, U.; Dragoni, F. Instrument Parameterization for Optimum Use of Commercial Direct Inlet Systems. *Org. Mass Spectrom.* **1982,** *17*, 587-592.
35. Traldi, P. Direct Electron Impact - a New Ionization Technique? *Org. Mass Spectrom.* **1982,** *17*, 245-246.
36. Udseth, H.R.; Friedman, L. Analysis of Styrene Polymers by Mass Spectrometry With Filament-Heated Evaporation. *Anal. Chem.* **1981,** *53*, 29-33.
37. Daves, G.D., Jr. Mass Spectrometry of Involatile and Thermally Unstable Molecules. *Accounts of Chemical Research* **1979,** *12*, 359-365.
38. Peltier, J.M.; MacLean, D.B.; Szarek, W.A. Determination of the Glycosidic Linkage in Peracetylated Disaccharides Comprised of D-Glucopyranose Units by Use of Desorption EI-MS. *Rapid Comm. Mass Spectrom.* **1991,** *5*, 446-449.
39. Kurlansik, L.; Williams, T.J.; Strong, J.M.; Anderson, L.W.; Campana, J.E. Desorption Ionization Mass Spectrometry of Synthetic Porphyrins. *Biomed. Mass Spectrom.* **1984,** *11*, 475-481.
40. Qian, K.; Killinger, W.E.; Casey, M.; Nicol, G.R. Rapid Polymer Identification by In-Source Direct Py-MS and Library Searching Techniques. *Anal. Chem.* **1996,** *68*, 1019-1027.
41. Meuzelaar, H.L.C.; Haverkamp, J.; Hileman, F.D. *Pyrolysis Mass Spectrometry of Recent and Fossil Biomaterials*; Elsevier: Amsterdam, 1982.
42. Guillo, C.; Lipp, M.; Radovic, B.; Reniero, F.; Schmidt, M.; Anklam, E. Use of Py-MS in Food Analysis: Applications in the Food Analysis Laboratory of the European Commissions' Joint Research Center. *J. Anal. Appl. Pyrolysis* **1999,** *49*, 329-335.
43. Schulten, H.-R.; Leinweber, P. Characterization of Humic and Soil Particles by Analytical Pyrolysis and Computer Modeling. *J. Anal. Appl. Pyrolysis* **1996,** *38*, 1-53.
44. Basile, F.; Beverly, M.B.; Voorhees, K.J. Pathogenic Bacteria: Their Detection and

Differentiation by Rapid Lipid Profiling With Pyrolysis Mass Spectrometry. *Trends Anal. Chem.* **1998,** *17*, 95-109.
45. Badawy, S.M. Identification of Some Polymeric Materials by Low-Temperature Py-MS. *Eur. J. Mass Spectrom.* **2004,** *10*, 613-617.
46. Message, G.M. *Practical Aspects of Gas Chromatography/Mass Spectrometry*; Wiley: New York, 1984.
47. Hübschmann, H.-J. *Handbuch Der GC-MS – Grundlagen und Anwendungen*; Verlag Chemie: Weinheim, 1996.
48. Budde, W.L. *Analytical Mass Spectrometry*; ACS and Oxford Univ. Press: Wash., D.C. and Oxford, 2001.
49. Gohlke, R.S.; McLafferty, F.W. Early Gas Chromatography/Mass Spectrometry. *J. Am. Soc. Mass Spectrom.* **1993,** *4*, 367-371.
50. McFadden, W.H.; Schwartz, H.L.; Evans, S. Direct Analysis of Liquid Chromatographic Effluents. *J. Chromatogr.* **1976,** *122*, 389-396.
51. Karger, B.L.; Kirby, D.P.; Vouros, P.; Foltz, R.L.; Hidy, B. On-Line Reversed Phase Liquid Chromatography-Mass Spectrometry. *Anal. Chem.* **1979,** *51*, 2324-2328.
52. Millington, D.S.; Yorke, D.A.; Burns, P. A New Liquid Chromatography-Mass Spectrometry Interface. *Adv. Mass Spectrom.* **1980,** *8B*, 1819-1825.
53. Games, D.E.; Hirter, P.; Kuhnz, W.; Lewis, E.; Weerasinghe, N.C.A.; Westwood, S.A. Studies of Combined Liquid Chromatography-Mass Spectrometry With a Moving-Belt Interface. *J. Chromatogr.* **1981,** *203*, 131-138.
54. Liang, Z.; Hsu, C.S. Molecular Speciation of Saturates by Online Liquid Chromatography-Field Ionization Mass Spectrometry. *Energy Fuels* **1998,** *12*, 637-643.
55. Willoughby, R.C.; Browner, R.F. Monodisperse Aerosol Generation Interface for Combining LC With MS. *Anal. Chem.* **1984,** *56*, 2625-2631.
56. Winkler, P.C.; Perkins, D.D.; Williams, D.K.; Browner, R.F. Performance of an Improved Monodisperse Aerosol Generation Interface for LC-MS. *Anal. Chem.* **1988,** *60*, 489-493.
57. Brauers, F.; von Bünau, G. Mass Spectrometry of Solutions: a New Simple Interface for the Direct Introduction of Liquid Samples. *Int. J. Mass Spectrom. Ion Proc.* **1990,** *99*, 249-262.
58. Cappiello, A. Is Particle Beam an Up-to-Date LC-MS Interface? State of the Art and Perspectives. *Mass Spectrom. Rev.* **1997,** *15*, 283-296.
59. Cappiello, A.; Famiglini, G. Capillary-Scale Particle-Beam LC-MS Interface: Can Electron Ionization Sustain the Competition? *J. Am. Chem. Soc. Mass Spectrom.* **1998,** *9*, 993-1001.
60. Cappiello, A.; Famiglini, G.; Mangani, F.; Palma, P. A Simple Approach for Coupling Liquid Chromatography and EI-MS. *J. Am. Chem. Soc. Mass Spectrom.* **2002,** *13*, 265-273.
61. Cappiello, A.; Famiglini, G.; Palma, P.; Siviero, A. LC-EI-MS: Fields of Application and Evaluation of the Performance of a Direct-EI Interface. *Mass Spectrom. Rev.* **2005,** *24*, 978-989.
62. Ludányi, K.; Dallos, A.; Kühn, Z.; Vékey, D. Mass Spectrometry of Very Large Saturated Hydrocarbons. *J. Mass Spectrom.* **1999,** *34*, 264-267.
63. Remberg, G.; Remberg, E.; Spiteller-Friedmann, M.; Spiteller, G. Massenspektren Schwach Angeregter Moleküle. 4. Mitteilung. *Org. Mass Spectrom.* **1968,** *1*, 87-113.
64. Bowen, R.D.; Maccoll, A. Low-Energy, Low-Temperature Mass Spectra. I. Selected Derivatives of Octane. *Org. Mass Spectrom.* **1983,** *18*, 576-581.
65. Brophy, J.J.; Maccoll, A. Low-Energy, Low-Temperature Mass Spectra. 9. The Linear Undecanols. *Org. Mass Spectrom.* **1988,** *23*, 659-662.
66. Melaku, A.; Maccoll, A.; Bowen, R.D. Low-Energy, Low-Temperature MS. Part 17: Selected Aliphatic Amides. *Eur. Mass Spectrom.* **1997,** *3*, 197-208.
67. *Handbook of Derivates for Chromatography*; Blau, G.; King, G.S., eds.; Heyden: London, 1977.
68. Poole, C.F. Recent Advances in the Silylation of Organic Compounds for Gas Chromatography, in *Handbook of derivates for chromatography*; Blau, G.; King, G.S., editors; Heyden: London, 1977; Chap. 4, pp. 152-200.
69. Svendsen, J.S.; Sydnes, L.K.; Whist, J.E. MS Study of Dimethyl Esters of Trimethylsilyl Ether Derivatives of Some 3-Hydroxy Dicarboxylic Acids. *Org. Mass Spectrom.* **1987,** *22*, 421-429.

70. Svendsen, J.S.; Whist, J.E.; Sydnes, L.K. A MS Study of the Dimethyl Ester Trimethylsilyl Enol Ether Derivatives of Some 3-Oxodicarboxylic Acids. *Org. Mass Spectrom.* **1987,** *22*, 486-492.
71. Scribe, P.; Guezennec, J.; Dagaut, J.; Pepe, C.; Saliot, A. Identification of the Position and the Stereochemistry of the Double Bond in Monounsaturated Fatty Acid Methyl Esters by GC-MS of Dimethyl Disulfide Derivatives. *Anal. Chem.* **1988,** *60*, 928-931.
72. Pepe, C.; Sayer, H.; Dagaut, J.; Couffignal, R. Determination of Double Bond Positions in Triunsaturated Compounds by Means of GC-MS of Dimethyl Disulfide Derivatives. *Rapid Commun. Mass Spectrom.* **1997,** *11*, 919-921.
73. Abrahamsson, S.; Stenhagen, E.; McLafferty, F.W. *Atlas of Mass Spectral Data*; Wiley: New York, 1969; Vol. 1-3.
74. *Eight Peak Index of Mass Spectra;* 3rd ed.; Royal Society of Chemistry: London, 1983; Vol. 1-3.
75. McLafferty, F.W.; Stauffer, D.B. *The Wiley/NBS Registry of Mass Spectral Data;* 2nd ed.; Wiley: New York, 1989; Vol. 1-7.
76. McLafferty, F.W.; Gohlke, R.S. Mass-Spectrometric Analysis: Spectral-Data File Utilizing Machine Filing and Manual Searching. *Anal. Chem.* **1959,** *31*, 1160-1163.
77. Stein, S.E.; Ausloos, P.; Lias, S.G. Comparative Evaluations of Mass Spectral Databases. *J. Am. Soc. Mass Spectrom.* **1991,** *2*, 441-443.
78. McLafferty, F.W.; Stauffer, D.B.; Twiss-Brooks, A.B.; Loh, S.Y. An Enlarged Data Base of EI Mass Spectra. *J. Am. Soc. Mass Spectrom.* **1991,** *2*, 432-437.
79. McLafferty, F.W.; Stauffer, D.B.; Loh, S.Y. Comparative Evaluations of Mass Spectral Data Bases. *J. Am. Soc. Mass Spectrom.* **1991,** *2*, 438-440.
80. Henneberg, D.; Weimann, B.; Zalfen, U. Computer-Aided Interpretation of Mass Spectra Using Databases With Spectra and Structures. I. Structure Searches. *Org. Mass Spectrom.* **1993,** *28*, 198-206.
81. Zhu, D.; She, J.; Hong, Q.; Liu, R.; Lu, P.; Wang, L. ASES/MS: an Automatic Structure Elucidation System for Organic Compounds Using Mass Spectrometric Data. *Analyst* **1988,** *113*, 1261-1265.
82. Kwiatkowski, J.; Riepe, W. A Combined Forward-Reverse Library Search System for the Identification of Low-Resolution Mass Spectra. *Anal. Chim. Acta* **1979,** *112*, 219-231.
83. Stein, S.E.; Heller, D.N. On the Risk of False Positive Identification Using Multiple Ion Monitoring in Qualitative MS: Large-Scale Intercomparisons With a Comprehensive Mass Spectral Library. *J. Am. Chem. Soc. Mass Spectrom.* **2006,** *17*, 823-835.
84. Milman, B.L. Towards a Full Reference Library of MS^n Spectra. Testing of a Library Containing 3126 MS^2 Spectra of 1743 Compounds. *Rapid Commun. Mass Spectrom.* **2005,** *19*, 2833-2839.
85. Stein, S.; Scott, D.R. Optimization and Testing of Mass Spectral Library Search Algorithms for Compound Identification. *J. Am. Soc. Mass Spectrom.* **1994,** *5*, 859-866.
86. Stein, S.E. Estimating Probabilities of Correct Identification From Results of Mass Spectral Library Searches. *J. Am. Soc. Mass Spectrom.* **1994,** *5*, 316-323.
87. Lebedev, K.S.; Cabrol-Bass, D. New Computer Aided Methods for Revealing Structural Features of Unknown Compounds Using Low Resolution Mass Spectra. *J. Chem. Inf. Comput. Sci.* **1998,** *38*, 410-419.
88. Halket, J.M.; Waterman, D.; Przyborowska, A.M.; Patel, R.K.P.; Fraser, P.D.; Bramley, P.M. Chemical Derivatization and MS Libraries in Metabolic Profiling by GC/MS and LC/MS/MS. *J. Exp. Bot.* **2005,** *56*, 219-243.

6 Fragmentation of Organic Ions and Interpretation of EI Mass Spectra

Learning Objectives

- Fragmentation reactions of organic ions
- Competing fragmentation pathways
- Bond cleavages of radical ions
- Bond cleavages of non-radical ions
- Rearrangement fragmentations
- Fragmentation reactions of important compound classes
- Characteristic ions and typical neutral losses
- Distonic ions and ion-neutral complexes
- Extracting structural information from mass spectra – tools and rules
- Interpreting mass spectra – systematic approaches

The following chapter introduces one of the key disciplines of organic mass spectrometry: the common fragmentation pathways of organic ions and the resulting methodology for the interpretation of *electron ionization* (EI) mass spectra. As a single chapter cannot be comprehensive, some other resources for further reading may be desirable [1,2,3]. There is also a dedicated monograph on applications of mass spectrometry to organic stereochemistry [4]. And of course, a vast number of original publications is dealing with classes of compounds or fragmentation pathways: these should be consulted to solve a particular problem.

Intended as a systematic introduction to the topic this chapter emphasizes the most important fragmentation pathways rather than dwelling on countless compounds. Basic skills are provided as a guideline for further "learning by doing". Throughout the chapter we will keep an eye on the relationships between fragmentation patterns and gas phase ion chemistry. As a prerequisite for successfully working through these pages, some knowledge is needed on the general concept of mass spectrometry (Chap. 1) and of the basics of electron ionization (Chap. 5). In addition, you should be familiar with the fundamentals of gas phase ion chemistry (Chap. 2) as well as with isotopic mass and isotopic distributions (Chap. 3).

Note: Although the discussion of common fragmentation pathways of organic ions is embedded here in the context of EI mass spectrometry, their occurrence is not restricted to this technique. The reactions of isolated gaseous ions do not directly depend on the ionization method, but are almost exclusively governed by intrinsic properties of the respective ion and by its internal energy (Chap. 2).

J. Gross, *Mass Spectrometry*, 2nd ed., DOI 10.1007/978-3-642-10711-5_6,
© Springer-Verlag Berlin Heidelberg 2011

6.1 Cleavage of a Sigma-Bond

6.1.1 Writing Conventions for Molecular Ions

Electron ionization mainly creates singly charged positive ions by ejection of one electron out of the neutral. If the precursor was a molecule, M, it will have an even number of electrons, i.e., be an *even-electron ion* (or *closed-shell ion*). The molecular ion formed upon EI must then be a positive *radical ion*, $M^{+\bullet}$, i.e., an *odd-electron ion* (or *open-shell ion*).

Definition: The *molecular ion* has the same formula as the corresponding neutral molecule. The neutral and its molecular ion only differ by one (or more) electron(s). A singly charged molecular ion can either be a positive radical ion, $M^{+\bullet}$, or a negative radical ion, $M^{-\bullet}$ (not in the case of EI). The nominal mass of this ion corresponds to the sum of the masses of the most abundant isotopes of the various atoms that make up the molecule [5,6].

Table 6.1. Symbolism for charge and radical states

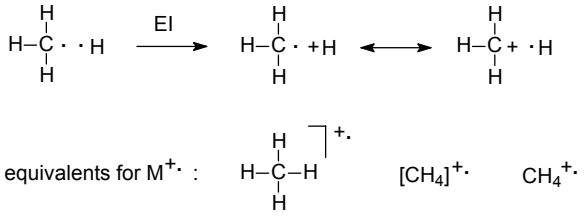
State of species	Symbol	Examples
Even-electron ion	+, –	CH_3^+, NH_4^+, EtO^-, CF_3^-
Odd-electron ion	+•, –•	$CH_4^{+\bullet}$, $C_{60}^{+\bullet}$, $C_{60}^{-\bullet}$, $CCl_4^{-\bullet}$
Radical, no charge	•	$CH_3^\bullet$, $OH^\bullet$, $H^\bullet$, $Br^\bullet$

Note: The symbol $M^{+\bullet}$ does *not mean one added electron*. The radical ($^\bullet$) symbol is added to the molecular ion only to *indicate the remaining unpaired* electron after ionization. Addition of one electron (electron capture) to a neutral would make it a negative radical ion, $M^{-\bullet}$.

When initially formulating the ionization process, one did not consider where the charge would reside (Chap. 2.2.1), e.g., for methane we wrote:

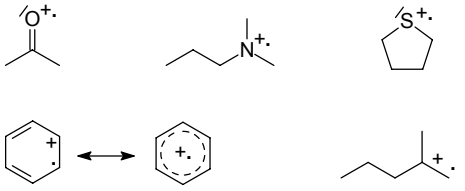
$$CH_4 + e^- \rightarrow CH_4^{+\bullet} + 2e^- \qquad (6.1)$$

The tremendous changes in electronic structure and bonding that arise with the loss of an electron are by far better depicted by a formula representation including the σ-bonding electrons of the C–H bond. In small nonfunctionalized molecules such as methane, it is not possible to avoid the loss of a valence electron from a σ-bond upon electron ionization. The same is true for all other saturated hydrocarbons or a hydrogen molecule, for example. The resulting methane molecular ion may *formally* be represented either as a species resembling a combination of a methyl cation plus a hydrogen radical or a methyl radical plus a proton. Nevertheless, one may still assume that it resembles more the intact molecule than the evolving fragments – a statement being also in accordance with the basic assumptions of the QET (Chap. 2.1). Otherwise, fragmentation would proceed almost spontaneously, thereby excluding the detection of the molecular ion.



Scheme 6.1.

Lone pairs or π-orbitals are the preferred sites of a molecule to deliver an electron. The ease of doing so is directly reflected by their effect on ionization energy (Chap. 2.2.2) [7]. Therefore, it is common practice to write the charge of a molecular ion as if localized at the position of lowest ionization energy. This is of course not in full agreement with the real charge distributions in ions, but it has been established as a useful first step when writing down a fragmentation scheme. Appropriate formula representations of molecular ions of acetone, *N,N*-dimethylpropylamine, tetrahydrothiophene, benzene, and 2-methyl-1-pentene are:



Scheme 6.2.

6.1.2 σ-Bond Cleavage in Small Nonfunctionalized Molecules

The most intense peaks in the EI mass spectrum of methane are the molecular ion at *m/z* 16 and the fragment ion at *m/z* 15 (Fig. 6.1). Explicitly writing the electrons helps to understand the subsequent dissociations of $CH_4^{+\bullet}$ to yield CH_3^+, *m/z* 15, by $H^\bullet$ loss (σ_1) or H^+ by $CH_3^\bullet$ loss (σ_2), respectively. In general, it is more convenient to write the molecular ion in one of the equivalent forms. The charge and radical state are then attached to the brackets (often abbreviated as ⌉) enclosing the molecule. (It is advised to review the rules of Chap. 1 for terminology in the description of mass spectra).

The CH_3^+ fragment ion can also be seen in its relation to the molecular ion, i.e., it may be described as an $[M–H]^+$ ion. Accordingly, the proton could be written as $[M–CH_3]^+$. The $[M–H_2]^{+\bullet}$ ion at *m/z* 14, i.e., carbene molecular ion in this case, results from a rearrangement fragmentation (*rd*). Rearrangements are discussed later in this chapter.

The σ-bond cleavage represents a simple but very common type of fragmentation. Its occurrence does neither require particular functional groups nor heteroa-

toms in a molecular ion. The σ-bond cleavage proceeds via a loose transition state and therefore can become very rapid, provided that ions have sufficient internal energy (Chap. 2.6.4). Even if additional and perhaps energetically more favorable fragmentation pathways prevail, σ-bond cleavages will not vanish completely.

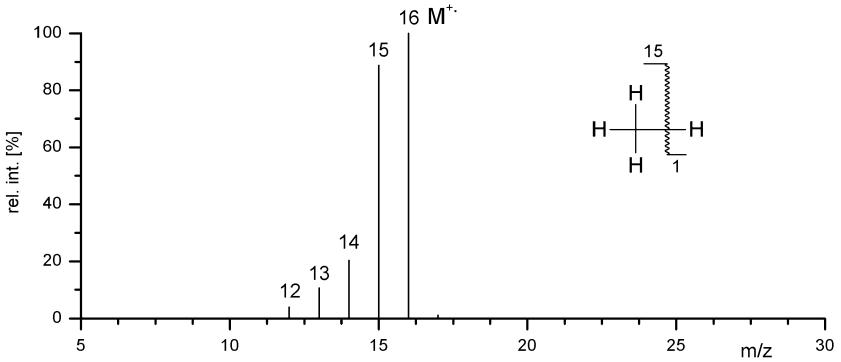
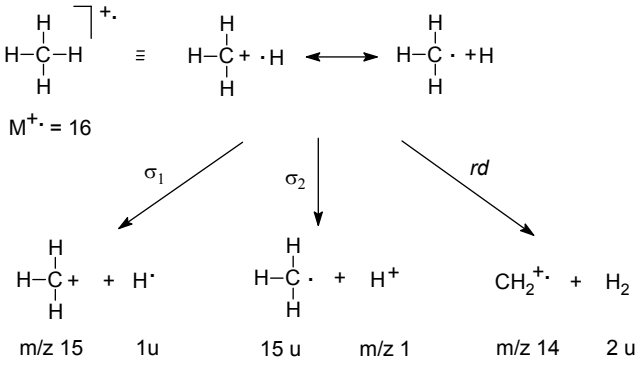


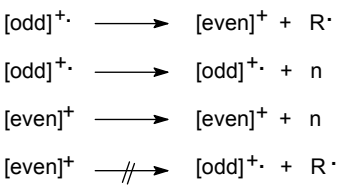
Fig. 6.1. EI mass spectrum of methane. Used by permission of NIST. © NIST 2002.



Scheme 6.3.

6.1.3 Even-Electron Rule

The *dissociation* or *fragmentation* of ions – as it is usually referred to in mass spectrometry – yields a fragment ion and a neutral. Depending on whether the fragmenting ion is an even-electron or an odd-electron species, certain fragmentation pathways may be allowed or forbidden. This has been generalized in the *even-electron rule* [8]. It serves as a reliable guideline rather than a strict rule for the fragmentation of ions, and thus for the interpretation of mass spectra. The even-electron rule can be summarized in the following scheme:



Scheme 6.4.

Even-electron rule: Odd-electron ions (such as molecular ions and fragment ions formed by rearrangements) may eliminate either a radical or an even-electron neutral species, but even-electron ions (such as protonated molecules or fragments formed by a single bond cleavage) will not usually lose a radical to form an odd-electron cation. In other words, the successive loss of radicals is forbidden [9].

Example: According to the even-electron rule the molecular ion of methane should undergo the following dissociations:

$$CH_4^{+\bullet} \rightarrow CH_3^+ + H^\bullet \quad (6.2)$$

$$CH_4^{+\bullet} \rightarrow CH_2^{+\bullet} + H_2 \quad (6.3)$$

Despite that it might initially be generated in a different electronic state and/or conformation, the $CH_2^{+\bullet}$ fragment ion can be expected to decompose further in a way identical to the molecular ion of carbene:

$$CH_2^{+\bullet} \rightarrow C^{+\bullet} + H_2 \quad (6.4)$$

$$CH_2^{+\bullet} \rightarrow CH^+ + H^\bullet \quad (6.5)$$

Loss of a radical from a radical ion creates an even-electron fragment ion, CH_3^+ in this case, which preferably may undergo subsequent loss of a molecule:

$$CH_3^+ \rightarrow CH^+ + H_2 \quad (6.6)$$

Loss of $H^\bullet$ from CH_3^+ should not occur. It is noteworthy that even such a simple fragmentation scheme offers two independent pathways for the generation of CH^+ (Eqs. 6.5 and 6.6).

Note: It is important to assign the correct charge and radical state to all species encountered and to carefully track them through a fragmentation scheme. Otherwise, "impossible" fragmentation pathways may be formulated, thereby misleading the assignment of elemental composition and molecular constitution.

Numerous exceptions of the even-electron rule have been described [9-11]. Violations tend to occur where the loss of a radical from an even-electron ion leads to the formation of an exceptionally stable ionic species or where highly excited ions are involved. Representatives of highly excited ions are small molecular ions,

ions having only a few degrees of freedom to randomize internal energy [10] or ions being subject to collision-induced dissociation (Chap. 9) [11,12].

Hint: In chemistry, there usually is no strict "either ... or" – instead the ions behave like "more ... than ...".

6.1.4 σ-Bond Cleavage in Small Functionalized Molecules

The introduction of a charge-localizing heteroatom into a molecule is accompanied by obvious changes in the appearance of the mass spectrum. Withdrawal of an electron upon EI does not necessarily affect a σ-bond, because the lone pairs of the heteroatom may now deliver an electron for ejection.

In the EI mass spectrum of iodomethane the molecular ion, $CH_3–I^{+\bullet}$, is detected as the base peak at *m/z* 142 (Fig. 6.2). An important new feature of the spectrum is the peak at *m/z* 127 due to an $[M–CH_3]^+$ ion. This signal is due to I^+ also formed by a process that can also be classified as σ-bond cleavage. Here, a single electron

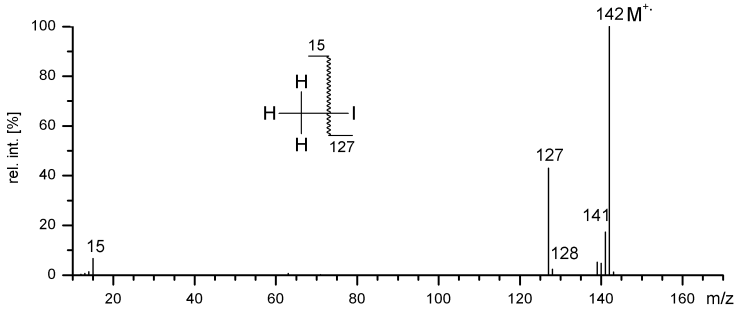
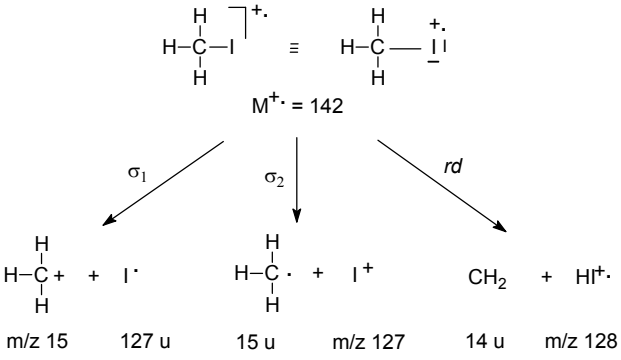


Fig. 6.2. EI mass spectrum of iodomethane. The molecular ion mainly decomposes to yield ionic fragments representing its major constituent groups, i.e., I^+, *m/z* 127 and CH_3^+, *m/z* 15. Spectrum used by permission of NIST. © NIST 2002.



Scheme 6.5.

shifts from the intact C–I bond to the radical site, thereby rupturing the bond. The peak is accompanied by a much less intense one at *m/z* 128 resulting from $HI^{+\bullet}$ by rearrangement. (The peak at *m/z* 128 should not be interpreted as an isotopic peak of *m/z* 127, because iodine is monoisotopic!) The remaining peaks can be explained as we already did for methane, i.e., peaks can be assigned as $[M–H]^+$, *m/z* 141, $[M–H_2]^{+\bullet}$, *m/z* 140, and $[M–H–H_2]^+$, *m/z* 139. Analogous to $H^\bullet$ loss, $I^\bullet$ loss also occurs generating the CH_3^+ ion, *m/z* 15.

Note: Halogenated compounds typically reveal the positive halogen ion and a less intense peak due to the hydrogen halogenide. In accordance with the incrementing electronegativities of the halogens their intensities follow the order $F^+ < Cl^+ < Br^+ < I^+$. In case of Br and Cl the isotopic patterns give additional evidence for their presence (Chap. 6.2.6) [13].

6.2 Alpha-Cleavage

6.2.1 α-Cleavage of Acetone Molecular Ion

The EI mass spectrum of acetone is rather simple: it shows three important peaks at *m/z* 58, 43, and 15. According to the formula C_3H_6O, the peak at *m/z* 58 corresponds to the molecular ion. The base peak at *m/z* 43 is related to this signal by a difference of 15 u, a neutral loss that can almost certainly be assigned to loss of a methyl radical, $CH_3^\bullet$. The peak at *m/z* 15 may then be expected to correspond to the ionic counterpart of the methyl radical, i.e., to the CH_3^+ carbenium ion (Fig. 6.3). In order to rationalize this mass spectrum in terms of ion chemistry, we consider the steps of electron ionization and subsequent fragmentation in detail.

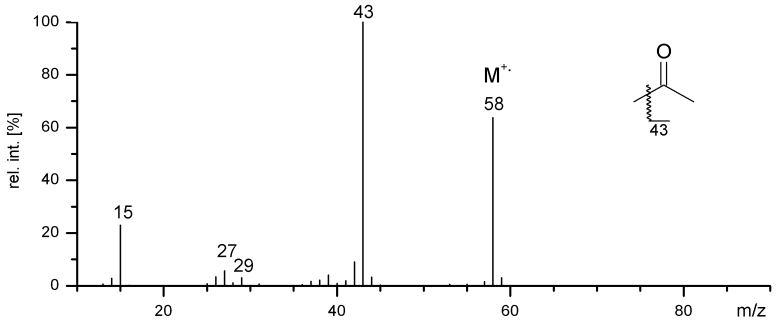
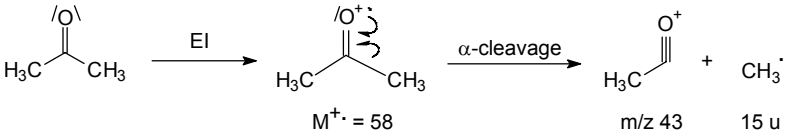


Fig. 6.3. EI mass spectrum of acetone. Used by permission of NIST. © NIST 2002.

The acetone molecule has two lone pairs at the oxygen that will at least formally be the preferred ones to remove an electron (Chap. 2.2.2). The excited molecular ion may then cleave off a methyl radical by simply shifting *one electron* (single-barbed arrow or "fishhook") from the CO–CH_3 bond to the radical site at

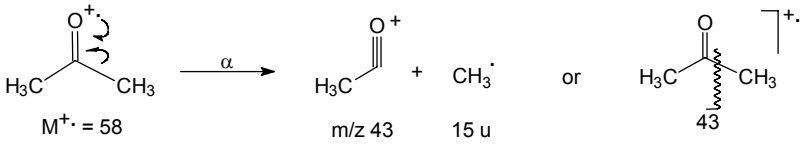
the oxygen atom allowing the products to drift apart (Scheme 6.6). This homolytic bond cleavage is a *radical-site initiated* process with *charge retention*, i.e., the ionic charge resides within the moiety where it was initially located. The process is also known as *α-cleavage*. The neutral fragment, $CH_3^{\bullet}$, is not detected by the mass spectrometer, while the charged fragment, $C_2H_3O^+$, leads to the base peak *m/z* 43:



Scheme 6.6.

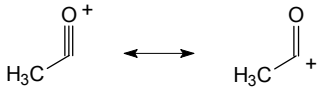
Note: The term *α-cleavage* for this widespread *radical-site initiated process* with *charge retention* can be misleading, because the bond cleaved is not directly attached to the radical site, but to the next neighboring atom.

Including the ionization process, the lone pairs, and single-barbed arrows for each moving electron in the scheme is not necessary but presents a valuable aid. Alternatively, the α-cleavage may be indicated in a simplified manner:



Scheme 6.7.

The first abbreviated form only shows the according electron shift, but it still explicitly gives the structures of the products. The second is useful to indicate which bond will be cleaved and what *m/z* the ionic product will have. Such a writing convention can of course be used for any other fragmentation pathway. The ionic product of the α-cleavage, an *acylium ion*, will not exactly have the angular structure as shown, however drawing it this way helps to identify the fragment as a part of the initial molecular ion. The charge in acylium ions can be substantially resonance-stabilized:



Scheme 6.8.

6.2.2 Stevenson's Rule

The origin of the peak at *m/z* 43 in the EI mass spectrum of acetone should be quite clear now and we may examine the formation of the CH_3^+ ion, *m/z* 15, next. In principle, the ionic charge may reside on either fragment, the acyclium or the alkyl. In case of acetone, the formation of the acylium ion, CH_3CO^+, *m/z* 43, is preferred over the formation of the small carbenium ion, CH_3^+, *m/z* 15. The question which of the two incipient fragments will preferably retain the charge can be answered by means of Stevenson's Rule.

Stevenson's rule: When a fragmentation takes place, the positive charge remains on the fragment with the lowest ionization energy.

This criterion was originally established for the fragmentation of alkanes by Stevenson [14] and was later demonstrated to be generally valid [15,16]. The rule can be rationalized on the basis of ion thermochemical considerations (Fig. 6.4). Assuming no reverse activation barrier, the difference in thermodynamic stability as expressed in terms of the difference of heats of formation of the respective products determines the preferred dissociation pathway:

$$\Delta H_{f(B+;A\bullet)} - \Delta H_{f(A+;B\bullet)} = \Delta\Delta H_{f(Prod)} = \Delta E_0 \qquad (6.7)$$

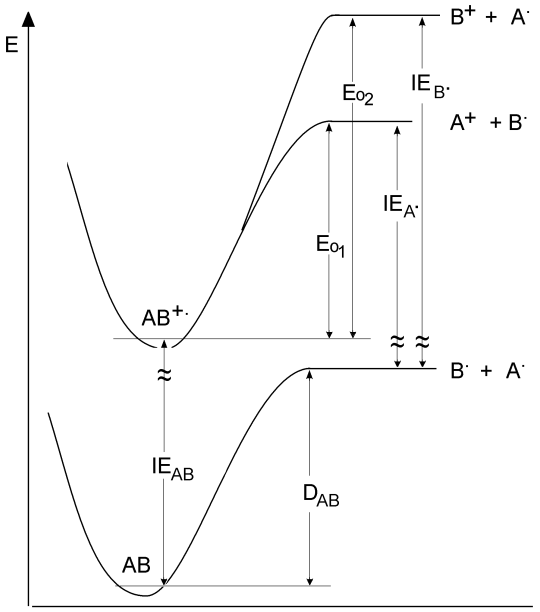


Fig. 6.4. Thermochemical description of Stevenson's rule (D_{AB} homolytic bond dissociation energy of bond A–B, *IE* ionization energy).

This can also be expressed in relation to the ionization energies of the radicals formed by both dissociations:

$$\Delta E_0 = IE_{B\bullet} - IE_{A\bullet} = E_{02} - E_{01} \tag{6.8}$$

Therefore, the radical having the lower ionization energy will dominate among the products [15,17]. For example, in case of the α-cleavage of acetone, $CH_3C^{\bullet}=O$ has a by 2.8 eV lower *IE* than $^{\bullet}CH_3$ (Table 6.2). As ion internal energies are subject to a wide distribution, there is a substantial fraction of ions that may also dissociate to form the energetically more demanding pair of fragments. This is the reason for the "soft" character of the rule.

Note: The homolytic dissociation of a bond generally proceeds to yield both product pairs, their relative abundances being basically governed by Stevenson's rule.

Without the thermochemical data, it is not easy to decide which pair of products will be preferred over the other. In general, the formation of the higher substituted and/or larger carbenium ion is preferred, because it can more easily stabilize a charge. However, the tendency is the same for the radicals and one may expect loss of ethyl to be favored over loss of methyl, for example. Thus, the formation of both the ionic and the radical fragments are of critical importance for the final distribution of products.

Table 6.2. Ionization energies of some radicals[a]

Radical	IE[b] [eV]	Radical	IE[b] [eV]
$H^{\bullet}$	13.6	$CH_3O^{\bullet}$	10.7
$^{\bullet}CH_3$	9.8	$^{\bullet}CH_2OH$	7.6
$^{\bullet}C_2H_5$	8.4	$CH_3C^{\bullet}=O$	7.0
n-$^{\bullet}C_3H_7$	8.2	$C_2H_5C^{\bullet}=O$	5.7
i-$^{\bullet}C_3H_7$	7.6	$^{\bullet}CH_2Cl$	8.8
n-$^{\bullet}C_4H_9$	8.0	$^{\bullet}CCl_3$	8.1
i-$^{\bullet}C_4H_9$	7.9	$C_6H_5^{\bullet}$	8.3
s-$^{\bullet}C_4H_9$	7.3	$C_6H_5CH_2^{\bullet}$	7.2
t-$^{\bullet}C_4H_9$	6.8	$^{\bullet}CH_2NH_2$	6.3

[a] IE data extracted from Ref. [18] with permission © NIST 2002
[b] all values rounded to one decimal

Note: The validity of Stevenson's rule requires no reverse activation energy barrier to exist for the fragmentation pathway. This requirement is usually fulfilled for simple bond cleavages, but not in case of rearrangement fragmentations.

6.2.3 α-Cleavage of Nonsymmetrical Aliphatic Ketones

When a ketone grows larger it does not necessarily imply that it has two identical alkyl groups at the carbonyl. In case of different alkyl groups, Stevenson's rule may help to decide which of them will mainly be detected as part of the acylium ion and which should preferably appear as carbenium ion. Overall, a nonsymmetrical ketone will yield four primary fragment ions in its EI mass spectrum.

The competing process of carbenium ion formation occurs as a companion of the α-cleavage and may be understood either as *charge site-induced cleavage* (also termed *inductive cleavage*, symbol *i*) or as σ-cleavage. In Scheme 6.9 the charge site-induced mechanism was chosen where the bonding electron pair is retained at the carbonyl fragment to yield an acyl radical and a carbenium ion. If the initial charge was directly assigned to the corresponding σ-bond, the very same products would also result from σ-cleavage.

Example: At *m/z* 43, the EI mass spectrum of butanone shows a fragment due to ethyl loss from the molecular ion, which is largely preferred over methyl loss leading to a minor peak at *m/z* 57 (Fig. 6.5). Furthermore, the $C_2H_5^+$ ion, *m/z* 29, is more abundant than the less stable CH_3^+ ion, *m/z* 15. If the alkyls become larger than ethyl, an additional dissociation pathway will occur (Chap. 6.7).

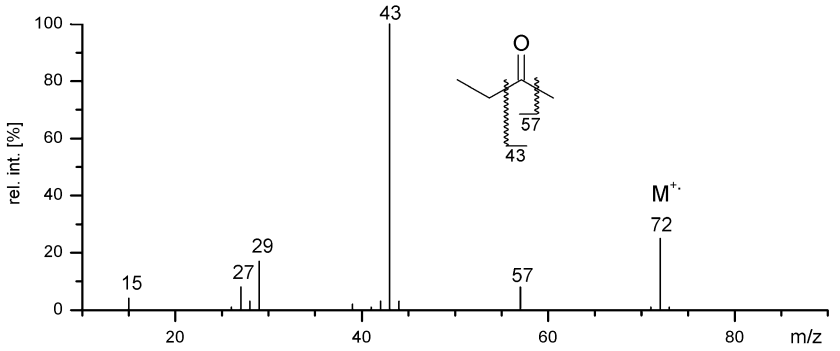
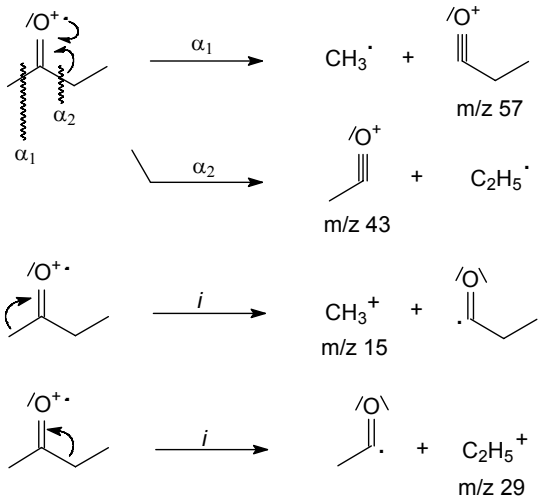


Fig. 6.5. EI mass spectrum of butanone. Used by permission of NIST. © NIST 2002.

In contrast to ketones [19] α-cleavage is less important as primary fragmentation for aliphatic aldehyde molecular ions [20,21]. This is because α-cleavage of aldehyde molecular ions forms energetically unfavorable products, i.e., by loss of $H^{\bullet}$ or formation of the formyl ion, CHO^+, *m/z* 29. It was demonstrated by high-resolution mass spectrometry (Chap. 3.3) that only a fraction of the peak at *m/z* 29 originates from CHO^+ ions, while the majority is due to $C_2H_5^+$ ions from σ-cleavage or charge site-induced cleavage, respectively [22].

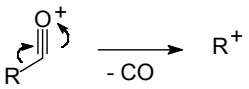


Scheme 6.9.

6.2.4 Acylium Ions and Carbenium Ions

For larger ketones one can also expect larger acylium and alkyl fragments to occur. Such *series of homologous ions* are useful for deducing structural information from mass spectra. Ions such as those from the acylium ion series and the carbenium ion series are also known as *characteristic ions*. It is advisable to learn the nominal masses of the first members of each series by heart (Tables 6.3 and 6.4).

Besides having different accurate mass, carbenium ions and acylium ions fortunately exhibit different dissociation pathways allowing their differentiation from the appearance of a mass spectrum. Acylium ions undergo charge-induced CO loss (–28 u), thereby forming carbenium ions, but they do not eliminate hydrogen molecules:



Scheme 6.10.

Example: The dissociation $CH_3CO^+ \rightarrow CH_3^+ + CO$ presents a second pathway for the generation of the peak at *m/z* 15 in the mass spectra of acetone (Fig. 6.3) and butanone (Fig. 6.5), and accordingly the process $CH_3CH_2CO^+ \rightarrow C_2H_5^+ + CO$ also causes a peak at *m/z* 29. Thus, this pathway competes with the one-step formation of carbenium ions from ketone molecular ions by charge migration.

Table 6.3. Carbenium ions

m/z (1 + 14*n*)	Carbenium ions $[C_nH_{2n+1}]^+$	Accurate mass [u][a]
15	CH_3^+	15.0229
29	$C_2H_5^+$	29.0386
43	*n*-$C_3H_7^+$, *i*-$C_3H_7^+$	43.0542
57	*n*-$C_4H_9^+$, *i*-$C_4H_9^+$, *sec*-$C_4H_9^+$, *tert*-$C_4H_9^+$	57.0699
71	$C_5H_{11}^+$ isomers	71.0855
85	$C_6H_{13}^+$ isomers	85.1011
99	$C_7H_{15}^+$ isomers	99.1168
113	$C_8H_{17}^+$ isomers	113.1325

[a] values rounded to four decimals

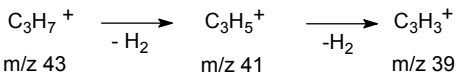
Table 6.4. Acylium ions

m/z (15 + 14*n*)	Acylium ions $[C_nH_{2n-1}O]^+$	Accurate mass [u][a]
29	HCO^+	29.0022
43	CH_3CO^+	43.0178
57	$C_2H_5CO^+$	57.0335
71	$C_3H_7CO^+$	71.0491
85	$C_4H_9CO^+$	85.0648
99	$C_5H_{11}CO^+$ isomers	99.0804
113	$C_6H_{13}CO^+$ isomers	113.0961
127	$C_7H_{15}CO^+$ isomers	127.1117

[a] values rounded to four decimals

Note: The acylium ions and the saturated carbenium ions are isobars, i.e., they have the same nominal mass. However, their exact masses are different, i.e., CH_3CO^+, *m/z* 43.0178, and $C_3H_7^+$, *m/z* 43.0542.

Carbenium ions, especially from ethyl to butyl show remarkable dehydrogenation that gives rise to a characteristic accompanying pattern of peaks at *m/z*–2 and *m/z*–4, i.e., at the low-mass side of the corresponding peak:



Scheme 6.11.

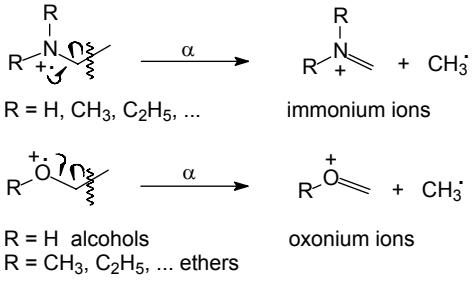
Example: The mass spectra of both acetone and butanone show typical acylium ion peaks at *m/z* 43, whereas the signals in the spectra of isopropyl ethyl thioether (Fig. 6.9), of 1-bromo-octane, (Fig. 6.10), and of isomeric decanes

(Fig. 6.18) may serve as examples for carbenium ion signals. The superimposition of both classes of ions causes signals representing an average pattern. The properties of larger carbenium ions are discussed in the section on alkanes (Chaps. 6.6.1 and 6.6.3).

6.2.5 α-Cleavage When Heteroatoms Belong to the Aliphatic Chain

The charge-localizing heteroatom can also be part of the aliphatic chain as it is the case with amines, ethers, and alcohols. The mechanism of the α-cleavage remains unaffected by this change, i.e., still the bond second to the charge site is cleaved. Nevertheless, the structure of the charged fragments is quite changed, and consequently their further fragmentation pathways are also different.

In case of amine molecular ions the α-cleavage is clearly the dominating primary fragmentation pathway. The strong charge-stabilizing properties of the nitrogen atom keeps the fraction of charge migration fragments very low. The product ions are termed *immonium ions* (also *iminium ions)*, because these can formally be obtained by electrophilic addition of a proton or carbenium ion to imines. Immonium ions represent the most stable $[C_nH_{2n+2}N]^+$ isomers [23] and preferably undergo further decomposition on two widespread and thus highly important pathways for alkene loss [24,25] (Chap. 6.11). *Oxonium ions* are the oxygen analogs of immonium ions. As oxygen is somewhat less charge-stabilizing than nitrogen, the competing formation of carbenium ions is more pronounced among the primary fragmentations of aliphatic ethers [26,27] and alcohols [28], but still the α-cleavage represents the favored dissociation.



Scheme 6.12.

6.2.6 α-Cleavage of Aliphatic Amines

The intensity of the molecular ion of aliphatic amines decreases with increasing molecular weight [29], the reason being their predisposition to α-cleavage. Analogous tendencies are observed for aliphatic ethers [27], hydrocarbons [30], aldehydes [20], and others.

A comparison of the relative strength of functional groups to cause α-cleavage is summarized in Table 6.5 [31]. This also corresponds to a rough measure of relative charge-stabilizing capability of the respective substituent, e.g., the ratio $H_2C{=}OH^+/H_2C{=}NH_2^+$ from 2-amino ethanol molecular ion is 2.3/100 and the ratio of $H_2C{=}OH^+/H_2C{=}SH^+$ from 2-thio ethanol molecular ion is 42/70 [16].

The mass spectrum of *N*-ethyl-*N*-methyl-propanamine, $C_6H_{15}N$, shows the molecular ion peak at *m/z* 101 (Fig. 6.6). The primary fragmentations of the molecular ion are explained in terms of the α-cleavage and accordingly, the peaks at *m/z* 72 and 86 can be assigned as immonium fragment ions due to ethyl and methyl loss, respectively. There are three other pathways for α-cleavage! In order to identify those missing pathways, we have to write down the fragmentation scheme carefully checking every possibility. And of course, we have to examine the mass spectrum with sufficient care in order not to overlook an indicative peak.

Table 6.5. Relative potential of functional groups to cause α-cleavage; from Ref. [31] with permission. © Georg Thieme Verlag, 2002.

Functional group	Relative value
–COOH	1
–Cl, –OH	8
–Br	13
–COOMe	20
–CO– (ketones)	43
–OMe	100
–I , –SMe	≈ 110
$-NHCOCH_3$	128
$-NH_2$	990
acetals	1600
$-NMe_2$	2100

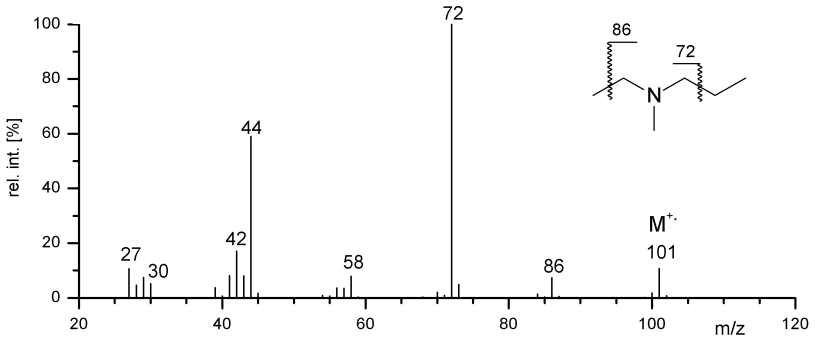
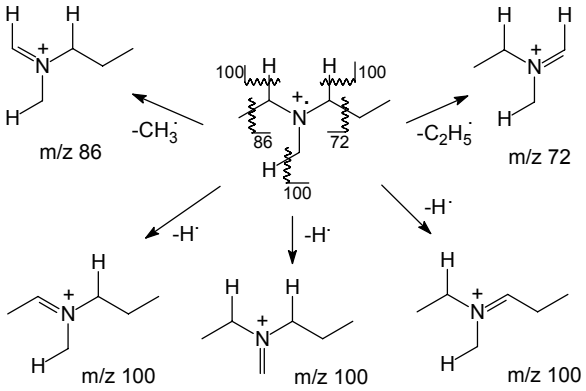


Fig. 6.6. EI mass spectrum of *N*-ethyl-*N*-methyl-propanamine. The molecular ion is detected at odd *m/z*, whereas the immonium fragment ions all have even *m/z* values. Spectrum used by permission of NIST. © NIST 2002.



Scheme 6.13.

The peak at *m/z* 100 corresponds to $H^{\bullet}$ loss and is also due to α-cleavage as can be easily recognized from Scheme 6.13. Three different positions to cleave off a $H^{\bullet}$ as one of seven almost equivalent hydrogens are available. Despite these options, the peak at *m/z* 100 is still weak, the reason for this being the unfavorable thermodynamics of $H^{\bullet}$ loss as compared to methyl loss (Table 2.2).

As with acylium ions and carbenium ions before, the series of homologous immonium ions is part of the mass spectrometrist's tool box. They can easily be recognized in the mass spectra and have even-numbered *m/z* values (Table 6.6). In the EI spectrum of *N*-ethyl-*N*-methyl-propanamine the series is completely present from *m/z* 30 up to *m/z* 100.

Table 6.6. Aliphatic immonium ions

m/z (16 + 14*n*)	Immonium ions $[C_nH_{2n+2}N]^+$	Accurate mass [u][a]
30	CH_4N^+	30.0338
44	$C_2H_6N^+$	44.0495
58	$C_3H_8N^+$	58.0651
72	$C_4H_{10}N^+$	72.0808
86	$C_5H_{12}N^+$	86.0964
100	$C_6H_{14}N^+$	100.1120
114	$C_7H_{16}N^+$	114.1277
128	$C_8H_{18}N^+$	128.1434

[a] values rounded to four decimals

Note: In the EI mass spectra of primary amines the methylene immonium ion, $CH_2{=}NH^+$, *m/z* 30, resulting from α-cleavage either represents the base peak or at least is the by far most abundant of the immonium ion series.

Even though α-cleavage seems to be a purely electronic process at first sight, the influence of ion internal energy and of the alkyl chain should not be neglected.

Whereas $CH_2{=}NH^+$, *m/z* 30, is the predominating ionic product of fragmentations of highly excited primary amine molecular ions within the ion source, the metastable decompositions of such molecular ions yield $CH_3CH^+NH_2$ ($CH_3CH{=}NH_2^+$), *m/z* 44, and $CH_3CH_2CH^+NH_2$ ($CH_3CH_2H{=}NH_2^+$) *m/z* 58. This has been attributed to isomerization via $H^\bullet$ shifts prior to dissociation [32].

6.2.7 Nitrogen Rule

When we restrict our selection to common elements in organic mass spectrometry (H, B, C, N, O, Si, S, P, F, Cl, Br, I, etc.) all but one of these elements having an odd number of valences also possess an odd mass number and those having an even number of valences also have even mass numbers. Nitrogen represents this only exception, which gives rise to the so-called *nitrogen rule* (Table 6.7).

Nitrogen rule: If a compound contains an even number of nitrogen atoms (0, 2, 4, ...), its monoisotopic molecular ion will be detected at an even-numbered nominal *m/z* value. Vice versa, an odd number of nitrogens (1, 3, 5, ...) is indicated by an odd-numbered nominal *m/z*.

Table 6.7. Examples illustrating the nitrogen rule

Number of nitrogens	Examples	$M^{+\bullet}$ at *m/z*
0	methane, CH_4	16
0	acetone, C_3H_6O	58
0	chloroform, $CHCl_3$	118
0	[60]fullerene, C_{60}	720
1	ammonia, NH_3	17
1	acetonitrile, C_2H_3N	41
1	pyridine, C_5H_5N	79
1	*N*-ethyl-*N*-methyl-propanamine, $C_6H_{15}N$	101
2	urea, CH_4N_2O	60
2	pyridazine, $C_4H_4N_2$	80
3	triazole, $C_2H_3N_3$	69
3	hexamethylphosphoric triamide, HMPTA, $C_6H_{18}N_3OP$	179

The rule may also be extended for use with fragment ions. This makes a practical tool to distinguish even-electron from odd-electron fragment ions and thus simple bond cleavages from rearrangements. However, some additional care has to be taken when applying the extended rule, because nitrogen might also be contained in the neutral, e.g., loss of NH_3, 17 u, or of $CONH_2^\bullet$, 44 u.

Rule: Cleaving off a radical (that contains no nitrogen) from any ion changes the nominal *m/z* value from odd to even or vice versa. Loss of a molecule (that contains no nitrogen) from an ion produces even nominal mass fragments from even mass ions and odd mass fragments from odd mass ions.

Example: To rationalize the mass spectrum of methane, reactions 6.2–6.6 were proposed. They all obey the rule. Just check the mass spectra and fragmentation schemes throughout this chapter for additional examples of the nitrogen rule:

$$CH_4^{+\bullet} \rightarrow CH_3^+ + H^\bullet;\ m/z\ 16 \rightarrow m/z\ 15 \tag{6.2}$$

$$CH_4^{+\bullet} \rightarrow CH_2^{+\bullet} + H_2;\ m/z\ 16 \rightarrow m/z\ 14 \tag{6.3}$$

$$CH_2^{+\bullet} \rightarrow C^{+\bullet} + H_2;\ m/z\ 14 \rightarrow m/z\ 12 \tag{6.4}$$

$$CH_2^{+\bullet} \rightarrow CH^+ + H^\bullet;\ m/z\ 14 \rightarrow m/z\ 13 \tag{6.5}$$

$$CH_3^+ \rightarrow CH^+ + H_2;\ m/z\ 15 \rightarrow m/z\ 13 \tag{6.6}$$

6.2.8 α-Cleavage of Aliphatic Ethers and Alcohols

The molecular ions of aliphatic ethers do not behave much different from those of amines [26,27]. However, oxygen is not directing their primary dissociations as strongly to the α-cleavage as nitrogen does in amines. Although α-cleavage is still dominant, there is a stronger tendency towards formation of carbenium ion fragments by charge migration. As can be expected, the structure of the alkyls also exerts a significant influence on the selection of a cleavage pathway.

Example: The 70-eV EI mass spectra of two aliphatic ethers are shown below (Fig. 6.7). Although being isomers, their spectra are clearly different. In case of methyl propyl ether, α-cleavage can occur by $H^\bullet$ loss, *m/z* 73, and preferably by $C_2H_5^\bullet$ loss resulting in the base peak at *m/z* 45. The thermodynamic advantage of $C_2H_5^\bullet$ loss over $CH_3^\bullet$ loss becomes evident from the diethyl ether spectrum. In accordance with Stevenson's rule, even two ethyl groups cleave off less $CH_3^\bullet$ than a single propyl looses $C_2H_5^\bullet$. It is tempting, although not trivial, to quantify the relative "ease" of fragmentation from the ratio of peak intensities. However, the primary fragment will undergo further fragmentation at an unknown rate, e.g., ethene loss from the oxonium ion at *m/z* 59 to yield the smaller one at *m/z* 31. Generally, oxonium ions are highly indicative of aliphatic ethers and alcohols. In the EI spectrum of diethyl ether the series from *m/z* 31 to *m/z* 73 is present (Table 6.8).

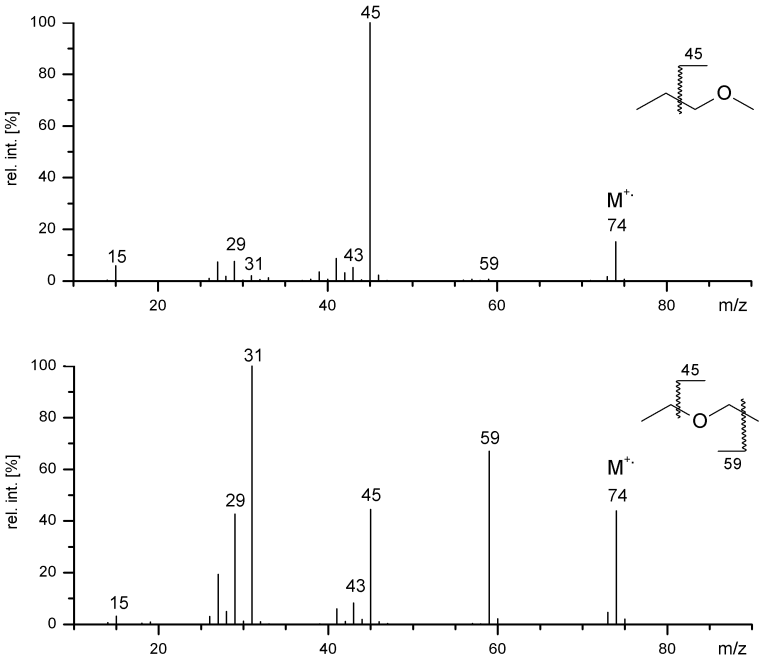


Fig. 6.7. EI mass spectra of methylpropylether and diethyl ether. Spectra used by permission of NIST. © NIST 2002.

In case of alkanols, the methylene oxonium ion, $CH_2{=}OH^+$, *m/z* 31, deserves special attention. Resulting from α-cleavage, it undoubtedly marks spectra of primary alkanols, where it either represents the base peak or at least is the by far most abundant of the oxonium ion series (Fig. 6.8) [28]. The second important fragmentation route of aliphatic alcohols, loss of H_2O, is discussed in Chap. 6.10.

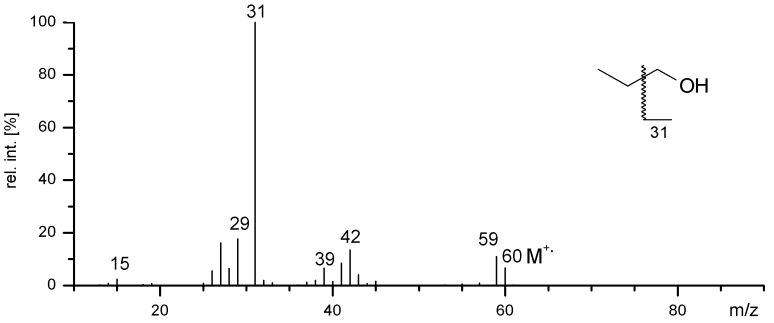


Fig. 6.8. EI mass spectrum of 1-propanol. Used by permission of NIST. © NIST 2002.

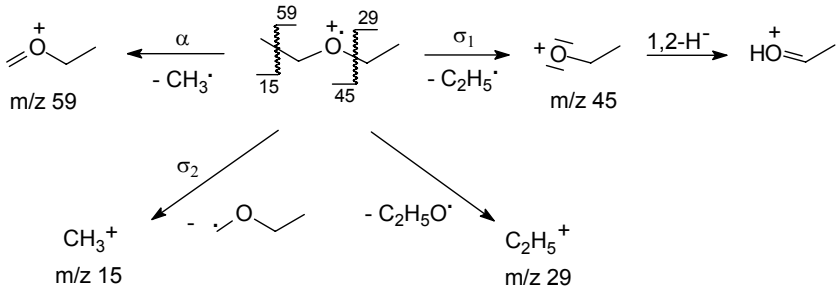
Table 6.8. Aliphatic oxonium ions

m/z (17 + 14*n*)	Oxonium ions $[C_nH_{2n+1}O]^+$	Accurate mass [u][a]
31	CH_3O^+	31.0178
45	$C_2H_5O^+$	45.0335
59	$C_3H_7O^+$	59.0491
73	$C_4H_9O^+$	73.0648
87	$C_5H_{11}O^+$	87.0804
101	$C_6H_{13}O^+$	101.0961
115	$C_7H_{15}O^+$	115.1117
129	$C_8H_{17}O^+$	129.1274

[a] values rounded to four decimals

6.2.9 Charge Retention at the Heteroatom

The peak at *m/z* 45 in the spectrum of diethyl ether can neither be explained by α-cleavage nor by α-cleavage plus a subsequent cleavage, because the latter would demand carbene loss to occur, which is almost never observed (one of the rare examples is presented by formation of $HI^{+\bullet}$ from $CH_3I^{+\bullet}$). Obviously, the C–O bond can access a direct pathway for cleavage. Although some C–N bond cleavage can be observed in EI spectra of aliphatic amines, the cleavage of the C–O bond is gaining importance for the molecular ions of aliphatic ethers. It is a simple σ-bond cleavage as discussed for methane molecular ions, the only difference being the fact that one of the atoms connected by the σ-bond is not a carbon atom. As the heteroatom can stabilize the charge better than a primary carbon, the RX^+ fragment is preferably formed in such a case (σ_1). The product ion may then rearrange by 1,2-hydride shift to form an oxonium ion [33]. The formation of $C_2H_5^+$ fragment ions, *m/z* 29, directly competes with σ_1.



Scheme 6.14.

6.2.10 α-Cleavage of Thioethers

The EI mass spectra of thiols and thioethers also show a series of onium ions generated by α-cleavage of the molecular ion (Table 6.9). *Sulfonium ions* can easily be recognized from the isotopic pattern of sulfur (Fig. 6.9). The fragmentation patterns of thioethers will be discussed in greater detail later (Chaps. 6.5.2 and 6.12.4).

Table 6.9. Aliphatic sulfonium ions

m/z (33 + 14*n*)	Sulfonium ions $[C_nH_{2n+1}S]^+$	Accurate mass [u][a]
47	CH_3S^+	46.9950
61	$C_2H_5S^+$	61.0106
75	$C_3H_7S^+$	75.0263
89	$C_4H_9S^+$	89.0419
103	$C_5H_{11}S^+$	103.0576
117	$C_6H_{13}S^+$	117.0732
131	$C_7H_{15}S^+$	131.0889
145	$C_8H_{17}S^+$	145.1045

[a] values rounded to four decimals

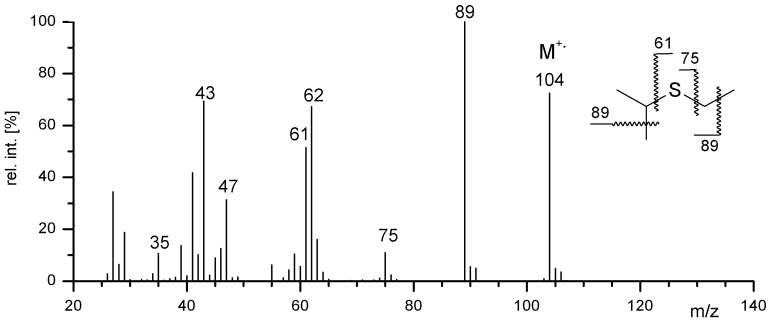


Fig. 6.9. EI mass spectrum of ethylisopropylthioether. Due to the isotopic composition of sulfur, the intensity of the $[M+2]^{+\bullet}$ ion is increased. The corresponding contributions can also be recognized for the sulfonium ions at *m/z* 47, 61, 75, and 89. The *m/z* 35 peak is due to H_3S^+ ions; also compare the spectrum of ethylpropylthioether (Fig. 6.43). Spectrum used by permission of NIST. © NIST 2002.

6.2.11 α-Cleavage of Halogenated Hydrocarbons

Aliphatic halogenated hydrocarbons do not show abundant fragment ions due to α-cleavage [13]. As was found with aliphatic amines and ethers before, the molecular ion peak decreases in intensity as the molecular weight and branching of the alkyl chain increase. In general, the relative intensity of the molecular ion peak

falls in the order I > Br > Cl > F (Chap. 6.1.4). For bromine the molecular ions are almost of the same relative intensity as for hydrogen, i.e., for the corresponding hydrocarbon. This corresponds to the inverse order of halogen electronegativities. Higher electronegativity of the halogen also causes a higher ionization energy of the RX molecule and an increase of α-cleavage products.

Example: The 70-eV EI mass spectrum of 1-bromo-octane incorporates the characteristic fragmentations of aliphatic halogenated hydrocarbons (Fig. 6.10). All bromine-containing fragments are readily recognized from their bromine isotopic pattern (Chap. 3.1, 3.2). The product of the α-cleavage, $[CH_2Br]^+$, *m/z* 91, 93, is of minor intensity, whereas a $[M–57]^+$ ion, *m/z* 135, 137, dominates the spectrum. The preference for the $[M–57]^+$ ion, $[C_4H_8Br]^+$, has been attributed to the possibility of forming a five-membered cyclic bromonium ion of low ring strain. This reaction differs from the preceding bond cleavages in that it is a displacement of an alkyl group, but it shares the common property of being a

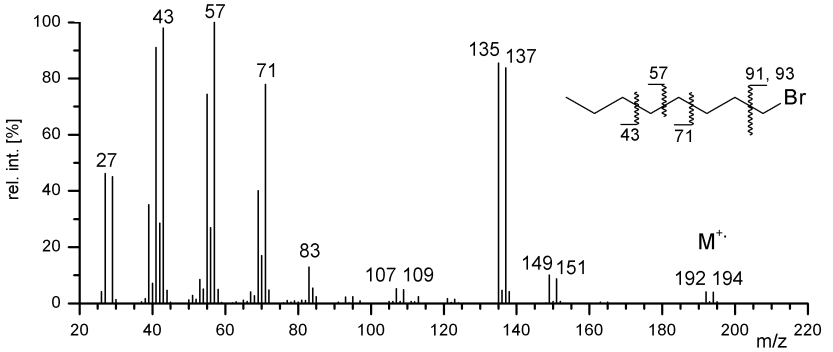
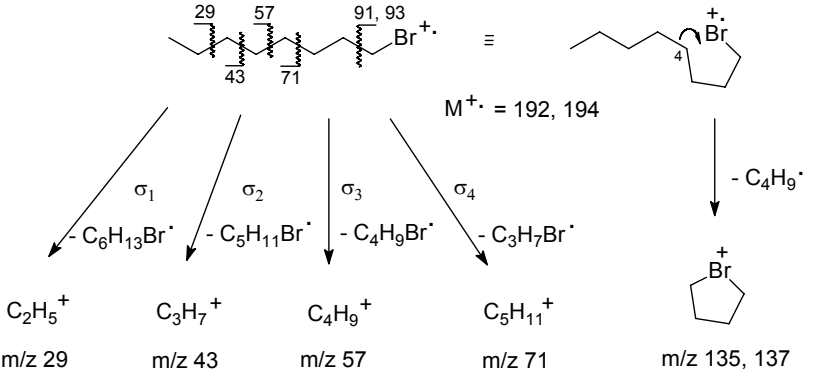


Fig. 6.10. EI mass spectrum of 1-bromo-octane. The product of the α-cleavage, *m/z* 91, 93 is of minor intensity, and the cyclic bromonium ion, *m/z* 135 and 137, dominates the spectrum. Spectrum used by permission of NIST. © NIST 2002.

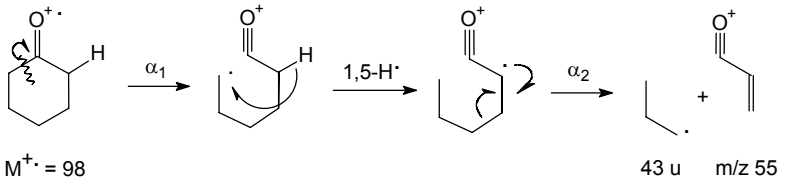


Scheme 6.15.

one-step process [34]. Analogous behavior is observed for the chlorohydrocarbons from hexyl through octadecyl that show the $[C_4H_8Cl]^+$ ion, *m/z* 91, 93. Fortunately, the isotopic patterns of Br and Cl are clearly different, thereby avoiding confusion of the isobaric $[C_4H_8Cl]^+$ and $[CH_2Br]^+$ ions. Iodo- and fluorohydrocarbons do not exhibit such cyclic halonium ions in their EI spectra. The remaining fragments can be explained by σ-cleavages leading to carbenium ions (Table 6.3).

6.2.12 Double α-Cleavage

Of course, α-cleavage can also occur in alicyclic ketones and other heteroatom-substituted alicyclic compounds. From a cycle, a single bond cleavage cannot release a neutral fragment, because this is still adhering to another valence of the functional group. To eliminate a propyl from cyclohexanone molecular ion, a three-step mechanism consisting of two α-cleavages and an intermediate 1,5-H$^\bullet$ shift is required.



Scheme 6.16.

Cyclohexanone has been examined by deuterium-labeling to reveal the mechanism of propyl loss, $[M–43]^+$, *m/z* 55, from its molecular ion, $M^{+\bullet} = 98$ [35,36]. The corresponding signal is the base peak of the spectrum (Fig. 6.11). Clearly, one deuterium is incorporated in the fragment that is shifted to *m/z* 56 in case of the [2,2,6,6-D_4]isotopolog, which is consistent with the above three-step mechanism.

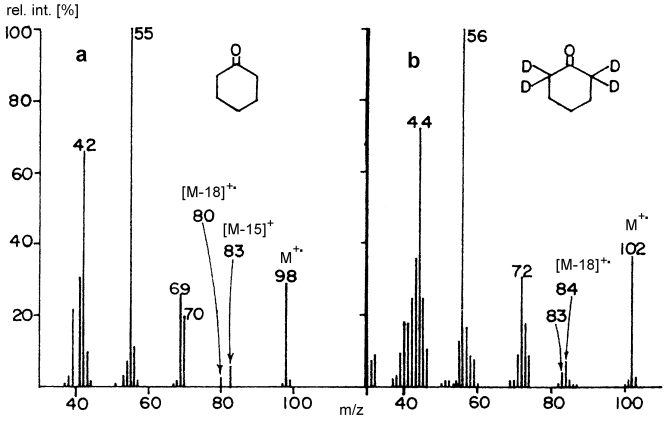


Fig. 6.11. 70-eV EI mass spectra of cyclohexanone (**a**) and its deuterated isotopolog [2,2,6,6-D_4] (**b**). Adapted from Ref. [35] with permission. © Springer-Verlag Wien, 1964.

Note: Early publications often oversimplified complex fragmentation processes. There are strong arguments that gas phase ionic reactions are generally stepwise processes. Thus, is more probable that complex fragmentations follow several discrete steps instead of single ones with simultaneous breaking and forming of several bonds [34].

6.2.13 Double α-Cleavage for the Identification of Regioisomers

Following the logic of deuterium labeling, regioisomers of cyclohexanones, cyclohexylamines, cyclohexylalcohols and others can be identified by strict application of the above mechanism. Regardless of some limitations of the method, e.g., that it is impossible to distinguish a 2,3-dimethyl from a 2-ethyl or 3-ethyl derivative, the method provides a valuable aid in structure elucidation.

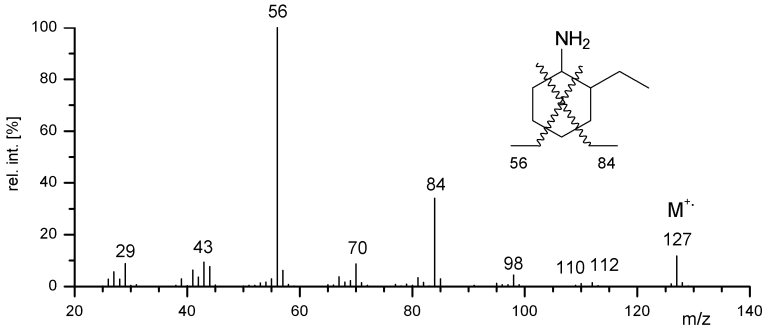
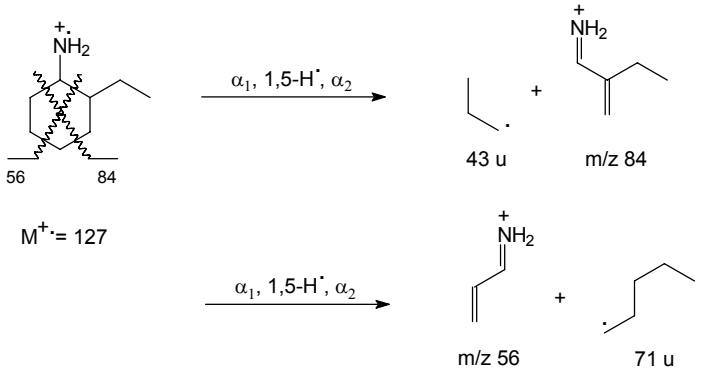


Fig. 6.12. EI mass spectrum of 2-ethyl-cyclohexylamine. Double α-cleavage allows to identify the substitution on one side of the ring. Spectrum used by permission of NIST. © NIST 2002.



Scheme 6.17.

Example: Propyl and pentyl losses from 2-ethyl-cyclohexylamine molecular ion, $M^{+\bullet}$ = 127 (odd *m/z*) are competitive (Fig. 6.12). Pentyl loss, *m/z* 56 (even *m/z*), is favored over propyl loss, *m/z* 84 (even *m/z*), in accordance with Stevenson's rule. The peak at *m/z* 98 may be explained by ethyl loss due to a minor contribution of 1,4-$H^{\bullet}$ shift, i.e., from 3-position instead of the predominant 1,5-$H^{\bullet}$ shift from 2-position. The $[M–CH_3]^+$ peak, *m/z* 112, is accompanied by a $[M–NH_3]^{+\bullet}$ signal, *m/z* 110, which is typical of primary (and to lower extent) secondary amines.

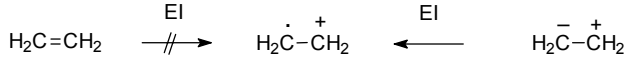
6.3 Distonic Ions

6.3.1 Definition of Distonic Ions

For the case of the intermediate fragmentation products resulting from the first α-cleavage of cyclohexyl compounds the charge and the radical are not located at the same atom as is the case of molecular ions, but at distant positions. The term *distonic ion* was derived from the Greek word for 'separate' to describe such ionic species [37]. Distonic ions represent an ionic class of their own [37-39].

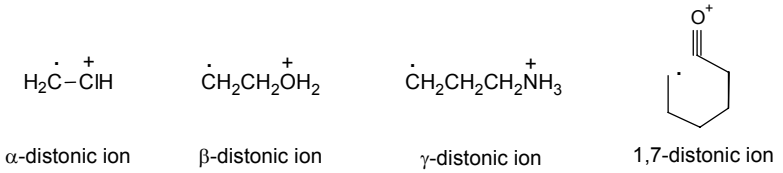
Definition: A *distonic ion* is a positive radical ion, which would formally arise by ionization of a zwitterion or a diradical, by isomerization or fragmentation of a 'classical' molecular ion, or by ion-molecule reactions. Consequently, distonic ions have charge and radical at different atoms in a conventional valence bond description [39,40].

However, bearing charge and radical at separate sites is not a sufficient condition for an ion to be denoted distonic, e.g., the ethylene molecular ion may be written as such, but the corresponding neutral is *not* best represented as zwitterion and therefore the ethylene molecular ion by definition is *not* a distonic ion:



Scheme 6.18.

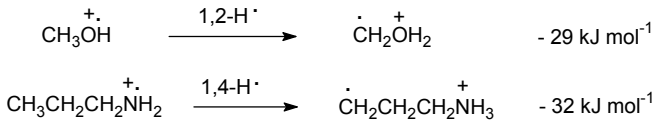
The expressions *nonclassical* and *hypervalent* ion have also been used by some authors to describe distonic ions, but these are incorrect and thus should no longer be used. The term *ylidion* is limited to species where charge and radical are in adjacent positions. Thus, to describe the distance between charge and radical site, the terms α- (1,2-) *distonic ion*, β- (1,3-) *distonic* ion, γ- (1,4-) *distonic ion*, and so forth are now in use [39,40]:



Scheme 6.19.

6.3.2 Formation and Properties of Distonic Ions

Cleavage of a bond without immediate dissociation of the precursor radical ion is one way for generating distonic ions. Isomerization of molecular ions by hydrogen radical shift frequently leads to distonic ions prior to fragmentation and, moreover, the distonic isomers are often thermodynamically more stable than their "classical" counterparts [37]:



Scheme 6.20.

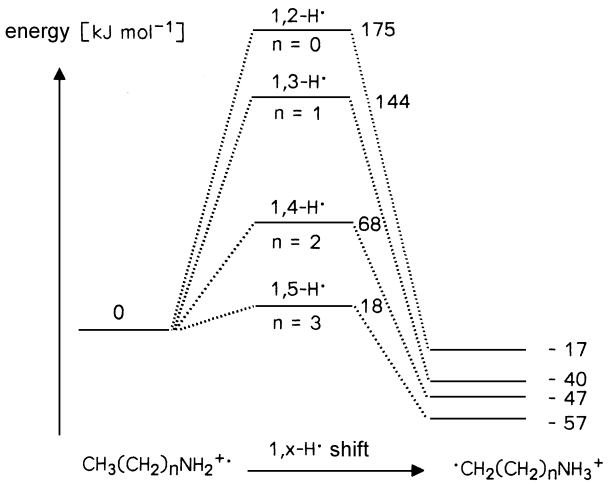


Fig. 6.13. Activation energies for isomerization of primary amine molecular ions to distonic isomers with the heats of formation of the precursor $M^{+\bullet}$ ions normalized to zero [42].

The mutual interconversion of "classical" and distonic ions is not a fast process, because the isomers are separated by a comparatively high energy barrier. The ac-

tivation energy for 1,2-H$^{\bullet}$ shifts is substantially larger than for longer distance shifts such as 1,4- or 1,5-H$^{\bullet}$ shifts. The activation energies and the heats of reaction have been determined for H$^{\bullet}$ shifts in primary amine molecular ions (Fig. 6.13) [32,41,42]. It has been argued that with increasing number of atoms between the positions, the ring strain in the respective C–H$^{\bullet}$–N transition states is reduced and that this is the reason for a significant decrease in activation energy [42]. In addition to the influence on transition states, the longer distance from charge to radical site also lowers the heats of formation of the distonic ions with respect to the "classical" ion precursors, i.e., any of these isomerizations is exothermic.

6.3.3 Distonic Ions as Intermediates

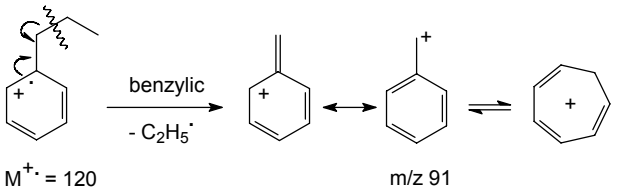
Distonic ions are of high relevance in the dissociation reactions of many ionized molecules as they play an important role as the central intermediates and products. It is likely that the long-lived molecular ions of many organic compounds exist in distonic form [40]. It has been shown, for example, that the long-lived radical ions of simple organophosphates spontaneously isomerize to distonic isomers, [43] and that the ring-opening product of cyclopropane molecular ion is also distonic [44]. The next distonic ions we are going to learn about are the intermediates of the McLafferty rearrangement (Chap. 6.7).

6.4 Benzylic Bond Cleavage

The α-cleavage in molecular ions of ketones, amines, ethers, and similar functionalized compounds yields specific cleavage products of high importance for structure elucidation. Analogous behavior is observed in the mass spectra of phenylalkanes [45].

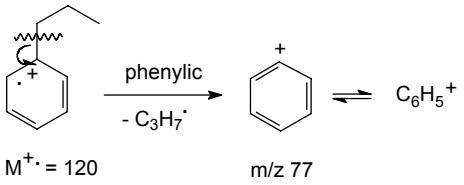
6.4.1 Cleavage of the Benzylic Bond in Phenylalkanes

Molecular ions of phenylalkanes are comparatively stable due to the good charge-stabilizing properties of the aromatic ring and thus, they normally give rise to intense peaks. Those molecular ions, possessing a benzylic bond preferably show cleavage of that bond as compared to the phenylic or homobenzylic position. As with the α-cleavage, the process is radical-initiated and follows the same basic scheme, i.e., dissociation of the bond second to the radical-site after transfer of a single electron towards the radical-site. The mass spectrum of *n*-propylbenzene is an example (Fig. 6.14).



Scheme 6.21.

The cleavages of the phenylic and homobenzylic bond are less important as can be seen from the minor peaks at *m/z* 77 and *m/z* 105 in the mass spectrum of *n*-propylbenzene. Nevertheless, phenylic bond cleavage does also occur and gives rise to further fragments. Due to its high thermodynamic stability, the $[C_7H_7]^+$ ion is not only formed by benzylic cleavage, but it is also obtained from many other fragmentation processes of phenylalkanes. The majority of mass spectra of such compounds clearly exhibit the corresponding peak at *m/z* 91.



Scheme 6.22.

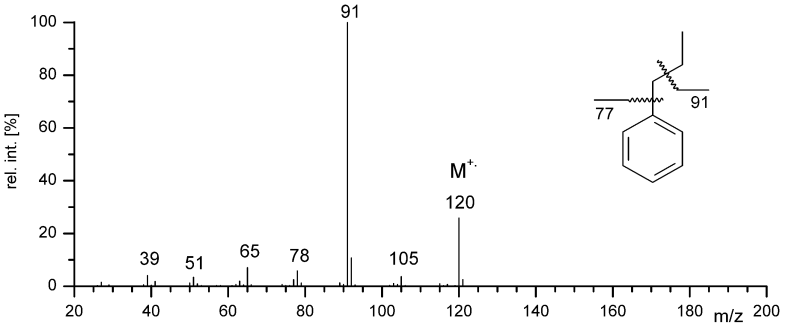
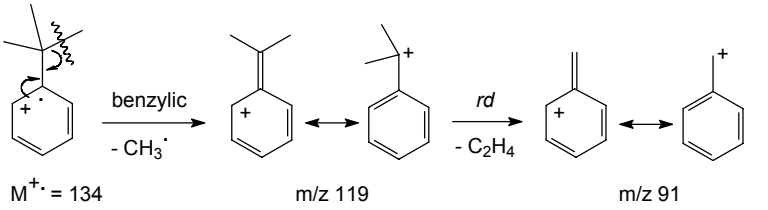


Fig. 6.14. EI mass spectrum of *n*-propylbenzene. The molecular ion peak and the primary fragment ion have significant intensity, whereas low-mass fragments are less abundant. Spectrum used by permission of NIST. © NIST 2002.

Example: In the mass spectrum of *tert*-butylbenzene, $C_{10}H_{14}$, the $[C_7H_7]^+$ ion is formed by C_2H_4 loss from the product of benzylic cleavage, *m/z* 119, though such a rearrangement would not be expected at first sight (Fig. 6.15).



Scheme 6.23.

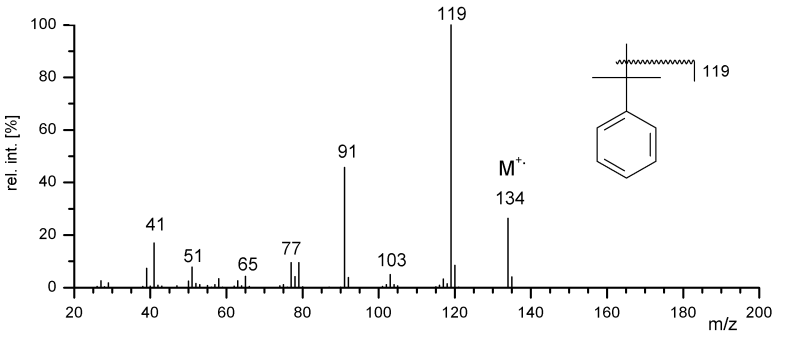
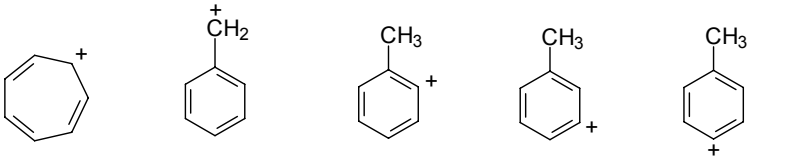


Fig. 6.15. EI spectrum of *tert*-butylbenzene. Again, molecular ion and primary fragment ion are dominating the spectrum. Spectrum used by permission of NIST. © NIST 2002.

Note: The mere occurrence of the $[C_7H_7]^+$ ion – especially when it is of low intensity – is *not sufficient* to prove that the analyte belongs to the phenylalkanes. This ion and its characteristic fragments may also be observed *if there is any means of* generating a $[C_7H_7]^+$ fragment ion.

6.4.2 The Further Fate of $[C_6H_5]^+$ and $[C_7H_7]^+$

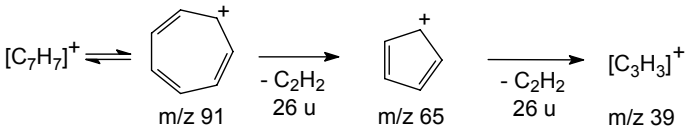
As already indicated in the preceding schemes, the resonance-stabilized benzyl ion, $[C_7H_7]^+$, initially formed by benzylic bond cleavage reversibly isomerizes to the tropylium and tolyl ion isomers. The isomerization of $[C_7H_7]^+$ ions has been the subject of numerous studies [46], revealing the tropylium ion as the thermodynamically most stable isomer [47,48]. Provided sufficient lifetime, the process of benzyl/tropylium isomerization can be reversible ($E_0 = 167$ kJ mol^{-1} [46]), and then it necessarily goes along with a *scrambling* of hydrogens and of carbons as can be demonstrated by use of isotopically labeled compounds [49]. The degree of scrambling also depends on ion internal energy and on ion lifetime.



Scheme 6.24.

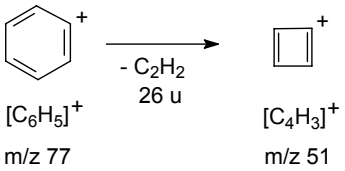
Note: The illustrative term *scrambling* is used in mass spectrometry to describe rapid processes of (intramolecular) positional interchange of atoms. Scrambling may occur with hydrogens or may involve the complete carbon skeleton of an ion. Aryl radical ions and protonated aryl compounds are well known for their numerous scrambling processes [50].

Whatever the initial or preferred structure, the $[C_7H_7]^+$ ions dissociate by loss of ethyne, C_2H_2, to yield the cyclopentadienyl ion, $[C_5H_5]^+$, *m/z* 65, which fragments to yield $[C_3H_3]^+$, *m/z* 39, upon repeated ethyne loss:



Scheme 6.25.

The phenyl ion $[C_6H_5]^+$, *m/z* 77, also undergoes C_2H_2 loss, thereby generating the cyclobutadienyl ion, $[C_4H_3]^+$, *m/z* 51:

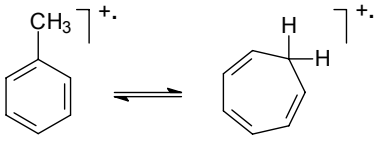


Scheme 6.26.

Note: Overall, the former two reaction lead to the typical appearance of the ion series *m/z* 39, 51, 65, 77, 91 in the EI mass spectra of phenylalkanes. However, one needs to be aware of the two competing reaction sequences leading to this series: *i*) $M^{+\bullet} \rightarrow 91 \rightarrow 65 \rightarrow 39$ and *ii*) $M^{+\bullet} \rightarrow 77 \rightarrow 51$; the latter usually being of lower intensity, which is in accordance with the preference for benzylic bond cleavage.

6.4.3 Isomerization of $[C_7H_8]^{+\bullet}$ and $[C_8H_8]^{+\bullet}$ Ions

The molecular ions of toluene and cycloheptatriene are capable of mutual isomerization prior to dissociation [45,49,51]. It has been known for long that hydrogen loss from toluene molecular ions takes place as if all eight positions within these ions were equivalent, and this has been interpreted in terms of complete hydrogen scrambling prior to dissociation [52]. The extent of isomerization becomes apparent from the close similarity of the toluene and cycloheptatriene EI mass spectra (Fig. 6.16). Loss of $H^{\bullet}$ from $[C_7H_8]^{+\bullet}$ leads to the formation of $[C_7H_7]^{+}$ ions, preferably of tropylium structure [50], and thus, to the typical fragment ion series described above.



$[C_7H_8]^{+\bullet}$, m/z 92

Scheme 6.27.

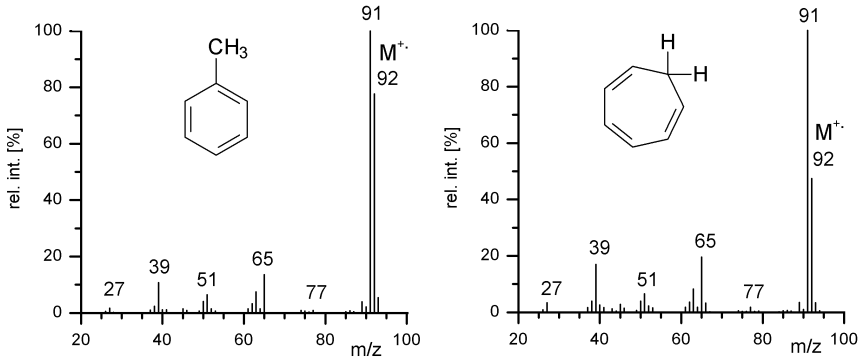
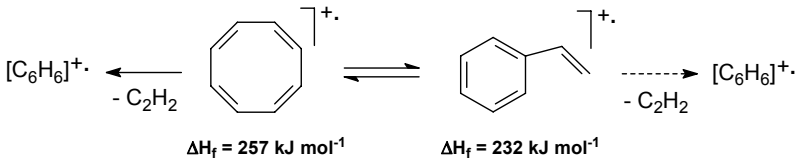


Fig. 6.16. Close similarity of the 70-eV EI mass spectra of toluene (*left*) and cycloheptatriene (*right*). Spectra used by permission of NIST. © NIST 2002.

Extensive isomerizations prior to dissociation are also observed for other ions having similar structural features. Deuterium labeling of some bicyclic aromatic systems has shown that complete or partial randomization of the aromatic hydrogens prior to dissociation can occur upon EI [53]. In detail, such observations were made in molecular ions of *i*) biphenyl prior to loss of $CH_3^{\bullet}$, C_2H_2, or $C_3H_3^{\bullet}$, *ii*) 1- and 2-cyanonaphthalenes before HCN expulsion, and *iii*) benzothiophene before C_2H_2 expulsion. Cyclooctatetraene and styrene molecular ions, $[C_8H_8]^{+\bullet}$, *m/z* 104, interconvert prior to loss of ethyne to yield benzene molecular ion, *m/z* 78. Because of the substantially lower overall activation energy, most of the

$[C_6H_6]^{+\bullet}$ ions formed result from dissociation of cyclooctatetraene molecular ion although this has the higher heat of formation [54].



Scheme 6.28.

6.4.4 Rings Plus Double Bonds

Based on valence rules, a general algorithm can be derived to distinguish between ions containing a different total number of double bonds and/or rings. As this algorithm does not allow to differentiate between a cyclic substructure and a double bond, the result is known as *double bond equivalents* (DBE) or simply *rings plus double bonds* ($r + d$). (The rarely used term *unsaturation* is not recommended because it does not imply cyclic structures.) The general equation for the determination of $r + d$ is:

$$r + d = 1 + 0.5 \times \sum_{i}^{i_{max}} N_i \ (V_i - 2) \tag{6.9}$$

where V_i represents the valence of an element and N_i is the number of atoms. For regular use, the expressions $0.5 \times (V_i - 2)$ should be calculated. For monovalent elements (H, F, Cl, Br, I) one obtains $0.5 \times (1 - 2) = -0.5$, for divalent elements (O, S, Se) $0.5 \times (2 - 2) = 0$ which is the reason why the contribution of divalent elements is cancelled. Proceeding with the higher valences yields:

$$r + d = 1 - 0.5\, N_{mono} + 0.5\, N_{tri} + N_{tetra} + 1.5\, N_{penta} + 2\, N_{hexa} + \ldots \tag{6.10}$$

Restriction to formulas of the general type $C_cH_hN_nO_o$ reduces the expression to:

$$r + d = 1 + c - 0.5h + 0.5n \tag{6.11}$$

Here, other monovalent elements than hydrogen (F, Cl, Br, I) are counted "as hydrogens", other trivalent elements such as phosphorus are counted "as nitrogen" and tetravalent elements (Si, Ge) are handled the same way as carbons.

The $r + d$ algorithm produces integers for odd-electron ions and molecules, but nonintegers for even-electron ions that have to be rounded to the next lower integer, thereby allowing to distinguish even- from odd-electron species.

Care has to be taken when elements of changing valence are encountered, e.g., S in sulfoxides and sulfones or P in phosphates. In such a case, Eqs. 6.9 or 6.10 have to be used, whereas Eq. 6.11 yields erroneous results.

Table 6.10. Examples for the application of the $r + d$ algorithm according to Eq. 6.11

Name	Formula	$r + d$	Comment
Decane	$C_{10}H_{22}^{+\bullet}$	1+ 10 – 11 = 0	
Cyclohexanone	$C_6H_{10}O^{+\bullet}$	1 + 6 – 5 = 2	1 r + 1 d
Benzene	$C_6H_6^{+\bullet}$	1 + 6 – 3 = 4	1 r + 3 d
Benzonitrile	$C_7H_5N^{+\bullet}$	1 + 7 – 2.5 + 0.5 = 6	1 r + 5 d
Butyl ion	$C_4H_9^+$	1 + 4 – 4.5 = 0.5[a]	fragment[a]
Acetyl ion	CH_3CO^+	1 + 2 – 1.5 = 1.5[a]	1 d for C=O[b]
Dimethylsulfoxide	$C_2H_6SO^{+\bullet}$	1 + 2 – 3 = 0	1 d expected[c]
		1 + 3 – 3 = 1[c]	1 d for tetravalent S

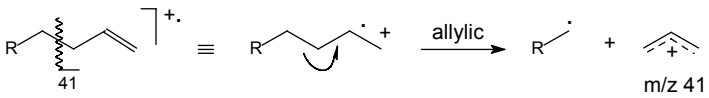
[a] even-electron ions have 0.5 $r + d$ more than expected; round to next lower integer
[b] values are correct for resonance structure with charge at carbon
[c] Attention! Sulfur is tetravalent in DMSO and should be handled as carbon

Note: Even-electron rule, Stevenson's rule, nitrogen rule, and $r + d$ algorithm belong to a collection of empirical rules and hints on how to systematically approach a mass spectrum of an unknown (Chap. 6.15). It is good practice to apply these during mass spectral interpretation, e.g., the $r + d$ algorithm as soon as the formula of a molecular ion or a fragment ion becomes apparent. This yields valuable information on possible substructures. You can practice their use while examining the numerous examples of spectra throughout this chapter!

6.5 Allylic Bond Cleavage

6.5.1 Cleavage of the Allylic Bond in Aliphatic Alkenes

The mass spectra of alkenes are governed by the alkyl moiety of the molecule and by the specific reactions characteristic for the double bond. Molecular ions are generally of low intensity – as is the case with all other purely aliphatic compounds discussed so far – and may even be fully absent [3,26]. There is some preference for the cleavage of the allylic bond in the alkene molecular ions which can be treated analogously to α-cleavage and benzylic cleavage, but the double bond is the weakest cleavage-directing functional group:



Scheme 6.29.

As hydrogen rearrangements prior to dissociation are prevalent in alkene molecular ions, the radical site migrates along the chain, thereby obscuring the original location of the double bond [55]. ^{2}H- and ^{13}C-labeling revealed that the mo-

lecular ions of 1-, 2-, 3-, and 4-octene completely interconvert within 10^{-9} s. The equilibration of double bond isomers by radical-site migration and concomitant hydrogen rearrangements do not involve the terminal hydrogens to a larger extent [56]. Generally, smaller unsaturated hydrocarbon ions undergo more extensive isomerization prior to decomposition than larger ones.

Note: Extensive isomerization prior to or between single steps of fragmentation makes the mass spectra of isomeric alkenes become very similar.

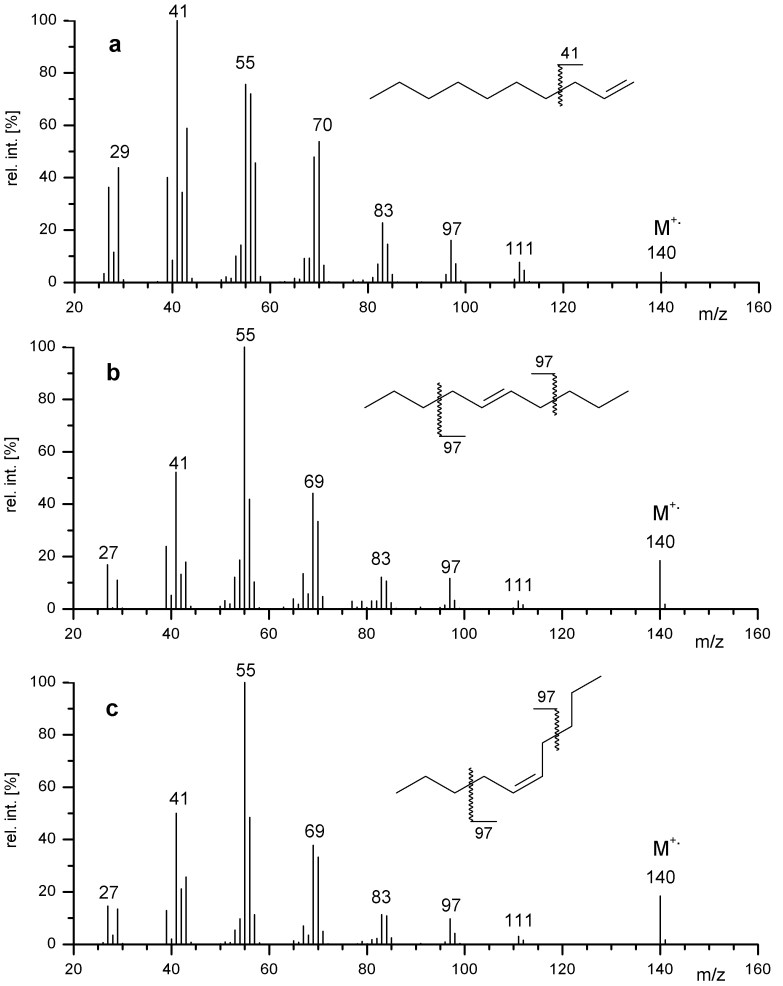


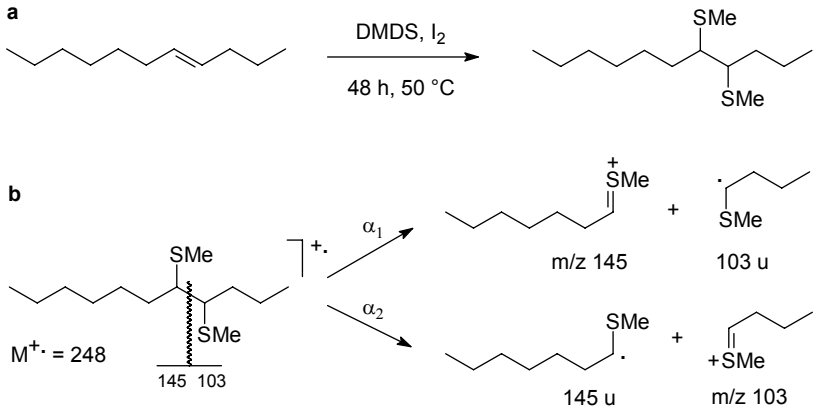
Fig. 6.17. EI mass spectra of isomeric decenes. The differences between 1-decene (**a**), (*E*)-5-decene (**b**), and (*Z*)-5-decene (**c**) are visible, but without reference spectra the isomers cannot be identified. Spectra used by permission of NIST. © NIST 2002.

Example: The spectra of 1-decene, (*E*)-5-decene, and (*Z*)-5-decene are shown in Fig. 6.17. Whereas in the spectrum of 1-decene the basepeak at *m/z* 41 can easily be explained as a result of allylic cleavage, the base peak of both stereoisomeric 5-decenes is at *m/z* 55, and therefore, cannot result from direct allylic cleavage. It is impossible to find evidence for a certain isomer without reference spectra. At *m/z* 97, there is only a minor signal from allylic cleavage, and unfortunately such a peak is also observed in the spectrum of 1-decene. Consecutive fragmentations of the primary cleavage product give one reason for this close similarity, another being the influence of $H^{\bullet}$ migrations prior to dissociation of the alkene molecular ions. Even comparison to reference spectra does not permit their proper identification as the differences between the stereoisomers are negligible.

6.5.2 Methods for the Localization of the Double Bond

The localization of a double bond is an important step in structure elucidation and therefore, it is not astonishing that numerous approaches have been made to overcome the above limitations. The methods "to freeze" isomerization include *i*) epoxidation [57], *ii*) iron and copper ion chemical ionization [58,59], *iii*) field ionization [60], *iv*) collision-induced dissociation [55], *v*) formation of thioether derivatives [61,62], and others.

Example: The oxidative addition of dimethyl disulfide (DMDS) transforms the double bond to its 1,2-bis-thiomethyl derivative (**a**). Induced by charge localization at either sulfur atom, the molecular ions of DMDS adducts are prone to α-cleavage at the former double bond position (**b**). This gives rise to sulfonium ions that are readily identified on the mass spectrum (Chap. 6.2.5). The method can be extended to dienes, trienes, and alkynes [63,64].

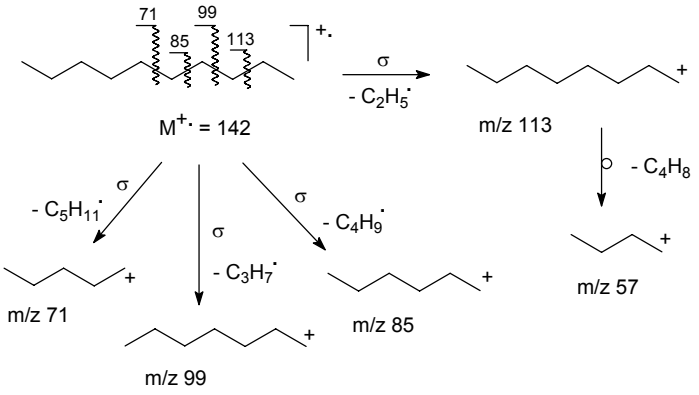


Scheme 6.30.

6.6. Cleavage of Non-Activated Bonds

6.6.1 Saturated Hydrocarbons

In a molecular ion of a straight-chain *n*-alkane there is no preferred position to localize the charge. Consequently, as in the case of methane, longer chain alkanes also suffer from substantial weakening of bonds upon electron ionization. The α-cleavage is not observed anymore. As expected, the primary step of dissociation is unspecific σ-bond cleavage at all but C_1–C_2 bonds, provided there are others. Methyl loss is negligible due to the unfavorable thermodynamics of this process. The resulting carbenium ions subsequently dissociate by loss of alkene molecules, preferably propene to pentene [65]. This process can occur repeatedly as long as the chain length of the fragment ion suffices [66]. As a result of these competing and consecutive ion dissociations, the base peak of aliphatic hydrocarbon spectra originates from low-mass carbenium ions, typically propyl, *m/z* 43, or butyl, *m/z* 57 (Table 6.3). Saturated carbenium ion fragments $[C_nH_{2n+1}]^+$ (n = 3–7) isomerize to common structures before decomposition, whereas the molecular ions retain their structure [67]. The molecular ion peak is usually apparent, but never as strong as in spectra of aromatic compounds [30]. For highly branched hydrocarbons it may even be absent:



Scheme 6.31.

Example: The EI mass spectrum of *n*-decane is typical for this class of hydrocarbons (Fig. 6.18a). Branching of the aliphatic chain supports cleavage of the bonds adjacent to the branching point, because then secondary or tertiary carbenium ions and/or alkyl radicals are obtained (Fig. 6.18b,c). This allows for the identification of isomers to a certain degree.

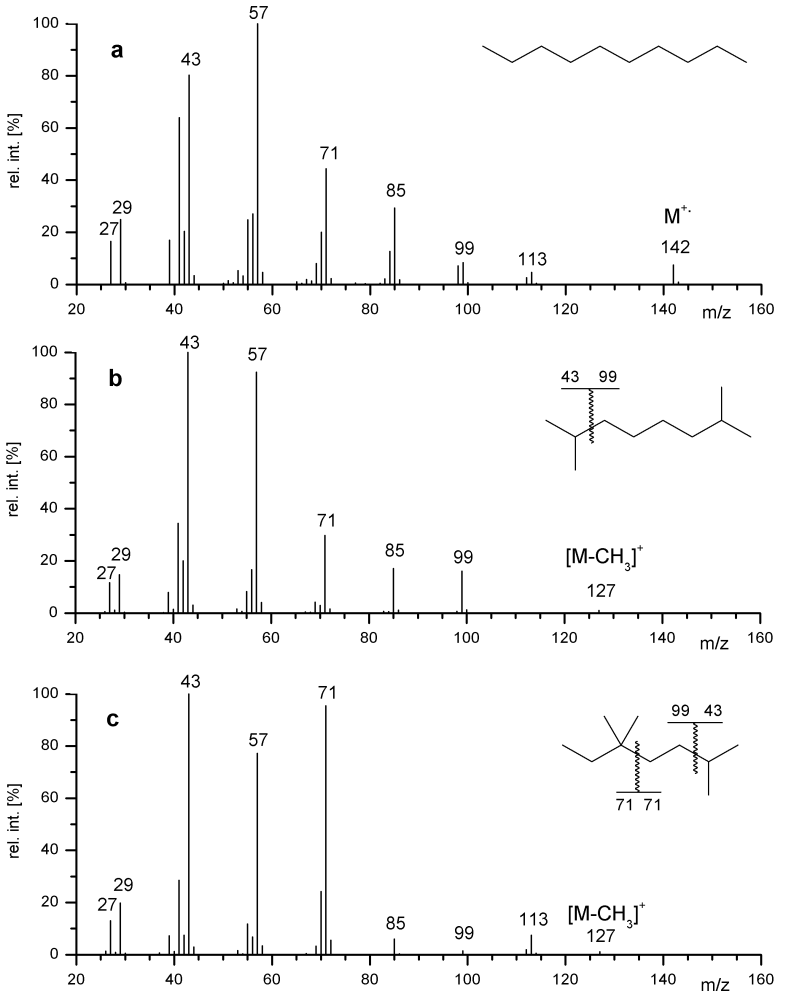
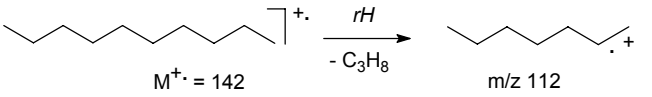


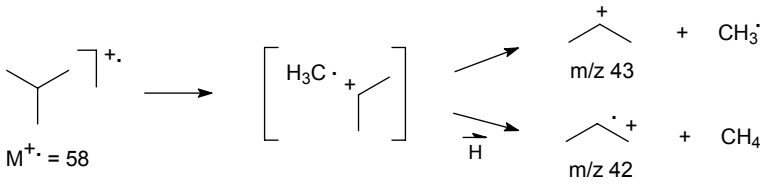
Fig. 6.18. EI mass spectra of *n*-decane (**a**), 2,7-dimethyloctane (**b**), and 2,5,5-trimethylheptane (**c**). Spectra used by permission of NIST. © NIST 2002.

A closer look at the spectrum of *n*-decane also reveals fragment ions at *m/z* 84, 98, and 112, i.e., rearrangement ions at even mass number. The origin by loss of $H^{\bullet}$ from the accompanying carbenium ions at *m/z* 85, 99, and 113, respectively, can be excluded by application of the even-electron rule. Instead, alkane molecular ions may undergo alkane loss [68]:



Scheme 6.32.

Theoretical and experimental studies revealed a common intermediate for the elimination of $CH_3^{\bullet}$ and CH_4 from isobutane and other alkanes of similar size. The additional hydrogen needed may originate from either one of the terminal positions of the propyl moiety [69,70]:



Scheme 6.33.

6.6.2 Carbenium Ions

Carbenium ions make up the largest portion of peaks in alkane mass spectra. They dissociate further by alkene loss with or without prior isomerization. Generally, such processes will yield a more stable isomer, e.g., the *tert*-butyl ion instead of other $[C_4H_9]^+$ isomers (Fig. 6.19).

Among the $[C_4H_9]^+$ isomers, only the *n*-butyl isomer can undergo fragmentations. It either yields an allyl ion, *m/z* 41, by loss of methane or an ethyl ion, *m/z* 29, by elimination of ethene. This is the reason why *tert*-butyl compounds exhibit strong *m/z* 41 and *m/z* 57 signals in their EI spectra (Figs. 6.20, 6.23). In case of metastable $[C_4H_9]^+$ ions, methane loss is about 20-fold stronger than ethene loss because of the 1 eV higher activation energy in case of ethene loss [71].

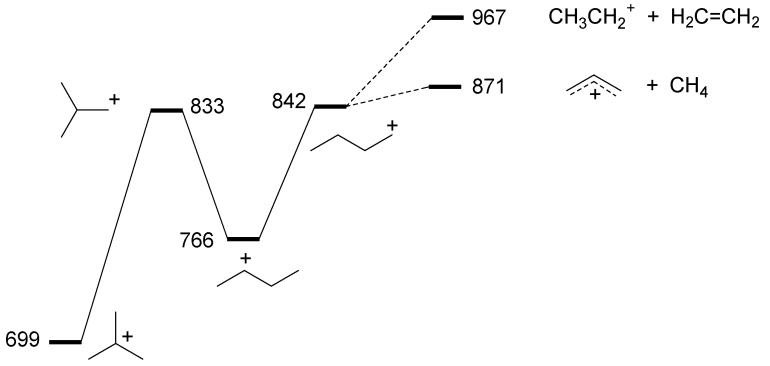


Fig. 6.19. Energetics of the isomerization and fragmentation pathways of $[C_4H_9]^+$ ions. Heat of formations are in kJ mol^{-1}. Redrawn from Ref. [71] with permission. © American Chemical Society, 1977.

Example: In the EI mass spectrum of *tert*-butylchloride the molecular ion peak is absent and the highest *m/z* signal is due to $[M\text{-}CH_3]^+$; note the Cl isotopic pat-

tern of this signal (Fig. 6.20). The remaining portion of the spectrum is determined by the *tert*-butyl group, causing the base peak at *m/z* 57. The *tert*-butyl ion directly originates from σ-cleavage of the C–Cl bond. The ratio of the $[C_3H_5]^+$, *m/z* 41, and $[C_2H_5]^+$, *m/z* 29, fragments correlates well with the energetically favorable CH_4 loss from $[C_4H_9]^+$ ions (Fig. 6.19).

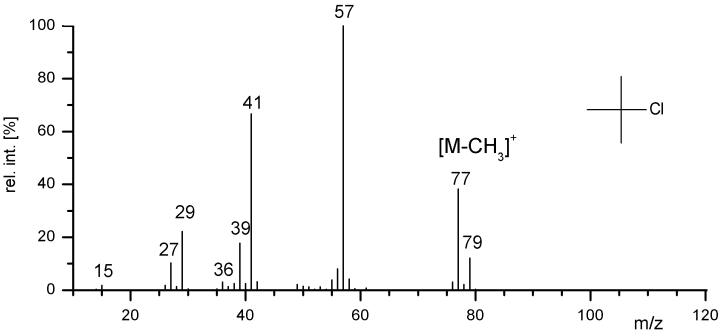


Fig. 6.20. EI mass spectrum of *tert*-butylchloride. Spectrum used by permission of NIST. © NIST 2002.

Besides alkene loss requiring sufficient chain length to occur, the smaller carbenium ions such as ethyl, propyl, or butyl ion exhibit remarkable dehydrogenation (Chap. 6.2.4.). These single and even double H_2 elimitations lead to the observation of characteristic accompanying peak patterns at *m/z*–2 and *m/z*–4, i.e., at the low-mass side of the corresponding carbenium ion peak.

Dirarylmethyl and triarylmethyl ions (trityl ions) are even more stable than the *tert*-butyl ion which is impressively demonstrated by the commercial availability of solid $[Ph_3C]^+[BF_4]^-$ and similar salts. Triphenylchloromethane dissociates in polar, inert solvents such as SO_2, and therefore, it is not surprising that EI spectra of triphenylmethyl compounds almost exclusively exhibit this ion together with some of its fragments, whereas the molecular ion peak is usually absent. Field desorption avoids this problem (Chap. 8.5).

6.6.3 Very Large Hydrocarbons

The mass spectra of very large hydrocarbons obey the same rules as their lower-mass counterparts. However, their peculiarities are worth mentioning. In case of linear chains, the EI spectrum shows an evenly expanding series of carbenium ion fragments of ever decreasing intensity. Given a clean background, the molecular ion (< 1% rel. int.) can be well recognized at even *m/z* followed by the first fragment ion, $[M-29]^+$ (Fig. 6.21).

Very large branched alkanes, such as 24,24-diethyl-19,29-dioctadecylheptatetracontane, $C_{87}H_{176}$, pose difficulties in obtaining useful mass spectra. Even 15-eV EI conditions are not sufficient for the detection of their molecular ions [72]. Beyond C_{40} alkanes, especially in case of mixtures such as hydrocarbon waxes or

polyethylenes of low molecular weight, field desorption and matrix-assisted laser desorption/ionization are the ionization methods of choice (Chaps. 8, 11).

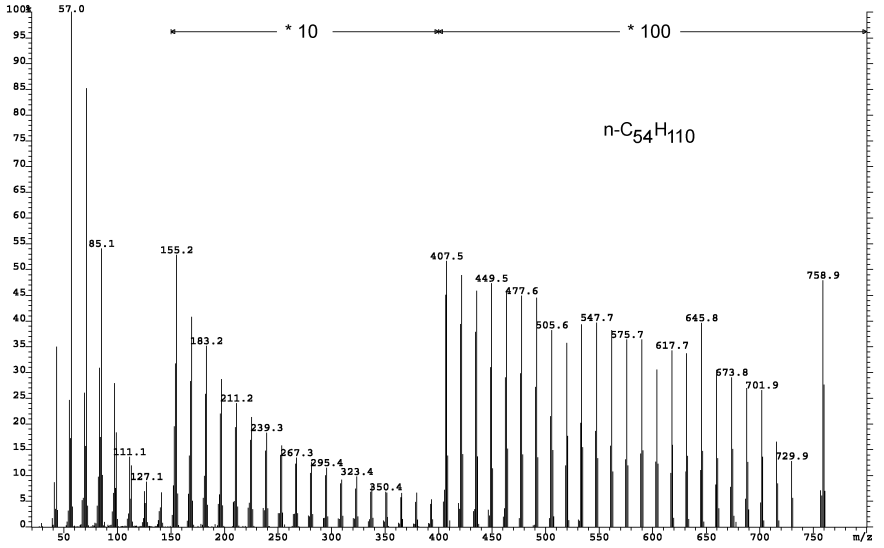


Fig. 6.21. DEI mass spectrum of tetrapentacontane, *n*-$C_{54}H_{110}$. The intensity scale is shown 10-fold from *m/z* 150–400 and 100-fold above *m/z* 400. Note how the first decimal of the *m/z* values continuously rises with increasing *m/z*. By courtesy of W. Amrein, Labor für Organische Chemie, ETH Zürich.

Note: The first decimal of the *m/z* values of carbenium ions continuously rises with increasing *m/z* as a result of the negative mass defect of hydrogen (Chap. 3.3). Theoretically from $C_{32}H_{65}^+$ onwards (*m/z* 449.5081), rounding of the *m/z* value causes a shift to the next integer *m/z*, and thus result in confusion due to the nitrogen rule. Therefore, integer *m/z* values should not be used above *m/z* 400; instead use of the decimal is recommended also for LR-MS.

6.6.4 Recognition of the Molecular Ion Peak

The molecular ion peak directly provides valuable information on the analyte. Provided the peak being of sufficient intensity, in addition to mere molecular mass, the accurate mass can reveal the molecular formula of the analyte, and the isotopic pattern may be used to derive limits of elemental composition (Chaps. 3.2 and 3.3). Unfortunately, the peak of highest *m/z* in a mass spectrum must not necessarily represent the molecular ion of the analyte. This is often the case with EI spectra either as a result of rapidly fragmenting molecular ions or due to thermal decomposition of the sample (Chap. 6.10) In general, the stability of the molecular

ion increases if π-bonding electrons for the delocalization of the charge are available and it decreases in the presence of preferred sites for bond cleavage.

Rule of thumb: The stability of molecular ions decreases roughly in the following order: aromatic compounds > conjugated alkenes > alkenes > alicyclic compounds > carbonyl compounds > linear alkanes > ethers > esters > amines > carboxylic acids > alcohols > branched alkanes [73].

In EI mass spectrometry, the molecular ion peak can be increased to a certain degree by measuring at low electron energy and ion source temperature (Chap. 5.1.5). However, some compounds thermally decompose prior to evaporation or simply cannot form nondissociating molecular ions at all. The use of soft ionization methods is often the best way for coping with these problems. Unfortunately, even for the softest ionization method, there is no guarantee that the peak at highest *m/z* corresponds to molecular mass.

In order to derive reliable analytical information, it is therefore important to have some criteria at hand to identify the molecular ion peak.

1. The molecular ion must be the ion of highest *m/z* in the mass spectrum (besides the corresponding isotopic peaks).
2. It has to be an odd-electron ion, $M^{+\bullet}$.
3. Peaks at the next lower *m/z* must be explainable in terms of reasonable losses, i.e., of common radicals or molecules. Signals at M–5 to M–14 and at M–21 to M–25 point towards a different origin of the presumed $M^{+\bullet}$ (Table 6.11).
4. Fragment ions may not show isotopic patterns due to elements that are not present in the presumed molecular ion.
5. No fragment ion may contain a larger number of atoms of any particular element than the molecular ion does.

Table 6.11. Commonly observed neutral losses from molecular ions

$[M–X]^+$	Radicals	$[M–XY]^{+\bullet}$	Molecules
–1	$H^\bullet$	–2	H_2
–15	$CH_3^\bullet$	–4	$2 \times H_2$
–17	$OH^\bullet$	–18	H_2O
–19	$F^\bullet$	–20	HF
–29	$C_2H_5^\bullet$	–27	HCN
–31	$OCH_3^\bullet$	–28	CO, C_2H_4, (N_2)
–33	$SH^\bullet$	–30	$H_2C{=}O$, NO
–35	$Cl^\bullet$	–32	CH_3OH
–43	$C_3H_7^\bullet$, $CH_3CO^\bullet$	–34	H_2S
–45	$OC_2H_5^\bullet$, $COOH^\bullet$	–36	HCl
–57	$C_4H_9^\bullet$	–42	C_3H_6, $H_2C{=}C{=}O$
–79	$Br^\bullet$	–44	CO_2
–91	$C_7H_7^\bullet$	–46	C_2H_5OH, NO_2
–127	$I^\bullet$	–60	CH_3COOH

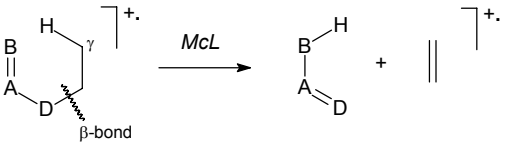
Example: The EI mass spectrum of 2,5,5-trimethylheptane (Fig. 6.18) shows no molecular ion peak. The peak of highest *m/z* is at *m/z* 113, which either demands for a nitrogen or its interpretation as a fragment ion. The remaining mass spectrum does not reveal any hint for nitrogen-containing ions, e.g., immonium ions are absent. Instead, the spectrum suggests that there are carbenium ions and their accompanying fragments only. Thus, the peak at *m/z* 113 should be due to a fragment ion, most probably created by loss of $C_xH_y^{\bullet}$. Here, it is explained as $[M–Et]^+$. However, $[M–Me]^+$ and other alkyl losses should also be taken into account.

6.7 McLafferty Rearrangement

Up to here, we have mainly discussed mass spectral fragmentations along the guideline of radical loss by simple cleavages, occasionally making some steps aside to learn about compound-specific reactions where appropriate. Next, we shall examine some pathways of alkene loss from molecular ions. Any loss of an intact molecule belongs to the rearrangement type of fragmentations. Among these, the *γ-H shift with β-cleavage*, commonly known as *McLafferty rearrangement (McL)*, surely is the most prominent.

6.7.1 McL of Aldehydes and Ketones

The loss of alkenes from molecular ions of carbonyl compounds was noticed early on [19,74]. Soon, a mechanism involving γ-H shift and β-cleavage was proposed and studied in detail [21,22,75,76]. Strictly speaking, the term *McLafferty rearrangement* (McL) only describes an alkene loss from molecular ions of saturated aliphatic aldehydes, ketones, and carboxylic acids, the mechanism of which is analogous to the Norrish type-II photofragmentation in condensed-phase chemistry. However, a more generous use of the term to include all alkene losses essentially following this mechanism is useful for the recognition of analogies from a wide variety of molecular ions. Below, any fragmentation that can be described as a transfer of a γ-hydrogen to a double-bonded atom through a six-membered transition state with β-bond cleavage is regarded as McLafferty rearrangement [77,78]: The requirements for McL in a broad sense are that *i*) the atoms A, B, and D can be carbons or heteroatoms, *ii*) A and B must be connected by a double bond, *iii*) at least one γ-hydrogen is available that *iv*) is selectively transferred to B via a six-membered transition state, *v*) causing alkene loss upon cleavage of the β-bond. In addition to these general requirements, the distance between the γ-hydrogen and the double-bonded atom must be less than 1.8×10^{-10} m [79,80] and the C_γ–H bond must be in plane with the acceptor group [81].



Scheme 6.34.

Example: The EI mass spectrum of butanal mainly shows carbenium fragment ions due to simple bond cleavage that can be easily recognized from their odd-numbered *m/z* values. Only the base peak is represented by a $[M–28]^{+\bullet}$ ion, *m/z* 44, obviously resulting from rearrangement.

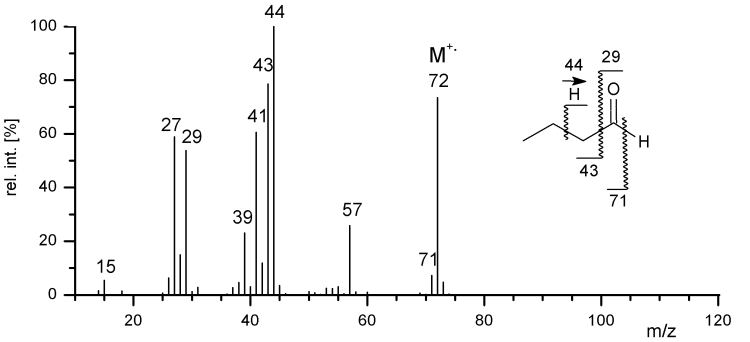
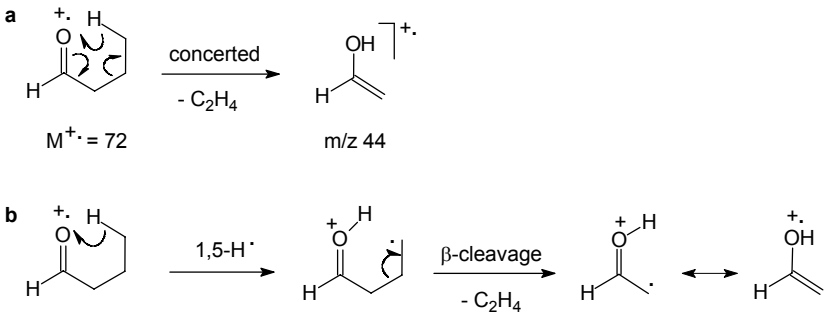


Fig. 6.22. EI mass spectrum of butanal. The base peak at *m/z* 44 is caused by the product of the McLafferty rearrangement. Note that here the peak at *m/z* 57 cannot result from $[C_4H_9]^+$, but is due to $[M–CH_3]^+$. Spectrum used by permission of NIST. © NIST 2002.

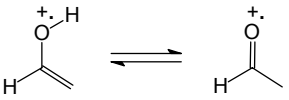
Following the above general description of the McLafferty rearrangement, the peak at *m/z* 44 in the mass spectrum of butanal can be explained by C_2H_4 loss from the molecular ion. The process may either be formulated in a concerted manner (**a**) or as a stepwise process (**b**):



Scheme 6.35.

While the concerted pathway has been preferred in early publications on the subject, evidence for a stepwise mechanism involving distonic ion intermediates is presented in more recent work taking kinetic isotope effects into account [82]. This is also in agreement with the postulation that reactions involving multiple bonds are generally stepwise processes [34,83]. Nevertheless, this question is still a matter of debate [82].

In principle, the enolic fragment ion may or may not tautomerize to the keto form before further fragmentation takes place:



Scheme 6.36.

The gas-phase heats of formation of several enol positive ions of aliphatic aldehydes, ketones, acids, and esters were measured and compared with those of the corresponding keto ions. The enolic ions were found to be thermodynamically more stable by 58–129 kJ mol^{-1}. This is in marked contrast to the neutral tautomers, in which the keto forms are generally more stable [84]. The experimental findings also are in good agreement with MNDO calculations [85], and support the hypothesis that reketonization does not play a major role for further fragmentation. Anyway, it is helpful to consider tautomerization when seeking for subsequent decomposition pathways.

The McLafferty rearrangement itself proceeds via charge retention, i.e., as alkene loss from the molecular ion, but depending on the relative ionization energies of the respective enol and alkene products, the charge migration product, i.e., the corresponding alkene molecular ion is also observed, e.g., $C_2H_4^{+\bullet}$, *m/z* 28, in the EI spectrum of butanal.

The occurrence of the McLafferty rearrangement is strictly limited to molecular ions possessing at least one γ-hydrogen for transfer to the terminal atom at the double bond. Thus, blocking the γ-position, e.g., by introduction of alkyl or halogen substituents, effectively excludes this dissociation pathway.

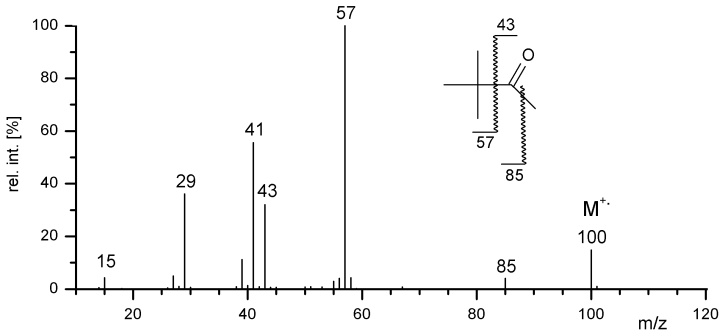
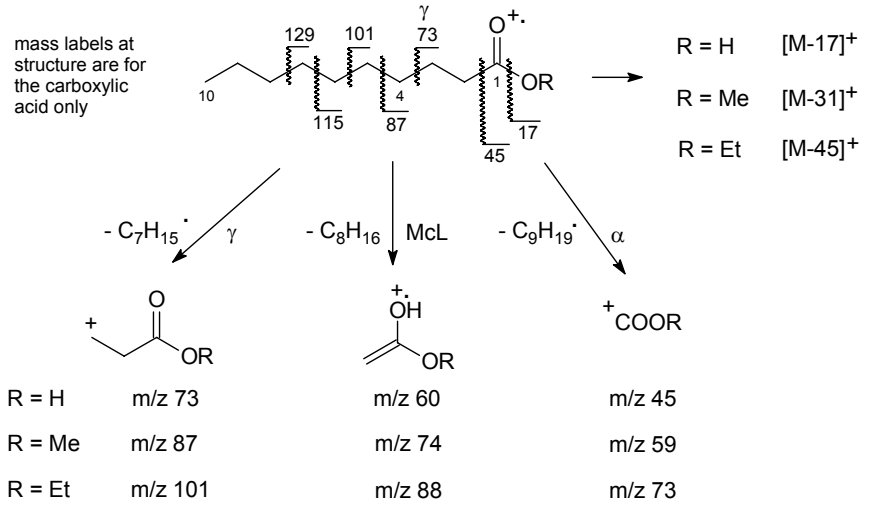


Fig. 6.23. EI spectrum of 3,3-dimethyl-2-butanone. The McLafferty rearrangement is suppressed, because there is no γ-hydrogen. Spectrum by permission of NIST. © NIST 2002.

Example: In the EI mass spectrum of 3,3-dimethyl-2-butanone no fragment ion due to McLafferty rearrangement can be observed, because there is no γ-hydrogen available (Fig. 6.23). Instead, the products are exclusively formed by simple cleavages as evident from their odd-numbered *m/z* values. The highly stable *tert*-butyl ion, *m/z* 57, predominates over the acylium ion at *m/z* 43 (Chap. 6.6.2).

6.7.2 Fragmentation of Carboxylic Acids and Their Derivatives

The mass spectra of carboxylic acids and their derivatives are governed by both α-cleavage and McLafferty rearrangement. As expected, α-cleavage may occur at either side of the carbonyl group causing $OH^{\bullet}$ loss, $[M–17]^+$, or alternatively alkyl loss. Whereas the α-cleavages can even be observed for formic acid where they are leading to $[M–OH]^+$, *m/z* 29, $[M–H]^+$, *m/z* 45, and the respective charge migration products, the McLafferty rearrangement can only occur from butanoic acid and its derivatives onwards [74]. Analogous to aliphatic aldehydes, the same fragment ions are obtained for a homologous series of carboxylic acids, provided they are not branched at the α-carbon. Thus, highly characteristic fragment ions make their recognition straightforward.



Scheme 6.37.

Example: The molecular ion of decanoic acid, $C_{10}H_{20}O_2^{+\bullet}$, preferably eliminates octene via McLafferty rearrangement yielding $C_2H_4O_2^{+\bullet}$, *m/z* 60, as the base peak of the spectrum (Fig. 6.24). This process is accompanied by several σ-bond cleavages among which cleavage of the γ-bond is clearly favored. Resulting from α-cleavage, $OH^{\bullet}$ loss can be expected, but is often represented by a very minor peak in the spectra of carboxylic acids. The other product, $[M–R]^+$, $COOH^+$,

m/z 45, is almost always observed together with the complementary $[M–45]^+$ ion, both of which normally belong to the ions of low abundance.

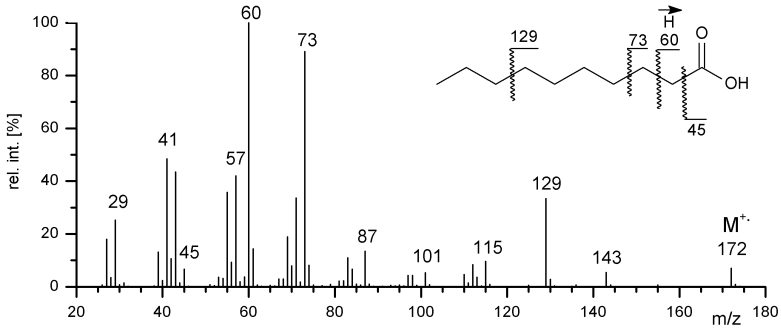


Fig. 6.24. EI mass spectrum of decanoic acid. Used by permission of NIST. © NIST 2002.

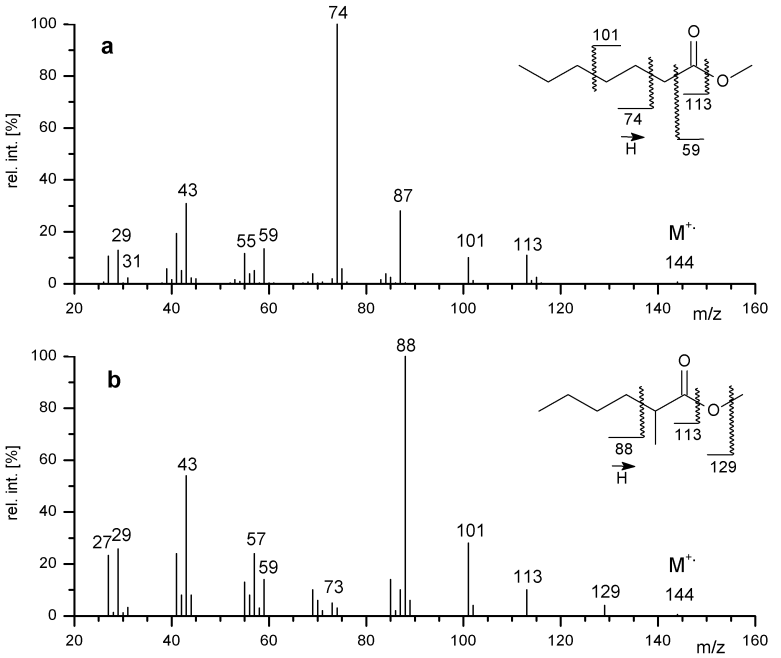
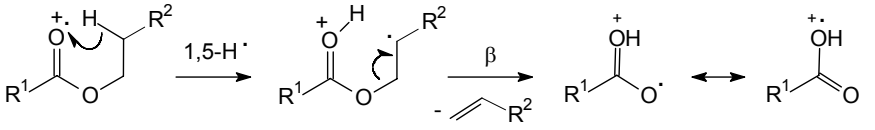


Fig. 6.25. EI mass spectra of methyl heptanoate (**a**) and methyl 2-methylhexanoate (**b**). Spectra used by permission of NIST. © NIST 2002.

In aliphatic esters the fragments typical for carboxylic acids are shifted by 14 u to higher mass upon transition from the free acid to the methyl ester and by further 14 u for the ethyl ester [77,78,86,87].

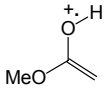
Examples: The mass spectrum of methyl heptanoate nicely meets the standard, and thus all peaks may be explained according to Scheme 6.37 (Fig. 6.25a). In principle, the same is true for the isomeric methyl 2-methylhexanoate, but here care has to be taken not to interpret the mass spectrum as belonging to an ethyl ester. This is because the 2-methyl substituent resides on the ionic products of McLafferty rearrangement and γ-cleavage, shifting both of them 14 u upwards. Nevertheless, a glance at the α-cleavage products, $[M–OMe]^+$ and $[COOMe]^+$, *m/z* 59, reveals the methyl ester.

For carboxylic acid ethyl and longer-chain aliphatic esters the McLafferty rearrangement can also occur on the alkoxy branch (R^2) of the molecular ion. It then competes as a second alkene loss with the reaction at R^1:



Scheme 6.38.

Table 6.12. Frequent product ions of the McLafferty rearrangement

Precursor	Product structure	Formula	Accurate mass [u][a]
Aldehyde		$C_2H_4O^{+\bullet}$	44.0257
Alkyl methyl ketone		$C_3H_6O^{+\bullet}$	58.0413
Carboxylic acid		$C_2H_4O_2^{+\bullet}$	60.0206
Carboxylic acid amide		$C_2H_5NO^{+\bullet}$	59.0366
Methyl carboxylates		$C_3H_6O_2^{+\bullet}$	74.0362
Ethyl carboxylates		$C_4H_8O_2^{+\bullet}$	88.0519

[a] values rounded to four decimals

Example: The base peak at *m/z* 88 in the mass spectrum of ethyl hexanoate results from butene loss from the molecular ion, $M^{+\bullet}$, *m/z* 144, via McLafferty rearrangement. This product ion may then undergo ethene loss to yield the fragment ion at *m/z* 60. The remaining fragments can be rationalized by propyl loss via γ-

cleavage, $[M–Pr]^+$, *m/z* 101, and α-cleavage products, $[M–OEt]^+$, *m/z* 99, respectively. The carbenium ions representing the alkyl portion of the molecule are formed by σ-bond cleavages.

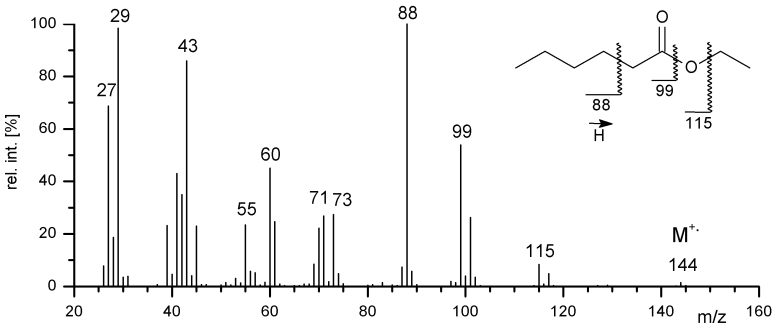
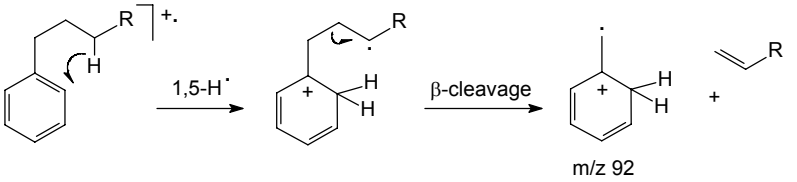


Fig. 6.26. EI spectrum of ethyl hexanoate. Used by permission of NIST. © NIST 2002.

6.7.3 McL of Aromatic Hydrocarbons

In addition to the previously described benzylic and phenylic cleavages (Chap. 6.4), phenylalkanes may undergo alkene loss by a mechanism that is perfectly analogous to the "true" McLafferty rearrangement, provided the alkyl substituent fulfills all requirements. The γ-hydrogen is transferred to the *ortho*-position where the aromatic ring serves as the accepting double bond:



Scheme 6.39.

Independent of the alkyl substituent, $[C_7H_8]^{+\bullet}$, *m/z* 92, is obtained as the product ion, provided there are no other substituents at the ring. The product is an isomer of toluene molecular ion, and as such it readily stabilizes by $H^\bullet$ loss to yield the even-electron $[C_7H_7]^+$ species, *m/z* 91, which then produces the well-known characteristic fragments (*m/z* 65, 39). Provided that there is no prior isomerization of the molecular ion, this dissociation is prohibited if both *ortho*-positions are substituted and/or if there is no γ-hydrogen in the alkyl group.

Example: The base peak in the EI mass spectrum of (3-methylpentyl)-benzene is formed by McLafferty rearrangement of the molecular ion (Fig. 6.27). As long as pentene loss may occur, there is not much difference to spectra of isomers like 2-methylpentyl-, 4-methylpentyl, or *n*-hexyl. Reference spectra are needed for dis-

tinguishing between those isomers, because the spectra only differ in relative peak intensities.

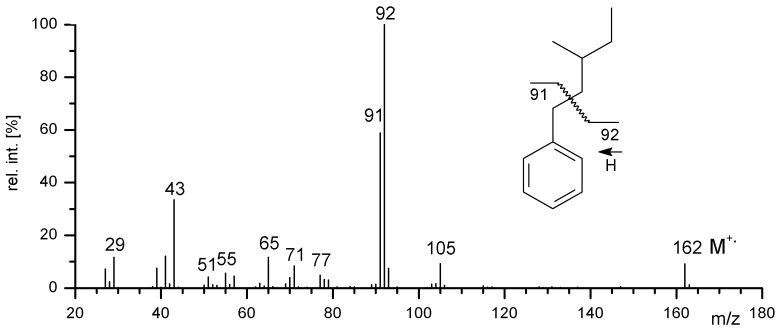


Fig. 6.27. EI mass spectrum of (3-methylpentyl)-benzene. McLafferty rearrangement and benzylic cleavage are clearly dominating. In the low-mass range carbenium ions and the "aromatic fragments" are present. Spectrum used by permission of NIST. © NIST 2002.

In case of alkyl benzylethers, aldehyde loss can occur following the same reaction pathway. For example, acetaldehyde is eliminated from the molecular ions of benzylethylether, thus producing $[C_7H_8]^{+\bullet}$ fragment ions. Again, evidence has been presented for a stepwise mechanism involving a distonic intermediate [88].

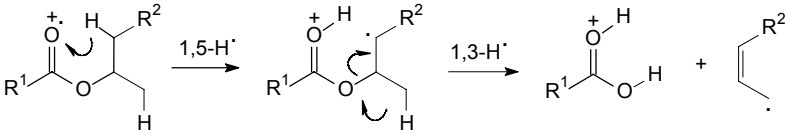
6.7.4 McL with Double Hydrogen Transfer

Alkene loss via McLafferty rearrangement at the alkoxy group of aliphatic and aromatic carboxylic acid esters competes with yet another reaction path, where two hydrogens instead of one as in the "normal McLafferty product" are transferred to the charge site. This second pathway leading to alkenyl loss has early been noticed [86] and has become known as *McLafferty rearrangement with double hydrogen transfer* (*r2H*):

$$[R^1COOR^2]^{+\bullet} \xrightarrow{r2H} [R^1C(OH)_2]^{+} + [R^2\text{-}2H]^{\bullet}$$

Scheme 6.40.

Labeling studies indicate that this process is by far not as site-specific as its better known counterpart [89,90]. Based on thermochemical data, evidence has been presented for a two-step mechanism that finally yields a carbonyl-protonated carboxylic acid and the unsaturated radical. While the final products are well described, the second step has not fully been elucidated [91,92]:



Scheme 6.41.

Example: The competition of alkene and alkenyl loss is demonstrated by the presence of peaks at *m/z* 122 (*McL*) and *m/z* 123 (*r2H*) in the EI mass spectrum of isopropyl benzoate (Fig. 6.28) [92]. Of course, both primary fragmentations are competing with the predominating α-cleavage at the carbonyl group yielding the highly characteristic *benzoyl ion*, $[C_7H_5O]^+$, *m/z* 105 [93]. The benzoyl ion, essentially an aromatic acylium ion, dissociates by CO loss to yield the phenyl ion, *m/z* 77, and finally by C_2H_2 loss the cyclobutadienyl ion, *m/z* 51 (Chap. 6.4.2).

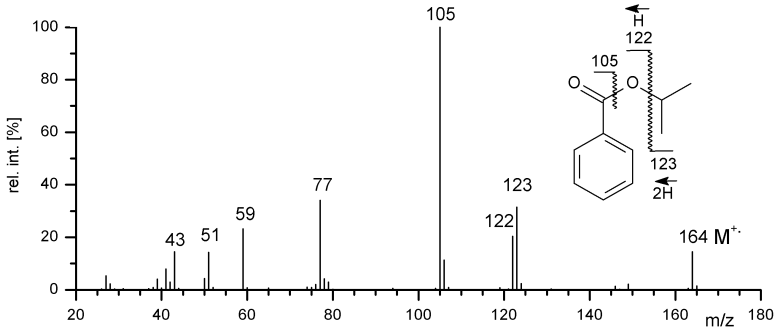
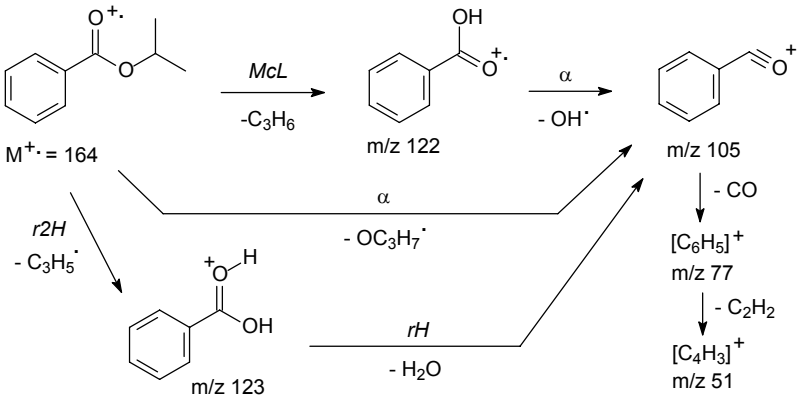


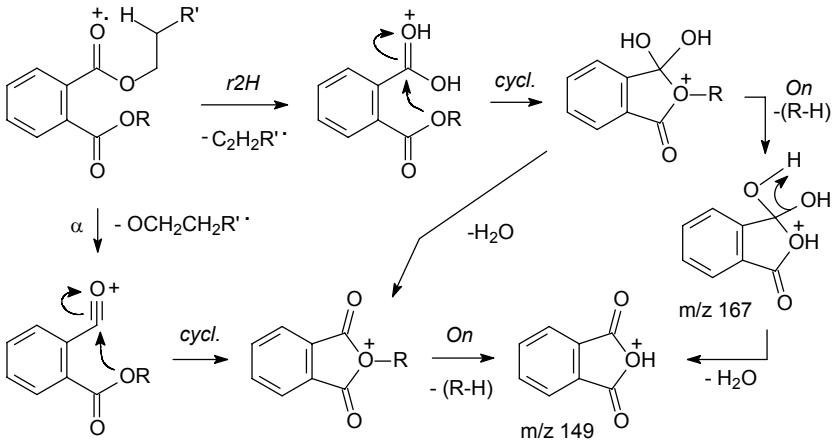
Fig. 6.28. EI spectrum of isopropyl benzoate. Used by permission of NIST. © NIST 2002.



Scheme 6.42.

Note: The ion series *m/z* 51, 77, 105 is a reliable indicator for benzoyl substructures, e.g., from benzaldehyde, benzoic acid and its derivatives, acetophenone, benzophenone etc. In contrast to benzylic compounds, the peaks at *m/z* 39, 65, and 91 are almost absent. If a peak at *m/z* 105 and the complete series *m/z* 39, 51, 65, 77, 91 are present, this strongly points towards the composition $[C_8H_9]^+$, and thus to phenylalkanes. In case of doubt, HR-MS is the method of choice for their differentiation.

The fragment ions at *m/z* 149, $[C_8H_5O_3]^+$, and 167, $[C_8H_7O_4]^+$, are especially prominent in the EI spectra of phthalates. The formation of the $[C_8H_5O_3]^+$ ion has initially been attributed to a McLafferty rearrangement followed by loss of an alkoxy radical and final stabilization to a cyclic oxonium ion [94]. However, it has been revealed that four other pathways in total lead to its formation excluding the above one [95,96]. The most prominent fragmentation pathways are:



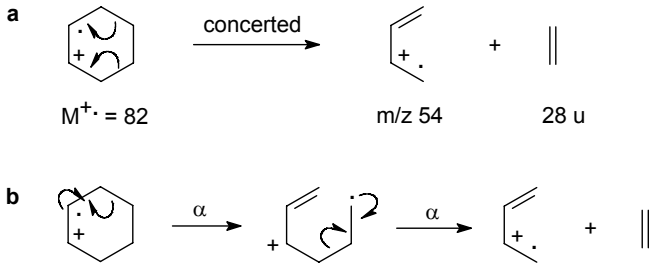
Scheme 6.43.

Note: Phthalates, especially di-2-ethylhexyl phthalate (also known as dioctyl phthalate, DOP), are commonly used plasticizers in synthetic polymers. Unfortunately, they are extracted from the polymers upon exposure to solvents such as dichloromethane, chloroform, or toluene, e.g., from syringes, tubing, vials etc. Therefore, they are often detected as impurities. They are easily recognized from their peaks at *m/z* 149 (often base peak), *m/z* 167, and $[M–(R–2H)]^+$ (*m/z* 279 in case of DOP). The molecular ion is often absent in their EI spectra.

6.8 Retro-Diels-Alder Reaction

6.8.1 Properties of the Retro-Diels-Alder Reaction

Molecular ions containing a cyclohexene unit may fragment to form conjugated di-olefinic (*diene*) and mono-olefinic (*ene*) products. This fragmentation pathway was first recognized by Biemann as formally analogous to the retro-Diels-Alder (RDA) reaction of neutrals in the condensed phase [73]. The fragmentation can in principle proceed in a concerted manner (**a**) or stepwise, i.e., it can be regarded as a double α-cleavage with the first being an allylic cleavage (**b**):



Scheme 6.44.

Note: The McLafferty rearrangement and the RDA reaction have several features in common: *i*) both belong to the rearrangement type of fragmentations, although the name conceals this fact in case of the latter, *ii*) both represent pathways for alkene loss from molecular ions, and *iii*) both are highly versatile in structure elucidation.

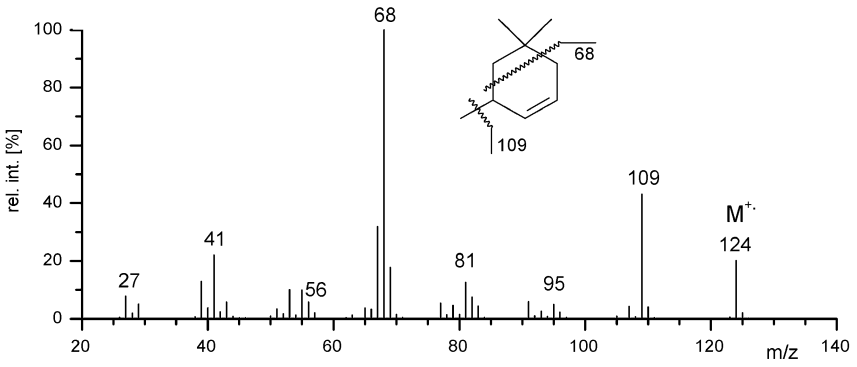
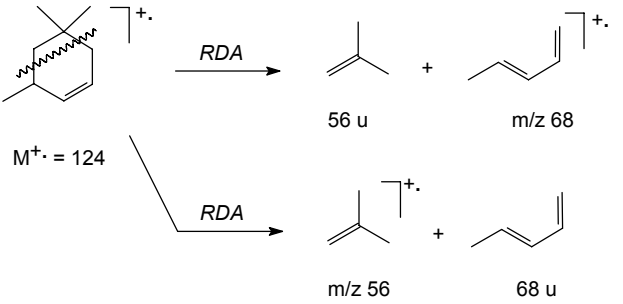


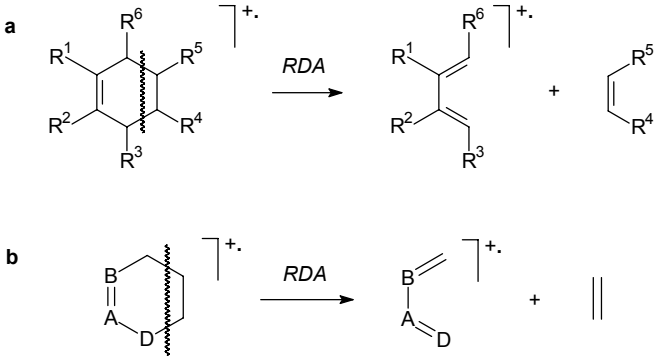
Fig. 6.29. EI mass spectrum of 3,5,5-trimethylcyclohexene. The molecular ion undergoes isobutene loss, 56 u, via RDA reaction yielding the base peak at *m/z* 68, which is also the only significant peak at even-numbered *m/z*. The charge migration product at *m/z* 56 is of low intensity. Spectrum used by permission of NIST. © NIST 2002.

As most ion dissociations, the RDA reaction is endothermic, e.g., by 185 kJ mol^{-1} in case of ethene loss from cyclohexene molecular ion [97]. The charge usually resides at the diene fragment, but the ene fragment is also frequently observed in the mass spectra (Fig. 6.29). The fraction of charge retention and charge migration products has been studied [98]. As may be expected, competition for the charge is greatly influenced by the substitution pattern of the cyclohexene derivative and by the presence or absence of heteroatoms in the respective fragments.



Scheme 6.45.

Provided the double bond does not migrate prior to RDA reaction, the alkene loss is perfectly regiospecific, and it does not really suffer from extensive substitution at the cyclohexene unit. Thus, substitution patterns can be revealed from the mass spectrum (**a**). The RDA reaction also proceeds independent of whether the six-membered ring contains heteroatoms or not (**b**):



Scheme 6.46.

Obviously, the RDA reaction has the potential needed for a widespread mass spectral fragmentation, and consequently, its analytical and mechanistical aspects have repeatedly been reviewed [97,99,100].

Note: Almost any molecular ion having a six-membered ring that contains one double bond can undergo the RDA reaction to eliminate a (substituted) alkene or a corresponding heteroanalog.

6.8.2 Influence of Positional Isomerism on the RDA Reaction

As often observed in mass spectrometry, seemingly small changes in ion structure may cause significant changes in the mass spectra of the respective analytes. This is impressively demonstrated by comparison of the mass spectra of α- and β-ionone (Fig. 6.30). While α-ionone significantly dissociates to yield the fragment ion at *m/z* 136 upon isobutene loss via RDA reaction, its isomer β-ionone mainly exhibits an intense $[M–CH_3]^+$ signal [73]. This is because the geminal methyl substituents are in allylic position to the ring double bond in the latter, and moreover, in this case methyl loss by allylic bond cleavage yields a thermodynamically favorable tertiary allyl ion.

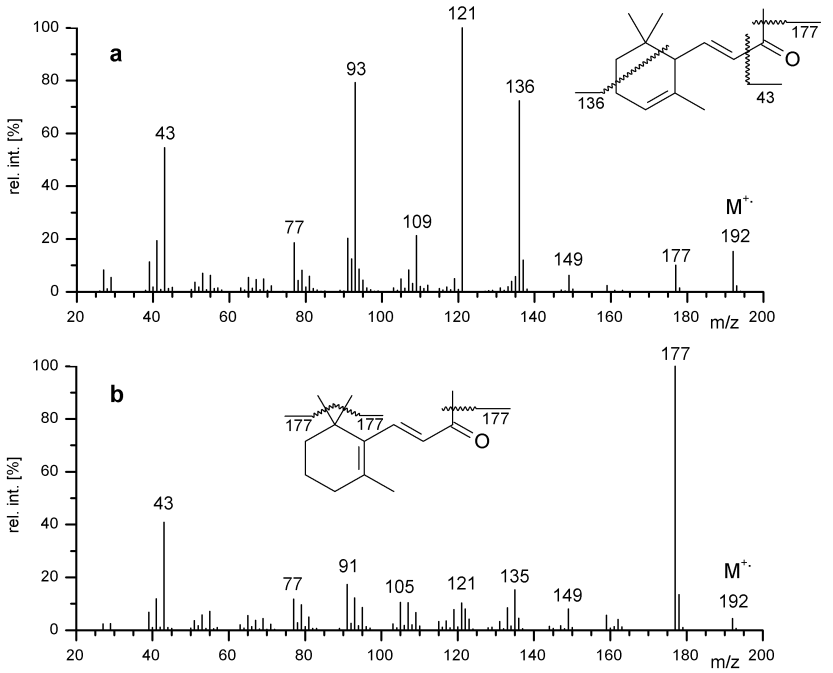
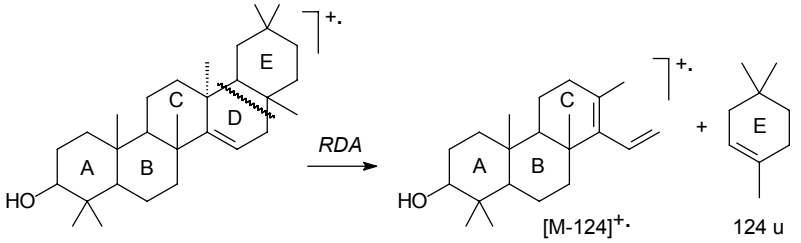


Fig. 6.30. EI mass spectra of α- (**a**) and β-ionone (**b**). RDA reaction proceeds via loss of isobutene, causing the peak at *m/z* 136 in case of α-ionone, whereas ethene loss is almost absent in the β-ionone spectrum. Spectra used by permission of NIST. © NIST 2002.

6.8.3 RDA Reaction in Natural Products

The RDA reaction is often observed from steroid molecular ions, and it can be very indicative of steroidal structure [97,100-102]. The extent of the RDA reaction depends on whether the central ring junction is *cis* or *trans*. The mass spectra of Δ^7-steroidal olefins, for example, showed a marked dependence upon the stereochemistry of the A/B ring juncture, in accordance with orbital symmetry rules for a thermal concerted process. In the *trans* isomer the RDA is much reduced as compared to the *cis* isomer. Moreoever, the differentiating effect increases at 12 eV. This represents the first example of apparent symmetry control in olefinic hydrocarbons [102].

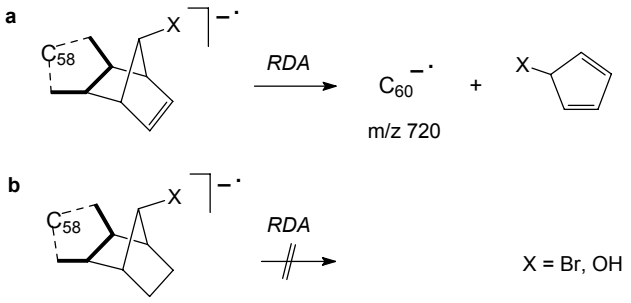
The RDA reaction is also a typical process of flavones, naphthoflavones, and methoxynaphthoflavones [103]. In many cases it provides intact A- and B-ring fragments, and therefore, it is of high relevance for structure elucidation. The intensity ratio of A- to B-ring fragments was found to be strongly influenced by the substituent position, i.e., to be very sensitive to the charge distribution within the molecular ion [104]. The pentacyclic triterpene molecular ion below also shows RDA:



Scheme 6.47.

6.8.4 Widespread Occurrence of the RDA Reaction

Any molecule that can at least formally be synthesized by a Diels-Alder reaction is a potential candidate for the mass spectral RDA reaction. In addition, the RDA reaction is not restricted to positive radical ions, but it may also occur from even-electron ions as well as from negative radical ions, $M^{-\bullet}$. These findings remind us of the fact that ionic reactions are determined by the intrinsic properties and the internal energy of the ions, and thus only indirectly by the ionization technique used for their creation.



Scheme 6.48.

Example: Certain [60]fullerene derivatives can be regarded as formal Diels-Alder adducts of [60]fullerene with cyclopentadienes. Their positive as well as negative radical ions undergo RDA reaction at extremely high rates almost precluding the detection of a molecular ion. Instead, $C_{60}^{+\bullet}$ and $C_{60}^{-\bullet}$ are detected [105,106]. However, using negative-ion FAB or MALDI allows for the detection of $M^{-\bullet}$ and the RDA product (**a**). Removal of the double bond by hydrogenation causes this fragmentation pathway to vanish (**b**) and enables the detection of intense molecular anions [105].

6.9 Elimination of Carbon Monoxide

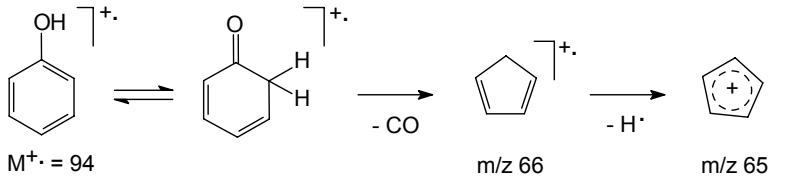
The elimination of small stable molecules represents a frequent fragmentation route of odd- and even-electron ions. Second to alkene loss, we will consider some of the numerous pathways for loss of carbon monoxide, CO. In contrast to the preceding reactions, CO does not follow a single mechanism. Instead, a wide range of molecular and fragment ions can undergo loss of CO. Therefore, this is rather a compound-specific view in the context of CO loss than a collection of compounds exhibiting a certain reaction mechanism. In retrospect, we actually already have encountered some CO losses (Chap. 6.2.4. and 6.7.4).

6.9.1 CO Loss from Phenols

Phenols exhibit a strong molecular ion peak often representing the base peak in their spectra. The most characteristic fragment ions of phenols are caused by loss of CO from the molecular ion [107], and subsequent $H^{\bullet}$ loss, thereby forming $[M–28]^{+\bullet}$ and $[M–29]^{+}$ ions, respectively (Fig. 6.31), the identity of which have been ascertained by HR-MS as $[M–CO]^{+\bullet}$ and $[M–CHO]^{+}$. [108] This initially unexpected fragmentation proceeds via ketonization of the molecular ion prior to elimination of CO. The mechanism has been verified by D-labeling. These experiments also revealed that only about one third of the $H^{\bullet}$ cleaved off from the

cyclopentadiene ion, *m/z* 66, originates from the former OH, whereas the majority is derived from the ring [109].

Note: The above mechanism of CO loss from phenols is perfectly analogous to HCN loss from aniline and other aminoarenes (Chap. 6.14.2).



Scheme 6.49.

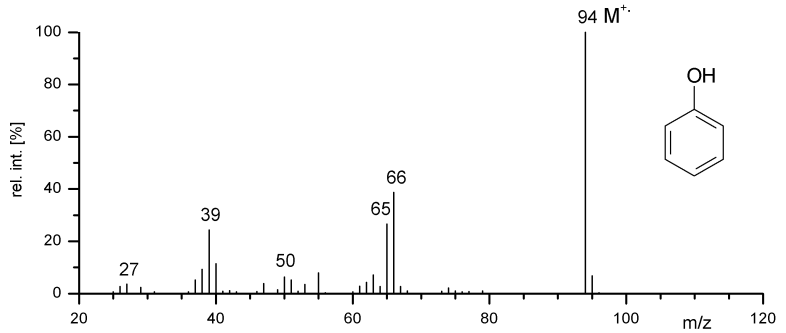
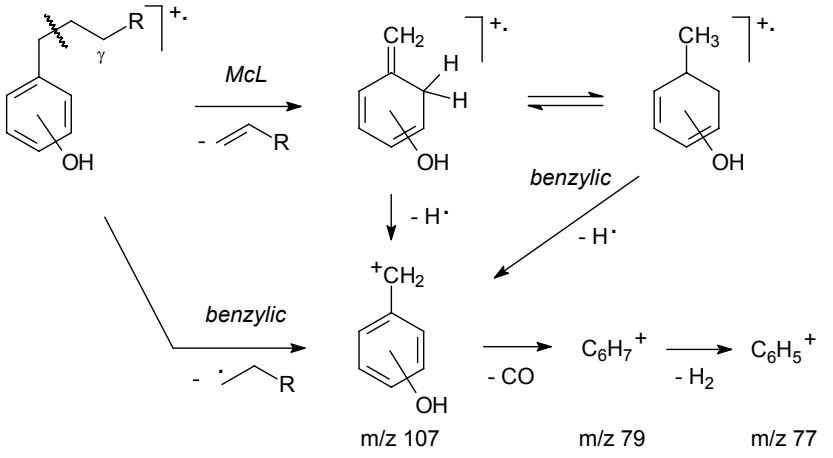


Fig. 6.31. EI mass spectrum of phenol showing an intense peak due to CO loss at *m/z* 66. Spectrum used by permission of NIST. © NIST 2002.



Scheme 6.50.

Alkylphenol molecular ions preferably dissociate by benzylic bond cleavage, e.g., $[M–H]^+$ ions are observed in case of methylphenols. Provided a γ-hydrogen is available in alkyl substituents of sufficient chain length, the benzylic bond cleavage competes with the McLafferty rearrangement [110], the product ion of this being an isomer of methylphenol molecular ion. Loss of $H^•$ from the latter yields a $[C_7H_7O]^+$ ion, *m/z* 107, that may dissociate further by CO loss, thus forming a protonated benzene ion, $[C_6H_7]^+$, *m/z* 79. This tells us that CO loss occurs equally well from even-electron phenolic ions.

Example: Ethyl loss clearly predominates over methyl loss in the EI mass spectrum of 2-(1-methylpropyl)phenol. It proceeds via benzylic bond cleavage, the products of which are detected as the base peak at *m/z* 121 and *m/z* 135 (3%), respectively (Fig. 6.32a). The McLafferty rearrangement does not play a role, as the peak at *m/z* 122 (8.8%) is completely due to the ^{13}C isotopic contribution to the peak at *m/z* 121. From the HR-EI spectrum (Fig. 6.32b) the alternative pathway for the formation of a $[M–29]^+$ peak, i.e., $[M–CO–H]^+$, can be excluded, because the measured accurate mass of this singlet peak indicates $C_8H_9O^+$. HR-MS data also reveal that the peak at *m/z* 107 corresponds to $[M–CH_3–CO]^+$ and that the one at *m/z* 103 corresponds to $[M–C_2H_5–H_2O]^+$. Although perhaps unexpected, the loss of H_2O from phenolic fragment ions is not unusual.

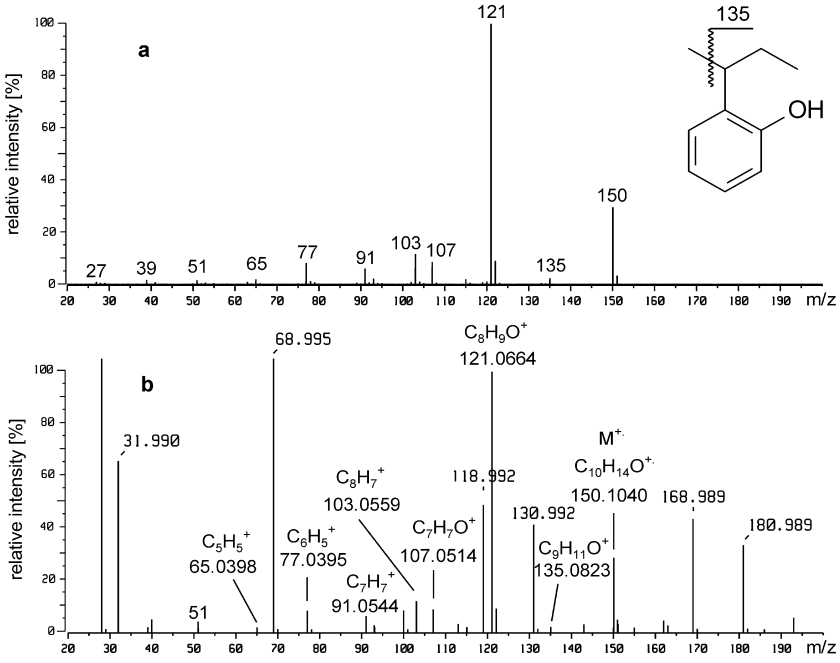
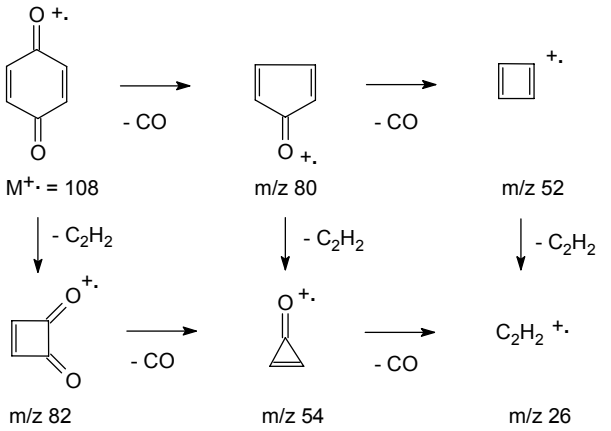


Fig. 6.32. LR- (**a**) and HR-EI (**b**) mass spectra of 2-(1-methylpropyl)phenol. The elemental compositions as obtained from accurate mass measurement are directly attached to the corresponding peaks. Peaks bearing smaller labels (e.g., 31.990) are due to PFK and residual air used for internal mass calibration (Chap. 3.3).

6.9.2 CO and C_2H_2 Loss from Quinones

Quinones [111] and aromatic ketones such as flavones [104], fluorenone, anthraquinone, and similar compounds [112] dissociate by competing and consecutive losses of CO and C_2H_2. Multiple CO losses may also occur subsequent to the RDA reaction of flavones [104]. As these molecules all have large π-electron systems to stabilize the charge, they show intense molecular ion peaks that often represent the base peak in those spectra. Typically any available carbonyl group is expelled as CO in the course of complete dissociation of the molecular ion; sometimes CO first, sometimes alternating with C_2H_2 loss.

Example: 1,4-Benzoquinone represents the perfect prototype of this fragmentation pattern. The subsequent eliminations of intact molecules causes a series comprising odd-electron fragment ions only (Fig. 6.33). This results in characteristic fragment ions from sequences such as $[M–28–26–28]^{+\bullet}$ or $[M–28–26–26]^{+\bullet}$.



Scheme 6.51.

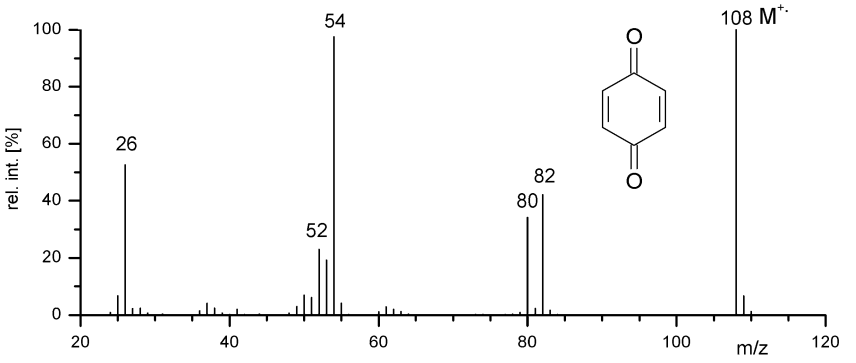
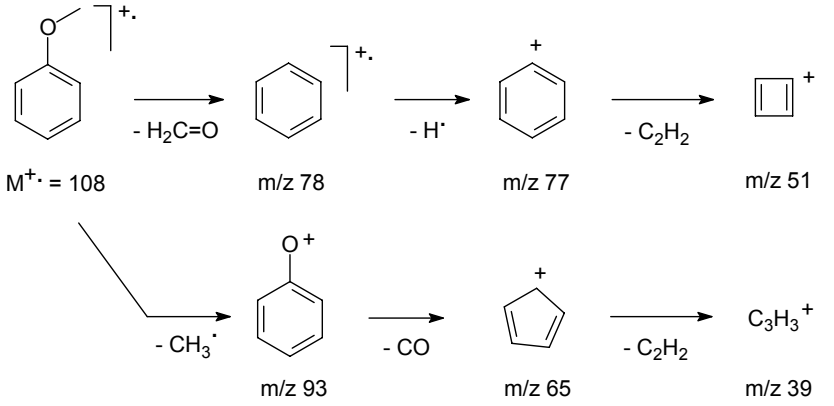


Fig. 6.33. EI mass spectrum of 1,4-benzoquinone. Spectrum used by permission of NIST. © NIST 2002.

6.9.3 Fragmentation of Arylalkylethers

The molecular ions of arylmethylethers preferably dissociate by loss of a formaldehyde molecule or by loss of the alkyl group [88,113], thereby yielding an even-electron phenolic ion, $C_6H_5O^+$, *m/z* 93, that readily expels CO (Fig. 6.34) [114,115]:



Scheme 6.52.

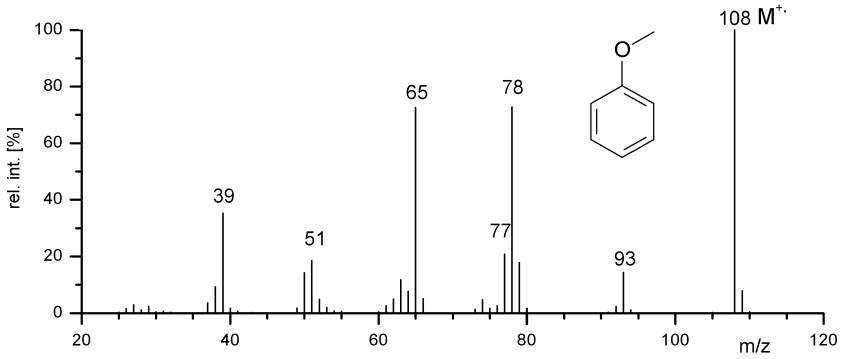


Fig. 6.34. EI mass spectrum of anisole exhibiting a strong $[M–H_2CO]^{+\bullet}$ peak at *m/z* 78. Spectrum used by permission of NIST. © NIST 2002.

Astonishingly, the study of the mechanism of formaldehyde loss from anisole revealed two different pathways for this process, one involving a four- and one a five-membered cyclic transition state (Fig. 6.35) [116]. The four-membered transition state conserves aromaticity in the ionic product, which therefore has the lower heat of formation. Prompted by the observation of a composite metastable peak, this rather unusual behavior could be uncovered by deconvolution of two different values of kinetic energy release with the help of metastable peak shape analysis (Chap. 2.8).

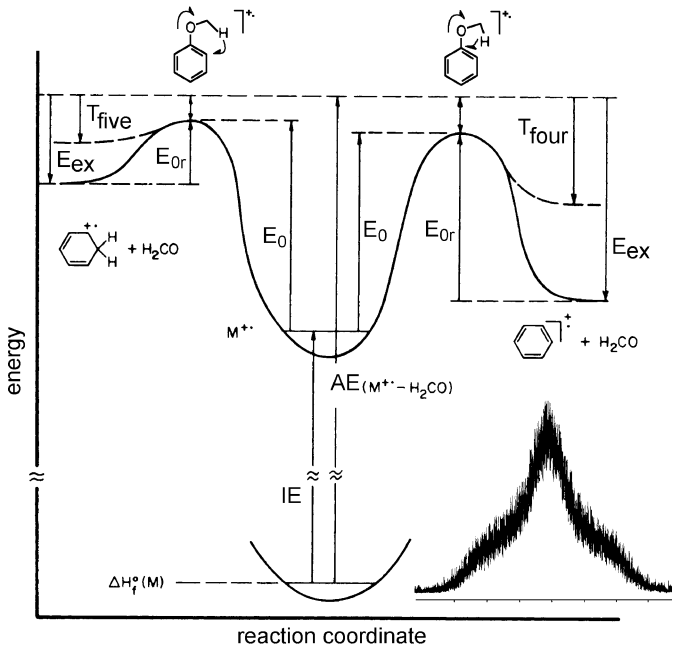


Fig. 6.35. Energetics of formaldehyde loss from anisole. The *inset* shows the composite metastable peak due to two different amounts of kinetic energy release. Adapted from Ref. [116] with permission. © American Chemical Society, 1973.

In case of longer-chain alkyl substituents, alkene loss can compete with the McLafferty rearrangement as is observed from suitably substituted phenylalkanes (Chap. 6.7.3), e.g., ethene loss from phenetole and its derivatives (Fig. 6.36) [113].

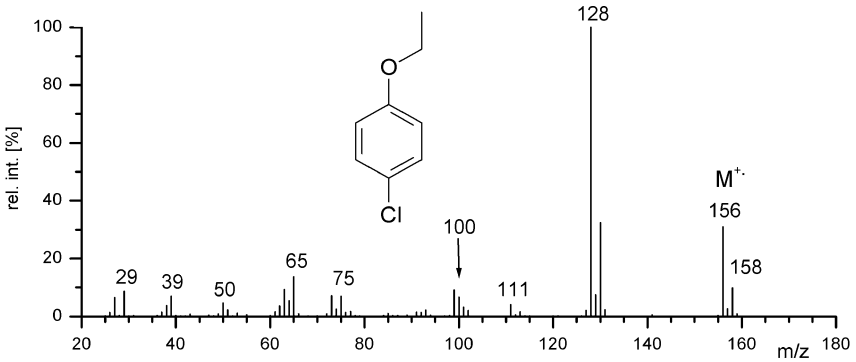
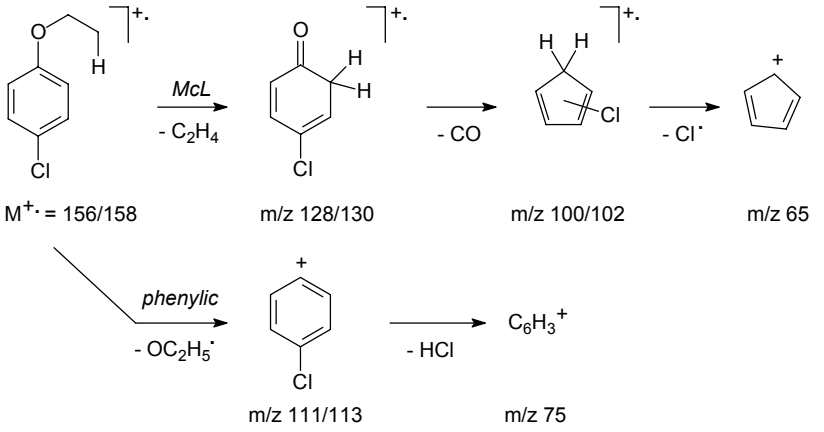


Fig. 6.36. EI mass spectrum of 4-chlorophenetole. The chlorine isotopic pattern is found in the signals corresponding to $M^{+\bullet}$, *m/z* 156, $[M–C_2H_4]^{+\bullet}$, *m/z* 128, $[M–OEt]^+$, *m/z* 111, and $[M–C_2H_4–CO]^{+\bullet}$, *m/z* 100. Spectrum used by permission of NIST. © NIST 2002.



Scheme 6.53.

6.9.4 CO Loss from Transition Metal Carbonyl Complexes

Transition metal carbonyl complexes successively eliminate all CO ligands upon electron ionization until the bare metal remains. Pure carbonyl complexes as well as many other complexes with carbonyl ligands can therefore be readily identified from their characteristic CO losses which are – dependent on the metal – often observed in combination with the eye-catching isotopic pattern of the respective metal (Fig. 6.37). According to ^{13}C-labeling experiments, extensive isomerization may precede the dissociation of the carbonyl complexes [117]. Furthermore, the different bond strength of the M–CO bond in heterometallic transition-metal dimers can be deduced from the mass spectral fragmentation pattern of the carbonyl complexes, e.g., selective ^{12}CO loss from Mn in $[Mn(CO)_5Re(^{13}CO)_5]$ has been interpreted in terms of stronger Re–CO bonds [118].

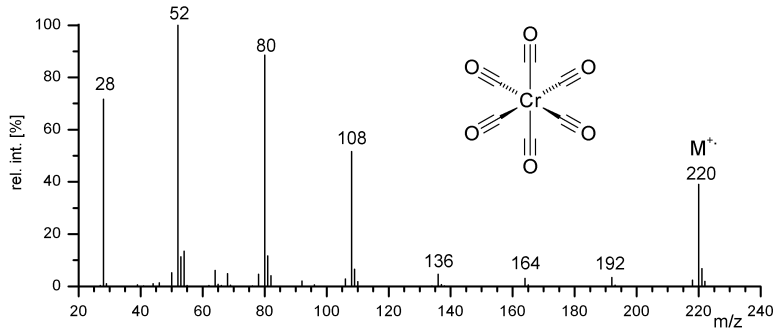


Fig. 6.37. EI mass spectrum of hexacarbonylchromium. All six CO ligands are eliminated until the bare metal ion, *m/z* 52, remains. The isotopic pattern of chromium can well be recognized from the more intense signals. Used by permission by NIST. © NIST 2002.

6.9.5 CO Loss from Carbonyl Compounds

A molecule of CO may also be eliminated from malonates [119], β-keto esters [120], phenoxyacetates [121], and many other compounds containing similar structural features. Whatever the mechanism of CO loss might be, in none of the above cases does CO loss proceed by a simple bond cleavage. Instead, multistep rearrangements are necessary to "cut" the CO moiety out of the precursor ion.

Note: The detection of CO loss from molecular or fragment ions usually indicates the presence of carbonyl groups. However, it is less indicative of molecular structure than the highly specific reactions discussed before, because a multitude of rearrangement processes can be effective. These might even lead to CO loss in cases where no carbonyl group exists, e.g., from phenols.

6.9.6 Differentiation Between Loss of CO, N_2, and C_2H_4

Carbon monoxide, CO, 27.9949 u, is a nominal isobar of ethene, C_2H_4, 28.0313 u, and nitrogen, N_2, 28.0061 u, and the separation of these gases themselves by means of HR-MS has already been described (Chap. 3.3). Accordingly, the difference in accurate mass for a given pair of peaks can be used to decide which of these neutrals has been eliminated, e.g., we employed HR-MS to uniquely identify the $[M–29]^+$ peak from 2-(1-methylpropyl)phenol as $[M–C_2H_5]^+$ (Chap. 6.9.1). The elimination of N_2, CO, and/or C_2H_4 can even occur on consecutive and competing fragmentation pathways from the very same analyte [122].

Example: The molecular ion of ethyl-*trans*-3-methyltetrazole-5-acrylate, $[C_7H_{10}O_2N_4]^{+\bullet}$, *m/z* 182.0798, exhibits two fragmentation sequences involving loss of N_2, C_2H_4, and/or CO, in different order. This way, isobaric fragment ions at *m/z* 98 and 126 are formed that cannot be distinguished by LR-MS. HR-MS resolves both signals as doublets and thus deconvolutes the competing pathways (Table 6.13) [122].

Table 6.13. Example of the differentiation of isobaric neutral losses

Generation of fragment	Type of peak	Sequence a) and *m/z*	Sequence b) and *m/z*
0th	singlet	$M^{+\bullet}$ = 182.0798	
		↓ – N_2	
1st	singlet	154.0737	
		↓ – N_2	↓ – C_2H_4
2nd	doublet	126.0675 (10%)	126.0424 (90%)
		↓ – C_2H_4	↓ – CO
3rd	doublet	98.0362 (61%)	98.0475 (39%)

Hint: In case of doubt which neutral loss(es) are effective, it is highly recommended to obtain HR-MS data to avoid ambiguities. Moreover, the differences in accurate mass for a given pair of peaks can be used to identify the neutral loss even though the composition of the ions themselves might still be unknown.

6.10 Thermal Degradation vs. Ion Fragmentation

Heating of the sample, a common procedure enforcing evaporation from the crucible placed onto a direct insertion probe, may cause unwanted reactions prior to ionization. Thus, non-mass spectral but thermal reactions can effect that the mass spectrum does not represent the analyte itself, but its decomposition product(s). Sometimes, those thermal reactions are difficult to recognize, because the same neutral loss may also occur by a true mass spectral fragmentation of the corresponding molecular ion. In even more disadvantageous circumstances, the thermal decomposition does not yield a single defined derivative, but a complex mixture of pyrolysis products. This is the case with highly polar natural products such as saccharides, nucleotides, and peptides or when ionic compounds such as organic salts or metal complexes are to be measured.

6.10.1 Decarbonylation and Decarboxylation

Thermal degradation prior to ionization can cause decarbonylation or decarboxylation of the analyte. Decarbonylation, is observed for α-ketocarboxylic acids and α-ketocarboxylic acid esters, while decarboxylation is typical for β-oxocarboxylic acids such as malonic acid and its derivatives and di-, tri-, or polycarboxylic acids.

6.10.2 Retro-Diels-Alder Reaction

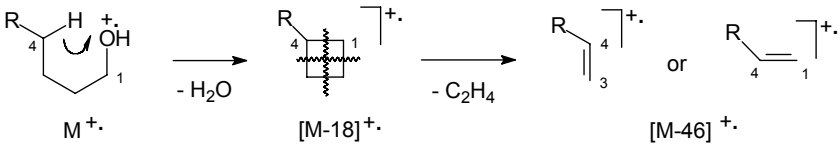
The Diels-Alder reaction is reversible at elevated temperatures, and therefore its products can decompose prior to evaporation by RDA reaction of the neutral in the condensed phase. The mass spectral RDA reaction has already been discussed in detail (Chap. 6.8).

6.10.3 Loss of H_2O from Alkanols

Aliphatic alcohols show a strong tendency to thermally eliminate water. This is of special relevance if volatile alkanols are introduced via the reference inlet system or by means of a gas chromatograph. Then, the mass spectra correspond to the re-

spective alkenes rather than to the alkanols that were intended to be analyzed. Water is often not detected, simply because mass spectra are frequently acquired starting from *m/z* 40 to omit background from residual air.

Interestingly, the molecular ions of alkanols also strongly tends to lose H_2O [28,123,124], which is their second important fragmentation route in addition to α-cleavage (Chap. 6.2.5). It has been demonstrated that the large majority of H_2O loss from the molecular ion proceeds by 1,4-elimination, whereas only some minor percentage of H_2O loss is due to other 1,x-eliminations. Following the labeling results, a cyclic intermediate can be assumed that decomposes further by loss of ethene [124]. These findings are not only supported by deuterium labeling studies but also by the fact that H_2O loss does play a less important role in the mass spectra of methanol, ethanol, and the propanols:



Scheme 6.54.

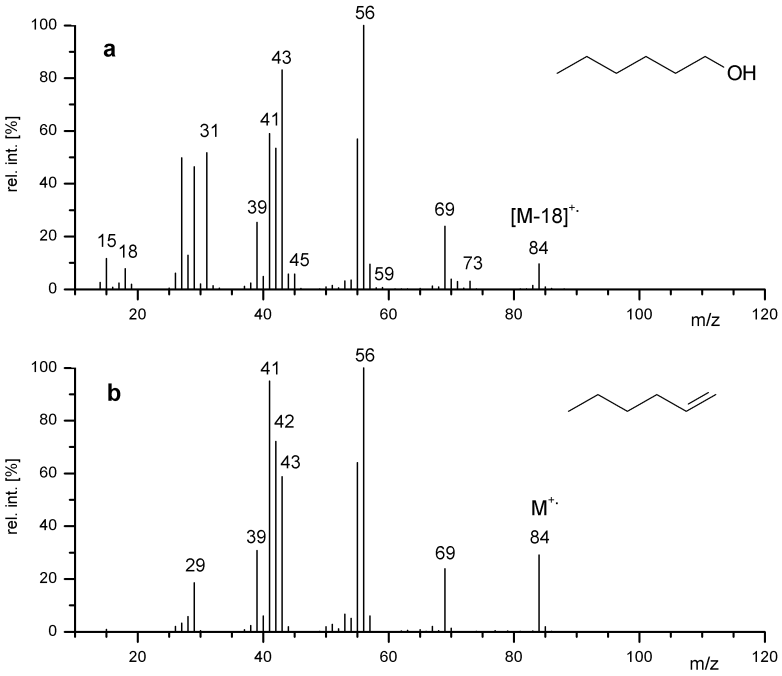


Fig. 6.38. Comparison of the EI mass spectra of 1-hexanol, $M_r = 102$ (**a**) and 1-hexene, $M_r = 84$ (**b**). Spectra used with permission by NIST. © NIST 2002.

Example: The EI mass spectra of 1-hexanol, $M_r = 102$, and 1-hexene, $M_r = 84$, are similar because the molecular ion peak is absent in the mass spectrum of hexanol (Fig. 6.38). However, a more careful examination of the hexanol spectrum reveals peaks at *m/z* 18, 19, 31, and 45 that are absent in the hexene spectrum. These are due to $H_2O^{+\bullet}$, H_3O^+, and to oxonium ions ($H_2C{=}OH^+$ and $H_3CCH{=}OH^+$ in this case) which are reliable indicators of aliphatic alcohols and ethers (Table 6.8).

In addition to the observation of oxonium ions, alkanols may occasionally be identified from the occurrence of a seemingly [M–3] peak while the molecular ion is absent (Fig. 6.39). The unusual difference of 3 u results from neighboring $[M–CH_3]^+$ and $[M–H_2O]^{+\bullet}$ peaks. In these cases, a [M–33] peak indicates consecutive losses of $CH_3^\bullet$ and H_2O in either order, i.e., $[M\text{-}H_2O\text{-}CH_3]^+$ and $[M\text{-}CH_3\text{-}H_2O]^+$. (Chap. 6.6.4). Alternatively, the sequence of $[M–H_2O]^{+\bullet}$ and $[M–H_2O–C_2H_4]^{+\bullet}$ may occur.

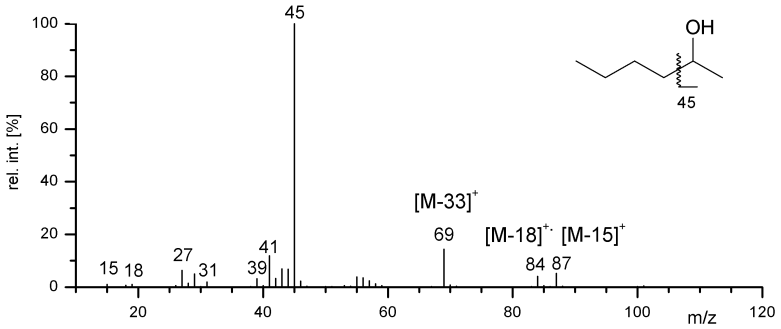


Fig. 6.39. EI mass spectrum of 2-hexanol, $M_r = 102$. Spectrum used with permission by NIST. © NIST 2002.

6.10.4 EI Mass Spectra of Organic Salts

Ammonium, phosphonium, oxonium salts and the like cannot be evaporated without substantial or complete decomposition, and thus EI-MS does not serve well for their characterization. Nevertheless, if a sample that happens to be an organic salt has incidentally been analyzed by EI-MS, it is helpful to know about their recognition. The EI mass spectra usually appear to result from the corresponding amines, phosphines, or ethers, but fortunately, the anion cannot 'hide'.

Example: The EI mass spectrum of tetrabutylammonium iodide shows a peak of low intensity (0.6%) for the $[Bu_4N]^+$ ion, *m/z* 242. A 'molecular ion' of the salt that would occur at *m/z* 369 is not observed. The majority of the sample decomposes and the spectrum closely resembles that of pure tributylamine showing its molecular ion peak at *m/z* 185 (the fragmentation of which is explained in Chap. 6.11.1). Closer inspection, however, reveals the existence of peaks at *m/z* 127 and 128 corresponding to I^+ and $HI^{+\bullet}$, respectively (Fig. 6.40).

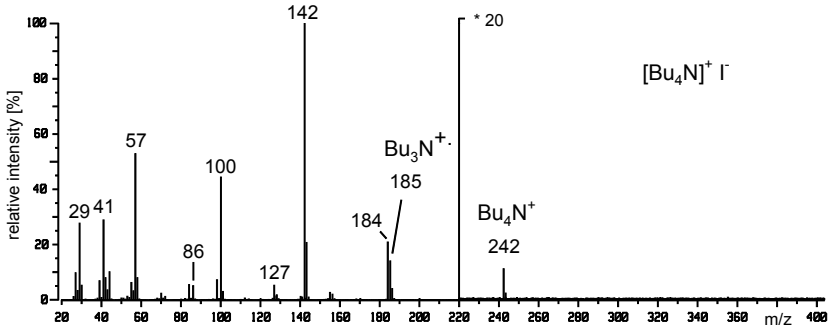


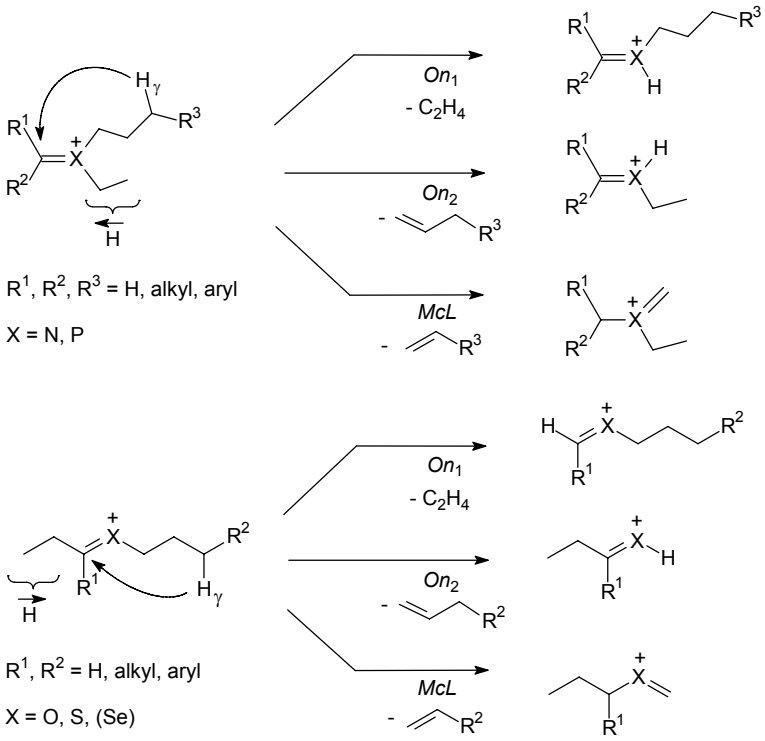
Fig. 6.40. EI mass spectrum of tetrabutylammonium iodide. The intensity scale is 20-fold above *m/z* 220, i.e., disregarding the peaks at *m/z* 127 and 128 this spectrum is very similar to the mass spectrum of pure tributylamine (Fig. 6.41b; for the field desorption mass spectrum cf. Chap. 8.5).

6.11 Alkene Loss from Onium Ions

Up to this point, aliphatic *onium ions* such as *immonium*, *oxonium*, and *sulfonium ions* have only been referred to as even-electron ionic products of the α-cleavage occurring from molecular ions of amines, alcohols, ethers, thiols, and thioethers (Chap. 6.2.5). All these and analogous onium ions are capable of further fragmentation reactions, the majority of which are alkene losses [125] yielding fragments of high relevance for structure elucidation.

The first of these reactions requires a γ-hydrogen, and thus at least one C_3-alkyl substitutent. It may either be regarded as the *even-electron analogy of the McLafferty rearrangement* (*McL*, Chap. 6.7) as it will be treated here [77,78,126], or alternatively, as a *retro-ene reaction* [127,128].

The second alkene loss can occur from any onium ion bearing at least one C_2-alkyl moiety, which obviously is the least demanding prerequisite for an alkene loss (ethene) to proceed. By this process, the whole substituent is cleaved off the heteroatom with concomitant nonspecific hydrogen transfer from the leaving group to the heteroatom [26,29]. In accordance with its occurrence from onium ions, this alkene loss is sometimes termed *onium reaction* (*On*) [3,31,129-132]. Thus, we obtain the following general fragmentation scheme for alkene losses from suitably substituted onium ions:

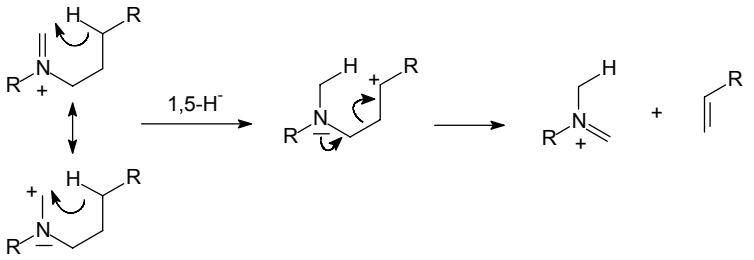


Scheme 6.55.

6.11.1 McL of Onium Ions

The McLafferty rearrangement of onium ions is accompanied by the same 100% regioselectivity for γ-H transfer as is observed for odd-electron ions which has repeatedly been demonstrated by deuterium labeling experiments [126,129,131,133]. This γ-selectivity also supports the general findings that immonium ions neither undergo random hydrogen nor carbon skeleton rearrangements prior to fragmentation [23,126,134]. The generally observed inertness of onium ions towards isomerization which is in contrast to $[C_nH_{2n+1}]^+$ (Chap. 6.6.1) and $[C_2H_{2n-1}]^+$ ions (Chap. 6.5.1) can be attributed to the preferred charge localization at the heteroatom [135].

Although the origin of the moving hydrogen and the structures of the product ions of the McLafferty rearrangement are well known, there is still some debate on whether it is *i*) concerted [128], *ii*) heterolytic stepwise [126,129,133,136-138], or even *iii*) stepwise involving homolytic bond cleavages [130]. A large amount of experimental data is in perfect agreement with the heterolytic stepwise mechanism, initiated by a 1,5-hydride shift:



Scheme 6.56.

The carbenium ion intermediate then eliminates the alkene by charge-induced cleavage of a C–C bond. The striking argument for a carbenium ion intermediate is presented by the influence of the γ-substituent R on the competition of onium reaction and McL. If R = H, i.e., for propyl-substituted iminum ions, the products of both reactions exhibit similar abundance. If R = Me or larger or if even two alkyls are present, McL becomes extremely dominant, because then its intermediate is a secondary or tertiary carbenium ion, respectively, in contrast to a primary carbenium ion intermediate in case of R = H. The importance of relative carbenium ion stability for onium ion fragmentations (Chap. 6.11.2) will become more apparent when dealing with the mechanism of the onium reaction.

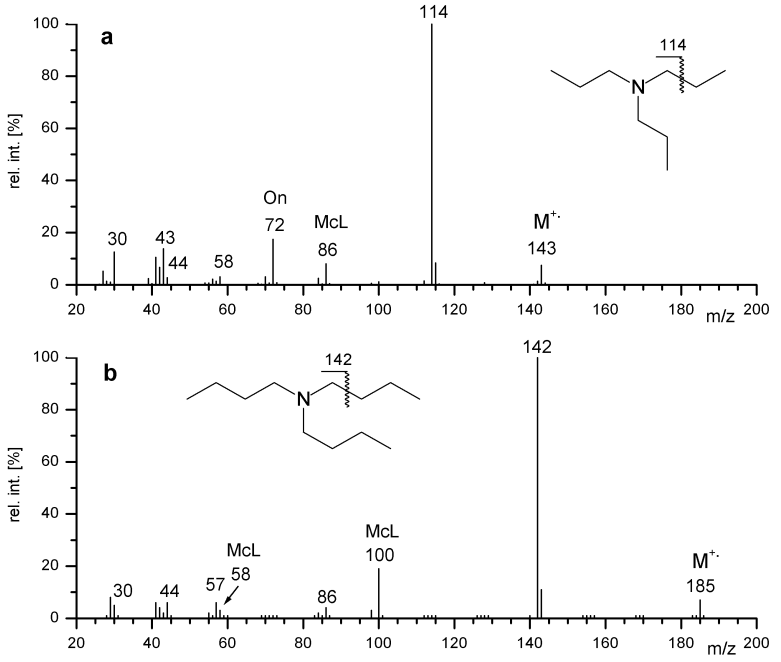
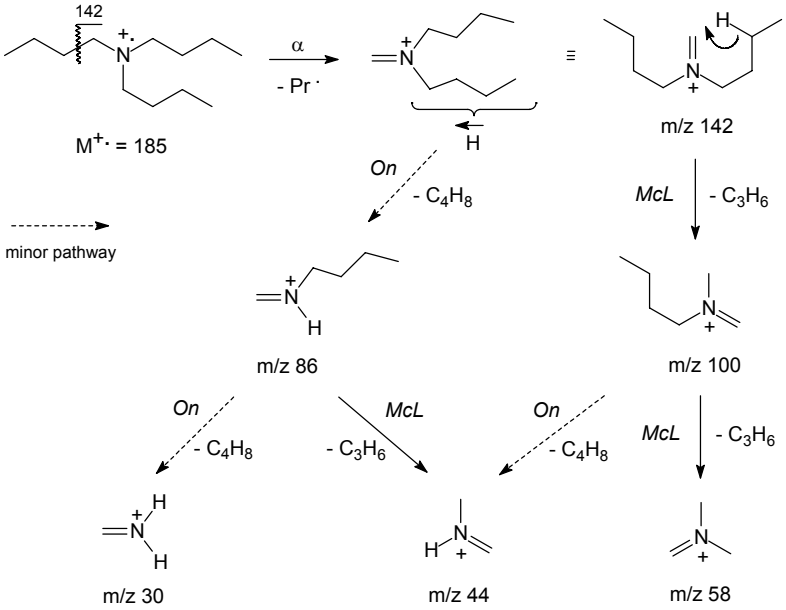


Fig. 6.41. EI mass spectra of tripropylamine (**a**) and tributylamine (**b**). For both compounds, the immonium ion series are completely present from *m/z* 30 onwards. Spectra used by permission of NIST. © NIST 2002.

Note: Regardless of the exact mechanism and regardless of whatever the correct name, the McLafferty rearrangement of onium ions is one of those processes allowing to reliably track ionic structures through a mass spectrum.

Example: Comparing the EI mass spectra of tripropylamine (Fig. 6.41a) and tributylamine [130] (Fig. 6.41b) shows that the latter basically can be explained by two reactions: α-cleavage of the molecular ion at *m/z* 185 forming a dibutylmethyleneimmonium ion, *m/z* 142, undergoing double propene loss (42 u) via consecutive McLafferty rearrangements. The propyl substitutents of the primary iminum ion fragment from tripropylamine, *m/z* 114, on the other side, allow for both fragmentations equally well, i.e., ethene loss via McL and propene loss via onium reaction, yielding peaks at *m/z* 86 and 72, respectively.



Scheme 6.57.

Example: The McLafferty rearrangement of onium ions is not necessarily as obvious as in the case of the immonium ions from aliphatic amines above. Especially, when other dissociation pathways are effectively competing, the corresponding signals can be of comparatively low intensity. The EI mass spectrum of butylisopropylether represents such a case: only the primary fragment ion at *m/z* 101 is able to undergo McL to form the oxonium ion at *m/z* 59 (Fig. 6.42 and Scheme 6.60). The peak at *m/z* 56 is due to $[C_4H_8]^{+\bullet}$ ions by loss of isopropanol from the molecular ion [139,140]. Eliminations of ROH from ionized ethers are usually of low abundance, but can gain importance in case of branching at the α-carbon.

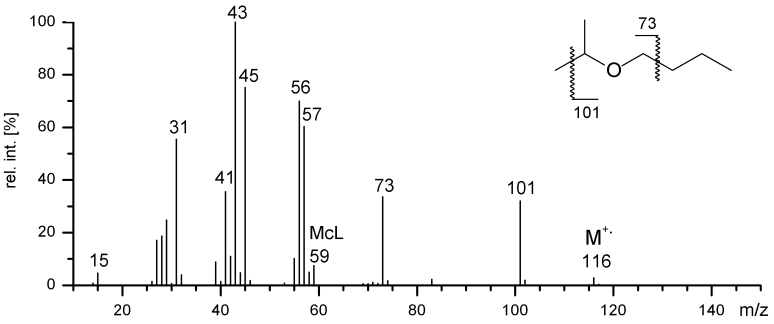


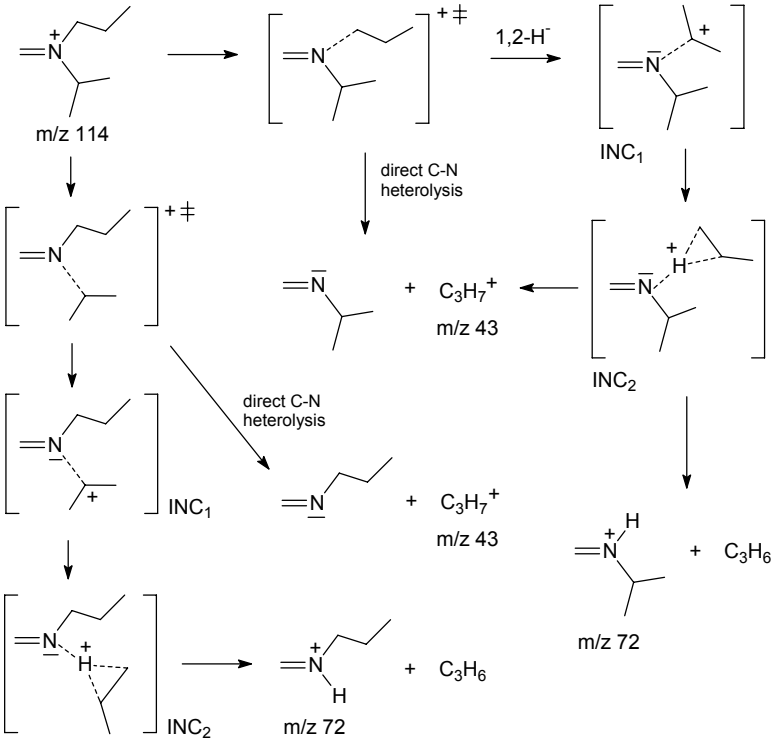
Fig. 6.42. EI mass spectrum of butylisopropylether. Spectrum used by permission of NIST. © NIST 2002.

6.11.2 Onium Reaction

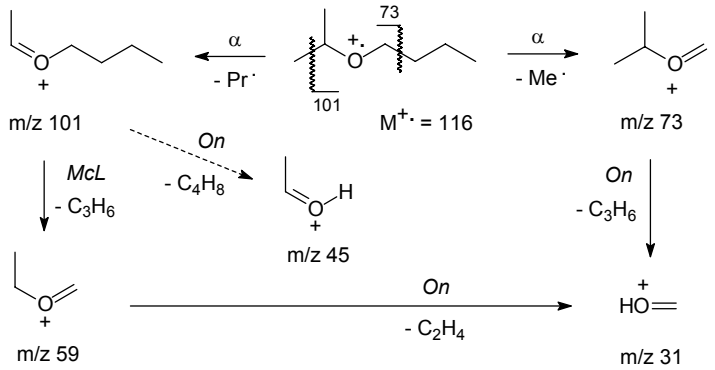
The loss of alkenes from aliphatic onium ions via onium reaction comprises scission of the C–X bond and concomitant transfer of a hydrogen from the leaving alkyl moiety to the heteroatom, and a merely phenomenological description of this reaction has already been included in the preceding schemes. This seemingly simple reaction has to be regarded as a multistep process that involves *ion-neutral complex* (INC) intermediates. The properties of ion-neutral complexes are discussed in detail below (Chap. 6.12). Here, we restrict ourselves to the application of this concept to achieve a full and consistent explanation of the behavior of onium ions.

The onium reaction of immonium ions [129,131,132,138,141,142] and oxonium ions [33,127,143,144] has been studied exhaustively. Imagine an isopropylpropylmethyleneimmonium ion, *m/z* 114, where the reaction is initiated by heterolytic elongation of the C–N bond (Scheme 6.60). Having passed the transition state, the reaction would normally be expected to proceed by direct dissociation to yield a $C_3H_7^+$ ion, *m/z* 43 (imine loss). Alternatively, the incipient propyl ion might stay with the imine, thus forming an ion-neutral complex INC_1. The decision which of these channels will be followed depends on the ion internal energy, i.e., the less energetic ions will prefer INC formation, whereas the highly excited ones are prone to dissociation. An INC can be regarded as the gas phase analog to solvation of ions in the condensed phase. Here, the lone pair of the imine acts as a donor for the carbenium ion. As ion and neutral are mutually free and mainly held together by coulombic attraction, isomerization of the incipient 1-propyl ion to a 2-propyl ion via 1,2-hydride shift can take place. This goes along with a stabilization of about 60 kJ mol^{-1} (Table 2.3). The stabilization energy must of course be stored in internal degrees of freedom, thereby contributing to some further excitation of INC_1. Direct dissociation of INC_1 is also detected as imine loss. By considering the propyl ion as a protonated propene molecule it becomes reasonable that within the INC a proton may be attracted by the imine having a by 100–140 kJ mol^{-1} higher proton affinity (*PA*, Chap. 2.11) than the leaving alkene

[126,145-147]. Therefore, the proton is almost quantitatively transferred to the imine, and the heat of reaction of 140 kJ mol^{-1} causes additional excitation. Thus, INC_2, also called *proton-bridged complex* (PBC), finally decomposes to give an immonium ion, *m/z* 72, and propene, 42 u.



Scheme 6.58.



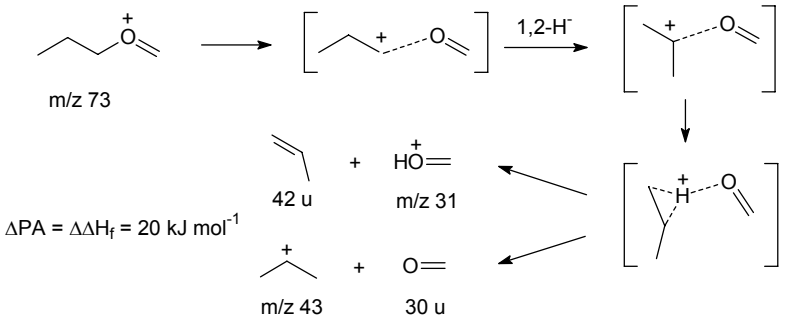
Scheme 6.59.

Example: The spectra of *N*-ethyl-*N*-methyl-propylamine (Fig. 6.6), tripropylamine, and tributylamine (Fig. 6.41) also exemplify alkene loss from immonium ions via an onium reaction. Oxonium ions are involved in the fragmentation of diethylether and methylpropylether (Fig. 6.7) and many others have been published (Scheme 6.59) [127,143,144,148].

The onium reaction and the McLafferty rearrangement of onium ions are closely related to each other in so far as that they often occur from the very same ion. However, the knowledge of the above mechanisms reveals significant differences in the way they proceed and it sheds light on the competition of onium reaction and McL: During the onium reaction alkyl substituents with no branch at C_α (adjacent to the heteroatom) have to be cleaved off via a transition state resembling a primary carbenium ion. Branching at C_α will effect dramatic change on the ease of bond heterolysis. As pointed out, analogous effects are observed for the McL in case of substitution at C_γ (Chap. 6.11.1 and Fig. 6.43). It becomes clear that the reaction pathway passing through the higher branched carbenium ion intermediate will be observed as the predominating process.

In case of immonium ion fragmentations, the large difference of proton affinities, ΔPA, between imine and alkene clearly favors the formation of immonium ion plus neutral alkene, whereas imine loss is restricted to highly energetic precursors.

In decomposing oxonium ions the situation is quite different, i.e., the preference for alkene loss is much less emphasized and aldehyde (ketone) loss is gaining importance. The observed changes are in good agreement with the postulated mechanism of the onium reaction [127,149]. The alternative pairs of oxonium ion plus alkene and aldehyde plus carbenium ion may be formed with a preference for the first one, because ΔPA is comparatively small (20–60 kJ mol^{-1}) or even zero, e.g., for the acetone/isobutene pair [127,147,149]:



Scheme 6.60.

6.12 Ion-Neutral Complexes

During the above discussion of the mechanism of the onium reaction we encountered another type of reactive intermediates of unimolecular ion fragmentations: *ion-neutral complexes* (INC) [25,38,150-153]. In contrast to *distonic ions* (Chap. 6.3) ion-neutral complex intermediates add some bimolecular reaction characteristics to fragmentation pathways of isolated ions. This is effected by allowing an incipient neutral fragment to remain some time with the ionic part, both derived from the same precursor ion, thus enabling processes that otherwise could only occur from bimolecular ion-molecule reactions. The final products of such fragmentations are governed by the properties of the species involved, e.g., by the relative proton affinities of the partners as was the case with the onium reaction.

6.12.1 Evidence for the Existence of Ion-Neutral Complexes

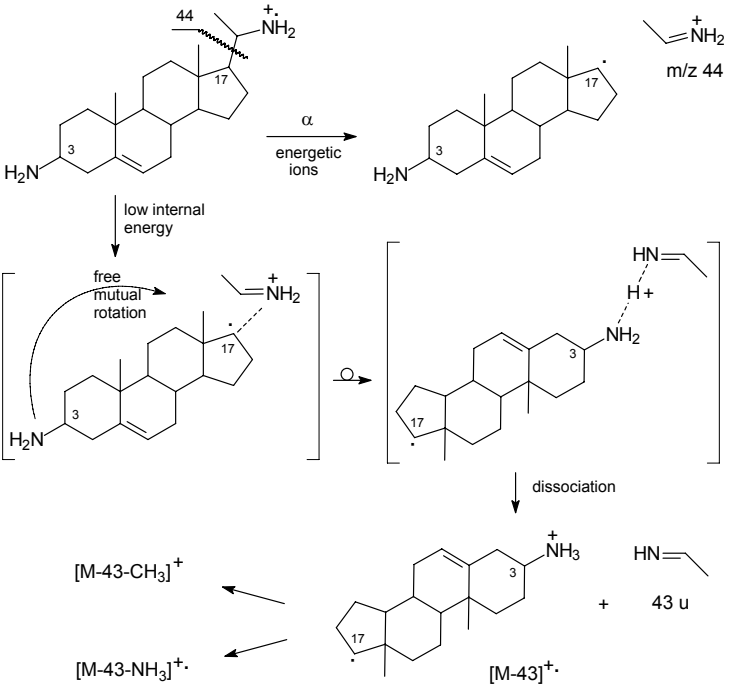
INCs were first referred to by Rylander and Meyerson [154,155]. Soon, the concept that the decomposition of oxonium and immonium ions involve INCs (Chap. 6.11.2) was put forth by Bowen and Williams [127,141,142,149], and the analogies to solvolysis were described by Morton [150]. Still, mass spectrometrists were too much used to strictly unimolecular reactions as to assimilate this concept without stringent proof.

Conclusive evidence for INCs was first presented by Longevialle and Botter [156,157] who demonstrated the transfer of a proton from an imine fragment to an amino group located on the opposite side of the rigid skeleton of bifunctional steroidal amines [157]. Such a proton transfer cannot proceed without the intermediacy of an INC; otherwise, a conventional hydrogen shift would have bridged the distance of about 10^{-9} m between the respective groups which is about five times too far.

The occurrence of this unexpected reaction chiefly depends on the ion's internal energy: energetic molecular ions undergo α-cleavage leading to an immonium ion, $[C_2H_6N]^+$, *m/z* 44, while less energetic ions and especially metastable ions show imine loss. Obviously, mutual rotation of the reacting partners has to precede the final acid-base reaction preferably causing imine loss, i.e., an $[M–C_2H_5N]^{+\bullet}$ fragment, $[M–43]^{+\bullet}$. This is possible because the attractive forces between the radical and the ion are strong enough to prevent spontaneous dissociation by forming an INC. Now, mutual rotation of the reacting partners allows additional dissociation channels to be explored. Finally, the proton transfer to the amine is thermodynamically favorable, because the proton affinity of ethylideneimine, 891 kJ mol^{-1}, is presumably lower than that of the steroidal amine radical (as estimated from the proton affinity of cyclohexylamine [145], this is about 920 kJ mol^{-1}, i.e., $\Delta PA \approx 29$ kJ mol^{-1}).

Proton transfer will be prevented when the initial fragments separate too rapidly for the partners to rotate into a suitable configuration. Here, the lower limit for the intermediate's lifetime can be estimated as 10^{-11} s. The competition between the

α-cleavage and the INC-mediated reaction is therefore governed by the amount of ion internal energy.



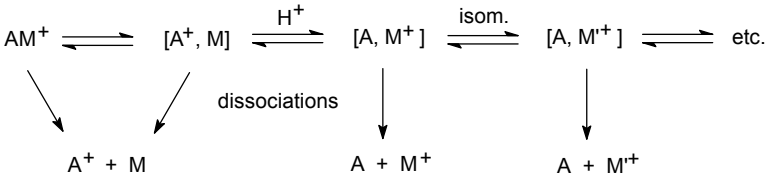
Scheme 6.61.

6.12.2 Attractive Forces in Ion-Neutral Complexes

The term ion-neutral complex is applied to species in which an ion and a neutral are held together mainly by electrostatic attraction [153]. The INC must be held together by attracting positive and negative charges and an electron-donating or -accepting group, respectively, rather than by the action of covalent bonds. This can accomplished by ion-dipole and ion-induced dipole interactions. The formation of an INC can be compared to solvolysis reactions in the condensed phase [150] with subsequent mutual solvation of the partners. Typically, stabilization energy V_r is in the range of 20–50 kJ mol^{-1}.

Consider the dissociation of an ion AM^+ that may either dissociate to form the fragments A^+ and M or the INC $[A^+, M]$ allowing free mutual rotation and thus reorientation of the particles. Within the INC, A^+ and M can recombine only if they attain a well-defined mutual orientation, i.e., the system has to freeze rotational degrees of freedom. Such a configuration allowing covalent bonds to be formed is termed *locked-rotor critical configuration* [151-153,158] and any reaction channel, e.g., proton transfer or recombination, has to pass this *entropic bot-*

tleneck. The INC $[A^+, M]$ can in principle undergo multiple isomerizations and may dissociate at any of these isomeric states:



Scheme 6.62.

Note: Any reaction depending on a certain configuration to be attained, i.e., "classical" rearrangement fragmentations and especially INC-mediated processes, exhibit comparatively low rate constants that are in part due to entropic bottlenecks that need to be passed (cf. *tight transition states*, Chap. 2.6.4). Therefore, high ion internal energies tend to discriminate between INC-mediated reactions, but favor direct bond cleavages.

6.12.3 Criteria for Ion-Neutral Complexes

A species can be considered as an INC if its lifetime is long enough to allow for other chemical reactions than the mere dissociation of the incipient particles. This is the minimum criterion that has to be fulfilled to term a reactive intermediate an ion-neutral complex, because otherwise any transition state would also represent an INC [153,159]. In addition, the *reorientation criterion* [25,151] should be met, i.e., free reorientation of the particles involved must be possible. Although still regarded provisional by the authors, McAdoo and Hudson have provided a useful collection of additional characteristics of ion-neutral complex-mediated decompositions [160,161]:

1. Complete dissociation by the bond cleavage that forms the INC will be observed and will increase in importance relative to the INC-mediated pathway as internal energy increases.
2. INC-mediated processes will be among the lowest energy reactions of an ion.
3. Reactions within and between partners may occur below the dissociation thresholds for simple dissociations.
4. Alternative mechanisms consistent with the observations would require much higher energy transition states – transition states in which multiple bond breakings and makings occur simultaneously, or even transition states of impossible geometries.
5. The observed kinetic isotope effects are usually large (because of low excess energy in the transition states).
6. The kinetic energy releases in corresponding metastable decompositions may be very small.

6.12.4 Ion-Neutral Complexes of Radical Ions

The intermediacy of ion-neutral complexes is neither restricted to even-electron fragmentations nor to complexes that consist of a neutral molecule and an ion. In addition, radical-ion complexes and radical ion-neutral complexes occur that may dissociate to yield the respective fragments or can even *reversibly interconvert* by hydride, proton, or hydrogen radical shifts. Many examples are known from aliphatic alcohols [162,163], alkylphenylethers [164-166], and thioethers [167].

Example: The unimolecular reactions of the molecular ion of ethyl-propylthioether (Fig. 6.43, Scheme 6.64) [167] chiefly are *i*) loss of a methyl from the ethyl or the propyl group, *ii*) loss of an ethyl from the propyl group, both leading to *sulfonium ions* [168] (Chap. 6.2.5), and *iii*) elimination of propene or an allyl radical by transfer of one or two hydrogen atoms, respectively, from the propyl group to the sulfur. On the microsecond time scale, the loss of $CH_3^{\bullet}$ involves only the propyl entity and is preceded by an isomerization of this group. Partial loss of the positional identity of the hydrogen atoms of the propyl group occurs, but incorporation of hydrogen or carbon atoms from the ethyl group into the formed neutral species does not occur. Cleavage of a C–S bond assisted by a 1,2-hydride shift in the incipient carbenium ion leads to an INC of a thioethoxy radical and a 2-propyl ion. The INC may recombine to form the molecular ion of ethylisopropylthioether (cf. Fig. 6.9) prior to $CH_3^{\bullet}$ loss, or react by proton transfer to give another INC, which may dissociate or undergo hydrogen atom transfer, followed by elimination of an allyl radical. The partial loss of positional identity of the hydrogen atoms during the decomposition of the metastable ions is mainly a result of reversible proton transfer between the constituents, which competes favorably with 1,2-hydride shifts within the carbenium ion entity of the complex.

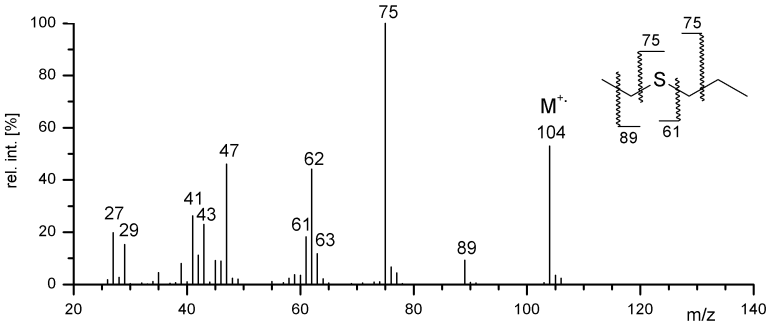
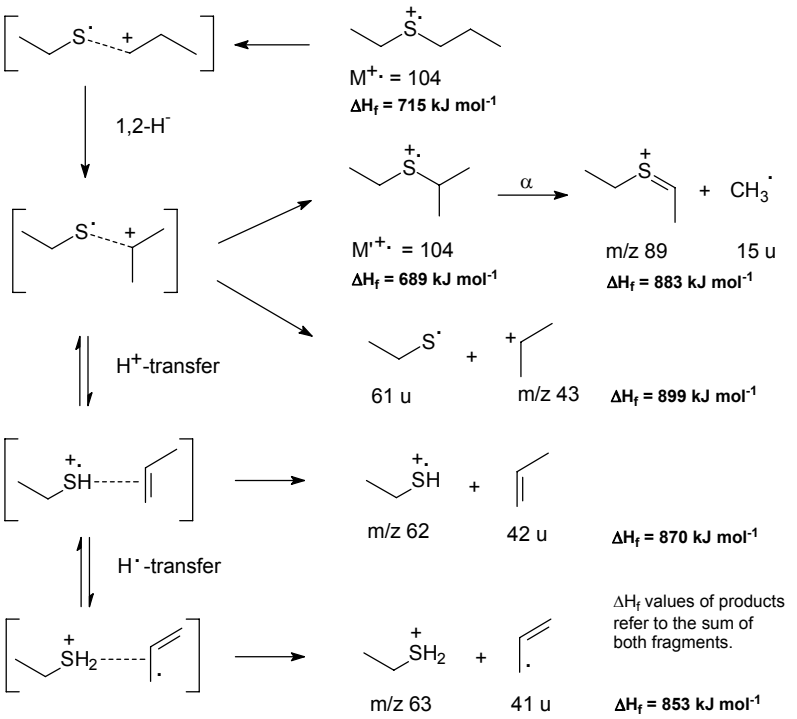


Fig. 6.43. EI mass spectrum of ethylpropylthioether. (Also compare to the spectrum of ethylisopropylthioether, Fig. 6.9. The isotopic pattern is discussed in Chap. 3.2.6). Spectrum used by permission of NIST. © NIST 2002.



Scheme 6.63.

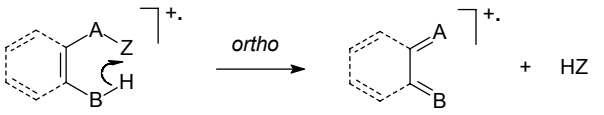
6.13 *Ortho* Elimination (*Ortho* Effect)

The *ortho elimination* (*ortho effect*) has been stated to belong to the diagnostically most important mass spectral fragmentations [169]. Indeed, from the first report on this process [94] until the present, there is a continuing interest in this topic concerning a wide range of compounds [170-175]. The driving force for these research activities stems from a strict relation of this process to the substitution pattern of aryl compounds. The existence of a suitably 1,2-disubstituted *cis*-double bond presents an essential structural requirement for this rearrangement-type fragmentation, and this double bond is usually part of an aromatic system, hence the name.

Note: Although not being correct to describe a reaction, the term *ortho effect* is well established, and another occasionally used term, *retro-1,4-addition*, is redundant; *1,4-elimination* would describe the same. Unfortunately, this might be confused with 1,4-H_2O-eliminations from aliphatic alcohols, for example. Therefore, the term *ortho elimination* is suggested and used here.

6.13.1 *Ortho* Elimination from Molecular Ions

Commonly, *ortho* elimination refers to a hydrogen transfer via a six-membered transition state at *ortho*-disubstituted aromatic compounds. In practice, the reacting entities are almost in position to form this six-membered transition state. The general mechanism of the *ortho* elimination is as follows:



Scheme 6.64.

The charge can reside on either product, but charge retention at the diene product is generally predominant. As the 1,2-disubstituted *cis*-double bond must not necessarily belong to an aryl group, the optional part of the molecule has been drawn in dashed style in the above scheme. In addition to the substitution pattern, the *ortho* elimination requires substituent A to bear a hydrogen-accepting leaving group, Z, and substituent B to be a hydrogen donor, e.g., hydroxyl, amino, thiol, or even alkyl [176].

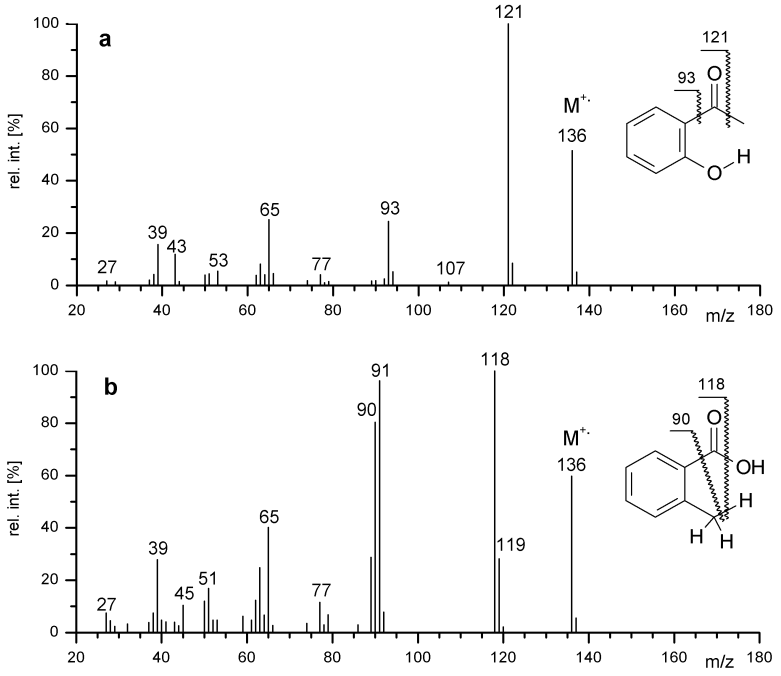
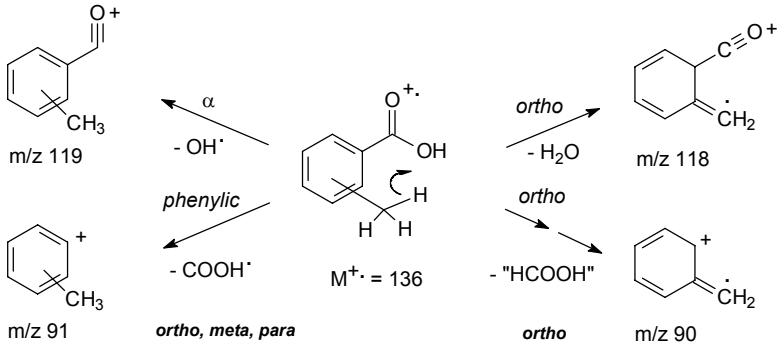


Fig. 6.44. EI mass spectra of 2-hydroxyacetophenone (**a**) and 2-methylbenzoic acid (**b**). Spectra used by permission of NIST. © NIST 2002.

Example: The leaving methyl of 2-hydroxyacetophenone (Fig. 6.44a) is not a suitable hydrogen acceptor, and therefore homolytic cleavages predominate. Here, these are loss of a methyl by α-cleavage, $[M–CH_3]^+$, *m/z* 121, and loss of an acyl by phenylic cleavage, $[M–COCH_3]^+$, *m/z* 93. On the other hand, all requirements for the *ortho* elimination are met in the 2-methylbenzoic acid molecular ion (Fig. 6.44b) [94]. As usual, homolytic cleavages are still competing with the *ortho* elimination [177], but the additional fragments due to loss of intact molecules containing one hydrogen from the donor site cannot be overlooked. Thus, α-cleavage, $[M–OH]^+$, *m/z* 119, is overrun by loss of water, $[M–H_2O]^{+\bullet}$, *m/z* 118, and phenylic cleavage, $[M–COOH]^+$, *m/z* 91, has to compete with formal loss of formic acid, $[M–HCOOH]^{+\bullet}$, *m/z* 90. Consequently, such neutral losses are absent in the mass spectra of the *meta* and *para* isomers.



Scheme 6.65.

As indicated by metastable ion studies of isopropylbenzoic acids [178], the formation of the ion at *m/z* 90 should be described as a two-step process, i.e., the product rather is $[M–OH–CHO]^{+\bullet}$ than $[M–HCOOH]^{+\bullet}$. This would add yet another example to the list of violations of the even-electron rule (Chap. 6.1.3).

6.13.2 *Ortho* Elimination from Even-Electron Ions

As with the McLafferty rearrangement and the retro-Diels-Alder reaction before, the occurrence of the *ortho* elimination is not restricted to molecular ions. It may equally well proceed in even-electron species.

Example: Examination of the mass spectrum of isopropylbenzoic acid reveals that the molecular ion, *m/z* 164, as well as the $[M–CH_3]^+$ ion, *m/z* 149, eliminate H_2O via *ortho* elimination yielding fragment ions at *m/z* 146 and 131, respectively (Fig. 6.45) [178]. The $[M–CH_3–H_2O]^+$ ion, a homolog of the benzoyl ion, decomposes further by loss of CO, thereby creating a fragment that overall corresponds to $[M–CH_3–HCOOH]^+$, *m/z* 103.

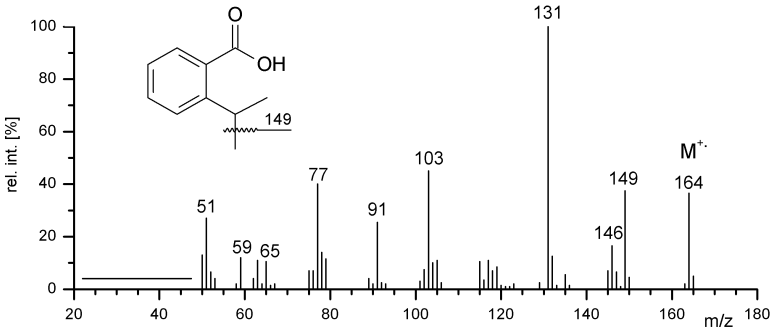
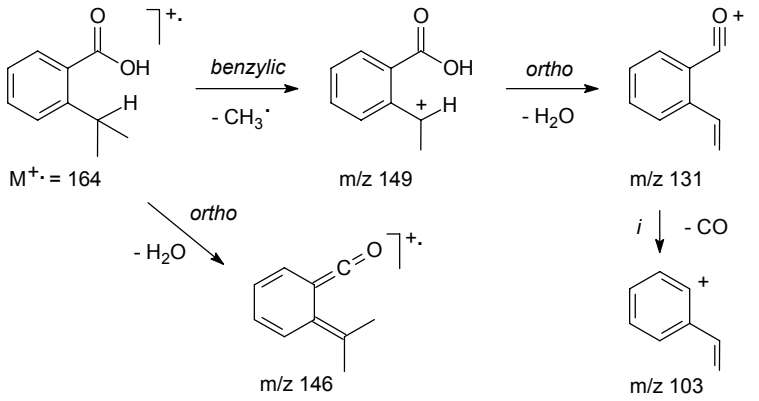
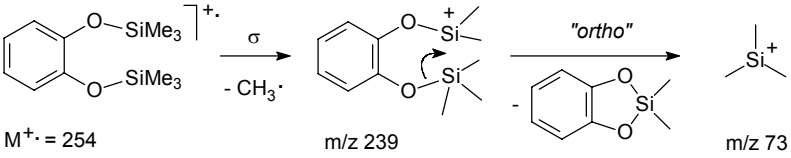


Fig. 6.45. EI mass spectrum of isopropylbenzoic acid. Spectrum used by permission of NIST. © NIST 2002.



Scheme 6.66.

Example: The molecular ion of 1,2-bis(trimethylsiloxy)benzene, *m/z* 254, undergoes methyl loss by Si–C bond cleavage as typically observed for silanes (Fig. 6.46). Rearrangement of the $[M–CH_3]^+$ ion then yields $[Si(Me)_3]^+$, *m/z* 73 (base peak). This is not an *ortho* elimination with concomitant $H^•$ transfer as defined in the strict sense, but the observed reaction is still specific for the *ortho*-isomer [169,179]. In the spectra of the *meta*- and *para*-isomers the $[Si(Me)_3]^+$ ion is of lower abundance, the $[M–CH_3]^+$ ion representing the base peak in their spectra. Moreover, the *m/z* 73 ion is then generated directly from the molecular ion which is clearly different from the two-step pathway of the *ortho*-isomer.



Scheme 6.67.

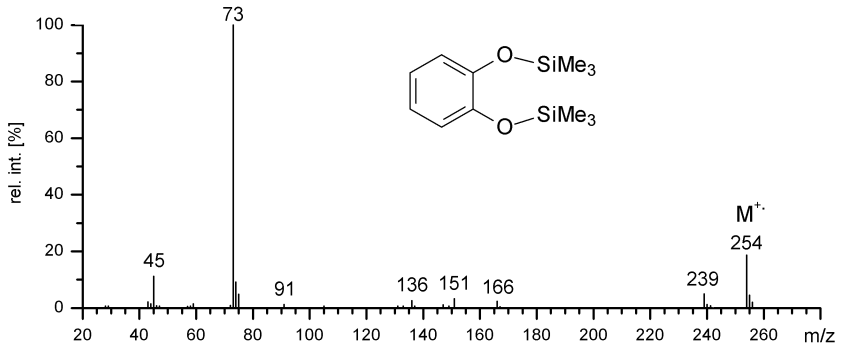
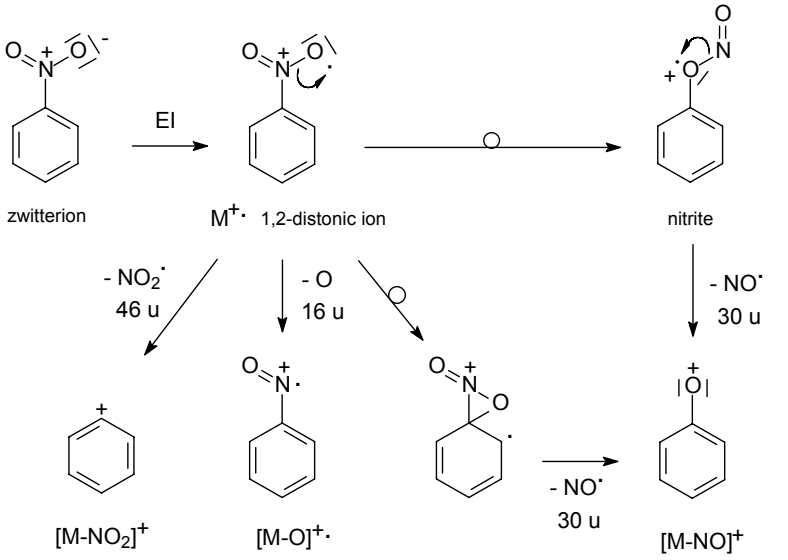


Fig. 6.46. EI mass spectrum of 1,2-bis(trimethylsiloxy)benzene. The isotopic pattern of silicon is clearly visible in the signals at *m/z* 73, 239, and 254 (Chap. 3.2.6). Spectrum used by permission of NIST. © NIST 2002.

Note: Trimethylsilyl (TMS) derivatives are frequently employed to volatize alcohols [179,180], carboxylic acids [181,182], and other compounds [183] for mass spectrometry, and for GC-MS applications in particular. The EI mass spectra of TMS derivatives exhibit weak molecular ion peaks, clearly visible $[M–CH_3]^+$ signals and often $[Si(Me)_3]^+$, *m/z* 73, as the base peak.

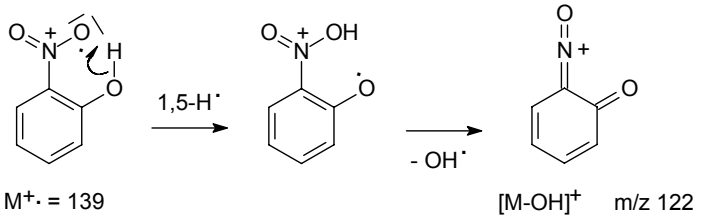


Scheme 6.68.

6.13.3 *Ortho* Elimination in the Fragmentation of Nitroarenes

Nitroarenes are recognized from their characteristic neutral losses due to the NO_2 substituent. Normally, all theoretically possible fragment ions, the plausible $[M–NO_2]^+$ and $[M–O]^{+\bullet}$ ions as well as the unexpected $[M–NO]^+$ ion, are observed. It is worth noting that molecular ions are 1,2-distonic by definition, because nitroarene molecules are best represented as zwitterion (Chap. 6.3). The molecular ion may either dissociate directly by loss of an oxygen atom or a NO_2 molecule or it may rearrange prior to loss of $NO^{\bullet}$. For the latter process, two reaction pathways have been suggested, one of them involving intermediate formation of a nitrite, the other proceeding via a three-membered cyclic intermediate [184]. Fragmentation of the nitrite then yields a phenolic-type ion that can decompose further by elimination of CO. Thus, the characteristic series of $[M–16]^{+\bullet}$ (generally weak signal), $[M–30]^+$, and $[M–46]^+$ ions is obtained (Fig. 6.47a,b), e.g., for nitrobenzene.

Ortho-substituted nitroarenes can be distinguished from *meta*- or *para*-substituted isomers due to a characteristic change in their mass spectra. In the precence of a hydrogen-donating *ortho* subtituent, $[M–OH]^+$ replaces the $[M–O]^{+\bullet}$ the fragment ion, e.g., in case of the above nitrophenols, the ion at *m/z* 122 appears in place of the one at *m/z* 123 (Fig. 6.47c). The mechanism of this $OH^{\bullet}$ loss is not quite clear [185], because different proposals [186-188] are in good accordance with the experimental data. Here, the mechanism which resembles the previously discussed *ortho* eliminations is shown [188]:



Scheme 6.69.

Ortho eliminations are widely considered in the structure elucidation of aromatic nitro compounds such as nitroanilines [175], dinitrophenols [189], or trinitroaromatic explosives [190].

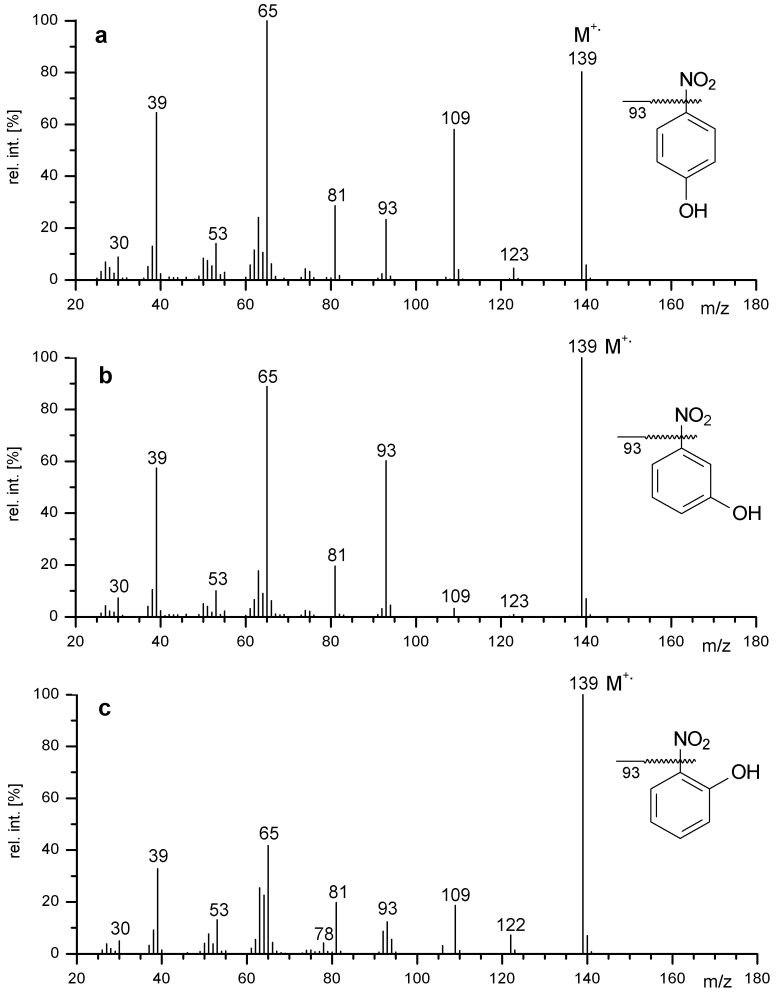


Fig. 6.47. EI mass spectra of isomeric nitrophenols. The fragment ion $[M–OH]^+$, *m/z* 122, instead of $[M–O]^{+\bullet}$, *m/z* 123, is only observed for the *ortho* isomer. Spectra used by permission of NIST. © NIST 2002.

6.14 Heterocyclic Compounds

As mentioned earlier in this chapter, it is not possible in this book to deliver a comprehensive treatment of the fragmentations of organic ions. Nevertheless, a short reference to MS of heterocyclic compounds should be made here, while being aware that this topic could easily fill an entire textbook of its own [191].

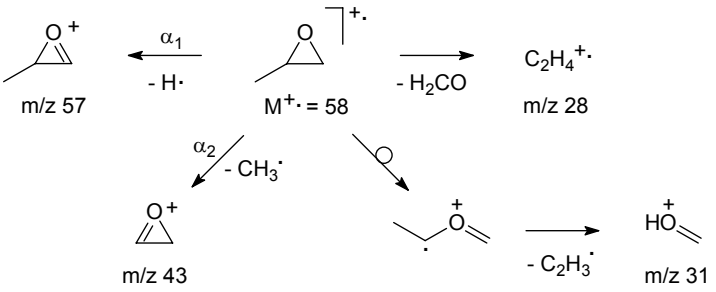
6.14.1 Saturated Heterocyclic Compounds

The molecular ions of small saturated heterocyclic compounds exhibit a strong tendency for *transannular cleavages* that often give rise to the base peak. These transannular cleavages can formally be regarded as clean cuts across the ring. Other fragmentation pathways including ring-opening bond scissions followed by consecutive cleavages and α-cleavage also play a role and start to compete effectively with the characteristic ring cleavage as the number of substituents at the ring increases [192-194].



Scheme 6.70.

The methyloxirane molecular ion, *m/z* 58, easily fragments by α-cleavage preferably yielding a $[M–CH_3]^+$ ion, *m/z* 43, and a $[M–H]^+$ ion, *m/z* 57 (Fig. 6.48). The more characteristic transannular ring cleavage leads to loss of formaldehyde, thus explaining the base peak at *m/z* 28 as a $C_2H_4^{+\bullet}$ ion. Ring opening and consecutive fragmentation leads to fragment ions such as $[CH_2OH]^+$, *m/z* 31, $[CHO]^+$, *m/z* 29, and $[CH_3]^+$, *m/z* 15:



Scheme 6.71.

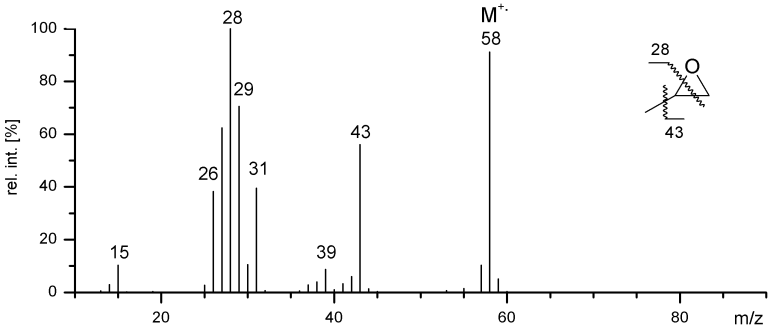
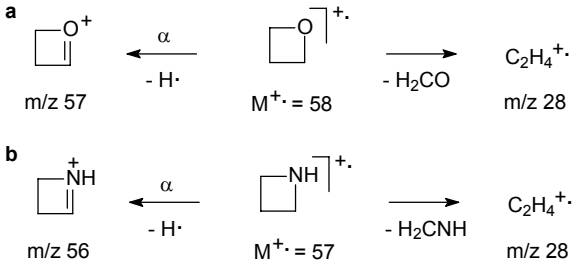


Fig. 6.48. EI mass spectrum of methyloxirane. Spectrum used by permission of NIST.

Example: Comparing the spectra of methyloxirane and its isomer oxetane reveals a clear difference in that the $[M–CH_3]^+$ ion, *m/z* 43, is almost absent because of the missing methyl group, whereas the $[M–H]^+$ ion, *m/z* 57, remains unaffected (Fig. 6.49a). The transannular ring cleavage, however, benefits from this reduced number of competing routes and thus, the $[M–H_2CO]^{+\bullet}$ ion, *m/z* 28, is definitely dominant. The better charge-localizing capability of nitrogen as in azetidine pronounces radical-induced cleavages as compared to the oxetane spectrum, i.e., a $[M–CH_3]^+$ ion, *m/z* 42, is observed due to ring opening and the $[M–H]^+$ ion, *m/z* 56, from α-cleavage (Chap. 6.2) is also more prominent (Fig. 6.49b). Here, transannular ring cleavage of the *N*-heterocycle effects loss of methyleneimine, and the $[M–H_2CNH]^{+\bullet}$ ion forms the base peak:



Scheme 6.72.

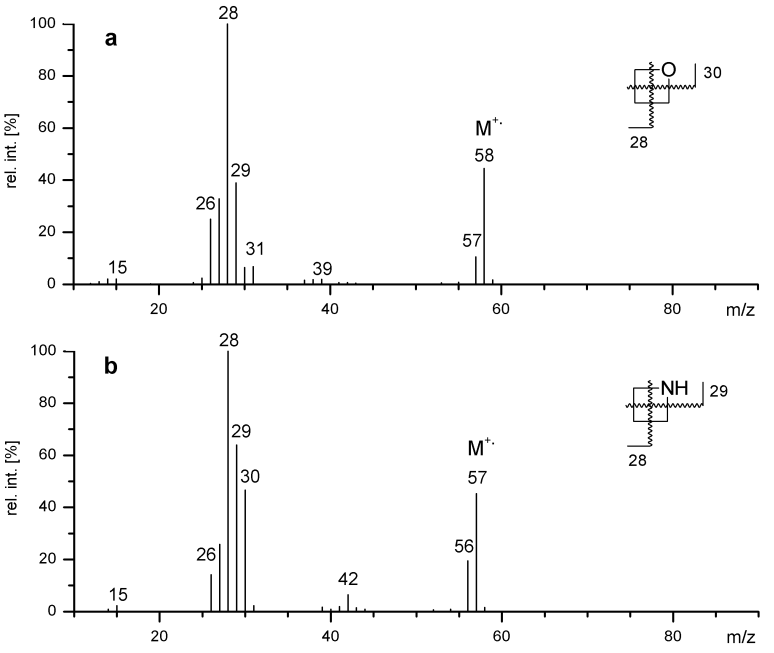


Fig. 6.49. EI mass spectra of oxetane (**a**) and azetidine (**b**). Spectra used by permission of NIST. © NIST 2002.

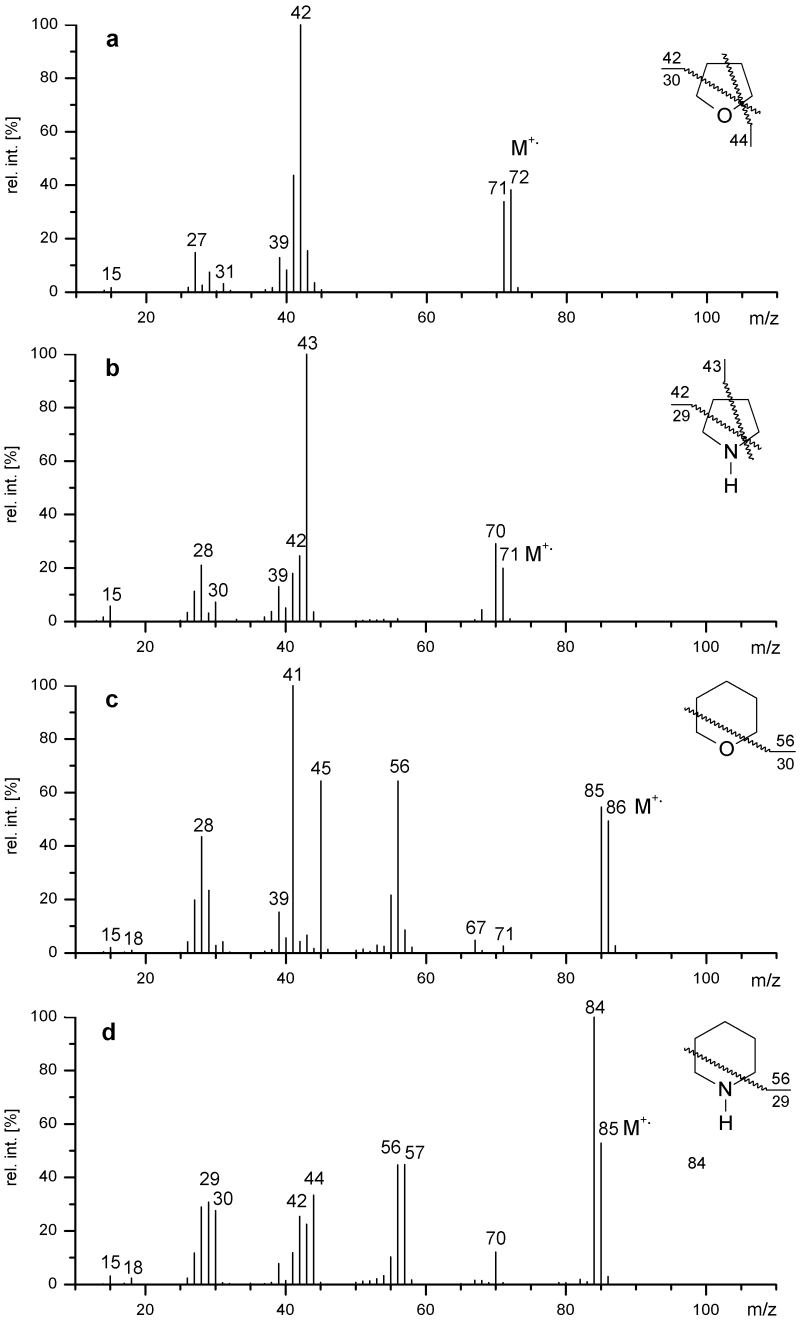


Fig. 6.50. EI mass spectra of tetrahydrofuran (**a**), pyrrolidine (**b**), tetrahydropyran (**c**), and piperidine (**d**). Spectra used by permission of NIST. © NIST 2002.

Note: Methyloxirane and oxetane are C_3H_6O isomers, but acetone, propanal, methyl vinylether, and 2-propenol also belong to this group. This reminds us to be careful when assigning structures to empirical formulas and when deducing structural information from $r + d$ values (Chap. 6.4.4).

Loss of formaldehyde is not only among the low critical energy processes of oxirane and oxetane molecular ions, but also of larger cyclic ethers such as tetrahydrofurane and tetrahydropyran [195]. Again, imine loss from *N*-heterocycles [196] behaves analogously. The mass spectra of tetrahydrofuran, pyrrolidine, tetrahydropyran, and piperidine are compared below (Fig. 6.50). The strong $[M–H]^+$ peaks in all of those four spectra are due to α-cleavage.

6.14.2 Aromatic Heterocyclic Compounds

Pyridine and other aromatic *N*-heterocycles eliminate a molecule of hydrogen cyanide, HCN, 27 u, from their molecular ions. It has been demonstrated that the molecule eliminated from pyridine molecular ions, *m/z* 79, definitely is HCN and not its isomer hydrogen isocyanide, HNC [197,198]. The fragmentation of pyridine molecular ions to form $[C_4H_4]^{+\bullet}$, *m/z* 52, and HCN was reported to proceed via a tight transition state [199], which is in some disagreement with the small kinetic energy release of 43 meV [200]. The fragmentation threshold of 12.1 eV for this process is well beyond the *IE* of 9.3 eV [18], thus demonstrating high energy requirements [199]. HCN loss from aromatic *N*-heterocycles is the equivalent to C_2H_2 loss from aromatic hydrocarbons. As anticipated, the peak at *m/z* 53 in the spectrum of pyridine reveals that (after subtraction of the isotopic contribution of ^{13}C) a fraction of the pyridine molecular ions eliminates C_2H_2, 26 u (Fig. 6.51).

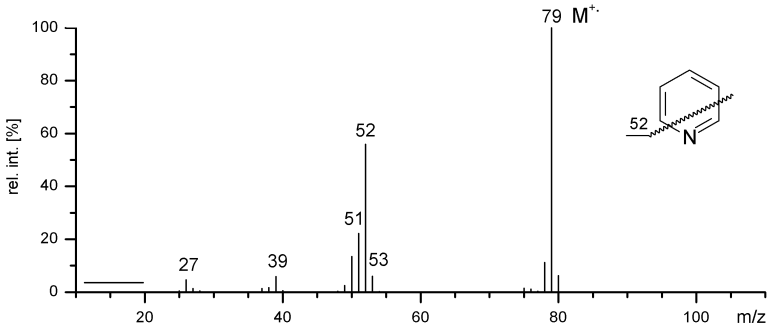
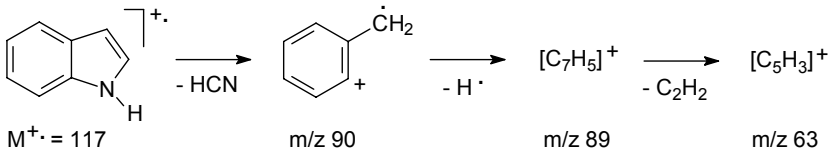


Fig. 6.51. EI mass spectrum of pyridine. HCN loss represents the most important primary fragmentation of the molecular ion. Spectrum used by permission of NIST. © NIST 2002.

Example: Indole molecular ions, *m/z* 117, preferably dissociate by loss of HCN (Fig. 6.52) [201]. The $[C_7H_6]^{+\bullet}$ fragment ion, *m/z* 90, then stabilizes by $H^\bullet$ loss to form an even-electron species, $[C_7H_5]^+$, *m/z* 89, which decomposes further by loss of ethyne:



Scheme 6.73.

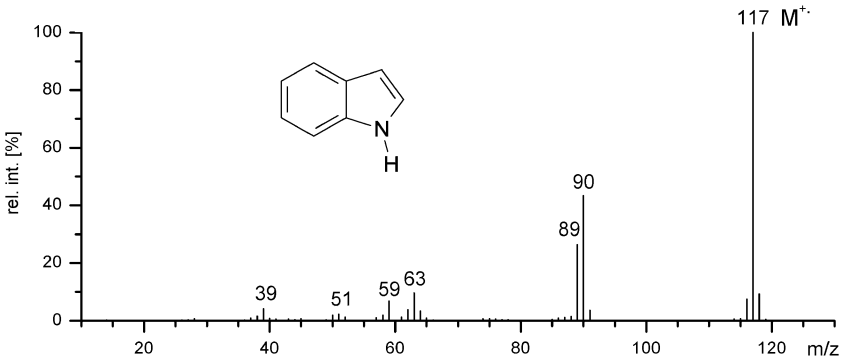
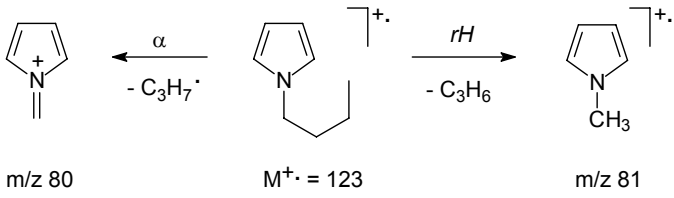


Fig. 6.52. EI mass spectrum of indole. Used by permission of NIST. © NIST 2002.

Indole derivatives are widespread natural compounds, and mass spectrometry of indoles [201,202], especially of indole alkaloids, has been of special interest ever since [203-205].

In case of the pyrrole molecular ion, HCN loss is somewhat less important than with indole, i.e., the $[M–C_2H_2]^{+\bullet}$ ion at *m/z* 41 is more abundant than the $[M–HCN]^{+\bullet}$ ion at *m/z* 40. This may in part be due to the twofold chance of C_2H_2 elimination (Fig. 6.53). The introduction of *N*-substituents has similar effects as observed for the saturated heterocycles mentioned earlier, i.e., rearrangement fragmentations and α-cleavage of the substituent take control [206]:



Scheme 6.74.

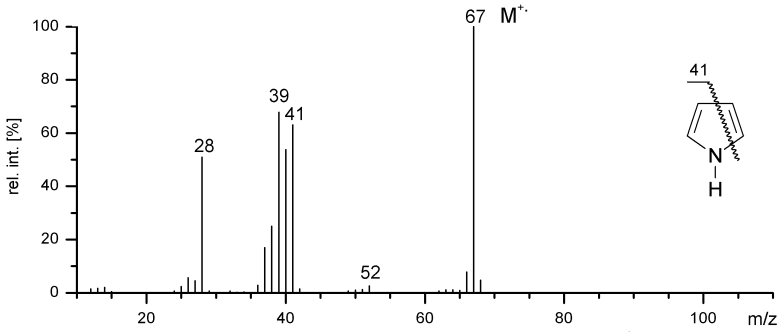


Fig. 6.53. EI mass spectrum of pyrrole. Elimination of C_2H_2 slightly predominates over loss of HCN. Spectrum used by permission of NIST. © NIST 2002.

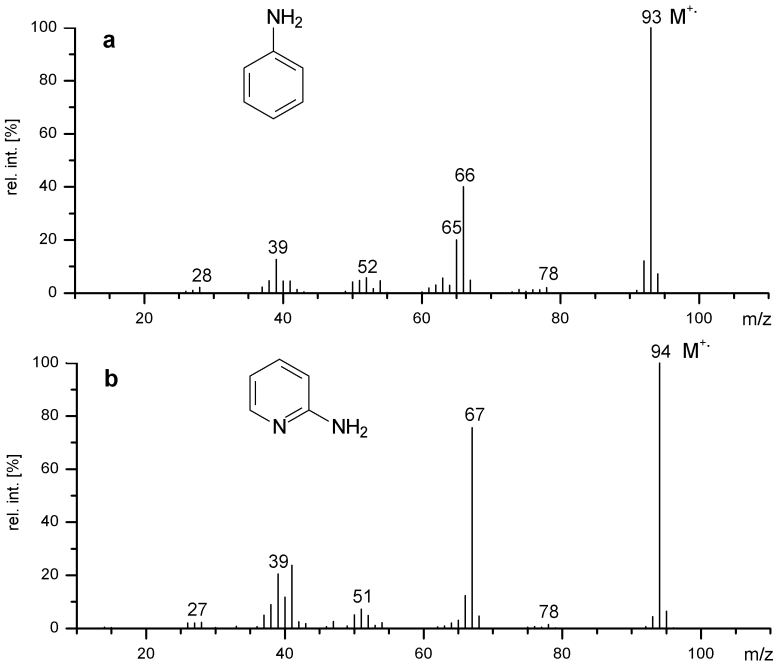
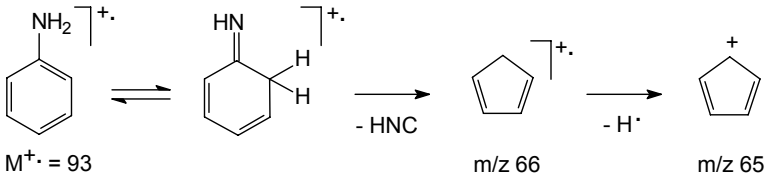


Fig. 6.54. EI mass spectra of aniline (**a**) and 2-aminopyridine (**b**). Different in mechanism from the *N*-heterocycles, but very similar in appearance: the aromatic amine molecular ions eliminate HNC. Spectra used by permission of NIST. © NIST 2002.

The mass spectrum of aniline has been known since the early days of mass spectrometry [109]. Initially, the observed $[M–27]^{+\bullet}$ ion was interpreted in terms of HCN loss (Fig. 6.54a). The mechanism for loss of the elements of H, N, and C from aminoarenes is perfectly analogous to CO loss from phenols (Chap. 6.9.1) [207]. More recently, it could be demonstrated that loss of hydrogen isocyanide,

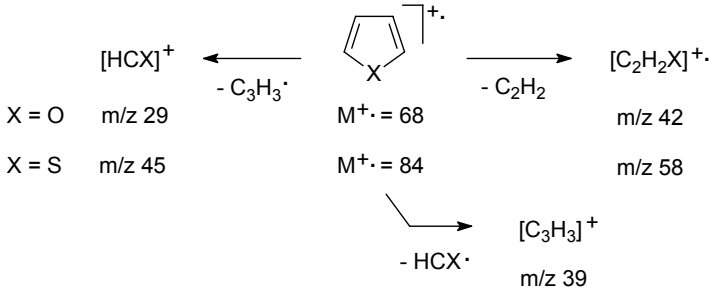
HNC, occurs rather than losing the more stable neutral species HCN, a behavior typical of ionized pyridine [198].

Interestingly, the three isomeric aminopyridine molecular ions display ion chemistry similar to aniline molecular ions, i.e., metastable HNC loss [198], instead of HCN loss which should also be possible due to the pyridine core of the molecule (Fig. 6.54b).



Scheme 6.75.

The mass spectra of furanes are governed by a strong $[M–HCO]^+$ signal and the corresponding, but weaker peak at *m/z* 29 belonging to the formyl ion [208]. Analogous behavior is observed for thiophene, i.e., the spectrum shows a $[M–HCS]^+$ peak, *m/z* 39, and the thioformyl ion, $[HCS]^+$, at *m/z* 45 (Fig. 6.55). Mass spectra of [2-^{13}C]thiophene and of [2-D]thiophene showed that the thioformyl ion is generated after carbon skeleton rearrangement, whereas hydrogen scrambling seemed to be absent [209]. In addition to this marked fragmentation route, the molecular ions of furanes and thiophenes preferably decompose by C_2H_2 loss [210], a behavior resembling that of pyrroles and quinones (Chap. 6.9.2). Mass spectra of substituted furanes and thiophenes are discussed in the literature [208,211,212].



Scheme 6.76.

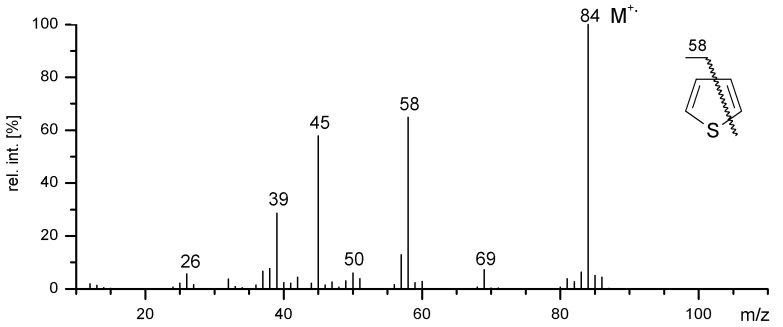


Fig. 6.55. EI mass spectrum of thiophene. The isotopic pattern of sulfur directly reveals its presence in the ions detected at *m/z* 45, 58, (69), and 84. Spectrum used by permission of NIST. © NIST 2002.

6.15 Guide to the Interpretation of Mass Spectra

6.15.1 Summary of Rules

1. Identify the molecular ion! This is an important inital step, because it is needed to derive the molecular composition (Chap. 6.6.4). If the EI spectrum does not allow for the identification of the molecular ion, soft ionization methods should be employed in addition.
2. The mass differences between the presumed molecular ion and primary fragments must correspond to realistic chemical compositions (Chap. 6.6.4, Table 6.12).
3. The calculated and experimental isotopic patterns have to agree with the molecular formula postulated (Chap. 3.2).
4. The derived molecular formula must obey the nitrogen rule (Chap. 6.2.5). An odd-numbered *m/z* value of the molecular ion requires 1, 3, 5, ... nitrogens to be contained, whereas an even *m/z* value belongs to 0, 2, 4, ... nitrogens.
5. Homolytic cleavages cause odd-numbered mass differences between fragment and molecular ion (Chap. 6.2.5). Rearrangement fragmentations cause even-numbered mass differences. This rule toggles if odd numbers of nitrogen are contained in the neutral loss.
6. In general, fragmentations obey the even-electron rule (Chap. 6.1.3). Odd-electron fragments from rearrangement fragmentations behave as if they were molecular ions of the respective smaller molecule.
7. The competition of homolytic cleavages is governed by Stevenson's rule (Chap. 6.2.2). Thermodynamic stability of the pairs of products formed is decisive in selecting the preferred fragmentation route.

8. Calculate $r + d$ to check formula proposals and to derive some structural characteristics (Chap. 6.4.4).
9. Write down a fragmentation scheme, thereby carefully tracking the origin of primary fragment ions and of characteristic ions used for structure assignment. From the purely analytical point of view this is very useful. However, one should keep in mind that any proposed fragmentation scheme remains a working hypothesis unless experimental confirmation is available.
10. Employ additional techniques, such as measurement of accurate mass (Chap. 3.3), tandem mass spectrometry, or other spectroscopic methods to crosscheck and to refine your assignments.

6.15.2 Systematic Approach to Mass Spectra

1. Collect background information such as origin of the sample, presumed compound class, solubility, thermal stability, or other spectroscopic information.
2. Write *m/z* labels for all relevant peaks and calculate mass differences between prominent peaks. Do you recognize characteristic ion series or mass differences that point to common neutral losses?
3. Check which ionization method was used and examine the general appearance of the mass spectrum. Is the molecular ion peak intense (as with aromatic, heterocyclic, polycyclic compounds) or weak (as with aliphatic and multifunctional compounds)? Are there typical impurities (solvent, grease, plasticizers) or background signals (residual air, column bleed in GC-MS)?
4. Is accurate mass data available for some of the peaks?
5. Now, follow the above rules to proceed.
6. Derive information on the presence/absence of functional groups.
7. Be careful when using collections of common neutral losses and *m/z*-to-structure relationship tables – they're never comprehensive. Moreover, one tends to get stuck on the first assumption.
8. Put together the known structural features and try to assign the structure to the unknown sample. Sometimes, only partial structures of the analyte can be derived or isomers cannot be distinguished.
9. Crosscheck proposed molecular structure and mass spectral data. This is also recommended between the single steps of mass spectral interpretation.
10. Are there reference spectra available (at least of similar compounds) either from the literature or from mass spectral databases (Chap. 5.7)?
11. Never rigidly follow this scheme! Sometimes, a step back or forth may accelerate the process or help to avoid pitfalls.
12. Good luck!

References

1. Budzikiewicz, H.; Djerassi, C.; Williams, D.H. *Mass Spectrometry of Organic Compounds*; Holden-Day: San Francisco, 1967.
2. McLafferty, F.W.; Turecek, F. *Interpretation of Mass Spectra;* 4th ed.; University Science Books: Mill Valley, 1993.
3. Budzikiewicz, H. *Massenspektrometrie - Eine Einführung;* 4th ed.; Wiley-VCH: Weinheim, 1998.
4. *Applications of Mass Spectrometry to Organic Stereochemistry*; Splitter, J.S.; Turecek, F. (eds.); Verlag Chemie: Weinheim, 1994.
5. Price, P. Standard Definitions of Terms Relating to Mass Spectrometry. A Report from the Committee on Measurements and Standards of the ASMS. *J. Am. Chem. Soc. Mass Spectrom.* **1991,** *2*, 336-348.
6. Todd, J.F.J. Recommendations for Nomenclature and Symbolism for Mass Spectroscopy Including an Appendix of Terms Used in Vacuum Technology. *Int. J. Mass Spectrom. Ion Proc.* **1995,** *142*, 211-240.
7. Svec, H.J.; Junk, G.A. Electron-Impact Studies of Substituted Alkanes. *J. Am. Chem. Soc.* **1967,** *89*, 790-796.
8. Friedman, L.; Long, F.A. Mass Spectra of Six Lactones. *J. Am. Chem. Soc.* **1953,** *75*, 2832-1836.
9. Karni, M.; Mandelbaum, A. The 'Even-Electron Rule'. *Org. Mass Spectrom.* **1980,** *15*, 53-64.
10. Bowen, R.D.; Harrison, A.G. Loss of Methyl Radical from Some Small Immonium Ions: Unusual Violation of the Even-Electron Rule. *Org. Mass Spectrom.* **1981,** *16*, 180-182.
11. Nizigiyimana, L.; Rajan, P.K.; Haemers, A.; Claeys, M.; Derrick, P.J. Mechanistic Aspects of High-Energy Collision-Induced Dissociation Proximate to the Charge in Saturated Fatty Acid *N*-Butyl Esters Cationized with Lithium. Evidence for Hydrogen Radical Removal. *Rapid Commun. Mass Spectrom.* **1997,** *11*, 1808-1812.
12. Veith, H.J.; Gross, J.H. Alkane Loss from Collisionally Activated Alkylmethyleneimmonium Ions. *Org. Mass Spectrom.* **1991,** *26*, 1061-1064.
13. McLafferty, F.W. Mass Spectrometric Analysis. I. Aliphatic Halogenated Compounds. *Anal. Chem.* **1962,** *34*, 2-15.
14. Stevenson, D.P. Ionization and Dissociation by Electronic Impact. Ionization Potentials and Energies of Formation of *sec*-Propyl and *tert*-Butyl Radicals. Some Limitations on the Method. *Discuss. Faraday Soc.* **1951,** *10*, 35-45.
15. Audier, H.E. Ionisation et Fragmentation en SM I. Sur La Répartition de la Charge Positive Entre Fragment Provenant des Mêmes Ruptures. *Org. Mass Spectrom.* **1969,** *2*, 283-298.
16. Harrison, A.G.; Finney, C.D.; Sherk, J.A. Factors Determining Relative Ionic Abundances in Competing Fragmentation Reactions. *Org. Mass Spectrom.* **1971,** *5*, 1313-1320.
17. Levsen, K. Reaction Mechanisms, in: *Fundamental Aspects of Organic Mass Spectrometry*; Verlag Chemie: Weinheim, 1978; pp. 152-208.
18. NIST NIST Chemistry Webbook. *http://webbook.nist.gov/* **2002**.
19. Sharkey, A.G., Jr.; Shultz, J.L.; Friedel, R.A. Mass Spectra of Ketones. *Anal. Chem.* **1956,** *28*, 934-940.
20. Gilpin, J.A.; McLafferty, F.W. Mass Spectrometric Analysis: Aliphatic Aldehydes. *Anal. Chem.* **1957,** *29*, 990-994.
21. Liedtke, R.J.; Djerassi, C. MS in Structural and Stereochemical Problems. CLXXXIII. A Study of the EI Induced Fragmentation of Aliphatic Aldehydes. *J. Am. Chem. Soc.* **1969,** *91*, 6814-6821.
22. Harrison, A.G. The High-Resolution Mass Spectra of Aliphatic Aldehydes. *Org. Mass Spectrom.* **1970,** *3*, 549-555.
23. Levsen, K.; McLafferty, F.W. Metastable Ion Characteristics. XXVII. Structure and Unimolecular Reactions of $[C_2H_6N]^+$ and $[C_3H_8N]^+$ Ions. *J. Am. Chem. Soc.* **1974,** *96*, 139-144.
24. Bowen, R.D. The Chemistry of $[C_nH_{2n+2}N]^+$ Ions. *Mass Spectrom. Rev.* **1991,** *10*, 225-279.
25. Bowen, R.D. Ion-Neutral Complexes. *Accounts of Chemical Research* **1991,** *24*, 364-371.
26. Djerassi, C.; Fenselau, C. Mass Spectrometry in Structural and Stereochemical Problems. LXXXIV. The Nature of

the Cyclic Transition State in Hydrogen Rearrangements of Aliphatic Ethers. *J. Am. Chem. Soc.* **1965,** *87*, 5747-5762.
27. McLafferty, F.W. Mass Spectrometric Analysis of Aliphatic Ethers. *Anal. Chem.* **1957,** *29*, 1782-1789.
28. Friedel, R.A.; Shultz, J.L.; Sharkey, A.G., Jr. Mass Spectra of Alcohols. *Anal. Chem.* **1956,** *28*, 927-934.
29. Gohlke, R.S.; McLafferty, F.W. MS Analysis of Aliphatic Amines. *Anal. Chem.* **1962,** *34*, 1281-1287.
30. O'Nier, M.J., Jr.; Wier, T.P., Jr. Mass Spectrometry of Heavy Hydrocarbons. *Anal. Chem.* **1951,** 830-843.
31. Hesse, M.; Meier, H.; Zeeh, B. Massenspektren, in: *Spektroskopische Methoden in der Organischen Chemie*, 6th ed.; Thieme: Stuttgart, 2002; Chap. 4, p. 243.
32. Audier, H.E.; Milliet, A.; Sozzi, G.; Denhez, J.P. The Isomerization Mechanisms of Alkylamines: Structure of $[C_2H_6N]^+$ and $[C_3H_8N]^+$ Fragment Ions. *Org. Mass Spectrom.* **1984,** *19*, 79-81.
33. Phillips, G.R.; Russell, M.E.; Solka, B.H. Structure of the $[C_2H_5O]^+$ Ion in the Mass Spectrum of Diethyl Ether. *Org. Mass Spectrom.* **1975,** *10*, 819-823.
34. McAdoo, D.J.; Hudson, C.E. Gas Phase Ionic Reactions Are Generally Stepwise Processes. *Int. J. Mass Spectrom. Ion Proc.* **1984,** *62*, 269-276.
35. Williams, D.H.; Budzikiewicz, H.; Pelah, Z.; Djerassi, C. MS and Its Application to Structural and Stereochemical Problems. XLIV. Fragmentation Behavior of Monocyclic Ketones. *Monatsh. Chem.* **1964,** *95*, 166-177.
36. Seibl, J.; Gäumann, T. Massenspektren Organischer Verbindungen. 2. Mitteilung: Cyclohexanone. *Helv. Chim. Acta* **1963,** *46*, 2857-2872.
37. Yates, B.F.; Bouma, W.J.; Radom, L. Detection of the Prototype Phosphonium (CH_2PH_3), Sulfonium (CH_2SH_2), and Chloronium (CH_2ClH) Ylides by Neutralization-Reionization Mass Spectrometry: a Theoretical Prediction. *J. Am. Chem. Soc.* **1984,** *106*, 5805-5808.
38. Grützmacher, H.-F. Unimolecular Reaction Mechanisms: the Role of Reactive Intermediates. *Int. J. Mass Spectrom. Ion Proc.* **1992,** *118/119*, 825-855.
39. Hammerum, S. Distonic Radical Cations in the Gaseous and Condensed Phase. *Mass Spectrom. Rev.* **1988,** *7*, 123-202.
40. Stirk, K.M.; Kiminkinen, M.L.K.; Kenttämaa, H.I. Ion-Molecule Reactions of Distonic Radical Cations. *Chem. Rev.* **1992,** *92*, 1649-1665.
41. Hammerum, S.; Derrick, P.J. Thermodynamics of Intermediate Ion-Molecule Complexes or Kinetics of Competing Reactions? The Reactions of Low-Energy Isobutylamine and Neopentylamine Molecular Ions. *J. Chem. Soc. ,Perkin Trans. 2* **1986,** 1577-1580.
42. Yates, B.F.; Radom, L. Intramolecular Hydrogen Migration in Ionized Amines: a Theoretical Study of the Gas-Phase Analogues of the Hofmann-Löffler and Related Rearrangements. *J. Am. Chem. Soc.* **1987,** *109*, 2910-2915.
43. Zeller, L.; Farrell, J., Jr.; Vainiotalo, P.; Kenttämaa, H.I. Long-Lived Radical Cations of Simple Organophosphates Isomerize Spontaneously to Distonic Structures in the Gas Phase. *J. Am. Chem. Soc.* **1992,** *114*, 1205-1214.
44. Sack, T.M.; Miller, D.L.; Gross, M.L. The Ring Opening of Gas-Phase Cyclopropane Radical Cations. *J. Am. Chem. Soc.* **1985,** *107*, 6795-6800.
45. Grubb, H.M.; Meyerson, S. Mass Spectra of Alkylbenzenes, in: *Mass Spectrometry of Organic Ions*; McLafferty, F.W. (ed.); Academic Press: New York, 1963; pp. 453-527.
46. McLafferty, F.W.; Bockhoff, F.M. Collisional Activation and Metastable Ion Characteristics. 67. Formation and Stability of Gaseous Tolyl Ions. *Org. Mass Spectrom.* **1979,** *14*, 181-184.
47. Cone, C.; Dewar, M.J.S.; Landman, D. Gaseous Ions. 1. MINDO/3 Study of the Rearrangement of Benzyl Cation to Tropylium. *J. Am. Chem. Soc.* **1977,** *99*, 372-376.
48. Traeger, J.C.; McLoughlin, R.G. Threshold Photoionization and Dissociation of Toluene and Cycloheptatriene. *J. Am. Chem. Soc.* **1977,** *99*, 7351-7352.
49. Howe, I.; McLafferty, F.W. Unimolecular Decomposition of Toluene and Cycloheptatriene Molecular Ions. Variation of the Degree of Scrambling and Isotope Effect with Internal Energy. *J. Am. Chem. Soc.* **1971,** *93*, 99-105.
50. Kuck, D. Half a Century of Scrambling in Organic Ions: Complete, Incomplete, Progressive and Composite Atom Interchange. *Int. J. Mass Spectrom.* **2002,** *213*, 101-144.

51. Mormann, M.; Kuck, D. Protonated 1,3,5-Cycloheptatriene and 7-Alkyl-1,3,5-Cycloheptatrienes in the Gas Phase: Ring Contraction to the Isomeric Alkylbenzenium Ions. *J. Mass Spectrom.* **1999,** *34*, 384-394.
52. Rylander, P.N.; Meyerson, S.; Grubb, H.M. Organic Ions in the Gas Phase. II. The Tropylium Ion. *J. Am. Chem. Soc.* **1957,** *79*, 842-846.
53. Cooks, R.G.; Howe, I.; Tam, S.W.; Williams, D.H. Studies in Mass Spectrometry. XXIX. Hydrogen Scrambling in Some Bicyclic Aromatic Systems. Randomization Over Two Rings. *J. Am. Chem. Soc.* **1968,** *90*, 4064-4069.
54. Borchers, F.; Levsen, K. Isomerization of Hydrocarbon Ions. III. $[C_8H_8]^+$, $[C_8H_8]^{2+}$, $[C_6H_6]^+$, and $[C_6H_5]^+$ Ions. *Org. Mass Spectrom.* **1975,** *10*, 584-594.
55. Nishishita, T.; McLafferty, F.W. Metastable Ion Characteristics. XXXXVII. Collisional Activation Mass Spectra of Pentene and Hexene Molecular Ions. *Org. Mass Spectrom.* **1977,** *12*, 75-77.
56. Borchers, F.; Levsen, K.; Schwarz, H.; Wesdemiotis, C.; Winkler, H.U. Isomerization of Linear Octene Cations in the Gas Phase. *J. Am. Chem. Soc.* **1977,** *99*, 6359-6365.
57. Schneider, B.; Budzikiewicz, H. A Facile Method for the Localization of a Double Bond in Aliphatic Compounds. *Rapid Commun. Mass Spectrom.* **1990,** *4*, 550-551.
58. Peake, D.A.; Gross, M.L. Iron(I) Chemical Ionization and Tandem Mass Spectrometry for Locating Double Bonds. *Anal. Chem.* **1985,** *57*, 115-120.
59. Fordham, P.J.; Chamot-Rooke, J.; Guidice, E.; Tortajada, J.; Morizur, J.-P. Analysis of Alkenes by Copper Ion GC-CI-MS and GC-MS/MS Mass Spectrometry. *J. Mass Spectrom.* **1999,** *34*, 1007-1017.
60. Levsen, K.; Weber, R.; Borchers, F.; Heimbach, H.; Beckey, H.D. Determination of Double Bonds in Alkenes by FI-MS. *Anal. Chem.* **1978,** *50*, 1655-1658.
61. Buser, H.-R.; Arn, H.; Guerin, P.; Rauscher, S. Determination of Double Bond Position in Mono-Unsaturated Acetates by MS of Dimethyl Disulfide Adducts. *Anal. Chem.* **1983,** *55*, 818-822.
62. Scribe, P.; Guezennec, J.; Dagaut, J.; Pepe, C.; Saliot, A. Identification of the Position and the Stereochemistry of the Double Bond in Monounsaturated Fatty Acid Methyl Esters by GC-MS of Dimethyl Disulfide Derivatives. *Anal. Chem.* **1988,** *60*, 928-931.
63. Pepe, C.; Dif, K. The Use of Ethanethiol to Locate the Triple Bond in Alkynes and the Double Bond in Substituted Alkenes by GC-MS. *Rapid Commun. Mass Spectrom.* **2001,** *15*, 97-103.
64. Pepe, C.; Sayer, H.; Dagaut, J.; Couffignal, R. Determination of Double Bond Positions in Triunsaturated Compounds by Means of GC-MS of Dimethyl Disulfide Derivatives. *Rapid Commun. Mass Spectrom.* **1997,** *11*, 919-921.
65. Levsen, K.; Heimbach, H.; Shaw, G.J.; Milne, G.W.A. Isomerization of Hydrocarbon Ions. VIII. The Electron Impact Induced Decomposition of *N*-Dodecane. *Org. Mass Spectrom.* **1977,** *12*, 663-670.
66. Lavanchy, A.; Houriet, R.; Gäumann, T. The Mass Spectrometric Fragmentation of *N*-Alkane. *Org. Mass Spectrom.* **1979,** *14*, 79-85.
67. Levsen, K. Isomerization of Hydrocarbon Ions. I. Isomeric Octanes. Collisional Activation Study. *Org. Mass Spectrom.* **1975,** *10*, 43-54.
68. Traeger, J.C.; McAdoo, D.J.; Hudson, C.E.; Giam, C.S. Why Are Alkane Eliminations from Ionized Alkanes so Abundant? *J. Am. Chem. Soc. Mass Spectrom.* **1998,** *9*, 21-28.
69. McAdoo, D.J.; Bowen, R.D. Alkane Eliminations from Ions in the Gas Phase. *Eur. Mass Spectrom.* **1999,** *5*, 389-409.
70. Olivella, S.; Solé, A.; McAdoo, D.J.; Griffin, L.L. Unimolecular Reactions of Ionized Alkanes: Theoretical Study of the Potential Energy Surface for CH_3·Bul. and CH_4 Losses from Ionized Butane and Isobutane. *J. Am. Chem. Soc.* **1994,** *94*, 11078-11088.
71. Williams, D.H. A Transition State Probe. *Accounts of Chemical Research* **1977,** *10*, 280-286.
72. Ludányi, K.; Dallos, A.; Kühn, Z.; Vékey, D. Mass Spectrometry of Very Large Saturated Hydrocarbons. *J. Mass Spectrom.* **1999,** *34*, 264-267.
73. Biemann, K. Application of MS in Organic Chemistry for Structure Determination of Natural Products. *Angew. Chem.* **1962,** *74*, 102-115.
74. Happ, G.P.; Stewart, D.W. Rearrangement Peaks in the Mass Spectra of Cer-

tain Aliphatic Acids. *J. Am. Chem. Soc.* **1952,** *74*, 4404-4408.
75. McLafferty, F.W. Mass Spectrometric Analysis. Broad Applicability to Chemical Research. *Anal. Chem.* **1956,** *28*, 306-316.
76. McLafferty, F.W. Mass Spectrometric Analysis: Molecular Rearrangements. *Anal. Chem.* **1965,** *31*, 82-87.
77. Kingston, D.G.I.; Bursey, J.T.; Bursey, M.M. Intramolecular Hydrogen Transfer in Mass Spectra. II. McLafferty Rearrangement and Related Reactions. *Chem. Industry* **1974,** *74*, 215-245.
78. Zollinger, M.; Seibl, J. McLafferty Reactions in Even-Electron Ions? *Org. Mass Spectrom.* **1985,** *11*, 649-661.
79. Djerassi, C.; Tökés, L. Mass Spectrometry in Structural and Stereochemical Problems. XCIII. Further Observations on the Importance of Interatomic Distance in the McLafferty Rearrangement. Synthesis and Fragmentation Behavior of Deuterium-Labeled 12-Oxo Steroids. *J. Am. Chem. Soc.* **1966,** *88*, 536-544.
80. Djerassi, C.; von Mutzenbecher, G.; Fajkos, J.; Williams, D.H.; Budzikiewicz, H. MS in Structural and Stereochemical Problems. LXV. Synthesis and Fragmentation Behavior of 15-Oxo Steroids. The Importance of Inter-Atomic Distance in the McLafferty Rearrangement. *J. Am. Chem. Soc.* **1965,** *87*, 817-826.
81. Henion, J.D.; Kingston, D.G.I. MS of Organic Compounds. IX. McLafferty Rearrangements in Some Bicyclic Ketones. *J. Am. Chem. Soc.* **1974,** *96*, 2532-2536.
82. Stringer, M.B.; Underwood, D.J.; Bowie, J.H.; Allison, C.E.; Donchi, K.F.; Derrick, P.J. Is the McLafferty Rearrangement of Ketones Concerted or Stepwise? The Application of Kinetic Isotope Effects. *Org. Mass Spectrom.* **1992,** *27*, 270-276.
83. Dewar, M.J.S. Multibond Reactions Cannot Normally Be Synchronous. *J. Am. Chem. Soc.* **1984,** *106*, 209-219.
84. Holmes, J.L.; Lossing, F.P. Gas-Phase Heats of Formation of Keto and Enol Ions of Carbonyl Compounds. *J. Am. Chem. Soc.* **1980,** *102*, 1591-1595.
85. Hrušák, J. MNDO Calculations on the Neutral and Cationic $[CH_3\text{-}CO\text{-}R]$ Systems in Relation to Mass Spectrometric Fragmentations. *Z. Phys. Chem.* **1991,** *172*, 217-226.
86. Beynon, J.H.; Saunders, R.A.; Williams, A.E. The High Resolution Mass Spectra of Aliphatic Esters. *Anal. Chem.* **1961,** *33*, 221-225.
87. Harrison, A.G.; Jones, E.G. Rearrangement Reactions Following Electron Impact on Ethyl and Isopropyl Esters. *Can. J. Chem.* **1965,** *43*, 960-968.
88. Wesdemiotis, C.; Feng, R.; McLafferty, F.W. Distonic Radical Ions. Stepwise Elimination of Acetaldehyde from Ionized Benzyl Ethyl Ether. *J. Am. Chem. Soc.* **1985,** *107*, 715-716.
89. Benoit, F.M.; Harrison, A.G. Hydrogen Migrations in MS. II. Single and Double Hydrogen Migrations in the EI Fragmentation of Propyl Benzoate. *Org. Mass Spectrom.* **1976,** 1056-1062.
90. Müller, J.; Krebs, G.; Lüdemann, F.; Baumgartner, E. Wasserstoff-Umlagerungen beim Elektronenstoß-induzierten Zerfall von H^6–Benzoesäure-*n*-Propylester-Tricarbonylchrom. *J. Organomet. Chem.* **1981,** *218*, 61-68.
91. Benoit, F.M.; Harrison, A.G.; Lossing, F.P. Hydrogen Migrations in Mass Spectrometry. III. Energetics of Formation of $[R'CO_2H_2]^+$ in the Mass Spectra of $R'CO_2R$. *Org. Mass Spectrom.* **1977,** *12*, 78-82.
92. Tajima, S.; Azami, T.; Shizuka, H.; Tsuchiya, T. An Investigation of the Mechanism of Single and Double Hydrogen Atom Transfer Reactions in Alkyl Benzoates by the Ortho Effect. *Org. Mass Spectrom.* **1979,** *14*, 499-502.
93. Elder, J.F., Jr.; Beynon, J.H.; Cooks, R.G. The Benzoyl Ion. Thermochemistry and Kinetic Energy Release. *Org. Mass Spectrom.* **1976,** *11*, 415-422.
94. McLafferty, F.W.; Gohlke, R.S. MS Analysis-Aromatic Acids and Esters. *Anal. Chem.* **1959,** *31*, 2076-2082.
95. Yinon, J. Mass Spectral Fragmentation Pathways in Phthalate Esters. A Tandem Mass Spectrometric Collision-Induced Dissociation Study. *Org. Mass Spectrom.* **1988,** *23*, 755-759.
96. Djerassi, C.; Fenselau, C. Mass Spectrometry in Structural and Stereochemical Problems. LXXXVI. The Hydrogen-Transfer Reactions in Butyl Propionate, Benzoate, and Phthalate. *J. Am. Chem. Soc.* **1965,** *87*, 5756-5762.
97. Turecek, F.; Hanus, V. Retro-Diels-Alder Reaction in Mass Spectrometry. *Mass Spectrom. Rev.* **1984,** *3*, 85-152.

98. Turecek, F.; Hanuš, V. Charge Distribution Between Formally Identical Fragments: the Retro-Diels-Alder Cleavage. *Org. Mass Spectrom.* **1980,** *15*, 4-7.
99. Kühne, H.; Hesse, M. The Mass Spectral Retro-Diels-Alder Reaction of 1,2,3,4-Tetrahydronaphthalene, Its Derivatives and Related Heterocyclic Compounds. *Mass Spectrom. Rev.* **1982,** *1*, 15-28.
100. Budzikiewicz, H.; Brauman, J.I.; Djerassi, C. Mass Spectrometry and Its Application to Structural and Stereochemical Problems. LXVII. Retro-Diels-Alder Fragmentation of Organic Molecules Under Electron Impact. *Tetrahedron* **1965,** *21*, 1855-1879.
101. Djerassi, C. Steroids Made It Possible: Organic Mass Spectrometry. *Org. Mass Spectrom.* **1992,** *27*, 1341-1347.
102. Dixon, J.S.; Midgley, I.; Djerassi, C. Mass Spectrometry in Structural and Stereochemical Problems. 248. Stereochemical Effects in EI-Induced Retro-Diels-Alder Fragmentations. *J. Am. Chem. Soc.* **1977,** *99*, 3432-3441.
103. Barnes, C.S.; Occolowitz, J.L. MS of Some Naturally Occurring Oxygen Heterocycles and Related Compounds. *Aust. J. Chem.* **1964,** *17*, 975-986.
104. Ardanaz, C.E.; Guidugli, F.H.; Catalán, C.A.N.; Joseph-Nathan, P. MS Studies of Methoxynaphthoflavones. *Rapid Commun. Mass Spectrom.* **1999,** *13*, 2071-2079.
105. Ballenweg, S.; Gleiter, R.; Krätschmer, W. Chemistry at Cyclopentene Addends on [60]Fullerene. MALDI-TOF-MS as a Quick and Facile Method for the Characterization of Fullerene Derivatives. *Synth. Met.* **1996,** *77*, 209-212.
106. Ballenweg, S.; Gleiter, R.; Krätschmer, W. Unusual Functionalization of C_{60} Via Hydrozirconation: Reactivity of the C_{60}-Zr(IV) Complex vs. Alkyl-Zr(IV) Complexes. *J. Chem. Soc. ,Chem. Commun.* **1994,** 2269-2270.
107. Aczel, T.; Lumpkin, H.E. Correlation of Mass Spectra With Structure in Aromatic Oxygenated Compounds. Aromatic Alcohols and Phenols. *Anal. Chem.* **1960,** *32*, 1819-1822.
108. Beynon, J.H. Correlation of Molecular Structure and Mass Spectra, in *Mass Spectrometry and its Applications to Organic Chemistry*; Elsevier: Amsterdam, 1960; pp. 352.
109. Momigny, J. The Mass Spectra of Monosubstituted Benzene Derivatives. Phenol, Monodeuteriophenol, Thiophenol, and Aniline. *Bull. Soc. Royal Sci. Liège* **1953,** *22*, 541-560.
110. Occolowitz, J.L. Mass Spectrometry of Naturally Occurring Alkenyl Phenols and Their Derivatives. *Anal. Chem.* **1964,** *36*, 2177-2181.
111. Stensen, W.G.; Jensen, E. Structural Determinationof 1,4-Naphthoquinones by Mass Spectrometry/Mass Spectrometry. *J. Mass Spectrom.* **1995,** *30*, 1126-1132.
112. Beynon, J.H.; Lester, G.R.; Williams, A.E. Specific Molecular Rearrangements in Mass Spectra of Organic Compounds. *J. Phys. Chem.* **1959,** *63*, 1861-1869.
113. Pelah, Z.; Wilson, J.M.; Ohashi, M.; Budzikiewicz, H.; Djerassi, C. Mass Spectrometry in Structural and Stereochemical Problems. XXXIV. Aromatic Methyl and Ethyl Ethers. *Tetrahedron* **1963,** *19*, 2233-2240.
114. Molenaar-Langeveld, T.A.; Ingemann, S.; Nibbering, N.M.M. Skeletal Rearrangements Preceding Carbon Monoxide Loss from Metastable Phenoxymethylene Ions Derived from Phenoxyacetic Acid and Anisole. *Org. Mass Spectrom.* **1993,** *28*, 1167-1178.
115. Zagorevskii, D.V.; Régimbal, J.-M.; Holmes, J.L. The Heat of Formation of the $[C_6,H_5,O]^+$ Isomeric Ions. *Int. J. Mass Spectrom. Ion Proc.* **1997,** *160*, 211-222.
116. Cooks, R.G.; Bertrand, M.; Beynon, J.H.; Rennekamp, M.E.; Setser, D.W. Energy Partitioning Data As an Ion Structure Probe. Substituted Anisoles. *J. Am. Chem. Soc.* **1973,** *95*, 1732-1739.
117. Alexander, J.J. Mechanism of Photochemical Decarbonylation of Acetyldicarbonyl-H^5-Cyclopentadienyliron. *J. Am. Chem. Soc.* **1975,** *97*, 1729-1732.
118. Coville, N.J.; Johnston, P. A Mass-Spectral Investigation of Site-Selective Carbon Monoxide Loss from Isotopically Labeled $[MnRe(CO)_{10}]^+$. *J. Organomet. Chem.* **1989,** *363*, 343-350.
119. Tobita, S.; Ogino, K.; Ino, S.; Tajima, S. On the Mechanism of Carbon Monoxide Loss from the Metastable Molecular Ion of Dimethyl Malonate. *Int. J. Mass Spectrom. Ion Proc.* **1988,** *85*, 31-42.
120. Moldovan, Z.; Palibroda, N.; Mercea, V.; Mihailescu, G.; Chiriac, M.; Vlasa, M. Mass Spectra of Some β-Keto Esters.

A High Resolution Study. *Org. Mass Spectrom.* **1981,** *16*, 195-198.
121. Vairamani, M.; Mirza, U.A. Mass Spectra of Phenoxyacetyl Derivatives. Mechanism of Loss of CO from Phenyl Phenoxyacetates. *Org. Mass Spectrom.* **1987,** *22*, 406-409.
122. Tou, J.C. Competitive and Consecutive Eliminations of Molecular Nitrogen and Carbon Monoxide (or Ethene) from Heterocyclics Under Electron Impact. *J. Heterocycl. Chem.* **1974,** *11*, 707-711.
123. Meyerson, S.; Leitch, L.C. Organic Ions in the Gas Phase. XIV. Loss of Water from Primary Alcohols Under Electron Impact. *J. Am. Chem. Soc.* **1964,** *86*, 2555-2558.
124. Bukovits, G.J.; Budzikiewicz, H. Mass Spectroscopic Fragmentation Reactions. XXVIII. The Loss of Water from *N*-Alkan-1-ols. *Org. Mass Spectrom.* **1983,** *18*, 219-220.
125. Bowen, R.D. The Role of Ion-Neutral Complexes in the Reactions of Onium Ions and Related Species. *Org. Mass Spectrom.* **1993,** *28*, 1577-1595.
126. Bowen, R.D. Potential Energy Profiles for Unimolecular Reactions of Isolated Organic Ions: Some Isomers of $[C_4H_{10}N]^+$ and $[C_5H_{12}N]^+$. *J. Chem. Soc. ,Perkin Trans. 2* **1980,** 1219-1227.
127. Bowen, R.D.; Derrick, P.J. Unimolecular Reactions of Isolated Organic Ions: the Chemistry of the Oxonium Ions $[CH_3CH_2CH_2CH_2O{=}CH_2]^+$ and $[CH_3CH_2CH_2CH{=}OCH_3]^+$. *Org. Mass Spectrom.* **1993,** *28*, 1197-1209.
128. Solling, T.I.; Hammerum, S. The Retro-Ene Reaction of Gaseous Immonium Ions Revisited. *J. Chem. Soc. ,Perkin Trans. 2* **2001,** 2324-2428.
129. Veith, H.J.; Gross, J.H. Alkene Loss from Metastable Methyleneimmonium Ions: Unusual Inverse Secondary Isotope Effect in Ion-Neutral Complex Intermediate Fragmentations. *Org. Mass Spectrom.* **1991,** *26*, 1097-1105.
130. Budzikiewicz, H.; Bold, P. A McLafferty Rearrangement in an Even-Electron System: C_3H_6 Elimination from the α-Cleavage Product of Tributylamine. *Org. Mass Spectrom.* **1991,** *26*, 709-712.
131. Bowen, R.D.; Colburn, A.W.; Derrick, P.J. Unimolecular Reactions of Isolated Organic Ions: Reactions of the Immonium Ions $[CH_2{=}N(CH_3)CH(CH_3)_2]^+$, $[CH_2{=}N(CH_3)CH_2CH_2CH_3]^+$ and $[CH_2{=}N(CH_2CH_2CH_3)_2]^+$. *J. Chem. Soc. ,Perkin Trans. 2* **1993,** 2363-2372.
132. Gross, J.H.; Veith, H.J. Propene Loss from Phenylpropylmethyleneiminium Ions. *Org. Mass Spectrom.* **1994,** *29*, 153-154.
133. Gross, J.H.; Veith, H.J. Unimolecular Fragmentations of Long-Chain Aliphatic Iminium Ions. *Org. Mass Spectrom.* **1993,** *28*, 867-872.
134. Uccella, N.A.; Howe, I.; Williams, D.H. Structure and Isomerization of Gaseous $[C_3H_8N]^+$ Metastable Ions. *J. Chem. Soc. ,B* **1971,** 1933-1939.
135. Levsen, K.; Schwarz, H. Influence of Charge Localization on the Isomerization of Organic Ions. *Tetrahedron* **1975,** *31*, 2431-2433.
136. Bowen, R.D. Unimolecular Reactions of Organic Ions: Olefin Elimination from Immonium Ions $[R^1R^2N{=}CH_2]^+$. *J. Chem. Soc.,Perkin Trans. 2* **1982,** 409-413.
137. Bowen, R.D. Reactions of Isolated Organic Ions. Alkene Loss from the Immonium Ions $[CH_3CH{=}NHC_2H_5]^+$ and $[CH_3CH{=}NHC_3H_7]^+$. *J. Chem. Soc. ,Perkin Trans. 2* **1989,** 913-918.
138. Bowen, R.D.; Colburn, A.W.; Derrick, P.J. Unimolecular Reactions of the Isolated Immonium Ions $[CH_3CH{=}NHC_4H_9]^+$, $[CH_3CH_2CH{=}NHC_4H_9]^+$,$[(CH_3)_2C{=}NHC_4H_9]^+$. *Org. Mass Spectrom.* **1990,** *25*, 509-516.
139. Bowen, R.D.; Maccoll, A. Unimolecular Reactions of Ionized Ethers. *J. Chem. Soc. ,Perkin Trans. 2* **1990,** 147-155.
140. Traeger, J.C.; Hudson, C.E.; McAdoo, D.J. Energy Dependence of Ion-Induced Dipole Complex-Mediated Alkane Eliminations from Ionized Ethers. *J. Phys. Chem.* **1990,** *94*, 5714-5717.
141. Bowen, R.D.; Williams, D.H. Non-Concerted Unimolecular Reactions of Ions in the Gas-Phase: the Importance of Ion-Dipole Interactions in Carbonium Ion Isomerizations. *Int. J. Mass Spectrom. Ion Phys.* **1979,** *29*, 47-55.
142. Bowen, R.D.; Williams, D.H. Unimolecular Reactions of Isolated Organic Ions. The Importance of Ion-Dipole Interactions. *J. Am. Chem. Soc.* **1980,** *102*, 2752-2756.
143. Bowen, R.D.; Derrick, P.J. The Mechanism of Ethylene Elimination from the Oxonium Ions $[CH_3CH_2CH{=}OCH_2CH_3]^+$ and $[(CH_3)_2C{=}OCH_2CH_3]^+$. *J. Chem. Soc. ,Perkin Trans. 2* **1992,** 1033-1039.

144. Nguyen, M.T.; Vanquickenborne, L.G.; Bouchoux, G. Energy Barrier for 1,2-Elimination of Methane from Dimethyloxonium Cation. *Int. J. Mass Spectrom. Ion Proc.* **1993,** *124*, R11-R14.
145. Lias, S.G.; Liebman, J.F.; Levin, R.D. Evaluated Gas Phase Basicities and Proton Affinities of Molecules; Heats of Formation of Protonated Molecules. *J. Phys. Chem. Ref. Data* **1984,** *13*, 695-808.
146. Lias, S.G.; Bartmess, J.E.; Liebman, J.F.; Holmes, J.L.; Levin, R.D.; Mallard, W.G. Gas-Phase Ion and Neutral Thermochemistry. *J. Phys. Chem. Ref. Data* **1988,** *17, Supplement 1*, 861 pp.
147. Hunter, E.P.L.; Lias, S.G. Evaluated Gas Phase Basicities and Proton Affinities of Molecules: An Update. *J. Phys. Chem. Ref. Data* **1998,** *27*, 413-656.
148. Bowen, R.D.; Colburn, A.W.; Derrick, P.J. Unimolecular Reactions of Isolated Organic Ions: the Chemistry of the Unsaturated Oxonium Ion $[CH_2{=}CHCH{=}OCH_3]^+$. *Org. Mass Spectrom.* **1992,** *27*, 625-632.
149. Bowen, R.D.; Stapleton, B.J.; Williams, D.H. Nonconcerted Unimolecular Reactions of Ions in the Gas Phase: Isomerization of Weakly Coordinated Carbonium Ions. *J. Chem. Soc. ,Chem. Commun.* **1978,** 24-26.
150. Morton, T.H. Gas Phase Analogues of Solvolysis Reactions. *Tetrahedron* **1982,** *38*, 3195-3243.
151. Morton, T.H. The Reorientation Criterion and Positive Ion-Neutral Complexes. *Org. Mass Spectrom.* **1992,** *27*, 353-368.
152. Longevialle, P. Ion-Neutral Complexes in the Unimolecular Reactivity of Organic Cations in the Gas Phase. *Mass Spectrom. Rev.* **1992,** *11*, 157-192.
153. McAdoo, D.J. Ion-Neutral Complexes in Unimolecular Decompositions. *Mass Spectrom. Rev.* **1988,** *7*, 363-393.
154. Rylander, P.N.; Meyerson, S. Organic Ions in the Gas Phase. I. The Cationated Cyclopropane Ring. *J. Am. Chem. Soc.* **1956,** *78*, 5799-5802.
155. Meyerson, S. Cationated Cyclopropanes As Reaction Intermediates in Mass Spectra: an Earlier Incarnation of Ion-Neutral Complexes. *Org. Mass Spectrom.* **1989,** *24*, 267-270.
156. Longevialle, P.; Botter, R. Electron Impact Mass Spectra of Bifunctional Steroids. The Interaction Between Ionic and Neutral Fragments Derived from the Same Parent Ion. *Org. Mass Spectrom.* **1983,** *18*, 1-8.
157. Longevialle, P.; Botter, R. The Interaction Between Ionic and Neutral Fragments from the Same Parent Ion in the Mass Spectrometer. *Int. J. Mass Spectrom. Ion Phys.* **1983,** *47*, 179-182.
158. Redman, E.W.; Morton, T.H. Product-Determining Steps in Gas-Phase Broensted Acid-Base Reactions. Deprotonation of 1-Methylcyclopentyl Cation by Amine Bases. *J. Am. Chem. Soc.* **1986,** *108*, 5701-5708.
159. Filges, U.; Grützmacher, H.-F. Fragmentations of Protonated Benzaldehydes Via Intermediate Ion/Molecule Complexes. *Org. Mass Spectrom.* **1986,** *21*, 673-680.
160. Hudson, C.E.; McAdoo, D.J. Alkane Eliminations from Radical Cations Through Ion-Radical Complexes. *Int. J. Mass Spectrom. Ion Proc.* **1984,** *59*, 325-332.
161. McAdoo, D.J.; Hudson, C.E. Ion-Neutral Complex-Mediated Hydrogen Exchange in Ionized Butanol: a Mechanism for Nonspecific Hydrogen Migration. *Org. Mass Spectrom.* **1987,** *22*, 615-621.
162. Hammerum, S.; Audier, H.E. Experimental Verification of the Intermediacy and Interconversion of Ion-Neutral Complexes As Radical Cations Dissociate. *J. Chem. Soc., Chem. Commun.* **1988,** 860-861.
163. Traeger, J.C.; Hudson, C.E.; McAdoo, D.J. Isomeric Ion-Neutral Complexes Generated from Ionized 2-Methylpropanol and *N*-Butanol: the Effect of the Polarity of the Neutral Partner on Complex-Mediated Reactions. *J. Am. Chem. Soc. Mass Spectrom.* **1991,** *3*, 409-416.
164. Sozzi, G.; Audier, H.E.; Mourgues, P.; Milliet, A. Alkyl Phenyl Ether Radical Cations in the Gas Phase: a Reaction Model. *Org. Mass Spectrom.* **1987,** *22*, 746-747.
165. Blanchette, M.C.; Holmes, J.L.; Lossing, F.P. The Fragmentation of Ionized Alkyl Phenyl Ethers. *Org. Mass Spectrom.* **1989,** *24*, 673-678.
166. Harnish, D.; Holmes, J.L. Ion-Radical Complexes in the Gas Phase: Structure and Mechanism in the Fragmentation of Ionized Alkyl Phenyl Ethers. *J. Am. Chem. Soc.* **1991,** *113*, 9729-9734.

167. Zappey, H.W.; Ingemann, S.; Nibbering, N.M.M. Isomerization and Fragmentation of Aliphatic Thioether Radical Cations: Ion-Neutral Complexes in the Reactions of Metastable Ethyl Propyl Thioether Ions. *J. Chem. Soc., Perkin Trans. 2* **1991,** 1887-1892.
168. Broer, W.J.; Weringa, W.D. Potential Energy Profiles for the Unimolecular Reactions of $[C_3H_7S]^+$ Ions. *Org. Mass Spectrom.* **1980,** 229-234.
169. Schwarz, H. Some Newer Aspects of Mass Spectrometric Ortho Effects. *Top. Curr. Chem.* **1978,** *73*, 231-263.
170. Meyerson, S.; Drews, H.; Field, E.K. Mass Spectra of Ortho-Substituted Diarylmethanes. *J. Am. Chem. Soc.* **1964,** *86*, 4964-4967.
171. Grützmacher, H.-F. Mechanisms of Mass Spectrometric Fragmentation Reactions. XXXII. The Loss of *Ortho* Halo Substituents from Substituted Thiobenzamide Ions. *Org. Mass Spectrom.* **1981,** *16*, 448-450.
172. Ramana, D.V.; Sundaram, N.; George, N. Ortho Effects in Organic Molecules on EI. 14. Concerted and Stepwise Ejections of SO_2 and N_2 from *N*-Arylidene-2-Nitrobenzenesulfen-amides. *Org. Mass Spectrom.* **1987,** *22*, 140-144.
173. Sekiguchi, O.; Noguchi, T.; Ogino, K.; Tajima, S. Fragmentation of Metastable Molecular Ions of Acetylanisoles. *Int. J. Mass Spectrom. Ion Proc.* **1994,** *132*, 172-179.
174. Barkow, A.; Pilotek, S.; Grützmacher, H.-F. *Ortho* Effects: A Mechanistic Study. *Eur. Mass Spectrom.* **1995,** *1*, 525-537.
175. Danikiewicz, W. Electron Ionization-Induced Fragmentation of *N*-Alkyl-*o*-Nitroanilines: Observation of New Types of *Ortho* Effects. *Eur. Mass Spectrom.* **1998,** *4*, 167-179.
176. Spiteller, G. The *Ortho* Effect in the Mass Spectra of Aromatic Compounds. *Monatsh. Chem.* **1961,** *92*, 1147-1154.
177. Martens, J.; Praefcke, K.; Schwarz, H. Spectroscopic Investigations. IX. Analytical Importance of the *Ortho* Effect in Mass Spectrometry. Benzoic and Thiobenzoic Acid Derivatives. *Z. Naturforsch. ,B* **1975,** *30*, 259-262.
178. Smith, J.G.; Wilson, G.L.; Miller, J.M. Mass Spectra of Isopropyl Benzene Derivatives. A Study of the *Ortho* Effect. *Org. Mass Spectrom.* **1975,** *10*, 5-17.
179. Schwarz, H.; Köppel, C.; Bohlmann, F. Electron Impact-Induced Fragmentation of Acetylene Compounds. XII. Rearrangement of Bis(Trimethylsilyl) Ethers of Unsaturated α,ω-Diols and Mass Spectrometric Identification of Isomeric Phenols. *Tetrahedron* **1974,** *30*, 689-693.
180. Krauss, D.; Mainx, H.G.; Tauscher, B.; Bischof, P. Fragmentation of Trimethylsilyl Derivatives of 2-Alkoxyphenols: a Further Violation of the 'Even-Electron Rule'. *Org. Mass Spectrom.* **1985,** *20*, 614-618.
181. Svendsen, J.S.; Sydnes, L.K.; Whist, J.E. MS Study of Dimethyl Esters of Trimethylsilyl Ether Derivatives of Some 3-Hydroxy Dicarboxylic Acids. *Org. Mass Spectrom.* **1987,** *22*, 421-429.
182. Svendsen, J.S.; Whist, J.E.; Sydnes, L.K. A Mass Spectrometric Study of the Dimethyl Ester Trimethylsilyl Enol Ether Derivatives of Some 3-Oxodicarboxylic Acids. *Org. Mass Spectrom.* **1987,** *22*, 486-492.
183. Halket, H.M.; Zaikin, V.G. Derivatization in Mass Spectrometry -1. Silylation. *Eur. J. Mass Spectrom.* **2003,** *9*, 1-21.
184. Beynon, J.H.; Bertrand, M.; Cooks, R.G. Metastable Loss of Nitrosyl Radical from Aromatic Nitro Compounds. *J. Am. Chem. Soc.* **1973,** *95*, 1739-1745.
185. McLuckey, S.A.; Glish, G.L. The Effect of Charge on Hydroxyl Loss from *Ortho*-Substituted Nitrobenzene Ions. *Org. Mass Spectrom.* **1987,** *22*, 224-228.
186. Beynon, J.H.; Saunders, R.A.; Topham, A.; Williams, A.E. The Dissociation of *O*-Nitrotoluene Under Electron Impact. *J. Chem. Soc.* **1965,** 6403-6405.
187. Herbert, C.G.; Larka, E.A.; Beynon, J.H. The Elimination of Masses 27 and 28 from the $[M\text{-}OH]^+$ Ion of 2-Nitrotoluene. *Org. Mass Spectrom.* **1984,** *19*, 306-310.
188. Meyerson, S.; Puskas, I.; Fields, E.K. Organic Ions in the Gas Phase. XVIII. Mass Spectra of Nitroarenes. *J. Am. Chem. Soc.* **1966,** *88*, 4974-4908.
189. Riley, J.S.; Baer, T.; Marbury, G.D. Sequential *Ortho* Effects: Characterization of Novel $[M\text{-}35]^+$ Fragment Ions in the Mass Spectra of 2-Alkyl-4,6-Dinitrophenols. *J. Am. Chem. Soc. Mass Spectrom.* **1991,** *2*, 69-75.
190. Yinon, J. Mass Spectral Fragmentation Pathways in 2,4,6-Trinitroaromatic Compounds. A Tandem-MS Collision-

Induced Dissociation Study. *Org. Mass Spectrom.* **1987,** *22*, 501-505.
191. Porter, Q.N.; Baldas, J. *Mass Spectrometry of Heterocyclic Compounds*; Wiley Interscience: New York, 1971.
192. Schwarz, H.; Bohlmann, F. Mass Spectrometric Investigation of Amides. II. EI Fragmentation of (Phenylacetyl)-Aziridine, -Pyrrolidine, and -Piperidine. *Tetrahedron Lett.* **1973,** *38*, 3703-3706.
193. Nakano, T.; Martin, A. Mass Spectrometric Fragmentation of the Oxetanes of 3,5-Dimethylisoxazole, 2,4-Dimethylthiazole, and 1-Acetylimidazole. *Org. Mass Spectrom.* **1981,** *16*, 55-61.
194. Grützmacher, H.-F.; Pankoke, D. Rearrangement Reactions of the Molecular Ions of Substituted Aliphatic Oxiranes. *Org. Mass Spectrom.* **1989,** *24*, 647-652.
195. Collin, J.E.; Conde-Caprace, G. Ionization and Dissociation of Cyclic Ethers by Electron Impact. *Int. J. Mass Spectrom. Ion Phys.* **1968,** *1*, 213-225.
196. Duffield, A.M.; Budzikiewicz, H.; Williams, D.H.; Djerassi, C. Mass Spectrometry in Structural and Stereochemical Problems. LXIV. A Study of the Fragmentation Processes of Some Cyclic Amines. *J. Am. Chem. Soc.* **1965,** *87*, 810-816.
197. Burgers, P.C.; Holmes, J.L.; Mommers, A.A.; Terlouw, J.K. Neutral Products of Ion Fragmentations: HCN and HNC Identified by Collisionally Induced Dissociative Ionization. *Chem. Phys. Lett.* **1983,** *102*, 1-3.
198. Hop, C.E.C.A.; Dakubu, M.; Holmes, J.L. Do the Aminopyridine Molecular Ions Display Aniline- or Pyridine-Type Behavior? *Org. Mass Spectrom.* **1988,** *23*, 609-612.
199. Rosenstock, H.M.; Stockbauer, R.; Parr, A.C. Unimolecular Kinetics of Pyridine Ion Fragmentation. *Int. J. Mass Spectrom. Ion Phys.* **1981,** *38*, 323-331.
200. Burgers, P.C.; Holmes, J.L. Kinetic Energy Release in Metastable-Ion Fragmentations. *Rapid Commun. Mass Spectrom.* **1989,** *2*, 279-280.
201. Cardoso, A.M.; Ferrer, A.J. Fragmentation Reactions of Molecular Ions and Dications of Indoleamines. *Eur. Mass Spectrom.* **1999,** *5*, 11-18.
202. Rodríguez, J.G.; Urrutia, A.; Canoira, L. EI-MS of Indoles. *Int. J. Mass Spectrom. Ion Proc.* **1996,** *152*, 97-110.
203. Hesse, M. *Indolalkaloide, Teil 1: Text;* VCH: Weinheim, 1974.
204. Hesse, M. *Indolalkaloide, Teil 2: Spektren*; VCH: Weinheim, 1974.
205. Biemann, K. Four Decades of Structure Determination by MS: from Alkaloids to Heparin. *J. Am. Chem. Soc. Mass Spectrom.* **2002,** *13*, 1254-1272.
206. Duffield, A.M.; Beugelmans, R.; Budzikiewicz, H.; Lightner, D.A.; Williams, D.H.; Djerassi, C. MS in Structural and Stereochemical Problems. H-Rearrangements Induced by EI on *N-n*-Butyl- and *N-n*-Pentylpyrroles. *J. Am. Chem. Soc.* **1965,** *87*, 805-810.
207. Aubagnac, J.L.; Campion, P. Mass Spectrometry of Nitrogen Heterocycles. X. Contribution to the Behavior of the Aniline Ion and Aminopyridine Ions Prior to Fragmentation by Loss of HCN. *Org. Mass Spectrom.* **1979,** *14*, 425-429.
208. Heyns, K.; Stute, R.; Scharmann, H. Mass Spectrometric Investigations. XII. Mass Spectra of Furans. *Tetrahedron* **1966,** *22*, 2223-2235.
209. De Jong, F.; Sinnige, H.J.M.; Janssen, M.J. Carbon Scrambling in Thiophene Under Electron Impact. *Rec. Trav. Chim. Pays-Bas* **1970,** *89*, 225-226.
210. Williams, D.H.; Cooks, R.G.; Ronayne, J.; Tam, S.W. Studies in Mass Spectrometry. XXVII. The Decomposition of Furan, Thiophene, and Deuterated Analogs Under EI. *Tetrahedron Lett.* **1968,** *14*, 1777-1780.
211. Riepe, W.; Zander, M. The Mass Spectrometric Fragmentation Behavior of Thiophene Benzologs. *Org. Mass Spectrom.* **1979,** *14*, 455-456.
212. Rothwell, A.P.; Wood, K.V.; Gupta, A.K.; Prasad, J.V.N.V. Mass Spectra of 2- and 3-Cycloalkenylfurans and -Cycloalkenylthiophenes and Their Oxy Derivatives. *Org. Mass Spectrom.* **1987,** *22*, 790-795.

7 Chemical Ionization

Learning Objectives

- Ion formation by ion–molecule reactions
- Processes of positive-ion formation other than electron ionization
- Pathways of negative-ion formation
- Softness of chemical ionization techniques
- Applications of chemical ionization mass spectrometry

Mass spectrometrists have ever been searching for ionization methods softer than EI, because molecular weight determination is key for structure elucidation. *Chemical ionization* (CI) is the first of the so-called *soft ionization methods* we are going to discuss (cf. Fig. 1.2). Historically, *field ionization* (FI, Chap. 8) is the elder technique, and thus CI can be regarded as the second soft ionization method introduced to organic mass spectrometry. Nonetheless, CI shares some similarities with EI making its discussion next to EI convenient. CI goes back to experiments of Talrose in the early 1950s [1] and was developed to an analytically useful technique by Munson and Field in the mid-1960s [2-5]. Since then, the basic concept of CI has been extended and applied in numerous different ways, meanwhile providing experimental conditions for a wide diversity of analytical tasks [5-7].

7.1 Basics of Chemical Ionization

7.1.1 Formation of Ions in Positive-Ion Chemical Ionization

In chemical ionization, new ionized species are formed when gaseous molecules interact with ions, i.e., chemical ionization is based on *ion–molecule reactions*. Chemical ionization may involve the transfer of an electron, proton, or other ions between the reactants [8]. These reactants are *i*) the neutral analyte M and *ii*) ions from a *reagent gas*.

CI differs from what we have encountered in mass spectrometry so far because *bimolecular processes* are used to generate analyte ions. The occurrence of bimolecular reactions requires a sufficiently large number of ion–molecule collisions during the dwell time of the reactants in the ion source. This is achieved by significantly increasing the partial pressure of the reagent gas. Assuming reasonable

J. Gross, *Mass Spectrometry*, 2nd ed., DOI 10.1007/978-3-642-10711-5_7,
© Springer-Verlag Berlin Heidelberg 2011

collision cross sections and an ion source residence time of 1 μs [9], a molecule will undergo 30–70 collisions at an ion source pressure of about 2.5×10^2 Pa [10]. The 10^3–10^4-fold excess of reagent gas also effectively shields the analyte molecules from direct ionization by primary electrons, a prerequisite to suppress competing EI of the analyte. In CI, there are four general pathways of positive-ion formation from a neutral analyte molecule M:

$$M + [BH]^+ \rightarrow [M+H]^+ + B \qquad \textit{proton transfer} \qquad (7.1)$$

$$M + X^+ \rightarrow [M+X]^+ \qquad \textit{electrophilic addition} \qquad (7.2)$$

$$M + X^+ \rightarrow [M-A]^+ + AX \qquad \textit{anion abstraction} \qquad (7.3)$$

$$M + X^{+\bullet} \rightarrow M^{+\bullet} + X \qquad \textit{charge exchange} \qquad (7.4)$$

Although *proton transfer* is generally considered to yield protonated analyte molecules, $[M+H]^+$, acidic analytes themselves may form both $[M+H]^+$ and $[M-H]^-$ ions by mutual proton exchange, a behavior exploited for *negative-ion chemical ionization* (NICI, Chap. 7.5). *Electrophilic addition* chiefly occurs by attachment of reagent ions to analyte molecules, e.g., $[M+NH_4]^+$ occurs when ammonia reagent gas is used. Hydride abstractions are abundant representatives of *anion abstraction*, e.g., aliphatic alcohols rather yield $[M-H]^+$ ions than $[M+H]^+$ ions [11,12]. While Eqs. 7.1–7.3 result in even-electron ions – *charge exchange* (CE) or *charge transfer* (CE), as it is also termed – Eq. 7.4 yields radical ions of low internal energy which behave similar to molecular ions in low-energy electron ionization (Chap. 5.6).

Note: It has been common to denote $[M+H]^+$ and $[M-H]^+$ ions as *quasimolecular ions* because they comprise the otherwise intact analyte molecule and are detected in place of a "true" molecular ion, $M^{+\bullet}$, when soft ionization methods are employed. The term was also applied to $[M+alkali]^+$ ions created by soft ionization methods other than CI. Recent recommendations deprecate the term *quasimolecular ion*. Now, $[M+H]^+$ ions are addressed as *protonated molecules*, $[M-H]^-$ as *deprotonated molecules*, and $[M+Na]^+$ ions as *sodiated molecules*.

7.1.2 Chemical Ionization Ion Sources

CI ion sources exhibit close similarity to EI ion sources (Chap. 5.1). In fact, modern EI ion sources can usually be switched to CI operation in seconds, i.e., they are constructed as *EI/CI combination ion sources*. Such a change requires the EI ion source to be modified according to the needs of holding a comparatively high pressure of reagent gas (some 10^2 Pa) without allowing too much leakage into the ion source housing [13]. This is accomplished by axially inserting some inner wall, e.g., a small cylinder, into the ion volume leaving only narrow entrances and exits of the ionizing primary electrons, the sample inlets, and the exiting ion beam. The ports for the reference inlet, the gas chromatograph (GC) and the direct inser-

tion probe (DIP) need to be tightly connected to the respective inlet system during operation, e.g., the empty DIP is inserted even when another inlet actually provides the sample flow into the ion volume. The reagent gas is introduced directly into the ion volume to ensure maximum pressure inside at minimum losses to the ion source housing (Fig. 7.1). During CI operation, the pressure in the ion source housing typically rises by a factor of 20–50 (5×10^{-4}–10^{-3} Pa) as compared to the background pressure of the instrument. Thus, a sufficient pumping speed of 200 l s^{-1} or more is necessary to maintain stable operation in CI mode. The energy of the primary electrons is preferably adjusted to some 200 eV, because electrons of lower energy experience difficulties in penetrating the reagent gas.

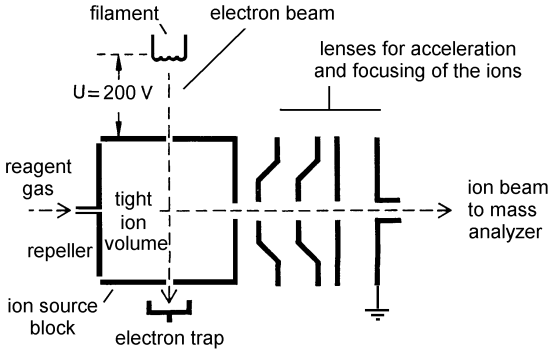


Fig. 7.1. Layout of a chemical ionization ion source. Adapted from Ref. [14] by permission. © Springer-Verlag Heidelberg, 1991.

7.1.3 Sensitivity of Chemical Ionization

Ionization in CI is the result of one or several competing chemical reactions. Therefore, the sensitivity (Chap. 1.4.1) in CI strongly depends on the conditions of the experiment. For comparison of sensitivity data, the reagent gas, its pressure, and the ion source temperature have to be stated in addition to primary electron energy and electron current. Specifications of actual magnetic sector instruments state a sensitivity of about 4×10^{-8} C μg^{-1} for the $[M+H]^+$ ion of methylstearate, *m/z* 299, at $R = 1000$ in positive-ion CI mode with methane reagent gas. This is approximately one order of magnitude less than for EI.

7.1.4 Chemical Ionization Techniques and Terms

In its original implementation, chemical ionization delivered positive ions [2-5], and therefore, for many practitioners the acronym CI used without further specifications still stands for *positive-ion chemical ionization* (PICI) where the latter term should be preferred; for negative ions the term *negative-ion chemical ionization* (NICI) should be used [8]. Table 7.1 provides an overview of CI terms and acronyms.

Table 7.1. Chemical ionization methods and terms

Polarity	Method	Acronym	Explication
Positive	Positive-ion chemical ionization (or positive chemical ionization)	PICI (or PCI)	Strictly speaking, any CI technique delivering even-electron positive analyte ions. Frequently used in the restricted sense of ion formation by protonation.
	Charge exchange	CE-CI	Positive radical ions are formed by exchange/transfer of an electron; these terms are interchangeable
	Charge transfer	CT-CI	
Negative	Negative-ion chemical ionization (or negative chemical ionization)	NICI (or NCI)	Any CI technique delivering even-electron negative analyte ions
	Electron capture	EC	Not a CI technique in the strict sense, but ion source operation is equal to NICI

7.2 Protonation in Chemical Ionization

7.2.1 Source of Protons

The formation of $[M+H]^+$ ions due to bimolecular processes between ions and their neutral molecular counterparts is called *autoprotonation*, a special form of *self-chemical ionization* (self-CI). Self-CI is a chemical ionization process, where the reagent ions are formed by an ionized species of the analyte itself [15]. In EI-MS, autoprotonation is an unwanted phenomenon. $[M+H]^+$ ions from autoprotonation are promoted by increasing the ion source pressure and lowering the temperature. Furthermore, the formation of $[M+H]^+$ ions is favored if the analyte is highly volatile and/or has acidic hydrogens. Thus, self-CI can cause a misinterpretation of mass spectra either by an overestimation of the number of carbon atoms from the ^{13}C isotopic peak due to exaggerated [M+1] ion abundance (Chap. 3.2.1) or by indicating a molecular mass which seems to be higher by 1 u than it really is (Fig. 7.6 and cf. *nitrogen rule* Chap. 6.2.7). In CI-MS with methane or ammonia reagent gas, however, the process of autoprotonation is intentionally exploited to generate the reactant ions.

Note: *Chemi-ionization* means ionization of internally excited molecules upon interaction with other neutrals by *electron detachment*. This corresponds to $M^* + X \rightarrow MX^{+\bullet} + e^-$. Chemi-ionization is different from CI in that there is no ion–molecule reaction involved (cf. Penning ionization, Chap. 2.1.3) [8,16].

7.2.2 Methane Reagent Gas Plasma

The EI mass spectrum of methane has already been discussed (Chap. 6.1). It shows peaks from all ionic species listed in Eq. 7.5. Raising the partial pressure of methane from the EI standard value of about 10^{-4} Pa to 10^{2} Pa significantly alters the ion population [1]. The molecular ion, $CH_4^{+\bullet}$, *m/z* 16, almost vanishes and a new species, CH_5^+, *m/z* 17, is detected instead [17]. Some additional ions occur at higher mass, the most prominent being $C_2H_5^+$, *m/z* 29, and $C_3H_5^+$, *m/z* 41 (Fig. 7.2) [18,19]. Clearly, the positive-ion CI spectrum of methane is governed by competing and consecutive bimolecular reactions in the ion source [4,6,10]:

$$CH_4 + e^- \rightarrow CH_4^{+\bullet}, CH_3^+, CH_2^{+\bullet}, CH^+, C^{+\bullet}, H_2^{+\bullet}, H^+ \quad (7.5)$$

$$CH_4^{+\bullet} + CH_4 \rightarrow CH_5^+ + CH_3^{\bullet} \quad (7.6)$$

$$CH_3^+ + CH_4 \rightarrow C_2H_7^+ \rightarrow C_2H_5^+ + H_2 \quad (7.7)$$

$$CH_2^{+\bullet} + CH_4 \rightarrow C_2H_4^{+\bullet} + H_2 \quad (7.8)$$

$$CH_2^{+\bullet} + CH_4 \rightarrow C_2H_3^+ + H_2 + H^{\bullet} \quad (7.9)$$

$$C_2H_3^+ + CH_4 \rightarrow C_3H_5^+ + H_2 \quad (7.10)$$

$$C_2H_5^+ + CH_4 \rightarrow C_3H_7^+ + H_2 \quad (7.11)$$

The relative abundances of the product ions change dramatically as the ion source pressure increases from EI conditions to 25 Pa. Above 100 Pa, the relative concentrations become stabilized at levels represented by the CI spectrum of methane reagent gas (Fig. 7.2) [4,20]. Fortunately, in CI the ion source pressure is usually in this range of 10^2 Pa and thus in this plateau region of relative ion abundances, thereby ensuring reproducible CI conditions. The influence of the ion source temperature is more pronounced than in EI because the high collision rate rapidly effects a thermal equilibrium.

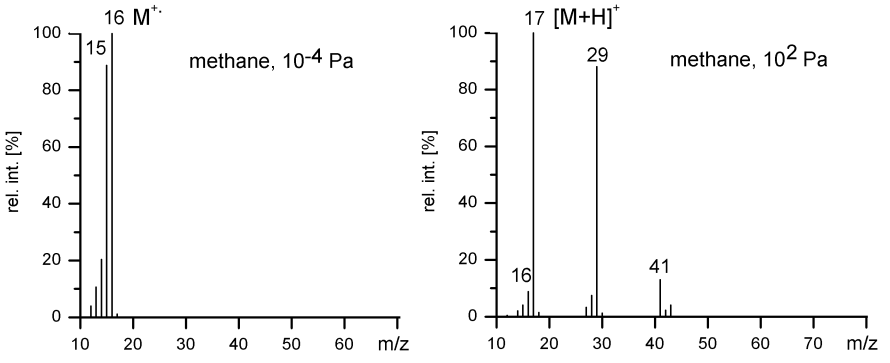
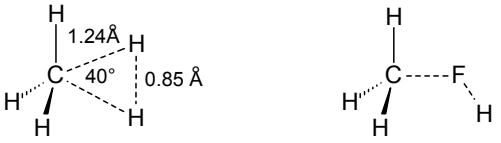


Fig. 7.2. Comparison of the methane spectrum upon electron ionization at different ion source pressures: (**a**) approx. 10^{-4} Pa, (**b**) approx. 10^2 Pa. The latter represents the typical methane reagent gas spectrum in positive-ion CI.

Note: The simultaneous presence of free electrons, protons, and numerous ionic and radical species in the ionized reagent gas has led to its description as a *reagent gas plasma*.

7.2.3 CH_5^+ and Related Ions

The protonated methane ion, CH_5^+, represents a reactive as well as fascinating species in the methane reagent gas plasma. In 1991, its structure had been calculated as shown in Scheme 7.1 [17] and the chemical behavior of the CH_5^+ ion indeed appears to be compatible with a stable structure, involving a three-center two-electron bond associating two hydrogens and the carbon atom.



Scheme 7.1.

Rearrangement of this structure due to exchange between one of these hydrogens and one of the three remaining hydrogens seemingly is a fast process induced by interactions with the chemical ionization gas. Recent work indicates that all five C–H bonds are rendered equal by extremely rapid zero-point motion thereby precluding the assignment of a unique CH_5^+ ion structure [21]. For the $C_2H_7^+$ intermediate during $C_2H_5^+$ ion formation several isomerizing structures are discussed [18,19]. In protonated fluoromethane, the conditions are quite different, promoting a weak C–F and a strong F–H bond [22].

7.2.4 Energetics of Protonation

The tendency of a (basic) molecule B to accept a proton is quantitatively described by its *proton affinity* (*PA*, Chap. 2.12). For such a protonation we have [3]:

$$B_g + H_g^+ \rightarrow [BH]_g^+; \qquad -\Delta H_r^0 = PA_{(B)} \tag{7.12}$$

To judge the chances of protonation under CI conditions, one has to compare the *PA* of the neutral analyte M with that of the complementary base B of the proton-donating reactant ion $[BH]^+$ (Brønsted acid). Protonation will occur as long as the process is exothermic, i.e., if $PA_{(B)} < PA_{(M)}$. The heat of reaction has basically to be distributed among the degrees of freedom of the $[M+H]^+$ analyte ion [12,23]. Accordingly, the minimum internal energy of the $[M+H]^+$ ions is well approximated by:

$$E_{int(M+H)} \approx \Delta PA = PA_{(M)} - PA_{(B)} \tag{7.13}$$

Some additional thermal energy will also be contained in the $[M+H]^+$ ions. Having *PA* data at hand (Table 2.6) one can easily judge whether a reagent ion will be able to protonate the analyte of interest and how much energy will be put into the $[M+H]^+$ ion.

Example: The CH_5^+ reactant ion will protonate C_2H_6 because Eq. 7.13 gives $\Delta PA = PA_{(C2H6)} - PA_{(CH4)} = 601 - 552 = 49$ kJ mol^{-1}. The product, protonated ethane, $C_2H_7^+$, is immediately stabilized by H_2 loss to yield $C_2H_5^+$ {Mackay, 1981 16 /id;Fisher, 2000 78 /id}. In case of tetrahydrofurane, protonation to yield $[C_4H_8O+H]^+$ is more exothermic: $\Delta PA = PA_{(C4H8O)} - PA_{(CH4)} = 831 - 552 = 279$ kJ mol^{-1}, and thus, yields stronger fragmentation of the $[M+H]^+$ ions.

7.2.5 Impurities of Higher *PA* than the Reagent Gas

Due to the above energetic considerations, impurities of the reagent gas having a higher *PA* than the neutral reagent gas are protonated by the reactant ion [3]. Residual water is a frequent source of contamination. Higher concentrations of water in the reagent gas may even alter its properties completely, i.e., H_3O^+ becomes the predominant species in a CH_4/H_2O mixture under CI conditions (Fig. 7.3) [24].

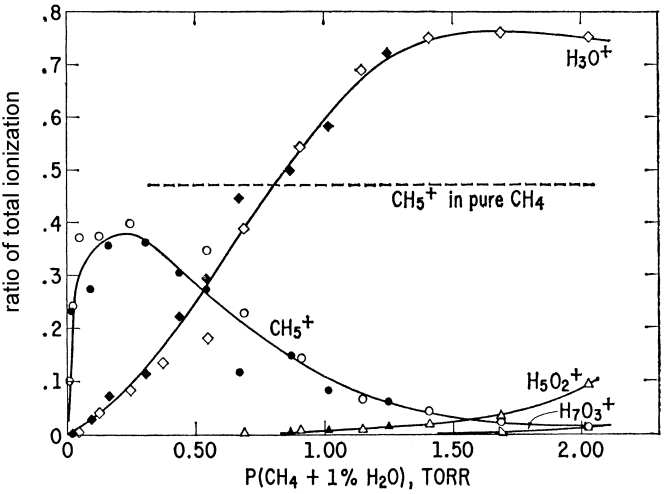


Fig. 7.3. Relative concentrations of CH_5^+ and H_3O^+ ions vs. pressure of a mixture of CH_4 (99%) and H_2O (1%). 1 Torr = 133 Pa. Reproduced from Ref. [24] by permission. © American Chemical Society, 1965. **H2O_in_methaneCI02.tif**

Note: Any analyte of suitable *PA* may be regarded as a basic impurity of the reagent gas, and thus becomes protonated in excellent yield. Heteroatoms and π-electron systems are the preferred sites of protonation. Nevertheless, the additional proton is often mobile within the ion, sometimes even accompanied by its exchange with otherwise fixed hydrogens [25,26].

7.2.6 Methane Reagent Gas PICI Spectra

The $[M+H]^+$ ion peak in methane reagent gas PICI spectra – generally denoted *methane-CI spectra* – is usually intense and often represents the base peak [27-29]. Although protonation in CI is generally exothermic by 1–4 eV, the degree of fragmentation of $[M+H]^+$ ions is much lower than that observed for the same analytes under 70-eV EI conditions. This is because $[M+H]^+$ ions have *i*) a narrow internal energy distribution, and *ii*) fast radical-induced bond cleavages are prohibited, because solely intact molecules are eliminated from these even-electron ions. Electrophilic addition fairly often gives rise to $[M+C_2H_5]^+$ and $[M+C_3H_5]^+$ adduct ions. Thus, [M+29] and [M+41] peaks are sometimes observed in addition to the expected – usually clearly dominating – [M+1] peak. Occasionally, hydride abstraction may occur instead of protonation.

Note: Hydride abstractions are difficult to recognize. To identify a $[M–H]^+$ peak occurring instead of a $[M+H]^+$ peak it is useful to examine the mass differences between the signal in question and the products of electrophilic addition. In that case, [M+29] and [M+41] appear as if they were [M+31] and [M+43] peaks, respectively. An apparent loss of 16 u might indicate an $[M+H–H_2O]^+$ ion instead of an $[M+H–CH_4]^+$ ion.

Example: EI vs. methane reagent gas PICI spectrum of methionine. The comparison shows greatly reduced fragmentation in the PICI spectrum (Fig. 7.4). Only small intact molecules such as NH_3, HCOOH, and MeSH are eliminated from the $[M+H]^+$ ion, *m/z* 150, which yields the base peak. In addition, the PICI spectrum perfectly reveals the isotopic pattern that indicates the presence of sulfur. The horizontal line (Fig. 7.4b) means that this range was not acquired in the PICI spectrum as to keep the spectrum free from reactant ion signals. The spectra were, however, plotted on the same *m/z* scales to simplify the comparison.

Note: Resulting from the large excess of reagent gas, its spectrum often is of higher intensity than that of the analyte. Therefore, CI spectra are usually acquired starting above the *m/z* range occupied by reactant ions, e.g., above *m/z* 50 for methane or above *m/z* 70 for isobutane. Background subtraction can alternatively be applied to remove these peaks, but this approach suffers from variations in the reactant ion abundances upon admission of the analyte.

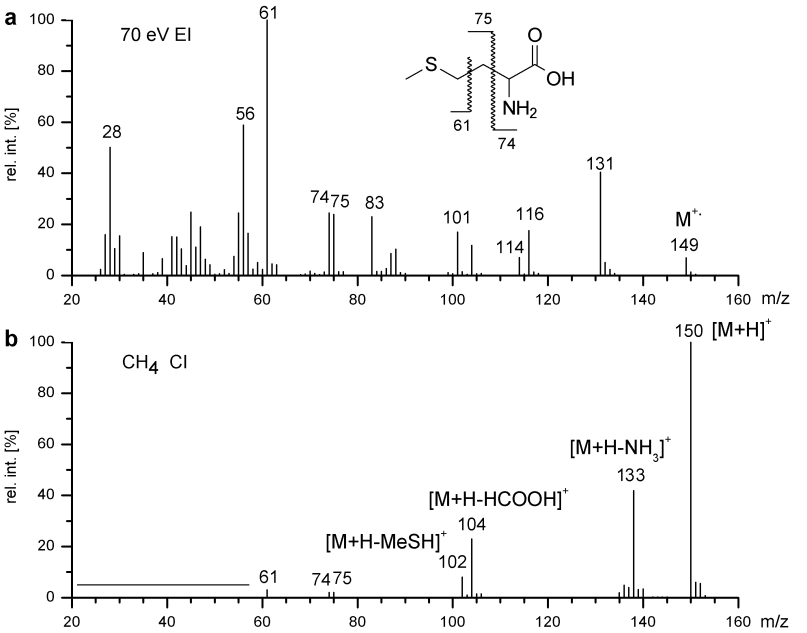


Fig. 7.4. Comparison of (**a**) 70-eV EI spectrum and (**b**) methane reagent gas PICI spectrum of the amino acid methionine.

7.2.7 Other Reagent Gases in PICI

As pointed out, the value of ΔPA determines whether a particular analyte can be protonated by a certain reactant ion and how exothermic the protonation will be. Considering other reagent gases than methane therefore allows some tuning of the PICI conditions. The systems employed include molecular hydrogen and hydrogen-containing mixtures [12,23,30], isobutane [31-35], ammonia [32,36-42], dimethylether [43], diisopropylether [44], acetone [11], acetaldehyde [11], benzene [45], and iodomethane [46]. Even transition metal ions such as Cu^+ [47] and Fe^+ [48] can be employed as reactant ions to locate double bonds. However, nitrous oxide reagent gas better serves that purpose [37,49,50].

The most common reagent gases are summarized in Table 7.2 and the EI and CI spectra of ammonia and isobutane reagent gas are compared in Fig. 7.5. Isobutane is an especially versatile reagent gas, because *i*) it provides low-fragmentation PICI spectra of all but the most nonpolar analytes, *ii*) gives almost exclusively one well-defined adduct ($[M+C_4H_9]^+$, [M+57]) if any (Fig. 7.6), and *iii*) can also be employed for electron capture (Chap. 7.4).

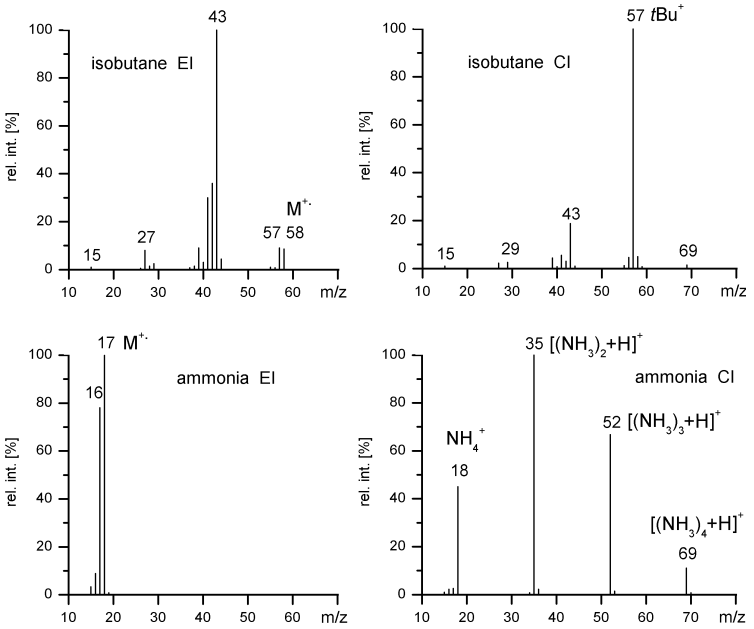


Fig. 7.5. Standard EI vs. positive-ion CI spectra of isobutane (*upper*) and ammonia (*lower part*). Ammonia forms abundant cluster ions upon CI.

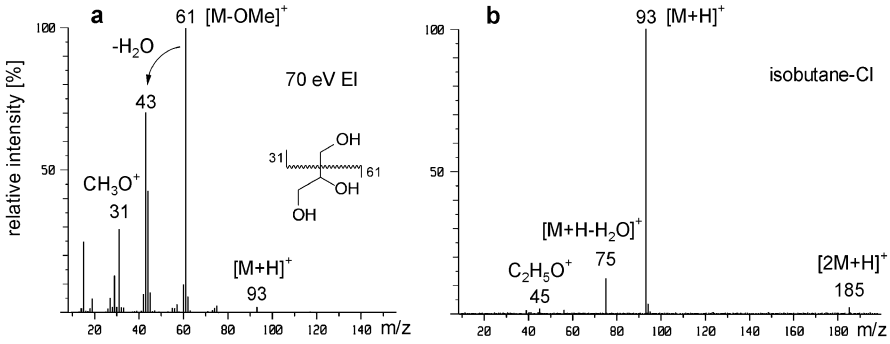


Fig. 7.6. 70-eV EI (**a**) vs. isobutane-PICI spectrum of glycerol (**b**). Even in EI mode, an $[M+H]^+$ ion by autoprotonation is observed rather than $M^{+\bullet}$. Besides $[M+H]^+$, the PICI spectrum shows only few fragment ions and a weak $[2M+H]^+$ cluster ion signal.

Example: In a drug overdose case evidence was available of ingestion of Percodan (a mixture of several common drugs). The isobutane-PICI spectrum of the gastric extract was obtained (Fig. 7.7) [31]. All drugs gave rise to an $[M+H]^+$ ion. Due to the low exothermicity of protonation by the *tert*-$C_4H_9^+$ ion, most $[M+H]^+$ ions did not fragment, solely that of aspirin showing intense fragment ion peaks assigned as $[M+H–H_2O]^+$, *m/z* 163; $[M+H–H_2C=CO]^+$, *m/z* 139; and the strongest

one, $[M+H–CH_3COOH]^+$, *m/z* 121. In addition to the $[M+H]^+$ ion at *m/z* 180, phenacetine formed a $[2M+H]^+$ cluster ion, *m/z* 359; such $[2M+H]^+$ cluster ions are frequent in CI-MS.

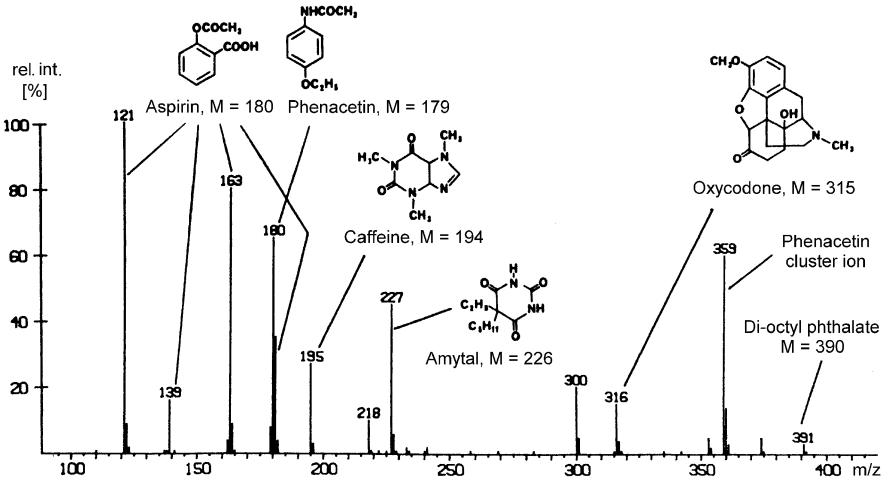


Fig. 7.7. Isobutane PICI mass spectrum of gastric contents in an overdose case. Reproduced from Ref. [31] by permission. © American Chemical Society, 1970.

Table 7.2. Common PICI reagent gases (chiefly protonating)

Reagent gas	Reactant ions	Neutral from reactant ions	*PA* of neutral product	Analyte ions
H_2	H_3^+	H_2	424	$[M+H]^+$, $[M–H]^+$
CH_4	CH_5^+ ($C_2H_5^+$ and $C_3H_5^+$)	CH_4	552	$[M+H]^+$ ($[M+C_2H_5]^+$ and $[M+C_3H_5]^+$)
i-C_4H_{10}	*t*-$C_4H_9^+$	*i*-C_4H_8	820	$[M+H]^+$, ($[M+C_4H_9]^+$, eventually $[M+C_3H_3]^+$, $[M+C_3H_5]^+$ and $[M+C_3H_7]^+$)
NH_3	NH_4^+	NH_3	854	$[M+H]^+$, $[M+NH_4]^+$

7.3 Proton Transfer Reaction Mass Spectrometry

By combining the principles of PICI with an apparatus derived from *selected-ion flow tube* (SIFT) experiments, the technique of *proton transfer reaction mass spectrometry* (PTR-MS) has been developed as a dedicated tool for the analysis of *volatile organic compounds* (VOCs) at parts-per-trillion by volume (pptv) level in air [51,52]. PTR-MS is highly useful as a fast and quantitative method for the determination of VOCs as proven by numerous applications in food control, envi-

ronmental and atmospheric research, as well as in medicine, e.g., to analyze the exhaled breath of patients [51-55].

7.3.1 Reactant Ion Formation in PTR-MS

When water vapor is passed through the discharge of a hollow-cathode ion source it is ionized by primary electrons, basically by EI. Due to ion–molecule reaction sequences the product ion mixture forms H_3O^+ ions with high selectivity of up to 99.5% (Chap. 7.2.5) [51,52]. Even $N_2^{+\bullet}$ or N^+ ions from nitrogen rapidly react with water molecules in the source region to result in more H_3O^+ ions. Thus, a high (typical count rates of $\approx 10^6$ counts s^{-1}) and almost pure flux of hydronium primary ions is provided that may then serve as reactant ions in a PICI process:

$$M + H_3O^+ \rightarrow [MH]^+ + H_2O \qquad (7.14)$$

Fortunately this proton transfer reaction can generally occur for all VOCs as their *PA*s exceed that of water (PA_{water} = 697 kJ mol^{-1}) allowing for their exothermic protonation.

7.3.2 Analyte Ion Formation in PTR-MS

Different from classical CI sources, PTR-MS separates reactant ion generation from the stage of analyte ion formation. For the latter step, PTR-MS makes use of an ion flow tube similar to a device used in IMS (Chap. 4.9.2), which provides sufficient time for effective reactions according to Eq. 7.14. Thus, ions are extracted from the hollow-cathode source, passed through a short drift region, and delivered to the extended reaction region, at the entrance of which the sample air containing the VOCs is continuously admitted (Fig. 7.8). Due to the purity of the H_3O^+ reactant ions delivered, there is no need for an ion flux-limiting quadrupole system to preselect reactant ions [51,52].

On its way from the Venturi-type inlet to the downstream end of the drift section, H_3O^+ ions undergo nonreactive and reactive collisions with any one of the components of air [51,52]. The water reagent gas PICI process causes the analyzed VOCs to be converted into $[M+H]^+$ ions.

The flow tube, which is about 20 cm long, acts as a reaction region that is maintained at about 1 mbar by action of a vacuum pump attached to its exit. These conditions afford thermalization and effective proton transfer as the hydronium ions drift along together with the VOC-loaded air. As PTR-MS does not necessitate an additional buffer gas, the analyte air is not diluted any further, a feature that contributes to the high sensitivity of the method. Furthermore, the original mole fraction of the analytes in the air is maintained.

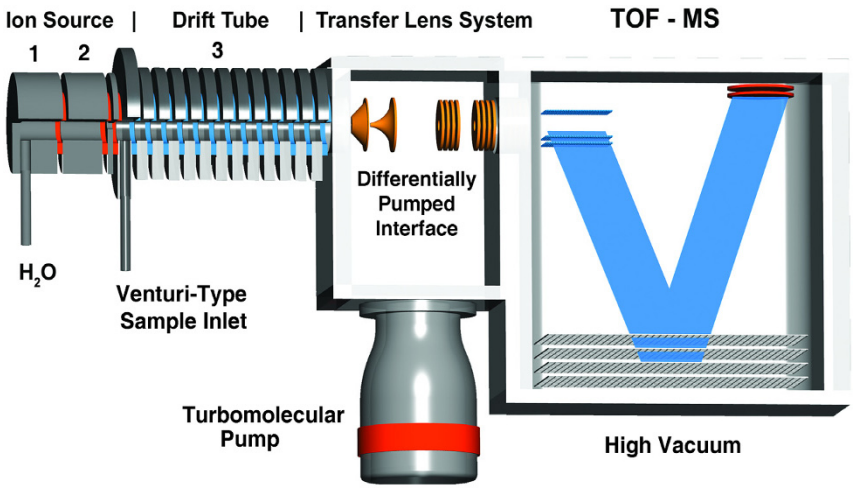


Fig. 7.8. PTR mass spectrometer. The ion source of the Ionicon PTR-TOF 2000™ is divided into a compartment for reactant ion generation from H_2O by (**1**) a hollow cathode and (**2**) a source drift region in front of the sample inlet, and (**3**) the drift tube for analyte ion formation. The TOF analyzer has its own turbomolecular pump to maintain high vacuum (*not shown*). By courtesy of Ionicon Analytik GmbH, Innsbruck, Austria.

Example: VOCs in air originate from natural (emission by plants and animals) and anthropogenic sources (usage of fossil fuels, evaporation of solvents, gases from landfill sites). Even without anthropogenic contributions, the Earth's atmosphere would consist of a complex mixture of VOCs [53]. Methane (2 pptv) is by far the most common organic compound in the Earth's atmosphere, while other VOCs are in the ppbv range [53]. Isoprene, C_5H_8, and monoterpenes are important VOCs for modeling atmospheric chemistry in Amazonia [56]. The model of *emissions of gases and aerosols from nature* (MEGAN), estimates VOC fluxes and can describe the large observed variations associated with land-use change in the region of Manaus. Airborne PTR-MS measurements of isoprene, detected as $[C_5H_9]^+$, *m/z* 69, were conducted by flying a racetrack pattern north-east of Manaus at constant altitude of 675 m above sea level. The racetrack of 320 km covered various landscapes such as primary forest, mixed water/forest, soybean plantations, and agricultural areas. In Fig. 7.9, the left panel depicts the isoprene emission map calculated from MEGAN, with the flight track plotted in gray. The right panel shows the surface flux calculated from airborne PRT-MS (Fig. 7.9) [56].

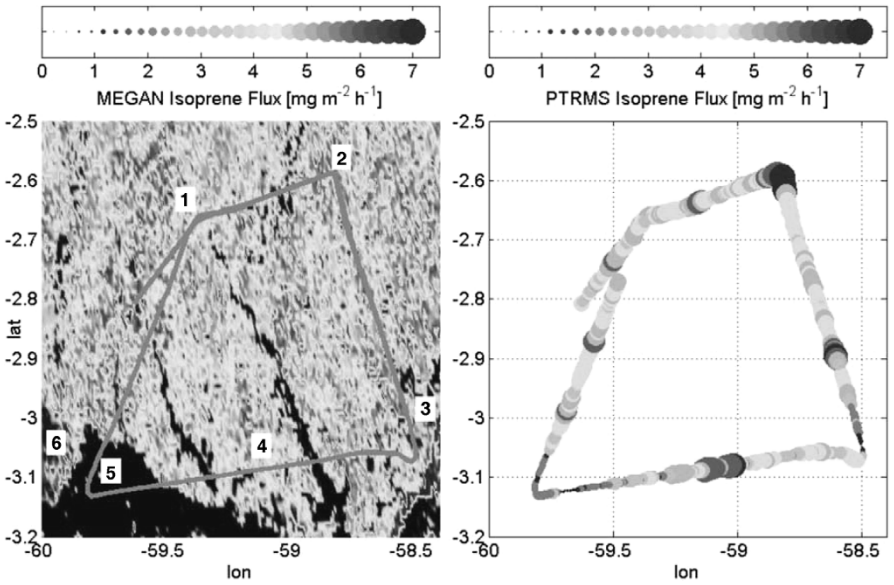


Fig. 7.9. Isoprene emission map generated for flight conditions from MEGAN (*left*) compared to airborne PTR-MS measurements (*right*). The *gray line* on the *left panel* depicts the flight track. Numbers **1–6** on the *left side* mark different land cover types: **1** mixed forest/plantation, **2** primary tropical forest, **3** soybean plantations, **4** mixed forest/plantation, **5** water, **6** Manaus urban region. Reproduced from Ref. [56] by permission. © The American Geophysical Union, 2007.

7.4 Charge Exchange Chemical Ionization

Charge exchange (CE) or *charge transfer* (CT) ionization occurs when an ion-neutral reaction takes place in which the ionic charge is transferred to the neutral [8]. In principle, any of the reagent systems discussed so far is capable of effecting CE because the respective reagent molecular ions $X^{+\bullet}$ are also present in the plasma:

$$X^{+\bullet} + M \rightarrow M^{+\bullet} + X \tag{7.15}$$

With methane, isobutane, or ammonia, however, proton transfer is still prevailing. Therefore, reagent gases suitable for CE should exhibit abundant molecular ions even under the conditions of CI, whereas potentially protonating species have to be absent or at least of minor abundance.

Note: The acronym CE is also used for *capillary electrophoresis*, a separation method. CE may be coupled to a mass spectrometer via an electrospray interface (Chaps. 12, 14), and thus CE-CI and CE-ESI-MS must not be confused.

7.4.1 Energetics of CE

The energetics of CE is determined by the *ionization energy* of the neutral analyte, $IE_{(M)}$, and the *recombination energy* of the reactant ion, $RE_{(X+\bullet)}$. Recombination of an atomic or molecular ion with a free electron is the inverse of its ionization. $RE_{(X+\bullet)}$ is defined as the exothermicity of the gas phase reaction [7]:

$$X^{+\bullet} + e^- \rightarrow X; \quad -\Delta H_r = RE_{(X+\bullet)} \tag{7.16}$$

For monoatomic ions, the *RE* has the same numeric value as the *IE* of the neutral; for diatomic or polyatomic species differences may occur due to storage of energy in internal modes or electronic excitation. Ionization of the analyte via CE is effected if [57]:

$$RE_{(X+\bullet)} - IE_{(M)} > 0 \tag{7.17}$$

Now, the heat of reaction, and thus the minimum internal energy of the analyte molecular ion, is given by [58]:

$$E_{int(M+\bullet)} \geq RE_{(X+\bullet)} - IE_{(M)} \tag{7.18}$$

(The $\geq$ sign indicates the additional contribution of thermal energy.) In summary, no CE is expected if $RE_{(X+\bullet)}$ is less than $IE_{(M)}$; $M^{+\bullet}$ ions are predominantly expected if $RE_{(X+\bullet)}$ is slightly above $IE_{(M)}$; extensive fragmentation occurs if $RE_{(X+\bullet)}$ is notably greater than $IE_{(M)}$ [58]. Accordingly, the "softness" of CE-CI can be adjusted by choosing a reagent gas of suitable *RE*. Fortunately, the differences between *RE*s and *IE*s are small, and unless highest accuracy is required, *IE* data may be used to estimate the effect of a CE reagent gas (Table 2.1).

7.4.2 Reagent Gases for CE-CI

Numerous gases are employed for CE-CI. Reagent gases such as hydrogen [23] or methane can also affect CE. Typically, pure compounds are employed as CE reagent gases, but occasionally they are diluted with nitrogen to act as an inert or sometimes reactive buffer gas (Table 7.3). Compared to protonating CI conditions, the reagent gas is typically admitted at somewhat lower pressure (15–80 Pa). Primary electron energies are reported in the 100–600 eV range. The major reagent gases include chlorobenzene [59], benzene [45,60,61], carbon disulfide [62,63], xenon [62,64], carbon oxysulfide [62-66], carbon monoxide [58,62,64], nitrogen oxide [58,67], dinitrogen oxide [63,67], nitrogen [62], and argon [62].

Example: Comparison of the CE-CI spectra of cyclohexene with that of the according 70-eV EI spectrum. Different CE reagent gases show different degrees of fragmentation (Fig. 7.10) [68]. The relative intensity of the molecular ion increases as the RE of the reagent gas decreases. CE-CI mass spectra closely resemble low-energy EI spectra (Chap. 5.6) because molecular ions are formed upon CE. As the sensitivity of CE-CI is superior to low-energy EI [57], CE-CI may be preferred over low-energy EI.

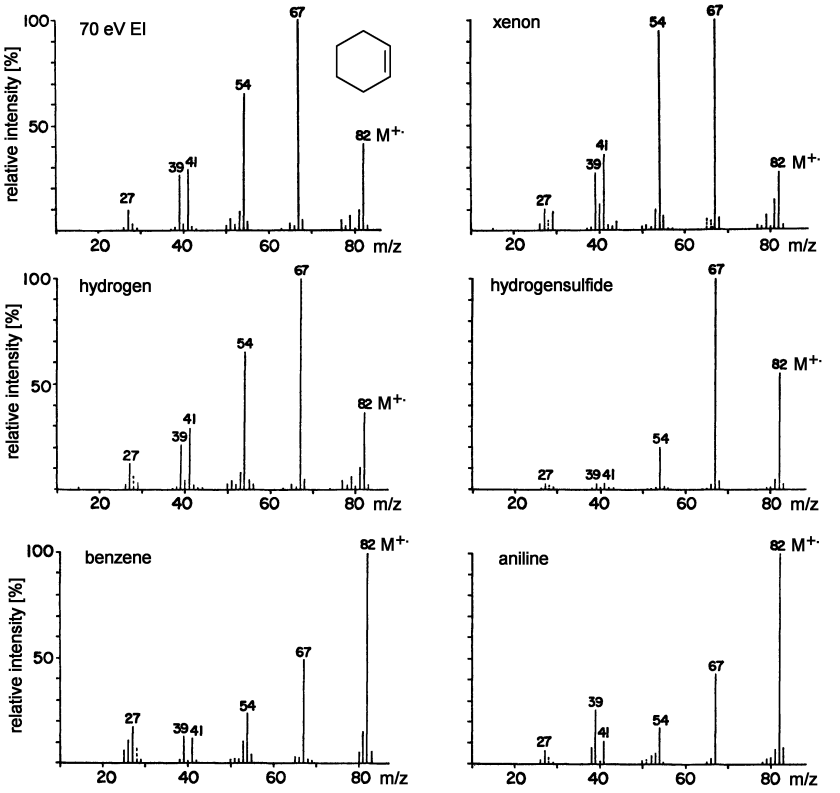


Fig. 7.10. Comparison of CE-CI spectra of cyclohexene with that of the according 70-eV EI spectrum recorded with different reagent gases. Adapted from Ref. [68] by permission. © John Wiley & Sons, 1976.

7.4.3 Compound Class-Selective CE-CI

The energy distribution upon CE largely differs from that obtained upon EI in that the CE process delivers an energetically well-defined ionization of the neutral. Choosing the appropriate reagent gas allows for the selective ionization of a targeted compound class contained in a complex mixture [57,59,61,70]. The differentiation is possible due to the characteristic range of *IE*s for each compound class. This property of CE-CI can also be applied to construct breakdown graphs (Chap. 2.11.2) from a set of CE-CI mass spectra by using reactant ions of stepwise increasing $RE_{(X+\bullet)}$, e.g., $C_6F_6^{+\bullet}$, $CS_2^{+\bullet}$, $COS^{+\bullet}$, $Xe^{+\bullet}$, $N_2O^{+\bullet}$, $CO^{+\bullet}$, $N_2^{+\bullet}$ [64,69].

Example: CE-CI allows for the direct determination of the molecular weight distributions of the major aromatic components in liquid fuels and other petroleum products [57,59,70]. The approach involves selective CE between $C_6H_5Cl^{+\bullet}$ and the substituted benzenes and naphthalenes in the sample. In this application, chlo-

chlorobenzene also serves as the solvent for the fuel to avoid interferences with residual solvent. Thus, the paraffinic components present in the fuel can be suppressed in the resulting CE-CI mass spectra (Fig. 7.11) [59].

Table 7.3. CE-CI reagent gases [7,58,59,62-64,69]

Reagent gas	Reactant ion	*RE* or *RE* range [eV]
$C_6H_5NH_2$	$C_6H_5NH_2^{+\bullet}$	7.7
C_6H_5Cl	$C_6H_5Cl^{+\bullet}$	9.0
C_6H_6	$C_6H_6^{+\bullet}$	9.2
$NO^{\bullet} : N_2 = 1 : 9$	NO^+	9.3
$C_6F_6 : CO_2 = 1 : 9$	$C_6F_6^{+\bullet}$	10.0
$CS_2 : N_2 = 1 : 9$	$CS_2^{+\bullet}$	9.5–10.2
H_2S	$H_2S^{+\bullet}$	10.5
$COS : CO = 1 : 9$	$COS^{+\bullet}$	11.2
Xe	$Xe^{+\bullet}$	12.1, 13.4
N_2O (: N_2 = 1 : 9)	$N_2O^{+\bullet}$	12.9
CO_2	$CO_2^{+\bullet}$	13.8
CO	$CO^{+\bullet}$	14.0
Kr	$Kr^{+\bullet}$	14.0, 14.7
N_2	$N_2^{+\bullet}$	15.3
H_2	$H_2^{+\bullet}$	15.4
Ar	$Ar^{+\bullet}$	15.8, 15.9
Ne	$Ne^{+\bullet}$	21.6, 21.7
He	$He^{+\bullet}$	24.6

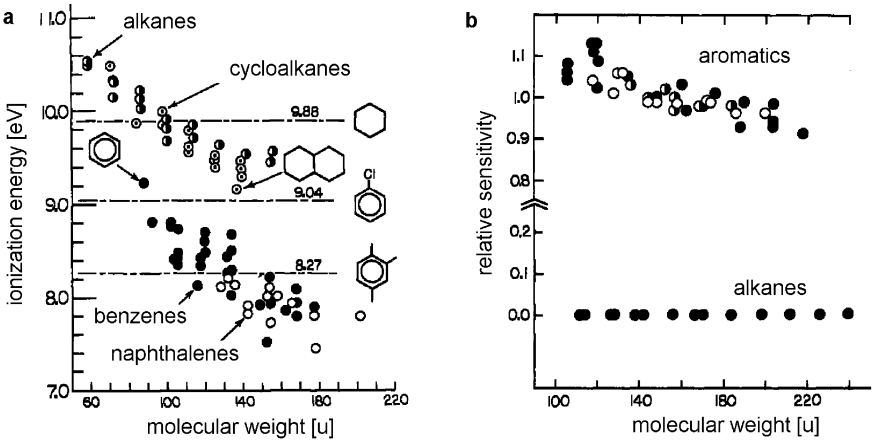
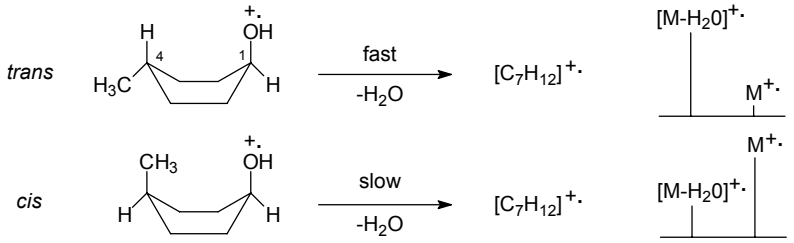


Fig. 7.11. (**a**) Ionization energies of certain classes of organic molecules as a function of their molecular weight, and (**b**) relative sensitivities for (○) alkylbenzenes, (●) polyolefines, and (◑) substituted naphthalenes in chlorobenzene CE-CI. Adapted from Ref. [59] by permission. © American Chemical Society, 1983.

7.4.4 Regio- and Stereoselectivity in CE-CI

Small differences in activation energy, E_0, that exist between analogous fragmentations of regioisomers [62,63,65,66] or stereoisomers do not cause significant differences in their 70-eV EI spectra. Pathways leading to fragments F_1 and $F_{1'}$ cannot be distinguished, because minor differences in the respective *appearance energies* (*AE*s) are overridden by the excess energy of the fragmenting ions (Chap. 2.5). The situation changes if an energy-tunable ionization method is applied, which in addition offers a narrow internal energy distribution of the ions. Then, a significant alteration of relative intensities of F_1 and $F_{1'}$ could be effected if the appearance energies $AE_{(F1)}$ and $AE_{(F1')}$ of the fragments F_1 and $F_{1'}$ from isomeric precursors were just below $RE_{(x+\bullet)}$.

Example: In epimeric 4-methylcyclohexanols the methyl and the hydroxyl group can either both reside in axial position (*cis*) or one is equatorial and the other axial (*trans*). In the *trans* isomer, stereospecific 1,4–H_2O elimination should proceed easily (Chap. 6.10.3), while H_2O loss from the *cis* isomer is more demanding. CE-CI using $C_6F_6^{+\bullet}$ reactant ions clearly reveals the difference between these stereoisomers from the according $M^{+\bullet}/[M–H_2O]^{+\bullet}$ ratio determined as *trans* : *cis* = 0.09 : 2.0 = 23) [69].



Scheme 7.2.

7.5 Negative-Ion Chemical Ionization

In any CI plasma, ions of both polarities, positive *and* negative, are formed simultaneously, e.g., $[M+H]^+$ and $[M–H]^-$ ions, and it is just a matter of the polarity of the acceleration voltage which ions are extracted from the ion source [71]. Thus, *negative-ion chemical ionization* (NICI) [72] mass spectra are readily obtained when one of the following processes occurs: *i*) dissociation (deprotonation) of acidic analytes such as carboxylic acids, diimides, or phenols, *ii*) nucleophilic addition (anion attachment), or *iii*) ion-pair formation [73-76]:

$$M \rightarrow [M–H]^- + H^+ \qquad \textit{dissociation of acids} \qquad (7.19)$$

$$M + A^- \rightarrow [M+A]^- \qquad \textit{nucleophilic addition} \qquad (7.20)$$

$$M + e^- \rightarrow [M–B]^- + B^+ + e^- \qquad \textit{ion-pair formation} \qquad (7.21)$$

Example: The NICI mass spectrum of tetraiodoethene, $I_2C{=}CI_2$, has been obtained using isobutane reagent gas (Fig. 7.12). The negative molecular ion, $M^{-\bullet}$, at *m/z* 531.6 has a relative intensity of just 0.15%, while the product of nucleophilic addition, $[M+I]^-$, *m/z* 658.5, yields the base peak [77]. Losses of $I^\bullet$ and I_2 from $M^{-\bullet}$ are also observed. The series of peaks at *m/z* 126.9, 253.8, and 380.7 corresponds to traces of iodine present as impurity of tetraiodoethene. The iodine is also ionized by both electron capture (EC, next paragraph) and iodide addition. The spectrum nicely exemplifies the superimposition of mass spectra of two components of a mixture. It is not always simple to tell the corresponding peaks apart; accurate mass measurements or tandem mass spectrometry may be required. It is worth noting the mass defect introduced by the iodine and the ^{13}C isotopic peak of merely 2% due to only two carbon atoms present.

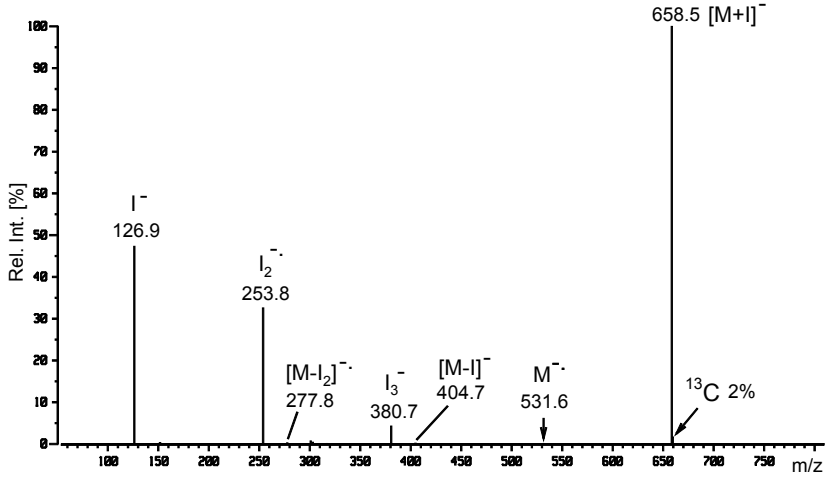


Fig. 7.12. NICI mass spectrum of tetraiodoethene (isobutane reagent gas, electron emission 300 μA at 200 eV, and ion source temperature of 200°C). Adapted from Ref. [77] with permission. © Wiley-VCH, Weinheim, 2007.

Note: Over the last decade, NICI applications have diminished because these analyses have mostly been carried out by negative-ion *atmospheric pressure chemical ionization* (APCI). APCI is compatible with liquid chromatography (Chap. 14) and can readily be implemented on instruments with electrospray ionization interface (ESI, Chap. 12). Such instruments have an enormous market share, and thus, it is often more convenient and economic to switch between ESI and APCI as required. Although being a type of CI, APCI will be dealt in conjunction with ESI.

7.6 Electron Capture

There is one further process of negative-ion formation that is of special interest, because it provides superior sensitivity towards many toxic and/or environmentally relevant substances [78-82]: *electron capture* (EC) or *electron attachment* [72]. EC is a resonance process whereby an external electron is incorporated into an orbital of an atom or molecule [8]. Strictly speaking, EC is not a subtype of CI because the electrons are not provided by a reacting ion, but are freely moving through the gas at thermal energy. Nonetheless, the ion source conditions to achieve EC are the same as for NICI [83].

7.6.1 Ion Formation by Electron Capture

When a neutral molecule interacts with an electron of high kinetic energy, the positive radical ion is generated by EI. If the electrons have less energy than the *IE* of the respective neutral, EI is prohibited. As the electrons approach thermal energy, EC can occur instead. Under EC conditions, there are three different mechanisms of ion formation [74,84-86]:

$$M + e^- \rightarrow M^{-\bullet} \qquad \textit{resonance electron capture} \qquad (7.22)$$

$$M + e^- \rightarrow [M\text{–}A]^- + A^\bullet \qquad \textit{dissociative electron capture} \qquad (7.23)$$

$$M + e^- \rightarrow [M\text{–}B]^- + B^+ + e^- \qquad \textit{ion-pair formation} \qquad (7.24)$$

Resonance electron capture directly yields the negative molecular ion, $M^{-\bullet}$, whereas even-electron fragment ions are formed by dissociative electron capture and ion-pair formation. Molecular ions are generated by capture of electrons with 0–2 eV kinetic energy, whereas fragment ions result from capture of electrons having 0 to 15 eV. Ion-pair formation tends to occur when electron energies exceed 10 eV [86].

7.6.2 Energetics of EC

The potential energy curves of a neutral molecule AB and the potential ionic products from Eqs. 7.22–7.24 are compared below (Fig. 7.13). These graphs reveal that the formation of negative molecular ions, $AB^{-\bullet}$, is energetically more favorable than homolytic bond dissociation of AB and that the $AB^{-\bullet}$ ions have internal energies close to the activation energy for dissociation [72,74,84]. The negative molecular ions from EC are therefore definitely less excited than their positive counterparts from 70-eV EI.

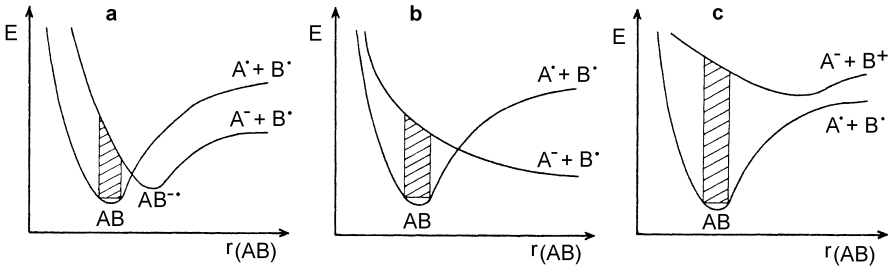


Fig. 7.13. Energetics of (**a**) resonance electron capture, (**b**) dissociative electron capture, and (**c**) ion-pair formation. Adapted from Ref. [84] by permission. © John Wiley & Sons, 1981.

Example: The EC mass spectrum of benzo[a]pyrene, $C_{20}H_{12}$, shows the negative molecular ion exclusively at *m/z* 252 (Fig. 7.14). This spectrum is representative for EC spectra of *polycyclic aromatic hydrocarbons* (PAHs) [87,88]. One particular PAH, fluoranthene, has recently received much attention as its $M^{-\bullet}$ ion serves as electron donating reactant ion in *electron transfer dissociation* (ETD, Chap. 9.15).

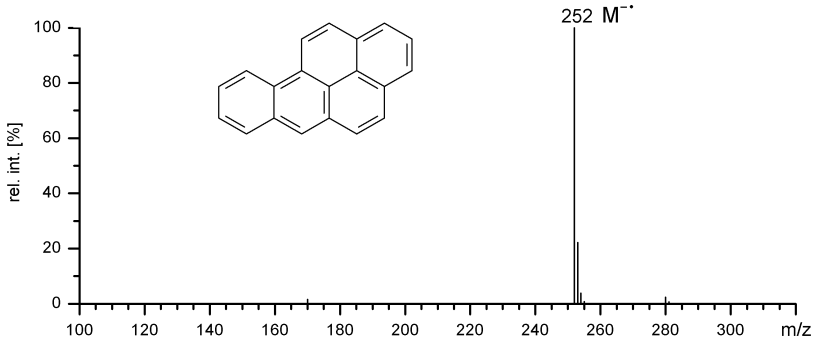


Fig. 7.14. EC spectrum of benzo[a]pyrene (isobutane buffer gas, ion source 200°C). The two additional minor signals correspond to impurities of the sample.

The energetics of EC are determined by the *electron affinity* (*EA*) of the neutral. *EA* is the negative of the enthalpy of the attachment of a zero kinetic energy electron to a neutral molecule or atom:

$$M + e^- \rightarrow M^{-\bullet} \qquad -\Delta H_r = EA_{(M)} \tag{7.25}$$

Just like the *IE* of a molecule is governed by the atom of lowest *IE* within that neutral (Chap. 2.1.4), the *EA* of a molecule is basically determined by the atom of highest electronegativity. This is why analytes with halogens, in particular fluorine and chlorine, as well as with nitro groups make attractive candidates for EC (Table 7.4) [89]. If EC occurs with a neutral of negative *EA*, the electron–molecule complex will have a short lifetime (*autodetachment*), but in case of positive *EA* a negative molecular ion can persist.

Example: Consider the dissociative EC process $CF_2Cl_2 + e^- \rightarrow F^- + CFCl_2^{\bullet}$ and let the potential energy of CF_2Cl_2 be zero. The homolytic bond dissociation energy $D_{(F–CFCl2)}$ has been calculated as 4.93 eV. Now, the potential energy of the products is 4.93 eV less the electron affinity of a fluorine atom ($EA_{(F\bullet)}$ = 3.45 eV), i.e., the process is endothermic by 1.48 eV. The experimental *AE* of the fragments is 1.8 eV. This yields a minimum excess energy of 0.32 eV (Fig. 7.15) [90].

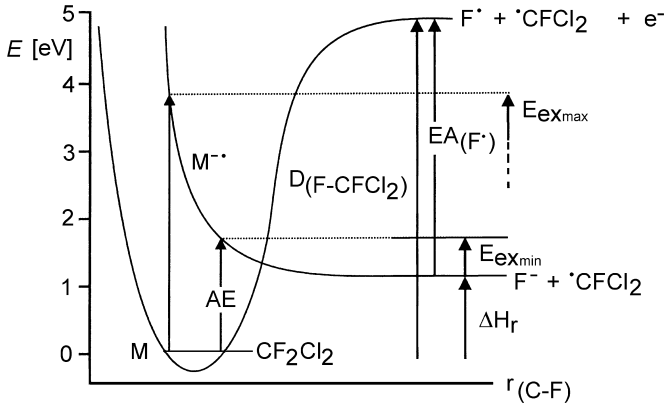


Fig. 7.15. Potential energy diagram of the dissociative EC process $CF_2Cl_2 + e^- \rightarrow F^- + CFCl_2^{\bullet}$.

Table 7.4. Selected electron affinities [91]

Compound	*EA* [eV]	Compound	*EA* [eV]
Carbon dioxide	–0.600	Pentachlorobenzene	0.729
Naphthalene	–0.200	Carbon tetrachloride	0.805
Acetone	0.002	Biphenylene	0.890
1,2-Dichlorobenzene	0.094	Nitrobenzene	1.006
Benzonitrile	0.256	Octafluorocyclobutane	1.049
Molecular oxygen	0.451	Pentafluorobenzonitrile	1.084
Carbon disulfide	0.512	2-Nitronaphthalene	1.184
Benzo[e]pyrene	0.534	1-Bromo-4-nitrobenzene	1.292
Tetrachloroethylene	0.640	Antimony pentafluoride	1.300

7.6.3 Creating Thermal Electrons

Thermionic emission from a heated metal filament is the standard source of free electrons. However, those electrons usually are significantly above thermal energy and need to be decelerated for EC. Buffer gases such as methane, isobutane, or carbon dioxide serve well for that purpose, but others have also been used [73,83,92]. The gases do not form negative ions themselves while effectively moderating the energetic electrons to thermal energy [79]. Despite inverse polarity

of the extraction voltage, the same conditions as for PICI can usually be applied. Lowering the ion source temperature provides lower-energy electrons, e.g., assuming Maxwellian energy distribution the mean electron energy is 0.068 eV at 250°C and 0.048 eV at 100°C [79].

EC is comparatively sensitive to ion source conditions [76,93]. The actual ion source temperature, the buffer gas, the amount of sample introduced, and ion source contaminations each play important roles. Regular cleaning of the ion source is important [80]. It much depends on the actual analyte whether EC is effective or whether competing processes (Eq. 7.19–7.21) are prevalent.

Alternatively to direct supply from a heated filament, electrons of well-defined low energy can be delivered into the ion volume by an electron monochromator [90,93-95].

7.6.4 Appearance of EC Spectra

EC spectra generally exhibit strong molecular ions and no primary fragment ions (Fig. 7.14) or in some cases just a few (Fig. 7.16). As $M^{-\bullet}$ is an odd-electron species, homolytic bond cleavages as well as rearrangement fragmentations may occur. Apart from the opposite charge, there are close similarities to the fragmentation pathways of positive molecular ions (Chap. 6) [76,85,86].

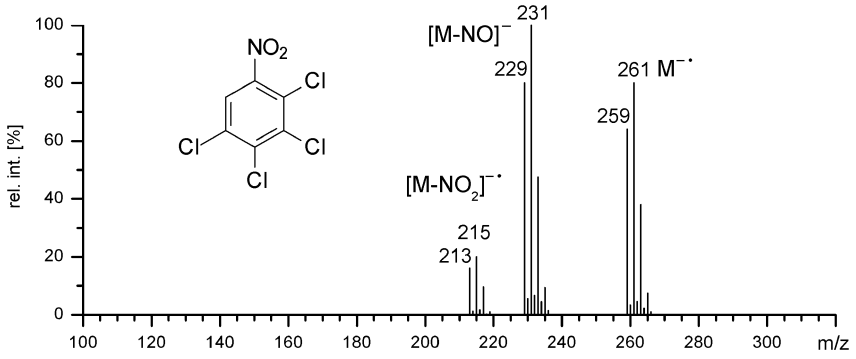


Fig. 7.16. Methane EC spectrum of 2,3,4,5-tetrachloronitrobenzene. Redrawn from Ref. [86] by permission. © John Wiley & Sons, 1988.

7.6.5 Applications of EC

EC, especially when combined with GC-MS, is commomly used in the monitoring of environmental pollutants such as dioxins [90,93,95], pesticides [90], halogenated metabolites [81], DNA adducts [89], explosives [75,96,97], and others [78,79,98,99].

7.7 Desorption Chemical Ionization

In CI, the analyte is generally introduced into the ion source via *direct insertion probe* (DIP), *gas chromatograph* (GC), or *reservoir inlet* (Chap. 5.2). However, CI can also be used in conjunction with sample introduction by a *direct exposure probe* (DEP). This is known as *desorption chemical ionization* (DCI) [32,100,101]. In DCI, the analyte is applied from solution or suspension to the outside of a thin resistively heated wire loop or coil. Then, the analyte is directly exposed to the reagent gas plasma while being rapidly heated at rates of several hundred °C s^{-1} and to temperatures up to about 1500°C (Chap. 5.2.5). The analytical result depends on the actual shape of the wire, the sample application method, and the heating rate [102,103]. The rapid heating of the sample plays an important role in promoting molecular species rather than pyrolysis products [104]. In contrast to *desorption electron ionization* (DEI), DCI is more frequently applied [103,105-107]. An appropriate experimental setup provided, accurate mass measurements can be achieved in DCI mode [108].

Note: DCI requires fast scanning of the mass analyzer because of the rather sudden evaporation of the analyte.

Example: The pyrolysis (Py) DCI mass spectrum of cellulose, $H(C_6H_{10}O_5)_nOH$, as acquired using NH_3 reagent gas, 100 eV of electron energy, and scanning *m/z* 140–700 at 2 s per cycle shows a series of distinct signals. The peaks are separated by 162 u, i.e., by $C_6H_{10}O_5$ saccharide units. The main signals are due to ions from anhydro-oligosaccharides, $[(C_6H_{10}O_5)_n+NH_4]^+$, formed upon heating of the cellulose in the ammonia CI plasma (Fig. 7.17) [102].

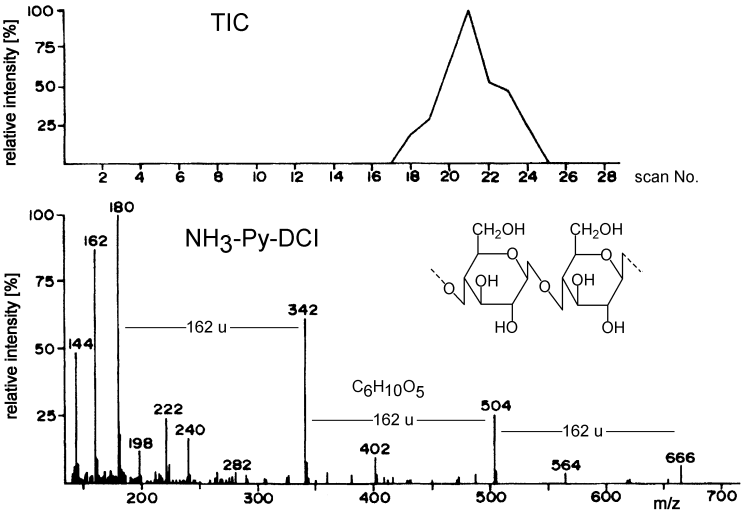


Fig. 7.17. Ammonia-Py-DCI mass spectrum of cellulose and total ion current. Adapted from Ref. [102] by permission. © Research Council of Canada, 1994.

Note: Although *desorption chemical ionization* being the correct term [103], DCI is sometimes referred to as *direct CI*, *direct exposure CI*, *in-beam CI*, or even *surface ionization*. Nowadays, DCI is rarely used, because in most instances one of the various desorption/ionization methods serves the purpose much better (Chaps. 8, 10–12).

7.8 Analytes for CI

Whether an analyte is suitable to be analyzed by CI depends on what particular CI technique is to be applied. Obviously, protonating PICI will be beneficial for other compounds than CE-CI or EC. In general, most analytes accessible to EI (Chap. 5.6) can be analyzed by protonating PICI, and PICI turns out to be especially useful when molecular ion peaks in EI are absent or very weak. CE-CI and EC play a role where selectivity and/or very high sensitivity for a certain compound class is desired (Table 7.5). The typical mass range for CI reaches from 80 to 1200 u. In DCI, molecules up to 2000 u are standard, but up to 6000 u may become feasible [103].

Table 7.5. CI methods for different groups of analytes

Analyte	Thermodynamic properties[a)]	Example	Suggested CI method
Low polarity, no heteroatoms	Low to high IE, low PA, low EA	Alkanes, alkenes, aromatic hydrocarbons	CE
Low to medium polarity, one or two heteroatoms	Low to medium IE, medium to high *PA*, low *EA*	Alcohols, amines, esters, heterocyclic compounds	PICI, CE
Medium to high polarity, some heteroatoms	Low to medium *IE*, high *PA* and low *EA*	Diols, triols, amino acids, disaccharides, substituted aromatic or heterocyclic compounds	PICI
Low to high polarity, halogens (especially F or Cl)	Medium *IE*, low *PA*, medium to high *EA*	Halogenated compounds, derivatives, e.g., trifluoroacetate, pentafluorobenzyl	EC
High polarity, medium to high molecular mass	Low to medium *IE*, high *PA* and low *EA*	Mono- to tetrasaccharides, low mass peptides, other polar oligomers	DCI
High polarity, very high molecular mass	Decomposition products of low to medium *IE*, high *PA* and low *EA*	Polysaccharides, humic compounds, synthetic polymers	Py-DCI

a) *IE*: ionization energy, *PA*: proton affinity, *EA*: electron affinity

References

1. Talrose, V.L.; Ljubimova, A.K. Secondary Processes in the Ion Source of a Mass Spectrometer (Reprint from 1952). *J. Mass Spectrom.* **1998,** *33*, 502-504.
2. Munson, M.S.B.; Field, F.H. Reactions of Gaseous Ions. XV. Methane + 1% Ethane and Methane + 1% Propane. *J. Am. Chem. Soc.* **1965,** *87*, 3294-3299.
3. Munson, M.S.B. Proton Affinities and the Methyl Inductive Effect. *J. Am. Chem. Soc.* **1965,** *87*, 2332-2336.
4. Munson, M.S.B.; Field, F.H. Chemical Ionization Mass Spectrometry. I. General Introduction. *J. Am. Chem. Soc.* **1966,** *88*, 2621-2630.
5. Munson, M.S.B. Development of Chemical Ionization Mass Spectrometry. *Int. J. Mass Spectrom.* **2000,** *200*, 243-251.
6. Richter, W.J.; Schwarz, H. Chemical Ionization - a Highly Important Productive Mass Spectrometric Analysis Method. *Angew. Chem.* **1978,** *90*, 449-469.
7. Harrison, A.G. *Chemical Ionization Mass Spectrometry,* 2nd ed.; CRC Press: Boca Raton, 1992.
8. Todd, J.F.J. Recommendations for Nomenclature and Symbolism for Mass Spectroscopy Including an Appendix of Terms Used in Vacuum Technology. *Int. J. Mass Spectrom. Ion. Proc.* **1995,** *142*, 211-240.
9. Griffith, K.S.; Gellene, G.I. A Simple Method for Estimating Effective Ion Source Residence Time. *J. Am. Soc. Mass Spectrom.* **1993,** *4*, 787-791.
10. Field, F.H.; Munson, M.S.B. Reactions of Gaseous Ions. XIV. Mass Spectrometric Studies of Methane at Pressures to 2 Torr. *J. Am. Chem. Soc.* **1965,** *87*, 3289-3294.
11. Hunt, D.F.; Ryan, J.F.I. Chemical Ionization Mass Spectrometry Studies. I. Identification of Alcohols. *Tetrahedron Lett.* **1971,** *47*, 4535-4538.
12. Herman, J.A.; Harrison, A.G. Effect of Reaction Exothermicity on the Proton Transfer Chemical Ionization Mass Spectra of Isomeric C_5 and C_6 Alkanols. *Can. J. Chem.* **1981,** *59*, 2125-2132.
13. Beggs, D.; Vestal, M.L.; Fales, H.M.; Milne, G.W.A. Chemical Ionization Mass Spectrometer Source. *Rev. Sci. Inst.* **1971,** *42*, 1578-1584.
14. Schröder, E. *Massenspektrometrie - Begriffe und Definitionen;* Springer-Verlag: Heidelberg, 1991.
15. Ghaderi, S.; Kulkarni, P.S.; Ledford, E.B., Jr.; Wilkins, C.L.; Gross, M.L. Chemical Ionization in Fourier Transform Mass Spectrometry. *Anal. Chem.* **1981,** *53*, 428-437.
16. Price, P. Standard Definitions of Terms Relating to Mass Spectrometry. A Report From the Committee on Measurements and Standards of the Amercian Society for Mass Spectrometry. *J. Am. Chem. Soc. Mass Spectrom.* **1991,** *2*, 336-348.
17. Heck, A.J.R.; de Koning, L.J.; Nibbering, N.M.M. Structure of Protonated Methane. *J. Am. Soc. Mass Spectrom.* **1991,** *2*, 454-458.
18. Mackay, G.I.; Schiff, H.I.; Bohme, K.D. A Room-Temperature Study of the Kinetics and Energetics for the Protonation of Ethane. *Can. J. Chem.* **1981,** *59*, 1771-1778.
19. Fisher, J.J.; Koyanagi, G.K.; McMahon, T.B. The $C_2H_7^+$ Potential Energy Surface: a Fourier Transform Ion Cyclotron Resonance Investigation of the Reaction of Methyl Cation With Methane. *Int. J. Mass Spectrom.* **2000,** *195/196*, 491-505.
20. Drabner, G.; Poppe, A.; Budzikiewicz, H. The Composition of the Methane Plasma. *Int. J. Mass Spectrom. Ion Proc.* **1990,** *97*, 1-33.
21. Thompson, K.C.; Crittenden, D.L.; Jordan, M.J.T. CH_5^+: Chemistry's Chameleon Unmasked. *J. Am. Chem. Soc.* **2005,** *127*, 4954-4958.
22. Heck, A.J.R.; de Koning, L.J.; Nibbering, N.M.M. On the Structure and Unimolecular Chemistry of Protonated Halomethanes. *Int. J. Mass Spectrom. Ion Proc.* **1991,** *109*, 209-225.
23. Herman, J.A.; Harrison, A.G. Effect of Protonation Exothermicity on the Chemical Ionization Mass Spectra of Some Alkylbenzenes. *Org. Mass Spectrom.* **1981,** *16*, 423-427.
24. Munson, M.S.B.; Field, F.H. Reactions of Gaseous Ions. XVI. Effects of Additives on Ionic Reactions in Methane. *J. Am. Chem. Soc.* **1965,** *87*, 4242-4247.

25. Kuck, D.; Petersen, A.; Fastabend, U. Mobile Protons in Large Gaseous Alkylbenzenium Ions. the 21-Proton Equilibration in Protonated Tetrabenzylmethane and Related "Proton Dances". *Int. J. Mass Spectrom.* **1998,** *179/180*, 129-146.
26. Kuck, D. Half a Century of Scrambling in Organic Ions: Complete, Incomplete, Progressive and Composite Atom Interchange. *Int. J. Mass Spectrom.* **2002,** *213*, 101-144.
27. Fales, H.M.; Milne, G.W.A.; Axenrod, T. Identification of Barbiturates by Chemical Ionization Mass Spectrometry. *Anal. Chem.* **1970,** *42*, 1432-1435.
28. Milne, G.W.A.; Axenrod, T.; Fales, H.M. Chemical Ionization Mass Spectrometry of Complex Molecules. IV. Amino Acids. *J. Am. Chem. Soc.* **1970,** *92*, 5170-5175.
29. Fales, H.M.; Milne, G.W.A. Chemical Ionization Mass Spectrometry of Complex Molecules. II. Alkaloids. *J. Am. Chem. Soc.* **1970,** *92*, 1590-1597.
30. Herman, J.A.; Harrison, A.G. Energetics and Structural Effects in the Fragmentation of Protonated Esters in the Gas Phase. *Can. J. Chem.* **1981,** *59*, 2133-2145.
31. Milne, G.W.A.; Fales, H.M.; Axenrod, T. Identification of Dangerous Drugs by Isobutane Chemical Ionization Mass Spectrometry. *Anal. Chem.* **1970,** *42*, 1815-1820.
32. Takeda, N.; Harada, K.-I.; Suzuki, M.; Tatematsu, A.; Kubodera, T. Application of Emitter Chemical Ionization Mass Spectrometry to Structural Characterization of Aminoglycoside Antibiotics. *Org. Mass Spectrom.* **1982,** *17*, 247-252.
33. McGuire, J.M.; Munson, B. Comparison of Isopentane and Isobutane As Chemical Ionization Reagent Gases. *Anal. Chem.* **1985,** *57*, 680-683.
34. McCamish, M.; Allan, A.R.; Roboz, J. Poly(Dimethylsiloxane) as Mass Reference for Accurate Mass Determination in Isobutane Chemical Ionization Mass Spectrometry. *Rapid Commun. Mass Spectrom.* **1987,** *1*, 124-125.
35. Maeder, H.; Gunzelmann, K.H. Straight-Chain Alkanes as Reference Compounds for Accurate Mass Determination in Isobutane Chemical Ionization Mass Spectrometry. *Rapid Commun. Mass Spectrom.* **1988,** *2*, 199-200.
36. Hunt, D.F.; McEwen, C.N.; Upham, R.A. Chemical Ionization Mass Spectrometry. II. Differentiation of Primary, Secondary, and Tertiary Amines. *Tetrahedron Lett.* **1971,** *47*, 4539-4542.
37. Busker, E.; Budzikiewicz, H. Studies in Chemical Ionization Mass Spectrometry. 2. Isobutane and Nitric Oxide Spectra of Alkynes. *Org. Mass Spectrom.* **1979,** *14*, 222-226.
38. Keough, T.; DeStefano, A.J. Factors Affecting Reactivity in Ammonia Chemical-Ionization Spectrometry. *Org. Mass Spectrom.* **1981,** *16*, 527-533.
39. Hancock, R.A.; Hodges, M.G. A Simple Kinetic Method for Determining Ion-Source Pressures for Ammonia CIMS. *Int. J. Mass Spectrom. Ion Phys.* **1983,** *46*, 329-332.
40. Rudewicz, P.; Munson, B. Effect of Ammonia Partial Pressure on the Sensitivities for Oxygenated Compounds in Ammonia Chemical Ionization Mass Spectrometry. *Anal. Chem.* **1986,** *58*, 2903-2907.
41. Lawrence, D.L. Accurate Mass Measurement of Positive Ions Produced by Ammonia Chemical Ionization. *Rapid Commun. Mass Spectrom.* **1990,** *4*, 546-549.
42. Brinded, K.A.; Tiller, P.R.; Lane, S.J. Triton X-100 As a Reference Compound for Ammonia High-Resolution Chemical Ionization Mass Spectrometry and as a Tuning and Calibration Compound for Thermospray. *Rapid Commun. Mass Spectrom.* **1993,** *7*, 1059-1061.
43. Wu, H.-F.; Lin, Y.-P. Determination of the Sensitivity of an External Source Ion Trap Tandem Mass Spectrometer Using Dimethyl Ether Chemical Ionization. *J. Mass Spectrom.* **1999,** *34*, 1283-1285.
44. Barry, R.; Munson, B. Selective Reagents in Chemical Ionization Mass Spectrometry: Diisopropyl Ether. *Anal. Chem.* **1987,** *59*, 466-471.
45. Allgood, C.; Lin, Y.; Ma, Y.C.; Munson, B. Benzene as a Selective Chemical Ionization Reagent Gas. *Org. Mass Spectrom.* **1990,** *25*, 497-502.
46. Srinivas, R.; Vairamani, M.; Mathews, C.K. Gase-Phase Halo Alkylation of C_{60}-Fullerene by Ion-Molecule Reaction Under Chemical Ionization. *J. Am. Soc. Mass Spectrom.* **1993,** *4*, 894-897.
47. Fordham, P.J.; Chamot-Rooke, J.; Guidice, E.; Tortajada, J.; Morizur, J.-P.

Analysis of Alkenes by Copper Ion Chemical Ionization Gas Chromatography/Mass Spectrometry and Gas Chromatography/Tandem Mass Spectrometry. *J. Mass Spectrom.* **1999,** *34*, 1007-1017.
48. Peake, D.A.; Gross, M.L. Iron(I) Chemical Ionization and Tandem Mass Spectrometry for Locating Double Bonds. *Anal. Chem.* **1985,** *57*, 115-120.
49. Budzikiewicz, H.; Blech, S.; Schneider, B. Studies in Chemical Ionization. XXVI. Investigation of Aliphatic Dienes by Chemical Ionization With Nitric Oxide. *Org. Mass Spectrom.* **1991,** *26*, 1057-1060.
50. Schneider, B.; Budzikiewicz, H. A Facile Method for the Localization of a Double Bond in Aliphatic Compounds. *Rapid Commun. Mass Spectrom.* **1990,** *4*, 550-551.
51. Lindinger, W.; Jordan, A. Proton-Transfer-Reaction Mass Spectrometry (PTR-MS): Online Monitoring of Volatile Organic Compounds at Pptv Levels. *Chemical Society Reviews* **1998,** *27*, 347-354.
52. Lindinger, W.; Hansel, A.; Jordan, A. Online Monitoring of Volatile Organic Compounds at Pptv Levels by Means of Proton-Transfer-Reaction Mass Spectrometry (PTR-MS). Medical Applications, Food Control and Environmental Research. *Int. J. Mass Spectrom. Ion Proc.* **1998,** *173*, 191-241.
53. Blake, R.S.; Monks, P.S.; Ellis, A.M. Proton-Transfer Reaction Mass Spectrometry. *Chem. Rev.* **2009,** *109*, 861-896.
54. de Gouw, J.; Warneke, C. Measurements of Volatile Organic Compounds in the Earth's Atmosphere Using Proton-Transfer-Reaction Mass Spectrometry. *Mass Spectrom. Rev.* **2007,** *26*, 223-257.
55. Fay, L.B.; Yeretzian, C.; Blank, I. Novel Mass Spectrometry Methods in Flavour Analysis. *Chimia* **2001,** *55*, 429-434.
56. Karl, T.; Guenther, A.; Yokelson, R.J.; Greenberg, J.; Potosnak, M.; Blake, D.R.; Artaxo, P. The Tropical Forest and Fire Emissions Experiment: Emission, Chemistry, and Transport of Biogenic Volatile Organic Compounds in the Lower Atmosphere Over Amazonia. *J. Geophys. Res. [Atmosphere]* **2007,** *112*, D18302-1-D18302/17.
57. Hsu, C.S.; Qian, K. Carbon Disulfide Charge Exchange as a Low-Energy Ionization Technique for Hydrocarbon Characterization. *Anal. Chem.* **1993,** *65*, 767-771.
58. Einolf, N.; Munson, B. High-Pressure Charge Exchange Mass Spectrometry. *Int. J. Mass Spectrom. Ion Phys.* **1972,** *9*, 141-160.
59. Sieck, L.W. Determination of Molecular Weight Distribution of Aromatic Components in Petroleum Products by Chemical Ionization Mass Spectrometry With Chlorobenzene as Reagent Gas. *Anal. Chem.* **1983,** *55*, 38-41.
60. Allgood, C.; Ma, Y.C.; Munson, B. Quantitation Using Benzene in Gas Chromatography/Chemical Ionization Mass Spectrometry. *Anal. Chem.* **1991,** *63*, 721-725.
61. Subba Rao, S.C.; Fenselau, C. Evaluation of Benzene as a Charge Exchange Reagent. *Anal. Chem.* **1978,** *50*, 511-515.
62. Li, Y.H.; Herman, J.A.; Harrison, A.G. Charge Exchange Mass Spectra of Some C_5H_{10} Isomers. *Can. J. Chem.* **1981,** *59*, 1753-1759.
63. Abbatt, J.A.; Harrison, A.G. Low-Energy Mass Spectra of Some Aliphatic Ketones. *Org. Mass Spectrom.* **1986,** *21*, 557-563.
64. Herman, J.A.; Li, Y.-H.; Harrison, A.G. Energy Dependence of the Fragmentation of Some Isomeric $C_6H_{12}^{+\cdot}$ Ions. *Org. Mass Spectrom.* **1982,** *17*, 143-150.
65. Chai, R.; Harrison, A.G. Location of Double Bonds by Chemical Ionization Mass Spectrometry. *Anal. Chem.* **1981,** *53*, 34-37.
66. Keough, T.; Mihelich, E.D.; Eickhoff, D.J. Differentiation of Monoepoxide Isomers of Polyunsaturated Fatty Acids and Fatty Acid Esters by Low-Energy Charge Exchange Mass Spectrometry. *Anal. Chem.* **1984,** *56*, 1849-1852.
67. Polley, C.W., Jr.; Munson, B. Nitrous Oxide As Reagent Gas for Positive Ion Chemical Ionization Mass Spectrometry. *Anal. Chem.* **1983,** *55*, 754-757.
68. Hsu, C.S.; Cooks, R.G. Charge Exchange Mass Spectrometry at High Energy. *Org. Mass Spectrom.* **1976,** *11*, 975-983.
69. Harrison, A.G.; Lin, M.S. Stereochemical Applications of Mass Spectrometry. 3. Energy Dependence of the Fragmenta-

tion of Stereoisomeric Methylcyclohexanols. *Org. Mass Spectrom.* **1984,** *19*, 67-71.
70. Roussis, S. Exhaustive Determination of Hydrocarbon Compound Type Distributions by High Resolution Mass Spectrometry. *Rapid Commun. Mass Spectrom.* **1999,** *13*, 1031-1051.
71. Hunt, D.F.; Stafford, G.C., Jr.; Crow, F.W. Pulsed Positive- and Negative-Ion Chemical Ionization Mass Spectrometry. *Anal. Chem.* **1976,** *48*, 2098-2104.
72. von Ardenne, M.; Steinfelder, K.; Tümmler, R. *Elektronenanlagerungs-Massenspektrographie Organischer Substanzen;* Springer-Verlag: Heidelberg, 1971.
73. Dougherty, R.C.; Weisenberger, C.R. Negative Ion Mass Spectra of Benzene, Naphthalene, and Anthracene. A New Technique for Obtaining Relatively Intense and Reproducible Negative Ion Mass Spectra. *J. Am. Chem. Soc.* **1968,** *90*, 6570-6571.
74. Dillard, J.G. Negative Ion Mass Spectrometry. *Chem. Rev.* **1973,** *73*, 589-644.
75. Bouma, W.J.; Jennings, K.R. Negative Chemical Ionization Mass Spectrometry of Explosives. *Org. Mass Spectrom.* **1981,** *16*, 330-335.
76. Budzikiewicz, H. Studies in Negative Ion Mass Spectrometry. XI. Negative Chemical Ionization (NCI) of Organic Compounds. *Mass Spectrom. Rev.* **1986,** *5*, 345-380.
77. Gross, J.H. Mass Spectrometry, in: Andrews, D.L. (ed.) *Encyclopedia of Applied Spectroscopy*, Wiley-VCH: Berlin, 2009; Chap. 29, pp. 989-1054.
78. Hunt, D.F.; Crow, F.W. Electron Capture Negative Ion Chemical Ionization Mass Spectrometry. *Anal. Chem.* **1978,** *50*, 1781-1784.
79. Ong, V.S.; Hites, R.A. Electron Capture Mass Spectrometry of Organic Environmental Contaminants. *Mass Spectrom. Rev.* **1994,** *13*, 259-283.
80. Oehme, M. Quantification of Fg-Pg Amounts by Electron Capture Negative Ion Mass Spectrometry – Parameter Optimization and Practical Advice. *Fresenius J. Anal. Chem.* **1994,** *350*, 544-554.
81. Bartels, M.J. Quantitation of the Tetrachloroethylene Metabolite *N*-Acetyl-*S*-(Trichlorovinyl)Cysteine in Rat Urine Via Negative Ion Chemical Ionization Gas Chromatography/Tandem Mass Spectrometry. *Biol. Mass Spectrom.* **1994,** *23*, 689-694.
82. Fowler, B. The Determination of Toxaphene in Environmental Samples by Negative Ion Electron Capture High Resolution Mass Spectrometry. *Chemosphere* **2000,** *41*, 487-492.
83. Laramée, J.A.; Arbogast, B.C.; Deinzer, M.L. Electron Capture Negative Ion Chemical Ionization Mass Spectrometry of 1,2,3,4-Tetrachlorodibenzo-*p*-Dioxin. *Anal. Chem.* **1986,** *58*, 2907-2912.
84. Budzikiewicz, H. Mass Spectrometry of Negative Ions. 3. Mass Spectrometry of Negative Organic Ions. *Angew. Chem.* **1981,** *93*, 635-649.
85. Bowie, J.H. The Formation and Fragmentation of Negative Ions Derived From Organic Molecules. *Mass Spectrom. Rev.* **1984,** *3*, 161-207.
86. Stemmler, E.A.; Hites, R.A. The Fragmentation of Negative Ions Generated by Electron Capture Negative Ion Mass Spectrometry: A Review with New Data. *Biomed. Environ. Mass Spectrom.* **1988,** *17*, 311-328.
87. Buchanan, M.V.; Olerich, G. Differentiation of Polycyclic Aromatic Hydrocarbons Using Electron Capture Negative Chemical Ionization. *Org. Mass Spectrom.* **1984,** *19*, 486-489.
88. Oehme, M. Determination of Isomeric Polycyclic Aromatic Hydrocarbons in Air Particulate Matter by High-Resolution Gas Chromatography/Negative Ion Chemical Ionization Mass Spectrometry. *Anal. Chem.* **1983,** *55*, 2290-2295.
89. Giese, R.W. Detection of DNA Adducts by Electron Capture Mass Spectrometry. *Chem. Res. Toxicol.* **1997,** *10*, 255-270.
90. Laramée, J.A.; Mazurkiewicz, P.; Berkout, V.; Deinzer, M.L. Electron Monochromator-Mass Spectrometer Instrument for Negative Ion Analysis of Electronegative Compounds. *Mass Spectrom. Rev.* **1996,** *15*, 15-42.
91. NIST NIST Chemistry Webbook. *http://webbook.nist. gov*.
92. Williamson, D.H.; Knighton, W.B.; Grimsrud, E.P. Effect of Buffer Gas Alterations on the Thermal Electron Attachment and Detachment Reactions of Azulene by Pulsed High Pressure Mass Spectrometry. *Int. J. Mass Spectrom.* **2000,** *195/196*, 481-489.
93. Carette, M.; Zerega, Y.; Perrier, P.; André, J.; March, R.E. Rydberg Elec-

tron-Capture Mass Spectrometry of 1,2,3,4-Tetrachlorodibenzo-*p*-Dioxin. *Eur. Mass Spectrom.* **2000,** *6*, 405-408.
94. Wei, J.; Liu, S.; Fedoreyev, S.A.; Vionov, V.G. A Study of Resonance Electron Capture Ionization on a Quadrupole Tandem Mass Spectrometer. *Rapid Commun. Mass Spectrom.* **2000,** *14*, 1689-1694.
95. Zerega, Y.; Carette, M.; Perrier, P.; André, J. Rydberg Electron Capture Mass Spectrometry of Organic Pollutants. *Organohal. Comp.* **2002,** *55*, 151-154.
96. Yinon, J. Mass Spectrometry of Explosives: Nitro Compounds, Nitrate Esters, and Nitramines. *Mass Spectrom. Rev.* **1982,** *1*, 257-307.
97. Cappiello, A.; Famiglini, G.; Lombardozzi, A.; Massari, A.; Vadalà, G.G. Electron Capture Ionization of Explosives With a Microflow Rate Particle Beam Interface. *J. Am. Soc. Mass Spectrom.* **1996,** *7*, 753-758.
98. Knighton, W.B.; Grimsrud, E.P. High-Pressure Electron Capture Mass Spectrometry. *Mass Spectrom. Rev.* **1995,** *14*, 327-343.
99. Aubert, C.; Rontani, J.-F. Perfluoroalkyl Ketones: Novel Derivatization Products for the Sensitive Determination of Fatty Acids by Gas Chromatography/Mass Spectrometry in Electron Impact and Negative Chemical Ionization Modes. *Rapid Commun. Mass Spectrom.* **2000,** *14*, 960-966.
100. Cotter, R.J. Mass Spectrometry of Nonvolatile Compounds by Desorption From Extended Probes. *Anal. Chem.* **1980,** *52*, 1589A-1602A.
101. Kurlansik, L.; Williams, T.J.; Strong, J.M.; Anderson, L.W.; Campana, J.E. Desorption Ionization Mass Spectrometry of Synthetic Porphyrins. *Biomed. Mass Spectrom.* **1984,** *11*, 475-481.
102. Helleur, R.J.; Thibault, P. Optimization of Pyrolysis-Desorption Chemical Ionization Mass Spectrometry and Tandem Mass Spectrometry of Polysaccharides. *Can. J. Chem.* **1994,** *72*, 345-351.
103. Vincenti, M. The Renaissance of Desorption Chemical Ionization Mass Spectrometry: Characterization of Large Involatile Molecules and Nonpolar Polymers. *Int. J. Mass Spectrom.* **2001,** *212*, 505-518.
104. Beuhler, R.J.; Flanigan, E.; Greene, L.J.; Friedman, L. Proton Transfer Mass Spectrometry of Peptides. Rapid Heating Technique for Underivatized Peptides Containing Arginine. *J. Am. Chem. Soc.* **1974,** *96*, 3990-3999.
105. Cullen, W.R.; Eigendorf, G.K.; Pergantis, S.A. Desorption Chemical Ionization Mass Spectrometry of Arsenic Compounds Present in the Marine and Terrestrial Environment. *Rapid Commun. Mass Spectrom.* **1993,** *7*, 33-36.
106. Juo, C.G.; Chen, S.W.; Her, G.R. Mass Spectrometric Analysis of Additives in Polymer Extracts by Desorption Chemical Ionization and Collisional Induced Dissociation With B/E Linked Scanning. *Anal. Chim. Acta* **1995,** *311*, 153-164.
107. Chen, G.; Cooks, R.G.; Jha, S.K.; Green, M.M. Microstructure of Alkoxy and Alkyl Substituted Isocyanate Copolymers Determined by Desorption Chemical Ionization Mass Spectrometry. *Anal. Chim. Acta* **1997,** *356*, 149-154.
108. Pergantis, S.A.; Emond, C.A.; Madilao, L.L.; Eigendorf, G.K. Accurate Mass Measurements of Positive Ions in the Desorption Chemical Ionization Mode. *Org. Mass Spectrom.* **1994,** *29*, 439-444.

8 Field Ionization and Field Desorption

Learning Objectives

- Ion formation by action of very strong electric fields
- Desorption of ions into the gas phase by strong electric fields
- Softness of field ionization and field desorption
- Methods of sample introduction for field ionization and field desorption
- General properties and fields of application of the title methods
- Applications to air- and moisture-sensitive samples
- Complex mixture analysis by combining gas chromatography and high-resolution mass spectrometry with field ionization and field desorption

---

The first observation of the desorption of positive ions from surfaces by high electrostatic fields was made by means of a field ion microscope [1,2]. The mass spectrometric analysis of some field-ionized gases followed soon [2-4]. In 1959, H.D. Beckey presented the first focusing field ionization ion source [5]. In these early experiments electric field strengths of about 10^8 V cm^{-1} (1 VÅ^{-1}) were generated at sharp tungsten tips [2,4,5]. The method of *field ionization* (FI) was soon extended to analyzing volatile liquids [6-11] and solids introduced by evaporation from a sample vial in close proximity to the ionizing tip or wire electrode [12]. FI, still embryonic in the mid-1960s, had soon to compete with chemical ionization (CI, Chap. 7) [13]. The major breakthrough came from its further development to *field desorption* (FD), because FD circumvents the evaporation of the analyte prior to ionization [14,15]. Instead, the processes of ionization *and* subsequent desorption of the formed ions are centered on the surface of the *field emitter*. The specific charm of FI-MS and especially of FD-MS arises from their extraordinary softness of ionization, in many cases yielding solely intact molecular ions, and from the capability of FD to handle neutral as well as ionic analytes [16-25]. FD-MS initially flourished from the mid-1970s to the mid-1980s, but soon suffered from the advent of fast-atom bombardment (FAB) and later electrospray ionization (ESI) mass spectrometry. [24] Then, however, the unique capabilities of FD-MS were rediscovered [26-28], even more so with the advent of advanced sample introduction [29,30] and the adaptation of FI and FD ion sources to oaTOF and FT-ICR mass analyzers [31-34].

J. Gross, *Mass Spectrometry*, 2nd ed., DOI 10.1007/978-3-642-10711-5_8,
© Springer-Verlag Berlin Heidelberg 2011

8.1 Field Ionization Process

Inghram and Gomer described and explained the process of *field ionization* of a single hydrogen atom [3,4,35]: If a hydrogen atom resides on a metal surface, its proton-electron potential is only slightly distorted. However, in the presence of an electric field in the order of 2 VÅ^{-1} with the metal at positive polarity, this distortion becomes remarkable (Fig. 8.1). As a result, the electron can become detached from the proton by tunneling into the bulk metal through a potential barrier that is only a few angstroms wide and some electronvolts high [20,36]. Thereby, the hydrogen atom becomes ionized, and the resulting proton is immediately driven away by action of the electric field. Interestingly, the situation is quite similar for an isolated hydrogen atom. Here, the electric field causes analogous distortion of the potential, and with sufficient field strength, the atom is field ionized, too. This means that atoms or molecules can be ionized by the mere action of a strong electric field independent of whether they have been adsorbed to the anodic surface or whether they are moving freely through the space between the electrodes.

Field ionization essentially is a autoionization-type process, i.e., an internally supra-excited atom or molecular moiety loses an electron spontaneously without further interaction with an energy source [37]. Different from electron ionization, there is no excess energy transferred onto the incipient ion, and thus, dissociation of the ions is reduced to a minimum.

$$M \rightarrow M^{+\bullet} + e^{-} \tag{8.1}$$

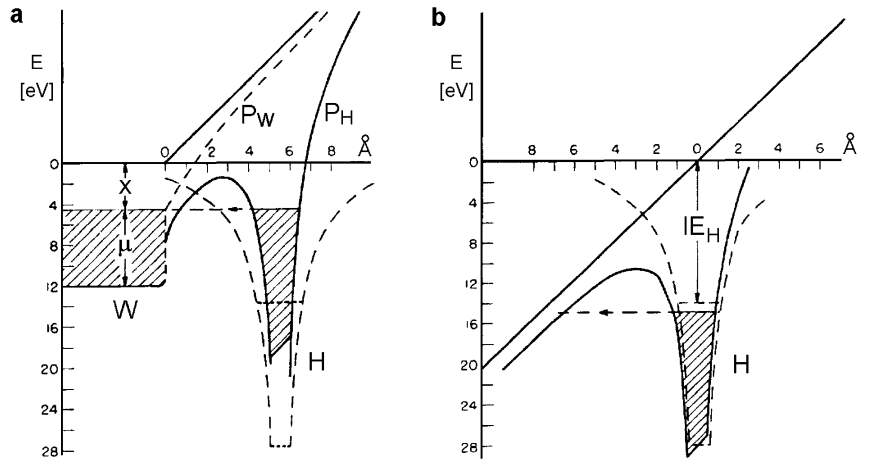


Fig. 8.1. Field ionization of a hydrogen atom (H) **a**) close to a tungsten surface (W), **b**) isolated. Conditions and symbols: electric field 2 VÅ^{-1}, P_W image potential of W distorted by the field, P_H potential of the hydrogen atom distorted by the field, X work function, μ Fermi level. *Dashed lines* represent potentials in absence of the electric field. Adapted from Ref. [4] by permission. © Verlag der Zeitschrift für Naturforschung, 1955.

Electric fields sufficient to effect field ionization are only obtained in close proximity to sharp tips, edges, or thin wires. The smaller the radius of the curvature of the anode, the further away (1–10 nm) the field sufficing to cause ionization. The importance of sufficient electric field strength is reflected by the extreme decrease in half-life calculated for a hydrogen atom: it is in the order of 0.1 s at 0.5 $VÅ^{-1}$, 0.1 ns at 1.0 $VÅ^{-1}$, and 0.1 fs at 2.5 $VÅ^{-1}$ [20].

Note: The field anode is usually referred to as *field emitter*, *FI emitter*, or *FD emitter*. The properties of the field emitter are of key importance for FI- and FD-MS. The electrode opposed to the emitter is called *field cathode* or simply *counter electrode*.

8.2 FI and FD Ion Sources

In FI- and FD-MS, a voltage of 8–12 kV is applied between *field emitter* (field anode) and *counter electrode* (field cathode) usually located 2–3 mm in front of the emitter. Thus, the desorbing ions are accelerated to 8–12 keV kinetic energy, clearly exceeding the amount which can be handled by a double-focusing magnetic sector instrument (typically used in conjunction with FI/FD ion sources). These contradictory requirements can be met by setting the counter electrode to negative potential to establish the high field gradient for ion generation while adjusting the difference between emitter and ground potential to the actual acceleration voltage (Fig. 8.2) [38]. With the emitter grounded and the counter electrode at high negative potential even slow ion beams can be delivered for mounting FD ion sources to FT-ICR or oaTOF instruments [31,39].

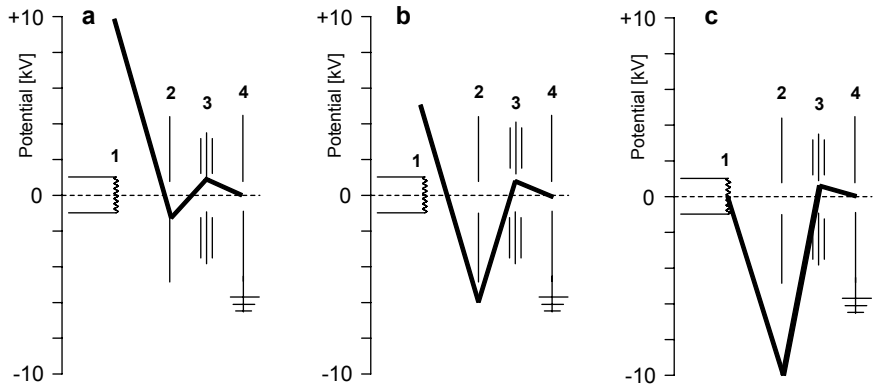


Fig. 8.2. Potentials (*bold lines*) along different FI/FD ion sources to realize full extraction voltage while delivering ions of defined kinetic energy to the analyzer. The part numbers correspond to: **1** emitter, **2** counter electrode, **3** optional electrostatic lenses, **4** analyzer entrance slit. (**a**) Instruments with high acceleration voltage, (**b**) instruments with medium acceleration voltage as is often the case in magnetic sector instruments, and (**c**) instruments requiring slow ions, e.g., FT-ICR or oaTOF instruments.

In FI mode, the analyte is introduced via external inlet systems such as a direct probe, a reservoir inlet, or a gas chromatograph (Chap. 5.3). In FD mode, the analyte is supplied directly on the surface of the field emitter. Doing so not only guarantees a more efficient usage of the sample, it also combines the steps of ionization and desorption, thereby minimizing the risk of thermal decomposition prior to ionization (Figs. 8.3, 8.4). This is especially important in case of highly polar or ionic analytes that cannot be evaporated without thermal degradation.

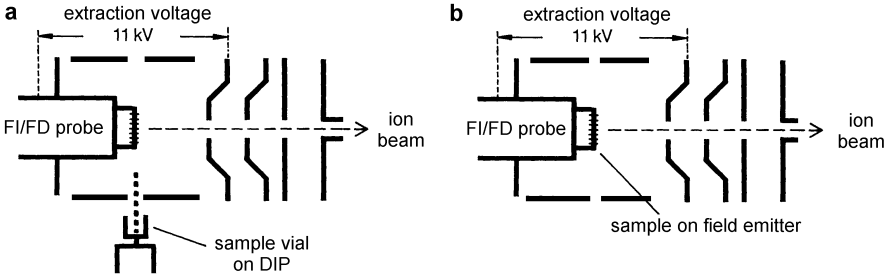


Fig. 8.3. Schematic of an FI/FD ion source (**a**) in FI mode, (**b**) in FD mode. The distance between emitter and counter electrode is exaggerated for clarity. Adapted from Ref. [40] by permission. © Springer-Verlag, Heidelberg, 1991.

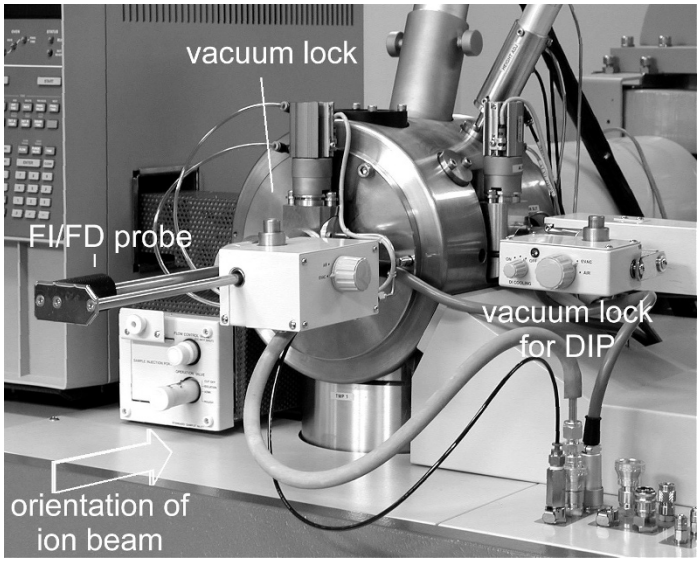


Fig. 8.4. FD probe inserted into the vacuum lock. FD probes are generally inserted in axial position to free the vacuum lock of the DIP for FI use. The emitter wire is now oriented vertically to comply with the beam geometry of the magnetic sector analyzer.

8.3 Field Emitters

8.3.1 Blank Metal Wires as Emitters

In the first FI experiments, the high electric field strength was obtained at sharply pointed tungsten tips [2,4,5]. Later, edges of sharp blades [41] and wires of a few micrometers in diameter were used. Wires are advantageous because the emitting surface of a smooth blade is approximately two orders of magnitude smaller than that of a smooth wire at the same field strength under normal working conditions (Fig. 8.5). Simple wire emitters can be used for field desorption of nonpolar [42] or electrolytic analytes [43]. As thin wires are fragile and can break during electric discharges, sharp edges should be avoided in their vicinity, e.g., by polishing the counter electrode [44].

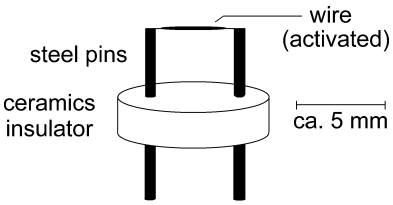


Fig. 8.5. A wire emitter: high voltage is supplied via the emitter-holding pins. These also serve to pass a current for resistive heating through the (activated) wire.

8.3.2 Activated Emitters

The electric field strength on the emitter can greatly be enhanced by creating dendritic microneedles (*whiskers*) on its surface, by a process known as *emitter activation*. FI- and FD-MS require emitters of reproducible high quality, and therefore the activation procedure has received much attention. The high-temperature activation of 10 μm tungsten wires with pure benzonitrile vapor takes 3–7 h [45], but it may be accelerated by reversal of the polarity of the high voltage during activation [46], or by using indane, indene, indole, or naphthalene as the activating agent [47]. An extremely fast activation of carbon fiber, tungsten, and platinum wire emitters is by heating to 600–900°C in an external field for a few seconds in the presence of benzene vapor [42,48]. The activation procedures with benzonitrile or indene are employed commercially to produce carbon whiskers on emitters (Fig. 8.6). Microneedle growth is also achieved by decomposition of hexacarbonyltungsten, $W(CO)_6$, on a cathode producing an electric discharge [49]. A self-controlling mechanism which draws ions preferably to the top of the growing tungsten needles has been suggested [49]. SEM pictures of activated emitter surfaces and single whiskers have an aesthetic appeal [46,47,49-52].

Alternative wire emitters other than activated tungsten are less commonly used. Cobalt and nickel [50,53] as well as silver [54] can be electrochemically deposited

on wires to produce activated FD emitters. Mechanically strong and efficient emitters can be made by growing fine silicon whiskers from silane gas on gold-coated tungsten or tantalum wires of 60 µm diameter [51]. The fracture-surface of graphite rods exposes fine microcrystallites, which are sharp enough to provide sufficiently high field strengths for ionization [55].

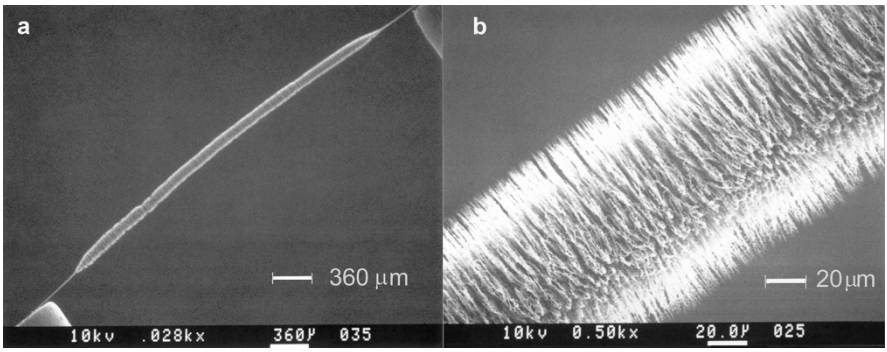


Fig. 8.6. SEM pictures of activated tungsten wire emitters; (**a**) overview showing the thin tungsten wire close to the holders and the whisker-bearing middle section, (**b**) detail of the central part revealing whiskers. By courtesy of Carbotec, Bergisch Gladbach, Germany.

8.3.3 Emitter Temperature

Emitters can be heated by applying an electric current via the emitter holders. It is somewhat difficult to establish a precise calibration of emitter temperature versus *emitter heating current* (EHC) [56,57]. The actual temperature not only depends on the emitter material, but also on diameter and length of the emitter as well as on length and area density of the whiskers. A useful estimate for tungsten emitters with carbon whiskers is given below (Fig. 8.7).

In practice, moderate heating of the emitter at constant current serves to reduce adsorption to its surface during FI measurements. Heating at a constant rate (1–20 mA min^{-1}) is frequently employed to enforce desorption of analytes from the emitter in FD-MS. Electric discharges resulting from too massive ion desorption can be avoided by emission-controlled emitter heating [58-60]. where the EHC is regulated as to achieve a constant ion emission current, typically in the range of 1–100 nA. At the end, the emitter is cleaned for subsequent measurements by baking for 2–5 s at 800–1000°C at 50–60 mA (activated tungsten emitters of 10 µm diameter) or at 80–100 mA (emitters of 13 µm)..

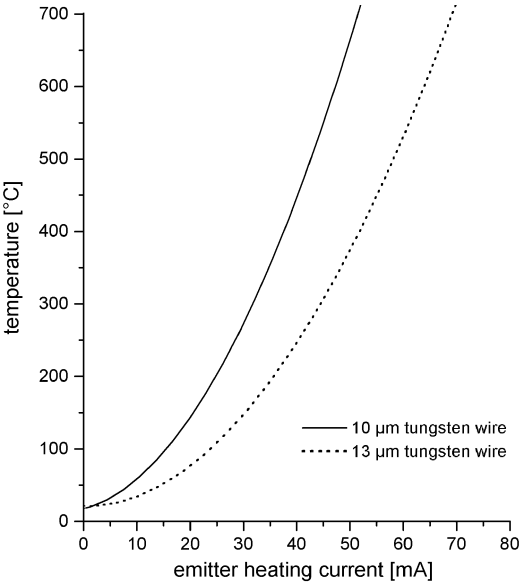


Fig. 8.7. Calibration of EHC vs. temperature for emitters activated with carbon needles on 10-µm and 13-µm tungsten wire. By courtesy of Carbotec, Bergisch Gladbach, Germany.

8.3.4 Handling of Activated Emitters

Activated wire emitters are extremely fragile, because after activation the material behaves more like ceramics than like a metal wire. The slightest touch with a syringe needle as well as electric discharges during operation cause immediate destruction of the emissive wire. Delicate handling of the emitter is therefore a prerequisite [24]; it includes *i*) using tweezers for its manipulation by grasping at the robust ceramics socket or at both pins simultaneously, *ii*) baking before first use in order to outgas and clean the emitter, *iii*) application of analytes by transfer of a drop of solution whereby only the liquid surface may contact the emitter wire (Fig. 8.8), *iv*) evaporation of the solvent usually before insertion into the vacuum lock (Fig. 8.4), *v*) switching on the high voltage only after the high vacuum has fully recovered, and finally after the measurement has been completed, *vi*) baking to remove residual sample only after switching off the high voltage. With adequate handling, an emitter can last for about 20 measurements.

Note: To apply a solution of the analyte, the emitter can either be *dipped into*, or alternatively, a drop of 1–2 µl can be *transferred onto* the emitter by means of a microliter syringe [52]. The latter method exhibits better reproducibility and avoids contamination of the emitter pins. Special micromanipulators are available to handle the syringe [15], but with some exercise a skilled operator can accomplish it manually.

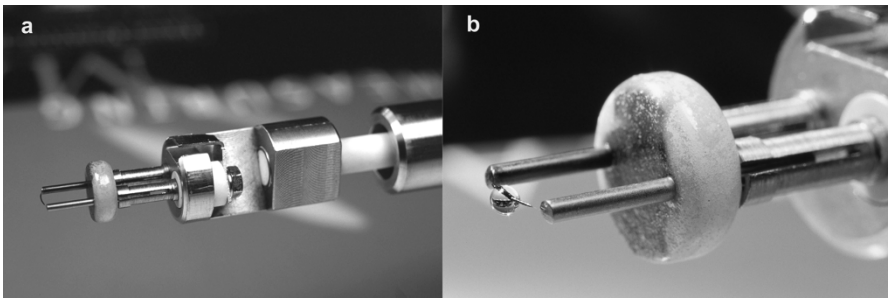


Fig. 8.8. FD probe. (**a**) Emitter holder of a JEOL FD probe tip, (**b**) a drop formed of 1–2 µl of analyte solution placed onto the activated emitter by means of a microliter syringe.

8.4 Field Ionization Mass Spectrometry

FI mass spectra are normally characterized by intense molecular ion peaks accompanied by no or in some cases just a few fragment ions [9,10,12]. Especially in case of nonpolar low-mass analytes, FI-MS can serve for molecular ion mass spectrometry (Fig. 8.9) [61]. This property made FI-MS a standard tool for hydrocarbon analysis in the petroleum industry [6,7,11,13,26,61-63]. FI performs nicely for samples that can reasonably be evaporized, but it exhibits poor sensitivity for polyhalogenated compounds such as $CHCl_3$ or PFK. FI usually fails with highly polar or even ionic compounds due to thermal decomposition. Nonetheless, there is no rule without exceptions: FI can, for example, create low-abundant "molecular ions", more appropriately described as cation-radical pairs $[C+A]^{+\bullet}$, of ionic liquids [64].

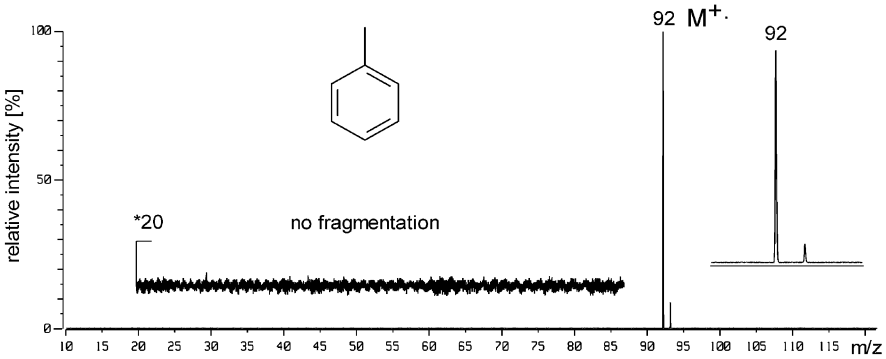


Fig. 8.9. FI spectrum of toluene. The molecular ion and its isotopolog are the only observed entities. (The CID spectrum of field-ionized toluene is shown in Chap. 9, the EI spectrum is discussed in Chap. 6.4.3).

Although convenient at first sight, the lack of fragment ion peaks in FI spectra also means a lack of structural information. If data beyond a mere estimate of the elemental composition based on the isotopic pattern are asked for, then tandem MS employing collision-induced dissociation (CID, Chap. 9) is the preferred standard of structure elucidation. Fortunately, the fragmentation pathways of $M^{+\bullet}$ ions in CID are the same as in EI-MS (Chap. 6).

Note: In FI-MS, the ionization efficiency is very low, because of the low probability for a neutral effusing from any inlet system towards the field emitter to come close enough to the whiskers. Consequently, FI-MS produces very low ion currents. The application of FI-MS is therefore restricted to samples that are too volatile for FD-MS or require prior gas chromatographic separation.

8.4.1 Origin of $[M+H]^+$ Ions in FI-MS

FI mass spectra can show signals due to reactions of the analyte with the emitter surface or between molecules adsorbed to that surface. In case of acetone, it was demonstrated that $[M+H]^+$ ions are produced mainly by a *field-induced proton-transfer* reaction in the physically adsorbed layer [65]. The mechanism of this field-induced reaction depends on the existence of tautomeric structures of the neutral molecule. Besides the $[M+H]^+$ ions, $[M–H]^\bullet$ radicals are formed in an overall reaction analogous to CH_5^+ formation in CI:

$$M^{+\bullet} + M \rightarrow [M+H]^+ + [M–H]^\bullet \qquad (8.2)$$

Furthermore, the radicals formed upon field-induced hydrogen abstraction can lead to polymerization products on the emitter surface [65]. Criteria to distinguish $M^{+\bullet}$ from $[M+H]^+$ ions have been published [66]. Besides analyte polarity and acidity of the solvent used for sample deposition onto the emitter, lower electric field strength and lower emitter temperature are likely to cause stronger $[M+H]^+$ ion contributions [66]. Analytes possessing exchangeable hydrogens strongly tend to form $[M+H]^+$ ions in FI-MS. Occasionally, the protonated molecule occurs in favor of the molecular ion that even may be hardly present (cf. Table 8.1).

8.4.2 Multiply-Charged Ions in FI-MS

Multiply charged ions of minor abundance are frequently observed in FI and FD mass spectra. Their increased abundance as compared to EI spectra can be rationalized by either of the following two-step processes: *i*) *Post-ionization* of gaseous $M^{+\bullet}$ ions can occur due to the probability for an $M^{+\bullet}$ ion to suffer a second or even third ionization while drifting away from the emitter surface [67,68]. Especially ions generated in locations not in close vicinity of the counter electrode pass numerous whiskers on their first 10–100 µm of flight:

$$M \rightarrow M^{+\bullet} + e^- \qquad (8.3)$$

$$M^{+\bullet} \rightarrow M^{2+} + e^- \tag{8.4}$$

ii) Alternatively, a surface-bound ion, $M^{+\bullet}_{(surf)}$, is formed and ionized for a second time before leaving the surface [69-71]:

$$M \rightarrow M^{+\bullet}_{(surf)} + e^- \tag{8.5}$$

$$M^{+\bullet}_{(surf)} \rightarrow M^{2+} + e^- \tag{8.6}$$

The most commonly formed types of ions in FI are summarized in Table 8.1.

Note: For recognizing multiply charged ions, it is important to keep in mind that the *m/z* scale is compressed by a factor equal to the number of charges *z* (Chaps. 3.5 and 4.2.2).

Table 8.1. Ions formed by FI

Analytes	Ions Formed
nonpolar	$M^{+\bullet}$, M^{2+}, occasionally $M^{3+\bullet}$, rarely $[M+H]^+$
medium polarity	$M^{+\bullet}$, M^{2+} and/or $[M+H]^+$
polar	$[M+H]^+$
ionic	generally thermal decomposition

8.4.3 Field-Induced Dissociation

In certain cases, the advantageous property of the strong electric field to effect soft ionization can be accompanied by *field-induced dissociation*, another type of field-induced reactions [9,72,73]. For example, the fragment ions in the FI spectra of low-mass aliphatic amines, ketones, and hydrocarbons are formed by field-induced dissociation [9,65]. Field-induced dehydrogenation [74,75] presents a severe problem to the FI and FD analysis of saturated hydrocarbon mixtures reaching beyond C_{40}, because signals from unsaturated compounds at low levels are superimposed by $[M–H_2]^{+\bullet}$ peaks [76-79]. A reduction of the emitter potential can reduce field-induced dehydrogenation to some degree.

8.4.4 Accurate Mass FI Spectra

Accurate mass complements FI with other valuable information. Unfortunately, FI delivers very low ion currents, which on scanning sector instruments make it difficult to achieve accurate mass measurements. This is because *i*) high resolution requires narrow slits, and thus, goes along with low transmission, and *ii*) internal reference masses have to be distributed over the entire range making interferences more likely. While HR-FI-MS on sector instruments is neither new nor impossible [80-83], it is generally outside routine operation [64]. The attachment of FI/FD ion

sources to oaTOF instruments has made it quite a bit easier, because a single point of reference, a so-called *lock mass*, is normally sufficient [31,32].

8.4.5 Coupling Gas Chromatography to FI-MS

In the early 1970s, the coupling of gas chromatography (GC) to FI-MS suffered from poor instrument capabilities of that time [84,85]. Recent advances with oa-TOF instrumentation allow for fast acquisition of spectra, high resolution, and straightforward accurate mass measurements in GC-FI-MS. Thus, GC-FI-MS has become a trusted tool in many laboratories, especially in the petroleum industry [31,32,86,87]. To maintain full ionization efficiency, it is common that an accumulation period of 1 s per spectrum is followed by flash-heating the emitter for 0.1–0.2 s [31,32]. These applications have also been driving the development of EI/FI/FD [39] and EI/CI/FI combination sources for GC-oaTOF instruments [88].

Example: GC-FI-oaTOF-MS was performed on paraffins from C_6 to C_{44}, covering the boiling range from 98 to 545°C, delivering GC separation and accurate mass in one run. Main components such as the C_{12}, C_{14}, and C_{16} alkanes caused some broadening of their GC peaks, eventually due to adsorption/desorption from the emitter surface resulting in a temporal spread [32]. Fig. 8.10 shows the gas chromatogram as represented by the total ion chromatogram and the mass spectrum averaged over the complete acquistion period. Although FI of the entire mixture would have yielded a similar mass spectrum, this approach avoids mutual interference during ionization and delivers isomer recognition from retention times.

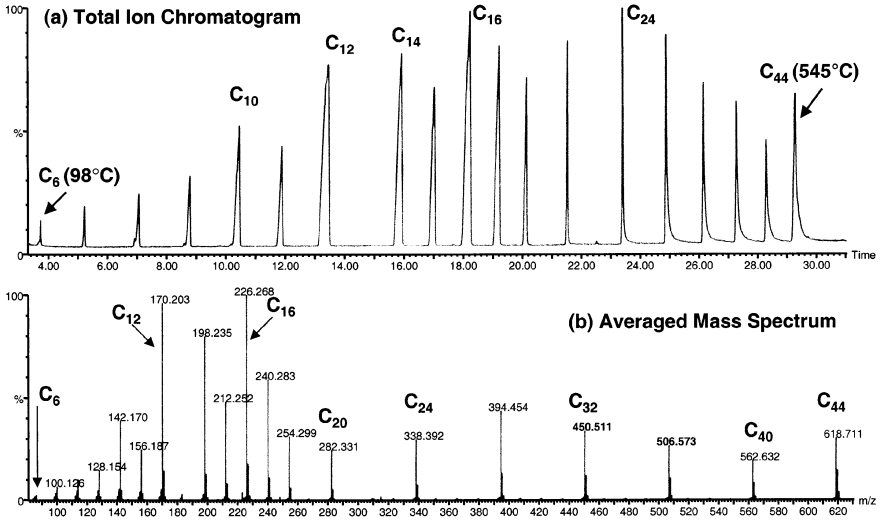


Fig. 8.10. GC-FI-oaTOF-MS total ion chromatogram and averaged mass spectrum of C_6–C_{44} *n*-paraffins. The masses of the paraffin molecular ions are all accurate. Reproduced from Ref. [32] with permission. © American Chemical Society, 2002.

8.5 FD Spectra

FD can be regarded the softest ionization method in mass spectrometry, even though electrospray ionization and matrix-assisted laser desorption ionization can transfer much larger ions into the gas phase [27,89]. This is mainly because the ionization process itself does not transfer any extra energy to the incipient ions. Problems normally arise above molecular weights of 3000 u where the heated emitter causes thermal decomposition of the sample.

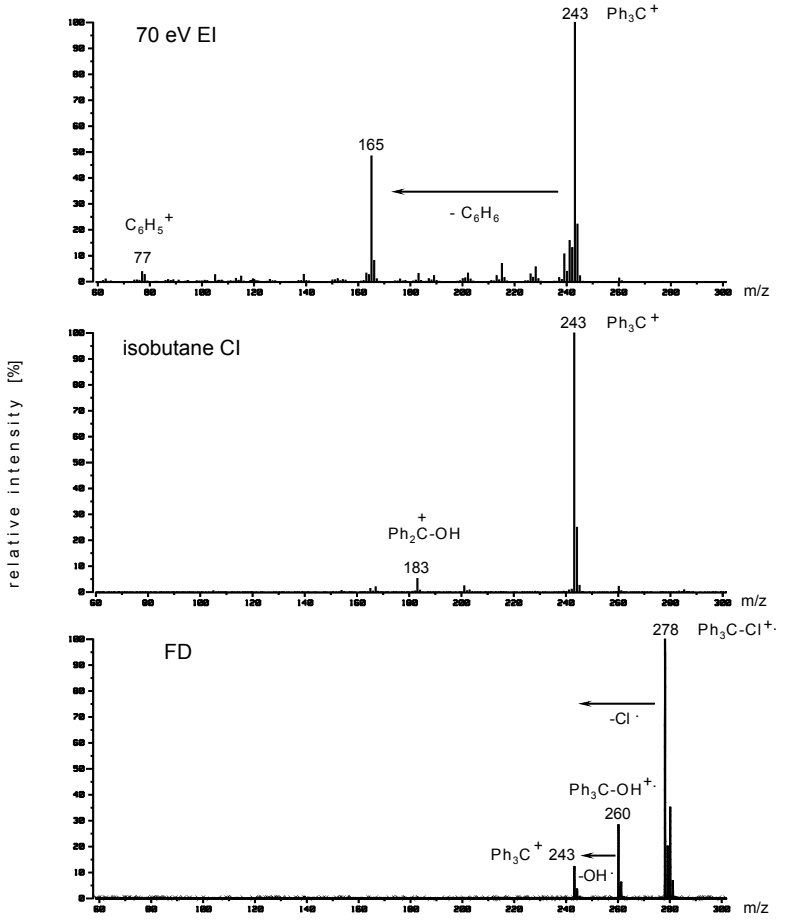


Fig. 8.11. Comparison of EI, PICI, and FD mass spectra of chlorotriphenylmethane containing some triphenylmethanol. By courtesy of C. Limberg, Humboldt University, Berlin.

Example: The extraordinarily stable trityl ion, Ph_3C^+, *m/z* 243, tends to dominate mass spectra (Chap. 6.6.2). Thus, neither the EI spectrum of chlorotriphenylmethane nor that of its impurity triphenylmethanol show molecular ions

(Fig. 8.11). An isobutane PICI spectrum also shows the trityl ion almost exclusively, although some hint is obtained from the Ph_2COH^+ ion, *m/z* 183, that cannot be explained as a fragment of a chlorotriphenylmethane ion. Only FD reveals the presence of the alcohol by its molecular ion at *m/z* 260, while that of the chloride is detected at *m/z* 278. Both molecular ions undergo some $OH^\bullet$ or $Cl^\bullet$ loss, respectively, to yield the Ph_3C^+ fragment ion of minor intensity.

8.5.1 Ion Formation by Field Ionization in FD-MS

In *field ionization* (as an experimental configuration) *field ionization* (the process) is the major pathway of ion generation. In *field desorption* from activated emitters, the analyte may also undergo *field ionization*. Presuming that the molecules are deposited in layers on the shanks of the whiskers or between them, this requires that *i*) analytes of low polarity are polarized by action of the electric field, *ii*) become mobile upon heating, and *iii*) finally reach the locations of ionizing electric field strength at the tips of the whiskers (Fig. 8.12). The requirement of mobility of the polarized molecules can either be fulfilled via gas phase transport or surface diffusion [52]. As the level of mobility to travel some ten micrometers along a whisker is clearly below that for evaporation from a separate inlet system, thermal decomposition of the field-ionized analyte in FD-MS is much reduced as compared to FI-MS. The relevance of the FI mechanism of ionization decreases as the polarity of the analyte increases. In certain cases such as sucrose, for example, it is not easy to decide whether gas phase mobility of the neutral and molecular ions jointly formed by FI still play a role [90,91] or not [92].

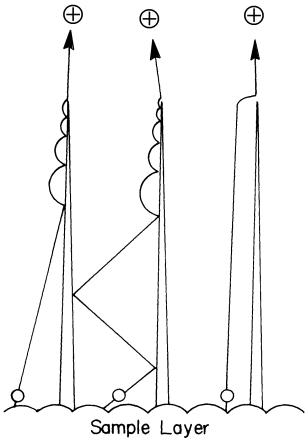


Fig. 8.12. The transport of neutrals to the tips of the field-enhancing whiskers. Reproduced from Ref. [52] by permission. © Elsevier Science, 1981.

Example: D-Glucose evaporates into the ion source without complete decomposition as demonstrated by its FI spectrum (Fig. 8.13). FD yields a spectrum with a very low degree of fragmentation that is most probably due to the required slight

heating of the emitter. The occurrence of $M^{+\bullet}$ ions, *m/z* 180, and $[M+H]^+$ ions, *m/z* 181, in the FD spectrum suggests that ion formation occurs via FI and field-induced proton transfer, respectively. However, thermal energy plus a hard ionization method (as EI) effect strong fragmentation. By comparing EI and FI spectra, the effects of thermal energy may roughly be distinguished from those of EI itself.

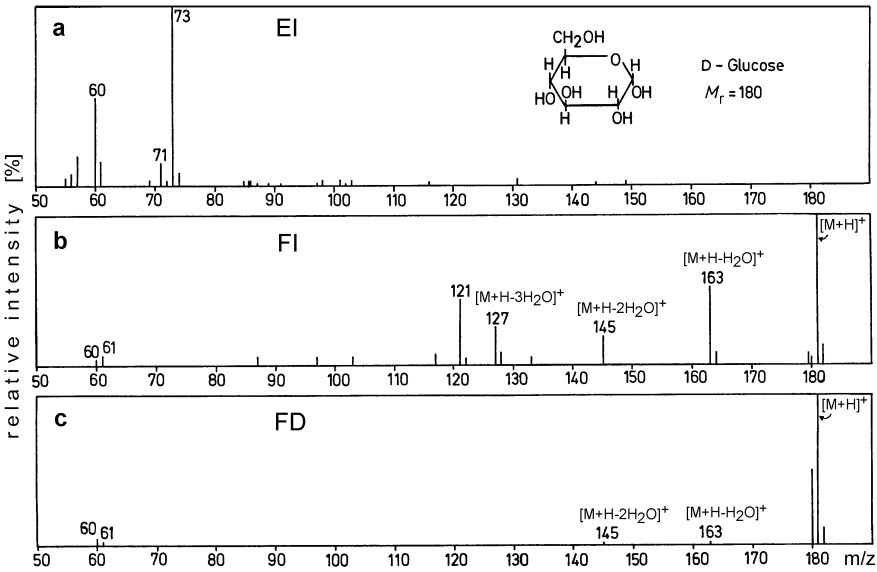


Fig. 8.13. D-Glucose mass spectra: (**a**) EI only yields ions that are due to decomposition and fragmentation, (**b**) FI still produces several fragments, and (**c**) FD almost exclusively gives ions related to the intact molecule. Adapted from Ref. [14] by permission. © Elsevier Science, 1969.

8.5.2 Desorption of Preformed Ions in FD-MS

Analytes of very high polarity are not further ionized by field ionization. Here, the prevailing pathways are *protonation* or *cationization*, i.e., the attachment of alkali ions to molecules [93]. The subsequent desorption of the ions from the surface is effected by the action of the electric field. As $[M+Na]^+$ and $[M+K]^+$ ions are already present in the condensed phase, the field strength required for their desorption is lower than that for field ionization or field-induced $[M+H]^+$ ion formation [43,94]. The desorption of ions is also effective in case of ionic analytes.

Example: FD from untreated wire emitters to which alkali metal salts were added was used to obtain mass spectra of tartaric acid, arginine, pentobarbital, and other compounds [93,95]. Besides $[M+H]^+$ ions, *m/z* 175, the FD mass spectrum of arginine exhibits $[M+Na]^+$, *m/z* 197, and $[M+K]^+$, *m/z* 213, ions due to alkali metal cationization as well as $[2M+H]^+$, *m/z* 349, cluster ions (Fig. 8.14) [43].

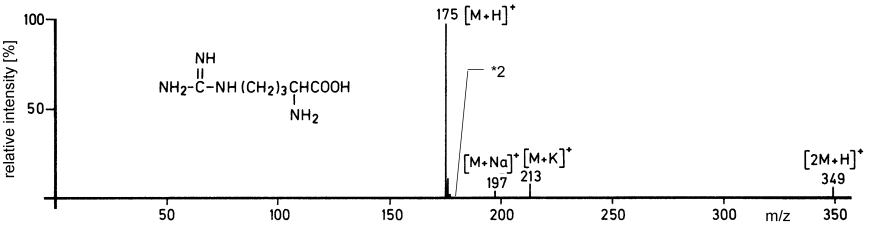


Fig. 8.14. The FD mass spectrum of arginine, $M_r = 174$, desorbed from an untreated metal wire emitter in the presence of alkali ions. Adapted from Ref. [43] by permission. © John Wiley & Sons, 1977.

Two major concepts of ion formation and desorption have been suggested, but it has remained a matter of debate whether the concept of *field-induced desolvation* [96-98] or that of *ion evaporation* [99,100] more appropriately describes the event. Although different in several aspects, the models are coherent in that ions are created in the condensed phase and subsequently desorbed into the gas phase. Both recognize the electric field as the driving force to effect extraction of ionic species after charge separation within the layer adsorbed onto the emitter surface.

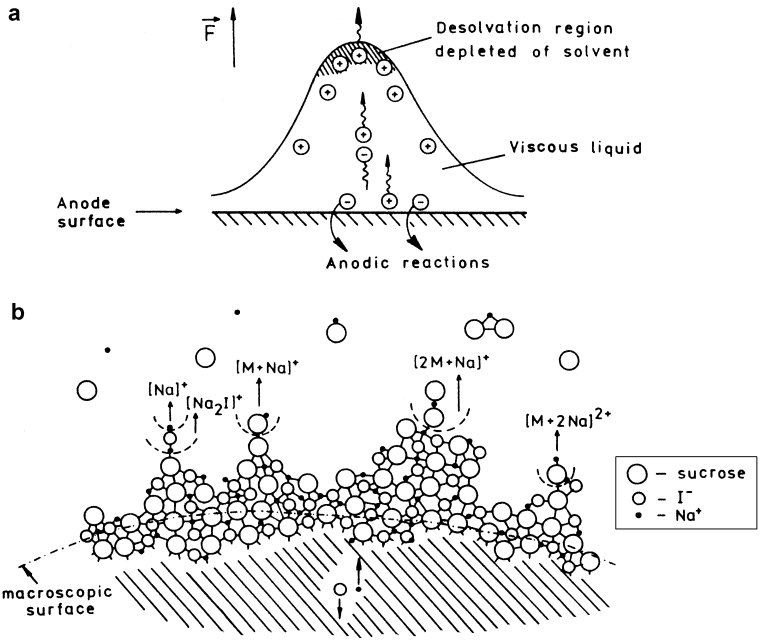


Fig. 8.15. The desolvation of ions. (**a**) Charge separation inside a protuberance, (**b**) continuous reconstruction of the surface allows for successive rupture of intermolecular bonds and stepwise desolvation of the ions. Reproduced from Ref. [98] by permission. © Elsevier Science, 1984.

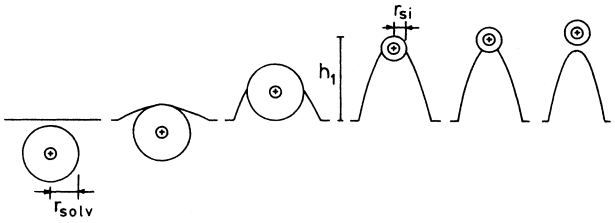


Fig. 8.16. Schematic model for ion evaporation. r_{solv} is the radius of the solvation sphere, r_{si} the radius of the separating ion, and h_1 the height of the protuberance when the radius of its parabolic tip equals r_{si}. Reproduced from Ref. [100] by permission. © Elsevier Science, 1987.

8.5.3 Cluster Ion Formation in FD-MS

Highly polar analytes which strongly tend towards cationization, frequently form cluster ions such as $[n\text{M+H}]^+$ and $[n\text{M+alkali}]^+$ in addition to $[\text{M+H}]^+$ and $[\text{M+alkali}]^+$ ions. A priori, there is no reason why these cluster ions should not be interpreted as resulting from "impurities". However, the sequence of events can serve as a reliable criterion to distinguish components of higher molecular weight from cluster ions. Cluster ions are preferably formed when the coverage of the emitter surface is still high, i.e., in the beginning of desorption. As desorption proceeds, the probability for cluster ion formation decreases, because the surface layer is diminished. In addition, a continuously rising emitter heating current leads to further thermal decomposition of clusters. Whereas cluster ions decrease in abundance, true higher-mass components require higher emitter temperature to become mobile and ionized thereafter (cf. Chap. 8.4.1). Doubly charged cluster ions, e.g., $[\text{M+2Na}]^{2+}$, may also occur. Such doubly or even multiply charged ions can serve to extend the mass range accessible by FD-MS [27].

Example: During the acquisition of an FD mass spectrum of a putatively clean disaccharide, a series of ions at higher *m/z* was observed in addition to $[\text{M+H}]^+$, *m/z* 341 and $[\text{M+Na}]^+$, *m/z* 363. Those ions could be interpreted either in terms of cluster ions or of higher oligosaccharides, respectively. The high-mass ions were only observed soon after the onset of desorption, while their abundance decreased remarkably at somewhat higher emitter current. Thereby, these signals could be assigned to cluster ions such as $[\text{2M+Na}]^+$, *m/z* 703, and $[\text{3M+Na}]^+$, *m/z* 1043 (Fig. 8.17).

Note: Pure analytes often show a comparatively sharp onset of desorption. Desorption then lasts for several scans until the sample is consumed. Finally, the intensity of the signals rapidly drops to zero again. In case of mixtures, some fractionation by molecular weight of the components is observed (Fig. 8.21).

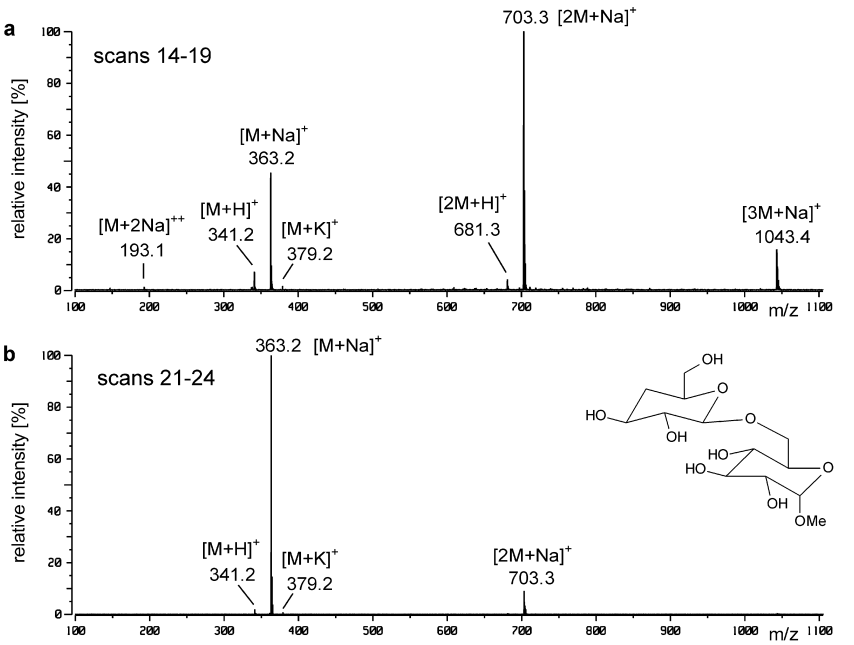


Fig. 8.17. FD mass spectra of a disaccharide (**a**) at the beginning of desorption, (**b**) towards end of desorption [101]. By courtesy of H. Friebolin, Heidelberg University.

8.5.4 FD-MS of Ionic Analytes

The intact cation C^+ of an ionic analyte of the general composition $[C^+A^-]$ always causes the base peak in positive-ion FD mass spectra. In addition, singly charged cluster ions of the $[C_nA_{n-1}]^+$ type are observed [102,103]. Their abundance and the maximum of n varies depending on the ionic species encountered as well as on the actual experimental parameters such as temperature and sample load of the emitter (Figs. 8.18, 8.19). The advantage of these cluster ions is that the mass difference between the members of the series corresponds to $[C^+A^-]$. Thus, the counterion A^- can be determined by subtraction of the mass of C^+. Moreover, the isotopic pattern of the anion is reflected in the cluster ion signals, facilitating the identification of chloride and bromide, for example. Interestingly, ionic species corresponding to some sort of "molecular ion of the salt" can also be formed. Usually, such ions are of much lower intensity than the even-electron cluster ions. Applications of FD-MS to detect cations are manifold and include organic cations [17,21,102-106] as well as inorganic ones [107,108] even down to the trace level [109], e.g., for trace-metal analysis in physiological fluids of patients suffering from multiple sclerosis [110].

Zwitterions are generally not easy to analyze by MS. Depending on the acidity of the proton-donating site and on the basicity of the proton-accepting site either the cationic or the anionic species can be formed preferentially. Adding acids to the solution of the analyte prior to loading of the emitter can significantly enhance the signal resulting from the protonated species [111].

Anions can be analyzed indirectly by FD-MS via the formation of cluster ions with their positive counterion. Negative-ion FD-MS for the direct detection of the anion A^- and cluster ions of the general composition $[C_{n-1}A_n]^-$ can be performed [112,113], but negative-ion FD-MS has remained an exception. This is due to the fact that electrons are easily emitted from activated emitters before negative ions desorb. Then, the strong emission of electrons causes the destruction of the emitter. Low emitter voltage and larger emitter–counter electrode distance help to avoid such problems [114]. Neutral analytes can give rise to $[M–H]^-$ ions or products of nucleophilic addition, e.g., $[M+Cl]^-$ ions [115]. Nowadays, fast atom bombardment (FAB, Chap. 9), matrix-assisted laser desorption/ionization (MALDI, Chap. 10), or electrospray ionization (ESI, Chap. 11) are preferred for the analysis of anions.

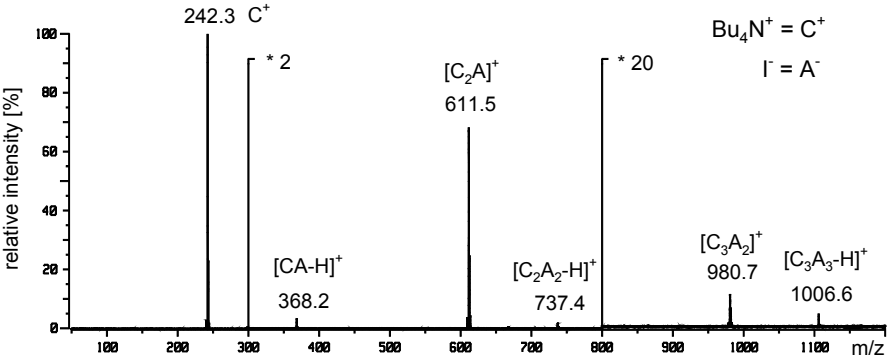


Fig. 8.18. FD mass spectrum of $[(n\text{-}C_4H_9)_4N]^+ I^-$. The intact ammonium ion is detected at *m/z* 242; additional signals are due to cluster ions. (For the EI spectrum cf. Chap. 6.10.4).

Example: Ionic liquids (ILs) are perfect representatives of ionic analytes. LIFDI (essentially FD, cf. Chap. 8.6) spectra of ILs such as *N*-hexylpyridinium tetrafluoroborate (Fig. 8.19) are dominated by the cation peak, C^+ here at *m/z* 164, that is accompanied by a strong first cluster ion signal, $[(C^+)_2+BF_4^-]^+$ at *m/z* 415, and by a weak second cluster ion signal. The corresponding boron isotopic patterns (B_1 and B_2) are clearly visible. Furthermore, the softness of the FD process is demonstrated by the fact that even the weakly bound cluster ions exhibit almost no fragmentation in metastable ion spectra, but require collisions to induce dissociation [116].

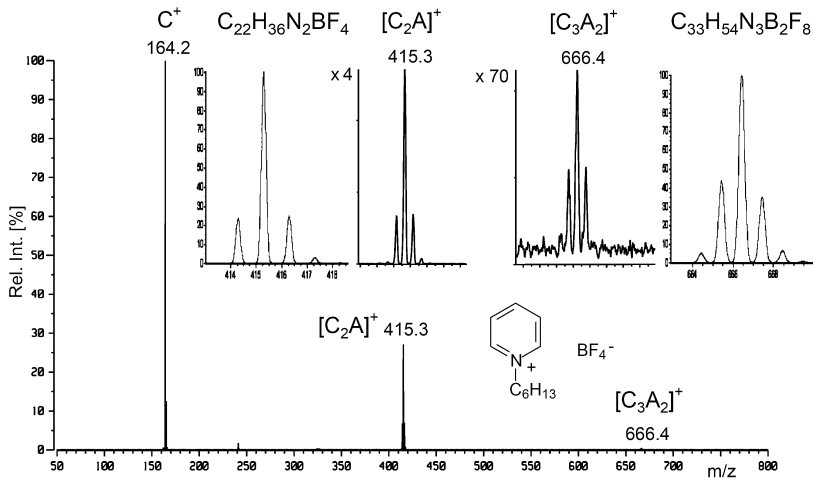


Fig. 8.19. LIFDI mass spectrum of *N*-hexylpyridinium tetrafluoroborate in methanol at a concentration of 0.1 µl ml^{-1} scanned over the *m/z* 50–800 range. The *insets* show the $[C_2A]^+$ and $[C_3A_2]^+$ cluster ions for comparison of the experimental and calculated isotopic patterns that are characteristic of one and two boron atoms, respectively. Reproduced from Ref. [116] with permission. © Elsevier Science Publishers, 2007.

8.5.5 Best Anode Temperature and Thermal Decomposition

The onset of desorption of an analyte depends not solely on its intrinsic properties, but also on the extraction voltage and the applied emitter heating current. FD spectra are typically acquired while the *emitter heating current* (EHC) is increased at a constant rate (1–8 mA min^{-1}). Alternatively, the heating can be regulated in a emission-controlled manner [58-60]. The desorption usually begins before the competing thermal decomposition of the analytes becomes severe. Nevertheless, increasing temperature of the emitter transfers additional thermal energy onto the desorbing ions, thereby effecting some fragmentation. The optimum temperature of the emitter where a sufficiently intense signal at the lowest level of fragmentation is obtained has been termed *best anode temperature* (BAT) [20,36].

Example: The FD spectrum of a ruthenium-carbonyl-porphyrin complex shows an isotopic pattern very close to the theoretical distribution (Chap. 3.2.8). The loss of the carbonyl ligand chiefly results from thermal decomposition. A spectrum accumulated close to BAT (scans 19–25, EHC 25–30 mA) is nearly devoid of CO loss, while a spectrum accumulated of scans 30–36 (35–40 mA) shows significant CO loss (Fig. 8.20). This is demonstrated by comparison of the total ion chromatogram (TIC) with the reconstructed ion chromatogram (RIC) of $M^{+\bullet}$ and $[M–CO]^{+\bullet}$ (Chap. 5.4). The FD spectrum of a lower-mass complex was essentially devoid of signals of CO loss because lower emitter currents were sufficient to effect desorption [117].

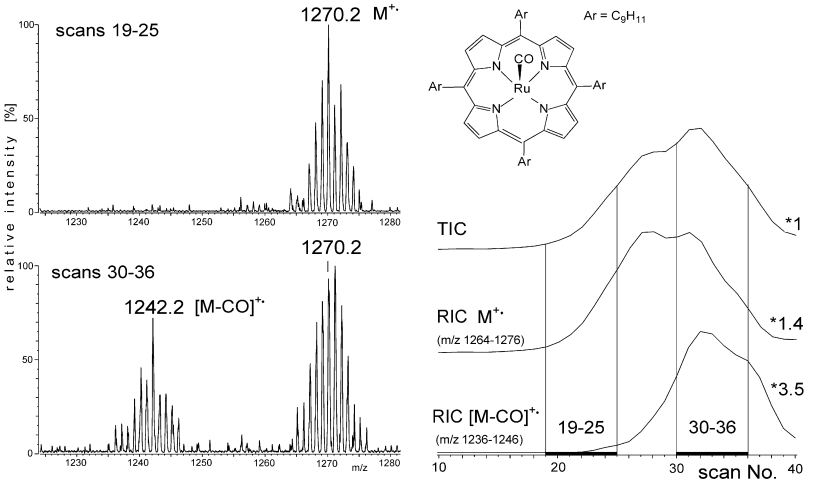


Fig. 8.20. Thermal CO loss during FD measurement of a ruthenium-carbonyl-porphyrin complex. Adapted from Ref. [117] by permission. © IM Publications, 1997.

8.5.6 FD-MS of Polymers

FD-MS is well suited for the analysis of low- to medium-polarity synthetic oligomers and polymers [27,28,72,76,77,79,118-120]. In advantageous cases, polymer molecules beyond molecular weights of 10,000 u can be measured [121]. Besides the mass analyzer used, limiting factors for the mass range are thermal decomposition of polymer and presence or absence of charge-stabilizing groups. Polystyrene, for example, with its combination of aromatic rings and low polarity is close to an ideal case for FD-MS. Heteroatoms are also useful because of their general capability to serve as proton- or metal ion-accepting sites. The worst case for MS is that of polyethylene (PE) [76,77,79]: the FD mass spectra of PE oligomers can be obtained up to *m/z* 3500; however, starting at around C_{40} hydrocarbons, field-induced and thermally induced dehydrogenation can no longer be suppressed and thermal decomposition of the hydrocarbon chains start playing a role above 2000 u.

Example: The FD mass spectrum of polyethylene of nominal average molecular weight 1000 u (PE 1000) was obtained by summing of all scans where desorption occurred, i.e., over the 4–45 mA EHC range (Fig. 8.21) [79]. The result represents the molecular weight distribution of the polymer. The according experimental average molecular weight can be calculated by means of Eq. 3.1 (Chap. 3.1.4). The fractionating effect of emitter heating and the significant changes in spectral appearance are demonstrated by the spectra in the lower part of the figure showing two selected portions of the total ion desorption.

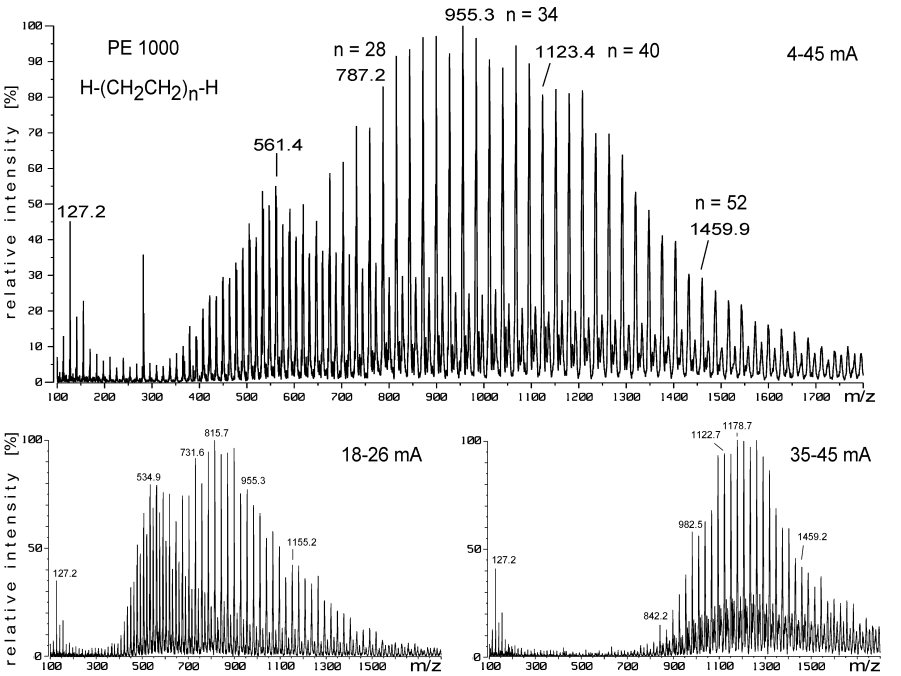


Fig. 8.21. FD spectra of PE 1000 (emitter potential 10 kV, EHC 4–45 mA). *Insets* show selected ranges corresponding to different EHCs. Adapted from Ref. [79] by permission. © IM Publications, 2000.

8.5.7 Types of Ions in FD-MS

At first sight, FD produces a disadvantageous variety of ions depending on the polarity of the analyte and on the presence or absence of impurities such as alkali metal ions that cause $[M+Na]^+$ and $[M+K]^+$ ions in addition to $M^{+\bullet}$ and $[M+H]^+$ ions. However, with some knowledge of the ions formed, the signals can be deconvoluted without difficulty (Table 8.2).

Note: One alkali adduct ion almost never occurs exclusively, i.e., $[M+H]^+$, $[M+Na]^+$ and $[M+K]^+$ (M+1, M+23 and M+39) are observed with varying relative intensities at 22 u and 16 u distance, respectively. This facilitates the recognition of those peaks and effectively allows for the assignment of the molecular weight.

Table 8.2. Ions formed by FD

Method	Analytes	Ions formed
FD	nonpolar	$M^{+\bullet}$, M^{2+}, occasionally $M^{3+\bullet}$
FD	medium polarity	$M^{+\bullet}$, M^{2+} and/or $[M+H]^+$, $[M+alkali]^+$, occasionally $[2M]^{+\bullet}$ and/or $[2M+H]^+$, $[2M+alkali]^+$, rarely $[M+2H]^{2+}$, $[M+2\ alkali]^{2+}$
FD	polar	$[M+H]^+$, $[M+alkali]^+$, often $[2M+H]^+$, $[2M+alkali]^+$, occasionally $[nM+H]^+$, $[nM+alkali]^+$, rarely $[M+2H]^{2+}$, $[M+2\ alkali]^{2+}$
FD	ionic[a]	C^+, $[C_n+A_{n-1}]^+$, rarely $[CA]^{+\bullet}$

[a] comprising cation C^+ and anion A^-

8.6 Liquid Injection Field Desorption Ionization

Numerous analytes could be good candidates for FD-MS, but undergo immediate decomposition by reacting with ambient air and/or water during conventional emitter loading. Emitter loading under inert conditions such as in a glove box does not really avoid the problem, because the emitter still needs to be mounted to the probe before insertion into the vacuum lock.

Liquid injection field desorption ionization (LIFDI) presents a major breakthrough for FD-MS of reactive analytes [30,122]. The risk of decomposition before starting the measurement is greatly reduced because the analyte, dissolved at about 0.1–0.2 mg ml^{-1}, can be handled under inert conditions. It is transported through a fused silica capillary by the sucking action of the ion source vacuum and then spreads out over the entire emitter driven by capillary forces and adsorption. Careful alignment of the sample transfer capillary with respect to the emitter axis is crucial for reliable wetting. The small volume of solvent transferred (ca. 40 nl) evaporates within seconds. As the sample is supplied from the "backside" to the emitter, there neither is a need to remove the capillary during the measurement, nor to change the adjustment of the emitter inside the ion source (Fig. 8.22). Instead, the emitter interrupts the contact to the capillary as it slightly bends toward the counter electrode as soon as the high voltage is switched on. Thus, LIFDI simplifies the delicate procedure of emitter loading and allows for its repeated loading without breaking the vacuum between successive measurements. This also avoids frequent focusing of the ion source [30,116,123]. Together with faster ramping of the EHC, up to 30 mA min^{-1} as enabled by lower sample load, this causes up to tenfold reduced measurement times in LIFDI as compared to conventional FD-MS. In any other respect, FD and LIFDI spectra are equivalent.

The majority of LIFDI applications either deals with sensitive compounds such as transition metal complexes [30,123,124] or belongs to the group of petroleomics applications [33,125-127]. Using an extremely low liquid flow rate even allows to continuously deliver sample solution to an emitter at high voltage, permiting continuous-flow (CF-)LIFDI experiments [34,128]. More recently, an automated LIFDI system has been introduced [129].

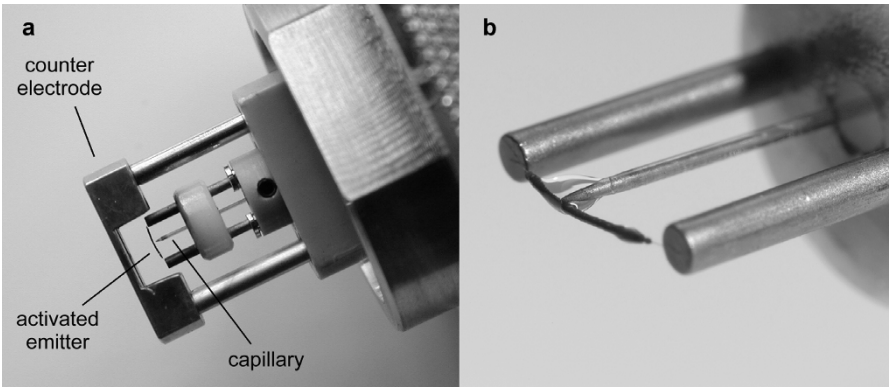


Fig. 8.22. (**a**) LIFDI probe tip with the fused silica capillary that delivers the sample to the "backside" of the activated emitter; here, the counter electrode is part of the probe, and (**b**) wetting of the emitter with solvent spreading out over the activated zone. The 13-µm tungsten wire connecting this section to the posts is barely visible. By courtesy of Linden CMS, Leeste, Germany.

Example: Transition metal complexes are readily analyzed by LIFDI-MS. A dichloro nickel carbene complex dissolved in acetonitrile not only forms the expected $[M–Cl]^+$ ion, *m/z* 375.3, but also a molecular ion, *m/z* 410.3, of somewhat lower abundance. The isotopic patterns of the signals are in very good agreement with the calculated isotopic distributions (Fig. 8.23). Peaks due to the free ligand and its oxide are also observed. The corresponding TIC is typical for FD experiments and clearly reveals the onset of desorption/ionization at medium EHC and the completion of the measurement when the sample is consumed [123].

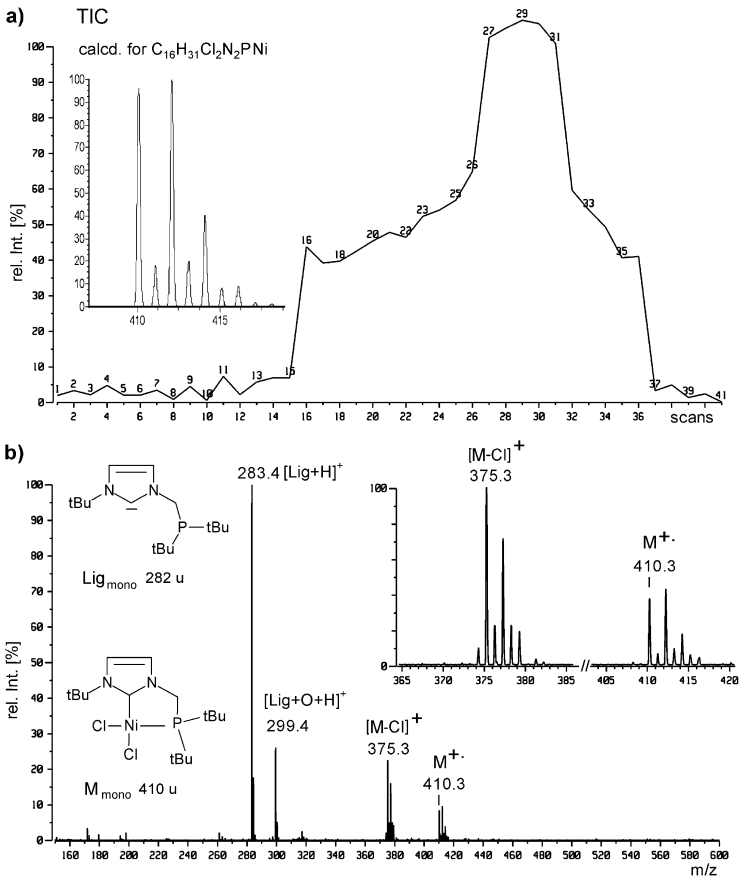


Fig. 8.23. (**a**) TIC and (**b**) LIFDI mass spectrum obtained from a nickel carbene complex in acetonitrile solution shows peaks due to excess free ligand $[Lig+H]^+$, *m/z* 283.4, and its oxide $[Lig+O+H]^+$, *m/z* 299.4, plus those corresponding to the complex. Note the intense $M^{+\bullet}$ ion at *m/z* 410.3 accompanying the $[M–Cl]^+$ ion at *m/z* 375.3. The isotopic pattern of the molecular ion is in good agreement with the calculated isotopic distribution (cf. inserts). Reproduced from Ref. [123] with permission. © Springer-Verlag, Heidelberg, 2006.

Example: Extremely complex crude oil fractions with each component at a very low concentration can be analyzed by continuous-flow LIFDI-FT-ICR-MS. CF-LIFDI delivers improved spectral quality as a stable FD-generated ion current can be sustained to allow for measurement times totaling up to 1 h. With the ionizing high voltage switched on, the sample solution (0.1 mg ml^{-1}) is delivered at 75 nl min^{-1} through a 10 µm i.d. capillary onto the emitter which is moderately heated using an EHC of 15 mA. The example shows the CF-LIFDI-FT-ICR spectrum of a refinery process stream sample (Fig. 8.24) [34].

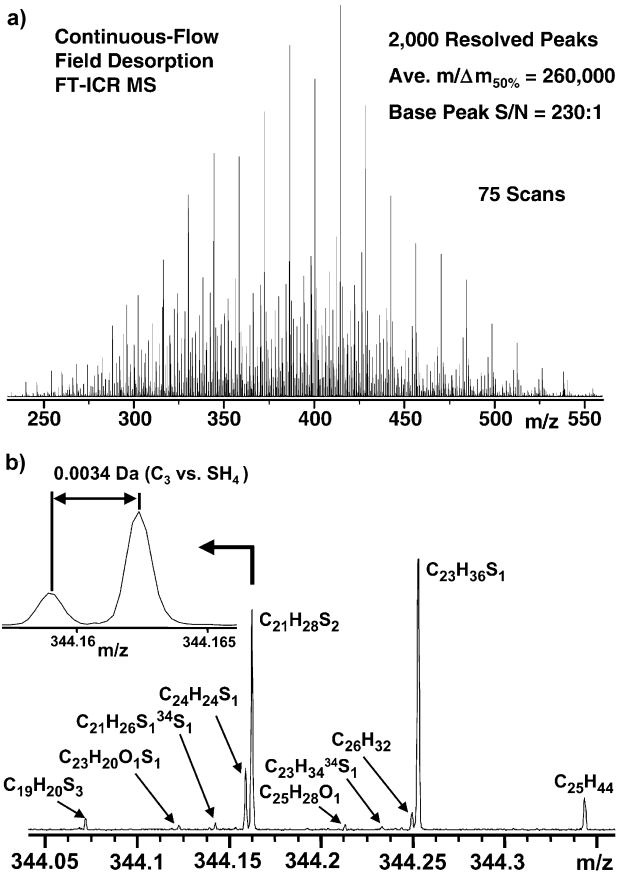


Fig. 8.24. CF-LIFDI-FT-ICR mass spectral analysis of a refinery process stream sample. (**a**) Spectrum as obtained from 75 single spectra accumulated during 1 h. (**b**) Extreme mass scale expansion at nominal *m/z* 344 from the broadband mass spectrum reveals the complexity of the sample. The resolution of the 3.4×10^{-3} u distant C_3 vs. SH_4 doublet can be observed at *m/z* 344.25 and separately in the inset at *m/z* 344.16. Adapted from Ref. [34] with permission. © John Wiley & Sons Ltd, 2004.

8.7 General Properties of FI-MS and FD-MS

8.7.1 Sensitivity of FI-MS and FD-MS

In FD mode, the sensitivity (Chap. 5.2.4) of actual magnetic sector instruments is about 4×10^{-11} C μg^{-1} for the $[M+H]^+$ ion of cholesterol, *m/z* 387, at $R = 1000$. This is 10^4 times less than specified for those instruments in EI mode and 10^3 times less than for CI mode.

In FI mode, the sensitivity of such instruments is about 4×10^{-9} A Pa^{-1} for the molecular ion of acetone, *m/z* 58, at $R = 1000$. This corresponds to an ion current of 4×10^{-13} A at a realized ion source pressure of 10^{-4} Pa.

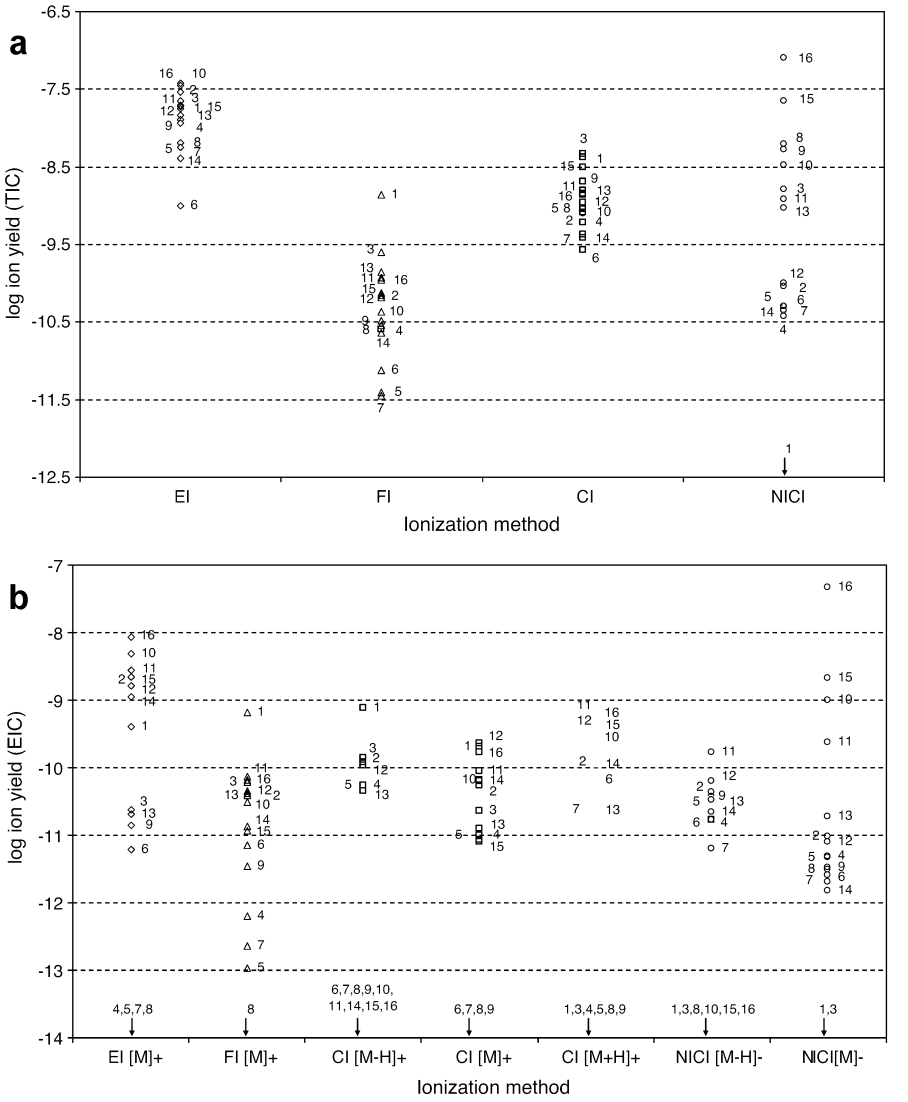


Fig. 8.25. Comparison of (**a**) total ion currents and (**b**) of molecular ion or quasimolecular currents of analytes typical for GC-MS as obtained by 70-eV EI, FI, positive-ion CI and negative-ion CI both using methane reagent gas. Reproduced from Ref. [88] with permission. © John Wiley & Sons, Ltd., 2009.

Although the ion currents produced by FI/FD ion sources are by orders of magnitude smaller than those from EI or CI ion sources, the detection limits are quite good. In general, about 0.1 ng of sample yield a sufficient signal-to-noise ratio (S/N $\geq$ 10) in FD-MS. This is because most of the ion current is collected in a single ionic species (including the isotopologs). Furthermore, the background of FI/FD ion sources is very clean, providing a good signal-to-background ratio.

Example: The comparison of 70-eV EI, CI, NICI and FI on the average reveals a 200-fold lower total ion current from FI as compared to EI. If only molecular ion peak intensities are compared, the FI spectra become much more appealing (Fig. 8.25) [88]. The concentration of the ion current on the molecular ions and the concomitant clarity of FI spectra are certainly the most attractive features of FI-MS.

8.7.2 Analytes and Practical Considerations for FI, FD, and LIFDI

Analytes for FI have to be evaporated prior to ionization, and thus any sample suitable for EI (Chap. 5.6) or CI (Chap. 7.6) yields low-fragmentation FI mass spectra. For FD and LIFDI, the analyte should be soluble to at least 0.01 mg ml^{-1} in some solvent. Concentrations of 0.1–2 mg ml^{-1} are ideal for FD and about 0.1–0.2 mg ml^{-1} should be used for LIFDI. Significantly higher sample loads result in overloading the emitter, and in turn cause its destruction due to electric discharge. In case of extremely low solubility, repeated application of solution to the emitter is also possible. For FD, fine suspensions or dispersions are acceptable, whereas these will block the capillary in LIFDI. Pure water tends not to wet the emitter surface – a problem that can be circumvented by addition of some methanol before transferring the solution to the emitter. Whatever the solvent for FD, it should be volatile enough to evaporate prior to introduction of the probe into the vacuum lock, while small volumes of dimethylformamide or dimethylsulfoxide, for example, can also be evaporated in the rough vacuum of the vacuum lock. The analyte may be neutral or ionic. However, anions are usually detected solely in an indirect manner, i.e., from corresponding cluster ions. Solutions containing metal salts, e.g., from buffers or excess of noncomplexed metals, are to be avoided, because sudden desorption of the metal ions at higher emitter current often leads to rupture of the emitter. A mass range up to 3000 u is easily covered by FD, and cases reaching up to 10,000 u have been reported.

8.7.3 Mass Analyzers for FI and FD

In FI and FD, ions of 10–12 keV kinetic energy are generated as a continuous ion current. Compared to EI or CI the ion current is weak and tends to fluctuate. The voltage drop across the whiskers (roughly proportional to the whisker length) causes an energy spread of the ions which results in poor resolution with single-

focusing magnetic sector instruments [44]. Therefore, double-focusing magnetic sector instruments were the standard in FD-MS for decades. Although linear quadrupoles have been adapted to FI/FD ion sources rather successfully [130,131], they never became widespread with FI/FD. More recently, oaTOF and FT-ICR analyzers have been equipped with FD/LIFDI sources with great success [125,128].

References

1. Müller, E.W. Feldemission. *Ergebnisse der exakten Naturwissenschaften* **1953,** *27*, 290-360.
2. Gomer, R.; Inghram, M.G. Applications of Field Ionization to Mass Spectrometry. *J. Am. Chem. Soc.* **1955,** *77*, 500.
3. Inghram, M.G.; Gomer, R. Mass-Spectrometric Analysis of Ions from the Field Microscope. *J. Chem. Phys.* **1954,** *22*, 1279-1280.
4. Inghram, M.G.; Gomer, R. Mass-Spectrometric Investigation of the Field Emission of Positive Ions. *Z. Naturforsch.* **1955,** *10A*, 863-872.
5. Beckey, H.D. Mass Spectrographic Investigations, Using a Field Emission Ion Source. *Z. Naturforsch.* **1959,** *14A*, 712-721.
6. Beckey, H.D. Field-Ionization Mass Spectra of Organic Molecules. Normal C_1 to C_9 Paraffins. *Z. Naturforsch.* **1962,** *17A*, 1103-1111.
7. Beckey, H.D.; Wagner, G. Analytical Use of an Ion Field Mass Spectrometer. *Fresenius Z. Anal. Chem.* **1963,** *197*, 58-80.
8. Beckey, H.D. Mass Spectrometric Analysis with a New Source for the Production of Ion Fields at Thin Wires or Metal Edges. *Fresenius Z. Anal. Chem.* **1963,** *197*, 80-90.
9. Beckey, H.D. Molecule Dissociation by High Electric Fields. *Z. Naturforsch.* **1964,** *19A*, 71-83.
10. Beckey, H.D.; Wagner, G. Field Ionization Mass Spectra of Organic Molecules. II. Amines. *Z. Naturforsch.* **1965,** *20A*, 169-175.
11. Beckey, H.D.; Schulze, P. Field Ionization Mass Spectra of Organic Molecules. III. *N*-Paraffins Up to C_{16} and Branched Paraffins. *Z. Naturforsch.* **1965,** *20A*, 1329-1335.
12. Beckey, H.D. Analysis of Solid Organic Natural Products by Field Ionization Mass Spectrometry. *Fresenius Z. Anal. Chem.* **1965,** *207*, 99-104.
13. Beckey, H.D. Comparison of Field Ionization and Chemical Ionization Mass Spectra of Decane Isomers. *J. Am. Chem. Soc.* **1966,** *88*, 5333-5335.
14. Beckey, H.D. Field Desorption Mass Spectrometry: A Technique for the Study of Thermally Unstable Substances of Low Volatility. *Int. J. Mass Spectrom. Ion Phys.* **1969,** *2*, 500-503.
15. Beckey, H.D.; Heindrichs, A.; Winkler, H.U. New Field Desorption Techniques. *Int. J. Mass Spectrom. Ion Phys.* **1970,** *3*, A9-A11.
16. Beckey, H.D. *Field-Ionization Mass Spectrometry*; Pergamon: Elmsford, 1971.
17. Sammons, M.C.; Bursey, M.M.; White, C.K. Field Desorption Mass Spectrometry of Onium Salts. *Anal. Chem.* **1975,** *47*, 1165-1166.
18. Beckey, H.D.; Schulten, H.-R. Field Desorption Mass Spectrometry. *Angew. Chem.* **1975,** *87*, 425-438.
19. Lehmann, W.D.; Schulten, H.-R. Physikalische Methoden in der Chemie: Massenspektrometrie II CI-, FI- und FD-MS. *Chem. Unserer Zeit.* **1976,** *10*, 163-174.
20. Beckey, H.D. *Principles of Field Desorption and Field Ionization Mass Spectrometry;* Pergamon Press: Oxford, 1977.
21. Larsen, E.; Egsgaard, H.; Holmen, H. Field Desorption Mass Spectrometry of 1-Methylpyridinium Salts. *Org. Mass Spectrom.* **1978,** *13*, 417-424.
22. Wood, G.W. Field Desorption Mass Spectrometry: Applications. *Mass Spectrom. Rev.* **1982,** *1*, 63-102.
23. Schulten, H.-R. Ion Formation from Organic Solids: Analytical Applications of

Field Desorption Mass Spectrometry, 25 ed.; Benninghoven, A. (ed.); Springer-Verlag: Heidelberg, 1983; pp. 14-29.
24. Lattimer, R.P.; Schulten, H.-R. Field Ionization and Field Desorption Mass Spectrometry: Past, Present, and Future. *Anal. Chem.* **1989,** *61*, 1201A-1215A.
25. Olson, K.L.; Rinehart, K.L. Field Desorption, Field Ionization, and Chemical Ionization Mass Spectrometry. *Methods Carbohyd. Chem.* **1993,** *9*, 143-164.
26. Del Rio, J.C.; Philp, R.P. Field Ionization Mass Spectrometric Study of High Molecular Weight Hydrocarbons in a Crude Oil and a Solid Bitumen. *Org. Geochem.* **1999,** *30*, 279-286.
27. Guo, X.; Fokkens, R.H.; Peeters, H.J.W.; Nibbering, N.M.M.; de Koster, C.G. Multiple Cationization of Polyethylene Glycols in Field Desorption Mass Spectrometry: A New Approach to Extend the Mass Scale on Sector Mass Spectrometers. *Rapid Commun. Mass Spectrom.* **1999,** *13*, 2223-2226.
28. Lattimer, R.P. Field Ionization (FI-MS) and Field Desorption (FD-MS), in *Mass Spectrometry of Polymers*; Montaudo, G.; Lattimer, R.P. (eds.); CRC Press: Boca Raton, 2001; pp. 237-268.
29. Linden, H. B. *Quick Soft Analysis of Sensitive Samples Under Inert Conditions by In-Source Liquid Injection FD*; ASMS: Orlando, 2002; pp. MPL 373.
30. Linden, H.B. Liquid Injection Field Desorption Ionization: a New Tool for Soft Ionization of Samples Including Air-Sensitive Catalysts and Non-Polar Hydrocarbons. *Eur. J. Mass Spectrom.* **2004,** *10*, 459-468.
31. Hsu, C.S.; Green, M. Fragment-Free Accurate Mass Measurement of Complex Mixture Components by Gas Chromatography/Field Ionization-Orthogonal Acceleration Time-of-Flight Mass Spectrometry: an Unprecedented Capability for Mixture Analysis. *Rapid Commun. Mass Spectrom.* **2001,** *15*, 236-239.
32. Qian, K.; Dechert, G.J. Recent Advances in Petroleum Characterization by GC Field Ionization Time-of-Flight High-Resolution Mass Spectrometry. *Anal. Chem.* **2002,** *74*, 3977-3983.
33. Schaub, T.M.; Hendrickson, C.L.; Qian, K.; Quinn, J.P.; Marshall, A.G. High-Resolution Field Desorption/Ionization Fourier Transform Ion Cyclotron Resonance Mass Analysis of Nonpolar Molecules. *Anal. Chem.* **2003,** *75*, 2172-2176.
34. Schaub, T.M.; Linden, H.B.; Hendrickson, C.L.; Marshall, A.G. Continuous-Flow Sample Introduction for Field Desorption/Ionization Mass Spectrometry. *Rapid Commun. Mass Spectrom.* **2004,** *18*, 1641-1644.
35. Gomer, R. Field Emission, Field Ionization, and Field Desorption. *Surf. Sci.* **1994,** *299/300*, 129-152.
36. Prókai, L. *Field Desorption Mass Spectrometry;* Marcel Dekker: New York, 1990.
37. Todd, J.F.J. Recommendations for Nomenclature and Symbolism for Mass Spectroscopy Including an Appendix of Terms Used in Vacuum Technology. *Int. J. Mass Spectrom. Ion. Proc.* **1995,** *142*, 211-240.
38. Ligon, W.V., Jr. Molecular Analysis by Mass Spectrometry. *Science* **1979,** *205*, 151-159.
39. Miyamoto, K.; Fujimaki, S.; Ueda, Y. Development of a New Electron Ionization/Field Ionization Ion Source for Gas Chromatography/Time-of-Flight Mass Spectrometry. *Rapid Commun. Mass Spectrom.* **2009,** *23*, 3350-3354.
40. Schröder, E. *Massenspektrometrie – Begriffe und Definitionen;* Springer-Verlag: Heidelberg, 1991.
41. Derrick, P.J.; Robertson, A.J.B. Field Ionization Mass Spectrometry With Conditioned Razor Blades. *Int. J. Mass Spectrom. Ion Phys.* **1973,** *10*, 315-321.
42. Giessmann, U.; Heinen, H.J.; Röllgen, F.W. Field Desorption of Nonelectrolytes Using Simply Activated Wire Emitters. *Org. Mass Spectrom.* **1979,** *14*, 177-179.
43. Heinen, H.J.; Giessmann, U.; Röllgen, F.W. Field Desorption of Electrolytic Solutions Using Untreated Wire Emitters. *Org. Mass Spectrom.* **1977,** *12*, 710-715.
44. Beckey, H.D.; Krone, H.; Röllgen, F.W. Comparison of Tips, Thin Wires, and Sharp Metal Edges as Emitters for Field Ionization Mass Spectrometry. *J. Sci. Instrum.* **1968,** *1*, 118-120.
45. Beckey, H.D.; Hilt, E.; Schulten, H.-R. High Temperature Activation of Emitters for Field Ionization and Field Desorption Spectrometry. *J. Phys. E:Sci. Instrum.* **1973,** *6*, 1043-1044.

46. Linden, H.B.; Hilt, E.; Beckey, H.D. High-Rate Growth of Dendrites on Thin Wire Anodes for Field Desorption Mass Spectrometry. *J. Phys. E:Sci. Instrum.* **1978,** *11*, 1033-1036.
47. Rabrenovic, M.; Ast, T.; Kramer, V. Alternative Organic Substances for Generation of Carbon Emitters for Field Desorption Mass Spectrometry. *Int. J. Mass Spectrom. Ion Phys.* **1981,** *37*, 297-307.
48. Okuyama, F.; Hilt, E.; Röllgen, F.W.; Beckey, H.D. Enhancement of Field Ionization Efficiency of 10-µm Tungsten Filaments Caused by the Nucleation of Carbide Particles. *J. Vac. Sci. Technol.* **1977,** *14*, 1033-1035.
49. Linden, H.B.; Beckey, H.D.; Okuyama, F. On the Mechanism of Cathodic Growth of Tungsten Needles by Decomposition of Hexacarbonyltungsten Under High-Field Conditions. *Appl. Phys.* **1980,** *22*, 83-87.
50. Bursey, M.M.; Rechsteiner, C.E.; Sammons, M.C.; Hinton, D.M.; Colpitts, T.; Tvaronas, K.M. Electrochemically Deposited Cobalt Emitters for Field Ionization and Field Desorption Mass Spectrometry. *J. Phys. E: Sci. Instrum.* **1976,** *9*, 145-147.
51. Matsuo, T.; Matsuda, H.; Katakuse, I. Silicon Emitter for Field Desorption Mass Spectrometry. *Anal. Chem.* **1979,** *51*, 69-72.
52. Okuyama, F.; Shen, G.-H. Ion Formation Mechanisms in Field-Desorption Mass Spectrometry of Semirefractory Metal Elements. *Int. J. Mass Spectrom. Ion Phys.* **1981,** *39*, 327-337.
53. Rechsteiner, C.E., Jr.; Mathis, D.E.; Bursey, M.M.; Buck, R.P. A Novel Inexpensive Device for the Electrochemical Generation of Metallic Emitters for Field Desorption. *Biomed. Mass Spectrom.* **1977,** *4*, 52-54.
54. Goldenfeld, I.V.; Veith, H.J. A New Emitter for Field-Desorption Mass Spectrometry With Silver-Electroplated Microneedles. *Int. J. Mass Spectrom. Ion Phys.* **1981,** *40*, 361-363.
55. Kosevich, M.V.; Shelkovsky, V.S. A New Type of Graphite Emitter for Field Ionization/Field Desorption Mass Spectrometry. *Rapid Commun. Mass Spectrom.* **1993,** *7*, 805-811.
56. Kümmler, D.; Schulten, H.-R. Correlation Between Emitter Heating Current and Emitter Temperature in Field Desorption Mass Spectrometry. *Org. Mass Spectrom.* **1975,** *10*, 813-816.
57. Winkler, H.U.; Linden, B. On the Determination of Desorption Temperatures in Field Desorption Mass Spectrometry. *Org. Mass Spectrom.* **1976,** *11*, 327-329.
58. Schulten, H.-R.; Lehmann, W.D. High-Resolution Field Desorption Mass Spectrometry. Part VII. Explosives and Explosive Mixtures. *Anal. Chim. Acta* **1977,** *93*, 19-31.
59. Schulten, H.-R.; Nibbering, N.M.M. An Emission-Controlled Field Desorption and Electron Impact Spectrometry Study of Some *N*-Substituted Propane and Butane Sultams. *Biomed. Mass Spectrom.* **1977,** *4*, 55-61.
60. Schulten, H.-R. Recent Advances in Field Desorption Mass Spectrometry. *Adv. Mass Spectrom.* **1978,** *7A*, 83-97.
61. Severin, D. Molecular Ion Mass Spectrometry for the Analysis of High- and Nonboiling Hydrocarbon Mixtures. *Erdöl und Kohle - Erdgas - Petrochemie vereinigt mit Brennstoff-Chemie* **1976,** *29*, 13-18.
62. Mead, L. Field Ionization Mass Spectrometry of Heavy Petroleum Fractions. Waxes. *Anal. Chem.* **1968,** *40*, 743-747.
63. Scheppele, S.E.; Hsu, C.S.; Marriott, T.D.; Benson, P.A.; Detwiler, K.N.; Perreira, N.B. Field-Ionization Relative Sensitivities for the Analysis of Saturated Hydrocarbons From Fossil-Energy-Related Materials. *Int. J. Mass Spectrom. Ion Phys.* **1978,** *28*, 335-346.
64. Gross, J.H. Molecular Ions of Ionic Liquids in the Gas Phase. *J. Am. Chem. Soc. Mass Spectrom.* **2008,** *19*, 1347-1352.
65. Röllgen, F.W.; Beckey, H.D. Surface Reactions Induced by Field Ionization of Organic Molecules. *Surf. Sci.* **1970,** *23*, 69-87.
66. Schulten, H.-R.; Beckey, H.D. Criteria for Distinguishing Between $M^{+\cdot}$ and $[M+H]^+$ Ions in Field Desorption Mass Spectra. *Org. Mass Spectrom.* **1974,** *9*, 1154-1155.
67. Goldenfeld, I.V.; Korostyshevsky, I.Z.; Nazarenko, V.A. Multiple Field Ionization. *Int. J. Mass Spectrom. Ion Phys.* **1973,** *11*, 9-16.
68. Helal, A.I.; Zahran, N.F. Field Ionization of Indene on Tungsten. *Int. J. Mass Spectrom. Ion Proc.* **1988,** *85*, 187-193.
69. Röllgen, F.W.; Heinen, H.J. Formation of Multiply Charged Ions in a Field Ioni-

zation Mass Spectrometer. *Int. J. Mass Spectrom. Ion Phys.* **1975,** *17*, 92-95.
70. Röllgen, F.W.; Heinen, H.J. Energetics of Formation of Doubly Charged Benzene Ions by Field Ionization. *Z. Naturforsch.* **1975,** *30A*, 918-920.
71. Röllgen, F.W.; Heinen, H.J.; Levsen, K. Doubly-Charged Fragment Ions in the Field Ionization Mass Spectra of Alkylbenzenes. *Org. Mass Spectrom.* **1976,** *11*, 780-782.
72. Neumann, G.M.; Cullis, P.G.; Derrick, P.J. Mass Spectrometry of Polymers: Polypropylene Glycol. *Z. Naturforsch.* **1980,** *35A*, 1090-1097.
73. McCrae, C.E.; Derrick, P.J. The Role of the Field in Field Desorption Fragmentation of Polyethylene Glycol. *Org. Mass Spectrom.* **1983,** *18*, 321-323.
74. Heine, C.E.; Geddes, M.M. Field-Dependent $[M-2H]^{+\cdot}$ Formation in the Field Desorption Mass Spectrometric Analysis of Hydrocarbon Samples. *Org. Mass Spectrom.* **1994,** *29*, 277-284.
75. Klesper, G.; Röllgen, F.W. Field-Induced Ion Chemistry Leading to the Formation of $[M-2_nH]^{+\cdot}$ and $[2M-2_mH]^{+\cdot}$ Ions in Field Desorption Mass Spectrometry of Saturated Hydrocarbons. *J. Mass Spectrom.* **1996,** *31*, 383-388.
76. Evans, W.J.; DeCoster, D.M.; Greaves, J. Field Desorption Mass Spectrometry Studies of the Samarium-Catalyzed Polymerization of Ethylene Under Hydrogen. *Macromolecules* **1995,** *28*, 7929-7936.
77. Evans, W.J.; DeCoster, D.M.; Greaves, J. Evaluation of Field Desorption Mass Spectrometry for the Analysis of Polyethylene. *J. Am. Soc. Mass Spectrom.* **1996,** *7*, 1070-1074.
78. Gross, J.H.; Vékey, K.; Dallos, A. Field Desorption Mass Spectrometry of Large Multiply Branched Saturated Hydrocarbons. *J. Mass Spectrom.* **2001,** *36*, 522-528.
79. Gross, J.H.; Weidner, S.M. Influence of Electric Field Strength and Emitter Temperature on Dehydrogenation and C–C Cleavage in Field Desorption Mass Spectrometry of Polyethylene Oligomers. *Eur. J. Mass Spectrom.* **2000,** *6*, 11-17.
80. Chait, E.M.; Shannon, T.W.; Perry, W.O.; Van Lear, G.E.; McLafferty, F.W. High-Resolution Field-Ionization Mass Spectrometry. *Int. J. Mass Spectrom. Ion Phys.* **1969,** *2*, 141-155.
81. Forehand, J.B.; Kuhn, W.F. High Resolution Field Ionization Mass Spectrometry of the Condensable Phase of Cigarette Smoke. *Anal. Chem.* **1970,** *42*, 1839-1841.
82. Schulten, H.R.; Beckey, H.D.; Meuzelaar, H.L.C.; Boerboom, A.J.H. High-Resolution Field Ionization Mass Spectrometry of Bacterial Pyrolysis Products. *Anal. Chem.* **1973,** *45*, 191-195.
83. Schulten, H.R.; Marzec, A.; Simmleit, N.; Dyla, P.; Mueller, R. Thermal Behavior and Degradation Products of Differently Ranked Coals Studied by Thermogravimetry and High-Resolution Field-Ionization Mass Spectrometry. *Energy & Fuels* **1989,** *3*, 481-487.
84. Games, D.E.; Jackson, A.H.; Millington, D.S. Applications of Field Ionization Mass Spectrometry in the Analysis of Organic Mixtures. *Tetrahedron Lett.* **1973,** 3063-3066.
85. Damico, J.N.; Barron, R.P. Application of Field Ionization to Gas-Liquid Chromatography-Mass Spectrometry (GLC-MS) Studies. *Anal. Chem.* **1971,** *43*, 17-21.
86. Briker, Y.; Ring, Z.; Iacchelli, A.; McLean, N.; Rahimi, P.M.; Fairbridge, C.; Malhotra, R.; Coggiola, M.A.; Young, S.E. Diesel Fuel Analysis by GC-FIMS: Aromatics, *N*-Paraffins, and Isoparaffins. *Energy & Fuels* **2001,** *15*, 23-37.
87. Qian, K.; Dechert, G.J.; Edwards, K.E. Deducing Molecular Compositions of Petroleum Products Using GC-Field Ionization High Resolution Time of Flight Mass Spectrometry. *Int. J. Mass Spectrom.* **2007,** *265*, 230-236.
88. Hejazi, L.; Ebrahimi, D.; Hibbert, D.B.; Guilhaus, M. Compatibility of Electron Ionization and Soft Ionization Methods in Gas Chromatography/Orthogonal Time-of-Flight Mass Spectrometry. *Rapid Commun. Mass Spectrom.* **2009,** *23*, 2181-2189.
89. Kane-Maguire, L.A.P.; Kanitz, R.; Sheil, M.M. Comparison of Electrospray Mass Spectrometry With Other Soft Ionization Techniques for the Characterization of Cationic Π-Hydrocarbon Organometallic Complexes. *J. Organomet. Chem.* **1995,** *486*, 243-248.

90. Rogers, D.E.; Derrick, P.J. Mechanisms of Ion Formation in Field Desorption of Oligosaccharides. *Org. Mass Spectrom.* **1984,** *19*, 490-495.
91. Derrick, P.J.; Nguyen, T.-T.; Rogers, D.E.C. Concerning the Mechanism of Ion Formation in Field Desorption. *Org. Mass Spectrom.* **1985,** *11*, 690.
92. Veith, H.J.; Röllgen, F.W. On the Ionization of Oligosaccharides. *Org. Mass Spectrom.* **1985,** *11*, 689-690.
93. Schulten, H.-R.; Beckey, H.D. Field Desorption Mass Spectrometry With High-Temperature Activated Emitters. *Org. Mass Spectrom.* **1972,** *6*, 885-895.
94. Davis, S.C.; Neumann, G.M.; Derrick, P.J. Field Desorption Mass Spectrometry With Suppression of the High Field. *Anal. Chem.* **1987,** *59*, 1360-1362.
95. Veith, H.J. Alkali Ion Addition in FD Mass Spectrometry. Cationization and Protonation-Ionization Methods in the Application of Nonactivated Emitters. *Tetrahedron* **1977,** *33*, 2825-2828.
96. Giessmann, U.; Röllgen, F.W. Electrodynamic Effects in Field Desorption Mass Spectrometry. *Int. J. Mass Spectrom. Ion Phys.* **1981,** *38*, 267-279.
97. Röllgen, F. W. *Ion Formation From Organic Solids: Principles of Field Desorption Mass Spectrometry*; Benninghoven, A. (ed.); Springer-Verlag: Heidelberg, 1983; pp. 2-13.
98. Wong, S.S.; Giessmann, U.; Karas, M.; Röllgen, F.W. Field Desorption of Sucrose Studied by Combined Optical Microscopy and Mass Spectrometry. *Int. J. Mass Spectrom. Ion Proc.* **1984,** *56*, 139-150.
99. Derrick, P.J. Mass Spectroscopy at High Mass. *Fresenius Z. Anal. Chem.* **1986,** *324*, 486-491.
100. Davis, S.C.; Natoli, V.; Neumann, G.M.; Derrick, P.J. A Model of Ion Evaporation Tested Through Field Desorption Experiments on Glucose Mixed With Alkali Metal Salts. *Int. J. Mass Spectrom. Ion Proc.* **1987,** *78*, 17-35.
101. Reichert, H. Monodesoxygenierte Glucosid-Synthese und Kinetikstudien der enzymatischen Spaltung. *Dissertation*, Organisch-Chemisches Institut, Universität Heidelberg, 1997.
102. Veith, H.J. Field Desorption Mass Spectrometry of Quaternary Ammonium Salts: Cluster Ion Formation. *Org. Mass Spectrom.* **1976,** *11*, 629-633.
103. Veith, H.J. Mass Spectrometry of Ammonium and Iminium Salts. *Mass Spectrom. Rev.* **1983,** *2*, 419-446.
104. Veith, H.J. Collision-Induced Fragmentations of Field-Desorbed Cations. 4. Collision-Induced Fragmentations of Alkylideneammonium Ions. *Angew. Chem.* **1980,** *92*, 548-550.
105. Fischer, M.; Veith, H.J. Collision-Induced Fragmentations of Field-Desorbed Cations. 5. Reactions of 2- and 3-Phenyl Substituted Alkylalkylidene Iminium Ions in the Gas Phase. *Helv. Chim. Acta* **1981,** *64*, 1083-1091.
106. Miermans, C.J.H.; Fokkens, R.H.; Nibbering, N.M.M. A Study of the Applicability of Various Ionization Methods and Tandem Mass Spectrometry in the Analyses of Triphenyltin Compounds. *Anal. Chim. Acta* **1997,** *340*, 5-20.
107. Röllgen, F.W.; Giessmann, U.; Heinen, H.J. Ion Formation in Field Desorption of Salts. *Z. Naturforsch.* **1976,** *31A*, 1729-1730.
108. Röllgen, F.W.; Ott, K.H. On the Formation of Cluster Ions and Molecular Ions in Field Desorption of Salts. *Int. J. Mass Spectrom. Ion Phys.* **1980,** *32*, 363-367.
109. Lehmann, W.D.; Schulten, H.-R. Determination of Alkali Elements by Field Desorption Mass Spectrometry. *Anal. Chem.* **1977,** *49*, 1744-1746.
110. Schulten, H.-R.; Bohl, B.; Bahr, U.; Mueller, R.; Palavinskas, R. Qualitative and Quantitative Trace-Metal Analysis in Physiological Fluids of Multiple Sclerosis Patients by Field Desorption Mass Spectrometer. *Int. J. Mass Spectrom. Ion Phys.* **1981,** *38*, 281-295.
111. Keough, T.; DeStefano, A.J. Acid-Enhanced Field Desorption Mass Spectrometry of Zwitterions. *Anal. Chem.* **1981,** *53*, 25-29.
112. Ott, K.H.; Röllgen, F.W.; Zwinselmann, J.J.; Fokkens, R.H.; Nibbering, N.M.M. Negative Ion Field Desorption Mass Spectra of Some Inorganic and Organic Compounds. *Org. Mass Spectrom.* **1980,** *15*, 419-422.
113. Daehling, P.; Röllgen, F.W.; Zwinselmann, J.J.; Fokkens, R.H.; Nibbering, N.M.M. Negative Ion Field Desorption Mass Spectrometry of Anionic Surfactants. *Fresenius Z. Anal. Chem.* **1982,** *312*, 335-337.
114. Mes, G.F.; Van der Greef, J.; Nibbering, N.M.M.; Ott, K.H.; Röllgen, F.W. The

Formation of Negative Ions by Field Ionization. *Int. J. Mass Spectrom. Ion Phys.* **1980,** *34*, 295-301.
115. Dähling, P.; Ott, K.H.; Röllgen, F.W.; Zwinselmann, J.J.; Fokkens, R.H.; Nibbering, N.M.M. Ionization by Proton Abstraction in Negative Ion Field Desorption Mass Spectrometry. *Int. J. Mass Spectrom. Ion Phys.* **1983,** *46*, 301-304.
116. Gross, J.H. Liquid Injection Field Desorption/Ionization Mass Spectrometry of Ionic Liquids. *J. Am. Chem. Soc. Mass Spectrom.* **2007,** *18*, 2254-2262.
117. Frauenkron, M.; Berkessel, A.; Gross, J.H. Analysis of Ruthenium Carbonyl-Porphyrin Complexes: a Comparison of Matrix-Assisted Laser Desorption/Ionization Time-of-Flight, Fast-Atom Bombardment and Field Desorption Mass Spectrometry. *Eur. Mass. Spectrom.* **1997,** *3*, 427-438.
118. Lattimer, R.P.; Harmon, D.J.; Welch, K.R. Characterization of Low Molecular Weight Polymers by Liquid Chromatography and Field Desorption Mass Spectroscopy. *Anal. Chem.* **1979,** *51*, 293-296.
119. Craig, A.C.; Cullis, P.G.; Derrick, P.J. Field Desorption of Polymers: Polybutadiene. *Int. J. Mass Spectrom. Ion Phys.* **1981,** *38*, 297-304.
120. Lattimer, R.P.; Schulten, H.-R. Field Desorption of Hydrocarbon Polymers. *Int. J. Mass Spectrom. Ion Phys.* **1983,** *52*, 105-116.
121. Matsuo, T.; Matsuda, H.; Katakuse, I. Use of Field Desorption Mass Spectra of Polystyrene and Polypropylene Glycol as Mass References up to Mass 10,000. *Anal. Chem.* **1979,** *51*, 1329-1331.
122. Linden, H. B. Germany DE 99-19963317, **2001,** 4 pp.
123. Gross, J.H.; Nieth, N.; Linden, H.B.; Blumbach, U.; Richter, F.J.; Tauchert, M.E.; Tompers, R.; Hofmann, P. Liquid Injection Field Desorption/Ionization of Reactive Transition Metal Complexes. *Anal. Bioanal. Chem.* **2006,** *386*, 52-58.
124. Monillas, W.H.; Yap, G.P.H.; Theopold, K.H. A Tale of Two Isomers: A Stable Phenyl Hydride and a High-Spin (S = 3) Benzene Complex of Chromium. *Angew. Chem., Intl. Ed.* **2007,** *46*, 6692-6694.
125. Schaub, T.M.; Hendrickson, C.L.; Quinn, J.P.; Rodgers, R.P.; Marshall, A.G. Instrumentation and Method for Ultrahigh Resolution Field Desorption Ionization Fourier Transform Ion Cyclotron Resonance Mass Spectrometry of Nonpolar Species. *Anal. Chem.* **2005,** *77*, 1317-1324.
126. Fu, J.; Klein, G.C.; Smith, D.F.; Kim, S.; Rodgers, R.P.; Hendrickson, C.L.; Marshall, A.G. Comprehensive Compositional Analysis of Hydrotreated and Untreated Nitrogen-Concentrated Fractions From Syncrude Oil by Electron Ionization, Field Desorption Ionization, and Electrospray Ionization Ultrahigh-Resolution FT-ICR Mass Spectrometry. *Energy & Fuels* **2006,** *20*, 1235-1241.
127. Stanford, L.A.; Rodgers, R.P.; Marshall, A.G.; Czarnecki, J.; Wu, X.A. Compositional Characterization of Bitumen/Water Emulsion Films by Negative- and Positive-Ion Electrospray Ionization and Field Desorption/Ionization Fourier Transform Ion Cyclotron Resonance Mass Spectrometry. *Energy & Fuels* **2007,** *21*, 963-972.
128. Schaub, T.M.; Rodgers, R.P.; Marshall, A.G.; Qian, K.; Green, L.A.; Olmstead, W.N. Speciation of Aromatic Compounds in Petroleum Refinery Streams by Continuous Flow Field Desorption Ionization FT-ICR Mass Spectrometry. *Energy & Fuels* **2005,** *19*, 1566-1573.
129. Smith, D.F.; Schaub, T.M.; Rodgers, R.P.; Hendrickson, C.L.; Marshall, A.G. Automated Liquid Injection Field Desorption/Ionization for Fourier Transform Ion Cyclotron Resonance Mass Spectrometry. *Anal. Chem.* **2008,** *80*, 7379-7382.
130. Heinen, H.J.; Hötzel, C.; Beckey, H.D. Combination of a Field Desorption Ion Source With a Quadrupole Mass Analyzer. *Int. J. Mass Spectrom. Ion Phys.* **1974,** *13*, 55-62.
131. Gierlich, H.H.; Heinen, H.J.; Beckey, H.D. The Application of Quadrupole Mass Filters in Field Desorption Mass Spectrometry. *Biomed. Mass Spectrom.* **1975,** *2*, 31-35.

9 Tandem Mass Spectrometry

Learning Objectives

- Tandem MS – concepts and terminology
- Modes of operation
- Different instrumental platforms
- Methods of ion activation to induce dissociation
- Applications to analytical problems
- A versatile tool for gas phase ion chemistry

Electron ionization mass spectra show a wealth of fragment ion peaks allowing to retrieve structural information, often though at the expense of abundance of the molecular ion. For decades, EI has served as the one and only ionization method of organic mass spectrometry. With the advent of soft ionization methods such as CI or FD we just dealt with, spectra exhibiting minor or even no fragment ion signals could be generated. While highly advantageous at first sight, in the long run, the lack of structural information presents a severe drawback for analytical applications. The development of numerous new techniques to store, manipulate, activate, fragment, and re-analyze ions in the gas phase by means of mass spectrometry have been driven both by the desire to understand the energetics, reactivity, and detailed fragmentation pathways of ions and the strong need for techniques to derive structural information from soft ionization mass spectra.

9.1 Concepts of Tandem Mass Spectrometry

The term *tandem mass spectrometry*, or briefly *tandem MS*, encompasses the numerous techniques where mass-selected ions are subjected to a second mass spectrometric analysis [1,2]. Tandem mass spectrometry comprises the acquisition and study of the spectra of ionic products or precursors of *m/z*-selected ions, or of precursor ions of a selected neutral mass loss. Tandem MS is also denoted as *mass spectrometry/mass spectrometry* from which the common acronym MS/MS is derived.

A mass spectrometer designed for MS/MS, also termed *tandem mass spectrometer*, requires to incorporate at least two stages of *m/z* analysis, often referred to as MS1 and MS2, respectively. Thus, many aspects of tandem MS are closely

J. Gross, *Mass Spectrometry*, 2nd ed., DOI 10.1007/978-3-642-10711-5_9,
© Springer-Verlag Berlin Heidelberg 2011

related to instrumentation [3]. In retrospect, we recognize that tandem MS has already been anticipated in some sections of the instrumentation chapter (Chaps. 4.4.4, 4.5, 4.7.11, 4.8.4, 4.9). Here, more principal considerations of the topic will follow.

9.1.1 Tandem-in-Space and Tandem-in-Time

There are two basic instrumental concepts for MS/MS. The first is *tandem mass spectrometry in space* (or *tandem-in-space* MS). In order to perform two consecutive mass-analyzing steps, two mass analyzers may be mounted in tandem. Thus, tandem-in-space refers to MS/MS instrumentation where product ion spectra are recorded using spatially separated *m/z* analyzers. Specific *m/z* separation is performed so that in one section of the instrument ions are selected, then dissociated in an intermediate region, and the products thereof are finally transmitted to a second analyzer for mass analysis (Fig. 9.1). All beam transmitting devices, e.g., multiple sector, ReTOF, TOF/TOF, QqQ, and QqTOF instruments follow this route to tandem MS (Fig. 9.2) [4]. The second approach, *tandem mass spectrometry in time* (or tandem-in-time MS), employs a single *m/z* analyzer (QIT, LIT, FT-ICR) that may be operated by executing the discrete steps of ion selection, activation, and product ion analysis in the very same place but sequentially in time [4].

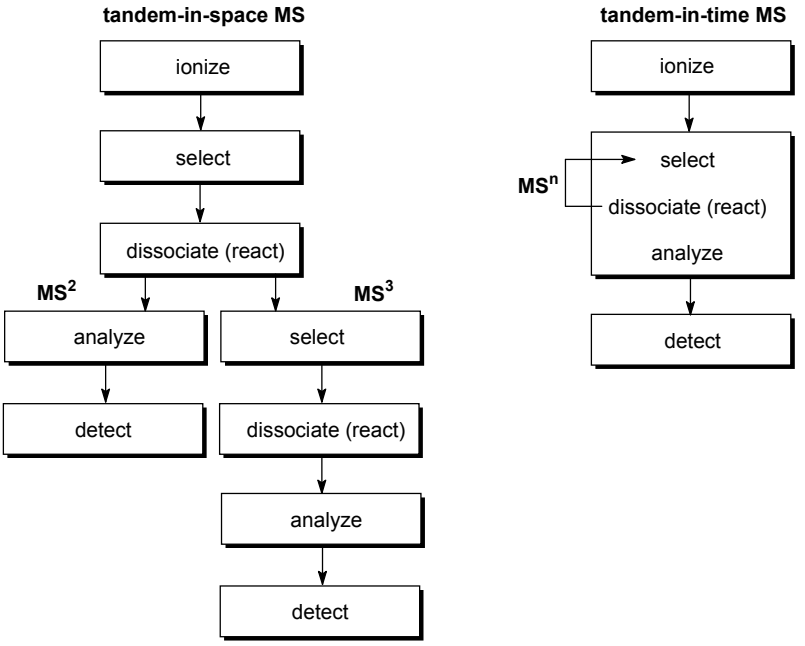


Fig. 9.1. Comparison of tandem-in-space and tandem-in-time MS. Obviously, higher order MS^n can be better realized by tandem-in-time setups, whereas tandem-in-space instrumentation is usually designed for MS^2 with MS^3 representing already the rare exception.

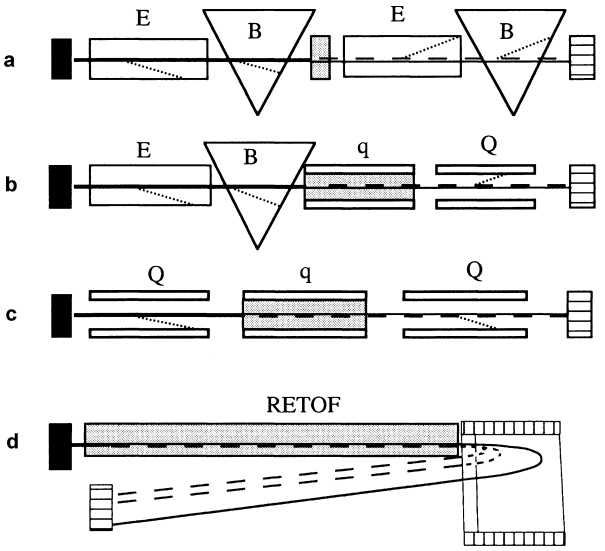


Fig. 9.2. Tandem-in-space setups for different beam instruments: (**a**) magnetic four-sector instrument of EB-EB geometry, (**b**) magnetic sector–quadrupole hybrid of EB-qQ geometry, (**c**) triple quadrupole (includes QqQ, QhQ, QoQ setups), and (**d**) ReTOF instrument. The line styles indicate —— stable precursor ions, - - - transmitted ions, and ····· non-transmitted fragment ions. *Shaded* areas show the region of analytically useful ion dissociations. Reproduced from Ref. [5] with permission. © Elsevier Science, 1994.

In principle, both instrumental concepts can be expanded to allow for multiple-stage mass spectrometry, i.e., multiple stages of precursor ion selection followed by product ion detection for successive n^{th} generation product ions [6]. While it is convenient to talk about MS/MS, acronyms like MS/MS/MS are clearly out of place. Therefore, it is common practice to use MS^2, MS^3, and generally MS^n to denote the number of stages of a tandem mass spectrometric experiment. Accordingly, in the sequential fragmentation scheme

$$m_1^+ \rightarrow m_2^+ \rightarrow m_3^+ \rightarrow m_4^+ \rightarrow m_5^+ \tag{9.1}$$

m_4^+ is the precursor ion of m_5^+, m_4^+ is a 1st generation product ion of m_3^+, a 2nd generation product ion of m_2^+, and also a 3rd generation product ion of m_1^+ [7,8]. The corresponding spectra are analogously termed n^{th} generation product ion spectra.

Clearly, the vast majority of tandem MS experiments is designed to deliver fragment ion data. Nonetheless, selected ions may also be allowed to react with neutrals to form products with a gain in mass:

$$m_1^+ + n \rightarrow m_2^+ \tag{9.2}$$

Ion–molecule reactions can thus be conducted under carefully controlled conditions. This sort of tandem MS is frequently employed in fundamental studies of ion reactivity.

Note: Obviously, tandem MS experiments can be adapted according to need. They can set up as ion fragmentations, typically by energetic collisions of fast ions with an inert gas (Chap. 9.3) or as addition reactions with an according increase in precursor ion mass by addition of a reactive gaseous neutral upon very low-energy collisions (Chap. 9.18). However, ion–neutral collisions can even be soft and still nonreactive as exploited for thermalizing ions by multiple low-energy collisions with a buffer gas (Chap. 4.4.4).

9.1.2 Pictograms for MS/MS Experiments

To facilitate the evaluation of tandem mass spectra, the particular type of experiment can be described by pictograms. Following a simplistic notation [6,9,10], the chosen analyzer (or stage of experiment) may be indicated by ●, a scanning analyzer (or stage of experiment) by ○. Information such as precursor ion mass, type of ion activation, or neutral loss may be indicated as required (Table 9.1).

Dissociations in transit through the mass analyzer may either occur spontaneously (*metastable*, Chap. 9.2) or can result from intentionally supplied additional activation, typically from collisions with neutrals (Chap. 9.3). Below follows a description of methods for activating or reacting otherwise stable ions in the *field-free region* (FFR) between the first stage, *m/z*-selection (MS1), and product ion analysis (MS2).

Thus, to include ionization mode, type of mass analyzers, scan mode, and conditions of ion activation, a more elaborate set of pictograms has been suggested by Lehmann (Fig. 9.3) [11]. Since then, such pictorial presentations of basic experimental parameters are occasionally given along with tandem mass spectra. Unfortunately, neither an authorized "character set" nor an update to include current equipment and modes are available at the time of this writing.

Table 9.1. Pictogram symbols for tandem MS experiments [6]

Mode	Product ion mode	Product ion mode	Precursor ion mode	Neutral loss scan
Level	MS^2	MS^3	MS^2	MS^2
Pictogram	● ↓ ○	● 228 ↓ ● 200 ↓ ○	○ ↓ CID ●	○ ↓ 32 ○
Notes		The *m/z* values of the selected ions may be noted	Conditions for activation may be added to arrow	Neutral loss can be indicated on arrow

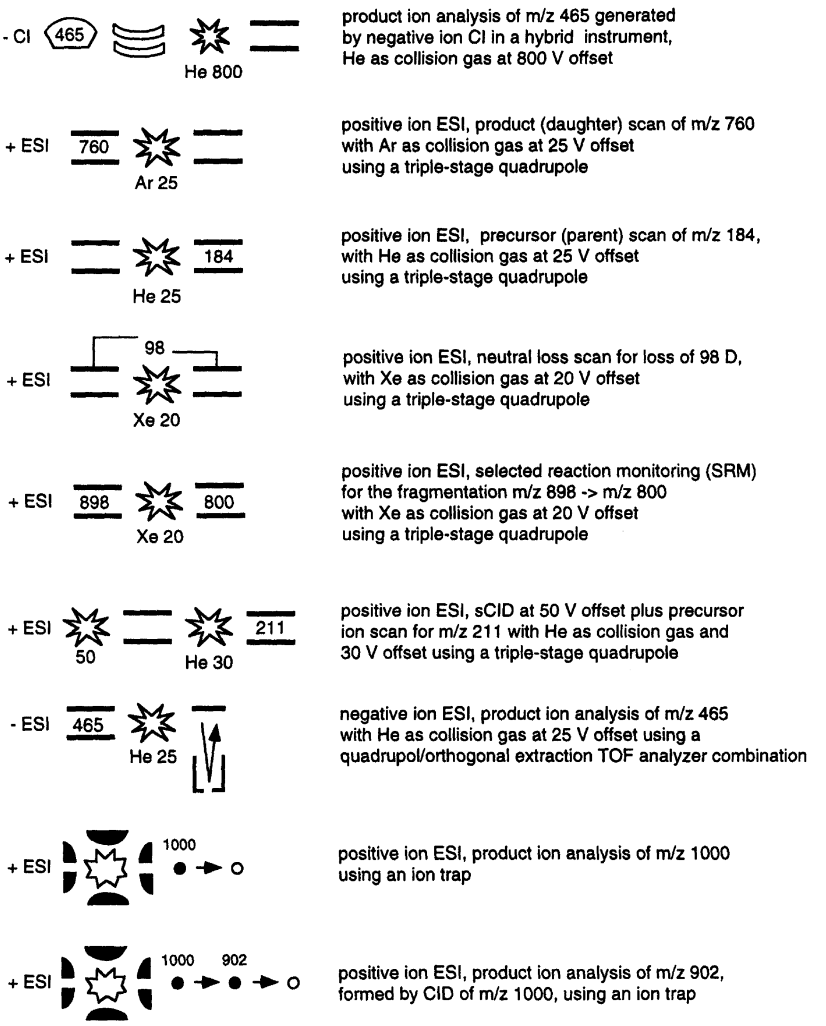


Fig. 9.3. Pictograms for tandem MS. Reproduced from Ref. [11] with permission. © Elsevier Science Inc., 1997.

Note: There is a close relationship between the type of mass analyzer and choice of method of ion activation that can be applied to the respective instrumental platform. It is therefore unfavorable to strictly separate the discussion of ion activation from that of instrumental setups and their modes of operation. Thus, the following passages of this chapter will reflect these mutual dependences by alternating discussions of activation methods and instrumental details in a way that is supposed to deliver convenient access to the subject matter.

9.2 Metastable Ion Dissociation

The success of any tandem mass spectrometric experiment depends on the occurrence of some kind of reaction between the consecutive steps of precursor ion selection and product ion analysis. This demands that ions entering the zone and/or period for reaction either possess or receive sufficient internal energy for doing so; alternatively, a partner for reaction may be presented.

As dealt with in Chap. 2.6, ions reacting sufficiently fast to dissociate while transiting the analyzer are termed *metastable ions* [12]. In classical beam instruments, this is correlated to lifetimes of roughly 10^{-6}–10^{-5} s, and thus, requires rate constants of unimolecular dissociation in the order of 10^{6}–10^{5} s^{-1}. EI, CI, and MALDI can provide a respectable fraction of ions, as to say in the afterglow of the ion source, falling into this range of internal energy and therefore into the lifetime of metastable decomposition. The fraction of metastable ion dissociations occurring in the *field-free region* (FFR) between MS1 and MS2 is accessible by means of tandem MS. Ions fragmenting during the very step of mass analysis are lost.

It is a generally accepted assumption that metastable ions possess internal energy close to threshold of ion dissociation. Interestingly, there are still differences even among metastable ion populations, depending on whether they are observed in close proximity to the ion source (1.FFR) or further away (2.FFR). Metastable ion spectra represent one of the indispensable tools for studying the mechanism and thermochemistry of ion dissociations [13,14]. Examples are given in the section on tandem MS on magnetic sector instruments.

9.3 Collision-Induced Dissociation

Even though collisions of ions with neutral gas atoms or molecules appear contradictory to the conditions of high vacuum, most mass spectrometers are equipped (or can be upgraded) to allow for their study. Consequently, fundamental and analytical studies make use of activating or reactive collisions within the mass spectrometer. The most prominent collision technique is *collision-induced dissociation* (CID) [15,16]; the terms *collisionally activated dissociation* (CAD) or *collisional activation* (CA) are also being used. CID allows for the fragmentation of gaseous ions that were otherwise perfectly stable. Thus, CID is especially useful for elucidating the structure of ions of low internal energy as for those created by soft ionization methods.

9.3.1 Effecting Collisions in a Mass Spectrometer

CID is generally realized by passing an ion beam through a *collision cell* where the collision gas (He, N_2, Ar) is set to a pressure considerably above that of the surrounding high vacuum. This can be achieved by introducing the gas via a needle valve into a comparatively tight compartment with narrow entrance and exit

slits for the ion beam (Fig. 9.4). A nearby vacuum pump removes effusing gas, thereby creating a *differentially pumped* region, due to the lack of laminar flow at some 10^{-4} Pa. Instead, expansion of the gas is diffusion-controlled. The reading of a pressure gauge can serve to reproduce the pressure adjustment, but it does not show the actual pressure inside the cell [17].

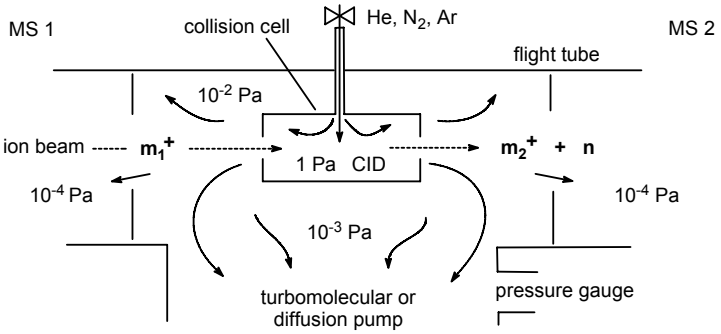


Fig. 9.4. Schematic of a collision cell for CID experiments in a beam instrument. Ions mass-selected in MS1 enter from the left.

9.3.2 Energy Transfer During Collisions

The collision of an ion AB^+ carrying some kiloelectronvolts of kinetic energy with a neutral N takes about 10^{-15} s. This allows to apply the assumptions of QET analogously to electron ionization (Chap. 2.1.1) [14,18-21]. The collision-induced dissociation of AB^+ can therefore be regarded as a two-step process [22]. First, the activated species AB^{+*} is formed. Second, after randomization of the internal energy has occurred, AB^{+*} will dissociate along any fragmentation pathway available at this specific level of internal energy:

$$AB^+ + N \rightarrow AB^{+*} + N \rightarrow A^+ + B + N \qquad (9.3)$$

The internal energy E_{AB+*} is composed of the internal energy prior to the collision, E_{AB+}, and of the amount of energy Q transferred during the collision:

$$E_{AB+*} = E_{AB+} + Q \qquad (9.4)$$

Thus, the collision marks a restart of the time scale for the activated ion. As $Q > E_{AB+}$ generally holds, the internal energy prior to the collision is of minor relevance – though not generally negligible – for the behavior of the activated ion. As may be expected, the CID spectra of stable molecular ions exhibit marked similarity to the 70-eV EI spectra of the respective compounds [15,16].

Example: Except for the intensities relative to the precursor ion, the B/E-linked scan CID spectrum of the toluene molecular ion, *m/z* 92, closely resembles the 70-eV EI mass spectrum (Fig. 9.5; for EI cf. Chap. 6.4.3). Here, all fragments are due

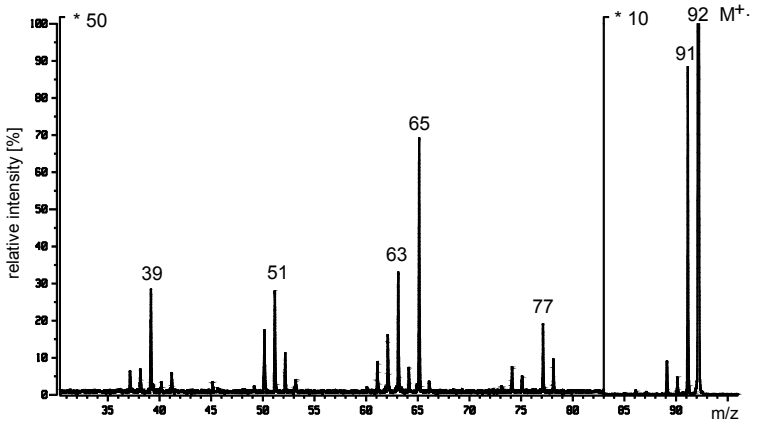


Fig. 9.5. CID spectrum of toluene molecular ion, *m/z* 92, as obtained at E_{lab} = 10 keV, B/E = *const.* linked scan on a magnetic sector instrument (cf. Chap. 9.6.4), collision gas He at about 50% transmission.

to CID because the molecular ion was generated by field ionization and did not show any metastable decomposition, i.e., $E_{AB+} = 0$ and $E_{AB+*} = Q$. The absolute upper limit for the value of Q is defined by the *center-of-mass collision energy*, E_{CM} [18,19],

$$E_{CM} = E_{LAB} \frac{m_N}{m_N + m_{AB}} \tag{9.5}$$

where m_N is the mass of the neutral, m_{AB} the mass of the ion, and E_{LAB}, the *ion kinetic energy in the laboratory frame of reference*.

Note: E_{LAB}, the ion kinetic energy in the laboratory frame of reference, simply represents the kinetic energy of the ion as received from passing through an acceleration stage that defines its kinetic energy, e.g., a singly charged ion initially at rest will have E_{LAB} = 10 eV after passing through a potential of 10 V. The collision event of the ion–neutral pair, however, is also determined by both ion mass, m_{AB}, and neutral mass, m_N, as expressed by the ratio $m_N / (m_N + m_{AB})$. The neutral is commonly treated as being at rest, which is a good approximation for the collision gas at thermal energy.

For a polyatomic ion consisting both of the atom B actually, involved in the collision process, and the remainder A, the maximum of Q is calculated to have a lower value than E_{CM}. Assuming central collisions we obtain [19]:

$$E_{\text{int max}} = 4E_{LAB}\, m_A\, m_B \left(\frac{m_N}{m_{AB}\,(m_B + m_N)} \right)^2 \tag{9.6}$$

However, most collisions are not "head-on", but occur at some angle θ. Increasing m_{AB} makes $E_{int\ max}$ decrease, whereas larger m_N is beneficial for energy transfer. In CID-MIKES the center of the peak is shifted to the low mass side, i.e., to the low ion translational energy side, because the uptake Q originates from a loss in E_{LAB} [23-28]. The relationship between ΔE_{LAB} and Q can be expressed as [25]:

$$Q = \frac{\Delta E_{LAB}(m_{AB} + m_N)}{m_N} - \left[\left(\frac{2m_{AB}E_{LAB}}{m_N}\right)\left(1 - \sqrt{\frac{E_{LAB} - \Delta E_{LAB}}{E_{LAB}}}\cos\theta\right)\right] \quad (9.7)$$

Several conclusions can be drawn from Eq. 9.7: *i*) Q has a broad distribution (0–15 eV) due to variations in θ and typically is in the order of some electronvolts [29]; *ii*) up to a certain ionic mass, the neutral penetrates the incident ion, i.e., the activated ion leaves the neutral behind (forward-scattered ion), but beyond the limit (> 10^2 atoms) the neutral is expelled in the direction of ion motion (backward-scattered ion) [25]; *iii*) at about *m/z* 1500 the translational energy loss is fully converted into vibrational excitation of the ion ($\Delta E_{LAB} = Q$); and *iv*) Q decreases beyond *m/z* 1500, thus explaining the difficulties in fragmenting heavy singly charged ions by CID (Fig. 9.6) [21,25,30].

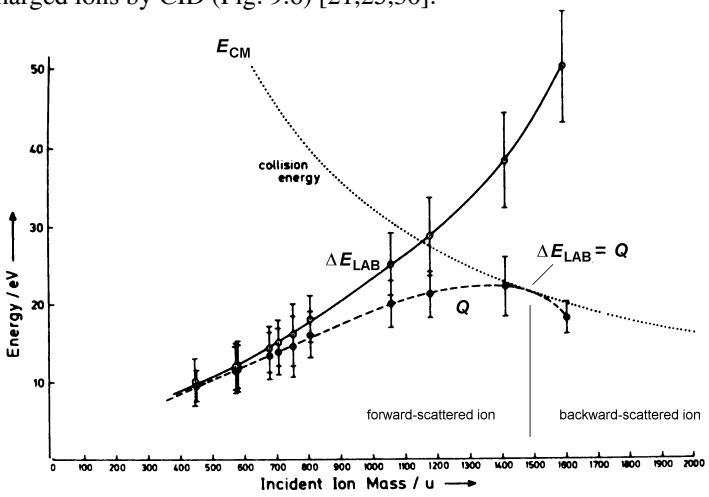


Fig. 9.6. The relationship between E_{CM}, ΔE_{LAB}, and Q. Adapted from Ref. [25] with permission. © Verlag der Zeitschrift für Naturforschung, 1984.

Note: In magnetic sector and TOF instruments, He is typically used as the collision gas because $E_{int\ max}$ from *high-energy collisions* (keV) is still comparatively large, and He reduces the risk of charge exchange due to its high IE. In the *low collision energy regime* [19] of quadrupole and ion trapping instruments (1–200 eV), heavier gases are frequently employed (N_2, Ar, Xe) to make CID more effective.

9.3.4 Single and Multiple Collisions in CID

Generally, the collision gas pressure is indirectly adjusted via the attenuation of the beam of mass-selected ions undergoing collisions. As the so-called *main beam* becomes increasingly attenuated, the probability for multiple collisions rises and so does the yield of fragments resulting from high activation energy processes. In a typical high-energy collision experiment a transmission of 90% for the main beam translates into 95% of the colliding ions to undergo single collisions while only about 5% encounter double collisions. At 50% transmission, about 68% of the colliding ions encounter a single, 23% two, and the remaining even three and four collisions (Fig. 9.7) [17]. To achieve sufficient activation of the ions in the low-energy collision regime, elongated collision cells are employed where Q is accumulated from numerous collision events.

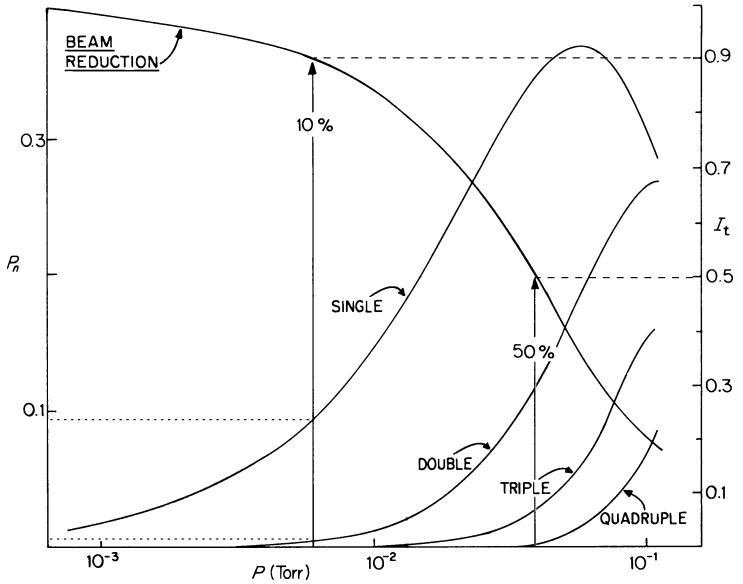


Fig. 9.7. Total collision probability P_n (*left* ordinate) and fractions of single, double, triple, and quadruple collisions vs. collision gas pressure. The transmission of the main beam I_t is given on the *right* ordinate. *Dotted lines* mark beam transmission and collision probabilities for 90% and 50% transmission, respectively. Values are calculated for an ion of collision cross section 5×10^{-16} cm^2 and 1 cm collision path; 10^{-2} Torr = 1.33 Pa. Adapted from Ref. [17] with permission. © John Wiley & Sons, 1985.

In beam-type analyzers, the collision event leading to ion activation can be considered in terms of the Lambert-Beer law, because the precursor ion beam flux $[M_p]_0$ is exponentially reduced when passing through a collision chamber of length l containing gas at target number density n

$$[M_p] = [M_p]_0 \times e^{-n\sigma l} \tag{9.8}$$

where σ is the collision cross section of the event [31].

In tandem-in-time experiments as performed in trapping instruments a description in terms of rate constants and reaction times is more appropriate, which leads to the expression

$$[M_p]_t = [M_p]_0 \times e^{-nkt} \tag{9.9}$$

where t is the activation time span, and k sums the rate constants of all processes leading to reduction in $[M_p]_0$, i.e., it includes fragmentation and scattering losses.

Note: It has turned out that medium transmission is optimal for structure elucidation. Too strong reduction of the main beam favors ion losses due to scattering, charge exchange ($M^{+\bullet} + N \rightarrow M + N^{+\bullet}$) or charge stripping processes ($M^{+\bullet} + N \rightarrow M^{2+} + N^{+\bullet}$) instead of delivering additional structural information.

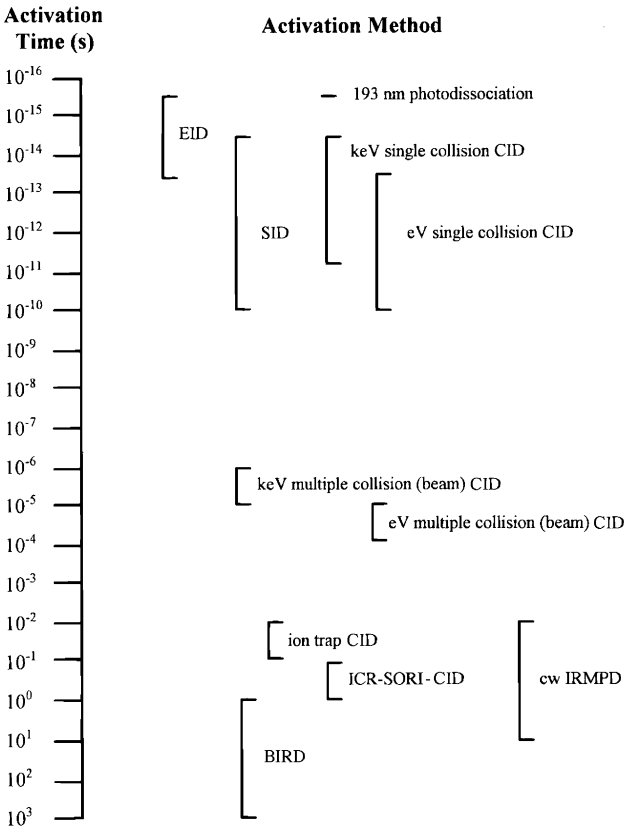


Fig. 9.8. Time scale of ion activation processes for tandem mass spectrometry. Adapted from Ref. [31] with permission. © Wiley & Sons, Ltd., 1997.

9.3.5 Time Scale of Ion Activating Processes

Collisions of energetic ions with gaseous molecules are very fast. Nonetheless, there is a considerable variation of the effective activation period, i.e., single collisions of ions of keV energy occur in the femtosecond range while those at eV energies tend to take picoseconds. If multiple collisions occur within one activation stage, the time scale is extended, because the span between collisions is then ruling the overall duration. Other activation techniques go along with even millisecond to second time spans (Fig. 9.8) [31]; most of these techniques will be addressed in this chapter [3]. While the fast ones can be treated by QET analogous to the event of electron ionization, the slower processes (SORI-CID, IRMPD, BIRD) tend to achieve an equilibrium of ion internal energy prior to dissociation.

9.4 Surface-Induced Dissociation

Instead of using gaseous atoms as the collision partners, collisions with solid surfaces can be employed to induce dissociation of the incident ions. This technique has become known as *surface-induced dissociation* (SID) [32,33]. Ions of some ten electronvolts kinetic energy are collided with a solid surface typically at an angle of 45° to effect SID. The evolving fragments are mass-analyzed by means of a linear quadrupole mass analyzer at right angles to the incident ion beam (Fig. 9.9) [32,34,35]. Such an experimental setup allows for the control of the energy of the incident ions, and therefore for adjusting the degree of fragmentation.

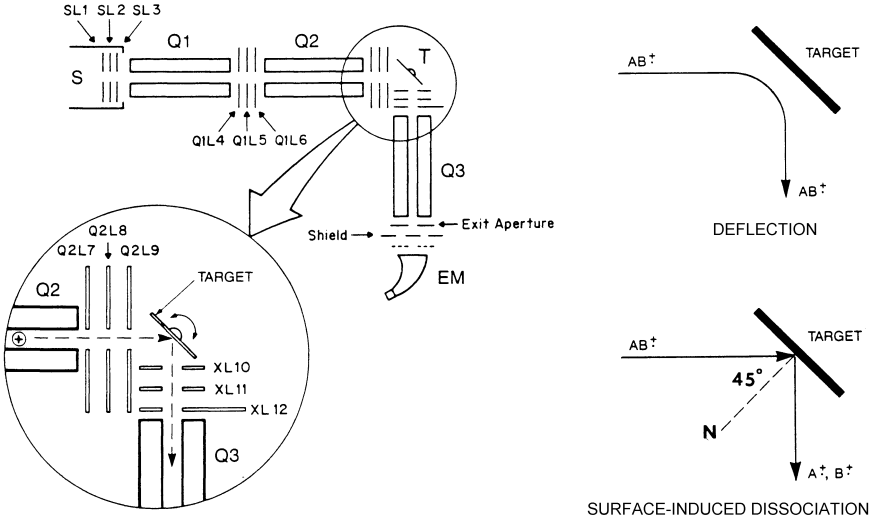


Fig. 9.9. Apparatus (*left*) and modes of operation (*right*) for SID with a modified triple quadrupole mass spectrometer. Reproduced from Ref. [34] with permission. © Elsevier Science, 1987.

SID conditions can be tuned to deliver spectra resembling either high- or low-energy CID spectra [32]. The absence of collision gas presents an advantage of SID over CID because losses of resolution due to high background pressure are avoided. SID has been successfully employed for structure elucidation of protonated peptides [36], and an SID mode of operation has even been implemented with a quadrupole ion trap [37]. However, apart from the quadrupole ion trap, SID requires substantial modifications of the instrumental hardware; circumstances that made SID lag behind the countless applications of CID.

9.5 Tandem MS on TOF Instruments

9.5.1 Utilizing a ReTOF for Tandem MS

Consider an ion m_1^+ decomposing in transit through a field-free region. Its kinetic energy is distributed among the product ion m_2^+ and the neutral fragment n according to their relative contribution to the mass of the precursor ion

$$E_{kin(m2+)} = E_{kin(m1+)} \frac{m_{i2}}{m_{i1}} \quad \text{and} \quad E_{kin(n)} = E_{kin(m1+)} \left(1 - \frac{m_{i2}}{m_{i1}}\right) \tag{9.10}$$

Fragment ions generated on the flight from the ion source to the reflector will have kinetic energies lower than intact precursor ions (Fig. 9.10). While the kinetic energy changes upon dissociation, the ion velocity remains constant, as already noted in the discussion on linear TOF (Chap. 4.2.3). A reflector is capable of handling ions bearing down to 70–90% of the energy to which it has been adjusted ($0.7–0.9 \times E_{\mathrm{kin(m1+)}}$). Stepwise reduction of the reflector potential allows acquisition of partial fragment ion spectra each covering several percent of the precursor ion mass [5,38,39]. Piecing the data together yields a spectrum of the product ions formed by metastable dissociation of m_1^+. To cover the range from m_1 to $0.1 \times m_{i1}$ the reflector must be stepped down from its potential V_0 to $0.1 \times V_0$ in some 10–20 increments.

The ReTOF analyzer alone supplies only the field-free region and MS2, i.e., the metastable dissociations of different precursor ion species leaving the ion source would be detected simultaneously. The precursor ion selection (MS1) – although technically demanding – follows a simple principle: first, ions below the selected precursor *m/z* value are electrostatically deflected, then the deflector is turned off to let the precursor ion pass, and finally the high voltage is switched on again to deflect heavier ions. As the deflector gate is located rather close to the ion source it acts as a short TOF analyzer providing only moderate precursor ion resolution. An early velocity-dependent ion selector has been introduced by Bradbury and Nielsen, thus often called *Bradbury-Nielsen gate* [40]. In modern instrumentation the term *timed ion selector* (TIS) is commonly used for the precursor ion-selecting device.

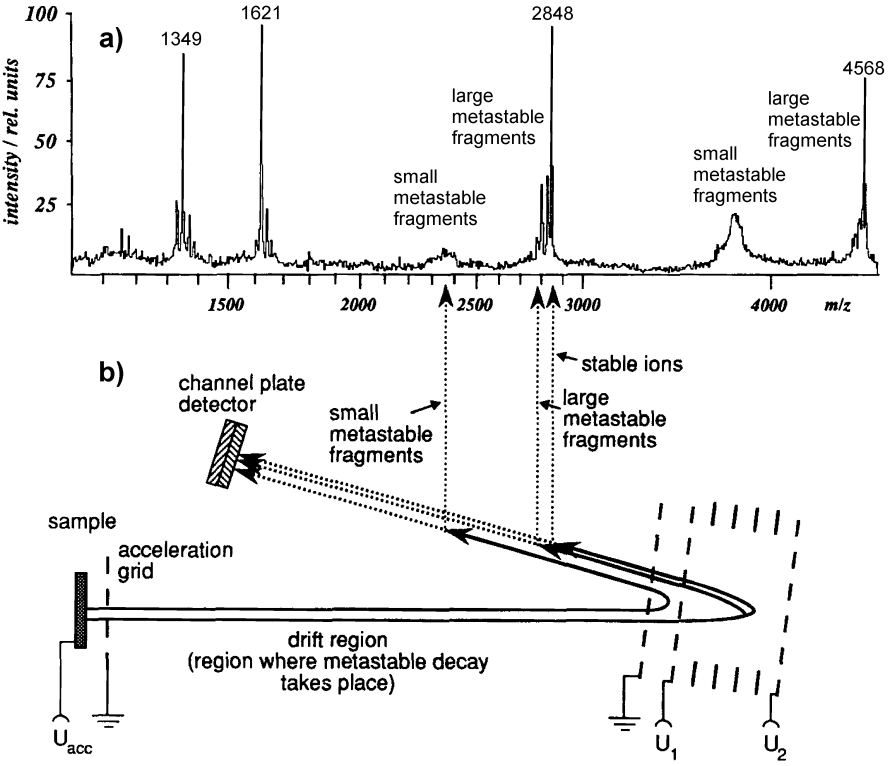


Fig. 9.10. Explanation of PSD fragment analysis by MALDI-ReTOF-MS. (**a**) The occurrence of peaks due to ions of different origin is indicated above the schematic in the MADLI spectrum of a mixture of substance P (*m/z* 1348), bombesin (*m/z* 1621), melittin (*m/z* 2848), and ACTH (*m/z* 4568). (**b**) The PSD mode translates the diffuse fragment ion peaks into an analytically useful spectrum. While the precursor ion and fragments of closely related mass penetrate deep into the reflector, those ions resulting from larger neutral losses return in the fringe field close to the reflector entry and are not properly focused onto the detector. To make these ions enter the useful reflector region, the reflector potential is stepped down to successively lower values. Reproduced from Ref. [38] with permission. © John Wiley & Sons, Ltd. 1992.

Despite the comparatively poor precursor ion resolution and being a time- and sample-consuming procedure, in comparison to the later true tandem TOF instruments, MS/MS of *post-source decay* (PSD) ions on the ReTOF had become established as one of the major tools of biomolecule sequencing for ions in the *m/z* 500–3000 range.

In particular the MALDI-TOF community has coined some sort of own terminology, e.g., *in-source decay* (ISD) for all fragmentations occurring within the ion source, *post-source decay* (PSD) instead of metastable ion dissociation, and *fragment analysis and structural TOF* (FAST) for the specific mode of operation of a ReTOF to detect metastable ions.

Note: Methods for the detection of metastable ion dissociations in ReTOF-MS in combination with *secondary ion mass spectrometry* (SIMS) and ^{252}Cf *plasma desorption* (^{252}Cf-PD) mass spectrometry were known before the advent of MALDI [41-44].

9.5.2 Curved-Field Reflectron

The laborious stepwise acquisition of PSD spectra could be circumvented by applying the newly developed *curved-field reflectron* (CFR) [45-48]. It offers advantages in speed and simplicity of operation when metastable fragmentations are to be studied as in the case of MALDI-TOF peptide sequencing. This type of ion reflector extends over a long section of the flight tube where it creates a nonlinear electric field that increases with its depth by steadily increasing the voltage difference between a comparatively large number of lenses (Fig. 9.11). Thus, the curved-field reflectron is capable of simultaneously focusing PSD fragments over the entire range of kinetic energies from 0.1–1.0 × $E_{kin(m1+)}$. It acts as a divergent ion mirror causing additional ion losses as compared to two-stage reflectors. CFR instruments have been available from Shimadzu Axima. An instrument with a quadratic field reflectron has also been introduced [49]. To enhance fragmentation of precursor ions via CID, a collision cell may be placed anywhere in the short flight path in front of the precursor ion-selecting gate [48].

Example: The curved-field reflectron of a coaxial ReTOF instrument occupies a large portion (D) of the total flight path ($s = l_1 + D$) and uses 86 lens elements whose voltages are set by 85 precision potentiometers located between them [47]. The distance l_1 between ion source and reflector entrance provides sufficient field-free flight path for metastable dissociations.

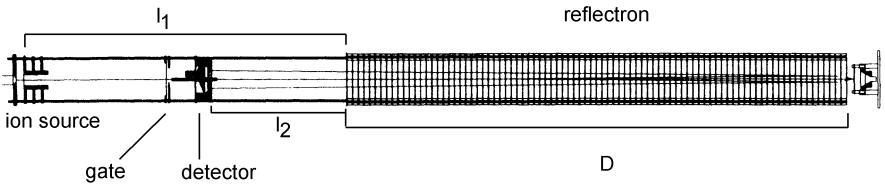


Fig. 9.11. Coaxial curved-field reflectron TOF spectrometer. The total length is about 1 m. Adapted from Ref. [47] with permission. © John Wiley & Sons, 1995.

9.5.3 Tandem MS on True Tandem TOF Instruments

Both limited precursor ion resolution and the need for stepwise acquisition of tandem mass spectra have driven the development of TOF/TOF instrumentation. Here, the MS1 functionality is achieved by a distinguished short linear TOF ana-

lyzer delivering ions *m/z*-selected by a *timed ion selector* (TIS) to a collision cell from where fragments are accelerated in a well-defined manner into the second flight tube that belongs to a ReTOF system. The first commercial TOF/TOF instruments of that class were available from Applied Biosystems [50] and Bruker Daltonik [51,52]. Although differing in detail, the basic idea of these TOF/TOF instruments is to operate TOF1 at comparatively low acceleration voltage and to accelerate fragment ions into a high-resolving ReTOF acting as MS2 designed to analyze ions of 20–27 keV kinetic energy (Fig. 9.12).

The lower velocity of precursor ions in TOF1 does not only simplify the operation of the TIS, it also permits sufficient time for the ions to dissociate (10–20 μs) [52] and it results in a narrow spread of the kinetic energies of the fragment ions arising thereof. After fragmentation, typically enforced by CID [53], the ions are passed into a second acceleration stage located behind the collision cell. By "lifting" all ions by a certain amount of kinetic energy, their relative spread in kinetic energy is reduced. For example, a precursor ion of 5 keV might yield fragments having 0.5–5 keV. Addition of another 15 keV to all fragment ions lifts them to 15.5–20 keV. In fact, the assembly comprising collision cell and acceleration lenses acts like a second DE ion source. Given a reflector of sufficient energy acceptance they can be analyzed without tedious stepping of the reflector voltage. The Bruker system employs 8-keV ions in TOF1 that are accelerated by another 19 kV after collision. For standard MALDI-MS operation, the ions are fully accelerated in the ion source and the TIS–collision cell–LIFT assembly is switched off (grounded). The Applied Biosystems instruments decelerate mass-analyzed ions to 1–2 keV prior to CID and then accelerate them to 20 keV for the ReTOF. Both concepts make use of delayed extraction for each stage and both require a metastable ion suppressor in the tube between collision cell and reflector. The metastable

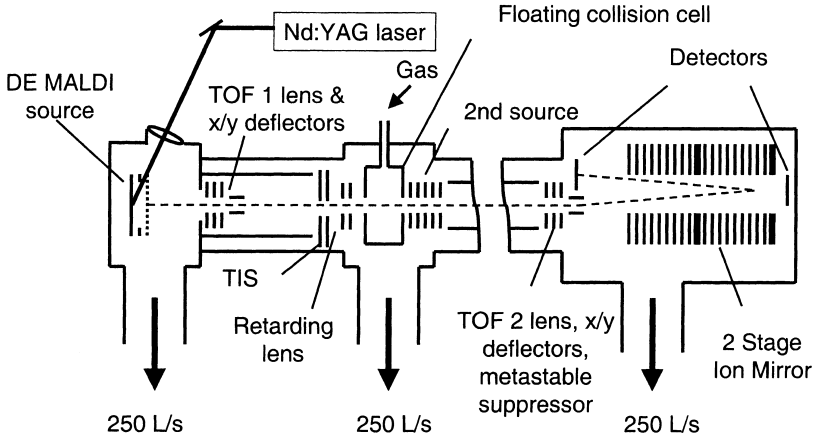


Fig. 9.12. Tandem TOF analyzer with linear TOF1 and ReTOF2. The ions from TOF1 are *m/z*-selected by a timed ion selector, decelerated, fragmented by CID, accelerated, and then passed into ReTOF2. Reproduced from Ref. [50] with permission. © Elsevier Science, 2002.

ion suppressor deflects precursor ions having survived the CID cell analogous to the TIS operation, because the 2.FFR metastable ions would otherwise interfere with the spectrum in the same way as shown in Fig. 9.10 [48,53].

9.6 Tandem MS with Magnetic Sector Instruments

There are multiple ways of detecting metastable and collision-induced dissociations with magnetic sector instruments [12]. In fact, the whole phenomenon of so-called "diffuse peaks" in mass spectra was discovered with this particular type of mass analyzer (Chap. 4.3.2). In the mid-1940s, these broad signals were correctly interpreted as ions decomposing in transit [54,55]. Metastable ion spectra still represent one of the indispensable tools for studying the mechanism and thermochemistry of ion dissociations [1,2,13,14].

9.6.1 Dissociations in the FFR Preceding the Magnetic Sector

Peaks from metastable ion decompositions are detected at non-integral *m/z* values. Instead, the peak corresponding to a fragment m_2^+ formed from m_1^+ upon decomposition in the field-free region in front of the magnetic sector is located at a magnet setting m* which is described by the relationship $m^* = m_2^2/m_1$ [54,55]. This is because dissociation in a *field-free region* (FFR) not only causes partitioning of ion kinetic energy (Eq. 9.10), but also goes with partitioning of momentum *p*

$$p_{(m2+)} = p_{(m1+)} \frac{m_{i2}}{m_{i1}} \tag{9.11}$$

Due to conservation of velocity, i.e., $v_1 = v_2 \equiv v$, the momentum of a fragment ion m_2^+ formed in a FFR preceding the magnetic sector is different from that of such a fragment ion arising from the ion source. The ion formed by metastable ion dissociation thus passes the magnet as if it had the virtual mass m*

$$m^* = \frac{m_2{}^2}{m_1} \tag{9.12}$$

This explains "diffuse" peaks at fractional *m/z* values in the *B* scan spectra of B and EB instruments as a result of metastable ion dissociations [54,55]. In turn, the mass spectra obtained from BE instruments do not show any metastable ion peaks in normal operation.

Example: The metastable decay of the *o*-nitrophenol molecular ion, *m/z* 139, by loss of NO to yield the $[M–NO]^+$ ion, *m/z* 109, has been studied on a single-focusing magnetic sector instrument (Fig. 9.13) [56]. The mass spectrum shows a flat-topped peak of low intensity expanding over three mass units. Some minor and narrow "regular" peaks corresponding to fragment ions formed within the ion

source are observed beside and on top of it. The peak due to the metastable dissociation is centered at *m/z* 85.5 which can be explained by the simple calculation $m^* = m_2^2/m_1 = 109^2/139 = 85.5$.

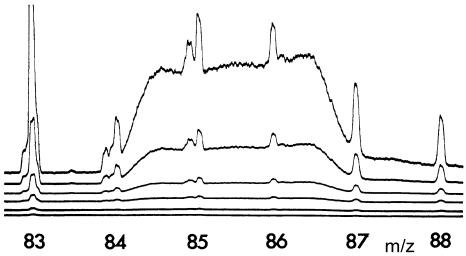


Fig. 9.13. Peak due to metastable NO loss of the *o*-nitrophenol molecular ion. The multiple traces correspond to different amplifier settings of a multi-channel recorder. Adapted from Ref. [56] with permission. © Verlag der Zeitschrift für Naturforschung, 1965.

9.6.2 Mass-Analyzed Ion Kinetic Energy Spectra

Mass-analyzed ion kinetic energy spectra (MIKES) [57,58] can be measured on BE geometry instruments only. The precursor ion is selected by the magnet and the fragments from dissociations of m_1^+ in the 2.FFR are analyzed by the ESA due to their kinetic energy. This is possible because the kinetic energy of the precursor is distributed among the product ion and the neutral. From Eq. 9.10 we have

$$\frac{E_2}{E_1} = \frac{m_{i2}}{m_{i1}} = \frac{m_{i2}v^2}{m_{i1}v^2} \tag{9.13}$$

Thus, scanning of the electric field (*E* scan) yields an energy spectrum which allows for the determination of the *kinetic energy release* (KER) from the peak width. The MIKE technique provides good precursor ion resolution, but poor product ion resolution due to the influence of KER on peak shapes.

Note: In MIKES E_1 represents the full electric field necessary to transmit the precursor ion m_1^+ through the ESA, and E_1 is often denoted as starting value E_0. Then, the abscissa of MIKE spectra is divided into units of $E/E_0 = m_2/m_1$.

9.6.3 Determination of Kinetic Energy Release

We just saw that peaks due to metastable ion dissociations are much broader than "regular" peaks (Fig. 9.13). In Chap. 2.8 we dealt with the *activation energy of the reverse reaction*, E_{or}, and *energy partitioning* as the thermochemical reasons for the occurrence of *kinetic energy release* (KER). The peak broadening is caused by the kinetic energy from KER grafted onto the kinetic energy of the ion beam as it

passes through the mass analyzer. Due to the free rotation of the dissociating ion, there is no preferred orientation of this superimposed motion. Given a suitable experimental setup of the analyzer system that allows to obtain a kinetic energy spectrum, the *x*-component of KER, i.e., along the flight axis, can be calculated from the peak width of metastable ion decompositions. *Mass-analyzed ion kinetic energy spectrometry* (MIKES) is an established technique for doing so (Fig. 9.14). The peak width at half height is related to KER by [13,14]:

$$T = \frac{m_2\, U_b\, e}{16n}\left(\frac{\Delta E}{E}\right)^2 \tag{9.14}$$

where T is the average kinetic energy released, m_2 is mass of the fragment ion, n the mass of the neutral, U_b the acceleration voltage, e the electron charge, E gives the position and ΔE the width of the peak on the kinetic energy scale. Correction of the width of the metastable peak, w_{50meta}, for the width of the main beam, w_{50main}, should be applied for smaller values of T [59,60]:

$$w_{50corr} = \sqrt{{w_{50meta}}^2 - {w_{50main}}^2} \tag{9.15}$$

Example: The observed KER values and also peak shapes may change dramatically as E_{0r} decreases (Fig. 9.14). In the McLafferty rearrangement of immonium ions (Chap. 6.11.1) the leaving alkene grows from ethene to hexene as the substituent varies from propyl to octyl. Nonetheless, the mechanism of the reaction by which the product ion at *m/z* 58 is formed remains unaffected [61].

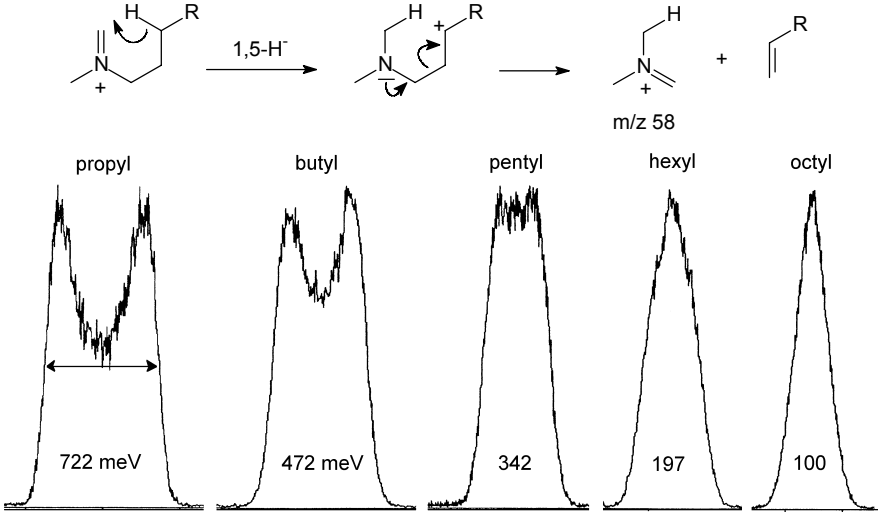


Fig. 9.14. Effect of decreasing E_{0r} on KER. The peaks from MIKE measurements result from the *m/z* 58 ion product ion of alkene loss (ethene to hexene) from homologous iminium ions. The KER is determined from peak width at half height.

Note: Before performing KER measurements, a "calibration" of the instrument(al parameters) against a well-established standard is recommended. Allylmethylether molecular ions, for example, decompose to yield three peaks of different shape and position in the spectrum [62-64].

9.6.4 B/E = *Const.* Linked Scan

Ions decomposing in the 1.FFR of BE and EB instruments can be detected using the $B/E = const.$ linked scan [65]. Due to the proportionality of B and p ($r_m = mv_i/qB$) ions are transmitted through the magnet if

$$\frac{B_2}{B_1} = \frac{m_2 v}{m_1 v} = \frac{p_2}{p_1} = \frac{m_2}{m_1} \tag{9.16}$$

where m_1 and m_2 denote the masses of the precursor and the product ion and v is their equal velocity. For their subsequent passage through the ESA, Eq. 9.13 has to be satisfied. Therefore, we have for the passage through both fields

$$\frac{B_2}{B_1} = \frac{E_2}{E_1} = \frac{m_2}{m_1} \tag{9.17}$$

which defines the conditions for a scan as $B/E = const.$ Thus, B and E have to be scanned together, i.e., in a *linked* fashion. The $B/E = const.$ linked scan provides good fragment ion resolution ($R \approx 1000$) but poor precursor ion resolution ($R \approx 200$). As with all linked scans, there is a risk of artefact peaks [66-69] because linked scan techniques represent no true tandem MS where MS1 and MS2 are clearly separate. The use of two complementary scan modes is therefore suggested to avoid ambiguities [67].

9.6.5 Additional Linked Scan Functions

Whereas TOF instruments solely allow for the detection of product ions of a selected precursor, sector instruments offer additional modes of operation: *i*) to exclusively identify product ions of a particular precursor ion, so-called *precursor ion scans* [70,71], or *ii*) to detect only ions formed by loss of a specific neutral mass, so-called *constant neutral loss* (CNL) scan [72]. This can be achieved by some technically more demanding linked scans (Table 9.2) [73-76].

Example: The $B^2E = const.$ linked scan [71] has been employed to quantify the caffeine content of coffee, black tea, and caffeinated softdrinks [77]. Caffeine, $M^{+\bullet} = 194$, was determined by spiking the sample with a known concentration of $[D_3]$caffeine, $M^{+\bullet} = 197$, as internal standard. Both molecular ions dissociate to form a fragment ion at *m/z* 109 which was selected as m_2^+. Then, the precursor ion scan showed both molecular ion, m_1^+ and $[D_3]m_1^+$, as precursor of the ion at *m/z* 109. The ratio of peak intensities was taken as a measure for the relative concen-

tration of analyte and labeled standard (Fig. 9.15). A modern approach would certainly involve a triple quadrupole instrument (Chap. 9.7).

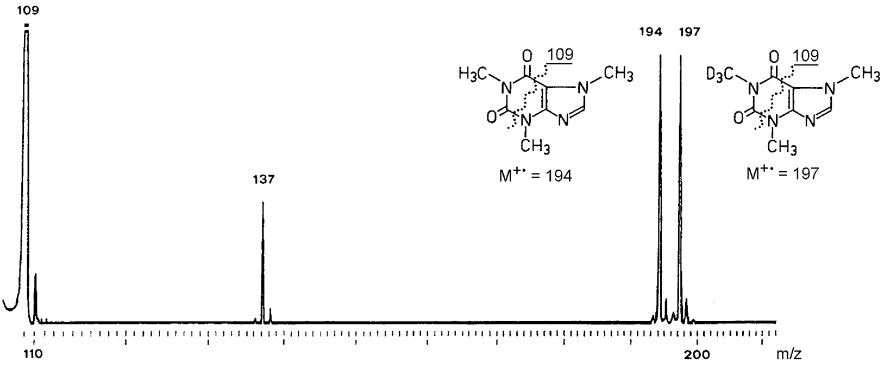


Fig. 9.15. CID B^2E spectrum of the ion *m/z* 109 of a caffeinated softdrink (cola) with [D_3]caffeine as internal standard. Different brands yielded 73–158 mg l^{-1}. Adapted from Ref. [77] with permission. © John Wiley & Sons, 1983.

Table 9.2. Common scan laws for the detection of metastable ion dissociations on magnetic sector mass spectrometers [a]

Selected mass	Scan law	KER from peak width?	Analyzer and FFR	Properties
m_1	$B = B_{m1}$, and $E/E_0 = m_2/m_1$	yes	BE 2.FFR	mass-analyzed ion kinetic energy spectrum (MIKES), E is scanned
m_1	$B/E = B_{0(1)}/E_0$ i.e., $B/E = const.$	no	BE or EB 1.FFR	linked scan, poor precursor but good product ion resolution
m_2	$B^2/E = B_2^2/E_0$ i.e., $B^2/E = const.$	yes	BE or EB 1.FFR	linked scan, poor product but good precursor ion resolution, demands precise control of B
m_2	$B^2 \times E = B_{0(2)} \times E_0$ i.e., $B^2 \times E = const.$	no	BE 2.FFR	linked scan, resolution controlled by that of B, needs precise control of B
m_n	$(B/E) \times [1-(E/E_0)]^{1/2}$ i.e., $E/E_0 = m_2/m_1 = 1-(m_n/m_1)$	no	BE or EB 1.FFR	constant neutral loss (CNL), linked scan

[a] all scans listed use constant acceleration voltage U. Scanning of U offers additional scan modes. However, scanning of U over a wide range causes detuning of the ion source

Note: *Precursor ion scanning* suggests some sort of measuring into the past. One should be aware that also in precursor ion scans the product ions are detected, but this is accomplished in a way that only fragments of a selected precursor ion mass can reach the detector, hence the term.

9.6.6 Multi-Sector Instruments

Multi-sector instruments, typically four-sector machines, were developed in the 1980s to combine high precursor ion resolution with high fragment ion resolution [78,79]. Their major field of application was sequencing of biomolecules by FAB-CID-MS/MS. Commercial representatives are (were) the JEOL HX110/HX110A (EBEB), the JEOL MStation-T (BEBE), or the Micromass AutospecT (EBEBE). As industrial laboratories are governed by high-throughput and other economic aspects, modern TOF/TOF, QqTOF, and hybrid FT-ICR instruments have mostly replaced these impressing "dinosaurs" weighing some 4–5 tons and having about 3×5 m footprint. Numerous custom-built four-sector instruments are still operated in laboratories devoted to gas-phase ion chemistry [80].

Example: The FAB-CID-MS/MS spectrum of thymosin-T1 $[M+H]^+$ ions, *m/z* 1427.7, as obtained from a magnetic four-sector instrument [81] shows numerous fragment ions due to *N*-terminal, *C*-terminal, and internal fragmentations (Fig. 9.16) [82]. It would be almost impossible to obtain sequence information from such a spectrum without generalizing rules to follow [83-88]. The most abundant ions obtained from the fragmenting peptide ion usually belong to six series named **a**, **b**, and **c** if the proton (charge) is kept in the *N*-terminus or **x**, **y**, and **z**, respectively, where the proton is located in the *C*-terminal part. Within each series the mass difference should only be one amino acid. Ideally, one can then count down the amino acids.

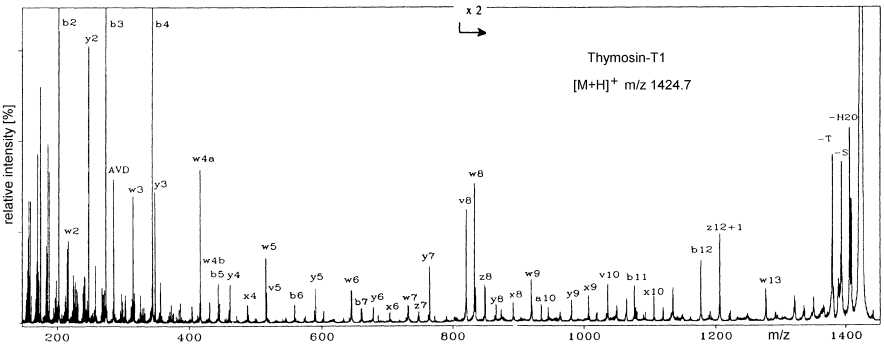


Fig. 9.16. FAB-CID tandem mass spectrum of thymosin-T1 $[M+H]^+$ ions, *m/z* 1427.7. Reproduced from Ref. [82] by permission. © American Chemical Society, 1993.

Note: One of the advantages of MS/MS techniques is that they do not require the full isolation of all compounds of interest, because the precursor ion selection of MS1 excludes accompanying ions from contributing to the CID spectrum of the actually selected precursor ion as acquired by MS2.

9.7 Tandem MS with Linear Quadrupole Analyzers

9.7.1 Triple Quadrupole Mass Spectrometers

Triple quadrupole mass spectrometers, QqQ, are becoming a standard analytical tool for GC-MS/MS and LC-MS/MS applications, in particular for cases where accurate quantitation is desired (Chap. 14). Ever since their introduction [89-91], they have continuously been improved in terms of mass range, resolution, and sensitivity [92-94]. In early triple quadrupole mass spectrometers, Q_1 served as MS1, followed by an intermediate RF-only quadrupole, q_2, acting as "field-free region" with ion-guiding capabilities for metastable dissociations or more often as collision cell for CID experiments, and finally Q_3 to analyze the fragment ions exiting from q_2 (Fig. 9.17). The transition of ions through the QqQ instrument is normally supported by Einzel lenses in the gaps separating the quadrupoles [95,96].

Note: Collision cells of simple short tube design like in tandem TOF or magnetic sector instruments (Chap. 9.3.1) cannot be combined with quadrupoles since the ions are rather dispersed at the exit and would be lost upon further collisional scattering.

In recent instruments, the collision region between MS1 and MS2 is not anymore an RF-only quadrupole, but a hexapole or octapole due to their steeper potential well (Chap. 4.4.4), which greatly improves their ion-guiding capabilities as compared to a true quadrupole. Today, most "triple quadrupole instruments" essentially present QhQ or QoQ designs. Since the introduction of the *traveling wave ion guide* (TWIG, Chap. 4.9.2), there are also instruments featuring a Q-TWIG-Q geometry.

In MS/MS operation, the mass-selected ions emerging from Q_1 are accelerated into the ion guide collision cell by a potential offset of typically 5–50 V where the collision gas (N_2, Ar) is provided at a pressure of 0.1–0.3 Pa. Careful optimization of all parameters allows for major improvements of CID efficiency and resolution [97]. If MS/MS is not intended, either Q_1 or Q_3 may be set to RF-only mode, thereby reducing its function to that of a simple flight tube with ion-guiding capabilities. The instrument then behaves as though it was a single quadrupole mass spectrometer.

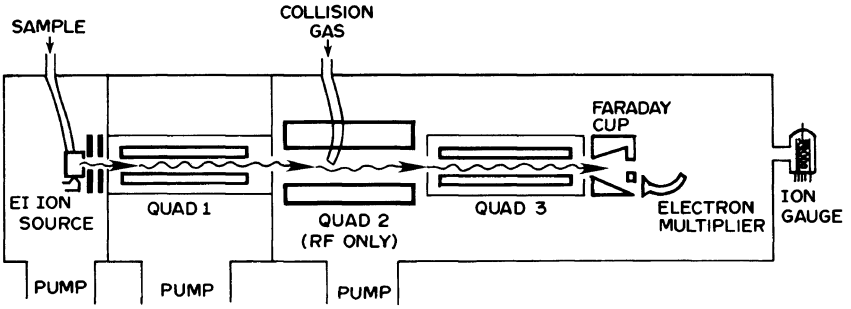


Fig. 9.17. Schematic of an early triple quadrupole mass spectrometer (QqQ). Reproduced from Ref. [90] with permission. © Elsevier Science, 1979.

Note: At first sight, there is no difference whether Q_1 or Q_3 is switched to RF-only for MS mode. However, for EI it seems better to operate Q_3 in RF-only mode. Otherwise, the ion source would effectively extend up to the entrance of Q_3 making fragment ions more abundant due to elongated time for dissociations. Soft ionization methods do not show such differences.

9.7.2 Scan Modes for Tandem MS with Triple Quadrupole Instruments

In triple quadrupole instruments Q_1 and Q_3 are operated independently as MS1 and MS2, respectively, making MS/MS straightforward. The experimental setups for product ion, precursor ion, and neutral loss scanning are summarized in Table 9.3 and depicted in Fig. 9.18. Definitely, this instrument class offers the most easily understandable tandem MS modes of operation.

9.7.3 Penta Quadrupole Instruments

The concept of the triple quadrupole instrument may be expanded by adding another RF-only quadrupole and a third mass-analyzing quadrupole to build a QqQqQ instrument. The penta quadrupole represents one of the rare tandem-in-space concepts to achieve MS^3. A commercial penta quadrupole instrument has once been offered by Extrel, but remained fairly exotic. Nonetheless, the penta quadrupole instrument may serve as a versatile tool for the study of gas phase ion chemistry and in particular ion-molecule reactions [99-102]. For the latter application the effective spatial separation of the zone with neutral reagent from that of preparation of the *m/z*-selected precursor ion presents a clear advantage over tandem-in-time concepts.

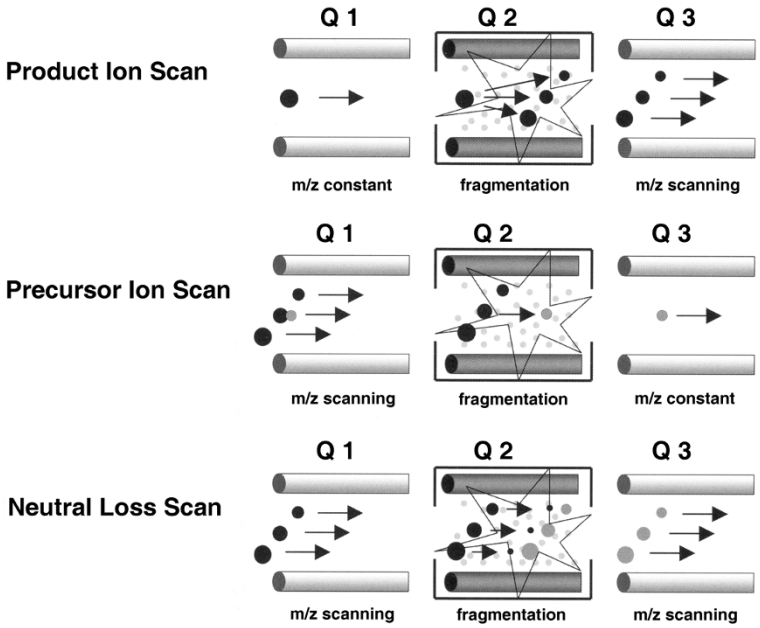


Fig. 9.18. Scan modes of triple quadrupole mass spectrometers. Adapted from Ref. [98] with permission. © Springer-Verlag, 2004.

Table 9.3. Scan modes of triple quadrupole instruments

Scan mode [a]	Operation of Q_1	Operation of q_2	Operation of Q_3
Product ion, define m_1	no scan, select m_1	metastable or CID	scan up to m_1 to collect its fragments
Precursor ion, define m_2	scan from m_2 upwards to cover potential precursors	metastable or CID	no scan, select m_2
Constant neutral loss, define n	scan desired range	metastable or CID	scan range shifted by Δm to low mass

[a] masses for reaction $m_1^+ \rightarrow m_2^+ + n$

9.8 Tandem MS with the Quadrupole Ion Trap

Ion traps are *tandem-in-time* instruments, i.e., they perform the steps of precursor ion selection, ion activation, and acquisition of fragment ion spectra in the very same place. This advantageous property allows the multiple use of a single QIT to perform not only MS^2 but also MS^3 and higher order MS^n experiments – indeed a very economic concept. Depending on the abundance of the initial precursor ion,

its fragmentation behavior – and of course, on the performance of the QIT – MS^6 experiments are possible [103].

In the QIT, MS^n is accomplished by using appropriate scan functions for the fundamental RF and the auxiliary modulation voltage (Chap. 4.6.7) [103-105]. At a sufficient level of sophistication, e.g., by combining slow and fast forward and reverse RF voltage scans with suitable settings of the auxiliary voltage, monoisotopic precursor ions can even be isolated in case of triply charged ions (Figs. 9.19, 9.20) [106]. The resonance excitation provided by moderate auxiliary voltages can be employed to effect low-energy CID of the trapped ions due to activating collisions with the buffer gas [107], i.e., no additional collision gas is required in a QIT. A full description of the numerous approaches to continuously improving scans can be found in the literature [106,108-113].

Unfortunately, there is one major disadvantage of QITs for fragment ion analysis in that they cannot simultaneously store ions over the full *m/z* range. It is a commonly accepted property of QITs to loose ions below an *m/z* value of about one third of the precursor ion. This phenomenon is known as *low-mass cutoff* (LMCO) [113].

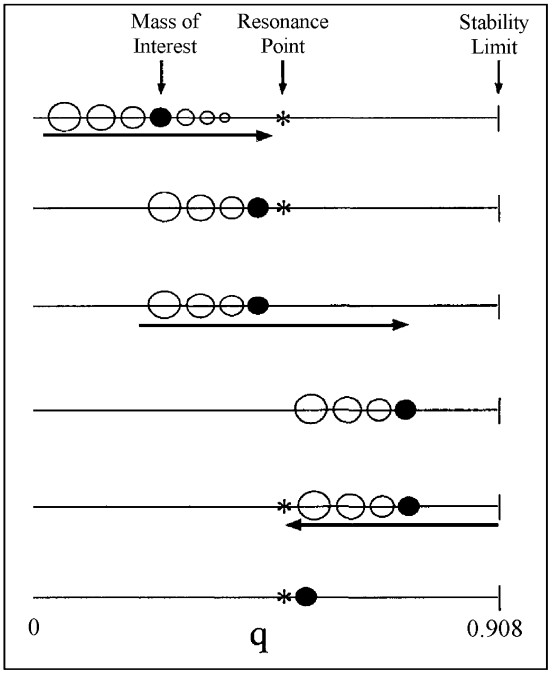


Fig. 9.19. The principle of isolation of a precursor ion by using forward and reverse scanning of a QIT. Ions smaller than the precursor are ejected by exciting them above the stability limit at $q = 0.908$, then settings are changed so that reduction of the RF amplitude causes ejection of the heavier ions. Reproduced from Ref. [106] with permission. © John Wiley & Sons, 1992.

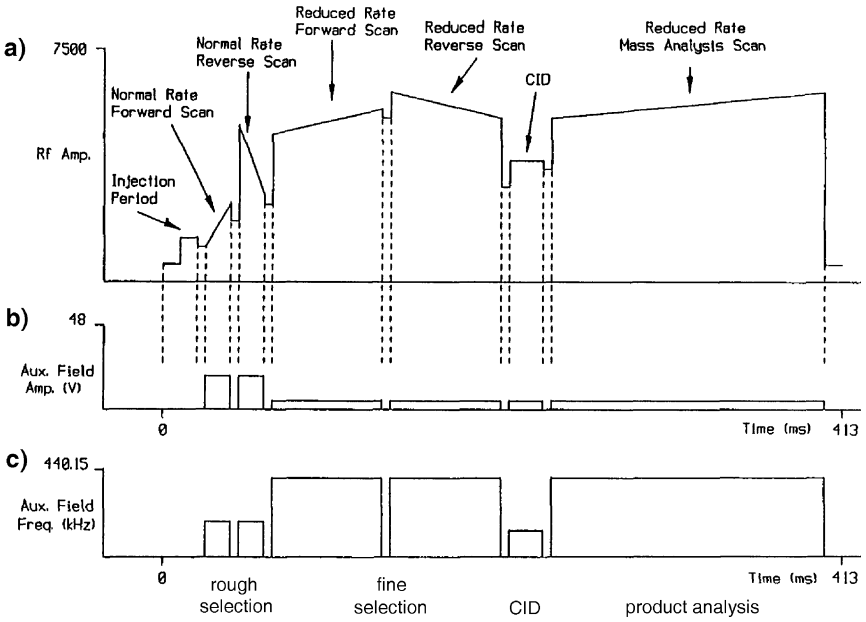


Fig. 9.20. Sequence of changes of (**a**) RF amplitude, (**b**) auxiliary voltage amplitude, and (**c**) auxiliary voltage frequency to first achieve a rough precursor ion selection, then a fine selection by repetition at slow rates, followed by CID, and product ion scan. Adapted from Ref. [106] with permission. © John Wiley & Sons, 1992.

Example I: The positive-ion electrospray tandem mass spectrum of the $[M+2H]^{2+}$ ion of the β-casein tryptic phosphopeptide FQpSEEQQQTEDELQDK was obtained on a Bruker Esquire 3000 quadrupole ion trap (Fig. 9.21) [98]. Sequential amino acid residue losses from both terminal ends of the peptide are labeled according to the b- and y-ion nomenclature. Due to the phosphoserine, the C- and N-terminal peptide ions ($b_3 - b_{15}$ and $y - y_{14}$) exhibit an increase of 80 u in mass as compared to the unphosphorylated form. In addition, most ions are accompanied by the corresponding fragments from H_3PO_4 loss (98 u).

Example II: MS^4 on a QIT was used for the identification of beauverolides, cyclic peptides from the fermentation broth of *Beauveria bassiana*, a pathogenic fungus of insects [114]. All MS^n (ESI-CID-QIT) experiments started from singly charged $[M+H]^+$ precursor ions (Fig. 9.22).

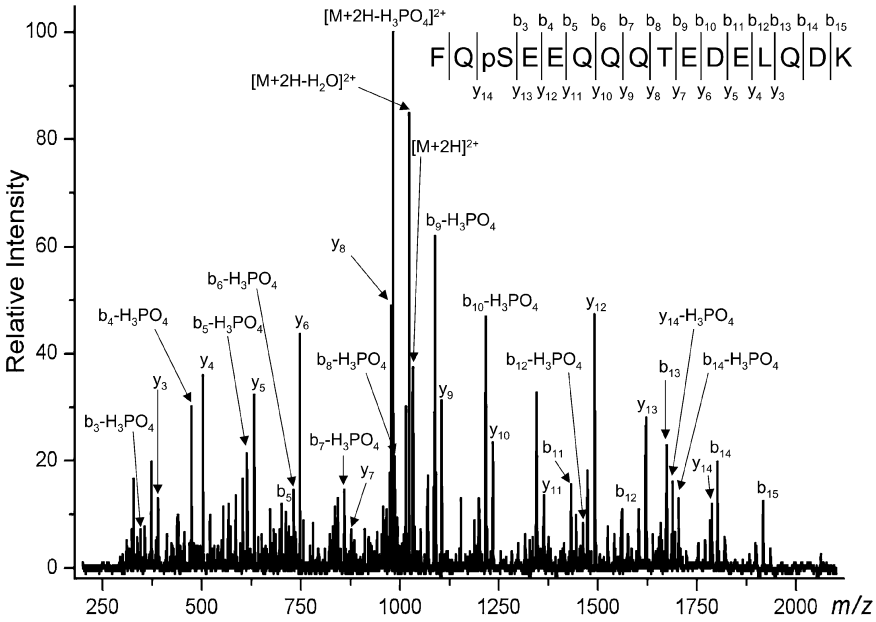


Fig. 9.21. Positive-ion electrospray tandem mass spectrum of the $[M+2H]^{2+}$ ion of the β-casein tryptic phosphopeptide FQpSEEQQQTEDELQDK as obtained upon HPLC coupling to a quadrupole ion trap. Reproduced from Ref. [98] with permission. © Springer-Verlag, 2004.

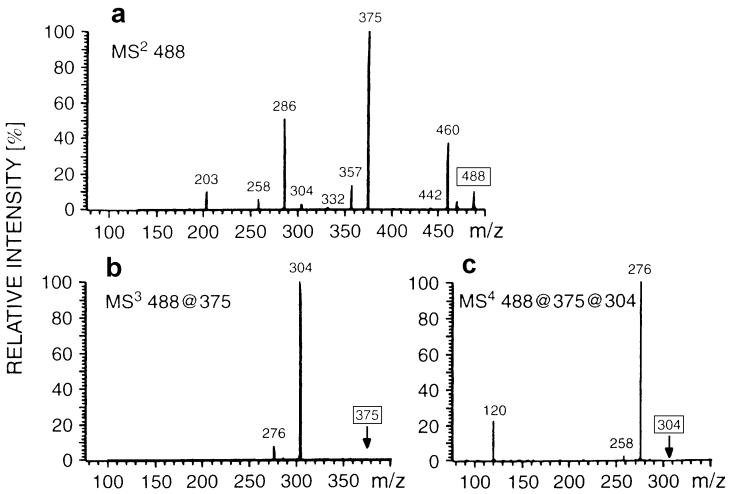
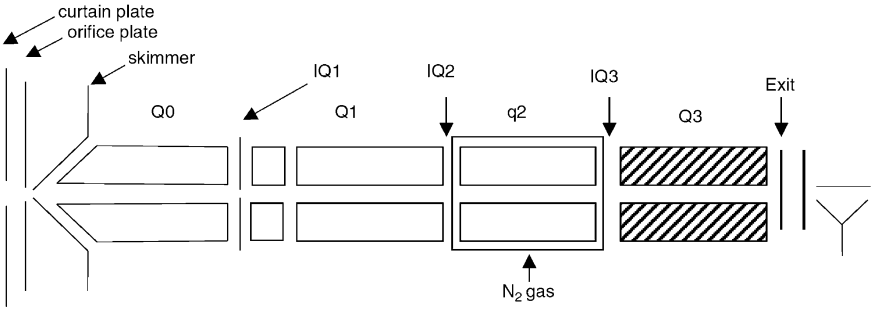


Fig. 9.22. Sequence of ESI-CID-QIT mass spectra of a beauverolide: (**a**) MS^2 of $[M+H]^+$, *m/z* 488, selected out of a full scan spectrum, (**b**) MS^3 of *m/z* 375 selected from (**a**), and (**c**) MS^4 of *m/z* 304 selected from (**b**). Adapted from Ref. [114] by permission. © John Wiley & Sons, 2001.

Note: In contrast to tandem-in-space instruments, tandem-in-time instruments neither support precursor ion nor constant neutral loss scanning. While product ion scans just need a precursor to be isolated prior to its fragmentation, both precursor ion and constant neutral loss scan rely on the simultaneous application of selection plus scanning or double scanning, respectively. Fulfilling two criteria at the same time requires two distinct analyzers at work.

9.9 Tandem MS with Linear Quadrupole Ion Traps

Mass spectrometers incorporating a linear quadrupole ion trap are highly flexible instruments. As discussed in Chap. 4.5, there are two competing concepts available on the market, one employing a LIT with axial ejection as part of a hybrid instrument [115], and another, featuring a pure LIT design with radial ejection [116,117].



Scan Type	Q1	q2	Q3
Q1 Scan	Resolving (Scan)	RF-only	RF-only
Q3 Scan	RF-only	RF-only	Resolving (Scan)
Product Ion Scan (PIS)	Resolving (Fixed)	Fragment	Resolving (Scan)
Precursor Ion Scan (PI)	Resolving (Scan)	Fragment	Resolving (Fixed)
Neutral Loss Scan (NL)	Resolving (Scan)	Fragment	Resolving (Scan Offset)
Selected Reaction Monitoring mode (SRM)	Resolving (Fixed)	Fragment	Resolving (Fixed)
Enhanced Product Ion (EPI)	Resolving (Fixed)	Fragment	Trap/scan
MS3	Resolving (Fixed)	Fragment	Isolation/frag trap/scan
Time delayed frag capture Product Ion (TDF)	Resolving (Fixed)	Trap/No frag	Frag/trap/scan
Enhanced Q3 Single MS (EMS)	RF-only	No frag	Trap/scan
Enhanced Resolution Q3 Single MS (ERMS)	RF-only	No frag	Trap/scan
Enhanced Multiply Charge (EMC)	RF-only	No frag	Trap/empty/scan

Fig. 9.23. Correlation of the instrumental setup of a QqLIT instrument (Applied Biosystems Q-Trap series) with the description of its various scan modes. The *upper part* of the table lists scan modes that are identical to triple quadrupole instruments, whereas the *lower part* contains those unique to the specific instrument design. Reproduced from Ref. [115] with permission. © John Wiley and Sons, Ltd., 2003.

9.9.1 Tandem MS on QqLIT Instruments

The QqLIT design basically presents a triple quadrupole instrument having Q3 exchanged for a linear ion trap. As such, it offers all scan modes and properties typical for QqQ instruments (Chap. 9.7) plus those additional ones that are enabled by the LIT, i.e., higher-order tandem MS and combinations of ion accumulation and subsequent scanning for enhanced sensitivity (Fig. 9.23) [115,118-120].

Example: The fragmentation pathways of ions of Trocade™, an antirheumatoid drug, $[trocade+H]^+$, *m/z* 437, were elucidated by sequential tandem MS up to MS^4 on a QqLIT instrument (Fig. 9.24). The protonated molecule first eliminates hydroxylamine, 33 u, to yield the acylium ion fragment at *m/z* 404, which in turn cleaves off the imidazolidinedione substituent at the α-carbon prior to loss of CO from the fragment ion at *m/z* 262 [115].

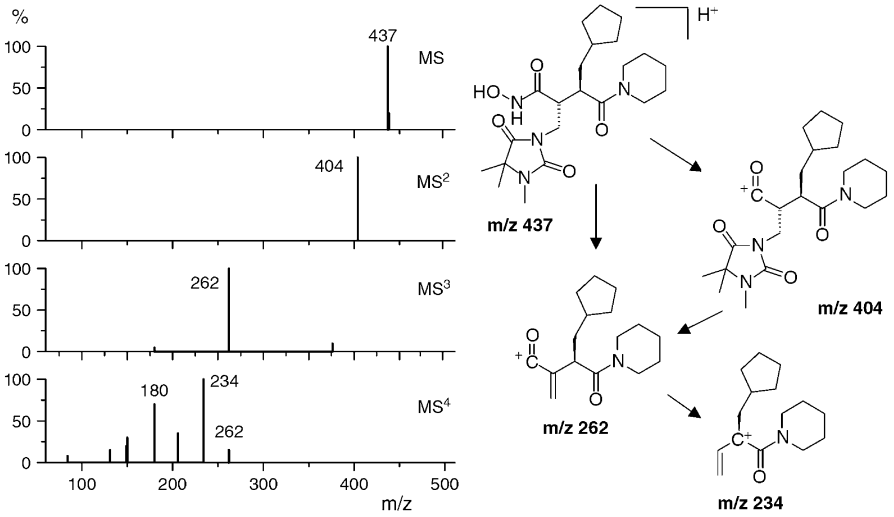


Fig. 9.24. Fragmentation pathways of $[trocade+H]^+$ ions, *m/z* 437, as elucidated by sequential tandem mass spectrometry up to MS^4 on a QqLIT instrument. Adapted from Ref. [115] with permission. © John Wiley and Sons, Ltd., 2003.

9.9.2 Tandem MS on LITs with Radial Ejection

A single LIT alone offers tandem MS along the tandem-in-time route. Improved trapping efficiency, more effective fragmentation, and trapping can be achieved when the LIT is operated with a higher buffer gas pressure, while higher scan rates and resolving power are obtained at lower pressure. The recent *dual-LIT* design introduced by the Thermo Fisher LTQ Velos™ series unites these requirements by operating two identical LITs in tandem that are connected to the same RF and auxiliary AC power supplies, whereas the DC offset for trapping is delivered sepa-

rately. Admission of the helium buffer gas into the high-pressure LIT allows to reduce its pressure in the neighboring mass-analyzing LIT (Fig. 9.25) [116]. The functional separation between the LITs not only allows to maintain unit resolution up to a scan rate of 33,000 u s^{-1}, it also more than doubles resolving power of the single-LIT version up to 25,000 when operated at very slow scan rates over a narrow *m/z* range. Such a dual-LIT design has also been incorporated in other hybrid instruments of this manufacturer that make use of LITs as MS1 (LTQ-Orbitrap Velos™ [121], LTQ-FT Velos™).

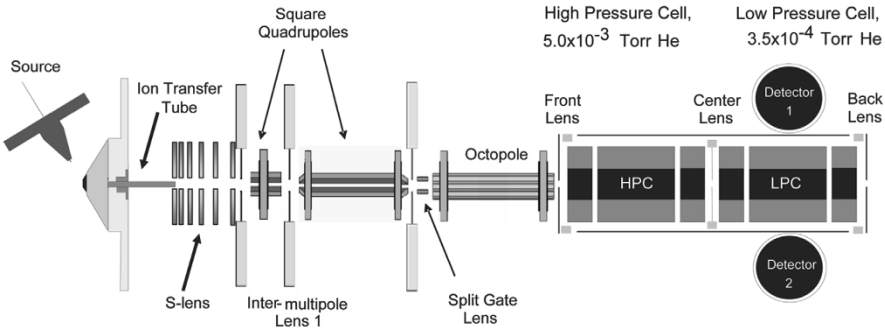


Fig. 9.25. The Thermo Fisher LTQ Velos instruments have a dual linear ion trap, the first section of which is operated at higher pressure (HPC), the second is run at lower pressure to achieve better resolving power (LPC). The dual LIT design also increases the speed of operation, because the first LIT can already prepare ions for the second while this is still mass-analyzing fragments from the previous cycle. Reprinted from Ref. [116] with permission. © American Chemical Society, 2009.

Note: With the introduction of QqLIT and dual-LIT instruments, even the concepts of tandem-in-space and tandem-in-time MS start to intermingle, because both tandem characteristics are part of each of these instruments. Once more, this demonstrates the ongoing highly dynamic development of mass spectrometry instrumentation.

9.10 Tandem MS with Orbitrap Instruments

The orbitrap analyzer itself does not provide for a mode of tandem MS operation. Instead, the steps of precursor ion isolation and dissociation are performed in a dedicated LIT as MS1 (Chap. 4.8.4) prior to high-resolution and accurate mass analysis of the fragments by the orbitrap. Multiple-collision CID (Chap. 9.3) in the LIT of the LTQ-orbitrap instrument is sometimes not hard enough to achieve fragmentation of comparatively stable precursor ions, e.g., it can be insufficient to generate immonium ion fragments from protonated peptides.

9.10.1 Higher-Energy C-Trap Dissociation

One approach towards harsher CID is to use the C-trap as a collision cell simply by raising the RF voltage from the standard setting of 1500 V peak-to-peak to 2500 V. The nitrogen present at about 1.3×10^{-3} mbar is sufficient to serve as the collision gas. After several oscillations, most of the precursor ions have undergone dissociating fragmentation, and all ions accumulate in the middle of the C-trap being confined by voltages on the gate aperture and trapping plate. This procedure has been termed *higher-energy C-trap dissociation* (HCD, Fig. 9.26a) [122]. An increase in RF voltage of the C-trap unfortunately goes along with a decrease in the *m/z* range that can be stored simultaneously in the C-trap.

These disadvantages are avoided by attaching an RF-only octopole collision cell with nitrogen at 5 mbar to the back end of the C-trap. To use this collision cell the C-trap passes through the ions from the LIT rather than ejecting them directly into the orbitrap. This octopole collision cell provides fragment trapping over a wide *m/z* range. The fragments generated are then filled back into the C-trap, thermalized, and transferred into the orbitrap for final *m/z* analysis (Fig. 9.26b) [122]. Such an instrument geometry is being offered as LTQ-orbitrapXL™.

Example: Peptide ions, $[HLVDEPQNLIK+2H]^{2+}$, *m/z* 653.36, were selected as precursor ions, accumulated and isolated in the LIT until 10^5 ions were reached. With HCD setup (**a**) spectrum (**c**) was obtained. Using the dedicated octopole collision cell as depicted in (**b**) delivered the spectrum shown as (**d**) that exhibits stronger and more fragment ion signals in the lower *m/z* range. In particular, the immonium fragment ion of histidine can be observed at *m/z* 110 (Fig. 9.26) [123].

9.10.2 Extended LIT-Orbitrap Hybrid Instruments

It makes sense to extend the HCD geometry towards the dual-LIT MS1 to arrive at an advanced hybrid instrument design that combines MS^n in several modes with a powerful final *m/z* analysis [121]. Such an instrument has become available in the form of the Thermo Scientific LTQ Orbitrap Velos (Fig. 9.27). One of the most important advantages of this instrumentation is speed for proteomics analysis, e.g., within 1.0 s the dual-LIT can deliver five complete tandem mass spectra simultaneously with the orbitrap running one high-resolution accurate mass scan of the whole *m/z* range.

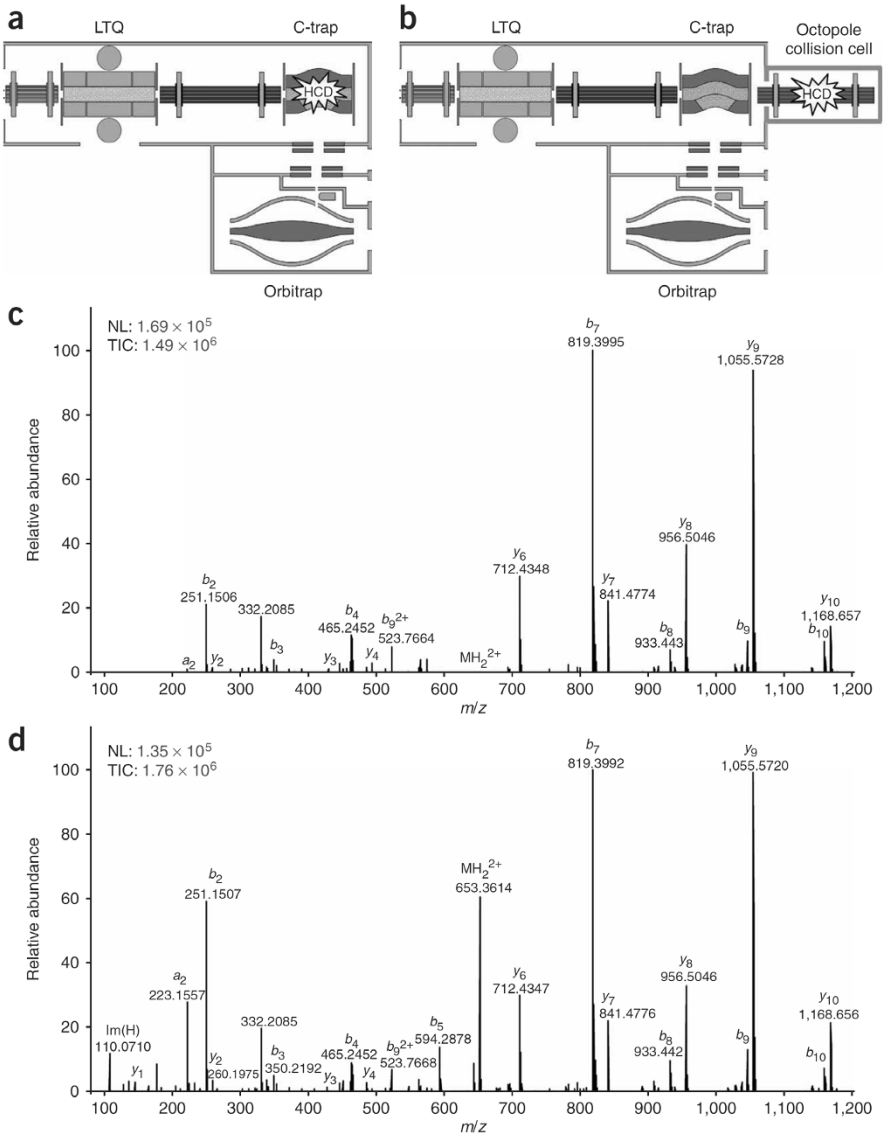


Fig. 9.26. Schematic of the hybrid LIT–orbitrap instrument indicating the electrostatic potentials used in HCD and comparison of CID spectra. (**a**) HCD operation of the C-trap; (**b**) with octopole collision cell; (**c**) CID spectrum of peptide $[HLVDEPQNLIK+2H]^{2+}$ ions from HCD as in (**a**); (**d**) spectrum as obtained by setup (**b**). NL: intensity in counts normalized to 1 s; TIC: total ion current. Reproduced from Ref. [123] with permission. © Nature Publishing Group, London, 2007.

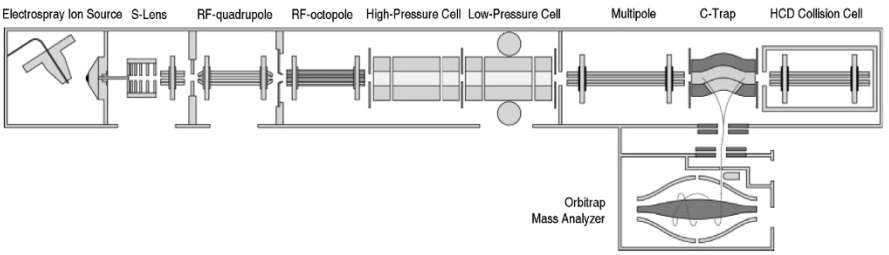


Fig. 9.27. Schematic of the Thermo Scientific LTQ Orbitrap Velos hybrid FT mass spectrometer combining dual-LIT and HCD with an Orbitrap mass analyzer. Courtesy of Thermo Fisher Scientific, Bremen.

9.11 Tandem MS with FT-ICR Instruments – Part I

As ion trapping devices, FT-ICR instruments belong to the *tandem-in-time* category of instruments. The stage of precursor ion selection (MS1) is accomplished by selectively storing the ions of interest, whereas all others are ejected by means of a suitably tailored excitation pulse. For this purpose, the SWIFT technique [124] or *correlated sweep excitation* (CHEF) [125,126] are used (Chap. 4.7.7). Both methods generate tailored waveforms that cause excitation of all but the selected ions. Like QITs and LITs, FT-ICR analyzers are also capable of MS^n.

Although hybrid designs such as Qh-FT-ICR or LIT-FT-ICR are prevalent in modern FT-ICR instrumentation (Chaps. 4.7.11 and 4.9.1), there is still the need for tandem MS experiments inside the ICR cell. Its dedicated abilities of very precise precursor ion selection, elongated ion storage in the order of tens of seconds, and possibility to admit gaseous reactants to perform even slow ion-molecule reactions make the ICR cell a unique tool [3].

9.11.1 Sustained Off-Resonance Irradiation-CID in ICR Cells

CID still is widely used as an activation technique for tandem MS in FT-ICR instruments. The collision gas is admitted into the ICR cell through a pulsed valve. To avoid detrimental effects of the collision gas on the ultra-high vacuum of the ICR cell ($\approx 10^{-10}$ mbar) the gas is admitted from a low pressure vessel (≈ 10 mbar) in short pulses (5–50 ms). This causes the cell pressure to rise to levels ($\approx 10^{-8}$ mbar) that do not compromise the resolving power of FT-ICR in a noteworthy manner. To further reduce the interference with collision gas, a pump delay (1–5 s) can be inserted between CID and *m/z* analysis. Generally, a set of such cycles is accumulated to obtain a spectrum.

For effective dissociation CID requires that the ions collide sufficiently fast with the collision gas. The increase in ion kinetic energy is classically effected by short (0.1–0.5 ms) excitation at the cyclotron frequency of the precursor ion

[127,128]. This is known as *resonance excitation* (RE). The uptake of kinetic energy by resonance excitation occurs very fast, and thus, care has to be taken to avoid ion ejection from the cell. On the other hand, RE offers access to fragmentation channels requiring comparatively high activation energy.

Nowadays, *sustained off-resonance irradiation* (SORI) has established as the standard CID method in FT-ICR [129,130], although there are others of comparable effect [131,132]. Irradiating slightly off resonance ($\Delta\nu \approx 1\%$ or 500–1500 Hz) makes ions undergo acceleration–deceleration cycles throughout the duration of the RF pulse (Fig. 9.28). The principle behind off-resonance irradiation is the occurrence of a beat frequency f_b induced by the alternating positive and negative interference of cyclotron frequency f_c and excitation frequency f_{exc} as given by

$$f_b = f_{exc} - f_c \tag{9.18}$$

As a consequence, the orbit does not exceed the cell dimensions but still maintains a high average translational energy for an extended activation period during which only small increments of internal energy are transferred to the ions. The ions can therefore be irradiated for a sustained period (0.1–1 s) without causing ejection, that otherwise at f_c was unavoidable. SORI-CID results in sequential activation of ions by multiple collisions of low (< 10 eV) kinetic energy ions with the collision gas, i.e., SORI-CID exploits slow internal heating of the ions [133]. Hence, SORI-CID addresses those fragmentation routes requiring rather low activation energy but benefit from sufficient reaction time.

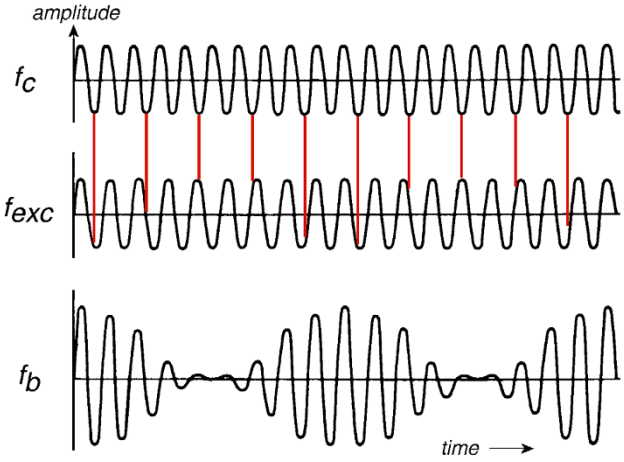


Fig. 9.28. Generation of an oscillation of ion kinetic energy as defined by a beat frequency due to off-resonance excitation; vertical connections are to locate points of positive and negative interferences, respectively. The larger the amplitude of f_b the more kinetic energy is contained in the circulating ions. One SORI-CID experiment consists of hundreds of beats.

Note: Both, RE-CID and SORI-CID are highly selective in precursor ion *m/z*, and therefore, activate only the precursor ion itself, normally even just a selected isotopolog. As a result, special pulse shapes are required to achieve activation of all isotopologs to preserve isotopic information in the fragment ion spectra. Furthermore, the high *m/z* selectivity causes only the precursor ion to dissociate while fragment ions do not receive any further energy to trigger second-generation cleavages.

Example: MALDI-SORI-FT-ICR spectra of the 2-aminobenzamide derivative of an unknown oligosaccharide were used for structure elucidation. First, the $[M+Na]^+$ ion, *m/z* 1240.5, was selected and fragmented (MS^2, Fig. 9.29a), then selected fragments thereof were subjected to further dissociation; to illustrate the principle, only one of these has been included here (MS^3, Fig. 9.29b). The frequency for SORI was chosen at 1.5% distant from the respective precursor ion's cyclotron frequency and supplied with an amplitude V_{SORI} = 10 V [133].

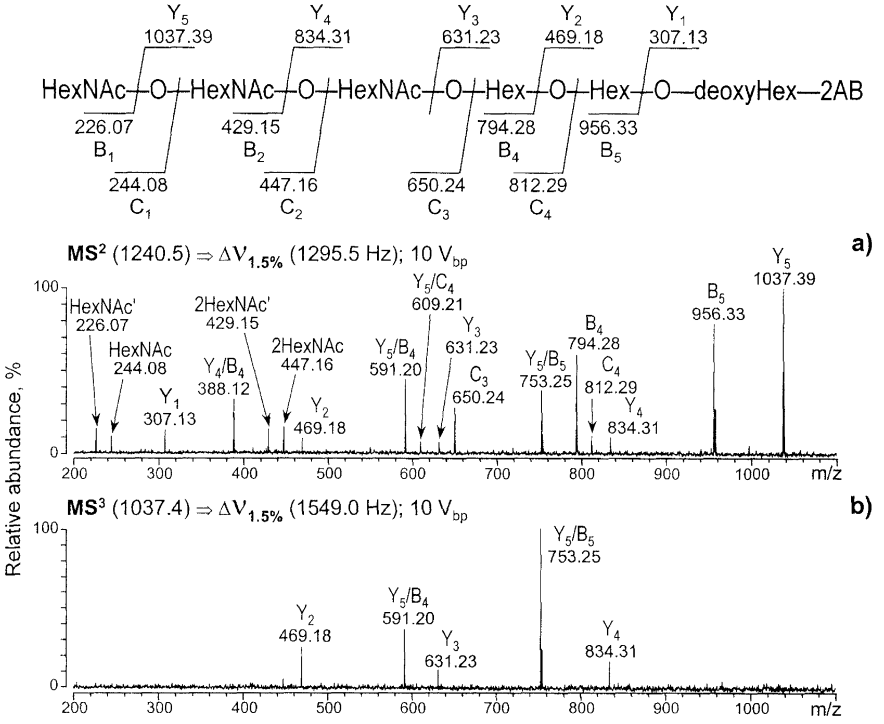


Fig. 9.29. MALDI-SORI-FT-ICR spectra of the $[M+Na]^+$ ion, *m/z* 1240.5, of the 2-aminobenzamide derivative of an unknown oligosaccharide (MS^2, **a**), and of the fragment at *m/z* 1037.4 obtained thereof (MS^3, **b**). Adapted from Ref. [134] with permission. © Elsevier Science Publishers, 2002.

Note: CID can rather easily be implemented on FT-ICR instruments because it only demands for a pulse valve and a reservoir. Although the collision gas in SORI-CID can be easily handled, its use is nonetheless in contradiction to the high vacuum requirements of the ICR cell. Thus, alternative ion activation techniques without the use of gas are desirable.

9.12 Infrared Multiphoton Dissociation

The energy received from multiple photon absorption may also be used to activate and dissociate otherwise stable gaseous ions [135]:

$$m_1^+ + x \times h\nu \rightarrow m_2^+ + n \tag{9.19}$$

Infrared multiphoton dissociation (IRMPD) was first described along with the dissociation of weakly bound protonated diethylether cluster ions [135]:

$$[(Et_2O)_2+H]^+ + x\ h\nu \rightarrow [Et_2O+H]^+ + Et_2O \tag{9.20}$$

IRMPD is a technique that can be conveniently applied to trapped ions as is the case in ICR cells. IRMPD normally employs a continuous wave carbon dioxide laser of 10.6 μm wavelength (2.83×10^{13} Hz) having a power of 25–40 W which is passed into the ICR cell through a ZnSe or BaF_2 window [136,137]. It is advantageous to combine FT-ICR with IRMPD because the amount of energy applied to the ions can be varied via the duration of laser irradiation, typically in the range of 5–300 ms [138]. This allows for the application of IRMPD to small ions [135] as well as to medium-sized [138] or high-mass ions [137].

Absorption of photon energy by a single normal mode of the ion is usually followed by dissipation among other vibrational modes, i.e., by *intramolecular vibrational relaxation* (IVR). The initial absorbing mode thereby returns to its ground state and gets ready to absorb another IR photon and so on (Fig. 9.30) [139]. IRMPD is regarded as a *slow heating method* because a large number of IR photons must be absorbed to effect fragmentation. In case of the usual carbon dioxide laser the energy of a single photon is just 0.116 eV, i.e., per electronvolt the absorption of 9 photons is required [140,141].

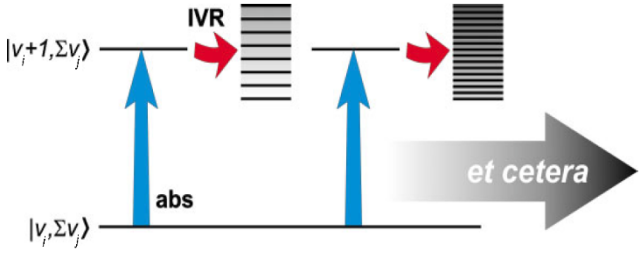


Fig. 9.30. IRMPD mechanism involving intramolecular vibrational relaxation (IVR). Reproduced from Ref. [139] with permission. © John Wiley Periodicals, Inc., 2009.

Note: For IRMPD, care must be taken to block the IR laser from abandoning its assigned optical path. The IR laser is extremely powerful and can instantaneously ignite objects or cause injuries from burns.

9.12.1 IRMPD in QITs and LITs

IRMPD is a valuable tool for gas phase ion studies and analytical applications which often do not necessarily require the full power of an extremely expensive FT-ICR instrument. Therefore, attempts have been made to apply IRMPD on three-dimensional (Fig. 9.33) [140,141] and linear quadrupole ion traps [142-144]. Due to the slow heating of ions, collisional cooling by the buffer gas required for quadrupole ion trap operation is counteracting the accumulation of ion internal energy. To circumvent this problem a dynamic pressure operation mode has been developed for IRMPD in QITs where initial ion storage and precursor ion selection are run at standard QIT pressure (3×10^{-2} mbar) while the buffer gas flow is interrupted several milliseconds prior to IRMPD ($< 10^{-4}$ mbar) and subsequent product ion scanning [141].

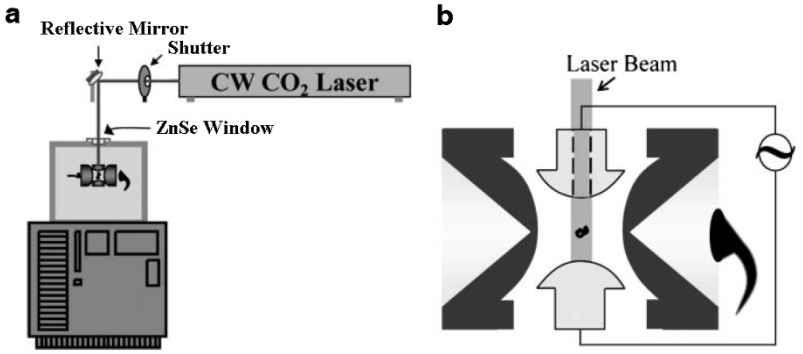


Fig. 9.31. IRMPD in a quadrupole ion trap; (**a**) relative to the entire instrument and (**b**) beam passage through a hole in the end cap electrodes of the QIT. Reproduced from Ref. [140] with permission. © John Wiley Periodicals, 2009.

9.13 Electron Capture Dissociation

9.13.1 Principles of Electron Capture Dissociation

For an ion, the cross section for *electron capture* (EC) roughly increases with the square of the ionic charge [145]. This makes multiply charged ions as produced by *electrospray ionization* (ESI, Chap. 12) the ideal targets for this process. When a UV laser of 193 nm wavelength (6.4 eV per photon) in the course of *ultraviolet photon dissociation* (UVPD) experiments erroneously hit a metal surface, elec-

trons were deliberated inside the ICR cell. Electron capture by the formed multiply charged protein ions shifted their charge state from 11^+ to 10^+ without affecting mass [145]:

$$[M+11H]^{11+} + e^- \rightarrow [M+11H]^{10+\bullet} \quad (9.21)$$

The product of EC is a radical ion (Fig. 9.34). The energy from neutralization of one ionic charge (5–7 eV) is transformed into ion internal energy that causes immediate fragmentation, so-called *electron capture dissociation* (ECD).

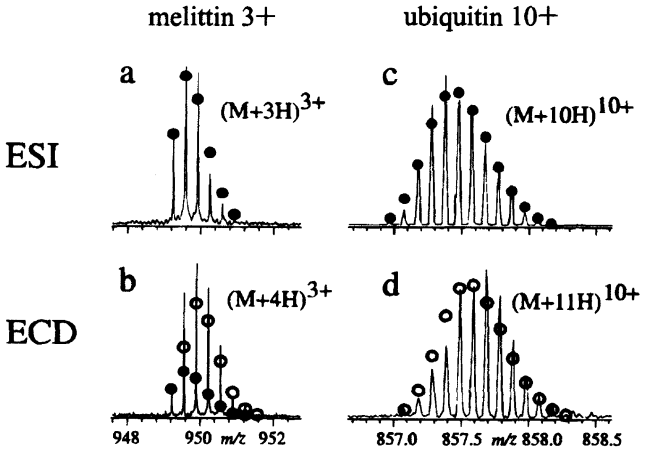


Fig. 9.32. Discovery of ECD by comparison of electrospray ionization (ESI) mass spectra of protein ions with those obtained when the UV laser was switched on to generate thermal electrons from the inner walls of the ICR cell. *Closed circles* mark the theoretically predicted isotopic abundances for the closed-shell ions of n^+ charge state, while *open circles* show those for the $(n-1)^{+\bullet}$ radical ions. The experimental patterns clearly show superimpositions of both. Reproduced from Ref. [145] with permission. © American Chemical Society, 1998.

Again, ECD is a technique for trapped ions only. To effectively achieve ECD the electrons must have energies < 0.2 eV. Therefore, they are supplied analogously to EI from a carefully regulated heated filament [146] externally mounted to the ICR cell. Although a rather recent discovery [145,147], ECD is now widely applied in biomolecule sequencing by means of ESI-FT-ICR-MS [146,148]. The motivation for those numerous ECD applications is due to the fact that ECD yields information complementary to CID [149] and IRMPD [136].

Note: As one electron charge is neutralized upon EC, the precursor ion for ECD must at least be a doubly charged positive even-electron ion to yield a singly charged radical ion for subsequent dissociation.

9.13.2 Peptide Ion Cleavages Upon ECD

In contrast to the prevalent generation of *b*- and *y*-type fragment ions from slow-heating activation methods, the fragmentation patterns in ECD contain mostly *c*- and *z*-type ions. These are generated by cleavage of an amine bond ($N–C_\alpha$ bond cleavage). Assuming a peptide ion $[M+zH]^{z+}$ having a lysine (Lys) residue, one can write the mechanism of ECD-induced peptide cleavage as depicted in Fig. 9.33 [150].

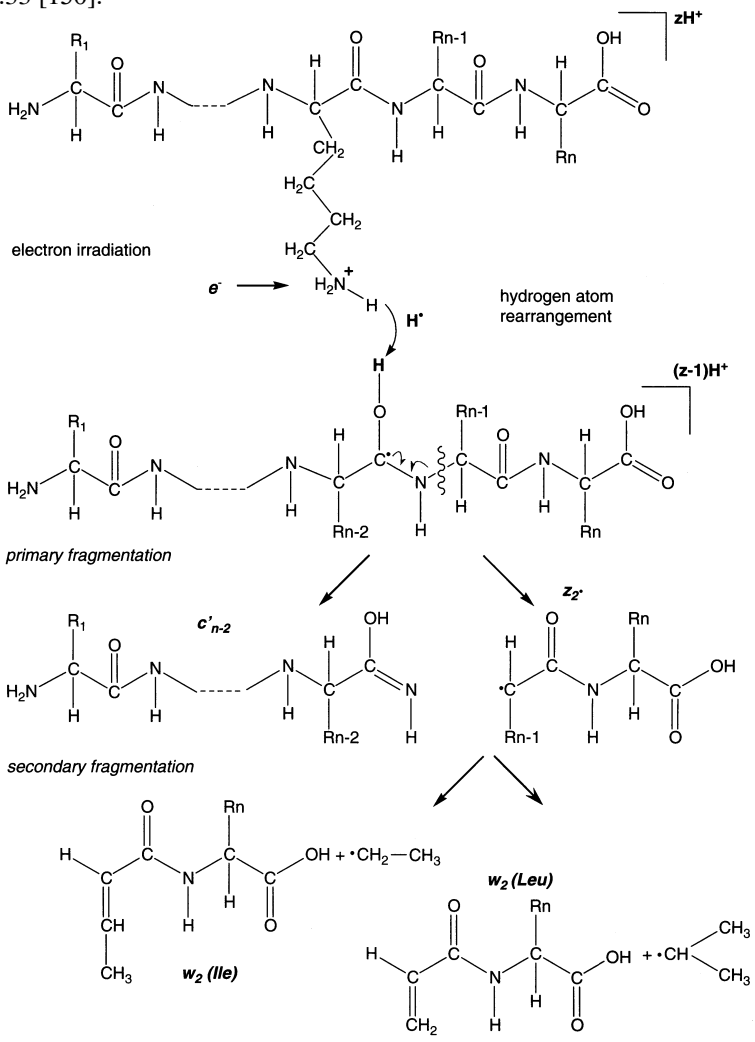


Fig. 9.33. Mechanism of fragmentation upon ECD following the hot hydrogen atom model. Here, a protonated lysine residue captures the electron and immediately transfers a hydrogen atom to its neighboring carbonyl-O. Primary and secondary fragmentation pathways of the ions are shown. Adapted from Ref. [150] by permission. © John Wiley & Sons, 2004.

This scheme follows the most widely used model for the ECD mechanism, the so-called *hot hydrogen atom model*, which states that the electron is captured in a high Rydberg state by action of a charged site in the ion. Typically, the charges reside on basic amino acid residues, i.e., on arginine (Arg), lysine (Lys), or histidine (His), or on *N*-terminal amino groups. The primary odd-electron ion immediately cleaves off a hydrogen radical by N–H bond cleavage, thereby creating a hydrogen atom with an excess energy of about 6 eV. This "hot" hydrogen atom may be transferred along the peptide chain to any amide carbonyl group or to disulfide groups [151,152]. Now, one of the electrons of the carbonyl-carbon atom is unpaired. Due to the excess energy this radical can dissociate by N–C_α bond cleavage. Thus, the amine-terminal peptide fragments are forming *c*-type fragment ions while the carboxylate-terminal fragments belong to the *z*-type fragment ion series.

The mechanism of peptide fragmentation upon ECD is still a matter of debate [152-154]. In particular, there is a discussion as to whether the ECD process is *nonergodic* (so fast that there is no internal equilibration of energy prior to dissociation) [145,147] or ergodic (following QET) [154].

Note: Peptide fragments formed after transfer of a hydrogen (atom) are marked by a prime after the letter, e.g., the fragments from ECD are *c*' and *z*' ions [152].

9.14 Tandem MS with FT-ICR Instruments – Part II

As obvious from the preceding pages, both IRMPD and ECD are intimately connected with FT-ICR instrumentation. Now having considered these methods for ion activation in some detail we may focus our attention on their practical realization on the FT-ICR platform and some illustrative applications.

9.14.1 IRMPD for Tandem FT-ICR-MS

IRMPD is optionally available on most commercial FT-ICR instruments. The absence of a collision gas preserves the ultra-high vacuum and circumvents time-consuming pump delays in the sequence of an experiment.

Example: Gangliosides such as GM1 contain a hydrophobic ceramide moiety that consists of sphingosine, a long-chain amino alcohol, which is acylated with a fatty acid on the amino group. The molecule has a polar oligosaccharide head that contains sialic acid. GM1 exists as two isomeric forms, GM1a and GM1b, differing in that the sialic acid is in branched or terminal position, respectively. The negative-ion IRMPD (200 ms, 14 W, 100 scans) spectrum of doubly deprotonated ganglioside GM1, $[M–2H]^{2–}$, exhibits a cleavage within the ceramide moiety that causes loss of the fatty acid. The presence of GM1b as a minor component is evident from *i*) the fragment ion peak at *m/z* 1091.722, which corresponds to a loss of

the disaccharide HexNeuAc' from the precursor and *ii*) its complementary peak at *m/z* 452.141 due to the disaccharide (Fig. 9.34) [155].

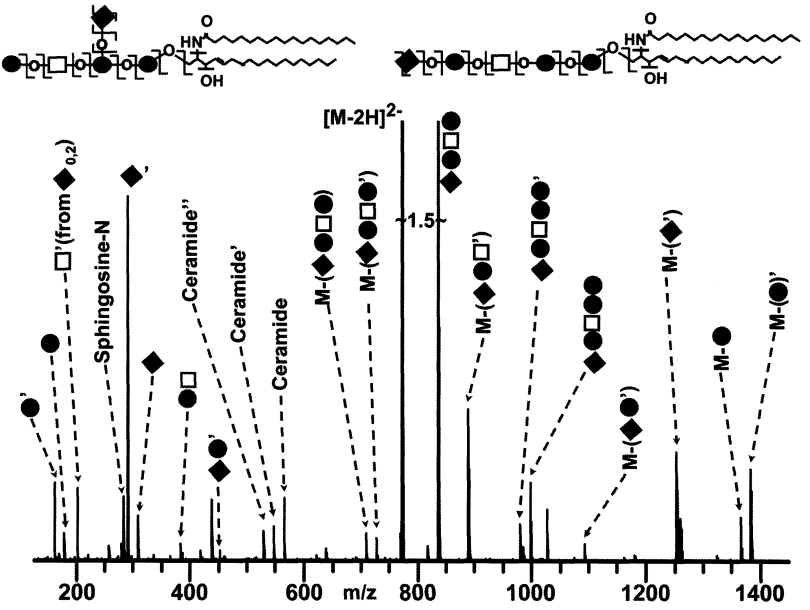


Fig. 9.34. IRMPD (200 ms, 14 W, 100 scans) spectrum of doubly deprotonated ganglioside GM1, $[M–2H]^{2–}$, occurring in two isomeric forms. Reproduced from Ref. [155] with permission. © Elsevier Science Publishers, 2005.

9.14.2 Infrared Photodissociation Spectroscopy

Provided a tunable laser light source is available, the IRMPD experiment can be performed in a wavelength-dependent manner to reveal the absorption characteristics of gaseous ions. Different from IR spectroscopy of condensed phase samples, in mass spectrometry the occurrence of IR absorption is observed by detection of specific fragment ions and their abundances as a function of laser wavelength. This technique is known as *infrared photodissociation spectroscopy* (IRPD) [139,156].

Unfortunately, powerful IR lasers tunable over a significant frequency range are difficult to obtain. Currently, the most effective but highly demanding approach to this end is represented by the *free-electron laser* (FEL). FEL facilities are limited and offer access for researchers to perform their experiments at dedicated ports on a tight schedule (Fig. 9.35). Alternatively, *optical parametric oscillator/amplifiers* (OPO/As) can serve as tunable IR light sources [139,156].

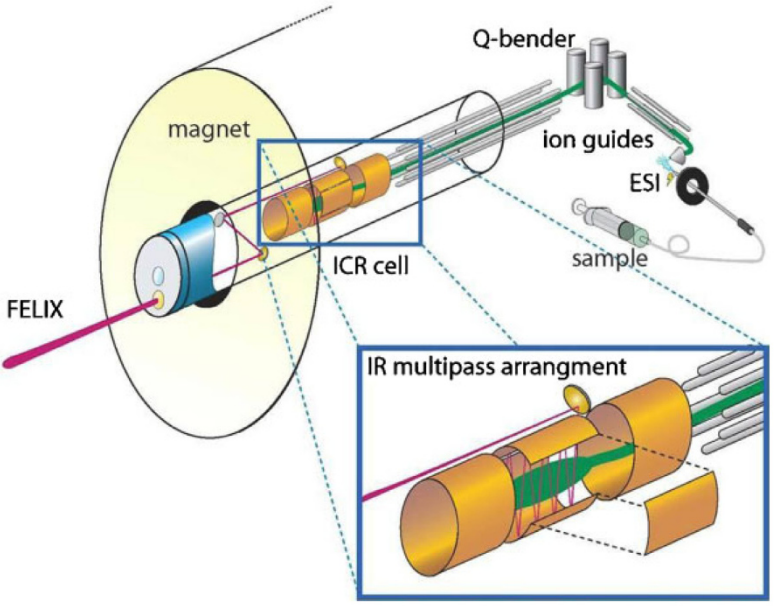


Fig. 9.35. Setup for infrared photodissociation spectroscopy. In this particular setup (FELIX at Utrecht, Netherlands) the light from a free-electron laser is guided into an open cylindrical ICR cell in a way that the IR light undergoes multiple reflections on the inner surfaces to extend its path for absorption by the ions inside the cell. Reproduced from Ref. [139] with permission. © John Wiley Periodicals, Inc., 2009.

9.14.3 Blackbody Infrared Radiative Dissociation

Even under essentially perfect vacuum where collisional activation is virtually absent ($< 10^{-9}$ mbar) ions can undergo slow unimolecular dissociation. As the energy for these fragmentations is provided by the emission of infrared photons by blackbody radiation of the vacuum housing, this process is termed *blackbody infrared radiative dissociation* (BIRD) [157]. Blackbody infrared radiation is always present above non-zero temperatures. BIRD dissociations are characterized by reaction times in the order of several seconds to even minutes. Therefore, ICR cells provide the most suitable environment for their study. To vary the wavelength and intensity of IR radiation both the ICR cell and the surrounding vacuum manifold have to be uniformly heated. Typically, temperatures up to about 250°C can be reached in dedicated instruments. This allows to study reaction kinetics where bonds of low to moderate strength are involved [157].

Note: Routine FT-ICR instruments are not suited for BIRD studies because of restrictions in heat resistance of electronic circuitry in proximity to the ICR cell and potential complications with the superconducting cryomagnet.

9.14.4 ECD for Tandem FT-ICR-MS

The implementation of ECD on ICR cells is nicely compatible with IRMPD. One approach uses a hollow cathode [158] instead of a filament to deliver the electrons. The hollow cathode offers a wider beam enlarging the volume where ECD can occur within the ICR cell. The IR laser then passes through the central hole – a setup that exerts some restrictions to the ICR radii where ions can interact with the laser beam. Several cathode designs are in use (Figs. 9.36 and 9.37) [159].

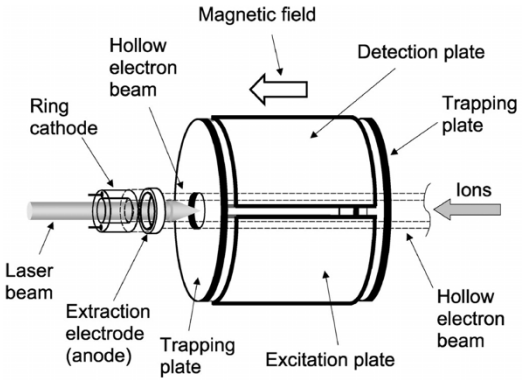


Fig. 9.36. Combined ECD and IRMPD setup for FT-ICR-MS. Reproduced from Ref. [159] by permission. © John Wiley & Sons, 2003.

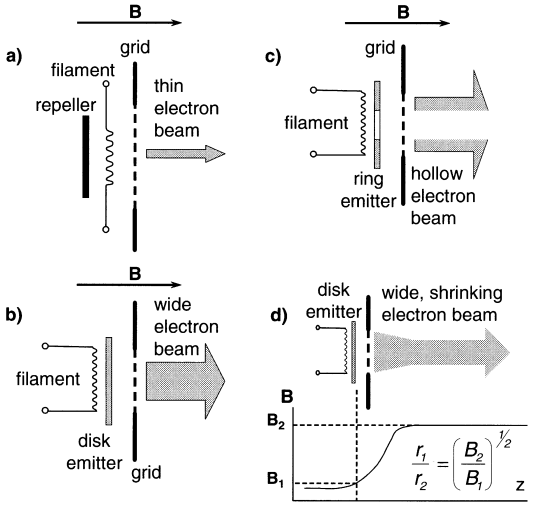


Fig. 9.37. Electron injection systems for ECD-FT-ICR instruments: (**a**) directly heated filament in homogeneous magnetic field, (**b**) disk-shaped indirectly heated cathode in homogeneous magnetic field, (**c**) ring-shaped indirectly heated cathode, and (**d**) cathode in fringing magnetic field region with beam collimation. Reproduced from Ref. [150] with permission. © John Wiley & Sons, Ltd., 2004.

Example: The direct bond cleavages upon ECD can be used to locate postranslational peptide modifications that would be disguised in CID or IRMPD spectra. The difference between CID and IRMPD on one side and ECD on the other arises from the loss of most posttranslational modifications prior to backbone cleavage to from *b*- and *y*-type ions, while in ECD the chain is immediately cleaved to yield *c*- and *z*-type ions, independent of the peptide sequence [160]. Thus, the neutral loss reflects the mass of the modification, e.g., additional 80 u (HPO_3) in case of the phosphorylation that can be identified to occur at the tyrosine of the peptide RLpYIFSCFR (Fig. 9.38) [150]. The opportunity to obtain complementary peptide sequence information is the reason why CID or IRMPD spectra are sometimes combined with ECD spectra for structure elucidation of peptides [136,149,161].

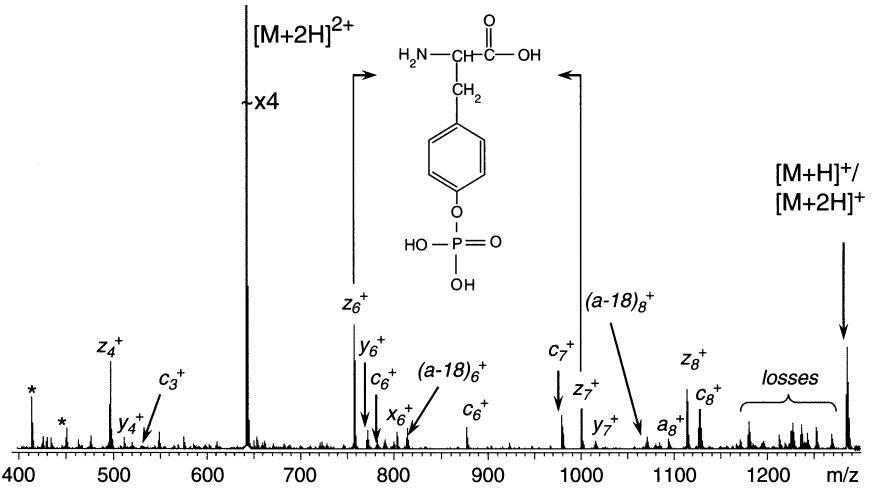
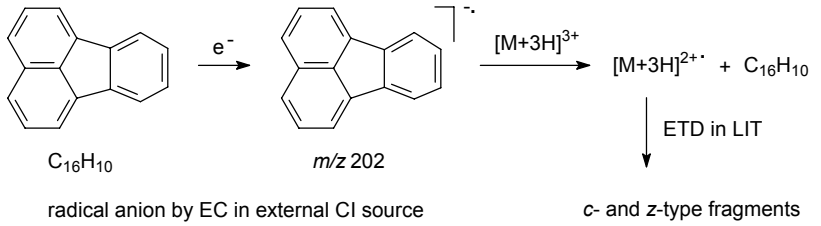


Fig. 9.38. Upon ECD, the $[M+2H]^{2+}$ ion of the peptide RLpYIFSCFR exhibits an increased mass difference of 80 u between its z_6^+ and z_7^+ fragments due to tyrosine phosphorylation. Adapted from Ref. [150] with permission. © John Wiley & Sons, Ltd., 2004.

9.15 Electron Transfer Dissociation

ECD can only take place in the ultra-high vacuum of FT-ICR mass spectrometers, while it is not possible to simultaneously store thermal electrons and peptide cations in quadrupole ion traps that utilize RF fields for ion manipulation and trapping. Furthermore, thermal electrons absorb energy from the RF field within milliseconds to become energetic. On the other hand, LITs can be operated as to store oppositely charged ions. Attempts for applying the advantages of ECD to LITs therefore make use of electron transfer via cation–anion reactions. In contrast to ECD, electron transfer may then occur at relatively high pressures ($\approx 10^{-3}$ mbar) [162]. This technique is termed *electron-transfer dissociation* (ETD) [160].

Anthracene radical anions as obtained by electron capture in a chemical ionization source with methane reagent gas were formerly employed as anions [160,163]. Meanwhile, fluoranthene has become more widely used (Scheme 9.1) [164,165].



Scheme 9.1

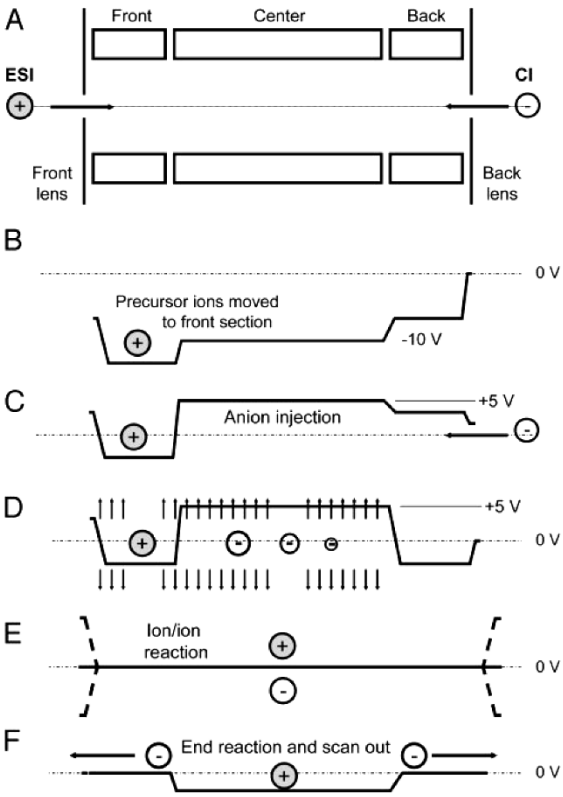


Fig. 9.39. Sequence of events to trap both positive peptide ions and reagent anions in a LIT, to react them, and to obtain an ETD spectrum showing the product ions. See text for discussion. Reproduced from Ref. [160] with permission. © The National Academy of Sciences of the USA, 2004.

Thus, ETD lends the capabilities of ECD to linear ion trap mass spectrometers. The individual steps involved in the operation of an LTQ instrument in ETD mode (Fig. 9.39) are: injection of multiply protonated peptides as delivered by an ESI source; application of a DC offset to store these ions in the front section of the LIT followed by injection of reagent anions from the CI source into the center of the LIT. Then all but the peptide precursor ions and the electron-donor reagent ions are ejected. Next the DC potential well is switched off and a secondary RF voltage is applied to the end lens plates of the LIT causing positive and negative ion populations to mix and react. The reaction period is ended by axial ejection of reagent anions while positive product ions are retained in the center section of the LIT. Finally, mass-selective radial ejection as usual yields the ETD spectrum [160]. The attractive ETD technique has also been implemented on LITs with axial ejection [144,166] and on LIT-orbitrap hybrids [167-169].

Unfortunately, ETD has limited applicability to doubly protonated peptide precursor ions, $[M+2H]^{2+}$, while triply protonated ions fragment to reveal the full sequence due to the higher exothermicity of the electron capture (Fig. 9.40) [162].

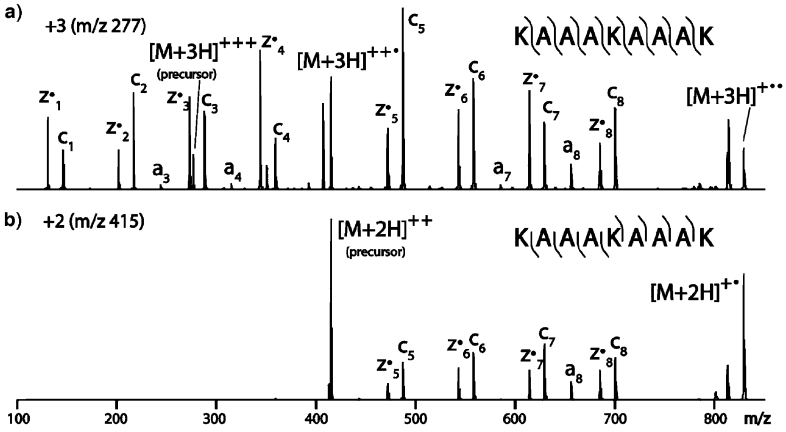


Fig. 9.40. Effect of precursor ion charge state on ETD product ion spectra of (**a**) the triply protonated peptide ion $[KAAAKAAAK+H]^{3+}$ and (**b**) the doubly protonated ion of the same peptide which only produces half of the possible *c*- and *z*-type fragments. Reproduced from Ref. [162] with permission. © American Chemical Society, 2007.

9.16 Electron Detachment Dissociation

Both ECD and ETD cause direct backbone cleavages in multiply positive peptide ions to deliver *c*- and *z*-type fragments which are highly informative for mass spectral sequencing. Especially when occurring more than once on a molecule, post-translational modifications like phosphorylation or sulfonation, reduce its tendency to form multiply protonated ions. Such analytes are best studied as negative ions, which are of course not amenable to ECD [170]. If the primary electrons

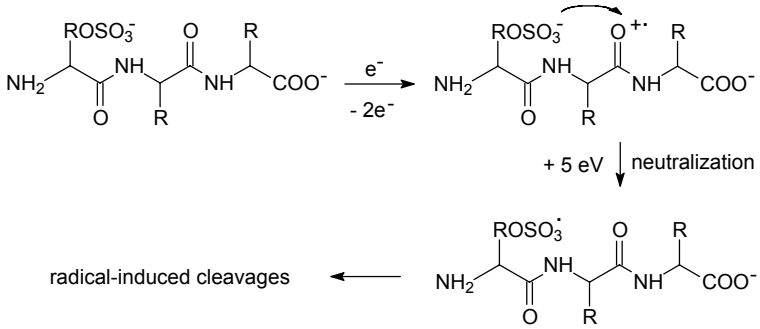
are energetic (about 20 eV) rather than thermal, there is a substantial chance to promote *electron detachment* from the anion [171]. In fact, the overall process can be regarded as electron ionization of an anion, which leads to formation of a neutral radical site (Chap. 6.3.1).

$$[M–nH]^{n-} + e^- \rightarrow [M–nH]^{(n-1)-\bullet} + 2e^- \quad (9.22)$$

Alternatively, electron ionization can occur anywhere along a polypeptide chain to locally form a positive radical ion that also may be regarded as an electron hole. This will attract an excess electron from one of the anionic sites of the ion and end up in mutual neutralization. The released energy effects electronic excitation, that, in turn, causes backbone cleavage [171]. This technique is termed *electron detachment dissociation* (EDD) [170-173].

EDD is not only useful for acidic peptides but also for oligonucleotides [174] and other analytes [152]. EDD has also been adapted to QITs [172]. Nonetheless, EDD is clearly less relevant in bioanalytical work than ECD or ETD.

A variation of EDD, termed *negative electron transfer dissociation* (NETD) employs fluoranthene, $C_{16}H_{10}^{+\bullet}$, or $Xe^{+\bullet}$ ions instead of energetic electrons to induce radical cationic sites by charge transfer rather than by electron ionization [175]. NETD yields selective backbone cleavage at the C_α–C bonds, similar to EDD, but leaves the phosphorylation sites intact, thereby enabling the localization of posttranslational modifications (PTMs).



Scheme 9.2

9.17 Summary of Ion Activation Techniques

Ideally, an all-purpose ion activation method would suffice to generate fragment ions for structure elucidation of any compound class. Moreover, the charge state of the precursor ion, its mass, and other characteristics would not interfere. In reality, however, no such method exists [162]. In case of peptides, for example, there is no single successful activation technique for delivering a sufficient number of sequence-informative product ions for sequence identification; instead, the amino acid composition and posttranslational modifications exhibit a strong influence on

the fragmentation pattern – justifying all the previous methods. Commonly available ion activation techniques are summarized and briefly described in Table 9.4 [31,176].

Table 9.4. Common ion activation techniques for tandem MS

Method	Instrumental platforms	Ionic charge and species accessible	Description and properties
CID	BE, ReTOF, TOF-TOF	+ / – precursor and fragments	collisions at keV-energies with inert gas. Several eV energy transfer in single collision within femtosecond
	QqQ, QqTOF, QqLIT etc.	+ / – precursor and fragments	tens of eV-collisions with inert gas. about eV energy transfer per collision; several events within about a millisecond
	FT-ICR	+ / – selected precursor only	some eV-collisions with inert gas; about eV energy transfer per collision; several events within a second
IRMPD	FT-ICR (QIT)	+ / – precursor and fragments	rather low-energy activation by IR laser; compatible with ECD
BIRD	FT-ICR	+ / – precursor and fragments	slow, low-energy activation by IR blackbody radiation close to equilibrium; to study kinetics and thermodynamics
ECD	FT-ICR	multiply + precursor and fragments	energy from partial neutralization by thermal electrons; extremely fast process causes radical ion cleavages
ETD	LIT and hybrids with LIT	multiply + precursor and fragments	energy from partial neutralization transferred by cation–anion reaction; result similar to ECD
EDD	FT-ICR	multiply – precursor and fragments	energy from partial neutralization delivered by electron detachment; results like “ECD for anions”

9.18 Special Applications of Tandem MS

Bimolecular reactions may take place when gaseous ions collide with neutrals at *thermal energy* rather than at multi- or even kiloelectronvolt energy. Proton transfer is one of the prominent representatives of an *ion-molecule reaction* in the gas phase. It is employed for the determination of *GB*s and *PA*s as described below. More sophisticated studies are enabled by reactions of gaseous ions with more complex reagents in the gas phase and the immediate mass spectral analysis of the reaction products [3].

9.18.1 Ion–Molecule Reactions in Catalytic Studies

The catalytic activities of a large pool of transition-metal carbene complexes have been screened by means of ion–molecule reactions in tandem-MS experiments [177-179]. Reactions of bare or solvated metal ions with organic molecules have been studied using mass spectrometers as reaction vessels [180-183]. In contrast to the concepts and methods discussed so far, the latter experiments are not designed to study the fundamentals of mass spectrometry. Instead, sophisticated methods of modern mass spectrometry are now employed to reveal the secrets of other complex chemical systems.

Example: Reaction of mass-selected $[Ni(H)(OH)]^+$ ions, *m/z* 76, with methane at 0 eV collision energy in the laboratory frame of reference yields a CH_2 insertion product, $[Ni(CH_3)(OH)]^+$, *m/z* 90. The experiments were carried out by using a QhQ mass spectrometer with an electrospray ion source. $[NiL]^+$ reactand ions were produced by ESI from solutions of NiL_2 (L = F, Cl, Br, I) in pure methanol and $[NiOH]^+$ ions from NiI_2 in H_2O. For the methane-activation study, the ions containing ^{58}Ni were mass selected in Q1 and reacted at thermal energy with methane in the RF-only hexapole at about 10^{-4} mbar. The ionic products were then detected by Q2 (Fig. 9.41) [183].

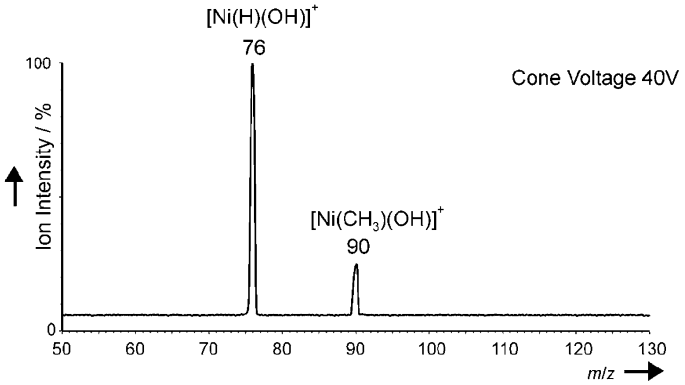


Fig. 9.41. Reaction of mass-selected $[Ni(H)(OH)]^+$ ions, *m/z* 76, with methane at 0 eV collision energy in the laboratory frame of reference yields a CH_2 insertion product, *m/z* 90. The cone voltage refers to the ESI conditions to produce optimum precursor ion abundance from Ni salt solutions. Reproduced from Ref. [183] with permission. © Wiley-VCH Verlag, Weinheim, 2007.

9.18.2 Gas Phase Hydrogen–Deuterium Exchange

Deuterium and other isotopic labeling prior to mass spectrometric analysis has been known from the early days of mass spectrometry (Chaps. 2.9 and 3.3). Modern methodology even allows labeling of gaseous ions, thereby yielding insight

into mechanistic details of reactions in a much more convenient way than by complicated synthetic routes. Furthermore, the gas phase exchange of hydrogen for deuterium can be applied to transient species that would otherwise remain inaccessible. So *hydrogen–deuterium exchange* (HDX) can be accomplished not only in solution (Chaps. 6, 7 in [184]), e.g., prior to analysis by electrospray ionization, but also in the gas phase. This is best achieved on ion traps of any kind as these provide extended and easily variable reaction times – circumstances that also enable kinetic studies.

Example: Gas phase HDX has been used to probe complete parent and fragment ion populations generated by CID of multiply charged protonated peptides [185]. The peptide ions were monoisotopically selected, dissociated by SORI-CID, and then subjected to HDX by repeated pulsed admission of CD_3OD to the ICR cell. Finally, the products were analyzed by FT-ICR-MS. HDX for variable reaction times revealed distinguished exchange kinetics for different types of ions, which allowed to deduce information on their structures. For example, *b*-type ions exhibited fast HDX while *a*-type ions showed only restricted exchange even at longer reaction times (Fig. 9.42) [185,186]. The observed exchange behavior was used to argue in favor of a oxazolone structure of the b_2 ions.

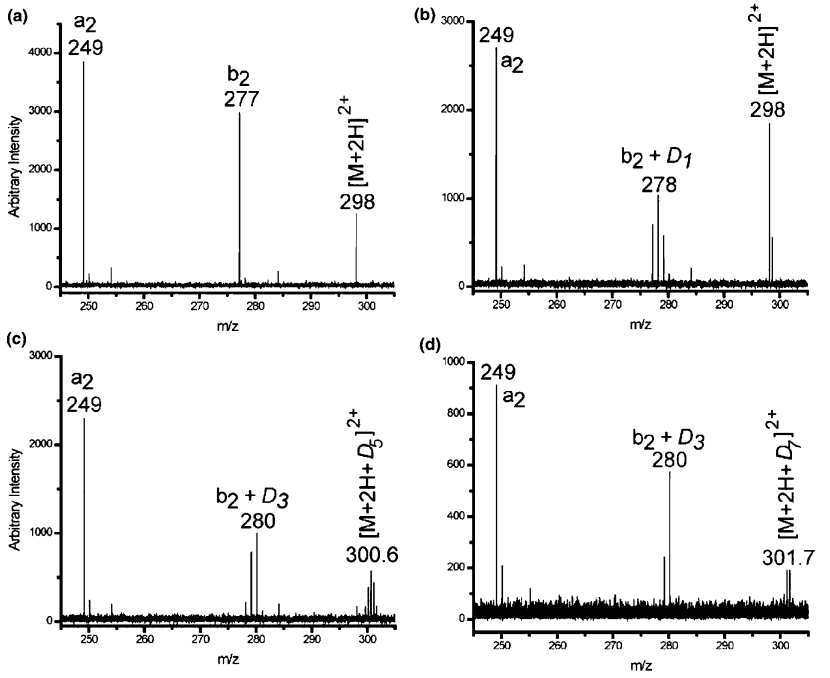


Fig. 9.42. The a_2-b_2 region of the product ion spectrum of doubly protonated YIGSR after (**a**) 0 s, (**b**) 1 s, (**c**) 10 s, and (**d**) 60 s gas phase HDX in an ICR cell. The uptake of deuterium is denoted by D_n in the formulas. Reproduced from Ref. [186] with permission. © Elsevier Science Publishers, 2009.

9.18.3 Determination of Gas Phase Basicities and Proton Affinities

The methods for the determination of *GB*s and *PA*s (Chap. 2.12) make use of their relation to K_{eq} (Eq. 9.23) and the shift of K_{eq} upon change of $[AH]^+$ or B, respectively [187,188]. Basically, the value of *GB* or *PA* is bracketed by measuring K_{eq} with a series of several reference bases ranging from lower to higher *GB* than the unknown. There are two methods we should address in brief, a detailed treatment of the topic being beyond the scope of the present book, however. The *kinetic method* makes use of the dissociation of proton-bound heterodimers, and the *thermokinetic method* determines the equilibrium constant of the acid-base reaction of gaseous ions. In general, proton transfer plays a crucial role in the formation of protonated molecules, e.g., in positive-ion chemical ionization mass spectrometry (Chap. 7).

The *kinetic method* [189-192] compares the relative rates of the competitive dissociations of a proton-bound adduct $[A–H–B]^+$ formed by admitting a mixture of A and B to a CI ion source [189,190]. There, the proton-bound adduct $[A–H–B]^+$ is generated amongst other products such as $[AH]^+$ and $[BH]^+$. Using standard tandem MS techniques, e.g., MIKES, the cluster ion $[A–H–B_{ref}]^+$ is selected and allowed to undergo metastable decomposition:

$$[AH]^+ + B_{ref} \leftarrow [A–H–B_{ref}]^+ \rightarrow A + [B_{ref}H]^+ \tag{9.23}$$

The relative intensities of the products $[AH]^+$ and $[B_{ref}H]^+$ are then used as a measure of relative rate constants of the competing reactions. In case the *PA* of the unknown was equal to that of the reference, both peaks would be of equal intensity. As this will almost never be the case, a series of reference bases is employed instead, and *PA* is determined by interpolation. The value of $PA_{(A)}$ is obtained from a plot of $\ln[AH]^+/[B_{ref}H]^+$ versus $PA_{(B)}$ at $\ln[AH]^+/[B_{ref}H]^+ = 0$.

The *thermokinetic method* [193,194] uses the measurement of the forward rate constant of the equilibrium

$$[AH]^+ + B_{ref} \rightleftharpoons A + [B_{ref}H]^+ \tag{9.24}$$

The thermokinetic method takes advantage of the correlation observed between k_{exp} and $\Delta G_2^{\,0}$ through the relationship

$$\frac{k_{exp}}{k_{coll}} = \frac{1}{1 + exp\left[\left(\Delta G_2^0 + \Delta G_a^0\right)/RT\right]} \tag{9.25}$$

where k_{coll} is the collision rate constant and $\Delta G_a^{\,0}$ a term close to *RT*. The *GB* of the unknown is then obtained from $\Delta G_2^{\,0} = GB - GB_{ref}$. The task to establish a proper value of the reaction efficiency $RE = k_{exp}/k_{coll}$, is solved by plotting the experimental values of *RE* versus $GB_{(B)}$ and interpolating these points with a parametric function. Although this can be done with high accuracy, it is still a matter of debate as to which value of *RE* yields the most realistic *GB*, suggestions being *RE* = 0.1–0.5 [187].

Example: *GB* and *PA* of cyclohexanecarboxamide were determined by both experimental methods. The kinetic method based on both metastable dissociation and CID yielded $GB = 862 \pm 7$ kJ mol^{-1} and $PA = 896 \pm 5$ kJ mol^{-1}, while the thermokinetic method gave $GB = 860 \pm 5$ kJ mol^{-1} and $PA = 891 \pm 5$ kJ mol^{-1}, i.e., both methods yield comparable results (Fig. 9.43).

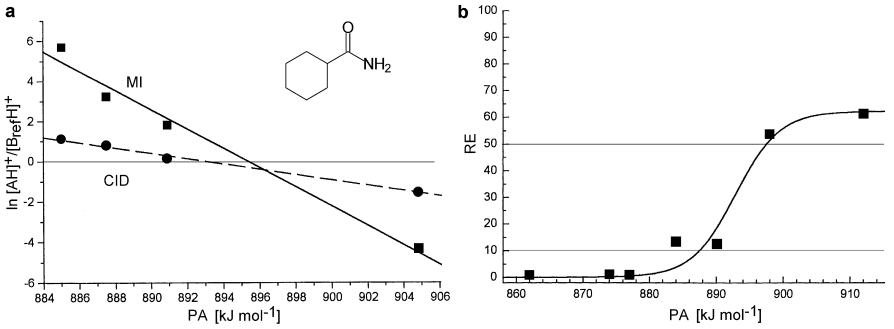


Fig. 9.43. Determination of the proton affinity of cyclohexanecarboxamide (**a**) by the kinetic method, and (**b**) by the thermokinetic method. The *horizontal lines* show the indicative values $\ln[AH]^+/[B_{ref}H]^+ = 0$ in (**a**) and *RE*s according to different authors in (**b**) [187]. Adapted from Ref. [195] by permission. © IM Publications, 2003.

9.18.4 Neutralization-Reionization Mass Spectrometry

In CID, charge exchange between the ions and the collision gas is an unwanted side reaction. However, it may become useful when employed in combination with a subsequent reionization step as in *neutralization-reionization mass spectrometry* (NR-MS) [196-204]. In NR-MS, the precursor ion of some kiloelectronvolts of kinetic energy is mass-selected in MS1 and passed through a first collision cell containing a reducing collision gas. A certain fraction of these ions will be reduced by charge exchange to become neutrals. As these neutrals basically retain their initial kinetic energy and direction, they leave the first collision cell along with the precursor ion beam. Remaining ions can then be removed from the beam by electrostatic deflection. Having traveled for some microseconds along a short path through the field-free region, the neutrals are subjected to ionizing collisions in a second collision cell. Finally, the mass spectrum of the reionized species is detected by means of MS2.

For the purpose of neutralization it is possible to employ *i*) noble gases of low IE such as Xe (12.1 eV) [198], *ii*) metal vapors effusing from an oven, e.g., Hg (10.4 eV), Zn (9.3 eV), and Cd (9.0 eV) [196,205], or *iii*) volatile organic molecules, e.g., benzene (9.2 eV) or triphenylamine (6.8 eV) [206]. Reionization of the neutrals in the second collision cell can be achieved *i*) using O_2 (12.1 eV) or He (24.6 eV) [205,206], or *ii*) some standard ionization method such as electron ionization or field ionization [200].

NR-MS ia applied in numerous ways [201,207-209]. In particular, NR-MS is a powerful tool where the existence of short-lived and otherwise unstable species has to be proved [210-212].

Example: The NR mass spectrum of acetone closely resembles its 70-eV EI mass spectrum (Chap. 6.2.1), thereby demonstrating that the molecular ion basically retains the structure of the neutral (Fig. 9.44) [198]. However, the isomeric $C_3H_6O^{+\bullet}$ ions formed by McLafferty rearrangement of 2-hexanone molecular ion are expected to have enol structure (Chap. 6.7.1), and thus the corresponding NR mass spectrum is easily distinguished from that of acetone.

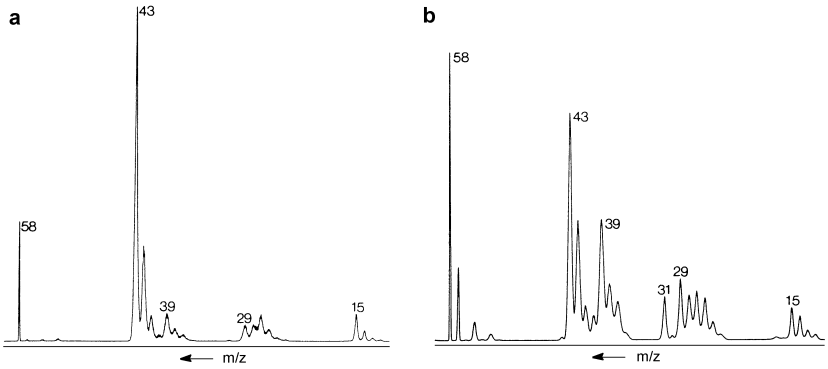


Fig. 9.44. NR-MS (Xe–He) of acetone (**a**) and its enol (**b**) from neutralization of the corresponding ions. Adapted from Ref. [198] with permission. © Elsevier Science, 1985.

References

1. *Tandem Mass Spectrometry;* McLafferty, F.W. (ed.); Wiley: New York, 1983.
2. Busch, K.L.; Glish, G.L.; McLuckey, S.A. *Mass Spectrometry/Mass Spectrometry;* Wiley VCH: New York, 1988.
3. Schalley, C.A.; Springer, A. *Mass Spectrometry and Gas-Phase Chemistry of Non-Covalent Complexes;* Wiley: Hoboken, 2009.
4. Johnson, J.V.; Yost, R.A.; Kelley, P.E.; Bradford, D.C. Tandem-in-Space and Tandem-in-Time Mass Spectrometry: Triple Quadrupoles and Quadrupole Ion Traps. *Anal. Chem.* **1990,** *62*, 2162-2172.
5. Kaufmann, R.; Kirsch, D.; Spengler, B. Sequencing of Peptides in a Time-of-Flight Mass Spectrometer: Evaluation of Postsource Decay Following Matrix-Assisted Laser Desorption Ionization (MALDI). *Int. J. Mass Spectrom. Ion Proc.* **1994,** *131*, 355-385.
6. Glish, G.L. Multiple Stage Mass Spectrometry: the Next Generation Tandem Mass Spectrometry Experiment. *Analyst* **1994,** *119*, 533-537.
7. Glish, G. Letter to the Editor [Concerning Terms in Mass Spectrometry]. *J. Am. Soc. Mass Spectrom.* **1991,** *2*, 349.
8. Thorne, G.C.; Ballard, K.D.; Gaskell, S.J. Metastable Decomposition of Peptide $[M+H]^+$ Ions Via Rearrangement Involving Loss of C-Terminal Amino Acid Residue. *J. Am. Soc. Mass Spectrom.* **1990,** *1*, 249-257.
9. Louris, J.N.; Wright, L.G.; Cooks, R.G.; Schoen, A.E. New Scan Modes Ac-

cessed With a Hybrid Mass Spectrometer. *Anal. Chem.* **1985,** *57*, 2918-2924.
10. Glish, G.L.; Burinsky, D.J. Hybrid Mass Spectrometers for Tandem Mass Spectrometry. *J. Am. Soc. Mass Spectrom.* **2008,** *19*, 161-172.
11. Lehmann, W.D. Pictograms for Experimental Parameters in Mass Spectrometry. *J. Am. Soc. Mass Spectrom.* **1997,** *8*, 756-759.
12. Cooks, R.G.; Beynon, J.H.; Caprioli, R.M. *Metastable Ions;* Elsevier: Amsterdam, 1973.
13. Cooks, R.G.; Beynon, J.H.; Caprioli, R.M. *Metastable Ions*; Elsevier: Amsterdam, 1973.
14. Levsen, K. *Fundamental Aspects of Organic Mass Spectrometry*; Verlag Chemie: Weinheim, 1978.
15. McLafferty, F.W.; Bente, P.F.I.; Kornfeld, R.; Tsai, S.-C.; Howe, I. Collisional Activation Spectra of Organic Ions. *J. Am. Chem. Soc.* **1973,** *95*, 2120-2129.
16. Levsen, K.; Schwarz, H. Collisional Activation Mass Spectrometry – A New Probe for Structure Determination of Ions in the Gaseous Phase. *Angew. Chem.* **1976,** *88*, 589-601.
17. Holmes, J.L. Assigning Structures to Ions in the Gas Phase. *Org. Mass Spectrom.* **1985,** *20*, 169-183.
18. Levsen, K.; Schwarz, H. Gas-Phase Chemistry of Collisionally Activated Ions. *Mass Spectrom. Rev.* **1983,** *2*, 77-148.
19. Bordas-Nagy, J.; Jennings, K.R. Collision-Induced Decomposition of Ions. *Int. J. Mass Spectrom. Ion Proc.* **1990,** *100*, 105-131.
20. McLuckey, S.A. Principles of Collisional Activation in Analytical Mass Spectrometry. *J. Am. Chem. Soc. Mass Spectrom.* **1992,** *3*, 599-614.
21. Shukla, A.K.; Futrell, J.H. Tandem Mass Spectrometry: Dissociation of Ions by Collisional Activation. *J. Mass Spectrom.* **2000,** *35*, 1069-1090.
22. Guevremont, R.; Boyd, R.K. Are Derrick Shifts Real? An Investigation by Tandem Mass Spectrometry. *Rapid. Commun. Mass Spectrom.* **1988,** *2*, 1-5.
23. Bradley, C.D.; Derrick, P.J. Collision-Induced Decomposition of Peptides. An Investigation into the Effect of Collision Gas Pressure on Translational Energy Losses. *Org. Mass Spectrom.* **1991,** *26*, 395-401.
24. Bradley, C.D.; Derrick, P.J. Collision-Induced Decomposition of Large Organic Ions and Inorganic Cluster Ions. Effects of Pressure on Energy Losses. *Org. Mass Spectrom.* **1993,** *28*, 390-394.
25. Neumann, G.M.; Sheil, M.M.; Derrick, P.J. Collision-Induced Decomposition of Multiatomic Ions. *Z. Naturforsch.* **1984,** *39A*, 584-592.
26. Alexander, A.J.; Thibault, P.; Boyd, R.K. Target Gas Excitation in Collision-Induced Dissociation: A Reinvestigation of Energy Loss in Collisional Activation of Molecular Ions of Chlorophyll-a. *J. Am. Chem. Soc.* **1990,** *112*, 2484-2491.
27. Kim, B.J.; Kim, M.S. Peak Shape Analysis for Collisionally Activated Dissociation in Mass-Analyzed Ion Kinetic Energy Spectrometry. *Int. J. Mass Spectrom. Ion Proc.* **1990,** *98*, 193-207.
28. Vékey, K.; Czira, G. Large Translational Energy Loss and Scattering in Collision-Induced Dissociation Processes. *Org. Mass Spectrom.* **1993,** *28*, 546-551.
29. Wysocki, V.H.; Kenttämaa, H.; Cooks, R.G. Internal Energy Distributions of Isolated Ions After Activation by Various Methods. *Int. J. Mass Spectrom. Ion Proc.* **1987,** *75*, 181-208.
30. Bradley, C.D.; Curtis, J.M.; Derrick, P.J.; Wright, B. Tandem Mass Spectrometry of Peptides Using a Magnetic Sector/Quadrupole Hybrid – The Case for Higher Collision Energy and Higher Radio-Frequency Power. *Anal. Chem.* **1992,** *64*, 2628-2635.
31. McLuckey, S.A.; Goeringer, D.E. Slow Heating Methods in Tandem Mass Spectrometry. *J. Mass Spectrom.* **1997,** *32*, 461-474.
32. Mabud, Md.A.; Dekrey, M.J.; Cooks, R.G. Surface-Induced Dissociation of Molecular Ions. *Int. J. Mass Spectrom. Ion Proc.* **1985,** *67*, 285-294.
33. Cooks, R.G.; Hoke, S.H., II; Morand, K.L.; Lammert, S.A. Mass Spectrometers: Instrumentation. *Int. J. Mass Spectrom. Ion Proc.* **1992,** *118-119*, 1-36.
34. Bier, M.E.; Amy, J.W.; Cooks, R.G.; Syka, J.E.P.; Ceja, P.; Stafford, G. A Tandem Quadrupole Mass Spectrometer for the Study of Surface-Induced Dissociation. *Int. J. Mass Spectrom. Ion Proc.* **1987,** *77*, 31-47.
35. Wysocki, V.H.; Ding, J.-M.; Jones, J.L.; Callahan, J.H.; King, F.L. Surface-Induced Dissociation in Tandem Quad-

rupole Mass Spectrometers: a Comparison of Three Designs. *J. Am. Chem. Soc. Mass Spectrom.* **1992,** *3*, 27-32.
36. Dongré, A.R.; Somogyi, A.; Wysocki, V.H. Surface-Induced Dissociation: an Effective Tool to Probe Structure, Energetics and Fragmentation Mechanisms of Protonated Peptides. *J. Mass Spectrom.* **1996,** *31*, 339-350.
37. Lammert, S.A.; Cooks, R.G. Surface-Induced Dissociation of Molecular Ions in a Quadrupole Ion Trap Mass Spectrometer. *J. Am. Chem. Soc. Mass Spectrom.* **1991,** *2*, 487-491.
38. Spengler, B.; Kirsch, D.; Kaufmann, R.; Jaeger, E. Peptide Sequencing by Matrix-Assisted Laser-Desorption Mass Spectrometry. *Rapid Commun. Mass Spectrom.* **1992,** *6*, 105-108.
39. Boesl, U.; Weinkauf, R.; Schlag, E. Reflectron Time-of-Flight Mass Spectrometry and Laser Excitation for the Analysis of Neutrals, Ionized Molecules and Secondary Fragments. *Int. J. Mass Spectrom. Ion Proc.* **1992,** *112*, 121-166.
40. Bradbury, N.E.; Nielsen, R.A. Absolute Values of the Electron Mobility in Hydrogen. *Phys. Rev.* **1936,** *49*, 388-393.
41. Tang, X.; Ens, W.; Standing, K.G.; Westmore, J.B. Daughter Ion Mass Spectra from Cationized Molecules of Small Oligopeptides in a Reflecting Time-of-Flight Mass Spectrometer. *Anal. Chem.* **1988,** *60*, 1791-1799.
42. Tang, X.; Ens, W.; Mayer, F.; Standing, K.G.; Westmore, J.B. Measurement of Unimolecular Decay in Peptides of Masses Greater Than 1200 Units by a Reflecting Time-of-Flight Mass Spectrometer. *Rapid Commun. Mass Spectrom.* **1989,** *3*, 443-448.
43. Schueler, B.; Beavis, R.; Ens, W.; Main, D.E.; Tang, X.; Standing, K.G. Unimolecular Decay Measurements of Secondary Ions From Organic Molecules by Time-of-Flight Mass Spectrometry. *Int. J. Mass Spectrom. Ion Proc.* **1989,** *92*, 185-194.
44. Brunelle, A.; Della-Negra, S.; Depauw, J.; Joret, H.; LeBeyec, Y. Time-of-Flight Mass Spectrometry With a Compact Two-Stage Electrostatic Mirror: Metastable-Ion Studies With High Mass Resolution and Ion Emission From Thick Insulators. *Rapid Commun. Mass Spectrom.* **1991,** *5*, 40-43.
45. Cornish, T.J.; Cotter, R.J. A Curved-Field Reflectron for Improved Energy Focusing of Product Ions in Time-of-Flight Mass Spectrometry. *Rapid Commun. Mass Spectrom.* **1993,** *7*, 1037-1040.
46. Cornish, T.J.; Cotter, R.J. A Curved Field Reflection Time-of-Flight Mass Spectrometer for the Simultaneous Focusing of Metastable Product Ions. *Rapid Commun. Mass Spectrom.* **1994,** *8*, 781-785.
47. Cordero, M.M.; Cornish, T.J.; Cotter, R.J.; Lys, I.A. Sequencing Peptides Without Scanning the Reflectron: Post-Source Decay With a Curved-Field Reflectron Time-of-Flight Spectrometer. *Rapid Commun. Mass Spectrom.* **1995,** *9*, 1356-1361.
48. Cotter, R.J.; Gardner, B.D.; Iltchenko, S.; English, R.D. Tandem Time-of-Flight Mass Spectrometry with a Curved Field Reflectron. *Anal. Chem.* **2004,** *76*, 1976-1981.
49. Giannakopulos, A.E.; Thomas, B.; Colburn, A.W.; Reynolds, D.J.; Raptakis, E.N.; Makarov, A.A.; Derrick, P.J. Tandem Time-of-Flight Mass Spectrometer (TOF-TOF) With a Quadratic-Field Ion Mirror. *Rev. Sci. Instrum.* **2002,** *73*, 2115-2123.
50. Yergey, A.L.; Coorssen, J.R.; Backlund, P.S.; Blank, P.S.; Humphrey, G.A.; Zimmerberg, J.; Campbell, J.M.; Vestal, M.L. De Novo Sequencing of Peptides Using MALDI/TOF-TOF. *J. Am. Soc. Mass Spectrom.* **2002,** *13*, 784-791.
51. Schnaible, V.; Wefing, S.; Resemann, A.; Suckau, D.; Bücker, A.; Wolf-Kümmeth, S.; Hoffmann, D. Screening for Disulfide Bonds in Proteins by MALDI in-Source Decay and LIFT-TOF/TOF-MS. *Anal. Chem.* **2002,** *74*, 4980-4988.
52. Suckau, D.; Resemann, A.; Schuerenberg, M.; Hufnagel, P.; Franzen, J.; Holle, A. A Novel MALDI LIFT-TOF/TOF Mass Spectrometer for Proteomics. *Anal. Bioanal Chem.* **2003,** *376*, 952-965.
53. Moneti, G.; Francese, S.; Mastrobuoni, G.; Pieraccini, G.; Seraglia, R.; Valitutti, G.; Traldi, P. Do Collisions Inside the Collision Cell Play a Relevant Role in CID-LIFT Experiments? *J. Mass Spectrom.* **2007,** *42*, 117-126.

54. Hipple, J.A. Detection of Metastable Ions With the Mass Spectrometer. *Phys. Rev.* **1945,** *68*, 54-55.
55. Hipple, J.A.; Fox, R.E.; Condon, E.U. Metastable Ions Formed by Electron Impact in Hydrocarbon Gases. *Phys. Rev.* **1946,** *69*, 347-356.
56. Beynon, J.H.; Saunders, R.A.; Williams, A.E. Formation of Metastable Ions in Mass Spectrometers With Release of Internal Energy. *Z. Naturforsch.* **1965,** *20A*, 180-183.
57. Beynon, J.H.; Cooks, R.G.; Amy, J.W.; Baitinger, W.E.; Ridley, T.Y. Design and Performance of a Mass-Analyzed Ion Kinetic Energy (MIKE) Spectrometer. *Anal. Chem.* **1973,** *45*, 1023A.
58. Amy, J.W.; Baitinger, W.E.; Cooks, R.G. Building Mass Spectrometers and a Philosophy of Research. *J. Am. Soc. Mass Spectrom.* **1990,** *1*, 119-128.
59. Ottinger, C. Fragmentation Energies of Metastable Organic Ions. *Phys. Lett.* **1965,** *17*, 269-271.
60. Baldwin, M.A.; Derrick, P.J.; Morgan, R.P. Correction of Metastable Peak Shapes to Allow for Instrumental Broadening and the Translational Energy Spread of the Parent Ion. *Org. Mass Spectrom.* **1976,** *11*, 440-442.
61. Gross, J.H.; Veith, H.J. Unimolecular Fragmentations of Long-Chain Aliphatic Iminium Ions. *Org. Mass Spectrom.* **1993,** *28*, 867-872.
62. Bowen, R.D.; Wright, A.D.; Derrick, P.J. Unimolecular Reactions of Ionized Methyl Allyl Ether. *Org. Mass Spectrom.* **1992,** *27*, 905-915.
63. Cao, J.R.; George, M.; Holmes, J.L. Fragmentation of 1- and 3-Methoxypropene Ions. Another Part of the $[C_4H_8O]^{+\cdot}$ Cation Radical Potential Energy Surface. *J. Am. Chem. Soc. Mass Spectrom.* **1992,** *3*, 99-107.
64. Gross, J.H.; Veith, H.J. Unimolecular Fragmentations of Long-Chain Aliphatic Iminium Ions. *Org. Mass Spectrom.* **1993,** *28*, 867-872.
65. Millington, D.S.; Smith, J.A. Fragmentation Patterns by Fast Linked Electric and Magnetic Field Scanning. *Org. Mass Spectrom.* **1977,** *12*, 264-265.
66. Morgan, R.P.; Porter, C.J.; Beynon, J.H. On the Formation of Artefact Peaks in Linked Scans of the Magnet and Electric Sector Fields in a Mass Spectrometer. *Org. Mass Spectrom.* **1977,** *12*, 735-738.
67. Lacey, M.J.; Macdonald, C.G. The Use of Two Linked Scanning Modes in Alternation to Analyze Metastable Peaks. *Org. Mass Spectrom.* **1980,** *15*, 134-137.
68. Lacey, M.J.; Macdonald, C.G. Interpreting Metastable Peaks From Double Focusing Mass Spectrometers. *Org. Mass Spectrom.* **1980,** *15*, 484-485.
69. Mouget, Y.; Bertrand, M.J. Graphical Method for Artefact Peak Interpretation, and Methods for Their Rejection, Using Double and Triple Sector Magnetic Mass Spectrometers. *Rapid Commun. Mass Spectrom.* **1995,** *9*, 387-396.
70. Evers, E.A.I.M.; Noest, A.J.; Akkerman, O.S. Deconvolution of Composite Metastable Peaks: a New Method for the Determination of Metastable Transitions Occurring in the First Field Free Region. *Org. Mass Spectrom.* **1977,** *12*, 419-420.
71. Boyd, R.K.; Porter, C.J.; Beynon, J.H. A New Linked Scan for Reversed Geometry Mass Spectrometers. *Org. Mass Spectrom.* **1981,** *16*, 490-494.
72. Lacey, M.J.; Macdonald, C.G. Constant Neutral Spectrum in Mass Spectrometry. *Anal. Chem.* **1979,** *51*, 691-695.
73. Boyd, R.K.; Beynon, J.H. Scanning of Sector Mass Spectrometers to Observe the Fragmentations of Metastable Ions. *Org. Mass Spectrom.* **1977,** *12*, 163-165.
74. Jennings, K.R. Scanning Methods for Double-Focusing Mass Spectrometers, Almoster Ferreira, M.A. (ed.); Reidel: Dordrecht, 1984; Chap. 118, pp. 7-21.
75. Fraefel, A.; Seibl, J. Selective Analysis of Metastable Ions. *Mass Spectrom. Rev.* **1984,** *4*, 151-221.
76. Boyd, R.K. Linked-Scan Techniques for MS/MS Using Tandem-in-Space Instruments. *Mass Spectrom. Rev.* **1994,** *13*, 359-410.
77. Walther, H.; Schlunegger, U.P.; Friedli, F. Quantitative Determination of Compounds in Mixtures by B^2E = Const. Linked Scans. *Org. Mass Spectrom.* **1983,** *18*, 572-575.
78. Futrell, J.H. Development of Tandem Mass Spectrometry. One Perspective. *Int. J. Mass Spectrom.* **2000,** *200*, 495-508.
79. Fenselau, C. Tandem Mass Spectrometry: the Competitive Edge for Pharmacology. *Ann. Rev. Pharmacol. Toxicol.* **1992,** *32*, 555-578.
80. Srinivas, R.; Sülzle, D.; Weiske, T.; Schwarz, H. Generation and Characteri-

zation of Neutral and Cationic 3-Silacyclopropenylidene in the Gas Phase. Description of a New BEBE Tandem Mass Spectrometer. *Int. J. Mass Spectrom. Ion Proc.* **1991,** *107*, 369-376.
81. Bordaz-Nagy, J.; Despeyroux, D.; Jennings, K.R.; Gaskell, S.J. Experimental Aspects of the Collision-Induced Decomposition of Ions in a Four-Sector Tandem Mass Spectrometer. *Org. Mass Spectrom.* **1992,** *27*, 406-415.
82. Stults, J.T.; Lai, J.; McCune, S.; Wetzel, R. Simplification of High-Energy Collision Spectra of Peptides by Amino-Terminal Derivatization. *Anal. Chem.* **1993,** *65*, 1703-1708.
83. Biemann, K.; Papyannopoulos, I.A. Amino Acid Sequencing of Proteins. *Acc. Chem. Res.* **1994,** *27*, 370-378.
84. Papyannopoulos, I.A. The Interpretation of Collision-Induced Dissociation Tandem Mass Spectra of Peptides. *Mass Spectrom. Rev.* **1995,** *14*, 49-73.
85. Lehmann, W.D. *Massenspektrometrie in der Biochemie;* Spektrum Akad. Verlag: Heidelberg, 1996.
86. *Mass Spectrometry of Proteins and Peptides;* Chapman, J.R. (ed.); Humana Press: Totowa, 2000.
87. Snyder, A.P. *Interpreting Protein Mass Spectra;* Oxford Univ. Press: New York, 2000.
88. Kinter, M.; Sherman, N.E. *Protein Sequencing and Identification Using Tandem Mass Spectrometry;* Wiley: Chichester, 2000.
89. Yost, R.A.; Enke, C.G. Selected Ion Fragmentation With a Tandem Quadrupole Mass Spectrometer. *J. Am. Chem. Soc.* **1978,** *100*, 2274-2275.
90. Yost, R.A.; Enke, C.G.; McGilvery, D.C.; Smith, D.; Morrison, J.D. High Efficiency Collision-Induced Dissociation in an Rf-Only Quadrupole. *Int. J. Mass Spectrom. Ion Phys.* **1979,** *30*, 127-136.
91. Yost, R.A.; Enke, C.G. Triple Quadrupole Mass Spectrometry for Direct Mixture Analysis and Structure Elucidation. *Anal. Chem.* **1979,** *51*, 1251A-1262A.
92. Hunt, D.F.; Shabanowitz, J.; Giordani, A.B. Collision Activated Decompositions in Mixture Analysis With a Triple Quadrupole Mass Spectrometer. *Anal. Chem.* **1980,** *52*, 386-390.
93. Dawson, P.H.; French, J.B.; Buckley, J.A.; Douglas, D.J.; Simmons, D. The Use of Triple Quadrupoles for Sequential Mass Spectrometry: The Instrument Parameters. *Org. Mass Spectrom.* **1982,** *17*, 205-211.
94. Dawson, P.H.; French, J.B.; Buckley, J.A.; Douglas, D.J.; Simmons, D. The Use of Triple Quadrupoles for Sequential Mass Spectrometry: A Detailed Case Study. *Org. Mass Spectrom.* **1982,** *17*, 212-219.
95. Inglebert, R.L.; Hennequin, J.F. Overall Transmission of Quadrupole Mass Spectrometers. *Adv. Mass Spectrom.* **1980,** *8B*, 1764-1770.
96. Cerezo, A.; Miller, M.K. Einzel Lenses in Atom Probe Designs. *Surface Sci.* **1991,** *246*, 450-456.
97. Thomson, B.A.; Douglas, D.J.; Corr, J.J.; Hager, J.W.; Jolliffe, C.L. Improved Collisionally Activated Dissociation Efficiency and Mass Resolution on a Triple Quadrupole Mass Spectrometer System. *Anal. Chem.* **1995,** *67*, 1696-1704.
98. Zeller, M.; Koenig, S. The Impact of Chromatography and Mass Spectrometry on the Analysis of Protein Phosphorylation Sites. Mass Spectrometric Phosphorylation Analysis. *Anal. Bioanal. Chem.* **2004,** *379*, 318.
99. Schwartz, J.C.; Schey, K.L.; Cooks, R.G. A Penta-Quadrupole Instrument for Reaction Intermediate Scans and Other MS-MS-MS Experiments. *Int. J. Mass Spectrom. Ion Proc.* **1990,** *101*, 1-20.
100. Gozzo, F.C.; Sorrilha, A.E.P.M.; Eberlin, M.N. The Generation, Stability, Dissociation and Ion/Molecule Chemistry of Sulfinyl Cations in the Gas Phase. *J. Chem. Soc., Perkin Trans. 2* **1995,** 587-596.
101. Juliano, V.F.; Gozzo, F.C.; Eberlin, M.N.; Kascheres, C.; do Lago, C.L. Fast Multidimensional (3D and 4D) MS^2 and MS^3 Scans in a High-Transmission Pentaquadrupole Mass Spectrometer. *Anal. Chem.* **1996,** *68*, 1328-1334.
102. Eberlin, M.N. Triple-Stage Pentaquadrupole (QqQqQ) Mass Spectrometry and Ion/Molecule Reactions. *Mass Spectrom. Rev.* **1997,** *16*, 113-144.
103. March, R.E. Quadrupole Ion Trap Mass Spectrometry: Theory, Simulation, Recent Developments and Applications. *Rapid Commun. Mass Spectrom.* **1998,** *12*, 1543-1554.
104. Griffiths, I.W. Recent Advances in Ion-Trap Technology. *Rapid Commun. Mass Spectrom.* **1990,** *4*, 69-73.

105. Siethoff, C.; Wagner-Redeker, W.; Schäfer, M.; Linscheid, M. HPLC-MS with an Ion Trap Mass Spectrometer. *Chimia* **1999,** *53*, 484-491.
106. Schwartz, J.C.; Jardine, I. High-Resolution Parent-Ion Selection/Isolation Using a Quadrupole Ion-Trap Mass Spectrometer. *Rapid Commun. Mass Spectrom.* **1992,** *6*, 313-317.
107. Remes, P.M.; Glish, G.L. On the Time Scale of Internal Energy Relaxation of AP-MALDI and Nano-ESI Ions in a Quadrupole Ion Trap. *J. Am. Soc. Mass Spectrom.* **2009,** *20*, 1801-1812.
108. Louris, J.N.; Cooks, R.G.; Syka, J.E.P.; Kelley, P.E.; Stafford, G.C., Jr.; Todd, J.F.J. Instrumentation, Applications, and Energy Deposition in Quadrupole Ion-Trap Tandem Mass Spectrometry. *Anal. Chem.* **1987,** *59*, 1677-1685.
109. McLuckey, S.A.; Glish, G.L.; Kelley, P.E. Collision-Activated Dissociation of Negative Ions in an Ion Trap Mass Spectrometer. *Anal. Chem.* **1987,** *59*, 1670-1674.
110. Cooks, R.G.; Amy, J.W.; Bier, M.; Schwartz, J.C.; Schey, K. New Mass Spectrometers, 1989; Chap. 11A, pp. 33-52.
111. Murrell, J.; Konn, D.O.; Underwood, N.J.; Despeyroux, D. Studies into the Selective Accumulation of Multiply Charged Protein Ions in a Quadrupole Ion Trap Mass Spectrometer. *Int. J. Mass Spectrom.* **2003,** *227*, 223-234.
112. Hashimoto, Y.; Hasegawa, H.; Yoshinari, K. Collision-Activated Infrared Multiphoton Dissociation in a Quadrupole Ion Trap Mass Spectrometer. *Anal. Chem.* **2003,** *75*, 420-425.
113. March, R.E.; Todd, J.F.J. *Quadrupole Ion Trap Mass Spectrometry;* Wiley: Hoboken, 2005.
114. Kuzma, M.; Jegorov, A.; Kacer, P.; Havlícek, V. Sequencing of New Beauverolides by High-Performance Liquid Chromatography and Mass Spectrometry. *J. Mass Spectrom.* **2001,** *36*, 1108-1115.
115. Hopfgartner, G.; Husser, C.; Zell, M. Rapid Screening and Characterization of Drug Metabolites Using a New Quadrupole-Linear Ion Trap Mass Spectrometer. *J. Mass Spectrom.* **2003,** *38*, 138-150.
116. Pekar Second, T.; Blethrow, J.D.; Schwartz, J.C.; Merrihew, G.E.; MacCoss, M.J.; Swaney, D.L.; Russell, J.D.; Coon, J.J.; Zabrouskov, V. Dual-Pressure Linear Ion Trap Mass Spectrometer Improving the Analysis of Complex Protein Mixtures. *Anal. Chem.* **2009,** *81*, 7757-7765.
117. Magparangalan, D.P.; Garrett, T.J.; Drexler, D.M.; Yost, R.A. Analysis of Large Peptides by MALDI Using a Linear Quadrupole Ion Trap With Mass Range Extension. *Anal. Chem.* **2010,** *82*, 930-934.
118. Londry, F.A.; Hager, J.W. Mass Selective Axial Ion Ejection From a Linear Quadrupole Ion Trap. *J. Am. Soc. Mass Spectrom.* **2003,** *14*, 1130-1147.
119. Hopfgartner, G.; Varesio, E.; Tschaeppaet, V.; Grivet, C.; Bourgogne, E.; Leuthold, L.A. Triple Quadrupole Linear Ion Trap Mass Spectrometer for the Analysis of Small Molecules and Macromolecules. *J. Mass Spectrom.* **2004,** *39*, 845-855.
120. Moberg, M.; Markides, K.E.; Bylund, D. Multi-Parameter Investigation of Tandem Mass Spectrometry in a Linear Ion Trap Using Response Surface Modelling. *J. Mass Spectrom.* **2005,** *40*, 317-324.
121. Olsen, J.V.; Schwartz, J.C.; Griep-Raming, J.; Nielsen, M.L.; Damoc, E.; Denisov, E.; Lange, O.; Remes, P.; Taylor, D.; Splendore, M.; Wouters, E.R.; Senko, M.; Makarov, A.; Mann, M.; Horning, S. A Dual Pressure Linear Ion Trap Orbitrap Instrument With Very High Sequencing Speed. *Mol. Cell. Proteomics* **2009,** *8*, 2759-2769.
122. Olsen, J.V.; Macek, B.; Lange, O.; Makarov, A.; Horning, S.; Mann, M. Higher-Energy C-Trap Dissociation for Peptide Modification Analysis. *Nature Methods* **2007,** *4*, 709-712.
123. Olsen, J.V.; de Godoy, L.M.F.; Li, G.; Macek, B.; Mortensen, P.; Pesch, R.; Makarov, A.; Lange, O.; Horning, S.; Mann, M. Parts Per Million Mass Accuracy on an Orbitrap Mass Spectrometer Via Lock Mass Injection into a C-Trap. *Mol. Cell. Proteomics* **2005,** *4*, 2010-2021.
124. Guan, S.; Marshall, A.G. Stored Waveform Inverse Fourier Transform (SWIFT) Ion Excitation in Trapped-Ion Mass Spectrometry: Theory and Applications. *Int. J. Mass Spectrom. Ion Proc.* **1996,** *157/158*, 5-37.

125. Heck, A.J.R.; Derrick, P.J. Ultrahigh Mass Accuracy in Isotope-Selective Collision-Induced Dissociation Using Correlated Sweep Excitation and Sustained Off-Resonance Irradiation: A FT-ICR-MS Case Study on the $[M+2H]^{2+}$ Ion of Bradykinin. *Anal. Chem.* **1997,** *69*, 3603-3607.
126. Heck, A.J.R.; Derrick, P.J. Selective Fragmentation of Single Isotopic Ions of Proteins Up to 17 KDa Using 9.4 Tesla Fourier Transform Ion Cyclotron Resonance. *Eur. Mass Spectrom.* **1998,** *4*, 181-188.
127. Cody, R.B.; Freiser, B.S. Collision-Induced Dissociation in a Fourier-Transform Mass Spectrometer. *Int. J. Mass Spectrom. Ion Phys.* **1982,** *41*, 199-204.
128. Cody, R.B.; Burnier, R.C.; Freiser, B.S. Collision-Induced Dissociation With Fourier Transform Mass Spectrometry. *Anal. Chem.* **1982,** *54*, 96-101.
129. Gauthier, J.W.; Trautman, T.R.; Jacobson, D.B. Sustained Off-Resonance Irradiation for Collision-Activated Dissociation Involving FT-ICR-MS. CID Technique That Emulates Infrared Multiphoton Dissociation. *Anal. Chim. Acta* **1991,** *246*, 211-225.
130. Senko, M.W.; Speir, J.P.; McLafferty, F.W. Collisional Activation of Large Multiply Charged Ions Using Fourier Transform Mass Spectrometry. *Anal. Chem.* **1994,** *66*, 2801-2808.
131. Boering, K.A.; Rolfe, J.; Brauman, J.I. Control of Ion Kinetic Energy in ICR-MS: Very-Low-Energy Collision-Induced Dissociation. *Rapid Commun. Mass Spectrom.* **1992,** *6*, 303-305.
132. Lee, S.A.; Jiao, C.Q.; Huang, Y.; Freiser, B.S. Multiple Excitation Collisional Activation in Fourier-Transform Mass Spectrometry. *Rapid Commun. Mass Spectrom.* **1993,** *7*, 819-821.
133. Mihalca, R.; van der Burgt, Y.E.M.; Heck, A.J.R.; Heeren, R.M.A. Disulfide Bond Cleavages Observed in SORI-CID of Three Nonapeptides Complexed With Divalent Transition-Metal Cations. *J. Mass Spectrom.* **2007,** *42*, 450-458.
134. Mirgorodskaya, E.; O'Connor, P.B.; Costello, C.E. A General Method for Precalculation of Parameters for Sustained Off Resonance Irradiation/Collision-Induced Dissociation. *J. Am. Soc. Mass Spectrom.* **2002,** *13*, 318-324.
135. Woodin, R.L.; Bomse, D.S.; Beauchamp, J.L. Multiphoton Dissociation of Molecules With Low Power Continuous Wave Infrared Laser Radiation. *J. Am. Chem. Soc.* **1978,** *100*, 3248-3250.
136. Håkansson, K.; Cooper, H.J.; Emmet, M.R.; Costello, C.E.; Marshall, A.G.; Nilsson, C.L. Electron Capture Dissociation and Infrared Multiphoton Dissociation MS/MS of an *N*-Glycosylated Tryptic Peptic to Yield Complementary Sequence Information. *Anal. Chem.* **2001,** *73*, 4530-4536.
137. Little, D.P.; Senko, M.W.; O'Conner, P.B.; McLafferty, F.W. Infrared Multiphoton Dissociation of Large Multiply-Charged Ions for Biomolecule Sequencing. *Anal. Chem.* **1994,** *66*, 2809-2815.
138. Watson, C.H.; Baykut, G.; Eyler, J.R. Laser Photodissociation of Gaseous Ions Formed by Laser Desorption. *Anal. Chem.* **1987,** *59*, 1133-1138.
139. Eyler, J.R. Infrared Multiple Photon Dissociation Spectroscopy of Ions in Penning Traps. *Mass Spectrom. Rev.* **2009,** *28*, 448-467.
140. Brodbelt, J.S.; Wilson, J.J. Infrared Multiphoton Dissociation in Quadrupole Ion Traps. *Mass Spectrom. Rev.* **2009,** *28*, 390-424.
141. Hashimoto, Y.; Hasegawa, H.; Waki, I. High Sensitivity and Broad Dynamic Range Infrared Multiphoton Dissociation for a Quadrupole Ion Trap. *Rapid Commun. Mass Spectrom.* **2004,** *18*, 2255-2259.
142. Madsen, J.A.; Gardner, M.W.; Smith, S.I.; Ledvina, A.R.; Coon, J.J.; Schwartz, J.C.; Stafford, G.C.; Brodbelt, J.S. Top-Down Protein Fragmentation by Infrared Multiphoton Dissociation in a Dual Pressure Linear Ion Trap. *Anal. Chem.* **2009,** *81*, 8677-8686.
143. Gardner, M.W.; Smith, S.I.; Ledvina, A.R.; Madsen, J.A.; Coon, J.J.; Schwartz, J.C.; Stafford, G.C.; Brodbelt, J.S. Infrared Multiphoton Dissociation of Peptide Cations in a Dual Pressure Linear Ion Trap Mass Spectrometer. *Anal. Chem.* **2009,** *81*, 8109-8118.
144. Campbell, J.L.; Hager, J.W.; Le Blanc, J.C.Y. On Performing Simultaneous Electron Transfer Dissociation and Collision-Induced Dissociation on Multiply

Protonated Peptides in a Linear Ion Trap. *J. Am. Soc. Mass Spectrom.* **2009,** *20*, 1672-1683.

145. Zubarev, R.A.; Kelleher, N.L.; McLafferty, F.W. Electron Capture Dissociation of Multiply Charged Protein Cations. A Nonergodic Process. *J. Am. Chem. Soc.* **1998,** *120*, 3265-3266.

146. Axelsson, J.; Palmblad, M.; Håkansson, K.; Håkansson, P. Electron Capture Dissociation of Substance P Using a Commercially Available Fourier Transform Ion Cyclotron Resonance Mass Spectrometer. *Rapid Commun. Mass Spectrom.* **1999,** *13*, 474-477.

147. Cerda, B.A.; Horn, D.M.; Breuker, K.; Carpenter, B.K.; McLafferty, F.W. Electron Capture Dissociation of Multiply-Charged Oxygenated Cations. A Nonergodic Process. *Eur. Mass Spectrom.* **1999,** *5*, 335-338.

148. Håkansson, K.; Emmet, M.R.; Hendrickson, C.L.; Marshall, A.G. High-Sensitivity Electron Capture Dissociation Tandem FTICR Mass Spectrometry of Microelectrosprayed Peptides. *Anal. Chem.* **2001,** *73*, 3605-3610.

149. Leymarie, N.; Berg, E.A.; McComb, M.E.; O'Conner, P.B.; Grogan, J.; Oppenheim, F.G.; Costello, C.E. Tandem Mass Spectrometry for Structural Characterization of Proline-Rich Proteins: Application to Salivary PRP-3. *Anal. Chem.* **2002,** *74*, 4124-4132.

150. Tsybin, Y.O.; Ramstroem, M.; Witt, M.; Baykut, G.; Hakansson, P. Peptide and Protein Characterization by High-Rate Electron Capture Dissociation Fourier Transform Ion Cyclotron Resonance Mass Spectrometry. *J. Mass Spectrom.* **2004,** *39*, 719-729.

151. Zubarev, R.A.; Horn, D.M.; Fridriksson, E.K.; Kelleher, N.L.; Kruger, N.A.; Lewis, M.A.; Carpenter, B.K.; McLafferty, F.W. Electron Capture Dissociation for Structural Characterization of Multiply Charged Protein Cations. *Anal. Chem.* **2000,** *72*, 563-573.

152. Zubarev, R.A. Reactions of Polypeptide Ions with Electrons in the Gas Phase. *Mass Spectrom. Rev.* **2003,** *22*, 57-77.

153. Leymarie, N.; Costello, C.E.; O'Connor, P.B. Electron Capture Dissociation Initiates a Free Radical Reaction Cascade. *J. Am. Chem. Soc.* **2003,** *125*, 8949-8958.

154. Turecek, F. N-C_α Bond Dissociation Energies and Kinetics in Amide and Peptide Radicals. Is the Dissociation a Non-Ergodic Process? *J. Am. Chem. Soc.* **2003,** *125*, 5954-5963.

155. McFarland, M.A.; Marshall, A.G.; Hendrickson, C.L.; Nilsson, C.L.; Fredman, P.; Mansson, J.E. Structural Characterization of the GM1 Ganglioside by Infrared Multiphoton Dissociation, Electron Capture Dissociation, and Electron Detachment Dissociation Electrospray Ionization FT-ICR MS/MS. *J. Am. Soc. Mass Spectrom.* **2005,** *16*, 752-762.

156. Oh, H.B.; Lin, C.; Hwang, H.Y.; Zhai, H.; Breuker, K.; Zabrouskov, V.; Carpenter, B.K.; McLafferty, F.W. Infrared Photodissociation Spectroscopy of Electrosprayed Ions in a Fourier Transform Mass Spectrometer. *J. Am. Chem. Soc.* **2005,** *127*, 4076-4083.

157. Dunbar, R.C. BIRD (Blackbody Infrared Radiative Dissociation): Evolution, Principles, and Applications. *Mass Spectrom. Rev.* **2004,** *23*, 127-158.

158. Tsybin, Y.O.; Hakansson, P.; Budnik, B.A.; Haselmann, K.F.; Kjeldsen, F.; Gorshkov, M.; Zubarev, R.A. Improved Low-Energy Electron Injection Systems for High Rate Electron Capture Dissociation in Fourier Transform Ion Cyclotron Resonance Mass Spectrometry. *Rapid Commun. Mass Spectrom.* **2001,** *15*, 1849-1854.

159. Tsybin, Y.O.; Witt, M.; Baykut, G.; Kjeldsen, F.; Hakansson, P. Combined Infrared Multiphoton Dissociation and Electron Capture Dissociation With a Hollow Electron Beam in Fourier Transform Ion Cyclotron Resonance Mass Spectrometry. *Rapid Commun. Mass Spectrom.* **2003,** *17*, 1759-1768.

160. Syka, J.E.P.; Coon, J.J.; Schroeder, M.J.; Shabanowitz, J.; Hunt, D.F. Peptide and Protein Sequence Analysis by Electron Transfer Dissociation Mass Spectrometry. *Proc. Natl. Acad. Sci. USA* **2004,** *101*, 9528-9533.

161. Cooper, H.J.; Hakansson, K.; Marshall, A.G. The Role of Electron Capture Dissociation in Biomolecular Analysis. *Mass Spectrom. Rev.* **2005,** *24*, 201-222.

162. Swaney, D.L.; McAlister, G.C.; Wirtala, M.; Schwartz, J.C.; Syka, J.E.P.; Coon, J.J. Supplemental Activation Method for High-Efficiency Electron-Transfer Dissociation of Doubly Protonated Peptide Precursors. *Anal. Chem.* **2007,** *79*, 477-485.

163. Coon, J.J.; Syka, J.E.P.; Schwartz, J.C.; Shabanowitz, J.; Hunt, D.F. Anion Dependence in the Partitioning Between Proton and Electron Transfer in Ion/Ion Reactions. *Int. J. Mass Spectrom.* **2004,** *236*, 33-42.
164. Good, D.M.; Wirtala, M.; McAlister, G.C.; Coon, J.J. Performance Characteristics of Electron Transfer Dissociation Mass Spectrometry. *Mol. Cell. Proteomics* **2007,** *6*, 1942-1951.
165. Chi, A.; Huttenhower, C.; Geer, L.Y.; Coon, J.J.; Syka, J.E.P.; Bai, D.L.; Shabanowitz, J.; Burke, D.J.; Troyanskaya, O.G.; Hunt, D.F. Analysis of Phosphorylation Sites on Proteins From Saccharomyces Cerevisiae by Electron Transfer Dissociation (ETD) Mass Spectrometry. *Proc. Natl. Acad. Sci. USA* **2007,** *104*, 2193-2198.
166. Liang, X.; Hager, J.W.; McLuckey, S.A. Transmission Mode Ion/Ion Electron-Transfer Dissociation in a Linear Ion Trap. *Anal. Chem.* **2007,** *79*, 3363-3370.
167. McAlister, G.C.; Berggren, W.T.; Griep-Raming, J.; Horning, S.; Makarov, A.; Phanstiel, D.; Stafford, G.; Swaney, D.L.; Syka, J.E.P.; Zabrouskov, V.; Coon, J.J. A Proteomics Grade Electron Transfer Dissociation-Enabled Hybrid Linear Ion Trap-Orbitrap Mass Spectrometer. *J. Prot. Res.* **2008,** *7*, 3127-3136.
168. Williams, D.K., Jr.; McAlister, G.C.; Good, D.M.; Coon, J.J.; Muddiman, D.C. Dual Electrospray Ion Source for Electron-Transfer Dissociation on a Hybrid Linear Ion Trap-Orbitrap Mass Spectrometer. *Anal. Chem.* **2007,** *79*, 7916-7919.
169. McAlister, G.C.; Phanstiel, D.; Good, D.M.; Berggren, W.T.; Coon, J.J. Implementation of Electron-Transfer Dissociation on a Hybrid Linear Ion Trap-Orbitrap Mass Spectrometer. *Anal. Chem.* **2007,** *79*, 3525-3534.
170. Haselmann, K.F.; Budnik, B.A.; Kjeldsen, F.; Nielsen, M.L.; Olsen, J.V.; Zubarev, R.A. Electronic Excitation Gives Informative Fragmentation of Polypeptide Cations and Anions. *Eur. J. Mass Spectrom.* **2002,** *8*, 117-121.
171. Budnik, B.A.; Haselmann, K.F.; Zubarev, R.A. Electron Detachment Dissociation of Peptide Di-Anions: an Electron-Hole Recombination Phenomenon. *Chem. Phys. Lett.* **2001,** *342*, 299-302.
172. Kjeldsen, F.; Silivra, O.A.; Ivonin, I.A.; Haselmann, K.F.; Gorshkov, M.; Zubarev, R.A. C_α-C Backbone Fragmentation Dominates in Electron Detachment Dissociation of Gas-Phase Polypeptide Polyanions. *Chem.- Eur. J.* **2005,** *11*, 1803-1812.
173. Anusiewicz, I.; Jasionowski, M.; Skurski, P.; Simons, J. Backbone and Side-Chain Cleavages in Electron Detachment Dissociation (EDD). *J. Phys. Chem. A* **2005,** *109*, 11332-11337.
174. Yang, J.; Mo, J.; Adamson, J.T.; Haakansson, K. Characterization of Oligodeoxynucleotides by Electron Detachment Dissociation Fourier Transform Ion Cyclotron Resonance Mass Spectrometry. *Anal. Chem.* **2005,** *77*, 1876-1882.
175. Huzarska, M.; Ugalde, I.; Kaplan, D.A.; Hartmer, R.; Easterling, M.L.; Polfer, N.C. Negative Electron Transfer Dissociation of Deprotonated Phosphopeptide Anions: Choice of Radical Cation Reagent and Competition Between Electron and Proton Transfer. *Anal. Chem.* **2010,** *82*, 2873-2878.
176. Sleno, L.; Volmer, D.A. Ion Activation Methods for Tandem Mass Spectrometry. *J. Mass Spectrom.* **2004,** *39*, 1091-1112.
177. Adlhart, C.; Hinderling, C.; Baumann, H.; Chen, P. Mechanistic Studies of Olefin Metathesis by Ruthenium Carbene Complexes Using Electrospray Ionization Tandem Mass Spectrometry. *J. Am. Chem. Soc.* **2000,** *122*, 8204-8214.
178. Hinderling, C.; Adlhart, C.; Chen, P. Mechanism-Based High-Throughput Screening of Catalysts. *Chimia* **2000,** *54*, 232-235.
179. Volland, M.A.O.; Adlhart, C.; Kiener, C.A.; Chen, P.; Hofmann, P. Catalyst Screening by Electrospray Ionization Tandem Mass Spectrometry: Hofmann Carbenes for Olefin Metathesis. *Chem. - Eur. J.* **2001,** *7*, 4621-4632.
180. Schwarz, H. Relativistic Effects in Gas-Phase Ion Chemistry: An Experimentalist's View. *Angew. Chem., Int. Ed.* **2003,** *42*, 4442-4454.
181. Schwarz, H. On the Spin-Forbiddeness of Gas-Phase Ion-Molecule Reactions: a Fruitful Intersection of Experimental and Computational Studies. *Int. J. Mass Spectrom.* **2004,** *237*, 75-105.

182. Boehme, D.K.; Schwarz, H. Gas-Phase Catalysis by Atomic and Cluster Metal Ions: The Ultimate Single-Site Catalysts. *Angew. Chem., Int. Ed.* **2005,** *44*, 2336-2354.
183. Schlangen, M.; Schroeder, D.; Schwarz, H. Pronounced Ligand Effects and the Role of Formal Oxidation States in the Nickel-Mediated Thermal Activation of Methane. *Angew. Chem., Int. Ed.* **2007,** *46*, 1641-1644.
184. Kaltashov, I.A.; Eyles, S.J. *Mass Spectrometry in Biophysics: Conformation and Dynamics of Biomolecules;* Wiley: Hoboken, 2005.
185. Somogyi, A. Probing Peptide Fragment Ion Structures by Combining Sustained Off-Resonance Collision-Induced Dissociation and Gas-Phase H/D Exchange (SORI-HDX) in Fourier Transform Ion-Cyclotron Resonance (FT-ICR) Instruments. *J. Am. Soc. Mass Spectrom.* **2008,** *19*, 1771-1775.
186. Bythell, B.J.; Somogyi, Á.; Paizs, B. What Is the Structure of B_2 Ions Generated From Doubly Protonated Tryptic Peptides? *J. Am. Soc. Mass Spectrom.* **2009,** *20*, 618-624.
187. Harrison, A.G. The Gas-Phase Basicities and Proton Affinities of Amino Acids and Peptides. *Mass Spectrom. Rev.* **1997,** *16*, 201-217.
188. McMahon, T.B. Thermochemical Ladders: Scaling the Ramparts of Gaseous Ion Energetics. *Int. J. Mass Spectrom.* **2000,** *200*, 187-199.
189. Cooks, R.G.; Kruger, T.L. Intrinsic Basicity Determination Using Metastable Ions. *J. Am. Chem. Soc.* **1977,** *99*, 1279-1281.
190. Cooks, R.G.; Wong, P.S.H. Kinetic Method of Making Thermochemical Determinations: Advances and Applications. *Acc. Chem. Res.* **1998,** *31*, 379-386.
191. Cooks, R.G.; Patrick, J.S.; Kotiaho, T.; McLuckey, S.A. Thermochemical Determinations by the Kinetic Method. *Mass Spectrom. Rev.* **1994,** *13*, 287-339.
192. Kukol, A.; Strehle, F.; Thielking, G.; Grützmacher, H.-F. Methyl Group Effect on the Proton Affinity of Methylated Acetophenones Studied by Two Mass Spectrometric Techniques. *Org. Mass Spectrom.* **1993,** *28*, 1107-1110.
193. Bouchoux, G.; Salpin, J.Y. Gas-Phase Basicity and Heat of Formation of Sulfine CH_2=S=O. *J. Am. Chem. Soc.* **1996,** *118*, 6516-6517.
194. Bouchoux, G.; Salpin, J.Y.; Leblanc, D. A Relationship Between the Kinetics and Thermochemistry of Proton Transfer Reactions in the Gas Phase. *Int. J. Mass Spectrom. Ion Proc.* **1996,** *153*, 37-48.
195. Witt, M.; Kreft, D.; Grützmacher, H.-F. Effects of Internal Hydrogen Bonds Between Amide Groups: Protonation of Alicyclic Diamides. *Eur. J. Mass Spectrom.* **2003,** *9*, 81-95.
196. Danis, P.O.; Wesdemiotis, C.; McLafferty, F.W. Neutralization-Reionization Mass Spectrometry (NRMS). *J. Am. Chem. Soc.* **1983,** *105*, 7454-7456.
197. Gellene, G.I.; Porter, R.F. Neutralized Ion-Beam Spectroscopy. *Acc. Chem. Res.* **1983,** *16*, 200-207.
198. Terlouw, J.K.; Kieskamp, W.M.; Holmes, J.L.; Mommers, A.A.; Burgers, P.C. The Neutralization and Reionization of Mass-Selected Positive Ions by Inert Gas Atoms. *Int. J. Mass Spectrom. Ion Proc.* **1985,** *64*, 245-250.
199. Holmes, J.L.; Mommers, A.A.; Terlouw, J.K.; Hop, C.E.C.A. The Mass Spectrometry of Neutral Species Produced From Mass-Selected Ions by Collision and by Charge Exchange. Experiments With Tandem Collision Gas Cells. *Int. J. Mass Spectrom. Ion Proc.* **1986,** *68*, 249-264.
200. Blanchette, M.C.; Holmes, J.L.; Hop, C.E.C.A.; Mommers, A.A. The Ionization of Fast Neutrals by Electron Impact in the Second Field-Free Region of a Mass Spectrometer of Reversed Geometry. *Org. Mass Spectrom.* **1988,** *23*, 495-498.
201. McLafferty, F.W. Neutralization-Reionization Mass Spectrometry. *Int. J. Mass Spectrom. Ion Proc.* **1992,** *118/119*, 221-235.
202. Goldberg, N.; Schwarz, H. Neutralization-Reionization Mass Spectrometry: a Powerful "Laboratory" to Generate and Probe Elusive Neutral Molecules. *Acc. Chem. Res.* **1994,** *27*, 347-352.
203. Schalley, C.A.; Hornung, G.; Schroder, D.; Schwarz, H. Mass Spectrometry As a Tool to Probe the Gas-Phase Reactivity of Neutral Molecules. *Int. J. Mass Spectrom. Ion Proc.* **1998,** *172*, 181-208.
204. Schalley, C.A.; Hornung, G.; Schroder, D.; Schwarz, H. Mass Spectrometric

Approaches to the Reactivity of Transient Neutrals. *Chem. Soc. Rev.* **1998,** *27*, 91-104.

205. Blanchette, M.C.; Bordas-Nagy, J.; Holmes, J.L.; Hop, C.E.C.A.; Mommers, A.A.; Terlouw, J.K. Neutralization-Reionization Experiments; A Simple Metal Vapor Cell for VG Analytical ZAB-2F Mass Spectrometers. *Org. Mass Spectrom.* **1988,** *23*, 804-807.
206. Zang, M.Y.; McLafferty, F.W. Organic Neutralization Agents for Neutralization-Reionization Mass Spectrometry. *J. Am. Chem. Soc. Mass Spectrom.* **1992,** *3*, 108-112.
207. Zhang, M.-Y.; McLafferty, F.W. Quantitative Analysis of Isomeric Ion Mixtures. *Org. Mass Spectrom.* **1992,** *27*, 991-994.
208. Zagorevskii, D.V.; Holmes, J.L. Neutralization-Reionization Mass Spectrometry Applied to Organometallic and Coordination Chemistry. *Mass Spectrom. Rev.* **1994,** *13*, 133-154.
209. Zagorevskii, D.V.; Holmes, J.L. Neutralization-Reionization Mass Spectrometry Applied to Organometallic and Coordination Chemistry (Update: 1994-1998). *Mass Spectrom. Rev.* **1999,** *18*, 87-118.
210. Weiske, T.; Wong, T.; Krätschmer, W.; Terlouw, J.K.; Schwarz, H. Proof of the Existence of an Endohedral Helium-Fullerene ($He@C_{60}$) Structure Via Gas-Phase Neutralization of $[HeC_{60}]^{+\cdot}$ *Angew. Chem., Int. Ed.* **1992,** *31*, 183-185.
211. Keck, H.; Kuchen, W.; Tommes, P.; Terlouw, J.K.; Wong, T. The Phosphonium Ylide CH_2PH_3 Is Stable in Gas Phase. *Angew. Chem., Int. Ed.* **1992,** *31*, 86-87.
212. Schröder, D.; Schwarz, H.; Wulf, M.; Sievers, H.; Jutzi, P.; Reiher, M. Experimental Evidence for the Existence of Neutral P_6: A New Allotrope of Phosphorus. *Angew. Chem., Int. Ed.* **1999,** *38*, 313-315.

10 Fast Atom Bombardment

Learning Objectives

- Ablating action of energetic particles on surfaces
- Secondary ion formation by impact of primary ions and neutrals
- Desorption of ions from condensed phase into the gas phase
- Moderating effect of a liquid matrix
- FAB and LSIMS – general properties and applications
- Air- and moisture-sensitive samples
- Related desorption/ionization techniques

When particles of kilo- or even megaelectronvolt kinetic energy are impinging on a surface, they cause the ejection of large numbers of neutrals and some ions from the surface material exposed to their bombardment.

Secondary ion mass spectrometry (SIMS) was first applied employing the sputtering effects of a beam of impacting ions on bulk, inorganic materials [1-3] and was later for the analysis of organic solids [9,10]. Prior to this, biomolecules were analyzed by ^{252}*Cf plasma desorption* (PD) time-of-flight (TOF) mass spectrometry and of *molecular beam solid analysis* (MBSA) using energetic neutrals [4-8]. Unfortunately, SIMS conditions disadvantageously interfered with ion source potentials as a result of electrostatic charging of organic surfaces upon ion impact. Employing a beam of energetic neutral atoms in analogy to the MBSA technique eliminated such problems and promoted further developments of this promising method [11,12] – the technique was later named *fast atom bombardment* (FAB) [7, 11-13].

It turned out that ions of intact molecular species could be generated even in case of highly polar compounds that definitely were no candidates for electron ionization (EI, Chaps. 5, 6) or chemical ionization (CI, Chap. 7). Early FAB-MS suffered from rapid radiolytic decomposition of the samples upon irradiation and from the comparatively harsh conditions of desorption/ionization. The use of a *liquid matrix* in which the analyte was dissolved meant a major breakthrough [14,15]. Today one would refer to this as "matrix-assisted fast atom bombardment" [16,17]. FAB-MS soon became the major competitor of field desorption (Chap. 8). It turned out that the properties of the liquid matrix are of key importance for the resulting FAB spectra [18-20]. Due to some electric conductivity of the matrix, primary ions could now again be employed successfully [21-24]. If primary ions instead of neutrals are used to provide the energy for secondary ion

J. Gross, *Mass Spectrometry*, 2nd ed., DOI 10.1007/978-3-642-10711-5_10,
© Springer-Verlag Berlin Heidelberg 2011

ejection from the liquid matrix, the technique is termed *liquid secondary ion mass spectrometry* (LSIMS, Table 10.1). Next to FAB and LSIMS, "inorganic" SIMS has tremendously developed to become a versatile method for surface analysis and more recently for molecular imaging applications (Chap. 15.5).

While FAB and LSIMS are useful and versatile "soft" methods, they have widely been replaced by matrix-assisted laser desorption/ionization (MALDI, Chap. 11), electrospray ionization (ESI, Chap. 12), and related API techniques. Therefore, we will restrict ourselves to a brief introduction of FAB and LSIMS.

Table 10.1. Desorption/ionization methods employing impact of energetic particles

Method	Acronym	Principle
Secondary ion mass spectrometry	SIMS	sputtering and ionization by a beam of ions impacting on solids [1-3]
Plasma desorption	PD-MS	desorption/ionization of biomolecules by impact of single megaelectronvolt nuclear fission fragments [4-6]
Molecular beam solid analysis	MBSA	ion formation by impact of energetic neutral molecules on organic solids [7,8]
Fast atom bombardment	FAB	desorption/ionization from solids and liquids by a beam of energetic neutral atoms [11,12]
Liquid secondary ion mass spectrometry	LSIMS	desorption/ionization from samples dissolved in a liquid matrix by a beam of energetic ions [21,22]
Massive cluster impact	MCI	generation of secondary ions by bombardment with massive clusters of up to 10^8 u [25]

Note: Apart from momentum, the characteristics of the primary particles is of minor importance [26] because only minor differences are observed between FAB and LSIMS spectra. In the following, because of the otherwise minor differences between the two methods, reference to FAB will be meant to include LSIMS.

10.1 Ion Sources for FAB and LSIMS

10.1.1 FAB Ion Sources

A FAB ion source basically is an EI ion source (Chap. 5.2.1) modified to give free access to the fast atom beam. The electron-emitting filament and the ion source heaters are switched off during FAB operation (Fig. 10.1). The FAB gas is introduced via a needle valve into the lower part of the *FAB gun* mounted above the ion source. From there, it effuses into the ionization chamber of the FAB gun and into the ion source housing. The *saddle field gun* [27] is the most common type of

FAB gun, delivering a primary particle flux of some 10^{10} s^{-1} mm^{-2} [28,29]. The gas is ionized and the ions are accelerated by a high voltage (4–8 kV) and focused onto the sample [11,13,17,30]. Neutralization of the energetic noble gas ions is effected by charge exchange with incoming neutrals (Chaps. 7.3 and 9.18.4). The kinetic energy of the atoms is mostly conserved during charge exchange, and thus the neutrals hit the exposed surface with high kinetic energy. Of course, neutralization is not quantitative, but this is not an issue as long electrostatic charging of the sample is avoided [26]. Ion guns for the generation of energetic noble gas ions can therefore be employed without disadvantage [31]. Xenon is preferred over argon and neon as FAB gas [32,33], because it transfers a higher momentum when impacting onto the surface at equal kinetic energy (Fig. 10.2).

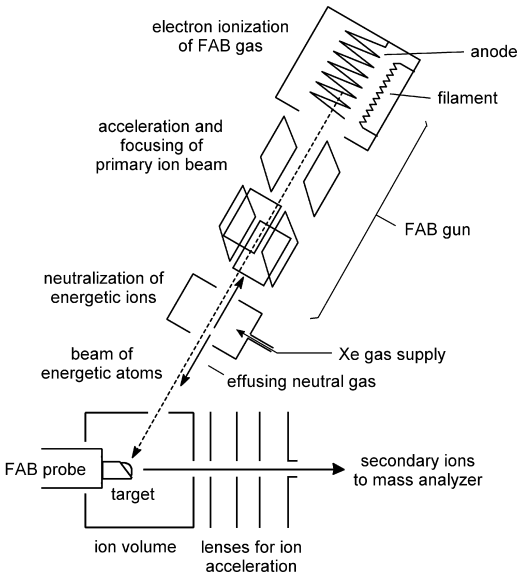


Fig. 10.1. Schematic of a FAB ion source and a FAB gun.

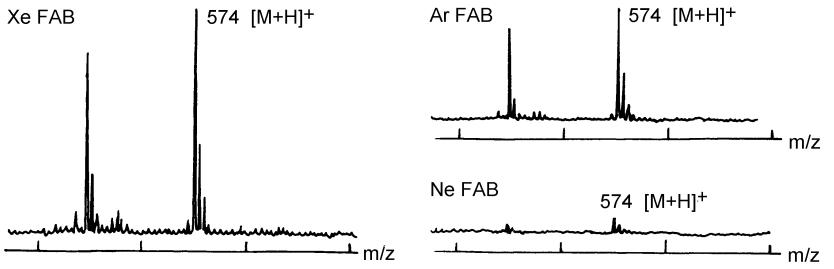


Fig. 10.2. Comparison of the efficiency of xenon, argon, and neon FAB gas for the FAB mass spectrum of the small peptide Met-enkephalin. The intensities are in scale. Reproduced from Ref. [32] by permission. © Elsevier Science, 1983.

Note: Effusing FAB gas and evaporating matrix present an additional load to the high vacuum pump of the ion source housing, affording sufficient pumping speed (300–500 l s^{-1}) for stable operation. In contrast to EI and CI ion sources, FAB ion sources are operated without heating to reduce evaporation of the matrix and thermal stress of the analyte. Accordingly, the ion source is contaminated with matrix. Often, ion sources are constructed as EI/CI/FAB combination ion sources. After FAB measurements, it is therefore recommended to heat and pump the ion source over night prior to EI or CI operation.

10.1.2 LSIMS Ion Sources

As mentioned before, primary ions can also be employed to provide the energy for secondary ion emission when organic compounds are admixed to a liquid matrix [21-23]. Cs^+ ions are preferentially used in organic *liquid secondary ion mass spectrometry* (LSIMS). The Cs^+ ions are produced by *thermal ionization* (Chap. 15.1) from a surface coated with cesium alumina silicate or other cesium salts [21]. Temperatures of about 1000°C are necessary to generate a sufficient flow of primary ions, and thus precautions must be taken to shield the LSIMS ion source from that heat. The Cs^+ ions are extracted, accelerated, and focused onto the target as usual by electrostatic lenses [34-36]. An advantage of Cs^+ ion guns is that the beam energy can be more widely varied, e.g., in the 5–25 keV range, in order to adjust for optimized secondary ion emission [37]. Especially with high-mass analytes, Cs^+ ion guns generally yield superior ion emission as compared to Xe FAB [26]. In order to further increase the momentum of the primary ions, gold negative atomic ions [38], as well as molecular and massive cluster ions (Chap. 10.6) have been used as primary ions.

10.1.3 FAB Probes

The analyte, either solid or admixed to some liquid matrix, is introduced into the FAB ion source by means of a probe bearing a sample holder or *FAB target*. The FAB target usually is a stainless steel or copper tip that exposes the analyte at some angle (30–60°) to the fast atom beam. The target can have a plane or more specifically cup-shaped surface to hold a 1–3 µl drop of matrix/analyte mixture (Fig. 10.3). Normally, the target is maintained at ion source temperature, i.e., only slightly above ambient temperature. Heating or – more importantly – cooling can be provided with special FAB probes only (Chap. 10.4.6).

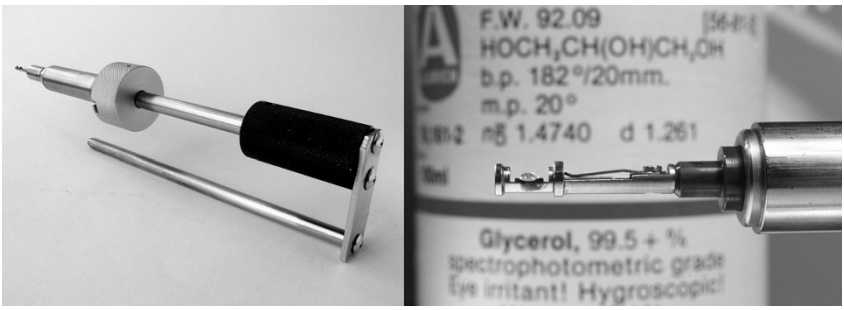


Fig. 10.3. FAB probe of a JEOL JMS-700 magnetic sector instrument (*left*). The probe tip with a drop of glycerol placed onto the exchangeable stainless steel FAB target (*right*).

10.2 Ion Formation in FAB and LSIMS

10.2.1 Ion Formation from Inorganic Samples

The energy provided by the impacting primary particle causes a collision cascade in the upper atomic or molecular layers of the sample. Within 30–60 ps, a cylindrical expansion is effected in the sample along the path of penetration [22]. Not all of this energy is dissipated and absorbed in deeper sample layers. A portion is directed toward the surface, where it effects ejection of material into the vacuum (Fig. 10.4) [24]. Due to the primary particle flux employed, this mode of operation corresponds to the *dynamic SIMS* mode as described in Chap. 15.5.1 in more detail.

In case of a bulk inorganic salt such as cesium iodide, Cs^+ and I^- ions are heading away from the surface [39]. Those ions having the suitable polarity are attracted by the extraction/acceleration voltage, those of opposite charge sign are pushed back onto the surface. Held together by strong interionic forces, ionic clusters may desorb as such or dissociate in the liquid–gas interface layer due to their internal energy content.

Example: Bombardment of cesium iodide or gold delivers cluster ion series which are useful for mass calibration of the instrument over a wide range. CsI works equally well in positive- and negative-ion mode to yield $[(CsI)_nCs]^+$ and $[(CsI)_nI]^-$ cluster ions, respectively (Fig. 10.5). Starting from $n = 0$, $[(CsI)_nCs]^+$ cluster ions have been observed up to *m/z* 90,000 [39]. Larger $[(CsI)_nCs]^+$ cluster ions dissociate to yield smaller ones: $[(CsI)_nCs]^+ \rightarrow [(CsI)_{n-x}Cs]^+ + (CsI)_x$ [40]. Gold produces a negative $Au_n^{-\bullet}$ cluster ion series up to about *m/z* 10,000 [41].

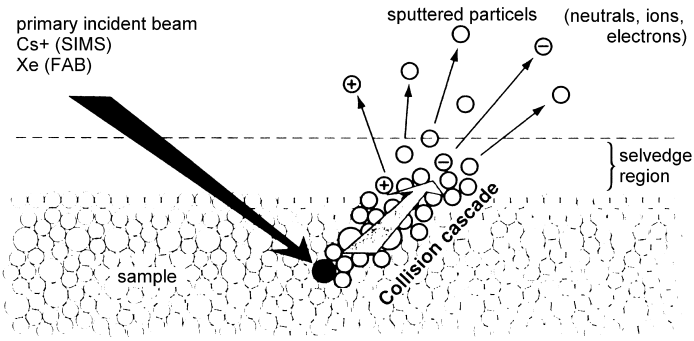


Fig. 10.4. Simple illustration of an instantaneous collision cascade generated as a result of primary particle impact in desorption/ionization mass spectrometry. Adapted from Ref. [24] by permission. © John Wiley & Sons, 1995.

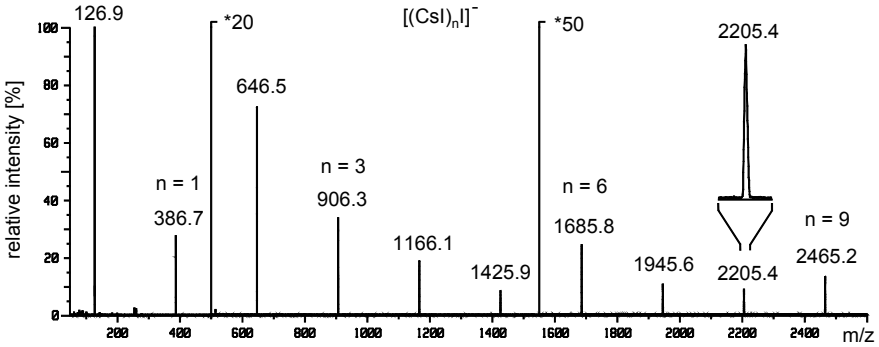


Fig. 10.5. Negative-ion FAB spectrum of solid CsI. The monoisotopic $[(CsI)_nI]^-$ cluster ion series (cf. expanded view of *m/z* 2205.4) is well suited for calibrating a wide mass range.

Note: CsI and Au both bear the advantage of being monoisotopic. This insures the peak top to exactly represent the theoretical isotopic mass of the respective cluster ion, independent of its *m/z* ratio or actual resolution (Chaps. 3.3.5, 3.4). CsI, KI, and other alkali salts that provide more narrow-spaced cluster ion series can alternatively be employed as saturated solutions in glycerol [42-44].

10.2.2 Ion Formation from Organic Samples

According to Todd "it is a common feature of FAB and LSIMS that they defy any generally acceptable mechanistic description" [45]. Unlike EI or CI, where ions are generated from gaseous molecules, desorption/ionization techniques involve a state transition from liquid or solid to the gas phase *and* ionization of neutral molecules. Nonetheless, reviews dealing with the processes of desorption and ion formation under FAB and LSIMS conditions offer some insight [22-24]. Basi-

cally, there are two major concepts, the *chemical ionization model* on one side [45-49], and the *precursor model* on the other [49-53].

The *chemical ionization model* of FAB assumes the formation of analyte ions to occur in the liquid–gas interface layer some micrometers above the liquid matrix. In this space, a plasma state similar to the reagent gas plasma in chemical ionization can exist powered by the quasi-continuous supply of energy from a stream of impacting primary particles. The present reactive species may undergo numerous bimolecular reactions, the most interesting of them being the protonation of analyte molecules to yield $[M+H]^+$ ions. Plasma conditions could also explain the observation of $M^{+\bullet}$ and $M^{-\bullet}$ radical ions as formed in case of low-polarity analytes. Here, the primary particle beam serves to sputter material from the liquid surface and to subsequently ionize neutrals by particle impact (cf. EI, Chap 5.1) in the gas phase. Matrix molecules, preferably ionized for statistical reasons, may then act as reagent ions to effect CI of the gaseous analyte. Striking arguments for this model are the facts that ion formation largely depends on the presence of gaseous matrix [46,47], and that FAB spectra of volatile analytes are closely similar to the corresponding CI spectra [49].

The *precursor model* of FAB applies well to ionic analytes and samples that are easily converted to ionic species within the liquid matrix, e.g., by protonation or deprotonation or due to cationization. Those *preformed ions* would simply have to be desorbed into the gas phase (Fig. 10.6). The promoting effect of decreasing pH (added acid) on $[M+H]^+$ ion yield of porphyrins and other analytes supports the precursor ion model [52,53]. The relative intensities of $[M+H]^+$ ions in FAB spectra of aliphatic amine mixtures also do not depend to the partial pressure of the amines in the gas phase, but are sensitive on the acidity of the matrix [54]. Furthermore, incomplete desolvation of preformed ions nicely explains the observation of matrix (Ma) adducts such as $[M+Ma+H]^+$ ions. The precursor model bears some similarities to ion evaporation in field desorption (Chap. 8.5.1).

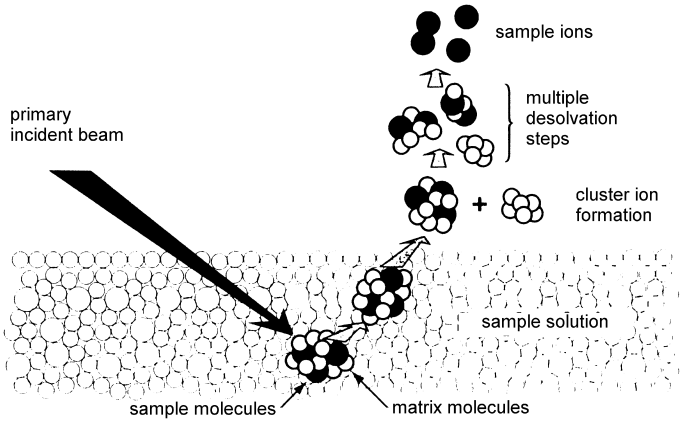


Fig. 10.6. In LSIMS and FAB, sample–matrix cluster ion formation and desolvation processes occur on a longer time scale. Adapted from Ref. [24] by permission. © John Wiley & Sons, 1995.

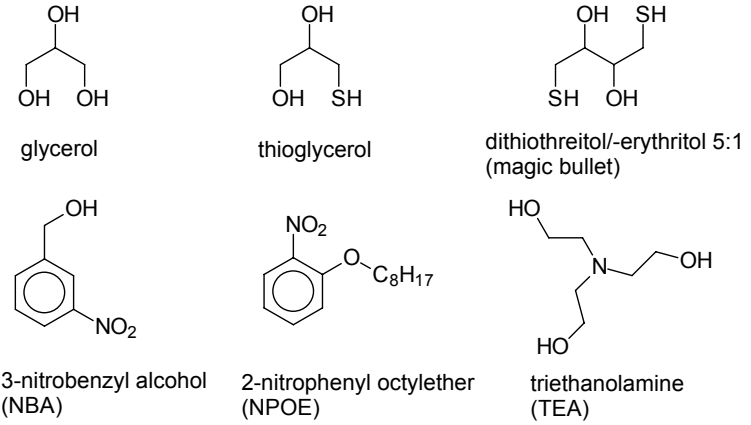
Note: It has been estimated that a single impact causes the eruption of about 10^3 secondary neutrals, but yields only 0.02–1.5 ions [43,45,54,55]. The ions are then heading away from the surface in a *supersonic expansion* at speeds of about 1000 m s^{-1} [22,43].

10.3 Liquid Matrices for FAB and LSIMS

10.3.1 The Role of the Liquid Matrix

Soon after the first use of a glycerol matrix, the importance of a liquid matrix for FAB was recognized [17]. Other organic solvents of low volatility were explored in order to obtain better spectra. The tasks of the matrix are numerous [22,23,33,56,57]: *i*) It has to absorb the primary energy. *ii*) By solvation it helps to overcome intermolecular forces between analyte molecules or ions. *iii*) The liquid matrix provides a continuously refreshing and long-lasting supply of analyte. *iv*) Finally, it assists analyte ion formation, e.g., by yielding proton donating/accepting or electron donating/accepting species upon bombardment.

Nowadays, numerous matrices are being used, especially 3-nitrobenzyl alcohol (NBA) [58-60], 2-nitrophenyl octylether (NPOE) [18,58], and thioglycerol [16]. In particular NBA is a good choice for a first trial with an unknown sample. Similar to thioglycerol, "magic bullet" (eutectic 5:1 mixture of dithiothreitol/dithioerythritol) is useful for polar high-mass analytes such as peptides [61]. Di-, tri-, and tetraethyleneglycols [16,18] and triethanolamine (TEA) [18] are also applied. Liquid paraffin [62-64], sulfolane [65,66], concentrated sulfuric acid [67], and others [18,68,69] serve for special purposes. Several reviews on FAB matrices have appeared [19,20,56,57,70].



Scheme 10.1.

An ideal FAB matrix should fulfill the following criteria [22,23,33,56,57]: *i*) The analyte should be soluble in the matrix. Otherwise, addition of co-solvents, e.g., dimethylformamide (DMF), dimethylsulfoxide (DMSO), or other additives [71,72] can become necessary. *ii*) Only low-vapor pressure solvents can be easily used as a matrix in FAB. In principle, volatile solvents can be employed, provided a stable surface can be obtained on the time scale of recording a mass spectrum. *iii*) The viscosity of the solvent must be low enough to ensure the diffusion of the solutes to the surface [73]. *iv*) Ions from the matrix itself should be as unobtrusive as possible in the resulting FAB spectrum. *v*) The matrix itself has to be chemically inert. However, specific ion formation reactions promoting secondary ion yield are advantageous.

Note: A great advantage of FAB is that the matrix can be perfectly adapted to the analyte's requirements. On the other hand, using the wrong matrix can result in complete suppression of analytically useful signals.

10.3.2 FAB Matrix Spectra – General Characteristics

FAB matrix spectra are generally characterized by a series of matrix (Ma) cluster ions accompanied by some more abundant fragment ions in the lower *m/z* range. In positive-ion FAB, $[Ma_n+H]^+$ cluster ions predominate, while $[Ma_n–H]^-$ cluster ions are preferably formed in negative-ion FAB (Fig. 10.7). The principal ion series may be accompanied by $[Ma_n+alkali]^+$ ions and some fragments of minor intensity, e.g., $[Ma_n+H–H_2O]^+$. The fragment ions detected below the $[Ma+H]^+$ ion, which normally also gives rise to the base peak, are almost the same as observed in the positive-ion CI mass spectrum of the respective matrix compound [43].

In addition to the prominent cluster ions, radiolytic decomposition of the matrix generates an enormous number of different ions, radicals, and cluster ions resulting thereof [74,75]. Despite being of minor intensity, they contribute to the "peak at every *m/z*-character" of FAB spectra, i.e., there is significant *chemical noise* (Chap. 5.2.4) [76,77]. During elongated measurements, the changes of the matrix spectrum due to increasing radiolytic decay are clearly visible [74]. High kinetic energy of impacting primary particles combined with reduced particle flux seem to diminish destructive effects of irradiation [78].

10.3.3 Unwanted Reactions in FAB-MS

The conditions of the FAB process also promote unwanted reactions between analyte and matrix. Even though such processes are not relevant in the majority of FAB measurements, one should be aware of them. Besides addition or condensation reactions with matrix fragment ions [79,80], reduction [81-84] and dehalogenation [85,86] of the analyte represent the more prominent side-reactions in FAB. Electron transfer causing the reduction of otherwise doubly charged ions have also been observed [44].

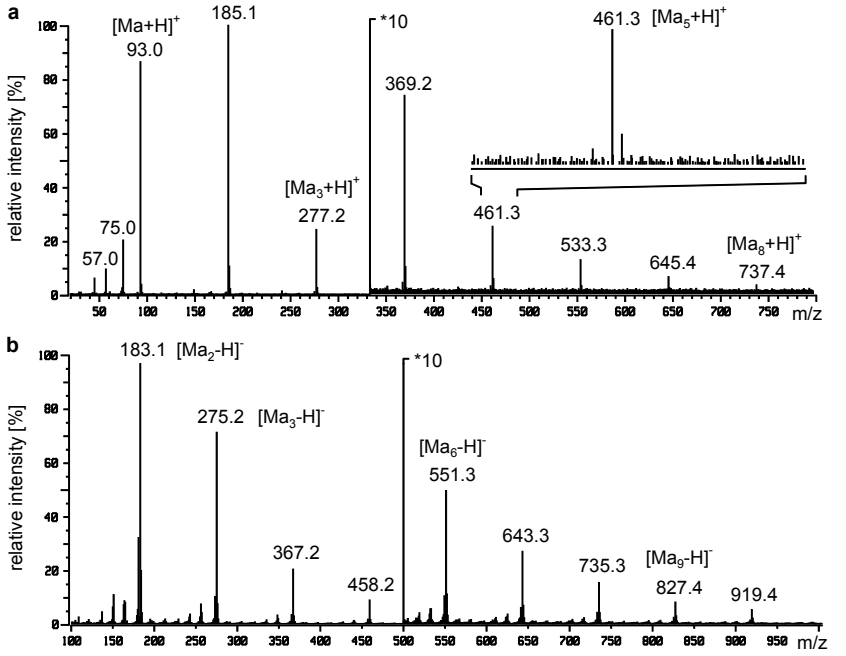


Fig. 10.7. FAB spectra of neat glycerol, M_r = 92 u. (**a**) Positive ions (for the positive-ion CI spectrum of glycerol, see Chap. 7.2.5); (**b**) negative ions. The expanded view in (**a**) shows the "peak at every *m/z*-character" of FAB spectra.

10.4 Applications of FAB-MS

10.4.1 FAB-MS of Analytes of Low to Medium Polarity

The FAB plasma provides conditions that allow to ionize molecules by either loss or addition of an electron to form positive molecular ions, $M^{+\bullet}$ [49,87], or negative molecular ions, $M^{-\bullet}$, respectively. Alternatively, protonation or deprotonation may result in $[M+H]^+$ or $[M–H]^-$ ions. Their occurrence is determined by the respective basicity or acidity of analyte and matrix. Cationization, preferably with alkali metal ions, is also frequently observed. Often, $[M+H]^+$ ions are accompanied by $[M+Na]^+$ and $[M+K]^+$ ions as already noted with FD-MS (Chap. 8.5.7). Furthermore, the joint occurrence of both $M^{+\bullet}$ and $[M+H]^+$ ions of one compound is not unusual [49]. In case of simple aromatic amines, for example, the peak intensity ratio $M^{+\bullet}/[M+H]^+$ increases as the ionization energy of the substrate decreases, whereas 4-substituted benzophenones show preferential formation of $[M+H]^+$ ions, regardless of the nature of the substituents [88]. It can be assumed that protonation is initiated when the benzophenone carbonyl groups form hydrogen bonds with the matrix.

Exchangeable protons can be replaced by alkali ions without affecting the charge state of a molecule. Thus, $[M–H_n+alkali_{n+1}]^+$ and $[M–H_n+alkali_{n–1}]^–$ ions can also be observed if one or more acidic hydrogens are easily exchanged [10,21,44,72,89,90]. The addition of cation exchange resins or crown ethers may help to reduce alkali ion contaminations [91]. Double protonation to yield $[M+2H]^{2+}$ ions or double cationization [44] are only observed with high-mass analytes [92,93] and otherwise remain an exception in FAB. Which of the above processes will most effectively contribute to the total ion yield strongly depends on the actual analyte–matrix pair.

Example: The positive-ion FAB spectrum of tetramesitylporphyrin, $C_{56}H_{54}N_4$, in NBA matrix exhibits $M^{+\bullet}$ and $[M+H]^+$ ions (Fig. 10.8) [94]. The presence of both species can be recognized by comparison of experimental and calculated M+1 ion intensity. This difference is due to about 20% $[M+H]^+$ ion formation. The diffuse groups of signals around *m/z* 900 reveal the formation of some adduct ions with the matrix, e.g., $[M+Ma+H–H_2O]^+$ at *m/z* 918.

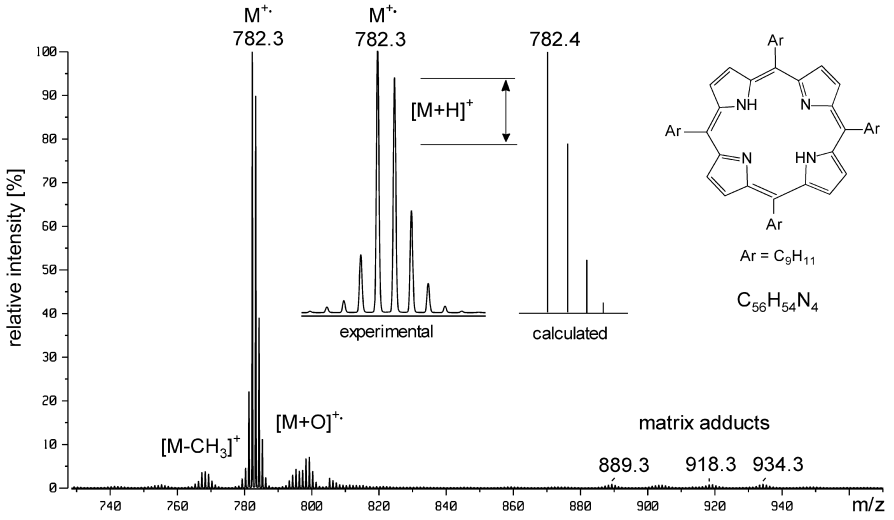


Fig. 10.8. Partial positive-ion FAB spectrum of a tetramesitylporphyrin in NBA matrix. Comparison of the experimental and calculated isotopic patterns reveals the presence of $M^{+\bullet}$ and $[M+H]^+$ ions. Adapted from Ref. [94] by permission. © IM Publications, 1997.

Example: Polyethyleneglycols (PEGs) of average molecular weights up to about 2000 u are well soluble in NBA. Resulting from their flexible polyether chain, $H(OCH_2CH_2)_nOH$, PEGs are easily cationized by loose complexation with Na^+ or K^+ ions. Traces of alkali salts are sufficient to prefer $[M+alkali]^+$ over $[M+H]^+$ ions. The positive-ion FAB spectrum of PEG 600 in NBA nicely shows the molecular weight distribution of the oligomer (Fig. 10.9). The peaks belonging to the same series are displayed at 44 u distance.

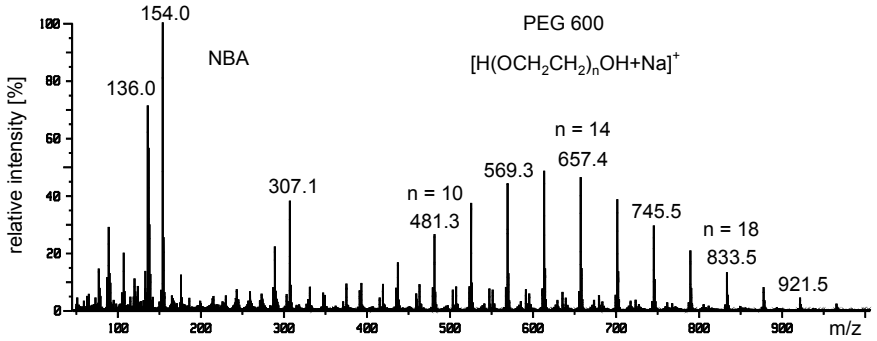


Fig. 10.9. Positive-ion FAB spectrum of polyethyleneglycol of average molecular weight 600 u (PEG 600) in NBA matrix.

10.4.2 FAB-MS of Ionic Analytes

FAB is well suited for the analysis of ionic analytes. In positive-ion mode, the spectrum is usually dominated by the cationic species, C^+, which is accompanied by cluster ions of the general composition $[C_n+A_{n-1}]^+$. Thus, the distance between these signals corresponds to the complete salt CA, i.e., yields its "molecular" weight. This behavior is perfectly analogous to FD (Chap. 8.5.3). In negative-ion FAB, the anion A^- will cause the base peak of the spectrum, and accordingly, cluster ions of the type $[C_{n-1}+A_n]^-$ are formed in addition. Consequently, both cation and anion are usually identified from the same FAB spectrum, irrespective of the chosen polarity. Nonetheless, it is common practice to select the polarity of the more interesting ion for the measurement.

Provided the salt is sufficiently soluble in the matrix, the signals normally exhibit high intensity as compared to those of the matrix. This result is consistent with the model of preformed ions in solution that only need to be desorbed into the gas phase.

Example I: The positive-ion FAB spectrum of an immonium perchlorate, $[C_{14}H_{16}N]^+ ClO_4^-$ [95], dissolved in NBA is dominated by the immonium ion (C^+) at *m/z* 198 (Fig. 10.10). The perchlorate counterion can well be identified from the cluster ions $[2C+A]^+$, *m/z* 495, and $[3C+2A]^+$, *m/z* 792. The signal at *m/z* 495 is expanded to demonstrate that chlorine is readily recognized from its isotopic pattern (Chap. 3.2.3).

Example II: The Bunte salt $[CH_3(CH_2)_{15}S\text{-}SO_3]^- Na^+$ yields a very useful negative-ion FAB spectrum from NBA matrix (Fig. 10.11). NBA forms $[Ma–H]^-$ and $Ma^{-\bullet}$ ions. The salt anion contributes the base peak at *m/z* 337.3. $[C+2A]^-$, *m/z* 697.5, and $[2C+3A]^-$, *m/z* 1057.6, cluster ions are observed in addition, their isotopic patterns being in good agreement with theoretical expectation. It is noteworthy that the matrix adduct at *m/z* 513.4 is a negative radical ion.

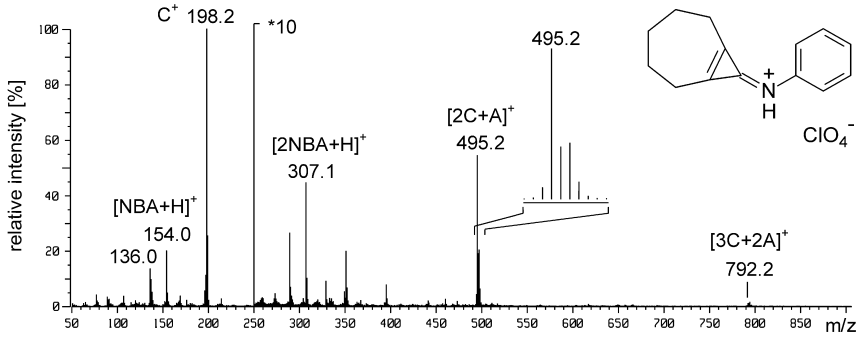


Fig. 10.10. Positive-ion FAB spectrum of an immonium salt [95]. The perchlorate counter-ion can well be identified from the first and second cluster ion. By courtesy of H. Irngartinger, Heidelberg University.

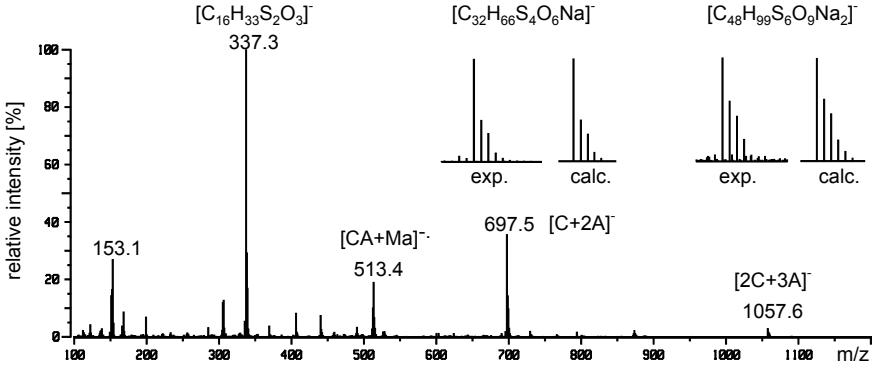


Fig. 10.11. Negative-ion FAB mass spectra of a Bunte salt. The *insets* compare experimental and calculated isotopic patterns of the $[C+2A]^-$ and $[2C+3A]^-$ cluster ions. By courtesy of M. Grunze, Heidelberg University.

10.4.3 High-Mass Analytes in FAB-MS

FAB is chiefly applied to analytes up to about *m/z* 3000, but significantly heavier ions are sometimes accessible. The upper limit surely has been demonstrated by the detection of $[(CsI)_nCs]^+$ cluster ions up to *m/z* 90,000 [39]. In case of organic molecules, $[M+H]^+$, $[M+2H]^{2+}$, and $[M+3H]^{3+}$ of porcine trypsin, a peptide of M_r = 23,463 u, have been the highest hitherto detected ions on record [93]. FAB spectra of peptides in the *m/z* 3000–6000 range are more commonly reported [16,92,96], and the FAB spectrum of a dendrimer of 7000 u has also been published [97].

Example: Inclusion complexes of [60]fullerene, C_{60} [61], of its oxides $C_{60}O$, $C_{60}O_2$, and $C_{60}O_3$ [98], and of several cycloaddition products of the fullerene [99]

in γ-cyclodextrin (γ-CD) can be analyzed by negative-ion FAB-MS using "magic bullet" matrix [61]. As one fullerene molecule is enclosed between two γ-CD units, the $[M–H]^-$ ions of these host-guest complexes [100] are detected starting from $[C_{156}H_{159}O_{80}]^-$ (monoisotopic peak expected at *m/z* 3311.8, Fig. 10.12).

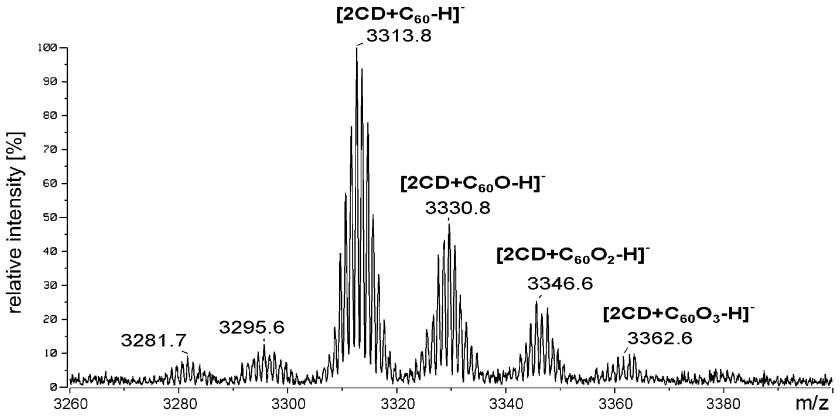


Fig. 10.12. Partial negative-ion FAB spectrum of γ–CD fullerene complexes in "magic bullet" matrix. Reproduced from Ref. [98] by permission. © IM Publications, 1998.

Note: The choice of the matrix is determined by the outer sphere of the analyte molecules, i.e., by γ-CD in case of the above inclusion complexes. [60]Fullerene and its oxides yield poor spectra in "magic bullet", but work well with less polar matrices such as NBA and NPOE.

10.4.4 Accurate Mass Measurements in FAB Mode

FAB produces long-lasting signals of sufficient intensity, thereby allowing to set magnetic sector instruments to 5,000–10,000 resolving power as needed for accurate mass measurements. In the range up to about *m/z* 600, internal calibration can sometimes be achieved by using the matrix peaks as mass reference, but the admixture of other mass calibrants to the matrix–analyte solution is normally preferred. PEGs are frequently employed for calibration purposes. Then, mass reference peaks are evenly spaced over the *m/z* range of interest (44 u distant in case of PEG, cf. Fig. 10.9) and their intensity can be adjusted to approximate those of the analyte. However, the mass calibrant can only be admixed if unwanted reactions with the analyte do not occur. In particular, in case of badly soluble analytes, complete suppression of the analyte signals by the added calibrant may pose a problem.

Example: The positive-ion high-resolution (HR) FAB spectrum of a cationic fluorescent marker dye shows the signal of the analyte ion enclosed by a set of mass reference peaks due to the admixture of PEG 600 (Fig. 10.13). The elemental

composition of the analyte can be assigned with good accuracy: exp. *m/z* 663.3182, calc. *m/z* 663.3153 for $[C_{37}H_{42}O_4N_4F_3]^+$; exp. *m/z* 664.3189, calc. *m/z* 664.3184 for $[^{13}C^{12}C_{36}H_{42}O_4N_4F_3]^+$.

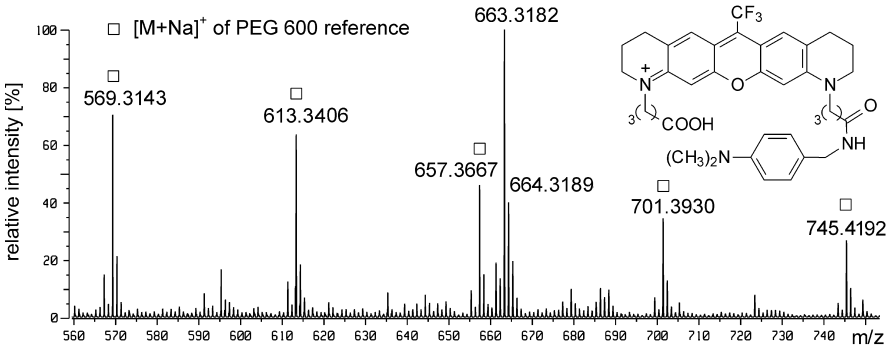


Fig. 9.13. Positive-ion FAB spectrum of a cationic fluorescent marker dye with PEG 600 admixed for internal mass calibration. By courtesy of K. H. Drexhage, Siegen University, and J. Wolfrum, Heidelberg University.

Provided a mass spectrometer offers very good scan-to-scan reproducibility of mass calibration, there is no absolute necessity to admix the mass calibrant to the analyte. Instead, alternating scans on analyte and calibrant offer almost the same level of accuracy. The simplest technical realization of such a *pseudo-internal calibration* is changing the target without interruption of the measurement [101]. The use of a *dual-target* FAB probe (DTP), having a split or double-sided target offering two separated positions, is preferable [102]. Switching between both positions is then achieved by rotating the probe axially between successive scans. The resulting *total ion chromatogram* (TIC) typically has a saw-tooth appearance (Fig. 10.14). Calibration of the analyte spectra is performed by transferring the internal calibration of the mass reference scan(s) to the successive scan(s) on the analyte. The advantages of a DTP are: *i*) interference of reference and analyte signals is excluded independent of resolution, *ii*) mutual suppression of reference and

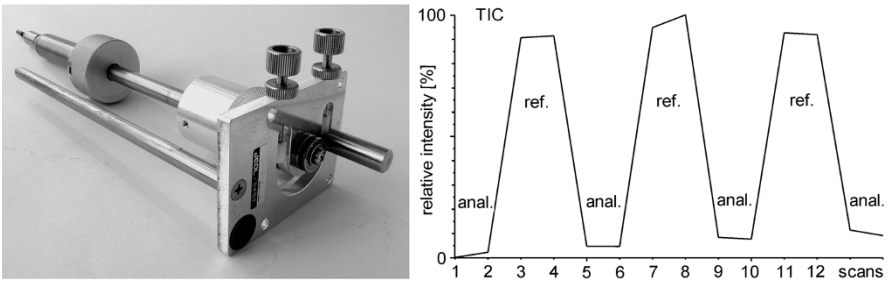


Fig. 10.14. FAB dual-target probe with handle for 180° axial turns (*left*) and TIC of a HR-FAB measurement using this probe (*right*).

analyte are avoided, *iii*) there is no need to adjust the relative intensities of analyte and calibrant peaks very closely, and *iv*) even otherwise reactive calibrants can be employed [103].

Note: Scanning of a magnet is affected by hysteresis. This improves the reproducibility of mass calibration after several scan cycles. For best results with dual-target probes, it is therefore recommended to skip the first few scans.

10.4.5 Continuous-Flow FAB

In standard FAB, the surface of the matrix solution is depleted of analyte and suffers from radiational damage during elongated measurements. Refreshment of the surface proceeds by diffusion (limited by the viscosity of the matrix) or evaporation. *Continuous-flow fast atom bombardment* (CF-FAB) continuously refreshes the surface exposed to the atom beam [104,105]. The same effect is obtained in a slightly different way by the *frit-fast atom bombardment* (frit-FAB) technique [106,107]. In addition, both CF-FAB and frit-FAB can be used for online-coupling of *liquid chromatography* (LC, Chap. 14) [108] or *capillary electrophoresis* (CE) to a FAB ion source [109].

In CF-FAB, a carrier solution, typically composed of 95% water and 5% glycerol, is passed through the CF-FAB interface via a fused silica capillary of 75 µm inner diameter at flow rates of 5–20 µl min^{-1}. Into this flow, a volume of 0.5–5 µl of liquid sample is injected. As the liquid reaches the end of the capillary inside the FAB ion source, it becomes exposed to the atom beam. The water evaporates while excess glycerol is typically absorbed by a small wick attached to the probe tip. The signal persists as long as it takes to completely elute the analyte from the interface (Fig. 10.15) [104,110]. Due to lower flow rates of 1–2 µl min^{-1}, the frit-FAB design does not need an absorbing pad (Fig 10.15). Generally, the open capillary yields less tailing after injections and can accommodate higher flow rates, whereas the frit-FAB technique operates at lower flow rates and is easier to stabilize during operation [110-112].

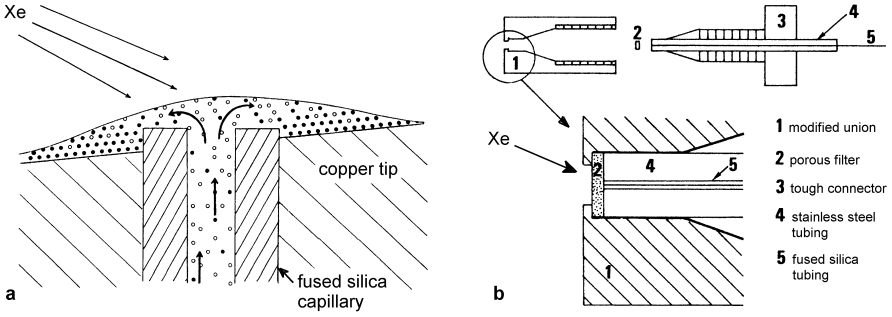


Fig. 10.15. Experimental setups of (**a**) CF-FAB and (**b**) frit-FAB. Reproduced from Ref. [105] by permission (**a**). © Academic Press, 1986. Reproduced from Ref. [107] by permission (**b**). © Elsevier Science, 1988.

10.4.6 Low-Temperature FAB

Originally, cooled FAB probes were designed to prolong the acquisition time for FAB measurements with more volatile matrices [113]. Research on sputtering processes from solid gases [114,115] and studies of cluster ion formation from solid or deeply cooled liquid alcohols [116-118] have contributed to FAB at cryogenic temperatures [119,120]. *Low-temperature fast atom bombardment* (LT-FAB) of frozen aqueous solutions of metal salts provides a source of abundant hydrated metal ions [121-123]. Organic molecules can also be detected from their frozen solutions [124]. Such LT-FAB applications are particularly interesting when enabling the detection of species that would otherwise not be accessible by mass spectrometry, because they are either extremely air- and/or water-sensitive [125,126] as the phosphaoxetane intermediate of the Wittig reaction [127] or insoluble in standard FAB matrices [103,128].

LT-FAB consumes somewhat higher amounts of sample than FAB at ambient temperature because standard solvents are less effective than conventional matrices. Thus, the analytes should be dissolved to yield 0.5–3.0 μg μl^{-1} solutions. About 3 μl of solution are deposited on the FAB probe tip and frozen. There are two modes for freezing the sample–matrix mixture: *i*) by cooling the target with cold nitrogen gas inside a custom-made vacuum lock before application of the sample [125,127] or *ii*) by simply immersing the target with the drop of solution into liquid nitrogen for about 30 s prior to transfer into the vacuum lock [103,119,120,126,129]. LT-FAB mass spectra are then obtained during thawing of frozen solutions inside the FAB ion source, which allows to employ almost any solvent as matrix in LT-FAB-MS. Consequently, neither volatility nor unwanted

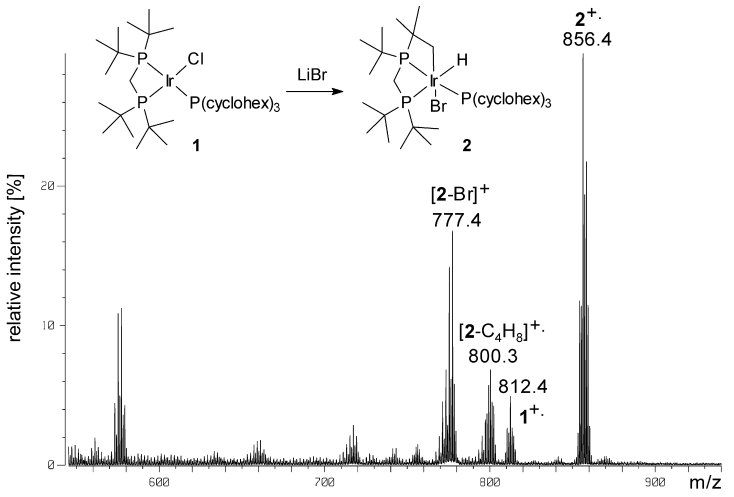


Fig. 10.16. Partial LT-FAB mass spectrum of the reaction mixture containing the iridium complexes **1** and **2** in toluene. In addition to the changes in mass, the isotopic pattern changes upon exchange of Cl by Br. By courtesy of P. Hofmann, Heidelberg University.

chemical reactions with the matrix restrict the choice of a matrix. Instead, the solvent matrix may be tailored to the analyte's requirements.

Example: Selective activation of C–H bonds is rarely observed in saturated alkyl groups. However, iridium complex **1** simply reacts by C–H insertion of the metal into a ligand bond upon treatment with LiBr in solution. The reaction can be tracked by LT-FAB-MS (Fig. 10.16). A decreasing intensity of the molecular ion of **1**, *m/z* 812.4, and increasing $M^{+\bullet}$ of **2**, *m/z* 856.4, indicate the progress of this reaction. Furthermore, the halogen exchange is indicated by the isotopic pattern.

10.4.7 FAB-MS and Peptide Sequencing

The ability of FAB mass spectra to deliver peptide sequence information was soon recognized [15,130]. Initially, the sequence was derived from fragment ions observed in the full scan spectra [15,96]. Another approach to sequence information is to subject the peptide to enzymatic hydrolysis by a mixture of several carboxypeptidases to produce a series of truncated molecules. The FAB spectrum of the mixture then reveals the *C*-terminal sequence [131,132]. In the MALDI community, this approach became known as *peptide ladder sequencing* [133].

As protein ions are too big to effect fragmentation by collision-induced dissociation (CID, Chap. 9), they are enzymatically degraded to peptides prior to their mass spectrometric examination, e.g., by tryptic digestion [134]. The digest may be used directly to obtain MS/MS spectra of peptide $[M+H]^+$ or $[M+Na]^+$ ions. Alternatively, the peptides may be separated by *liquid chromatography* (LC), *capillary electrophoresis* (CE) [135], or *2D gel electrophoresis* prior to MS.

Nowadays, sequencing of peptides and other biopolymers by tandem mass spectrometry represents a major field of work for many mass spectrometrists [136-139]; FAB and LSIMS no longer play a role here (for an example of peptide sequencing by FAB-MS cf. Chap. 9.6.6).

10.5 FAB and LSIMS – General Characteristics

10.5.1 Sensitivity of FAB-MS

In FAB mode, the sensitivity (Chap. 5.2.4) is more difficult to specify than for other ionization methods, because the intensity of a signal strongly depends on the actual preparation on the target. Magnetic sector instruments yield ion currents of about 10^{-11}–10^{-10} A on matrix ions at $R = 1000$. Significantly lower figures (10^{-15}–10^{-14} A) are obtained for the $[M+H]^+$ ion of bovine insulin, *m/z* 5734.6, at $R = 6000$. Accordingly, the detection limits vary depending on the solubility of the analyte and the ease to achieve some sort of ionization if not already ionic at all.

10.5.2 Types of Ions in FAB-MS

FAB produces a variety of ions depending on the polarity and on the ionization energy of the analyte as well as on the presence or absence of impurities such as alkali metal ions. [136] However, with some knowledge of the types of ions formed, reasonable compositions can be assigned to the signals (Table 10.2).

Table 10.2. Ions formed by FAB/LSIMS

Analytes	Positive ions	Negative ions
Nonpolar	$M^{+\bullet}$	$M^{-\bullet}$
Medium polarity	$M^{+\bullet}$ and/or $[M+H]^+$, $[M+alkali]^+$, *clusters* $[2M]^{+\bullet}$ and/or $[2M+H]^+$, $[2M+alkali]^+$, *adducts* $[M+Ma+H]^+$, $[M+Ma+alkali]^+$	$M^{-\bullet}$ and/or $[M-H]^-$, *clusters* $[2M]^{-\bullet}$ and/or $[2M-H]^-$ *adducts* $[M+Ma]^{-\bullet}$, $[M+Ma-H]^-$
Polar	$[M+H]^+$, $[M+alkali]^+$, *clusters* $[nM+H]^+$, $[nM+alkali]^+$, *adducts* $[M+Ma+H]^+$, $[M+Ma+alkali]^+$ *exchange* $[M-H_n+alkali_{n+1}]^+$ *high-mass anal.* $[M+2H]^{2+}$, $[M+2alkali]^{2+}$	$[M-H]^-$, *clusters* $[nM-H]^-$ *adducts* $[M+Ma-H]^-$ *exchange* $[M-H_n+alkali_{n-1}]^-$
Ionic[a]	C^+, $[C_n+A_{n-1}]^+$, rarely $[CA]^{+\bullet}$	A^-, $[C_{n-1}+A_n]^-$, rarely $[CA]^{-\bullet}$

[a] comprising cation C^+ and anion A^-

10.5.3 Analytes for FAB-MS

For FAB/LSIMS, the analyte should be soluble to at least 0.1 mg ml^{-1} in some solvent or even better directly in the matrix; concentrations of 0.1–3 µg $µl^{-1}$ in the matrix are ideal. In case of extremely low solubility, additives such as other solvents, acids, or surfactants can help [72].

The analyte may be neutral or ionic. Solutions containing metal salts, e.g., from buffers or excess of noncomplexed metals, may cause a confusingly large number of signals due to multiple proton/metal exchange and adduct ion formation [89]. The mass range up to 3000 u is easily covered by FAB, samples reaching up to about twice that mass still may work if sufficient solubility and some ease of ionization are combined.

10.5.4 Mass Analyzers for FAB-MS

Double-focusing magnetic sector instruments represent the standard in FAB-MS, because they combine a suitable mass range with the ability to perform high-resolution and accurate mass measurements. Until the advent of ESI and MALDI, FAB-MS/MS on magnetic four-sector instruments was the method of choice for

biomolecule sequencing [140-142]. Linear quadrupole [143] and triple quadrupole instruments have also been adapted to FAB ion sources. Other types of mass analyzers are rare exceptions with FAB or LSIMS ion sources.

10.6 Massive Cluster Impact

Massive cluster impact (MCI) mass spectrometry presents an additional means of generating secondary ions by bombardment of a surface [25]. Massive clusters of up to 10^8 u are generated by electrohydrodynamic emission (Chap. 12.1.3) of an electrolyte/glycerol solution, e.g., 0.75 M ammonium acetate in glycerol. The resulting clusters consisting of about 10^6 glycerol molecules and bearing about 200 electron charges on the average are accelerated by a 10–20 kV high voltage [144]. Although those highly charged microdroplets carry megaelectronvolt kinetic energies, the translational energy per nucleon is only in the order of 1 eV, whereas it is about 50 eV per nucleon in the case of Xe FAB. A shock wave model is proposed to explain ion formation in MCI [145]. According to this model both the impacting cluster and the surface of the bulk or matrix-dissolved analyte are compressed to gigapascal pressures upon impact. Some mixing of analyte and impacting microdroplet can be demonstrated by the occurrence of analyte species cationized by the same ions used as electrolyte in the solution from which the massive clusters are generated. Nonetheless, a matrix effect due to accumulation of a thin layer of glycerol on the surface can be excluded [144]. Instead, dry sample preparations work equally well in MCI [144].

MCI has successfully been applied to analyze proteins up to about 17,000 u [146]. These form multiply charged ions, e.g., $[M+6Na]^{6+}$, under the conditions of MCI [146]. Especially in the mass range of about 10^4 u, MCI is superior to FAB and LSIMS because it combines good signal intensity due to the enormous momentum of the impinging species with a remarkably low degree of ion fragmentation. Despite of its promising capabilities, MCI has been superseded by MALDI and ESI before it could receive widespread acceptance.

10.7 ^{252}Californium Plasma Desorption

^{252}*Californium plasma desorption* (^{252}Cf-PD) dates back to 1973 [4-6,22,147-149] and was the first method to yield ions of bovine insulin [150]. Practically, ^{252}Cf-PD served for protein characterization, an application which is now fully transferred to MALDI or ESI (Chaps. 11, 12) [151].

In ^{252}Cf-PD-MS, particles of megaelectronvolt translational energy are created from radioactive decay of ^{252}Cf nuclides, the nuclear process being the source of their kinetic energy. Each event yields two nuclides of varying identity, the sum of their masses being the mass of the former nucleus. The fission fragments of similar mass are travelling in opposite directions. Thus, only one of each pair can be

employed to effect desorption of ions from a thin film of analyte on a support foil. The ionization process in ^{252}Cf-PD is different from FAB with some closer relations to dry SIMS. The incident particles are normally travelling from the backside through a thin sample layer on a support foil [24,152]. The initial interaction of the fission fragment with a solid produces approximately 300 electron–hole pairs per angstrom along its track. Recombination of these pairs releases a large amount of energy to the surrounding medium. Within an organic layer, the resulting sudden heat is dissipated by lattice vibrations (phonons) that finally effect desorption of ions from that layer [6,153,154]. In addition to spontaneous ion desorption, ionization processes can occur on the nanosecond timescale in the gas phase [155].

Deposition of the analyte on nitrocellulose films instead of metal foils allows the removal of alkali ion contaminations by washing of the sample layer which results in better PD spectra [156]. Further improvements can be achieved by adsorption of the analyte molecules on top of an organic low-molecular-weight matrix layer [157,158].

Obviously, ^{252}Cf-PD creates ions in a pulsed manner – one burst of ions per fission event – analogous to laser desorption, a fact that restricted the adaptation of ^{252}Cf-PD to time-of-flight (TOF) analyzers (Chap. 4.2). The second fission fragment is not wasted as it serves to trigger the time measurement of the TOF analyzer if the fission fragment source is placed between sample and fission fragment detector (Fig. 10.18) [24,153]. The ^{252}Cf-PD mass spectrum of bovine insulin, for example, exhibits the $[M+H]^+$ ion as well as doubly charged $[M+2H]^{2+}$ and triply charged $[M+3H]^{3+}$ ions [149].

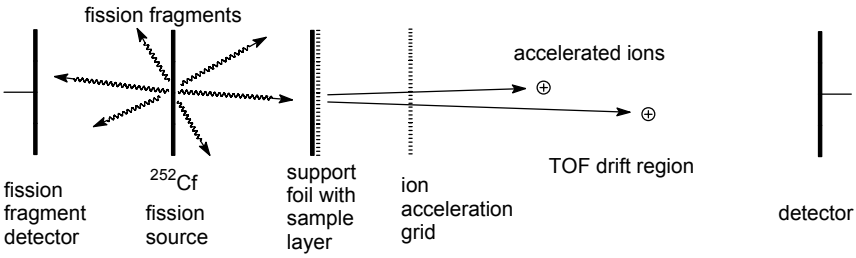


Fig. 10.17. Schematic of a ^{252}Cf-plasma desorption TOF instrument [153].

References

1. Benninghoven, A.; Kirchner, F. The Energy Distribution of Atomized Neutral and Charged Products. *Z. Naturforsch.* **1963,** *18A*, 1008-1010.
2. Honig, R.E. The Development of Secondary Ion Mass Spectrometry (SIMS): a Retrospective. *Int. J. Mass Spectrom. Ion Proc.* **1985,** *66*, 31-54.
3. Honig, R.E. Stone-Age Mass Spectrometry: the Beginnings of "SIMS" at RCA Laboratories, Princeton. *Int. J. Mass Spectrom. Ion Proc.* **1995,** *143*, 1-10.
4. Macfarlane, R.D.; Torgerson, D.F. Californium-252-Plasma Desorption Time-of-Flight Mass Spectrometry. *Int. J. Mass Spectrom. Ion Phys.* **1976,** *21*, 81-92.

5. Macfarlane, R.D.; Torgerson, D.F. Californium-252 Plasma Desorption Mass Spectroscopy. *Science* **1976,** *191*, 920-925.
6. Macfarlane, R. D. Ion Formation from Organic Solids: High Energy Heavy-Ion Induced Desorption. Benninghoven, A. Springer Series in Chemical Physics **1983,** *25*, 32-46.
7. Devienne, F.M.; Roustan, J.-C. "Fast Atom Bombardment" – A Rediscovered Method for Mass Spectrometry. *Org. Mass Spectrom.* **1982,** *17*, 173-181.
8. Devienne, F.M. Different Uses of High Energy Molecular Beams. *Entropie* **1967,** *18*, 61-67.
9. Barber, M.; Vickerman, J.C.; Wolstenholme, J. Secondary Ion Mass Spectra of Some Simple Organic Molecules. *J. Chem. Soc. , Faraday Trans. 1* **1980,** *76*, 549-559.
10. Benninghoven, A. Ion Formation from Organic Solids: Secondary ion mass spectrometry of organic compounds. Benninghoven, A. Springer Series in Chemical Physics **1983,** *25*, 64-89.
11. Barber, M.; Bordoli, R.S.; Sedgwick, R.D.; Tyler, A.N. Fast Atom Bombardment of Solids As an Ion Source in Mass Spectrometry. *Nature* **1981,** *293*, 270-275.
12. Barber, M.; Bordoli, R.S.; Sedgwick, R.D.; Tyler, A.N. Fast Atom Bombardment Mass Spectrometry of Cobalamines. *Biomed. Mass Spectrom.* **1981,** *8*, 492-495.
13. Surman, D.J.; Vickerman, J.C. Fast Atom Bombardment Quadrupole Mass Spectrometry. *J. Chem. Soc. , Chem. Commun.* **1981,** 324-325.
14. Barber, M.; Bordoli, R.S.; Sedgwick, R.D.; Tyler, A.N.; Bycroft, B.W. Fast Atom Bombardment Mass Spectrometry of Bleomycin A2 and B2 and Their Metal Complexes. *Biochem. Biophys. Res. Commun.* **1981,** *101*, 632-638.
15. Morris, H.R.; Panico, M.; Barber, M.; Bordoli, R.S.; Sedgwick, R.D.; Tyler, A.N. Fast Atom Bombardment: a New Mass Spectrometric Method for Peptide Sequence Analysis. *Biochem. Biophys. Res. Commun.* **1981,** *101*, 623-631.
16. Barber, M.; Bordoli, R.S.; Elliott, G.J.; Sedgwick, R.D.; Tyler, A.N.; Green, B.N. Fast Atom Bombardment Mass Spectrometry of Bovine Insulin and Other Large Peptides. *J. Chem. Soc. , Chem. Commun.* **1982,** 936-938.
17. Barber, M.; Bordoli, R.S.; Elliott, G.J.; Sedgwick, R.D.; Tyler, A.N. Fast Atom Bombardment Mass Spectrometry. *Anal. Chem.* **1982,** *54*, 645A-657A.
18. Meili, J.; Seibl, J. Matrix Effects in Fast Atom Bombardment (FAB) Mass Spectrometry. *Int. J. Mass Spectrom. Ion Phys.* **1983,** *46*, 367-370.
19. Gower, L.J. Matrix Compounds for Fast Atom Bombardment Mass Spectrometry. *Biomed. Mass Spectrom.* **1985,** *12*, 191-196.
20. De Pauw, E.; Agnello, A.; Derwa, F. Liquid Matrices for Liquid Secondary Ion Mass Spectrometry-Fast Atom Bombardment [LSIMS-FAB]: an Update. *Mass Spectrom. Rev.* **1991,** *10*, 283-301.
21. Aberth, W.; Straub, K.M.; Burlingame, A.L. Secondary Ion Mass Spectrometry With Cesium Ion Primary Beam and Liquid Target Matrix for Analysis of Bioorganic Compounds. *Anal. Chem.* **1982,** *54*, 2029-2034.
22. Sundqvist, B.U.R. Desorption Methods in Mass Spectrometry. *Int. J. Mass Spectrom. Ion Proc.* **1992,** *118/119*, 265-287.
23. Sunner, J. Ionization in Liquid Secondary Ion Mass Spectrometry (LSIMS). *Org. Mass Spectrom.* **1993,** *28*, 805-823.
24. Busch, K.L. Desorption Ionization Mass Spectrometry. *J. Mass Spectrom.* **1995,** *30*, 233-240.
25. Mahoney, J.F.; Perel, J.; Ruatta, S.A.; Martino, P.A.; Husain, S.; Lee, T.D. Massive Cluster Impact Mass Spectrometry: a New Desorption Method for the Analysis of Large Biomolecules. *Rapid Commun. Mass Spectrom.* **1991,** *5*, 441-445.
26. Miller, J.M. Fast Atom Bombardment Mass Spectrometry of Organometallic, Coordination, and Related Compounds. *Mass Spectrom. Rev.* **1989,** *9*, 319-347.
27. Franks, J.; Ghander, A.M. Saddle Field Ion Source of Spherical Configuration for Etching and Thinning Applications. *Vacuum* **1974,** *24*, 489-491.
28. Alexander, A.J.; Hogg, A.M. Characterization of a Saddle-Field Discharge Gun for FABMS Using Different Discharge Vapors. *Int. J. Mass Spectrom. Ion Proc.* **1986,** *69*, 297-311.

29. Boggess, B.; Cook, K.D. Determination of Flux From a Saddle Field Fast-Atom Bombardment Gun. *J. Am. Soc. Mass Spectrom.* **1994,** *5*, 100-105.
30. Barber, M.; Bordoli, R.S.; Sedgwick, R.D.; Tyler, A.N. Fast Atom Bombardment of Solids (F.A.B.): a New Ion Source for Mass Spectrometry. *J. Chem. Soc. , Chem. Commun.* **1981,** 325-327.
31. McDowell, R.A.; Morris, H.R. Fast Atom Bombardment Mass Spectrometry: Biological Analysis Using an Ion Gun. *Int. J. Mass Spectrom. Ion Phys.* **1983,** *46*, 443-446.
32. Morris, H.R.; Panico, M.; Haskins, N.J. Comparison of Ionization Gases in FAB Mass Spectra. *Int. J. Mass Spectrom. Ion Phys.* **1983,** *46*, 363-366.
33. Fenselau, C. Ion Formation from Organic Solids: Fast Atom Bombardment. Benninghoven, A. Springer Series in Chemical Physics **1983,** *25*, 90-100.
34. Burlingame, A. L.; Aberth, W. Ion Formation from Organic Solids: Use of a cesium primary beam for liquid SIMS analysis of bio-organic compounds. Benninghoven, A. Springer Series in Chemical Physics **1983,** *25*, 167-171.
35. Burlingame, A.L. Comparison of Three Geometries for a Cesium Primary Beam Liquid Secondary Ion Mass Spectrometry Source. *Anal. Chem.* **1984,** *56*, 2915-2918.
36. Aberth, W.; Burlingame, A.L. Comparison of Three Geometries for a Cesium Primary Beam Liquid Secondary Ion Mass Spectrometry Source. *Anal. Chem.* **1984,** *56*, 2915-2918.
37. Aberth, W.H.; Burlingame, A.L. Effect of Primary Beam Energy on the Secondary-Ion Sputtering Efficiency of Liquid Secondary-Ionization Mass Spectrometry in the 5-30-KeV Range. *Anal. Chem.* **1988,** *60*, 1426-1428.
38. McEwen, C.N.; Hass, J.R. Negative Gold Ion Gun for Liquid Secondary Ion Mass Spectrometry. *Anal. Chem.* **1985,** *57*, 890-892.
39. Katakuse, I.; Nakabushi, H.; Ichihara, T.; Sakurai, T.; Matsuo, T.; Matsuda, H. Generation and Detection of Cluster Ions $[(CsI)_NCs]^+$ Ranging Up to M/z = 90,000. *Int. J. Mass Spectrom. Ion Proc.* **1984,** *57*, 239-243.
40. Katakuse, I.; Nakabushi, H.; Ichihara, T.; Sakurai, T.; Matsuo, T.; Matsuda, H. Metastable Decay of Cesium Iodide Cluster Ions. *Int. J. Mass Spectrom. Ion Proc.* **1984,** *62*, 17-23.
41. Sim, P.G.; Boyd, R.K. Calibration and Mass Measurement in Negative-Ion Fast-Atom Bombardment Mass Spectrometry. *Rapid Commun. Mass Spectrom.* **1991,** *5*, 538-542.
42. Rapp, U.; Kaufmann, H.; Höhn, M.; Pesch, R. Exact Mass Determinations Under FAB Conditions. *Int. J. Mass Spectrom. Ion Phys.* **1983,** *46*, 371-374.
43. Sunner, J. Role of Ion-Ion Recombination for Alkali Chloride Cluster Formation in Liquid Secondary Ion Mass Spectrometry. *J. Am. Soc. Mass Spectrom.* **1993,** *4*, 410-418.
44. Cao, Y.; Haseltine, J.N.; Busch, K.L. Double Cationization With Alkali Ions in Liquid Secondary Ion Mass Spectrometry. *Spectroscopy Lett.* **1996,** *29*, 583-589.
45. Todd, P.J. Secondary Ion Emission From Glycerol Under Continuous and Pulsed Primary Ion Current. *Org. Mass Spectrom.* **1988,** *23*, 419-424.
46. Schröder, E.; Münster, H.; Budzikiewicz, H. Ionization by Fast Atom Bombardment - a Chemical Ionization (Matrix) Process Ion the Gas Phase? *Org. Mass Spectrom.* **1986,** *21*, 707-715.
47. Münster, H.; Theobald, F.; Budzikiewicz, H. The Formation of a Matrix Plasma in the Gas Phase Under Fast Atom Bombardment Conditions. *Int. J. Mass Spectrom. Ion Proc.* **1987,** *79*, 73-79.
48. Rosen, R.T.; Hartmann, T.G.; Rosen, J.D.; Ho, C.-T. Fast-Atom-Bombardment Mass Spectra of Low-Molecular-Weight Alcohols and Other Compounds. Evidence for a Chemical-Ionization Process in the Gas Phase. *Rapid Commun. Mass Spectrom.* **1988,** *2*, 21-23.
49. Miller, J.M.; Balasanmugam, K. Fast Atom Bombardment Mass Spectrometry of Some Nonpolar Compounds. *Anal. Chem.* **1989,** *61*, 1293-1295.
50. Benninghoven, A. Organic Secondary Ion Mass Spectrometry (SIMS) and Its Relation to Fast Atom Bombardment (FAB). *Int. J. Mass Spectrom. Ion Phys.* **1983,** *46*, 459-462.
51. van Breemen, R.B.; Snow, M.; Cotter, R.J. Time-Resolved Laser Desorption Mass Spectrometry. I. Desorption of Pre-

formed Ions. *Int. J. Mass Spectrom. Ion Phys.* **1983,** *49*, 35-50.
52. Musselman, B.; Watson, J.T.; Chang, C.K. Direct Evidence for Preformed Ions of Porphyrins in the Solvent Matrix for Fast Atom Bombardment Mass Spectrometry. *Org. Mass Spectrom.* **1986,** *21*, 215-219.
53. Shiea, J.; Sunner, J. The Acid Effect in Fast Atom Bombardment. *Org. Mass Spectrom.* **1991,** *26*, 38-44.
54. Todd, P.J. Solution Chemistry and Secondary Ion Emission From Amine-Glycerol Solutions. *J. Am. Soc. Mass Spectrom.* **1991,** *2*, 33-44.
55. Wong, S.S.; Röllgen, F.W. Sputtering of Large Molecular Ions by Low Energy Particle Impact. *Nulc. Instrum. Methods Phys. Res. ,B* **1986,** *B14*, 436-447.
56. Baczynskyi, L. New Matrices for Fast Atom Bombardment Mass Spectrometry. *Adv. Mass Spectrom.* **1985,** *10*, 1611-1612.
57. De Pauw, E.; Agnello, A.; Derwa, F. Liquid Matrices for Liquid Secondary Ion Mass Spectrometry. *Mass Spectrom. Rev.* **1986,** *5*, 191-212.
58. Meili, J.; Seibl, J. A New Versatile Matrix for Fast Atom Bombardment Analysis. *Org. Mass Spectrom.* **1984,** *19*, 581-582.
59. Barber, M.; Bell, D.; Eckersley, M.; Morris, M.; Tetler, L. The Use of *M*-Nitrobenzyl Alcohol As a Matrix in Fast Atom Bombardment Mass Spectrometry. *Rapid Commun. Mass Spectrom.* **1988,** *2*, 18-21.
60. Aubagnac, J.-L. Use of *M*-Nitrobenzyl Alcohol As a Matrix in Fast-Atom-Bombardment Negative-Ion Mass Spectrometry of Polar Compounds. *Rapid Commun. Mass Spectrom.* **1990,** *4*, 114-116.
61. Andersson, T.; Westman, G.; Stenhagen, G.; Sundahl, M.; Wennerström, O. A Gas Phase Container for C_{60}; a Γ-Cyclodextrin Dimer. *Tetrahedron Lett.* **1995,** *36*, 597-600.
62. Dube, G. The Behavior of Aromatic Hydrocarbons Under Fast Atom Bombardment. *Org. Mass Spectrom.* **1984,** *19*, 242-243.
63. Abdul-Sada, A.K.; Greenway, A.M.; Seddon, K.R. The Extent of Aggregation of Air-Sensitive Alkyllithium Compounds As Determined by Fast-Atom-Bombardment Mass Spectrometry. *J. Organomet. Chem.* **1989,** *375*, C17-C19.
64. Abdul-Sada, A.K.; Greenway, A.M.; Seddon, K.R. The Application of Liquid Paraffin and 3,4-Dimethoxybenzyl Alcohol As Matrix Compounds to Fast Atom Bombardment Mass Spectrometry. *Eur. Mass Spectrom.* **1996,** *2*, 77-78.
65. Bandini, A.L.; Banditelli, G.; Minghetti, G.; Pelli, B.; Traldi, P. Fast Atom Bombardment Induced Decomposition Pattern of the Gold(III) Bis(Carbene) Complex $[[(p\text{-}MeC_6H_4NH)(EtO)C]_2AuI_2]ClO_4$, a Retrosynthetic Process? *Organometallics* **1989,** *8*, 590-593.
66. Dobson, J.C.; Taube, H. Coordination Chemistry and Redox Properties of Polypyridyl Complexes of Vanadium(II). *Inorg. Chem.* **1989,** *28*, 1310-1315.
67. Leibman, C.P.; Todd, P.J.; Mamantov, G. Enhanced Positive Secondary Ion Emission From Substituted Polynuclear Aromatic Hydrocarbon/Sulfuric Acid Solutions. *Org. Mass Spectrom.* **1988,** *23*, 634-642.
68. Staempfli, A.A.; Schlunegger, U.P. A New Matrix for Fast-Atom Bombardment Analysis of Corrins. *Rapid Commun. Mass Spectrom.* **1991,** *5*, 30-31.
69. Visentini, J.; Nguyen, P.M.; Bertrand, M.J. The Use of 4-Hydroxybenzenesulfonic Acid As a Reduction-Inhibiting Matrix in Liquid Secondary-Ion Mass Spectrometry. *Rapid Commun. Mass Spectrom.* **1991,** *5*, 586-590.
70. Gower, L.J. Matrix Compounds for Fast Atom Bombardment: a Further Review. *Adv. Mass Spectrom.* **1985,** *10*, 1537-1538.
71. Rozenski, J.; Herdewijn, P. The Effect of Addition of Carbon Powder to Samples in Liquid Secondary Ion Mass Spectrometry: Improved Ionization of Apolar Compounds. *Rapid Commun. Mass Spectrom.* **1995,** *9*, 1499-1501.
72. Huang, Z.-H.; Shyong, B.-J.; Gage, D.A.; Noon, K.R.; Allison, J. *N*-Alkylnicotinium Halides: a Class of Cationic Matrix Additives for Enhancing the Sensitivity in Negative Ion Fast-Atom Bombardment Mass Spectrometry of Polyanionic Analytes. *J. Am. Soc. Mass Spectrom.* **1994,** *5*, 935-948.

73. Shiea, J.T.; Sunner, J. Effects of Matrix Viscosity on FAB Spectra. *Int. J. Mass Spectrom. Ion Proc.* **1990,** *96*, 243-265.
74. Field, F.H. Fast Atom Bombardment Study of Glycerol: Mass Spectra and Radiation Chemistry. *J. Phys. Chem.* **1982,** *86*, 5115-5123.
75. Caldwell, K.A.; Gross, M.L. Origins and Structures of Background Ions Produced by FAB of Glycerol. *J. Am. Soc. Mass Spectrom.* **1994,** *5*, 72-91.
76. Busch, K.L. Chemical Noise in Mass Spectrometry. Part I. *Spectroscopy* **2002,** *17*, 32-37.
77. Busch, K.L. Chemical Noise in Mass Spectrometry. Part II - Effects of Choices in Ionization Methods on Chemical Noise. *Spectroscopy* **2003,** *18*, 56-62.
78. Reynolds, J.D.; Cook, K.D. Improving Fast Atom Bombardment Mass Spectra: the Influence of Some Controllable Parameters on Spectral Quality. *J. Am. Soc. Mass Spectrom.* **1990,** *1*, 149-157.
79. Barber, M.; Bell, D.J.; Morris, M.; Tetler, L.W.; Woods, M.D.; Monaghan, J.J.; Morden, W.E. The Interaction of *M*-Nitrobenzyl Alcohol With Compounds Under Fast-Atom-Bombardment Conditions. *Rapid Commun. Mass Spectrom.* **1988,** *2*, 181-183.
80. Tuinman, A.A.; Cook, K.D. Fast Atom Bombardment-Induced Condensation of Glycerol With Ammonium Surfactants. I. Regioselectivity of the Adduct Formation. *J. Am. Soc. Mass Spectrom.* **1992,** *3*, 318-325.
81. Aubagnac, J.-L.; Claramunt, R.-M.; Sanz, D. Reduction Phenomenon on the FAB Mass Spectra of *N*-Aminoazoles With a Glycerol Matrix. *Org. Mass Spectrom.* **1990,** *25*, 293-295.
82. Murthy, V.S.; Miller, J.M. Suppression Effects on a Reduction Process in Fast-Atom Bombardment Mass Spectrometry. *Rapid Commun. Mass Spectrom.* **1993,** *7*, 874-881.
83. Aubagnac, J.-L.; Gilles, I.; Lazaro, R.; Claramunt, R.-M.; Gosselin, G.; Martinez, J. Reduction Phenomenon in Frit Fast-Atom Bombardment Mass Spectrometry. *Rapid Commun. Mass Spectrom.* **1995,** *9*, 509-511.
84. Aubagnac, J.-L.; Gilles, I.; Claramunt, R.M.; Escolastico, C.; Sanz, D.; Elguero, J. Reduction of Aromatic Fluorine Compounds in Fast-Atom Bombardment Mass Spectrometry. *Rapid Commun. Mass Spectrom.* **1995,** *9*, 156-159.
85. Théberge, R.; Bertrand, M.J. Beam-Induced Dehalogenation in LSIMS: Effect of Halogen Type and Matrix Chemistry. *J. Mass Spectrom.* **1995,** *30*, 163-171.
86. Théberge, R.; Bertrand, M.J. An Investigation of the Relationship Between Analyte Surface Concentration and the Extent of Beam-Induced Dehalogenation in LSIMS. *Rapid Commun. Mass Spectrom.* **1998,** *12*, 2004-2010.
87. Vetter, W.; Meister, W. Fast Atom Bombardment Mass Spectrum of B-Carotene. *Org. Mass Spectrom.* **1985,** *20*, 266-267.
88. Nakata, H.; Tanaka, K. Structural and Substituent Effects on $M^{+\cdot}$ Vs. $[M+H]^+$ Formation in FAB Mass Spectra of Simple Organic Compounds. *Org. Mass Spectrom.* **1994,** *29*, 283-288.
89. Moon, D.-C.; Kelly, J.A. A Simple Desalting Procedure for FAB-MS. *Biomed. Environ. Mass Spectrom.* **1988,** *17*, 229-237.
90. Prókai, L.; Hsu, B.-H.; Farag, H.; Bodor, N. Desorption Chemical Ionization, Thermospray, and Fast Atom Bombardment Mass Spectrometry of Dihydropyridine - Pyridinium Salt-Type Redox Systems. *Anal. Chem.* **1989,** *61*, 1723-1728.
91. Kolli, V.S.K.; York, W.S.; Orlando, R. Fast Atom Bombardment Mass Spectrometry of Carbohydrates Contaminated With Inorganic Salts Using a Crown Ether. *J. Mass Spectrom.* **1998,** *33*, 680-682.
92. Desiderio, D.M.; Katakuse, I. Fast Atom Bombardment Mass Spectrometry of Insulin, Insulin A-Chain, Insulin B-Chain, and Glucagon. *Biomed. Mass Spectrom.* **1984,** *11*, 55-59.
93. Barber, M.; Green, B.N. The Analysis of Small Proteins in the Molecular Weight Range 10-24 KDa by Magnetic Sector Mass Spectrometry. *Rapid Commun. Mass Spectrom.* **1987,** *1*, 80-83.
94. Frauenkron, M.; Berkessel, A.; Gross, J.H. Analysis of Ruthenium Carbonyl-Porphyrin Complexes: a Comparison of Matrix-Assisted Laser Desorption/Ionization Time-of-Flight, Fast-Atom Bombardment and Field Desorption Mass Spectrometry. *Eur. Mass. Spectrom.* **1997,** *3*, 427-438.

95. Irngartinger, H.; Altreuther, A.; Sommerfeld, T.; Stojanik, T. Pyramidalization in Derivatives of Bicyclo[5.1.0]Oct-1(7)-Enes and 2,2,5,5-Tetramethylbicyclo[4.1.0]Hept-1(6)-Enes. *Eur. J. Org. Chem.* **2000,** 4059-4070.
96. Barber, M.; Bordoli, R.S.; Elliott, G.J.; Tyler, A.N.; Bill, J.C.; Green, B.N. Fast Atom Bombardment (FAB) Mass Spectrometry: a Mass Spectral Investigation of Some of the Insulins. *Biomed. Mass Spectrom.* **1984,** *11*, 182-186.
97. Rajca, A.; Wongsriratanakul, J.; Rajca, S.; Cerny, R. A Dendritic Macrocyclic Organic Polyradical With a Very High Spin of $S = 10$. *Angew. Chem. ,Int. Ed.* **1998,** *37*, 1229-1232.
98. Giesa, S.; Gross, J.H.; Krätschmer, W.; Gleiter, R. Experiments Towards an Analytical Application of Host-Guest Complexes of [60] Fullerene and Its Derivatives. *Eur. Mass. Spectrom.* **1998,** *4*, 189-196.
99. Juo, C.-G.; Shiu, L.-L.; Shen, C.K.F.; Luh, T.-J.; Her, G.-R. Analysis of C_{60} Derivatives by FAB-MS As Γ-Cyclodextrin Inclusion Complexes. *Rapid Commun. Mass Spectrom.* **1995,** *9*, 604-608.
100. Vincenti, M. Host-Guest Chemistry in the Mass Spectrometer. *J. Mass Spectrom.* **1995,** *30*, 925-939.
101. Morgan, R.P.; Reed, M.L. Fast Atom Bombardment (FAB)-Accurate Mass Measurement. *Org. Mass Spectrom.* **1982,** *17*, 537.
102. Münster, H.; Budzikiewicz, H.; Schröder, E. A Modified Target for FAB Measurements. *Org. Mass Spectrom.* **1987,** *22*, 384-385.
103. Gross, J.H.; Giesa, S.; Krätschmer, W. Negative-Ion Low-Temperature Fast-Atom Bombardment Mass Spectrometry of Monomeric and Dimeric [60]Fullerene Compounds. *Rapid Commun. Mass Spectrom.* **1999,** *13*, 815-820.
104. Caprioli, R.M.; Fan, T.; Cottrell, J.S. A Continuous-Flow Sample Probe for Fast Atom Bombardment Mass Spectrometry. *Anal. Chem.* **1986,** *58*, 2949-2954.
105. Caprioli, R.M.; Fan, T. High Sensitivity Mass Spectrometric Determination of Peptides: Direct Analysis of Aqueous Solutions. *Biochem. Biophys. Res. Commun.* **1986,** *141*, 1058-1065.
106. Ito, Y.; Takeuchi, T.; Ishii, D.; Goto, M. Direct Coupling of Micro High-Performance Liquid Chromatography With FAB-MS. *J. Chromatogr.* **1985,** *346*, 161-166.
107. Takeuchi, T.; Watanabe, S.; Kondo, N.; Ishii, D.; Goto, M. Improvement of the Interface for Coupling of FAB-MS and Micro High-Performance Liquid Chromatography. *J. Chromatogr.* **1988,** *435*, 482-488.
108. Siethoff, C.; Nigge, W.; Linscheid, M.W. The Determination of Ifosfamide in Human Blood Serum Using LC/MS. *Fresenius J. Anal. Chem.* **1995,** *352*, 801-805.
109. Suter, M.J.F.; Caprioli, R.M. An Integral Probe for Capillary Zone Electrophoresis/Continuous-Flow Fast Atom Bombardment Mass Spectrometry. *J. Am. Soc. Mass Spectrom.* **1992,** *3*, 198-206.
110. Caprioli, R.M. Continuous-Flow Fast Atom Bombardment Mass Spectrometry. *Anal. Chem.* **1990,** *62*, 477A-485A.
111. *Continuous-Flow Fast Atom Bombardment Mass Spectrometry;* Caprioli, R.M., editor; John Wiley & Sons: Chichester, 1990.
112. Caprioli, R.M.; Suter, M.J.F. Continuous-Flow FAB: Recent Advances and Applications. *Int. J. Mass Spectrom. Ion Proc.* **1992,** *118/119*, 449-476.
113. Falick, A.M.; Walls, F.C.; Laine, R.A. Cooled Sample Introduction Probe for Liquid SIMS. *Anal. Biochem.* **1986,** *159*, 132-137.
114. Jonkman, H.T.; Michl, J. Secondary Ion Mass Spectrometry of Small-Molecule Solids at Cryogenic Temperatures. 1. Nitrogen and Carbon Monoxide. *J. Am. Chem. Soc.* **1981,** *103*, 733-737.
115. Orth, R.G.; Jonkman, H.T.; Michl, J. Secondary Ion Mass Spectrometry of Small-Molecule Solids at Cryogenic Temperatures. 2. Rare Gas Solids. *J. Am. Chem. Soc.* **1981,** *103*, 6026-6030.
116. Katz, R.N.; Chaudhary, T.; Field, F.H. Particle Bombardment (FAB) Mass Spectra of Methanol at Sub-Ambient Temperatures. *J. Am. Chem. Soc.* **1986,** *108*, 3897-3903.
117. Katz, R.N.; Chaudhary, T.; Field, F.H. Particle Bombardment (KeV) Mass Spectra of Ethylene Glycol, Glycerol, and Water at Sub-Ambient Temperatures. *Int. J. Mass Spectrom. Ion Proc.* **1987,** *78*, 85-97.
118. Johnstone, R.A.W.; Wilby, A.H. Fast Atom Bombardment at Low Tempera-

tures. Part 2. Polymerization in the Matrix. *Int. J. Mass Spectrom. Ion Proc.* **1989,** *89*, 249-264.
119. Kosevich, M.V.; Czira, G.; Boryak, O.A.; Shelkovsky, V.S.; Vékey, K. Comparison of Positive and Negative Ion Clusters of Methanol and Ethanol Observed by Low Temperature Secondary Ion MS. *Rapid Commun. Mass Spectrom.* **1997,** *11*, 1411-1416.
120. Kosevich, M.V.; Czira, G.; Boryak, O.A.; Shelkovsky, V.S.; Vékey, K. Temperature Dependences of Ion Currents of Alcohol Clusters Under Low-Temperature Secondary Ion Mass Spectrometric Conditions. *J. Mass Spectrom.* **1998,** *33*, 843-849.
121. Magnera, T.F.; David, D.E.; Stulik, D.; Orth, R.G.; Jonkman, H.T.; Michl, J. Production of Hydrated Metal Ions by Fast Ion or Atom Beam Sputtering. Collision-Induced Dissociation and Successive Hydration Energies of Gaseous Cu^+ With 1-4 Water Molecules. *J. Am. Chem. Soc.* **1989,** *111*, 5036-5043.
122. Boryak, O.A.; Stepanov, I.O.; Kosevich, M.V.; Shelkovsky, V.S.; Orlov, V.V.; Blagoy, Y.P. Origin of Clusters. I. Correlation of Low Temperature FAB Mass Spectra With the Phase Diagram of NaCl-Water Solutions. *Eur. Mass Spectrom.* **1996,** *2*, 329-339.
123. Kosevich, M.V.; Boryak, O.A.; Stepanov, I.O.; Shelkovsky, V.S. Origin of Clusters. II. Distinction of Two Different Processes of Formation of Mixed Metal/Water Clusters Under Low-Temperature Fast Atom Bombardment. *Eur. Mass Spectrom.* **1997,** *3*, 11-17.
124. Boryak, O.A.; Kosevich, M.V.; Shelkovsky, V.S.; Blagoy, Y.P. Study of Frozen Solutions of Nucleic Acid Nitrogen Bases by Means of Low Temperature FAB-MS. *Rapid Commun. Mass Spectrom.* **1996,** *10*, 197-199.
125. Huang, M.-W.; Chei, H.-L.; Huang, J.P.; Shiea, J. Application of Organic Solvents As Matrixes to Detect Air-Sensitive and Less Polar Compounds Using Low-Temperature Secondary Ion Mass Spectrometry. *Anal. Chem.* **1999,** *71*, 2901-2907.
126. Hofmann, P.; Volland, M.A.O.; Hansen, S.M.; Eisenträger, F.; Gross, J.H.; Stengel, K. Isolation and Characterization of a Monomeric, Solvent Coordinated Ruthenium(II) Carbene Cation Relevant to Olefin Metathesis. *J. Organomet. Chem.* **2000,** *606*, 88-92.
127. Wang, C.H.; Huang, M.-W.; Lee, C.-Y.; Chei, H.-L.; Huang, J.P.; Shiea, J. Detection of a Thermally Unstable Intermediate in the Wittig Reaction Using Low-Temperature Liquid Secondary Ion and Atmospheric Pressure Ionization Mass Spectrometry. *J. Am. Soc. Mass Spectrom.* **1998,** *9*, 1168-1174.
128. Giesa, S.; Gross, J.H.; Hull, W.E.; Lebedkin, S.; Gromov, A.; Krätschmer, W.; Gleiter, R. $C_{120}OS$: the First Sulfur-Containing Dimeric [60]Fullerene Derivative. *Chem. Commun.* **1999,** 465-466.
129. Gross, J.H. Use of Protic and Aprotic Solvents of High Volatility As Matrixes in Analytical Low-Temperature FAB-MS. *Rapid Commun. Mass Spectrom.* **1998,** *12*, 1833-1838.
130. König, W.A.; Aydin, M.; Schulze, U.; Rapp, U.; Höhn, M.; Pesch, R.; Kalikhevitch, V.N. Fast-Atom-Bombardment for Peptide Sequencing - a Comparison With Conventional Ionization Techniques. *Int. J. Mass Spectrom. Ion Phys.* **1983,** *46*, 403-406.
131. Caprioli, R.M. Enzymes and Mass Spectrometry: a Dynamic Combination. *Mass Spectrom. Rev.* **1987,** *6*, 237-287.
132. Caprioli, R.M. Analysis of Biochemical Reactions With Molecular Specificity Using FAB-MS. *Biochemistry* **1988,** *27*, 513-521.
133. Chait, B.T.; Wang, R.; Beavis, R.C.; Kent, S.B. Protein Ladder Sequencing. *Science* **1993,** *262*, 89-92.
134. Naylor, S.; Findeis, A.F.; Gibson, B.W.; Williams, D.H. An Approach Towards the Complete FAB Analysis of Enzymic Digests of Peptides and Proteins. *J. Am. Chem. Soc.* **1985,** *108*, 6359-6363.
135. Deterding, L.J.; Tomer, K.B.; Wellemans, J.M.Y.; Cerny, R.L.; Gross, M.L. Capillary Electrophoresis/Tandem Mass Spectrometry With Array Detection. *Eur. Mass Spectrom.* **1999,** *5*, 33-40.
136. Lehmann, W.D. *Massenspektrometrie in Der Biochemie;* Spektrum Akademischer Verlag: Heidelberg, 1996.
137. *Mass Spectrometry of Proteins and Peptides;* Chapman, J.R., editor; Humana Press: Totowa, 2000.
138. Snyder, A.P. *Interpreting Protein Mass Spectra;* Oxford University Press: New York, 2000.

139. Kinter, M.; Sherman, N.E. *Protein Sequencing and Identification Using Tandem Mass Spectrometry;* John Wiley & Sons: Chichester, 2000.
140. Stults, J.T.; Lai, J.; McCune, S.; Wetzel, R. Simplification of High-Energy Collision Spectra of Peptides by Amino-Terminal Derivatization. *Anal. Chem.* **1993,** *65*, 1703-1708.
141. Bordaz-Nagy, J.; Despeyroux, D.; Jennings, K.R.; Gaskell, S.J. Experimental Aspects of the Collision-Induced Decomposition of Ions in a Four-Sector Tandem Mass Spectrometer. *Org. Mass Spectrom.* **1992,** *27*, 406-415.
142. Karlsson, N.G.; Karlsson, H.; Hansson, G.C. Sulfated Mucin Oligosaccharides From Porcine Small Intestine Analyzed by Four-Sector Tandem MS. *J. Mass Spectrom.* **1996,** *31*, 560-572.
143. Caprioli, R.M.; Beckner, C.F.; Smith, L.A. Performance of a Fast-Atom Bombardment Source on a Quadrupole Mass Spectrometer. *Biomed. Mass Spectrom.* **1983,** *10*, 94-97.
144. Cornett, D.S.; Lee, T.D.; Mahoney, J.F. Matrix-Free Desorption of Biomolecules Using Massive Cluster Impact. *Rapid Commun. Mass Spectrom.* **1994,** *8*, 996-1000.
145. Mahoney, J.F.; Perel, J.; Lee, T.D.; Martino, P.A.; Williams, P. Shock Wave Model for Sputtering Biomolecules Using Massive Cluster Impact. *J. Am. Soc. Mass Spectrom.* **1992,** *3*, 311-317.
146. Mahoney, J.F.; Cornett, D.S.; Lee, T.D. Formation of Multiply Charged Ions From Large Molecules Using Massive-Cluster Impact. *Rapid Commun. Mass Spectrom.* **1994,** *8*, 403-406.
147. Sundqvist, B.; Macfarlane, R.D. Californium-252-Plasma Desorption Mass Spectrometry. *Mass Spectrom. Rev.* **1985,** *4*, 421-460.
148. Macfarlane, R.D. Californium-252-Plasma Desorption Mass Spectrometry I - a Historical Perspective. *Biol. Mass Spectrom.* **1993,** *22*, 677-680.
149. Macfarlane, R.D.; Hu, Z.-H.; Song, S.; Pittenauer, E.; Schmid, E.R.; Allmaier, G.; Metzger, J.O.; Tuszynski, W. ^{252}Cf-PD-MS II - a Perspective of New Directions. *Biol. Mass Spectrom.* **1994,** *23*, 117-130.
150. Håkansson, P.; Kamensky, I.; Sundqvist, B.; Fohlman, J.; Peterson, P.; McNeal, C.J.; Macfarlane, R.D. Iodine-127-PD-MS of Insulin. *J. Am. Chem. Soc.* **1982,** *104*, 2948-2949.
151. Macfarlane, R.D. Mass Spectrometry of Biomolecules: From PDMS to MALDI. *Brazilian J. Phys.* **1999,** *29*, 415-421.
152. Sundqvist, B.; Håkansson, P.; Kamensky, I.; Kjellberg, J. Ion Formation from Organic Solids: Fast heavy ion induced desorption of molecular ions from small proteins. Benninghoven, A. Springer Series in Chemical Physics **1983,** *25*, 52-57.
153. Macfarlane, R.D. ^{252}Californium Plasma Desorption Mass Spectrometry. *Biomed. Mass Spectrom.* **1981,** *8*, 449-453.
154. Wien, K.; Becker, O. Ion Formation from Organic Solids: Secondary ion emission from metals under fission fragment bombardment. Benninghoven, A. Springer Series in Chemical Physics **1983,** *25*, 47-51.
155. Zubarev, R.A.; Abeywarna, U.K.; Demirev, P.; Eriksson, J.; Papaléo, R.; Håkansson, P.; Sundqvist, B.U.R. Delayed, Gas-Phase Ion Formation in PD-MS. *Rapid Commun. Mass Spectrom.* **1997,** *11*, 963-972.
156. Jonsson, G.P.; Hedin, A.B.; Håkansson, P.; Sundqvist, B.U.R.; Säve, B.G.S.; Nielsen, P.; Roepstorff, P.; Johansson, K.-E.; Kamensky, I.; Lindberg, M.S.L. PD-MS of Peptides and Proteins Adsorbed on Nitrocellulose. *Anal. Chem.* **1986,** *58*, 1084-1087.
157. Wolf, B.; Macfarlane, R.D. Small Molecules As Substrates for Adsorption/Desorption in Californium-252 PD-MS. *J. Am. Soc. Mass Spectrom.* **1990,** *2*, 29-32.
158. Song, S.; Macfarlane, R.D. PDMS-Chemistry of Angiotensin II and Insulin in Glucose Glass Thin Films. *Anal. Bioanal. Chem.* **2002,** *373*, 647-655.

11 Matrix-Assisted Laser Desorption/Ionization

Learning Objectives

- Pulsed laser light as a source of energy for desorption and ionization
- Ion formation from thin solid layers
- Matrix assistance as a key to soft desorption/ionization
- Inherently pulsed ionization method
- Applications and uses
- Fine vacuum and atmospheric pressure sources for MALDI
- MALDI imaging techniques

The technique of *laser desorption/ionization* (LDI) was introduced in the late 1960s [1-3], long before the advent of field desorption (FD, Chap. 8), *californium plasma desorption* (^{252}Cf-PD, Chap. 10.7) or *fast atom bombardment* (FAB, Chap. 10). While low-mass organic salts and light-absorbing organic molecules are easily accessible by LDI [2,3], it takes a serious effort to obtain useful mass spectra of biomolecules [4], in particular when the mass of the analyte exceeds 2000 u [5,6]. FAB and ^{252}Cf-PD therefore represented the standard in biomolecular and biomedical mass spectrometry until the late 1980s, while LDI was regarded rather exotic [7].

The admixture of strongly light-absorbing compounds to the sample prior to preparation for laser desorption effected a tremendous change of what was possible in mass spectrometry (Fig. 11.1).

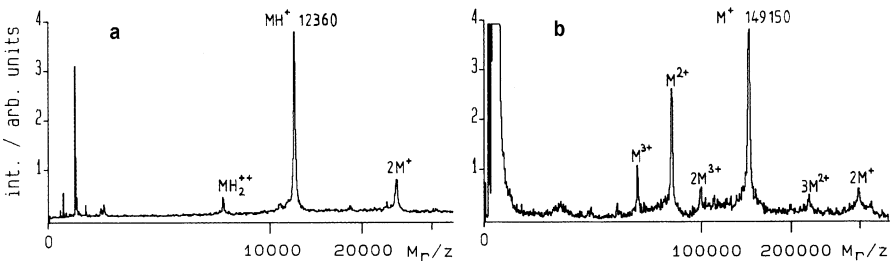


Fig. 11.1. MALDI-TOF mass spectra of (**a**) porcine cytochrome C from 2,5-dihydroxybenzoic acid matrix at 337 nm and (**b**) a monoclonal antibody from nicotinic acid matrix at 266 nm. These spectra from one of the landmark papers during the early phase of MALDI development impressingly demonstrate the enormous potential of the method. Reproduced from Ref. [16] by permission. © John Wiley & Sons, 1991.

J. Gross, *Mass Spectrometry*, 2nd ed., DOI 10.1007/978-3-642-10711-5_11,
© Springer-Verlag Berlin Heidelberg 2011

Two approaches were independently developed: *i*) the admixture of ultrafine cobalt powder (particle size about 30 nm) to analyte solutions in glycerol [8,9], and *ii*) the cocrystallization of the analyte with an organic matrix [10-13]. When combined with a *time-of-flight* (TOF, Chap. 4.2) mass analyzer, both methods are capable of producing mass spectra of proteins of about 100,000 u molecular weight. Nonetheless, the application of the "*ultrafine-metal-plus-liquid-matrix*" method remained an exception because the versatility of an organic matrix and the sensitivity of *matrix-assisted laser desorption/ionization* (MALDI) [10,11,14,15] made it by far superior to the admixture of cobalt powder [16-19]. In its present status, MALDI represents a major analytical tool in the modern life sciences [15,20-22] and in polymer science [23,24].

11.1 Ion Sources for LDI and MALDI

The general setup of LDI/MALDI ion sources is comparatively simple (Fig. 11.2) [25]. Both LDI and MALDI make use of the absorption of laser light by a solid sample layer. The energy uptake upon laser irradiation then causes evaporation and eventually ionization of the sample. The pulse of laser light is focused onto a small spot which is typically 0.05–0.2 mm in diameter [26]. As laser irradiance is a critical parameter in MALDI, a variable beam attenuator in the laser optical path is employed to adjust the irradiance, e.g., by means of a rotatable absorbing filter of variable transmittance from close to 100% down to about 1%. Then, the laser attenuation is individually optimized for each measurement. LDI/MALDI ion sources are generally operated at ambient temperature.

Although lasers of both ultraviolet (UV) and infrared (IR) wavelengths are in use, UV lasers are by far the most important light sources in analytical LDI-MS and MALDI-MS. Among these, nitrogen lasers and frequency-tripled or quadrupled Nd:Yag lasers serve for the majority of applications [27]. IR-MALDI is dominated by Er:Yag lasers [27,28] while TEA-CO_2 lasers (cf. IRMPD in Chap. 9.12) are rarely used (Table 11.1) [17,29].

UV lasers are emitting pulses of 3–10 ns duration, while those of IR lasers are in the range of 6–200 ns. Short pulses are needed to effect sudden ablation of the sample layer. In addition, an extremely short time interval of ion generation basically avoids thermal degradation of the analyte, e.g., a 10 ns laser pulse would require the high rate constant of $10^8\ s^{-1}$ to complete decomposition. On the other hand, much longer irradiation would simply cause heating of the bulk material. In case of IR-MALDI, a slight decrease in threshold fluence has been observed with shorter laser pulses [30]. Furthermore, a short time interval of ion generation means a better definition of the starting pulse, which is relevant when a TOF analyzer is being used. Fortunately, the introduction of delayed extraction techniques (Chap. 4.2.6) has greatly reduced the influence of the laser pulse duration on resolving power and mass accuracy [30].

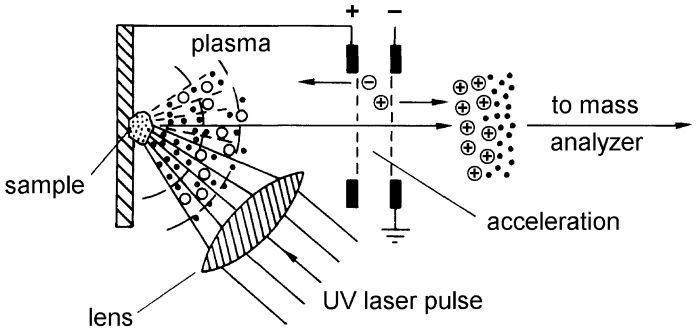


Fig. 11.2. Simplistic laser desorption ion source for nonresonant light absorption by a solid. In practice, the solid is supplied as a thin microcrystalline layer. Here, positive ions are continuously being extracted as long as the supply is sustained by the laser desorption plasma. Reproduced from Ref. [25] by permission. © Elsevier Science, 1994.

Table 11.1. Lasers for laser desorption/ionization

Spectral range	Wavelength	Photon energy	Laser type
UV	193 nm	6.4 eV	ArF Excimer laser
UV	248 nm	5.0 eV	KrF Excimer laser
UV	266 nm	4.7 eV	Frequency-quadrupled Nd:YAG laser
UV	308 nm	3.8 eV	XeCl Excimer laser
UV	337 nm	3.7 eV	Nitrogen laser[a]
UV	355 nm	3.5 eV	Frequency-tripled Nd:YAG laser[a]
IR	1.06 μm	1.2 eV	Nd:YAG laser[b]
IR	2.94 μm	0.4 eV	Er:YAG laser[b]
IR	1.7–2.5 μm	0.7–0.5 eV	Optical parametric oscillator (OPO) laser
IR	10.6 μm	0.1 eV	CO_2 laser

[a] most frequently used UV lasers; [b] most frequently used IR lasers

Note: The majority of MALDI applications are run with UV lasers. IR-MALDI has been restricted to applications where the deeper penetration of IR radiation offers advantages, e.g., for the direct desorption of analytes from *sodium dodecyl sulfate* (SDS) gels or *thin layer chromatography* (TLC) plates.

11.2 Ion Formation

The mechanisms of ion formation in MALDI are a subject of continuing research [31-35]. The major concerns are the relationship between ion yield and laser fluence [26,36], the temporal evolution of the desorption process and its implications

upon ion formation [37], the initial velocity of the desorbing ions [30,38,39], and the question whether preformed ions or ions generated in the gas phase provide the major source of the ionic species detected in MALDI [40-42].

11.2.1 Ion Yield and Laser Fluence

Ion formation does not occur below a *threshold laser irradiance* of about 10^6 W cm^{-2}. At threshold, a sharp onset of desorption/ionization occurs and ion abundances rise to a high power (5th to 9th) of laser irradiance [17,36,43]. The threshold *laser fluence* for the detection of matrix and analyte ions not only depends on the actual matrix, but also on the molar matrix-to-analyte ratio, e.g., the minimum threshold laser fluence for cytochrome C was found at a molar matrix-to-sample ratio of 4000 : 1. Significantly higher or lower ratios require almost twice that laser fluence (Fig. 11.3) [44]. The increase at low analyte concentrations can be attributed to a decreasing detection efficiency because a larger volume of material has to be ablated in order to generate a sufficient number of analyte ions. At high analyte concentrations, the energy absorption per volume is reduced as the matrix becomes diluted with analyte molecules causing a higher threshold fluence. The total particle yield from laser desorption as a function of *laser fluence* has been determined by collecting the desorbed neutrals on a quartz crystal microbalance [45]. The study by Quist *et al.* [26] indicates that the desorption of neutrals occurs by thermal evaporation starting at laser fluences of about 11 mJ cm^{-2}. However, the ion-to-neutral ratio of the MALDI process was determined to be less than 10^{-5} [45].

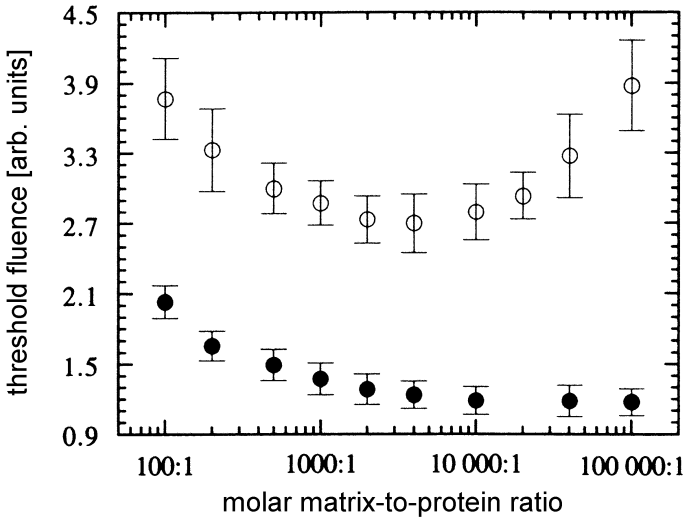


Fig. 11.3. Threshold fluence for positive ions of (○) cytochrome c and (●) sinapinic acid as a function of the molar matrix-to-protein ratio. Reproduced from Ref. [44] by permission. © John Wiley & Sons, 1994.

Note: The *fluence* is defined as energy per unit area; in MALDI typical fluences are in the range of 10–100 mJ cm^{-2}. The *irradiance* is fluence divided by the laser pulse duration; in MALDI the irradiances are in the range of 10^6–10^7 W cm^{-2} [34].

11.2.2 Effect of Laser Irradiation on the Surface

Best MALDI spectra in terms of resolution and low to absent ion fragmentation are obtained slightly above threshold for analyte ion formation [17,43]. An evenly distributed shallow ablation of material from the upper layers of the sample is achieved if a comparatively homogeneous laser fluence is irradiated onto the target [26,36,46]. Ideal laser spot sizes are 100–200 μm as realized by 100–200 mm focal length of the commonly employed lenses [47]. Numerous single-shot spectra are then obtained from one spot. Such a laser spot size is also advantageous because a number of micrometer-sized crystrals are illuminated simultaneously thereby averaging out the effects of mutual orientation of crystal surfaces and laser beam axis [46,48,49]. On the other hand, an extremely sharp laser spot causes the eruption of material from a small area upon formation of a deep crater (Fig. 11.4). The MALDI spectra of cytochrome C (M_r = 12,360 u) demonstrate the superior quality of spectra obtained using an optimized spot size [50].

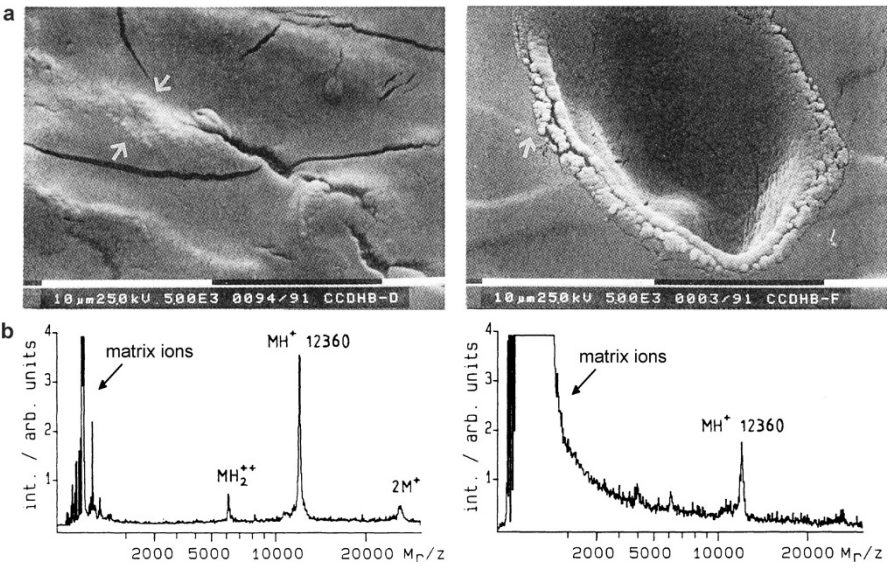


Fig. 11.4. Effect of focused and defocused laser beam. (**a**) SEM micrographs of DHB single crystals after exposure to 10 laser shots (337 nm) under focused (*right column*) and defocused (*left column*) irradiation with corresponding sum spectra of horse heart cytochrome C (M_r = 12,360 u); *black and white bars* correspond to 10 μm. (**b**) Resulting MALDI spectra. Reproduced from Ref. [50] by permission. © Elsevier Science, 1991.

Although established over the years, nitrogen lasers inherently possess disadvantages in that *i*) their maximum repetition rate is limited to about 50 Hz, and *ii*) their average lifespan is only several 10^7 shots. Diode-pumped solid-state lasers such as the frequency-tripled Nd:YAG laser can deliver rates of > 1 kHz and have a hundred times longer lifespan. Especially in MALDI imaging and automated high-throughput proteomics this number of shots is easily reached. Frequency-tripled Nd:YAG lasers unfortunately suffer from poor MALDI performance, e.g., they are of limited use with certain matrices and with highly relevant thin layer preparations. Their inferiority is not caused by the slight change from 337 nm to 355 nm wavelength but simply by their too small spot size. The insertion of a beam modulator to create beam profiles delivering a diffuse multispot pattern of similar overall diameter as a nitrogen laser solves this problem. This way, Bruker's Smartbeam™ Nd:YAG lasers may even surpass the MALDI performance of nitrogen lasers [51].

Note: MALDI spectra are acquired just above the threshold laser fluence for ion formation. Single-shot spectra therefore tend to exhibit a low signal-to-noise ratio (Chap. 1.4.3) due to poor ion statistics. Thus, 50–200 single-shot spectra are usually accumulated to create the final spectrum [49].

11.2.3 Temporal Evolution of a Laser Desorption Plume

The desorption of ions and neutrals into the vacuum upon irradiation of a laser pulse proceeds as a jet-like *supersonic expansion* [39]: a small, but initially hot and very rapidly expanding plume is generated [15,52]. The description of MALDI as an *energy-sudden* method [42] nicely expresses the explosive character of the plume formed by the nanosecond laser pulse. As the expansion is adiabatic, the process is accompanied by fast cooling of the plume [39].

Although the initial velocity of the desorbed ions is difficult to measure, reported values generally are in the range of 400–1200 m s^{-1}. The initial velocity is almost independent of the mass of the analyte ions but dependent on the matrix [34,37-39,48,53,54]. On the other hand, the initial analyte ion velocity is not independent of the compound class, i.e., peptides show a behavior different from oligosaccharides [15,54]. The essential independence of mean ion velocities on the molecular weight of the analyte leads to an approximate linear increase of the mean initial kinetic energies of the analyte ions with mass. High-mass ions therefore carry tens of electronvolts of translational energy *before* ion acceleration [34,43,53]. The initial velocity of the ions is superimposed onto that obtained from ion acceleration, thereby causing considerable losses in resolution with continuous extraction TOF analyzers, in particular when operated in the linear mode.

Example: Laser flash light photographs of the temporal evolution of a laser desorption plume are highly illustrative [55,56]. The plume shown in Fig. 11.5 was generated from neat glycerol by an Er:Yag (2.94 μm) laser of 100 ns pulse width. Such laser pulse durations are typical for IR-MALDI. Glycerol was employed as a

liquid matrix to provide a homogeneous sample and reproducible plume formation. Pulses of a frequency-doubled Nd:YAG laser (532 nm, 8 ns duration) served as the flashing light source for obtaining the photographs. Dark-field illumination was used to show the particulate components of the plume. In the beginning, the plume appears to consist of a continuous cloud of material of varying density, whereas individual micrometer-sized particles dominate later images. Interestingly, even after the exposure there was still some ejection of material [57].

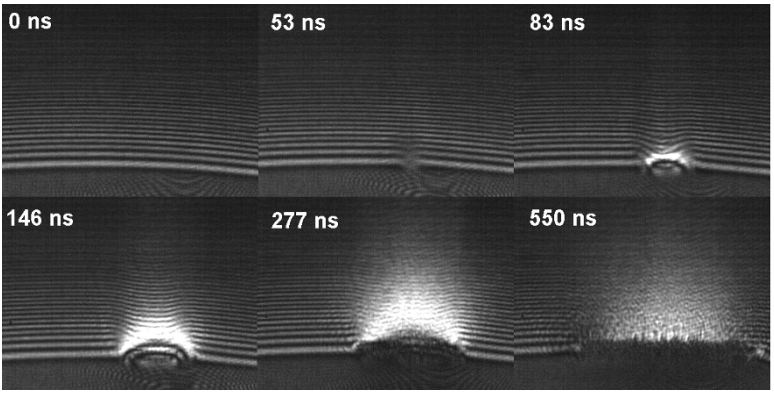


Fig. 11.5. Temporal evolution of a laser desorption plume generated by an Er:Yag laser pulse from neat glycerol [56]. Courtesy of F. Hillenkamp, A. Leisner, Münster University.

11.2.4 Processes of Ion Formation in MALDI

The pathways of ion formation in MALDI are numerous, i.e., no single process applies [15,41,42]. The promoting effect of decreasing pH of matrix-analyte solutions upon peptide ion yield indicates desorption of preformed $[M+H]^+$ ions. Similar observations are made for cationization products such as $[M+alkali]^+$ ions from oxygen-rich analytes. Nonetheless, gas phase processes cannot be excluded, because ions may be formed in the plasma plume even some hundred micrometers above the sample surface [58,59]. Another study reveals a gradual increase of the initial ion velocities as the mass of oligosaccharides and synthetic polymers increases; they may even reach the high level characteristic for peptides and proteins. Introduction of a charged functional group via derivatization has the same effect on small oligosaccharides. This indicates that typical MALDI analytes require their incorporation as preformed ions into the matrix crystal to effectively become released into the gas phase, whereas gas phase cationization is viable for low-molecular-weight neutrals [39]. When non-carboxylic acid matrices are being used to protonate slightly basic analyte molecules, excited states of the matrix molecules may account for proton transfer [59,60].

In case of UV light-absorbing analytes, direct photoionization can also occur. The frequently observed positive and negative radical ions $M^{+\bullet}$ [61,62] and $M^{-\bullet}$ [63-65] can only be generated by removal or capture of an electron. Thus, $M^{+\bullet}$ and

$M^{-\bullet}$ ions point towards the occurrence of photoionization [61], charge exchange, and electron capture in the gas phase [42,61]. Which of the above processes contributes most to ion formation depends on the actual combination of matrix, analyte, and possibly present additives or contaminants.

11.2.5 "Lucky Survivor" Model of Ion Formation

The plasma emerging from a surface upon laser irradiation contains both positive and negative ions – it is neutral in total. Depending only on the polarity of the acceleration voltage one may either extract positive or negative ions, a situation similar to CI where an isobutane reagent gas plasma works equally well to deliver protonated species in PICI or deprotonated ions in NICI (Chap. 7.5). The starting conditions in MALDI, however, are quite different in that the analyte can be *multiply* protonated, deprotonated or otherwise charged by ion attachment in solution before its incorporation into the matrix crystals [15,42]. Proof of multiple charging of macromolecules in solution phase is directly obtained from electrospray ionization mass spectra (Chap. 12).

Example: Although peptides and proteins are generally prepared for MALDI from acidified solutions, both singly protonated or deprotonated ions can normally be observed solely depending on the polarity of the extraction voltage. However, negative ion spectra tend to be less intensive for the same laser fluence, i.e., positive- and negative-ion mass spectra are not analogous (Fig. 11.6). Interestingly, the relative ion yields of both polarities are basically independent of the solvent composition, its pH, and of the solution phase acidity/basicity of the analyte.

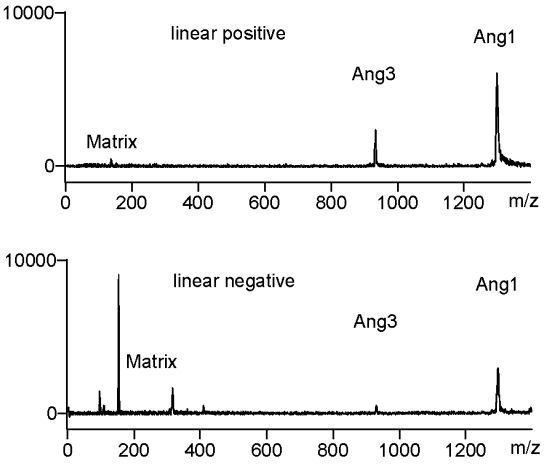


Fig. 11.6. MALDI mass spectra of a mixture of the small peptides angiotensin 1 (Ang1) and angiotensin 3 (Ang3) from DHB matrix as obtained on a linear TOF instrument in (**a**) positive-ion and (**b**) negative-ion mode under otherwise identical conditions. Reproduced from Ref. [42] with permission. © John Wiley & Sons, Ltd., 2000.

So why are singly charged ions the (almost) only species observed in MALDI? How can charge separation be accomplished when mutual neutralization is considered to be the preferred process inside the plume? What are the fundamental processes essentially limiting the ionic charge state to just one – either positive or negative?

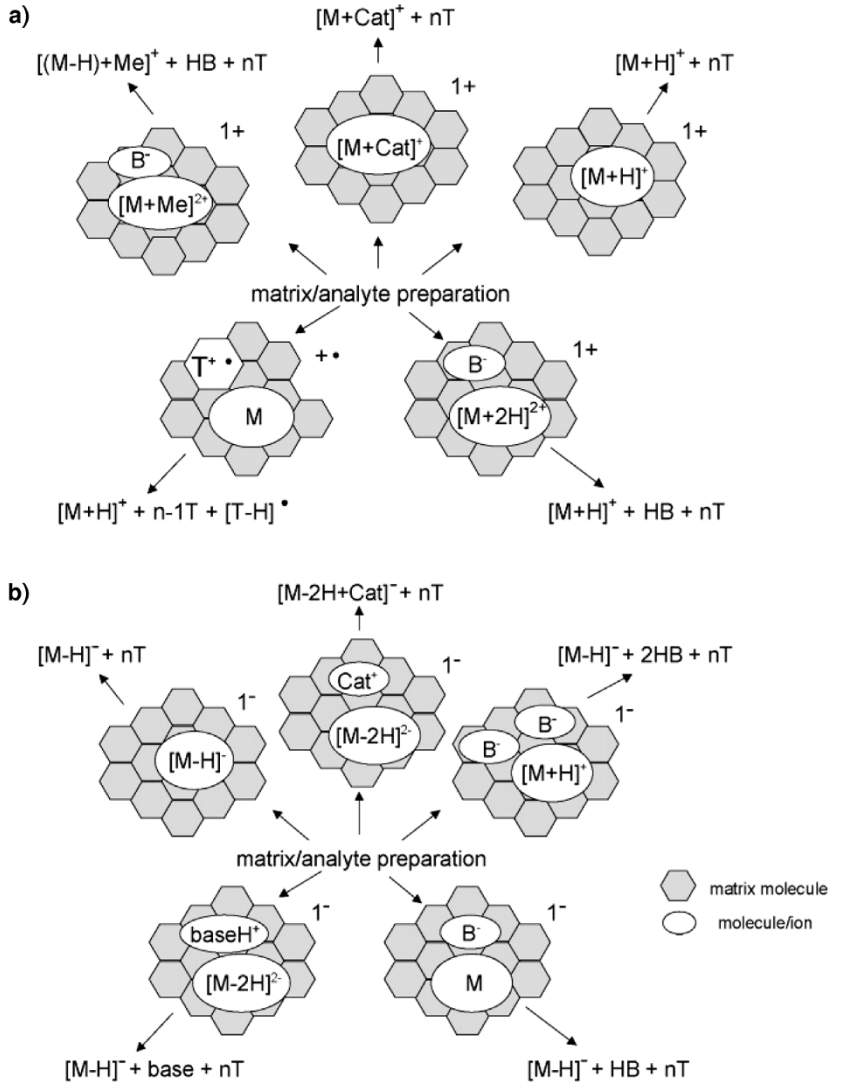


Fig. 11.7. Pathways of formation of singly charged ions from sample–matrix preparations according to the lucky survivor model. (**a**) Positive ion formation, (**b**) negative ion formation; M: analyte molecule, T: matrix molecule, Cat: small cation, Me: metal^{2+}, B: base. Adapted from Ref. [42] with permission. © John Wiley & Sons., Ltd., 2000.

The so-called *lucky survivor model* [42] explains this behavior in terms of mutual neutralization by recombination of cationic and anionic components of the plasma. Re-neutralization rates are higher, the higher the initial charge state of an ion. Thus, re-neutralization is slower for singly charged ions representing a late stage of the sequence, and therefore less probable to occur. Hence, singly charged ions generally are the "lucky survivors of the re-neutralization conflict" inside the laser plume (Fig. 11.7). As the fast moving electrons are most rapidly lost from the laser plume, an excess positive charge is established over time, which explains the lower abundance of negative ions in MALDI.

11.3 MALDI Matrices

11.3.1 Role of the Solid Matrix

The role of the matrix in MALDI is analogous to that in FAB (Chap. 10.3). In contrast to FAB, MALDI matrices are generally crystalline solids of low vapor pressure in order not to be volatized in the ion source vacuum. While in principle any liquid can serve as a FAB matrix to moderate the energy of the impacting primary particles, the matrix in MALDI has to effectively absorb the laser light of the wavelength intended for use [66]. In UV-MALDI, the molecules need to possess a suitable chromophore, because energy uptake is based on the strong absorption, and thus the resulting electronic excitation of the matrices. Therefore, the structure of UV-MALDI matrices is based on some aromatic core suitably functionalized to achieve the desired properties.

In case of IR-MALDI, fewer restrictions apply because wavelengths around 3 μm are effectively absorbed by O–H and N–H stretch vibrations, while wavelengths around 10 μm cause excitation of C–O stretch and O–H bending vibrations [30,33]. Therefore, malonic acid, succinic acid, malic acid, urea, and glycerol serve well as matrices in IR-MALDI [28,29]. A matrix can serve as protonating or deprotonating agent or as electron-donating or -accepting agent.

Note: It is evident that the first function of the matrix essentially is to dilute and isolate analyte molecules from each other. This occurs during solvent evaporation and concomitant formation of a solid solution. Then, upon laser irradiation, it functions as a mediator for energy absorption [42].

11.3.2 Matrices in UV-MALDI

Nicotinic acid (NA) was the first organic compound to be successfully employed as a matrix in UV-MALDI of peptides and proteins [12-14]. Ever since, better matrices have been sought, the following now being widespread in use (Fig. 11.8): picolinic acid (PA) [67], 3-hydroxypicolinic acid (HPA) [68], 3-aminopicolinic acid (3-APA) [69], and 6-aza-2-thiothymine (ATT) [70,71] for oligonucleotides

and DNA [72]; 2,5-dihydroxybenzoic acid (DHB, gentisic acid) [17,50] and combined matrices having DHB as the main component [73-76], e.g., "super-DHB" [77], as well as 3-amino-quinoline (3-AQ) [78-80] for oligosaccharides; α-cyano-4-hydroxycinnamic acid (α-CHC, α-CHCA, 4-HCCA, CCA,) for peptides, smaller proteins [81], triacylglycerols [82], and numerous other compounds [83,84]; 3,5-dimethoxy-4-hydroxycinnamic acid (SA, sinapinic acid) for proteins [85]; 2-(4-hydroxyphenylazo)benzoic acid (HABA) for peptides, proteins, glycoproteins [66], and polystyrene [86]; 2-mercaptobenzothiazole (MBT) and 5-chloro-2-mercaptobenzothiazole (CMBT) for peptides, proteins, and synthetic polymers [87]; 2,6-dihydroxyacetophenone (DHAP) for glycopeptides, phosphopeptides,

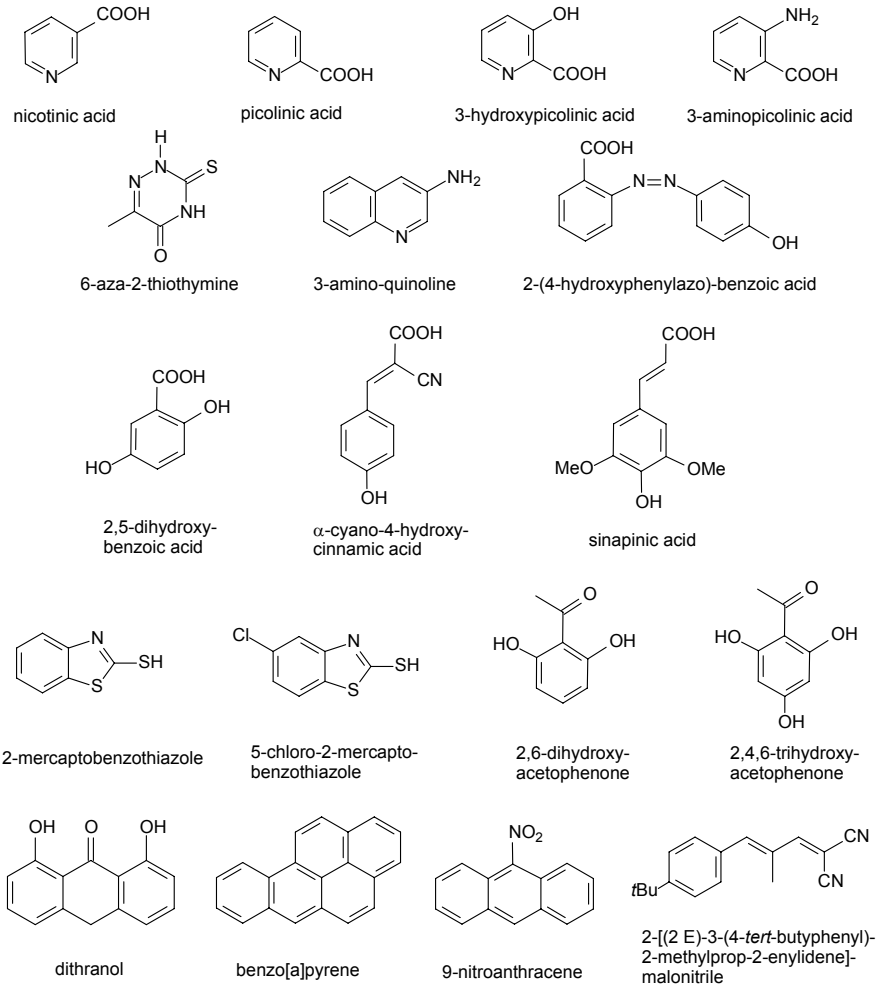


Fig. 11.8. Collection of common MALDI matrices.

and proteins [88,89]; 2,4,6-trihydroxyacetophenone (THAP) for solid-supported oligonucleotides [90]; 1,8,9-anthracenetriol (dithranol) for synthetic polymers [91,92]; and 9-nitroanthracene (9-NA) [65,93,94], benzo[a]pyrene [64], and 2-[(2 E)-3-(4-*tert*-butylphenyl)-2-methylprop-2-enylidene]malonitrile (DCTB) [95] for fullerenes and their derivatives. Even [60]fullerene itself [96] and porphyrins [97] have been used as matrix. Liquid matrices have been used either due to the specific advantages of the particular matrix or to employ the self-refreshing surface for achieving long-lasting signals in MALDI-magnetic sector experiments [98,99], and thus, even *ionic liquids* (ILs) have been used as liquid MALDI matrices [100,101].

Note: It is common to use acronyms rather than compound names for matrices. However, these are not always consistently used, e.g., α-CHC, 4-HCCA, CHCA, and CCA all refer to α-cyano-4-hydroxycinnamic acid. Others may be easily confused, e.g., nicotinic acid (NA) and 9-nitroanthracene (9-NA).

Example: The choice of a matrix and optimized conditions of sample preparation have substantial influence on the analytical value of MALDI spectra. Even when employing standard matrices such as CHCA or DHB, significant improvements can be achieved, e.g., by appropriate mixing of the two matrices to analyze ribonuclease B (Fig. 11.9) [76].

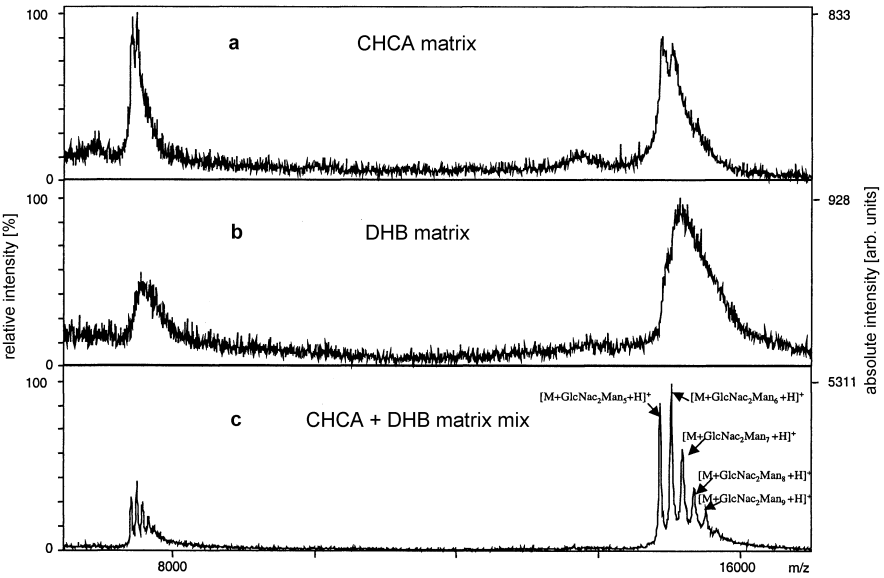


Fig. 11.9. Linear mode positive-ion MALDI-TOF spectra of ribonuclease B in 80 mM urea. (**a**) 300 fmol in CHCA, (**b**) 600 fmol in DHB, and (**c**) 300 fmol in CHCA/DHB matrix mix. Reproduced from Ref. [76] by permission. © Elsevier Science, 2003.

Hint: The choice of the right matrix is key to success in MALDI – and at the same time appears to be some kind of magic. For a first approach to a new analytical problem, it is recommended to try a matrix from this collection. In general, highly polar analytes work better with highly polar matrices, and nonpolar analytes are preferably combined with nonpolar matrices. Matrix acidity data may help to judge its protonating effect [102,103]. In unfortunate cases, only one specific analyte-matrix combination might yield useful MALDI spectra.

11.3.3 Characteristics of MALDI Matrix Spectra

MALDI matrix (Ma) spectra are characterized by strong molecular and/or ions from protonation, cationization etc. The signals are accompanied by series of matrix cluster ions and some more abundant fragment ions [33]. In positive-ion MALDI, $[Ma_n+H]^+$ cluster ions predominate, while $[Ma_n–H]^-$ cluster ions are preferably formed in negative-ion MALDI. The principal ion series may be accompanied by $[Ma_n+alkali]^+$ ions and some fragments of minor intensity, e.g., $[Ma_n+H–H_2O]^+$. In particular with aprotic matrices, radical ions tend to dominate. In addition, a "continuous" background is formed by clustering of radiolytic decomposition products of the matrix. In general, the spectrum of the neat matrix, i.e., its LDI spectrum, strongly depends on the actual laser fluence and on the presence of impurities. Thus, the "correct" LDI spectrum of the matrix compound largely differs from what is obtained under conditions applied to form analyte ions from that matrix, because then, a 10–100-fold increased matrix ion density causes numerous secondary processes to occur. This dramatic change in mass spectral appearance bears some similarity to the transition observed from EI to CI spectra of reagent gases (Chap. 7.2.2).

11.4 Sample Preparation

The standard method of sample preparation in LDI and MALDI involves deposition and subsequent evaporation of 0.5–2 µl of dilute sample(–matrix) solution on the surface of a *sample holder* or *MALDI target*, as it is often referred to. Both composition of the solution and surface characteristics of the target strongly effect the outcome of the MALDI-MS experiment.

11.4.1 MALDI Target

Sample introduction has undergone a dramatic change in MALDI. In first experiments, single samples were supplied on MALDI probes designed similar to FAB probes (Chap. 10.1.3). Soon, multisample probes were developed. Early commercial products provided approximately twenty spots on one target which could be rotated, shifted, or freely moved in *x*- and *y*-directions to bring any spot on its sur-

face into the laser's focus. Driven by the needs of combinatorial chemistry, 96-spot targets were developed to allow for the transfer of samples from a complete standard well plate. Soon after, the current standard of 384-spot, occasionally even 1536-spot, targets was established (Fig. 11.10). To take full advantage of such targets it is recommended to combine robotic sample preparation with automated measurement of the MALDI spectra.

The spot size of MALDI preparations and thus the amount of sample necessary to yield a useful layer can be substantially reduced by so-called *AnchorChip*™ targets (Bruker Daltonik). Such targets bear small hydrophilic spots on a hydrophobic surface. As a result, the evaporating drop of matrix–analyte solution is "anchored" to such a point where it shrinks until the onset of crystallization exactly within this hydrophilic area (Fig. 11.11c) [104]. The resulting preparation covers a much smaller surface than that from a freely spreading drop. In addition to improved detection limits, this technique simplifies automated spot finding due to their precisely defined location on the target.

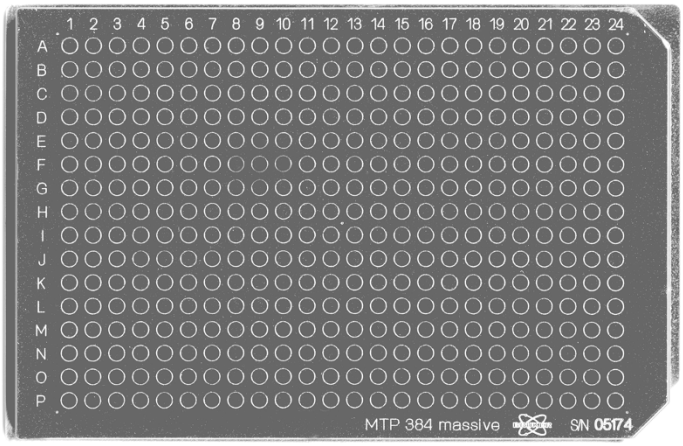


Fig. 11.10. Typical MALDI target. The Bruker Scout384™ target offers a 16 × 24 spot array with 384 positions for sample preparation. Here, a standard nickel-coated massive aluminum version is shown; its dimensions are 84 × 128 mm with marks of 3 mm in diameter.

11.4.2 Standard Sample Preparation

The analyte should be soluble to about 0.1 mg ml^{-1} in some solvent. If a matrix is used, the matrix is dissolved to yield either a saturated solution or a concentration of about 10 mg ml^{-1}. The solution of the analyte is then admixed to that of the matrix. For optimized MALDI spectra, the molar matrix-to-analyte ratio is normally adjusted as to fall into the range from 1000 : 1 to 100,000 : 1 [16,17,50]. In this range, a good signal-to-noise ratio and a low degree of ion fragmentation are preserved. At very high sample concentrations the "matrix effect" is dimished and the spectra start resembling LDI spectra. Too low sample concentrations require addi-

tional laser irradiance for sufficient analyte ion production [44]. However, given a proper preparation, even a matrix-to-analyte ratio of 10^8 : 1 will produce useful results. A sufficient miscibility of analyte and matrix is always required [91].

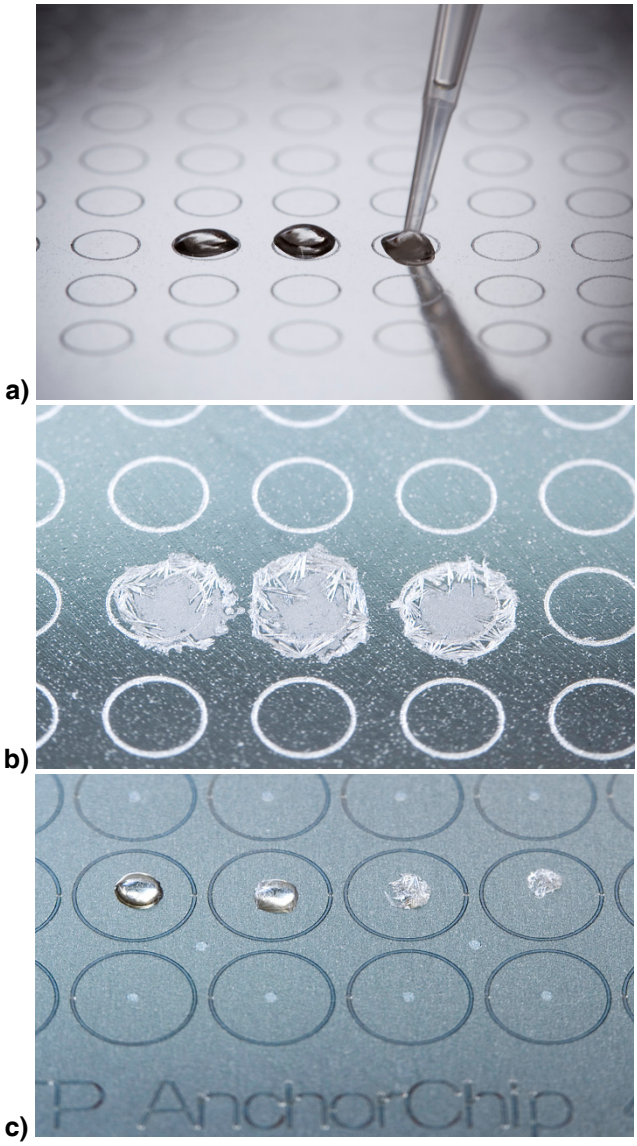


Fig. 11.11. Sample preparation for MALDI. (**a**) Pipetting of 1 µl of sample–matrix solution onto a standard MALDI target; (**b**) same spots after DHB has crystallized show large crystals on the rim and evenly distributed small crystals in the center; (**c**) cummulative effect of hydrophilic spots (*bright areas in circles*) present on a hydrophobic surface of an AnchorChip™ target on crystallizing DHB matrix.

Example: Assuming a typical MALDI matrix with an M_r of about 200 g mol^{-1}, dissolution at 10 mg ml^{-1} in a suitable solvent yields a matrix solution that is 0.05 M in concentration, which is equal to 5×10^{-8} mol µl^{-1}. An average peptide of M_r around 2000 g mol^{-1} dissolved at 0.01 mg ml^{-1} results in 5×10^{-12} mol µl^{-1} (5 pmol µl^{-1}). Mixing the matrix with the analyte solution 1:1 (v/v) results in a molar matrix-to-analyte ratio of 10,000 : 1 for preparation on a target. Pipetting 1 µl of this mixture per spot onto a MALDI target corresponds to 2.5 pmol of sample per spot (Fig. 11.11). In fact, MALDI-TOF-MS of peptides can be extended to 1/1000th of this amount, and thus, may routinely deliver useful spectra down to a few fmol of peptide per spot, which is equal to a molar matrix-to-analyte ratio of 10,000,000 : 1.

The crystallization process is a critical parameter in LDI and MALDI sample preparation [50,105,106]. The conventional co-crystallization is usually termed *dried droplet preparation*. Dried droplet preparation yields comparatively large crystals, especially when slow evaporation, e.g., from aqueous solutions, is involved. Unfortunately, large crystals are detrimental for good shot-to-shot reproducibility and mass accuracy.

Evenly distributed thin layers of microcrystallites are therefore preferred [105,107]. The original so-called *thin layer technique* involves preparation of a thin HCHA layer from solution in acetone on top of which the analyte is placed in a second step without re-dissolving the matrix [108,109]. The formation of thin layers can also be assisted by *i*) using volatile solvent(s) such as acetone, *ii*) by eventually enforcing evaporation by gentle heating of the target or by a softly blowing hair dryer, and finally *iii*) by using polished targets. Thus, the thin layer technique had a significant impact on MALDI sample preparation [108,110].

Finally, (nano)electrospray deposition can be used to deposit the analytes onto different kinds of predeposited matrix layers. MALDI sample preparations where the analyte solution is deposited on top of a previously prepared matrix layer are generally termed *sandwich methods*. The base layer of matrix may be prepared either by the standard dried droplet technique or by thin layer preparation. For (nano)electrospray deposition of peptides, for example, a 10^{-5} M solution is sprayed from a (nano)electrospray capillary onto the solid matrix layer. The advantage of nanoelectrospray over conventional electrospray is that very small droplets are formed, which arrive at the target as dry particles, and thus, do not wet and redissolve the matrix surface [41].

11.4.3 Cationization

Metal ions, in particular singly charged ions such as Na^+, K^+, Cs^+, and Ag^+ are sometimes added to the matrix–analyte solution to effect cationization of the neutral analyte [111]. This is advantageous when the analyte has a high affinity to a certain metal ion, e.g., towards alkali ions in case of oligosaccharides [6]. Addition of individual cations can also lead to a concentration of ions of a particular

kind, e.g., promoting $[M+K]^+$ ions over all other alkali ion adducts upon addition of a potassium salt (Fig. 11.12).

Silver ions (from silver trifluoroacetate or trifluoromethanesulfonate), Cu^+, and other transition metal ions in their 1+ oxidation state [112,113] are frequently employed to obtain $[M+metal]^+$ ions from nonfunctionalized or at least nonpolar hydrocarbons [114], polyethylene [115,116], or polystyrene (for an example see Chap. 11.6.1) [112,113,117-119].

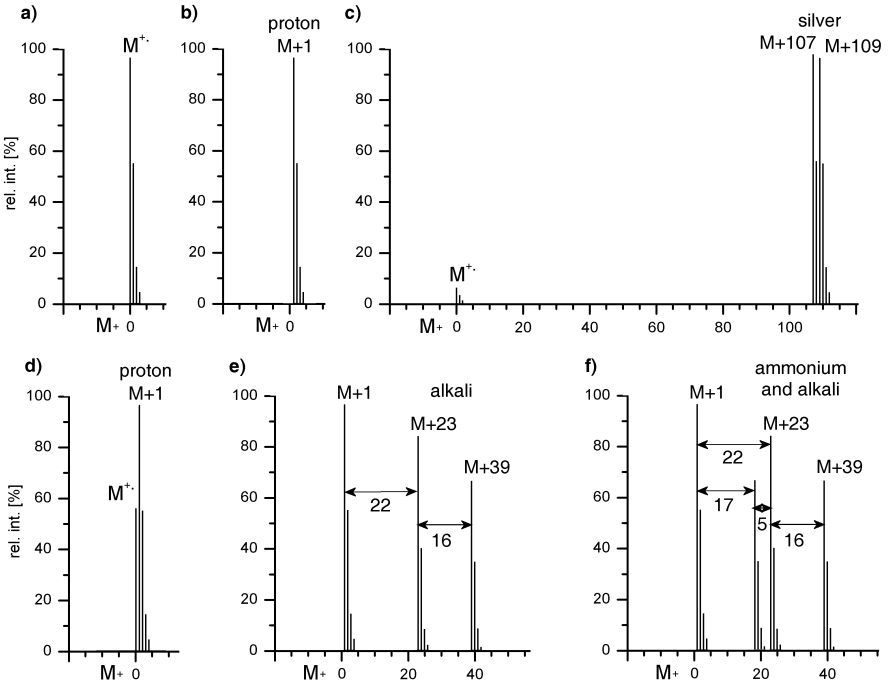


Fig. 11.12. Typical appearances of signals representing the intact molecular mass in case of (**a**) molecular ion formation, (**b**) protonation, (**c**) silver cationization, **d**) molecular ion and protonation, (**e**) protonation plus alkali cationization, and (**f**) protonation, ammonium plus alkali adduct formation. The relative abundances of the respective contributions are subject to wide variations. The abscissa gives the corresponding M+X nominal mass value; artificial isotopic patterns are added for more realistic appearance.

Note: Sodium and potassium are ubquitous and the corresponding adducts are almost omnipresent given the analyte has some alkali ion affinity [120]. It is therefore advisable to know these typical mass differences by heart. Searching a spectrum for those frequent peak distances, e.g., +22 u and +16 u in case of $[M+Na]^+$ and $[M+K]^+$ ions accompanying $[M+H]^+$, reveals the true molecular mass. Other cations, e.g., Li^+ or Ag^+, are easily identifiable by their isotopic pattern.

Accurate mass data provided, the $\Delta m/z$ values between suspect pairs of peaks can be used to unequivocally identify $[M+Na]^+$, $[M+K]^+$, and other frequent cationization product ions the same way as we used the corresponding differences to verify the presence of certain elements by their characteristic $\Delta m/z$ between isotopes (Table 3.2) [121]. The most frequent pairs to be distinguished are collected below (Table 11.2).

Table 11.2. Characteristic mass differences to identify frequent cationization products

Pair of ions	Δm [u]
$M^{+\bullet}$ vs. $^{13}C\text{-}M^{+\bullet}$	1.0033
$M^{+\bullet}$ vs. $[M+H]^+$	1.0078
$[M+H]^+$ vs. $[M+NH_4]^+$	17.0265
$[M+H]^+$ vs. $[M+Na]^+$	21.9819
$[M+H]^+$ vs. $[M+K]^+$	37.9559
$[M+Na]^+$ vs. $[M+K]^+$	15.9739
$[M+H]^+$ vs. $[M+O+H]^+$	15.9949

11.4.4 Cation Removal

If an analyte molecule like an oligonucleotide contains several acidic hydrogens, these can be exchanged by alkali ions without generating a charged species, e.g., [M–H+K] or [M–2H+2Na]. As a result, a single analyte will form numerous ionic species thereby significantly decreasing the abundance of each species involved, e.g., $[M-2H+Na]^-$, $[M-2H+K]^-$, $[M-3H+Na+K]^-$ etc. Thus, hydrogen-to-metal exchange may even result in complete suppression of a signal [122].

On-target washing presents a simple but very effective approach to reduce the alkali ion content of MALDI sample preparations [123,124]. For this purpose, 2–5 µl of alkali ion-free water containing 0.1–1% formic or trifluoroacetic acid is placed on top of the crystalline layer and removed after a few seconds by a microliter pipette or by blowing it off with a stream of pressurized air. The acidification avoids dissolution of the crystals in case of carboxylic acid matrix preparations.

Cation exchange resins can be added prior to preparation to substitute alkali ions for ammonium (Fig. 11.13) [27]. To take full effect, it is important to keep the cation exchange beads even on the target in order to capture the alkali ion contamination of the metal surface, too. No useful signals are obtained when the laser hits the cation exchange beads. Furthermore, there is a risk of ion source contamination as beads may occasionally fall off the surface, even as a result of laser shots.

Another approach is to use tips of microliter pipettes as miniature columns by filling them with *size exclusion chromatography* (SEC) stationary phase material or standard C_{18} reversed phase material [125,126]. Such tips are also commercially available as ZipTips™ [122]. There is a risk of sample absorption on the

column material, which is particularly critical for minor components of complex mixtures – and the cost factor of these consumables should also be kept in mind.

Finally, it is advantageous to add a surfactant blend (Invitrosol-MALDI protein solubilizer B, IMB) prior to preparation (Fig. 11.14) [127].

Equally, sodium dodecyl sulfate contaminations should be removed from 2D gel electrophoresis before subjecting samples to MALDI-MS [128].

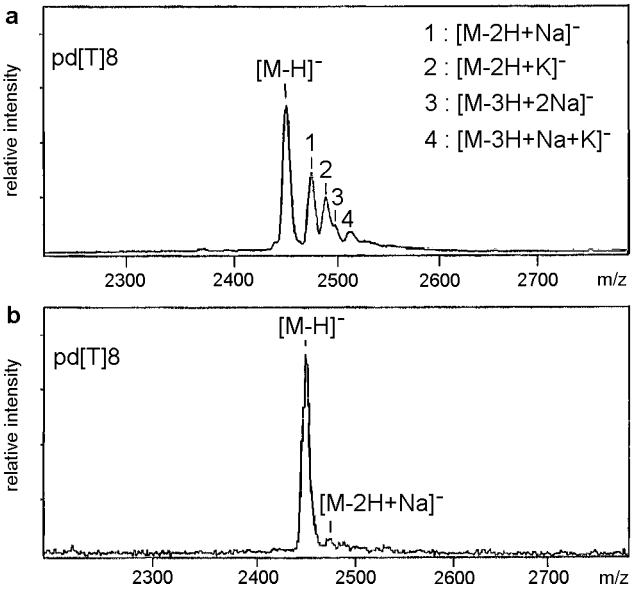


Fig. 11.13. Negative-ion MALDI spectra of the oligonucleotide pd[T]$_8$; (**a**) 5 pmol, (**b**) same as (**a**) after addition of 5–10 cation exchange beads to the sample preparation. Adapted from Ref. [27] by permission. © John Wiley & Sons, 1992.

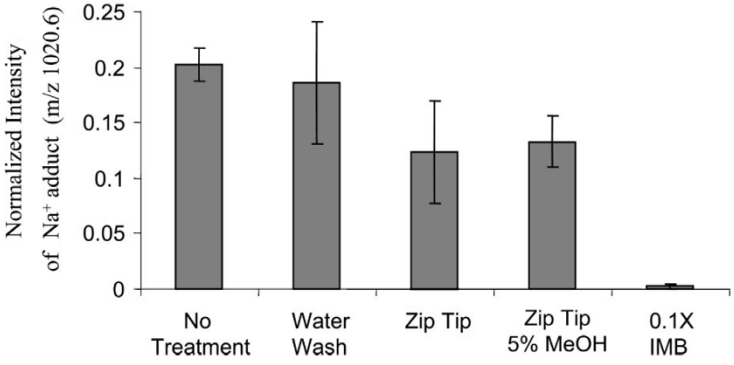


Fig. 11.14. Comparison of common alkali adduct suppression techniques. The ratio of the intensity of a peptide $[M+Na]^+$ peak, *m/z* 1020.56, to the sum of $[M+H]^+$ and $[M+Na]^+$ signal intensities is shown. *Error bars* represent standard deviation of three measurements. Adapted from Ref. [127] with permission. © John Wiley & Sons, Ltd, 2004.

11.4.5 Solvent-Free Sample Preparation

If an analyte is absolutely insoluble or only soluble in solvents that are not acceptable for the standard MALDI sample preparation technique, it can alternatively be ground together with the solid matrix, preferably in a vibrating ball mill. The resulting fine powder is then spread onto the target. To avoid contamination, non-adherent material should be gently blown away from the target before insertion into the ion source [116,129,130]. This preparation technique is obviously restricted to situations where sufficient sample is available.

Example: The organic dye Pigment Red 144, has been subjected to mass analysis by LDI, solvent-based MALDI, and solvent-free MALDI [130]. Its monoisotopic molecular ion, $[C_{40}H_{23}Cl_5O_4N_6]^{+\bullet}$, is expected at *m/z* 826.0. Due to the strong light absorption of the pigment, the uptake of energy in LDI causes quantitative fragmentation to yield solely $[M–OH]^+$ ions. Here, solvent-based MALDI results in a poor sample preparation because of the unfavorable solvents needed, whereas solvent-free sample preparation yields a better spectrum exhibiting mainly $M^{+\bullet}$ and $[M+Na]^+$ ions of the pigment (Fig. 11.15).

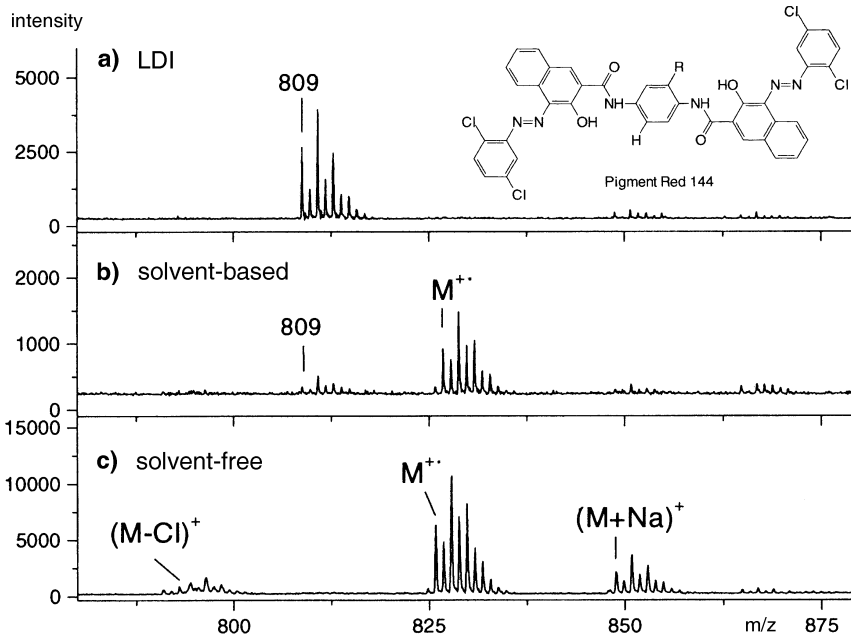


Fig. 11.15. Comparison of spectra of the organic dye Pigment Red 144 as obtained by (**a**) LDI, (**b**) solvent-based, and (**c**) solvent-free MALDI sample preparation. Adapted from Ref. [130] by permission. © John Wiley & Sons, 2001.

11.4.6 Additional Methods of Sample Supply

Surface-adsorbed analytes can be examined by laser desorption techniques if they are supplied on a metal foil, a TLC plate [131], or at least on semiconducting material. Even the foil itself can be subject to LDI. This requires the foil to be fixed on top of a sample target, e.g., by means of (conducting) double-sided adhesive tape or some general-purpose adhesive. Care has to be taken not to produce sharp edges protruding from the surface because these might cause discharges in the ion source when the accelerating voltage is switched on. Furthermore, the mass calibration can be affected by such an unusually thick "sample layer". The latter two limitations are only relevant in case of on-axis MALDI-TOF analysis, while oa-TOF analyzers and other setups with external MALDI ion sources are by far more robust in this respect.

Safety notice: Unconventional sample supply techniques on commercial MALDI instruments require great care. Possible pitfalls include *i*) blocking of the vacuum lock due to unacceptable thickness of the target, *ii*) loss of the sample inside the ion source or inside the vacuum lock, *iii*) damage to the instrument from electric discharges.

11.5 Applications of LDI

Although LDI is also possible for peptides [5] and oligosaccharides [4,6], it is suited much better for analyzing organic and inorganic salts [132-134], molecules with large conjugated π-electron systems [135-137], organic dyes as contained in ballpoint pen inks [138], porphyrins [139], or UV light-absorbing synthetic polymers [5,52]. As interferences with matrix ions are excluded, LDI presents a useful and quick alternative to MALDI in the low-mass range. In addition, solvent-free sample preparation can be employed with insoluble analytes by simply grinding the solid onto the sample holder. However, LDI is a "harder" ionization method than MALDI and fragmentation has to be taken into account.

Example I: Polycyclic aromatic hydrocarbons (PAHs) are easily detected by LDI due to their strong UV absorbance. The positive-ion LDI-TOF mass spectrum of 1,2,3,4,5,6-hexahydrophenanthro[1,10,9,8-*opqra*]perylene exclusively presents the molecular ion at *m/z* 356 (Fig. 11.16; for the EI spectrum cf. Chap. 5.2) [137].

Example II: Fullerene soots as obtained by the Huffman-Krätschmer synthesis [140] can be characterized by positive- as well as negative-ion LDI-MS [135]. Such LDI spectra can exhibit fullerene molecular ion signals well beyond *m/z* 3000; among these, $C_{60}^{+\bullet}$ and $C_{70}^{+\bullet}$ are clearly accentuated (Fig. 11.17). Furthermore, such samples provide experimental carbon-only isotopic patterns over a wide mass range (Chap. 3.2.1). The spectrum below was obtained on a FT-ICR mass spectrometer; hence the resolution is 175,000 at *m/z* 840, i.e., almost by a factor of 1000 higher than on early TOF instruments as used for the discovery of

C_{60} and larger fullerenes [141]. The insets show expanded views of the $M^{+\bullet}$ ions for C_{60}, C_{70}, and C_{120} together with the corresponding calculated isotopic patterns. Note, that the accurate masses are lower than the nominal values by the mass of an electron, while the difference in mass of 1.0033 u between ^{12}C and ^{13}C can be recognized from the mass increment of the 1st and 2nd isotopic peaks.

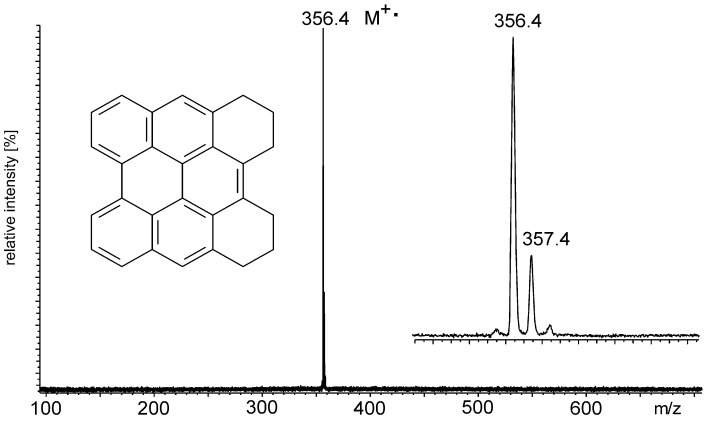


Fig. 11.16. Positive-ion LDI-TOF mass spectrum of 1,2,3,4,5,6-hexahydrophenanthro-[1,10,9,8-*opqra*]perylene. The *inset* shows an expanded view of the molecular ion signal. Adapted from Ref. [137] with permission. © Elsevier Science, 2002.

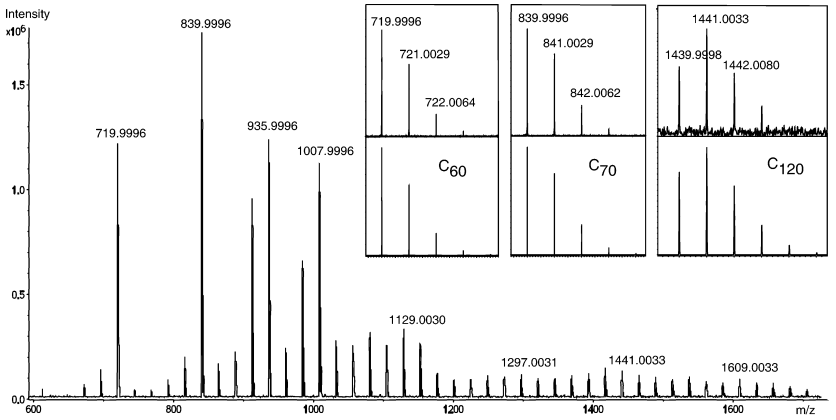


Fig. 11.17. Positive-ion LDI-FT-ICR mass spectrum of a fullerene soot. The *insets* show expanded views of the experimental (*upper parts*) and calculated (*lower parts*) isotopic patterns of $C_{60}^{+\bullet}$, $C_{70}^{+\bullet}$,and $C_{120}^{+\bullet}$. Sample courtesy of W. Krätschmer, Max Planck Institute for Nuclear Physics, Heidelberg. Reproduced from Ref. [142] by permission. © Wiley-VCH, Weinheim, 2009.

11.6 Applications of MALDI

MALDI applications are growing at a rapid pace with over 3000 publications annually since 2006 (Fig. 11.18). A single book chapter thus can impossibly cover all aspects of these developments. However, there are several excellent monographs on different aspects of MALDI which are highly recommended to anyone intending to pursue further studies of MALDI-MS [15,23,143-145]. The following section will merely outline some flagship applications of MALDI-MS.

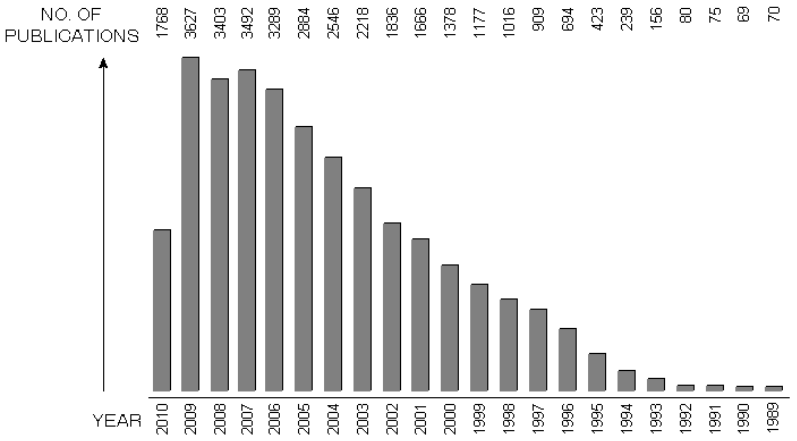


Fig. 11.18. Annual number of publications between 1989 and 2010 containing the concept "MALDI" sorted by year as analyzed by Chemical Abstracts Scifinder Software. The value for 2010 only includes papers up to June of that year.

11.6.1 Protein Analysis by MALDI-MS

The success story of MALDI started with MALDI-TOF-MS on intact proteins. Hillenkamp and Karas showed that MALDI is unique in that it can combine the ability for *i*) desorbing ions of biomacromolecule into the gas phase, *ii*) preserving their structural integrity, and *iii*) being perfectly compatible with mass analyzers with almost unlimited *m/z* range and extraordinary sensitivity (Figs. 11.1 and 11.4) [11,13,14].

The analysis of intact proteins is often the first step in a series of analytical procedures revealing characteristics of cells, physiological pathways, diseases, or other aspects of interest in a biological or biomedical context. Often, the proteins are separated prior to MALDI-MS, e.g., by 2D gel electrophoresis. MALDI experiments must be carried out with highly purified proteins or mixtures containing only a limited number of proteins. In cases where the full mass range of proteins is needed, MALDI-TOF-MS would be the preferred choice.

Commonly, 3,5-dimethoxy-4-hydroxycinnamic acid (sinapinic acid, SA) [85] and 2,5-dihydroxybenzoic acid (DHB) [17,50] are suitable for MALDI of pro-

teins, 2-(4-hydroxyphenylazo)benzoic acid (HABA) for peptides, proteins, and glycoproteins [66], and 2-mercaptobenzothiazole (MBT) or 5-chloro-2-mercaptobenzothiazole (CMBT) are also used of proteins. For smaller proteins, α-cyano-4-hydroxycinnamic acid (α-CHCA) can be used as well [81].

Any organism bears a characteristic *protein fingerprint*. Protein fingerprints (and also those of carbohydrates) can be readily obtained by means of MALDI-MS. The necessary purification steps prior to MALDI analysis depend on the individual sample. For instance, the protein composition of a Mozzarella cheese will be able to reveal whether it was made from cow's milk or of that of a water buffalo [146], or whether feta cheese is "contaminated" with cow's milk [147]. MALDI spectra of protein extracts from different *Bacillus* species can be used to distinguish pathogenic from nonpathogenic bacteria, e.g., the protein fingerprints of chemically lysed *B. anthracis* (Sterne), *B. thuringiensis* (4A1), and *B. cereus* (6E1) are clearly different [148]; even different strains are distinguishable on the basis of particular biomarker proteins.

Example: In food analysis of fish and seafood products, differentiating between individual species of pathogenic and food-spoilage microorganisms and their rapid identification are particularly important.. MALDI-TOF-MS protein

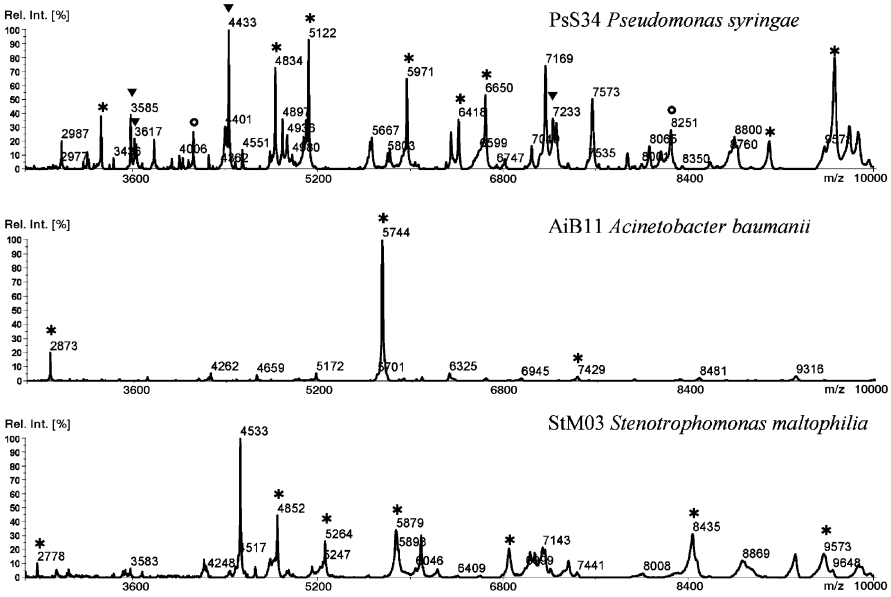


Fig. 11.19. Protein fingerprint MALDI-TOF spectra of *Pseudomonas syringae* (*top*), *Acetinobacter baumannii* (*center*) and *Stenotrophomonas maltophilia* (*bottom*) have clearly different appearances; species-specific peaks are indicated by ✱, genus-specific peaks by ○, and other characteristic peaks by ▼. Adapted from Ref. [149] with permission. © American Chemical Society, 2010.

fingerprinting was used to characterize the main 26 species responsible for seafood spoilage and associated pathogenic bacteria such as *Acinetobacter baumanii* and *Pseudomonas* species (Fig. 11.19) [149]. For this purpose, low-mass proteins were extracted from intact bacterial cells and subjected to MALDI analysis using α-CHCA matrix on a linear TOF instrument. Then, a library of specific MS fingerprints was compiled by comparing 10–35 characteristic peaks per organism in a range of *m/z* 2,000–10,000 from the protein fingerprint MALDI spectra.

11.6.2 Peptide Sequencing and Proteomics

Analysis of the total of all proteins expressed by a living organism, a type of tissue, or certain cells is a tremendous task, as we are dealing with thousands of proteins with relative abundances in range of > 1000 : 1. This field of research called *proteomics* aims at quantitative analysis of entire proteomes of individual organisms, ,and requires complex analytical approaches involving different separation techniques along with MS and MS/MS [150-159]. Of course, in proteomics there are no restrictions as to ionization methods, while MALDI (together with ESI; see Chap. 12) accomplish 99.9% of all MS analyses in proteomics.

A standardized workflow for the complete analysis of a protein by using a pure MALDI strategy comprises several steps (Fig. 11.20). It commences with the measurement of the intact protein's mass, preferably by MALDI-TOF-MS as this combination offers inexpensive and reliable access to the full *m/z* range where proteins may occur. Next, a proteolytic digestion is performed to cut the macromolecule into smaller peptide subunits, typically in the range of 800–2500 u. Generally, the enzyme trypsin is employed to deliver these peptides, a so-called *tryptic digest*, which are then analyzed in a survey measurement by MALDI-TOF-MS. The resulting MALDI spectrum presents a so-called *peptide mass map*. Such peptide mass maps usually suffice to identify the protein [160].

The next stage is to subject as many as possible peptides of the peptide mass map to tandem MS to reveal their individual amino acid sequences. Interpreting the amino acid sequences requires substantial knowledge of the fragmentation behavior of peptide ions [154,158,161]. Automated sequencing is widely used. This involves automated precursor ion selection for tandem MS, e.g., by selecting several abundant $[M+H]^+$ ions of a survey spectrum and generating peak lists from those tandem mass spectra. The experimental results are finally compared with large peptide databases. The number of potential proteins and its tryptic peptides can further be narrowed down using accurate mass data of the protein and the peptides. While MALDI-MS and MALDI-MS/MS could serve this pupose almost alone, electrospray ionization and liquid chromatography coupling to MS today contribute to a larger extent to the instrumental and methodological mix in proteomics, because the LC-MS technique is more efficient in detecting trace proteins than approaches starting from 2D gels [15,22,162,163].

Only the peptide subunits of a protein can be efficiently fragmented by CID for tandem MS analysis. Identifying a protein from such a peptide "jumble" is called *bottom-up* protein analysis. The corresponding tandem MS of the entire protein

ions is called *top-down* protein analysis. As the *top-down* approach requires larger amounts of purified protein, it is more widely applied in protein biochemistry. ECD-FT-ICR-MS, assisted by IRMPD heating of the protein ions, is currently the exclusive tool for this purpose (Chap. 9.14.4).

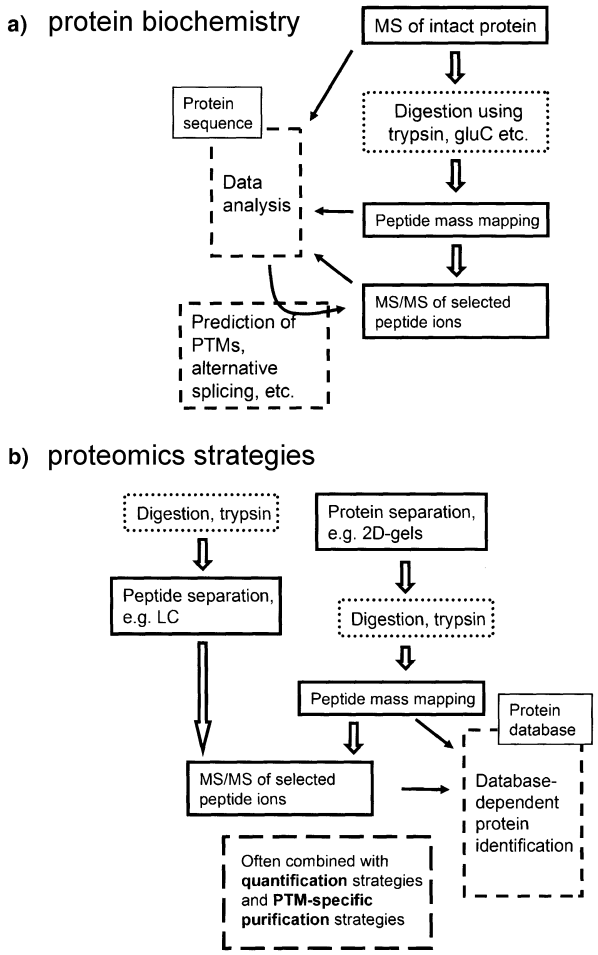
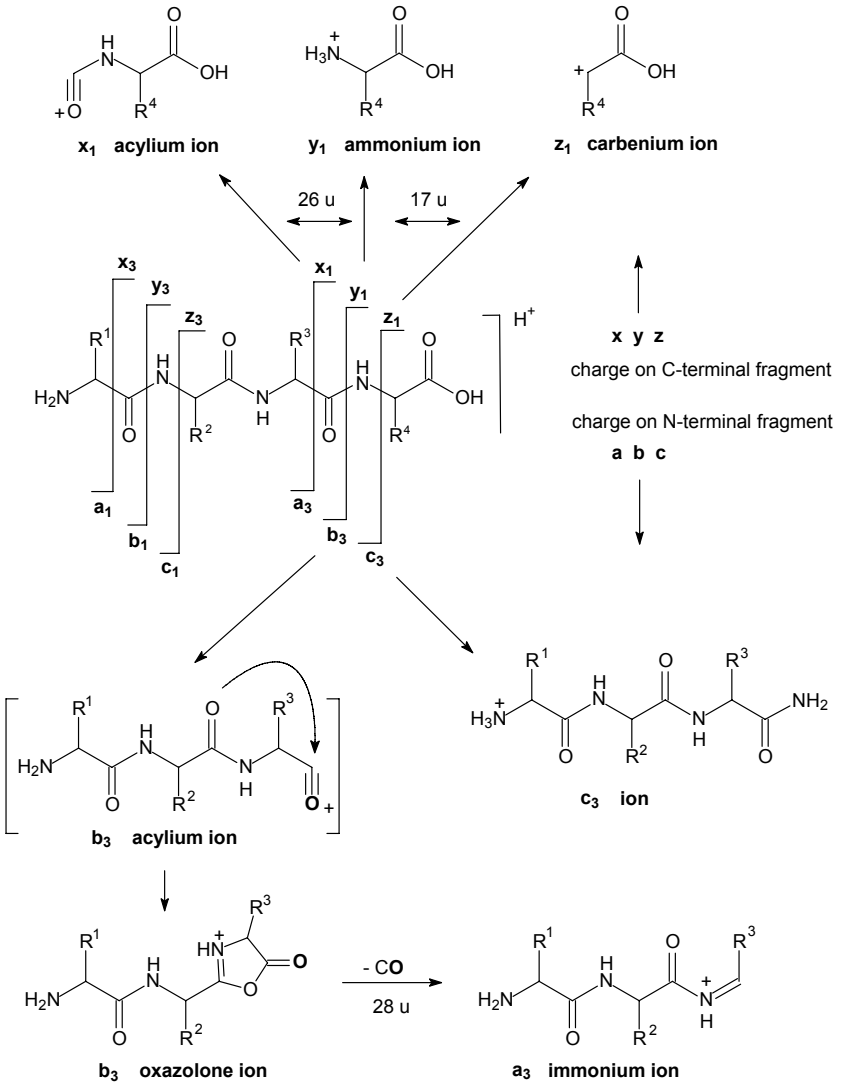


Fig. 11.20. Analytical strategies in (**a**) protein biochemistry requiring highly purified proteins and (**b**) proteomics addressing the entire proteome of a living cell. Adapted from Chap. 3 by Hjernø and Jensen in Ref. [15] by permission. © Wiley-VCH, Weinheim, 2007.

Note: Examples and mechanistic aspects of peptide fragmentation are also covered in the context of tandem MS (see Chaps. 9.6.6, 9.8, and 9.10.1). The mechanism of peptide cleavage upon ECD is discussed in Chap. 9.13.2 with an example in Chap. 9.14.4; peptide ETD spectra are given in Chap. 9.15. Some further examples will follow in Chap. 12.

Peptide ions are comparatively large, and thus assume various fragmentation pathways. The most obvious and analytically useful fragmentation routes involve the cleavage of the peptide backbone. Following the nomenclature for peptide backbone cleavages originally suggested by Roepstoff and Fohlman [164] and modified by Biemann [165] fragments bearing the charge (due to protonation) at the N-terminus are denoted as a-, b-, and c-ions depending on the actual bond cleaved. If C-terminal fragment ions are formed, the ions are termed x-, y-, and z-ions, respectively (Scheme 11.1). Further, a number index counting from 1 to *n*–1



Scheme 11.1 (One carbonyl-*O* is set in bold for better tracking)

for a peptide composed of *n* amino acids is used to indicate which bond is cleaved. Within each ion series, peaks are seperated by $\Delta m/z$ values directly reflecting the *amino acid residue* (Table A.9) between them.

The base fragment ion series due to amide bond cleavages are formed by b-ions on the N-terminus and y-ions on the C-terminus. The signals of the a-ions are set off to lower mass by 28 u (CO loss) from the b-ions, while c-ions are 17 u (NH_3) heavier than b-ions as the adjacent N–C_α bond is cleaved. The x-ions of the C-terminal series are by 26 u lighter than y-ions (minus CO, plus H_2) and z-ions are again by 17 u (NH_3) heavier than y-ions.

Example I: Scheme 11.1 depicts the most likely structures for the main peptide fragment ions. For example, the nominal acylium form of the b_3 ions is not stable, rather it is stabilized by formation of a 5-membered oxazolone ring [166-169] at its C-terminus. Note that this ion contains the amino acid residues up to the third (R^3) including the carbonyl group of R^3 and that the charge is carried by the nitrogen of the ring. The corresponding a_3 ion is formed by elimination of the carbonyl group (CO) from the oxazolone ring.

Example II: The purified octapeptide QAMNKFTF–NH_2 was subjected to positive-ion MALDI-TOF/TOF analysis. The spectrum shown (Fig. 11.21) was obtained from the $[M+H]^+$ precursor ion, *m/z* 985.53. The fragment at *m/z* 968.33 corresponds to ammonia loss from $[M+H]^+$. All seven ions belonging to the b-ion series are detected at *m/z* 821.25, 720.23, 573.19, 445.12, 331.08, 200.04, and 129.02. In addition b–NH_3 ions, referred to as b* ions, accompany the first four ions at *m/z* 804.24, 703.22, 556.17, and 428,10 because the N-terminal glutamine (Q) has a tendency to lose NH_3.Thus, we have ions consistent with the expected b_7 to b_1 and b_7* to b_4* fragments, although the ion at *m/z* 129 can also be formed from lysine (K). The four additional fragment ions at *m/z* 857.29, 786.25, 655.25, and 541.23 belong to the y-series and represent the y_7 to y_4 ions, whereas smaller y ions are absent (only their hypothetical positions are indicated as y_1^a to y_3^a) [170].

Note: Peptides show marked differences, though having a great deal in common. Biochemists always emphasize the enormous variability of peptides and proteins assembled from as just twenty amino acids and the plethora of resulting functional characteristics. Accordingly, one should stay aware of the fact, that every (peptide) molecule has intrinsic properties also determining their fragmentation into ions.

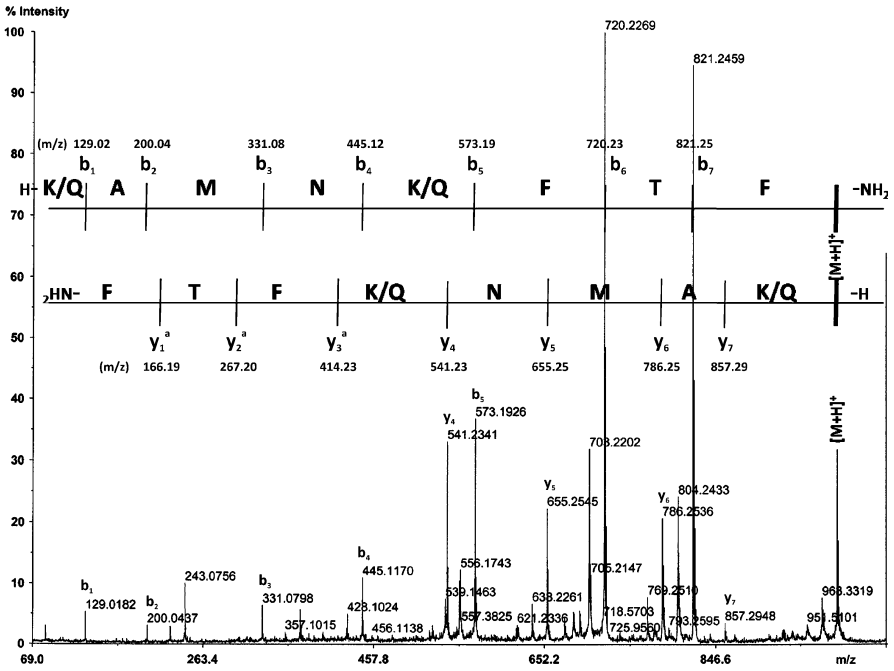


Fig. 11.21. MALDI-TOF/TOF mass spectrum of the purified octapeptide H-QAMNKFTF-NH_2 showing the experimental b_j and y_j peptide fragment ion series; y^a ions are only hypothetical in this case. Adapted from Ref. [170] with permission. © John Wiley & Sons, 2010.

The appearance of a tandem mass spectrum may vary greatly. First, it depends to some extent on the ionization method employed to generate a $[M+H]^+$ precursor ion, because ions from MALDI are entering the activation process with already somewhat higher internal energy than those from ESI. Second, the charge state of the selected prescursor ion is of utmost importance. With increasing number of charges the Coulombic repulsion also contributes to drive the incipient fragments apart, and thus, less energy needs to be provided by the activation method used. Besides the activation technique, other instrumental factors such as ion life time or internal energy distribution also effect the appearance of the spectrum. In tandem MS, quadrupole ion trap analyzers tend to suppress the lower third of the *m/z* range, whereas TOF and magnetic sector analyzers do not. Together with the intrinsic properties of the ion under study these specific differences introduced into the sequencing experiment cause certain fragments to occur in the final spectrum while others may be missed. This is commonly referred to as *sequence coverage* of a given intrumental configuration.

11.6.3 Carbohydrate Analysis by MALDI-MS

Starting from simple mono- and disaccharides to oligo- and polysaccharides, carbohydrates play an important role in organisms and nutrition. MALDI-MS (typically using DHB or some DHB-containing matrix [17,73-75,77]), is a powerful tool for their characterization [171]. Applications include the characterization of maltose chains in "gummy bears" [73], fructans in onions [172], high-molecular-weight oligosaccharides in human milk [74,75], and others [111,173]. MALDI-MS of carbohydrates from fungal spores [174] allows for the characterization of the corresponding fungus.

Example: The maltose chains in the confectionery "gummy bears" consist of up to about 30 maltose units [73]. The signals originating from $[M+Na]^+$ ions are spaced 162 u apart, i.e., by $C_6H_{10}O_5$ monomer units (Fig. 11.22). The difference between biopolymer or synthetic polymer is of minor significance when it comes to MALDI.

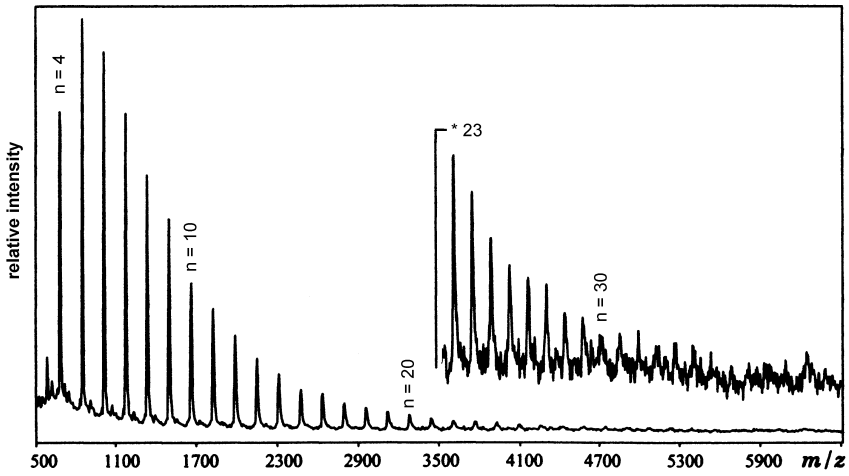
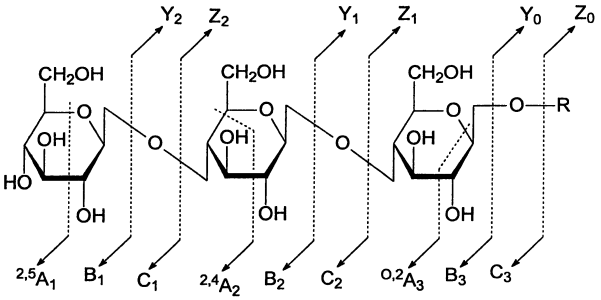


Fig. 11.22. Positive-ion MALDI spectrum of the maltose chains in "gummy bears". Reproduced from Ref. [73] by permission. © John Wiley & Sons, 1995.

The structure of linear as well as complex branched oligosaccharides can be sequenced by tandem MS analogous to peptide sequencing [171,175]. If the carbohydrate ions are generated by MALDI, sufficient energy for their fragmentation can be provided in two ways: *i*) Higher laser irradiance can effect *in-source decay* (ISD) or *metastable dissociation* [118]; the latter being termed *post-source decay* (PSD) in the MALDI-TOF community. *ii*) *Collision-induced dissociation* (CID) of selected precursor ions can be employed alternatively. (Of course, other compound classes such as peptides, oligonucleotides, or synthetic polymers can be treated analogously.) The general scheme of carbohydrate fragmentation is as follows (from Ref. [171] by permission, © Elsevier Science, 2003):



Scheme 11.2.

Example: The PSD-MALDI-TOF spectrum of the $[M+Na]^+$ ion, *m/z* 1418.9, of high-mannose *N*-linked glycan $(Man)_6(GlcNAc)_2$ from chicken ovalbumin shows distinct cleavages of the branched carbohydrate skeleton (Fig. 11.23). [171] The spectrum was obtained using DHB matrix.

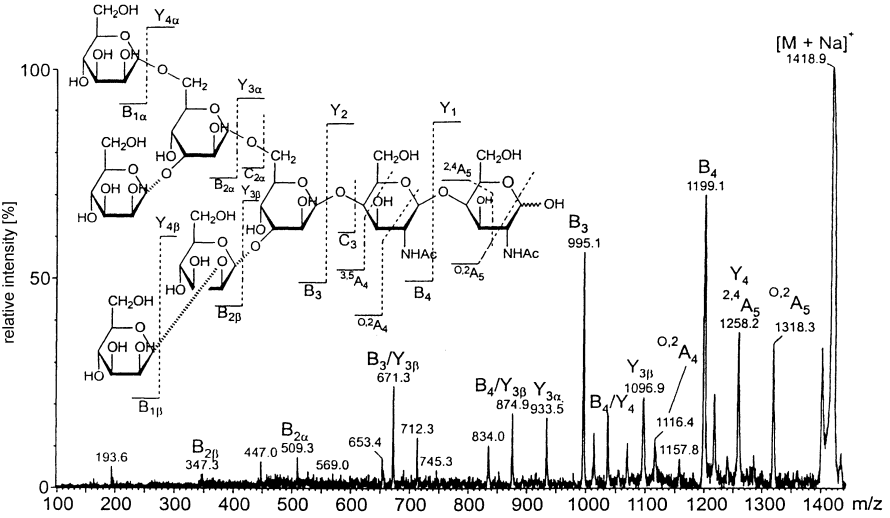


Fig. 11.23. PSD-MALDI-TOF spectrum of *N*-linked glycan $(Man)_6(GlcNAc)_2$ from chicken ovalbumin. Reproduced from Ref. [171] by permission. © Elsevier Science, 2003.

Note: Carbohydrates possess a high affinity towards alkali metal ions, and thus in MALDI spectra $[M+Na]^+$ and/or $[M+K]^+$ are normally observed instead of or in addition to $[M+H]^+$ ions of very low abundance. Radical ions are not observed. It generally depends on the relative amount of alkali ion impurities or dopant which ionic species will dominate the spectrum.

11.6.4 Oligonucleotide Analysis by MALDI-MS

Oligonucleotides and DNA represent the highest polarity class of biopolymers. Therefore, it is of special importance that isolation in an organic matrix allows to overcome their strong intermolecular interaction. MALDI analysis of oligonucleotides is further complicated by the numerous acidic hydrogens present in a single molecule. In particular the phosphate groups easily exchange protons with the ubiqitous alkali ions [27]. Thus, MALDI of this compound class requires to follow proven experimental protocols to obtain clean spectra of intact quasimolecular ions. The acidity of the phosphates makes oligonucleotides and DNA accessible as $[M–H]^-$ ions if measured in the negative ion mode [27].

Due to their numerous acidic hydrogens, oligonucleotides require desalting prior to MALDI, e.g., by using cation exchange resins [27]. Similar procedures are necessary when other ionization methods are applied to this compound class [72,90,176,177].

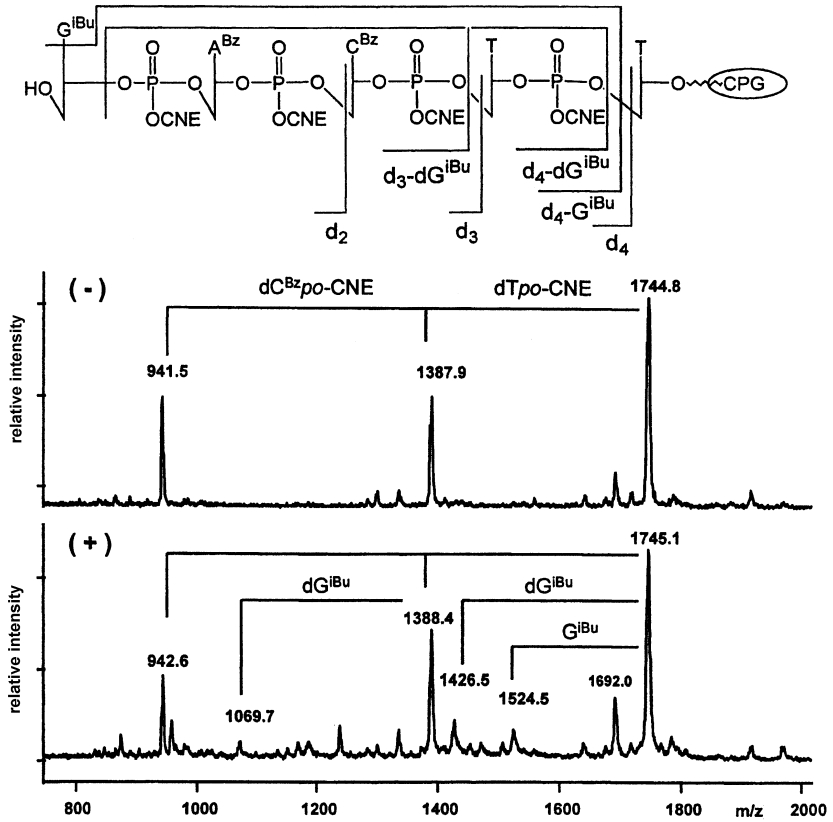


Fig. 11.24. Comparison of the negative- and positive-ion mode MALDI-TOF spectra of the 5-meric *po*-CNE 5′-GACTT-3′ oligodeoxynucleotide. Both show fragment ions by ISD. Adapted from Ref. [90] by permission. © John Wiley & Sons, 2000.

Example: The negative- and positive-ion mode MALDI-TOF spectra of the solid-supported 5-meric oligodeoxynucleotide *po*-CNE 5′-GACTT-3′ [90]: comparison shows that both exhibit fragment ions due to cleavages of the phosphotriester backbone (Fig. 11.24). As oligonucleotides normally do not exhibit such a distinct level of ISD in MALDI spectra, it has been argued that the linking to the solid support plays a role for the generation of this mass ladder of peaks which differ by one nucleotide residue.

11.6.5 MALDI-MS of Synthetic Polymers

MALDI is the method of choice for the analysis of synthetic polymers. MALDI is soft enough to provide intact molecular ions or intimately related ions by cationization and gives access to an essentially unlimited mass range [23,24,145]. As ions from MALDI are almost always singly charged [42] the spectrum may represent a very good approximation to the molecular weight distribution of the examined polymer. While polar polymers such as poly(methylmethacrylate) (PMMA) [91,178], polyethylene glycol (PEG) [178,179], and others [87,180,181] readily form $[M+H]^+$ or $[M+alkali]^+$ ions, nonpolar polymers like polystyrene (PS) [112,113,118,119] or nonfunctionalized polymers like polyethylene (PE) [115,116] can only be cationized by transition metal ions in their 1+ oxidation state [112,113]. The formation of evenly spaced oligomer ion series can also be employed to establish an internal mass calibration of a spectrum [180].

The most important parameters that can be determined by MALDI are *number-average molecular weight* (M_n), *weight-average molecular weight* (M_w), and the molecular weight distribution expressed as *polydispersity* (*PD*) [119,182]:

$$M_n = \frac{\sum M_i I_i}{\sum I_i} \tag{11.1}$$

$$M_w = \frac{\sum M_i^2 I_i}{\sum M_i I_i} \tag{11.2}$$

$$PD = \frac{M_w}{M_n} \tag{11.3}$$

where M_i and I_i represent the molecular weights of the oligomeric components and their signal intensities (assuming a linear relationship between number of ions and signal intensity) of the detected species. The formula for M_n is identical to that used for the calculation of the molecular weight from isotopic masses and their abundances as represented by an isotopic pattern (Eq. 3.2 in Chap. 3.1.5).

Example: Polystyrenes ranging from PS 2200 to PS 12500 form $[M+metal]^+$ ions with Ag^+ and Cu^+ ions when silver or copper(I) salts are admixed to the sample preparation. In case of PS 12500, both metal ions were found to effect cationi-

zation equally well, i.e., without causing differences in average molecular weight or ionic abundances (Fig. 11.25) [119].

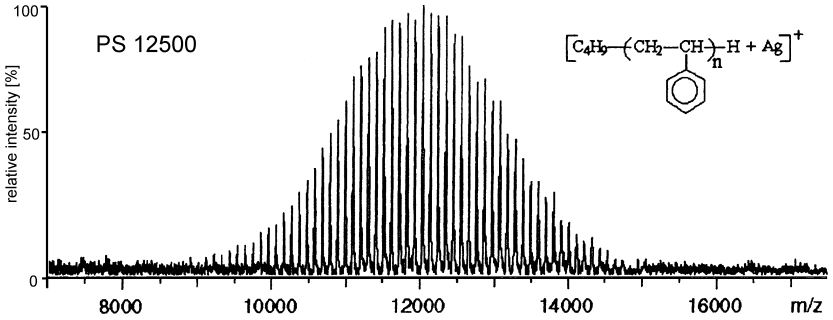


Fig. 11.25. MALDI-TOF spectrum of polystyrene 12500 doped with Ag^+ ions . The isotopic pattern of silver does not affect the spectrum as isotopic resolution here is not achieved anyway. Adapted from Ref. [119] by permission. © John Wiley & Sons, 2001.

In addition, the determination of a polymer's endgroup(s) [183,184] and the analysis of random and block-copolymers [185,186] can be achieved by MALDI. However, care has to be taken when judging the MALDI spectra because of the mass-dependent desorption and detection characteristics of the experiment. In case of higher polydispersity ($PD > 1.1$) high-mass ions are underestimated from MALDI spectra [106,182]. The current practice to deal with such samples is to fractionate them by *gel permeation chromatography* (GPC) [181] or *size-exclusion chromatography* (SEC) prior to MALDI analysis [182,187].

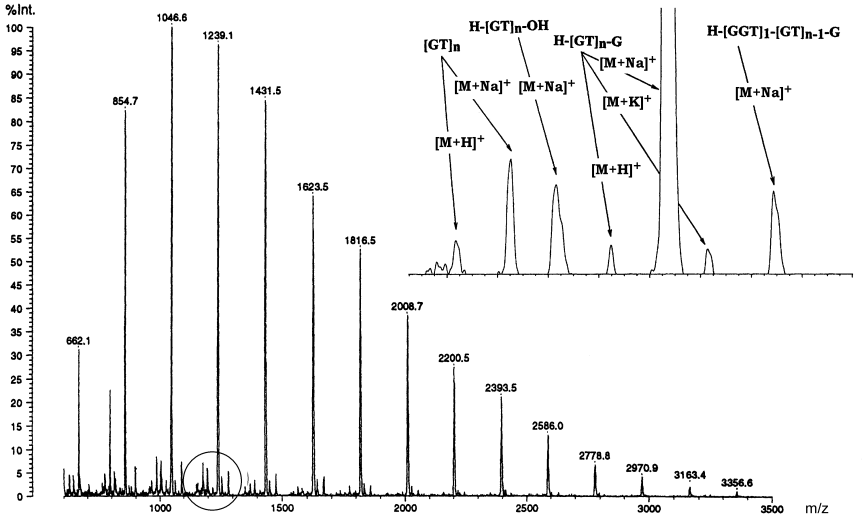


Fig. 11.26. Oligo(ethylene terephthalate diol)s: MALDI-TOF spectrum of the model compound. The *inset* shows an expanded view of the low-intensity peaks *m/z* 940–1120 (*circled*). Adapted from Ref. [184] by permission. © John Wiley & Sons, 1995.

Example: Extracted and synthesized oligo(ethylene terephthalate)s were compared by MALDI-MS [184]. Using the symbols G for ethylene glycol units, GG for diethylene glycol units, and T for terephthalic acid units, the detected oligomers were *i*) cyclic oligomers $[GT]_n$, *ii*) linear chains H-$[GT]_n$-G, and *iii*) some other distributions such as linear H-$[GH]_n$-OH and H-$[GGT]_1$-$[GT]_{n-1}$-G oligomers and cyclic H-$[GGT]_1$-$[GT]_{n-1}$ oligomers. Type *i*) was mainly contained in technical yarns and tiles, whereas types *ii*) and *iii*) were constituents of the model oligomers (Fig. 11.26).

11.7 Special Surfaces to Mimic the Matrix

MALDI is so unique in offering a wide range of applications from small molecule analysis over peptides and synthetic polymers to large biomacromolecules that efforts have been made to mimic the matrix effect in other ways without having the specific disadvantages of matrixes, such as background peaks (which are particularly disturbing in the low-mass range). Here, alternative techniques are briefly discussed.

11.7.1 Desorption/Ionization on Silicon

In *desorption/ionization on silicon* (DIOS), the analyte is absorbed by a micrometers-thick porous surface layer on a silicon chip, i.e., the porous silicon is used as substitute of an organic matrix [188,189]. Porous silicon surfaces with high UV absorptivity can be generated with varying properties from flat crystalline silicon by using a galvanostatic etching procedure [190]. Stabilization of the freshly prepared surfaces is achieved by hydrosilylation. Porous silicon surfaces can be reused several times after washing. Arrays of 100–1000 sample positions can be realized on a 3×3 cm silicon chip [190]. The DIOS technique offers picomole detection limits for peptides, comparatively simple sample preparation, and – most importantly for small molecule analysis – the absence of matrix peaks in the spectra [191,192]. DIOS plates are commerically available and normally used via an adapter sample plate.

Example: DIOS-TOF/TOF experiments on the tryptic digest of 100 fmol of the protein bovine serum albumine (BSA) demonstrate this technique. Using conductive tape the DIOS chip was directly attached to the MALDI target plate of an Applied Biosystems 4700 tandem TOF instrument equipped with a frequency-tripled Nd:YAG laser (355 nm). The resulting DIOS-TOF spectrum of the digest and the DIOS-TOF/TOF spectrum of one selected peptide, $[YLYEIAR+H]^+$, *m/z* 927.5 are shown in Fig. 11.27. The tandem mass spectrum provides complete detection of the *y* and *b* ion series [192].

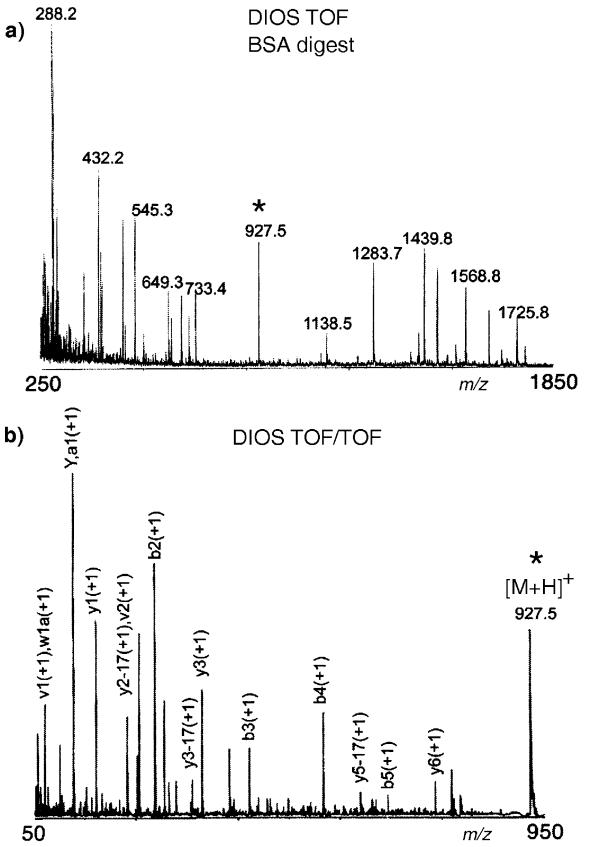


Fig. 11.27. DIOS applied to a tryptic BSA digest. (**a**) DIOS spectrum of the tryptic peptides from BSA; (**b**) DIOS tandem mass spectrum of the $[YLEIAR+H]^+$ peptide ion, *m/z* 927.5, to demonstrate sensitivity and sequence coverage of DIOS. Adapted from Ref. [192] with permission. © American Chemical Society, 2003.

11.7.2 Nano-Assisted Laser Desorption/Ionization

A more recent approach, also from the Suizdak group, is to modify silicon surfaces with *single-crystal silicon nanowires* (SiNWs), which also happen to provide a good platform for surface-based mass spectrometry. Those silicon nanowires are directly synthesized on the surface of a silicon wafer. The formation of SiNW can be well controlled to define physical dimensions, composition, density, and position of the nanowires on the surface [193,194].

The synthesis of SiNWs starts from gold nanoparticles with diameters of 10, 20, or 40 nm that are distributed on a silicon substrate. The nanoclusters are required to catalyze SiNW growth. The method employs an elaborate series of steps of growth, etching, oxidation, and finally silylation to generate a perfluorophenyl-

derivatized SiNW surface. Like DIOS targets, the SiNW-coated plates are attached to a modified sample plate. The procedure of measuring a spectrum is then analogous to LDI or DIOS, i.e., the special surface replaces the organic matrix.

The term *nano-assisted laser desorption/ionization* (NALDI) [195,196] has been coined for techniques using nanostructured surfaces to mimic MALDI. NALDI™ sample plates are commerically available from a major manufacturer of MALDI-TOF instrumentation (Fig. 11.28). Like DIOS, NALDI is particularly useful for small molecule analysis in high-throughput analytics [195,195,196].

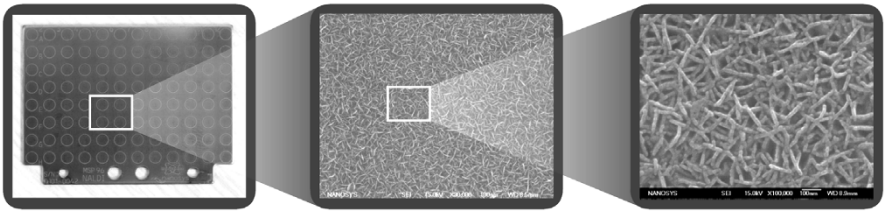


Fig. 11.28. NALDI target plate. The figure shows the NALDI target plate (*left*) and increasing magnification SEM images (*center* and *right*) of the nanostructured coating that provides the active surface for desorption/ionization of deposited analytes. Courtesy of Bruker Daltonik GmbH, Bremen.

11.7.3 Further Variations of the MALDI Theme

The properties of a surface may to a certain extent be tailored to optimize its performance for a particular field of application. Basically, the matrix–analyte pair is replaced by a customized surface–analyte pair that is subjected to laser irradiation. While this approach, on the one hand, simplifies sample preparation, on the other it necessitates preparation of a set of delicate surfaces to be used for different needs.

Silica gel can be derivatized in multiple ways, e.g., by covalently binding ligands via Si–O bonds to its surface. Both *surface-enhanced laser desorption/ionization* (SELDI) and *material-enhanced laser desorption/ionization* (MELDI) make use of the presence of metal complexes on a silica gel surface to selectively adsorb target compounds via complex formation from solution to a target surface [197]. Besides silica gel, also cellulose or glycidyl methacrylate particles, and even diamond powder have been employed as carriers for the metal complex-functionalized groups [198,199].

Note: Surfaces for DIOS, NALDI, or MELDI are active and rather sensitive. They require proper storage, handling, and processing, e.g., washing, before use. As the sample holder is of one type of customized surface only, this sort of targets is merely useful when performing a large number of very similar analyses. Increased cost at reduced robustness as compared to simple stainless steel plates may need to be taken into account.

11.8 MALDI Imaging

MALDI-MS can be used to generate ion images of samples thus providing the capability of mapping specific molecules to two-dimensional coordinates of the original sample [200]. This approach to surface analysis has long been known in *secondary ion mass spectrometry* (SIMS, Chap. 15.5.4) and was introduced in MALDI-MS as *MALDI imaging* by the Caprioli group in 1997 [200]. Since then, MALDI imaging has undergone a tremendous development [201-204] (Chap. 4 in [15] and Chap. 12 in [205]). The high sensitivity of the technique ranging down to the low femtomole to even attomole levels for proteins and peptides gives access to the study of intricate biochemical processes. In fact, MALDI imaging is most frequently used to map local concentrations of target analytes in tissue samples, but it can also be applied to analyze paint or ink on paper or valuable artwork.

The preparation procedure is critical for the outcome of MALDI imaging. It consists of coating of the tissue section or a blotted imprint of the section with an evenly distributed thin matrix layer before the sample can be placed into the mass spectrometer (Fig. 11.29) [218]. The matrix solution is preferably sprayed onto the sample, e.g., by a pneumatic or electrostatic nebulizer delivering very fine droplets to assure homogeneous coating [206]. Alternatively, a picoliter volume spotter can be used to deposit matrix spots in a fixed pattern onto the sample slice [201]. Variations in matrix crystallization or layer thickness result in erroneous images, because the intensity of the signals would rather be determined by the quality of the matrix layer on the actual pixel than by the concentration of the analyte underneath. Microcrystalline layers and laser spot focus diameter also determine the spatial resolution of the imaging process, which can resolve structures to about 10 µm [202,206,207].

Note: The term *imaging mass spectrometry* (IMS) is correlated to the same acronym as *ion mobility spectrometry* (IMS, Chap. 4.9.2), thus one must be aware of the context in which IMS is being used.

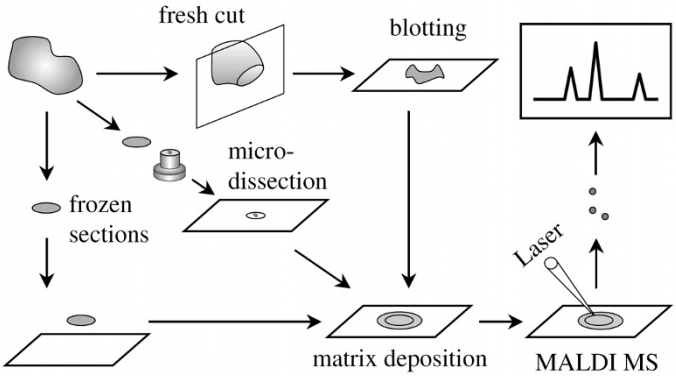


Fig. 11.29. Sample preparation strategies for MALDI imaging of tissues. Reproduced from Ref.[218] with permission. © John Wiley & Sons, Ltd., 2001.

MALDI imaging creates an array of mass spectra, i.e., each "pixel" of the image, often of an 256 × 256 spot array, is represented by a MALDI spectrum of its own. Images are then obtained by extracting ionic abundances of certain *m/z* or eventually *m/z* ranges for display. In other words, reconstructed ion chromatograms (Chap. 1.3) are plotted two-dimensionally rather than just along a time axis. Often, color coding is used to simplify the recognition of patterns, e.g., a certain color may represent a certain compound or *m/z* range, its brightness may reveal the abundance of the compound. It is obvious from this approach that only a few components or compound groups can be displayed in one image at a time. This is why MALDI imaging results are often represented by a set of images each of them composed to highlight a topic of its own (Fig. 11.30). It is furthermore required to correlate the MALDI mass spectral image with the optical image of the sample as obtained by light microscopy immediately before matrix coating.

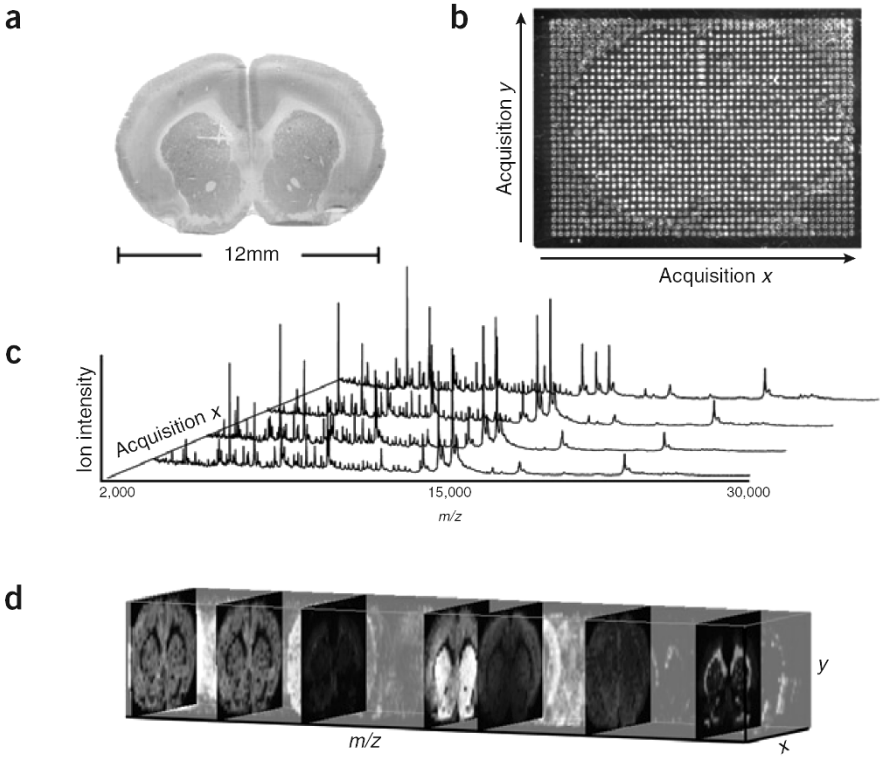


Fig. 11.30. Conceptual overview of MALDI imaging. (**a**) Freshly cut tissue section (here: mouse brain); (**b**) mounted section after application of matrix, here by a robotic picoliter volume spotter; (**c**) partial series of mass spectra along the *x*-axis of the sample; (**d**) three-dimensional volumetric plot of the complete dataset with selected *m/z* ranges per image. Reproduced from Ref. [201] with permission. © Nature Publishing Group, 2007.

IMS instrumentation can be classified according to how ions are generated from the sample, i.e., either by irradiation with a pulsed laser as in MALDI or by bombardment with energetic particles as in SIMS [201]. SIMS uses a continuous particle beam that can be precisely focused, and thus, SIMS can deliver images offering a spatial resolution in the order of 100 nm, however, at the cost of fragmentation upon impact of the energetic particles. MALDI imaging is generally limited to yield a resolution of about 20 μm, but it can access an *m/z* range over 100,000 [201].

11.9 Atmospheric Pressure MALDI

In *atmospheric pressure MALDI* (AP-MALDI) the MALDI process takes place under atmospheric pressure in dry nitrogen gas. The desorbed ions are then transferred into the vacuum of the mass analyzer by means of an *atmospheric pressure ionization* (API) interface which is typically provided by an electrospray ionization (ESI, Chap. 11) source. AP-MALDI was first presented in combination with an orthogonal acceleration TOF (oaTOF, Chap. 4.2.6) analyzer where the original ESI ion source was modified to accommodate a simple MALDI target plus laser instead of the ESI spray capillary [208]. AP-MALDI has also been adapted to a quadrupole ion trap (QIT, Chap. 4.5) [209] where an improved design was realized by extending the heated transfer capillary of a Finnigan LCQ ion trap instru

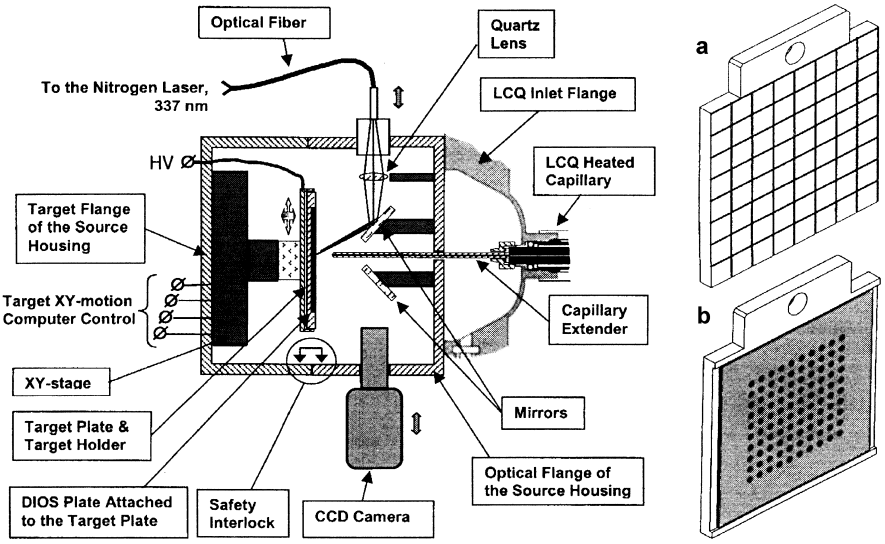


Fig. 11.31. AP-MALDI ion source with extended transfer capillary. *Insets*: (**a**) the target holder can be equipped with a 64-spot MALDI target or (**b**) a 10 × 10-spot DIOS chip. Adapted from Ref. [191] by permission. © John Wiley & Sons, 2002.

ment. Thus, a multi-sample target on an *xy*-movable target holder and observation optics could be incorporated on the atmospheric pressure side (Fig. 11.31) [210]. The entrance of the capillary extender is held at 1.5–3 kV to attract the ions from the target surface located about 2 mm away. By modifying the target an AP-DIOS arrangement can also be accomplished on such an AP-MALDI source [191].

Compared to vacuum MALDI, AP-MALDI has a larger tolerance to laser fluence variations and exhibits reduced fragmentation due to the collisional cooling of the expanding plume. As a result of this cooling process, clustering between matrix and analyte ions is more pronounced. Declustering can be achieved by employing higher laser fluences or adapting the parameters of the atmospheric pressure interface [211].

11.10 General Characteristics of MALDI

11.10.1 Sample Consumption and Detection Limit

In MALDI, the minimum sample load or the detection limit is usually specified instead of sensitivity. Sample loads of 50–500 fmol of a protein for one sample preparation have been communicated earlier [13,14] and 1 fmol can normally be achieved. As thousands of single-shot spectra can be obtained from one preparation spread over some square millimeters, the sample consumption has been estimated to approximate 10^{-17} mol per laser shot, i.e., normally more than 99% of the sample can theoretically be recovered from the target. Improved ion extraction and detection as well as miniaturized sample preparation, e.g., by means of the anchor target technology, can provide attomole detection limits for peptides.

Note: In MALDI-MS, the combination of the actual analyte and the procedure of sample preparation represent the true limiting factors for sample consumption and detection limit.

11.10.2 Analytes for MALDI

For standard MALDI sample preparation, the analyte should be soluble to about 0.1 mg ml^{-1} in some solvent. If an analyte is completely insoluble, solvent-free sample preparation may alternatively be applied (Chap. 11.4.3). The analyte may be neutral or ionic. Solutions containing metal salts, e.g., from buffers or excess of noncomplexated metals, may cause a confusingly large number of signals due to multiple proton/metal exchange and adduct ion formation; even complete suppression of the analyte can occur. The mass range of MALDI is theoretically almost unlimited; in practice, limits can be as low as 3000 u, e.g., with polyethylene, or as high as 300,000 u in case of antibodies.

11.10.3 Types of Ions in LDI and MALDI-MS

Very similar to FAB/LSIMS, LDI ,and MALDI produce a variety of ions depending on the polarity of the analyte, its ionization energy, the characteristics of the matrix (if any) and on the presence or absence of impurities such as alkali metal ions [20,33,34]. The tendency to form radical ions is somewhat lower than in case of FAB/LSIMS (Table 11.3).

Table 11.3. Ions formed by LDI and MALDI

Analytes	Positive ions	Negative ions
nonpolar	$M^{+\bullet}$	$M^{-\bullet}$
medium polarity	$M^{+\bullet}$ and/or $[M+H]^+$, $[M+alkali]^+$, {*clusters* $[2M]^{+\bullet}$ and/or $[2M+H]^+$, $[2M+alkali]^+$, *adducts* $[M+Ma+H]^+$, $[M+Ma+alkali]^+$}[b]	$M^{-\bullet}$ and/or $[M-H]^-$, {*clusters* $[2M]^{-\bullet}$ and/or $[2M-H]^-$ *adducts* $[M+Ma]^{-\bullet}$, $[M+Ma-H]^-$}
polar	$[M+H]^+$, $[M+alkali]^+$, *exchange* $[M-H_n+alkali_{n+1}]^+$ *high-mass anal.* $[M+2H]^{2+}$, $[M+2alkali]^{2+}$ {*clusters* $[nM+H]^+$, $[nM+alkali]^+$, *adducts* $[M+Ma+H]^+$, $[M+Ma+alkali]^+$}	$[M-H]^-$, *exchange* $[M-H_n+alkali_{n-1}]^-$ {*clusters* $[nM-H]^-$ *adducts* $[M+Ma-H]^-$}
ionic[a]	C^+, $[C_n+A_{n-1}]^+$, $\{[CA]^{+\bullet}\}$	A^-, $[C_{n-1}+A_n]^-$, $\{[CA]^{-\bullet}\}$

[a] comprising of cation C^+ and anion A^-
[b] enclosure in parentheses denotes rarely observed species

11.10.4 Mass Analyzers for MALDI-MS

Laser desorption intrinsically is a pulsed ionization process, which is therefore ideally combined with time-of-flight (TOF) analyzers (Chap. 4.2) [17,52]. Ever since the first MALDI experiments, MALDI and TOF have been forming a unit, and the majority of MALDI applications are MALDI-TOF measurements. Vice versa, it was the success of MALDI that pushed forth the tremendous delevopment of TOF mass analyzers. More recently, MALDI has also been adapted to orthogonal acceleration TOF analyzers [212].

Fourier transform ion cyclotron resonance (FT-ICR, Chap. 4.7) is much better suited for laser desorption [5,6]. Best results are obtained when the ions are generated in an external ion source and subsequently transferred into the ICR cell for mass analysis [213]. MALDI-FT-ICR has become a mature combination [214,215]. Modern MALDI-FT-ICR instruments make use of collisional cooling of the plasma plume before transferring the ions into the ICR cell [216,217].

References

1. Fenner, N.C.; Daly, N.R. Laser Used for Mass Analysis. *Rev. Sci. Instrum.* **1966,** *37*, 1068-1070.
2. Vastola, F.J.; Pirone, A.J. Ionization of Organic Solids by Laser Irradiation. *Adv. Mass Spectrom.* **1968,** *4*, 107-111.
3. Vastola, F.J.; Mumma, R.O.; Pirone, A.J. Analysis of Organic Salts by Laser Ionization. *Org. Mass Spectrom.* **1970,** *3*, 101-104.
4. Posthumus, M.A.; Kistemaker, P.G.; Meuzelaar, H.L.C.; Ten Noever de Brauw, M.C. Laser Desorption-Mass Spectrometry of Polar Nonvolatile Bio-Organic Molecules. *Anal. Chem.* **1978,** *50*, 985-991.
5. Wilkins, C.L.; Weil, D.A.; Yang, C.L.C.; Ijames, C.F. High Mass Analysis by Laser Desorption Fourier Transform Mass Spectrometry. *Anal. Chem.* **1985,** *57*, 520-524.
6. Coates, M.L.; Wilkins, C.L. Laser Desorption Fourier Transform Mass Spectra of Malto-Oligosaccharides. *Biomed. Mass Spectrom.* **1985,** *12*, 424-428.
7. Macfarlane, R.D. Mass Spectrometry of Biomolecules: From PDMS to MALDI. *Brazilian J. Phys.* **1999,** *29*, 415-421.
8. Tanaka, K.; Waki, H.; Ido, Y.; Akita, S.; Yoshida, Y.; Yhoshida, T. Protein and Polymer Analyses Up to *M/z* 100,000 by Laser Ionization Time-of-Flight Mass Spectrometry. *Rapid Commun. Mass Spectrom.* **1988,** *2*, 151-153.
9. Tanaka, K. The Origin of Macromolecule Ionization by Laser Irradiation (Nobel Lecture). *Angew. Chem., Int. Ed.* **2003,** *42*, 3861-3870.
10. Karas, M.; Bachmann, D.; Hillenkamp, F. Influence of the Wavelength in High-Irradiance Ultraviolet Laser Desorption Mass Spectrometry of Organic Molecules. *Anal. Chem.* **1985,** *57*, 2935-2939.
11. Karas, M.; Bachmann, D.; Bahr, U.; Hillenkamp, F. Matrix-Assisted Ultraviolet Laser Desorption of Non-Volatile Compounds. *Int. J. Mass Spectrom. Ion Proc.* **1987,** *78*, 53-68.
12. Karas, M.; Hillenkamp, F. Laser Desorption Ionization of Proteins With Molecular Masses Exceeding 10,000 Daltons. *Anal. Chem.* **1988,** *60*, 2299-2301.
13. Karas, M.; Bahr, U.; Ingendoh, A.; Hillenkamp, F. Laser-Desorption Mass Spectrometry of 100,000–250,000-Dalton Proteins. *Angew. Chem.* **1989,** *101*, 805-806.
14. Karas, M.; Ingendoh, A.; Bahr, U.; Hillenkamp, F. Ultraviolet-Laser Desorption/Ionization Mass Spectrometry of Femtomolar Amounts of Large Proteins. *Biomed. Environ. Mass Spectrom.* **1989,** *18*, 841-843.
15. *MALDI-MS. A Practical Guide to Instrumentation, Methods and Applications;* Hillenkamp, F.; Peter-Katalinic, J., editors; Wiley-VCH: Weinheim, 2007.
16. Karas, M.; Bahr, U.; Gießmann, U. Matrix-Assisted Laser Desorption Ionization Mass Spectrometry. *Mass Spectrom. Rev.* **1991,** *10*, 335-357.
17. Hillenkamp, F.; Karas, M.; Beavis, R.C.; Chait, B.T. Matrix-Assisted Laser Desorption/Ionization Mass Spectrometry of Biopolymers. *Anal. Chem.* **1991,** *63*, 1193A-1203A.
18. Beavis, R.C. Matrix-Assisted Ultraviolet Laser Desorption: Evolution and Principles. *Org. Mass Spectrom.* **1992,** *27*, 653-659.
19. Hillenkamp, F.; Karas, M. Matrix-Assisted Laser Desorption/Ionisation, an Experience. *Int. J. Mass Spectrom.* **2000,** *200*, 71-77.
20. Lehmann, W.D. *Massenspektrometrie in der Biochemie;* Spektrum Akad. Verlag: Heidelberg, 1996.
21. Cotter, R.J. *Time-of-Flight Mass Spectrometry: Instrumentation and Applications in Biological Research;* American Chem. Soc.: Washington, DC, 1997.
22. Siuzdak, G. *The Expanding Role of Mass Spectrometry in Biotechnology;* 2nd ed.; MCC Press: San Diego, 2006.
23. *Mass Spectrometry of Polymers;* Montaudo, G.; Lattimer, R.P., editors; CRC Press: Boca Raton, 2001.
24. Murgasova, R.; Hercules, D.M. MALDI of Synthetic Polymers - an Update. *Int. J. Mass Spectrom.* **2003,** *226*, 151-162.
25. Mamyrin, B.A. Laser Assisted Reflectron Time-of-Flight Mass Spectrometry. *Int. J. Mass Spectrom. Ion Proc.* **1994,** *131*, 1-19.
26. Dreisewerd, K.; Schürenberg, M.; Karas, M.; Hillenkamp, F. Influence of the Laser Intensity and Spot Size on the Desorption of Molecules and Ions in Ma-

trix-Assisted Laser Desorption/Ionization With a Uniform Beam Profile. *Int. J. Mass Spectrom. Ion Proc.* **1995,** *141*, 127-148.
27. Nordhoff, E.; Ingendoh, A.; Cramer, R.; Overberg, A.; Stahl, B.; Karas, M.; Hillenkamp, F.; Crain, P.F. Matrix-Assisted Laser Desorption/Ionization Mass Spectrometry of Nucleic Acids With Wavelengths in the Ultraviolet and Infrared. *Rapid Commun. Mass Spectrom.* **1992,** *6*, 771-776.
28. Overberg, A.; Karas, M.; Bahr, U.; Kaufmann, R.; Hillenkamp, F. Matrix-Assisted Infrared-Laser (2.94 Mm) Desorption/Ionization Mass Spectrometry of Large Biomolecules. *Rapid Commun. Mass Spectrom.* **1990,** *4*, 293-296.
29. Overberg, A.; Karas, M.; Hillenkamp, F. Matrix-Assisted Laser Desorption of Large Biomolecules With a TEA-CO_2-Laser. *Rapid Commun. Mass Spectrom.* **1991,** *5*, 128-131.
30. Berkenkamp, S.; Menzel, C.; Hillenkamp, F.; Dreisewerd, K. Measurements of Mean Initial Velocities of Analyte and Matrix Ions in Infrared Matrix-Assisted Laser Desorption Ionization Mass Spectrometry. *J. Am. Soc. Mass Spectrom.* **2002,** *13*, 209-220.
31. Zenobi, R.; Knochenmuss, R. Ion Formation in MALDI Mass Spectrometry. *Mass Spectrom. Rev.* **1999,** *17*, 337-366.
32. Menzel, C.; Dreisewerd, K.; Berkenkamp, S.; Hillenkamp, F. Mechanisms of Energy Deposition in Infrared Matrix-Assisted Laser Desorption/Ionization Mass Spectrometry. *Int. J. Mass Spectrom.* **2001,** *207*, 73-96.
33. Dreisewerd, K.; Berkenkamp, S.; Leisner, A.; Rohlfing, A.; Menzel, C. Fundamentals of Matrix-Assisted Laser Desorption/Ionization Mass Spectrometry With Pulsed Infrared Lasers. *Int. J. Mass Spectrom.* **2003,** *226*, 189-209.
34. Dreisewerd, K. The Desorption Process in MALDI. *Chem. Rev.* **2003,** *103*, 395-425.
35. Karas, M.; Krüger, R. Ion Formation in MALDI: The Cluster Ionization Mechanism. *Chem. Rev.* **2003,** *103*, 427-439.
36. Westmacott, G.; Ens, W.; Hillenkamp, F.; Dreisewerd, K.; Schürenberg, M. The Influence of Laser Fluence on Ion Yield in Matrix-Assisted Laser Desorption Ionization Mass Spectrometry. *Int. J. Mass Spectrom.* **2002,** *221*, 67-81.
37. Menzel, C.; Dreisewerd, K.; Berkenkamp, S.; Hillenkamp, F. The Role of the Laser Pulse Duration in Infrared Matrix-Assisted Laser Desorption/Ioniza-tion Mass Spectrometry. *J. Am. Soc. Mass Spectrom.* **2002,** *13*, 975-984.
38. Juhasz, P.; Vestal, M.L.; Martin, S.A. On the Initial Velocity of Ions Generated by Matrix-Assisted Laser Desorption Ionization and Its Effect on the Calibration of Delayed Extraction Time-of-Flight Mass Spectra. *J. Am. Soc. Mass Spectrom.* **1997,** *8*, 209-217.
39. Karas, M.; Bahr, U.; Fournier, I.; Glückmann, M.; Pfenninger, A. The Initial Ion Velocity as a Marker for Different Desorption-Ionization Mechanisms in MALDI. *Int. J. Mass Spectrom.* **2003,** *226*, 239-248.
40. Horneffer, V.; Dreisewerd, K.; Ludemann, H.-C.; Hillenkamp, F.; Lage, M.; Strupat, K. Is the Incorporation of Analytes into Matrix Crystals a Prerequisite for Matrix-Assisted Laser Desorption/Ionization Mass Spectrometry? A Study of Five Positional Isomers of Dihydroxybenzoic Acid. *Int. J. Mass Spectrom.* **1999,** *185/186/187*, 859-870.
41. Glückmann, M.; Pfenninger, A.; Krüger, R.; Thierolf, M.; Karas, M.; Horneffer, V.; Hillenkamp, F.; Strupat, K. Mechanisms in MALDI Analysis: Surface Interaction or Incorporation of Analytes? *Int. J. Mass Spectrom.* **2001,** *210/211*, 121-132.
42. Karas, M.; Gluckmann, M.; Schäfer, J. Ionization in Matrix-Assisted Laser Desorption/Ionization: Singly Charged Molecular Ions Are the Lucky Survivors. *J. Mass Spectrom.* **2000,** *35*, 1-12.
43. Ens, W.; Mao, Y.; Mayer, F.; Standing, K.G. Properties of Matrix-Assisted Laser Desorption. Measurements With a Time-to-Digital Converter. *Rapid Commun. Mass Spectrom.* **1991,** *5*, 117-123.
44. Medina, N.; Huth-Fehre, T.; Westman, A.; Sundqvist, B.U.R. Matrix-Assisted Laser Desorption: Dependence of the Threshold Fluence on Analyte Concentration. *Org. Mass Spectrom.* **1994,** *29*, 207-209.
45. Quist, A.P.; Huth-Fehre, T.; Sundqvist, B.U.R. Total Yield Measurements in Matrix-Assisted Laser Desorption Using a Quartz Crystal Microbalance. *Rapid Commun. Mass Spectrom.* **1994,** *8*, 149-154.

46. Beavis, R.C.; Chait, B.T. Factors Affecting the Ultraviolet Laser Desorption of Proteins. *Rapid Commun. Mass Spectrom.* **1989,** *3*, 233-237.
47. Ingendoh, A.; Karas, M.; Hillenkamp, F.; Giessmann, U. Factors Affecting the Resolution in Matrix-Assisted Laser Desorption-Ionization Mass Spectrometry. *Int. J. Mass Spectrom. Ion Proc.* **1994,** *131*, 345-354.
48. Aksouh, F.; Chaurand, P.; Deprun, C.; Della-Negra, S.; Hoyes, J.; Le Beyec, Y.; Pinho, R.R. Influence of the Laser Beam Direction on the Molecular Ion Ejection Angle in Matrix-Assisted Laser Desorption/Ionization. *Rapid Commun. Mass Spectrom.* **1995,** *8*, 515-518.
49. Liao, P.-C.; Allison, J. Dissecting Matrix-Assisted Laser Desorption/Ionization Mass Spectra. *J. Mass Spectrom.* **1995,** *30*, 763-766.
50. Strupat, K.; Karas, M.; Hillenkamp, F. 2,5-Dihydroxybenzoic Acid: a New Matrix for Laser Desorption-Ionization Mass Spectrometry. *Int. J. Mass Spectrom. Ion Proc.* **1991,** *111*, 89-102.
51. Holle, A.; Haase, A.; Kayser, M.; Hoehndorf, J. Optimizing UV Laser Focus Profiles for Improved MALDI Performance. *J. Mass Spectrom.* **2006,** *41*, 705-716.
52. Cotter, R.J. Laser Mass Spectrometry: an Overview of Techniques, Instruments and Applications. *Anal. Chim. Acta* **1987,** *195*, 45-59.
53. Pan, Y.; Cotter, R.J. Measurement of Initial Translational Energies of Peptide Ions in Laser Desorption/Ionization Mass Spectrometry. *Org. Mass Spectrom.* **1992,** *27*, 3-8.
54. Glückmann, M.; Karas, M. The Initial Ion Velocity and Its Dependence on Matrix, Analyte and Preparation Method in Ultraviolet Matrix-Assisted Laser Desorption/Ionization. *J. Mass Spectrom.* **1999,** *34*, 467-477.
55. Puretzky, A.A.; Geohegan, D.B.; Hurst, G.B.; Buchanan, M.V.; Luk'yanchuk, B.S. Imaging of Vapor Plumes Produced by Matrix Assisted Laser Desorption: A Plume Sharpening Effect. *Phys. Rev. Lett.* **1999,** *83*, 444-447.
56. Leisner, A.; Rohlfing, A.; Berkenkamp, S.; Röhling, U.; Dreisewerd, K.; Hillenkamp, F. IR-MALDI With the Matrix Glycerol: Examination of the Plume Expansion Dynamics for Lasers of Different Pulse Duration. *36. DGMS Jahrestagung* **2003,** Poster.
57. Leisner, A.; Rohlfing, A.; Roehling, U.; Dreisewerd, K.; Hillenkamp, F. Time-Resolved Imaging of the Plume Dynamics in Infrared Matrix-Assisted Laser Desorption/Ionization With a Glycerol Matrix. *J. Phys. Chem. B* **2005,** *109*, 11661-11666.
58. Wang, B.H.; Dreisewerd, K.; Bahr, U.; Karas, M.; Hillenkamp, F. Gas-Phase Cationization and Protonation of Neutrals Generated by Matrix-Assisted Laser Desorption. *J. Am. Soc. Mass Spectrom.* **1993,** *4*, 393-398.
59. Liao, P.-C.; Allison, J. Ionization Processes in Matrix-Assisted Laser Desorption/Ionization Mass Spectrometry: Matrix-Dependent Formation of $[M+H]^+$ Vs. $[M+Na]^+$ Ions of Small Peptides and Some Mechanistic Comments. *J. Mass Spectrom.* **1995,** *30*, 408-423.
60. Gimon, M.E.; Preston, L.M.; Solouki, T.; White, M.A.; Russel, D.H. Are Proton Transfer Reactions of Excited States Involved in UV Laser Desorption Ionization? *Org. Mass Spectrom.* **1992,** *27*, 827-830.
61. Juhasz, P.; Costello, C.E. Generation of Large Radical Ions From Oligometallocenes by Matrix-Assisted Laser Desorption Ionization. *Rapid Commun. Mass Spectrom.* **1993,** *7*, 343-351.
62. Lidgard, R.O.; McConnell, B.D.; Black, D.S.C.; Kumar, N.; Duncan, M.W. Fragmentation Observed in Continuous Extraction Linear MALDI: a Cautionary Note. *J. Mass Spectrom.* **1996,** *31*, 1443-1445.
63. Irngartinger, H.; Weber, A. Twofold Cycloaddition of [60]Fullerene to a Bifunctional Nitrile Oxide. *Tertrahedron Lett.* **1996,** *37*, 4137-4140.
64. Gromov, A.; Ballenweg, S.; Giesa, S.; Lebedkin, S.; Hull, W.E.; Krätschmer, W. Preparation and Characterization of C_{119}. *Chem. Phys. Lett.* **1997,** *267*, 460-466.
65. Giesa, S.; Gross, J.H.; Hull, W.E.; Lebedkin, S.; Gromov, A.; Krätschmer, W.; Gleiter, R. $C_{120}OS$: the First Sulfur-Containing Dimeric [60]Fullerene Derivative. *Chem. Commun.* **1999,** 465-466.
66. Juhasz, P.; Costello, C.E.; Biemann, K. Matrix-Assisted Laser Desorption Ionization Mass Spectrometry With 2-(4-

Hydroxyphenylazo)Benzoic Acid Matrix. *J. Am. Soc. Mass Spectrom.* **1993,** *4*, 399-409.

67. Tang, K.; Taranenko, N.I.; Allman, S.L.; Chen, C.H.; Chang, L.Y.; Jacobson, K.B. Picolinic Acid as a Matrix for Laser Mass Spectrometry of Nucleic Acids and Proteins. *Rapid Commun. Mass Spectrom.* **1994,** *8*, 673-677.
68. Wu, K.J.; Steding, A.; Becker, C.H. Matrix-Assisted Laser Desorption Time-of-Flight Mass Spectrometry of Oligonucleotides Using 3-Hydroxypicolinic Acid As an Ultraviolet-Sensitive Matrix. *Rapid Commun. Mass Spectrom.* **1993,** *7*, 142-146.
69. Taranenko, N.I.; Tang, K.; Allman, S.L.; Ch'ang, L.Y.; Chen, C.H. 3-Aminopicolinic Acid As a Matrix for Laser Desorption Mass Spectrometry of Biopolymers. *Rapid Commun. Mass Spectrom.* **1994,** *8*, 1001-1006.
70. Terrier, P.; Tortajada, J.; Zin, G.; Buchmann, W. Noncovalent Complexes Between DNA and Basic Polypeptides or Polyamines by MALDI-TOF. *J. Am. Soc. Mass Spectrom.* **2007,** *18*, 1977-1989.
71. Lecchi, P.; Le, H.M.; Pannell, L.K. 6-Aza-2-Thiothymine: a Matrix for MALDI Spectra of Oligonucleotides. *Nucl. Acids Res.* **1995,** *23*, 1276-1277.
72. Taranenko, N.I.; Potter, N.T.; Allman, S.L.; Golovlev, V.V.; Chen, C.H. Gender Identification by Matrix-Assisted Laser Desorption/Ionization Time-of-Flight Mass Spectrometry. *Anal. Chem.* **1999,** *71*, 3974-3976.
73. Mohr, M.D.; Börnsen, K.O.; Widmer, H.M. Matrix-Assisted Laser Desorption/Ionization Mass Spectrometry: Improved Matrix for Oligosaccharides. *Rapid Commun. Mass Spectrom.* **1995,** *9*, 809-814.
74. Finke, B.; Stahl, B.; Pfenninger, A.; Karas, M.; Daniel, H.; Sawatzki, G. Analysis of High-Molecular-Weight Oligosaccharides From Human Milk by Liquid Chromatography and MALDI-MS. *Anal. Chem.* **1999,** *71*, 3755-3762.
75. Pfenninger, A.; Karas, M.; Finke, B.; Stahl, B.; Sawatzki, G. Matrix Optimization for Matrix-Assisted Laser Desorption/Ionization Mass Spectrometry of Oligosaccharides from Human Milk. *J. Mass Spectrom.* **1999,** *34*, 98-104.
76. Laugesen, S.; Roepstorff, P. Combination of Two Matrices Results in Improved Performance of MALDI MS for Peptide Mass Mapping and Protein Analysis. *J. Am. Soc. Mass Spectrom.* **2003,** *14*, 992-1002.
77. Karas, M.; Ehring, H.; Nordhoff, E.; Stahl, B.; Strupat, K.; Hillenkamp, F.; Grehl, M.; Krebs, B. Matrix-Assisted Laser Desorption/Ionization Mass Spectrometry With Additives to 2,5-Dihydroxybenzoic Acid. *Org. Mass Spectrom.* **1993,** *28*, 1476-1481.
78. Rohmer, M.; Meyer, B.; Mank, M.; Stahl, B.; Bahr, U.; Karas, M. 3-Aminoquinoline Acting as Matrix and Derivatizing Agent for MALDI MS Analysis of Oligosaccharides. *Anal. Chem.* **2010,** *82*, 3719-3726.
79. Stahl, B.; Thurl, S.; Zeng, J.; Karas, M.; Hillenkamp, F.; Steup, M.; Sawatzki, G. Oligosaccharides From Human Milk as Revealed by Matrix-Assisted Laser Desorption/Ionization Mass Spectrometry. *Anal. Biochem.* **1994,** *223*, 218-226.
80. Metzger, J.O.; Woisch, R.; Tuszynski, W.; Angermann, R. New Type of Matrix for Matrix-Assisted Laser Desorption Mass Spectrometry of Polysaccharides and Proteins. *Fresenius' Journal of Analytical Chemistry* **1994,** *349*, 473-474.
81. Beavis, R.C.; Chaudhary, T.; Chait, B.T. α-Cyano-4-Hydroxycinnamic Acid as a Matrix for Matrix-Assisted Laser Desorption Mass Spectrometry. *Org. Mass Spectrom.* **1992,** *27*, 156-158.
82. Ayorinde, F.O.; Elhilo, E.; Hlongwane, C. Matrix-Assisted Laser Desorption/Ionization Time-of-Flight Mass Spectrometry of Canola, Castor and Olive Oils. *Rapid Commun. Mass Spectrom.* **1999,** *13*, 737-739.
83. George, M.; Wellemans, J.M.Y.; Cerny, R.L.; Gross, M.L.; Li, K.; Cavalieri, E.L. Matrix Design for Matrix-Assisted Laser Desorption Ionization: Sensitive Determination of PAH-DNA Adducts. *J. Am. Soc. Mass Spectrom.* **1994,** *5*, 1021-1025.
84. Lidgard, R.O.; Duncan, M.W. Utility of Matrix-Assisted Laser Desorption/Ionization Time-of-Flight Mass Spectrometry for the Analysis of Low Molecular Weight Compounds. *Rapid Commun. Mass Spectrom.* **1995,** *9*, 128-132.
85. Beavis, R.C.; Chait, B.T. Cinnamic Acid Derivatives As Matrices for Ultraviolet

Laser Desorption Mass Spectrometry of Proteins. *Rapid Commun. Mass Spectrom.* **1989,** *3*, 432-435.

86. Montaudo, G.; Montaudo, M.S.; Puglisi, C.; Samperi, F. 2-(4-Hydroxyphenylazo)benzoic acid: a Solid Matrix for Matrix-Assisted Laser Desorption/Ionization of Polystyrene. *Rapid Commun. Mass Spectrom.* **1994,** *8*, 1011-1015.
87. Xu, N.; Huang, Z.-H.; Watson, J.T.; Gage, D.A. Mercaptobenzothiazoles: A New Class of Matrixes for Laser Desorption Ionization Mass Spectrometry. *J. Am. Soc. Mass Spectrom.* **1997,** *8*, 116-124.
88. Pitt, J.J.; Gorman, J.J. Matrix-Assisted Laser Desorption/Ionization Time-of-Flight Mass Spectrometry of Sialylated Glycopeptides and Proteins Using 2,6-Dihydroxyacetophenone as a Matrix. *Rapid Commun. Mass Spectrom.* **1996,** *10*, 1786-1788.
89. Gorman, J.J.; Ferguson, B.L.; Nguyen, T.B. Use of 2,6-Dihydroxyacetophenone for Analysis of Fragile Peptides, Disulfide Bonding and Small Proteins by Matrix-Assisted Laser Desorption/Ionization. *Rapid Commun. Mass Spectrom.* **1996,** *10*, 529-536.
90. Meyer, A.; Spinelli, N.; Imbach, J.-L.; Vasseur, J.-J. Analysis of Solid-Supported Oligonucleotides by Matrix-Assisted Laser Desorption/Ionization Time-of-Flight Mass Spectrometry. *Rapid Commun. Mass Spectrom.* **2000,** *14*, 234-242.
91. Kassis, C.M.; DeSimone, J.M.; Linton, R.W.; Lange, G.W.; Friedman, R.M. An Investigation into the Importance of Polymer-Matrix Miscibility Using Surfactant Modified Matrix-Assisted Laser Desorption/Ionization Mass Spectrometry. *Rapid Commun. Mass Spectrom.* **1997,** *11*, 1462-1466.
92. Carr, R.H.; Jackson, A.T. Preliminary Matrix-Assisted Laser Desorption Ionization Time-of-Flight and Field Desorption Mass Spectrometric Analyses of Polymeric Methylene Diphenylene Diisocyanate, Its Amine Precursor and a Model Polyether Prepolymer. *Rapid Commun. Mass Spectrom.* **1998,** *12*, 2047-2050.
93. Lebedkin, S.; Ballenweg, S.; Gross, J.H.; Taylor, R.; Krätschmer, W. Synthesis of $C_{120}O$: a New Dimeric [60]Fullerene Derivative. *Tetrahedron Lett.* **1995,** *36*, 4971-4974.
94. Ballenweg, S.; Gleiter, R.; Krätschmer, W. Chemistry at Cyclopentene Addends on [60]Fullerene. Matrix-Assisted Laser Desorption-Ionization Time-of-Flight Mass Spectrometry (MALDI-TOF MS) As a Quick and Facile Method for the Characterization of Fullerene Derivatives. *Synth. Met.* **1996,** *77*, 209-212.
95. Brown, T.; Clipston, N.L.; Simjee, N.; Luftmann, H.; Hungebühler, H.; Drewello, T. Matrix-Assisted Laser Desorption/Ionization of Amphiphilic Fullerene Derivatives. *Int. J. Mass Spectrom.* **2001,** *210/211*, 249-263.
96. Hopwood, F.G.; Michalak, L.; Alderdice, D.S.; Fisher, K.J.; Willett, G.D. C_{60}-Assisted Laser Desorption/Ionization Mass Spectrometry in the Analysis of Phosphotungstic Acid. *Rapid Commun. Mass Spectrom.* **1994,** *8*, 881-885.
97. Jones, R.M.; Lamb, J.H.; Lim, C.K. 5,10,15,20-*Meso*-Tetra(Hydroxyphenyl)-Chlorin As a Matrix for the Analysis of Low Molecular Weight Compounds by Matrix-Assisted Laser Desorption/Ionization Time-of-Flight Mass Spectrometry. *Rapid Commun. Mass Spectrom.* **1995,** *9*, 968-969.
98. Kumar, N.; Kolli, V.S.; Orlando, R. A New Matrix for Matrix-Assisted Laser Desorption/Ionization on Magnetic Sector Instruments With Point Detectors. *Rapid Commun. Mass Spectrom.* **1996,** *10*, 923-926.
99. Harvey, D.J.; Hunter, A.P. Use of a Conventional Point Detector to Record Matrix-Assisted Laser Desorption/Ionization Spectra From a Magnetic Sector Instrument. *Rapid Commun. Mass Spectrom.* **1998,** *12*, 1721-1726.
100. Armstrong, D.W.; Zhang, L.K.; He, L.; Gross, M.L. Ionic Liquids as Matrixes for Matrix-Assisted Laser Desorption/Ionization Mass Spectrometry. *Anal. Chem.* **2001,** *73*, 3679-3686.
101. Li, Y.L.; Gross, M.L. Ionic-Liquid Matrices for Quantitative Analysis by MALDI-TOF Mass Spectrometry. *J. Am. Soc. Mass Spectrom.* **2004,** *15*, 1833-1837.
102. Mirza, S.P.; Raju, N.P.; Vairamani, M. Estimation of the Proton Affinity Values of Fifteen Matrix-Assisted Laser Desorption/Ionization Matrices Under Electrospray Ionization Conditions Using the

Kinetic Method. *J. Am. Soc. Mass Spectrom.* **2004,** *15*, 431-435.
103. Burton, R.D.; Watson, C.H.; Eyler, J.R.; Lang, G.L.; Powell, D.H.; Avery, M.Y. Proton Affinities of Eight Matrixes Used for Matrix-Assisted Laser Desorption/Ionization. *Rapid Commun. Mass Spectrom.* **1997,** *11*, 443-446.
104. Nordhoff, E.; Schürenberg, M.; Thiele, G.; Lübbert, C.; Kloeppel, K.-D.; Theiss, D.; Lehrach, H.; Gobom, J. Sample Preparation Protocols for MALDI-MS of Peptides and Oligonucleotides Using Prestructured Sample Supports. *Int. J. Mass Spectrom.* **2003,** *226*, 163-180.
105. Westman, A.; Huth-Fehre, T.; Demirev, P.A.; Sundqvist, B.U.R. Sample Morphology Effects in Matrix-Assisted Laser Desorption/Ionization Mass Spectrometry of Proteins. *J. Mass Spectrom.* **1995,** *30*, 206-211.
106. Arakawa, R.; Watanabe, S.; Fukuo, T. Effects of Sample Preparation on Matrix-Assisted Laser Desorption/Ionization Time-of-Flight Mass Spectra for Sodium Polystyrene Sulfonate. *Rapid Commun. Mass Spectrom.* **1999,** *13*, 1059-1062.
107. Chan, P.K.; Chan, T.-W.D. Effect of Sample Preparation Methods on the Analysis of Dispersed Polysaccharides by Matrix-Assisted Laser Desorption/Ionization Time-of-Flight Mass Spectrometry. *Rapid Commun. Mass Spectrom.* **2000,** *14*, 1841-1847.
108. Vorm, O.; Mann, M. Improved Mass Accuracy in Matrix-Assisted Laser Desorption/Ionization Time-of-Flight Mass Spectrometry of Peptides. *J. Am. Soc. Mass Spectrom.* **1994,** *5*, 955-958.
109. Ayorinde, F.O.; Keith, Q.L., Jr.; Wan, L.W. Matrix-Assisted Laser Desorption/Ionization Time-of-Flight Mass Spectrometry of Cod Liver Oil and the Effect of Analyte/Matrix Concentration on Signal Intensities. *Rapid Commun. Mass Spectrom.* **1999,** *13*, 1762-1769.
110. Vorm, O.; Roepstorff, P.; Mann, M. Improved Resolution and Very High Sensitivity in MALDI-TOF of Matrix Surfaces Made by Fast Evaporation. *Anal. Chem.* **1994,** *66*, 3281-3287.
111. Bashir, S.; Derrick, P.J.; Critchley, P.; Gates, P.J.; Staunton, J. Matrix-Assisted Laser Desorption/Ionization Time-of-Flight Mass Spectrometry of Dextran and Dextrin Derivatives. *Eur. J. Mass Spectrom.* **2003,** *9*, 61-70.
112. Rashidezadeh, H.; Baochuan, G. Investigation of Metal Attachment to Polystyrenes in Matrix-Assisted Laser Desorption Ionization. *J. Am. Soc. Mass Spectrom.* **1998,** *9*, 724-730.
113. Rashidezadeh, H.; Hung, K.; Baochuan, G. Probing Polystyrene Cationization in Matrix-Assisted Laser/Desorption Ionization. *Eur. Mass Spectrom.* **1998,** *4*, 429-433.
114. Kühn, G.; Weidner, S.; Decker, R.; Holländer, A. Derivatization of Double Bonds Investigated by Matrix-Assisted Laser Desorption/Ionization Mass Spectrometry. *Rapid Commun. Mass Spectrom.* **1997,** *11*, 914-918.
115. Kühn, G.; Weidner, S.; Just, U.; Hohner, S. Characterization of Technical Waxes. Comparison of Chromatographic Techniques and Matrix-Assisted Laser-Desorption/Ionization Mass Spectrometry. *J. Chromatogr. A* **1996,** *732*, 111-117.
116. Pruns, J.K.; Vietzke, J.-P.; Strassner, M.; Rapp, C.; Hintze, U.; König, W.A. Characterization of Low-Molecular-Weight Hydrocarbon Oligomers by Laser Desorption/Ionization Time-of-Flight Mass Spectrometry Using a Solvent-Free Sample Preparation Method. *Rapid Commun. Mass Spectrom.* **2002,** *16*, 208-211.
117. Mowat, I.A.; Donovan, R.J. Metal-Ion Attachment to Non-Polar Polymers During Laser Desorption/Ionization at 337 Nm. *Rapid Commun. Mass Spectrom.* **1995,** *9*, 82-90.
118. Goldschmitt, R.J.; Wetzel, S.J.; Blair, W.R.; Guttman, C.M. Post-Source Decay in the Analysis of Polystyrene by Matrix-Assisted Laser Desorption/ Ionization Time-of-Flight Mass Spectrometry. *J. Am. Soc. Mass Spectrom.* **2000,** *11*, 1095-1106.
119. Kéki, S.; Deák, G.; Zsuga, M. Copper(I) Chloride: a Simple Salt for Enhancement of Polystyrene Cationization in Matrix-Assisted Laser Desorption/Ionization Mass Spectrometry. *Rapid Commun. Mass Spectrom.* **2001,** *15*, 675-678.
120. Zhang, J.; Zenobi, R. Matrix-Dependent Cationization in MALDI Mass Spectrometry. *J. Mass Spectrom.* **2004,** *39*, 808-816.

121. Thurman, E.M.; Ferrer, I. The Isotopic Mass Defect: a Tool for Limiting Molecular Formulas by Accurate Mass. *Analytical and Bioanalytical Chemistry* **2010,** *DOI 10.1007/s00216-010-3562-6*.
122. Salplachta, J.; Rehulka, P.; Chmelik, J. Identification of Proteins by Combination of Size-Exclusion Chromatography With Matrix-Assisted Laser Desorption/Ionization Time-of-Flight Mass Spectrometry and Comparison of Some Desalting Procedures for Both Intact Proteins and Their Tryptic Digests. *J. Mass Spectrom.* **2004,** *39*, 1395-1401.
123. Jensen, O.N.; Wilm, M.; Shevchenko, A.; Mann, M. Sample Preparation Methods for Mass Spectrometric Peptide Mapping Directly From 2-DE Gels. *Methods Mol. Biol.* **1999,** *112*, 513-530.
124. Rehulka, P.; Salplachta, J.; Chmelik, J. Improvement of Quality of Peptide Mass Spectra in Matrix-Assisted Laser Desorption/Ionization Time-of-Flight Mass Spectrometry and Post-Source Decay Analysis of Salty Protein Digests by Using on-Target Washing. *J. Mass Spectrom.* **2003,** *38*, 1267-1269.
125. Zhang, L.; Orlando, R. Solid-Phase Extraction/MALDI-MS: Extended Ion-Pairing Surfaces for the On-Target Cleanup of Protein Samples. *Anal. Chem.* **1999,** *71*, 4753-4757.
126. Gobom, J.; Nordhoff, E.; Mirgorodskaya, E.; Ekman, R.; Roepstorff, P. Sample Purification and Preparation Technique Based on Nano-Scale Reversed-Phase Columns for the Sensitive Analysis of Complex Peptide Mixtures by Matrix-Assisted Laser Desorption/Ionization Mass Spectrometry. *J. Mass Spectrom.* **1999,** *34*, 105-116.
127. Leite, J.F.; Hajivandi, M.R.; Diller, T.; Pope, R.M. Removal of Sodium and Potassium Adducts Using a Matrix Additive During Matrix-Associated Laser Desorption/Ionization Time-of-Flight Mass Spectrometric Analysis of Peptides. *Rapid Commun. Mass Spectrom.* **2004,** *18*, 2953-2959.
128. Puchades, M.; Westman, A.; Blennow, K.; Davidsson, P. Removal of Sodium Dodecyl Sulfate From Protein Samples Prior to Matrix-Assisted Laser Desorption/Ionization Mass Spectrometry. *Rapid Commun. Mass Spectrom.* **1999,** *13*, 344-349.
129. Trimpin, S.; Grimsdale, A.C.; Räder, H.J.; Müllen, K. Characterization of an Insoluble Poly(9,9-Diphenyl-2,7-Fluorene) by Solvent-Free Sample Preparation for MALDI-TOF Mass Spectrometry. *Anal. Chem.* **2002,** *74*, 3777-3782.
130. Trimpin, S.; Rouhanipour, A.; Az, R.; Räder, H.J.; Müllen, K. New Aspects in Matrix-Assisted Laser Desorption/Ionization Time-of-Flight Mass Spectrometry: a Universal Solvent-Free Sample Preparation. *Rapid Commun. Mass Spectrom.* **2001,** *15*, 1364-1373.
131. Guittard, J.; Hronowski, X.L.; Costello, C.E. Direct Matrix-Assisted Laser Desorption/Ionization Mass Spectrometric Analysis of Glycosphingolipids on Thin Layer Chromatographic Plates and Transfer Membranes. *Rapid Commun. Mass Spectrom.* **1999,** *13*, 1838-1849.
132. McCrery, D.A.; Ledford, E.B., Jr.; Gross, M.L. Laser Desorption Fourier Transform Mass Spectrometry. *Anal. Chem.* **1982,** *54*, 1435-1437.
133. Claereboudt, J.; Claeys, M.; Geise, H.; Gijbels, R.; Vertes, A. Laser Microprobe Mass Spectrometry of Quaternary Phosphonium Salts: Direct Versus Matrix-Assisted Laser Desorption. *J. Am. Soc. Mass Spectrom.* **1993,** *4*, 798-812.
134. Gromer, S.; Gross, J.H. Methylseleninate Is a Substrate Rather Than an Inhibitor of Mammalian Thioredoxin Reductase: Implications for the Antitumor Effects of Selenium. *J. Biol. Chem.* **2002,** *277*, 9701-9706.
135. Wood, T.D.; Van Cleef, G.W.; Mearini, M.A.; Coe, J.V.; Marshall, A.G. Formation of Giant Fullerene Gas-Phase Ions (C_{2n}^+, n = 60–500): Laser Desorption/ Electron Ionization Fourier-Trans-form Ion Cyclotron Resonance Mass Spectrometric Evidence. *Rapid Commun. Mass Spectrom.* **1993,** *7*, 304-311.
136. Beck, R.D.; Weis, P.; Hirsch, A.; Lamparth, I. Laser Desorption Mass Spectrometry of Fullerene Derivatives: Laser-Induced Fragmentation and Coalescence Reactions. *J. Phys. Chem.* **1994,** *98*, 9683-9687.
137. Wolkenstein, K.; Gross, J.H.; Oeser, T.; Schöler, H.F. Spectroscopic Characterization and Crystal Structure of the 1,2,3,4,5,6-Hexahydrophenanthro-[1,10,9,8-*opqra*]Perylene. *Tetrahedron Lett.* **2002,** *43*, 1653-1655.

138. Grim, D.M.; Siegel, J.; Allison, J. Does Ink Age Inside of a Pen Cartridge? *J. Forensic Sci.* **2002,** *47*, 1294-1297.
139. Jones, R.M.; Lamb, J.H.; Lim, C.K. Urinary Porphyrin Profiles by Laser Desorption/Ionization Time-of-Flight Mass Spectrometry Without the Use of Classical Matrixes. *Rapid Commun. Mass Spectrom.* **1995,** *9*, 921-923.
140. Krätschmer, W.; Lamb, L.D.; Fostiropoulos, K.; Huffman, D.R. Solid C_{60}: a New Form of Carbon. *Nature* **1990,** *347*, 354-358.
141. Kroto, H. Symmetry, Space, Stars and C_{60}. *Rev. Mod. Phys.* **1997,** *69*, 703-722.
142. Gross, J.H. Mass Spectrometry, in *Encyclopedia of Applied Spectroscopy*, Andrews, D.L. (ed.); Wiley-VCH: Berlin, 2009; Chap. 29, pp. 989-1054.
143. *Mass Spectrometry of Proteins and Peptides;* Chapman, J.R. (ed.); Humana Press: Totowa, 2000.
144. Snyder, A.P. *Interpreting Protein Mass Spectra;* Oxford University Press: New York, 2000.
145. Pasch, H.; Schrepp, W. *MALDI-TOF Mass Spectrometry of Synthetic Polymers;* Springer: Heidelberg, 2003.
146. Angeletti, R.; Gioacchini, A.M.; Seraglia, R.; Piro, R.; Traldi, P. The Potential of Matrix-Assisted Laser Desorption/Ionization Mass Spectrometry in the Quality Control of Water Buffalo Mozzarella Cheese. *J. Mass Spectrom.* **1998,** *33*, 525-531.
147. Fanton, C.; Delogu, G.; Maccioni, E.; Podda, G.; Seraglia, R.; Traldi, P. Matrix-Assisted Laser Desorption/Ionization Mass Spectrometry in the Dairy Industry 2. The Protein Fingerprint of Ewe Cheese and Its Application to Detection of Adulteration by Bovine Milk. *Rapid Commun. Mass Spectrom.* **1998,** *12*, 1569-1573.
148. Krishnamurthy, T.; Ross, P.L.; Rajamani, U. Detection of Pathogenic and Non-Pathogenic Bacteria by Matrix-Assisted Laser Desorption/Ionization Time-of-Flight Mass Spectrometry. *Rapid Commun. Mass Spectrom.* **1996,** *10*, 883-888.
149. Bohme, K.; Fernandez-No, I.C.; Barros-Velazquez, J.; Gallardo, J.M.; Calo-Mata, P.; Canas, B. Species Differentiation of Seafood Spoilage and Pathogenic Gram-Negative Bacteria by MALDI-TOF Mass Fingerprinting. *J. Proteome Res.* **2010,** *9*, 3169-3183.
150. Gevaert, K.; Vandekerckhove, J. Protein Identification Methods in Proteomics. *Electrophoresis* **2000,** *21*, 1145-1154.
151. Peng, J.; Gygi, S.P. Proteomics: The Move to Mixtures. *J. Mass Spectrom.* **2001,** *36*, 1083-1096.
152. Aebersold, R.; Mann, M. Mass Spectrometry-Based Proteomics. *Nature* **2003,** *422*, 198-207.
153. Reinders, J.; Lewandrowski, U.; Moebius, J.; Wagner, Y.; Sickmann, A. Challenges in Mass Spectrometry-Based Proteomics. *Proteomics* **2004,** *4*, 3686-3703.
154. Paizs, B.; Suhai, S. Fragmentation Pathways of Protonated Peptides. *Mass Spectrom. Rev.* **2005,** *24*, 508-548.
155. Khidekel, N.; Ficarro, S.B.; Clark, P.M.; Bryan, M.C.; Swaney, D.L.; Rexach, J.E.; Sun, Y.E.; Coon, J.J.; Peters, E.C.; Hsieh-Wilson, L.C. Probing the Dynamics of O-GlcNAc Glycosylation in the Brain Using Quantitative Proteomics. *Nature Chem. Biol.* **2007,** *3*, 339-348.
156. Vestal, M.; Hayden, K. High Performance MALDI-TOF Mass Spectrometry for Proteomics. *Int. J. Mass Spectrom.* **2007,** *268*, 83-92.
157. Nesvizhskii, A.I.; Vitek, O.; Aebersold, R. Analysis and Validation of Proteomic Data Generated by Tandem Mass Spectrometry. *Nature Methods* **2007,** *4*, 787-797.
158. Paizs, B.; Van, S.M. Focus Issue on Peptide Fragmentation. *J. Am. Soc. Mass Spectrom.* **2008,** *19*, 1717-1718.
159. Seidler, J.; Zinn, N.; Boehm, M.E.; Lehmann, W.D. De Novo Sequencing of Peptides by MS/MS. *Proteomics* **2010,** *10*, 634-649.
160. Henzel, W.J.; Watanabe, C.; Stults, J.T. Protein Identification: the Origins of Peptide Mass Fingerprinting. *J. Am. Soc. Mass Spectrom.* **2003,** *14*, 931-942.
161. Bleiholder, C.; Osburn, S.; Williams, T.D.; Suhai, S.; Van, S.M.; Harrison, A.G.; Paizs, B. Sequence-Scrambling Fragmentation Pathways of Protonated Peptides. *J. Am. Chem. Soc.* **2008,** *130*, 17774-17789.
162. Kinter, M.; Sherman, N.E. *Protein Sequencing and Identification Using Tandem Mass Spectrometry;* Wiley: Chichester, 2000.
163. Kaltashov, I.A.; Eyles, S.J. *Mass Spectrometry in Biophysics: Conformation*

and Dynamics of Biomolecules; Wiley: Hoboken, 2005.
164. Roepstorff, P. Proposal for a Common Nomenclature for Sequence Ions in Mass Spectra of Peptides. *Biomed. Mass Spectrom.* **1984,** *11*, 601.
165. Biemann, K. Contributions of Mass Spectrometry to Peptide and Protein Structure. *Biomed. Environ. Mass Spectrom.* **1988,** *16*, 99-111.
166. Yalcin, T.; Khouw, C.; Csizmadia, I.G.; Peterson, M.R.; Harrison, A.G. Why Are b Ions Stable Species in Peptide Spectra? *J. Am. Soc. Mass Spectrom.* **1995,** *6*, 1165-1174.
167. Yalcin, T.; Csizmadia, I.G.; Peterson, M.R.; Harrison, A.G. The Structure and Fragmentation of B_n (n >= 3) Ions in Peptide Spectra. *J. Am. Soc. Mass Spectrom.* **1996,** *7*, 233-242.
168. Harrison, A.G. Peptide Sequence Scrambling Through Cyclization of B5 Ions. *J. Am. Soc. Mass Spectrom.* **2008,** *19*, 1776-1780.
169. Harrison, A.G. To b or Not to B: the Ongoing Saga of Peptide b Ions. *Mass Spectrom. Rev.* **2009,** *28*, 640-654.
170. Amadei, G.A.; Cho, C.F.; Lewis, J.D.; Luyt, L.G. A Fast, Reproducible and Low-Cost Method for Sequence Deconvolution of "on-Bead" Peptides Via "on-Target" Maldi-TOF/TOF Mass Spectrometry. *J. Mass Spectrom.* **2010,** *45*, 241-251.
171. Harvey, D.J. Matrix-Assisted Laser Desorption/Ionization Mass Spectrometry of Carbohydrates and Glycoconjugates. *Int. J. Mass Spectrom.* **2003,** *226*, 1-35.
172. Stahl, B.; Linos, A.; Karas, M.; Hillenkamp, F.; Steup, M. Analysis of Fructans From Higher Plants by Matrix-Assisted Laser Desorption/Ionization Mass Spectrometry. *Anal. Biochem.* **1997,** *246*, 195-204.
173. Garrozzo, D.; Impallomeni, G.; Spina, E.; Sturiale, L.; Zanetti, F. Matrix-Assisted Laser Desorption/Ionization Mass Spectrometry of Polysaccharides. *Rapid Commun. Mass Spectrom.* **1995,** *9*, 937-941.
174. Welham, K.J.; Domin, M.A.; Johnson, K.; Jones, L.; Ashton, D.S. Characterization of Fungal Spores by Laser Desorption/Ionization Time-of-Flight Mass Spectrometry. *Rapid Commun. Mass Spectrom.* **2000,** *14*, 307-310.
175. Harvey, D.J.; Naven, T.J.P.; Küster, B.; Bateman, R.; Green, M.R.; Critchley, G. Comparison of Fragmentation Modes for the Structural Determination of Complex Oligosaccharides Ionized by Matrix-Assisted Laser Desorption/Ionization Mass Spectrometry. *Rapid Commun. Mass Spectrom.* **1995,** *9*, 1556-1561.
176. Lin, H.; Hunter, J.M.; Becker, C.L. Laser Desorption of DNA Oligomers Larger Than One Kilobase From Cooled 4-Nitrophenol. *Rapid Commun. Mass Spectrom.* **1999,** *13*, 2335-2340.
177. Bartolini, W.P.; Johnston, M.V. Characterizing DNA Photo-Oxidation Reactions by High-Resolution Mass Measurements With Matrix-Assisted Laser Desorption/Ionization Time-of-Flight Mass Spectrometry. *J. Mass Spectrom.* **2000,** *35*, 408-416.
178. Jackson, A.T.; Yates, H.T.; Scrivens, J.H.; Critchley, G.; Brown, J.; Green, M.R.; Bateman, R.H. The Application of Matrix-Assisted Laser Desorption/Ionization Combined With Collision-Induced Dissociation to the Analysis of Synthetic Polymers. *Rapid Commun. Mass Spectrom.* **1996,** *10*, 1668-1674.
179. Tang, X.; Dreifuss, P.A.; Vertes, A. New Matrixes and Accelerating Voltage Effects in Matrix-Assisted Laser Desorption/Ionization of Synthetic Polymers. *Rapid Commun. Mass Spectrom.* **1995,** *9*, 1141-1147.
180. Montaudo, G.; Montaudo, M.S.; Puglisi, C.; Samperi, F. Self-Calibrating Property of Matrix-Assisted Laser Desorption/Ionization Time-of-Flight Spectra of Polymeric Materials. *Rapid Commun. Mass Spectrom.* **1994,** *8*, 981-984.
181. Williams, J.B.; Chapman, T.M.; Hercules, D.M. Matrix-Assisted Laser Desorption/Ionization Mass Spectrometry of Discrete Mass Poly(Butylene Glutarate) Oligomers. *Anal. Chem.* **2003,** *75*, 3092-3100.
182. Nielen, M.F.W.; Malucha, S. Characterization of Polydisperse Synthetic Polymers by Size-Exclusion Chromatography/Matrix-Assisted Laser Desorption/Ionization Time-of-Flight Mass Spectrometry. *Rapid Commun. Mass Spectrom.* **1997,** *11*, 1194-1204.
183. de Koster, C.G.; Duursma, M.C.; van Rooij, G.J.; Heeren, R.M.A.; Boon, J.J. Endgroup Analysis of Polyethylene Glycol Polymers by Matrix-Assisted Laser

Desorption/Ionization Fourier-Transform Ion Cyclotron Resonance Mass Spectrometry. *Rapid Commun. Mass Spectrom.* **1995,** *9*, 957-962.
184. Weidner, S.; Kühn, G.; Just, U. Characterization of Oligomers in Poly(Ethylene Terephthalate) by Matrix-Assisted Laser Desorption/Ionization Mass Spectrometry. *Rapid Commun. Mass Spectrom.* **1995,** *9*, 697-702.
185. Montaudo, M.S. Sequence Constraints in a Glycine-Lactic Acid Copolymer Determined by Matrix-Assisted Laser Desorption/Ionization Mass Spectrometry. *Rapid Commun. Mass Spectrom.* **1999,** *13*, 639-644.
186. Montaudo, M.S. Mass Spectra of Copolymers. *Mass Spectrom. Rev.* **2002,** *21*, 108-144.
187. Murgasova, R.; Hercules, D.M. Quantitative Characterization of a Polystyrene/Poly(α-Methylstyrene) Blend by MALDI Mass Spectrometry and Size-Exclusion Chromatography. *Anal. Chem.* **2003,** *75*, 3744-3750.
188. Wei, J.; Buriak, J.M.; Siuzdak, G. Desorption-Ionization Mass Spectrometry on Porous Silicon. *Nature* **1999,** *399*, 243-246.
189. Go, E.P.; Shen, Z.; Harris, K.; Siuzdak, G. Quantitative Analysis With Desorption/Ionization on Silicon Mass Spectrometry Using Electrospray Deposition. *Anal. Chem.* **2003,** *75*, 5475-5479.
190. Shen, Z.; Thomas, J.J.; Averbuj, C.; Broo, K.M.; Engelhard, M.; Crowell, J.E.; Finn, M.G.; Siuzdak, G. Porous Silicon As a Versatile Platform for Laser Desorption/Ionization Mass Spectrometry. *Anal. Chem.* **2001,** *73*, 612-619.
191. Laiko, V.V.; Taranenko, N.I.; Berkout, V.D.; Musselman, B.D.; Doroshenko, V.M. Atmospheric Pressure Laser Desorption/Ionization on Porous Silicon. *Rapid Commun. Mass Spectrom.* **2002,** *16*, 1737-1742.
192. Go, E.P.; Prenni, J.E.; Wei, J.; Jones, A.; Hall, S.C.; Witkowska, H.E.; Shen, Z.; Siuzdak, G. Desorption/Ionization on Silicon Time-of-Flight/Time-of-Flight Mass Spectrometry. *Anal. Chem.* **2003,** *75*, 2504-2506.
193. Kang, M.J.; Pyun, J.C.; Lee, J.C.; Choi, Y.J.; Park, J.H.; Park, J.G.; Lee, J.G.; Choi, H.J. Nanowire-Assisted Laser Desorption and Ionization Mass Spectrometry for Quantitative Analysis of Small Molecules. *Rapid Commun. Mass Spectrom.* **2005,** *19*, 3166-3170.
194. Go, E.P.; Apon, J.V.; Luo, G.; Saghatelian, A.; Daniels, R.H.; Sahi, V.; Dubrow, R.; Cravatt, B.F.; Vertes, A.; Siuzdak, G. Desorption/Ionization on Silicon Nanowires. *Anal. Chem.* **2005,** *77*, 1641-1646.
195. Vidova, V.; Novak, P.; Strohalm, M.; Pol, J.; Havlicek, V.; Volny, M. Laser Desorption-Ionization of Lipid Transfers: Tissue Mass Spectrometry Imaging Without MALDI Matrix. *Anal. Chem.* **2010,** *82*, 4994-4997.
196. Shenar, N.; Cantel, S.; Martinez, J.; Enjalbal, C. Comparison of Inert Supports in Laser Desorption/Ionization Mass Spectrometry of Peptides: Pencil Lead, Porous Silica Gel, DIOS-Chip and NALDI Target. *Rapid Commun. Mass Spectrom.* **2009,** *23*, 2371-2379.
197. Hashir, M.A.; Stecher, G.; Bakry, R.; Kasemsook, S.; Blassnig, B.; Feuerstein, I.; Abel, G.; Popp, M.; Bobleter, O.; Bonn, G.K. Identification of Carbohydrates by Matrix-Free Material-Enhanced Laser Desorption/Ionisation Mass Spectrometry. *Rapid Commun. Mass Spectrom.* **2007,** *21*, 2759-2769.
198. Rainer, M.; Muhammad, N.N.-H.; Huck, C.W.; Feuerstein, I.; Bakry, R.; Huber, L.A.; Gjerde, D.T.; Zou, X.; Qian, H.; Du, X.; Fang, W.G.; Ke, Y.; Bonn, G.K. Ultra-Fast Mass Fingerprinting by High-Affinity Capture of Peptides and Proteins on Derivatized Poly(Glycidyl Methacrylate/Divinylbenzene) for the Analysis of Serum and Cell Lysates. *Rapid Commun. Mass Spectrom.* **2006,** *20*, 2954-2960.
199. Feuerstein, I.; Najam-ul-Haq, M.; Rainer, M.; Trojer, L.; Bakry, R.; Aprilita, N.H.; Stecher, G.; Huck, C.W.; Bonn, G.K.; Klocker, H.; Bartsch, G.; Guttman, A. Material-Enhanced Laser Desorption/Ionization (MELDI)-A New Protein Profiling Tool Utilizing Specific Carrier Materials for Time of Flight Mass Spectrometric Analysis. *J. Am. Soc. Mass Spectrom.* **2006,** *17*, 1203-1208.
200. Caprioli, R.M.; Farmer, T.B.; Gile, J. Molecular Imaging of Biological Samples: Localization of Peptides and Proteins Using MALDI-TOF MS. *Anal. Chem.* **1997,** *69*, 4751-4760.
201. Cornett, D.S.; Reyzer, M.L.; Chaurand, P.; Caprioli, R.M. MALDI Imaging

Mass Spectrometry: Molecular Snapshots of Biochemical Systems. *Nature Methods* **2007,** *4*, 828-833.
202. Chaurand, P.; Schriver, K.E.; Caprioli, R.M. Instrument Design and Characterization for High Resolution MALDI-MS Imaging of Tissue Sections. *J. Mass Spectrom.* **2007,** *42*, 476-489.
203. Franck, J.; Arafah, K.; Elayed, M.; Bonnel, D.; Vergara, D.; Jacquet, A.; Vinatier, D.; Wisztorski, M.; Day, R.; Fournier, I.; Salzet, M. MALDI Imaging Mass Spectrometry: State of the Art Technology in Clinical Proteomics. *Mol. Cell. Proteomics* **2009,** *8*, 2023-2033.
204. Francese, S.; Dani, F.R.; Traldi, P.; Mastrobuoni, G.; Pieraccini, G.; Moneti, G. MALDI Mass Spectrometry Imaging, From Its Origins Up to Today: the State of the Art. *Comb. Chem. High Throughput Scr.* **2009,** *12*, 156-174.
205. *Mass Spectrometry in Drug Metabolism and Pharmacokinetics;* Ramanathan, R., editor; Wiley: Hoboken, 2009.
206. Sugiura, Y.; Shimma, S.; Setou, M. Two-Step Matrix Application Technique To Improve Ionization Efficiency for Matrix-Assisted Laser Desorption/Ionization in Imaging Mass Spectrometry. *Anal. Chem.* **2006,** *78*, 8227-8235.
207. Guenther, S.; Koestler, M.; Schulz, O.; Spengler, B. Laser Spot Size and Laser Power Dependence of Ion Formation in High Resolution MALDI Imaging. *Int. J. Mass Spectrom.* **2010,** *294*, 7-15.
208. Laiko, V.V.; Baldwin, M.A.; Burlingame, A.L. Atmospheric Pressure Matrix-Assisted Laser Desorption/Ionization Mass Spectrometry. *Anal. Chem.* **2000,** *72*, 652-657.
209. Laiko, V.V.; Moyer, S.C.; Cotter, R.J. Atmospheric Pressure MALDI/Ion Trap Mass Spectrometry. *Anal. Chem.* **2000,** *72*, 5239-5243.
210. Moyer, S.C.; Marzilli, L.A.; Woods, A.S.; Laiko, V.V.; Doroshenko, V.M.; Cotter, R.J. Atmospheric Pressure Matrix-Assisted Laser Desorption/Ionization (AP MALDI) on a Quadrupole Ion Trap Mass Spectrometer. *Int. J. Mass Spectrom.* **2003,** *226*, 133-150.
211. Doroshenko, V.M.; Laiko, V.V.; Taranenko, N.I.; Berkout, V.D.; Lee, H.S. Recent Developments in Atmospheric Pressure MALDI Mass Spectrometry. *Int. J. Mass Spectrom.* **2002,** *221*, 39-58.
212. Krutchinsky, A.N.; Loboda, A.V.; Spicer, V.L.; Dworschak, R.; Ens, W.; Standing, K.G. Orthogonal Injection of Matrix-Assisted Laser Desorption/Ioniza-tion Ions into a Time-of-Flight Spectrometer Through a Collisional Damping Interface. *Rapid Commun. Mass Spectrom.* **1998,** *12*, 508-518.
213. McIver, R.T., Jr.; Li, Y.; Hunter, R.L. Matrix-Assisted Laser Desorption/Ionization With an External Ion Source Fourier-Transform Mass Spectrometer. *Rapid Commun. Mass Spectrom.* **1994,** *8*, 237-241.
214. Li, Y.; McIver, R.T., Jr.; Hunter, R.L. High-Accuracy Molecular Mass Determination for Peptides and Proteins by Fourier Transform Mass Spectrometry. *Anal. Chem.* **1994,** *66*, 2077-2083.
215. Li, Y.; Tang, K.; Little, D.P.; Koester, H.; McIver, R.T., Jr. High-Resolution MALDI Fourier Transform Mass Spectrometry of Oligonucleotides. *Anal. Chem.* **1996,** *68*, 2090-2096.
216. Baykut, G.; Jertz, R.; Witt, M. Matrix-Assisted Laser Desorption/Ionization Fourier Transform Ion Cyclotron Resonance Mass Spectrometry With Pulsed in-Source Collision Gas and in-Source Ion Accumulation. *Rapid Commun. Mass Spectrom.* **2000,** *14*, 1238-1247.
217. O'Connor, P.B.; Costello, C.E. A High Pressure Matrix-Assisted Laser Desorption/Ionization Fourier Transform Mass Spectrometry Ion Source for Thermal Stabilization of Labile Biomolecules. *Rapid Commun. Mass Spectrom.* **2001,** *15*, 1862-1868.
218. Todd, P.J.; Schaaff, G., Chaurand, P.; Caprioli, R.M. Organic Ion Imaging of Biological Tissue with SIMS and MALDI *J. Mass Spectrom.* **2001,** *36*, 355-369.

12 Electrospray Ionization

Learning Objectives

- Atmospheric pressure ionization (API) methods in MS
- Interfacing atmospheric pressure ionization to analyzer high vacuum
- Spraying of electrolytic solutions by action of an electrostatic field
- Processes of ion liberation from electrolytic solutions
- Softness and mass range of electrospray ionization (ESI)
- Applications of ESI-MS
- Applications of alternative API methods

Electrospray ionization (ESI) is the most prominent technique among the group of *atmospheric pressure ionization* (API) methods and the leading method of choice for *liquid chromatography-mass spectrometry coupling* (LC-MS, Chap. 14) [1-4]. In fact, ESI and MALDI (Chap. 11) have provided the means for extending the analytical procedures of MS into the fields of biology and the biomedical sciences, and currently, they are the most frequently employed ionization methods in MS [1,2,4-9].

ESI "is a soft ionization technique that accomplishes the transfer of ions from solution to the gas phase. The technique is extremely useful for the analysis of large, non-volatile, chargeable molecules such as proteins and nucleic acid polymers" [10-13]. In contrast to fast atom bombardment (FAB, Chap. 10), in ESI the solution is composed of a volatile solvent containing the ionic analyte at very low concentration, typically 10^{-6}–10^{-4} M. In addition, the transfer of ions from the condensed phase into the state of isolated gas-phase ions starts at atmospheric pressure and incrementally proceeds into the high vacuum of the mass analyzer [6,14-16]. This results in a marked softness of ionization and makes ESI the "wings for molecular elephants" [17]. Another reason for the extraordinary high-mass capability of ESI [13,18,19] is founded in the characteristic formation of multiply charged ions in case of high-mass analytes [13,16,20]. Multiple charging also folds up the *m/z* scale by the number of charges, and thus, shifts the ions into an *m/z* range accessible by most mass analyzers (Fig. 12.1 and Chap. 3.8)

ESI serves equally well for small polar molecules, ionic metal complexes [21-23], and other soluble inorganic analytes [24].

J. Gross, *Mass Spectrometry*, 2nd ed., DOI 10.1007/978-3-642-10711-5_12,
© Springer-Verlag Berlin Heidelberg 2011

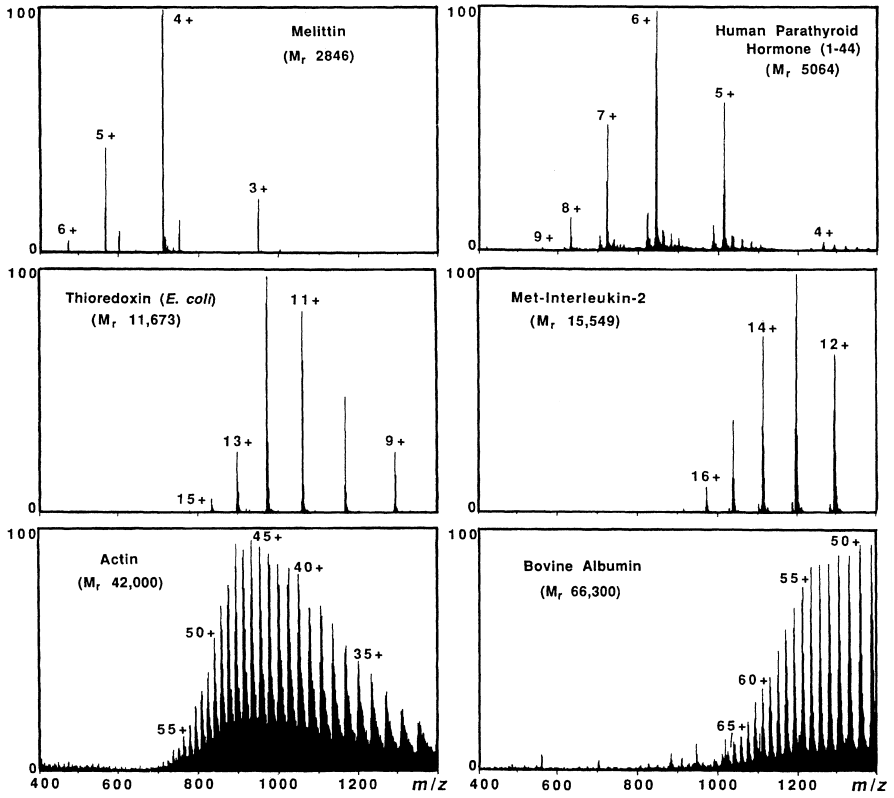


Fig. 12.1. Relationship between the mass of peptides and proteins and the number of ionic charges under ESI conditions. Adapted from Ref. [16] by permission. © American Chemical Society, 1990.

Note: In ESI the range up to *m/z* 3000 is normally employed for the detection of ions. Nonetheless, ESI can deliver ions of much higher *m/z* [25,26]; even ions at *m/z* 85,000 have been observed [27].

12.1 Development of ESI and Related Methods

ESI in its current state-of-the-art has not resulted from a straightforward development. It has many predecessors, some of which having been successful at their time, while others were rather short-lived methods replaced as soon as more sensitive or more robust techniques appeared [28]. Nonetheless, the development of all those techniques aimed at both the direct coupling of liquid chromatography to mass spectrometry and the access to highly polar or even ionic analytes.

Following this historical sketch of milestones along the way to ESI, the below sections will emphasize the construction of ESI interfaces, the process of electrospray as such, and the pathways of ion liberation from the liquid phase into the state of isolated gas phase ions.

12.1.1 Atmospheric Pressure Ionization

Atmospheric pressure ionization (API) was the first technique to directly connect solution phase analyte supply with a mass analyzer [29]. In API, a solution of the analyte is injected at atmospheric pressure into a stream of hot nitrogen (≈ 200°C) to rapidly evaporate the solvent. The vapor passes through a β-emitter where electrons from radioactive ^{63}Ni start a complex sequence of ionizing processes (Fig. 12.2).

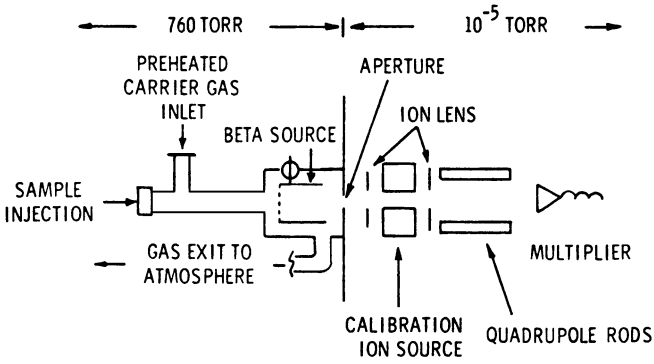


Fig. 12.2. The original implementation of API where primary electrons are delivered by a ^{63}Ni foil. For API, the filament of the EI calibration source was switched off and only the electrostatic lenses where used to pass the ions into the quadrupole mass analyzer chosen for its tolerance to moderate vacuum conditions. Reproduced from Ref. [29] with permission. © The American Chemical Society, 1973.

Beginning with the ionization of N_2, consecutive ion–molecule reactions eventually lead to the formation of $[(H_2O)_n+H]^+$ cluster ions:

$$N_2 + e^- \rightarrow N_2^{+\bullet} + 2e^- \tag{12.1}$$

$$N_2^{+\bullet} + 2N_2 \rightarrow N_4^{+\bullet} + N_2 \tag{12.2}$$

$$N_4^{+\bullet} + H_2O \rightarrow H_2O^{+\bullet} + 2N_2 \tag{12.3}$$

$$H_2O^{+\bullet} + H_2O \rightarrow H_3O^+ + OH^\bullet \tag{12.4}$$

$$H_3O^+ + H_2O + N_2 \rightarrow [H_2O)_2+H]^+ + N_2 \tag{12.5}$$

Here only the first reaction step of $[(H_2O)_n+H]^+$ cluster ion formation is explicitly formulated. As the *PA* of H_2O (697 kJ mol^{-1}) is actually below that of any analyte (Table 2.6), water cluster ions protonate the analyte molecules by a chemical ionization process at atmospheric pressure [29-31]:

$$[H_2O)_n+H]^+ + M \rightarrow [M+H]^+ + n\,H_2O \qquad (12.6)$$

Note: Reaction sequences analogous to API do occur whenever ionization is performed in a moist atmosphere. The initiating source of ionization can be delivered by a corona discharge as in *atmospheric pressure chemical ionization* (APCI, Chap. 12.8), by UV photons as in *atmospheric pressure photoionization* (APPI, Chap. 12.9), or by a glow-discharge in helium or argon as used in *direct analysis in real time* (DART, Chap. 13.5).

12.1.2 Thermospray

In *Thermospray* (TSP) [32-34] a solution of the analyte and a volatile buffer, usually 0.1 M ammonium acetate, is evaporated from a heated capillary at a flow rate of 1–2 ml min^{-1} into a heated chamber (> 600°C), hence the term. As the solvent evaporates, the analyte starts to form adducts with ions from the buffer salt. While most of the neutrals are removed by a vacuum pump, the ions are extracted orthogonally from their main axis of motion by use of an electrostatic potential. The ions are transferred into a quadrupole mass analyzer through a pinhole of about 25 μm in diameter (Fig. 12.3).

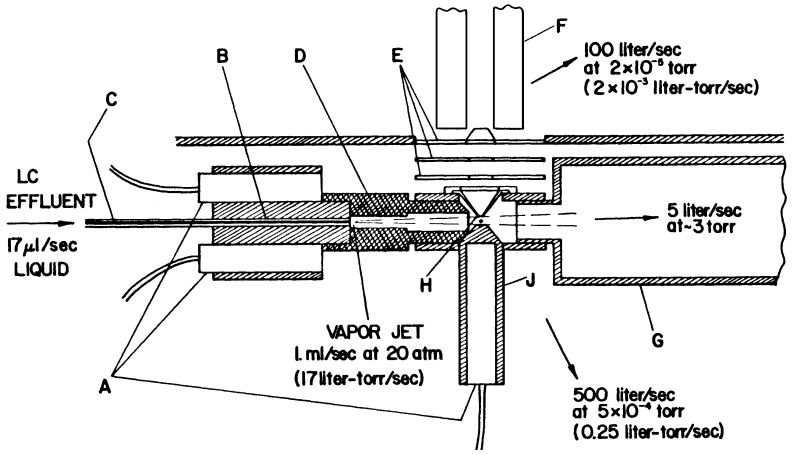


Fig. 12.3. Thermospray interface. **A** cartridge heater; **B** copper block brazed to stainless steel capillary; **C** capillary; **D** copper tube; **E** ion lenses; **F** quadrupole mass analyzer; **G** line to rotary vane pump; **H** ion exit aperture; **J** source heater. Reproduced from Ref. [33] by permission. © American Chemical Society, 1983.

Again a quadrupole is employed due to its tolerance to poor vacuum conditions. As the pure TSP mode only works with high-polarity solvents in the presence of a buffer salt, modified modes of operation were developed to expand the use of TSP ion sources to lower-polarity systems: *i*) use of an electrical discharge in the vapor phase [35] or *ii*) an electron-emitting filament as used in EI (Chap. 5) or CI (Chap. 7). With this added versatility, TSP meant a breakthrough for LC-MS [36]. Nonetheless, with the advent of ESI, TSP interfaces vanished rather quickly from the laboratories.

Note: Strictly speaking, thermospray is not really an API method because the analyte solution is sprayed into a rough vacuum of several hundred Pa instead of spraying at full atmospheric pressure.

12.1.3 Electrohydrodynamic Ionization

An electrolytic solution of sufficiently low volatility can be transferred into the vacuum without sudden evaporation and then be sprayed from a fine capillary by the action of a strong electrostatic field. This is known as *electrohydrodynamic ionization* (EHI) [37,38]. EHI results from the interaction of the field with the liquid meniscus at the end of the capillary tube [39,40]. A mist of micrometer-sized electrically charged droplets expands into the vacuum at supersonic speed. The droplets shrink upon evaporation of solvent. Shrinking causes the charge density on their surface to exceed the *Rayleigh limit* of stability [41], i.e., the surface tension is overcome by electrostatic repulsion. The electric forces then tear the droplets apart. The sequence of droplet shrinking and subsequent disintegration into smaller subunits occurs repeatedly and eventually leads to the formation of isolated gas-phase ions. Convenient EHI ion sources are at hand due to the compatibility of EHI to FD ion sources by simply replacing the field emitter with a capillary tube (Chap. 8.2) [42,43]. However, EHI never managed to become established in organic mass spectrometry. This is most probably due to its limitation to low-volatile solvents. Nonetheless, EHI has been applied to analyze polymers [44] and is used to generate primary ions in massive cluster impact (MCI) mass spectrometry (Chap. 10.6).

Note: EHI has important features in common with ESI: *i*) an electrolytic solution is sprayed by the mere action of an electrostatic field, *ii*) upon which it forms a mist of electrically highly charged droplets, from which *iii*) the analyte ions are liberated into the gas phase for subsequent mass analysis.

12.1.4 Electrospray Ionization

Actually, the development of electrospray ionization itself by the Dole group [45] preceded API, TSP, and EHI by several years [46]. The underlying principle of ESI, which it shares with EHI, even dates back to work by Zeleny [39] and Taylor

[40]. Again, a mist of micrometer-sized electrically charged droplets is generated and the repetitive shrinking and droplet disintegration are also observed under ESI conditions. In contrast to EHI, the electrostatic sprayer is operated at atmospheric pressure. The electrostatically charged mist is then continuously passed into the mass analyzer by means of a differentially pumped interface. The limitation of Dole's experiments was that the ions of the electrosprayed high-molecular-weight polystyrene used by his group could not be detected with his mass spectrometers [45-47]. It took years of work for the Fenn group and lasted until the late 1980s to fully realize that analytes of 100–2000 u molecular weight can be readily analyzed with a quadrupole attached to a properly constructed ESI interface [14,17,48]. To avoid freezing of the aerosol droplets under the conditions of adiabatic expansion on their transition from the atmosphere into the vacuum, sufficient energy supply turned out to be crucial. The heat may either be delivered by a heated countercurrent gas stream or by a heated capillary being part of the interface. Until today, all ESI sources make use of the one or the other way of heating the aerosol. The fact that ESI can be run with almost any standard solvent is another key to its tremendous success [17].

Note: It should be emphasized that atmospheric pressure ionization methods differ from all other techniques discussed so far in that they require an uninterrupted flow from ambient pressure into the high vacuum of a mass analyzer. This can only be accomplished by means of powerful differential pumping.

12.2 Ion Sources for ESI

12.2.1 Basic Design Considerations

The first electrospray–mass spectrometry interface was designed by the Fenn group in the mid 1980s [14,48-50]. The dilute sample solution is supplied by a syringe pump through a hypodermic needle – the spray capillary – at a rate of 5–20 µl min^{-1}. The spray capillary is kept at a potential of 3–4 kV relative to a surrounding cylindrical electrode (Fig. 12.4). Then, the electrosprayed aerosol expands into a countercurrent stream of hot nitrogen gas serving as a heat supply for vaporization of the solvent. A small portion of the sprayed material enters the aperture of a short capillary (0.2 mm inner diameter, 60 mm length) interfacing the atmospheric pressure spray zone to the first pumping stage ($\approx 10^2$ Pa) that is entered by the gas in a free jet expansion. Most of the gas expanding from the desolvating aerosol is pumped off by a rotary vane pump as it exits from the capillary. A minor portion passes through the orifice of a skimmer (a cone-shaped electrode with a small aperture at its apex) into the high vacuum behind ($\approx 10^{-3}$–10^{-4} Pa). At this stage, desolvation of the ions is completed, while the ions are focused into the

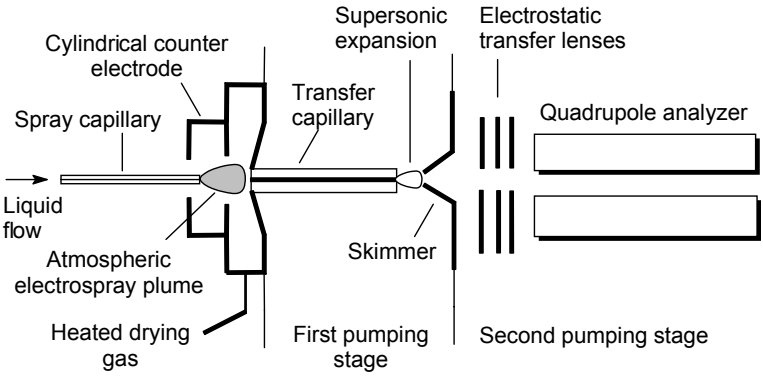


Fig. 12.4. Schematic of an early electrospray ion source design [14].

mass analyzer. Suitable potentials applied to capillary, skimmer, and lenses behind provide an effective transfer of ions through the interface, while the neutral gas is not affected and exits via the vacuum system.

Modern ESI sources – also termed *ESI interfaces* – are designed in many variations of this basic scheme [51,52]. They may either use a *heated transfer capillary* or a *countercurrent stream of hot nitrogen* (sometimes called *curtain gas*) to enforce solvent evaporation [53]. These differences can effect a system's robustness and the degree of cluster ion formation with a particular ESI interface [54,55]. Whatever the details, they are all derived from a *nozzle-skimmer system* initially proposed by Kantrowitz and Grey [56] that delivers an intense cool molecular jet into the high vacuum environment [45,48,57]. The adiabatic expansion of the gas upon entering the first pumping stage reduces random motion of the particles due to extensive cooling. Furthermore, a portion of the thermal motion is converted into directed flow by the nozzle-skimmer arrangement. In summary, this causes the heavier analyte ion-containing solvent clusters to travel close to the center of the flight path through the interface, while light solvent molecules escape from the jet [46]. Thus, the skimmer orifice is not just statistically passed by all sorts of particles but rather selectively by ionic constituents of the adiabatically expanding plume.

Note: One should be aware of the fact that ESI requires analyte ions to be present in the sample solution because ESI does not actively create ions as EI, CI, FAB, FD, or MALDI do. Thus, ESI is rather a method of ion transfer than a true ionization method. Therefore, *electrospray ionization* (ESI) is also simply referred to as *electrospray* (ES) and *ESI ion sources* are also termed *ESI interface* or *ES interface*.

12.2.2 Adaptation to Different Flow Rates

The actual process of "electrospraying" disperses a liquid into an aerosol, which works best at flow rates of 1–20 µl min^{-1}. This sets certain limits to its use as an LC-MS interface in respect to solvent properties such as volatility and polarity. Consequently, a number of sprayer design modifications have led to an expansion of the range of ESI applications (Fig. 12.5).

The design of a *pneumatically assisted* ESI interface differs from the simple electrospray interface in that it provides a pneumatic assistance for the spray process. This is achieved by supplying a concentric flow of an inert gas such as nitrogen around the electrospray plume [58-60]. Assistance by a *nebulizer gas* stream of about 1–2 l min^{-1} allows for higher liquid flow and for a reduced influence of the surface tension of the solvent [61]. Pneumatically assisted ESI can accommodate flows of 10–200 µl min^{-1}. In fact, all modern ESI interfaces equipped with a nebulizer gas or *sheath gas* line enclosing the spray capillary. Thus, most routine ESI measurements are done using pneumatically assisted ESI.

In addition to high LC flow rates, solutions of high conductivity and/or high surface tension are unsuitable for use with conventional ESI. An *ultrasonic nebulizer* can minimize such problems because it mechanically creates the spray. Unfortunately, the ultrasonically created droplets are comparatively large and this hinders ion formation, i.e., the ion yield is reduced. Nonetheless, the ultrasonic nebulizer handles liquid flow rates of 50–1000 µl min^{-1} and minimizes the restrictions of the range of mobile-phase compositions amenable to ESI. For example, a mobile-phase gradient beginning at water : methanol = 95 : 5 falls outside the solvent range that can be used with conventional ESI, while an ultrasonic nebulizer will work satisfactorily [62,63]. With both pneumatically assisted ESI and ultrasonic nebulizer ESI the purpose of the high voltage is almost reduced to the mere supply of electric charging of the droplets. For highly polar solutions at low flow rate, nanoESI provides the better technique (next section). Today, ultrasonic nebulizers are rarely used.

For *capillary zone electrophoresis* (CZE) mass spectrometry coupling, another modification of an ESI interface has been developed. This interface uses a *sheath flow* of liquid for establishing the electrical contact at the CZE terminus, thus defining both the CZE and electrospray field gradients. This way, the composition of the electrosprayed liquid can be controlled independently of the CZE buffer, thereby enabling operation with buffers that could not be used previously, e.g., aqueous and high ionic strength buffers. In addition, the interface operation becomes independent of the CZE flow rate [64].

Note: *Pneumatically assisted electrospray* is also termed *ion spray* (ISP). However, the term ISP is not recommended in place of pneumatically assisted ESI because ISP represents a mere modification of the ESI setup and is a company-specific term [65].

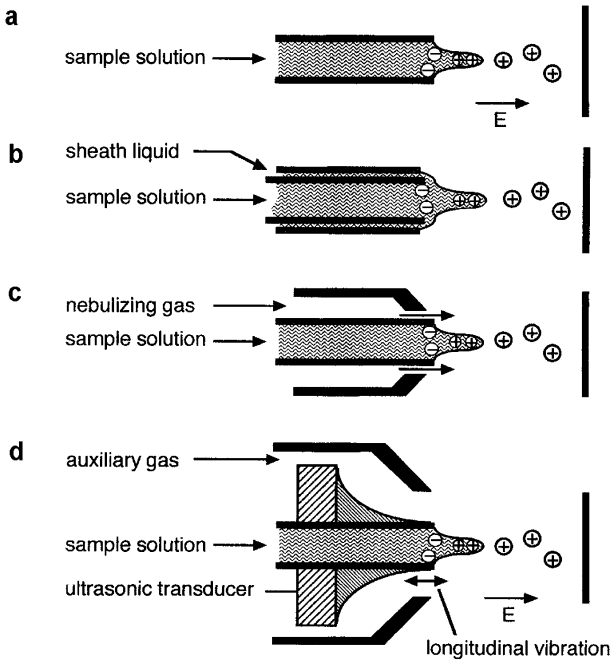


Fig. 12.5. Different sprayers for ESI. (**a**) Pure electrospray, (**b**) ESI with sheath liquid, (**c**) pneumatically assisted ESI, and (**d**) ultrasonic nebulizer. Adapted from Ref. [6] (p. 109) by permission. © John Wiley & Sons, Inc., 1997.

12.2.3 Improved Electrospray Configurations

Since the original design by the Fenn group, the ESI interface has been variously improved in *i*) robustness of operation, *ii*) ion transmission, *iii*) softness of ion desolvation, and *iv*) effectiveness of differential pumping. Nonetheless, whatever the actual design, all of those interfaces still have some basic characteristics in common: *i*) electrostatic spraying of an electrolytic solution at atmospheric pressure, *ii*) a source of heat supply for desolvation, *iii*) supersonic expansion into the first pumping stage of *iv*) a differentially pumped setup.

An intuitive adaptation of the geometry of the atmospheric pressure sprayer has been implemented: while early interfaces were aligned along the central paths from the spray capillary to the analyzer entrance, recent designs employ off-axis sprayers and even spraying at right angles to the vacuum entrance (or close to it for patent reasons). These latter alternative arrangements have the advantage of largely reducing possible contamination, especially by preventing the clogging of capillaries and skimmers, which formerly was one of the most severe problems with the otherwise easy-to-use ESI interfaces. When analytes are accompanied by

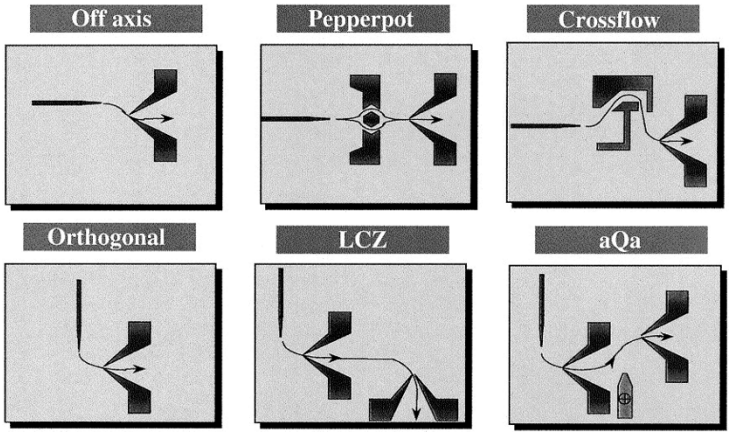


Fig. 12.6. Some strategies used in commercial API ion sources to increase solvent compatibility and system robustness. Some of these designs are commercial brands: Pepperpot, Crossflow, and LCZ ("z-spray", Micromass); AQA (Thermo Finnigan). Reproduced from Ref. [65] by permission. © John Wiley & Sons, 1999.

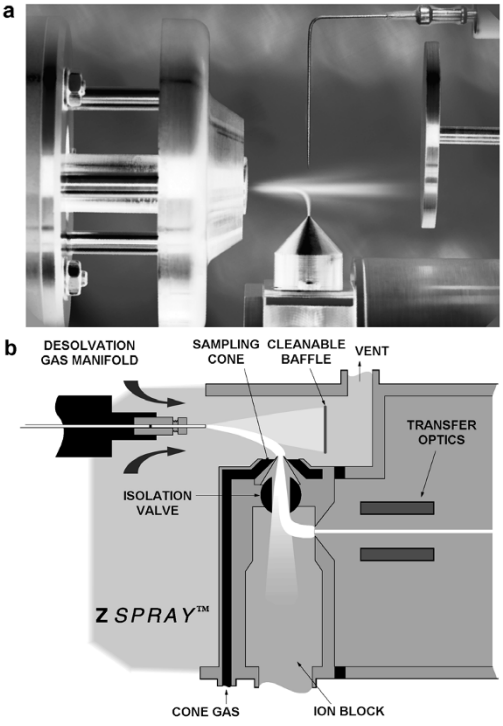


Fig. 12.7. Micromass z-spray interface. (**a**) Photograph of the actual spray from which charged constituents are extracted downwards into the entrance orifice, (**b**) schematic drawing. By courtesy of Waters Corporation, MS Technologies, Manchester, UK.

nonvolatile impurities, e.g., by buffer salts used to improve liquid chromatography or organic material as present in blood or urine samples, the deposition of this material can cause the rapid breakdown of the ESI interface. The principle of improved designs is to achieve spatial separation of the deposition site of nonvolatized material and the location of the ion entrance into the mass spectrometer. Such designs include *i*) spraying *off-axis*, *ii*) spraying at some angle up to *orthogonal*, and *iii*) guiding the desolvating microdroplets through *inflected paths* (Fig. 12.6) [65]. A most successful design of a modern commercial ESI interface is the Micromass *z-spray*™ interface (Fig. 12.7). Another advantage of orthogonal spraying is that it selectively collects small highly charged droplets which are the preferred source of analyte ions. Large and less-charged droplets are not sufficiently attracted by the extraction field at 90° angle and therefore miss the orifice.

12.2.4 Advanced Electrospray Interface Designs

We have already briefly encountered some of the modern electrospray interfaces as front-ends of advanced mass analyzers in the context of instrumentation (Chap. 4) and tandem MS (Chap. 9). The actual configuration of such interfaces largely depends on the high vacuum requirements of the mass analyzer attached, e.g., simple two-stage differential pumping is sufficient for linear quadrupoles and quadrupole ion traps, while others demand for virtual absence of residual gas. Furthermore, company-specific technologies will govern certain parts of the ion transfer optics such as RF-only ion guides (Fig. 12.8).

In recent years, so-called *ion funnels* are being used in place of the conventional skimmer cone electrode [66-68]. Ion funnels are radio frequency devices (≤ 1 MHz) composed of a stack of dozens of ring electrodes, typically spaced about 3 mm apart along the ion funnel axis, with a central aperture of increasingly smaller diameter, e.g., from 20 mm at the opening to 1 mm at the exit. An RF voltage of equal amplitude but opposite phase (200–400 V) is supplied between adjacent electrodes. Similar to stacked ring ion guides (Chap. 4.9.2) this alignment of electrodes creates a field that pushes ions down a low electric field gradient far more effectively than the field gradient alone could do. As the apertures decrease along the device the ion packages are not only transported but – more importantly – are also radially confined. This is employed to focus ion beams through narrow apertures into the next differential pumping stage or into a mass analyzer [69,70]. As ion funnels are best operated under the conditions of collisionally damped ion motion, i.e., at rough vacuum of 1–10 mbar (Chap. 4.4.4), they are perfectly compatible with the first pumping stage of ESI interfaces. Ion funnels increase the transmission of ESI interfaces, and accordingly, result in at least tenfold improved overall sensitivity of the mass spectrometer as compared to sources with a skimmer electrode. An example of an ESI interface with ion funnel is presented in the following section (Fig. 12.10).

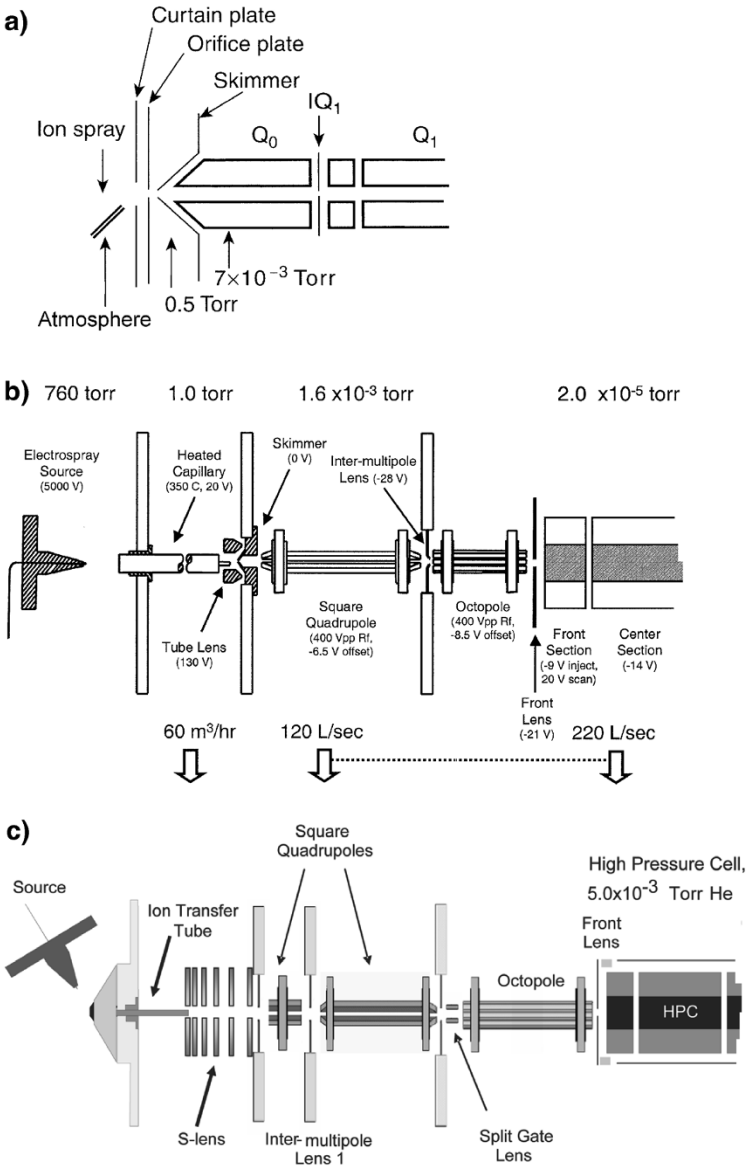


Fig. 12.8. Modern electrospray interfaces: (**a**) Setup for linear quadrupole and triple quadrupole instruments with 45° spray, heated countercurrent desolvation gas ("curtain gas"), orifice–skimmer setup for the first pumping stage, and RF-only quadrupole as ion guide in the second pumping stage. (**b**) On-axis spray on entrance of heated capillary serving as counter electrode, nozzle-skimmer arrangement, and RF-only multipole ion guides in front of an LIT. (**c**) Similar to (**b**) but the skimmer has been replaced by an ion-focusing lens system to improve transmission. This figure uses the front parts from Figs. 4.37, 4.41, and 9.25, respectively; reference to the according sources is given there.

12.2.5 Nozzle-Skimmer Dissociation

The rough vacuum zone of the first pumping stage between nozzle and skimmer of an electrospray interface does not only provide space for effective desolvation [71,72], but can also be used to achieve fragmentation of the ions by CID (Chap. 9.3). While a comparatively high pressure in this region can effect collisional cooling (Chap. 4.4.4) rather than dissociative collisions [73], an increased voltage difference between nozzle and skimmer enhances ion fragmentation by CID [71,73,74].

Nozzle-skimmer dissociation (NSD) or simply *skimmer CID* can *i*) strip off residual solvent molecules, *ii*) achieve fragmentation of electrosprayed ions resulting in spectra similar to CI mode [75], and *iii*) generate first-generation fragment ions for further tandem MS experiments. The latter method provides a *pseudo* MS^3 operation on triple quadrupole mass spectrometers [76-78]. Real MS^3 would require mass-selection prior to the first CID stage, too (for an example of pseudo MS^3 using NSD cf. Chap. 12.5.1). A programmable skimmer CID routine delivers ESI mass spectra with a variable degree of fragmentation from a single run [74,76,77,79].

Example: Even a moderate voltage drop between nozzle and skimmer can cause the elimination of weakly bonded substituents such as CO_2 in case of carbon dioxide-protected deprotonated *N*-heterocycles. In particular, $SnMe_3$-substituted anions such as 2-(trismethylstannyl)pyrrole-*N*-carbamate exhibit strong variations in the $[A–CO_2]^-/A^-$ ratio of up to a factor of 30 preventing the detection of A^- at slightly elevated voltages (Fig. 12.9) [80].

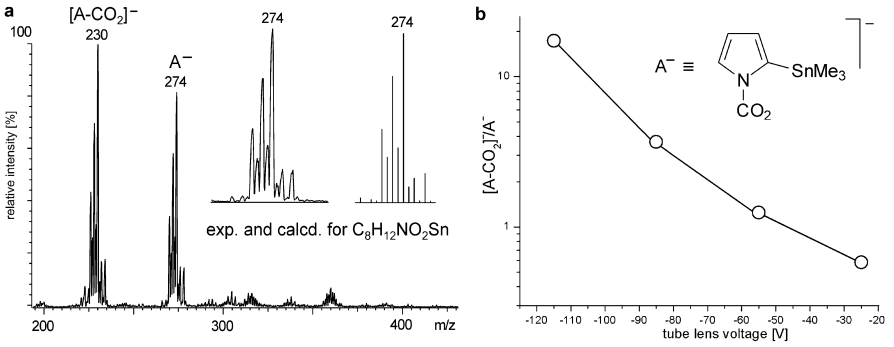


Fig. 12.9. (**a**) Partial negative-ion ESI spectrum of 2-(trismethylstannyl)pyrrole-*N*-carbamate (A^-) from tetrahydrofurane at low nozzle-skimmer voltage drop and (**b**) dependence of the $[A–CO_2]^-/A^-$ ratio variation on this voltage.

For NSD it is not required to have a true nozzle–skimmer arrangement. Instead, a potential drop of 20–100 V across a suitable pressure region of any ESI interface design suffices to induce this sort of CID. The Bruker Apollo II™ ESI source, for example, features a dual ion funnel setup with the first ion funnel in the rough vacuum of the supersonic expansion plume (≈ 3–4 mbar) and the second ion funnel prior to an RF-only hexapole used to alternatively guide or accumulate ions.

Here NSD or *in-source CID* as it is termed by the manufacturer, is achieved by shifting the DC potentials as to have the largest voltage drop at the entrance into the second ion funnel where a pressure of ≈ 0.1 mbar is suitable for low-energy CID (Fig. 12.10).

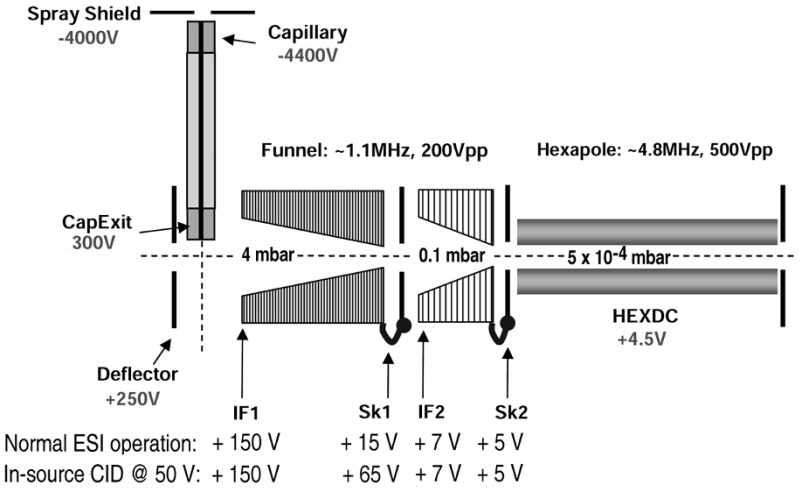


Fig. 12.10. ESI interface with differential pumping in a dual ion funnel arrangement (Bruker Apollo II™). In normal ESI operation the main DC gradient is located in the first ion funnel while ions drop only by about 8 V into the second. Lifting the exit potential of the first funnel causes the ions to enter the second ion funnel at much higher velocity, which is sufficient for NSD. Courtesy of Bruker Daltonik GmbH, Bremen.

12.3 Nanoelectrospray

Miniaturization of electrospray is even more attractive than access to high flow rates. A more narrow spray capillary results in smaller droplets and, moreover, in much reduced flow rates, as theoretically described and experimentally demonstrated by Wilm and Mann [81]. Such a downscaling can be achieved by replacing the spray needle by a borosilicate glass capillary of some microliters volume to which a fine tip is pulled with a micropipette puller. The tip has a narrow bore exit of 1–4 µm diameter making flow rates of 20–50 nl min^{-1} sufficient to provide a stable electrospray [82]. Derived from the nanoliter flow rates, the term *nanoelectrospray* (nanoESI) has become established for that technique. While conventional ESI produces initial droplets of 1–2 µm in diameter, the droplet size from nanoESI is less than 200 nm, i.e., their volume is about 100–1000 times smaller. NanoESI allows for high-polarity solvents such as pure water in both positive- and negative-ion mode, has extremely low sample consumption [83], and tolerates even higher loads with buffer salts than conventional ESI [53,84].

Example: In the pioneering nanoESI work, the minuscule sample consumption was demonstrated along an attempt to sequence tryptic peptides (Chap. 11.5.2) of the protein bovine serum albumin (BSA, $M_r \approx 66{,}400$ u). Each of the BSA-derived peptide ions shown in the full scan spectrum (Fig. 12.11) was subjected to fragment ion analysis by means of CID-MS/MS on a triple quadrupole instrument. Merely 800 fmol of BSA was consumed for the tryptic digest used in this analysis [83], a type of nanoESI application that is still highly attractive [85].

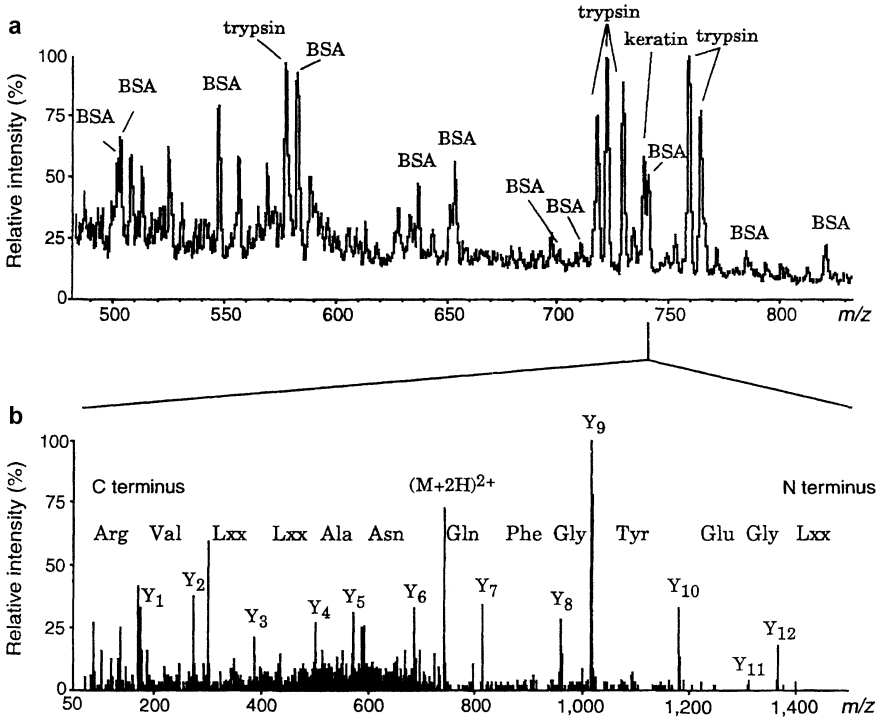


Fig. 12.11. Peptide sequencing by nanoESI-CID-MS/MS from a tryptic digest of BSA; 800 fmol of BSA were used: (**a**) full scan spectrum, (**b**) fragmentation of the selected doubly charged peptide ion at *m/z* 740.5. Adapted from Ref. [83] by permission. © Nature Publishing Group, 1996.

12.3.1 Practical Considerations for NanoESI

For the measurement, the nanoESI capillary is adjusted to locate at about 1 mm distance from the entrance of the counter electrode by means of a micromanipulator. Thus, precise optical control is needed during positioning to prevent crashing of the tip or electric discharges during operation. Commercial nanoESI sources are therefore equipped with a built-in microscope or camera (Fig. 12.12). The spray voltage of 0.7–1.2 kV is normally applied via an electrically conducting coating

on the outer surface of the spray capillaries, usually a sputtered gold film. Occasionally, wider capillaries with a fine metal filament inside are used. With the high voltage switched on, the liquid sample flow is solely driven by capillary forces refilling the aperture as droplets are leaving the tip. Sometimes, liquid flow is slightly supported by a gentle backing pressure on the capillary. Meanwhile, numerous specialized *nanoelectrospray emitters* – as these capillaries are often termed – have been developed to deliver optimum performance under various conditions of operation including nanoLC-MS coupling [86].

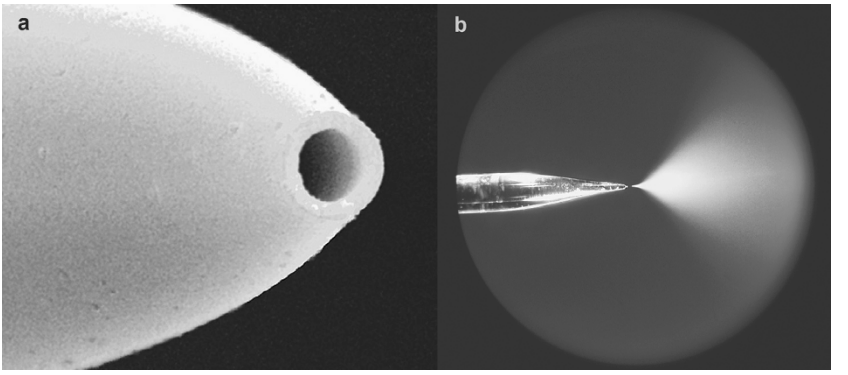


Fig. 12.12. Nanoelectrospray; (**a**) SEM micrograph of the open end of a glass nanoESI capillary having a 2-µm aperture, (**b**) microscopic view of the spray from a nanoESI capillary as provided by observations optics. By courtesy of New Objective, Woburn, MA.

Note: Besides its low sample consumption, nanoESI is free of *memory effects* because each sample is supplied in a fresh capillary by means of disposable micropipettes. Furthermore, the narrow exits of nanoESI capillaries prevent air-sensitive samples from rapidly decomposing.

12.3.2 Spray Modes of NanoESI

The onset of electrospray as well as the spatial and temporal characteristics of the spray plume largely depend on the experimental parameters. Strong effects are exerted by surface tension and polarity of the solvent, sample concentration, and electric field strength at the tip of the spray capillary. The latter parameter can easily be adjusted, and as demonstrated in Fig. 12.13, demands for careful control as to avoid disadvantageous spray conditions. At low electric field strength some spray will occur, but mostly by multiple discontinuous jets (dripping mode, D) not accompanied by useful aerosol formation [87]. Increasing the spray voltage initiates the formation of the charged mist, which is still accompanied by a spindle-like jet (S) taking away most of the liquid flow. Further increase of the spray voltage forms a wide cone-jet (C) purely consisting of charged microdroplets. As the

voltage exceeds a certain limit, the electrostatically driven dissipation of liquid surmounts the solvent flow attainable through the narrow capillary orifice, and thus, the cone-jet starts pulsing (P). Finally, at very high voltages any rough edge around the capillary orifice may initiate a cone-jet of its own. This multi-jet mode (M) causes losses due to overly wide dissipation of the sample flow. Any further increase of the spray voltage results in electric discharges not only detrimental for the capillary tip but eventually also causing failures of the intrument's electronics.

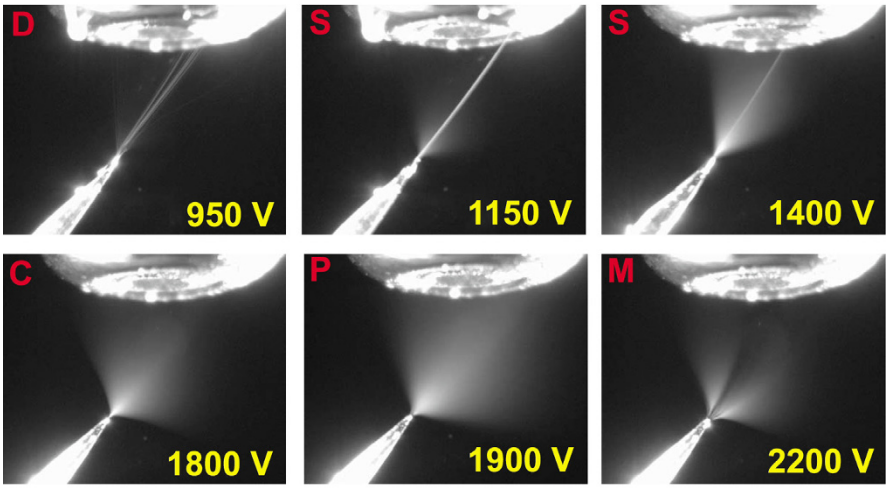


Fig. 12.13. Photographs of nanoelectrospray plumes as effected by different spray voltages. The modes observed starting from the *upper left* are dripping (**D**), spindle (**S**), cone-jet (**C**), pulsed cone-jet (**P**), and multi-jet (**M**). Only pure cone-jet mode will deliver stable electrospray for analytical work. Reproduced from Ref. [87] with permission. © Elsevier, 2004.

Note: These observations are equally relevant to (pneumatically assisted) ESI at standard flow rates [88]. Then, the corresponding voltages are just higher by a factor of ≥ 2, which is mostly due to the increased gap between spray capillary and counter electrode to accommodate the larger plume. The optimization of the electrospray for temporal stability by adjustment of liquid flow, nebulizer gas pressure, and spray voltage is therefore necessary for any analytical ESI work.

12.3.3 Nanoelectrospray from a Chip

The sample throughput of nanoESI is limited by the comparatively time-consuming procedure of manual capillary loading. A chip-based nanoESI sprayer on an etched silicon wafer allows for the automated loading of the sprayer array by a pipetting robot (Fig. 12.14). The chip provides a 10×10 array of nanoESI spray nozzles of 10 µm inner diameter. Volumes up to 10 µl are supplied directly

from a pipette contacting the chip from the backside. An electrically conducting coating of the pipette tip is used to connect the sprayer to high voltage. Pipetting robot and automated chip handling are united in a common housing that replaces the conventional (nano)ESI spray unit.

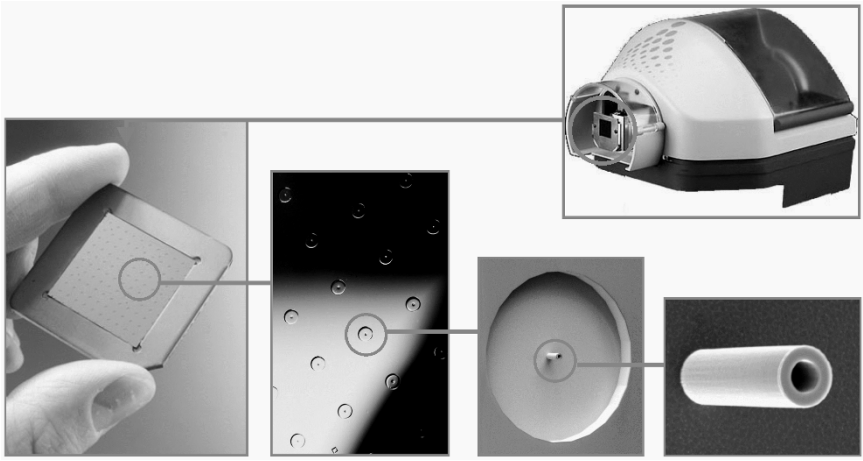


Fig. 12.14. Chip-based Advion nanoESI system. The pictures stepwise zoom in from the pipetting unit to the spray capillary on the silicon chip. By courtesy of G. Schultz, Advion BioSciences, Ithaca, NY.

12.4 Ion Formation in ESI

Until now, our discussion of electrospray was rather technical with an emphasis on interface design and occasional reference to applications. Next we shall consider the physicochemical aspects of the ESI process. This section presents answers to basic questions such as to why an electrospray does occur at all, how isolated gas phase ions are formed from droplets, and what rules are governing the charge state (distribution) of those incipient gas phase ions [88-90]. Ion formation in ESI can be considered to be composed of three steps: *i*) creation of an electrically charged spray, *ii*) dramatic reduction of the droplets' size, and finally *iii*) liberation of fully desolvated ions.

12.4.1 Formation of the Electrospray Plume

To understand the formation of a continuous spray, consider the surface of an electrolytic solution when exiting an electrically conducting capillary held at high electric potential with reference to a nearby counter electrode. In practice, the spray capillary has about 75 μm inner diameter and is kept at 3–4 kV with reference to the sampling orifice at approx. 1 cm distance. At the open end of the capillary the emerging liquid is thus exposed to an electric field of about 10^6 V m^{-1}.

The electric field causes charge separation in the electrolytic solution and finally deformation of the meniscus into a cone. The phenomenon of cone formation has been discovered by Zeleny [39] and first theoretically described by Taylor [40], hence it was termed *Taylor cone*.

The process of Taylor cone formation starts when the spherical surface forms an oval under the influence of increasing field strength. In turn, a sharper curvature of the oval increases the field strength. The Taylor cone forms as soon as the critical electric field strength is reached and starts ejecting a fine jet of liquid from its apex towards the counter electrode when surface tension is overcome by the

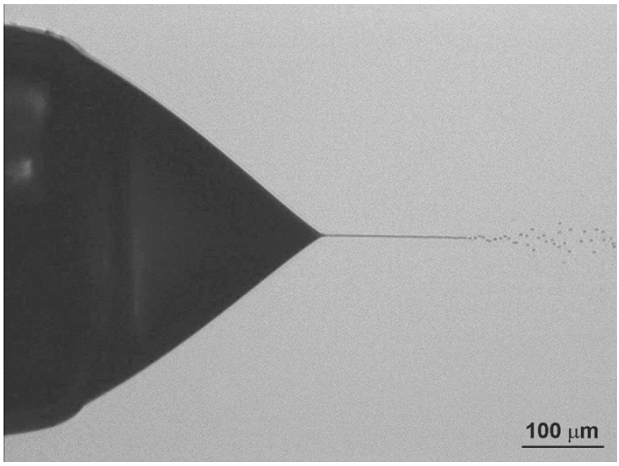


Fig. 12.15. Microphotograph of the meniscus shape during electrospray in stable cone-jet mode for optimum analytical operation. The shape and the emerging jet remain stationary and continuously delivering numerous small droplets upon breaking up of the jet. Adapted from Ref. [92] with permission. © American Chemical Society, 2007.

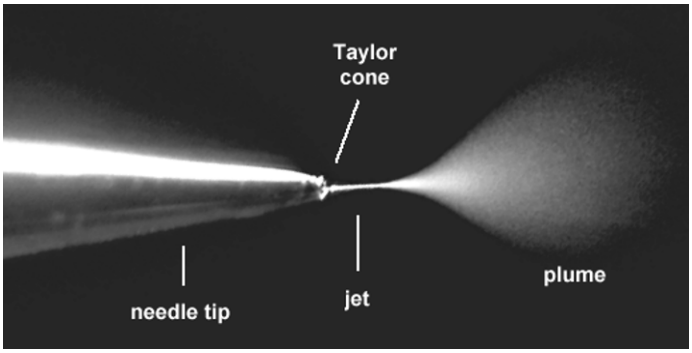


Fig. 12.16. Electrospray from a nanoESI capillary. The jet emitted from the Taylor cone is clearly visible and separate from the region of rapid expansion into a plume of microdroplets. By courtesy of New Objective, Woburn, MA.

electrostatic forces [81]. The jet carries a large excess of ions of one particular charge sign, because it emerges from the point of highest charge density, i.e., from the cone's apex [91]. Such a jet, however, cannot remain stable for an elongated period of time but breaks up into small droplets (Fig. 12.15) [92]. Due to their charge, these droplets are driven apart by Coulombic repulsion. Overall, this process causes the generation of a fine spray, and thus gave rise to the term *electrospray* (Figs. 12.16). This mode of operation is termed *cone-jet mode* [6].

The ESI process overall represents an electrolytic flow cell where the connection from the spray capillary to the counter electrode is created by charge transportation via the electrically charged aerosol (Fig. 12.17) [93-95]. In positive-ion mode, neutralization at the sampling orifice is effected by electrons from the high voltage power supply, which in turn originate from oxidation of anions on the inner wall of the spray capillary. In negative-ion mode, reduction of cations will occur in place of oxidation [61].

In rare cases, the electrolytic processes during electrospray can cause molecular ion, $M^{+\bullet}$, formation by electrolytic oxidation [95]. This is more probable if nonpolar molecules of very low ionization energy are precluded from other ionization pathways such as protonation or cationization. Electrolytic $M^{+\bullet}$ ion formation normally requires nonprotic solvents, low liquid flow for increased reaction time, and preferably metal spray capillaries rather than fused silica capillaries. ESI may also result in changes of the oxidation state of metal ions, e.g., $Ag^{+} \rightarrow Ag^{0}$, $Cu^{2+} \rightarrow Cu^{+}$.

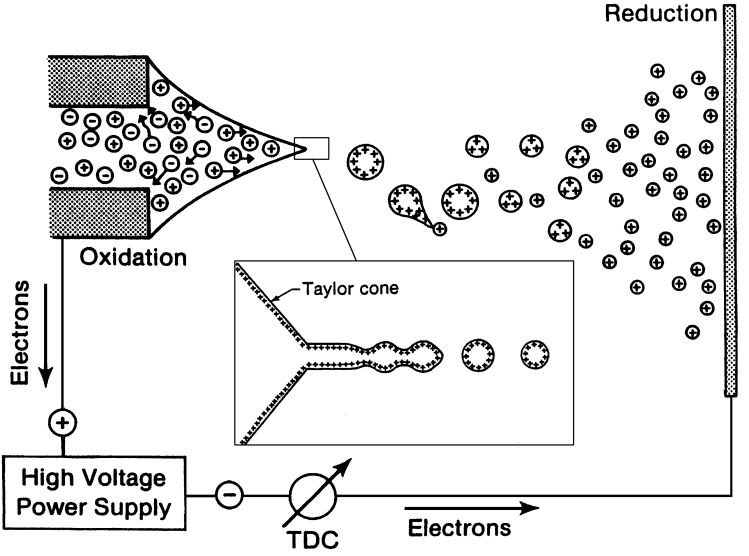


Fig. 12.17. Schematic of Taylor cone formation, ejection of a jet, and its disintegration into a fine spray. The electrochemical processes of ESI [93,94] are also assigned. Adapted from Ref. [52] by permission of the authors.

12.4.2 Disintegration of Charged Droplets

When a micrometer-sized droplet carrying a large excess of ions of one particular charge sign – some 10^4 charges can be considered to be a realistic value – evaporates some solvent, the charge density on its surface is continuously increased. As soon as electrostatic repulsion exceeds the conservative force of surface tension, disintegration of the droplet into smaller subunits will occur. The point at which this occurs is known as the *Rayleigh limit* [41]. Originally, it has been assumed that the droplets would then be degraded by *Coulomb fission* (or *Coulomb explosion*). This process then occurs repeatedly to generate increasingly smaller microdoplets. While the model of a cascading reduction in size holds valid, more recent work has demonstrated that the microdroplets do not explode, but eject a series of much smaller microdroplets from an elongated end (Fig. 12.18) [52,89,96]. The ejection from an elongated end can be explained by deformation of the flying microdroplets, i.e., they have no perfect spherical shape. Thus, the charge density on their surface is not homogeneous, but significantly increased in the region of sharper curvature. The smaller offspring droplets carry off only about 1–2% of the mass, but 10–18% of the charge of the parent droplet [89]. This process resembles the initial ejection of a jet from the Taylor cone. The concept of this so-called *droplet jet fission* is not only based on theoretical considerations but has been proven by flash microphotographs of droplet shadows [96,97]. The total series of events from the initially sprayed droplet to the isolated ion takes less than one millisecond. Micro-shadowgraphs also show that neutral droplets exhibit an analogous distortion of their shapes followed by ejection of off-spring droplets when field ionized by an electric field of about 2.5×10^6 V m^{-1} [98].

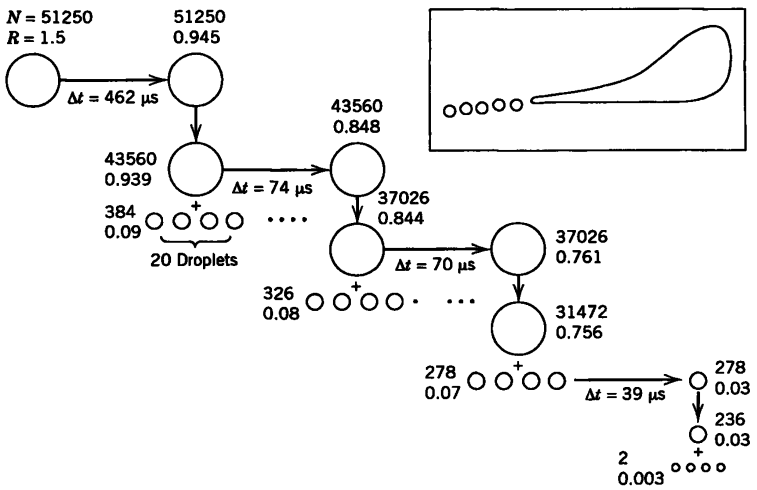


Fig. 12.18. Droplet jet fission. The average number of charges on a droplet, the radii of the droplets [μm], and the timescale of events are assigned. The *inset* shows a drawing of droplet jet fission based on an actual flash microphotograph published by Gomez and Tang [96]. Reproduced from Ref. [52] by permission of the authors.

12.4.3 Formation of Ions from Charged Droplets

The process of droplet jet fission starts on a macroscopic scale and eventually leads to states that might be regarded as large clusters or multiply solvated ions. The final step of the creation of isolated gas phase ions from these multimolecular entities is not addressed by this model, however.

The elder model of ion formation, the *charged-residue model* (CRM), assumes complete desolvation of ions to occur by successive loss of all solvent molecules from droplets that are sufficiently small to contain just one analyte molecule at the end of a droplet fission cascade [20,45,99]. The charges, e.g., protons, being part of this ultimate droplet are then transferred onto the (macro)molecule, especially if this exposes some basic sites. According to CRM, even large proteins should at least be able to form singly charged ions, although the formation of multiply charged species should be of higher probability. In fact, all charge states down to 1+ have been observed [25].

A later theory, the *ion evaporation model* (IEM) [100,101], describes the formation of desolvated ions as direct evaporation from the surface of highly charged microdroplets [102] (for ion evaporation in FD-MS cf. Chap. 8.5.1). Ionic solvation energies are in the range of 3–6 eV, but at 300 K thermal energy can only contribute about 0.03 eV to their escape from solution. Thus, the electric force has to provide the energy needed. It has been calculated that a field of 10^9 V m^{-1} is required for ion evaporation, which corresponds to a final droplet diameter of 10 nm [101]. The IEM nicely corresponds to the observation that the number of charges is related to the fraction of the microdroplet's surface that a (macro)molecule can cover. Upon shrinking of the droplet, the size of such a molecule and number of droplet charges remain constant. Now, the increasing charge density brings more charges within the reach of an analyte molecule as the spacing of the surface charges decreases [103,104]. Flat and planar molecules therefore exhibit higher average charge states than compact ones, e.g., the unfolding of (globular) proteins is accompanied by higher charge states under otherwise identical ESI conditions [105,106].

Further support of IEM comes from the effect of the droplet evaporation rate on the charge state distribution of proteins. Fast evaporation (more drying gas, higher temperature) favors higher average charge states, while slower evaporation results in fewer charges. This is in accordance with the reduced time available for ion evaporation from the shrinking droplet. It leads to a relative enrichment of charge on the droplet, and thus, on the leaving ions [103].

Example: The cleavage of disulfide bonds by reduction with 1,4-dithiothreitol causes the unfolding of the protein. This exposes additional basic sites to protonation, and therefore results in higher average charge states in the corresponding positive-ion ESI spectrum (Fig. 12.19) [105].

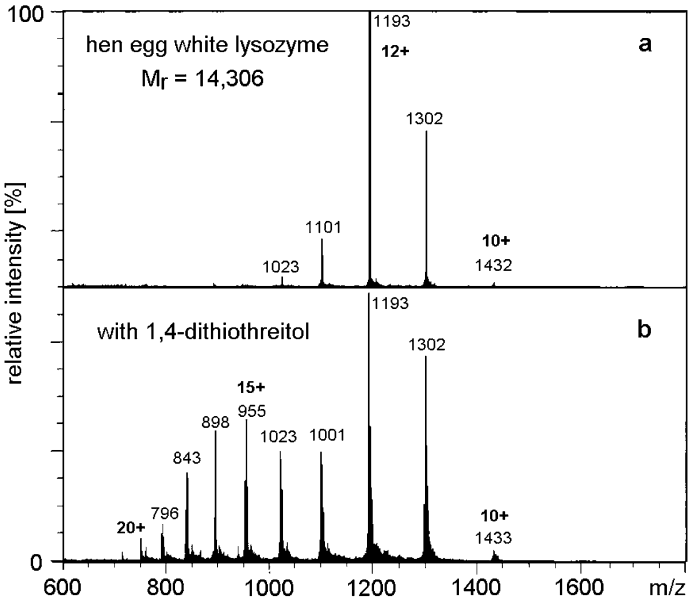


Fig. 12.19. Positive-ion ESI spectra of (**a**) hen egg white lysozyme and (**b**) the protein after addition of 1,4-dithiothreitol. Reproduced from Ref. [105] by permission. © American Chemical Society, 1990.

In contradiction to IEM, the electric field strength locally necessary to evaporate ions from a droplet cannot be attained, because the droplet would be crossing the Rayleigh limit before [25,107].

More recent work revealed the importance of gas-phase proton transfer reactions [108-111]. This implies that multiply charged peptide ions do not exist as preformed ions in solution, but are generated by gas-phase ion–ion reactions (Chap. 12.4.4). The proton exchange is driven by the difference in proton affinities (*PA*, Chaps. 2.12 and 9.18.3) of the species encountered, e.g., a protonated solvent molecule of low *PA* will protonate a peptide ion with some basic sites left. Under equilibrium conditions, the process would continue until the peptide ion is "saturated" with protons, a state that also marks its maximum number of charges.

Note: There is a continuing debate about ion formation in ESI [89,90,104]. In summary, it may be assumed that CRM holds valid for large molecules [20] while the formation of smaller ions is better described by IEM [89,90].

Independent of the "true" mechanism of ion liberation, the close correlation between the number of charge states and the surface a macromolecule exposes to its surrounding solvent can be used to observe these changes by ESI-MS [105,106,112-114].

Example: The average charge state of a protein depends on whether it is denatured or not and on the actual solvent; lower pH causes more protons to be attached to the protein than neutral conditions [106,114]. The degree of denaturization in turn depends on the pH of the electrosprayed solution. Resulting conformational changes of the protein, e.g., unfolding upon protonation, make additional basic sites accessible, thereby effecting an increase of the average charge state (Fig. 12.20) [106]. The maximum number of charges that can be placed upon peptide and protein molecules is directly related to the number of basic amino acid residues (arginine, lysine, histidine) present (Fig. 12.21) [105].

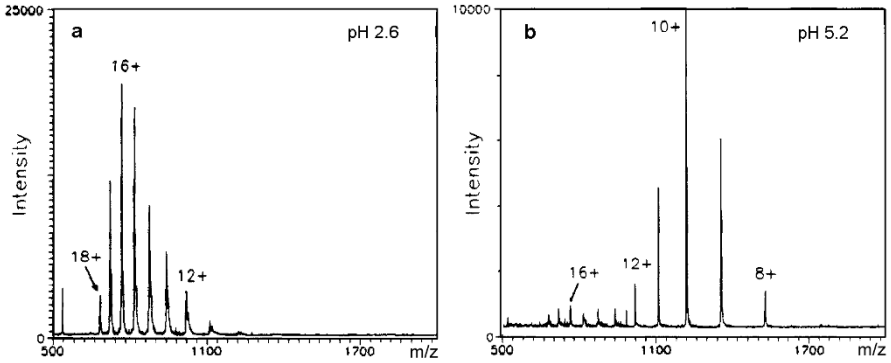


Fig. 12.20. Positive-ion ESI mass spectra of cytochrome c at different pH of the sprayed solution: (**a**) at pH 2.6, (**b**) at pH 5.2. Adapted from Ref. [106] by permission. © American Chemical Society, 1990.

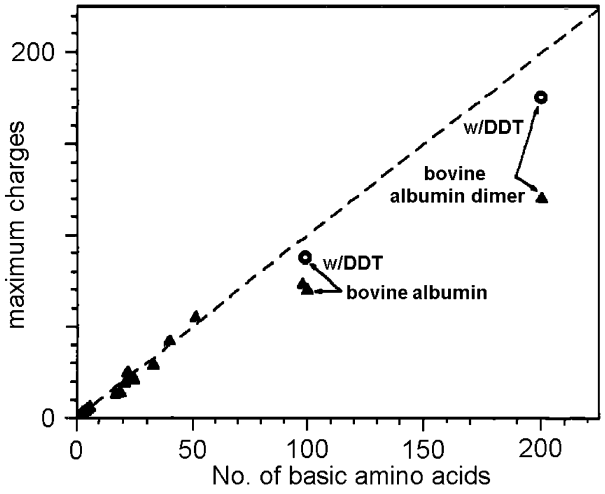


Fig. 12.21. Correlation between the number of basic amino acid residues and the maximum number of charges observed for a set of peptides and proteins under ESI conditions. Reproduced from Ref. [105] by permission. © American Chemical Society, 1990.

12.5 Multiply Charged Ions and Charge Deconvolution

12.5.1 Dealing with Multiply Charged Ions

The discussion of ion formation in ESI has revealed that – beside compound class – the actual experimental conditions exert significant influence on the appearance of an ESI spectrum. The most influential factors are *i*) pH of the sprayed solution, *ii*) flow of sample solution, *iii*) flow (or pressure) of nebulizing gas, and *iv*) flow and temperature of the desolvation gas or the temperature of the heated desolvation capillary, respectively (also cf. Figs. 12.1 and 12.19).

In general, the number of charges on a molecule in ESI depends on its molecular weight [20,115] and on the number of potential charge sites available, e.g., sites for protonation [10,20,105,106], deprotonation [116,117] or cationization [118]. On the one hand, this behavior advantageously folds up the *m/z* scale to make even extremely large molecules accessible to standard mass analyzers (Fig. 12.22). On the other hand, it creates a confusingly large number of peaks and requires tools to deal with in order to enable reliable mass assignments of unknowns.

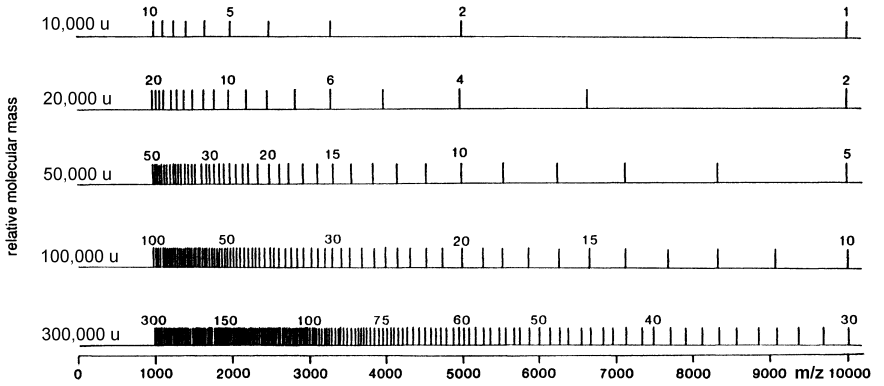


Fig. 12.22. Calculated *m/z* values for the different charge states of molecules of different molecular weight. Representative peaks are labeled with their corresponding charge state. Adapted from Ref. [115] by permission. © John Wiley & Sons, 1992.

While low-mass polymers exhibit only singly charged ions in ESI, polymers of higher mass form doubly, triply, and multiply charged ions [14]. Basically, the number of charges on those molecules increases in parallel to their average molecular weight. For example, PEG 400 exclusively exhibits singly charged ions in positive-ion ESI, PEG 1000 about equally forms 1+ and 2+ charge states, and with PEG 1500 the 3+ charge state starts to dominate [14,104].

Furthermore, charge distributions depend on the sample concentration, e.g., PEG 1450 yields triply and few doubly charged ions at 0.005 mg ml^{-1} in MeOH : H_2O = 1 : 1, triply and doubly charged ions of equal abundance plus few singly charged ions at 0.05 mg ml^{-1}, but mainly doubly charged ions accompanied by few singly and triply charged ions at 0.5 mg ml^{-1} [104]. This demonstrates that

a comparatively fixed number of charges in a droplet is distributed among few or many analyte molecules contained, and thus, supports IEM.

Example: PEGs and related oxygen-rich compounds form $[M+alkali_n]^{n+}$ ions [14,118,119] or $[M+nNH_4]^{n+}$ ions. Triton X-405, a commercial detergent, a.o. used in acrylic paints for stabilization of the suspension, has been analyzed by positive-ion nanoESI-MS. The molecular weight distribution appeared trifold; in this case, due to the presence of ammonium acetate as $[M+NH_4]^+$, $[M+2NH_4]^{2+}$, and $[M+3NH_4]^{3+}$ ion series (Fig. 12.23a). For endgroup analysis *nozzle-skimmer dissociation* (NSD) was applied at 60 V offset upon which only the $[M+3NH_4]^{3+}$ ions (least stable due to highest internal Coulombic repulsion) underwent significant dissociation to yield some low-mass fragment ions (Fig. 12.23b). The occurrence of $[C_8H_{17}\text{-}C_6H_4\text{-}(OC_2H_4)_n]^+$ ions at *m/z* 233 and 277 pointed towards octophenyl endgroups. Their presence was verified in a pseudo MS^3 experiment by CID-MS/MS of the fragment at *m/z* 233 at 20 V collision offset (Fig. 12.23c) [78].

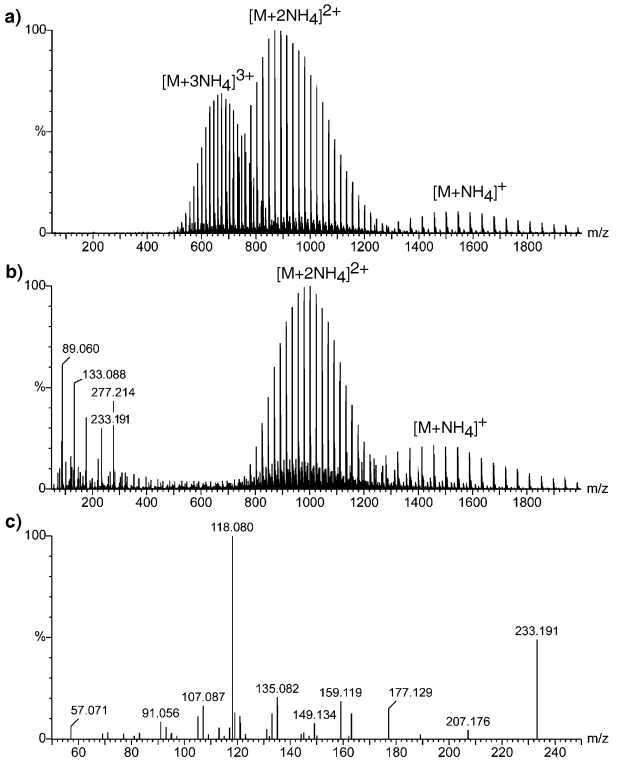


Fig. 12.23. Triton X-405 analyzed by positive-ion nanoESI-MS. (**a**) Molecular weight distribution appears trifold as $[M+NH_4]^+$, $[M+2NH_4]^{2+}$, and $[M+3NH_4]^{3+}$ ions series; (**b**) only the triply charged ions undergo significant dissociation upon NSD to yield low-mass fragment ions; (**c**) CID spectrum of the fragment ion at *m/z* 233 for endgroup analysis. Reproduced from Ref. [78] with permission. © Elsevier, 2009.

Note: In ESI spectra of (synthetic) polymers, multiple charging causes the simultaneous occurrence of superimposing ion series each of them representing the molecular weight distribution of the polymer. Therefore, MALDI is generally preferred for polymer analysis as it delivers only singly charged ions.

12.5.2 Mathematical Charge Deconvolution

How would we be able to retrieve the correct molecular weight from spectra as just presented in Figs. 12.20, 12.23 or even in Fig. 12.1 if the charge states corresponding to individual peaks were not yet assigned? A systematic treatment of these ion series reveals that adjacent signal groups (to include isotopic patterns) in an ESI mass spectrum of a pure compound belong to charge states differing exactly by one, i.e., distributions have no gaps or jumps. This renders the calculation of the number of charges corresponding to individual peaks straightforward and thus permits to deduce an unknown molecular weight M_r [60,115,120].

For the charge states of neighboring peaks belonging to a pair at m/z_1 (higher value) and m/z_2 (lower value) we have :

$$n_2 = n_1 + 1 \tag{12.7}$$

Assuming all charges from protonation and using m_H for the mass of a proton, m/z_1 is determined by

$$m/z_1 = \frac{M_r + n_1 m_H}{n_1} \tag{12.8}$$

and m/z_2 of the peak at lower mass is given by

$$m/z_2 = \frac{M_r + n_2 m_H}{n_2} = \frac{M_r + (n_1 + 1)\, m_H}{n_1 + 1} \tag{12.8a}$$

where n_2 can be expressed by inserting Eq. 12.7. The charge state n_1 can then be obtained from

$$n_1 = \frac{m/z_2 - m_H}{m/z_1 - m/z_2} \tag{12.9}$$

Having calculated n_1, M_r is given by

$$M_r = n_1 (m/z_1 - m_H) \tag{12.10}$$

In case of cationization instead of protonation, m_H has to be replaced by the corresponding mass of the cationizing agent, e.g., NH_4^+, Na^+, or K^+. (The recognition of cationized species is addressed in Chaps. 8.5.7 and 11.4.3).

Example: For the ease of calculation we use nominal mass (Chap. 3.1.5) and assume the charges from protonation. Consider the first peak at m/z 1001, the second at m/z 501. Now n_1 is obtained according to Eq. 12.9 by calculating it from

$n_1 = (501 - 1) / (1001 - 501) = 500 / 500 = 1$. Therefore, M_r is calculated from Eq. 12.10 to be $M_r = 1 \times (1001 - 1) = 1000$. (The doubly protonated ion is detected at *m/z* 501 because (1000 + 2) / 2 = 501.)

Note: As each pair of signals delivers an independent mass value for the hypothetical singly charged ion, mass accuracy can greatly be enhanced in ESI by multiple determination of this value and subsequent calculation of the average.

12.5.3 Computerized Charge Deconvolution

The above procedure may be time-consuming but works well for pure compounds and simple mixtures. When complex mixtures are to be addressed, proper manual assignment of all peaks becomes increasingly difficult. Additional problems arise from the simultaneous presence of peaks due to protonation and cation attachment. Therefore, numerous refined procedures have been developed to cope with these requirements [121-124]. The data systems of modern ESI instruments are normally equipped with elaborate computerized *charge deconvolution*. The efficiency of these computer programs can largely be improved by specifying some limitations, e.g., the expected range of charge numbers, the type of ions or presumed adducts, and the resolving power employed for the measurement. The resolving power is relevant to assist the algorithm in distinguishing neighboring peaks of other charge state from isotopic contributions.

Example I: The low-resolution (LR) positive-ion ESI mass spectrum and the charge-deconvoluted molecular weight spectrum (*inset*) of bovine serum albumin (BSA) as obtained from a quadrupole ion trap instrument are compared below (Fig. 12.24). In case of such high-mass ions the resolving power of a quadrupole ion trap is insufficient to separate different cationization products of equal charge state. Nonetheless, charge deconvolution reveals that ion series A belongs to the noncovalent BSA dimer, while series B results from the monomer [26].

Example II: A mixture of the proteins bovine ubiquitin, horse cytochrome c, and horse myoglobin, each at a concentration of 10 μM, was analyzed by positive-ion ESI-FT-ICR-MS. While the first analysis was carried out with only 16 k data, the second was obtained from a 512 k transient, resulting in $R = 2000$ and $R = 60{,}000$, respectively (Chap. 4.7.5). Charge deconvolution by the *Zscore* algorithm delivered "zero-charge spectra" clearly separating the proteins (Fig. 12.25) [122]. The program used here handles LR spectra to yield unresolved isotopic distribution envelopes as well as HR spectra to show the full isotopic information in the resulting zero-charge spectrum.

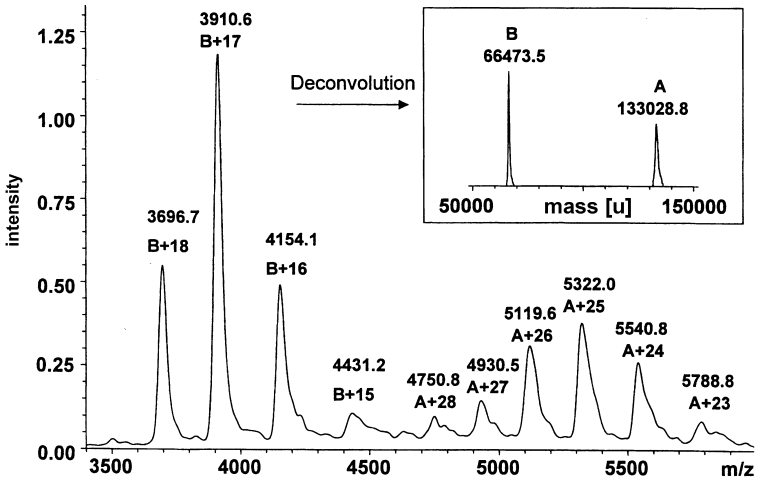


Fig. 12.24. Partial ESI mass spectrum of BSA and molecular weights of the neutrals after charge deconvolution (*inset*). Charge states are assigned to both series of peaks in the ESI spectrum. Reproduced from Ref. [26] by permission. © John Wiley & Sons, 2000.

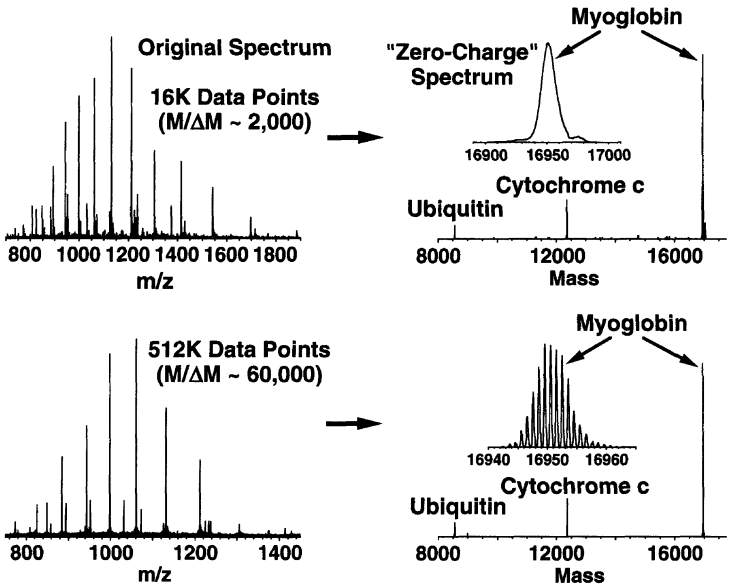


Fig. 12.25. Charge deconvolution of LR (*upper part*) and HR (*lower part*) positive-ion ESI spectra of an artificial protein mixture. The "zero charge" peak of myoglobin is also shown in expanded view to reveal the delineation of the isotopic pattern. Reproduced from Ref. [122] by permission. © Elsevier, 1998.

Note: The output of computerized charge deconvolution can often be customized to either display the mass spectrum as it would appear with singly charged ions or to deliver the molecular weights of the corresponding neutrals (as in the above example). The output of neutral M_r represents the only case where the abscissa has to be labeled "*mass* [u]", while mass spectra strictly require "*m/z*" on the *x*-axis!

12.5.4 Hardware Charge Deconvolution

The most effective technique to deal with complex spectra due to multiply charged ions is to achieve the full separation between signals corresponding to different charge states and to resolve their isotopic patterns. Beyond a molecular weight of about a few thousand u this requires high-resolving mass analyzers, because the isotopic distribution of organic ions then becomes several mass units wide (Fig. 12.26). The minimum resolution needed for full isotopic separation is always equal to the ion's mass number (Chaps. 3.4, 3.7, and 3.8), independent of the charge state of the ion. Lower resolution only envelops the isotopic distribution. At insufficient resolution, the resulting peak may even be wider than the envelope [115].

Magnetic sector instruments (Chap. 4.3) were used first to demonstrate the beneficial effects of resolution on ESI spectra of biomolecules [119,125,126]. Today, FT-ICR instruments (Chap. 4.7) [127,128] and more recently orthogonal acceleration time-of-flight (oaTOF, Chaps. 4.2.8 and 4.9) or orbitrap (Chap. 4.8) analyzers offer by far more effective means to resolve such signals.

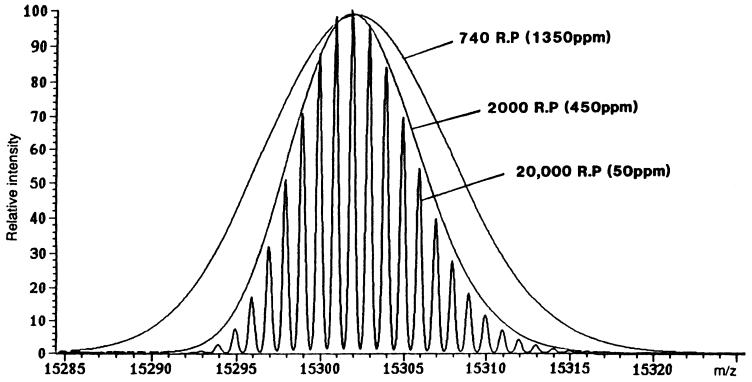


Fig. 12.26. Theoretical peak shape for a hypothetical singly charged protein ion of M_r = 15,300 u at different settings of resolution. Reproduced from Ref. [115] by permission. © John Wiley & Sons, 1992.

Example I: ESI on a magnetic sector instrument set to $R = 20{,}000$ allows for the full resolution of isotopic peaks in case of medium-molecular weight proteins (Fig. 12.27). This enables the direct determination of the charge state of the ions from the spacing of the isotopic peaks, i.e., 11+ for the lysozyme ion due to the average spaces of $\Delta m = 0.091$ u and 13+ for the myoglobin ion due to $\Delta m = 0.077$ u. In this particular case, the lysozyme $[M+11H]^{11+}$ ion serves as a mass reference for the accurate mass measurement of the "unknown" $[M+13H]^{13+}$ ion [125].

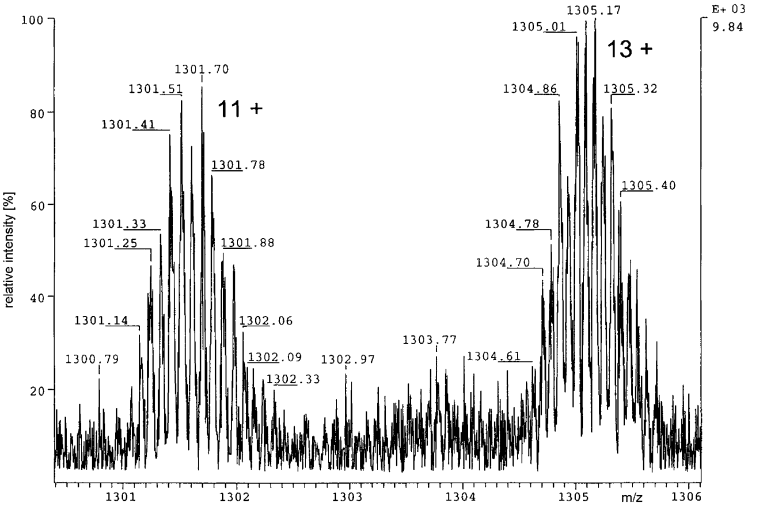


Fig. 12.27. Partial high-resolution ESI spectrum ($R = 20{,}000$) of a mixture of lysozyme and myoglobin on a magnetic sector instrument. Although a masterpiece at its time, today this approach is not anymore relevant. Reproduced from Ref. [125] by permission. © John Wiley & Sons, 1993.

Example II: ESI-orbitrap mass spectra of intact proteins show fully resolved isotopic patterns when 100 transients at a resolving power setting of $R = 100{,}000$ are acquired and charge deconvoluted. Figure 12.28 shows the results for the $[M+10H]^{10+}$ ion of horse heart apomyoglobin, $m = 16{,}940.965$ u (neutral mass of monoisotopic molecule) and of the $[M+21H]^{21+}$ ion of carbonic anhydrase, $m = 29{,}006.683$ u, both in very good agreement with the calculated isotopic patterns and masses [129]. A comparison with the previous example also demonstrates the great advances made in MS instrumentation that now allows to routinely resolve such signals. (Further examples are given by the ESI-ECD-FT-ICR spectra of proteins in Chap. 9.13.1 or by example II in the preceding section 12.5.3.)

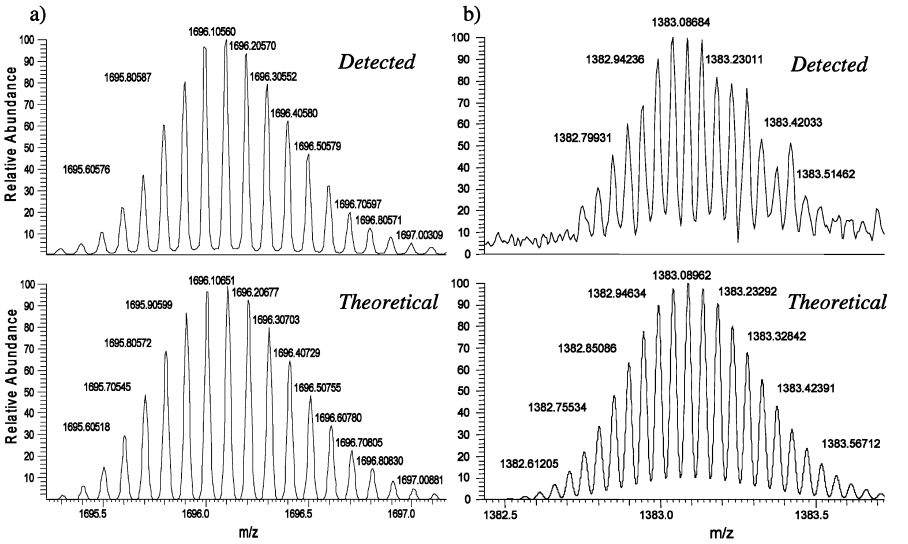


Fig. 12.28. ESI-orbitrap-MS of proteins. Fully resolved isotopic patterns as obtained upon charge deconvolution of (**a**) the $[M+10H]^{10+}$ ion of horse heart apomyoglobin, m = 16,940.965 u (neutral mass of monoisotopic molecule) and (**b**) the $[M+21H]^{21+}$ ion of carbonic anhydrase, m = 29,006.683 u. Reproduced from Ref. [129] by permission. © American Chemical Society, 2006.

Note: The resolving power required to fully resolve isotopic patterns is independent of the charge state of the ion. The minimum numerical value of R is always equal to the ion's mass number.

12.5.5 Controlled Charge Reduction in ESI

The complexity of ESI spectra of mixtures with all components forming series of multiply charged ions is apparent. An alternative approach to high resolution and data reduction by charge deconvolution is presented by the controlled reduction of the charge states themselves. *Charge reduction electrospray* (CRE) results in a significantly reduced number of peaks per component at the cost of their detection being required at substantially higher *m/z* [130,131]. In particular oaTOF analyzers provide a sufficient mass range for such an experimental approach at reasonable cost.

Charge reduction can be accomplished by neutralizing ion-molecule reactions during the desolvation step of ESI. The reducing ions needed for such neutralizations can either be generated by irradiating the gas with a ^{210}Po α-particle source [130,132] or more conveniently by a corona discharge [133,134]. Besides being nonradiative, the corona discharge offers the advantage of being tunable to achieve varying degrees of neutralization (Fig. 12.29) [133,134].

Ion-ion chemistry of oppositely charged ions presents another approach to charge reduction and charge state determination [108]. Such studies were done *i*) by employing the region preceding the skimmer of an ESI interface as a flow reactor and *ii*) inside a quadrupole ion trap. In the first case, both the substrate ion and the oppositely charged reactant ion are created by means of two separate ESI sprayers attached to a common interface [135]. The approach in a quadrupole ion trap makes use of the in-trap generation of proton-transferring reactant ions, while substrate ions are admitted via the ESI interface [136]. Finally, a noninstrumental approach is to derivatize the analytes as to reduce their ability of binding protons at basic functional groups [131].

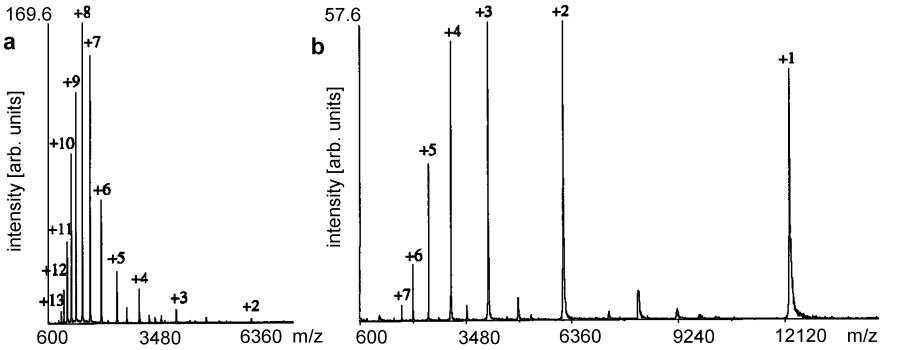


Fig. 12.29. Positive-ion ESI mass spectra of cytochrome c (**a**) under standard ESI conditions from acidic solution, (**b**) same but with medium setting of charge-reducing corona discharge. Adapted from Ref. [133] by permission. © American Chemical Society, 2000.

12.6 Applications of ESI-MS

ESI-MS is not only a versatile tool for any aspects of peptide and protein characterization including their complete sequencing, it also offers a tremendous variety of other applications some of which are highlighted below [4,9,23,137-140].

12.6.1 ESI-MS of Small Molecules

Polar analytes in the *m/z* 100–1500 range are often involved in pharmaceutical analytics including metabolism studies. The types of ions formed are various and depend on the ion polarity, the pH of the solution, the presence of salts, and the concentration of the sprayed solution. Multiply charged ions are rarely observed.

Example: The compound below represents the functional part of an effective drug (BM 50.0341) inhibiting HIV-1 infection by suppression of the unfolding of the gp120 glycoprotein (Fig. 12.30). Its positive-ion nanoESI spectrum from ethanol in the presence of ammonium chloride exhibits signals due to the formation of $[M+H]^+$, $[M+NH_4]^+$, and $[M+Na]^+$ ions. In addition, cluster ions of the type

$[2M+H]^+$, $[2M+NH_4]^+$, and $[2M+Na]^+$ are observed as typical for samples at comparatively high concentration. In negative-ion mode [141-144], the $[M–H]^-$ ion is accompanied by $[M+Cl]^-$ and $[M+EtO]^-$ adduct ions; the corresponding cluster ion series is also observed.

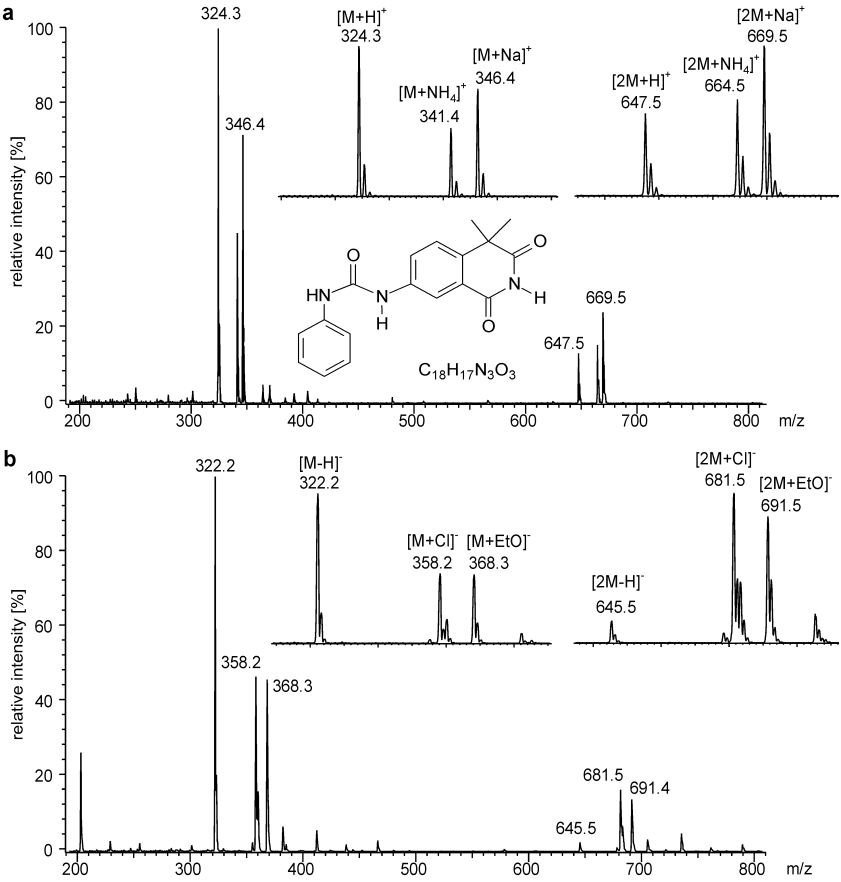


Fig. 12.30. Positive- (**a**) and negative-ion (**b**) nanoESI spectra of an anti-HIV drug from ethanol in the presence of ammonium chloride. By courtesy of H.-C. Kliem and M. Wiessler, German Cancer Research Center, Heidelberg.

12.6.2 ESI of Metal Complexes

In general, ESI can be well applied to ionic metal complexes and related compounds if these are soluble to at least 10^{-6} M in solvents suitable for the method [21-23]. Whether conventional or nanoESI should be employed basically depends on the tendency of the respective compounds towards decomposition. Labile complexes or compounds that are strongly adhesive to surfaces are preferably ana-

lyzed by nanoESI to avoid long-lasting contamination of the sample supply line. Illustrative examples in this field are presented by the application of ESI to isopoly metal oxyanions [145], polyphosphates [146], transition metal complexes (Fig. 12.31) [24,147,148], and cadmium sulfide clusters [149]. Furthermore, the gas-phase reactions of electrosprayed metal complexes can be directly examined by tandem MS techniques (Chap. 9.18.1) [150-152].

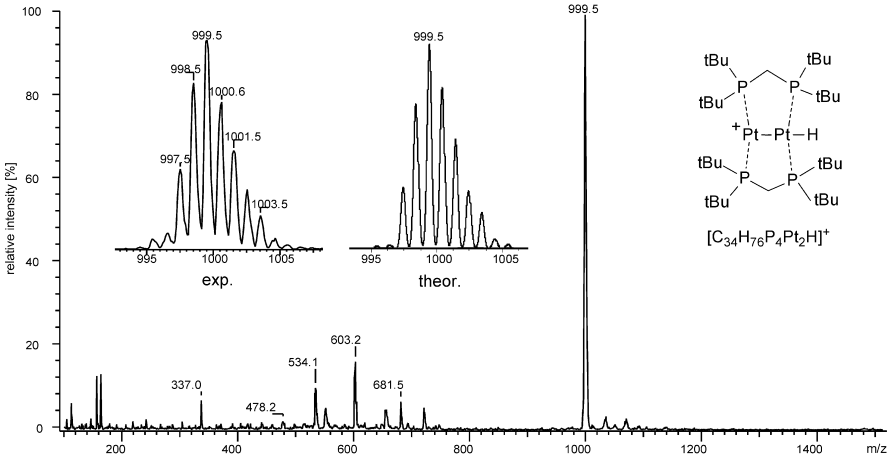


Fig. 12.31. Positive-ion ESI spectrum of a cationic dinuclear platinum hydride complex from dichloromethane solution. The *insets* compare experimental and theoretical isotopic patterns. By courtesy of P. Hofmann, Heidelberg University.

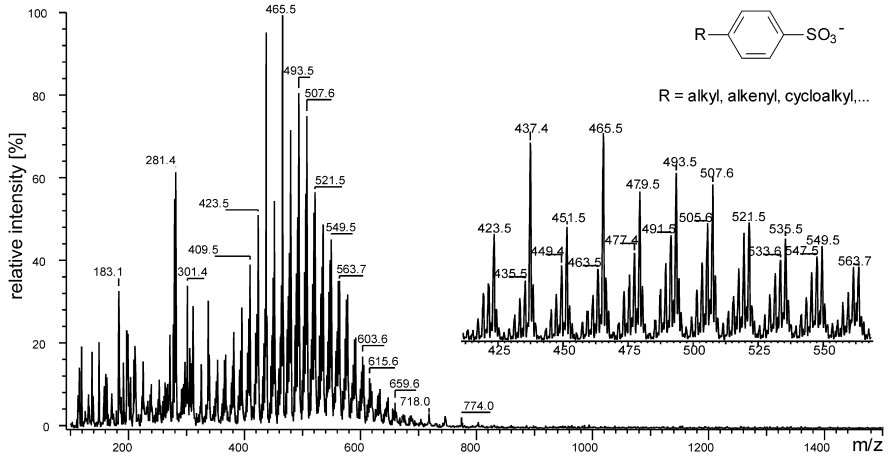


Fig. 12.32. Negative-ion ESI spectrum of an industrial cooling lubricant dissolved in 1-propanol at 1 : 1000. The dominant ions belong to alkylbenzene sulfonates. The *inset* expands the *m/z* 420–555 range, the most intensive peaks belonging to saturated alkyl chains. By courtesy of OMTEC GmbH, Eberbach.

12.6.3 ESI of Surfactants

Surfactants belong to a group of products where a low price is crucial, and therefore they are usually synthesized from coarsely defined mineral oil fractions or vegetable oils both of which represent (sometimes complex) mixtures (Fig. 12.32). Cationic and anionic surfactants are readily detected by ESI, but it also serves well for the detection of nonionic surfactants which tend to form $[M+alkali]^+$ or $[M–H]^-$ ions, respectively [153-157].

12.6.4 Oligonucleotides, DNA, and RNA

Negative-ion ESI is best suited for the analysis of *oligonucleotides*, *DNA*, and *RNA* [140]. While MALDI becomes difficult beyond oligonucleotide 20-mers, ESI can handle much larger molecules [158-161]. The problems associated with mass spectrometry of oligonucleotides are due to the often multiple exchange of protons versus alkali ions (Chap. 11.4.3). Instead of ion exchange beads, nitrogen bases have proven very helpful in removing alkali ions from solutions [162]. In particular, the addition of 25 mM imidazole and piperidine yields very clean spectra (Fig. 12.33) [163]. Even after cation removal, these polyanionic species are demanding targets for MS.

Conventionally, oligonucleotides are presented by starting from the 5-hydroxyl terminus and writing along the phosphodiester chain towards the 3-hydroxyl terminus, i.e., from the 5′ to the 3′ end or from the phosphate to the ribose, respectively (Fig. 12.34).

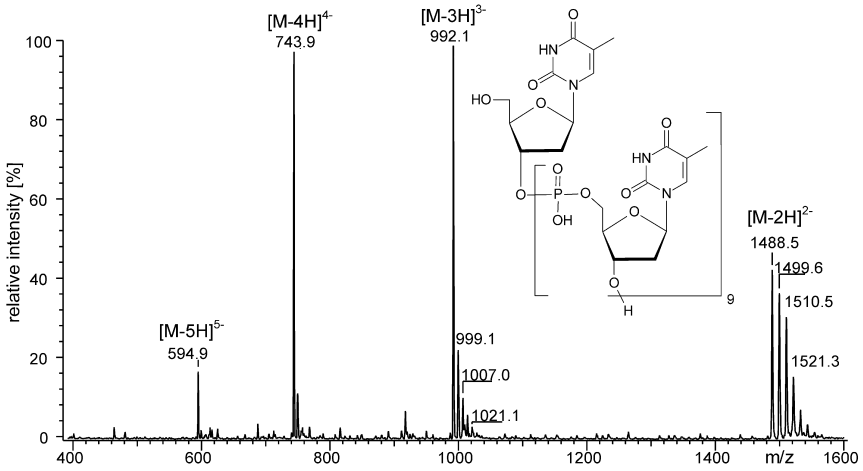


Fig. 12.33. Negative-ion ESI spectrum of the oligonucleotide dT_{10} in the presence of imidazole and piperidine. Here, H^+/Na^+ exchange is not completely suppressed. By courtesy of T. Krüger, University of Heidelberg.

Oligonucleotides built from *nucleotides* based on the furanose ribose are termed *ribonucleic acids* (RNAs), those based on deoxyribose are termed *deoxyribonucleic acids* (DNAs). The bases attached to the pentose moieties are nitrogen-rich heterocyclic compounds.

Sequencing of oligonucleotides by ESI-MS/MS techniques is also feasible [158,160,164,165]. Charged fragments of the 5′ end are denoted with letters and numerical subscripts from the beginning of the alphabet (*a*- to *d*-type ions) while fragments of the 3′ end are labeled as *w*- to *z*-type ions (Fig. 12.34) [166]. The bases on the riboses are denoted either without qualification as base B_n with the subscripts starting on the 5′ end or by using the one-letter code of the entire nucleotides.

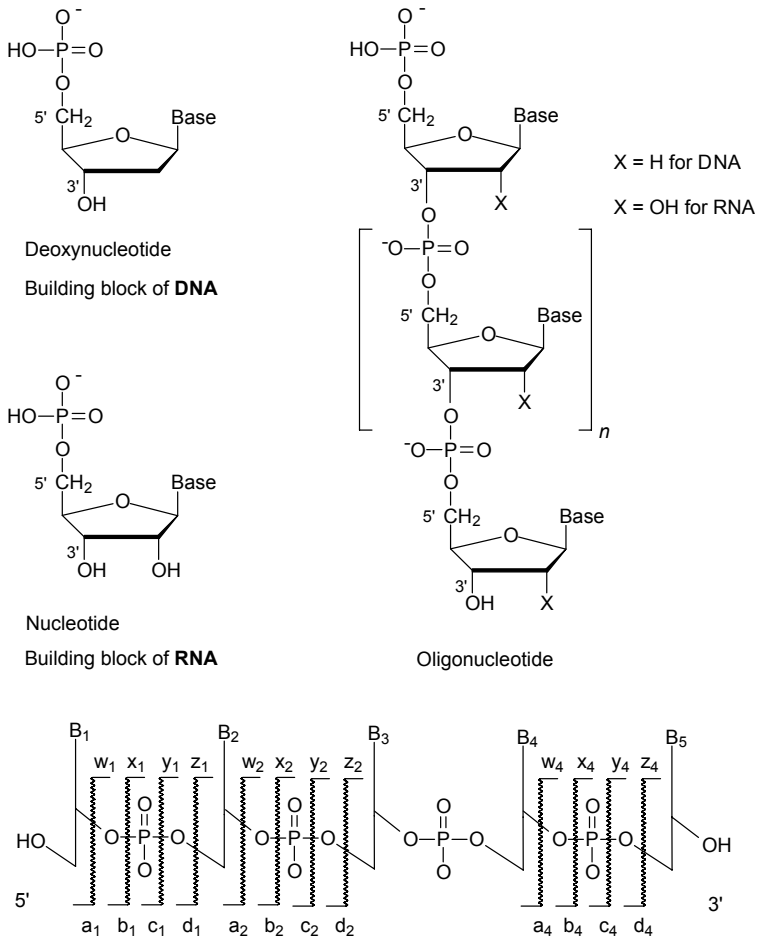


Fig. 12.34. Structures of nucleotides of DNA and RNA (*upper left*), general structure of oligonucleotides (*upper right*), and basic fragmentation scheme of oligonucleotides using the symbolized writing convention for the oligonucleotide backbone comprising furanose and *base (bottom*).

Example: The ESI-FT-ICR spectrum of $[M–4H]^{4–}$ ions of the phosphorothioate deoxyoligonucleotide 5′-GCCCAAGCTGGCATCCGTCA-3′ upon IRMPD exhibits numerous peaks corresponding to fragment ions of charge states from 1– to 4– (Fig. 12.35). This mass spectrum is greatly simplified upon charge deconvolution. Thanks to the resolving power of FT-ICR-MS, the assignment of charge states is absolutely reliable. In the resulting zero-charge spectrum, a_n-*B* and w_n fragment ions can be retrieved and the sequence thus derived [164].

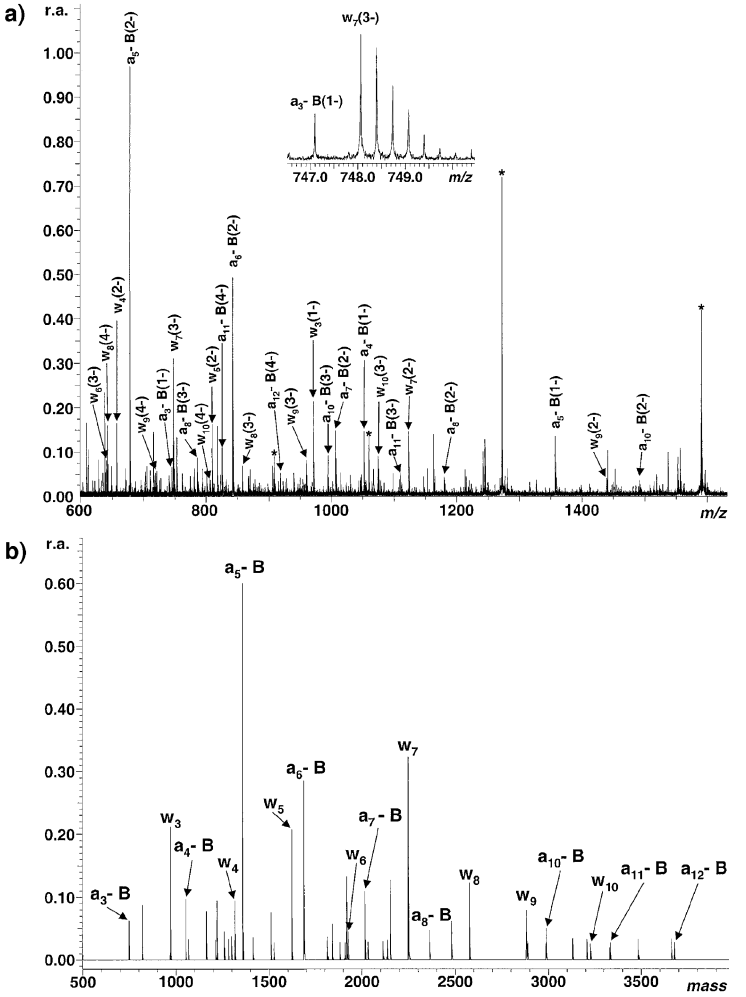


Fig. 12.35. ESI-FT-ICR IRMPD spectrum of negative ions of the phosphorothioate deoxyoligonucleotide 5′-GCCCAAGCTGGCATCCGTCA-3′. (**a**) The mass spectrum as obtained and (**b**) after charge deconvolution. Only the a_n-B and w_n fragment ions are labeled. In (**a**) peaks corresponding to residual precursor ions are labeled with an asterisk. The *inset* shows that closely spaced fragment ions can be resolved by FT-ICR-MS. Adapted from Ref. [164] with permission. © Elsevier, 2003.

12.6.5 ESI-MS of Oligosaccharides

Oligosaccharides [53,73,167,168] as well as closely related compounds such as glycoproteins [72,169], gangliosides [170], liposaccharides etc. are similar to oligonucleotides in that they require polar solvents and very soft ionization, in particular when the molecules are branched. As demonstrated by a large number of applications, ESI permits molecular weight determination and structure elucidation in these cases (Fig. 12.36; for a general fragmentation scheme cf. Chap. 11.5.3) [5].

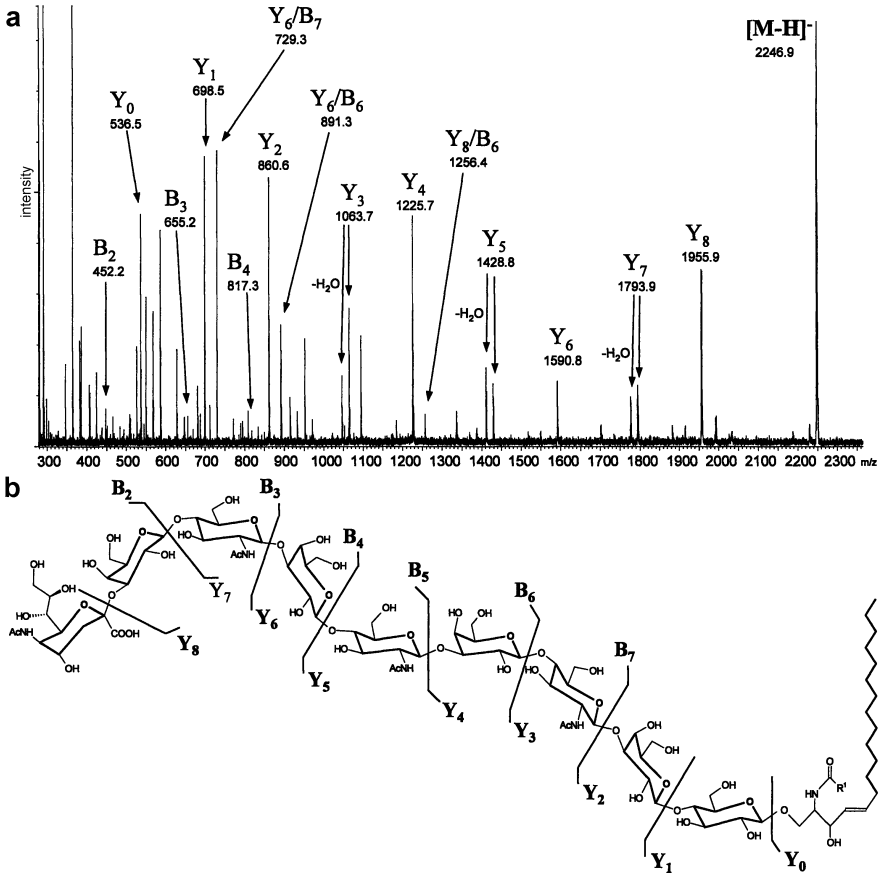


Fig. 12.36. (**a**) NanoESI-CID-MS/MS spectrum of the $[M–H]^-$ ion, *m/z* 2246.9, of a modified nonasaccharide obtained in a Q-TOF hybrid instrument and (**b**) proposed structure with fragments indicated. Reproduced from Ref. [170] by permission. © Elsevier Science, 2001.

12.6.6 High-Mass Proteins and Protein Complexes

The extraordinary high-mass capabilities of ESI allow for the analysis of proteins and protein complexes far beyond 10^6 u (> 1 MDa) [12,13,19,171,172]. Even though the resulting ions are formed in very high charge states special mass analyzers with an expanded *m/z* range are required for this type of research.

Example: The gram-negative spiral bacterium *Helicobacter pylori* is infecting almost half of the world's population. *H. pylori* possesses a very large multiprotein complex urease, which is essential for its survival in the acidic environment of the stomach. NanoESI has been used to establish the molecular weight of the 12-mer urease complex of 1,063,900 ± 600 u (Fig. 12.37) [13]. Spraying urease at higher concentration results in the formation of even larger protein complexes up to 48-mers of > 4 MDa that are detected at up to about *m/z* 27,000 corresponding to charge states of > 180+.

a)

m/z	charge	mass	org.
12364	86	1063226	$(\alpha\beta)_{12}$
12510	85	1063297	$(\alpha\beta)_{12}$
12660	84	1063434	$(\alpha\beta)_{12}$
12816	83	1063653	$(\alpha\beta)_{12}$
12976	82	1064003	$(\alpha\beta)_{12}$
13141	81	1064344	$(\alpha\beta)_{12}$

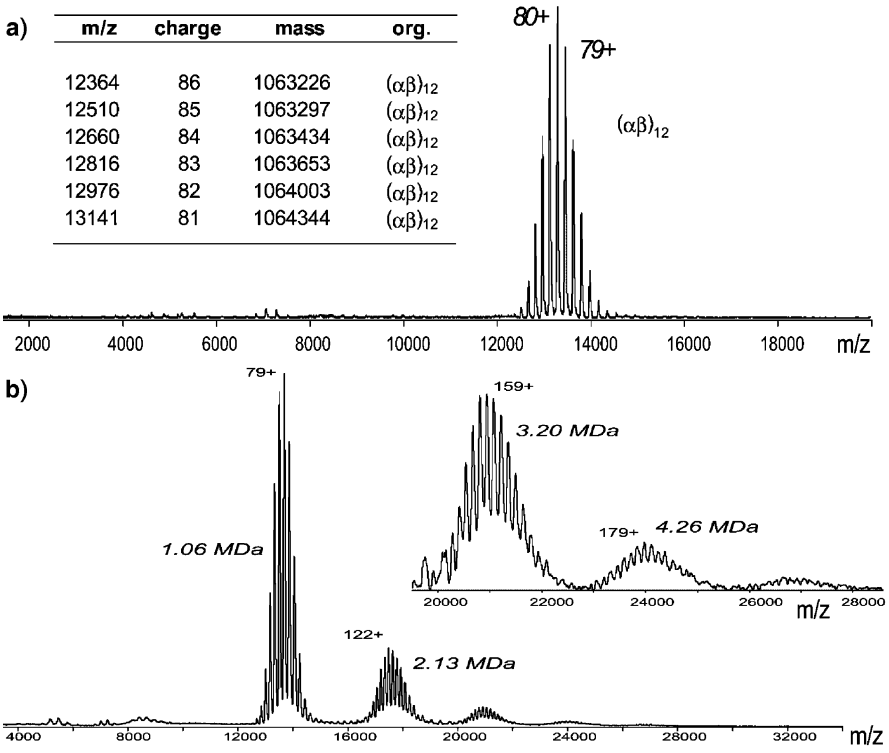


Fig. 12.37. NanoESI spectra of urease in 200 μM ammonium acetate at pH 8.0. (**a**) Using 20 μM urease mainly delivers $(\alpha\beta)_{12}$ subunits while (**b**) 40 μM concentration of the urease monomer also yield 24-, 36-, and even 48-mers. Adapted from Ref. [13] with permission. © Wiley Periodicals, Inc., 2004.

Note: ESI is soft enough to preserve noncovalent bonds during the sequence of ion liberation from solution into the gas phase. This can be observed by the formation of solvent adducts, cluster ions, and in particular, by its ability to deliver protein complexes and other supramolecular systems into the gas phase [139,171,172].

The question of whether or not proteins preserve their solution structure during ESI-MS has been addressed by Breuker and McLafferty [172]. According to their discussion, a protein ion loses the last hundred or so water molecules that are forming a monolayer around it during the very last steps of ion desolvation on the nanosecond timescale. The loss of water is accompanied by strong cooling of the protein ion, which finally collapses within several picoseconds as its exterior ionic interactions have been lost. Then, much slower during several milliseconds, the protein undergoes loss of hydrophobic bonding and of electrostatic interactions before it stabilizes over seconds to a final gas-phase conformation that is different from its native structure in solution. Due to the limited life time of the ions in normal ESI operation only the steps down to the cold exterior-collapsed structure can take place (Fig. 12.38).

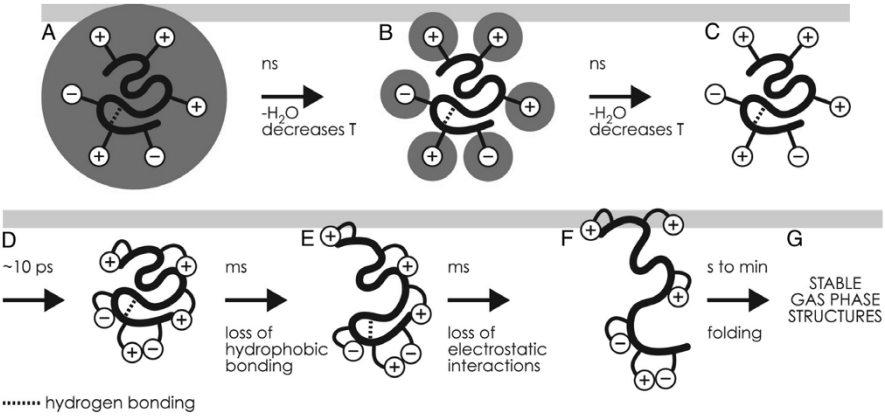


Fig. 12.38. Stepwise protein desolvation (A → C), denaturization to an exterior-collapsed structure (D) and refolding to a stable gas-phase structure (D → G) in transit from native solution phase to gas phase. Reproduced from Ref. [172] with permission. © The National Academy of Sciences of the USA, 2008.

12.7 Summary of ESI Characteristics

As a general rule, ESI-MS can successfully be applied when the analyte is intrinsically ionic or can easily be transformed in solution phase to become ionic by protonation, deprotonation, cation attachment, or anion attachment. Thus, ESI can handle medium polar to ionic analytes from as low as 10 u to as high as 10^6 u in

mass. ESI can deal equally well with ions of both polarities, whereas neutral analytes are not suitable (Table 12.1). The solvent may vary from volatile, nonpolar, and aprotic to moderately volatile, highly polar, and protic, e.g., diethylether, tetrahydrofuran, dichloromethane, trichloromethane, isopropanol, methanol, acetonitrile, water, and mixtures of these. Up to about 10% of dimethylsulfoxide or dimethylformamide can be tolerated in aqueous or methanolic solution. The addition of volatile acids or bases to promote ion formation is frequently employed. Volatile buffers and low concentrations of alkali ions ($< 10^{-3}$ M) to promote cationization can be tolerated.

As a rule of thumb, less volatile solvents call for more sheath (nebulizer) gas (typical range is 0–2 l min^{-1}) and higher temperature of the desolvation gas or heated capillary (typical range is 120–250°C), respectively. Both, insufficient desolvation and too strong desolvation will cause the ion formation to cease.

The importance of ESI for LC-MS can be inferred from its wide range of analyte acceptance in terms of both polarity and mass. A graphical representation of the molecular weight and analyte polarity ranges covered by ESI, APCI, and APPI is best suited to give and impression of the preferred fields of application for these methods (Fig. 12.39). APCI and APPI, on the other hand, are very similar in coverage as both are accessing the lower left segment of the polarity-mass plane in this illustration. (APCI and APPI will be discussed in Sects. 12.8 and 12.9 following below.)

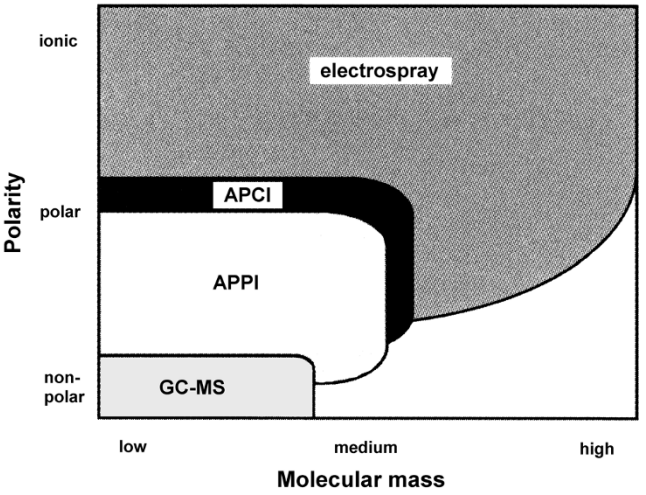


Fig. 12.39. ESI features a wide range of analyte acceptance in terms of both polarity and mass to handle medium polar to ionic analytes while APCI and APPI give access to the lower left segment of the polarity-mass plane. Adapted with permission of U. Karst from cover illustration of *Anal. Bioanal. Chem.* **378**(4), 2004. © Springer, Heidelberg, 2004.

12.7.1 Sample Consumption

Sample consumption is chiefly determined by the concentration of the analyte solution and the liquid flow. For example, during a 1-min measurement conventional ESI consumes 4 pmol of sample when a 10^{-6} M solution is delivered at a flow rate of 4 µl min^{-1}. For nanoESI this reduces to 40 fmol for the same solution at 40 nl min^{-1}. Modern instruments often allow for much lower sample consumption.

12.7.2 Types of Ions in ESI

Very similar to the previously introduced desorption methods ESI produces a variety of ions depending on the polarity of the analyte, the characteristics of the solvent, and on the presence or absence of impurities such as alkali metal ions. Radical ions are normally not observed. (Table 12.1).

Table 12.1. Ions formed by ESI

Analytes	Positive ions	Negative ions
nonpolar	$[M+H]^+$, $[M+alkali]^+$ if any	$[M–H]^–$, $[M+A]^–$ if any
medium to high polarity	$[M+H]^+$, $[M+alkali]^+$ *exchange* $[M–H_n+alkali_{n+1}]^+$ {*clusters* $[2M+H]^+$, $[2M+alkali]^+$, *adducts* $[M+solv+H]^+$, $[M+solv+alkali]^+$}[b]	$[M–H]^–$, $[M+A]^–$ *exchange* $[M–H_n+alkali_{n–1}]^–$ {*clusters* $[2M–H]^–$ *adducts* $[M+solv–H]^–$}
ionic[a]	C^+, $[C_n+A_{n–1}]^+$	$A^–$, $[C_{n–1}+A_n]^–$

[a] comprising cation C^+ and anion $A^–$
[b] enclosure in parentheses denotes less abundant species

12.7.3 Mass Analyzers for ESI

ESI ion sources are offered in combination with all types of mass analyzers, i.e., one is essentially free to choose any mass analyzer according to the analytical requirements. As fragment ions in ESI are often absent or at least exhibit very low abundance, analyzers capable of tandem MS are preferred.

12.8 Atmospheric Pressure Chemical Ionization

Ion–molecule reactions occurring at atmospheric pressure are employed for analyte ion production in *atmospheric pressure chemical ionization* (APCI). Basically, APCI represents an atmospheric pressure variant of vacuum chemical ionization (CI, Chap. 7). In APCI the reagent ion plasma is maintained by a corona discharge between the sharp tip of a needle and the spray chamber serving as the counter electrode.

12.8.1 Ion Sources for APCI

The ions are transferred into the mass analyzer by use of the same atmosphere-to-vacuum interface as employed in ESI. Therefore, ESI sources can easily be switched to APCI operation. To do so, the ESI spray head is exchanged for a unit comprising a pneumatic nebulizer and a heated spray chamber with a needle electrode mounted in front of the sampling orifice, while the atmosphere-to-vacuum interface stays in place (Fig. 12.40) [51,173]. Different from ESI, APCI requires high liquid flow (200–1000 µl min^{-1}) for effective vaporization.

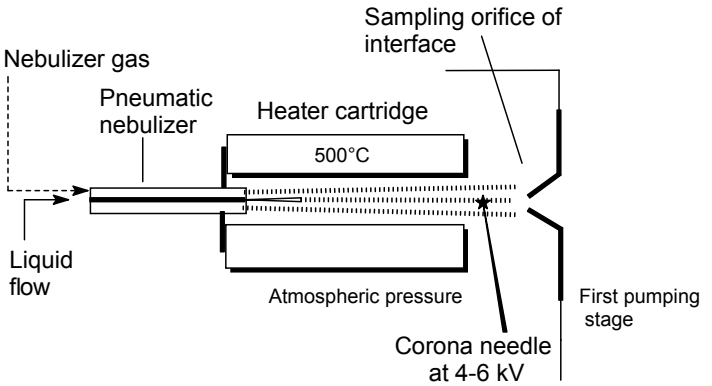


Fig. 12.40. APCI source. The liquid flow is pneumatically sprayed into a heated vaporizer where ionization is initiated by a corona discharge at atmospheric pressure. The sampling orifice and interface region behind remain unaltered by ESI.

Note: The significant enhancement of primary ion formation by a corona discharge as compared to a ^{63}Ni source has been implemented in early API sources, a context in which a basic APCI process has already been described (Eqs. 12.1–12.6 in Chap. 12.1.1) [174,175]. The corona needle employed to expand the acceptance range of TSP basically represents an APCI mode for these sources, too [28].

12.8.2 Ion Formation in APCI

In APCI, there is no spray voltage as nebulization is effected by action of the pneumatic nebulizer alone. The transformation of the aerosol into a vapor composed of solvent and highly diluted sample is then performed in a heater cartridge set to about 500°C. Although rather high temperature is used for vaporization, APCI is normally softer than conventional CI because *i*) the sample does not necessarily achieve the thermal equilibrium with the heater cartridge and *ii*) thermalization of the ions by soft collisions provide an effective "drain" for the energy liberated by exothermal protonation.

It is the greatest advantage of APCI over ESI that it actively generates ions from neutrals. Thus, APCI provides the means of applying low- to medium-polarity analytes eluting from a liquid chromatograph to mass spectrometry [176]. The use of APCI rapidly grew in the mid-1990, perhaps because by then elaborate vacuum interfaces had become available from ESI technology. Nowadays, APCI is used where LC separation is required, but ESI is not applicable to the compound class of interest [28,176-178].

12.8.3 APCI Spectra

The nature of the APCI plasma varies widely as both solvent and nebulizing gas contribute to the composition of the CI plasma, and thus, APCI spectra can resemble PICI, CECI, NICI, or EC spectra (Chap. 7.2–7.4) depending on the actual conditions and ion polarity. The influence of solvent components, temperature and other parameters explains why APCI conditions suffer from comparatively low reproducibility as compared to other ionization methods.

Example I: Liquid chromatographic separation of triacylglycerols from soybean oil delivered dozens of fats differing in type and combination of fatty acids. The positive-ion APCI mass spectra of two selected triacylglycerols, triolein (OOO) and 1(3)-palmitoyl-2-stearoyl-3(1)-linoleoyl glycerol (PSL), are shown in Fig. 12.41 [177]. The APCI spectra exhibit $[M+H]^+$ ions and fragment ions characteristic of fatty acid composition and – to a certain degree – of isomers. While triolein can only form one distinctive diacyl fragment $[OO]^+$, the other fat yields $[PS]^+$, $[PL]^+$, and $[LS]^+$ as primary fragment ions. The fatty acids themselves are also revealed by their acylium ions in the low-mass range.

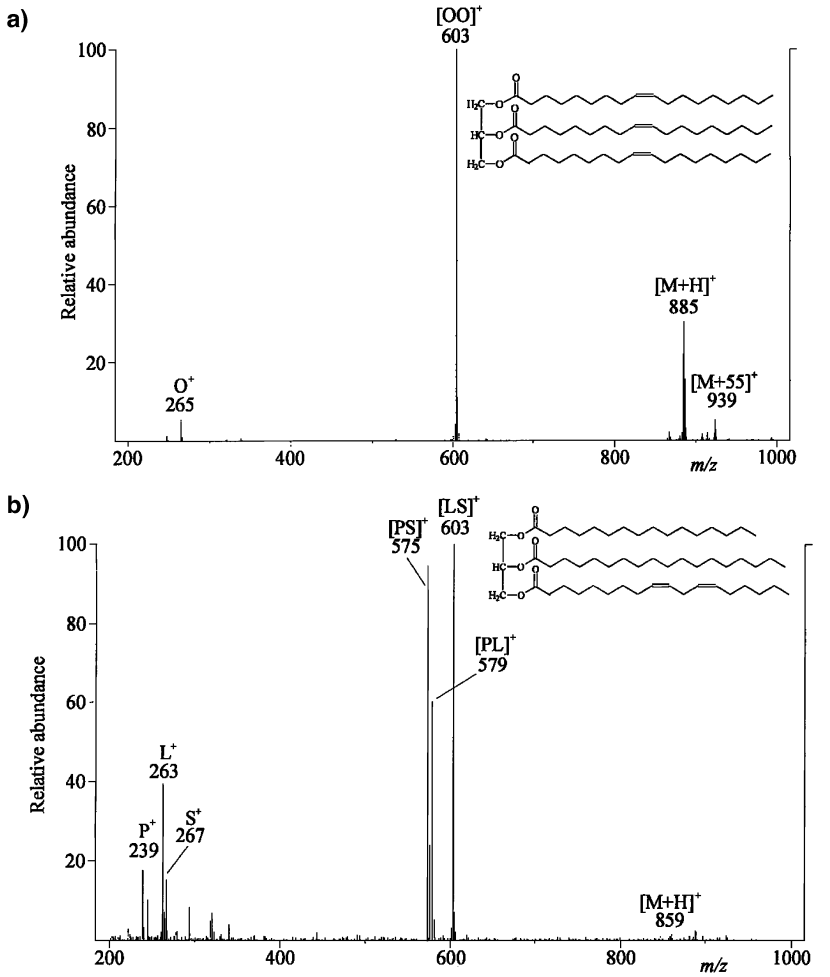


Fig. 12.41. Positive-ion APCI mass spectra of (**a**) triolein (OOO) and (**b**) 1(3)-palmitoyl-2-stearoyl-3(1)-linoleoyl glycerol (PSL) from soybean oil. The $[M+55]^+$ ion in (**a**) is a solvent (proprionitrile) adduct. Reproduced from Ref. [177] with permission. © John Wiley & Sons, Ltd, 1997.

Example II: Negative-ion APCI spectra of alkylamino derivatives of 4-chloro-7-nitrobenzofurazan (NBDCl) were measured from acetonitrile/methanol solution. Wile the *N*,*N*-dimethylamino derivative preferably forms the radical anion, $M^{-\bullet}$, *m/z* 208, the *N*-ethyl isomer prefers the $[M–H]^-$ ion, *m/z* 207. This major change in spectral appearance is due to the missing slightly acidic hydrogen in the NBDCl isomer with the tertiary amino group. This demonstrates the strong influence of analyte structure on negative-ion (AP)CI spectra (Fig. 12.42) [179,180].

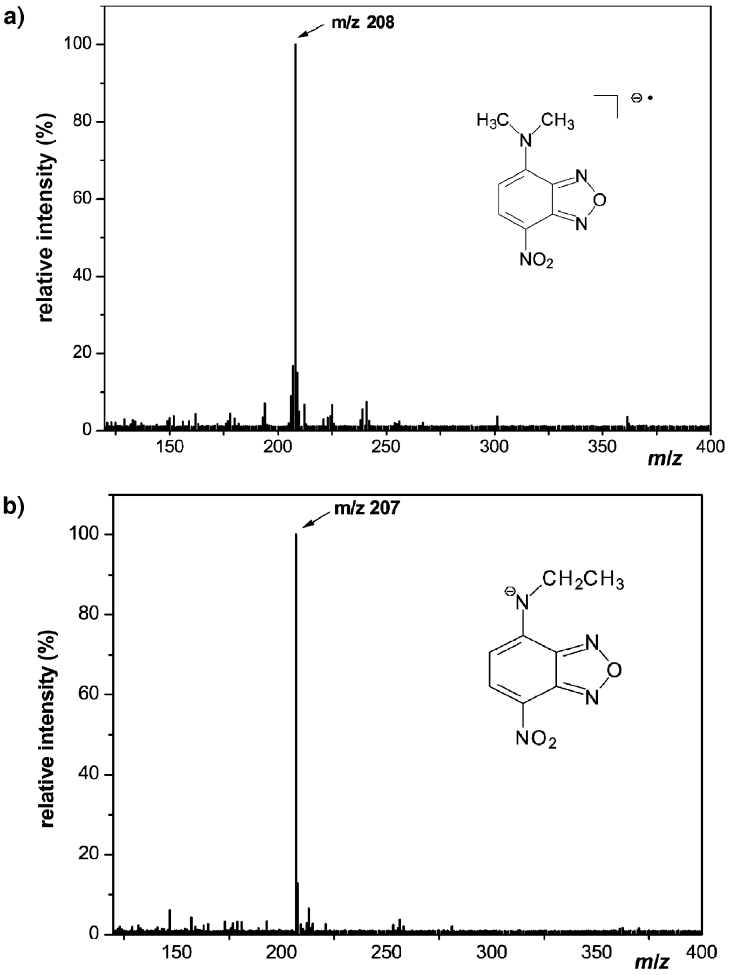


Fig. 12.42. Negative-ion APCI spectra of alkylamino derivatives of 4-chloro-7-nitrobenzofurazan (NBDCl). (**a**) The *N*,*N*-dimethylamino derivative preferably forms the radical anion, $M^{-\bullet}$, while (**b**) the *N*-ethyl form prefers the $[M–H]^-$ ion. Adapted from Ref. [180] with permission. © The Royal Society of Chemistry, 2002.

12.9 Atmospheric Pressure Photoionization

More recently, *atmospheric pressure photoionization* (APPI) has been introduced [181] as a complement or alternative to APCI [176,182,183]. In APPI, a UV light source replaces the corona discharge-powered plasma, while the pneumatic sprayer and the heated vaporizer remain almost unaffected (Fig. 12.43) [184-186]. The most relevant modification is the use of a quartz tube to guide the hot vapor toward the sampling orifice. Quartz is required to transmit the UV light emitted by a noble gas discharge lamp.

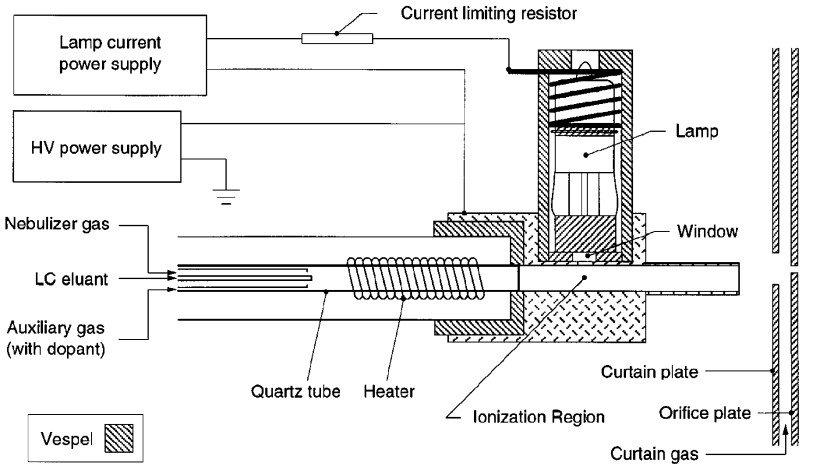


Fig. 12.43. APPI source comprising the heated nebulizer probe, photoionization UV lamp and mounting bracket. Reproduced from Ref. [181] by permission. © American Chemical Society, 2000.

Note: Modern instruments with atmospheric pressure ion sources are all constructed as to permit easy exchange of spray heads for rapid switching between ESI, APCI, and APPI [184]. There is no interruption of instrument vacuum and mounting of spray heads takes just a minute, but there is a 10–15-min delay for APCI or APPI vaporizers to fully heat up for operation or to sufficiently cool down before removal is possible without risk of injury from hot parts.

12.9.1 Ion Formation in APPI

Statistically, the light emitted by the UV lamp will be absorbed by solvent molecules or eventually by nitrogen used for spraying rather than by the analyte molecules. Therefore, the energy of the UV photons and the ionization energies of the compounds are decisive for the initiation of the APPI process (Fig. 12.44) [186].

Provided the analyte (AB) has a UV chromophore, direct *photoionization* of AB may occur (Chap. 2.10.4), but as explained above, is rarely observed. Often, photon absorption just causes photoexcitation instead of photoionization [186]:

$$AB + h\nu \rightarrow AB^* \qquad \textit{photoexcitation} \qquad (12.11)$$

$$AB + h\nu \rightarrow AB^* \rightarrow AB^{+\bullet} + e^- \qquad \textit{photoionization} \qquad (12.12)$$

Electronically excited molecules AB* can either undergo radiative decay, photodissociation, or collisional quenching with neutrals (N), or can form ions by ejection of an electron:

$$AB^* \rightarrow AB + h\nu \qquad \textit{radiative decay} \qquad (12.13)$$

$$AB^* \rightarrow A^{\bullet} + B^{\bullet} \qquad \textit{photodissociation} \qquad (12.14)$$

$$AB^* + N \rightarrow AB + N^* \qquad \textit{collisional quenching} \qquad (12.15)$$

$$AB^* \rightarrow AB^{+\bullet} + e^- \qquad \textit{ionization} \qquad (12.16)$$

Even if ions $AB^{+\bullet}$ have formed they can be neutralized by recombination with free electrons present in the plasma, eventually along with moderating ion–neutral collisions:

$$AB^{+\bullet} + e^- \rightarrow AB^* \qquad \textit{recombination} \qquad (12.17)$$

$$AB^{+\bullet} + e^- + N \rightarrow AB + e^- + N \qquad \textit{moderated recombination} \qquad (12.18)$$

Instead of relying on one of the above ionization processes to occur, a chemical ionization process where the reactant ions are formed by photoionization of a reagent gas is normally preferred. If the solvent (S) cannot be photoionized to play this role, a UV-absorbing dopant (D) may be added [185,187-189]. The dopant ions may then react with the analyte by charge transfer

$$D^{+\bullet} + AB \rightarrow AB^{+\bullet} + D \qquad \textit{charge transfer} \qquad (12.19)$$

or lead to the formation of solvent ions that finally act as reactant ions to protonate the analyte molecules [186]:

$$D^{+\bullet} + S \rightarrow [D\text{–}H]^{\bullet} + [S+H]^+ \qquad \textit{reactant ion formation} \qquad (12.20)$$

$$[S+H]^+ + AB \rightarrow S + [AB+H]^+ \qquad \textit{proton transfer} \qquad (12.21)$$

For example, methanol cannot be ionized by the frequently employed krypton lamp, but addition of some acetone as dopant will allow the processes described in Eqs. 12.19–12.21 to occur. Obviously, rich chemistry is involved until the neutral analyte has been transformed into $AB^{+\bullet}$ or $[AB+H]^+$ ions with sufficient efficiency.

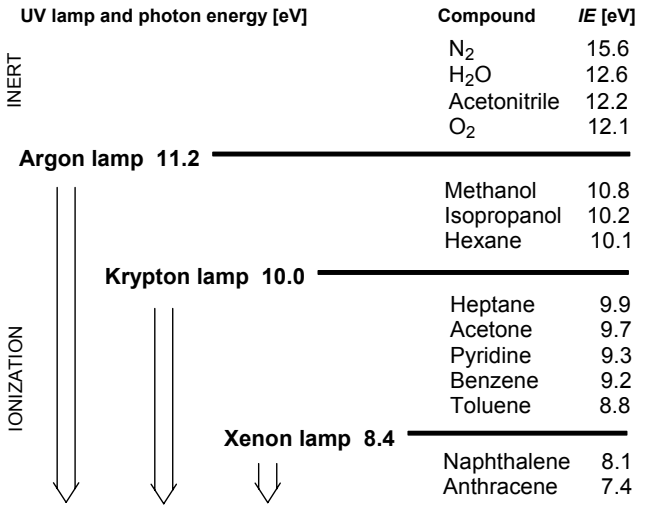


Fig. 12.44. Relationship between UV lamps and their photon energies used for APPI and ionization energies of typical compounds.

12.9.2 APPI Spectra

The appearance of APPI spectra strongly depends on the actual combination of UV lamp, solvent, analyte, and eventually dopant. It is not always straightforward to predict whether protonation or molecular ion formation will dominate a positive-ion APPI spectrum, and analogously, whether deprotonation or radical anion formation will be observed in negative-ion mode. As a rule of thumb, basic molecules tend to appear as $[M+H]^+$ ions while nonpolar analytes preferably form $M^{+\bullet}$ ions. Vice versa, acidic molecules easily deliver $[M–H]^-$ ions in negative-ion mode while those of high electron affinity may undergo electron capture to yield $M^{-\bullet}$ ions. Unfortunately, APPI tends towards mixed ion formation, e.g., $M^{+\bullet}$ beside $[M+H]^+$ ions, a property it has in common with FAB (Chap. 10). Some typical APPI spectra are compiled below (Fig. 12.45) [181,185,187,190].

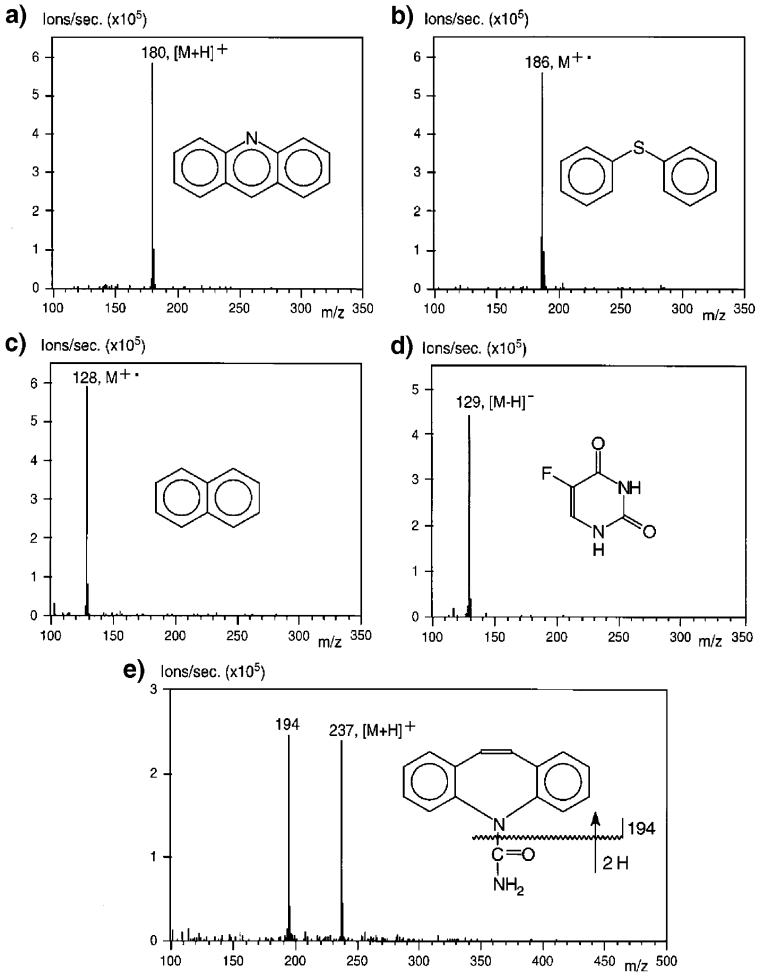


Fig. 12.45. APPI spectra of (**a**) acridine, (**b**) diphenyl sulfide, (**c**) naphthalene, (**d**) 5-fluorouracil, and (**e**) carbamazepine. Adapted from Ref. [181] with permission. © American Chemical Society, 2000.

References

1. *Mass Spectrometry in Drug Discovery;* Rossi, D.T.; Sinz, M.W. (eds.); Marcel Dekker: New York, 2002.
2. *Modern Mass Spectrometry;* Schalley, C.A. (ed.); Springer: New York, 2003.
3. Ardrey, R.E. *Liquid Chromatography-Mass Spectrometry – An Introduction;* Wiley: Chichester, 2003.
4. Siuzdak, G. *The Expanding Role of Mass Spectrometry in Biotechnology,* 2nd ed.; MCC Press: San Diego, 2006.
5. Lehmann, W.D. *Massenspektrometrie in der Biochemie;* Spektrum Akademischer Verlag: Heidelberg, 1996.
6. *Electrospray Ionization Mass Spectrometry – Fundamentals, Instrumentation and Applications;* Dole, R.B. (ed.); Wiley: Chichester, 1997.
7. Roboz, J. *Mass Spectrometry in Cancer Research;* CRC Press: Boca Raton, 1999.
8. *Mass Spectrometry of Proteins and Peptides;* Chapman, J.R. (ed.); Humana Press: Totowa, 2000.
9. *Applied Electrospray Mass Spectrometry;* Pramanik, B.N.; Ganguly, A.K.; Gross, M.L. (eds.); Marcel Dekker: New York, 2002.
10. Amad, M.H.; Cech, N.B.; Jackson, G.S.; Enke, C.G. Importance of Gas-Phase Proton Affinities in Determining the Electrospray Ionization Response for Analytes and Solvents. *J. Mass Spectrom.* **2000,** *35*, 784-789.
11. Schalley, C.A. Supramolecular Chemistry Goes Gas Phase: the Mass Spectrometric Examination of Noncovalent Interactions in Host-Guest Chemistry and Molecular Recognition. *Int. J. Mass Spectrom.* **2000,** *194*, 11-39.
12. Cristoni, S.; Bernardi, L.R. Development of New Methodologies for the Mass Spectrometry Study of Bioorganic Macromolecules. *Mass Spectrom. Rev.* **2003,** *22*, 369-406.
13. Heck, A.J.R.; van den Heuvel, R.H.H. Investigation of Intact Protein Complexes by Mass Spectrometry. *Mass Spectrom. Rev.* **2004,** *23*, 368-389.
14. Fenn, J.B.; Mann, M.; Meng, C.K.; Wong, S.F.; Whithouse, C.M. *Science* **1989,** *246*, 64-71.
15. Fenn, J.B.; Mann, M.; Meng, C.K.; Wong, S.F. Electrospray Ionization – Principles and Practice. *Mass Spectrom. Rev.* **1990,** *9*, 37-70.
16. Smith, R.D.; Loo, J.A.; Edmonds, C.G.; Barinaga, C.J.; Udseth, H.R. New Developments in Biochemical Mass Spectrometry: Electrospray Ionization. *Anal. Chem.* **1990,** *62*, 882-899.
17. Fenn, J.B. Electrospray: Wings for Molecular Elephants (Nobel Lecture). *Angew. Chem. Int. Ed.* **2003,** *42*, 3871-3894.
18. Fuerstenau, S.D.; Benner, W.H. Molecular Weight Determination of Megadalton DNA Electrospray Ions Using Charge Detection Time-of-Flight Mass Spectrometry. *Rapid Commun. Mass Spectrom.* **1995,** *9*, 1528-1538.
19. Fuerstenau, S.D.; Benner, W.H.; Thomas, J.J.; Brugidou, C.; Bothner, B.; Suizdak, G. Mass Spectrometry of an Intact Virus. *Angew. Chem., Int. Ed.* **2001,** *40*, 541-544.
20. Felitsyn, N.; Peschke, M.; Kebarle, P. Origin and Number of Charges Observed on Multiply-Protonated Native Proteins Produced by ESI. *Int. J. Mass Spectrom.* **2002,** *219*, 39-62.
21. Colton, R.; D'Agostino, A.; Traeger, J.C. Electrospray Mass Spectrometry Applied to Inorganic and Organometallic Chemistry. *Mass Spectrom. Rev.* **1995,** *14*, 79-106.
22. Traeger, J.C. Electrospray Mass Spectrometry of Organometallic Compounds. *Int. J. Mass Spectrom.* **2000,** *200*, 387-401.
23. Henderson, W.; McIndoe, S.J. *Mass Spectrometry of Inorganic and Organometallic Compounds;* Wiley: Chichester, 2005.
24. Poon, G.K.; Bisset, G.M.F.; Mistry, P. Electrospray Ionization Mass Spectrometry for Analysis of Low-Molecular-Weight Anticancer Drugs and Their Analogs. *J. Am. Soc. Mass Spectrom.* **1993,** *4*, 588-595.
25. Winger, B.E.; Light-Wahl, K.J.; Ogorzalek Loo, R.R.; Udseth, H.R.; Smith, R.D. Observation and Implications of High Mass-to-Charge Ratio Ions from Electrospray Ionization Mass Spectrometry. *J. Am. Soc. Mass Spectrom.* **1993,** *4*, 536-545.

26. Wang, Y.; Schubert, M.; Ingendoh, A.; Franzen, J. Analysis of Non-Covalent Protein Complexes Up to 290 KDa Using Electrospray Ionization and Ion Trap Mass Spectrometry. *Rapid Commun. Mass Spectrom.* **2000,** *14*, 12-17.
27. Sobott, F.; Hernández, H.; McCammon, M.G.; Tito, M.A.; Robinson, C.V. A Tandem Mass Spectrometer for Improved Transmission and Analysis of Large Macromolecular Assemblies. *Anal. Chem.* **2002,** *74*, 1402-1407.
28. Covey, T.R.; Thomson, B.A.; Schneider, B.B. Atmospheric Pressure Ion Sources. *Mass Spectrom. Rev.* **2009,** *28*, 870-897.
29. Horning, E.C.; Horning, M.G.; Carroll, D.I.; Dzidic, I.; Stillwell, R.N. New Picogram Detection System Based on a Mass Spectrometer with an External Ionization Source at Atmospheric Pressure. *Anal. Chem.* **1973,** *45*, 936-943.
30. Horning, E.C.; Carroll, D.I.; Dzidic, I.; Haegele, K.D.; Horning, M.G.; Stillwell, R.N. Atmospheric Pressure Ionization (API) Mass Spectrometry. Solvent-Mediated Ionization of Samples Introduced in Solution and in a Liquid Chromatograph Effluent Stream. *J. Chromatogr. Sci.* **1974,** *12*, 725-729.
31. Carroll, D.I.; Dzidic, I.; Stillwell, R.N.; Horning, M.G.; Horning, E.C. Subpicogram Detection System for Gas Phase Analysis Based Upon Atmospheric Pressure Ionization (API) Mass Spectrometry. *Anal. Chem.* **1974,** *46*, 706-704.
32. Blakley, C.R.; Carmody, J.J.; Vestal, M.L. A New Soft Ionization Technique for Mass Spectrometry of Complex Molecules. *J. Am. Chem. Soc.* **1980,** *102*, 5931-5933.
33. Blakley, C.R.; Vestal, M.L. Thermospray Interface for Liquid Chromatography/Mass Spectrometry. *Anal. Chem.* **1983,** *55*, 750-754.
34. Vestal, M.L. Studies of Ionization Mechanisms Involved in Thermospray LC-MS. *Int. J. Mass Spectrom. Ion Phys.* **1983,** *46*, 193-196.
35. Wilkes, J.G.; Freeman, J.P.; Heinze, T.M.; Lay, J.O., Jr.; Vestal, M.L. AC Corona-Discharge Aerosol-Neutralization Device Adapted to Liquid Chromatography/Particle Beam/Mass Spectrometry. *Rapid Commun. Mass Spectrom.* **1995,** *9*, 138-142.
36. Vestal, M.L. High-Performance Liquid Chromatography-Mass Spectrometry. *Science* **1984,** *226*, 275-281.
37. Evans, C.A., Jr.; Hendricks, C.D. Electrohydrodynamic Ion Source for the Mass Spectrometry of Liquids. *Rev. Sci. Inst.* **1972,** *43*, 1527-1530.
38. Simons, D.S.; Colby, B.N.; Evans, C.A., Jr. Electrohydrodynamic Ionization Mass Spectrometry. Ionization of Liquid Glycerol and Nonvolatile Organic Solutes. *Int. J. Mass Spectrom. Ion Phys.* **1974,** *15*, 291-302.
39. Zeleny, J. Instability of Electrified Liquid Surfaces. *Phys. Rev.* **1917,** *10*, 1-7.
40. Taylor, G.I. Disintegration of Water Drops in an Electric Field. *Proc. Royal Soc. London A* **1964,** *280*, 383-397.
41. Lord Rayleigh on the Equilibrium of Liquid Conducting Masses Charged with Electricity. *London, Edinburgh, Dublin Phil. Mag. J. Sci.* **1882,** *14*, 184-186.
42. Dülcks, T.; Röllgen, F.W. Ionization Conditions and Ion Formation in Electrohydrodynamic Mass Spectrometry. *Int. J. Mass Spectrom. Ion Proc.* **1995,** *148*, 123-144.
43. Dülcks, T.; Röllgen, F.W. Ion Source for Electrohydrodynamic Mass Spectrometry. *J. Mass Spectrom.* **1995,** *30*, 324-332.
44. Cook, K.D. Electrohydrodynamic Mass Spectrometry. *Mass Spectrom. Rev.* **1986,** *5*, 467-519.
45. Dole, M.; Mack, L.L.; Hines, R.L.; Mobley, R.C.; Ferguson, L.D.; Alice, M.B. Molecular Beams of Macroions. *J. Chem. Phys.* **1968,** *49*, 2240-2249.
46. Dole, M.; Hines, R.L.; Mack, L.L.; Mobley, R.C.; Ferguson, L.D.; Alice, M.B. Gas Phase Macroions. *Macromolecules* **1968,** *1*, 96-97.
47. Gieniec, J.; Mack, L.L.; Nakamae, K.; Gupta, C.; Kumar, V.; Dole, M. Electrospray Mass Spectroscopy of Macromolecules: Application of an Ion-Drift Spectrometer. *Biomed. Mass Spectrom.* **1984,** *11*, 259-268.
48. Yamashita, M.; Fenn, J.B. Electrospray Ion Source. Another Variation on the Free-Jet Theme. *J. Phys. Chem.* **1984,** *88*, 4451-4459.
49. Yamashita, M.; Fenn, J.B. Negative Ion Production with the Electrospray Ion Source. *J. Phys. Chem.* **1984,** *88*, 4671-4675.

50. Whitehouse, C.M.; Robert, R.N.; Yamashita, M.; Fenn, J.B. Electrospray Interface for Liquid Chromatographs and Mass Spectrometers. *Anal. Chem.* **1985,** *57*, 675-679.
51. Bruins, A.P. Mass Spectrometry with Ion Sources Operating at Atmospheric Pressure. *Mass Spectrom. Rev.* **1991,** *10*, 53-77.
52. Kebarle, P.; Tang, L. From Ions in Solution to Ions in the Gas Phase – The Mechanism of Electrospray Mass Spectrometry. *Anal. Chem.* **1993,** *65*, 972A-986A.
53. Karas, M.; Bahr, U.; Dülcks, T. Nano-Electrospray Ionization Mass Spectrometry: Addressing Analytical Problems Beyond Routine. *Fresenius J. Anal. Chem.* **2001,** *366*, 669-676.
54. Anacleto, J.F.; Pleasance, S.; Boyd, R.K. Calibration of Ion Spray Mass Spectra Using Cluster Ions. *Org. Mass Spectrom.* **1992,** *27*, 660-666.
55. Hop, C.E.C.A. Generation of High Molecular Weight Cluster Ions by Electrospray Ionization; Implications for Mass Calibration. *J. Mass Spectrom.* **1996,** *31*, 1314-1316.
56. Kantrowitz, A.; Grey, J. High Intensity Source for the Molecular Beam. I. Theoretical. *Rev. Sci. Inst.* **1951,** *22*, 328-332.
57. Fenn, J.B. Mass Spectrometric Implications of High-Pressure Ion Sources. *Int. J. Mass Spectrom.* **2000,** *200*, 459-478.
58. Bruins, A.P.; Covey, T.R.; Henion, J.D. Ion Spray Interface for Combined Liquid Chromatography/Atmospheric Pressure Ionization Mass Spectrometry. *Anal. Chem.* **1987,** *59*, 2642-2646.
59. Covey, T.R.; Bruins, A.P.; Henion, J.D. Comparison of Thermospray and Ion Spray Mass Spectrometry in an Atmospheric Pressure Ion Source. *Org. Mass Spectrom.* **1988,** *23*, 178-186.
60. Covey, T.R.; Bonner, R.F.; Shushan, B.I.; Henion, J.D. The Determination of Protein, Oligonucleotide, and Peptide Molecular Weights by Ion-Spray Mass Spectrometry. *Rapid Commun. Mass Spectrom.* **1988,** *2*, 249-256.
61. Ikonomou, M.G.; Blades, A.T.; Kebarle, P. Electrospray – Ion Spray: A Comparison of Mechanisms and Performance. *Anal. Chem.* **1991,** *63*, 1989-1998.
62. Banks, J.F., Jr.; Quinn, J.P.; Whitehouse, C.M. LC/ESI-MS Determination of Proteins Using Conventional Liquid Chromatography and Ultrasonically Assisted Electrospray. *Anal. Chem.* **1994,** *66*, 3688-3695.
63. Banks, J.F., Jr.; Shen, S.; Whitehouse, C.M.; Fenn, J.B. Ultrasonically Assisted Electrospray Ionization for LC/MS Determination of Nucleosides from a Transfer RNA Digest. *Anal. Chem.* **1994,** *66*, 406-414.
64. Smith, R.D.; Barinaga, C.J.; Udseth, H.R. Improved Electrospray Ionization Interface for Capillary Zone Electrophoresis-Mass Spectrometry. *Anal. Chem.* **1988,** *60*, 1948-1952.
65. Abian, J. The Coupling of Gas and Liquid Chromatography With Mass Spectrometry. *J. Mass Spectrom.* **1999,** *34*, 157-168.
66. Shaffer, S.A.; Tang, K.; Anderson, G.A.; Prior, D.C.; Udseth, H.R.; Smith, R.D. A Novel Ion Funnel for Focusing Ions at Elevated Pressure Using Electrospray Ionization Mass Spectrometry. *Rapid Commun. Mass Spectrom.* **1997,** *11*, 1813-1817.
67. Shaffer, S.A.; Prior, D.C.; Anderson, G.A.; Udseth, H.R.; Smith, R.D. An Ion Funnel Interface for Improved Ion Focusing and Sensitivity Using Electrospray Ionization Mass Spectrometry. *Anal. Chem.* **1998,** *70*, 4111-4119.
68. Kim, T.; Tolmachev, A.V.; Harkewicz, R.; Prior, D.C.; Anderson, G.; Udseth, H.R.; Smith, R.D.; Bailey, T.H.; Rakov, S.; Futrell, J.H. Design and Implementation of a New Electrodynamic Ion Funnel. *Anal. Chem.* **2000,** *72*, 2247-2255.
69. Ibrahim, Y.; Belov, M.E.; Tolmachev, A.V.; Prior, D.C.; Smith, R.D. Ion Funnel Trap Interface for Orthogonal Time-of-Flight Mass Spectrometry. *Anal. Chem.* **2007,** *79*, 7845-7852.
70. Ibrahim, Y.M.; Belov, M.E.; Liyu, A.V.; Smith, R.D. Automated Gain Control Ion Funnel Trap for Orthogonal Time-of-Flight Mass Spectrometry. *Anal. Chem.* **2008,** *80*, 5367-5376.
71. Smith, R.D.; Loo, J.A.; Barinaga, C.J.; Edmonds, C.G.; Udseth, H.R. Collisional Activation and Collision-Activated Dissociation of Large Multiply Charged Polypeptides and Proteins Produced by Electrospray Ionization. *J. Am. Soc. Mass Spectrom.* **1990,** *1*, 53-65.
72. Harvey, D.J. Collision-Induced Fragmentation of Underivatized *N*-Linked

Carbohydrates Ionized by Electrospray. *J. Mass Spectrom.* **2000,** *35*, 1178-1190.
73. Schmidt, A.; Bahr, U.; Karas, M. Influence of Pressure in the First Pumping Stage on Analyte Desolvation and Fragmentation in Nano-ESI MS. *Anal. Chem.* **2001,** *71*, 6040-6046.
74. Jedrzejewski, P.T.; Lehmann, W.D. Detection of Modified Peptides in Enzymatic Digests by Capillary Liquid Chromatography/Electrospray Mass Spectrometry and a Programmable Skimmer CID Acquisition Routine. *Anal. Chem.* **1997,** *69*, 294-301.
75. Weinmann, W.; Stoertzel, M.; Vogt, S.; Svoboda, M.; Schreiber, A. Tuning Compounds for Electrospray Ionization/in-Source Collision-Induced Dissociation and Mass Spectra Library Searching. *J. Mass Spectrom.* **2001,** *36*, 1013-1023.
76. Huddleston, M.J.; Bean, M.F.; Carr, S.A. Collisional Fragmentation of Glycopeptides by Electrospray Ionization LC/MS and LC/MS/MS: Methods for Selective Detection of Glycopeptides in Protein Digests. *Anal. Chem.* **1993,** *65*, 877-884.
77. Chen, H.; Tabei, K.; Siegel, M.M. Biopolymer Sequencing Using a Triple Quadrupole Mass Spectrometer in the ESI Nozzle-Skimmer/Precursor Ion MS/MS Mode. *J. Am. Soc. Mass Spectrom.* **2001,** *12*, 846-852.
78. Hoogland, F.G.; Boon, J.J. Development of MALDI-MS and Nano-ESI-MS Methodology for the Full Identification of Poly(ethylene glycol) Additives in Artists' Acrylic Paints. *Int. J. Mass Spectrom.* **2009,** *284*, 66-71.
79. Miao, X.-S.; Metcalfe, C.D. Determination of Carbamazepine and Its Metabolites in Aqueous Samples Using Liquid Chromatography-Electrospray Tandem Mass Spectrometry. *Anal. Chem.* **2003,** *75*, 3731-3738.
80. Gross, J.H.; Eckert, A.; Siebert, W. Negative-Ion Electrospray Mass Spectra of Carbon Dioxide-Protected *N*-Heterocyclic Anions. *J. Mass Spectrom.* **2002,** *37*, 541-543.
81. Wilm, M.S.; Mann, M. Electrospray and Taylor-Cone Theory, Dole's Beam of Macromolecules at Last? *Int. J. Mass Spectrom. Ion Proc.* **1994,** *136*, 167-180.
82. Wilm, M.; Mann, M. Analytical Properties of the Nanoelectrospray Ion Source. *Anal. Chem.* **1996,** *68*, 1-8.
83. Wilm, M.; Shevshenko, A.; Houthaeve, T.; Breit, S.; Schweigerer, L.; Fotsis, T.; Mann, M. Femtomole Sequencing of Proteins from Polyacrylamide Gels by Nano-Electrospray Mass Spectrometry. *Nature* **1996,** *379*, 466-469.
84. Juraschek, R.; Dülcks, T.; Karas, M. Nanoelectrospray – More Than Just a Minimized-Flow Electrospray Ionization Source. *J. Am. Soc. Mass Spectrom.* **1999,** *10*, 300-308.
85. Guo, M.; Huang, B.X.; Kim, H.Y. Conformational Changes in Akt1 Activation Probed by Amide Hydrogen/Deuterium Exchange and Nano-Electrospray Ionization Mass Spectrometry. *Rapid Commun. Mass Spectrom.* **2009,** *23*, 1885-1891.
86. Gibson, G.T.T.; Mugo, S.M.; Oleschuk, R.D. Nanoelectrospray Emitters: Trends and Perspective. *Mass Spectrom. Rev.* **2009,** *28*, 918-936.
87. Valaskovic, G.A.; Murphy, J.P.; Lee, M.S. Automated Orthogonal Control System for Electrospray Ionization. *J. Am. Soc. Mass Spectrom.* **2004,** *15*, 1201-1215.
88. Kebarle, P.; Verkerk, U.H. Electrospray: From Ions in Solution to Ions in the Gas Phase – What We Know Now. *Mass Spectrom. Rev.* **2009,** *28*, 898-917.
89. Cole, R.B. Some Tenets Pertaining to Electrospray Ionization Mass Spectrometry. *J. Mass Spectrom.* **2000,** *35*, 763-772.
90. Kebarle, P. A Brief Overview of the Present Status of the Mechanisms Invol-ved in Electrospray Mass Spectrometry. *J. Mass Spectrom.* **2000,** *35*, 804-817.
91. Marginean, I.; Nemes, P.; Parvin, L.; Vertes, A. How Much Charge Is There on a Pulsating Taylor Cone? *Appl. Phys. Lett.* **2006,** *89*, 064104-1-064104/3.
92. Nemes, P.; Marginean, I.; Vertes, A. Spraying Mode Effect on Droplet Formation and Ion Chemistry in Electrosprays. *Anal. Chem.* **2007,** *79*, 3105-3116.
93. de la Mora, J.F.; Van Berkel, G.J.; Enke, C.G.; Cole, R.B.; Martinez-Sanchez, M.; Fenn, J.B. Electrochemical Processes in Electrospray Ionization Mass Spectrometry. *J. Mass Spectrom.* **2000,** *35*, 939-952.
94. Van Berkel, G.J. Electrolytic Deposition of Metals on to the High-Voltage Contact in an Electrospray Emitter: Implica-

tions for Gas-Phase Ion Formation. *J. Mass Spectrom.* **2000,** *35*, 773-783.
95. Schaefer, M.; Drayue, M.; Springer, A.; Zacharias, P.; Meerholz, K. Radical Cations in Electrospray Mass Spectrometry: Formation of Open-Shell Species, Examination of the Fragmentation Behavior in ESI-MS^n and Reaction Mechanism Studies by Detection of Transient Radical Cations. *Eur. J. Org. Chem.* **2007,** 5162-5174.
96. Gomez, A.; Tang, K. Charge and Fission of Droplets in Electrostatic Sprays. *Phys. Fluids* **1994,** *6*, 404-414.
97. Duft, D.; Achtzehn, T.; Müller, R.; Huber, B.A.; Leisner, T. Coulomb Fission. Rayleigh Jets from Levitated Microdroplets. *Nature* **2003,** *421*, 128.
98. Grimm, R.L.; Beauchamp, J.L. Dynamics of Field-Induced Droplet Ionization: Time-Resolved Studies of Distortion, Jetting, and Progeny Formation from Charged and Neutral Methanol Droplets Exposed to Strong Electric Fields. *J. Phys. Chem. B* **2005,** *109*, 8244-8250.
99. Mack, L.L.; Kralik, P.; Rheude, A.; Dole, M. Molecular Beams of Macroions. II. *J. Chem. Phys.* **1970,** *52*, 4977-4986.
100. Iribarne, J.V.; Thomson, B.A. On the Evaporation of Small Ions from Charged Droplets. *J. Chem. Phys.* **1976,** *64*, 2287-2294.
101. Thomson, B.A.; Iribarne, J.V. Field-Induced Ion Evaporation from Liquid Surfaces at Atmospheric Pressure. *J. Chem. Phys.* **1979,** *71*, 4451-4463.
102. Labowsky, M.; Fenn, J.B.; de la Mora, J.F. A Continuum Model for Ion Evaporation from a Drop: Effect of Curvature and Charge on Ion Solvation Energy. *Anal. Chim. Acta* **2000,** *406*, 105-118.
103. Fenn, J.B. Ion Formation from Charged Droplets: Roles of Geometry, Energy, and Time. *J. Am. Soc. Mass Spectrom.* **1993,** *4*, 524-535.
104. Fenn, J.B.; Rosell, J.; Meng, C.K. In Electrospray Ionization, How Much Pull Does an Ion Need to Escape its Droplet Prison? *J. Am. Soc. Mass Spectrom.* **1997,** *8*, 1147-1157.
105. Loo, J.A.; Edmonds, C.G.; Udseth, H.R.; Smith, R.D. Effect of Reducing Disulfide-Containing Proteins on Electrospray Ionization Mass Spectra. *Anal. Chem.* **1990,** *62*, 693-698.
106. Chowdhury, S.K.; Katta, V.; Chait, B.T. Probing Conformational Changes in Proteins by Mass Spectrometry. *J. Am. Chem. Soc.* **1990,** *112*, 9012-9013.
107. Schmelzeisen-Redeker, G.; Bütfering, L.; Röllgen, F.W. Desolvation of Ions and Molecules in Thermospray Mass Spectrometry. *Int. J. Mass Spectrom. Ion Proc.* **1989,** *90*, 139-150.
108. Williams, E.R. Proton Transfer Reactivity of Large Multiply Charged Ions. *J. Mass Spectrom.* **1996,** *31*, 831-842.
109. Iavarone, A.T.; Jurchen, J.C.; Williams, E.R. Supercharged Protein and Peptide Ions Formed by Electrospray Ionization. *Anal. Chem.* **2001,** *73*, 1455-1460.
110. Iavarone, A.T.; Williams, E.R. Supercharging in Electrospray Ionization: Effects on Signal and Charge. *Int. J. Mass Spectrom.* **2002,** *219*, 63-72.
111. Iavarone, A.T.; Williams, E.R. Mechanism of Charging and Supercharging Molecules in Electrospray Ionization. *J. Am. Chem. Soc.* **2003,** *125*, 2319-2327.
112. Youhnovski, N.; Matecko, I.; Samalikova, M.; Grandori, R. Characterization of Cytochrome c Unfolding by Nano-Electrospray Ionization Time-of-Flight and Fourier Transform Ion Cyclotron Resonance Mass Spectrometry. *Eur. J. Mass Spectrom.* **2005,** *11*, 519-524.
113. Dobo, A.; Kaltashov, I.A. Detection of Multiple Protein Conformational Ensembles in Solution via Deconvolution of Charge-State Distributions in ESI-MS. *Anal. Chem.* **2001,** *73*, 4763-4773.
114. Nemes, P.; Goyal, S.; Vertes, A. Conformational and Noncovalent Complexation Changes in Proteins During Electrospray Ionization. *Anal. Chem.* **2008,** *80*, 387-395.
115. Chapman, J.R.; Gallagher, R.T.; Barton, E.C.; Curtis, J.M.; Derrick, P.J. Advantages of High-Resolution and High-Mass Range Magnetic-Sector Mass Spectrometry for Electrospray Ionization. *Org. Mass Spectrom.* **1992,** *27*, 195-203.
116. Cole, R.B.; Harrata, A.K. Solvent Effect on Analyte Charge State, Signal Intensity, and Stability in Negative Ion Electrospray Mass Spectrometry; Implications for the Mechanism of Negative Ion Formation. *J. Am. Soc. Mass Spectrom.* **1993,** *4*, 546-556.
117. Straub, R.F.; Voyksner, R.D. Negative Ion Formation in Electrospray Mass

Spectrometry. *J. Am. Soc. Mass Spectrom.* **1993,** *4*, 578-587.
118. Saf, R.; Mirtl, C.; Hummel, K. Electrospray Mass Spectrometry Using Potassium Iodide in Aprotic Organic Solvents for the Ion Formation by Cation Attachment. *Tetrahedron Lett.* **1994,** *35*, 6653-6656.
119. Cody, R.B.; Tamura, J.; Musselman, B.D. Electrospray Ionization/Magnetic Sector Mass Spectrometry: Calibration, Resolution, and Accurate Mass Measurements. *Anal. Chem.* **1992,** *64*, 1561-1570.
120. Mann, M.; Meng, C.K.; Fenn, J.B. Interpreting Mass Spectra of Multiply Charged Ions. *Anal. Chem.* **1989,** *61*, 1702-1708.
121. Labowsky, M.; Whitehouse, C.M.; Fenn, J.B. Three-Dimensional Deconvolution of Multiply Charged Spectra. *Rapid Commun. Mass Spectrom.* **1993,** *7*, 71-84.
122. Zhang, Z.; Marshall, A.G. A Universal Algorithm for Fast and Automated Charge State Deconvolution of Electrospray Mass-to-Charge Ratio Spectra. *J. Am. Soc. Mass Spectrom.* **1998,** *9*, 225-233.
123. Maleknia, S.D.; Downard, K.M. Charge Ratio Analysis Method to Interpret High Resolution Electrospray Fourier Transform-Ion Cyclotron Resonance Mass Spectra. *Int. J. Mass Spectrom.* **2005,** *246*, 1-9.
124. Maleknia, S.D.; Downard, K.M. Charge Ratio Analysis Method: Approach for the Deconvolution of Electrospray Mass Spectra. *Anal. Chem.* **2005,** *77*, 111-119.
125. Dobberstein, P.; Schroeder, E. Accurate Mass Determination of a High Molecular Weight Protein Using Electrospray Ionization with a Magnetic Sector Instrument. *Rapid Commun. Mass Spectrom.* **1993,** *7*, 861-864.
126. Haas, M.J. Fully Automated Exact Mass Measurements by High-Resolution Electrospray Ionization on a Sector Instrument. *Rapid Commun. Mass Spectrom.* **1999,** *13*, 381-383.
127. Hofstadler, S.A.; Griffey, R.H.; Pasa-Tolic, R.; Smith, R.D. The Use of a Stable Internal Mass Standard for Accurate Mass Measurements of Oligonucleotide Fragment Ions Using Electrospray Ionization Fourier Transform Ion Cyclotron Resonance Mass Spectrometry with Infrared Multiphoton Dissociation. *Rapid Commun. Mass Spectrom.* **1998,** *12*, 1400-1404.
128. Stenson, A.C.; Landing, W.M.; Marshall, A.G.; Cooper, W.T. Ionization and Fragmentation of Humic Substances in Electrospray Ionization Fourier Transform-Ion Cyclotron Resonance Mass Spectrometry. *Anal. Chem.* **2002,** *74*, 4397-4409.
129. Makarov, A.; Denisov, E.; Kholomeev, A.; Balschun, W.; Lange, O.; Strupat, K.; Horning, S. Performance Evaluation of a Hybrid Linear Ion Trap/Orbitrap Mass Spectrometer. *Anal. Chem.* **2006,** *78*, 2113-2120.
130. Scalf, M.; Westphall, M.S.; Krause, J.; Kaufmann, S.L.; Smith, L.M. Controlling Charge States of Large Ions. *Science* **1999,** *283*, 194-197.
131. Krusemark, C.J.; Frey, B.L.; Belshaw, P.J.; Smith, L.M. Modifying the Charge State Distribution of Proteins in Electrospray Ionization Mass Spectrometry by Chemical Derivatization. *J. Am. Soc. Mass Spectrom.* **2009,** *20*, 1617-1625.
132. Scalf, M.; Westphall, M.S.; Smith, L.M. Charge Reduction Electrospray Mass Spectrometry. *Anal. Chem.* **2000,** *72*, 52-60.
133. Ebeling, D.D.; Westphall, M.S.; Scalf, M.; Smith, L.M. Corona Discharge in Charge Reduction Electrospray Mass Spectrometry. *Anal. Chem.* **2000,** *72*, 5158-5161.
134. Ebeling, D.D.; Scalf, M.; Westphall, M.S.; Smith, L.M. A Cylindrical Capacitor Ionization Source: Droplet Generation and Controlled Charge Reduction for Mass Spectrometry. *Rapid Commun. Mass Spectrom.* **2001,** *15*, 401-405.
135. McLuckey, S.A.; Stephenson, J.L., Jr. Ion/Ion Chemistry of High-Mass Multiply Charged Ions. *Mass Spectrom. Rev.* **1998,** *17*, 369-407.
136. Herron, W.J.; Goeringer, D.E.; McLuckey, S.A. Product Ion Charge State Determination via Ion/Ion Proton Transfer Reactions. *Anal. Chem.* **1996,** *68*, 257-262.
137. *Analytical Methods in Supramolecular Chemistry;* Schalley, C.A. (ed.); Wiley-VCH: Weinhein, 2007.
138. *Mass Spectrometry in Drug Metabolism and Pharmacokinetics;* Ramanathan, R. (ed.); Wiley: Hoboken, 2009.

139. Schalley, C.A.; Springer, A. *Mass Spectrometry and Gas-Phase Chemistry of Non-Covalent Complexes;* Wiley: Hoboken, 2009.
140. *Mass Spectrometry of Nucleosides and Nucleic Acids;* Banoub, J.H.; Limbach, P.A. (eds.); CRC/Taylor & Francis: Boca Raton, 2009.
141. Williams, T.T.J.; Perreault, H. Selective Detection of Nitrated Polycyclic Aromatic Hydrocarbons by Electrospray Ionization Mass Spectrometry and Constant Neutral Loss Scanning. *Rapid Commun. Mass Spectrom.* **2000,** *14*, 1474-1481.
142. Zhu, J.; Cole, R.B. Formation and Decompositions of Chloride Adduct Ions, $[M+Cl]^-$, in Negative Ion Electrospray Ionization Mass Spectrometry. *J. Am. Soc. Mass Spectrom.* **2000,** *11*, 932-941.
143. Yang, C.; Cole, R.B. Stabilization of Anionic Adducts in Negative Ion Electrospray Mass Spectrometry. *Anal. Chem.* **2002,** *74*, 985-991.
144. Schalley, C.A.; Ghosh, P.; Engeser, M. Mass Spectrometric Evidence for Catenanes and Rotaxanes from Negative-ESI FT-ICR Tandem-MS Experiments. *Int. J. Mass Spectrom.* **2004,** *232*, 249-258.
145. Truebenbach, C.S.; Houalla, M.; Hercules, D.M. Characterization of Isopoly Metal Oxyanions Using Electrospray Time-of-Flight Mass Spectrometry. *J. Mass Spectrom.* **2000,** *35*, 1121-1127.
146. Choi, B.K.; Hercules, D.M.; Houalla, M. Characterization of Polyphosphates by Electrospray Mass Spectrometry. *Anal. Chem.* **2000,** *72*, 5087-5091.
147. Favaro, S.; Pandolfo, L.; Traldi, P. The Behavior of $[Pt(H^3\text{-Allyl})XP(C_6H_5)_3]$ Complexes in Electrospray Ionization Conditions Compared with those Achieved by other Ionization Methods. *Rapid Commun. Mass Spectrom.* **1997,** *11*, 1859-1866.
148. Feichtinger, D.; Plattner, D.A. Direct Proof for Mn^V-Oxo-Salen Complexes. *Angew. Chem. ,Int. Ed.* **1997,** *36*, 1718-1719.
149. Løver, T.; Bowmaker, G.A.; Henderson, W.; Cooney, R.P. Electrospray Mass Spectrometry of Some Cadmium Thiophenolate Complexes and of a Thiophenolate Capped CdS Cluster. *Chem. Commun.* **1996,** 683-685.
150. Hinderling, C.; Feichtinger, D.; Plattner, D.A.; Chen, P. A Combined Gas-Phase, Solution-Phase, and Computational Study of C-H Activation by Cationic Iridium(III) Complexes. *J. Am. Chem. Soc.* **1997,** *119*, 10793-10804.
151. Reid, G.E.; O'Hair, R.A.J.; Styles, M.L.; McFadyen, W.D.; Simpson, R.J. Gas Phase Ion-Molecule Reactions in a Modified Ion Trap: H/D Exchange of Non-Covalent Complexes and Coordinatively Unsaturated Platinum Complexes. *Rapid Commun. Mass Spectrom.* **1998,** *12*, 1701-1708.
152. Volland, M.A.O.; Adlhart, C.; Kiener, C.A.; Chen, P.; Hofmann, P. Catalyst Screening by Electrospray Ionization Tandem Mass Spectrometry: Hofmann Carbenes for Olefin Metathesis. *Chem. Eur. J.* **2001,** *7*, 4621-4632.
153. Jewett, B.N.; Ramaley, L.; Kwak, J.C.T. Atmospheric Pressure Ionization Mass Spectrometry Techniques for the Analysis of Alkyl Ethoxysulfate Mixtures. *J. Am. Soc. Mass Spectrom.* **1999,** *10*, 529-536.
154. Benomar, S.H.; Clench, M.R.; Allen, D.W. The Analysis of Alkylphenol Ethoxysulphonate Surfactants by High-Performance Liquid Chromatography, Liquid Chromatography-Electrospray Ionisation-Mass Spectrometry and Matrix-Assisted Laser Desorption Ionisation-Mass Spectrometry. *Anal. Chim. Acta* **2001,** *445*, 255-267.
155. Eichhorn, P.; Knepper, T.P. Electrospray Ionization Mass Spectrometric Studies on the Amphoteric Surfactant Cocamidopropylbetaine. *J. Mass Spectrom.* **2001,** *36*, 677-684.
156. Levine, L.H.; Garland, J.L.; Johnson, J.V. HPLC/ESI-Quadrupole Ion Trap Mass Spectrometry for Characterization and Direct Quantification of Amphoteric and Nonionic Surfactants in Aqueous Samples. *Anal. Chem.* **2002,** *74*, 2064-2071.
157. Barco, M.; Planas, C.; Palacios, O.; Ventura, F.; Rivera, J.; Caixach, J. Simultaneous Quantitative Analysis of Anionic, Cationic, and Nonionic Surfactants in Water by Electrospray Ionization Mass Spectrometry with Flow Injection Analysis. *Anal. Chem.* **2003,** *75*, 5179-5136.
158. Little, D.P.; Chorush, R.A.; Speir, J.P.; Senko, M.W.; Kelleher, N.L.; McLaffer-

McLafferty, F.W. Rapid Sequencing of Oligonucleotides by High-Resolution Mass Spectrometry. *J. Am. Chem. Soc.* **1994,** *116*, 4893-4897.

159. Limbach, P.A.; Crain, P.F.; McCloskey, J.A. Molecular Mass Measurement of Intact Ribonucleic Acids via Electrospray Ionization Quadrupole Mass Spectrometry. *J. Am. Soc. Mass Spectrom.* **1995,** *6*, 27-39.
160. Little, D.P.; Thannhauser, T.W.; McLafferty, F.W. Verification of 50- to 100-Mer DNA and RNA Sequences With High-Resolution Mass Spectrometry. *Proc.Nat.Acad.Sci. USA* **1995,** *92*, 2318-2322.
161. Hanson, L.; Fucini, P.; Ilag, L.L.; Nierhaus, K.H.; Robinson, C.V. Dissociation of Intact *Escherichia coli* Ribosomes in a Mass Spectrometer. Evidence for Conformational Change in Ribosome Elongation Factor G Complex. *J. Biol. Chem.* **2003,** *278*, 1259-1267.
162. De Bellis, G.; Salani, G.; Battaglia, C.; Pietta, P.; Rosti, E.; Mauri, P. Electrospray Ionization Mass Spectrometry of Synthetic Oligonucleotides Using 2-Propanol and Spermidine. *Rapid Commun. Mass Spectrom.* **2000,** *14*, 243-249.
163. Greig, M.; Griffey, R.H. Utility of Organic Bases for Improved Electrospray Mass Spectrometry of Oligonucleotides. *Rapid Commun. Mass Spectrom.* **1995,** *9*, 97-102.
164. Sannes-Lowery, K.A.; Hofstadler, S.A. Sequence Confirmation of Modified Oligonucleotides Using IRMPD in the External Ion Reservoir of an Electrospray Ionization Fourier Transform Ion Cyclotron Mass Spectrometer. *J. Am. Soc. Mass Spectrom.* **2003,** *14*, 825-833.
165. Andersen, T.E.; Kirpekar, F.; Haselmann, K.F. RNA Fragmentation in MALDI Mass Spectrometry Studied by H/D-Exchange: Mechanisms of General Applicability to Nucleic Acids. *J. Am. Soc. Mass Spectrom.* **2006,** *17*, 1353-1368.
166. McLuckey, S.A.; Van Berkel, G.J.; Glish, G.L. Tandem Mass Spectrometry of Small, Multiply Charged Oligonucleotides. *J. Am. Soc. Mass Spectrom.* **1992,** *3*, 60-70.
167. Pfenninger, A.; Karas, M.; Finke, B.; Stahl, B. Structural Analysis of Underivatized Neutral Human Milk Oligosaccharides in the Negative Ion Mode by Nano-Electrospray MS^n (Part 1: Methodology). *J. Am. Soc. Mass Spectrom.* **2002,** *13*, 1331-1340.
168. Pfenninger, A.; Karas, M.; Finke, B.; Stahl, B. Structural Analysis of Underivatized Neutral Human Milk Oligosaccharides in the Negative Ion Mode by Nano-Electrospray MS^n (Part 2: Application to Isomeric Mixtures). *J. Am. Soc. Mass Spectrom.* **2002,** *13*, 1341-1348.
169. Weiskopf, A.S.; Vouros, P.; Harvey, D.J. Electrospray Ionization-Ion Trap Mass Spectrometry for Structural Analysis of Complex *N*-Linked Glycoprotein Oligosaccharides. *Anal. Chem.* **1998,** *70*, 4441-4447.
170. Metelmann, W.; Peter-Katalinic, J.; Müthing, J. Gangliosides from Human Granulocytes: a Nano-ESI QTOF Mass Spectrometry Fucosylation Study of Low Abundance Species in Complex Mixtures. *J. Am. Soc. Mass Spectrom.* **2001,** *12*, 964-973.
171. van Duijn, E.; Bakkes, P.J.; Heeren, R.M.A.; van den Heuvel, R.H.H.; van Heerikhuizen, H.; van der Vies, S.M.; Heck, A.J.R. Monitoring Macromolecular Complexes Involved in the Chaperonin-Assisted Protein Folding Cycle by Mass Spectrometry. *Nature Methods* **2005,** *2*, 371-376.
172. Breuker, K.; McLafferty, F.W. Stepwise Evolution of Protein Native Structure with Electrospray into the Gas Phase, 10^{-12} to 10^{2} s. *Proc. Natl. Acad. Sci. USA* **2008,** *105*, 18145-18152.
173. Tsuchiya, M. Atmospheric Pressure Ion Sources, Physico-Chemical and Analytical Applications. *Adv. Mass Spectrom.* **1995,** *13*, 333-346.
174. Carroll, D.I.; Dzidic, I.; Stillwell, R.N.; Haegele, K.D.; Horning, E.C. Atmospheric Pressure Ionization Mass Spectrometry. Corona Discharge Ion Source for Use in a Liquid Chromatograph-Mass Spectrometer-Computer Analytical System. *Anal. Chem.* **1975,** *47*, 2369-2373.
175. Dzidic, I.; Stillwell, R.N.; Carroll, D.I.; Horning, E.C. Comparison of Positive Ions Formed in Nickel-63 and Corona Discharge Ion Sources Using Nitrogen, Argon, Isobutane, Ammonia and Nitric Oxide as Reagents in Atmospheric Pressure Ionization Mass Spectrometry. *Anal. Chem.* **1976,** *48*, 1763-1768.

176. Hayen, H.; Karst, U. Strategies for the Liquid Chromatographic-Mass Spectrometric Analysis of Non-polar Compounds. *J. Chromatogr. A* **2003,** *1000*, 549-565.
177. Mottram, H.; Woodbury, S.E.; Evershed, R.P. Identification of Triacylglycerol Positional Isomers Present in Vegetable Oils by High Performance Liquid Chromatography/Atmospheric Pressure Chemical Ionization Mass Spectrometry. *Rapid Commun. Mass Spectrom.* **1997,** *11*, 1240-1252.
178. Reemtsma, T. Liquid Chromatography-Mass Spectrometry and Strategies for Trace-Level Analysis of Polar Organic Pollutants. *J. Chromatogr. A* **2003,** *1000*, 477-501.
179. Hayen, H.; Jachmann, N.; Vogel, M.; Karst, U. LC-Electron Capture-APCI(-)-MS Determination of Nitrobenzoxadiazole Derivatives. *Analyst* **2003,** *128*, 1365-1372.
180. Hayen, H.; Jachmann, N.; Vogel, M.; Karst, U. LC-Electron Capture APCI-MS for the Determination of Nitroaromatic Compounds. *Analyst* **2002,** *127*, 1027-1030.
181. Robb, D.B.; Covey, T.R.; Bruins, A.P. Atmospheric Pressure Photoionization: an Ionization Method for Liquid Chromatography-Mass Spectrometry. *Anal. Chem.* **2000,** *72*, 3653-3659.
182. Keski-Hynnilä, H.; Kurkela, M.; Elovaara, E.; Antonio, L.; Magdalou, J.; Luukkanen, L.; Taskinen, J.; Koistiainen, R. Comparison of Electrospray, Atmospheric Pressure Chemical Ionization, and Atmospheric Pressure Photoionization in the Identification of Apomorphine, Dobutamine, and Entacapone Phase II Metabolites in Biological Samples. *Anal. Chem.* **2002,** *74*, 3449-3457.
183. Syage, J.A.; Hanold, K.A.; Lynn, T.C.; Horner, J.A.; Thakur, R.A. Atmospheric Pressure Photoionization. II. Dual Source Ionization. *J. Chromatogr. A* **2004,** *1050*, 137-149.
184. Yang, C.; Henion, J.D. Atmospheric Pressure Photoionization Liquid Chromatographic-Mass Spectrometric Determination of Idoxifene and its Metabolites in Human Plasma. *J. Chromatogr. A* **2002,** *970*, 155-165.
185. Kauppila, T.J.; Kuuranne, T.; Meurer, E.C.; Eberlin, M.N.; Kotiaho, T.; Koistiainen, R. Atmospheric Pressure Photoionization Mass Spectrometry. Ionization Mechanism and the Effect of Solvent on the Ionization of Naphthalenes. *Anal. Chem.* **2002,** *74*, 5470-5479.
186. Raffaeli, A.; Saba, A. Atmospheric Pressure Photoionization Mass Spectrometry. *Mass Spectrom. Rev.* **2003,** *22*, 318-331.
187. Kauppila, T.J.; Kostiainen, R.; Bruins, A.P. Anisole – A New Dopant for Atmospheric Pressure Photoionization Mass Spectrometry of Low Proton Affinity, Low Ionization Energy Compounds. *Rapid Commun. Mass Spectrom.* **2004,** *18*, 808-815.
188. Robb, D.B.; Covey, T.R.; Bruins, A.P. Atmospheric Pressure Photoionization: an Ionization Method for Liquid Chromatography-Mass Spectrometry. *Anal. Chem.* **2000,** *72*, 3653-3659.
189. Robb, D.B.; Covey, T.R.; Bruins, A.P. Atmospheric Pressure Photoionization (APPI): A New Ionization Technique for LC/MS. *Adv. Mass Spectrom.* **2001,** *15*, 391-392.
190. Kauppila, T.J.; Kotiaho, T.; Kostiainen, R.; Bruins, A.P. Negative Ion-Atmospheric Pressure Photoionization-Mass Spectrometry. *J. Am. Soc. Mass Spectrom.* **2004,** *15*, 203-211.

13 Ambient Mass Spectrometry

Learning Objectives

- Ion formation under ambient conditions
- Interfaces for ambient mass spectrometry
- Screening techniques for rapid quality control and safety applications
- Real time examination of samples during physical manipulation

---

All methods for the generation of ions for mass spectrometry described up to this point require the analyte for ionization to be presented either directly under high vacuum (EI, CI, FI, FD) or contained in a sort of solution from which ions are to be extracted into or generated in the gas phase (FAB, LDI, MALDI). Even the atmospheric pressure ionization techniques employ processes that create ions from dilute (solid) solutions of the sample (ESI, APCI, APPI, AP-MALDI). This chapter deals with the manifold methods and interfaces which are allowing to overcome these limitations, and which have developed at a breathtaking pace within the short time since the publication of the first edition of this book.

Desorption electrospray ionization (DESI) [1] was introduced at the end of 2004, and *direct analysis in real time* (DART) [2] soon after in 2005. The apparent potential of both DESI and DART in high-throughput applications soon led to the development of some "derivatives" with the intention to broaden the field of applications or to adapt the underlying methodology to specific analytical needs. Now, the repertoire of methods includes variations of the DESI theme such as *desorption sonic spray ionization* (DeSSI) [3], later renamed *easy sonic spray ionization* (EASI) [4] or *extractive electrospray ionization* (EESI) [5,6]. Then, there are the DESI analogs of APCI and APPI, i.e., *desorption atmospheric-pressure chemical ionization* (DAPCI) [7,8] and *desorption atmospheric pressure photoionization* (DAPPI) [9].

All these methods have one important characteristic in common: they direct a stream of ionizing or at least ion-desorbing fluid medium onto a sample surface from which analyte ions are withdrawn and transported through air into the mass analyzer via a standard API interface. The beauty of this approach lies in the fact that a sample needs just to be exposed to the ionizing medium under ambient conditions. In other words, DESI, DART and those numerous related methods enable the detection of surface materials like waxes, alkaloids, flavors, or pesticides from plants as well as explosives, pharmaceuticals, or drugs of abuse from luggage or banknotes. These and many more analytical applications are readily accessible by

J. Gross, *Mass Spectrometry*, 2nd ed., DOI 10.1007/978-3-642-10711-5_13,
© Springer-Verlag Berlin Heidelberg 2011

plainly exposing the corresponding items to the ionization region of the interface – even without harm to living organisms [10]. This reduced need for sample pre-treatment is key to the success of *ambient MS*. In ambient MS, samples are accessible to observation and may even be subjected to some kind of processing, either mechanical manipulations or chemical treatments, while mass spectra are continuously being measured. Recently, a fieldable ion trap mass spectrometer for use with commercial DESI and DART ion sources has been constructed [11].

Note: Although the features of DESI and DART are in many ways superior and "revolutionary", one should be aware of intrinsic limitations. The detection of a compound largely depends on the matrix, e.g., whether it is *on* or eventually *in* skin, fruit, bark, stone etc. This also results in a lack of quantification abilities. However, also no other single ionization method, especially when used under just one set of conditions, can deliver ions of all constituents of a complex sample. Nonetheless, DESI, DART and related methods can deliver a wealth of chemical information with unprecedented ease.

13.1 Desorption Electrospray Ionization

The novel feature of *desorption electrospray ionization* (DESI) is that it allows ambient MS without sample preparation or sample pre-treatment. Furthermore, "ambient" means here not only the mere operation at atmospheric pressure, e.g., as is the case with AP-MALDI, but the operation in a freely accessible open space in front of the atmospheric pressure interface [12]. DESI is applicable to solids, liquid samples, frozen solutions, and to loosely surface-bound species like adsorbed gases. It can detect low-molecular-weight organic compounds as well as comparatively large biomolecules. The material presented to DESI may be a single compound suitably prepared on a sample target analogous to LDI or it can be a complex biological material like tissue, blood, whole leaves, or fruit [13].

Note: Although it appears that the results of DESI analyses are almost instantaneously available, DESI spectra tend to require more thorough examination than standard ESI spectra in order to draw the right analytical conclusions.

13.1.1 Experimental Setup for DESI

In a standard ESI experiment the spray capillary is set to high voltage in respect to a counter electrode that is essentially represented by the atmospheric pressure entrance of the interface. Sample ions are already contained in the solution that is supplied to the sprayer (Chap. 12). For desorption electrospray, only a solvent or solvent mixture is sprayed under strong pneumatic assistance onto a surface at an impact angle α. Driven by the high-velocity gas stream, the highly charged microdroplets receive sufficient kinetic energy to be forced onto the sample surface

even while an electrostatic charge is constituting there. The resulting interaction may dissolve and take up analyte ions. Local electrostatic charging and the reflected gas stream may now act in concert and transport analyte ions away from the surface at an angle β (Fig. 13.1). A nearby sampling orifice may then inhale a portion of the mist in the same way as it normally would do when the sample is already admixed to the solvent system. To bridge the gap between the sampling area and the entrance into the interface, a transfer line or extension tube is mounted in front of the orifice. This tube, e.g., 3 mm o.d. stainless steel, simplifies handling and particularly accessibility of the sample and also improves desolvation of the ions, probably due to different droplet sizes as compared to standard ESI conditions [1,12]. DESI practice has shown that interfaces with a heated transfer capillary are superior to those employing a counter-current desolvation gas and corresponding modifications have been suggested [14].

Note: In principle, any mass spectrometer equipped with an ESI source can be modified for DESI operation by mounting the sprayer on an adjustable frame and placing a *x*,*y*-movable sample stage between sprayer and entrance of the interface (Chap. 13.1.3) [15]. For safety, a GΩ–resistor should be welded in the high-voltage supply cord. However, for successful analytical application, only sensitive modern instruments are suitable.

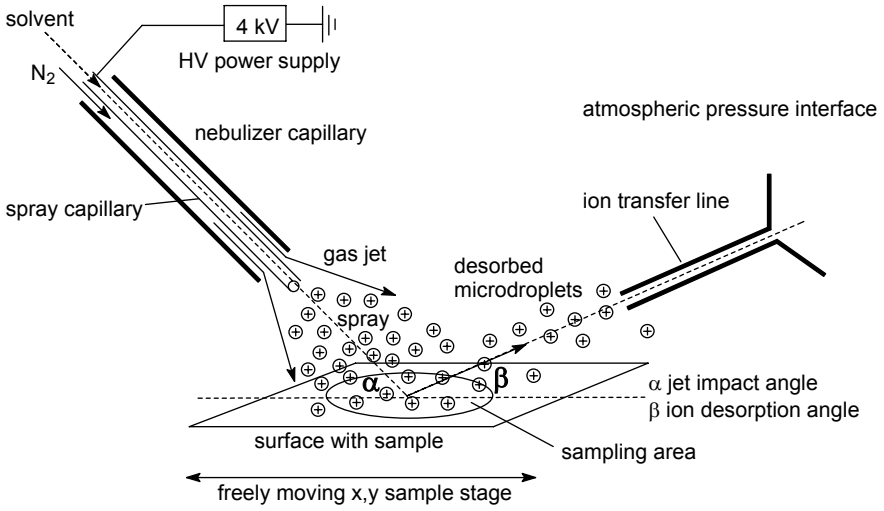


Fig. 13.1. Schematic of a DESI interface. A jet of gas and charged microdroplets is created by means of a standard pneumatic ESI sprayer and directed onto a sample surface at angle α. As a result, charged microdroplets containing ions of the surface material are created and transported away due to the action of the reflected gas stream and electric repulsion at angle β. A portion of the "secondary ESI spray" may be taken up by the atmospheric pressure interface of the mass spectrometer. Although at the expense of optimum sensitivity, an extended ion transfer line is normally employed to bridge the gap from surface to interface sampling orifice [1,12].

Obviously, DESI introduces new parameters to the ESI experiment. In particular, the velocity of the spray gas (represented by the supply pressure), the sprayer-to-surface and sampling orifice-to-surface distances, and the angles of impact and desorption are contributing to the effectivity of ion generation and subsequent uptake into the mass spectrometer. Accordingly, these parameters need to be carefully optimized for any DESI application as they exhibit rather wide variations (Table 13.1) [12,13]. It has also been found that optimum settings differ between API interfaces with counter-current drying gas and those employing the heated desolvation capillary design [16]. The transit of charged particles from the sample surface into the ion transfer line of the interface is determined, among others, by the dragging action of the mass analyzer's vacuum.

Additional parameters associated with DESI are the electrical conductivity, the chemical composition, and the texture of the sample surface. Neutralization of the droplets landing at the surface must be avoided to maintain continuous release of charged particles from the surface. Conductive sample supports need to be either isolated or floated at a potential equal to or slightly lower than the spray voltage. The electrostatic properties of the surface are also relevant for an insulator, because the signal stability depends on its preferred polarity. A highly electronegative polymer like PTFE, for example, yields better signal stability in negative-ion mode, whereas PMMA performs bettter in positive-ion mode. The chemical composition of the surface can affect crystallization of the analyte, and thus, as observed in MALDI preparations, lead to the occurrence of "sweet spots". Therefore,

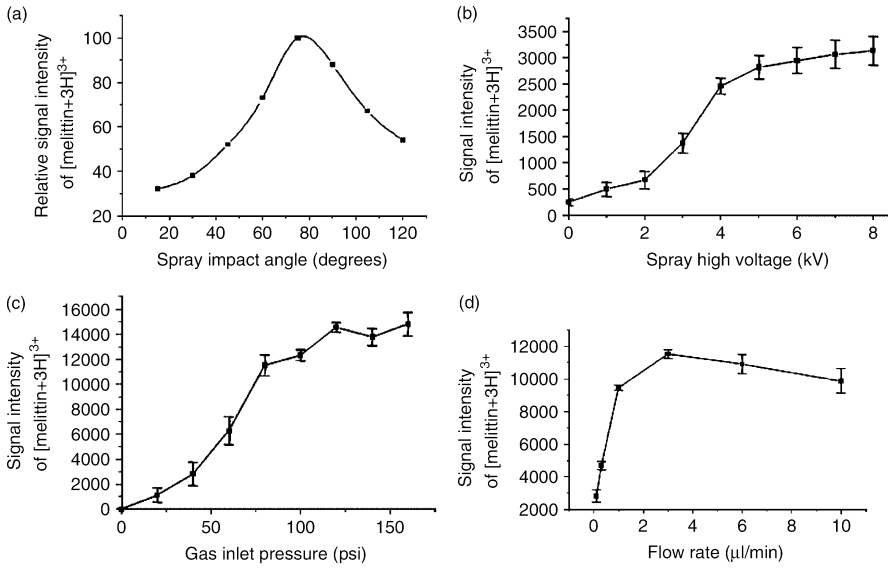


Fig. 13.2. Influence of experimental parameters on the intensity of the $[M+3H]^{3+}$ ion of melittin: (**a**) spray impact angle, (**b**) spray high voltage, (**c**) nebulizing gas pressure (14.5 psi ≈ 1 bar), (**d**) solvent flow rate. Reprinted from Ref. [12] with permission. © John Wiley & Sons, Ltd. 2005.

high affinity of analyte molecules to the surface needs to be avoided as it is detrimental for the release of analyte. Finally, the surface texture plays a role. The use of HF etched glass slides as DESI substrates instead of untreated ones delivered a dramatic increase in signal stability and eliminated "sweet spot" effects. Generally, rough surfaces like paper or textiles give superior sensitivity [12].

Example: Examinations have been carried out on the dependence of the signal intensity of the $[M+3H]^{3+}$ ion of melittin on basic experimental DESI parameters such as spray impact angle, spray high voltage, nebulizing gas inlet pressure, and solvent flow rate. Methanol : water = 1 : 1 was sprayed onto a sample of 10 ng melittin deposited on a PMMA surface at fixed spray tip-to-surface distance of 1 mm. While one parameter was varied, the others were kept constant at about their average value. The results reveal optimum conditions for each parameter that are rather typical for DESI and, as far a flow rate and spray high voltage are concerned, also for ESI (Fig. 13.2) [12].

DESI parameters can be grouped in a compound class-specific manner. It was found that proteins, for example, yield stronger signals when the spray is pointed onto the sample from close to vertical at about 1 mm distance while small molecules such as caffeine work best at an angle around 45° and several millimeters distance from the spray needle (Fig. 13.3) [12].

Early on, commercial DESI sources have become available and have meanwhile reached a level of maturity. They feature ESI sprayers adjustable in both angle and distance towards sample plates that can be operated under data system control (Fig. 13.4).

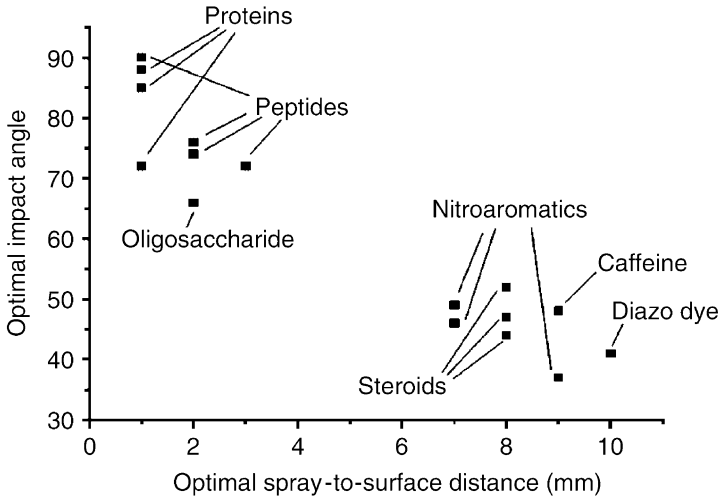


Fig. 13.3. Compound class-specific optima of spray impact angle and spray needle distance to surface. The *upper left* group of analytes would preferably be analyzed by ESI whereas the *lower right* group would rather demand for APCI (cf. Chap. 13.1.2). Reprinted from Ref. [12] with permission. © John Wiley & Sons, Ltd. 2005.



Fig. 13.4. A commercial DESI ion source. This one here is the Prosolia Omni Spray 2D source coupled to a Thermo Fisher LTQ mass spectrometer. The surface shown is a 96-spot Omni Slide HC having the standard microtiter plate dimensions. Note the extended desolvation capillary and the adjustable sprayer. Courtesy Prosolia, Inc., Indianapolis, In USA.

Table 13.1. Typical parameters for DESI

Parameter	Range of useful settings
Solvent flow rate	3–5 µl min^{-1}
Nebulizer gas pressure	8–12 bar
Spray voltage	2–6 kV
Sprayer-to-surface distance	1–5 mm
Sprayer-to-surface angle	30–70°
Surface-to-desolvation capillary distance	1–5 mm
Surface-to-desolvation capillary angle	10–30°
Temperature of desolvation capillary	200–300°C

13.1.2 Mechanisms of Ion Formation in DESI

DESI combines features of ESI with various desorption ionization devices [12], while also obviously displaying a resemblance to spray ionization methods, as an electrospray plume is usually generated by applying a potential of several kilovolts to an electrolytic solution under (strong) pneumatic assistance. The mist comprising charged microdroplets, ionic clusters, and gas phase solvent ions is then directed onto the sample surface. Therefore, the physical state of the sample distinguishes DESI from ESI. In this respect, DESI shows some phenomenological relationships to desorption ionization, because methods such as plasma desorption (PD), (matrix-assisted) laser desorption ionization ((MA)LDI), as well as fast atom bombardment (FAB) and its inorganic variant secondary ion mass spectrometry (SIMS, Chap. 15.5) all involve the impact of projectiles on condensed

phase samples. Depending on the method, these projectiles are either photons, energetic atoms, or ions. In contrast to those desorption methods, DESI is performed in the ambient atmosphere, and therefore, the projectiles in DESI can only possess low kinetic energies.

Three processes of ion formation have been proposed for DESI [17]; depending on the conditions and applied solvent-analyte pair one of these will predominate: *i*) droplet pickup, *ii*) condensed phase charge transfer, and *iii*) gas phase charge transfer.

i) *Droplet pickup* involves impact of electrosprayed droplets on the surface followed by dissolution of the analyte from the surface into the droplets. The droplets are again released from the surface and subsequent evaporation of the solvent and Coulomb fission generates ions by processes analogous to conventional ESI. The droplet pickup mechanism accounts for the similarity of DESI spectra with those of standard ESI in case of proteins. Interestingly, peptide ions can be observed even when the target and the sprayer are held at equal electrical potential. This has been attributed to the effect that offspring droplets will emerge mainly from the edges of a spreading primary droplet. In this case, charged droplet formation would essentially occur by electrospray driven by the potential between the edges and the extended desolvation capillary.

ii) *Condensed phase charge transfer* involves gaseous ions delivered by the electrospray and the analyte on the surface. The desorption of the analyte ions from the surface is thought to occur by a type of *chemical sputtering*. (Chemical sputtering is a process in which ion bombardment induces chemical reactions that finally lead to the formation of volatile erosion products [18].) This way, ions can be formed by transfer of electrons, protons, or other small ions from the impacting microdroplet to the surface bearing the analyte. A surface charge builds up and the momentum delivered from the impact event may then suffice to effect direct release of analyte ions from the surface. This proceeds at very low impact energy if the reactions are exothermic, while somewhat higher energies (adjusted via gas pressure) are required to achieve lift-off in case of endothermic reactions.

iii) *Gas phase charge transfer* means that ion formation occurs after volatilization or desorption of neutral species from the surface into the gas phase through ionization via proton/electron transfer or other ion–molecule reactions at atmospheric pressure. Indeed, the assumption of ion–molecule reactions, eventually purely in the gas phase above the sample, has led to the development of an DAPCI source (Chap. 13.2), in the first place to prove this mechanism of ion formation [7]. The solvent pH can be used to positively affect the vapor pressure of the analyte, e.g., the vapor pressure of volatile plant alkaloids is increased by addition of a base.

13.1.3 Analytical Features of DESI

DESI can serve for the identification of natural products in plant material [1,12,13], of lipids in animal tissue [16,19], for high-throughput analyses of pharmaceutical preparations [20], and for drug metabolite identification or even quan-

titation in blood and other biological fluids [12,14], as well as for the direct monitoring of biological tissue for biomarkers and in vivo analysis [10,16,19]. DESI is applicable to the analysis of proteins, carbohydrates, and oligonucleotides [12], as well as small organic molecules. Potential DESI applications are also in forensics and public safety such as the detection of explosives, toxic compounds, and chemical warfare agents on a variety of common surfaces, e.g., paper, plastics, cloth or luggage [17,21]. Plastic explosives, i.e., formulated explosive mixtures, can also be analyzed [10,17,21]. Even the transfer of ion-loaded gas from the sample to the API source through an up to three-meter-long stainless-steel tubing, termed non-proximate sampling, has been demonstrated [22].

The limit of detection for small peptides is in the order of 1 pg absolute or < 0.1 pg mm^{-2}, for proteins in the order of < 1 ng absolute or < 0.1 ng mm^{-2}; small molecules such as pharmaceuticals and explosives are detectable in the range of 10–100 pg absolute or 1–10 pg mm^{-2} [10,12]. These numbers indicate a footprint of about 10 mm^{-2} roughly corresponding to a circular spot of 3 mm in diameter. Smaller footprints can be realized – sample and sensitivity of the instrument permitting. The number of DESI papers is steadily growing. A few representative examples of DESI applications are compiled below.

Example: The negative-ion DESI mass spectrum of the over-the-counter drug acetylsalicylic acid (aspirin) was measured with a home-built DESI source attached to a seasoned triple quadrupole instrument (Fig. 13.5). The sample was presented on paper to a methanol spray. Whereas this sample even allowed tandem mass spectra of the $[M–H]^-$ ion, *m/z* 179, to be readily obtained, other samples were beyond the instrument's sensitivity limits [15].

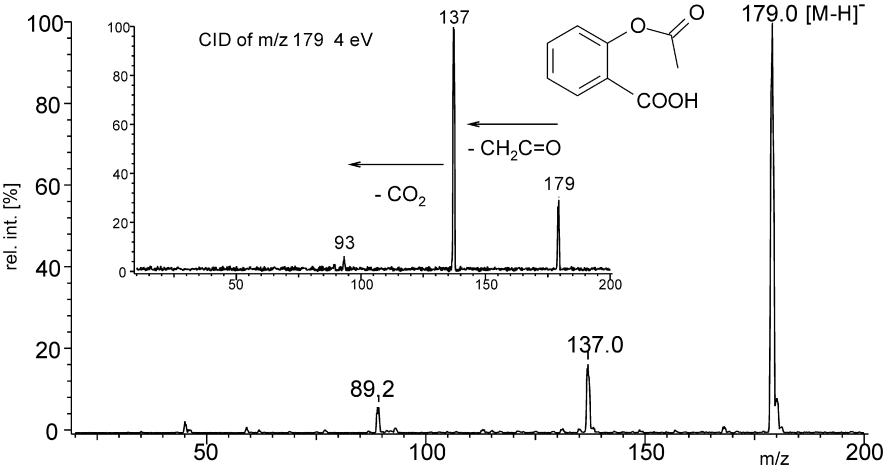


Fig. 13.5. Testing of a home-built DESI source. DESI mass spectrum of acetylsalicylic acid from paper analyzed by negative-ion DESI using methanol spray. The *inset* shows the tandem mass spectrum of the deprotonated ion.

Example: Plant alkaloids can be identified from DESI mass spectra of seeds, leaves, flowers, or roots. Here seeds of deadly nightshade (*Atropa belladonna*) were subjected to DESI for the identification of their principal alkaloids atropine and scopolamine (Fig. 13.6) [13]. (Atropine is the name of the racemic mixture of (R)- and (S)-hyoscyamine. It is a tropane alkaloid also extracted from jimsonweed (*Datura stramonium*), mandrake (*Mandragora officinarum*) among other plants of the Solanaceae family.) The inset in Fig. 13.4 shows tandem mass spectra of the ions at *m/z* 290 and 304, thereby confirming them as corresponding to protonated hyoscyamine and scopolamine, respectively. The confirmation of the ion at *m/z* 304 as $[M+H]^+$ ion of scopolamine was obtained by comparing the tandem mass spectrum with that of the standard alkaloid.

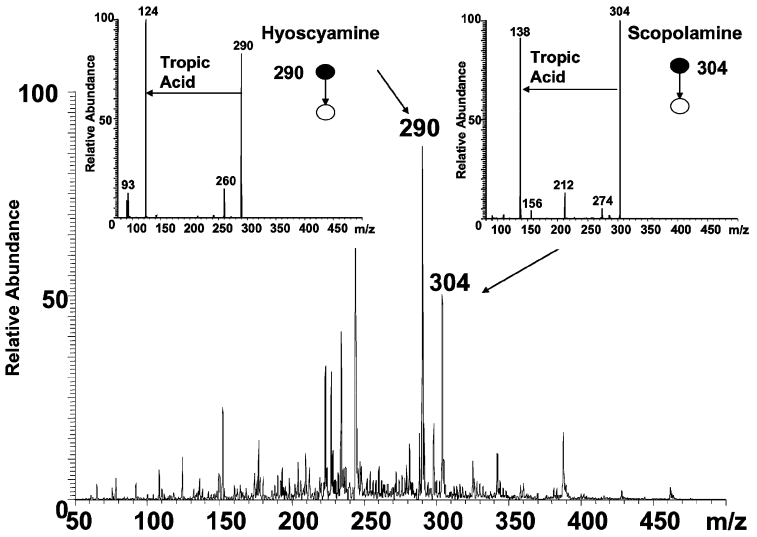


Fig. 13.6. DESI mass spectrum of *Atropa belladonna* seeds using methanol : water = 1 : 1 as spray solvent. The *insets* show tandem mass spectra of the protonated alkaloids hyoscamine, *m/z* 290 and scopolamine, *m/z* 304. Both protonated alkaloids have the characteristic loss of tropic acid, 166 u, in common. Reprinted from Ref. [13] with permission. © The Royal Society of Chemistry, 2005.

Example: Mouse liver sections were analyzed by DESI-FT-ICR-MS. The spectra of the tissue samples exhibited strong signals for phospholipids and lysophospholipids that were detected either as $[M+H]^+$, $[M+K]^+$, or $[M+K]^+$ ions. The mass accuracy of generally 1 ppm of the FT-ICR instrument allowed for assigning unique molecular formulas to most signals (Fig. 13.7) [16].

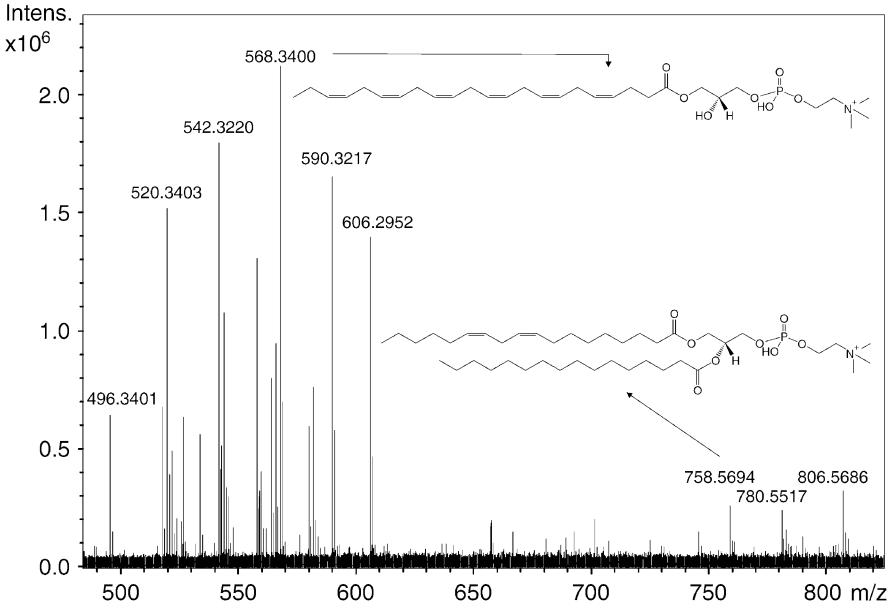


Fig. 13.7. Lipid profile of murine liver tissue sections as acquired by DESI-FT-ICR-MS using methanol : water = 1 : 1 (v/v) with 1% acetic acid as spray solvent. Reproduced from Ref. [16] with permission. © John Wiley & Sons, Ltd., 2008.

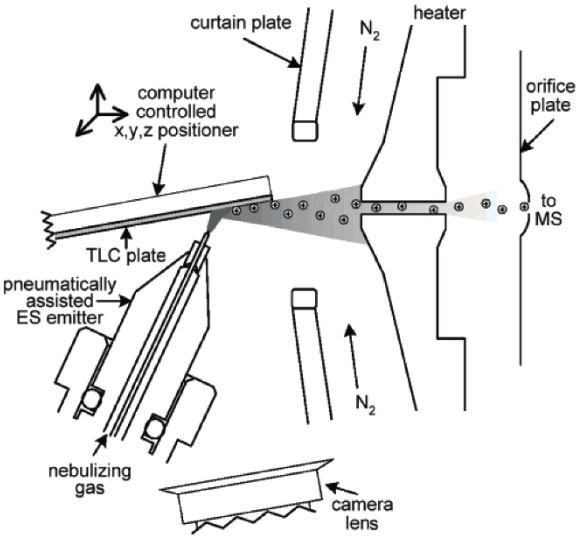


Fig. 13.8. Fully computer-controlled TLC-DESI unit attached to an ESI interface using the curtain gas design. Reprinted with permission from Ref. [23]. © The American Chemical Society, 2005.

Example: TLC-DESI was developed in the van Berkel group [23]. The sprayer was positioned about 4 mm from the curtain plate of the mass spectrometer at a 50° angle relative to the TLC plate surface. The TLC plates were cut to align the sample bands with the DESI plume. Methanol was sprayed at about 5 µl min^{-1} while a *x*-*y*-*z* robotic platform and control software were used to move the TLC plate relative to the stationary DESI emitter at about 50 µm min^{-1}. The position of the TLC plate relative to the sprayer was monitored with a camera, the image of which was output to a PC so as to correlate staining, position, and DESI spectral data (Fig. 13.8).

13.2 Desorption Atmospheric Pressure Chemical Ionization

The first report on *desorption atmospheric pressure chemical ionization* (DAPCI) appeared in a paper on the analysis of nitroaromatic explosives by negative-ion DESI [7]. These molecules all possess high electron affinities and thus they are prone to electron capture and deprotonation. From the positive effect of the DAPCI mode of operation for their detection, it was inferred that a chemical ionization mechanism should be effective if analytes are volatilized in the course of DESI analysis. So the main difference between DESI and DAPCI is the substitution of the charged solvent mist by a (hot) solvent vapor and the application of a corona discharge as the initial source of electric charge in DAPCI [17]. As usual in APCI, the corona discharge is created by applying a high DC voltage (3–6 kV) to a tapered tip stainless steel needle. Reactant ions are created in the solvent vapor upon passing the discharge. Then, the ionized gas streams onto the surface to be analyzed. Obviously, the droplet-pickup mechanism (Chap. 13.1.2) is precluded in DAPCI, while charge transfer to the surface and gas phase ionization of the analyte present the two possible mechanisms of ion formation [22].

It has been shown that addition of solvents can be avoided if the moisture of the ambient air is sufficient to generate H_3O^+ reagent ions [8,24]. The setup for DAPCI (using ambient air only) is shown in Fig. 13.9. A comparison of spectra of Proctosedyl, an ointment containing cinchocaine (M_r = 343 u) and hydrocortisone (M_r = 362 u), as obtained by DESI, DAPCI with ambient air, and DAPCI with solvent is presented in Fig. 13.10.

Applications of DAPCI include the comparative analysis of different teas such as green tea, oolong, and jasmine tea by their chemical fingerprints [24,25] and the direct rapid analysis of melamine and cyanuric acid in milk products delivering detection limits of 1–20 pg melamine mm^{-2} [26]. Furthermore, DAPCI has been successfully employed for the detection of peroxide explosives [21] or of illicit ingredients in food such as sudan red dyes in tomato sauce [24]. Analogous to DESI, DAPCI analyses can be performed with remote sampling [22].

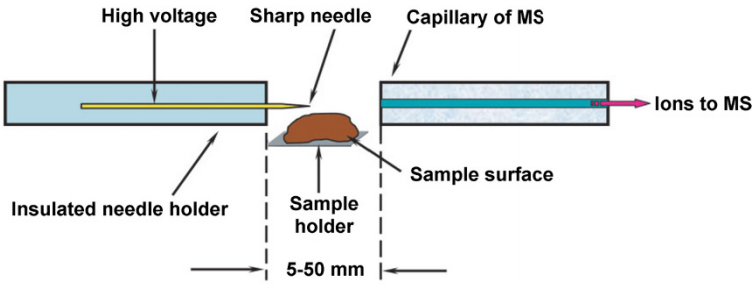


Fig. 13.9. Schematic of a DAPCI source for operation with moist ambient air as reagent gas. The sharp needle discharge electrode is coaxially centered in a capillary of 3 mm i.d. delivering humidified nitrogen gas if the ambient air is below 20% relative humidity. Adapted from Ref. [24] with permission. © John Wiley & Sons, Ltd., 2007.

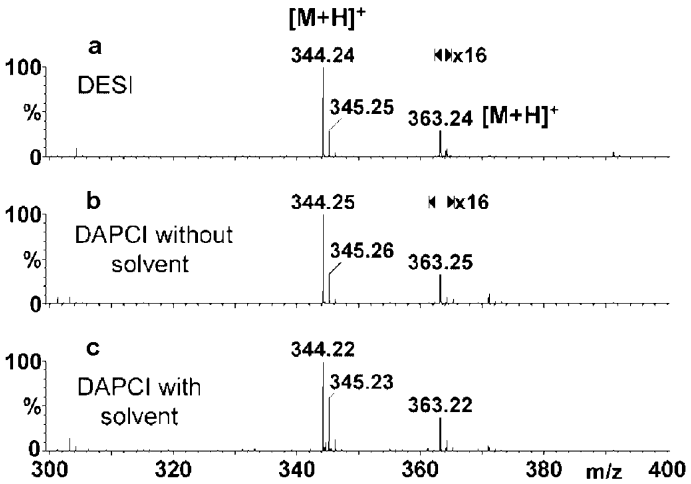


Fig. 13.10. Comparison of DESI, solvent-free DAPCI and DAPCI of Proctosedyl ointment. **(a)** Positive-ion DESI spectrum with the intensity of *m/z* 363, protonated hydrocortisone, 16-fold expanded to show the low-abundant ion. **(b)** Positive-ion DAPCI spectrum of the ointment obtained without solvent and same expansion as above. c) Positive-ion DAPCI spectrum obtained with solvent. Reproduced from Ref. [8] with permission. © John Wiley & Sons, Ltd., 2006.

13.3 Desorption Atmospheric Pressure Photoionization

DESI works best with polar analytes that are easy to protonate or deprotonate, although analytes of low polarity are accessible to a certain extent. This was the rationale for developing DAPCI. In order to improve the efficiency of ambient MS in the regime of low-polarity compounds even further, *desorption atmospheric*

pressure photoionization (DAPPI) has been developed. DAPPI represents the adaptation of APPI for the ambient analysis of surfaces analogous to the conversion of APCI to DAPCI.

In DAPPI, a heated jet of solvent vapor and nebulizer gas desorbs solid analytes from the surface. Using a microchip nebulizer turned out to be advantageous for handling and for highly responsive temperature control of the gas. The microchip nebulizer is a small glass device for mixing gas and solvent flow (dopant) and for heating the fluid medium during its passage along a platinum wire (Fig. 13.11) [9]. A krypton discharge lamp is directed toward the sample so as to irradiate the vapor phase immediately above the surface with UV photons of 10 eV where ionization of the analyte occurs. Like DESI and DAPCI, DAPPI uses a standard API interface to collect the ions [9,27].

The mechanism of ion generation in DAPPI has been proposed to be a combination of thermal and chemical processes. After thermal desorption of the analytes from the surface they can be photoionized in the gas phase. However, analytes with no UV chromophore may only be ionized by ion–molecule reactions with dopant ions. Dopant molecular ions, as formed from toluene for example, may promote charge exchange, while protonated dopant ions will yield $[M+H]^+$ ions.

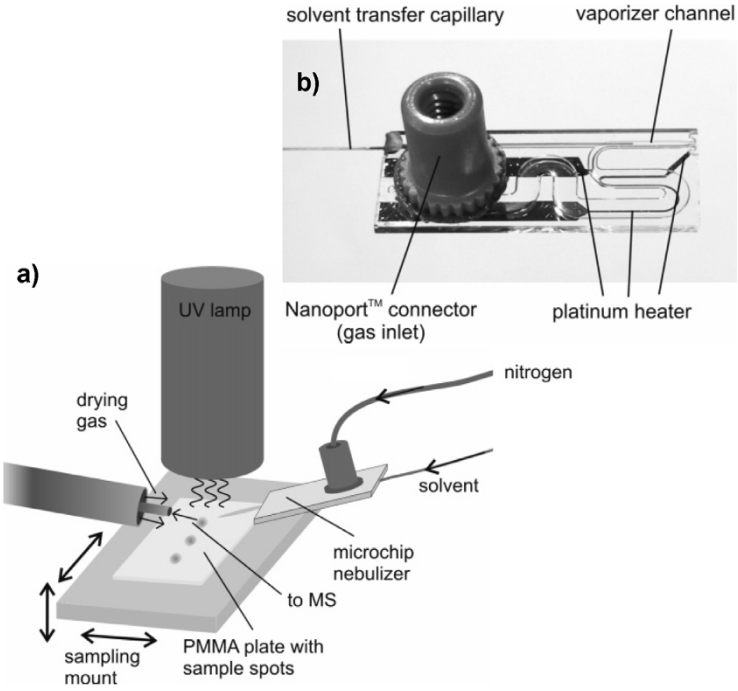


Fig. 13.11. Schematic of (**a**) the DAPPI setup and (**b**) photograph of the microchip nebulizer. The small solvent flow is mixed with nitrogen gas and vaporized in the microchip nebulizer by resistive heating of the platinum wire. The krypton UV lamp irradiates the sample surface that is in contact with the hot reagent gas. Reproduced from Ref. [9]with permission. © The American Chemical Society, 2007.

Acidic analytes can undergo deprotonation, while electronegative molecules are prone to anion addition or electron capture [27]. (The rules governing these processes have already been dealt with in Chap. 7.) The factors influencing the desorption and ionization in DAPPI such as the microfluidic jet impinging geometry, the thermal characteristics of the DAPPI surfaces, as well as chemical aspects like spray solvent have been examined for both positive- and negative-ion mode [27].

Example: DAPPI is capable of analyzing dried sample spots of compounds of different polarities from various surfaces, may serve for the direct analysis of pharmaceuticals and illicit drugs from tablets and other preparations (Fig. 13.12), and of many other applications [9,27-29].

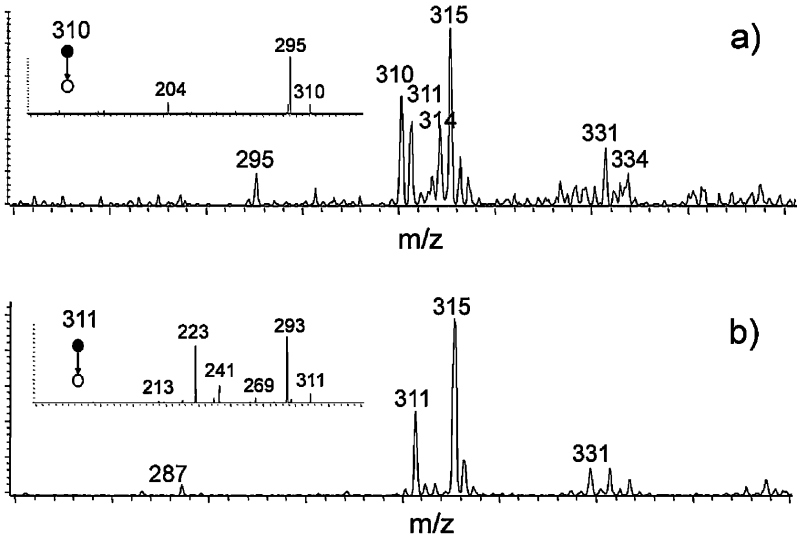


Fig. 13.12. Analysis of a hashish slab with DAPPI using toluene **(a)**and acetone **(b)** at flow rates of 2 ml min^{-1} as spray solvents. The insets show the tandem mass spectra of **(a)** the $M^{+\bullet}$ ion of cannabinol and **(b)** the $[M+H]^+$ ion of cannabinol; the ions at *m/z* 314 and 315 are attributed to the respective ionic species of tetrahydrocannabinol (THC). Reproduced from Ref. [29] with permission. © John Wiley Sons, Ltd., 2008.

13.4 Other Methods Related to DESI

Variation of the DESI theme by changing the mode of sample supply opens up a large variety of partially awe-inspiring, partially slightly odd, but always interesting analytical applications, some of which are so new that even the term is not finally coined at the time of their first publication.

13.4.1 Desorption Sonic Spray Ionization

In ESI an electrolytic solution is sprayed mainly by the action of an electric field inducing charge separation and subsequent disintegration of a bulk liquid into an electrostatically charged mist. A nebulizing gas flow at sonic speed coaxially to the liquid flow can also create a statistical imbalance of charges, i.e., a charge separation sufficient for the purpose of forming charged droplets. This is known as *sonic spray ionization* (SSI) [30-32]. The advantage of SSI is that it operates free of a high voltage and thus appears ideal for handling under ambient conditions [3]. An adaptation of SSI for ambient mass spectrometry was thus made and initially termed *desorption sonic spray ionization* (DeSSI) [3].

Note: Soon after its introduction, DeSSI was renamed *easy ambient sonic-spray ionization* (EASI) [33], the superfluous inclusion of the adjective "easy" and the generation of a rather blatant acronym (EASI) seem to have driven this change.

DeSSI (or EASI) requires unusually high backpressure of ca. 30 bar to achieve the sonic velocity of the nebulizer gas stream resulting in a flow of about 3 l min^{-1} to dissipate the liquid flow of 20 µl min^{-1} methanol/water solution. The curtain gas pressure of the API interface is also set to a rather high value of 5 bar.

The method has shown to deliver good results for the fingerprinting of biodiesel fuel [34] and perfumes [33], for the analysis of fabric softeners and surfactants [35], coupling to membrane inlet systems (MIMS-DeSSI) [4], and to analyze components separated on TLC plates [36]. However, the method appears to exhibit low inter-system compatibility; in some laboratories high voltages were needed to obtain a signal.

13.4.2 Extractive Electrospray Ionization

Analyte ions can also be efficiently generated when sample vapor or finely dispersed sample droplets transported by a carrier gas stream are admixed to the expanding electrospray plume. This technique, simple yet effective, has been introduced as *extractive electrospray ionization* (EESI) [37]. It utilizes two separate sprayers, one conventional ESI sprayer to provide the electrostatically charged mist and another to supply the sample vapor or mist (Fig. 13.13). While this approach is suggested for API interfaces with the heated transfer capillary design, the sample carrier stream may alternatively be passed into the desolvation gas of interfaces employing the heated curtain gas design (Fig. 13.14) [6,38].

Instead of a separate sample sprayer, an ultrasonic nebulizer may also deliver a sample-containing aerosol, which is transported and admixed to the electrospray mist by action of a mild stream of nitrogen. As the droplets of both origins are "fused" inside a small housing enclosing the spray, this approach has been termed *fused-droplet electrospray ionization*, and thus, led to the the somewhat confusing acronym FD-ESI [39,40].

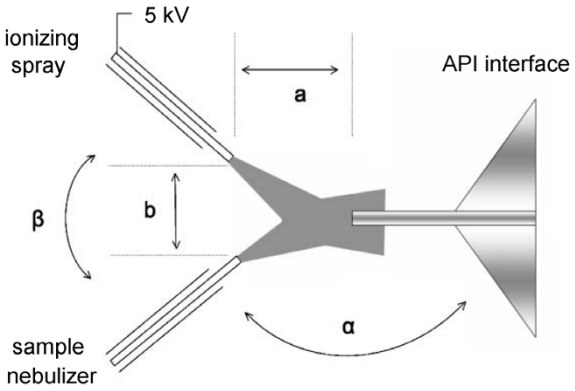


Fig. 13.13. Extractive electrospray ionization interface with two mixing sprays in front of a heated transfer capillary. The distances a and b and the angles α and β are adjusted as required for optimum signal intensity. Adapted from Ref. [37] with permission. © The Royal Society of Chemistry, 2006.

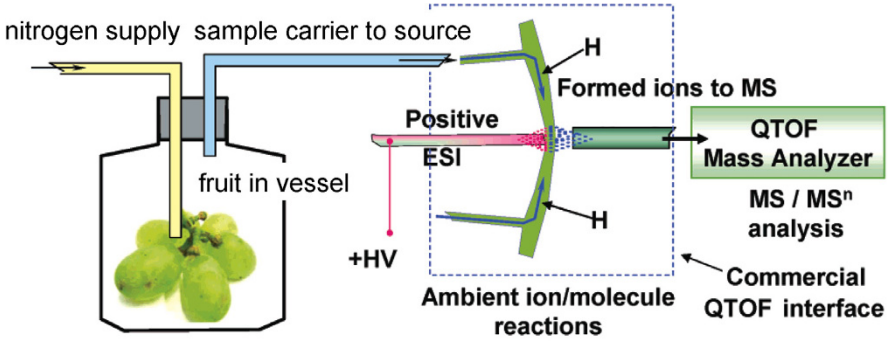


Fig. 13.14. Schematic of an EESI source where the sample carrier gas is fed into the curtain gas of the API interface. Here, the experiment is designed to determine the ripening of fruit from its headspace, i.e., odor. Adapted from Ref. [41] with permission. © The American Chemical Society, 2007.

EESI has its strengths in headspace analytical applications; it has been employed to classify authentic perfumes and to detect counterfeit products from chemical fingerprints of the fragrances after their application on paper strips as usually performed for customer's testing [42]. It may serve for the rapid determination of the ripening of fruit via headspace analysis as pointed out in Fig. 13.14 [41], or to identify spoiled food, either vegetables or meat samples, even in the frozen state, by detection of typical degradation products or metabolites from bacterial growth [5,38]. It is also possible to detect melamine in milk [43] (a sort of analysis one never would have assumed to be necessary until after the Olympic games in China in 2008). Finally, as the location of the extraction can be several

meters away from the mass spectrometer, traces of toxic chemicals, explosives, or drugs on skin can be detected by EESI without any hazard to a person [6,44].

13.4.3 Electrospray-Assisted Laser Desorption/Ionization (ELDI)

The technique of *electrospray-assisted laser desorption/ionization* (ELDI) combines two well-matured techniques of ionization for the benefit of improved analysis of samples under ambient conditions. The development of ELDI emanates from the fact that in (MA)LDI by far more neutrals than ions are released from the sample layer (Chap. 11) [45]. Consequently, post-ionization of laser-desorbed neutrals is promising and such methods have indeed been developed (cf. Refs. in [46]). The unique feature of ELDI is to laser-irradiate the sample in the ambient close to the ESI plume, wherein the neutrals are then ionized by ion–molecule reactions [46].

Standard conditions of ESI for ELDI involve a methanol : water = 1 : 1 mixture with 0.1% acetic acid sprayed at 3–5 µl min^{-1} from a grounded needle as to pass closely over an also grounded sample support. The orifice of the API interfaces acting as the counter electrode is held at 4–5 kV negative voltage. The UV nitrogen laser is adjusted to irradiate the sample sideward at an angle of about 45° while spraying (Fig. 13.15).

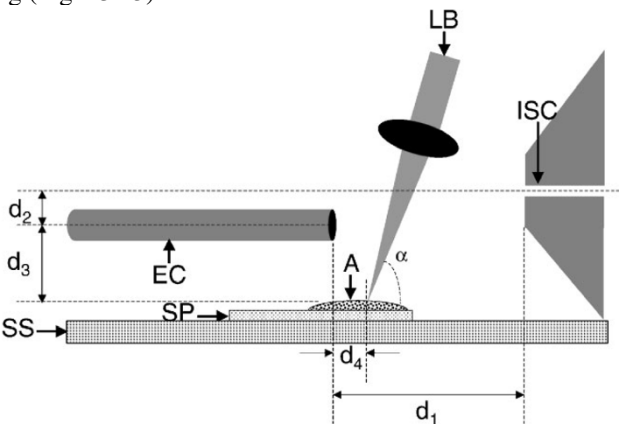


Fig. 13.15. ELDI setup. **A**: analyte, **SP**: stainless steel sample support plate, **SS**: mobile sample stage, **EC**: electrospray capillary, **LB**: UV laser beam, **ISC**: ion sampling capillary of the API interface. The distances $\mathbf{d_1}$ through $\mathbf{d_4}$ are all in the order of millimeters. Reproduced from Ref. [46] with permission. © John Wiley & Sons, Ltd., 2005.

Example: The combined use of ESI and LDI in ELDI is demonstrated for a sample of neat bovine cytochrome c on a stainless steel target (Fig. 13.16). The first spectrum (**A**), basically a blank spectrum, was obtained under pure LDI conditions. Spectrum **B** was measured with ESI on, but no laser irradiation. Finally, spectrum **C** was generated with both ESI and LDI active. It clearly shows the charge state distribution of the protein as typical for ESI spectra. The advantage of

ELDI is that samples can be presented to the inlet nozzle directly from the outside as compared to ESI or MALDI that require additional sample preparation [46]. ELDI has also been applied to the analysis of peptides and proteins [47] even from biological media [48], to detect chemicals on different surfaces [49], and of course, for compound identification on TLC plates [50]. It has been found that addition of a matrix is beneficial for the laser desorption part of the method. This gave rise to *matrix-assisted laser desorption electrospray ionization* (MALDESI) [51].

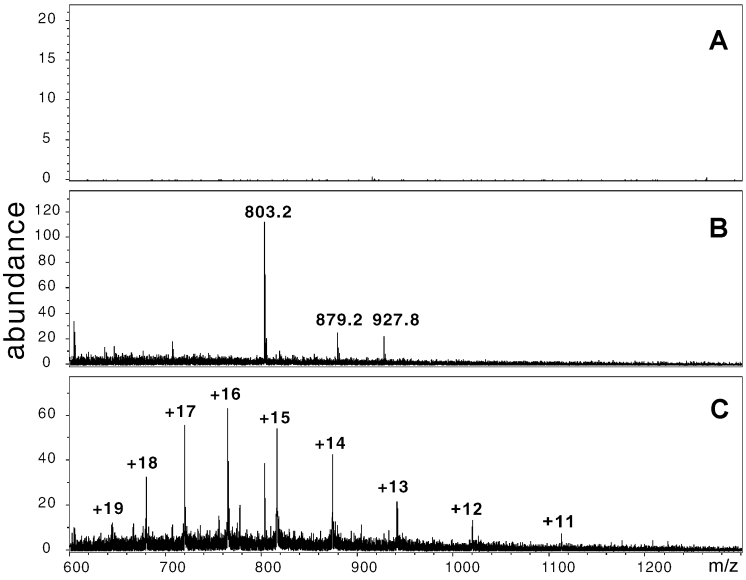


Fig. 13.16. Effect of the combined use of ESI and LDI in ELDI for a sample of neat bovine cytochrome c. Spectrum **(A)** was obtained under laser desorption only; **(B)** under ESI only; and **(C)** with both ESI and LDI active. Reproduced from Ref. [46] with permission. © John Wiley & Sons, Ltd., 2005.

13.4.4 Laser Ablation Electrospray Ionization

As just described, ELDI and MALDESI require pretreated samples, making them unfavorable for the (*in vivo*) analysis of water-rich biological samples that would preferentially be examined under ambient conditions. By replacing the UV laser with an IR laser (Er:YAG laser of 2.94 μm wavelength), the energy may directly be coupled into the OH vibrational modes of water-rich samples such as tissues. This experimental approach has been termed *laser ablation electrospray ionization* (LAESI) [52-54]. In contrast to AP-IR-MALDI, in LAESI the infrared laser only ablates neutrals from the sample, a noteworthy amount of them even in particulate state, which could be ascertained by flash shadowgraphy [52]. The laser impinging on the sample surface at 90° creates a plume that intercepts an electros-

pray operating in the cone-jet mode parallel to and at about 25 mm distance from the sample surface. The electrospray post-ionizes the neutrals and the particulate matter in that plume and transports the incipient analyte ions along the spray axis into the sampling orifice of an orthogonal acceleration time-of-flight (oa-TOF) mass spectrometer [52]. Apart from the IR laser, the experimental setup is sufficiently similar to ELDI to omit a schematic here.

Example: For LAESI, tissue samples are mounted on microscope slides, positioned 10–30 mm below the spray axis and 3–5 mm ahead of the emitter tip, and ablated using an Er:YAG laser with a pulse length of < 100 ns and 5 Hz repetition rate. The scanning electron microscope (SEM) image of the ablation crater produced by a single laser pulse on the adaxial leaf surface of a Zebra plant (*Aphelandra squarrosa*) is shown below (Fig. 13.17). The waxy cuticle and some of the upper epidermal and palisade cells were removed from a slightly elliptical area with axes of 300 and 280 µm indicating effective ablation of tissue [53]. This way, LAESI offers lateral mapping of metabolite distributions and their variations with depth on plant leaves. However, at present, LAESI cannot compete with vacuum imaging methods such as SIMS or MALDI [52].

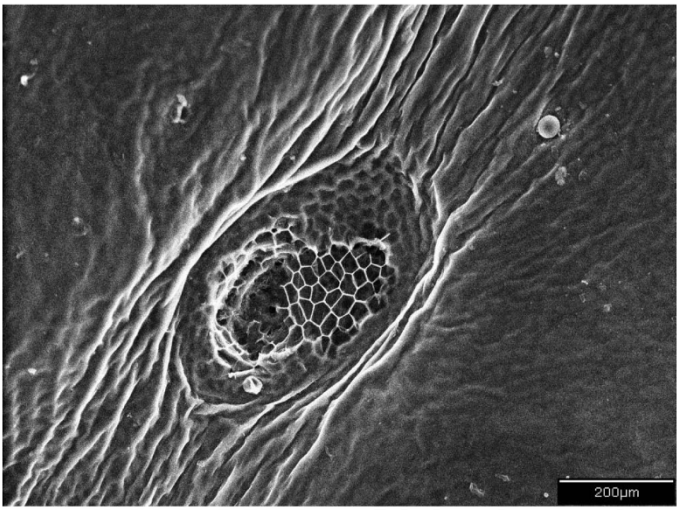


Fig. 13.17. SEM image of the ablation crater produced by a single laser pulse on the adaxial leaf surface of a Zebra plant (*Aphelandra squarrosa*). Scale bar indicates 200 µm. Multiple laser pulses penetrated deeper. The wrinkles on the cuticle were caused by the collapse of the underlying cells due to water loss in the vacuum environment during SEM imaging. Adapted from Ref. [53] with permission. © The American Chemical Society, 2008.

Note: In order to minimize the interference of external electromagnetic fields and air currents the LAESI system is shielded by a Faraday cage and a plastic enclosure, respectively. The enclosure also provides protection from potential health hazards of the fine particulates generated in the laser ablation process.

13.4.5 Atmospheric Pressure Solids Analysis Probe

The *atmospheric pressure solids analysis probe* (ASAP) [55,56] addresses a more classical field of application as it aims to offer an alternative to EI or CI using a direct insertion probe to introduce the analyte into the vacuum. By simply inserting a melting point tube into a stream of hot nitrogen gas, the solid is evaporated from the tube's surface and then ionized at atmospheric pressure by the corona discharge of an APCI source. The hot gas stream (350–500°C) may either be provided by the APCI sprayer or by an ESI sprayer. In contrast to DESI or DAPCI, no solvent is employed in ASAP. The only modification of a commercial API source is the creation of a small port in the housing around the spray region to insert the tube or to seal the hole by a plug to switch back to standard ESI operation.

13.5 Direct Analysis in Real Time

This section on *direct analysis in real time* (DART) [2] has not been placed at the end of this chapter because it would be inferior to the preceding techniques, but because DART relies on much different phenomena. In fact, DART delivers analytical results very similar to those of DESI, even more so to those of DAPCI or DAPPI, and thus presents an alternative concept of ambient MS.

13.5.1 Experimental Setup for DART

A gas flow, typically helium or nitrogen, is guided through a tube divided into three segments. In the first section, a corona discharge between a needle electrode and a first perforated disk electrode produces ions, electrons, and excited atoms (Fig. 13.18). The cold plasma passes through a second chamber where a second perforated electrode can remove cations from the gas stream that is subsequently heated and passed through a final grid electrode removing oppositely charged species. The ionizing neutral gas may either be directed towards the sampling orifice of an API interface, or analogous to DESI, may hit the sample surface at an angle suitable for its reflection into the entrance of the mass spectrometer [2].

Typical operating conditions for DART use a positive discharge needle potential of 1–5 kV while the counter electrode (first perforated disk electrode) is grounded. The potentials of the second perforated electrode and the exit grid electrode are set to positive potentials for positive-ion DART and to negative potentials in the order of a hundred volts for negative-ion mode. The insulator cap protects sample and operator from any high voltage. The gas flow is adjusted to about 1 l min^{-1} and the gas temperature may vary from room temperature up to 250°C. The DART source is adjustable over a range of angles and distances. Typically, a gap of 5–25 mm is established to insert the sample (Fig. 13.19). However, in certain circumstances ions can be detected even when the DART process occurred 1 m away from the mass spectrometer.

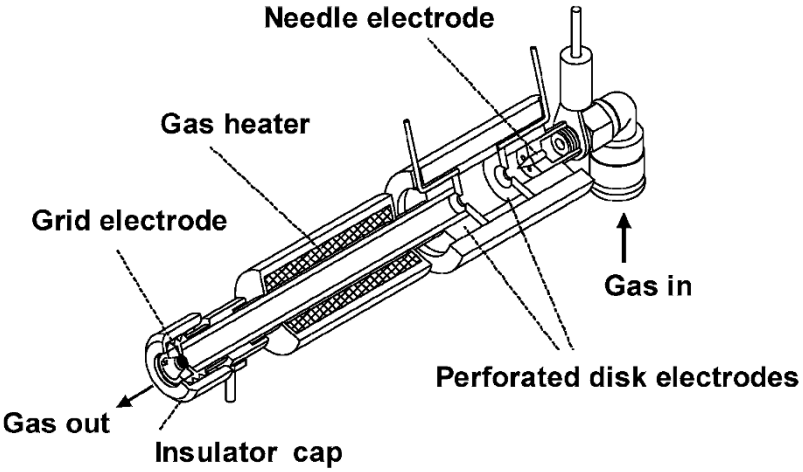


Fig. 13.18. Cutaway view of the DART source. The emanating gas effects ionization of sample independent of its state of aggregation. Reproduced from Ref. [2] with permission. © The American Chemical Society, 2005.



Fig. 13.19. Commercial DART source. Here it is used for the analysis of volatiles from a garlic clove. The sample is simply held in the open gap between the metastable atom source (*lower right part*) and the orifice of the API interface (*upper left*). Photograph by courtesy of JEOL USA.

13.5.2 Ion Formation in DART

The electrical discharge in helium produces a stream of gas-containing electronically excited atoms (metastable atoms), ions, and electrons. The cold plasma gas is then heated and fully depleted of ions by passing it through electrically charged grids. When the stream exits to the open, it may effect ionization of gases, and by direct contact also liquids and solids. It has been proposed that the metastable helium atoms (He*) induce *Penning ionization* (Chap. 2.1.3) of nitrogen and atmospheric water [2,57]:

$$He^* + N_2 \rightarrow He + N_2^{+\bullet} + e^- \quad (13.1)$$

$$He^* + H_2O \rightarrow He + H_2O^{+\bullet} + e^- \quad (13.2)$$

By ion–molecule reactions, the primary ions then deliver protonated water clusters, the most abundant being $H_5O_2^+$. These clusters act as reagent ions for analyte ion generation by chemical ionization mechanisms [58].

Note: The DART discharge belongs to the corona-to-glow (C-G) discharge type that operates with discharge currents in the order of 2 mA at a temperature of 50–60°C [59]. Recently, efforts have been made to provide a more efficient source for metastable atoms. A direct current *atmospheric pressure glow discharge* (APGD) sustained in helium and used in the *flowing afterglow* (FA) mode seems promising [57,59,60].

In negative ion mode, thermal electrons are presumed to generate mostly $O_2^{-\bullet}$ ions from air that serve as reagent ions. Of course, direct electron capture by the analyte as well as dissociative electron capture, deprotonation, or anion attachment are also feasible [58]. Thus, it has been inferred from the close similarity of the negative-ion products of DART and APPI that the same group of mechanisms of ion formation are effective.

13.5.3 Analytical Applications of DART

From the very beginning, DART has been applied variously. This includes the typical safety-related and forensic usages of ambient MS like detection of explosives, warfare agents, or pharmaceuticals and drugs of abuse from cloth, bank notes etc. [2,58,61]. DART also serves for clinical studies of compounds from plasma and urine [62,63] or for examining ballpoint-pen inks on paper, e.g., signatures in cases of check fraud [64]. At the borderline between forensic and environmental applications one finds the analysis of flavors and fragrances even including residues from cosmetic products such as from shampoo on a single hair [65]. In the life sciences, DART is applied for the rapid analysis of fatty acid methyl esters from whole cells [66] or for the recognition of different hydrocarbon profiles on living flies before and after courtship [67]. DART is sensitive enough to analyze self-assembled thiol and dithioether monolayers on gold surfaces [68].

Finally, the analysis of nonpolar compounds such as steroids and hydrocarbons makes DART a very strong competitor for DAPPI [69].

Example: Still under the impression of the 2001 terrorist attack on the World Trade Center, ambient MS initially had a strong focus on the detection of explosives. Negative-ion DART is very sensitive for the analysis of explosives exhibiting extremely low but non-zero vapor pressure [58]. Nitroglycerin has been detected on a man's necktie 8 h after exposure to the plume from blasting at a construction site (Fig. 13.20a) and various explosives present at about 3 ppm in a contaminated pond water sample have been detected; placing a small open bottle with 0.1% aqueous trifluoroacetic acid (H-TFA) in proximity to the sampling zone caused them to appear as $[M+TFA]^-$ adduct peaks in the DART spectrum (Fig. 13.20b) [2].

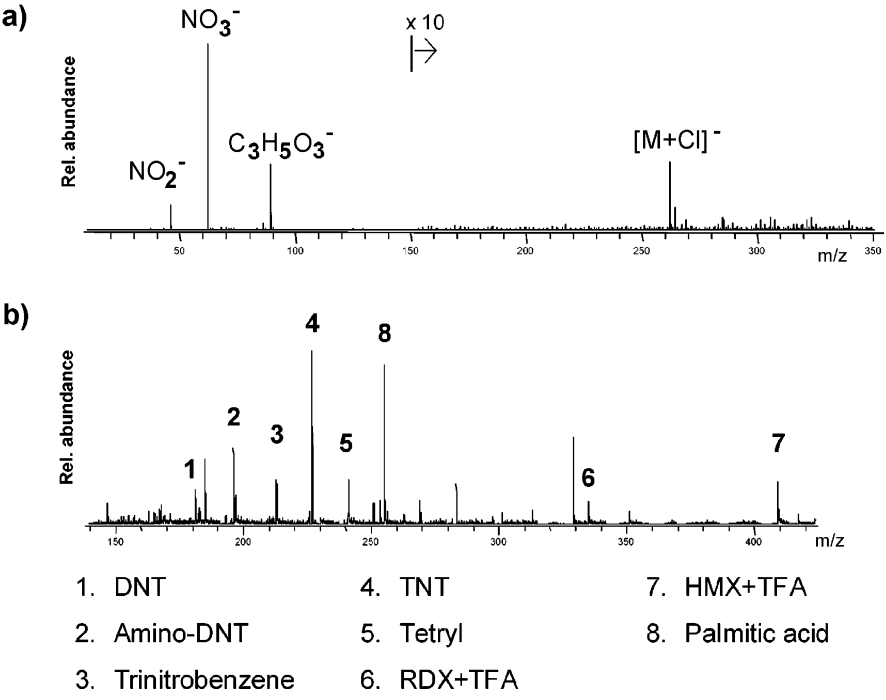


Fig. 13.20. DART spectra of explosives. Spectrum (**a**) shows nitroglycerin detected on a man's necktie 8 h after exposure to the plume from blasting at a construction site. In (**b**) a sample of contaminated pond water exhibits $[M+TFA]^-$ peaks for various explosives that are present at about 3 ppm. Reproduced from Ref. [2] with permission. © The American Chemical Society, 2005.

Example: DART allows for the cuticular hydrocarbon analysis of active fruit flies *Sophophora melanogaster (Drosophila melanogaster)*. The hydrocarbon profile as measured from the exterior of female flies comprises alkenes and alkadienes in the C_{18} to C_{29} range that are detected as $[M+H]^+$ ions. The profile has been

found to vary depending on whether the flies are observed as virgin females, 45 min or 90 min after courtship (Fig. 13.21). There is also a difference between males and females. The advantage of DART is that the fly can be exposed to the ionizing gas stream without risk of electrical shock to both fly and researcher [67].

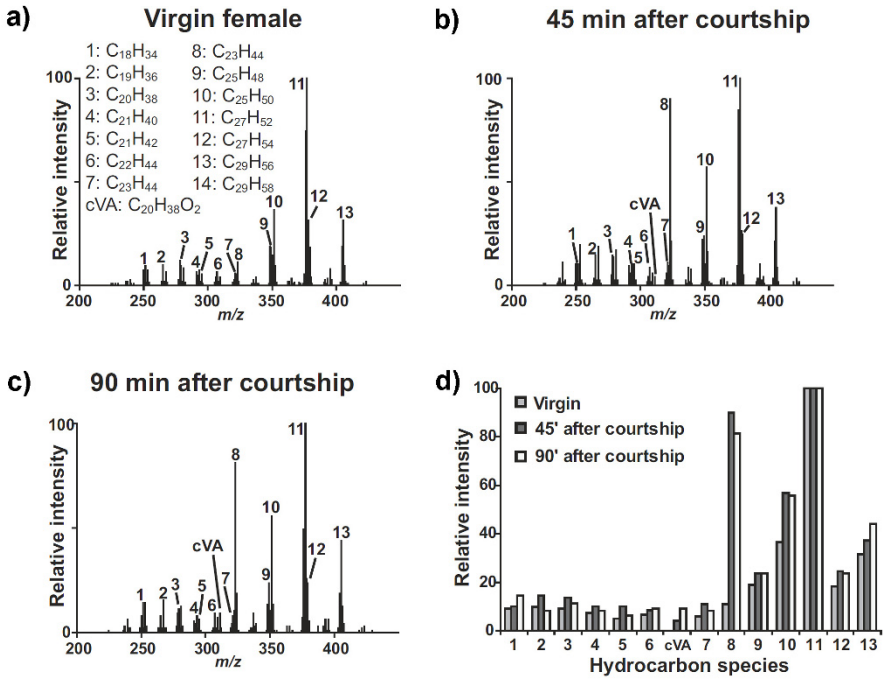


Fig. 13.21. Chemical profile changes in the same individual female fly as observed **(a)** before, **(b)** 45 min after, and **(c)** 90 min after copulation. **(d)** A histogram shows the changes in hydrocarbon concentrations, in particular, an increase in tricosene (peak 8) and pentacosene (peak 10). Reproduced from Ref. [67] with permission. © The National Academy of Sciences of the USA, 2008.

13.6 Overview of Ambient Mass Spectrometry

In closing this chapter, the below short table summarizes ambient MS methods. They are listed in alphabetical order of their acronyms together with a key reference (Table 13.2). It should be noted however, that only the truly simple-to-operate yet effective and rugged interfaces will survive over the years. Most probably, DESI and DART are the ones to persist in the long term.

Table 13.2. Methods of ambient mass spectrometry

Acronym	Full term	Basic principle and key reference
ASAP	Atmospheric pressure solids analysis probe	Evaporation of solids in hot gas stream and ionization by corona discharge [55]
DAPCI	Desorption atmospheric pressure chemical ionization	Sample surface exposed to APCI [17]
DAPPI	Desorption atmospheric pressure photoionization	Sample surface exposed to APPI [9]
DART	Direct analysis in real time	Sample surface exposed to ionizing noble gas stream [2]
DESI	Desorption electrospray ionization	Sample surface exposed to electrospray plume [1,12]
DeSSI	Desorption sonic spray ionization	Sample surface exposed to sonic spray ionization plume; equal to EASI [3]
ELDI	Electrospray-assisted laser desorption ionization	LDI with post-ionization by ESI plume [46]
EASI	Easy ambient sonic-spray ionization	Sample surface exposed to sonic spray ionization plume; equal to DeSSI [33]
EESI	Extractive electrospray ionization	Sample vapor or mist admixed to electrospray plume [6,37]
LAESI	Laser ablation electrospray ionization	IR laser ablation with postionization by ESI plume [53]
MALDESI	Matrix-assisted laser desorption electrospray ionization	Uptake of AP-MALDI plume by ESI spray and transport into API interface [51]

References

1. Takats, Z.; Wiseman, J.M.; Gologan, B.; Cooks, R.G. Mass Spectrometry Sampling Under Ambient Conditions with Desorption Electrospray Ionization. *Science* **2004,** *306*, 471-473.
2. Cody, R.B.; Laramee, J.A.; Durst, H.D. Versatile New Ion Source for the Analysis of Materials in Open Air Under Ambient Conditions. *Anal. Chem.* **2005,** *77*, 2297-2302.
3. Haddad, R.; Sparrapan, R.; Eberlin, M.N. Desorption Sonic Spray Ionization for (High) Voltage-Free Ambient Mass Spectrometry. *Rapid Commun. Mass Spectrom.* **2006,** *20*, 2901-2905.
4. Haddad, R.; Sparrapan, R.; Kotiaho, T.; Eberlin, M.N. Easy Ambient Sonic-Spray Ionization-Membrane Interface Mass Spectrometry for Direct Analysis of Solution Constituents. *Anal. Chem.* **2008,** *80*, 898-903.

5. Chen, H.; Zenobi, R. Direct Analysis of Living Objects by Extractive Electrospray Mass Ionization Spectrometry. *Chimia* **2007,** *61*, 843.
6. Chen, H.; Yang, S.; Wortmann, A.; Zenobi, R. Neutral Desorption Sampling of Living Objects for Rapid Analysis by Extractive Electrospray Ionization Mass Spectrometry. *Angew. Chem., Int. Ed.* **2007,** *46*, 7591-7594.
7. Takats, Z.; Cotte-Rodriguez, I.; Talaty, N.; Chen, H.; Cooks, R.G. Direct, Trace Level Detection of Explosives on Ambient Surfaces by Desorption Electrospray Ionization Mass Spectrometry. *Chem. Commun.* **2005,** 1950-1952.
8. Williams, J.P.; Patel, V.J.; Holland, R.; Scrivens, J.H. The Use of Recently Described Ionisation Techniques for the Rapid Analysis of Some Common Drugs and Samples of Biological Origin. *Rapid Commun. Mass Spectrom.* **2006,** *20*, 1447-1456.
9. Haapala, M.; Pol, J.; Saarela, V.; Arvola, V.; Kotiaho, T.; Ketola, R.A.; Franssila, S.; Kauppila, T.J.; Kostiainen, R. Desorption Atmospheric Pressure Photoionization. *Anal. Chem.* **2007,** *79*, 7867-7872.
10. Cooks, R.G.; Ouyang, Z.; Takats, Z.; Wiseman, J.M. Ambient Mass Spectrometry. *Science* **2006,** *311*, 1566-1570.
11. Wells, J.M.; Roth, M.J.; Keil, A.D.; Grossenbacher, J.W.; Justes, D.R.; Patterson, G.E.; Barket, D.J. Implementation of DART and DESI Ionization on a Fieldable Mass Spectrometer. *J. Am. Soc. Mass Spectrom.* **2008,** *19*, 1419-1424.
12. Takats, Z.; Wiseman, J.M.; Cooks, R.G. Ambient Mass Spectrometry Using Desorption Electrospray Ionization (DESI): Instrumentation, Mechanisms and Applications in Forensics, Chemistry, and Biology. *J. Mass Spectrom.* **2005,** *40*, 1261-1275.
13. Talaty, N.; Takats, Z.; Cooks, R.G. Rapid in Situ Detection of Alkaloids in Plant Tissue Under Ambient Conditions Using Desorption Electrospray Ionization. *Analyst* **2005,** *130*, 1624-1633.
14. Denes, J.; Katona, M.; Hosszu, A.; Czuczy, N.; Takats, Z. Analysis of Biological Fluids by Direct Combination of Solid Phase Extraction and Desorption Electrospray Ionization Mass Spectrometry. *Anal. Chem.* **2009,** *81*, 1669-1675.
15. Drayß, M. Oberflächenanalytik mittels Desorptions Elektrospray Ionisation an einem Tripelquadrupolmassenspektrometer. Diploma Thesis, Heidelberg University, 2005.
16. Takats, Z.; Kobliha, V.; Sevcik, K.; Novak, P.; Kruppa, G.; Lemr, K.; Havlicek, V. Characterization of DESI-FTICR Mass Spectrometry – From ECD to Accurate Mass Tissue Analysis. *J. Mass Spectrom.* **2008,** *43*, 196-203.
17. Cotte-Rodriguez, I.; Takats, Z.; Talaty, N.; Chen, H.; Cooks, R.G. Desorption Electrospray Ionization of Explosives on Surfaces: Sensitivity and Selectivity Enhancement by Reactive Desorption Electrospray Ionization. *Anal. Chem.* **2005,** *77*, 6755-6764.
18. Hopf, C.; Schlueter, M.; Schwarz-Selinger, T.; von Toussaint, U.; Jacob, W. Chemical Sputtering of Carbon Films by Simultaneous Irradiation with Argon Ions and Molecular Oxygen. *New J. Phys.* **2008,** *10*, 093022.
19. Wiseman, J.M.; Puolitaival, S.M.; Takats, Z.; Cooks, R.G.; Caprioli, R.M. Mass Spectrometric Profiling of Intact Biological Tissue by Using Desorption Electrospray Ionization. *Angew. Chem., Int. Ed.* **2005,** *44*, 7094-7097.
20. Chen, H.; Talaty, N.N.; Takats, Z.; Cooks, R.G. Desorption Electrospray Ionization Mass Spectrometry for High-Throughput Analysis of Pharmaceutical Samples in the Ambient Environment. *Anal. Chem.* **2005,** *77*, 6915-6927.
21. Cotte-Rodriguez, I.; Hernandez-Soto, H.; Chen, H.; Cooks, R.G. In Situ Trace Detection of Peroxide Explosives by Desorption Electrospray Ionization and Desorption Atmospheric Pressure Chemical Ionization. *Anal. Chem.* **2008,** *80*, 1512-1519.
22. Cotte-Rodriguez, I.; Mulligan, C.C.; Cooks, R.G. Non-Proximate Detection of Small and Large Molecules by Desorption Electrospray Ionization and Desorption Atmospheric Pressure Chemical Ionization Mass Spectrometry: Instrumentation and Applications in Forensics, Chemistry, and Biology. *Anal. Chem.* **2007,** *79*, 7069-7077.
23. Van Berkel, G.J.; Ford, M.J.; Deibel, M.A. Thin-Layer Chromatography and Mass Spectrometry Coupled Using De-

sorption Electrospray Ionization. *Anal. Chem.* **2005,** *77*, 1207-1215.
24. Chen, H.; Zheng, J.; Zhang, X.; Luo, M.; Wang, Z.; Qiao, X. Surface Desorption Atmospheric Pressure Chemical Ionization Mass Spectrometry for Direct Ambient Sample Analysis Without Toxic Chemical Contamination. *J. Mass Spectrom.* **2007,** *42*, 1045-1056.
25. Chen, H.; Liang, H.; Ding, J.; Lai, J.; Huan, Y.; Qiao, X. Rapid Differentiation of Tea Products by Surface Desorption Atmospheric Pressure Chemical Ionization Mass Spectrometry. *J. Agric. Food Chem.* **2007,** *55*, 10093-10100.
26. Yang, S.; Ding, J.; Zheng, J.; Hu, B.; Li, J.; Chen, H.; Zhou, Z.; Qiao, X. Detection of Melamine in Milk Products by Surface Desorption Atmospheric Pressure Chemical Ionization Mass Spectrometry. *Anal. Chem.* **2009,** *81*, 2426-2436.
27. Luosujarvi, L.; Arvola, V.; Haapala, M.; Pol, J.; Saarela, V.; Franssila, S.; Kotiaho, T.; Kostiainen, R.; Kauppila, T.J. Desorption and Ionization Mechanisms in Desorption Atmospheric Pressure Photoionization. *Anal. Chem.* **2008,** *80*, 7460-7466.
28. Luosujarvi, L.; Laakkonen, U.M.; Kostiainen, R.; Kotiaho, T.; Kauppila, T.J. Analysis of Street Market Confiscated Drugs by Desorption Atmospheric Pressure Photoionization and Desorption Electrospray Ionization Coupled with Mass Spectrometry. *Rapid Commun. Mass Spectrom.* **2009,** *23*, 1401-1404.
29. Kauppila, T.J.; Arvola, V.; Haapala, M.; Pol, J.; Aalberg, L.; Saarela, V.; Franssila, S.; Kotiaho, T.; Kostiainen, R. Direct Analysis of Illicit Drugs by Desorption Atmospheric Pressure Photoionization. *Rapid Commun. Mass Spectrom.* **2008,** *22*, 979-985.
30. Hirabayashi, Y.; Takada, Y.; Hirabayashi, A.; Sakairi, M.; Koizumi, H. Direct Coupling of Semi-Micro Liquid Chromatography and Sonic Spray Ionization Mass Spectrometry for Pesticide Analysis. *Rapid Commun. Mass Spectrom.* **1996,** *10*, 1891-1893.
31. Hiraoka, K. Sonic Spray Ionization Mass Spectrometry. *J. Mass Spectrom. Soc. of Japan* **1996,** *44*, 279-284.
32. Hirabayashi, A.; Fernandez de la Mora, J. Charged Droplet Formation in Sonic Spray. *Int. J. Mass Spectrom. Ion Proc.* **1998,** *175*, 277-282.
33. Haddad, R.; Catharino, R.R.; Marques, L.A.; Eberlin, M.N. Perfume Fingerprinting by Easy Ambient Sonic-Spray Ionization Mass Spectrometry: Nearly Instantaneous Typification and Counterfeit Detection. *Rapid Commun. Mass Spectrom.* **2008,** *22*, 3662-3666.
34. Abdelnur, P.V.; Eberlin, L.S.; de Sa, G.F.; de Souza, V.; Eberlin, M.N. Single-Shot Biodiesel Analysis: Nearly Instantaneous Typification and Quality Control Solely by Ambient Mass Spectrometry. *Anal. Chem.* **2008,** *80*, 7882-7886.
35. Saraiva, S.A.; Abdelnur, P.V.; Catharino, R.R.; Nunes, G.; Eberlin, M.N. Fabric Softeners: Nearly Instantaneous Characterization and Quality Control of Cationic Surfactants by Easy Ambient Sonic-Spray Ionization Mass Spectrometry. *Rapid Commun. Mass Spectrom.* **2009,** *23*, 357-362.
36. Haddad, R.; Milagre, H.M.S.; Catharino, R.R.; Eberlin, M.N. Easy Ambient Sonic-Spray Ionization Mass Spectrometry Combined with Thin-Layer Chromatography. *Anal. Chem.* **2008,** *80*, 2744-2750.
37. Chen, H.; Venter, A.; Cooks, R.G. Extractive Electrospray Ionization for Direct Analysis of Undiluted Urine, Milk and other Complex Mixtures Without Sample Preparation. *Chem. Commun.* **2006,** 2042-2044.
38. Chen, H.; Wortmann, A.; Zenobi, R. Neutral Desorption Sampling Coupled to Extractive Electrospray Ionization Mass Spectrometry for Rapid Differentiation of Biosamples by Metabolomic Fingerprinting. *J. Mass Spectrom.* **2007,** *42*, 1123-1135.
39. Chang, D.Y.; Lee, C.C.; Shiea, J. Detecting Large Biomolecules from High-Salt Solutions by Fused-Droplet Electrospray Ionization Mass Spectrometry. *Anal. Chem.* **2002,** *74*, 2465-2469.
40. Shieh, I.F.; Lee, C.Y.; Shiea, J. Eliminating the Interferences from TRIS Buffer and SDS in Protein Analysis by Fused-Droplet Electrospray Ionization Mass Spectrometry. *J. Proteome Res.* **2005,** *4*, 606-612.
41. Chen, H.; Sun, Y.; Wortmann, A.; Gu, H.; Zenobi, R. Differentiation of Maturity and Quality of Fruit Using Noninva-

sive Extractive Electrospray Ionization Quadrupole Time-of-Flight Mass Spectrometry. *Anal. Chem.* **2007,** *79*, 1447-1455.
42. Chingin, K.; Gamez, G.; Chen, H.; Zhu, L.; Zenobi, R. Rapid Classification of Perfumes by Extractive Electrospray Ionization Mass Spectrometry (EESI-MS). *Rapid Commun. Mass Spectrom.* **2008,** *22*, 2009-2014.
43. Zhu, L.; Gamez, G.; Chen, H.; Chingin, K.; Zenobi, R. Rapid Detection of Melamine in Untreated Milk and Wheat Gluten by Ultrasound-Assisted Extractive Electrospray Ionization Mass Spectrometry (EESI-MS). *Chem. Commun.* **2009,** 559-561.
44. Chen, H.; Hu, B.; Hu, Y.; Huan, Y.; Zhou, Z.; Qiao, X. Neutral Desorption Using a Sealed Enclosure to Sample Explosives on Human Skin for Rapid Detection by EESI-MS. *J. Am. Soc. Mass Spectrom.* **2009,** *20*, 719-722.
45. Quist, A.P.; Huth-Fehre, T.; Sundqvist, B.U.R. Total Yield Measurements in Matrix-Assisted Laser Desorption Using a Quartz Crystal Microbalance. *Rapid Commun. Mass Spectrom.* **1994,** *8*, 149-154.
46. Shiea, J.; Huang, M.Z.; Hsu, H.J.; Lee, C.Y.; Yuan, C.H.; Beech, I.; Sunner, J. Electrospray-Assisted Laser Desorption/Ionization Mass Spectrometry for Direct Ambient Analysis of Solids. *Rapid Commun. Mass Spectrom.* **2005,** *19*, 3701-3704.
47. Peng, I.X.; Shiea, J.; Loo, R.R.O.; Loo, J.A. Electrospray-Assisted Laser Desorption/Ionization and Tandem Mass Spectrometry of Peptides and Proteins. *Rapid Commun. Mass Spectrom.* **2007,** *21*, 2541-2546.
48. Huang, M.Z.; Hsu, H.J.; Lee, J.Y.; Jeng, J.; Shiea, J. Direct Protein Detection from Biological Media Through Electrospray-Assisted Laser Desorption Ionization/Mass Spectrometry. *J. Proteome Res.* **2006,** *5*, 1107-1116.
49. Huang, M.Z.; Hsu, H.J.; Wu, C.I.; Lin, S.Y.; Ma, Y.L.; Cheng, T.L.; Shiea, J. Characterization of the Chemical Components on the Surface of Different Solids with Electrospray-Assisted Laser Desorption Ionization Mass Spectrometry. *Rapid Commun. Mass Spectrom.* **2007,** *21*, 1767-1775.
50. Lin, S.Y.; Huang, M.Z.; Chang, H.C.; Shiea, J. Using Electrospray-Assisted Laser Desorption/Ionization Mass Spectrometry to Characterize Organic Compounds Separated on Thin-Layer Chromatography Plates. *Anal. Chem.* **2007,** *79*, 8789-8795.
51. Sampson, J.S.; Hawkridge, A.M.; Muddiman, D.C. Generation and Detection of Multiply-Charged Peptides and Proteins by Matrix-Assisted Laser Desorption Electrospray Ionization (MALDESI) Fourier Transform Ion Cyclotron Resonance Mass Spectrometry. *J. Am. Soc. Mass Spectrom.* **2006,** *17*, 1712-1716.
52. Nemes, P.; Vertes, A. Laser Ablation Electrospray Ionization for Atmospheric Pressure, in Vivo, and Imaging Mass Spectrometry. *Anal. Chem.* **2007,** *79*, 8098-8106.
53. Nemes, P.; Barton, A.A.; Li, Y.; Vertes, A. Ambient Molecular Imaging and Depth Profiling of Live Tissue by Infrared Laser Ablation Electrospray Ionization Mass Spectrometry. *Anal. Chem.* **2008,** *80*, 4575-4582.
54. Sripadi, P.; Nazarian, J.; Hathout, Y.; Hoffman, E.P.; Vertes, A. In Vitro Analysis of Metabolites from the Untreated Tissue of *Torpedo Californica* Electric Organ by Mid-Infrared Laser Ablation Electrospray Ionization Mass Spectrometry. *Metabolomics* **2009,** *5*, 263-276.
55. McEwen, C.N.; McKay, R.G.; Larsen, B.S. Analysis of Solids, Liquids, and Biological Tissues Using Solids Probe Introduction at Atmospheric Pressure on Commercial LC/MS Instruments. *Anal. Chem.* **2005,** *77*, 7826-7831.
56. McEwen, C.; Gutteridge, S. Analysis of the Inhibition of the Ergosterol Pathway in Fungi Using the Atmospheric Solids Analysis Probe (ASAP) Method. *J. Am. Soc. Mass Spectrom.* **2007,** *18*, 1274-1278.
57. Andrade, F.J.; Shelley, J.T.; Wetzel, W.C.; Webb, M.R.; Gamez, G.; Ray, S.J.; Hieftje, G.M. Atmospheric Pressure Chemical Ionization Source. 1. Ionization of Compounds in the Gas Phase. *Anal. Chem.* **2008,** *80*, 2646-2653.
58. Song, L.; Dykstra, A.B.; Yao, H.; Bartmess, J.E. Ionization Mechanism of Negative Ion-Direct Analysis in Real Time: A Comparative Study with Negative Ion-Atmospheric Pressure

Photoionization. *J. Am. Soc. Mass Spectrom.* **2009,** *20*, 42-50.
59. Shelley, J.T.; Wiley, J.S.; Chan, G.C.Y.; Schilling, G.D.; Ray, S.J.; Hieftje, G.M. Characterization of Direct-Current Atmospheric-Pressure Discharges Useful for Ambient Desorption/Ionization Mass Spectrometry. *J. Am. Soc. Mass Spectrom.* **2009,** *20*, 837-844.
60. Andrade, F.J.; Shelley, J.T.; Wetzel, W.C.; Webb, M.R.; Gamez, G.; Ray, S.J.; Hieftje, G.M. Atmospheric Pressure Chemical Ionization Source. 2. Desorption-Ionization for the Direct Analysis of Solid Compounds. *Anal. Chem.* **2008,** *80*, 2654-2663.
61. Fernandez, F.M.; Cody, R.B.; Green, M.D.; Hampton, C.Y.; McGready, R.; Sengaloundeth, S.; White, N.J.; Newton, P.N. Characterization of Solid Counterfeit Drug Samples by Desorption Electrospray Ionization and Direct-Analysis-in-Real-Time Coupled to Time-of-Flight Mass Spectrometry. *ChemMedChem* **2006,** *1*, 702-705.
62. Zhao, Y.; Lam, M.; Wu, D.; Mak, R. Quantification of Small Molecules in Plasma with Direct Analysis in Real Time Tandem Mass Spectrometry, Without Sample Preparation and Liquid Chromatographic Separation. *Rapid Commun. Mass Spectrom.* **2008,** *22*, 3217-3224.
63. Jagerdeo, E.; Abdel-Rehim, M. Screening of Cocaine and Its Metabolites in Human Urine Samples by Direct Analysis in Real-Time Source Coupled to Time-of-Flight Mass Spectrometry After Online Preconcentration Utilizing Microextraction by Packed Sorbent. *J. Am. Soc. Mass Spectrom.* **2009,** *20*, 891-899.
64. Jones, R.W.; Cody, R.B.; McClelland, J.F. Differentiating Writing Inks Using Direct Analysis in Real Time Mass Spectrometry. *J. Forensic Sci.* **2006,** *51*, 915-918.
65. Haefliger, O.P.; Jeckelmann, N. Direct Mass Spectrometric Analysis of Flavors and Fragrances in Real Applications Using DART. *Rapid Commun. Mass Spectrom.* **2007,** *21*, 1361-1366.
66. Yu, S.; Crawford, E.; Tice, J.; Musselman, B.; Wu, J.T. Bioanalysis Without Sample Cleanup or Chromatography: The Evaluation and Initial Implementation of Direct Analysis in Real Time Ionization Mass Spectrometry for the Quantification of Drugs in Biological Matrixes. *Anal. Chem.* **2009,** *81*, 193-202.
67. Yew, J.Y.; Cody, R.B.; Kravitz, E.A. Cuticular Hydrocarbon Analysis of an Awake Behaving Fly Using Direct Analysis in Real-Time Time-of-Flight Mass Spectrometry. *Proc. Natl. Acad. Sci. U.S.A.* **2008,** *105*, 7135-7140.
68. Kpegba, K.; Spadaro, T.; Cody, R.B.; Nesnas, N.; Olson, J.A. Analysis of Self-Assembled Monolayers on Gold Surfaces Using Direct Analysis in Real Time Mass Spectrometry. *Anal. Chem.* **2007,** *79*, 5479-5483.
69. Cody, R.B. Observation of Molecular Ions and Analysis of Nonpolar Compounds with the Direct Analysis in Real Time Ion Source. *Anal. Chem.* **2009,** *81*, 1101-1107.

14 Hyphenated Methods

Learning Objectives

- Coupling of separation methods to MS
- Basics of quantitation by MS
- Tandem MS modes for improved selectivity
- Tandem MS as a complement for chromatography coupling
- Ultrahigh resolution as a complement for chromatography coupling

---

The analysis of complex mixtures generally requires the combination of both separation techniques and mass spectrometry [1-3]. The first step in this direction was made by *gas chromatography-mass spectrometry* (GC-MS) coupling [4]. Soon, GC-MS became a routine method for mixture analysis [5-7]. The aim and attempt to also handle highly polar nonvolatile compounds by *liquid chromatography-mass spectrometry* (LC-MS) [8-11] eventually led to the development of API methods (Chap. 12) [12-15]. The expansion of this approach to coupling of other liquid-phase separation techniques to mass spectrometry followed as *capillary zone electrophoresis-mass spectrometry* (CZE-MS) [16-20] and *supercritical fluid chromatography-mass spectrometry* (SFC-MS) [21-25]. Regardless of the type of separation technique, it always adds an additional dimension to the analytical measurement. The hyphen used to indicate the coupling of a separation technique to mass spectrometry led to the group term *hyphenated methods*.

Mass spectrometry itself also offers two additional "degrees of freedom". The complexity of a sample can either be resolved by high or even ultrahigh mass resolution or by employing tandem MS techniques (Chap. 9), e.g., by separating the fragmentation pattern of one component from that of others in a mixture [2,3]. In practice, the coupling of separation techniques to mass spectrometry often involves advanced MS techniques to achieve the desired level of selectivity. This altogether ensures accuracy and reliability of analytical information [1,6,26-29]. (For *accuracy* and *precision* cf. Chap. 3.5.4.)

This chapter is about extending the range of samples that can be analyzed by mass spectrometry and about increasing the specificity of analytical information thereof. It briefly explains the basic concepts and methodologies such as handling of chromatograms, quantitation, as well as chromatography-mass spectrometry interfaces.

J. Gross, *Mass Spectrometry*, 2nd ed., DOI 10.1007/978-3-642-10711-5_14,
© Springer-Verlag Berlin Heidelberg 2011

Note: From an MS-centered view, any chromatographic system simply is another type of sample inlet, whereas from the chromatographer's point of view mass spectrometers are just detectors for their separation technique. Here, we deal with the peculiarities of those analyte-separating inlets and the associated implications for the operation of the attached mass spectrometers.

14.1 Concept of Chromatography-Mass Spectrometry

Chromatography separates the components of a mixture by their *retention times*, i.e., by the point in time when they are eluting from the chromatographic column. Simple chromatographic detectors such as the *flame ionization detector* (FID), frequently employed in GC, deliver a *chromatogram* that represents the mass flow eluting from the chromatographic column. Using a mass spectrometer instead, offers a third dimension of information, i.e., the mass spectra associated to any of the eluting components (Fig. 14.1). When a mass spectrometer is employed as the chromatographic detector (also cf. Chaps. 5.4, 5.5) its output must somehow represent the chromatogram that would have been obtained with other chromatographic detectors. The chromatogram as produced by the mass spectrometer is composed of a large set of consecutively acquired mass spectra. Because mass spectral chromatograms represent ionic abundances as a function of retention time, these are termed *ion chromatograms*.

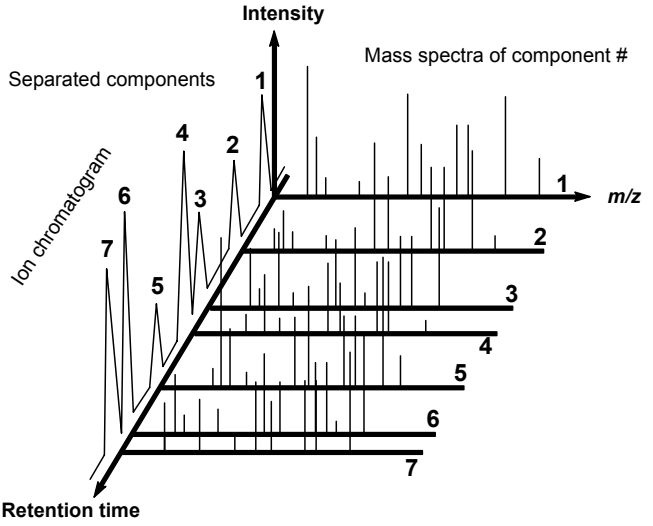


Fig. 14.1. Three dimensions of chromatography-mass spectrometry: retention time, intensity, and *m/z*. Each compound eluting from the chromatographic column is characterized by its own mass spectrum. The sum of all peak intensities of a mass spectrum at any point in retention time is used to construct the ion chromatogram.

14.1.1 Ion Chromatograms

Several decades ago, the *total ion current* (TIC) used to be measured by a *hardware TIC monitor* before mass analysis (nA to μA range). Today, its equivalent can be *reconstructed* or *extracted* after mass analysis [30]. Both adjectives, *reconstructed* and *extracted*, serve to illustrate that the chromatogram was obtained from a set of spectra by a computational process selecting user-defined signals to build the trace. For convenience, let us here again define some of the relevant terminology introduced in Chap. 1.3: The TIC represents a measure of the overall intensity of ion production as a function of time. The TIC obtained by means of *data reduction* [31], i.e., by summation of peak intensities of each mass spectrum as successively acquired during analysis, is termed *total ion chromatogram* (also abbreviated TIC). For this purpose, the sum of all ion intensities of each of the spectra is plotted as a function of time or scan number, respectively (Fig. 14.1). The term *total ion current chromatogram* (TICC) refers to a chromatogram obtained by plotting the total ion current detected in each of a series of mass spectra recorded as a function of retention times of the chromatographically separated components of a mixture (which essentially is implicated by: TIC). Unfortunately one also finds combinations such as *reconstructed total ion current* (RTIC), *reconstructed total ion current chromatogram* (RTICC), and *extracted ion chromatogram* (EIC, Table 14.1).

Table 14.1. Types of ion chromatograms

Acronym	Full name	Comment
TIC	Total ion chromatogram	Sum of ionic abundances or intensities per spectrum vs. retention time. In practice used interchangeably. TIC is recommended here as the least complicated form.
TICC	Total ion current chromatogram	
RTIC	Reconstructed total ion chromatogram	
RTICC	Reconstructed total ion current chromatogram	
RIC	Reconstructed ion chromatogram	Signal intensity at selected *m/z* vs. retention time. In practice used interchangeably.
EIC	Extracted ion chromatogram	
BPC	Base peak chromatogram	Base peak intensity of each spectrum plotted vs. retention time.

The term *reconstructed ion chromatogram* (RIC) was and still is used by many to describe the intensity of a given *m/z* or *m/z* range plotted as a function of time or scan number. Recently, the term *extracted ion chromatogram* (EIC) has been used to describe a chromatogram created by plotting the intensity of the signal observed at a chosen *m/z* value or set of values in a series of mass spectra recorded as a function of retention time. Plotting RICs or EICs is especially useful to identify a target compound of known *m/z* from complex GC-MS or LC-MS data. In other words, the RIC allows to retrieve the retention time of the target compound. RICs can also be used to elucidate the relationship of certain *m/z* values to differ-

ent mass spectra obtained from the measurement of a single (impure) sample. Thus, RICs (EICs) often reveal valuable information on impurities accompanying the main product, e.g., remaining solvents, plasticizers, vacuum grease, or synthetic by-products (Chap. 5.2.4). Finally, the *base peak chromatogram* (BPC) is a chromatogram obtained by plotting the signal of the base-peak ions detected in each of a series of mass spectra recorded as a function of retention time.

14.1.2 Repetitive Acquisition of Mass Spectra During Elution

A widespread mode of chromatography-mass spectrometry operation is to repetitively scan the mass analyzer over the *m/z* range of interest during the chromatographic run [32-34]. As explained above, this generates a relationship between chromatogram and mass spectra of the eluting components. Knowledgeable handling of the TIC and suitable RICs presents the key to the effective assignment of chromatographic peaks to target compounds.

Example: 4-Hydroxynon-2-enal (4-HNE) is a major aldehydic product of lipid peroxidation (LPO), its products being indicators for oxidative stress. In order to introduce LPO products as biomarkers, a GC-MS method for 4-HNE detection in clinical studies [35] was developed using a sample volume of 50 µl of plasma. For improved GC separation and subsequent mass spectral detection the aldehyde is converted into the pentafluorobenzyl-hydroxylimine and the hydroxy group is trimethylsilylated [36]. The TIC acquired in electron capture mode (EC, Chap. 7.4) exhibits 50 chromatographic peaks (Fig. 14.2). Those related to the target compounds can easily be identified from suitable RICs. The choice of potentially useful *m/z* values for RICs is made from the EC mass spectrum of the pure 4-HNE derivative (below). In this case, $[M–HF]^{-\bullet}$, *m/z* 403, $[M–HOSiMe_3]^{-\bullet}$, *m/z* 333, and $[C_6F_5]^-$, *m/z* 167, are indicative, while $[CH_2C_6F_5]^-$, *m/z* 181, is not.

Note: The abscissa of the TIC or RIC can either be plotted on the time scale, i.e., in units of seconds or minutes, or be labeled with scan numbers. Scan numbers are useful during data processing, while the time scale is better suited for comparison with other chromatography-mass spectrometry data.

When the experiment is performed in the repetitive scanning mode, each point of the TIC corresponds to a full mass spectrum. The time for the acquisition of a mass spectrum has to be shorter than the time to elute a component from the chromatographic column. In capillary GC-MS, this requires scan cycle times in the order of one second. A 20-minute run at one scan per second, for example, delivers a set of 1200 mass spectra. Nonetheless, the concentration of the eluting components still varies rapidly in time as compared to the time for a scan cycle. This affects the relative intensities of mass spectral peaks, i.e., high-mass ions are emphasized in an upwards mass scan at the onset of elution, but are underrepresented when elution fades out (Fig. 14.3).

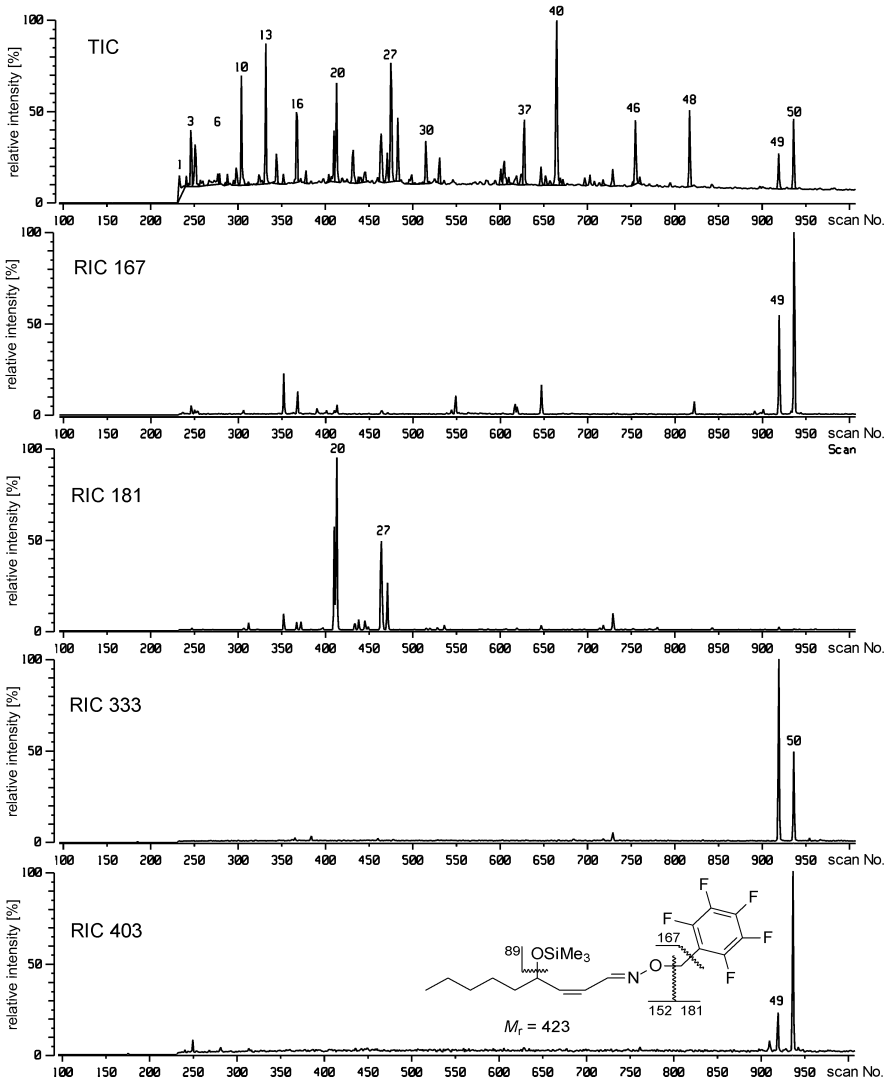


Fig. 14.2. TIC and RICs (*m/z* 167, 181, 333, and 403) obtained from a GC-EC-MS run of a plasma sample spiked with 4-HNE [36]. (The EC spectrum of the 4-HNE derivative is show in Fig. 14.3.).

Averaging or *accumulation* of the scans contributing to a specific chromatographic peak compensates for that source of error. Additional *background subtraction* can substantially improve the signal-to-noise ratio (Chap. 5.2.3.) of the final spectrum [33]. It is also obvious from this procedure that the number of final spectra is always lower than the actual number of scans.

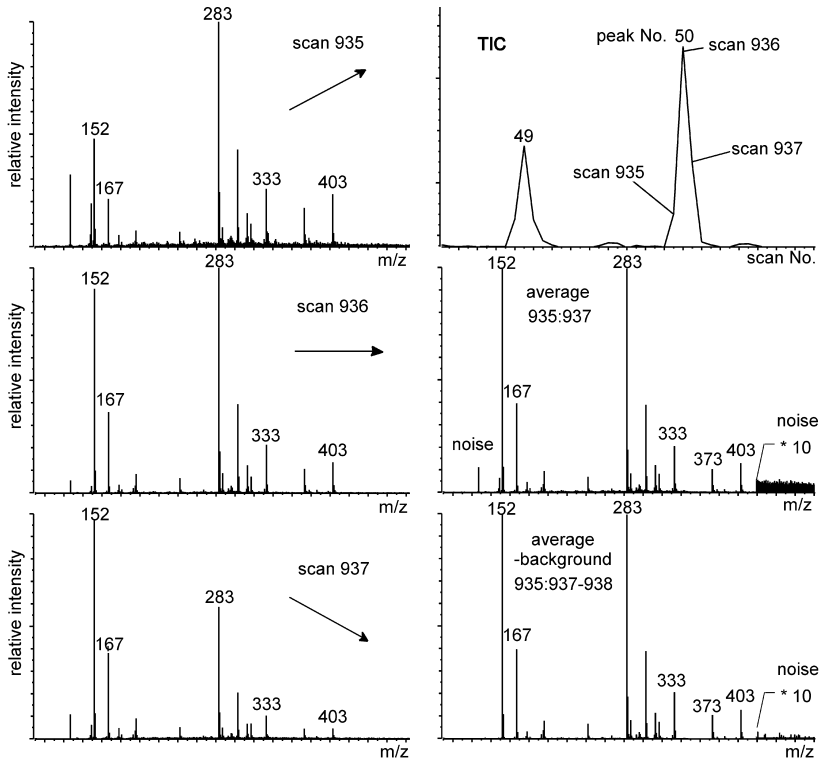


Fig. 14.3. Extraction of spectra from chromatographic peak No. 50 in the TIC of a plasma sample spiked with 4-HNE. *Left column*: single scan spectra from scans No. 935, 936, and 937 show changing relative intensities; averaging scans 935:937 levels intensity but leaves noise; background subtraction reduces noise additionally. (For explication, TIC, and RICs see preceding example and Fig. 14.2.)

Note: High-quality mass spectra suitable for interpretation and/or data base search (Chap. 5.7) are only obtained from summing/averaging plus subsequent background subtraction. Particularly for components of low concentration the value of background subtraction cannot be overestimated.

14.1.3 Selected Ion Monitoring

The operation of mass spectrometers in the repetitive scanning mode is useful for the identification of the components of a mixture. If *quantitation* is a major issue (below), *selected ion monitoring* (SIM) is preferably employed; the term *multiple ion detection* (MID) and some others are also in use [37]. In the SIM mode, the mass analyzer is operated in a way that it alternately acquires only the ionic masses of interest, i.e., it "jumps" from one *m/z* to the next [38-43]. The informa-

tion obtained from a SIM trace is equivalent to that from a RIC, but no mass spectra are recorded in SIM mode. Thus, the scan time spent on diagnostically useless *m/z* ranges or even on mere noise in the gaps between peaks is almost reduced to zero while the detector time for the ions of interest is increased by a factor of 10–100 (Fig. 14.4) [44]. An analogous improvement in sensitivity (Chap. 1.4.1) is also observed.

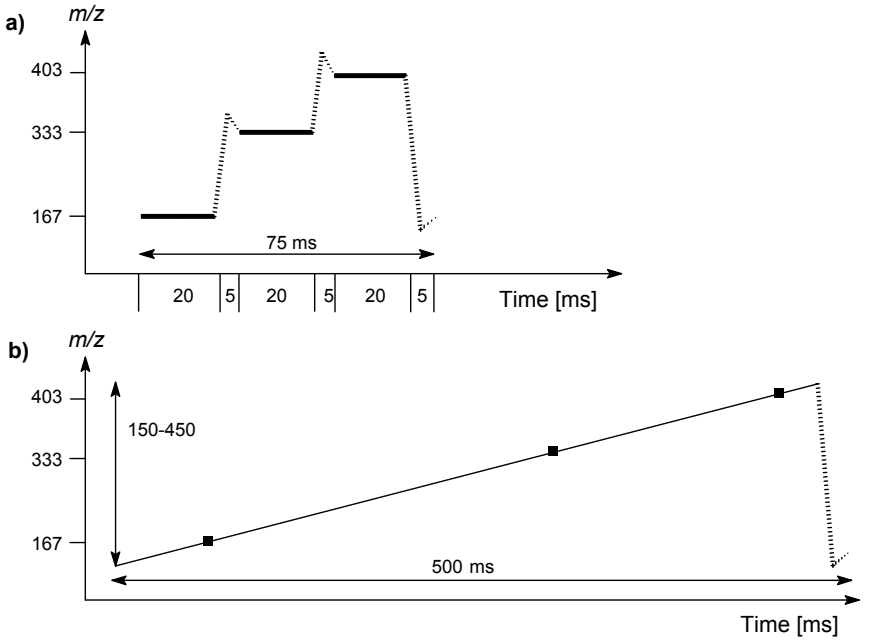


Fig. 14.4. SIM advantage over scanning mode. (**a**) Hypothetical SIM experiment to analyze 4-HNE in a plasma sample by *m/z* 167, 333, and 403 compared to (**b**) 500 ms-scan over the *m/z* 150–450 range. Only about 1.5 ms would be spent on each of the three signals during a 500 ms-scan while 20 ms are achieved for each in a much shorter 75 ms-SIM cycle with 5 ms settling time. (Time axes are not to scale.)

As the monitored *m/z* values are selected to best represent the target compound, SIM exhibits good selectivity that can be further increased by *high-resolution SIM* (HR-SIM) because HR-SIM almost eliminates isobaric interferences [45-48]. To ensure precise and drift-free positioning on narrow peaks, HR-SIM requires one or several *lock masses* to be employed although those are rarely explicitly mentioned in the literature [48,49]. The role of the lock mass is to serve as internal mass reference for accurate mass measurement. (For examples cf. Chap. 14.2.)

Only scanning instruments like magnetic sector and (triple) quadrupole mass spectrometers show improved sensitivity in SIM mode. Quadrupole ion traps (QIT and LIT) might be operated as to deliver a SIM output, the time to achieve ion selection is, however, essentially identical to their full scan cycle time, thus cancel-

ing out the sensitivity advantage. With oaTOF analyzers the SIM mode can neither be realized nor would it offer any improvement over getting a RIC.

Note: Normally, three to ten *m/z* values are monitored 20–100 ms each in one SIM cycle. Some settling time is needed for the mass analyzer after switching to the next value, e.g., 1–2 ms for pure electric scanning, 20–50 ms for a magnet scan. Due to the comparatively slow axial ion velocity in (triple) quadrupole instruments, the time to empty the quadrupole from one ionic species prior to setting it to the next has to be taken into account.

14.1.4 Selected Reaction Monitoring

Tandem MS adds a fourth dimension to the chromatography-MS experiment in that it allows to acquire a spectrum selectively, revealing the fragmentation of one specific ion generated of the target compound (Fig. 14.5). Like SIM, the approach of *selected reaction monitoring* (SRM, Table 14.2) requires useful ionic fragmentation pathways to be explored before their use in SRM analyses. If two or more ionic fragmentations are covered in one cycle the experiment is termed *multiple reaction monitoring* (MRM). Triple quadrupole instruments are preferred for SRM and MRM operation as they combine straightforward tandem MS operation and fast switching of *m/z* with a high linear dynamic range (10^4–10^5). (Examples of MRM and SRM are given in Chaps. 14.4 and 14.6, respectively.)

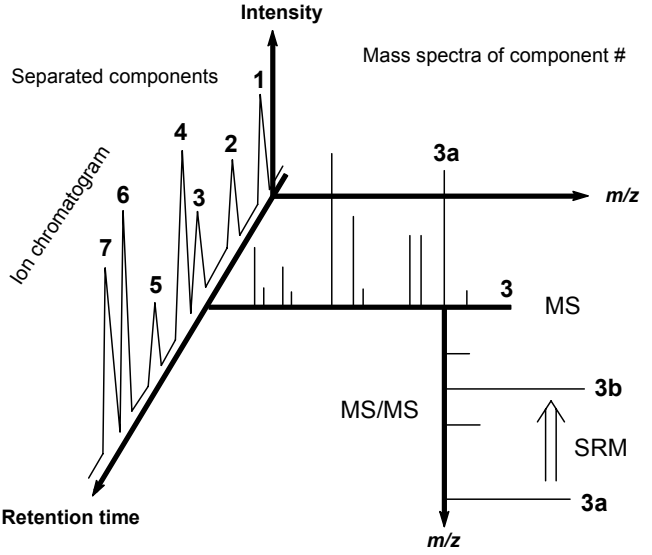


Fig. 14.5. The fourth dimension added by chromatography-tandem MS. Compound **3** has been chosen to illustrate the effect of selectively measuring the fragmentation of one precursor ion, **3a**, defined by its *m/z*. If the instrument is operated as to only detect one characteristic product ion, **3b**, the mode is termed *selected reaction monitoring* (SRM).

Table 14.2. Discontinuous modes of operation

Acronym	Full name	Comment
SIM MID	Selected ion monitoring Multiple ion detection	In practice used interchangeably; the term SIM is recommended.
HR-SIM	High-resolution selected ion monitoring	To avoid isobaric interferences
SRM MRM	Selected reaction monitoring Multiple reaction monitoring	SIM in a tandem MS mode More than one reaction per cycle

14.2 Quantitation

Every ionization method exhibits compound-dependent ionization efficiencies (Chap. 2.4). Whether a specific compound is rather preferred or suppressed relative to another greatly depends on the ionization process employed to deliver the ions to the mass analyzer. These circumstances require a careful calibration of the instrument's response versus the sample concentration for correct *quantitation* [6,7,50]. While relative signal intensities are perfect for qualitative analysis, i.e., for compound characterization, some means of measuring absolute intensities would be preferred in quantitation. Basic considerations on how to approach a quantitative analysis by mass spectrometry are given below [51-54]. Readers interested in a treatment of all aspects of quantitative analysis by mass spectrometry may refer to the highly recommended book by Boyd, Basic, and Bethem [50].

14.2.1 Quantitation by External Standardization

External standardization is obtained by constructing a *calibration curve*, i.e., plotting measured intensities versus rising concentration of the target compound. Calibration curves are generally linear over a wide range of concentrations. When the concentration approaches the detection limit (Chap. 1.4.2) the graph deviates from linearity, either towards underestimation or towards overestimation. Underestimation can be due to losses by adsorption, overestimation may either be due to "memory" from previous injections or result from chemical background. In the regime of high concentration, saturation of the detector or of the ion source cause an upper limit (Fig. 14.6). The preparation of a calibration curve requires repeated measurements which can be very time-consuming in case of a slow chromatographic separation. In addition, drifts in instrument sensitivity, e.g., due to ion source contamination, can deteriorate the quantitation result. Depending on the instrument's dynamic range (Chap. 4.2.11), the range of linear response is in the order of two to four orders of magnitude.

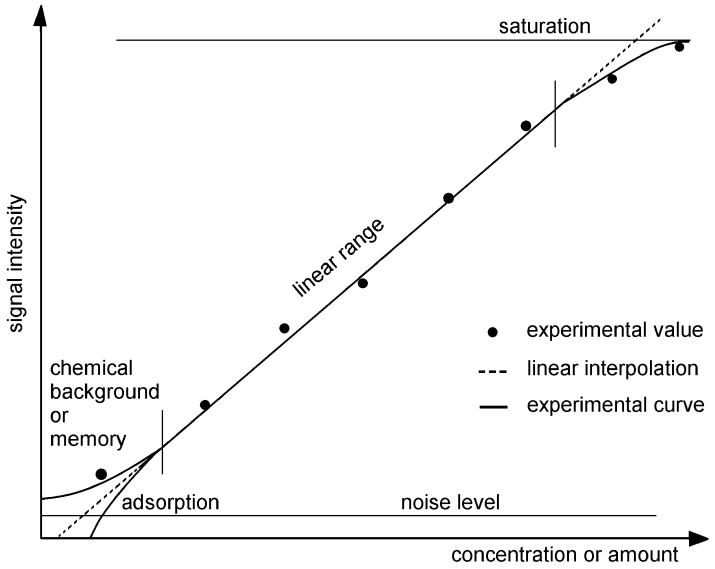


Fig. 14.6. General appearance of a calibration curve. The upper limit of the linear range is defined by saturation, the lower by memory and chemical background or adsorption. In addition, the noise level plays a role for the detection limit.

Note: In practice, four or five runs at increasing concentration of the standard, preferably from well above the detection limit to close to saturation, should be run in a sequence to obtain the data for the construction of a calibration curve. Extrapolation to concentrations outside the range covered has to be strictly avoided. One should also bear in mind that the *limit of quantitation* (LOQ) of a compound is found at higher concentration than its *limit of detection* (LOD).

14.2.2 Quantitation by Internal Standardization

Internal standardization circumvents the effects of time-variant instrument response, but does not compensate for different ionization efficiencies of analyte and standard. For internal standardization, a compound exhibiting close similarity in terms of ionization efficiency and retention time is added to the sample at a known level of concentration, e.g., an isomer or a homolog eluting closely to the analyte may serve that purpose.

It is important to add the internal standard before any clean-up procedure in order not to alter the concentration of the analyte without affecting that of the standard in the very same way. For reliable results, the relative concentration of analyte and standard should not differ by more than a factor of about ten.

14.2.3 Quantitation by Isotope Dilution

Virtually identical ionization efficiency for a pair of compounds is only given for isotopologs. As these differ from the nonlabeled target compound in mass, they can be added to the mixture at known concentration to result in a special case of internal standardization, hence the term *isotope dilution* [55]. The ratio of intensities of the peaks corresponding to target compound and labeled standard as delivered by the RICs, SIM, or MRM traces is then taken as the relative concentration of labeled internal standard and target compound. As the absolute concentration of the standard added before the analysis is known, the concentration of the analyte can reliably be calculated.

Example I: A potential drug (M) and its metabolite (M′) in a liver sample are quantified by LC-ESI-MS with internal standardization using trideuterated standards for each analyte (Fig. 14.7) [27]. Under these conditions it neither presents a problem that both analytes and their isotopic standards are almost co-eluting from the LC column, nor does the completely unspecific TIC play a role. If required for sensitivity reasons, this analysis could also have been performed in the SIM mode using the *m/z* values of the RICs shown.

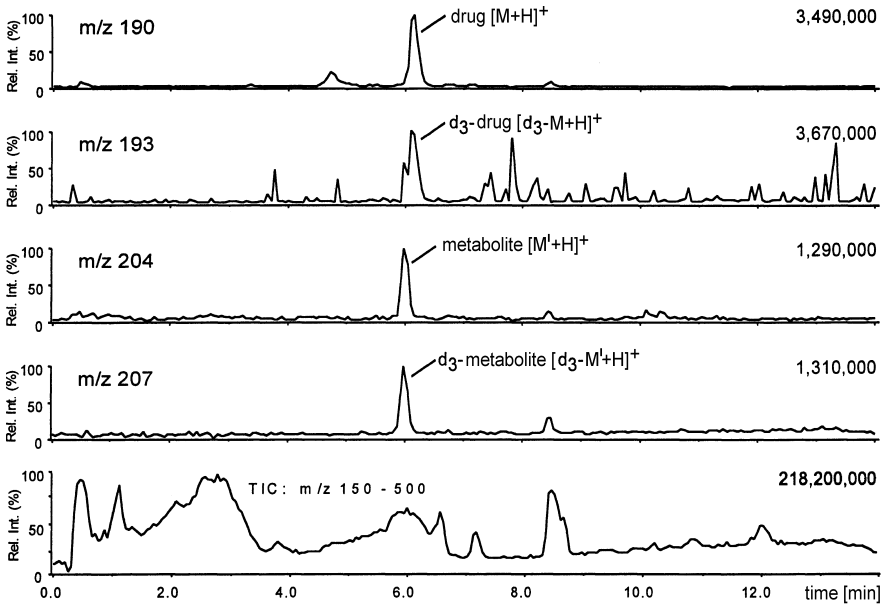


Fig. 14.7. RICs and TIC of an LC-ESI-MS quantification of a drug, $[M+H]^+$ at *m/z* 190, and its metabolite, $[M'+H]^+$ at *m/z* 204, by isotope dilution with trideuterated standards. The numbers on the top right of each trace give their absolute intensity values. Reproduced from Ref. [27] by permission. © Elsevier Science, 2001.

Example II: The number of *m/z* values to be monitored in SIM is limited. Such limitations are more severe when additional lock mass peaks have to be included in case of HR-SIM. Therefore, it is commonplace to monitor different sets of SIM traces during consecutive time windows leading to a sequence of different SIM setups during a single chromatographic separation. The quantitation of halogenated dibenzo-*p*-dioxins in municipal waste incinerator fly ash at concentrations in the ppb to low-ppm range requires such a setup (Fig. 14.8) [47]. Here, a combined approach of external standardization for the $BrCl_3$-species and internal standardization for the Cl_4-species has been realized.

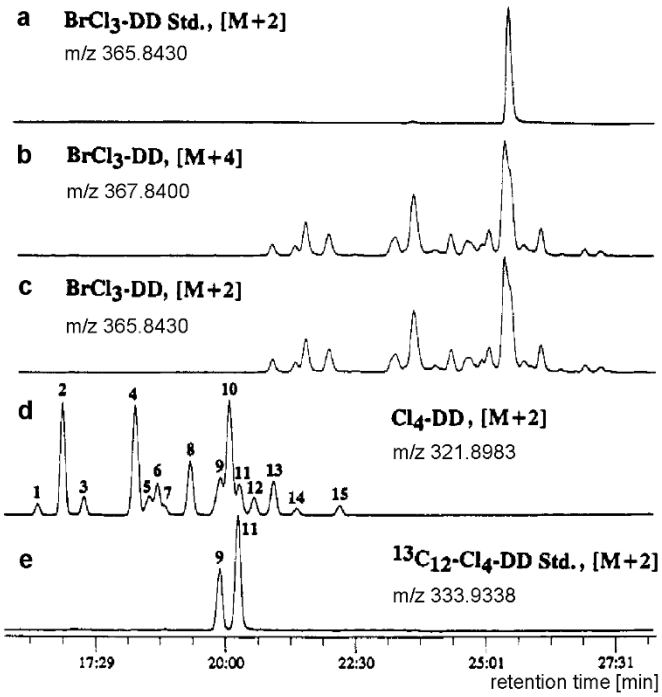


Fig. 14.8. Quantification of $BrCl_3$- and Cl_4-dibenzodioxins by HR-SIM. A $^{13}C_{12}$-labeled internal standard is added for the Cl_4-congener. Adapted from Ref. [47] by permission. © American Chemical Society, 1991.

Note: According to the enormous usage of isotope dilution, ^{2}H- (D) and ^{13}C-labeled standards [56] are commercially available for a wide range of applications. Often, a methyl is exchanged for a trideuteromethyl as this safely avoids overlap with isotopic peaks of the analyte. It is also important not to select compounds with acidic hydrogens exchanged for deuterons. Other restrictions for internal standards also apply.

14.2.4 Retention Times of Isotopologs

Isotopologs exhibit somewhat different retention times in chromatography. Deuterated compounds, for example, elute from chromatographic columns at slightly shorter retention times than their nonlabeled isotopologs. Normally, the difference is less than the peak width of the corresponding chromatographic peaks, but may still be large enough to require their integration over separate time windows (Fig. 14.9).

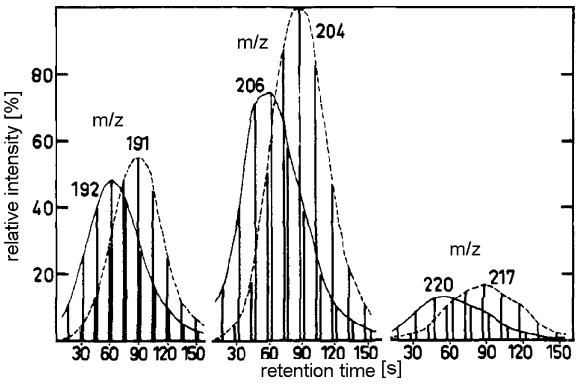


Fig. 14.9. Shorter retention times are observed for [D_7]glucose than for glucose eluting from a SE30 GC column as demonstrated for three pairs of peaks. Reproduced from Ref. [39] by permission. © American Chemical Society, 1966.

14.3 Gas Chromatography-Mass Spectrometry

14.3.1 GC-MS Interfaces

In early GC with packed columns several tens of milliliters of carrier gas per minute were eluted. Thus, most of the flow had to be separated before entering the ion source to prevent the mass spectrometer vacuum system from breakdown [4,33,38]. Flow reduction was either effected by a simple split to divide the effluent in the inlet system by a factor of about 1 : 100 or by means of a more elaborate *separator*, the *jet separator* being the best-known of those [57,58]. The advantage of separators over a simple split is the enrichment of the analyte relative to the carrier gas; in case of the jet separator this effect is based on a principle related to that of the nozzle-skimmer system in ESI (Chap. 12.2.1).

With the advent of capillary GC [59-63] the need for separators and the concomitant risk of suppression of certain components vanished. Capillary columns are operated at gas flow rates in the order of 1 ml min^{-1}, and therefore can be directly interfaced to EI or CI ion sources [57,58]. Although the pressure inside the ion source rises due to the continuous gas load, the conditions for EI are still properly maintained. Sufficient pumping speed ($\approx 200\,l\,s^{-1}$) is recommended to keep the pressure in the ion source housing below 10^{-5} mbar. Helium is the preferred

carrier gas for GC-EI-MS. If CI is intended, hydrogen or methane may be used instead as these can at the same time serve as reagent gas.

Note: Capillary columns are operated at constant carrier gas pressure rather than at constant gas flow. The temperature dependence of gas viscosities thus causes high ion source pressure at low temperature of the GC oven. Vice versa, the vacuum is better at the upper temperature limit of the GC program.

To interface the GC column to the ion source the capillary column is guided by a heated glass line (Fig. 14.10). The evacuated glass line is sealed toward the atmosphere by a graphite ferrule where the GC capillary leaves the oven. Guided by the glass line the exit of the capillary column is positioned at the entrance of the ionization volume. Most EI or CI ion sources have a dedicated entrance port opposite the direct probe port for that purpose (Chap. 5.1.1). Thus, a modern GC-MS interface basically consists of a heated glass line bridging the distance (≈ 30 cm) between GC oven and ion source. The interface should be operated at the highest temperature employed in the actual GC separation or at the highest temperature the column can tolerate (200–350°C). Keeping the transfer line at lower temperature causes condensation of eluting components inside the end of the column.

In contrast to sample introduction via direct probe (Chap. 5.2), the components eluting from a GC capillary are quantitatively transferred into the ion source during a short time interval just sufficient to acquire about five mass spectra. Consequently, the partial pressure of the analyte is comparatively high during elution for sample amounts in the picogram range to be analyzed by capillary GC-MS.

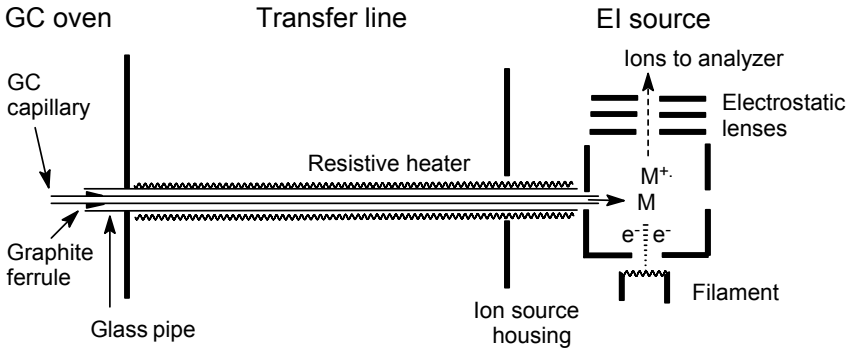


Fig. 14.10. Interfacing a capillary GC column to an EI ion source.

14.3.2 Volatility and Derivatization

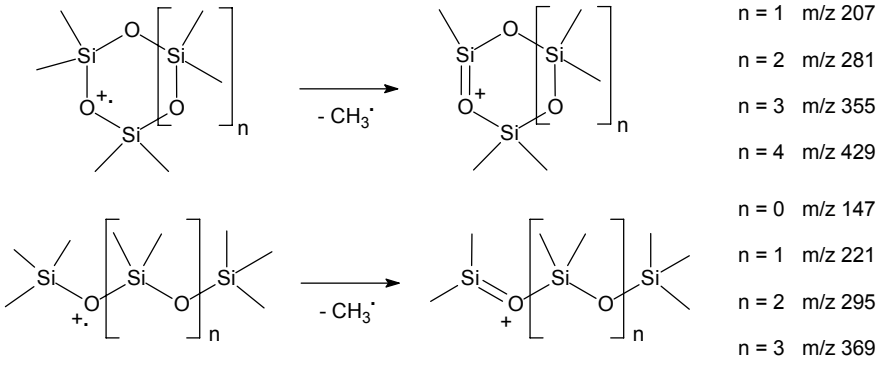
Gas chromatography requires a certain level of volatility and thermal robustness of the analyte. Both injection block of the gas chromatograph and interface to the mass spectrometer ion source are always at high temperature even while the column oven is not. In order to adapt an analyte to these needs, *derivatization* is well

established [64,65], the most frequent derivatization procedures being silylation, acetylation, methylation, and fluoroalkylation. As derivatization transforms XH groups into $XSiR_3$, XC=OMe, XMe, or $XCOCF_3$ groups, for example, polarity of the molecules largely decreases. This causes an improved volatility even though the molecular weight increases upon derivatization. Derivatization suppresses thermal decomposition, e.g., it protects alcohols from thermal dehydration. In particular fluoroalkyl and fluoroaryl groups are extremely useful to improve detection limits in EC-MS [36,66,67]. There is a complete series of reviews by John Halket covering the different derivatives and their uses in mass spectrometry [68-75].

Derivatization can also introduce functional groups that induce a controlled fragmentation of the ion [76], e.g., by α-cleavage at the new functional group. This way, 3-picolinyl esters of fatty acids reveal double bond positions because the charge localizing substituent largely reduces double bond rearrangement prior to fragmentation. The alternative use of dimethyldisulfide adducts for double bond localization has already been explained in Chap. 6.5.2.

14.3.3 Column Bleed

Rising temperature of the GC column not only assists transport of less volatile components, it also causes the slow release of the liquid phase from the inner wall of the capillary. As a result of slow thermal degradation, even chemically bonded liquid phases show such *column bleed* at elevated temperature. It is a characteristic of column bleed that it continuously rises as the temperature of the GC oven is raised and it falls again upon cooling of the system. Of course, the peaks from column bleed observed in the mass spectrum depend on the liquid phase of the GC capillary in use. In case of the frequently employed methyl-phenyl-siloxane liquid phases, abundant ions at *m/z* 73, 147, 207, 281, 355, 429, etc. are observed. Within one series the peaks are aligned at Δ*m/z* 74 ($OSiMe_2$) and exhibit characteristic silicon isotopic patterns. Fortunately, column bleed is easily recognized and can be removed by careful background subtraction. Similar background ions are also obtained from *septum bleed* and silicon grease [7,77].



Scheme 14.1.

Example: A portion of the TIC as obtained by GC-EI-MS of an unknown mixture on a 30-m HP-5 capillary column shows a rather small chromatographic peak at a retention time of 32.6 min (Fig. 14.11), while the chromatogram shows a rather high baseline due to continuous elution of column material. Extracting scan No. 2045 at the GC peak's apex yields a spectrum that is dominated by background ions from column bleed. This becomes obvious by averaging scans 2068 to 2082, which delivers the spectrum of column bleed alone. Averaging of all scans covering the GC peak followed by background subtraction ((2035:2052)–(2013:2020)) delivers a mass spectrum of reasonable quality, even though some background peaks are still present.

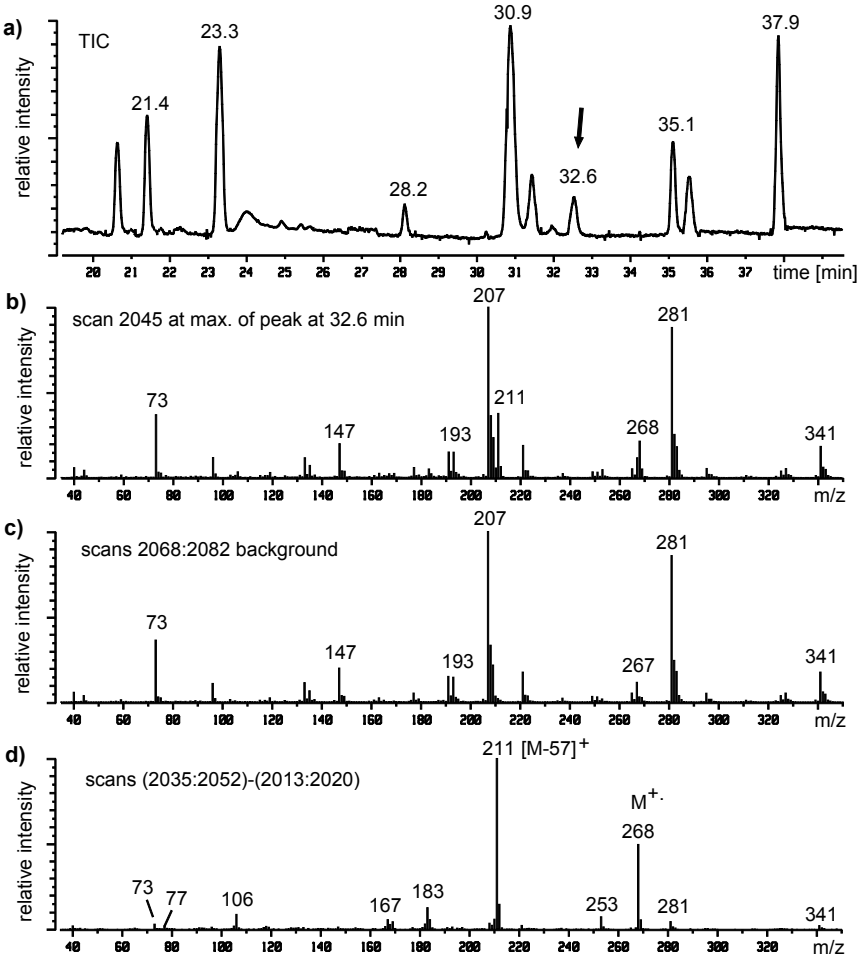


Fig. 14.11. Background subtraction to remove peaks from column bleed in GC-MS of an unknown mixture. (**a**) Partial TIC, (**b**) single scan mass spectrum from peak top at 32.6 min, (**c**) summation of scans from pure column bleed between GC peaks, and (**d**) final spectrum after averaging of scans and background subtraction.

14.3.4 Fast GC-MS

When a high sample throughput is of importance, *fast GC-MS* offers a time-saving concept for mixture analysis [78-80]. The GC separation can be accelerated by replacing standard size (20–60 m × 0.25–0.53 mm i.d.) capillary columns by short narrow-bore columns (2–5 m × 50 µm i.d.) and by applying sufficient pressure (8–10 bar) and rapid heating (50–200°C min^{-1}). Thus, a conventional 30-min separation is compressed into a 3-min or even shorter time frame. However, in fast GC the half-life of an eluting peak is too short for use with scanning quadrupole or magnetic sector analyzers. In fast GC-MS, oaTOF analyzers (Chap. 4.2.6) are typically employed because of their ability to acquire about a hundred spectra per second. Furthermore, the high duty cycle of oaTOFs offsets the difference in sensitivity between repetitive scanning and SIM analysis. At somewhat lower rates, advanced oaTOF systems even enable accurate mass determination at good accuracy.

14.3.5 Multiplexing for Increased Throughput

Even in fast GC operation the capacity of the capillary column is not fully exploited, because gaps between loaded zones inevitably occur as the separation proceeds. In the context of the duty cycle of TOF instruments the approach of Hadamard transform MS has already been mentioned (Chap. 4.2.10) [81]. The same principle can also be applied for GC separation, i.e., the next injection onto the column is made long before all components of the preceding injection have left the column. In contrast to conventional chromatographic separation, the chromatogram then consists of several chromatograms overlapping in time. Key to mathematical deconvolution by Hadamard transform is to inject rapidly and precisely by a *multiplexing* injector according to an *n*-bit pseudorandom sequence (Fig. 14.12) [82,83]. These pseudorandom injections are further divided into subsets of different concentrations, which may later serve for control of the time-shifted repetitive injections. Thus, a computer-controlled injection sequence combined with Hadamard transform of the detector output delivers the concentrations of all components at enhanced sample throughput. Using a multiplexing injector capable of up to 3000 injections per hour allowed for a 50% duty cycle of the chromatograph to be achieved.

Note: The term *multiplexing* refers to the use of one separation device for multiple samples at the same time. To achieve an improved duty cycle of the device multiplexing requires a complex mathematical deconvolution of the detector output. In contrast, *multiplexed* chromatographic systems are using one detector for multiple parallel chromatographs in a simple alternating mode (Chap. 14.4.2). Multiplexed systems use high-speed detection and are based on the assumption not to miss relevant information while the detector connects to other lines between sampling intervals.

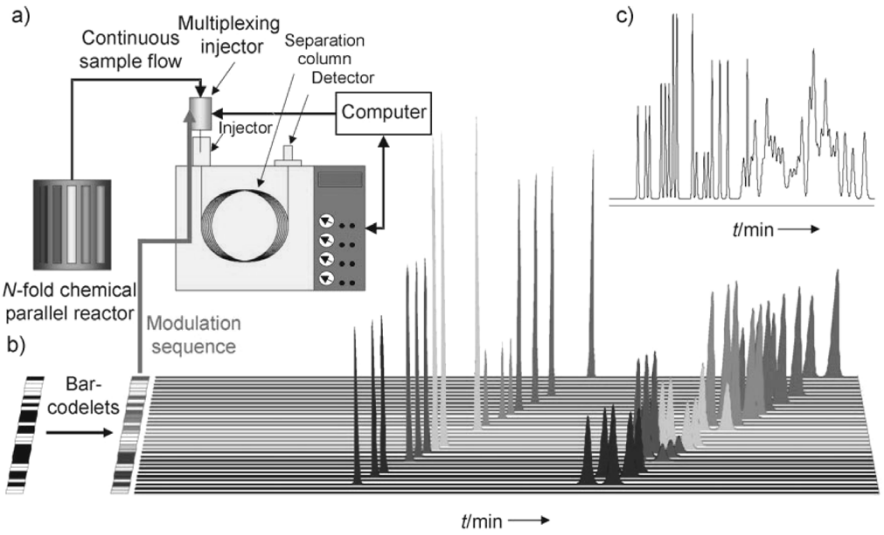


Fig. 14.12. High-throughput multiplexing gas chromatography. (**a**) Experimental setup for the analysis of the sample composition from an *N*-fold parallel reactor. The multiplexing injector is loading the column by short pressure pulses (1–5 ms) according to an *n*-bit binary pseudorandom sequence. (**b**) Temporally shifted chromatograms obtained by repetitive sample injections following the bar codelets of an *n*-bit sequence. (**c**) Convoluted chromatogram which is the sum of the chromatograms shown in (**b**). Reproduced from Ref. [83] with permission. © Wiley-VCH, 2007.

14.4 Liquid Chromatography-Mass Spectrometry

Coupling of liquid chromatography to mass spectrometry has not only led to a wide variety of interfaces, it also fostered the development of new ionization methods (Chap. 12) [8,9,12-15,84]. ESI, APCI, or APPI are suitable for LC-MS, their selection depending on sample properties like molecular mass and polarity (Chap. 12.7).

Most frequently, *high-pressure liquid chromatography* (HPLC) is used in LC-MS work, while more recently *ultrahigh-pressure liquid chromatography* (UHPLC or *ultra performance liquid chromatography*, UPLC, as it is termed by one manufacturer) has come into use. For very low sample amounts, nanoLC, i.e., capillary LC, can directly be interfaced to nanoESI.

In the analytical practice, LC-MS plays a tremendous role that could be testified here by a large number of applications [9-11,50,85]. However, other than proper adjustment of the interface to the liquid flow from the chromatograph the operation of LC-MS does not require dedicated techniques on the MS side. All scanning and ion monitoring techniques discussed so far in this chapter can equal-

equally well be employed for LC-MS analyses. Three examples shall highlight representative applications of LC-MS and LC-MS/MS.

Example I: Impurities in pharmaceutical preparations. UV *photodiode array* (PDA) and ESI-TOF detection can be combined if the LC effluent is split or the PDA precedes the ESI interface. The detection methods complement each other in that their different sensitivities towards components of a mixture prevent substances from being overlooked. RICs help to differentiate a targeted compound – an unknown impurity in this case – from others and to identify eventually present isomers. Finally, accurate mass measurement helps in the identification of the unknown, the $[M+H]^+$ ion of which was assigned as $[C_{20}H_{21}N_{10}]^+$. The mass error in the order of 5 ppm was considered perfect for the oaTOF instruments of that time (Fig. 14.13) [27].

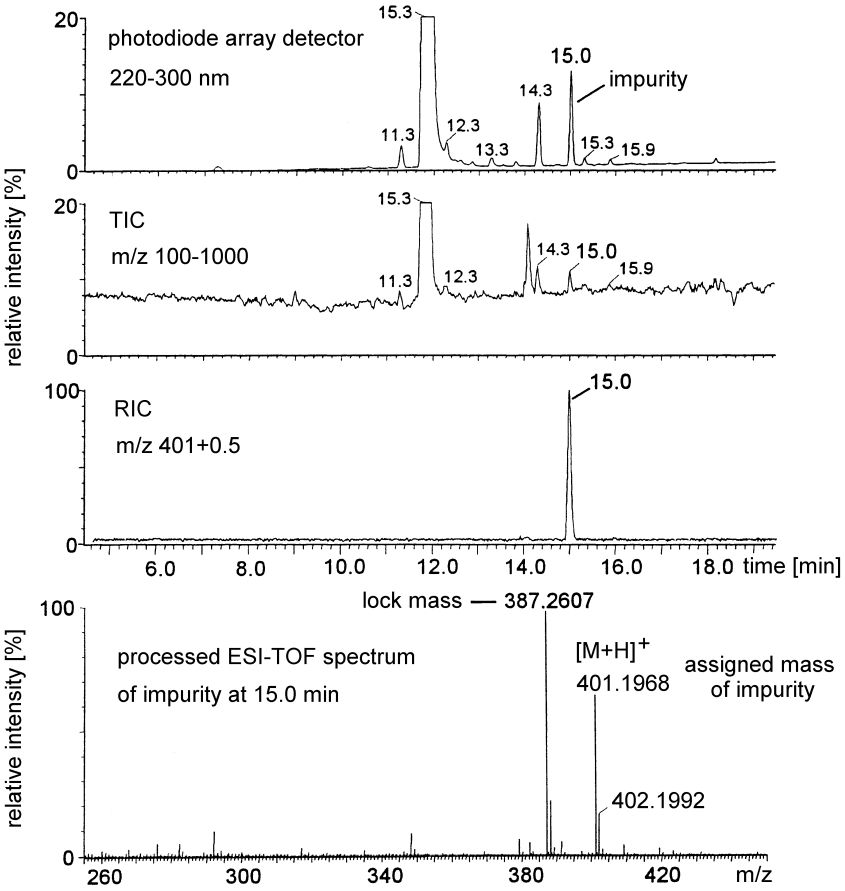


Fig. 14.13. Liquid chromatograms (*from top*) by photodiode array detection, TIC and RIC (*m/z* 401) from LC-ESI-MS, and accurate mass measurement (*bottom*) of the unknown impurity based on a one-point internal mass calibration. Adapted from Ref. [27] by permission. © Elsevier Science, 2001.

Example II: Illicit drugs in waste water. An LC-ESI-MS/MS method for the simultaneous determination of 16 illicit drugs and their metabolites in wastewater was developed [86]. Based on tandem mass spectra of the compounds, MRM experiments were set up to detect each drug by a characteristic transition (Fig. 14.14). Among others, cocaine, amphetamines, morphine, and 11-nor-9-carboxy-Δ9-tetrahydrocannabinol were found in substantial amounts in waste water treatment plants at Milan (Italy) and Lugano (Switzerland). Quantification was achieved by addition of several deuterated internal standards. Quantification ranges were found to be 0.2–1 ng l^{-1} for cocaine and 60–90 ng l^{-1} for 11-nor-9-carboxy-Δ9-THC. Illicit drugs were therefore considered ubiquitous contaminants, discharged into the environment together with pharmaceuticals presenting an environmental risk. Moreover, the concentrations of illicit drugs in wastewater reflect their consumption by the local population.

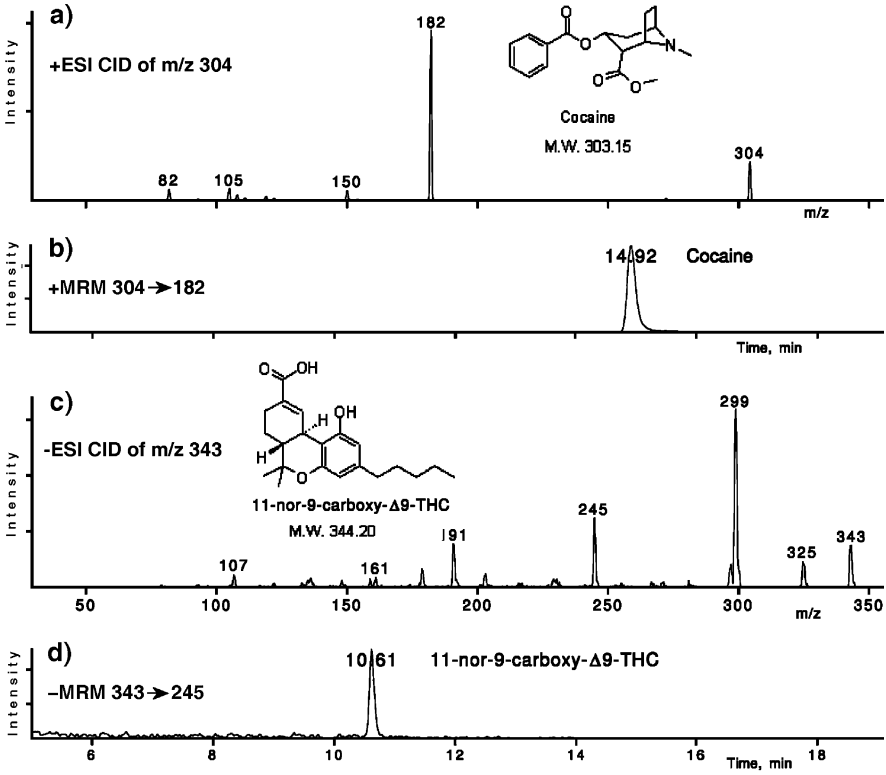


Fig. 14.14. Two examples from the analysis of illicit drugs in waste water by LC-MS/MS and MRM. (**a**) Positive-ion ESI-CID spectrum of the $[M+H]^+$ ion of cocaine and (**b**) the MRM trace derived thereof. (**c**) Negative-ion ESI-CID spectrum of the $[M+H]^-$ ion of 11-nor-9-carboxy-Δ9-THC and (**d**) the corresponding MRM trace. Adapted from Ref. [86] with permission. © American Chemical Society, 2006.

Example III: Peptide identification from biological samples. Colorectal cancer cells have been lysed and the protein fraction thereof has been subjected to 2D gel electrophoresis. A gastrointestinal-specific A33 antigen was expected in the molecular mass range of 40–45 kDa. The corresponding slice of the 2D gel was cut out and the proteins on it were subjected to tryptic digestion. Capillary column (150 × 0.2 mm C8 reversed phase) HPLC-ESI-MS of this total tryptic digest delivered a complex and mostly unresolved TIC (Fig. 14.16). A mass spectrum of a retention time span around 25.20 min still showed numerous peaks of protonated peptides requiring identification by mass spectrometric sequencing. One of these, an $[M+2H]^{2+}$ ion at *m/z* 1198.4, was identified as the A33 antigen peptide YNILNQEQPLAQPASGQPVSLK using SEQUEST database search.

14.4.1 Multiplexed LC-ESI-MS

Combinatorial chemistry and other high-throughput screening applications have contributed to the development of *multiplexed electrospray inlet systems* (MUX). Up to eight chromatographs can be connected in parallel to a single mass spectrometer by means of a MUX interface (Fig. 14.15) [88,89]. As in fast GC-MS, this requires a sufficiently high speed of spectral acquisition and a high sensitivity of the instrument to compensate for the loss of sample by the alternating mode of operation [90].

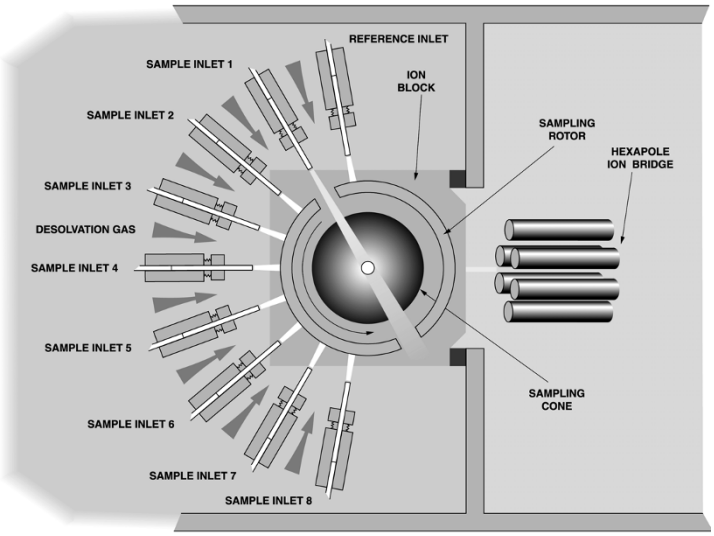


Fig. 14.15. Micromass z-spray with MUX technology. Eight ESI sprayers plus one reference sprayer are adjusted around the sampling orifice. However, only one sprayer has access to the orifice at a time, the others are blinded by a rotating aperture. By courtesy of Waters Corporation, MS Technologies, Manchester, UK.

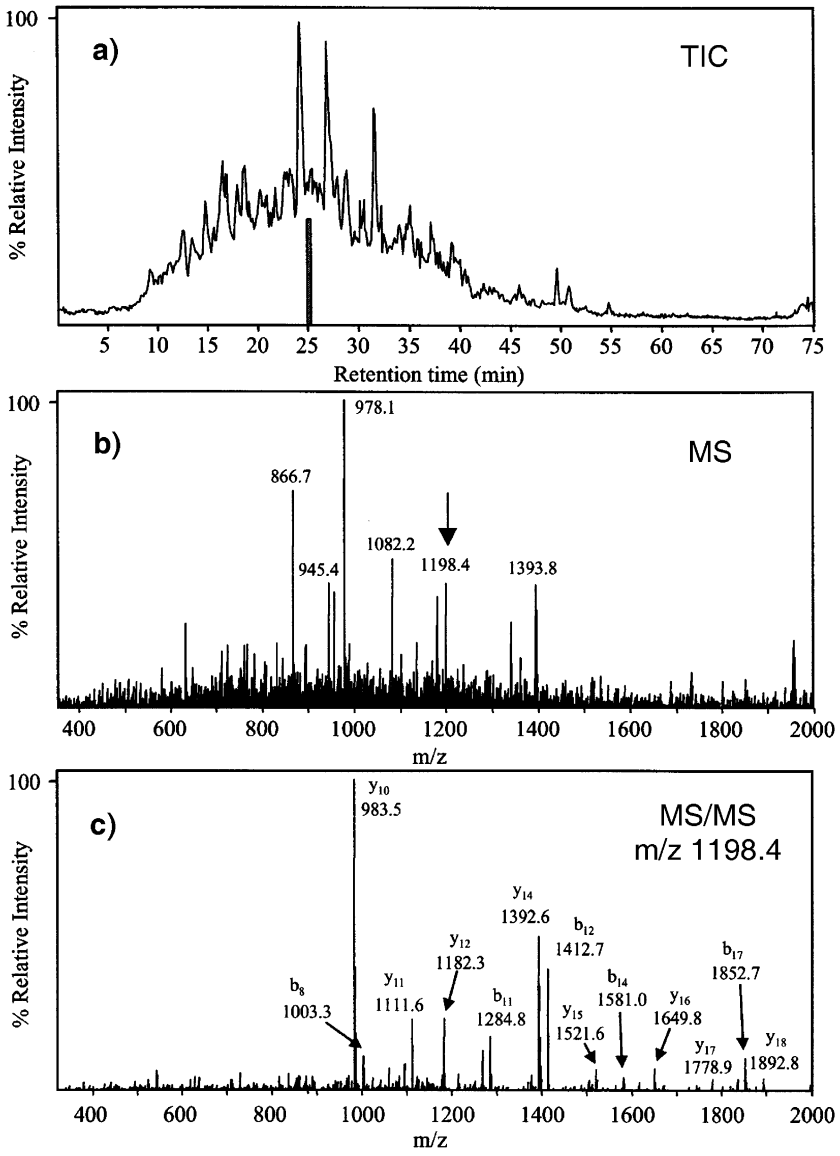


Fig. 14.16. Capillary column HPLC-ESI-MS/MS of a tryptic digest. (**a**) An unresolved TIC trace, (**b**) mass spectrum around retention time of 25.20 min, and (**c**) CID spectrum of an $[M+2H]^{2+}$ ion at *m/z* 1198.4, identified as the A33 antigen peptide. Adapted from Ref. [87] with permission of publisher and author. © Wiley-VCH, Weinheim, 2000.

14.5 Ion Mobility Spectrometry-Mass Spectrometry

Ion mobility spectrometry (IMS) presents an effective means of separating gaseous ions in an electric field according to their collision cross sections. From the perspective of its working principle, IMS could be regarded as gas-phase electrophoresis. As IMS is a separation method normally coupled to MS for ion detection, IMS-MS might completely be dealt with in line with GC-MS and LC-MS. However, IMS is different from GC and LC in that its instrumental implementation is strongly dependent on the features of the mass analyzer attached. Accordingly, we have already discussed IMS-MS systems in the context of hybrid mass spectrometers (Chap. 4.9.2) [91,92].

To complement this purely instrumental approach to IMS-MS, this section presents some applications: IMS-MS can be used to *i*) distinguish compound classes, *ii*) to separate different charge states of one species, *iii*) tell apart different gas phase conformations of otherwise identical ions, and *iv*) even to separate chiral compounds when a chiral modifier is added to the inert drift gas [91-96].

Example I: Biomolecule classification by IMS-MS. Singly charged ions of biologically relevant molecular classes (96 oligonucleotides, 192 carbohydrates, 610 peptides, and 53 lipids) were generated by MALDI and subjected to IMS. Then a plot of this data, i.e., of their collision cross sections vs. *m/z* allowed for the calculation of distinct curves marking average collision cross sections vs. *m/z* distinct for each compound class. Figure 14.17 shows a plot of the MALDI-IMS-MS conformation space as obtained for a mixture of model species (roughly a dozen species for each class in the range up to 1500 u) [95]. Dashed lines correspond to regression curves for each molecular class in conformation space. There was some fragmentation of the parent ions causing the signals in the vicinity of the asterisk in the upper left corner of the diagram.

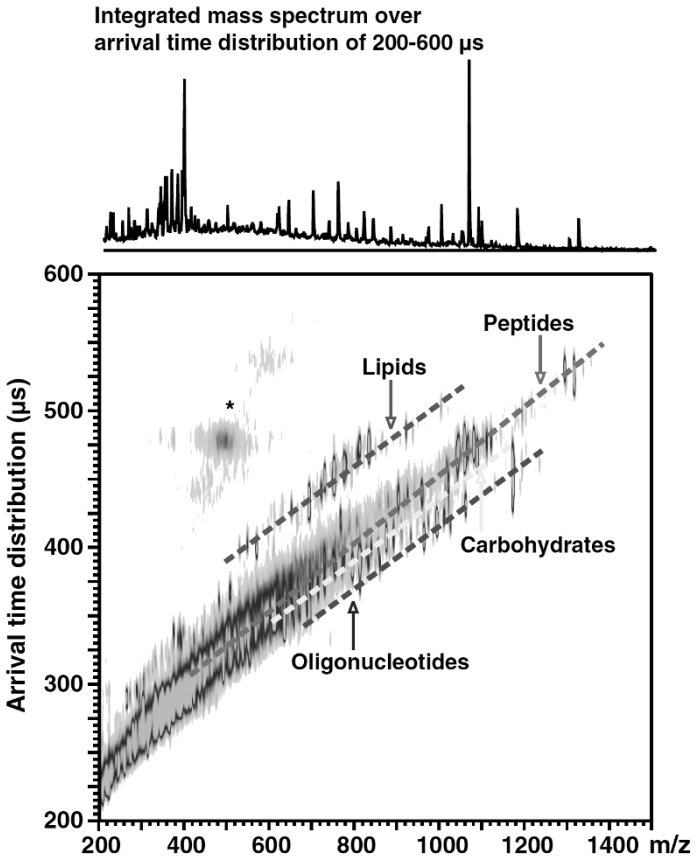


Fig. 14.17. Plot of MALDI-IMS-MS conformation space as obtained for a mixture of biomolecular model species. *Dashed lines* are for visualization purposes of where each molecular class occurs in conformation space. Signals in the vicinity of the *asterisk* arise from limited post-IM fragmentation of the parent ion species. Reproduced from Ref. [95] by permission. © Springer, 2009.

Example II: Separation of chiral compounds by IMS-MS. Amino acids and other small chiral molecules can be separated by IMS-MS if a chiral modifier is admixed to the inert nitrogen drift gas (Fig. 14.18) [93]. To achieve separation of L- and D-tryptophan, (*S*)-(+)-2-butanol at a concentration as low as 10 ppm has been used as chiral modifier. The differences in drift times of the amino acid enantiomers are large enough to deliver two peaks if the mixture is subjected to chiral IMS.

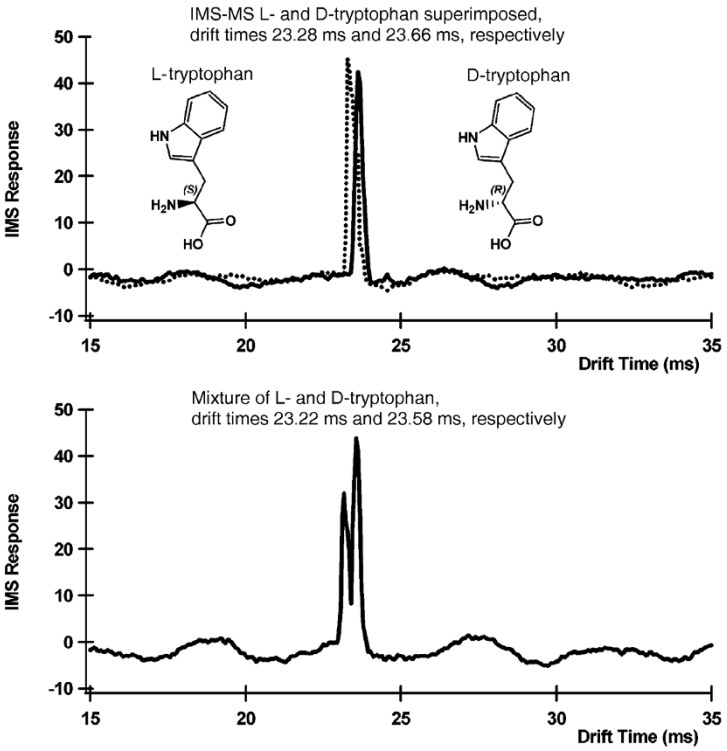


Fig. 14.18. Chiral separation of L- and D-tryptophan by IMS-MS using (*S*)-(+)-2-butanol as chiral modifier of the carrier gas. Adapted from Ref. [93] by permission. © American Chemical Society, 2006.

14.6 Tandem MS as a Complement to LC-MS

The principles of tandem mass spectrometry have been discussed in Chap. 9 and many different uses of tandem MS have been shown throughout this book (Table 14.3). More examples are following in this chapter showing how tandem MS offers increased selectivity [97], simplified clean-up procedures, or faster analysis as a direct result of the forth dimension added to the analytical measurement.
In tandem MS each stage of mass analysis provides an added step of selectivity or structural information to the analysis. Therefore, one tandem MS stage is to a certain degree equivalent to a chromatographic separation, provided the separation of isomers is not required. While chromatography separates components by their retention time, tandem MS isolates them by *m/z*. The next example illustrates how far MS/MS alone may go. The analysis presented in example III in Chap. 14.4, however, would have been impossible without using LC prior to MS/MS.

Note: SRM (and MRM) is preferably performed on triple quadrupole instruments due to their ease of setting up the experiment and to their speed of switching between channels if monitoring of multiple reactions plays a role.

Table 14.3. Tandem MS methods and spectra referred to throughout the book

Chapter	Aspect of tandem MS
2.9.3	MIKES of amine molecular ions in the context of H/D isotope effects
9.3.2	CID spectrum of toluene molecular ion on a magnetic sector instrument
9.5.1	MALDI-PSD spectrum of a peptide
9.6.5	Tandem MS with magnetic sector instruments; example: $B^2E = constant$ linked scan for caffeine quantitation using $[D_3]$caffeine internal standard
9.6.6	CID-FAB-MS/MS with magnetic sector instrument for peptide sequencing
9.8	Tandem MS with the quadrupole ion trap; examples: peptide sequencing by ESI-MS and LC-MS^4 to identify cyclic peptides
9.9.1	MS^4 on a QqLIT instrument for structure elucidation of a drug
9.10.1	Peptide sequencing by ESI-CID-MS/MS on LIT-orbitrap instrument
9.11.1	Sequencing of an oligosaccharide by MALDI-SORI-FT-ICR
9.14.1	ESI-IRMPD-MS/MS of gangliosides on a FT-ICR instrument
9.14.4	ECD of doubly charged peptide ions on a FT-ICR instrument
9.15	ETD of triply protonated peptide ions on a LIT instruments
9.18	Ion–molecule reactions: in catalysis research, to elucidate peptide fragmentation, and to study short-lived species in the gas phase
11.5.2	Peptide sequencing; mechanisms and applications of MALDI-MS/MS
11.5.3	Structure elucidation of carbohydrates by PSD-MALDI-MS
11.6.1	Peptide sequencing by DIOS-TOF-MS/MS
12.3	Peptide sequencing by nanoESI-MS/MS
12.6.4	Oligonucleotide sequencing by ESI-IRMPD-FT-ICR-MS
12.6.5	Structure elucidation of a nonasaccharide by nanoESI-CID-MS/MS on a Q-TOF hybrid instrument
13.1.3	DESI-MS/MS of aspirin

Example: Improved selectivity by tandem MS: SIM is not sufficient for the LC-MS detection of 100 pg dextrometorphan (DEX) spiked into 1 ml of human plasma. The corresponding signal of the $[M+H]^+$ ion in the SIM trace at *m/z* 272 is barely detectable, whereas the SRM chromatogram obtained from the reaction $[M+H]^+ \rightarrow [M–C_8H_{15}N]^+$ shows a clean background and a signal-to-noise enhancement of more than 50-fold (Fig. 14.19) [27].

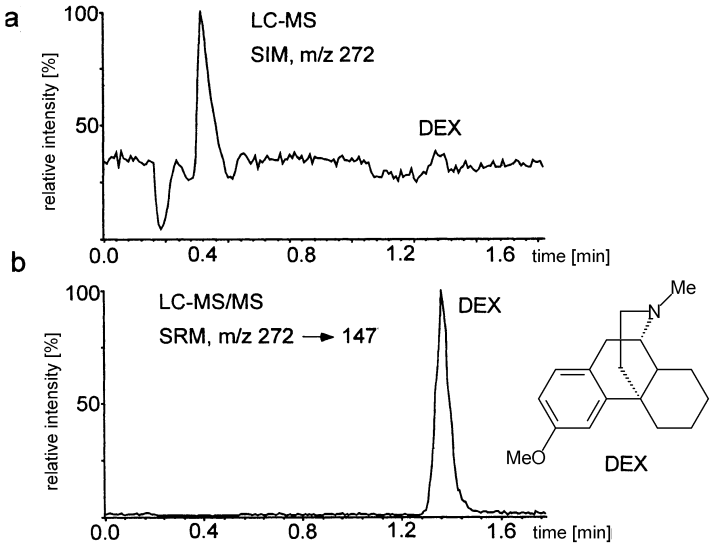


Fig. 14.19. Effect of SRM as compared to SIM in the detection of dextrometorphan. (**a**) LC-SIM and (**b**) LC-SRM. Reproduced from Ref. [27] by permission. © Elsevier Science, 2001.

Example: Tandem MS replacing LC: Akt is a key serine/threonine kinase controlling cellular processes such as cell survival, differentiation, proliferation, and metabolism. Three isoforms (Akt1, Akt2, and Akt3) are known in mammals. The nanoESI mass spectrum of all peptides obtained upon digestion of Akt3 with pepsin (peptic peptides) showed a large number of multiply charged ions (Fig. 14.20) [98]. The peptides were then characterized by tandem MS. The $[M+3H]^{3+}$ ions at *m/z* 797, for example, corresponded to a peptide of a neutral mass of 2388 u. As low-abundant peptides were difficult to identify by nanoESI-MS/MS alone, nanoLC/ESI-MS/MS was used in addition. Combining these approaches, a total of 24 peptide peaks were identified in both inactive and active Akt covering 70% of the amino acid sequence of Akt.

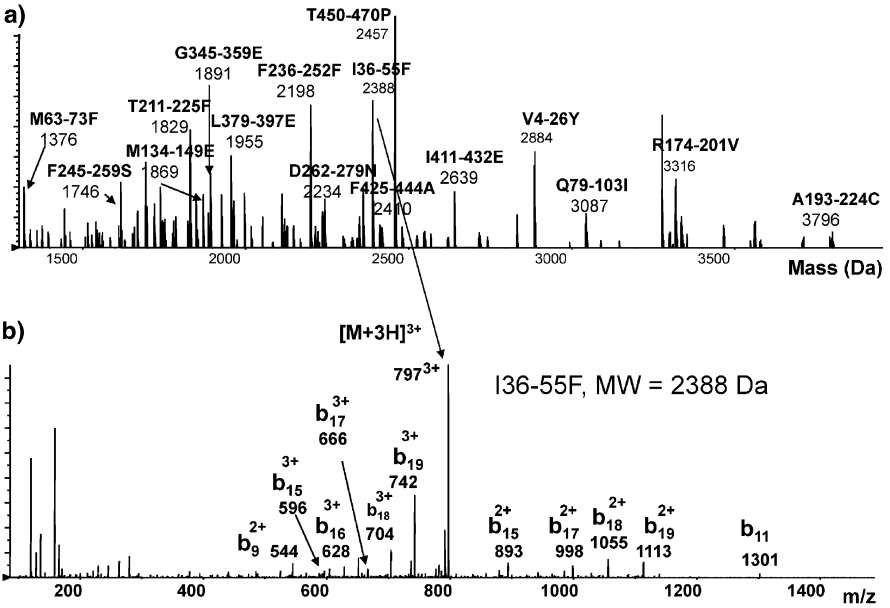


Fig. 14.20. Analysis of Akt by nanoESI-MS/MS. (**a**) Charge deconvoluted nanoESI spectrum of the complete peptic digest. (**b**) Tandem mass spectrum of the $[M+3H]^{3+}$ peptic peptide ion (I36-55F) at *m/z* 797 corresponding to a neutral peptide of 2388 u. Reproduced from Ref. [98] with permission. © John Wiley & Sons Ltd, 2009.

14.7 Ultrahigh-Resolution Mass Spectrometry

High and, in particular, ultrahigh resolution (Chap. 3.7) in combination with a soft ionization method such as ESI, MALDI, or FD present another way to achieve the separation of the molecular species contained in a mixture. Given a sufficient level of resolution, isobaric ions are displayed separately in the range of their common nominal mass value (Chap. 3.3.2, 3.4).

The potential of ultrahigh-resolution mass spectrometry for the analysis of complex chemical mixtures is particularly illustrated by FT-ICR-MS, which currently is the definite standard. Ultrahigh resolution was applied to separate several thousand components in crude oil [99,100], fuels [101,102], or explosion residues [103]. Actually, the attempts to analyze dissolved organic matter (DOM) and similar complex humic systems present another prominent field of application requiring the ultimate performance of FT-ICR instruments equipped with magnets of up to 15 T field strength [104].

Example: In a sample of South American crude oil positive-ion ESI selectively delivers $[M+H]^+$ ions of the basic compounds, i.e., only a small fraction of the entire chemical composition. Nevertheless, the positive-ion ESI-FT-ICR mass spec-

trum exhibits more than 11,100 resolved peaks, of which >75% may be assigned to a unique elemental composition ($C_cH_hO_oN_nS_s$). Such a separation in mass is possible because the average mass resolution in the *m/z* 225–1000 broadband spectrum is approximately 350,000 (Fig. 14.21). This demonstrates the current upper limit for the number of chemically distinct components resolved and identified in a single step [100].

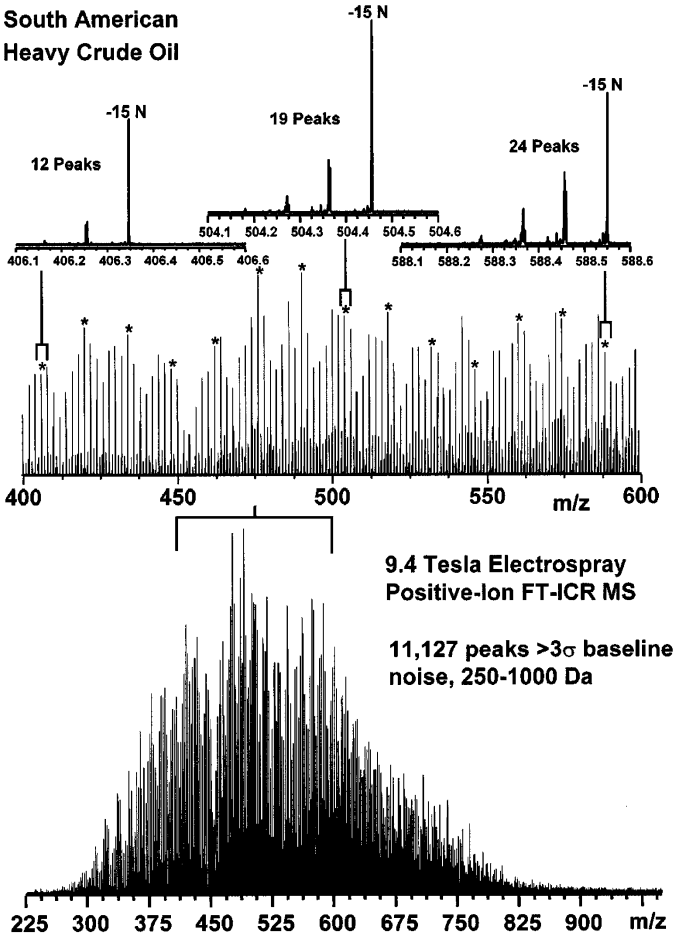


Fig. 14.21. Positive-ion ESI-FT-ICR spectrum of crude oil. The mass scale is successively expanded from the broadband spectrum to a more detailed one at three nominal mass values. Adapted from Ref. [100] by permission. © American Chemical Society, 2002.

References

1. Williams, J.D.; Burinsky, D.J. Mass Spectrometric Analysis of Complex Mixtures Then and Now: The Impact of Linking Liquid Chromatography and Mass Spectrometry. *Int. J. Mass Spectrom.* **2001,** *212*, 111-133.
2. McLafferty, F.W. Tandem Mass Spectrometric Analysis of Complex Biological Mixtures. *Int. J. Mass Spectrom.* **2001,** *212*, 81-87.
3. Kondrat, R.W. Mixture Analysis by Mass Spectrometry: Now's the Time. *Int. J. Mass Spectrom.* **2001,** *212*, 89-95.
4. Gohlke, R.S.; McLafferty, F.W. Early Gas Chromatography/Mass Spectrometry. *J. Am. Soc. Mass Spectrom.* **1993,** *4*, 367-371.
5. Message, G.M. *Practical Aspects of Gas Chromatography/Mass Spectrometry;* Wiley: New York, 1984.
6. Budde, W.L. *Analytical Mass Spectrometry;* ACS/Oxford Univ. Press: Washington, DC/Oxford, 2001.
7. Hübschmann, H.-J. *Handbook of GC/MS: Fundamentals and Applications;* 2nd ed.; Wiley-VCH: Weinheim, 2009.
8. *Current Practice of Liquid Chromatography-Mass Spectrometry;* Niessen, W.M.A.; Voyksner, R.D. (eds.); Elsevier: Amsterdam, 1998.
9. Ardrey, R.E. *Liquid Chromatography-Mass Spectrometry – An Introduction;* Wiley: Chichester, 2003.
10. Chowdhury, S.K. *Identification and Quantification of Drugs, Metabolites and Metabolizing Enzymes by LC-MS;* Elsevier: Amsterdam, 2005.
11. *Mass Spectrometry in Drug Metabolism and Pharmacokinetics;* Ramanathan, R., editor; Wiley: Hoboken, 2009.
12. Horning, E.C.; Carroll, D.I.; Dzidic, I.; Haegele, K.D.; Horning, M.G.; Stillwell, R.N. Atmospheric Pressure Ionization (API) Mass Spectrometry. Solvent-Mediated Ionization of Samples Introduced in Solution and in a Liquid Chromatograph Effluent Stream. *J. Chromatogr. Sci.* **1974,** *12*, 725-729.
13. Blakley, C.R.; Vestal, M.L. Thermospray Interface for Liquid Chromatography/Mass Spectrometry. *Anal. Chem.* **1983,** *55*, 750-754.
14. Vestal, M.L. High-Performance Liquid Chromatography-Mass Spectrometry. *Science* **1984,** *226*, 275-281.
15. Abian, J. The Coupling of Gas and Liquid Chromatography with Mass Spectrometry. *J. Mass Spectrom.* **1999,** *34*, 157-168.
16. Smith, R.D.; Barinaga, C.J.; Udseth, H.R. Improved Electrospray Ionization Interface for Capillary Zone Electrophoresis-Mass Spectrometry. *Anal. Chem.* **1988,** *60*, 1948-1952.
17. Schrader, W.; Linscheid, M. Styrene Oxide DNA Adducts: In Vitro Reaction and Sensitive Detection of Modified Oligonucleotides Using Capillary Zone Electrophoresis Interfaced to Electrospray Mass Spectrometry. *Arch. Toxicol.* **1997,** *71*, 588-595.
18. Tanaka, Y.; Kishimoto, Y.; Otsuga, K.; Terabe, S. Strategy for Selecting Separation Solutions in Capillary Electrophoresis-Mass Spectrometry. *J. Chromatogr. A* **1998,** *817*, 49-57.
19. Siethoff, C.; Nigge, W.; Linscheid, M. Characterization of a Capillary Zone Electrophoresis/Electrospray-Mass Spectrometry Interface. *Anal. Chem.* **1998,** *70*, 1357-1361.
20. Hsieh, F.; Baronas, E.; Muir, C.; Martin, S.A. A Novel Nanospray Capillary Zone Electrophoresis/Mass Spectrometry Interface. *Rapid Commun. Mass Spectrom.* **1999,** *13*, 67-72.
21. Smith, R.D.; Felix, W.D.; Fjeldsted, J.C.; Lee, M.L. Capillary Column Supercritical Fluid Chromatography Mass Spectrometry. *Anal. Chem.* **1982,** *54*, 1883-1885.
22. Arpino, P.J.; Haas, P. Recent Developments in Supercritical Fluid Chromatography-Mass Spectrometry Coupling. *J. Chromatogr. A* **1995,** *703*, 479-488.
23. Pinkston, J.D.; Chester, T.L. Guidelines for Successful SFC/MS. *Anal. Chem.* **1995,** *67*, 650A-656A.
24. Sjöberg, P.J.R.; Markides, K.E. New Supercritical Fluid Chromatography Interface Probe for Electrospray and Atmospheric Pressure Chemical Ionization Mass Spectrometry. *J. Chromatogr. A* **1997,** *785*, 101-110.
25. Combs, M.T.; Ashraf-Khorassani, M.; Taylor, L.T. Packed Column Supercriti-

cal Fluid Chromatography-Mass Spectroscopy: A Review. *J. Chromatogr. A* **1998,** *785*, 85-100.
26. *Forensic Applications of Mass Spectrometry;* Yinon, J. (ed.); CRC Press: Boca Raton, 1994.
27. Hoke, S.H.II.; Morand, K.L.; Greis, K.D.; Baker, T.R.; Harbol, K.L.; Dobson, R.L.M. Transformations in Pharmaceutical Research and Development, Driven by Innovations in Multidimensional Mass Spectrometry-Based Technologies. *Int. J. Mass Spectrom.* **2001,** *212*, 135-196.
28. *Mass Spectrometry in Drug Discovery;* Rossi, D.T.; Sinz, M.W. (ed.); Marcel Dekker: New York, 2002.
29. *Modern Mass Spectrometry;* Schalley, C.A. (ed.); Springer: New York, 2003.
30. Price, P. Standard Definitions of Terms Relating to Mass Spectrometry. A Report from the Committee on Measurements and Standards of the Amercian Society for Mass Spectrometry. *J. Am. Chem. Soc. Mass Spectrom.* **1991,** *2*, 336-348.
31. Todd, J.F.J. Recommendations for Nomenclature and Symbolism for Mass Spectroscopy Including an Appendix of Terms Used in Vacuum Technology. *Int. J. Mass Spectrom. Ion Proc.* **1995,** *142*, 211-240.
32. Hites, R.A.; Biemann, K. A Computer-Compatible Digital Data Acquisition System for Fast-Scanning, Single-Focusing Mass Spectrometers. *Anal. Chem.* **1967,** *39*, 965-970.
33. Hites, R.A.; Biemann, K. Mass Spectrometer-Computer System Particularly Suited for Gas Chromatography of Complex Mixtures. *Anal. Chem.* **1968,** *40*, 1217-1221.
34. Hites, R.A.; Biemann, K. Computer Evaluation of Continuously Scanned Mass Spectra of Gas Chromatographic Effluents. *Anal. Chem.* **1970,** *42*, 855-860.
35. Bertholf, R.L. Gas Chromatography and Mass Spectrometry in Clinical Chemistry, in *Encyclopedia of Analytical Chemistry*, Meyers, R.A. (ed.); Wiley: Chichester, 2000; pp. 1314-1336.
36. Spies-Martin, D.; Sommerburg, O.; Langhans, C.D.; Leichsenring, M. Measurement of 4-Hydroxynonenal in Small Volume Blood Plasma Samples: Modification of a Gas Chromatographic-Mass Mass Spectrometric Method for Clinical Settings. *J. Chromatogr.. B* **2002,** *774*, 231-239.
37. Price, P. Standard Definitions of Terms Relating to Mass Spectrometry. A Report from the Committee on Measurements and Standards of the Amercian Society for Mass Spectrometry. *J. Am. Soc. Mass Spectrom.* **1991,** *2*, 336-348.
38. Henneberg, D. Combination of Gas Chromatography and Mass Spectrometry for the Analysis of Organic Mixtures. *Z. Anal. Chem.* **1961,** *183*, 12-23.
39. Sweeley, C.C.; Elliot, W.H.; Fries, I.; Ryhage, R. Mass Spectrometric Determination of Unresolved Components in Gas Chromatographic Effluents. *Anal. Chem.* **1966,** *38*, 1549-1553.
40. Crosby, N.T.; Foreman, J.K.; Palframan, J.F.; Sawyer, R. Estimation of Steam-Volatile *N*-Nitrosamines in Foods at the 136μg/Kg Level. *Nature* **1972,** *238*, 342-343.
41. Brooks, C.J.W.; Middleditch, B.S. Uses of Chloromethyldimethylsilyl Ethers as Derivatives for Combined Gas Chromatography-Mass Spectrometry of Steroids. *Anal. Lett.* **1972,** *5*, 611-618.
42. Young, N.D.; Holland, J.F.; Gerber, J.N.; Sweeley, C.C. Selected Ion Monitoring for Multicomponent Analyses by Computer Control of Accelerating Voltage and Magnetic Field. *Anal. Chem.* **1975,** *47*, 2373-2376.
43. Tanchotikul, U.; Hsieh, T.C.Y. An Improved Method for Quantification of 2-Acetyl-1-Pyrroline, a "Popcorn"-Like Aroma, in Aromatic Rice by High-Resolution Gas Chromatography/Mass Spectrometry/Selected Ion Monitoring. *J. Agr. Food Chem.* **1991,** *39*, 944-947.
44. Middleditch, B.S.; Desiderio, D.M. Comparison of Selective Ion Monitoring and Repetitive Scanning During Gas Chromatography-Mass Spectrometry. *Anal. Chem.* **1973,** *45*, 806-808.
45. Millington, D.S.; Buoy, M.E.; Brooks, G.; Harper, M.E.; Griffiths, K. Thin-Layer Chromatography and High Resolution Selected Ion Monitoring for the Analysis of C_{19} Steroids in Human Hyperplastic Prostate Tissue. *Biomed. Mass Spectrom.* **1975,** *2*, 219-224.
46. Thorne, G.C.; Gaskell, S.J.; Payne, P.A. Approaches to the Improvement of Quantitative Precision in Selected Ion Monitoring: High Resolution Applica-

tions. *Biomed. Mass Spectrom.* **1984,** *11*, 415-420.
47. Tong, H.Y.; Monson, S.J.; Gross, M.L.; Huang, L.Q. Monobromopolychlorodibenzo-*p*-Dioxins and Dibenzofurans in Municipal Waste Incinerator Fly Ash. *Anal. Chem.* **1991,** *63*, 2697-2705.
48. Shibata, A.; Yoshio, H.; Hayashi, T.; Otsuki, N. Determination of Phenylpyruvic Acid in Human Urine and Plasma by Gas Chromatography/Negative Ion Chemical Ionization Mass Spectrometry. *Shitsuryo Bunseki* **1992,** *40*, 165-171.
49. Tondeur, Y.; Albro, P.W.; Hass, J.R.; Harvan, D.J.; Schroeder, J.L. Matrix Effect in Determination of 2,3,7,8-Tetrachlorodibenzodioxin by Mass Spectrometry. *Anal. Chem.* **1984,** *56*, 1344-1347.
50. Boyd, R.K.; Basic, C.; Bethem, R.A. *Trace Quantitative Analysis by Mass Spectrometry;* Wiley: Chichester, 2008.
51. Busch, K.L. Mass Spectrometry Forum: Quantitative Mass Spectrometry Part IV: Deviations from Linearity. *Spectroscopy* **2008,** *23*, 18-24.
52. Busch, K.L. Mass Spectrometry Forum: Quantitative Mass Spectrometry. Part III: An Overview of Regression Analysis. *Spectroscopy* **2008,** *23*, 16-20.
53. Bush, K.L. Quantitative Mass Spectrometry: Part II. *Spectroscopy* **2007,** *22*, 14-19.
54. Busch, K.L. Quantitative Mass Spectrometry: Part I. *Spectroscopy* **2007,** *22*, 13-19.
55. Heumann, K.G. Isotope Dilution Mass Spectrometry of Inorganic and Organic Substances. *Z. Anal. Chem. Fresenius* **1986,** *325*, 661-666.
56. Calder, A.G.; Garden, K.E.; Anderson, S.E.; Lobley, G.E. Quantitation of Blood and Plasma Amino Acids Using Isotope Dilution Electron Impact Gas Chromatography/Mass Spectrometry with U-^{13}C Amino Acids as Internal Standards. *Rapid Commun. Mass Spectrom.* **1999,** *13*, 2080-2083.
57. Gudzinowicz, B.J.; Gudzinowizc, M.J.; Martin, H.F. The GC-MS Interface, in: *Fundamentals of integrated GC-MS Part III*, Marcel Dekker: New York, 1977; Chapter B, pp. 58-181.
58. McFadden, W.H. Interfacing Chromatography and Mass Spectrometry. *J. Chromatogr. Sci.* **1979,** *17*, 2-16.
59. Lindeman, L.P.; Annis, J.L. A Conventional Mass Spectrometer as a Detector for Gas Chromatography. *Anal. Chem.* **1960,** *32*, 1742-1749.
60. Gohlke, R.S. Time-of-Flight Mass Spectrometry: Application to Capillary-Column Gas Chromatography. *Anal. Chem.* **1962,** *34*, 1332-1333.
61. McFadden, W.H.; Teranishi, R.; Black, D.R.; Day, J.C. Use of Capillary Gas Chromatography With a Time-of-Flight Mass Spectrometer. *J.Food Sci.* **1963,** *28*, 316-319.
62. Dandeneau, R.D.; Zerenner, E.H. An Investigation of Glasses for Capillary Chromatography. *J. High Res. Chromatogr./Chromatogr. Commun.* **1979,** *2*, 351-356.
63. Dandeneau, R.D.; Zerenner, E.H. The Invention of the Fused-Silica Column: an Industrial Perspective. *LC-GC* **1990,** *8*, 908-912.
64. *Handbook of Derivatives for Chromatography;* 2nd ed.; Blau, K.; King, G.S.; Halket, J.M. (eds.); Wiley: Chichester, 1993.
65. Zaikin, V.; Halket, J.M. *A Handbook of Derivatives for Mass Spectrometry;* IM Publ.: Chichester, 2009.
66. Aubert, C.; Rontani, J.-F. Perfluoroalkyl Ketones: Novel Derivatization Products for the Sensitive Determination of Fatty Acids by Gas Chromatography/Mass Spectrometry in Electron Impact and Negative Chemical Ionization Modes. *Rapid Commun. Mass Spectrom.* **2000,** *14*, 960-966.
67. Shin, H.S.; Jung, D.G. Sensitive Analysis of Malondialdehyde in Human Urine by Derivatization with Pentafluorophenylhydrazine then Headspace GC-MS. *Chromatographia* **2009,** *70*, 899-903.
68. Halket, J.M.; Zaikin, V.G. Derivatization in Mass Spectrometry: 1. Silylation. *Eur. Mass Spectrom.* **2003,** *9*, 1-21.
69. Zaikin, V.G.; Halket, J.M. Derivatization in Mass Spectrometry: 2. Acylation. *Eur. Mass Spectrom.* **2003,** *9*, 421-434.
70. Halket, J.M.; Zaikin, V.G. Derivatization in Mass Spectrometry: 3. Alkylation (Arylation). *Eur. Mass Spectrom.* **2004,** *10*, 1-19.
71. Zaikin, V.G.; Halket, J.M. Derivatization in Mass Spectrometry: 4. Formation of Cyclic Derivatives. *Eur. Mass Spectrom.* **2004,** *10*, 555-568.

72. Halket, J.M.; Zaikin, V.G. Derivatization in Mass Spectrometry: 5. Specific Derivatization of Monofunctional Compounds. *Eur. Mass Spectrom.* **2005,** *11*, 127-160.
73. Zaikin, V.G.; Halket, J.M. Derivatization in Mass Spectrometry: 6. Formation of Mixed Derivatives of Polyfunctional Compounds. *Eur. Mass Spectrom.* **2005,** *11*, 611-636.
74. Halket, J.M.; Zaikin, V.G. Derivatization in Mass Spectrometry: 7. On-Line Derivatization/Degradation. *Eur. Mass Spectrom.* **2006,** *12*, 1-13.
75. Zaikin, V.G.; Halket, J.M. Derivatization in Mass Spectrometry: 8. Soft Ionization Mass Spectrometry of Small Molecules. *Eur. Mass Spectrom.* **2006,** *12*, 79-115.
76. Anderegg, R.J. Derivatization in Mass Spectrometry: Strategies for Controlling Fragmentation. *Mass Spectrom. Rev.* **1988,** *7*, 395-424.
77. Spiteller, G. Contaminants in Mass Spectrometry. *Mass Spectrom. Rev.* **1982,** *1*, 29-62.
78. Leclerq, P.A.; Camers, C.A. High-Speed GC-MS. *Mass Spectrom. Rev.* **1998,** *17*, 37-49.
79. Prazen, B.J.; Bruckner, C.A.; Synovec, R.E.; Kowalski, B.R. Enhanced Chemical Analysis Using Parallel Column Gas Chromatography with Single-Detector Time-of-Flight Mass Spectrometry and Chemometric Analysis. *Anal. Chem.* **1999,** *71*, 1093-1099.
80. Hirsch, R.; Ternes, T.A.; Bobeldijk, I.; Weck, R.A. Determination of Environmentally Relevant Compounds Using Fast GC/TOF-MS. *Chimia* **2001,** *55*, 19-22.
81. Trapp, O.; Kimmel, J.R.; Yoon, O.K.; Zuleta, I.A.; Fernandez, F.M.; Zare, R.N. Continuous Two-Channel Time-of-Flight Mass Spectrometric Detection of Electrosprayed Ions. *Angew. Chem.,Int. Ed.* **2004,** *43*, 6541-6544.
82. Trapp, O.; Weber, S.K.; Bauch, S.; Hofstadt, W. High-Throughput Screening of Catalysts by Combining Reaction and Analysis. *Angew. Chem.,, Int. Ed.* **2007,** *46*, 7307-7310.
83. Trapp, O. Boosting the Throughput of Separation Techniques by "Multiplexing". *Angew. Chem., Int. Ed.* **2007,** *46*, 5609-5613, S5609-1.
84. van der Greef, J.; Niessen, W.M.A.; Tjaden, U.R. Liquid Chromatography-Mass Mass Spectrometry. The Need for a Multidimensional Approach. *J. Chromatogr.* **1989,** *474*, 5-19.
85. Siuzdak, G. *The Expanding Role of Mass Spectrometry in Biotechnology;* 2nd ed.; MCC Press: San Diego, 2006.
86. Castiglioni, S.; Zuccato, E.; Crisci, E.; Chiabrando, C.; Fanelli, R.; Bagnati, R. Identification and Measurement of Illicit Drugs and Their Metabolites in Urban Wastewater by Liquid Chromatography-Tandem Mass Spectrometry. *Anal. Chem.* **2006,** *78*, 8421-8429.
87. Simpson, R.J.; Connolly, L.M.; Eddes, J.S.; Pereira, J.J.; Moritz, R.L.; Reid, G.E. Proteomic Analysis of the Human Colon Carcinoma Cell Line (LIM 1215): Development of a Membrane Protein Database. *Electrophoresis* **2000,** *21*, 1707-1732.
88. Sage, A.B.; Giles, K. High Throughput Parallel LC/MS Analysis of Multiple Liquid Streams. *GIT Lab. J.* **2000,** *4*, 35-36.
89. Schrader, W.; Eipper, A.; Pugh, D.J.; Reetz, M.T. Second-Generation MS-Based High-Throughput Screening System for Enantioselective Catalysts and Biocatalysts. *Can. J. Chem.* **2002,** *80*, 626-632.
90. Morrison, D.; Davies, A.E.; Watt, A.P. An Evaluation of a Four-Channel Multiplexed Electrospray Tandem Mass Spectrometry for Higher Throughput Quantitative Analysis. *Anal. Chem.* **2002,** *74*, 1896-1902.
91. Bohrer, B.C.; Merenbloom, S.I.; Koeniger, S.L.; Hilderbrand, A.E.; Clemmer, D.E. Biomolecule Analysis by Ion Mobility Spectrometry. *Annual Review of Analytical Chemistry* **2008,** *1*, 293-327.
92. Kanu, A.B.; Dwivedi, P.; Tam, M.; Matz, L.; Hill, H.H., Jr. Ion Mobility-Mass Spectrometry. *J. Mass Spectrom.* **2008,** *43*, 1-22.
93. Dwivedi, P.; Wu, C.; Matz, L.M.; Clowers, B.H.; Seims, W.F.; Hill, H.H., Jr. Gas-Phase Chiral Separations by Ion Mobility Spectrometry. *Anal. Chem.* **2006,** *78*, 8200-8206.
94. Bohrer, B.C.; Merenbloom, S.I.; Koeniger, S.L.; Hilderbrand, A.E.; Clemmer, D.E. Biomolecule Analysis by Ion Mobility Spectrometry. *Ann. Rev. Anal. Chem.* **2008,** *1*, 293-327.
95. Fenn, L.S.; Kliman, M.; Mahsut, A.; Zhao, S.R.; McLean, J.A. Characterizing

Ion Mobility-Mass Spectrometry Conformation Space for the Analysis of Complex Biological Samples. *Anal. Bioanal. Chem.* **2009,** *394*, 235-244.
96. Enders, J.R.; McLean, J.A. Chiral and Structural Analysis of Biomolecules Using Mass Spectrometry and Ion Mobility-Mass Spectrometry. *Chirality* **2009,** *21*, e253-e264.
97. Moritz, T.; Olsen, J.E. Comparison Between High-Resolution Selected Ion Monitoring, Selected Reaction Monitoring, and Four-Sector Tandem Mass Spectrometry in Quantitative Analysis of Gibberellins in Milligram Amounts of Plant Tissue. *Anal. Chem.* **1995,** *67*, 1711-1716.
98. Guo, M.; Huang, B.X.; Kim, H.Y. Conformational Changes in Akt1 Activation Probed by Amide Hydrogen/Deuterium Exchange and Nano-Electrospray Ionization Mass Spectrometry. *Rapid Commun. Mass Spectrom.* **2009,** *23*, 1885-1891.
99. Hughey, C.A.; Hendrickson, C.L.; Rodgers, R.P.; Marshall, A.G. Kendrick Mass Defect Spectrum: A Compact Visual Analysis for Ultrahigh-Resolution Broadband Mass Spectra. *Anal. Chem.* **2001,** *73*, 4676-4681.
100. Hughey, C.A.; Rodgers, R.P.; Marshall, A.G. Resolution of 11,000 Compositionally Distinct Components in a Single Electrospray Ionization FT-ICR Mass Spectrum of Crude Oil. *Anal. Chem.* **2002,** *74*, 4145-4149.
101. Hsu, C.S.; Liang, Z.; Campana, J.E. Hydrocarbon Characterization by Ultrahigh Resolution Fourier Transform Ion Cyclotron Resonance Mass Spectrometry. *Anal. Chem.* **1994,** *66*, 850-855.
102. Hughey, C.A.; Hendrickson, C.L.; Rodgers, R.P.; Marshall, A.G. Elemental Composition Analysis of Processed and Unprocessed Diesel Fuel by Electrospray Ionization Fourier Transform Ion Cyclotron Resonance Mass Spectrometry. *Energy Fuels* **2001,** *15*, 1186-1193.
103. Wu, Z.; Hendrickson, C.L.; Rodgers, R.P.; Marshall, A.G. Composition of Explosives by Electrospray Ionization Fourier Transform Ion Cyclotron Resonance Mass Spectrometry. *Anal. Chem.* **2002,** *74*, 1879-1883.
104. Hertkorn, N.; Benner, R.; Frommberger, M.; Schmitt-Kopplin, P.; Witt, M.; Kaiser, K.; Kettrup, A.; Hedges, J.I. Characterization of a Major Refractory Component of Marine Dissolved Organic Matter. *Geochim. Cosmochim. Acta* **2006,** *70*, 2990-3010.

15 Inorganic Mass Spectrometry

Learning Objectives

- Ionization of inorganic samples
- Elemental analysis by MS – special instrumentation
- Accurate isotopic compositions
- Lateral distribution of elements
- Elemental MS for assessing biological systems
- Element speciation in organic materials and biological tissues

---

Mass spectrometry resulted from an endeavor to analyze gaseous ionic matter. The discovery of isotopes and the determination of their masses and relative abundances, i.e., *isotope ratios,* were a direct result of the pioneering work of Thomson, Aston, Dempster, and many others [1,2]. Soon, the results of such measurements became the driving force for new discoveries in physics. The detection of mass defect, for example, was direct proof of the mass–energy equivalence as postulated by Einstein's special theory of relativity. It was not until the late 1940s that mass spectrometry was developed as a tool for the analysis of organic compounds, but within a decade or two, this branch flourished. In 1968, the journal *Organic Mass Spectrometry* was founded, and soon, the leap into *biomedical mass spectrometry* (also a journal title from 1974 to 1985) was taken. The majority of mass spectrometrists is now working in proteomics or metabolomics, in environmental, clinical and forensic trace analysis to name a few. Meanwhile, what became known as *inorganic mass spectrometry* [3-7] has experienced equally revolutionary developments [8,9] as its organic and biomedical counterpart – of which it could be considered a "sibling".

The determination of molecular formulas via accurate mass measurements relies on isotopic masses accurate to at least 1 in 10^8 [10]. Elemental trace analysis is required for the detection of radioactive nuclides in the environment, of transition metals such as Pt in exhaust fumes from automobiles [11], and in the quality control of low-sulfur fuels for the same. All electronic devices demand for high-purity semiconductors and the properties of alloys are critically influenced by trace elements [12]. Age determinations from isotope ratios are applied in archeology, paleontology, and geology [4,13,14]. More recently, elemental MS and biomedical MS are jointly employed to unveil the presence and preferably location of metals in proteins or DNA as well as their lateral distribution in tissues [15-18], a field of research basically going back to seminal work by Houk in 1980

J. Gross, *Mass Spectrometry*, 2nd ed., DOI 10.1007/978-3-642-10711-5_15,
© Springer-Verlag Berlin Heidelberg 2011

[19]. Moreover, the prominent role of metal ions in physiological processes gave rise to a new field of research: *metallomics* [20,21]. Finally, we are witnessing a rapid expansion of imaging techniques based on former methods of element MS into the exploration of complex biological systems [22-25]. This altogether made it mandatory to include at least a compact chapter on *inorganic mass spectrometry* in this book.

Example: The function of metalloproteins critically depends on their interaction with a metal, e.g., Cu, Zn, Fe, Mo, or metalloid such as Se or As. The living cell not only depends on its genome and proteome, but also on its metallome, i.e., the distribution of those elements among different biomolecules. The complexity of speciation analysis demands for a combined approach of separation techniques and different methods of mass spectrometry. This is best illustrated by the metallomics toolbox that reflects the current understanding of how the metallome can be explored (Fig. 15.1) [21].

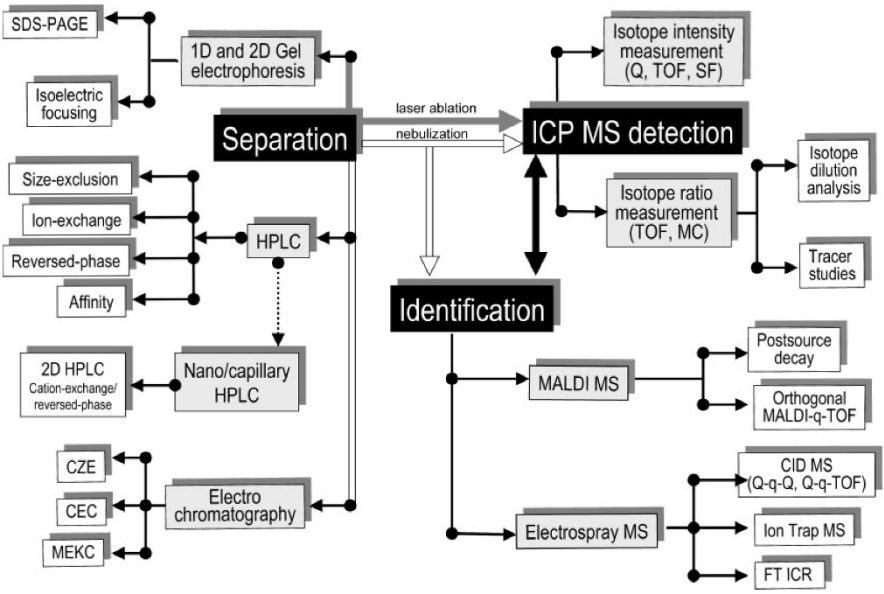


Fig. 15.1. The state-of-the art toolbox with hyphenated techniques for element speciation analysis and metallomics. The *upper right* section presents the tools of inorganic mass spectrometry. Reproduced from Ref. [21] with permission. © Wiley Periodicals Inc., 2006.

Example: The speciation of selenium incorporated in yeast proteins shows the high degree to which elemental and biomedical MS are interrelated by now. The analysis started with a tryptic digest of the water-soluble protein fraction that had been isolated by size-exclusion chromatography. Analysis of the digest by reversed-phase HPLC-*inductively coupled plasma mass spectrometry* (ICP-MS) provided identification of the selenopeptide fraction, which was then analyzed by

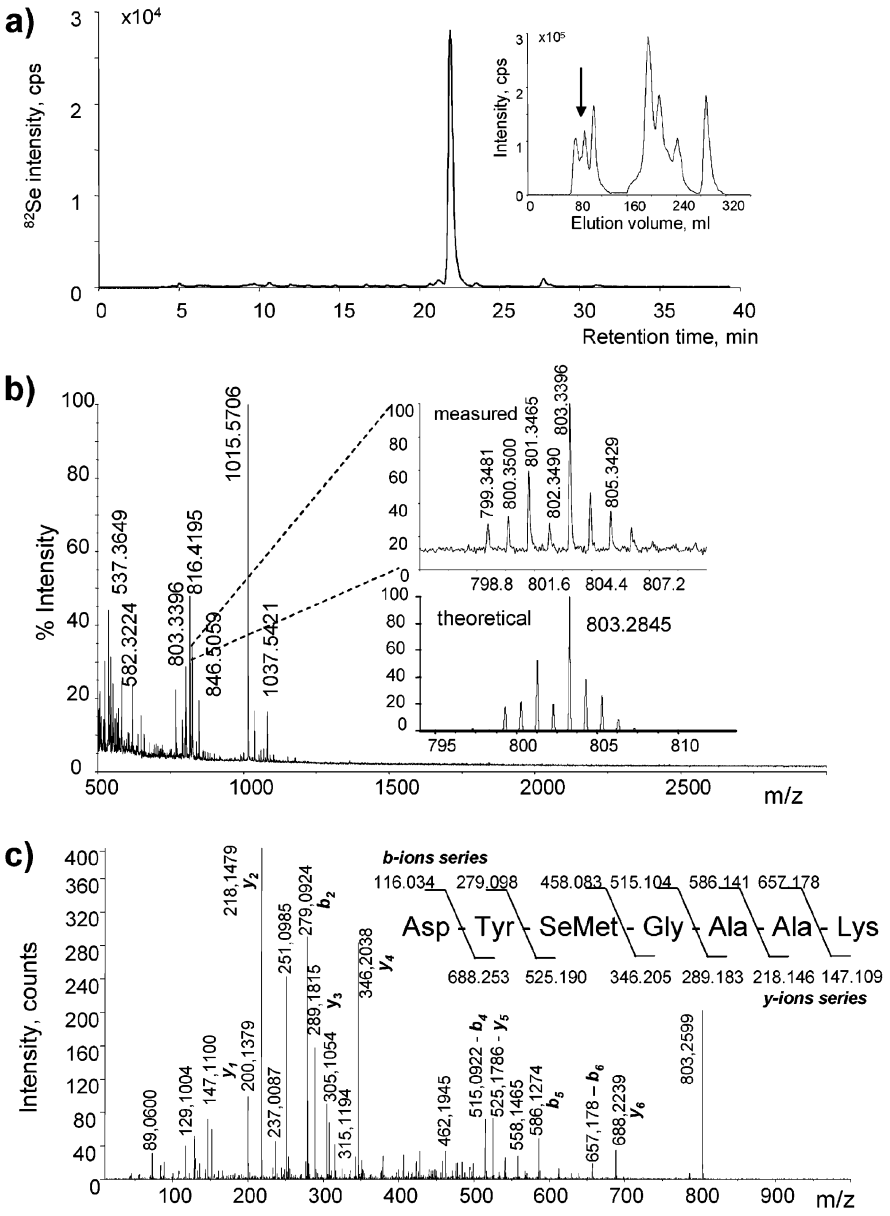


Fig. 15.2. Identification of the selenopeptide of the HSP12 protein: (**a**) Reconstructed ion chromatogram based on ^{77}Se and ^{82}Se from reversed-phase HPLC-ICP-MS of the Se-containing protein fraction (as obtained from the marked region in the size-exclusion chromatogram in the inset); (**b**) MALDI-TOF mass spectrum of the fraction producing the peak correlated to Se in (**a**); (**c**) ESI-CID spectrum of the $[M+H]^+$ ion, *m/z* 803.25, of the selenopeptide. Reproduced from Ref. [26] with permission. © American Chemical Society, 2003.

MALDI-TOF-MS in order to select target ions for tandem MS. Finally, the sequences of the selected selenopeptides were derived from ESI-CID spectra. This combined approach using ICP-MS, MALDI-MS, and ESI-MS allowed for the first time the identification of the heat-shock protein HSP12 (M_r = 11,693 u) in which the only methionine residue was replaced by selenomethionine (Fig. 15.2) [26].

Both the reliable determination of isotope ratios and the quantitation of trace elements generally accompanied by complete destruction of all molecular entities. Opposed to what is normally desired in organic and bio-organic mass spectrometry, ionization methods in inorganic mass spectrometry therefore use conditions which erase any molecular structure, i.e., inorganic mass spectrometry particularly employs high temperature plasmas to achieve atomization prior to ionization and mass analysis [27]. Furthermore, ion-neutral reactions need to be suppressed or their products destroyed in order to ensure isotopic patterns free from interferences with isobars [28,29].

It does not surprise that neither a single type of mass spectrometer nor a single method of ion generation can fulfill all of the requirements for measuring all varying sample types and compositions equally well. While accelerator mass spectrometers, for example, deliver very high abundance sensitivity and low background, they have low sample throughput and need larger samples. ICP mass spectrometers, on the other side, tend to have higher sample throughput while being more susceptible to isobaric interferences. These different types of instruments are best viewed as complementing each other in their analytical capabilities (Fig. 15.3) [30,31].

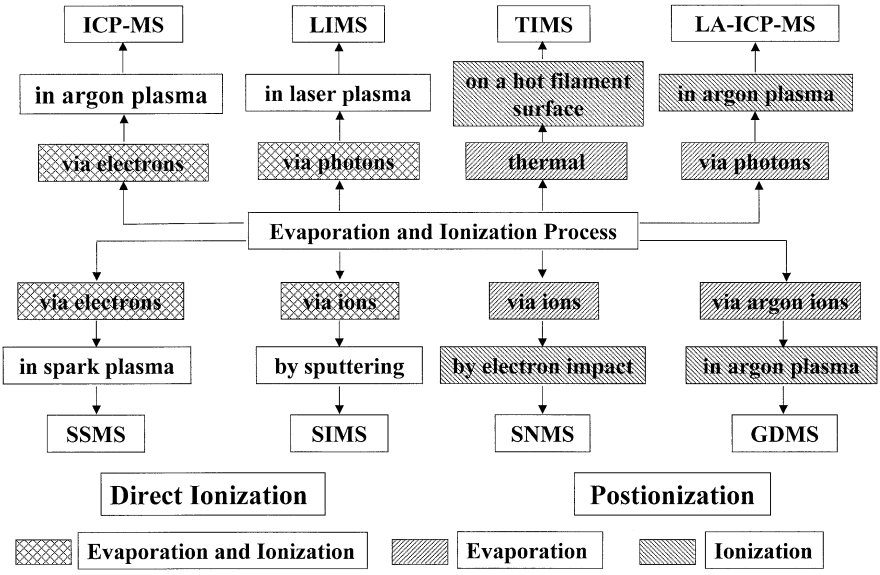


Fig. 15.3. Elemental MS techniques classified with respect to their evaporation and ionization processes. Reproduced from Ref. [30] with permission. © Elsevier Science Publishers, 2000.

15.1 Thermal Ionization Mass Spectrometry

Atomic and eventually molecular ions can be formed by *thermal ionization* (TI), also known as *surface ionization* (SI). For *thermal ionization mass spectrometry* (TI-MS), a metal salt, metal oxide, or metal is placed onto the surface of a rhenium or tungsten filament where it is heated in vacuum to 400–2300°C. In practice, an assembly of one to three ribbon filaments in close proximity is employed for TI (Fig. 15.4). The first filament is loaded with the sample and heated to evaporate the analyte. The neutral atoms or molecules emerging thereof may then be ionized on the second filament. Electron transfer to the bulk metal results in positive ions while electron transfer from the filament yields anions. The third filament of a triple filament assembly is normally used to deliver a standard that can be analyzed in alteration to the unknown under virtually identical ion source conditions. Double and triple filament assemblies have the advantage that evaporation and ionization temperature can be independently controlled. While evaporation is preferably performed at comparatively low temperature in order to obtain long-lasting signals and minor isotopic fractionation, ionization requires high temperatures for good ionization efficiency. Careful control of filament temperature [32] ensures that nanogram to microgram amounts of sample yield signals for hours because evaporation rates are in the order of picograms per second. Thoroughly chosen evaporation conditions are also vital for the reliability of the results [31]. Normally, 10 to 20 filament assemblies are mounted on one carousel-like sample turret in order to avoid frequent breaking of the vacuum. Once loaded and pumped to high vacuum, the instrument may be operated for days until all samples are measured.

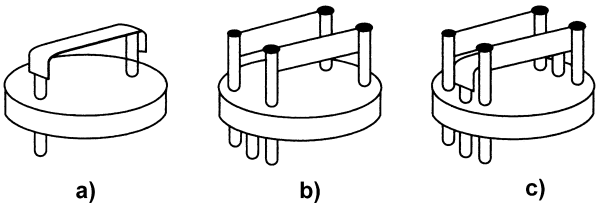


Fig. 15.4. From left (**a**) single filament, (**b**) double filament, and (**c**) triple filament assemblies for thermal ionization of metal salts and oxides. Reproduced from Ref. [3] with permission. © John Wiley & Sons Ltd, 1997.

Ion formation in TI relies on the blurring of the discrete electronic states of the neutral at high temperature. This way, the Fermi levels of adsorbed neutral and bulk metal can merge into a common band causing the charge state of the weakly surface-bound particle to be purely determined by Fermi statistics. In other words, as the electrons move freely between the adsorbed atom and the surface the atom is positive at times. Assuming ideal conditions, the degree of ionization, i.e., the ratio of ions and neutrals leaving the surface, is described by the *Saha-Langmuir equation*. The degree of positive ionization α^+ is given as

$$\alpha^+ = \frac{N^+}{N^0} = \frac{g^+}{g^0}\, exp\left[\frac{e(\Phi - IE)}{kT}\right] \tag{15.1}$$

$$= \frac{g^+}{g^0}\, exp\left[1.16\times10^4\,\frac{(\Phi - IE)}{T}\right] \tag{15.2}$$

where g^+/g^0 is the ratio of electronic states of the ion and the neutral, *IE* is the ionization energy of the atom or molecule to be ionized, Φ is the work function of the filament material, and *T* is the temperature of the ionizing filament. Best ionization efficiency is therefore obtained when metals of low *IE* are exposed to high temperature on filament materials that have large Φ. This is achieved by using filaments made of rhenium (Φ_{Re} = 4.98 eV, *m.p.* = 3180°C) or tungsten (Φ_W = 4.58 eV, *m.p.* = 3410°C; Fig. 15.5).

Vice versa, nonmetallic elements with high *IE* and metal oxides may form negative ions [33,34]. The degree of ionization α^- is then obtained from the modified Saha-Langmuir equation

$$\alpha^- = \frac{g^-}{g^0}\, exp\left[1.16\times10^4\,\frac{(EA - \Phi)}{T}\right] \tag{15.3}$$

where *EA* is the electron affinity of the adsorbed atom.

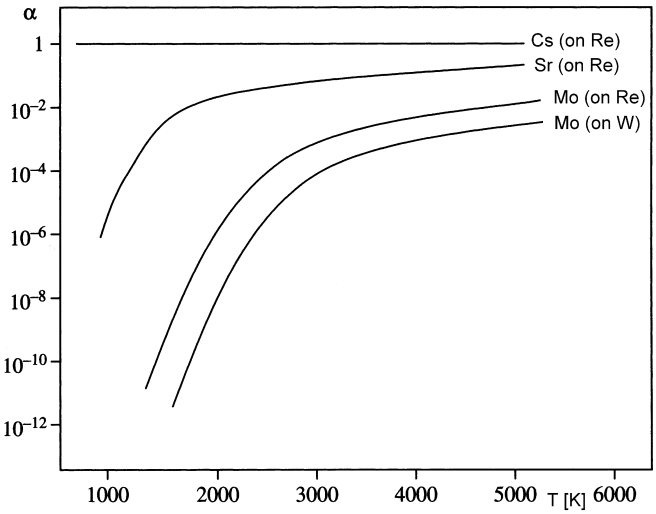


Fig. 15.5. Thermal ionization efficiency α^+ vs. filament temperature. The curves for Mo reflect the dependence of α^+ on the filament material. The advantage of the Re over the W filament follows from Eqs. 15.1–2. Reproduced from Ref. [7] with permission. © John Wiley & Sons Ltd, 2008.

Due to the low spatial and energetic spread of ions from TI, the method can be combined with single-focusing magnetic sector mass analyzers or quadrupoles [35]. Nonetheless, TI ion sources require dedicated instrumentation, frequently equipped with *multicollector* (MC) systems to insure the highest accuray for the isotope ratios measured (Chaps. 3.3.2 and 7.2 in [3]).

The favorite application of TI is *isotope ratio mass spectrometry* (IR-MS) and trace elemental analysis of metals and inorganic metal compounds. This is, however, in no way limiting the applicability of TI-MS to the elemental analysis of organic material including food. Such samples are transformed into suitable compounds by (extensive) work-up such as freeze-drying, oxidative treatment with concentrated HNO_3 or HNO_3/H_2O_2, ashing, or electrolytic deposition [36,37]. TI of organic salts remained a rare exception [38]. TI-MS is not suitable for mixture analysis and multi-element determinations where ICP-MS is normally employed. Due to its high precision, TI-MS is important as a reference method to calibrate other techniques of isotope ratio MS, such as MC-ICP-MS that, while also requiring matrix separation, is still able to deliver higher sample throughput (Chap. 15.4). TI-MS also serves for the certification of reference materials because accuracy and precision of the method are excellent [39].

Note: In the element MS community it is common to use the acronym TIMS without hyphen rather than the form TI-MS. The same is observed in case of other techniques employed for element MS, e.g., *secondary ion mass spectrometry* is abbreviated SIMS rather than SI-MS.

15.2 Spark Source Mass Spectrometry

The *spark source* (SS) developed by Dempster in 1935, provided the first truly multi-element and isotopic trace element method [40]. In *spark source mass spectrometry* (SS-MS), a solid sample is vaporized under vacuum by a high-voltage radiofrequency spark. The electric discharge is maintained between two pin-shaped electrodes (about 10 mm in length and 1–2 mm in diameter) in vacuum.

SS-MS is best suited for conducting samples, because the electrodes may then be directly prepared from the solid to be analyzed. Prior to insertion into the ion source, the electrodes have to be carefully cleaned, e.g., by etching, to avoid surface contamination (Chap. 5.2 in [6], Chap. 2.2 in [7]). If the sample is not itself conducting, high-purity graphite, or if neccessary silver or gold powder are used as scaffolding for the electrodes. Often, an *internal standard element* or an *isotopically enriched spike* are admixed to this powder before the finely ground analyte-containing material is added. Typically, 50 mg of powdered material, e.g., a rock sample, is mixed with the graphite powder and then compressed into electrode pins [41].

The detection limits for the elements from Rb through U generally vary between 0.001 and 0.1 ppm (equivalent to 0.001 to 0.1 $\mu g\ g^{-1}$). Certain elements

such as Nb, Zr, Y, Sn, Sb, and Th can even be measured at the ppb (ng g^{-1}) level [42].

Obviously, SS-MS is not suited for elemental analysis of small sample amounts, but SS-MS offers a high dynamic range making it very powerful for multiple element analysis including those present at trace level in alloys, ores, and similar samples. SS-MS also offers wide element coverage, an extensive concentration range and analysis of solids without dissolution.

Note: Although an element may be detected at the ultratrace level by SS-MS, the amount of sample required is comparatively large, as electrodes lasting for several hours of operation are needed.

The spark is initiated by emission of electrons from the cathode by field emission (opposite process to FI), which becomes possible due to the high local field strengths (10^8–10^9 V m^{-1}) at edges of the microscopically rough surface. The electrons are then accelerated towards the anode. There, the energy of the impinging electrons causes evaporation of the anode material (sample) that is subsequently ionized in the gas phase by electron ionization.

Proper operation of a spark source is not simple. It requires a high voltage supply of several tens of kilovolts, normally at 1 MHz radiofrequency that is generated in short pulses of variable length (20–200 μs) with a repetition frequency of 1–10^4 s^{-1} to achieve uniform ablation of both electrodes (Fig. 15.6) [41]. In order to maintain a stable ion current, the electrodes need to be carefully adjusted and dynamically re-adjusted during the measurement (0.1–0.5 mm tip to tip) [43], and special techniques such as *gliding spark source mass spectrometry* (GSS-MS) are sometimes employed for the analysis of nonconducting materials [44]. Finally, the ions emerge from the discharge with a wide kinetic energy distribution (keV range), which makes a double-focusing mass analyzer mandatory for SS-MS. To partially compensate for this high energy spread, accelerating voltages on the order of 20–25 kV are typical.

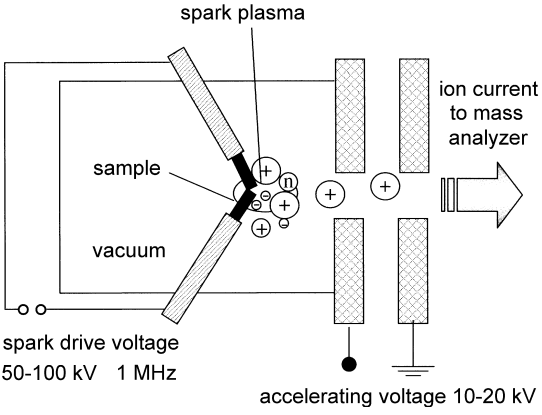


Fig. 15.6. RF spark source. Reproduced from Ref. [7] with permission. © John Wiley & Sons Ltd, 2008.

Opposed to all other current MS techniques, photoplate detection and subsequent densiometry on a series of exposures is still widespread in SS-MS. In practice, 15 consecutive spectra are acquired by exposing the plate streak-by-streak in a range from 0.001 to 300–2000 nCi, requiring total measurement times of about 0.5 to 3 h per sample. Translation of densiometric data into ion abundances is not trivial and detailed procedures have been developed for this crucial step of SS-MS analysis [40-42].

More recently, *multi-ion counting* (MIC) systems have been due to their improved sensitivity, precision, and sample throughput (Fig. 15.7) [42,43]. Simultaneous detection in Mattauch-Herzog geometry SS-MS instruments using MIC is also advantageous for applications such as isotope dilution analysis of several isotopes. Furthermore, SS-MS is well suited for C, N, O determination in semiconductors, because the combination of a high vacuum source without sputter gas with a high frequency discharge allows for the analysis of samples even at high resistivities [45].

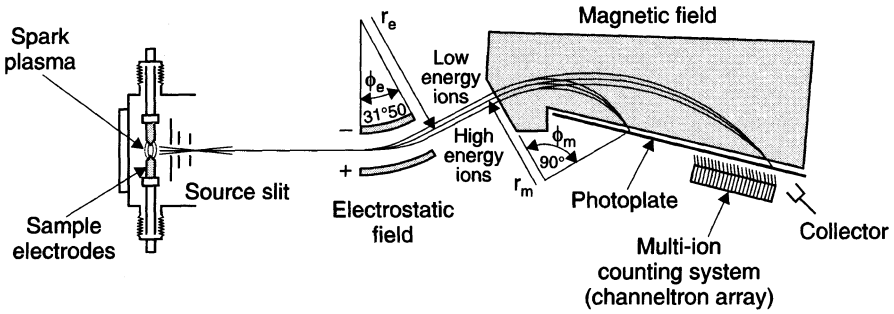


Fig. 15.7. Spark source mass spectrometer of Mattauch-Herzog design offering alternative detection on photoplate or by channeltron array for multi-ion counting. Reproduced from Ref. [42] with permission. © Addison Wesley Longman, 1997.

Example: SS-MS has been used for the quantification of carbon in a gallium arsenide (GaAs) sample produced by high-pressure liquid-encapsulated Czochralski (HP-LEC) crystal growth. The carbon might originate from the graphite susceptor, the ambient gas, or be present as a trace element in both gallium and arsenic starting material. The partial SS mass spectrum shows strong signals due to $^{69}Ga^{6+}$, $^{71}Ga^{6+}$, and $^{75}As^{6+}$ in close proximity to the carbon peak at *m/z* 12 (Fig. 15.8) [46].

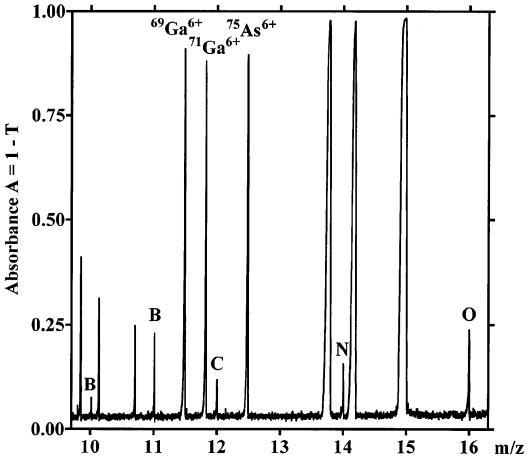


Fig. 15.8. Partial SS mass spectrum of a HP-LEC GdAs sample by photoplate detection after exposure to $Q = 3 \times 10^{-7}$ Ci. Reproduced from Ref. [46] with permission. © Springer-Verlag, 1999.

15.3 Glow Discharge Mass Spectrometry

The first report of the formation of positive ions of gases from a *glow discharge* (GD) in his so-called channel ray tube was by Goldstein in 1886 [7]. Since the launch of the first commercial instrument for *glow discharge mass spectrometry* (GD-MS) in 1984, GD-MS has become sort of industry standard for the analysis of trace elements in metals and semiconductors [47,48]. The pioneering work and much of the development of GD-MS has been done by Harrison and Marcus [49-53]. In fact, GD-MS appears as the successor to SS-MS, and at present, GD-MS is one of the most powerful solid-state analytical methods for the determination of trace impurities and depth profiling of solids. It allows direct trace element determination in solids down to concentrations as low as 1 ppb (ng g^{-1}) [30]. GD-MS is an essential technique for the quality control and characterization of high-purity metals in the electronics industry.

The direct current (DC) glow discharge is a self-sustaining low pressure gas discharge dominated by space charges and represents a low-energy plasma making the GD ion source a compact small volume source that operates a low wattage. It is inexpensive to build and maintain, and plasma gases are modestly consumed (ml min^{-1}). Also, unlike the spark source, the GD source is inherently stable [54]. Typically, in a GD ion source [45,48,54-58] a discharge current of 1–5 mA is maintained through a low-pressure argon atmosphere (10^1–10^3 Pa) by applying a DC voltage of 500–2000 V across the ionization volume. The cathode is represented by the solid sample which may either be a disk (so-called *Grimm-type GD source* [54]) or a stick and an anode present as the housing and the ion source exit plate (Chap. 5.3 in [6], Chap. 7.5 in [3]) .

The low-temperature Ar plasma serves as a source of primary ions, excited atoms and electrons. In the cathode dark space, a region where a large potential drop exists, the positive argon ions are accelerated towards the sample cathode and the sample material is sputtered from the cathode's surface by ion bombardment (cf. FAB, LSIMS, Chap. 10). The kinetic energies of the impinging ions are in the range of 100–500 eV [48]. Sputtered atoms and molecules depart from the surface with kinetic energies of 5–15 eV and are then ionized in the quasineutral glow discharge plasma (so-called *afterglow*). The electron density in the plasma can reach up to 10^{14} cm^{-3} [59] and their energy covers a wide distribution from thermal to energetic. Although they are by about a factor of 1000 less abundant in the plasma, metastable Ar* atoms are also effective for ionization because they carry 11.55 eV. Therefore, Penning ionization, electron ionization, and charge transfer contribute to ionize the neutrals (Fig. 15.9).

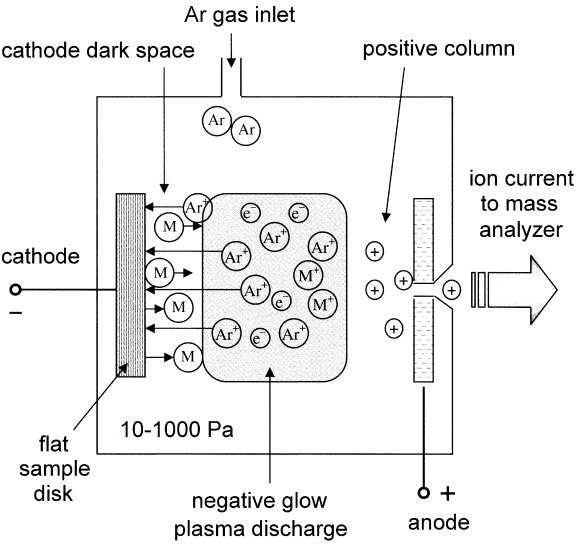


Fig. 15.9. GD ion source with disk-shaped cathode. Reproduced from Ref. [7] with permission. © John Wiley & Sons Ltd, 2008.

Note: The *afterglow* (or negative-glow) region shines brightly because excited atoms are emitting their characteristic visible radiation. This phenomenon not only gave rise to the method's name but also led to the construction of the neon lamp. For more applications of GDs a review by A. Bogearts is highly recommended [60].

Due to its general setup, GD has the advantage that the atomization and ionization processes are separated in space and time, resulting in only minor variations in sensitivity and a low matrix dependence. This enables the quantification of elements without the need for standards tailored to the actual type of sample matrix [45,48].

On the downside, there are isobaric interferences such as $[XAr]^{+\bullet}$ and $[XH]^{+}$ ions that require $R > 5000$ to avoid overlap with pure atomic ions $X^{+\bullet}$ [48]. Therefore, double-focusing magnetic sector instruments present the most successful mass analyzers in GD-MS [45]. Another disadvantage of GD-MS as compared to LA-ICP-MS or SIMS (Chaps. 15.4 and 15.5), for example, is the lack of spatial resolution.

Example: In the manufacture of aircraft engines and gas turbines superalloy is widely used due to its excellent performance, which to a great extent depends on the content of trace elements in the alloy. Critical control of the alloy's composition is therefore essential for the safe operation of such engines. The obvious method to avoid isobaric interferences is to select isotopes where no interferences exist. While Tl, Pb, and Bi meet this criterion, in case of Sn only the $^{118}Sn^{+\bullet}$ ion is free of superimpositions, whereas $^{120}Sn^{+\bullet}$ has serious interferences from $^{40}Ar_3^{+\bullet}$, $^{92}Mo^{14}N_2^{+\bullet}$, and $^{120}Te^{+\bullet}$. To determine the correct content of elements in superalloy on a quadrupole GD instrument also when no suitable isotope exists, both matching the sample matrix by use of external standards and multivariable linear regression have extensively been used (Fig. 15.10) [61].

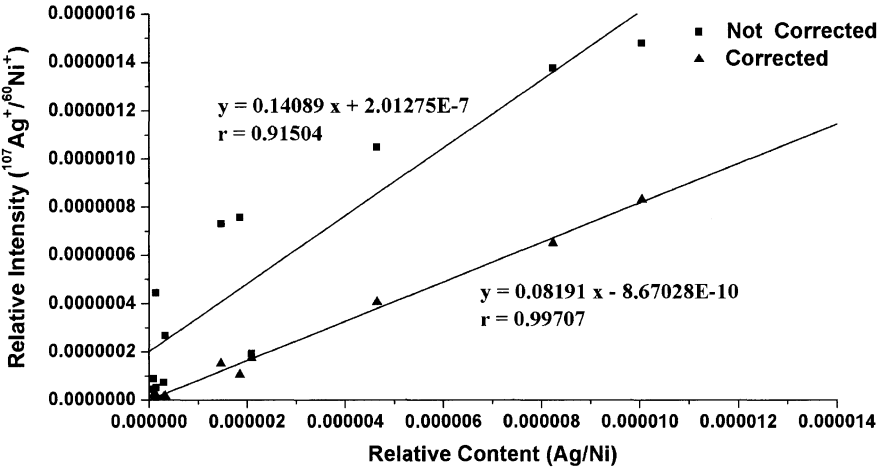


Fig. 15.10. Comparision of ^{107}Ag calibration curves in superalloy between the uncorrected results and those corrected by multivariable linear regression. The relevance of corrections when no separation by high-resolution is available is immediately apparent. Adapted from Ref. [61] with permission. © IM Publications, 2008.

In a DC GD, nonconducting samples would rapidly cause the breakdown of the discharge due to electrostatic charging. Radiofrequency (RF) discharges circumvent this problem [51-53,56,62]. By applying an RF voltage at one of the two electrodes (called the *RF-electrode*), the accumulated positive charge on the sample surface will be neutralized by the negative charge accumulation during the second part of the RF-cycle thereby avoiding net charges. Typically voltages of 2 kV at an RF of 13 MHz are employed.

The atomic collision processes in the GD are sufficiently robust to break many tenaciously bonded species [54]. Nonetheless, GC-GD-TOF-MS has even been demonstrated to be capable of delivering spectra of organic molecules and elemental information [63-65].

Note: The analytical problems of inorganic MS often require only certain selected isotopes or narrow *m/z* ranges to be measured. Multicollector systems, for example, are adjusted to simultaneously detect a few isotopes for the purpose of accurate isotope ratio determinations or to quantify a low-abundant isotope together with an isotopic standard for internal reference. Thus, the data is more often presented in tabular form or in plots of concentration versus variables such as depth of invasion, age of samples, or location on a surface. Mass spectra covering a wider range are only acquired for survey multi-element detection.

15.4 Inductively Coupled Plasma Mass Spectrometry

In *inductively coupled plasma mass spectrometry* (ICP-MS), atomization and ionization are achieved in a radiofrequency argon plasma at atmospheric pressure. Since a seminal publication in 1980 [19], ICP-MS has become one of the most frequently employed methods of elemental MS (Chap. 7.3 in [3], Chap. 4 in [6], Chap. 5 in [7]). The wide acceptance of ICP-MS is due to its comparatively robust, yet versatile sampling mode. An ICP not only offers high ionization efficiency for elements of low *IE*, e.g., 98% for $IE = 7$ eV, it is still applicable to nonmetals such as P and even Cl (ionization efficiency is 1% for $IE = 13$ eV).

The core of an ICP source is formed by a so-called *plasma torch*. It consists of three coaxially aligned quartz tubes that are inserted along the central axis of a water-cooled RF coil. After ignition by an electric spark discharge, the coil (typically RF of 27 MHz) feeds the plasma by coupling electric energy (1–2 kW) into the gas, because the fluctuating magnetic field causes ion motion which in turn heats up the gas and maintains a continuously flowing plasma. The outer quartz tube is about 20 mm in diameter and has its walls cooled by an argon gas flow of 12–20 l min^{-1}. The middle tube supplies another stream of argon, the so-called auxiliary gas flow of 1–2 l min^{-1} that is feeding the plasma. The sample is then introduced into the center of the toroidal plasma by an argon carrier gas flow of 1–1.5 l min^{-1}. This carrier gas passes through a nebulizer and leads to the dissipation and transfer of a liquid sample as micrometer-sized droplets (depending on the type of nebulizer), which can be vaporized, atomized, and ionized within the ICP. Typical sample consumption is in the order of 0.02–1 ml min^{-1} (Fig. 15.11).

The ICP approaches a temperature of 10,000 K in the induction zone close to the coil, in the center of which evaporation and atomization occur at about 8000 K. While the plasma flows away from the coil, excitation of the neutrals is effected at 7500 K followed by ionization in a zone well after the coil at about 6500 K (Fig. 15.11). Thereafter, recombination in the plasma's tail causes molecu-

lar interferences, which can be reduced by placing a collision cell in the ion beam, for example [28,29,66,67].

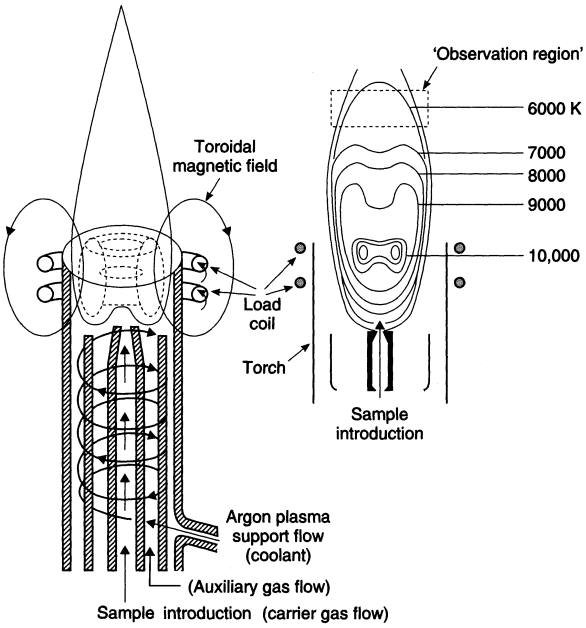


Fig. 15.11. ICP plasma torch (*left*) and the temperature distribution inside the plasma (*right*). Reproduced from Ref. [68] with permission. © Addison Wesley Longman, 1997.

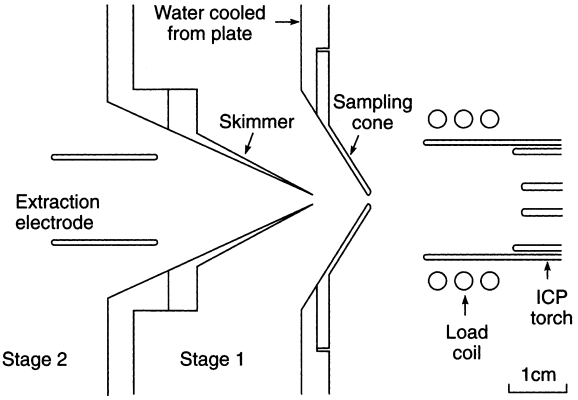


Fig. 15.12. Ion extraction interface for ICP-MS. Ions arrive from the right, a small portion is transmitted through the water-cooled sampling cone into the first pumping stage (rotary pump), the center of the free-jet expansion is then transmitted through the second skimmer cone, behind which it is guided by electric potentials through the second pumping stage into the mass analyzer. Reprinted with permission from Ref. [3]. © John Wiley & Sons Ltd., 1997.

Analogous to ESI (Chap. 12), ion transfer into the mass analyzer is accomplished via a differentially pumped interface. A small portion of the plasma enters the first pumping stage through a hole in the center of the sampling cone. Water cooling of the sampling cone preserves its surface from rapid destruction due to the exposure to the hot plasma. Next, the ions are guided through the entrance of the skimmer by application of an electric potential, while most neutrals are pumped off the supersonic expansion in this region (Fig. 15.12). Analogous to early atmospheric pressure ion sources of organic MS, the first implementation of ICP-MS was attached to a quadrupole analyzer due to its acceptance of moderate vacuum conditions [19].

Nowadays, ICP sources are used with magnetic sector [12,69], to an important extent time-of-flight (TOF) [70-75], and even Fourier transform ion cyclotron resonance (FT-ICR) mass analyzers [76].

The interest in high-resolution ICP instruments is driven by polyatomic interferences between the plasma gas and the matrix introduced, which are indeed limiting factors for ICP-QMS. Isobaric interferences are less problematic than it might appear on first sight, since most of the elements have more than two isotopes to select from. Anyway, none of the isobaric interferences can be resolved by the current sector or TOF mass spectrometers since they require a mass resolution above 12,000 [77].

Note: Occasionally, the type of mass analyzer is part of the acronym: a quadrupole leads to ICP-QMS, a (magnetic) sector field, also termed double-focusing instrument, leads to ICP-SFMS or ICP-DFMS, respectively, and a time-of-flight analyzer to ICP-TOFMS. Again, this is slightly different from the customs in organic and biomedical mass spectrometry where only TOF and FT-ICR tend to be included in the acronym and normally are separated by a hyphen from MS.

Liquid sample introduction is still the standard in ICP-MS. Consequently, the coupling of liquid chromatography or capillary electrophoresis to ICP instruments is straightforward. This way, not only the presence of an element in a sample can be detected, but also the assignment to molecular species becomes feasible. This explains the relevance of ICP-MS for the identification of non-C,H,N,O elements in proteins, i.e., for metallomics (cf. first two examples of this chapter).

Example: Three categories of signals are contributing to the ICP mass spectrum of brass. The background peaks due to $^{14}N^+$, $^{16}O^+$, $^{1}H_2{}^{16}O^{+\bullet}$, $^{40}Ar^{2+}$, $^{36,38,40}Ar^+$, and $^{40}Ar_2{}^+$ are contributions of the ICP background spectrum. Then, the polyisotopic elements Cu and Zn represent the main components of brass, and thus, cause strong peaks. Finally, Si, Mn, Fe, Ni, Sn, Sb, Pb, and Bi are present at low concentration (Fig. 15.13). Instead of nebulizing a solution of the alloy, in this particular case the brass has been fed into the ICP by in-torch laser ablation [75].

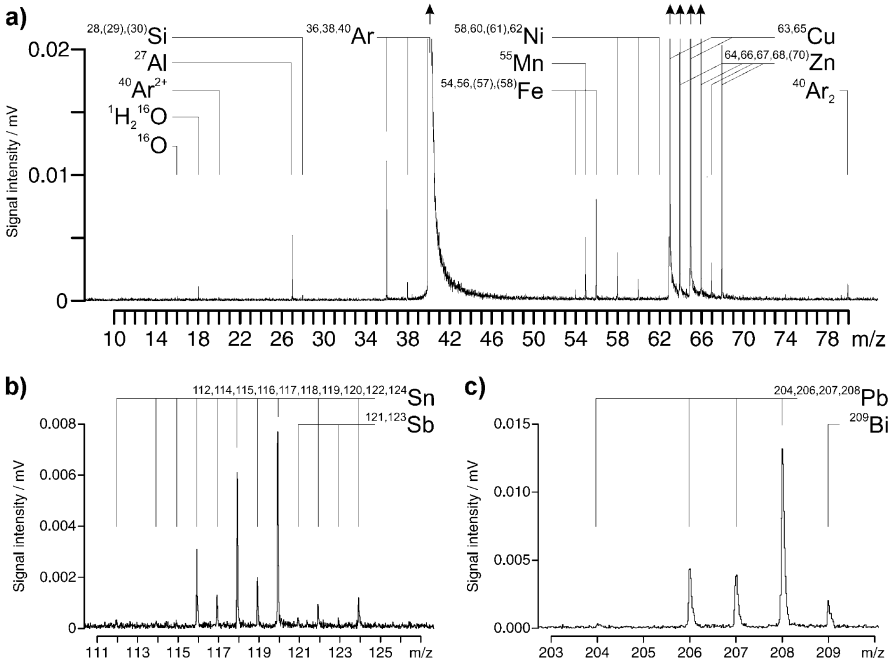


Fig. 15.13. The ICP-TOF mass spectrum of brass. The peaks due to N, O, H_2O, Ar^{2+}, Ar^+, and Ar_2^+ are present as a blank spectrum of the ICP. In range (**a**) up to *m/z* 80, Si, Mn, Fe, and Ni are detected at low levels while Cu and Zn are dominant as expected for brass. The sections (**b**) and (**c**) show overlapping signals from Sn and Sb as well as Pb and Bi, respectively. Adapted from Ref. [75] with permission. © Springer-Verlag, 2008.

Note: ICP-MS is commonly mentioned in the context of high throughput and claimed to have no need for extensive sample preparation. In analytical practice, however, every sample needs to be treated individually; digestion prior to analysis usually takes about 2 h per sample. Furthermore, as is the case with TIMS for example, matrix separation is required for precise and accurate isotope ratio determinations. In particular, if MC-ICP-MS is going to be used as a complementary technique for TIMS, high throughput is only achieved on the expense of precision.

15.4.1 Laser Ablation ICP-MS

To further complement the sampling repertoire for ICP-MS, a gas stream, typically helium, may be employed to take up a laser-generated aerosol. This technique is known as *laser ablation* (LA) ICP-MS. Its first realization by the Hieftje group in 1996 [78] was based on the previously introduced ICP-TOF instrumentation [70-72]. LA-ICP-TOF-MS can be used for sampling from solid surfaces of

bulk material, or alternatively, for imaging of element distributions. LA-ICP mass spectral imaging allows to monitor the lateral distribution of elements across a solid structure [79], to identify metals and metalloids on a 2D gel [80,81], or to reveal element concentrations in biological tissues and similar samples (Fig. 15.14) [16,17,81].

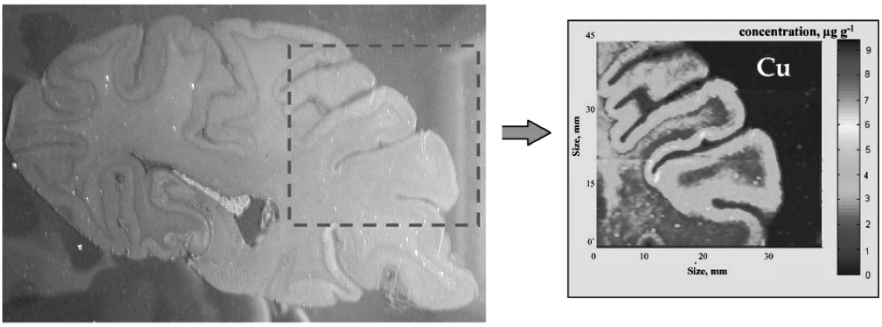


Fig. 15.14. Mass spectral imaging to unveil the quantitative distribution of Cu in tissue. The average concentration of Cu was 3–7 µg g^{-1} tissue. Light photograph of a thin tissue section of human brain (*left*) and the Cu distribution in the marked region as obtained by LA-ICP-MS (*right*). Adapted from Ref. [17] with permission. © Royal Society of Chemistry, 2007.

15.5 Secondary Ion Mass Spectrometry

When a beam of (primary) ions possessing keV-energies strikes a surface, the energy transferred by the incident particles causes a collision cascade that sets several atomic layers in motion and is accompanied by complex processes of energy transfer and electronic interaction in the surface zone of the solid. It results in the emission of electrons, photons, atoms, and molecules, both of the latter either neutral or ionic, whereby the surface under bombardment experiences irreversible changes [82]. The ions that are emitted are termed *secondary ions* and the method is therefore called *secondary ion mass spectrometry* (SIMS). Nearly the same processes of sputtering and ion formation are effective in FAB and LSIMS (Chap. 10) [83], and in fact, SIMS paved the road for the development of FAB and LSIMS to analyze organic samples. Nonetheless, SIMS is not simply a precursor of FAB, but a reputable method of its own serving nicely for analyzing inorganic samples that range from rocks to alloys and semiconductors [84,85].

The emission of secondary ions of both polarities from instrument construction materials produced as a by-product of ion source operation was first observed by Arnot [86,87] and was developed into an analytical instrument by Herzog and Vieböck [88]. Inspired by these experiments, an early SIMS instrument was constructed in the 1960s to analyze lunar rocks from NASA's Apollo missions. Much of the breakthrough of SIMS for *i*) bulk analysis of solids, *ii*) depth profiling of thin layers, *iii*) imaging, and *iv*) monolayer analysis is also the merit of the Benninghoven group [82,84,89,90].

15.5.1 Atomic SIMS

Applied to solid materials, especially semiconductors and thin films, SIMS can determine trace levels of all elements in the periodic table. Spatial microanalysis is provided by collimating the primary ion beam to about 1 μm in diameter and control of where the beam strikes the sample surface. This way, SIMS provides lateral and depth distributions of these elements within the sample. Currently, SIMS is being adapted to achieve lateral resolutions well below 100 nm. The driving force comes from the progress in microelectronics aiming at structures that approach 10 nm. Also, the depth resolution needs to come close to the atomic scale [91].

SIMS surface analysis is classified into two modes of operation, the so-called *static SIMS* and *dynamic SIMS* mode. Static SIMS employs an extremely low sputtering rate, often with a pulsed primary ion beam, for better sensibility to the characteristics of the top monolayer and even may reveal molecular information (see below) [92]. In static SIMS, the primary ion dose is kept below 10^{12} ions s^{-1} cm^{-2}. Dynamic SIMS uses high sputtering rates of a constant primary ion beam (10^{17} ions s^{-1} cm^{-2}) resulting in very high sensitivities to trace impurities (ppm to ppb). It delivers elemental and isotopic information as do the other methods of inorganic mass spectrometry. Magnetic sector or quadrupole mass analyzers are frequently in use for dynamic SIMS. Continuous analysis while sputtering yields information as a function of depth, called a *depth profile*.

Note: A single sputtering event, i.e., penetration, lattice perturbation by impact cascades, and final particle ejection, takes less than 10^{-12} s. Interestingly, for primary ion beam densities $< 10^{-6}$ A cm^{-2} (equal to 6×10^{12} ions s^{-1} cm^{-2}) no interference of processes caused by different primary ions will occur, because the maximum cross section of an impact is only in the order of 10 nm^2. In other words, each impact is independent of prior, subsequent, or nearby synchroneous hits [82,83]. In the time domain this means that a given surface area suffers 10–100 hits min^{-1} in dynamic SIMS, but only 0.01–0.1 hits min^{-1} in static SIMS. For a monoatomic layer, observation times in the order of 1 h can thus be realized in static SIMS, i.e., the attribute *static* refers to the extended preservation of the surface.

15.5.2 Instrumentation for Atomic SIMS

The primary ions for SIMS are usually generated by either a thermal ionization source delivering Cs^+ ions or by a *duoplasmatron source*. Depending on its mode of operation, the duoplasmatron is working somewhere between electron ionization and a glow discharge. It can be used to generate a collimated beam of positive (Ar^+, O^+) as well as negative primary ions ($O_2^{-\bullet}$) [93,94]. Positive oxygen ion bombardment increases the concentration of oxygen in the surface layer and creates M–O bonds there. Breaking these bonds during the process of bombardment and ion desorption builds up negative charge that is readily consumed by the oxy-

gen because of its high electron affinity. Thus, more metal atoms remain positively charged. Strongly electropositive elements are therefore analyzed as positive secondary ions from oxygen bombardment for best sensitivity. Opposed to oxygen, cesium ions implanted into the sample surface reduce its work function, thereby providing more secondary electrons, which enable effective negative ion formation. Consequently, semimetals and nonmetals as well as group VIII transition metals are preferably analyzed by Cs^+ bombardment as negative ions.

Another well-established class of primary ion sources are *liquid metal ion guns* (LMIG) delivering Ga^+ or In^+ ions. They offer very fine beams to achieve high lateral resolution. The Ga^+ LMIG currently provides the smallest probe size (less than 10 nm) with the highest current density (1–10 A cm^{-2}) of any ion gun. The LMIG normally consists of a field emitter tip coated with Ga from where a high electric field extracts Ga^+ ions. To ensure optimal focusing of the beam, the Ga^+ ions are accelerated by 20–60 kV (Fig. 15.15) [95].

Sputtering as a result of primary ion bombardment delivers diverse ion species ranging from monoatomic ions of various charge states to multi-atomic clusters and eventually simple molecular ions. Sputtering is generally accompanied by isotopic and chemical fractionation, i.e., the secondary ion yield is not independent of

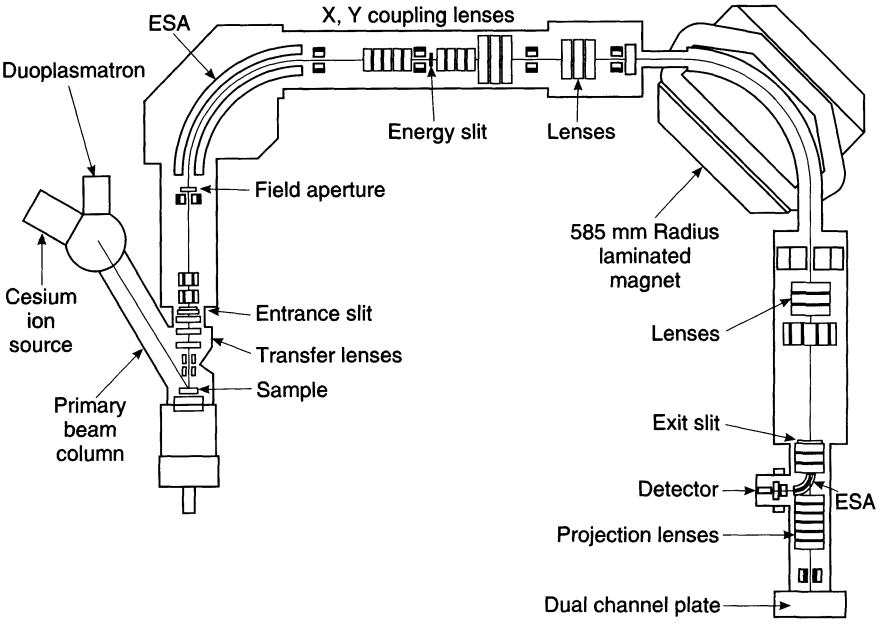


Fig. 15.15. Schematic of the Cameca IMS 1270, showing the main components of a high-resolution ion microprobe SIMS instrument. From the magnet radius, the footprint of the instrument can be estimated to about 4 × 3 m. For flexibility, the sample can be bombarded with either Cs^+ ions (by TI) or ions from a duoplasmatron source, which can deliver noble gas or oxygen ions. Reproduced from Ref. [96] with permission. © Addision Wesley Longman, 1997.

the material to be analyzed. SIMS produces spectra that are characterized by numerous interferences between different charge states of atomic ions and simple reaction products such as oxides, hydroxides, halides, etc. As with any other elemental MS technique before, high-resolution instruments provide the most effective and reliable means of dealing with superimposing isobars.

Examples: The positive secondary ion spectrum of a silicon surface shows peaks that can be assigned to Si^{2+}, Si^{+}, Si_2^{+}, Si_3^{+}, Si_4^{+}, etc. while the negative secondary ion spectrum yields signals corresponding to Si^{-}, Si_2^{-}, Si_3^{-}, and Si_4^{-}. In case of a two-component lattice such as a metal (M) oxide, SIMS will deliver positive ions of the type $[M_nO_{n-1}]^{x+}$ (normally $x = 1$) and negative ions of the general type $[M_{n-1}O_n]^{-}$. The number ratios of M and O will naturally depend on the metals' prevailing oxidation state. Accordingly, more complex systems result in additional cluster ion compositions. SIMS of salts preferably yields the cation or anion and corresponding cluster ion series as already mentioned for FD, FAB, or ESI (Chaps. 8, 10, 12, respectively) [82,89,90].

15.5.3 Molecular SIMS

Static SIMS, i.e., conditions of low primary ion flux, can preserve molecular information, but this is effected at the expense of correspondingly low secondary ion yields. The combination of static SIMS conditions with scanning mass analyzers is therefore disadvantageous and the outcome of experiments with SIMS for organic molecules such as amino acids in the "pre-FAB era" was not too exciting [92]. Here again, the TOF analyzer plays to its strength as it is capable of analyzing all ions contained in a package created by a short primary ion pulse. As only few ions are lost (due to imperfect transmission) there is a more than 1000-fold gain in sensitivity when using a TOF rather than a quadrupole analyzer [97].

The first TOF-SIMS instrument [98] employed a pulsed alkali primary ion source. The primary ions were created from alkali aluminosilicate by thermionic emission, accelerated by up to 25 keV and focused onto the monomolecular sample layer on gold or silver surfaces in bursts of 5–50 ns. (This type of Cs^{+} primary ion sources is still in use for LSIMS.) Useful spectra of amino acids and nucleosides [98,99] and even peptides [100] were obtained in this way. Soon, TOF-SIMS became a major competitor of PD-MS [101-103] and the development of FAB and LSIMS led to fruitful approaches such as TOF-LSIMS [104].

Note: In the 1980s FAB, LSIMS and PDMS were the methods of choice for the analysis of biomolecules, and there was mutually fostering research on these methods. After the advent of MALDI and ESI in the late 1980s, they were rapidly superseded, and by now, have been almost quantitatively replaced.

Modern TOF-SIMS applications are often in the field of synthetic polymer analysis, but rarely for the determination of molecular weight distributions which is the domain of MALDI. More frequently, low-molecular-weight additives or surface modifications are analyzed as there is no interference with a matrix as would

be the case with MALDI [105-109]. In essence, only SIMS can truly analyze the native surface.

Example: Additives are intentionally added to a polymer to stabilize or improve different polymer properties. They act as antioxidants, UV stabilizers, antistatic agents, flame retardants, etc. However, their migration towards the surface may result in blooming, thereby negatively affecting surface properties that are required for specific applications. TOF-SIMS is ideally suited to characterize surface compositions because it offers molecular information on the uppermost monolayers at high sensitivity. Here, the antioxidant Irgafos 168 (0.3 wt.%) has been analyzed on the copolymer PETi, a poly(ethylene terephthalate (60%) isophthalate (40%)) (Fig. 15.16) [109].

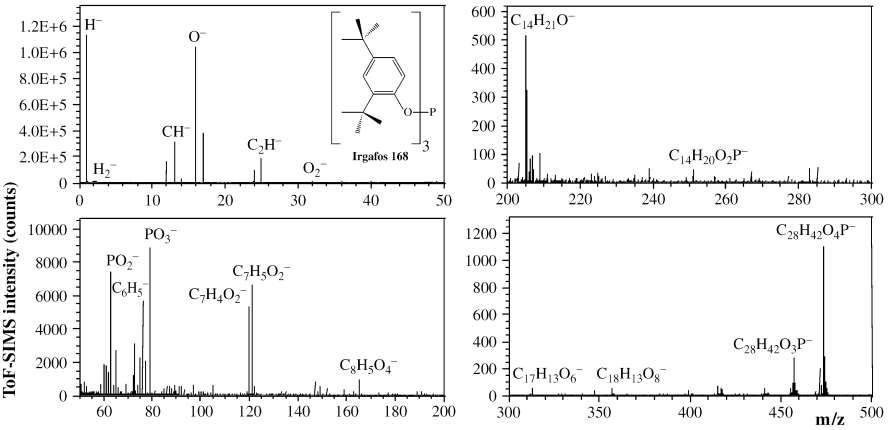


Fig. 15.16. Negative-ion TOF-SIMS analysis of Irgafos 168 on PETi. The compound undergoes significant fragmentation, and thus, no $[M–H]^-$ peak (*m/z* 645) is included. Note the tremendously decreasing ion abundances with rising *m/z*, which is also the reason for the segmented representation of the mass spectrum. Reproduced from Ref. [109] with permission. © John Wiley & Sons, Ltd., 2002.

15.5.4 Polyatomic Primary Ion Beams

More recently, SIMS has gained enormous impetus from the introduction of heavy primary ion beams such as gold [110] or bismuth clusters [111-113] or fullerene molecular ions [24,114-116]. Especially their combination with TOF-SIMS instrumentation has rejuvenated the whole field of SIMS. As we already know from FAB and LSIMS, and as has been veryfied also for SIMS [117], higher-mass xenon beams create a higher yield of secondary ions and are more effective for larger molecules than argon or neon, for example. Before the advent of heavy primary ion sources, the ions which could be detected by TOF-SIMS were limited to a mass range of about 300 u mainly because the primary ions where very inefficient in desorbing larger molecular species. With polyatomic primary ion beams

the secondary ion emission is drastically enhanced while the surface damage is not as severe [118]. Polyatomic primary ion beams can effectively cover the range up to *m/z* 1500 at lateral resolutions in the order of 1 μm.

Experiments and molecular dynamics theory suggest that the efficient ionization of large molecular species requires the concerted action of a number of collision cascades. Atomic primary particles focus the energy deposition in a very small area but quite deep into the solid. Polyatomic primary ions, on the other side, break apart upon collision with the surface, this way creating numerous weaker impacts over a wider range [115]. The concerted action of a number of soft impacts can effect the desorption of the molecule [97]. Molecular dynamics simulations suggest that an acoustic wave is generated that essentially pushes the secondary ions off the surface. Especially fullerene ion sources ($C_{60}^{+\bullet}$ primary ions [97]) lead to energy deposition in the uppermost sample layers.

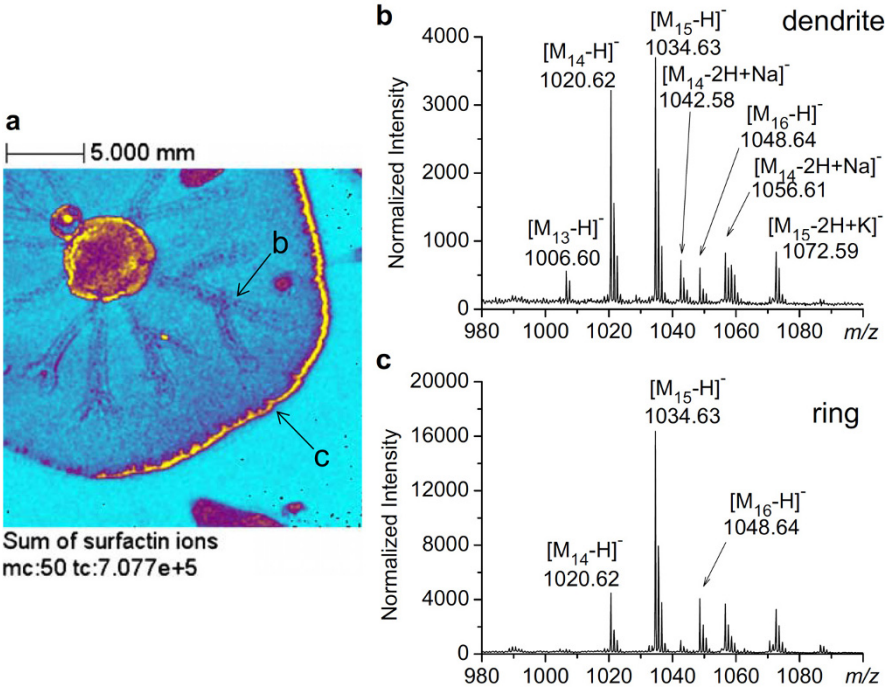


Fig. 15.17. (**a**) TOF-SIMS image of the sum of surfactin ions at the surface of a *Bacillus subtilis* swarming community. The maximal number of counts in a pixel (mc) and the total number of counts (tc) are indicated below the image. Field of view 23 × 23 mm^2, 256 × 256 pixels, pixel size 90 μm, Bi_3^+ primary ion fluence 1×10^9 ions cm^{-2}. (**b**) Partial mass spectrum obtained from a region of interest drawn around a dendrite. (**c**) Partial mass spectrum obtained from a region of interest drawn around the ring. M_n refers to compounds possessing an alkyl chain being n carbon atoms long. Adapted from Ref. [118] with permission. © Springer-Verlag 2009.

Example: Even with the advent of cluster ion sources, TOF-SIMS imaging favors hydrophobic molecules. Surfactins are a family of heptacyclodepsipeptides where the C-terminal carbonyl is linked with the β-hydroxy group of a fatty acid that is acylating the N-terminal function of a glutamic acid residue. The fatty acyl chain is 12–16 carbon atoms long. These compounds are secreted by the Gram-positive bacterium *Bacillus subtilis* and play an important role in the formation of dendritic patterns. Mapping of these surfactins by TOF–SIMS imaging showed that they were mainly located in the central mother colony, in a 'ring' surrounding the pattern and along the edges of the dendrites (Fig. 15.17). Surfactins with shorter chain lengths are found in the interior of the dendrites, whereas surfactins with longer fatty acyl chain lengths were found in the ring surrounding the swarm community [118].

Note: Mass spectral imaging creates sort of a "chemical map" filled with enormous amounts of data. A standard image of 256×256 pixels requires 65,536 mass spectra each possessing about 10^5 data points. Therefore, effective software tools for data evaluation, representation, and eventually compression for long-term storage are necessary to deal with those gigabytes of data.

The future for SIMS seems bright and promising. From a seemingly disappearing technology at the very beginning of this millennium [24], it has stood up to deliver impressing results such as the imaging of bones, tissues, and even single cells [22,24,113,115,119,120]. Advanced sample preparation techniques such as cryofreezing of tissues open up the new capabilities of holding these samples under low vacuum conditions for the time span of the experiment. Recently, MALDI and SIMS imaging are seen as complementary techniques to assess complex biological systems [23]. While MALDI can deliver imformation on peptides, proteins, oligosaccharides, and other high-mass constituents, TOF-SIMS is the tool of choice for the analysis of lipids, unaltered surfaces, and extremely fine structures [23,25,95,116,118]. The imaging community is now also using common instrumentation such as a SIMS/ESI/MALDI quadrupole-TOF instrument [121].

15.6 Accelerator Mass Spectrometry

The methodology of *accelerator mass spectrometry* (AMS) clearly differs from all other approaches to analyzing of atomic mass so far referred to in this book. While ions to be analyzed by a quadrupole analyzer are injected at kinetic energies of about 10 eV, those for a sector instrument at 5–10 keV, and those for TOFs at 15–30 keV, in AMS ions have several MeV. Another unique and key feature of the technique is that the ions experience dramatic changes in kinetic energy and charge state during the experiment.

AMS is an extremely sensitive technique for isotopic analysis, in particular for measuring isotope ratios over an extreme dynamic range. For some elements such as carbon, isotope ratios of as low as 1 in 10^{15} can be determined. This is by a fac-

tor of 10^5 lower than by any other MS technique [4]. Moreover, about 1 mg of sample is sufficient for AMS, which is equivalent to a content of only about 10^6 atoms of the isotope of interest. Thus, AMS is ideally suited for isotope ratio measurements of low-abundant isotopes, especially those having too long half-lives for determining radioactive decay from small sample amounts such as carbon-14. In fact, carbon-14 dating led to AMS [122,123] and is still applied in various ways [13,124,125]. AMS is nowadays also employed for determination of isotopes such as ^{10}B, ^{26}Al, ^{36}Cl, ^{41}Ca, ^{129}I and others including stable isotopes. The versatility of AMS has led to impressing applications in the life sciences, geosciences, archeology, and extraterrestrial research [14,18,125-128].

In order to achieve such extraordinary performance features, the accelerator mass spectrometer consists of several stages. First, negative secondary ions of the sample are created by Cs^+ ion bombardment (Fig. 15.18). The first step of mass analysis is conducted in a more-or-less conventional double-focusing magnetic sector unit. Mass-selected ions are then passed into a linear *Van de Graaff accelerator* or a *tandem accelerator*. These devices are frequent in nuclear physics. In a tandem accelerator, negative ions are attracted by high positive voltage towards the high voltage terminal in the center of the vessel where they are passed through a so-called (charge) *stripper*. Two types of charge stripping devices are in use: *i*) foil strippers, where the beam is shot through a thin carbon foil, and *ii*) gas strippers, essentially gas collision cells. Both serve to strip off all electrons from the anion, thereby converting it into a multiply charged positive ion. This extreme degree of charge inversion is the main purpose of the high collision energy – a very welcome side effect being the highly effective ion counting in the detector. The atomic cations are then pushed away from the high voltage terminal towards the exit of the accelerator on its opposite side. Due to their individual charge states the multiply charged positive ions gather different amounts of kinetic energy on the second stage of acceleration. They are then separated according to their momentum, charge, and energy, and finally counted individually. This second unit also represents a sort of large magnetic sector instrument. In particular, due to the accelerator, the classical AMS facility requires an area of some hundred square meters for instrumentation (Fig. 15.19). In recent years, the increasing demand for AMS measurements has led to the design of significantly smaller AMS instruments for dedicated purposes; this “miniaturization” has much been driven by Suter in Zurich [129-131]. The concise review by Hellborg and Skog is recommended for further readings [125].

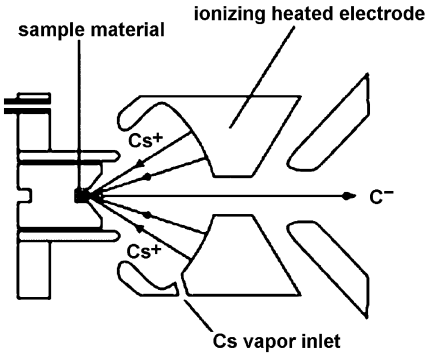


Fig. 15.18. High-intensity Cs sputter source for AMS. Cs^+ ions are created by thermal ionization of Cs vapor on a large heated tantalum anode that is placed over the sample like a dome. Secondary (analyte) ions exit through an axial aperture. Having the sample at negative high voltage accelerates the Cs^+ ions away from the anode to bombard the sample and also forces the analyte anions out of the source. Reproduced from Ref. [125] with permission. © Wiley Periodicals Inc., 2008.

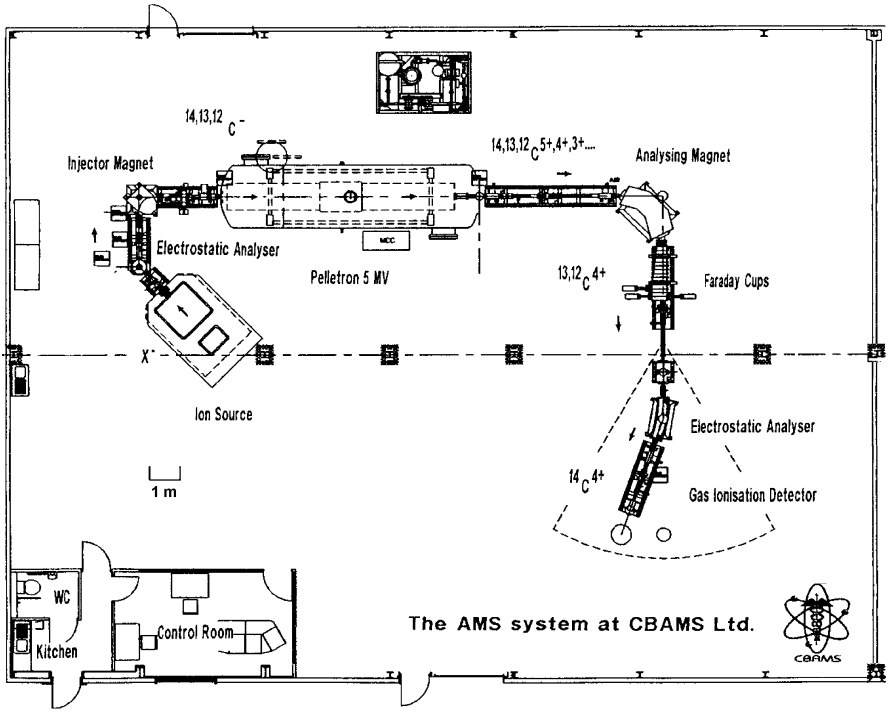


Fig. 15.19. AMS facility of CBAMS. The instrument is typical for its kind. Note the scale bar for 1 m. CBAMS, founded in 1997, is the first private company in the world to offer a fully commercial analytical service using an accelerator mass spectrometer. Reproduced from Ref. [13] with permission. © John Wiley & Sons, Ltd., 1999.

The great advantage of these MeV-energies is that they are able to help avoiding ambiguities in identification of atomic ions, because eventually interfering molecular species are completely destroyed at the stage of the charge stripper. Furthermore, selection of a suitable high charge state characteristic of the isotope to be analyzed allows to unequivocally identify the species. For example, the nuclei of ^{14}C, ^{26}Al, and ^{129}I are free of superimpositions from isobaric ^{14}N, ^{26}Mg, and ^{129}Xe, because the negative ions of the latter are unstable.

Example: To illustrate the capabilities of AMS, we compare carbon-14 determination by radioactive counting to AMS. A sample of 1 g of environmental carbon contains 6×10^{10} atoms of ^{14}C (and 1.2×10^{12} times more ^{12}C atoms). Due to the 5730 years half-life of ^{14}C, only 13 atoms will decay per minute. For a statistical precision of 0.5% as normally required in radiocarbon dating, decays from 1 g of carbon need to be counted for more than 48 h. AMS does not have to wait for the decays, it is more efficient because it uses the whole sample. A sample of 1 mg carbon, only one thousandth of the material needed for decay counting, is completely sputtered in the ion source within 1–2 h and delivers about 6×10^5 atoms, which is 1% of the total ^{14}C content, to the AMS detector system. Conventional mass spectrometers can not be used here, because the ^{14}C ions are superimposed by atomic and molecular isobars that are by orders of magnitude more abundant. These are $^{14}N^+$ and small fragments such as $^{13}CH^+$, $^{12}CH_2^{+\bullet}$, $^{12}CD^+$, and $^{7}Li_2^+$. Abundance sensitivity also plays a role by limiting the ^{14}C detection due to minor overlap with stretching peak bases from ^{12}C and ^{13}C. Conventional MS is therefore limited to isotope ratios of $^{14}C/^{12}C$ of approximately 10^{-7} at best. AMS achieves $^{14}C/^{12}C$ detection down to approximately 10^{-15}.

15.7 Conclusion

Mass spectrometry is no longer just organic, inorganic, physicochemical, biomedical, or environmental. On the contrary, mass spectrometry comprises a large number of facets and applications. The success of LA-ICP-MS, TOF-SIMS with polyatomic primary ion beams, and AMS in both the biomedical and the geological field marvelously exemplifies how a certain methodology can bridge the gap between extremes. The exploration of increasingly complex systems from cells and tissues to soils, ocean waters, and the atmosphere demands for the joint use of all techniques that enable crossing of interdisciplinary boundaries.

While working as a mass spectrometrist is necessarily correlated to a certain field of personal expertise, one should also be aware – at least to the degree of a good educational background in mass spectrometry – of the entire spectrum of this impressingly versatile method – mass spectrometry, a domain of science in itself.

References

1. de Laeter, J.R.; Kurz, M.D. Alfred Nier and the Sector Field Mass Spectrometer. *J. Mass Spectrom.* **2006,** *41*, 847-854.
2. Budzikiewicz, H.; Grigsby, R.D. Mass Spectrometry and Isotopes: A Century of Research and Discussion. *Mass Spectrom. Rev.* **2006,** *25*, 146-157.
3. Platzner, I.T.; Habfast, K.; Walder, A.J.; Goetz, A. *Modern Isotope Ratio Mass Spectrometry;* Platzner, I.T. (ed.); Wiley: Chichester, 1997.
4. Tuniz, C.; Bird, J.R.; Fink, D.; Herzog, G.F. *Accelerator Mass Spectrometry – Ultrasensitive Analysis for Global Science;* CRC Press: Boca Raton, 1998.
5. Taylor, H.E. *Inductively Coupled Plasma Mass Spectroscopy;* Academic Press: London, 2000.
6. de Laeter, J.R. *Applications of Inorganic Mass Spectrometry;* Wiley: New York, 2001.
7. Becker, J.S. *Inorganic Mass Spectrometry: Principles and Applications;* Wiley: Chichester, 2008.
8. Douthitt, C.B. Commercial Development of HR-ICPMS, MC-ICPMS and HR-GDMS. *J. Anal. Atom. Spectrom.* **2008,** *23*, 685-689.
9. Hieftje, G.M. Emergence and Impact of Alternative Sources and Mass Analyzers in Plasma Source MS. *J. Anal. Atom. Spectrom.* **2008,** *23*, 661-672.
10. de Laeter, J.R.; De Bièvre, P.; Peiser, H.S. Isotope Mass Spectrometry in Metrology. *Mass Spectrom. Rev.* **1992,** *11*, 193-245.
11. Ma, R.; Staton, I.; McLeod, C.W.; Gomez, M.B.; Gomez, M.M.; Palacios, M.A. Assessment of Airborne Platinum Contamination via ICP-Mass Spectrometric Analysis of Tree Bark. *J. Anal. Atom. Spectrom.* **2001,** *16*, 1070-1075.
12. Stuewer, D.; Jakubowski, N. Elemental Analysis by Inductively Coupled Plasma Mass Spectrometry with Sector Field Instruments: a Progress Report. *J. Mass Spectrom.* **1998,** *33*, 579-590.
13. Barker, J.; Garner, R.C. Biomedical Applications of Accelerator Mass Spectrometry-Isotope Measurements at the Level of the Atom. *Rapid Commun. Mass Spectrom.* **1999,** *13*, 285-293.
14. Kutschera, W. Progress in Isotope Analysis at Ultra-Trace Level by AMS. *Int. J. Mass Spectrom.* **2005,** *242*, 145-160.
15. Becker, J.S.; Zoriy, M.; Becker, J.S.; Pickhardt, C.; Przybylski, M. Determination of Phosphorus and Metals in Human Brain Proteins After Isolation by Gel Electrophoresis by Laser Ablation Inductively Coupled Plasma Source Mass Spectrometry. *J. Anal. Atom. Spectrom.* **2004,** *19*, 149-152.
16. Guenther, D.; Hattendorf, B. Solid Sample Analysis Using Laser Ablation Inductively Coupled Plasma Mass Spectrometry. *Trends Anal. Chem.* **2005,** *24*, 255-265.
17. Becker, J.S.; Zoriy, M.; Becker, J.S.; Dobrowolska, J.; Matusch, A. LA-ICP-MS in Elemental Imaging of Biological Tissues and in Proteomics. *J. Anal. Atom. Spectrom.* **2007,** *22*, 736-744.
18. Cheah, E.L.C.; Koh, H.L. Biomedical Applications of Accelerator Mass Spectrometry. *Current Anal. Chem.* **2008,** *4*, 102-110.
19. Houk, R.S.; Fassel, V.A.; Flesch, G.D.; Svec, H.J.; Gray, A.L.; Taylor, C.E. Inductively Coupled Argon Plasma As an Ion Source for Mass Spectrometric Determination of Trace Elements. *Anal. Chem.* **1980,** *52*, 2283-2289.
20. Szpunar, J. Metallomics: A New Frontier in Analytical Chemistry. *Anal. Bioanal. Chem.* **2004,** *378*, 54-56.
21. Lobinski, R.; Schaumlöffel, D.; Szpunar, J. Mass Spectrometry in Bioinorganic Analytical Chemistry. *Mass Spectrom. Rev.* **2006,** *25*, 255-289.
22. Walker, A.V. Why Is SIMS Underused in Chemical and Biological Analysis? Challenges and Opportunities. *Anal. Chem.* **2008,** *80*, 8865-8870.
23. Cassiday, L. SIMS and MALDI: Better Together. *Anal. Chem.* **2008,** *80*, 8860.
24. Griffiths, J. Secondary Ion MS. *Anal. Chem.* **2008,** *80*, 7194-7197.
25. McDonnell, L.A.; Heeren, R.M.A. Imaging Mass Spectrometry. *Mass Spectrom. Rev.* **2007,** *26*, 606-643.
26. Encinar, J.R.; Ouerdane, L.; Buchmann, W.; Tortajada, J.; Lobinski, R.; Szpunar,

J. Identification of Water-Soluble Selenium-Containing Proteins in Selenized Yeast by Size-Exclusion-Reversed-Phase HPLC-ICP-MS Followed by MALDI-TOF and ESI-Q-TOF-MS. *Anal. Chem.* **2003,** *75*, 3765-3774.

27. Adams, F.; Vertes, A. Inorganic Mass Spectrometry of Solid Samples. *Fresenius J. Anal. Chem.* **1990,** *337*, 638-647.
28. Tanner, S.D.; Baranov, V.I.; Bandura, D.R. Reaction Cells and Collision Cells for ICP-MS: a Tutorial. *Spectrochim. Acta, Part B* **2002,** *57B*, 1361-1452.
29. Koppenaal, D.W.; Eiden, G.C.; Barinaga, C.J. Collision and Reaction Cells in Atomic MS: Development, Status, and Applications. *J. Anal. Atom. Spectrom.* **2004,** *19*, 561-570.
30. Becker, J.S.; Dietze, H.J. Inorganic Mass Spectrometric Methods for Trace, Ultratrace, Isotope, and Surface Analysis. *Int. J. Mass Spectrom.* **2000,** *197*, 1-35.
31. Richter, S.; Goldberg, S.A. Improved Techniques for High Accuracy Isotope Ratio Measurements of Nuclear Materials Using Thermal Ionization Mass Spectrometry. *Int. J. Mass Spectrom.* **2003,** *229*, 181-197.
32. Halas, S.; Durakiewicz, T. Filament Temperature Stabilizer for a Thermal Ionization Mass Spectrometer. *Int. J. Mass Spectrom.* **1998,** *181*, 167-171.
33. Kawano, H.; Page, F.M. Experimental Methods and Techniques for Negative-Ion Production by Surface Ionization. Part I. Fundamental Aspects of Surface Ionization. *Int. J. Mass Spectrom. Ion Phys.* **1983,** *50*, 1-33.
34. Kawano, H.; Hidaka, Y.; Page, F.M. Experimental Methods and Techniques for Negative-Ion Production by Surface Ionization. Part II. Instrumentation and Operation. *Int. J. Mass Spectrom. Ion Phys.* **1983,** *50*, 35-75.
35. Heumann, K.G.; Schindlmeier, W.; Zeininger, H.; Schmidt, M. Application of an Economical and Small Thermal Ionization Mass Spectrometer for Accurate Anion Trace Analyses. *Fresenius' Zeitschrift für Analytische Chemie* **1985,** *320*, 457-462.
36. Heumann, K.G.; Kastenmayer, P.; Zeininger, H. Lead and Thallium Trace Determination in the Ppm and Ppb Range in Biological Material by Mass Spectrometric Isotope Dilution Analysis. *Fresenius' Zeitschrift für Analytische Chemie* **1981,** *306*, 173-177.
37. Waidmann, E.; Emons, H.; Duerbeck, H.W. Trace Determination of Tl, Cu, Pb, Cd, and Zn in Specimens of the Limnic Environment Using Isotope Dilution Mass Spectrometry with Thermal Ionization. *Fresenius J. Anal. Chem.* **1994,** *350*, 293-297.
38. Schade, U.; Stoll, R.; Röllgen, F.W. Thermal Surface Ionization Mass Spectrometry of Organic Salts. *Int. J. Mass Spectrom. Ion Phys.* **1983,** *46*, 337-340.
39. Moens, L. Applications of Mass Spectrometry in the Trace Element Analysis of Biological Materials. *Fresenius J. Anal. Chem.* **1997,** *359*, 309-316.
40. Koppenaal, D.W. Atomic Mass Spectrometry. *Anal. Chem.* **1990,** *62*, 303R-324R.
41. Verlinden, J.; Gijbels, R.; Adams, F. Application of Spark-Source Mass Spectrometry in the Analysis of Semiconductor Materials. A Review. *J. Anal. Atom. Spectrom.* **1986,** *1*, 411-419.
42. Jochum, K.P. Elemental Analysis by Spark Source Mass Spectrometry, in *Modern Analytical Geochemistry*, Gill, R. (ed.); Addison Wesley Longman: Harlow, 1997; Chap. 11, pp. 188-199.
43. Jochum, K.P.; Stoll, B.; Pfänder, J.A.; Seufert, M.; Flanz, M.; Maissenbacher, P.; Hofmann, M.; Hofmann, A.W. Progress in Multi-Ion Counting Spark-Source Mass Spectrometry (MIC-SSMS) for the Analysis of Geological Samples. *Fresenius J. Anal. Chem.* **2001,** *370*, 647-653.
44. Saprykin, A.I.; Becker, J.S.; Dietze, H.J. Investigation of the Analytical Performance of Gliding Spark Source Mass Spectrometry for the Trace Analysis of Nonconducting Materials. *Fresenius J. Anal. Chem.* **1999,** *364*, 763-767.
45. Hoffmann, V.; Kasik, M.; Robinson, P.K.; Venzago, C. Glow Discharge Mass Spectrometry. *Anal. Bioanal. Chem.* **2005,** *381*, 173-188.
46. Wiedemann, B.; Alt, H.C.; Meyer, J.D.; Michelmann, R.W.; Bethge, K. Spark Source Mass Spectrometric Calibration of the Local Vibrational Mode Absorption of Carbon in Gallium Arsenide on Arsenic Sublattice Sites. *Fresenius J. Anal. Chem.* **1999,** *364*, 768-771.
47. Gijbels, R.; Bogaerts, A. Recent Trends in Solid Mass Spectrometry. GDMS and

Other Methods. *Fresenius J. Anal. Chem.* **1997,** *359*, 326-330.
48. Stuewer, D. Glow Discharge Mass Spectrometry – A Versatile Tool for Elemental Analysis. *Fresenius J. Anal. Chem.* **1990,** *337*, 737-742.
49. Marcus, R.K.; King, F.L., Jr.; Harrison, W.W. Hollow Cathode Plume as an Atomization/Ionization Source for Solids Mass Spectrometry. *Anal. Chem.* **1986,** *58*, 972-974.
50. Harrison, W.W.; Hess, K.R.; Marcus, R.K.; King, F.L. Glow Discharge Mass Spectrometry. *Anal. Chem.* **1986,** *58*, 341A-342A, 344A, 346A, 348A, 350A, 352A.
51. Duckworth, D.C.; Marcus, R.K. Radio Frequency Powered Glow Discharge Atomization/Ionization Source for Solids Mass Spectrometry. *Anal. Chem.* **1989,** *61*, 1879-1886.
52. Marcus, R.K. Radiofrequency Powered Glow Discharges for Emission and MS: Operating Characteristics, Figures of Merit and Future Prospects. *J. Anal. Atom. Spectrom.* **1994,** *9*, 1029-1037.
53. Marcus, R.K. Radiofrequency Powered Glow Discharges: Opportunities and Challenges. Plenary Lecture. *J. Anal. Atom. Spectrom.* **1996,** *11*, 821-828.
54. Harrison, W.W.; Klingler, J.A.; Ratliff, P.H.; Mei, Y.; Barshick, C.M. Glow Discharge Techniques in Analytical Chemistry. *Anal. Chem.* **1990,** *62*, 943A-949A.
55. King, F.L.; Harrison, W.W. Glow Discharge Mass Spectrometry: An Introduction to the Technique and its Utility. *Mass Spectrom. Rev.* **1990,** *9*, 285-317.
56. Bogaerts, A.; Gijbels, R. New Developments and Applications in GDMS. *Fresenius J. Anal. Chem.* **1999,** *364*, 367-375.
57. Nelis, T.; Pallosi, J. Glow Discharge as a Tool for Surface and Interface Analysis. *Appl. Spectrosc. Rev.* **2006,** *41*, 227-258.
58. Jakubowski, N.; Dorka, R.; Steers, E.; Tempez, A. Trends in Glow Discharge Spectroscopy. *J. Anal. Atom. Spectrom.* **2007,** *22*, 722-735.
59. Penning, F.M. Ionization by Metastable Atoms. *Naturwissenschaften* **1927,** *15*, 818.
60. Bogaerts, A. The Glow Discharge: an Exciting Plasma! *J. Anal. Atom. Spectrom.* **1999,** *14*, 1375-1384.
61. Xing, Y.; Xiaojia, L.; Haizhou, W. Determination of Trace Elements and Correction of Mass Spectral Interferences in Superalloy Analyzed by Glow Discharge Mass Spectrometry. *Eur. J. Mass Spectrom.* **2008,** *14*, 211-218.
62. Winchester, M.R.; Payling, R. Radio-Frequency Glow Discharge Spectrometry: A Critical Review. *Spectrochimica Acta, Part B: Atomic Spectroscopy* **2004,** *59B*, 607-666.
63. Majidi, V.; Moser, M.; Lewis, C.; Hang, W.; King, F.L. Explicit Chemical Speciation by Microsecond Pulsed Glow Discharge TOF-MS: Concurrent Acquisition of Structur-al, Molecular and Elemental Information. *J. Anal. Atom. Spectrom.* **2000,** *15*, 19-25.
64. Lewis, C.L.; Moser, M.A.; Dale, D.E., Jr.; Hang, W.; Hassell, C.; King, F.L.; Majidi, V. Time-Gated Pulsed Glow Discharge: Real-Time Chemical Speciation at the Elemental, Structural, and Molecular Level for Gas Chromatography Time-of-Flight Mass Spectrometry. *Anal. Chem.* **2003,** *75*, 1983-1996.
65. Fliegel, D.; Fuhrer, K.; Gonin, M.; Guenther, D. Evaluation of a Pulsed Glow Discharge Time-of-Flight Mass Spectrometer as a Detector for Gas Chromatography and the Influence of the Glow Discharge Source Parameters on the Information Volume in Chemical Speciation Analysis. *Anal. Bioanal. Chem.* **2006,** *386*, 169-179.
66. Bandura, D.R.; Baranov, V.I.; Tanner, S.D. Reaction Chemistry and Collisional Processes in Multipole Devices for Resolving Isobaric Interferences in ICP-MS. *Fresenius J. Anal. Chem.* **2001,** *370*, 454-470.
67. Wilbur, S. A Pragmatic Approach to Managing Interferences in ICP-MS. *Spectroscopy* **2008,** *23*, 18-23.
68. Walsh, J.N. Inductively Coupled Plasma-Atomic Emission Spectrometry (ICP-AES), in *Modern Analytical Geochemistry*, Gill, R. (ed.); Addison Wesley Longman: Harlow, 1997; pp. 41-86.
69. Becker, J.S.; Dietze, H.J. Application of Double-Focusing Sector Field ICP Mass Spectrometry with Shielded Torch Using Different Nebulizers for Ultratrace and Precise Isotope Analysis of Long-Lived Radionuclides. *J. Anal. Atom. Spectrom.* **1999,** *14*, 1493-1500.

70. Myers, D.P.; Hieftje, G.M. Preliminary Design Considerations and Characteristics of an Inductively Coupled Plasma-Time-of-Flight Mass Spectrometer. *Microchem. Journ.* **1993,** *48*, 259-277.
71. Myers, D.P.; Li, G.; Yang, P.; Hieftje, G.M. An Inductively Coupled Plasma-Time-of-Flight Mass Spectrometer for Elemental Analysis. Part I: Optimization and Characteristics. *J. Am. Soc. Mass Spectrom.* **1994,** *5*, 1008-1016.
72. Myers, D.P.; Mahoney, P.P.; Li, G.; Hieftje, G.M. Isotope Ratios and Abundance Sensitivity Obtained with an Inductively Coupled Plasma-Time-of-Flight Mass Spectrometer. *J. Am. Soc. Mass Spectrom.* **1995,** *6*, 920-927.
73. Hieftje, G.M.; Myers, D.P.; Li, G.; Mahoney, P.P.; Burgoyne, T.W.; Ray, S.J.; Guzowski, J.P. Toward the Next Generation of Atomic Mass Spectrometers. *J. Anal. Atom. Spectrom.* **1997,** *12*, 287-292.
74. Westphal, C.S.; McLean, J.A.; Acon, B.W.; Allen, L.A.; Montaser, A. Axial Inductively Coupled Plasma TOF-MS Using Direct Liquid Sample Introduction. *J. Anal. Atom. Spectrom.* **2002,** *17*, 669-675.
75. Tanner, M.; Guenther, D. A New ICP-TOFMS. Measurement and Readout of Mass Spectra with 30 Ms Time Resolution, Applied to in-Torch LA-ICP-MS. *Anal. Bioanal. Chem.* **2008,** *391*, 1211-1220.
76. Milgram, K.E.; White, F.M.; Goodner, K.L.; Watson, C.H.; Koppenaal, D.W.; Barinaga, C.J.; Smith, B.H.; Winefordner, J.D.; Marshall, A.G.; Houk, R.S.; Eyler, J.R. High-Resolution Inductively Coupled Plasma Fourier Transform Ion Cyclotron Resonance Mass Spectrometry. *Anal. Chem.* **1997,** *69*, 3714-3721.
77. Becker, J.S.; Dietze, H.J. Ultratrace and Precise Isotope Analysis by Double-Focusing Sector Field Inductively Coupled Plasma Mass Spectrometry. *J. Anal. Atom. Spectrom.* **1998,** *13*, 1057-1063.
78. Mahoney, P.P.; Li, G.; Hieftje, G.M. Laser Ablation-Inductively Coupled Plasma Mass Spectrometry with a Time-of-Flight Mass Analyzer. *J. Anal. Atom. Spectrom.* **1996,** *11*, 401-405.
79. Pisonero, J.; Kroslakova, I.; Guenther, D.; Latkoczy, C. Laser Ablation Inductively Coupled Plasma Mass Spectrometry for Direct Analysis of the Spatial Distribution of Trace Elements in Metallurgical-Grade Silicon. *Anal. Bioanal. Chem.* **2006,** *386*, 12-20.
80. Neilsen, J.L.; Abildtrup, A.; Christensen, J.; Watson, P.; Cox, A.; McLeod, C.W. Laser Ablation Inductively Coupled Plasma-Mass Spectrometry in Combination with Gel Electrophoresis: A New Strategy for Speciation of Metal Binding Serum Proteins. *Spectrochim. Acta, Part B* **1998,** *53B*, 339-345.
81. Chery, C.C.; Moens, L.; Cornelis, R.; Vanhaecke, F. Capabilities and Limitations of Gel Electrophoresis for Elemental Speciation: a Laboratory's Experience. *Pure Appl. Chem.* **2006,** *78*, 91-103.
82. Benninghoven, A. Developments in Secondary Ion Mass Spectroscopy and Applications to Surface Studies. *Surf. Sci.* **1975,** *53*, 596-625.
83. Pachuta, S.J.; Cooks, R.G. Mechanisms in Molecular SIMS. *Chem. Rev.* **1987,** *87*, 647-669.
84. Benninghoven, A.; Werner, H.W.; Rudenauer, F.G. *Secondary Ion Mass Spectrometry: Basic Concepts, Instrumental Aspects, Applications and Trends;* Benninghoven, A., (ed.); Wiley: New York, 1987.
85. Briggs, D.; Brown, A.; Vickerman, J.C. *Handbook of Static Secondary Ion Mass Spectrometry;* Wiley: Chichester, 1989.
86. Arnot, F.L.; Beckett, C. Formation of Negative Ions at Surfaces. *Nature* **1938,** *141*, 1011-1012.
87. Arnot, F.L.; Milligan, J.C. A New Process of Negative-Ion Formation. *Proc. Royal Soc. London, Series A: Mathematical, Physical and Engineering Sci.* **1936,** *156*, 538-560.
88. Herzog, R.F.K.; Viehbock, F.P. Ion Source for Mass-Spectrography. *Phys. Rev.* **1949,** *76*, 855-856.
89. Benninghoven, A. Mechanism of Ion Formation and Ion Emission During Sputtering. *Zeitschrift fuer Physik* **1969,** *220*, 159-180.
90. Benninghoven, A. Analysis of Monomolecular Surface Layers of Solids by Secondary Ion Emission. *Zeitschrift fuer Physik* **1970,** *230*, 403-417.
91. Adams, F. Analytical Atomic Spectrometry and Imaging: Looking Backward from 2020 to 1975. *Spectrochimica Acta, Part B: Atomic Spectroscopy* **2008,** *63B*, 738-745.

92. Benninghoven, A.; Sichtermann, W.K. Detection, Identification and Structural Investigation of Biologically Important Compounds by Secondary Ion Mass Spectrometry. *Anal. Chem.* **1978,** *50*, 1180-1184.
93. Coath, C.D.; Long, J.V.P. A High-Brightness Duoplasmatron Ion Source for Microprobe Secondary-Ion Mass Spectrometry. *Rev. Scientific Instr.* **1995,** *66*, 1018-1023.
94. Konarski, P.; Kalczuk, M.; Koscinski, J. Bakeable Duoplasmatron Ion Gun for SIMS Microanalysis. *Rev. Scientific Instr.* **1992,** *63*, 2397-2399.
95. Pacholski, M.L.; Winograd, N. Imaging with Mass Spectrometry. *Chem. Rev.* **1999,** *99*, 2977-3005.
96. Shimizu, N. Principles of SIMS and Modern Ion Microprobes, in *Modern Analytical Geochemistry*, Gill, R. (ed.); Addison Wesley Longman: Harlow, 1997; Chap. 15, pp. 235-242.
97. Weibel, D.; Wong, S.; Lockyer, N.; Blenkinsopp, P.; Hill, R.; Vickerman, J.C. A C_{60} Primary Ion Beam System for Time of Flight Secondary Ion Mass Spectrometry: Its Development and Secondary Ion Yield Characteristics. *Anal. Chem.* **2003,** *75*, 1754-1764.
98. Chait, B.T.; Standing, K.G. A Time-of-Flight Mass Spectrometer for Measurement of Secondary Ion Mass Spectra. *Int. J. Mass Spectrom. Ion Phys.* **1981,** *40*, 185-193.
99. Standing, K.G.; Chait, B.T.; Ens, W.; McIntosh, G.; Beavis, R. Time-of-Flight Measurements of Secondary Organic Ions Produced by 1 keV to 16 keV Primary Ions. *Nucl. Instr. & Meth. Phys. Res.* **1982,** *198*, 33-38.
100. Jabs, H.U.; Assmann, G.; Greifendorf, D.; Benninghoven, A. High Performance Liquid Chromatography and Time-of-Flight Secondary Ion Mass Spectrometry: A New Dimension in Structural Analysis of Apolipoproteins. *J. Lipid Res.* **1986,** *27*, 613-621.
101. Ens, W.; Standing, K.G.; Chait, B.T.; Field, F.H. Comparison of Mass Spectra Obtained with Low-Energy Ion and High-Energy ^{252}Californium Fission Fragment Bombardment. *Anal. Chem.* **1981,** *53*, 1241-1244.
102. Lafortune, F.; Beavis, R.; Tang, X.; Standing, K.G.; Chait, B.T. Narrowing the Gap Between keV and Fission Fragment Secondary Ion Yields with Nitrocellulose. *Rapid Commun. Mass Spectrom.* **1987,** *1*, 114-116.
103. Ens, W.; Main, D.E.; Standing, K.G.; Chait, B.T. Comparison of Relative Quasi-Molecular Ion Yields for 8-KeV Ion and ^{252}Cf Fission Fragment Bombardment. *Anal. Chem.* **1988,** *60*, 1494-1498.
104. Olthoff, J.K.; Honovich, J.P.; Cotter, R.J. Liquid Secondary Ion TTOF-MS. *Anal. Chem.* **1987,** *59*, 999-1002.
105. Linton, R.W.; Mawn, M.P.; Belu, A.M.; DeSimone, J.M.; Hunt, M.O., Jr.; Menceloglu, Y.Z.; Cramer, H.G.; Benninghoven, A. Time-of-Flight Secondary Ion Mass Spectrometric Analysis of Polymer Surfaces and Additives. *Surf. Interface Anal.* **1993,** *20*, 991-999.
106. Galuska, A.A. ToF-SIMS Determination of Molecular Weights from Polymeric Surfaces and Microscopic Phases. *Surf. Interface Anal.* **1997,** *25*, 790-798.
107. Bullett, N.A.; Short, R.D.; O'Leary, T.; Beck, A.J.; Douglas, C.W.I.; Cambray-Deakin, M.; Fletcher, I.W.; Roberts, A.; Blomfield, C. Direct Imaging of Plasma-Polymerized Chemical Micropatterns. *Surf. Interface Anal.* **2001,** *31*, 1074-1076.
108. Liu, S.; Weng, L.T.; Chan, C.M.; Li, L.; Ho, N.K.; Jiang, M. Quantitative Surface Characterization of Poly(Styrene)/Poly-(4-Vinyl Phenol) Random and Block Copolymers by ToF-SIMS and XPS. *Surf. Interface Anal.* **2001,** *31*, 745-753.
109. Médard, N.; Poleunis, C.; Vanden Eynde, X.; Bertrand, P. Characterization of Additives at Polymer Surfaces by TOF-SIMS. *Surf. Interface Anal.* **2002,** *34*, 565-569.
110. Davies, N.; Weibel, D.E.; Blenkinsopp, P.; Lockyer, N.; Hill, R.; Vickerman, J.C. Development and Experimental Application of a Gold Liquid Metal Ion Source. *Appl. Surface Sci.* **2003,** *203-204*, 223-227.
111. Nagy, G.; Walker, A.V. Enhanced Secondary Ion Emission with a Bismuth Cluster Ion Source. *Int. J. Mass Spectrom.* **2007,** *262*, 144-153.
112. Touboul, D.; Kollmer, F.; Niehuis, E.; Brunelle, A.; Laprevote, O. Improvement of Biological Time-of-Flight-SIMS Imaging with a Bismuth Cluster Ion Source. *J. Am. Soc. Mass Spectrom.* **2005,** *16*, 1608-1618.

113. Malmberg, P.; Nygren, H. Methods for the Analysis of the Composition of Bone Tissue, with a Focus on Imaging Mass Spectrometry (TOF-SIMS). *Proteomics* **2008,** *8*, 3755-3762.
114. Wong, S.C.C.; Hill, R.; Blenkinsopp, P.; Lockyer, N.P.; Weibel, D.E.; Vickerman, J.C. Development of a C_{60}^+ Ion Gun for Static SIMS and Chemical Imaging. *Appl. Surface Sci.* **2003,** *203-204*, 219-222.
115. Fletcher, J.S.; Lockyer, N.P.; Vickerman, J.C. C_{60}, Buckminsterfullerene: Its Impact on Biological ToF-SIMS Analysis. *Surf. Interface Anal.* **2006,** *38*, 1393-1400.
116. Mas, S.; Perez, R.; Martinez-Pinna, R.; Egido, J.; Vivanco, F. Cluster TOF-SIMS Imaging: A New Light for in Situ Metabolomics? *Proteomics* **2008,** *8*, 3735-3745.
117. Briggs, D.; Hearn, M.J. Analysis of Polymer Surfaces by SIMS. Part 5. The Effects of Primary Ion Mass and Energy on Secondary Ion Relative Intensities. *Int. J. Mass Spectrom. Ion Proc.* **1985,** *67*, 47-56.
118. Brunelle, A.; Laprevote, O. Lipid Imaging with Cluster Time-of-Flight Secondary Ion Mass Spectrometry. *Anal. Bioanal. Chem.* **2009,** *393*, 31-35.
119. Herrmann, A.M.; Ritz, K.; Nunan, N.; Clode, P.L.; Pett-Ridge, J.; Kilburn, M.R.; Murphy, D.V.; O'Donnell, A.G.; Stockdale, E.A. Nano-Scale Secondary Ion Mass Spectrometry – A New Analytical Tool in Biogeochemistry and Soil Ecology: A Review Article. *Soil Biol. & Biochem.* **2007,** *39*, 1835-1850.
120. Fletcher, J.S.; Rabbani, S.; Henderson, A.; Blenkinsopp, P.; Thompson, S.P.; Lockyer, N.P.; Vickerman, J.C. A New Dynamic in Mass Spectral Imaging of Single Biological Cells. *Anal. Chem.* **2008,** *80*, 9058-9064.
121. Carado, A.; Passarelli, M.K.; Kozole, J.; Wingate, J.E.; Winograd, N.; Loboda, A.V. C_{60} SIMS with a Hybrid-Quadrupole Orthogonal TOF Mass Spectrometer. *Anal. Chem.* **2008,** *80*, 7921-7929.
122. Nelson, D.E.; Korteling, R.G.; Stott, W.R. Carbon-14: Direct Detection at Natural Concentrations. *Science* **1977,** *198*, 507-508.
123. Bennett, C.L.; Beukens, R.P.; Clover, M.R.; Grove, H.E.; Liebert, R.B.; Litherland, A.E.; Purser, K.H.; Sondheim, W.E. Radiocarbon Dating Using Electrostatic Accelerators: Negative Ions Provide the Key. *Science* **1977,** *198*, 508-510.
124. Lappin, G.; Garner, R.C. Current Perspectives of ^{14}C-Isotope Measurement in Biomedical Accelerator Mass Spectrometry. *Anal. Bioanal. Chem.* **2004,** *378*, 356-364.
125. Hellborg, R.; Skog, G. Accelerator Mass Spectrometry. *Mass Spectrom. Rev.* **2008,** *27*, 398-427.
126. Brown, K.; Dingley, K.H.; Turteltaub, K.W. Accelerator Mass Spectrometry for Biomedical Research. *Methods in Enzymology* **2005,** *402*, 423-443.
127. Ikeda, T. Instruments for Radiation Measurement in Life Sciences. VI. Use of AMS in Studies on Drug Metabolism and Pharmacokinetics. *Radioisotopes* **2005,** *54*, 15-21.
128. Brown, K.; Tompkins, E.M.; White, I.N.H. Applications of Accelerator Mass Spectrometry for Pharmacological and Toxicological Research. *Mass Spectrom. Rev.* **2006,** *25*, 127-145.
129. Suter, M. 25 Years of AMS - a Review of Recent Developments. *Nucl. Instrum. Methods Phys. Res., Sect. B* **2004,** *223-224*, 139-148.
130. Stocker, M.; Doebeli, M.; Grajcar, M.; Suter, M.; Synal, H.A.; Wacker, L. A Universal and Competitive Compact AMS Facility. *Nucl. Instrum. Methods Phys. Res., Sect. B* **2005,** *240*, 483-489.
131. Wacker, L.; Fifield, L.K.; Olivier, S.; Suter, M.; Synal, H.A. Compact AMS: A Powerful Tool to Measure Actinides in the Environment. *Special Publ. Royal Society of Chemistry* **2006,** *305*, 44-46.

Appendix

A.1 Units, Physical Quantities, and Physical Constants

The *International System of Units* (SI) provides the advantage of establishing uniformity and consistency of units for physical quantities – a prerequisite for communication in science.

Table A.1. SI base units

Physical base quantity	SI unit	Symbol
Length/Distance	meter[a]	m
Mass	kilogram[b]	kg
Time	second	s
Electric current	ampere	A
Thermodynamic temperature	kelvin[c]	K
Amount of substance	mole	mol
Luminous intensity	candela	cd

[a] 1 m = 3.2808; ft = 39.3701 in; 1 in = 2.54 cm; 1 ft = 0.3048 m
[b] 1 kg = 2.2046 lb; 1 lb = 0.4536 kg
[c] T[°C] = T[K] – 273.15; T[°F] = 1.8 × T[°C] + 32

Table A.2. Derived SI units with special names

Quantity	Name	Symbol	Expression in terms of base units	Expression in terms of other SI units
Frequency	hertz	Hz	s^{-1}	
Force	newton	N	m kg s^{-2}	J m^{-1}
Pressure	pascal[a]	Pa	kg m^{-1} s^{-2}	N m^{-2}
Volume	liter	l	10^{-3} m^3	
Energy	joule[b]	J	m^2 kg s^{-2}	N m
Power	watt	W	m^2 kg s^{-3}	J s^{-1}
Electric charge	coulomb	C	A s	
Electric potential	volt	V	m^2 kg A^{-1} s^{-3}	W A^{-1}
Magnetic flux density	tesla	T	kg A^{-1} s^{-2}	

[a] 1 bar = 1000 mbar = 10^5 Pa; 1 Torr = 133 Pa; 1 psi = 6895 Pa = 68.95 mbar
[b] 1 cal = 4.1868 J; 1 eV = 1.60219 × 10^{-19} J = 96.485 kJ mol^{-1}

J. Gross, *Mass Spectrometry*, 2nd ed., DOI 10.1007/978-3-642-10711-5,
© Springer-Verlag Berlin Heidelberg 2011

Table A.3. Physical constants and frequently used quantities (from NIST)

Physical constant/quantity	Symbol	Quantity
Charge of the electron	e	$1.60217648 \times 10^{-19}$ C
Mass of the electron	m_e	$9.1093822 \times 10^{-31}$ kg
Mass of the proton	m_p	$1.67262164 \times 10^{-27}$ kg
Mass of the neutron	m_n	$1.67492721 \times 10^{-27}$ kg
Unified atomic mass	u	$1.66053878 \times 10^{-27}$ kg
Speed of light in vacuum	c	2.99792458×10^{8} m s^{-1}
Avogadro's constant	N_A	$6.02214179 \times 10^{23}$ mol^{-1}
Boltzmann constant	k_B	$1.38065042 \times 10^{-23}$ J K^{-1}

Table A.4. SI number prefixes

a	f	p	n	μ	m	c	d	k	M	G	T
atto	femto	pico	nano	micro	milli	centi	deci	kilo	mega	giga	tera
10^{-18}	10^{-15}	10^{-12}	10^{-9}	10^{-6}	10^{-3}	10^{-2}	10^{-1}	10^{3}	10^{6}	10^{9}	10^{12}

A.2 Isotopic Composition of the Elements

Table A.5 comprises the stable elements from hydrogen to bismuth with the radioactive elements technetium and promethium omitted. Natural variations in isotopic composition of some elements such as carbon or lead do not allow for more accurate values, a fact also reflected in the accuracy of their relative atomic mass. However, exact masses of the isotopes are not affected by varying abundances. The isotopic masses listed may differ up to some 10^{-6} u in other publications.

Table A.5. Isotopic mass, isotopic composition, and relative atomic mass [u] of non-radioactive elements. © IUPAC 2001.

Atomic symbol	Name	Atomic No.	Mass No.	Isotopic mass	Isotopic comp.	Relative atomic mass
H	Hydrogen	1	1	1.007825	100	1.00795
			2	2.014101	0.0115	
He	Helium	2	3	3.016029	0.000137	4.002602
			4	4.002603	100	
Li	Lithium	3	6	6.015122	8.21	6.941
			7	7.016004	100	
Be	Beryllium	4	9	9.012182	100	9.012182
B	Boron	5	10	10.012937	24.8	10.812
			11	11.009306	100	
C	Carbon	6	12	12.000000	100	12.0108
			13	13.003355	1.08	

N	Nitrogen	7	14	14.003074	100	14.00675
			15	15.000109	0.369	
O	Oxygen	8	16	15.994915	100	15.9994
			17	16.999132	0.038	
			18	17.999116	0.205	
F	Fluorine	9	19	18.998403	100	18.998403
Ne	Neon	10	20	19.992402	100	20.1798
			21	20.993847	0.30	
			22	21.991386	10.22	
Na	Sodium	11	23	22.989769	100	22.989769
Mg	Magnesium	12	24	23.985042	100	24.3051
			25	24.985837	12.66	
			26	25.982593	13.94	
Al	Aluminium	13	27	26.981538	100	26.981538
Si	Silicon	14	28	27.976927	100	28.0855
			29	28.976495	5.0778	
			30	29.973770	3.3473	
P	Phosphorus	15	31	30.973762	100	30.973762
S	Sulfur	16	32	31.972071	100	32.067
			33	32.971459	0.80	
			34	33.967867	4.52	
			36	35.967081	0.02	
Cl	Chlorine	17	35	34.968853	100	35.4528
			37	36.965903	31.96	
Ar	Argon	18	36	35.967546	0.3379	39.948
			38	37.962776	0.0635	
			40	39.962383	100	
K	Potassium	19	39	38.963706	100	39.0983
			40	39.963999	0.0125	
			41	40.961826	7.2167	
Ca	Calcium	20	40	39.962591	100	40.078
			42	41.958618	0.667	
			43	42.958769	0.139	
			44	43.955481	2.152	
			46	45.953693	0.004	
			48	47.952534	0.193	
Sc	Scandium	21	45	44.955910	100	44.955910
Ti	Titanium	22	46	45.952629	11.19	47.867
			47	46.951764	10.09	
			48	47.947947	100	
			49	48.947871	7.34	
			50	49.944792	7.03	
V	Vanadium	23	50	49.947163	0.250	50.9415
			51	50.943964	100	
Cr	Chromium	24	50	49.946050	5.187	51.9962
			52	51.940512	100	

	Cr continued		53	52.940654	11.339	
			54	53.938885	2.823	
Mn	Manganese	25	55	54.938050	100	54.938050
Fe	Iron	26	54	53.939615	6.37	55.845
			56	55.934942	100	
			57	56.935399	2.309	
			58	57.933280	0.307	
Co	Cobalt	27	59	58.933200	100	58.933200
Ni	Nickel	28	58	57.935348	100	58.6934
			60	59.930791	38.5198	
			61	60.931060	1.6744	
			62	61.928349	5.3388	
			64	63.927970	1.3596	
Cu	Copper	29	63	62.929601	100	63.546
			65	64.927794	44.57	
Zn	Zinc	30	64	63.929147	100	65.39
			66	65.926037	57.37	
			67	66.927131	8.43	
			68	67.924848	38.56	
			70	69.925325	1.27	
Ga	Gallium	31	69	68.925581	100	69.723
			71	70.924705	66.367	
Ge	Germanium	32	70	69.924250	56.44	72.61
			72	71.922076	75.91	
			73	72.923459	21.31	
			74	73.921178	100	
			76	75.921403	20.98	
As	Arsenic	33	75	74.921596	100	74.921596
Se	Selenium	34	74	73.922477	1.79	78.96
			76	75.919214	18.89	
			77	76.919915	15.38	
			78	77.917310	47.91	
			80	79.916522	100	
			82	81.916700	17.60	
Br	Bromine	35	79	78.918338	100	79.904
			81	80.916291	97.28	
Kr	Krypton	36	78	77.920387	0.61	83.80
			80	79.916378	4.00	
			82	81.913485	20.32	
			83	82.914136	20.16	
			84	83.911507	100	
			86	85.910610	30.35	
Rb	Rubidium	37	85	84.911789	100	85.4678
			87	86.909183	38.56	
Sr	Strontium	38	84	83.913425	0.68	87.62
			86	85.909262	11.94	

	Sr continued		87	86.908879	8.48	
			88	87.905614	100	
Y	Yttrium	39	89	88.905848	100	88.905848
Zr	Zirconium	40	90	89.904704	100	91.224
			91	90.905645	21.81	
			92	91.905040	33.33	
			94	93.906316	33.78	
			96	95.908276	5.44	
Nb	Niobium	41	93	92.906378	100	92.906378
Mo	Molybdenum	42	92	91.906810	61.50	95.94
			94	93.905088	38.33	
			95	94.905841	65.98	
			96	95.904679	69.13	
			97	96.906021	39.58	
			98	97.905408	100	
			100	99.907478	39.91	
Ru	Ruthenium	44	96	95.907599	17.56	101.07
			98	97.905288	5.93	
			99	98.905939	40.44	
			100	99.904229	39.94	
			101	100.905582	54.07	
			102	101.904350	100	
			104	103.905430	59.02	
Rh	Rhodium	45	103	102.905504	100	102.905504
Pd	Palladium	46	102	101.905608	3.73	106.42
			104	103.904036	40.76	
			105	104.905084	81.71	
			106	105.903484	100	
			108	107.903894	96.82	
			110	109.905151	42.88	
Ag	Silver	47	107	106.905094	100	107.8682
			109	108.904756	92.90	
Cd	Cadmium	48	106	105.906459	4.35	112.412
			108	107.904184	3.10	
			110	109.903006	43.47	
			111	110.904182	44.55	
			112	111.902757	83.99	
			113	112.904401	42.53	
			114	113.903358	100	
			116	115.904755	26.07	
In	Indium	49	113	112.904061	4.48	114.818
			115	114.903879	100	
Sn	Tin	50	112	111.904822	2.98	118.711
			114	113.902782	2.03	
			115	114.903346	1.04	
			116	115.901744	44.63	
			117	116.902954	23.57	

	Sn continued		118	117.901606	74.34	
			119	118.903309	26.37	
			120	119.902197	100	
			122	121.903440	14.21	
			124	123.905275	17.77	
Sb	Antimony	51	121	120.903818	100	121.760
			123	122.904216	74.79	
Te	Tellurium	52	120	119.904021	0.26	127.60
			122	121.903047	7.48	
			123	122.904273	2.61	
			124	123.902819	13.91	
			125	124.904425	20.75	
			126	125.903306	55.28	
			128	127.904461	93.13	
			130	129.906223	100	
I	Iodine	53	127	126.904468	100	126.904468
Xe	Xenon	54	124	123.905896	0.33	131.29
			126	125.904270	0.33	
			128	127.903530	7.14	
			129	128.904779	98.33	
			130	129.903508	15.17	
			131	130.905082	78.77	
			132	131.904154	100	
			134	133.905395	38.82	
			136	135.907221	32.99	
Cs	Caesium	55	133	132.905447	100	132.905447
Ba	Barium	56	130	129.906311	0.148	137.328
			132	131.905056	0.141	
			134	133.904503	3.371	
			135	134.905683	9.194	
			136	135.904570	10.954	
			137	136.905821	15.666	
			138	137.905241	100	
La	Lanthanum	57	138	137.907107	0.090	138.9055
			139	138.906348	100	
Ce	Cerium	58	136	135.907145	0.209	140.116
			138	137.905991	0.284	
			140	139.905434	100	
			142	141.909240	12.565	
Pr	Praseodymium	59	141	140.907648	100	140.907648
Nd	Neodymium	60	142	141.907719	100	144.24
			143	142.909810	44.9	
			144	143.910083	87.5	
			145	144.912569	30.5	
			146	145.913112	63.2	
			148	147.916889	21.0	
			150	149.920887	20.6	

Sm	Samarium	62	144	143.911995	11.48	150.36
			147	146.914893	56.04	
			148	147.914818	42.02	
			149	148.917180	51.66	
			150	149.917271	27.59	
			152	151.919728	100	
			154	153.922205	85.05	
Eu	Europium	63	151	150.919846	91.61	151.964
			153	152.921226	100	
Gd	Gadolinium	64	152	151.919788	0.81	157.25
			154	153.920862	8.78	
			155	154.922619	59.58	
			156	155.922120	82.41	
			157	156.923957	63.00	
			158	157.924101	100	
			160	159.927051	88.00	
Tb	Terbium	65	159	158.925343	100	158.925343
Dy	Dysprosium	66	156	155.924279	0.21	162.50
			158	157.924405	0.35	
			160	159.925194	8.30	
			161	160.926930	67.10	
			162	161.926795	90.53	
			163	162.928728	88.36	
			164	163.929171	100	
Ho	Holmium	67	165	164.930319	100	164.930319
Er	Erbium	68	162	161.928775	0.42	167.26
			164	163.929197	4.79	
			166	165.930290	100	
			167	166.932045	68.22	
			168	167.932368	79.69	
			170	169.935460	44.42	
Tm	Thulium	69	169	168.934211	100	168.934211
Yb	Ytterbium	70	168	167.933894	0.41	173.04
			170	169.934759	9.55	
			171	170.936322	44.86	
			172	171.936378	68.58	
			173	172.938207	50.68	
			174	173.938858	100	
			176	175.942568	40.09	
Lu	Lutetium	71	175	174.940768	100	174.967
			176	175.942682	2.66	
Hf	Hafnium	72	174	173.940040	0.46	178.49
			176	175.941402	14.99	
			177	176.943220	53.02	
			178	177.943698	77.77	
			179	178.944815	38.83	
			180	179.946549	100	
Ta	Tantalum	73	180	179.947466	0.012	180.9479

	Ta continued		181	180.947996	100	
W	Tungsten	74	180	179.946707	0.40	183.84
			182	181.948206	86.49	
			183	182.950224	46.70	
			184	183.950933	100	
			186	185.954362	93.79	
Re	Rhenium	75	185	184.952956	59.74	186.207
			187	186.955751	100	
Os	Osmium	76	184	183.952491	0.05	190.23
			186	185.953838	3.90	
			187	186.955748	4.81	
			188	187.955836	32.47	
			189	188.958145	39.60	
			190	189.958445	64.39	
			192	191.961479	100	
Ir	Iridium	77	191	190.960591	59.49	192.217
			193	192.962924	100	
Pt	Platinum	78	190	189.959931	0.041	195.078
	Pt continued		192	191.961035	2.311	
			194	193.962664	97.443	
			195	194.964774	100	
			196	195.964935	74.610	
			198	197.967876	21.172	
Au	Gold	79	197	196.966552	100	196.966552
Hg	Mercury	80	196	195.965815	0.50	200.59
			198	197.966752	33.39	
			199	198.968262	56.50	
			200	199.968309	77.36	
			201	200.970285	44.14	
			202	201.970626	100	
			204	203.973476	23.00	
Tl	Thallium	81	203	202.972329	41.892	204.3833
			205	204.974412	100	
Pb	Lead	82	204	203.973029	2.7	207.2
			206	205.974449	46.0	
			207	206.975881	42.2	
			208	207.976636	100	
Bi	Bismuth	83	209	208.980383	100	208.980383
Th	Thorium*	90	232	232.038050	100	232.038050
U	Uranium*	92	234	234.040946	0.0055	238.0289
			235	235.043923	0.73	
			238	238.050783	100	

A.3 Carbon Isotopic Patterns

Provided no other element contributing to M+1 is present, reading out the P_{M+1}/P_M ratio from a mass spectrum yields the approximate number of carbon atoms, n_C, from $n_C \approx (P_{M+1}/P_M) \times 91$. If M+1 has an intensity of 24% of that of M, for example, we can calculate the presence of $(24/100) \times 91 \approx 22$ carbons.

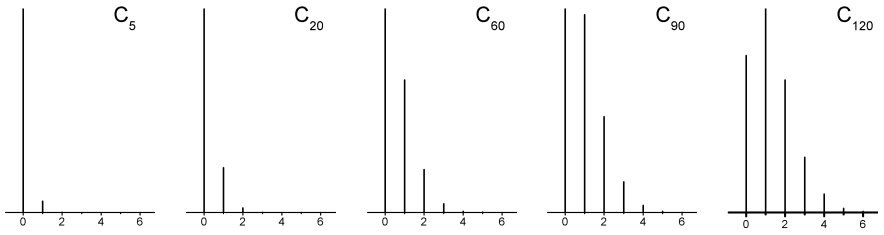


Fig. A.1. Calculated isotopic patterns for carbon. Note the steadily expanding width of the pattern as X+2, X+3, X+4,... become visible. At about C_{90} the X+1 peak reaches the same intensity as the X peak. At higher carbon number it becomes the base peak of the pattern.

Table A.6. Calculated isotopic distributions for carbon

Number of carbons	X+1	X+2	X+3	X+4	X+5
1	1.1	0.00			
2	2.2	0.01			
3	3.3	0.04			
4	4.3	0.06			
5	5.4	0.10			
6	6.5	0.16			
7	7.6	0.23			
8	8.7	0.33			
9	9.7	0.42			
10	10.8	0.5			
12	13.0	0.8			
15	16.1	1.1			
20	21.6	2.2	0.1		
25	27.0	3.5	0.2		
30	32.3	5.0	0.5		
40	43.2	9.0	1.3	0.1	
50	54.1	14.5	2.5	0.2	0.1
60	65.0	20.6	4.2	0.6	0.2
90	97.2	46.8	14.9	3.5	0.6
120[a]	100.0	64.4	27.3	8.6	2.2

[a] The X peak has an intensity of 77.0% in that case

A.4 Chlorine and Bromine Isotopic Patterns

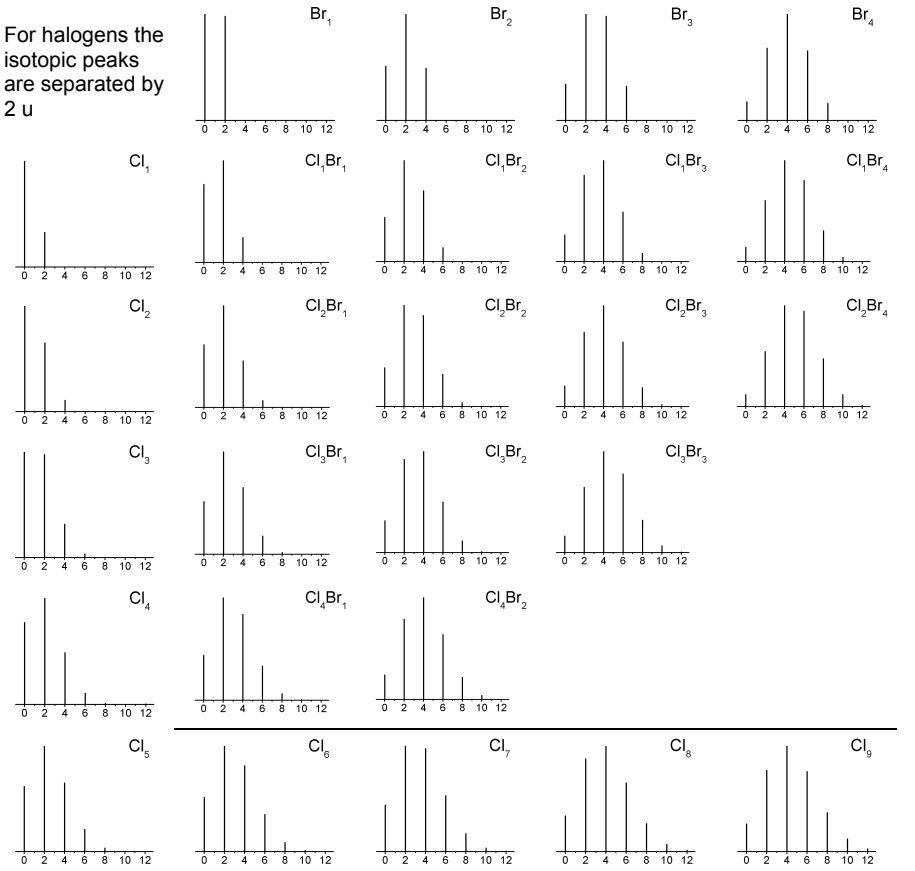


Fig. A.2. Calculated isotopic patterns for combinations of bromine and chlorine. The peak shown at zero position corresponds to the monoisotopic ion at *m/z* X. The isotopic peaks are then located at *m/z* = X+2, 4, 6, ... The numeric value of X is given by the mass number of the monoisotopic combination, e.g., 70 u for Cl_2.

A.5 Silicon and Sulfur Isotopic Patterns

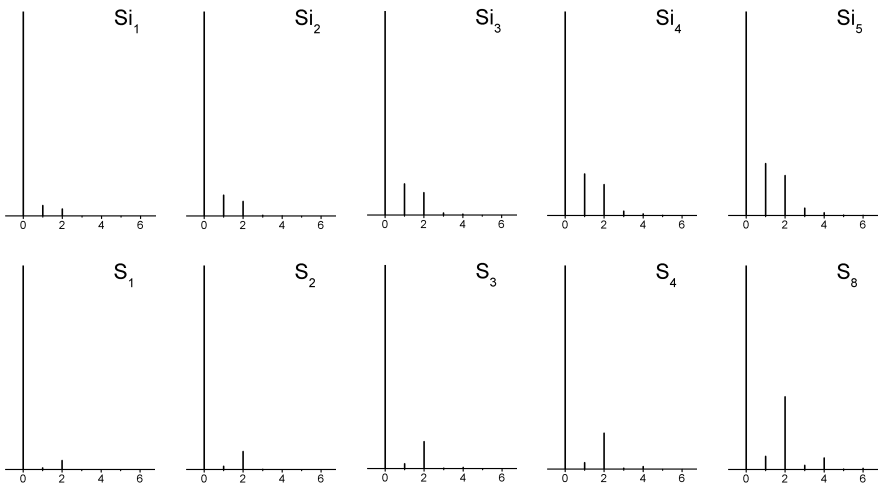


Fig. A.3. Isotopic patterns for silicon and sulfur. The peak at zero position corresponds to the monoisotopic ion at *m/z* X. The isotopic peaks are then located at *m/z* = X+1, 2, 3, ...

A.6 Isotopologs and Accurate Mass

If isotopolog ions are resolved and sufficient mass accuracy is available, the distance between isotopic peaks can yield a new type of analytical information: the differences between isotopic masses are characteristic for certain elements.

Table A.7. Characteristic mass differences to identify the presence of elements

Pair of isotopes or modification	Δm [u]
^{6}Li vs. ^{7}Li	1.0009
^{10}B vs. ^{11}B	0.9964
^{12}C vs. ^{13}C	1.0033
^{32}S vs. ^{34}S	1.9958
^{35}Cl vs. ^{37}Cl	1.9970
^{58}Ni vs. ^{60}Ni	1.9955
^{63}Cu vs. ^{65}Cu	1.9982
^{79}Br vs. ^{81}Br	1.9980
^{191}Ir vs. ^{193}Ir	2.0023
gain or loss of H	1.0078
gain or loss of H_2	2.0156

A.7 Characteristic Ions

Care should be taken when using tables of characteristic ions and neutral losses as the values listed represent only a minor fraction of the fragmentations possible.

Table A.8. Characteristic ion series and neutral losses

Ion series	*m/z* and $[M–X]^+$ ions	Remarks
Carbenium ions	15, 29, 43, 57, 71, 85, 99, 113, 127, 141, ...	any alkyl group
Acylium ions	29, 43, 57, 71, 85, 99, 113, 127, 141, 155, ...	aliphatic aldehydes, ketones, carboxylic acids and their derivatives
Immonium ions	30, 44, 58, 72, 86, 100, 114, 128, 142, 156, ...	aliphatic amines
Oxonium ions	31, 45, 59, 73, 87, 101, 115, 129, 143, 157, ...	aliphatic alcohols and ethers
Sulfonium ions	47, 61, 75, 89, 103, 117, 131, 145, 159, ...	aliphatic thiols and thioethers
From benzyl	39, 51, 65, 77, 91	phenylalkanes
From benzoyl	51, 77, 105	aromatic aldehydes, ketones, carboxylic acids and derivatives
	$[M–16]^{+\bullet}$, $[M–30]^+$, $[M–46]^{+\bullet}$	nitroarenes
	45, 60, 73, $[M–17]^+$, $[M–45]^+$	carboxylic acids
	59, 74, 87, $[M–31]^+$, $[M–59]^+$	methyl carboxylates
	73, 88, 101, $[M–45]^+$, $[M–73]^+$	ethyl carboxylates
By McL	44	McL of aldehydes
	58	McL of methyl ketones
	60	McL of carboxylic acids
	59	McL of carboxylic acid amides
	74	McL of methyl carboxylates
	88	McL of ethyl carboxylates
Halogens	$[M–19]^+$, $[M–20]^{+\bullet}$	fluorine compounds
	35, $[M–35]^+$, $[M–36]^{+\bullet}$	chlorine compounds (Cl pattern)
	79, $[M–79]^+$, $[M–80]^{+\bullet}$	bromine compounds (Br pattern)
	127, $[M–127]^+$, $[M–128]^{+\bullet}$	iodine compounds
General losses	$[M–1]^+$	loss of $H^\bullet$ (strong → α-cleavage)
	$[M–2]^{+\bullet}$	loss of H_2
	$[M–3]^+$	loss of $H^\bullet$ and H_2
	$[M–15]^+$	loss of methyl

continued →

Ion series	*m/z* and $[M–X]^+$ ions	Remarks
General losses	$[M–16]^{+\bullet\bullet}$	loss of O from nitroarenes
	$[M–17]^{+\bullet}$	loss of ammonia from amines,
	$[M–17]^+$	loss of $OH^\bullet$ from (*tert*)alcohols
	$[M–18]^{+\bullet}$	loss of water from alcohols
	$[M–27]^{+\bullet}$	loss of HCN from heterocycles or HNC from aromatic amines
	$[M–28]^{+\bullet}$	loss of CO, C_2H_4 or N_2
	$[M–29]^+$	loss of $CHO^\bullet$ or $C_2H_5^\bullet$
	$[M–30]^{+\bullet}$	loss of H_2CO from aromatic methyl ethers etc.; check for nitroarenes
	$[M–44]^{+\bullet}$	loss of CO_2
	$[M–46]^{+\bullet}$	loss of HCOOH, EtOH or NO_2
	$[M–48]^{+\bullet}$	loss of SO from sulfoxides
	$[M–64]^{+\bullet}$	loss of SO_2 from sulfolanes
	$[M–77]^+$	loss of phenyl
	$[M–91]^+$	loss of benzyl

A.8 Common Impurities

Table A.9. Recognizing common impurities by *m/z*

m/z	Source
18, 28, 32, 40, 44	residual air
149, 167, 279	phthalic acid esters (plasticizers)
149, 177, 222	diethyl phthalate (plasticizers)
73, 147, 207, 281, 355, 429	silicon grease or GC column bleed (Si_x isotopic pattern)
27, 29, 41, 43, 55, 57, 69, 71, 83, 85, 97, 99, 109, 111, 113, 125, 127, ..., up to *m/z* 500	hydrocarbons from grease or from suspensions in paraffin
32, 64, 96, 128, 160, 192, 224, 256	sulfur (S_x isotopic pattern)
51, 69, 119, 131, 169, 181, 219, 231, 243, 281, 317, 331, ...	background from PFK

A.9 Amino Acids

Table A.10. Amino acids (by order of residue mass)

Amino acid	Codes	Polarity	Charge[a]	Formula of residue	Residue nominal mass [u]	Residue accurate mass [u]
Glycine	Gly, G	nonpolar	O	C_2H_3NO	57	57.0520
Alanine	Ala, A	nonpolar	O	C_3H_5NO	71	71.0371
Serine	Ser, S	polar	O	$C_3H_5NO_2$	87	87.0320
Proline	Pro, P	nonpolar	O	C_5H_7NO	97	97.0528
Valine	Val, V	nonpolar	O	C_5H_9NO	99	99.0684
Threonine	Thr, T	polar	O	$C_4H_7NO_2$	101	101.0477
Cysteine	Cyc, C	nonpolar	O	C_2H_5NOS	103	103.0092
Leucine	Leu, L	nonpolar	O	$C_6H_{11}NO$	113	113.0841
Isoleucine	Ile, I	nonpolar	O	$C_6H_{11}NO$	113	113.0841
Asparagine	Asn, N	polar	O	$C_4H_6N_2O_2$	114	114.0429
Aspartic acid	Asp, D	polar	–	$C_4H_5NO_3$	115	115.0269
Glutamine	Gln, Q	polar	O	$C_5H_8N_2O_2$	128	128.0586
Lysine	Lys, K	polar	+	$C_6H_{12}N_2O$	128	128.0950
Glutamic acid	Glu, E	polar	–	$C_5H_7NO_3$	129	129.0426
Methionine	Met, M	nonp.	O	C_5H_9NOS	131	131.0405
Histidine	His, H	polar	(+)	$C_6H_7N_3O$	137	137.0589
Phenylalanine	Phe, F	nonpolar	O	C_9H_9NO	147	147.0684
Arginine	Arg, R	polar	+	$C_6H_{12}N_4O$	156	156.1011
Tyrosine	Tyr, Y	polar	O	$C_9H_9NO_2$	163	163.0633
Tryptophan	Trp, W	nonpolar	O	$C_{11}H_{10}N_2O$	186	186.0793

[a] Neutral amino acids are marked by O, basic AAs (+) tend to assume positive charge from protonation, acidic AAs (–) tend to be negative by dissociation of the acidic group.

A.10 Method Selection Guide

This diagram (Fig. A4) may help in selecting the right ionization method for analysis of a sample by MS. Often, there are several reasonable choices and it is advisable to make the best use possible of what is available at your local facility. MS results also depend on user input. Discuss your options with the MS staff at your facility.

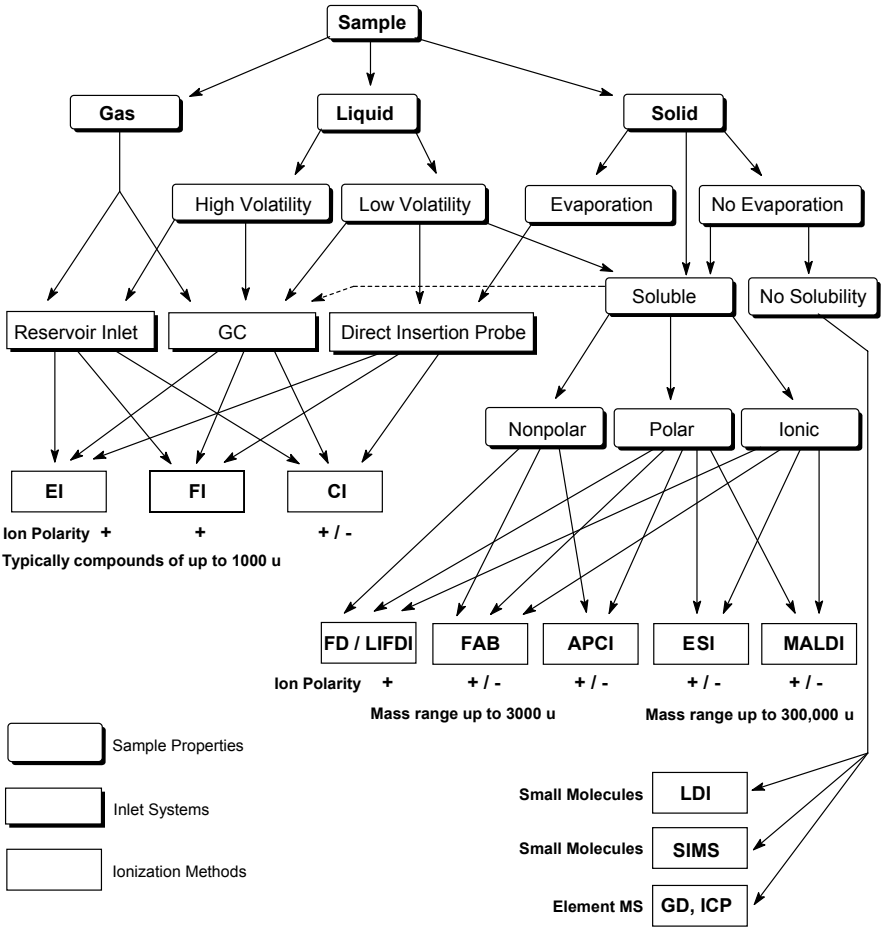


Fig. A.4. Method selection guide.

A.11 How to Recognize Cationization

Soft ionization methods like FAB, FD, ESI, and MALDI often cause cationization by Na^+, K^+, Cs^+, and Ag^+. Especially Na^+, K^+ adducts are almost omnipresent. Searching a spectrum for those peak distances reveals the true molecular mass.

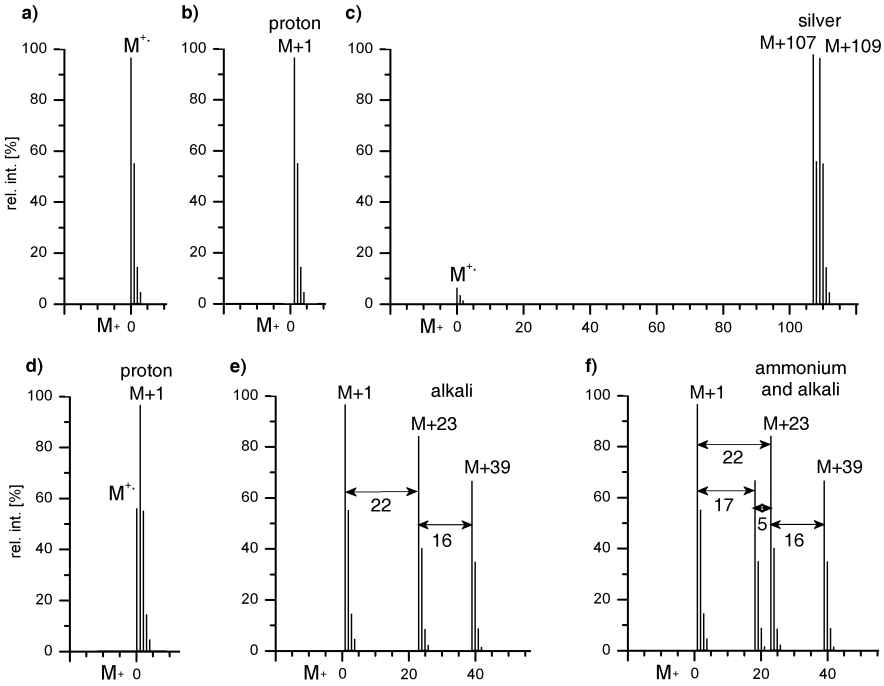


Fig. A.5. Signals representing the intact molecular mass in case of (**a**) molecular ion formation, (**b**) protonation, (**c**) silver cationization, (**d**) molecular ion and protonation, (**e**) protonation plus alkali cationization, and (**f**) protonation, ammonium plus alkali adduct formation. The relative abundances of the respective contributions are subject to wide variations. The abscissa gives the corresponding M+X nominal mass value; artificial isotopic patterns are added for more realistic appearance.

Table A.11. Characteristic mass differences to identify frequent cationization products

Pair of ions	Δm [u]
$M^{+\bullet}$ vs. ^{13}C-$M^{+\bullet}$	1.0033
$M^{+\bullet}$ vs. $[M+H]^+$	1.0078
$[M+H]^+$ vs. $[M+NH_4]^+$	17.0265
$[M+H]^+$ vs. $[M+Na]^+$	21.9819
$[M+H]^+$ vs. $[M+K]^+$	37.9559
$[M+Na]^+$ vs. $[M+K]^+$	15.9739

A.12 Systematic Approach to Mass Spectra

1. Collect background information such as origin of the sample, presumed compound class, solubility, thermal stability, or other spectroscopic information.
2. Write *m/z* labels for all relevant peaks and calculate mass differences between prominent peaks. Do you recognize characteristic ion series or mass differences that point to common neutral losses?
3. Check which ionization method was used and examine the general appearance of the mass spectrum. Is the molecular ion peak intense (as with aromatic, heterocyclic, polycyclic compounds) or weak (as with aliphatic and multifunctional compounds)? Are there typical impurities (solvent, grease, plasticizers) or background signals (residual air, column bleed in GC-MS)?
4. Is accurate mass data available for some of the peaks?
5. Now, follow the above rules to proceed.
6. Derive information on the presence/absence of functional groups.
7. Be careful when using Table A.8 as it cannot be comprehensive. Moreover, one tends to get stuck on the first assumption.
8. Put together the known structural features and try to assign the structure to the unknown sample. Sometimes, only partial structures of the analyte can be derived or isomers cannot be distinguished.
9. Crosscheck proposed molecular structure and mass spectral data. This is also recommended between the single steps of mass spectral interpretation.
10. Are there reference spectra available (at least of similar compounds) either from the literature or from mass spectral databases (Chap. 5.7)?
11. Never rigidly follow this scheme! Sometimes, a step back or forth may accelerate the process or help to avoid pitfalls.

A.13 Rules for the Interpretation of Mass Spectra

1. Identify the molecular ion! This is an important inital step, because it is needed to derive the molecular composition (Chap. 6.6.4). If the EI spectrum does not allow for the identification of the molecular ion, soft ionization methods should be employed in addition.
2. The mass differences between the presumed molecular ion and primary fragments must correspond to realistic chemical compositions (Chap. 6.6.4, Table 6.12).
3. The calculated and experimental isotopic patterns have to agree with the molecular formula postulated (Chap. 3.2).
4. The derived molecular formula must obey the nitrogen rule (Chap. 6.2.5). An odd-numbered *m/z* value of the molecular ion requires 1, 3, 5, ... nitrogens to be contained, whereas an even *m/z* value belongs to 0, 2, 4, ... nitrogens.

5. Homolytic cleavages cause odd-numbered mass differences between fragment and molecular ion (Chap. 6.2.5). Rearrangement fragmentations cause even-numbered mass differences. This rule toggles if odd numbers of nitrogen are contained in the neutral loss.
6. In general, fragmentations obey the even-electron rule (Chap. 6.1.3). Odd-electron fragments from rearrangement fragmentations behave as if they were molecular ions of the respective smaller molecule.
7. The competition of homolytic cleavages is governed by Stevenson's rule (Chap. 6.2.2). Thermodynamic stability of the pairs of products formed is decisive in selecting the preferred fragmentation route.
8. Calculate $r + d$ to check formula proposals and to derive some structural characteristics (Chap. 6.4.4).
9. Write down a fragmentation scheme, thereby carefully tracking the origin of primary fragment ions and of characteristic ions used for structure assignment. From the purely analytical point of view this is very useful. However, one should keep in mind that any proposed fragmentation scheme remains a working hypothesis unless experimental confirmation is available.
10. Employ additional techniques, such as measurement of accurate mass (Chap. 3.3), tandem mass spectrometry, or other spectroscopic methods to crosscheck and to refine your assignments.
11. Good luck!

A.14 Nobel Prizes for Mass Spectrometry

Laureate	Category and year	Prize motivation
Joseph John Thomson	Physics 1906	In recognition of the great merits of his theoretical and experimental investigations on the conduction of electricity by gases
Francis William Aston	Chemistry 1922	For his discovery, by means of his mass spectrograph, of isotopes in a large number of non-radioactive elements, and for his enunciation of the whole-number rule
Wolfgang Paul	Physics 1989	For the development of the ion trap technique
John B. Fenn jointly with Koichi Tanaka	Chemistry 2002	For their development of soft desorption ionization methods for mass spectrometric analyses of biological macromolecules

Subject Index

A

α-cleavage
  of acetone 255
  of amines, ethers, and alcohols 262
  of halogenated hydrocarbons 269
  of ketones 259
  of thioethers 269
about this book 3
  chapters overview 4
  problems and solutions website 5
accelerator mass spectrometry 707
  application 710
  facility 709
accumulation
  of spectra 655
accuracy 96
accurate mass 72, 92
  for formula assignment 102
  for isotopolog separation 110
  in FI-MS 390
  measurement 92
activation energy of the reverse reaction 47, 432
acylium ion 256
acylium ions 261
ADC *See* analog-to-digital converter, *See* time-to-analog converter
adiabatic ionization 29
AE *See* appearance energy
afterglow
  in GD-MS 695
AGHIS *See* all-glass heated inlet system
aliasing
  in FT 181
alkali ion adducts
  recognition 523
alkenes
  mass spectra 281
allylic bond cleavage
  isomerization prior to 281
  of alkenes 281
ambient MS 621, 622
  overview 644
amino acid residue 534
AMS *See* accelerator mass spectrometry
amu *See* atomic mass unit
analog-to-digital converter 131
analysis of complex mixtures 651
analyte ion formation
  in PTR-MS 362
analyte polarity
  ESI vs APCI vs APPI 602
AP *See* appearance energy
APCI *See* atmospheric pressure chemical ionization
APCI spectra 605
APGD *See* atmospheric pressure glow discharge
API *See* atmospheric pressure ionization
AP-MALDI *See* atmospheric pressure MALDI
apodization in FT 180
appearance energy
  definition 33
  determination 58

influence on selectivity 368
appearance potential *See* appearance energy
APPI *See* atmospheric pressure photoionization
APPI spectra 610
array detector 207
ASAP *See* atmospheric pressure solids analysis probe
aspirin
DESI spectrum 628
associative ionization *See* Penning ionization
atmospheric pressure chemical ionization 564, 604
atmospheric pressure glow discharge 642
atmospheric pressure ionization 563
interface for AP-MALDI 546
ion formation 563
atmospheric pressure ionization methods 561
atmospheric pressure MALDI 546
atmospheric pressure photoionization 564, 608
ion formation 608
atmospheric pressure solids analysis probe 640
atmospheric-pressure chemical ionization
ion formation 605
ion source 604
atomic mass unit 71
atomic number 67
atomic weight *See* relative atomic mass
atomization
of analytes 688
autodetachment 371
autoprotonation 354
average molecular mass 111
averaging of spectra 655

B

Bacillus subtilis
SIMS imaging 707
background subtraction
from spectra 655
bar graph representation of spectra 10
base peak
definition 9
base peak chromatogram 12, 654
BAT *See* field desorption
benzo[a]pyrene
EC spectrum 371
benzyl ion
dissociation 277
benzyl/tropylium isomerization 277
benzylic bond cleavage 275
phenylalkanes 275
BEqQ 196
binding energy per nucleon 94
biomolecule classification
by IMS-MS 673
BIRD *See* blackbody infrared radiative dissociation
blackbody infrared radiative dissociation 457
Boltzmann distribution 30
bond dissociation enthalpies
heterolytic 35
homolytic 34
Born-Oppenheimer approximation 27
bottom-up protein analysis 531
BPC *See* base peak chromatogram
Bradbury-Nielsen gate 427
breakdown graph 59
butyl ion isomers 286

C

C_{60}
primary ions for SIMS 706
RDA reaction of derivatives 304
CA *See* collision-induced dissociation
CAD *See* collision-induced dissociation
calibration file 99
^{252}Californium plasma desorption 498
^{252}Cf plasma desorption 498
capillary GC 663
interface to EI source 664
capillary zone electrophoresis 568
capillary zone electrophoresis-mass spectrometry 651
carbenium ions 261
stability of isomers 286
carrier gas
for GC-MS 664

in ICP-MS 697
CE *See* charge exchange
CE-CI *See* charge exchange chemical ionization
CEM *See* detectors
center-of-mass collision energy 422
CF-FAB 494
CH_5^+ 356
characteristic ions 260
charge deconvolution
computerized 588
in ESI 587
charge exchange 364
charge exchange *See* charge exchange chemical ionization
charge exchange chemical ionization
energetics 365
reagent gases 365
regio- and stereoselectivity 368
selective ionization 366
charge reduction electrospray 592
charge retention 256
charge states
in ESI *vs*. molecular weight 585
charge transfer ionization See charge exchange chemical ionization
charge-deconvoluted spectrum 588
charged-residue model
in ESI 582
charge-localization 25
chemical ionization 351
analytes for CI 375
ion formation 351
ion source 352
positive-ion formation 352
reagent gas 352
chemical noise
in FAB-MS 487
chemi-ionization 354
Chevron plate 205
chromatogram 652
chromatograms 651
chromatography-mass spectrometry interfaces 651
chromatography-tandem MS 658
CI *See* chemical ionization
CID *See* collision-induced dissociation
closed-shell ion *See* even-electron ion
cluster ions
for mass calibration 483
in FAB-MS 483
in FD-MS 396
CO loss 304
differentiation from N_2, C_2H_4 311
of arylmethylethers 308
of carbonyl compounds 311
of phenols 304
of quinones 307
of transition metal carbonyl complexes 310
collector slit 143
collision cascade
in SIMS 701
collision cell 153, 420
collisional activation *See* collision-induced dissociation
collisional cooling 153, 154
collisional focusing 154
collisionally activated dissociation *See* collision-induced dissociation
collision-induced dissociation 420
energy transfer 421
multiple collisions 424
colorectal cancer cells 671
column bleed
in GC-MS 665
combination ion source 224
composite metastable peak 309
cone-jet mode
in ESI 580
constant neutral loss scan 434, 438
consumption of analyte
by MS in general 8
continuous wave mode 178
continuous-flow FAB *See* fast atom bombardment
conversion dynode 207
correlated sweep excitation 448
CRE *See* charge reduction ESI
critical slope method 54
CRM *See* charged-residue model
crude oil
analysis 678
analysis by FD-MS 404
cryopump 209
Cs sputter source
for AMS 709
C-terminal fragment ions 533
C-trap 192
curved-field reflectron 429
cuticular hydrocarbons
by DART 643

cycloheptatriene 279
cyclopentadienyl ion 278
CZE *See* capillary zone electrophoresis
CZE-MS *See* capillary zone electrophoresis-mass spectrometry

D

Da *See* dalton
dalton 9
DAPCI See desorption atmospheric-pressure chemical ionization
DAPCI source 632
DAPPI *See* desorption atmospheric pressure photoionization
dark matter See neutral loss
DART *See* direct analysis in real time
DART source 641
data reduction 10, 11, 653
daughter ion 15
DBE *See* double bond equivalents
DBIS *See* dynamic batch inlet systems
DCI *See* desorption chemical ionization
DE *See* delayed extraction
decimal places
  calculation of exact mass 73
degrees of freedom
  external 31
  internal 31
  of an analysis 651
degrees of freedom effect 49
DEI *See* direct electron ionization
delayed extraction 129
delta notation 74
delta value *See* delta notation
deltamass 104
deoxyribonucleic acids 597
DEP *See* direct exposure probe
deprotonated molecules
  in CI 352
depth profile
  by SIMS 702
DESI *See* desorption electrospray ionization
DESI interface 623
DESI ion source 626
desorption atmospheric pressure chemical ionization 631
  setup 631
desorption atmospheric pressure photoionization 621, 633
desorption atmospheric-pressure chemical ionization 621
desorption chemical ionization 236, 374
desorption electron ionization 374
desorption electrospray *See* desorption electrospray ionization
desorption electrospray ionization 621
  features 627
  ion formation 627
  parameters 624
  sampling mode 623
  solvents 625
desorption sonic spray ionization 621, 635
desorption/ionization on silicon 541
DeSSI *See* desorption sonic spray ionization
destructive detection 177
detection limit 14
detector slit 143
detectors 202
  channel electron multiplier 204
  channeltron (CEM) 204
  conversion dynode 207
  cryogenic detector 203
  Faraday cup 202
  focal plane detector (FPD) 207
  microchannel plate (MCP) 205
  post-acceleration detector 206
  secondary electron multiplier (SEM) 203
differential pumping 162, 421
differentially pumped interface
  in ICP-MS 699
digital ion trap 173
digitization rate 131
di-isotopic element
  definition 68
dimensions
  of GC-MS 652
dimethyldisulfide adducts 665
DIOS *See* desorption/ionization on silicon
DIP *See* direct insertion probe
dirarylmethyl 287
direct analysis in real time 564, 621, 640
  applications 642
  ion formation 642

setup 640
direct analysis of daughter ions *See* mass-analyzed ion kinetic energy spectrometry
direct electron ionization 236
direct exposure probe 235, 374
direct insertion probe 231
discontinuous modes of operation 659
dissolved organic matter 106
distonic ions 273
formation 274
distonic ions
as intermediates 275
DIT *See* digital ion trap
DMDS adducts 283
DNA
by ESI 596
DOF *See* degrees of freedom effect
DOM *See* dissolved organic matter
double bond equivalents 280
examples 281
double zero-filling 180
double α-cleavage
identification of regioisomers 272
of alicyclic compounds 271
double-focusing *See* magnetic sector analyzer
double-focusing instruments 136
doubly charged ion
in EI 22
dried droplet preparation 522
droplet jet fission
in ESI 581
Drosophila melanogaster 643
DTP *See* dual-target FAB probe
dual-LIT 444
dual-target FAB probe 493
duoplasmatron source 702
duty cycle 133, 134
dynamic batch inlet systems 229
dynamic range 131
dynamic SIMS 702

E

EA *See* electron affinity
EASI *See* easy sonic spray ionization
easy ambient sonic-spray ionization 635
easy sonic spray ionization 621
EBqQ 196
EC *See* electron capture
ECD *See* electron capture dissociation
EDD *See* electron detachment dissociation
EESI *See* extractive electrospray ionization
EESI source 636
EHC *See* field desorption
EHI *See* electrohydrodynamic ionization
EI *See* electron ionization
EI ion source 223
contamination 224
efficiency 226
emission-controlled filament 226
filament 225
ionization chamber 224
repeller 224
EI mass spectral libraries 242
EI/CI combination ion sources
EI/CI 352
EIC *See* reconstructed ion chromatogram
ELDI *See* electrospray-assisted laser desorption/ionization
ELDI setup 637
electric field
to effect FI 383
electrohydrodynamic ionization 565
electron affinity 371
selected values 372
electron attachment *See* electron capture
electron capture 23, 370
creating thermal electrons 372
cross section 452
dissociative 372
EC spectra 373
energetics 370
ionization process 370
electron capture dissociation 453
of peptide ions 454
electron detachment 462
electron detachment dissociation 462
electron impact *See* electron ionization
electron impact ionization *See* electron ionization
electron ionization 22, 223, 249
doubly charged ions 22
fragment ions 23
fragmentation pathways 45

ionization process 22
layout of EI ion source 223
low-energy, low-temperature 239
primary electrons 225
processes 24
rearrangement ions 23
timescale 42
electron mass
in calculation of exact mass 72, 73
electron monochromator 55
electron-transfer dissociation 459
electrospray *See* electrospray ionization
electrolytic processes 580
electrospray interfaces 572
electrospray ionization 561
charge deconvolution 587
charge reduction 592
conventional *vs.* nanoESI 574
design of sprayers 568
disintegration of droplets 581
formation of a spray 578
high-mass capabilities 600
ion formation 582
ion source/interface 566
ionic metal complexes 594
oligosaccharides 599
principle 565
sample consumption 603
small molecules 593
spray plume 576
surfactants 596
Taylor cone 579
types of ions 603
electrospray-assisted laser desorption/ionization 637
electrostatic analyzer 136, 139
energy dispersion 140
electrostatic sector *See* electrostatic analyzer, *See* electrostatic analyzer
elemental MS
overview 688
elemental trace analysis 685
elimination of carbon monoxide *See* CO loss
emitter heating current 399
end cap electrodes *See* quadrupole ion trap
energy partitioning 432
energy-sudden methods
in contrast to slow heating 236
energy-time uncertainty principle 178
entrance slit 143
ES *See* electrospray ionization
ESA *See* electrostatic analyzer
ESI *See* electrospray ionization
ESI interface *See* electrospray ionization
ETD *See* electron-transfer dissociation
even-electron ion 22, 250
even-electron rule 253
exact mass 92
definition 72
excess energy
definition 36
exit slit 143
explosives
by DART 643
external ion source
for quadrupole ion trap 173
external ion sources
in FT-ICR-MS 187
external mass calibration 99
extracted ion chromatogram 653
extractive electrospray ionization 621, 635

F

FAB *See* fast atom bombardment
FAB gun 480
FAB matrix 486
Faraday cup *See* detectors
fast atom bombardment 479, 480
accurate mass 492
continuous-flow (CF) FAB 494
criteria for the liquid matrix 487
FAB gas 481
FAB target 482
frit-FAB 494
high-mass analytes 491
ion formation 483, 484
ion source 480
ionic analytes 490
low- to medium polarity analytes 488
low-temperature (LT) FAB 495
matrix spectra 487
peptide sequencing 496
role of the liquid matrix 486
side-reactions 487
types of ions 497

fast GC-MS 667
FC43 *See* perfluorotributylamine
FD *See* field desorption
FD emitter *See* field desorption
FFR *See* field-free region
FI *See* field ionization
FI/FD ion source 383
  counter electrode 383
  field emitter 383
FID *See* flame ionization detector
field anode/emitter *See* FI/FD ion source
field desorption 381
  best anode temperature (BAT) 399
  cationization 394
  cluster ions 396
  emitter activation 385
  emitter handling 387
  emitter heating current (EHC) 386
  FD spectra 392
  field-induced desolvation 395
  ion evaporation 395
  ion formation 393
  ionic analytes 397
  liquid injection field desorption ionization (LIFDI) 402
  of reactive analytes 402
  protonation 394
  surface mobility 393
  types of ions 402
  wire emitters 385
field ionization 381
  $[M+H]^+$ ions 389
  electric field strength 383
  emitter activation 385
  field emitter/field anode 383
  field-induced dissociation 390
  mass spectra 388
  multiply charged ions 389
  of hydrogen atom 382
  post-ionization 389
  process 382
  wire emitters 385
field-free region 418, 420, 431
flame ionization detector 652
fluence 511
forward library search 242
Fourier transform 179
Fourier transform ion cyclotron resonance 174
  axial trapping 183
  cyclotron frequency 175
  cyclotron motion 175
  ECD 455
  Fourier transformation 186
  free induction decay 186
  frequency domain 186
  frequency sweep (chirp) 182
  image current detection 186
  infrared multiphoton dissociation 452
  principle 174
  stored wavefrom inverse Fourier transform (SWIFT) 183
  sustained off-resonance irradiation (SORI) 449
  time domain 186
  time scale 44
Fourier transformation *See* Fourier transform ion cyclotron resonance
FPD *See* detectors
fragment ion peaks
  definition 9
fragment ions
  definition 9
Franck-Condon factor 27
Franck-Condon principle 27
frequency bandwidth
  in FT-ICR 177
frequency domain 179
frit-FAB 494
FT See Fourier transform
FT-ICR See Fourier transform ion cyclotron resonance
fused-droplet electrospray ionization 635
FWHM
  full width at half maximum 89

G

γ-H shift with β-cleavage *See* McLafferty rearrangement
gas chromatograph 237
gas chromatography
  coupled to FI-MS 391
gas chromatography-mass spectrometry 651
  derivatization 664
  fast GC-MS 667

interface 663
jet separator 663
narrow-bore columns 667
separators 663
gas phase basicity 61
determination 466
of some molecules 62
gas phase ion chemistry 21
GB *See* gas phase basicity
GC *See* gas chromatograph
GC columns
fused silica capillaries 663
narrow bore capillaries 667
packed 663
GC-MS *See* gas chromatography-mass spectrometry
GD *See* glow discharge
GD-MS *See* glow discharge mass spectrometry
glass heated inlet system 229
gliding spark source mass spectrometry 692
glow discharge 694
glow discharge mass spectrometry 694
Grimm type source 694
GSS-MS *See* gliding spark source mass spectrometry

H

H_2O loss
of alkanols 313
Hadamard transform 667
in TOF-MS 134
hashish slab
analysis by DAPPI 634
HCD *See* higher-energy C-trap dissociation
HCN loss 336, 337
HDX *See* hydrogen–deuterium exchange
headspace analysis 636
heats of formation
of small molecules 47
heavy primary ion beams
for SIMS 705
Helicobacter pylori 600
heterocyclic compounds 332
aromatic heterocycles 339
aromatic *N*-heterocycles 336
HCN loss 336
saturated heterocycles 333
heterolytic bond dissociation 33
high energy collisions 423
high mass
resolution requirements 110
higher-energy C-trap dissociation 446
high-pressure liquid chromatography 668
high-resolution 90, 92
high-resolution mass spectrometry 99
high-resolution SIM 657, 662
high-resolving mass analyzers
for charge deconvolution in ESI 590
histogram *See* bar graph
HNC loss 339
hollow-cathode
in PTR ion source 362
homologous ions
series 260
homolytic bond cleavage
$k_{(E)}$ functions 41
homolytic bond dissociation 33
Hornbeck-Molnar process 24
hot hydrogen atom model 455
HPLC *See* high-pressure liquid chromatography
HR *See* high resolution
HR-MS *See* high-resolution mass spectrometry
in FAB/LSIMS 492
hybrid instruments 160, 194
hybrid mass analyzers 197
hydrogen–deuterium exchange 465
hypervalent ions *See* distonic ions
hyphenated methods 651

I

ICP source 697
ICP-MS *See* inductively coupled plasma mass spectrometry
IE *See* ionization energy
IEM *See* ion evaporation model
illicit drugs
in waste water 670
ILs *See* ionic liquids
image current detection 177

image slit 143
immonium ions 262, 264
IM-MS *See* ion mobility-mass spectrometry
IMS *See* ion mobility spectrometry
IMS-MS 673
INC *See* ion-neutral complexes
inductively coupled plasma mass spectrometry 686, 697
  ICP source 697
infrared multiphoton dissociation 451, 452
  on LITs and QITs 452
infrared photodissociation spectroscopy 456
inlet *See* inlet system
inlet system 228
  direct exposure probe (DEP) 235
  direct insertion probe (DIP) 231
  liquid introduction system 231
  particle beam interface 238
  reservoir inlet 229
  sample vials for DIP 232
inorganic mass spectrometry 685
in-source CID *See* nozzle-skimmer dissociation
in-source decay 428, 536
integer mass *See* nominal mass
internal energy 29
  consequences 45
  influence on rate constants 38
  of $[M+H]^+$ ions 356
  randomization 35
internal mass calibration 101
internal standard
  isotopes 691
interpretation of EI mass spectra 249
interpretation of mass spectra
  rules 340, 733
  systematic approach 341, 733
intramolecular vibrational relaxation 451
ion activation methods
  comparison 462
ion beam 119
ion chromatograms 652
  concept 11
  types and akronyms 653
ion current-controlled heaters
  for direct probes 232
ion evaporation model
  in ESI 582
ion funnels
  in ESI interfaces 571
ion guides *See* RF-only quadrupole
ion mobility spectrometry 198, 673
ion mobility-mass spectrometry 198
ion pherogram *See* ion chromatogram
ion profile *See* ion chromatogram
ion source
  simple implementation 119
ion spray *See* pneumatically assisted ESI
ion trajectory calculations 227
ion trap array 173
ion volume *See* EI ion source
ionic liquids
  analysis by FD-MS 398
ionization cross section 29
ionization efficiency 29
  curves 55
ionization energy
  definition 25
  determination 54
  of radicals 258
  ranges 25
ionization potential *See* ionization energy
ion-molecule reaction 463
  for charge state reduction 592
  of transition metal complexes 464
  in CI 351
ion-neutral complexes 322
  electrostatic attraction 323
  evidence 322
  intermediacy 325
  intermediates of onium reaction 319
  of radical ions 325
  reorientation criterion 324
IP *See* ionization energy
IR-MALDI 516
IRMPD 452 *See* infrared multiphoton dissociation
IR-MS *See* isotope ratio mass spectrometry
IRPD *See* infrared photodissociation spectroscopy
irradiance 511
ISD *See* in-source decay
isobaric ions 261
isomeric nitrophenols
  EI spectra 332

isotope dilution 661
isotope effect 50
  determination 51
  intermolecular 50
  intramolecular 50
  kinetic 50
  primary 51
  secondary 53
isotope ratio mass spectrometry 74, 691
isotope ratio measurements
  by AMS 708
  accurate determination 688
isotopes
  definition 67
isotopic abundance
  representation 69
isotopic cluster *See* isotopic pattern
isotopic compositions *See* isotopic abundance
isotopic distribution *See* isotopic pattern
isotopic enrichment 87
isotopic homologs 77
isotopic ions 77
isotopic labeling 88
isotopic mass 92
  definition 71
isotopic molecular ion 77
isotopic pattern 69, 74
  at very high resolution 107
  average molecular mass 111
  calculation 74
  carbon 74
  distinguishing 79
  effect of charge state 112
  effect of resolution 112
  halogens 78
  oxygen, silicon, sulfur 81
  polyisotopic elements 81, 84, 86
isotopic patterns
  bookkeeping 85
isotopically enriched ion *See* isotopic enrichment
isotopolog ion 77
isotopologs 77
ISP *See* ion spray
ITA *See* ion trap array

K

$k_{(E)}$ function 40
Kendrick mass
  conversion to IUPAC mass 105
  defect 105
  nominal 105
  scale 105
KER *See* kinetic energy release
kinetic energy release 48, 432
kinetic method
  for detn. of GB 466
kinetic shift 59
Kingdon trap 189
  ideal 189
Kovats retention index 243

L

ladder sequencing *See* peptide sequencing
LAESI *See* laser ablation electrospray ionization
LA-ICP-MS *See* laser ablation
laser ablation
  for ICP-MS 700
laser ablation electrospray ionization 638
laser desorption/ionization 527
  applications 527
  introduction 507
lasers
  for MALDI 508
LC *See* liquid chromatograph
LC-MS *See* liquid chromatography-mass spectrometry
LDI *See* laser desorption/ionization
LIFDI *See* liquid injection field desorption
LIFT *See* TOF/TOF instruments
limit of detection 14
limit of quantitation 660
linear ion trap
  ETD 461
  tandem MS 444
linear quadrupole analyzer 146
  hyperbolic *vs*. cylindrical rods 151
  principle 147

triple quadrupole 437
unit resolution 151
linear quadrupole ion trap 155
axial ejection 158
mass-analyzing 158
radial ejection 160
scan function 160
segmented 161
tandem MS 443
time scale 44
liquid chromatograph 238
liquid chromatography-mass spectrometry
interfaces 668
moving belt interface 238
multiplexed electrospray inlet systems (MUX) 671
liquid chromato-graphy-mass spectrometry 651
liquid injection field desorption ionization 402
liquid matrix
in FAB/LSIMS 479
liquid metal ion guns
for SIMS 703
liquid secondary ion mass spectrometry 480
ion source 482
primary ions 482
LIT *See* linear quadrupole ion trap
LIT-FT-ICR hybrid instrument 197
LITICR 196
localization of double bonds 283
lock mass
in SIM 657
one-point calibration 391
LOD *See* limit of detection
loose transition state 41
Lorentz force 174
Lorentz Force 136
loss of ethyne 278
low resolution 90
low-energy collisions 423
low-energy EI spectra 239
low-temperature EI spectra 239
LR *See* low resolution
LSIMS *See* fast atom bombardment and liquid secondary ion mass spectrometry
LT-FAB *See* fast atom bombardment
lucky survivor model 516

M

m/z *See* mass-to-charge ratio
$M^{+\bullet}$ *See* molecular ion
[M–3] peak
seemingly occurrence 314
magnetic field scan 142
magnetic sector
illustration 139
magnetic sector analyzer
Bainbridge-Jordan 141
double-focusing 141
forward geometry 142
four-sector 436
lamination of the yoke 144
linked scans 434
magnet scan 142
Mattauch-Herzog 141
Nier-Johnson 142
principle 136
reversed geometry 142
setting resolution 143
tandem MS 431
magnetic sector instrument *See* magnetic sector analyzer
magnetic sector-oaTOF 196
magnetic sector-QIT 196
magnetic sector-quadrupole hybrid 196
magnetron frequency 185
main beam
attenuation in CID 424
MALDESI *See* matrix-assisted laser desorption electrospray ionization
MALDI *See* matrix-assisted laser desorption/ionization
MALDI imaging 544
mass accuracy 95
limits 97
requirements 97
specification 104
mass analyzer 118
ideal 119
for EI-MS 241
types 117
mass calibration 99
reference list 103
calibration compound 99
mass defect 93
negative 93
positive 93

vs. nominal mass 95
mass deficiency 93
mass number 68
in definition of *m/z* 8
mass reference compound *See* mass calibration compound
mass reference list 99
mass resolution 88
mass spectra
general description 10
mass spectral imaging
by LA-ICP-MS 701
by SIMS 706
mass spectrograph 138
term 6
mass spectrometer 138
as a chemical laboratory 21
components of 7
general scheme 8
term 6
mass spectrometric time scale
of modern instrumentation 45
mass spectrometrist 6
pioneers 1
mass spectrometry
aims 1
fields of application 2
principle of 6
techniques overview 7
term 6
things to understand 5
mass spectrometry/mass spectrometry *See* tandem mass spectrometry
mass spectroscopy *See* mass spectrometry
bad term 6, 15
mass spectrum
definition 9
mass uncertainty
state-of-the-art 98
mass-analyzed ion kinetic energy spectrometry *See*
determination of KER 433
mass-analyzed ion kinetic energy spectrum 432
mass-analyzed threshold ionization 57
mass–energy equivalence 98
massive cluster impact 480, 498
mass-to-charge ratio
definition 8
material-enhanced laser desorption/ionization 543
Mathieu equations 148, 166
MATI *See* mass-analyzed threshold ionization
matrix
in FAB-MS 486
matrix-assisted laser desorption electrospray ionization 638
matrix-assisted laser desorption/ionization 508
applications 529
carbohydrates 536
cationization 522
characteristic fingerprint 530
delayed extraction 508
desalting/cation exchange 524, 538
detection limit 547
expansion of plume 512
for proteins 529
imaging 545
ion formation 509, 513
ion source 508
laser fluence 510
laser irradiance 510
laser spot size 511
MALDI target 519
matrices in IR-MALDI 516
matrices in UV-MALDI 516
matrix spectra 519
oligonucleotides and DNA 538
oligosaccharide structures 536
polymer endgroups 540
role of the matrix 516
sample holder 519
sample introduction 519
sample load 547
sample preparation 519
solvent-free preparation 526
synthetic polymers 539
thin layer technique 522
types of ions in LDI/MALDI 548
Mattauch-Herzog geometry 141
for SS-MS 693
MBSA *See* molecular beam solid analysis
MCI *See* massive cluster impact
McL *See* McLafferty rearrangement
McLafferty rearrangement 290
concerted or stepwise 291
even-electron analogy 315

frequent product ions 295
of aldehydes and ketones 290
of aromatic hydrocarbons 296
of carboxylic acids and derivatives 293
requirements 290
role of the γ-hydrogen 292
with double hydrogen transfer 297
MCP *See* detectors
MELDI *See* material-enhanced laser desorption/ionization
memory effect 240
metallomics 686
metalloproteins 686
metastable dissociation 536
metastable ion 428
metastable ion suppressor *See* TOF/TOF instruments
metastable ions 44, 420
methane
EI spectrum 252
MIC *See* multi-ion counting
microchip nebulizer
for DAPPI 633
MID *See* multiple ion detection
MIKES *See* mass-analyzed ion kinetic energy spectrometry
molecular beam solid analysis 479, 480
molecular ion 22, 250
criteria 289
definition 9
recognition 288
writing conventions 250
molecular ion peak
definition 9
molecular ions
relative stability 289
molecular weight *See* relative molecular mass
monoatomic layer
analysis by SIMS 702
monoisotopic elements
definition 68
monoisotopic mass 111
definition 72
most abundant mass 77, 111
mouse liver sections
by DESI 629
MRM *See* multiple reaction monitoring
MS/MS *See* tandem mass spectrometry
MS^2 *See* tandem mass spectrometry
MS^3 *See* tandem mass spectrometry
MS^n 439, *See* tandem mass spectrometry
multi-ion counting 693
multiphoton ionization 56
multiple ion detection *See* selected ion monitoring
multiple reaction monitoring 658
multiplexed
term 667
multiplexing 667
term 667
multiply charged ions
isotopic patterns 112
resolving isotopic patterns 590
MUX *See* liquid chromatography-mass spectrometry

N

NALDI *See* nano-assisted laser desorption/ionization
nano-assisted laser desorption/ionization 543
nanoelectrospray 574
chip-based 577
droplet size 574
memory effects 576
spray capillaries 576
emitters 576
nanoESI *See* nanoelectrospray
nebulizer
for ICP-MS 697
negative electron transfer dissociation 462
negative-ion APCI spectra 606
negative-ion chemical ionization 353, 368
negative-ion electrospray ionization 596
NETD *See* electron detachment dissociation
neutral loss 16
neutral losses 289
neutralization-reionization mass spectrometry 467
NICI 368, *See* negative-ion chemical ionization
NIST/EPA/NIH Mass Spectral Database 242

nitroarenes 331
nitrogen rule 265
  effect of autoprotonation 354
nominal mass
  definition 71
  deviations 93
nonclassical ions *See* distonic ions
nondestructive detection 177
nozzle-skimmer dissociation 573, 586
nozzle-skimmer system
  in ESI source 567
NR-MS *See* neutralization-reionization mass spectrometry
NSD *See* nozzle-skimmer dissociation
N-terminal fragment ions 533
nucleon number *See* mass number
nucleotides 597
number of charges
  in definition of *m/z* 8
number-average molecular weight
  of polymers 539
Nyquist criterion 181
Nyquist limit frequency 181

O

oaTOF *See* orthogonal acceleration TOF
object slit 143
odd-electron ion 22, 250
oil diffusion pump 209
oligonucleotides
  by ESI 596
onium ions 315
  immonium ions 315
  McLafferty rearrangement 315, 316
  onium reaction 315, 319
  oxonium ions 315
  sulfonium ions 315
onium reaction 315
open-shell ion *See* odd-electron ion
orbitrap 189
  in ESI 591
  ion detection 191
  ion injection 192
  resolving power 191
  tandem MS 445
  time scale 44
orbitrap mass spectrometer 194
organic salts
  EI mass spectra 314
ortho effect *See* ortho elimination
ortho elimination 326
  of aromatic molecular ions 327
  of even-electron ions 328
  of nitroarenes 331
orthogonal acceleration TOF 132
oxonium ions 262, 268

P

PA *See* proton affinity
PAN *See* panoramic pulsed ion extraction
panoramic pulsed ion extraction 129
parent ion 15
particle beam interface 238
parts per billion 96
parts per million 95, 96
parts per trillion 96
parts-per-trillion by volume 361
PBI *See* particle beam interface
PD *See* ^{252}Californium plasma desorption
peak shapes
  and KER 433
Penning ionization 24
  in DART 642
penta quadrupole 438
peptide fragmentation pathways 533
peptide mass map 531
peptide sequencing 496
perfluorokerosene 229
  mass calibration in EI 99
perfluorotributylamine 229
PFK *See* perfluorokerosene
phenanthroperylene
  EI spectrum 23
photodiode array 669
photoelectron spectroscopy 57
photoionization
  for determination of IEs 55
  in APPI 609
  process 55
  schemes 56
photon energies
  of UV lamps for APPI 610
phthalates

EI spectra 299
physical quantities
units for 17, 717
PI *See* photoionization
PICI *See* positive-ion chemical ionization
PIE *See* pulsed ion extraction
plant alkaloids
by DESI 629
plasma chromatography 198
plasma torch
for ICP-MS 697
plasticizers *See* phthalates
pneumatically assisted ESI 568
polydispersity
of polymers 539
polyisotopic elements
definition 69
polymers
analysis by FD-MS 400
positive-ion chemical ionization 353
ammonia reagent gas 359
energetics of protonation 356
isobutane reagent gas 359
methane reagent gas 355, 358
post-acceleration detector *See* detectors
post-source decay 428, 536
ppb *See* parts per billion
ppm 95, *See* parts per million
ppt *See* parts per trillion
pptv *See* parts-per-trillion by volume
precision 96
precursor ion 15
precursor ion scan 434, 438
problems and solutions 5
product ion 15
product ion scan 438
profile data
representation of spectra 10
protein molecules
charge state in ESI 584
protein structure
during ESI 601
proteomics 531
proton affinity 61, 356
determination 466
of some molecules *See* proton transfer reaction 61
proton transfer reaction mass spectrometry 361
protonated molecules
in CI 352
protonation
in CI 352
proton-bridged complex 320
PSD *See* post-source decay
pseudo MS^3 573
PTR mass spectrometer 363
PTR-MS *See* proton transfer reaction-MS
pulse excitation 178
pulsed ion extraction 129
Py-MS *See* pyrolysis mass spectrometry
pyrolysis DCI 374
pyrolysis mass spectrometry 237

Q

QET *See* quasi-equilibrium theory
QIT *See* quadrupole ion trap
QITTOF 196
QqICR 196
QqLIT 196
QqTOF 196
Q-TWIG-Q geometry 437
quadrupole analyzer *See* linear quadrupole analyzer
quadrupole ion trap 164
automatic gain control 170
axial modulation 170
mass-selective instability 168
mass-selective stability 168
MS^n 440
nonlinear resonances 171
principle 164
resonant ejection 169
shape of electrodes 164
trajectories 167
quadrupole mass filter *See* linear quadrupole analyzer
quantitation 651, 656, 659
calibration curve 659
external standardization 659
internal standardization 660
isotope dilution 661
quasi-equilibrium theory 37
basic assumptions 37
quasimolecular ions 352
QUISTOR See quadrupole ion trap

R

r + d *See* rings plus double bonds
radical ion 22, 250
radical-site initiated process 256
radiofrequency discharges
  in GD-MS 696
rate constants 38
  meaning 39
Rayleigh limit 565, 581
RDA *See* retro-Diels-Alder reaction
reagent gases
  in CI 359
rearrangement fragmentation 251
  $k_{(E)}$ functions 41
recombination energy 365
reconstructed ion chromatogram 12, 233, 653
reconstructed total ion current *See* total ion chromatogram
reconstructed total ion current chromatogram *See* total ion chromatogram
reduced cyclotron frequency 185
reference inlet system *See* reservoir inlet system
reflector
  in TOF-MS 126
reflectron *See* reflector
relative atomic mass
  definition 72
  variations 73
relative intensity
  definition 9
relative molecular mass
  definition 72
REMPI *See* resonance-enhanced multiphoton ionization
repeatability 96
reproducibility 96
reservoir inlet system 228
residual air
  EI spectrum 90
resolution
  10 % valley definition 89
  determination 90
  full width at half maximum definition 89
resolving power 89, 91
  effect of vacuum 128
resonance excitation 449
resonant excitation 175
retention times
  of isotopologs 663
ReTOF *See* time-of-flight analyzer
retro-1,4-addition *See* ortho elimination
retro-Diels-Alder reaction 300
  of isomeric ions 302
  of natural products 303
  requirements 300
retro-ene reaction 315
reverse library search 242
RF-only 152
RF-only hexapoles 152
RF-only octopoles 152
RF-only quadrupole 152
  collisional cooling 154
  collisional focusing 154
ribonucleic acids 597
RIC *See* reconstructed ion chromatogram, *See* reconstructed ion chromatogram, *See* reconstructed ion chromatogram, *See* reconstructed ion chromatogram
Rice-Ramsperger-Marcus-Kassel theory 37
RICs
  using RICs 234
ring electrode See quadrupole ion trap
rings plus double bonds 280
RNA
  by ESI 596
RRKM *See* Rice-Ramsperger-Marcus-Kassel theory
rules for interpretation 340, 733

S

σ-bond cleavage
  of functionalized molecules 254
  of non-functionalized molecules 251
  of saturated hydrocarbons 284
S/N *See* signal-to-noise ratio
saddle field gun 480
Saha-Langmuir equation 689
sample introduction system *See* inlet system
sample vial 232
sampling rate 131

sandwich methods 522
scan rate 142
scrambling 278
secondary ion mass spectrometry 479, 701
  dynamic 702
  imaging 544
  static 702, 704
SELDI *See* surface-enhanced laser desorption/ionization
selected ion monitoring 656
selected reaction monitoring *See*
selected-ion flow tube 361
self-CI 354
SEM *See* detectors
sensitivity 13
  of CI 353
  of EI sources 227
  of FAB-MS 496
  of FI and FD 405
separation of chiral compounds
  by IMS-MS 674
septum bleed
  in GC-MS 665
sequence coverage
  in peptide analysis 535
sequencing of oligonucleotides 597
SFC-MS *See* supercritical fluid chromatography-mass spectrometry
sheath flow
  ESI sprayers for CZE 568
SI *See* thermal ionization
SI units 17
SID *See* surface-induced dissociation
SIFT *See* selected-ion flow tube
signal-to-background ratio 14
signal-to-noise ratio 14, 655
SIM *See* selected ion monitoring
SIMION 227
  simulation of LIT 162
SIMS *See* secondary ion mass spectrometry
single-crystal silicon nanowires 542
single-LIT 445
SiNWs *See* single-crystal silicon nanowires
skimmer
  in ICP source 699
skimmer CID *See* nozzle-skimmer dissociation
slow heating method 451
soft ionization
  chemical ionization 351
  ESI 561
  field desorption 381
soft ionization methods 240
sonic spray ionization 635
Sophophora melanogaster 643
SORI *See* Fourier transform ion cyclotron resonance
SORI-CID 449
source slit 143
spark source
  for SS-MS 692
spark source mass spectrometry 691
spike
  isotopic enrichment 691
sputtering
  in SIMS 702
SRM *See* selected reaction monitoring
SSI *See* sonic spray ionization
SS-MS *See* spark source mass spectrometry
stability diagram *See* linear quadrupole analyzer
  of two-dimensional quadrupole field 148
stable ions 43
stacked ring ion guide 201
static SIMS 702
Stevenson's rule 257
sulfonium ions 269
supercritical fluid chromatography-mass spectrometry 651
supersonic expansion
  in FAB-MS 486
  in MALDI 512
surface ionization *See* thermal ionization
surface-enhanced laser desorption/ionization 543
surface-induced dissociation 426
SWIFT 448, *See* Fourier transform ion cyclotron resonance
symbols in MS 16
systematic approach to interpretation 341, 733

T

tabular listing
representation of spectra 10
tandem accelerator
for AMS 708
tandem mass spectrometry 415
on a ReTOF 427
pictograms 418
tandem-in-space 416
tandem-in-time 416
tandem MS *See* tandem mass spectrometry
for structure elucidation 675
in mixture analysis 651
on FT-ICR instruments 448
on quadrupole ion traps 439
on ReTOF instruments 429
on TOF instruments 418
on triple quadrupole instruments 438
table of examples 676
tandem-in-space MS *See* tandem mass spectrometry
tandem-in-time MS 439, 448
Taylor cone
in ESI 579
TDC *See* time-to-digital converter
temperature programed heaters
for direct probes 232
tetraiodoethene
NICI spectrum 369
Th *See* thomson
thermal degradation
decarbonylation 312
decarboxylation 312
elimination of water 312
of organic salts 314
RDA reaction 312
thermal ionization 689
efficiency 690
ion formation 689
thermal ionization mass spectrometry 689
thermionic emission 225
thermodynamic stability 257
thermokinetic method
for detn. of GB 466
thermospray 564
thin layer technique 522
thomson 9
three-dimensional quadrupole field *See* quadrupole ion trap
three-dimensional quadrupole ion trap
time scale 44
threshold laser irradiance
in MALDI 510
TIC *See* total ion chromatogram
tight transition state 42
time domain 179
time-lag focusing 128
time scale of ion activation 425
time scale of MS 42
timed ion selector 427
time-of-flight *See* time-of-flight analyzer
time-of-flight analyzer
flight times 122
linear TOF 124
principle 120
properties 121
reflector TOF 126
time-to-analog converter 124
time-to-digital converter 135
TIMS *See* thermal ionization
TI-MS *See* thermal ionization mass spectrometry
TLC-DESI 630
TLF *See* time-lag focusing
TMS *See* trimethylsilyl
TOF *See* time-of-flight analyzer
TOF/TOF instruments 430
TOF-SIMS imaging 707
top-down protein analysis 532
total ion chromatogram 12, 653
total ion current 11, 653
total ion current chromatogram *See* total ion chromatogram
transannular cleavages 333
traveling wave 199
traveling wave ion guide 199, 437
triarylmethyl ions 287
trimethylsilyl
derivatives 330
triple quadrupole
scan modes 439
triple quadrupole analyzer *See* linear quadrupole analyzer
triple quadrupole mass spectrometer
RF-only multipoles in 155
triply charged ion
in EI 22

trityl ion
  as fragment 392
tropylium ions 279
tryptic digest 531
TSP *See* thermospray
tuning of the instrument 227
turbomolecular pump 209
T-wave *See* traveling wave
TWIGs *See* traveling wave ion guide

U

u *See* unified atomic mass
UHPLC *See* ultrahigh-pressure liquid chromatography
ultra performance liquid chromatography 668
ultrafine-metal-plus-liquid-matrix method 508
ultrahigh-resolution 108
  applications 678
  isotopolog separation 108
ultrahigh-pressure liquid chromatography 668
ultrasonic expansion
  in ESI 567
ultrasonic nebulizer
  for ESI 568
ultraviolet photon dissociation 452
unified atomic mass
  definition 9, 71
unit resolution *See* linear quadrupole analyzer
units
  for physical quantities 17, 717
unperturbed cyclotron frequency 185
unstable ions 44
UPLC *See* ultra performance liquid chromatography
UV lamps
  in APPI 610
UV-MALDI 516

V

vacuum 208
  cryopump 209
  oil diffusion pump 209
  pumping speed 209
  rotary vane pump 209
  turbomolecular pump 209
vacuum lock 231
van de Graaff accelerator 708
van Krevelen diagram 106
  of DOM 107
velocity of ions 121
vertical transitions 27
very large hydrocarbons
  EI spectra 287
VOCs *See* volatile organic compounds
  above rain forrest 363
volatile organic compounds 361

W

weight-average molecular weight
  of polymers 539
wiggles
  from FT 180
Wiley/NBS Mass Spectral Database 242
World Trade Center 643

Z

zero-filling 180
zoom scans 164
z-spray 571
z-stack 205
zwitterions
  analysis by FD-MS 398